

University of Alberta

Biological Activity of Nanostructured Silver

by

Patricia L. Nadworny

A thesis submitted to the Faculty of Graduate Studies and Research
in partial fulfillment of the requirements for the degree of

Doctor of Philosophy

Department of Chemical and Materials Engineering
Medical Sciences - Biomedical Engineering

©Patricia Nadworny
Spring 2010
Edmonton, Alberta

Permission is hereby granted to the University of Alberta Libraries to reproduce single copies of this thesis and to lend or sell such copies for private, scholarly or scientific research purposes only. Where the thesis is converted to, or otherwise made available in digital form, the University of Alberta will advise potential users of the thesis of these terms.

The author reserves all other publication and other rights in association with the copyright in the thesis and, except as herein before provided, neither the thesis nor any substantial portion thereof may be printed or otherwise reproduced in any material form whatsoever without the author's prior written permission.

Examining Committee

Dr. Robert Burrell, Biomedical Engineering and Chemical and Materials Engineering

Dr. William McCaffrey, Chemical & Materials Engineering

Dr. Elaine Yacyshyn, Rheumatology

Dr. JianFei Wang, Surgery

Dr. Walied Moussa, Mechanical Engineering and Biomedical Engineering

Dr. Gregory Schultz, Biochemistry and Molecular Biology, University of Florida

Dedication

I would like to dedicate this work to my husband, Stephen Nadworny; my sister and her husband, Celeste and Brent Adrian; and my parents, Ross and Coleen Taylor. They have been a huge support to me.

Abstract

Although nanocrystalline silver is used commercially to treat burns and wounds, the mechanisms of action (MOA) for its activity are not clear. The purposes of this work were to determine if nanocrystalline silver has anti-inflammatory activity, determine physicochemical properties critical for its MOA, and develop nanocrystalline silver-derived solutions for use in the treatment of lung diseases, including ARDS and pneumonia. In a porcine contact dermatitis model, nanocrystalline silver had anti-inflammatory activity independent of antimicrobial activity, with increased apoptosis induction in inflammatory cells, but not keratinocytes; decreased expression of TNF- α , TGF- β , IL-8, and MMPs; and increased expression of IL-4, EGF, KGF, and KGF-2. Treatment with AgNO₃ (Ag⁺) increased inflammation, and caused apoptosis induction in keratinocytes. Thus, nanocrystalline silver releases additional species, perhaps Ag⁽⁰⁾-containing clusters, resulting in anti-inflammatory activity. SIMS analysis showed significant deposition of Ag-clusters after nanocrystalline silver, but not AgNO₃, treatment. Nanocrystalline silver had a systemic effect, despite SIMS analysis showing minimal skin penetration by silver, suggesting that nanocrystalline silver interacts with cells near tissue surfaces that release signals altering the inflammatory cascade. Relative to various Ag⁺-releasing dressings, nanocrystalline silver had significantly enhanced antimicrobial activity, Ag⁺-resistant bacteria kill, and was not prone to development of resistant bacteria, indicating that nanocrystalline silver releases antimicrobial species additional to Ag⁺, and has multiple bactericidal MOA. Single silver nanocrystals are inactive,

and heat treatment of nanocrystalline silver resulting in crystallites over ~30 nm caused loss of antimicrobial activity, soluble silver, silver oxide, and oxygen. This indicates a poly-nanocrystalline silver structure is necessary for optimal antimicrobial activity, as is having silver oxide to pin the nanostructure, preventing its growth. While oxygen is necessary during sputtering to produce silver oxide, too much oxygen reduces antimicrobial activity, as silver oxide is predominantly deposited. Sufficient total silver, modifiable with current and time, is also important for activity. Nanocrystalline silver-derived solution properties vary significantly with dissolution conditions. Solutions generated at pH 4-6 have stronger antimicrobial activity, and solutions generated at pH 9 have stronger anti-inflammatory activity. Overall, nanocrystalline silver-derived solutions have biological properties similar to nanocrystalline silver, indicating that they may be useful in a variety of medical applications.

Acknowledgements

I would like to thank my supervisors Dr. Robert Burrell and Dr. William McCaffrey for their help and advice. I would also like to thank my supervisory, candidacy (Dr. Jon Meddings and Dr. Carlos Lange), and defense committees for their efforts. Jay Willis, Dr. Craig Wilkinson, Tamara Staska, Janes Goller, Dianna Agate, and the rest of the SRTC staff provided excellent technical assistance, as well as help and advice throughout the porcine contact dermatitis studies (Chapters 2, 3, and 7). Dr. Merle Olsen and Nick Allen from Innovotech, Inc., as well as the Nagel Veterinary Clinic staff were very helpful throughout the rat pulmonary studies (Chapter 6). Meenaxi Kaheri and Michelle Adrian provided support with silver dissolution assays (Chapters 5, 6, 7) and sputtering (Chapter 8). Qin Fu, and Frank Pau from Sherritt Technologies, Inc., provided help with spectrophotometry and AAS. Wayne Moffat from Spectral Services at the University of Alberta provided help with spectrofluorimetry and spectrometry. Dr. Yeong Kim provided general assistance as lab manager. I would like to acknowledge the summer students who have collaborated with me in some of these studies: Breanne Landry (Chapters 3 and 9), Marion Cavanagh (Chapters 4 and 5), Jessica Burrell (Chapter 9), Anne-Marie Burrell (Chapter 8), Laura Kim (Chapter 8), Jeff Shrum (Chapter 4), Nicole Christensen (Chapter 4), Thulasy Balasubramaniam (Chapter 4), Tara Nord (Chapter 4), Corrie Olson (Chapter 4), and Asha Olmstead (Chapter 4). I would like to thank Dr. Tredget for providing space and equipment in the Plastic Surgery Lab, and the staff of the Plastic Surgery Lab for their support. Anna Szenthe and Rich Mah (Biological Sciences)

provided support with antimicrobial assays. Dr. Dimitre Karpusov and the rest of the ACSES staff provided assistance with XPS, SEM, and SIMS testing. Dr. Oladipo Omotoso provided assistance with XRD, and Randy Mikula provided assistance with SEM for Chapter 5 (Canmet ENERGY, NRC). Shiraz Merali provided much appreciated AAS analysis. Daniel Salamons (NINT) provided assistance with SEM imaging (Chapter 4). Coleen Taylor provided much appreciated editorial assistance. Ross Taylor provided technical support with spectrophotometry, and various other electronic/computing issues. The following sources of assistance funded this work: NSERC CGS-D2, NSERC CGS-M (prior to September 1, 2006), Alberta Ingenuity Graduate Scholarship in Nanotechnology, Alberta Ingenuity Studentship (prior to 2008), and Isaac Walton Killam Memorial Scholarship. Thank you God for helping me through everything.

Table of Contents

Volume 1

Chapter 1 – Introduction and Review of the Literature	1
Introduction.....	1
Background.....	4
Chemistry of Silver	4
Chemical Reactivity (Bio-availability) of Silver	5
Physical and Chemical Properties of Nanocrystalline Silver	7
Infection and Inflammation in Wound Healing	11
Antimicrobial Activity of Silver	14
Minimum Inhibitory Concentrations Required for Silver	
Treatments.....	14
Minimum Bactericidal Concentrations Required for Silver	
Treatments.....	16
Bactericidal Activity of Various Silver-Containing Dressings....	17
Bactericidal Activity of Nanocrystalline Silver	18
<i>In Vivo</i> and Clinical Outcomes Related to the Antimicrobial	
Activity of Nanocrystalline Silver	22
Anti-Inflammatory/Pro-Healing Activity of Nanocrystalline	
Silver	24
Purpose.....	35
Bibliography	39
Chapter 2 – Testing Nanocrystalline Silver Dressings For Anti-	

Inflammatory Activity	46
Introduction.....	46
Materials and Methods.....	53
Materials	53
Animals.....	53
Sensitization to DNCB and Elicitation of Inflammatory Reaction....	54
Treatment	55
Visual Observations	57
Histopathology	58
Gelatinase Zymography	59
Apoptosis Detection.....	62
Mast Cell Staining and Counts	67
mRNA Signal Detection	68
Tissue powdering.....	68
RNA extraction.....	69
RNA quantification.....	70
Reverse transcription (creation of cDNA)	70
Primers	71
Traditional RT-PCR amplification	73
Electrophoresis.....	73
Real time RT-PCR	74
Immunohistochemistry	76
Statistics	78

Results.....	78
Visual Assessment	78
Biopsy Bleeding.....	83
Weight.....	84
Histology.....	85
Skin Thickness	87
Gelatinase Zymography	90
Apoptosis Detection.....	96
Mast Cell Counts.....	100
Primer Testing.....	102
Semi-quantitative Analysis of mRNA expression	105
Immunohistochemistry	124
Discussion.....	126
Bibliography	136
Chapter 3 – Systemic Effect of Nanocrystalline Silver Dressings	140
Introduction.....	140
Materials and Methods.....	141
Materials	141
Samples.....	141
Testing for Silver Deposition in Tissues.....	141
XPS and SIMS	141
Testing for Remote Anti-inflammatory/Pro-healing Effects	143
Animals.....	143

Sensitization to DNCB and Elicitation of Inflammatory	
Reaction	144
Treatment	144
Visual Observations	145
Storage of Blood Samples.....	146
Histopathology	146
Apoptosis Detection and Quantification.....	146
Immunohistochemistry	148
Testing for Systemic Effect Via the Blood.....	150
IL-10 Detection (Tissue) and Quantification (Serum).....	150
Serum c-Reactive Protein Quantification	155
Statistics	157
Results.....	158
Testing for Silver Deposition in Tissues.....	158
XPS and SIMS	158
Testing for Remote Anti-inflammatory/Pro-healing Effects	169
Visual Observations	169
Biopsy Bleeding.....	172
Weight Change.....	173
Histopathology	174
Apoptosis Detection and Quantification.....	175
Immunohistochemical Detection of Cytokines and	
Growth Factors.....	177

Testing for Systemic Effects Via the Blood	186
IL-10 Tissue and Serum Levels	186
CRP Serum Levels	189
Discussion	191
Bibliography	204

Chapter 4 – Understanding Nanocrystalline Silver Antimicrobial

Mechanisms of Action Via Comparison to Other Silver Products	207
Introduction.....	207
Study #1: Comparison of Antimicrobial Efficacy of New Commercially Available Silver Dressings Relative to Nanocrystalline Silver Dressings	208
Background.....	208
Materials and Methods.....	213
Materials	213
Bactericidal Efficacy – Log Reduction Assay	215
Silver Dissolution Assay.....	217
Bacteriostatic Longevity – Day-to-Day Corrected Zone of Inhibition (CZOI) Assay	218
Statistics	219
Results.....	219
Discussion.....	224
Study #2: Development of Silver Resistance and Ability to Kill Ag ⁺ - Resistant Bacteria: Comparison of Nanocrystalline Silver to	

Other Silver Treatments	234
Background	234
Materials and Methods.....	250
Materials	250
Micro-organisms	254
MIC Testing	254
MBC Testing.....	254
Development of Ag ⁺ Resistant Bacteria using Silver Nitrate.....	255
Development of Silver-Dressing Resistant Bacteria.....	256
Testing for Ability of Silver Dressings to Kill Ag ⁺	
Resistant Bacteria.....	258
Growth Rates of Silver Resistant Strains.....	259
Testing for Stability of Mutation	260
Antibiotic Sensitivity Testing in Ag ⁺ Resistant <i>Pseudomonas</i>	
<i>aeruginosa</i>	260
Statistical Analyses	262
Results.....	262
Original MICs	262
Development of Ag ⁺ Resistant Bacteria	262
Development of Silver-Dressing Resistant Bacteria.....	285
Testing for Ability of Silver Dressings to Kill Ag ⁺	
Resistant Bacteria.....	294
Growth Rates of Silver Resistant Strains.....	296

Testing for Stability of SRPA Mutation	300
Antibiotic Sensitivity Testing in SRPA	302
Discussion.....	302
Study #3: Improving Understanding of Nanocrystalline Silver	
Mechanisms of Action: Structure Versus Size	312
Background.....	312
Materials and Methods.....	314
Materials	314
Microorganism.....	314
Log Reduction Assay	315
Scanning Electron Microscopy (SEM)	316
X-ray Photoelectron Spectroscopy (XPS)	316
Statistics	317
Results.....	317
Bactericidal Efficacy.....	317
SEM	318
XPS	320
Discussion.....	321
Conclusions.....	323
Bibliography	325

Volume 2

Chapter 5 – Releasing Biologically Active Nanocrystalline Silver

Species – Effect of Dissolution Conditions.....	333
--	------------

Introduction.....	333
Materials and Methods.....	338
Materials	338
Setup for Carbonated Water Dissolution Experiments.....	338
Procedure for Dissolutions.....	340
Spectrophotometric Analysis	341
Effect of Sampling	342
Spectrofluorimetry	343
Total Silver Profiles – Atomic Absorption.....	344
Ag ⁺ Profiles.....	344
Antimicrobial Activity	347
Effect of Dissolution on Nanocrystalline Silver Dressings	350
Scanning Electron Microscopy (SEM).....	350
X-ray Photoelectron Spectroscopy (XPS)	350
X-ray Diffraction (XRD)	351
Effect of Storage Under Vacuum.....	351
Statistics	352
Results and Discussion	352
Spectrophotometric Analysis	352
Effect of Sampling	387
Spectrofluorimetry	388
Total Silver Profiles	405
pH Profiles	424

Antimicrobial Activity	441
XPS	448
SEM	462
XRD	473
Conclusions.....	476
Bibliography	479

Chapter 6 – Testing for Anti-inflammatory and Antimicrobial

Activity of Nanocrystalline Silver-Derived Solutions in the Lung	483
Introduction.....	483
Materials and Methods.....	502
Materials	502
Anti-inflammatory Activity Study	503
Animals.....	503
Preparation of Nanocrystalline Silver Solutions.....	504
Induction of Inflammation	504
Treatment	505
Cryopreservation.....	506
Serum Preservation	506
Bacterial Cell Count.....	506
Histopathology	507
Lipopolysaccharide Titration Study.....	507
Animals.....	507
Induction of Inflammation	508

Pseudomonas Aeruginosa Titration Study.....	508
Animals.....	508
Induction of Infection.....	509
Bacterial Cell Counts.....	509
Antimicrobial Activity Study.....	510
Preparation of Tobramycin Solutions.....	510
Preparation of Silver Nitrate Solutions.....	510
Preparation of Nanocrystalline Silver Solutions.....	510
Animals.....	511
Induction of Infection.....	511
Treatment.....	512
Cryopreservation.....	513
Bacterial Cell Counts.....	513
Histopathology.....	514
Real Time RT-PCR.....	514
Tissue powdering.....	514
RNA extraction.....	514
RNA quantification.....	515
Reverse transcription (creation of cDNA).....	515
Primers.....	516
Real time RT-PCR.....	516
Nanocrystalline Silver-Derived Solution Controls.....	517
Animals.....	517

Treatment	517
Cryopreservation.....	518
Histopathology	518
Confirming Solution Properties	518
Bacteriostatic Activity, Silver Content, and Wetability.....	518
Characterization of Microsprayer Particle Size	519
Statistical Analysis.....	519
Results and Discussion (By Study).....	520
Anti-inflammatory Activity Study	520
Visual observations.....	520
Total Silver.....	521
Digital Images	521
Histology.....	522
Discussion.....	524
Lipopolysaccharide Titration Study.....	531
Visual Observations	531
Histology.....	531
Discussion.....	534
<i>Pseudomonas Aeruginosa</i> Titration Study.....	536
Visual Observations	537
Digital Images	537
Bacterial Counts.....	538
Antimicrobial Activity Study.....	539

<i>P. aeruginosa</i> dose.....	539
Visual Observations up to 24 Hours	539
Digital Images at 24 Hours	540
Histological Images at 24 Hours.....	541
Visual Observations From 24 to 72 Hours	545
Digital Images at 72 Hours	546
Histology at 72 Hours	547
Bacterial Load at 24 and 72 Hours	550
Real Time RT-PCR.....	551
Total Silver.....	556
Nanocrystalline Silver Controls.....	556
Visual Observations	556
Histology.....	557
Total Silver.....	558
Analyzing Solution Properties	558
Wetability.....	558
Bacteriostatic Activity	559
Total Silver.....	561
Microsprayer Characterization.....	563
Conclusions.....	563
Bibliography	570
Chapter 7 – Anti-inflammatory Activity of Nanocrystalline Silver-	
Derived Solutions Varies with Dissolution Conditions.....	577

Introduction.....	577
Materials and Methods.....	579
Materials	579
Animals.....	579
Sensitization to DNCB and Elicitation of Inflammatory Reaction....	580
Treatment	580
Total Silver Analysis.....	582
Visual Observations	582
Histopathology	583
mRNA Signal Detection and Quantification	583
Tissue Powdering.....	583
RNA Extraction	584
RNA Quantification	585
Reverse Transcription (creation of cDNA).....	585
Primers	586
Real Time RT-PCR.....	587
Gelatinase Zymography	588
Apoptosis Detection.....	590
Immunohistochemistry	592
Statistics	593
Results.....	594
Visual Assessment	594
Histology.....	605

Semi-quantitative Analysis of mRNA Expression	608
Gelatinase Zymography	631
Apoptosis Detection and Quantification.....	635
Immunohistochemistry	641
Average Solution Volume, Silver, and Calcium Delivered.....	666
Discussion.....	668
Bibliography	683

Chapter 8 – Effect of Sputtering Parameters on Resulting

Nanocrystalline Silver Thin Film Properties.....	686
Introduction.....	686
Materials and Methods.....	689
Generation of Nanocrystalline Silver Thin Films.....	689
Total Silver Digest	691
Ammonia Silver Digest.....	692
X-ray Diffraction (XRD)	692
Bactericidal Efficacy.....	693
Results and Discussion	694
Total and Ammonia Soluble Silver.....	694
XRD	743
Log Reductions	749
Conclusions.....	772
Bibliography	774

Chapter 9 – Using the kinetics of heat treatment to determine critical

physicochemical properties for nanocrystalline silver

antimicrobial activity	775
Introduction.....	775
Materials and Methods.....	786
Dressing Materials	786
Biological Assays.....	786
Bacterial Preparation.....	786
Log Reduction.....	787
Corrected Zone of Inhibition (CZOI)	788
Physical and Chemical Methods.....	789
Silver Dissolution.....	789
Scanning Electron Microscopy (SEM)	790
X-ray Diffraction (XRD)	791
X-ray Photoelectron Spectroscopy (XPS)	791
Thermal Analysis	792
Differential Scanning Calorimetry.....	792
Statistical Analysis.....	796
Results.....	796
Biological Assays.....	796
Log Reduction.....	796
Corrected Zones of Inhibition.....	797
Physical and Chemical Assays.....	799
Silver Dissolution.....	799

SEM Analysis	800
XRD Analysis	806
XPS Analysis	812
Thermal Analysis	815
Differential Scanning Calorimetry (DSC)	815
Discussion	819
Bibliography	830
Chapter 10 – Conclusions	832
Conclusions.....	832
Future Directions	840
Bibliography	842
Appendix 1 – HSLAS Protocol	843
Health Sciences Laboratory Animal Services Standard Operating Procedure Medical Sciences Building Necropsy M-B74	843
Appendix 2 – Lipopolysaccharide Isolation Protocol	847
Collection of Biomass and Lyophilization	847
LPS Extraction with Hot Phenol.....	849
Removal of Phenol from the LPS-Rich Aqueous Layer by Dialysis.....	849
Concentration of the LPS-Rich Aqueous Layer via Centrifugation	850
Reduction of Contaminants via Enzymatic Digestion	850
Final Centrifugation for Purification and Isolation of LPS	850
Assessment of LPS Purity.....	851
Bibliography	852

List of Tables

Volume 1

Table 1-1. Characteristics of noble metals.....	5
Table 1-2. ICE table for Ag ⁺ =1 ppm	6
Table 1-3. ICE table for Ag ⁺ =25 ppm	6
Table 3-1. Weights used in SIMS analysis	143
Table 3-2. XPS analysis of tissue composition after direct nanocrystalline silver treatment (24h)	158
Table 4-1. Dressing saturation volumes.....	220
Table 4-2. Bactericidal efficacy	221
Table 4-3. 24 hour silver release.....	221
Table 4-4. Comparison of various commercial silver dressings.....	239-40
Table 4-5. Water holding capacities of various silver containing dressings.....	258
Table 4-6. Minimum inhibitory concentrations for micro-organisms tested for the development of resistance to Ag ⁺	262
Table 4-7. Results of Ag ⁺ resistance development assay in <i>P. aeruginosa</i> ..	263-5
Table 4-8. Periodically measured MICs for <i>P. aeruginosa</i> during step-wise exposure to Ag ⁺	267
Table 4-9. Results of Ag ⁺ resistance development assay in <i>E. coli</i> (11303)	268-70
Table 4-10. Results of Ag ⁺ resistance development assay in <i>E. coli</i> (B/5).....	270-72
Table 4-11. Periodically measured MICs for <i>E. coli</i> 11303 and	

<i>E. coli</i> B/5 during step-wise exposure to silver nitrate (Ag ⁺)	274
Table 4-12. Results of Ag ⁺ resistance development assay in <i>E. aerogenes</i>	275
Table 4-13. Results of Ag ⁺ resistance development assay in <i>P. vulgaris</i>	277
Table 4-14. Results of Ag ⁺ resistance development assay in <i>S. aureus</i>	279-81
Table 4-15. Results of the Ag ⁺ resistance development assay in <i>S. epidermidis</i>	283-4
Table 4-16. MICs during attempts to develop resistance to silver hydrocolloid dressings	291
Table 4-17. Bactericidal efficacy of silver dressings against SRPA and its parent strain	295
Table 4-18. Bactericidal efficacy of silver dressings against SRSA and its parent strain	296
Table 4-19. Comparison of the bactericidal efficacy of various silver nanostructured materials	318

Volume 2

Table 5-1. Results of statistical analyses of the effect of varying dissolution conditions (the ratio of silver dressing to solution volume, and whether or not the solution was stirred) at starting pHs of 4 or 5.6 on the total silver dissolved.....	407-9
Table 5-2. Results of statistical analyses of the effect of varying the ratio of silver dressing to solution volume, at starting pHs of 7 or 9, on the total silver dissolved in stirred solutions.....	413

Table 5-3. Results of statistical analyses of the effect of starting pH (pH 4 versus pH 5.6) on the total silver dissolved in solutions generated in the absence of stirring	416
Table 5-4. Results of statistical analyses of the effect of starting pH (pH 4, pH 5.6, pH 7, or pH 9) on the total silver dissolved in solutions generated under stirring	418-21
Table 5-5. Results of statistical analyses of the effect of dissolution time on the total silver dissolved under various conditions	423
Table 5-6. Results of statistical analyses on the effect of varying dissolution conditions (stirred or unstirred, ratio of nanocrystalline silver dressing to solution) on the pH during dissolution using a starting pH of 4 or 5.6	425-7
Table 5-7. Results of statistical analyses on the effect of varying the ratio of nanocrystalline silver dressing to solution on the pH during dissolution using a starting pH of 7 or 9	430
Table 5-8. Results of statistical analyses of the effect of varying the starting pH (4 or 5.6), during dissolution without stirring, on pH over time	433
Table 5-9. Results of statistical analyses on the effect of varying the starting pH (4, 5.6, 7, or 9) during dissolution, with stirring, on the pH over time	435-8
Table 5-10. Results of the statistical analysis of the effect of dissolution time on the pH of solutions generated under various conditions.....	441

Table 5-11. Results of log reductions generated using nanocrystalline silver-derived solutions generated under a variety of conditions against <i>S. aureus</i>	443
Table 5-12. Results of statistical analyses of the effect of starting pH (pH 4 versus pH 5.6) on the bactericidal efficacy of solutions generated in the absence of stirring	443
Table 5-13. Results of statistical analyses on the effect of starting pH on the bactericidal efficacy of solutions generated under stirring for 24h.....	444
Table 5-14. Results of statistical analyses of the effect of stirring on the bactericidal efficacy of solutions	444
Table 5-15. Results of statistical analyses of the effect of varying the ratio of silver dressing to solution volume on bactericidal efficacy, holding other variables constant	445
Table 5-16. Results of statistical analyses of the effect of dissolution for 1 or 24 hours on bactericidal efficacy, holding other variables constant	446
Table 5-17. Summary of XRD analysis for nanocrystalline silver dressings dissolved at 35°C for 24 hours in various solutions.....	475
Table 5-18. Summary of XRD analysis for nanocrystalline silver dressings dissolved at 35°C for 24 hours in various solutions, followed by storage under vacuum.....	476

Table 6-1. Comparison of the IA-1B® and IA-1C® MicroSprayers by PennCentury™, Inc.....	503
Table 6-2. Bacterial counts from lungs of acute inflammation study at 24 hours.....	526
Table 6-3. Bacterial counts for <i>P. aeruginosa</i> titration study.....	539
Table 6-4. Bacterial counts for the antimicrobial activity study.....	551
Table 6-5. Total silver in solutions under various conditions.....	563
Table 8-1. Effect of substrate location on the total silver deposited when sputtering at 4% O ₂ and 0.75A for various lengths of time	720
Table 8-2. Effect of substrate sample location on the total silver deposited when sputtering for 10 minutes at various currents and oxygen concentrations	723-4
Table 8-3. Effect of oxygen concentration on the total silver deposited when sputtering for 10 minutes at various currents at substrate locations W3 and W4.....	725
Table 8-4. Effect of substrate sample location on the percent ammonia soluble silver deposited when sputtering for 10 minutes at various currents and oxygen concentrations.....	727-8
Table 8-5. Effect of oxygen concentration on the percent ammonia soluble silver deposited when sputtering for 10 minutes at various currents at substrate locations W3 and W4.....	729
Table 8-6. The effect of current on the total silver deposited when sputtering for 10 minutes at various oxygen concentrations at substrate	

locations W3 and W4.....	738
Table 8-7. The effect of current on the ammonia soluble silver deposited when sputtering for 10 minutes at various oxygen concentrations at substrate locations W3 and W4.....	740
Table 8-7. Results of XRD analysis of nanocrystalline silver thin films generated under a variety of sputtering conditions. All samples were sputtered for 10 minutes statically	747
Table 8-8. The effect of substrate location on the resulting log reduction generated against <i>P. aeruginosa</i> for nanocrystalline silver thin films generated at various oxygen concentrations, web speeds, and currents ..	751-3
Table 8-9. The effect of current on the log reductions generated against <i>P. aeruginosa</i> at substrate locations W3 and W4 when sputtering at various oxygen concentrations and web speeds.....	754
Table 8-10. The effect of web speed on log reductions produced against <i>P. aeruginosa</i> for nanocrystalline silver thin films generated at 4% oxygen and various currents	764
Table 8-11. The effect of percent oxygen on log reductions produced against <i>P. aeruginosa</i> for nanocrystalline silver thin films generated at various currents for dynamic runs at 20 mm/min	765
Table 8-12. Effect of substrate location on log reduction against <i>S. aureus</i> for nanocrystalline silver dressings generated using 10 minute static sputtering runs at various oxygen concentrations and currents.....	767

Table 8-13. The effect of 4, 8, 10, and 12% oxygen on log reductions generated against <i>S. aureus</i> for nanocrystalline silver thin films generated using 10 minute static sputtering runs at various currents	768
Table 8-14. The effect of current (0.75, 1, or 1.5 A) on log reductions generated against <i>S. aureus</i> for nanocrystalline silver thin films generated using 10 minute static sputtering runs at various currents	769
Table 9-1. Summary of XRD analysis, including domain size, composition, and microstrain for nanocrystalline silver dressings heat-treated for 24 hours at various temperatures.....	784
Table 9-2. XRD analysis of nanocrystalline silver dressings heat-treated at 90, 100, and 110°C for various times	808

List of Figures or Illustrations

Volume 1

Figure 1-1. The effect of varying chloride concentrations in solution on the free silver (Ag^+) concentrations generated from 40 mg/L silver nitrate.	7
Figure 1-2. Timeline of wound healing and corresponding cell populations in the wounds.	12
Figure 1-3. Study flow diagram for the thesis	37-8
Figure 2-1. Comparison of control animal data from two excisional mouse models of re-epithelialization, a partial thickness porcine wound model of re-epithelialization, and a clinical study of meshed skin graft re-epithelialization	52
Figure 2-2. Comparison of the effect of treatment with nanocrystalline silver dressings on an excisional mouse model of re-epithelialization, a partial thickness porcine wound model of re-epithelialization, and a clinical study of meshed skin graft re-epithelialization	52
Figure 2-3. Images of application of a nanocrystalline silver dressing over a DNCB-induced rash.	56
Figure 2-4. Images of porcine DNCB-induced rashes at various time points during elicitation of the rash	79
Figure 2-5. Representative images of porcine DNCB-induced rashes after one day of treatment	80
Figure 2-6. Representative images of porcine DNCB-induced rashes	

after two days of treatment	81
Figure 2-7. Representative images of porcine DNCB-induced rashes	
after three days of treatment	82
Figure 2-8. Erythema and edema scores for pigs with DNCB-induced	
contact dermatitis treated for three days with nanocrystalline silver,	
silver nitrate, or saline.....	83
Figure 2-9. Biopsy bleeding scores for pigs with DNCB-induced contact	
dermatitis treated for three days with nanocrystalline silver, silver	
nitrate, or saline.....	84
Figure 2-10. Weight change over three days for pigs with DNCB-induced	
contact dermatitis treated with nanocrystalline silver, silver nitrate,	
or saline.....	85
Figure 2-11. Representative images of tissue sections stained with	
hematoxylin and eosin for pigs with DNCB-induced contact	
dermatitis treated with saline, silver nitrate, or nanocrystalline silver	86
Figure 2-12. Total skin thickness in millimeters measured over time	
for DNCB- induced rashes treated with saline, silver nitrate, or	
nanocrystalline silver	88
Figure 2-13. Epidermal thickness in millimeters measured over time	
for DNCB- induced porcine rashes treated with saline, silver nitrate,	
or nanocrystalline silver.....	89
Figure 2-14. Standard curve of optical density versus protein	
Concentration created using BSA standards.....	91

Figure 2-15. Total protein ($\mu\text{g/mL}$) in biopsies from DNCB-induced rashes treated with saline, silver nitrate, or nanocrystalline silver at different time points	92
Figure 2-16. Gelatinase activity of tissue samples from DNCB-induced rashes treated with saline, silver nitrate, or nanocrystalline silver, along with negative controls	93
Figure 2-17. Semi-quantitative analysis of gelatinase activity in DNCB-induced porcine rashes treated with saline, silver nitrate, or nanocrystalline silver, as well as in negative controls	95
Figure 2-18. Representative fluorescence images for immunohistochemical detection of apoptotic cells in positive and negative controls for the experiment.....	96
Figure 2-19. Representative fluorescence images for immunohistochemical detection of apoptotic cells in the epidermis and upper dermis of DNCB- induced porcine rashes treated with saline, silver nitrate, or nanocrystalline silver, as well as negative controls.....	98
Figure 2-20. Semi-quantitative analysis of apoptotic staining after treatment of DNCB-induced rashes with saline, silver nitrate, or nanocrystalline silver	99
Figure 2-21. Representative fluorescence images for immunohistochemical detection of apoptotic cells in the deep dermis of DNCB-induced rashes treated with silver nitrate or	

nanocrystalline silver	100
Figure 2-22. Mast cell detection in DNCB-induced rashes after treatment with saline or silver nitrate.....	101
Figure 2-23. Mast cell quantification in DNCB-induced rashes after treatment with saline, silver nitrate, or nanocrystalline silver	101
Figure 2-24. Testing for successful primer design and cDNA synthesis.....	103-4
Figure 2-25. Relative expression of IL-1 β mRNA in negative controls and DNCB-induced porcine rashes treated with saline, silver nitrate, or nanocrystalline silver.....	107
Figure 2-26. Relative expression of IL-8 mRNA in negative controls and DNCB-induced porcine rashes treated with saline, silver nitrate, or nanocrystalline silver	108
Figure 2-27. Relative expression of IL-10 mRNA in negative controls and DNCB-induced porcine rashes treated with saline, silver nitrate, or nanocrystalline silver.....	109
Figure 2-28. Relative expression of IL-12 mRNA in negative controls and DNCB-induced porcine rashes treated with saline, silver nitrate, or nanocrystalline silver	110
Figure 2-29. Relative expression of TNF- α mRNA in negative controls and DNCB-induced porcine rashes treated with saline, silver nitrate, or nanocrystalline silver.....	111
Figure 2-30. Relative expression of TGF- β mRNA in negative controls and DNCB-induced porcine rashes treated with saline, silver nitrate,	

or nanocrystalline silver	112
Figure 2-31. Relative expression of IL-1 β mRNA in negative controls and DNCB-induced porcine rashes treated with saline, silver nitrate, or nanocrystalline silver	115
Figure 2-32. Relative expression of IL-8 mRNA in negative controls and DNCB-induced porcine rashes treated with saline, silver nitrate, or nanocrystalline silver	116
Figure 2-33. Relative expression of IL-12 mRNA in negative controls and DNCB-induced porcine rashes treated with saline, silver nitrate, or nanocrystalline silver	117
Figure 2-34. Relative expression of TNF- α mRNA in negative controls and DNCB-induced porcine rashes treated with saline, silver nitrate, or nanocrystalline silver	118
Figure 2-35. Relative expression of TGF- β mRNA in negative controls and DNCB-induced porcine rashes treated with saline, silver nitrate, or nanocrystalline silver	119
Figure 2-36. Relative expression of IL-8 mRNA in negative controls and DNCB-induced porcine rashes treated with saline, silver nitrate, or nanocrystalline silver	122
Figure 2-37. Relative expression of IL-12 mRNA in negative controls and DNCB-induced porcine rashes treated with saline, silver nitrate, or nanocrystalline silver	123
Figure 2-38. Relative expression of TNF- α mRNA in negative controls	

and DNCB-induced porcine rashes treated with saline, silver nitrate, or nanocrystalline silver	124
Figure 2-39. Representative images for immunohistochemical detection of cytokines after 72 hours of treatment of DNCB-induced porcine rashes with saline, silver nitrate, or nanocrystalline silver, as well as negative controls.....	125
Figure 2-40. Representative images for immunohistochemical detection of TGF- β after 24 hours of treatment with saline, silver nitrate, or nanocrystalline silver	126
Figure 3-1. Standard curve for the optical densities of the lowest concentration standards versus pIL-10 concentration (pg/mL)	154
Figure 3-2. Standard curve for the optical densities of all standards versus pIL-10 concentration (pg/mL)	155
Figure 3-3. Standard curve for the optical densities of the highest concentration standards versus CRP concentration (ng/mL).....	157
Figure 3-4. Representative images of SIMS analysis of summed weights of various silver species deposited in porcine epidermis and upper dermis.....	162-5
Figure 3-5. Comparison of maximum count measurements for silver species deposited in the upper dermis and epidermis of pigs receiving various treatments for DNCB-induced rashes	166-8
Figure 3-6. Representative images of porcine DNCB-induced rashes over three days of treatment with remote nanocrystalline silver	170

Figure 3-7. Erythema scores with remote treatment.....	171
Figure 3-8. Edema scores with remote treatment	172
Figure 3-9. Biopsy bleeding scores for pigs with DNCB-induced contact dermatitis treated for three days with remote nanocrystalline silver	173
Figure 3-10. Representative histological images of remotely-treated tissue	175
Figure 3-11. Representative fluorescence images obtained via confocal microscopy for immunohistochemical detection of apoptotic cells in the epidermis and upper dermis of pigs with contact dermatitis undergoing remote treatments.....	177
Figure 3-12. Representative images for immunohistochemical detection of TNF- α after 24h and 72h treatment of DNCB-induced porcine contact dermatitis rashes with saline, or remote nanocrystalline silver...	178
Figure 3-13. Representative images for immunohistochemical detection of IL-8 after 24h and 72h treatment with DNCB-induced porcine contact dermatitis rashes with saline, or remote nanocrystalline silver...	179
Figure 3-14. Representative images for immunohistochemical detection of IL-4 after 24h and 72h treatment of DNCB-induced porcine contact dermatitis rashes with saline, remote nanocrystalline silver, or direct nanocrystalline silver	180
Figure 3-15. Representative images for immunohistochemical detection of IL-10 (using a monoclonal antibody) after 24h and 72h treatment of DNCB-induced porcine contact dermatitis rashes with saline,	

remote nanocrystalline silver, or direct nanocrystalline silver	181
Figure 3-16. Representative images for immunohistochemical detection of TGF- β after 24h and 72h treatment of DNCB-induced porcine contact dermatitis rashes with saline, or remote nanocrystalline silver ...	182
Figure 3-17. Representative images for immunohistochemical detection of EGF after 24h and 72h treatment of DNCB-induced porcine contact dermatitis rashes with saline, remote nanocrystalline silver, or direct nanocrystalline silver	183
Figure 3-18. Representative images for immunohistochemical detection of KGF after 24h and 72h treatment of DNCB-induced porcine contact dermatitis rashes with saline, remote nanocrystalline silver, or direct nanocrystalline silver	184
Figure 3-19. Representative images for immunohistochemical detection of KGF-2 after 24h and 72h treatment of DNCB-induced porcine contact dermatitis rashes with saline, remote nanocrystalline silver, or direct nanocrystalline silver	186
Figure 3-20. Representative images for immunohistochemical detection of IL-10 (using a polyclonal antibody) after 24h, 48h, or 72h of treatment with saline, silver nitrate, or direct nanocrystalline silver	188
Figure 3-21. Serum IL-10 levels measured from pigs with DNCB- induced rashes before treatment, and treated for three days with saline, silver nitrate, direct nanocrystalline silver, or remote nanocrystalline silver	189

Figure 3-22. Serum CRP levels measured for pigs with DNCB-induced rashes before treatment, and treated for three days with saline, silver nitrate, direct nanocrystalline silver, or remote nanocrystalline silver	190
Figure 3-23. Serum CRP levels with outliers removed	191
Figure 4-1. Corrected zone of inhibition (CZOI) of <i>S. aureus</i> over a series of days for nanocrystalline silver dressings, silver collagen matrix dressings, and silver alginate dressings	223-4
Figure 4-2. Diffraction pattern of Aquacel Ag®	253
Figure 4-3. Decision tree for the incremental development of silver-resistant organisms.....	256
Figure 4-4. The Ag ⁺ (silver nitrate) concentration that <i>Pseudomonas aeruginosa</i> (ATCC 27317) was exposed to during silver-resistance development experiments	266
Figure 4-5. The Ag ⁺ (silver nitrate) concentration that <i>Escherichia coli</i> (ATCC 11393) was exposed to during silver-resistance development experiments	273
Figure 4-6. The Ag ⁺ (silver nitrate) concentration that <i>Escherichia coli</i> (B/5) was exposed to during silver-resistance development experiments.....	273
Figure 4-7. The Ag ⁺ (silver nitrate) concentration that <i>Enterobacter aerogenes</i> (62-1) was exposed to during three silver-resistance development experiments	276

Figure 4-8. The Ag ⁺ (silver nitrate) concentration that <i>Proteus vulgaris</i> was exposed to during two silver-resistance development experiments.....	278
Figure 4-9. The Ag ⁺ (silver nitrate) concentration that <i>Staphylococcus aureus</i> (ATCC 25923) was exposed to during four silver-resistance development experiments	282
Figure 4-10. The Ag ⁺ (silver nitrate) concentration that <i>Staphylococcus epidermidis</i> (ATCC e15J) was exposed to during silver-resistance development experiments	284
Figure 4-11. Corrected zones of inhibition are plotted over time for six attempts to develop <i>P. aeruginosa</i> which were resistant to a nanocrystalline silver dressing.....	286
Figure 4-12. Corrected zones of inhibition are plotted over time for two attempts to develop <i>P. aeruginosa</i> which were resistant to a silver alginate dressing.....	287
Figure 4-13. Corrected zones of inhibition are plotted over time for an attempt to develop <i>P. aeruginosa</i> which were resistant to a silver chloride dressing.....	288
Figure 4-14. Corrected zones of inhibition are plotted over time for three attempts to develop <i>P. aeruginosa</i> which were resistant to a silver NaCMC dressing.....	289
Figure 4-15. Corrected zones of inhibition are plotted over time for two attempts to develop <i>P. aeruginosa</i> which were resistant to a silver	

hydrocolloid dressing.....	290
Figure 4-16. Corrected zones of inhibition are plotted over time for an attempt to develop <i>P. aeruginosa</i> which were resistant to a silver nylon dressing.....	292
Figure 4-17. Corrected zones of inhibition are plotted over time for an attempt to develop <i>P. aeruginosa</i> which were resistant to an ionic silver foam dressing.....	293
Figure 4-18. Corrected zones of inhibition are plotted over time for four attempts to develop <i>S. aureus</i> which were resistant to a nanocrystalline silver dressing.....	294
Figure 4-19. Optical densities are shown over time for SRPA and its parent strain grown up in TSB.....	297
Figure 4-20. Viable cell counts are shown over time for SRPA and its parent strain grown up in TSB.....	298
Figure 4-21. Optical densities are shown over time for SRSA and its parent strain grown up in TSB.....	299
Figure 4-22. Viable cell counts are shown over time for SRSA and its parent strain grown up in TSB.....	300
Figure 4-23. MICs to Ag ⁺ (silver nitrate) are shown over time for SRPA grown up daily in TSB (with no exposure to Ag ⁺).....	302
Figure 4-24. Scanning electron microscopy (SEM) images of silver exchanged zeolites.....	319
Figure 4-25. Representative SEM image of a nanocrystalline silver	

dressing	319
Figure 4-26. Representative XPS spectra for silver exchanged zeolites and nanocrystalline silver dressings.....	320
Volume 2	
Figure 5-1. Setup for generating and testing nanocrystalline silver- derived solutions	340
Figure 5-2. Initial testing of the antimicrobial activity of nanocrystalline silver-derived solutions.....	349
Figure 5-3. Example of effect of starting pH on absorbance of nanocrystalline silver-derived solutions	353
Figure 5-4. Relationship between peak height at 210 nm in spectrophotometric scans and total silver in nanocrystalline silver- derived solutions	354
Figure 5-5. Example of spikes generated from a nanocrystalline silver- derived solution started at pH 4 using an Ultrospec 3000	355
Figure 5-6. Example of spikes generated from a nanocrystalline silver- derived solution started at pH 4.5 using an Ultrospec 3000	356
Figure 5-7. Example of spikes generated from a nanocrystalline silver- derived solution started at pH 5.6 using an Ultrospec 3000	357
Figure 5-8. Example of spikes generated in a quartz cuvette after it held a nanocrystalline silver-derived solution started at pH 5.6 using an Ultrospec 3000	359
Figure 5-9. Example of a spectrophotometric scan of a nanocrystalline	

silver-derived solution using an Ultrospec 2000	361
Figure 5-10. Effect of multiple spectrophotometric scan on a nanocrystalline silver-derived solution	361
Figure 5-11. Spectrophotometric analysis of a nanocrystalline-silver derived solution, generated at a starting pH of 4, performed using a diode array	362
Figure 5-12. Spectrophotometric analysis of a nanocrystalline silver- derived solution, generated at a starting pH of 5.6, performed using a diode array	363
Figure 5-13. Spectrophotometric scan of a nanocrystalline silver-derived solution, generated at a starting pH of 4, using an Ultrospec 3000	363
Figure 5-14. Spectrophotometric scan of a nanocrystalline silver-derived solution, generated at a starting pH of 5.6, using an Ultrospec 3000	364
Figure 5-15. Spectrophotometric scan of nanocrystalline silver dissolved in nitric acid for one hour.....	365
Figure 5-16. Spectrophotometric scan of nanocrystalline silver dissolved in nitric acid for 17 hours.....	366
Figure 5-17. Spectrophotometric scan of 0.25% nitric acid	366
Figure 5-18. Spectrophotometric scan of sodium nitrate.....	367
Figure 5-19. Spectrophotometric scans of silver nitrate	367
Figure 5-20. Spectrophotometric scan of silver nitrate in sodium hydroxide	368
Figure 5-21. Spectrophotometric scan of high density polyethylene	

backing in nitric acid.....	369
Figure 5-22. Spectrophotometric scan of nanocrystalline silver dissolved in nitric acid (HDPE reference)	370
Figure 5-23. Spectrophotometric scan of nanocrystalline silver dissolved in sodium nitrate	371
Figure 5-24. Spectrophotometric scan of nanocrystalline silver dissolved in acetic acid	373
Figure 5-25. Spectrophotometric scan of nanocrystalline silver dissolved in carbonic acid.....	374
Figure 5-26. Spectrophotometric scan of nanocrystalline silver dissolved in phosphoric acid.....	375
Figure 5-27. Spectrophotometric scan of nanocrystalline silver dissolved in glacial acetic acid with sodium nitrate for one hour.....	376
Figure 5-28. Spectrophotometric scan of nanocrystalline silver dissolved in glacial acetic acid with sodium nitrate for 24 hours	377
Figure 5-29. Spectrophotometric scan of ammonia.....	378
Figure 5-30. Spectrophotometric scan of a nanocrystalline silver dissolved in ammonia for different periods of time.....	379
Figure 5-31. Spectrophotometric scan of silver nitrate in nitric acid	380
Figure 5-32. Spectrophotometric scan of silver nitrate in glacial acetic acid.....	381
Figure 5-33. Excitation scans for various nanocrystalline silver-derived solutions using a spectrofluorimeter	391

Figure 5-34. Emission scans for various nanocrystalline silver-derived solutions using a spectrofluorimeter	392
Figure 5-35. Excitation scans for examination of the effect of allowing a nanocrystalline silver-derived solution to sit in a cuvette for various lengths of time (without exposure to further nanocrystalline silver)	393
Figure 5-36. Emission scans for examination of the effect of allowing a nanocrystalline silver-derived solution to sit in a cuvette for various lengths of time (without exposure to further nanocrystalline silver)	394
Figure 5-37. Excitation scans for examination of the effect of rinsing a cuvette with a nanocrystalline silver-derived solution	395
Figure 5-38. Emission scans for studying the effect of rinsing a cuvette with a nanocrystalline silver-derived solution	396
Figure 5-39. Excitation scans testing for the presence of adsorbed species on cuvettes after exposure to nanocrystalline silver-derived solutions ...	397
Figure 5-40. Emission scans testing for the presence of adsorbed species on cuvettes after exposure to nanocrystalline silver-derived solutions ...	398
Figure 5-41. Total silver profiles over time for nanocrystalline silver-derived solutions generated at a starting pH of 4 under various conditions	407
Figure 5-42. Total silver profiles over time for nanocrystalline silver-derived solutions generated at a starting pH of 5.6 under various conditions	411
Figure 5-43. Total silver profiles over time for nanocrystalline silver-	

<p>derived solutions generated at a starting pH of 7 at different silver:solution ratios.....</p>	412
<p>Figure 5-44. Total silver profiles over time for nanocrystalline silver-derived solutions generated at a starting pH of 9 at different silver:solution ratios.....</p>	414
<p>Figure 5-45. Comparison of total silver profiles over time of nanocrystalline silver-derived solutions generated at starting pHs of 4 (carbonated water) and 5.6 (distilled water), unstirred, at a ratio of 1:5 in² Ag/mL solution.....</p>	415
<p>Figure 5-46. Comparison of total silver profiles over time of nanocrystalline silver-derived solutions generated at starting pHs of 4 (carbonated water) and 5.6 (distilled water), unstirred, at a ratio of 1:1 in² Ag/mL solution.....</p>	417
<p>Figure 5-47. Comparison of total silver profiles over time of nanocrystalline silver-derived solutions generated at starting pHs of 4 (carbonated water), 5.6 (distilled water), 7 (adjusted using calcium hydroxide), or 9 (adjusted using calcium hydroxide), stirred, at a ratio of 1:5 in² Ag/mL solution</p>	418
<p>Figure 5-48. Comparison of total silver profiles over time of nanocrystalline silver-derived solutions generated at starting pHs of 4 (carbonated water), 5.6 (distilled water), 7 (adjusted using calcium hydroxide), or 9 (adjusted using calcium hydroxide), stirred, at a ratio of 1:1 in² Ag/mL solution</p>	422

Figure 5-49. pH profiles over time for nanocrystalline silver-derived solutions generated at a starting pH of 4 under various conditions	425
Figure 5-50. pH profiles over time for nanocrystalline silver-derived solutions generated at a starting pH of 5.6 under various conditions	428
Figure 5-51. pH profiles over time for nanocrystalline silver-derived solutions generated at a starting pH of 7 at different silver:solution ratios.....	429
Figure 5-52. pH profiles for nanocrystalline silver-derived solutions generated at a starting pH of 9 at different silver:solution ratios.....	431
Figure 5-53. Comparison of pH profiles over time for nanocrystalline silver-derived solutions generated at starting pHs of 4 (carbonated water) and 5.6 (distilled water), unstirred, at a ratio of 1:5 in ² Ag/mL solution.....	432
Figure 5-54. Comparison of pH profiles over time for nanocrystalline silver-derived solutions generated at starting pHs of 4 (carbonated water) and 5.6 (distilled water), unstirred, at a ratio of 1:1 in ² Ag/mL solution.....	434
Figure 5-55. Comparison of pH profiles over time for nanocrystalline silver-derived solutions generated at starting pHs of 4 (carbonated water), 5.6 (distilled water), 7 (adjusted using calcium hydroxide), or 9 (adjusted using calcium hydroxide), stirred, at a ratio of 1:5 in ² Ag/mL solution	435
Figure 5-56. Comparison of pH profiles over time for nanocrystalline	

silver-derived solutions generated at starting pHs of 4 (carbonated water), 5.6 (distilled water), 7 (adjusted using calcium hydroxide), or 9 (adjusted using calcium hydroxide), stirred, at a ratio of 1:1 in ² Ag/mL solution.....	439
Figure 5-57. Unusual growth of <i>P. aeruginosa</i> with the appearance of plaques, suggesting infection of the culture by a bacteriophage	447
Figure 5-58. Summary of XPS intensities of C 1s peaks for nanocrystalline silver dressings after heating dry at 37°C (control dressings), or dissolution at 37°C in solutions at starting pHs of 4 (adjusted using HCl), 5.6 (reverse osmosis water), 9 (adjusted using NaOH), or fetal calf serum.....	449
Figure 5-59. Examples of deconvolution of C 1s XPS spectra for nanocrystalline silver dressings after dissolution under various conditions.....	450-2
Figure 5-60. Summary of XPS intensities of O 1s peaks for nanocrystalline silver dressings after heating dry at 37°C (control dressings), or dissolution at 37°C in solutions at starting pHs of 4 (adjusted using HCl), 5.6 (reverse osmosis water), 9 (adjusted using NaOH), or fetal calf serum.....	453
Figure 5-61. Examples of deconvolution of O 1s XPS spectra for nanocrystalline silver dressings after dissolution under various conditions.....	454-6
Figure 5-62. Summary of XPS intensities of Ag 3d peaks for	

nanocrystalline silver dressings after heating dry at 37°C (control dressings), or dissolution at 37°C in solutions at starting pHs of 4 (adjusted using HCl), 5.6 (reverse osmosis water), 9 (adjusted using NaOH), or fetal calf serum.....	457
Figure 5-63. Examples of deconvolution of Ag 3d XPS spectra for nanocrystalline silver dressings after dissolution under various conditions.....	458-60
Figure 5-64. Measurement of total oxygen and silver oxide via XPS	461-2
Figure 5-65. SEM images of nanocrystalline silver dressings heated dry at 37°C (controls)	463-4
Figure 5-66. SEM images of nanocrystalline silver dressings dissolved at a starting pH of 4 (adjusted using HCl) at 37°C	464-5
Figure 5-67. SEM images of nanocrystalline silver dressings dissolved at a starting pH of 5.6 (reverse osmosis water) at 37°C.....	466-7
Figure 5-68. SEM images of nanocrystalline silver dressings dissolved at a starting pH of 9 (adjusted using sodium hydroxide) at 37°C	468-9
Figure 5-69. SEM image of nanocrystalline silver dressings dissolved in fetal calf serum at 37°C for 2 hours	470
Figure 5-70. SEM images of nanocrystalline silver dressings heated dry at 37°C, followed by placement in a vacuum chamber.....	471-2
Figure 6-1. Images of lungs in the lung cavities of rats after euthanasia at the end of the anti-inflammatory activity study (24 hours)	522
Figure 6-2. Representative histological images of the lungs of each rat	

24 hours after treatment in the anti-inflammatory activity study	523-4
Figure 6-3. Images from the literature demonstrating the techniques for visualizing the trachea and using microsyringes in rats.....	525
Figure 6-4. Histological images showing the range of inflammation present in the upper left lung lobe of each rat used in the lipopolysaccharide (LPS) titration study	532-34
Figure 6-5. Representative digital images showing the upper left lung lobe of rats used in the <i>Pseudomonas aeruginosa</i> titration study.....	538
Figure 6-6. Representative digital images showing the portions of lung lobes of rats used for bacterial counts in the antimicrobial activity study 24 hours after inoculation of a 1:30 dilution of <i>Pseudomonas aeruginosa</i> incubated at 37°C overnight, followed four hours later by various treatments	541
Figure 6-7. Histological images showing the range of inflammation present in the upper left lung lobe of each rat euthanized 24 hours into the antimicrobial activity study	543-5
Figure 6-8. Representative digital images showing the portions of lung lobes of rats used for bacterial counts in the antimicrobial activity study 72 hours after inoculation of a 1:30 dilution of <i>Pseudomonas aeruginosa</i> incubated at 37°C overnight, followed four hours later by various treatments	547
Figure 6-9. Histological images showing the range of inflammation present in the upper left lung lobe of each rat euthanized at 72 hours	

in the antimicrobial activity study.....	548-50
Figure 6-10. Real time RT-PCR reaction rates.....	552
Figure 6-11. Relative expression of TNF- α mRNA in negative controls, <i>P. aeruginosa</i> infected rat lungs treated for 24 hours with 100 μ L of distilled water (positive controls), 2.4 mg/mL tobramycin in 0.9% saline, 0.31 mg/mL silver nitrate in distilled water, or nanocrystalline silver-derived solution (starting pH of 4, 24 hour dissolution time, ~100 rpm, 1 in ² /mL).....	553
Figure 6-12. Real time RT-PCR reaction rates.....	554-5
Figure 6-13. Relative expression of TNF- α mRNA in negative controls, <i>P. aeruginosa</i> infected rat lungs treated for 72 hours with 100 μ L of distilled water (positive controls), 2.4 mg/mL tobramycin in 0.9% saline, 0.31 mg/mL silver nitrate in distilled water, or nanocrystalline silver-derived solution (starting pH of 4, 24 hour dissolution time, ~100 rpm, 1 in ² /mL)	556
Figure 6-14. Histological images showing the range of inflammation present in the upper left lung lobe of each nanocrystalline silver control rat euthanized after 24 hours	558
Figure 6-15. Solution watability	559
Figure 6-16. Bacteriostatic activity of nanocrystalline silver-derived solutions	560-1
Figure 7-1. Digital images of rashes exposed to DNCB four times and then treated with various nanocrystalline silver-derived solutions.....	595

Figure 7-2. Digital images of rashes treated with various nanocrystalline silver-derived solutions on skin exposed once to DNCB after sensitization of the animal	597-9
Figure 7-3. Erythema scores for porcine skin exposed to DNCB four times over two weeks and then treated with various nanocrystalline silver-derived solutions.....	600
Figure 7-4. Edema scores for porcine skin exposed to DNCB four times over two weeks and then treated with various nanocrystalline silver-derived solutions.....	601
Figure 7-5. Biopsy bleeding scores for skin exposed to DNCB four times over two weeks and then treated various nanocrystalline silver-derived solutions	602
Figure 7-6. Erythema scores for porcine skin exposed to DNCB once (after sensitization of the animal) and then treated with various nanocrystalline silver-derived solutions	603
Figure 7-7. Edema scores for porcine skin exposed to DNCB once (after sensitization of the animal) and then treated with various nanocrystalline silver-derived solutions	604
Figure 7-8. Biopsy bleeding scores for skin exposed to DNCB once (after sensitization of the animal) and then treated various nanocrystalline silver-derived solutions.....	605
Figure 7-9. Representative histological images for skin exposed to DNCB four times over two weeks and then treated with various	

nanocrystalline silver-derived solutions	606-7
Figure 7-10. Representative histological images for skin exposed to DNCB once (after sensitization of the animal) and then treated with various nanocrystalline silver-derived solutions.....	609
Figure 7-11. Real time RT-PCR reaction rates for 24h samples	610-14
Figure 7-12. Real time RT-PCR reaction rates for 72h samples	614-18
Figure 7-13. Relative expression of TNF- α mRNA in negative controls and DNCB-induced porcine rashes treated for 24 hours with distilled water (positive controls), or nanocrystalline silver-derived solutions generated at starting pHs of 4, 5.6, 7, and 9.....	619
Figure 7-14. Relative expression of IL-1 β mRNA in negative controls and DNCB-induced porcine rashes treated for 24 hours with distilled water (positive controls), or nanocrystalline silver-derived solutions generated at starting pHs of 4, 5.6, 7, and 9	620
Figure 7-15. Relative expression of IL-8 mRNA in negative controls and DNCB-induced porcine rashes treated for 24 hours with distilled water (positive controls), or nanocrystalline silver-derived solutions generated at starting pHs of 4, 5.6, 7, and 9.....	621
Figure 7-16. Relative expression of IL-10 mRNA in negative controls and DNCB-induced porcine rashes treated for 24 hours with distilled water (positive controls), or nanocrystalline silver-derived solutions generated at starting pHs of 4, 5.6, 7, and 9.....	622
Figure 7-17. Relative expression of IL-12 mRNA in negative controls and	

<p>DNCB-induced porcine rashes treated for 24 hours with distilled water (positive controls), or nanocrystalline silver-derived solutions generated at starting pHs of 4, 5.6, 7, and 9.....</p>	623
<p>Figure 7-18. Relative expression of IL-17 mRNA in negative controls and DNCB-induced porcine rashes treated for 24 hours with distilled water (positive controls), or nanocrystalline silver-derived solutions generated at starting pHs of 4, 5.6, 7, and 9.....</p>	624
<p>Figure 7-19. Relative expression of TNF-α mRNA in negative controls and DNCB-induced porcine rashes treated for 72 hours with distilled water (positive controls), or nanocrystalline silver-derived solutions generated at starting pHs of 4, 5.6, 7, and 9.....</p>	625
<p>Figure 7-20. Relative expression of IL-1β mRNA in negative controls and DNCB-induced porcine rashes treated for 72 hours with distilled water (positive controls), or nanocrystalline silver-derived solutions generated at starting pHs of 4, 5.6, 7, and 9.....</p>	626
<p>Figure 7-21. Relative expression of IL-8 mRNA in negative controls and DNCB-induced porcine rashes treated for 72 hours with distilled water (positive controls), or nanocrystalline silver-derived solutions generated at starting pHs of 4, 5.6, 7, and 9.....</p>	627
<p>Figure 7-22. Relative expression of IL-10 mRNA in negative controls and DNCB-induced porcine rashes treated for 72 hours with distilled water (positive controls), or nanocrystalline silver-derived solutions generated at starting pHs of 4, 5.6, 7, and 9.....</p>	628

Figure 7-23. Relative expression of IL-12 mRNA in negative controls and DNCB-induced porcine rashes treated for 72 hours with distilled water (positive controls), or nanocrystalline silver-derived solutions generated at starting pHs of 4, 5.6, 7, and 9.....	629
Figure 7-24. Relative expression of IL-17 mRNA in negative controls and DNCB-induced porcine rashes treated for 72 hours with distilled water (positive controls), or nanocrystalline silver-derived solutions generated at starting pHs of 4, 5.6, 7, and 9.....	630
Figure 7-25. Zymogram showing gelatinase activity in biopsies from DNCB-induced rashes treated with various nanocrystalline silver-derived solutions	631
Figure 7-26. Quantitation of MMP band intensities from biopsies of DNCB-induced rashes treated with various nanocrystalline silver-derived solutions	633-4
Figure 7-27. Apoptosis detection in biopsies of DNCB-induced rashes treated for 24 hours with various nanocrystalline silver-derived solutions	636-40
Figure 7-28. Immunohistochemical detection of TNF- α in biopsies of DNCB-induced rashes treated with various nanocrystalline silver-derived solutions for 24 hours.....	642
Figure 7-29. Immunohistochemical detection of TNF- α in biopsies of DNCB-induced rashes treated with various nanocrystalline silver-derived solutions for 72 hours.....	643

Figure 7-30. Semi-quantitative analyses of immunohistochemical staining for TNF- α in biopsies of DNCB-induced rashes treated with various nanocrystalline silver-derived solutions	643-4
Figure 7-31. Immunohistochemical detection of TGF- β in biopsies of DNCB-induced rashes treated with various nanocrystalline silver-derived solutions for 24 hours.....	645
Figure 7-32. Immunohistochemical detection of TGF- β in biopsies of DNCB-induced rashes treated with various nanocrystalline silver-derived solutions for 72 hours.....	646
Figure 7-33. Semi-quantitative analyses of immunohistochemical staining for TGF- β in biopsies of DNCB-induced rashes treated with various nanocrystalline silver-derived solutions	647
Figure 7-34. Immunohistochemical detection of IL-8 in biopsies of DNCB-induced rashes treated with various nanocrystalline silver-derived solutions for 24 hours.....	649
Figure 7-35. Immunohistochemical detection of IL-8 in biopsies of DNCB-induced rashes treated with various nanocrystalline silver-derived solutions for 72 hours.....	650
Figure 7-36. Semi-quantitative analyses of immunohistochemical staining for IL-8 in biopsies of DNCB-induced rashes treated with various nanocrystalline silver-derived solutions	650-1
Figure 7-37. Immunohistochemical detection of IL-4 in biopsies of DNCB-induced rashes treated with various nanocrystalline silver-	

derived solutions for 24 hours.....	652
Figure 7-38. Immunohistochemical detection of IL-4 in biopsies of DNCB-induced rashes treated with various nanocrystalline silver- derived solutions for 72 hours.....	653
Figure 7-39. Semi-quantitative analyses of immunohistochemical staining for IL-4 in biopsies of DNCB-induced rashes treated with various nanocrystalline silver-derived solutions	653-4
Figure 7-40. Immunohistochemical detection of IL-10 in biopsies of DNCB-induced rashes treated with various nanocrystalline silver- derived solutions for 24 hours.....	655
Figure 7-41. Immunohistochemical detection of IL-10 in biopsies of DNCB-induced rashes treated with various nanocrystalline silver- derived solutions for 72 hours.....	656
Figure 7-42. Semi-quantitative analyses of immunohistochemical staining for IL-10 in biopsies of DNCB-induced rashes treated with various nanocrystalline silver-derived solutions	656-7
Figure 7-43. Immunohistochemical detection of EGF in biopsies of DNCB-induced rashes treated with various nanocrystalline silver- derived solutions for 24 hours.....	658
Figure 7-44. Immunohistochemical detection of EGF in biopsies of DNCB-induced rashes treated with various nanocrystalline silver- derived solutions for 72 hours.....	659
Figure 7-45. Semi-quantitative analyses of immunohistochemical staining	

for EGF in biopsies of DNCB-induced rashes treated with various nanocrystalline silver-derived solutions	659-60
Figure 7-46. Immunohistochemical detection of KGF in biopsies of DNCB-induced rashes treated with various nanocrystalline silver-derived solutions for 24 hours.....	661
Figure 7-47. Immunohistochemical detection of KGF in biopsies of DNCB-induced rashes treated with various nanocrystalline silver-derived solutions for 72 hours.....	662
Figure 7-48. Semi-quantitative analyses of immunohistochemical staining for KGF in biopsies of DNCB-induced rashes treated with various nanocrystalline silver-derived solutions	662-3
Figure 7-49. Immunohistochemical detection of KGF-2 in biopsies of DNCB-induced rashes treated with various nanocrystalline silver-derived solutions for 24 hours.....	664
Figure 7-50. Immunohistochemical detection of KGF-2 in biopsies of DNCB-induced rashes treated with various nanocrystalline silver-derived solutions for 72 hours.....	665
Figure 7-51. Semi-quantitative analyses of immunohistochemical staining for KGF-2 in biopsies of DNCB-induced rashes treated with various nanocrystalline silver-derived solutions	665-6
Figure 7-52. Average volume of solution delivered per day per side for treatment of DNCB-induced rashes	667
Figure 7-53. Average weight of silver delivered per day per side to	

DNCB-induced rashes via various nanocrystalline silver-derived solutions	668
Figure 8-1. Substrate sampling locations.....	691
Figure 8-2. Preliminary results showing total silver deposited on samples sputtered at 4% O ₂ for a 10 minute static run	695
Figure 8-3. Preliminary results showing ammonia-soluble silver deposited on samples sputtered at 4% O ₂ for a 10 minute static run	696
Figure 8-4. Effect of current on total silver deposited on samples sputtered at 4% O ₂ for a 20 mm/min dynamic run.....	697
Figure 8-5. Effect of current on ammonia-soluble silver deposited on samples sputtered at 4% O ₂ for a 20 mm/min dynamic run	698
Figure 8-6. Effect of current on total silver deposited on samples sputtered at 4% O ₂ for a 43 mm/min dynamic run.....	699
Figure 8-7. Effect of current on ammonia-soluble silver deposited on samples sputtered at 4% O ₂ for a 43 mm/min dynamic run	700
Figure 8-8. Effect of current on total silver deposited on samples sputtered at 4% O ₂ for an 80 mm/min dynamic run at 1.5A	701
Figure 8-9. Effect of current on ammonia-soluble silver deposited on samples sputtered at 4% O ₂ for an 80 mm/min dynamic run at 1.5A.....	702
Figure 8-10. Effect of web speed for dynamic runs on total silver deposited on samples sputtered at 4% O ₂	703
Figure 8-11. Effect of web speed for dynamic runs on ammonia-soluble silver deposited on samples sputtered at 4% O ₂	704

Figure 8-12. Effect of current on total silver deposited on samples sputtered at 2% O ₂ for a 20 mm/min dynamic run	705
Figure 8-13. Effect of current on ammonia-soluble silver deposited on samples sputtered at 2% O ₂ for a 20 mm/min dynamic run	706
Figure 8-14. Effect of current on total silver deposited on samples sputtered at 0% O ₂ for a 20 mm/min dynamic run	708
Figure 8-15. Effect of current on ammonia-soluble silver deposited on samples sputtered at 0% O ₂ for a 20 mm/min dynamic run	709
Figure 8-16. Effect of percent oxygen on total silver deposited on samples sputtered for a 20 mm/min dynamic run.....	710
Figure 8-17. Effect of percent oxygen on ammonia-soluble silver deposited on samples sputtered for a 20 mm/min dynamic run.....	711
Figure 8-18. Effect of solid versus meshed substrate on total silver deposited on samples sputtered at 4% O ₂ for a 10 minute static run.....	712
Figure 8-19. Effect of solid versus meshed substrate on ammonia-soluble silver deposited on samples sputtered at 4% O ₂ for a 10 minute static run	713
Figure 8-20. Preliminary study of the effect of percent oxygen on total silver deposited on samples sputtered at 1.5A for a 10 minute static run	714
Figure 8-21. Effect of percent oxygen on ammonia-soluble silver deposited on samples sputtered at 1.5A for a 10 minute static run.....	715
Figure 8-22. Preliminary study of the effect of current and percent	

oxygen on total silver deposited on samples sputtered in a 10 minute static run.....	716
Figure 8-23. Preliminary study of the effect of current and percent oxygen on ammonia-soluble silver deposited on samples sputtered in a 10 minute static run.....	717
Figure 8-24. The effect of sputtering time on total silver deposited on samples sputtered at 0.75A and 4% oxygen	719
Figure 8-25. Effect of sputtering time on ammonia-soluble silver deposited on samples sputtered at 0.75A and 4% oxygen.....	721
Figure 8-26. The effect of percent oxygen on total silver deposited on samples sputtered at 0.75A in a 10 minute static run	722
Figure 8-27. Effect of percent oxygen on ammonia-soluble silver deposited on samples sputtered at 0.75A in a 10 minute static run	726
Figure 8-28. The effect of percent oxygen on total silver deposited on samples sputtered at 1A in a 10 minute static run	730
Figure 8-29. Effect of percent oxygen on ammonia-soluble silver deposited on samples sputtered at 0.75A in a 10 minute static run	733
Figure 8-30. The effect of percent oxygen on total silver deposited on samples sputtered at 1.5A in a 10 minute static run	734
Figure 8-31. Effect of percent oxygen on ammonia-soluble silver deposited on samples sputtered at 1.5A in a 10 minute static run	736
Figure 8-32. Total silver deposited on samples sputtered at 0.9A and 4% O ₂ in a 30 minute static run	742

Figure 8-33. Ammonia-soluble silver deposited on samples sputtered at 0.9A and 4% O ₂ in a 30 minute static run.....	743
Figure 8-34. Example of an XRD footprint for a nanocrystalline silver thin film generated in-house	746
Figure 8-35. An XRD footprint for Acticoat™	746
Figure 8-36. Preliminary study of the effect of current on the log reduction of <i>Pseudomonas aeruginosa</i> produced by nanocrystalline silver thin films generated at 4% oxygen during a 10 minute static run.....	750
Figure 8-37. Log reductions of <i>P. aeruginosa</i> produced by nanocrystalline silver thin films generated at 4% oxygen and 1.5A during an 80 mm/min dynamic run.....	755
Figure 8-38. The effect of current on the log reductions of <i>P. aeruginosa</i> produced by nanocrystalline silver thin films generated at 4% oxygen during a 43 mm/min dynamic run.....	757
Figure 8-39. The effect of current on the log reductions of <i>P. aeruginosa</i> produced by nanocrystalline silver thin films generated at 4% oxygen during a 20 mm/min dynamic run.....	759
Figure 8-40. The effect of current on the log reductions of <i>P. aeruginosa</i> produced by nanocrystalline silver thin films generated at 2% oxygen during a 20 mm/min dynamic run.....	761
Figure 8-41. The effect of current on the log reductions of <i>P. aeruginosa</i> produced by nanocrystalline silver thin films generated at 0% oxygen	

during a 20 mm/min dynamic run.....	762
Figure 8-42. The effect of percent oxygen on the log reductions of <i>S. aureus</i> produced by nanocrystalline silver thin films generated at various currents during a 10 minute static run.....	766
Figure 9-1. Total release of silver in water versus time for nanocrystalline silver dressings heat treated at various temperatures for 24 hours	777
Figure 9-2. Total silver released after 24 hours in water for nanocrystalline silver dressings heat treated at various temperatures for 24 hours.....	777
Figure 9-3. Log reduction of <i>S. aureus</i> exposed to nanocrystalline silver dressings heated at various temperatures for 24 hours	778
Figure 9-4. Log reduction of <i>P. aeruginosa</i> exposed to nanocrystalline silver dressings heat treated at various temperatures for 24 hours	778
Figure 9-5. Corrected zone of inhibition (CZOI) of <i>S. aureus</i> over a series of days using nanocrystalline dressings heat treated at various temperatures for 24 hours	779
Figure 9-6. Corrected zones of inhibition (CZOI) of <i>P. aeruginosa</i> over a series of days using nanocrystalline silver dressings heat treated at various temperatures for 24 hours.....	779
Figure 9-7. Days of nanocrystalline silver dressing antibacterial activity for dressing heat treatment at various temperatures for 24 hours.....	780
Figure 9-8. SEM images of nanocrystalline silver dressings heat-treated for 24 hours.....	780-84

Figure 9-9. Comparison of atomic concentration of total oxygen and oxygen bonded to silver (determined via XPS, in percent), to crystallite size (determined via XRD, in nm/10, n=3), silver dissolution (in [mg/L]/10, n=3) and biological activity (<i>S. aureus</i> log reduction and days of activity data, n=3) after exposure of the dressing to various temperatures for 24 hours	785
Figure 9-10. Log reductions of <i>P. aeruginosa</i> exposed to nanocrystalline silver dressings heat-treated at 90, 100, or 110°C for various times	797
Figure 9-11. Corrected zones of inhibition for <i>P. aeruginosa</i> over a series of days in response to nanocrystalline silver dressings heat-treated for various times.....	798-9
Figure 9-12. Total release of silver in water after a 24 hour dissolution versus nanocrystalline silver dressing heat treatment time at temperatures of 90, 100, and 110°C	800
Figure 9-13. SEM images of heat-treated nanocrystalline silver dressings.....	802-6
Figure 9-14. Diffraction patterns of nanocrystalline silver dressings after isothermal holds at indicated times and temperatures	807
Figure 9-15. Comparison of the ratio of silver oxide to metallic silver over time and relative to crystallite size	809
Figure 9-16. Grain growth curves and exponents.....	811
Figure 9-17. Raw XPS data of heat-treated dressings	813-14
Figure 9-18. Oxygen percentage in heat-treated nanocrystalline silver	

dressing samples at 90, 100, and 110°C for various times	815
Figure 9-19. Differential scanning calorimetry of nanocrystalline silver oxide sputtered on an aluminum sample cell.....	816
Figure 9-20. Differential scanning calorimetry of nanocrystalline silver sputtered on aluminum foil layered in a nanocrystalline silver- sputtered sample cell.....	817-18
Figure 9-21. Diffraction patterns of nanocrystalline silver thin films sputtered onto aluminum foil for 30 minutes at 4% oxygen, 0.9 A, 40 mTorr pressure, and a working distance of 10 cm.....	819
Figure 10-1. Hypotheses about the mechanisms of action of nanocrystalline silver anti-inflammatory activity	837-9
Figure A2-1. pH, temperature, airflow, and stirring data over time for <i>Pseudomonas aeruginosa</i> growth in a fermentor	848

LIST OF SYMBOLS, ABBREVIATIONS, AND NOMENCLATURE

Abbreviation	Definition
AAS	atomic absorption spectroscopy
ACES	Alberta Center for Surface Engineering and Science
ALI	acute lung injury
ANOVA	analysis of variance
ARDS	adult respiratory distress syndrome
AP	alkaline phosphatase
APS	ammonium persulphate
ATCC	American Type Culture Collection
ATP	adenosine triphosphate
BAL	bronchoalveolar lavage
BSA	bovine serum albumin
CCAC	Canadian Council of Animal Care
CD	cluster of differentiation
cDNA	complementary DNA
CF	cystic fibrosis
CFU	colony forming unit
CMC	carboxymethylcellulose
COPD	chronic obstructive pulmonary disease
CPR	cardiopulmonary resuscitation

CPS	counts per second
CRP	c-reactive protein
CT	cycle time
CZOI	corrected zone of inhibition
d	distilled
d	isothermal holding time grain size
dd	double distilled
d ₀	initial grain size
DAB	diaminobenzoate
DAPI	4'6-diamidino-2-phenylindole
DEPC	diethyl pyrocarbonate
DNA	deoxyribonucleic acid
DNCB	2,4-dinitrochlorobenzene
DNFB	dinitrofluorobenzene
dNTP	deoxynucleotide triphosphate
DSC	differential scanning calorimetry
dUTP	deoxyuridine triphosphate
eAMV-RT	enhanced avian reverse transcriptase
ECM	extracellular matrix
EDTA	ethylenediaminetetraacetic acid
EGF	epidermal growth factor
ELISA	enzyme-linked immunosorbent assay
FAM	carboxyfluorescein

FGF	fibroblast growth factor
FITC	fluorescein isothiocyanate
FWHM	full width half maximum
GAPDH	glyceraldehyde 3-phosphate dehydrogenase
GFP	green fluorescent protein
GSD	geometric standard deviation
HDPE	high density polyethylene
HEPA	high efficiency particulate air
HPRT	hypoxanthine-guanine phosphoribosyltransferase
HRP	horse radish peroxidase
HSAPWC	Health Sciences Animal Policy and Welfare Committee
HSLAS	Health Sciences Lab Animal Services
IBD	inflammatory bowel disease
ICE	Initial, Change, Equilibrium
ICP-MS	inductively coupled plasma mass spectroscopy
ID	inner diameter
IDV	integrated density value
IFN	interferon
Ig	immunoglobulin
IL	interleukin
ISA	ion strength adjustment
ISE	ion specific electrode

JCPDS	Joint Committee on Powder Diffraction Standards
KGF	keratinocyte growth factor
ksp	solubility product constant
LPS	lipopolysaccharide
MBC	minimum bactericidal concentration
mc	maximum count
MHA	Mueller Hinton agar
MHB	Mueller Hinton broth
MIC	minimum inhibitory concentration
MMD	mass median diameter
MMAD	mass median aerodynamic diameter
MMP	matrix metalloproteinase
MOA	mechanism of action
MPC	mutant prevention concentration
mRNA	messenger ribonucleic acid
MR-CNS	methicillin resistant coagulase-negative <i>Staphylococci</i>
MRSA	methicillin resistant <i>Staphylococcus aureus</i>
MRSE	methicillin resistant <i>E. coli</i>
MSSA	methicillin sensitive <i>Staphylococcus aureus</i>
n	grain growth exponent
NIR	near infrared

NF- κ B	nuclear factor κ -light-chain-enhancer of activated B cells
OCT	optimal cutting temperature
OD	optical density
OD	outer diameter
PBS	phosphate buffered saline
PBST	phosphate buffered saline with Tween 20
PCR	polymerase chain reaction
PFA	paraformaldehyde
PIA	<i>Pseudomonas</i> isolation agar
PMN	polymorphonuclear leukocyte
PVL	Panton-Valentine Leukocidin
Q	activation energy for grain growth
R	gas constant
RA	rheumatoid arthritis
REO	Research Ethics Office
Rn	reaction
RNA	ribonucleic acid
ROS	reactive oxygen species
rpm	revolutions per minute
RT	reverse transcriptase
RT-PCR	reverse transcription polymerase chain reaction
SD	standard deviation

SDS	sequence detection software
SDS	sodium dodecyl sulphate
SECM	scanning electrochemical microscopy
SEM	scanning electron microscopy
SERS	surface enhanced Raman scattering
SIE	selective ion electrode
SIMS	secondary ion mass spectrometry
SOP	standard operating procedure
SPS	salt/polysorbate/sodium thioglycollate solution
SPR	surface plasmon resonance
SRPA	Silver (Ag ⁺) Resistant <i>Pseudomonas aeruginosa</i>
SRSA	Silver (Ag ⁺) Resistant <i>Staphylococcus aureus</i>
SRTC	Swine Research and Technology Centre
TAMRA	tetramethyl-6-carboxyrhodamine
t	isothermal hold time
T	temperature
tc	total count
TBE	tris-borate-EDTA buffer
TdT	terminal deoxynucleotidyl transferase
TEM	transmission electron microscopy
TEMED	<i>N,N,N',N'</i> -tetramethylethylenediamine
TENS	toxic epidermal necrolysis syndrome
TGF-β	transforming growth factor beta

TNF- α	tumor necrosis factor alpha
ToF-SIMS	time-of-flight secondary ion mass spectrometry
TSB	tryptic soy broth
TUNEL	TdT mediated Biotin-dUTP Nick End Labeling
UV	ultraviolet
VEGF	vascular endothelial growth factor
VRE	vancomycin resistant <i>E. coli</i>
wt	weight
XPS	x-ray photoelectron spectroscopy
XRD	x-ray diffraction

Volume 1

Chapter 1 – Introduction and Review of the Literature¹

Introduction

Silver has been used medicinally for centuries. In the 1700s, solid silver nitrate was used for opening abscesses, removing warts, and treating a variety of ulcers[1]. This use of solid silver nitrate continued into the 1900s[2]. In the 1800s, the use of silver nitrate-containing solution became more common. These solutions were used to remove hypertrophic granulation tissue, promote crust formation on burn wounds, and prepare wound surfaces for skin grafting[1]. Shortly after the discovery of the existence of microbes, the antibacterial properties of silver were demonstrated, and in 1880, Crede recommended the use of 2% silver nitrate for the treatment of ophthalmia neonatorum[3]. A few years later, Halsted began using silver wire stitches and silver foil dressings for their antibacterial effect during the treatment of hernias[4]. After the early 1940s, with the development and use of antibiotics, there was less interest in the use of silver, although silver foil was still used in burn and graft wounds for its pain-reducing effects, bactericidal activity, stimulation of granulation tissue growth, and good cosmetic results[1]. In 1965, Moyer *et al.*[5] introduced the use of 0.5% silver nitrate in the treatment of burns as the lowest concentration that remained active against bacteria *in vitro* and *in vivo* but, according to their work, did not have a toxic effect on growing epidermal cells (0.1% silver nitrate was not active against bacteria, while 1% killed epidermal cells)[5]. They recommended wetting the

¹ A version of this chapter has been published in: Nadworny and Burrell 2008, *Journal of Wound Technology*, 2:6-13, and Nadworny and Burrell 2008, *Journal of Wound Technology*, 2:14-22.

dressings with fresh silver nitrate solution every three to four hours, and changing the dressings one to two times per day[5]. In 1967, Fox[6] introduced the use of silver sulfadiazine, which is still used as a 1% cream, and is generally applied one to three times per day[7]. Some of the benefits of silver sulfadiazine (or SSD) included decreased frequency of sepsis in burn patients, and the fact that the dressings didn't need to be attended to every three to four hours. However, SSD did not provide sufficient protection against gram negative bacteria in badly burnt patients, and slowed wound healing[8]. This led, in the late 1990s, to the testing of various combinations of SSD with other agents, including cerium nitrate[9], and the testing of silver nylon dressings containing about 25% metallic silver, with[10] or without[11] attempts to increase silver ion concentrations by electrolysis.

Nanocrystalline silver dressings, one of the world's first applications of medical nanotechnology, were also developed in the late 1990s by Burrell and coworkers. The dressings, designed to release bactericidal levels of silver continuously over a period of days[12], were initially introduced into burn care as antimicrobial dressings. However, both clinical and lab studies indicated that the antimicrobial activity observed was beyond that expected for an Ag^+ releasing dressing[13-16]. As well, it was discovered that nanocrystalline silver dressings caused dramatic improvements in wound healing, possibly due to anti-inflammatory activity of the nanocrystalline silver[17-19]. While the exceptional antimicrobial activity of nanocrystalline silver has been lifesaving, as nanocrystalline silver has proven effective against fungi and many types of

bacteria including those resistant to antibiotics and heavy metals[12-16, 20], its anti-inflammatory activity could prove even more valuable clinically. Evidence suggests that nanocrystalline silver could be used to treat inflammatory skin diseases such as allergic contact dermatitis, atopic contact dermatitis, and psoriasis[21, 22], and to treat inflammatory bowel disease[23]. If nanocrystalline silver can be used to treat skin conditions, it is likely that it can also be used to treat other organs which derive from epithelium. If the correct structure and delivery system were designed, nanocrystalline silver could be delivered to the lung to treat inflammatory diseases such as pneumonia and adult respiratory distress syndrome, or to the gastrointestinal tract to treat diseases such as inflammatory bowel diseases.

To utilize fully the unique biological properties of nanocrystalline silver – its antimicrobial and anti-inflammatory activity – a better understanding of its mechanisms of action is necessary. This would allow for the creation of silver products designed specifically for each body system and application. For example, to treat inflammatory diseases in the lung, a form of silver could be developed which has a higher concentration of the species responsible for anti-inflammatory activity, with less of the species responsible for antimicrobial activity. It could also be designed specifically for delivery to the lung, such that it could be inhaled and these species would reach the deep lung in their active form.

Since the development of nanocrystalline silver dressings, there has been a rapid increase in the number of silver dressings available to physicians, including dressings containing pure metallic silver, and silver compounds such as silver

carboxymethylcellulose, silver phosphate, and silver chloride. The large number of dressings now available can make it confusing for caregivers to decide which product to use. This is another important reason to improve the understanding of the impact of the silver structure on its activity. As storage, processing, and conditions of use may modify the structure of nanocrystalline silver, the impact of heat on the dressings is important, and may also provide clues as to which properties are important for the activity of the thin films. With the development of antibiotic resistance, clinicians are seeking alternative antimicrobial treatments. If nanocrystalline silver kills bacteria by multiple mechanisms of action, as has been suggested, it may be difficult for bacteria to develop resistance to nanocrystalline silver, making nanocrystalline silver a good replacement therapy for antibiotics. This provides yet another reason to improve understanding of the antimicrobial mechanisms of action of nanocrystalline silver.

Background

Chemistry of Silver

Silver is a noble metal, in the same family as gold, platinum, and palladium. Some properties of these metals are shown in Table 1-1, which shows that they are structurally very similar. Silver is most commonly available in the form of silver metal, $\text{Ag}^{(0)}$, which, in bulk, is unreactive. Ionic silver is most commonly found in the form of Ag^+ (ionization energy: 731 kJ/mol), but it can also be ionized to Ag^{2+} (ionization energy: 2070 kJ/mol) and Ag^{3+} (ionization energy: 3361 kJ/mol)[24].

Table 1-1. Characteristics of noble metals (data from reference [25])

Metal	Atomic Number	Atomic Weight	Group in Periodic Table	Period in Periodic Table	Structure	Cell Parameters (pm)
Pd	46	106.4	10	5	CCP	a=b=c=389.07 $\alpha=\beta=\gamma=90^\circ$
Ag	47	107.8	11	5	CCP	a=b=c=408.53 $\alpha=\beta=\gamma=90^\circ$
Pt	78	195.1	10	6	CCP	a=b=c=392.42 $\alpha=\beta=\gamma=90^\circ$
Au	79	197.0	11	6	CCP	a=b=c=407.82 $\alpha=\beta=\gamma=90^\circ$

CCP=cubic close-packed, also known as face-centered cubic (FCC)

Chemical Reactivity (Bio-availability) of Silver

Ionic silver (Ag^+) reacts strongly with amino acids, proteins, and chloride to form low solubility compounds. For example, the K_{sp} for AgCl is 1.8×10^{-10} M [26]. This means that in a pure AgCl /water solution, the free silver concentration would be about 1.4 mg/L. However, the chloride contents of bacterial growth media (e.g. Tryptic Soy Agar, which has ~3050 mg/L chloride) and serum (which contains 3500 mg/L chloride[27]) are on the order of 1×10^{-1} M. Therefore, in these solutions, the free silver concentration is much lower, and thus the silver is unavailable for antimicrobial activity. For example, if silver is utilized at concentrations of about the mg/L level ($\sim 10^{-5}$ M) in either of these situations, a 1:10 000 $\text{Ag}^+:\text{Cl}^-$ ratio exists, and the free silver falls to less than 0.3 $\mu\text{g/L}$ (see I.C.E. table calculations for 1 ppm and 25 ppm in Tables 1-2 and 1-3), as it is converted to insoluble silver chloride. These calculations have been confirmed experimentally by measuring silver ion concentration using a specific ion electrode both during application of silver dressings to exuding burn surfaces, and in bacteriological broth containing various concentrations of sodium chloride[28]

(see Figure 1-1), and the resulting AgCl formed has been shown experimentally not to be bactericidal, as Ricketts *et al.*[28] concluded that the antibacterial effect of silver in burn dressings was dependent on the availability of silver ions, and not silver chloride. Thus, it is very important to consider the quantity of bioavailable silver, as opposed to total silver, when developing or selecting silver-containing dressings for clinical applications.

Table 1-2. ICE table for $\text{Ag}^+ = 1 \text{ ppm}$

	$[\text{Ag}^+_{\text{aq}}]$	$[\text{Cl}^-_{\text{aq}}]$
I	$9.25926 \times 10^{-6} \text{ M}$	$9.85915 \times 10^{-2} \text{ M}$
C	$-X$	$-X$
E	$9.25926 \times 10^{-6} - X \text{ M}$	$9.85915 \times 10^{-2} - X \text{ M}$

$$K_{\text{sp}} = [\text{Ag}^+]\text{s}$$

$$1.8 \times 10^{-10} = (9.25926 \times 10^{-6} - X)(9.85915 \times 10^{-2} - X)$$

$$X = 9.25743 \times 10^{-6} \text{ mol/L} \rightarrow \text{Ag}^+ \text{ at equilibrium} = 1.8259 \times 10^{-9} \text{ M or } 0.1981 \text{ } \mu\text{g/L}$$

Table 1-3. ICE table for $\text{Ag}^+ = 25 \text{ ppm}$

	$[\text{Ag}^+_{\text{aq}}]$	$[\text{Cl}^-_{\text{aq}}]$
I	$2.31481 \times 10^{-4} \text{ M}$	$9.85915 \times 10^{-2} \text{ M}$
C	$-X$	$-X$
E	$2.31481 \times 10^{-4} - X \text{ M}$	$9.85915 \times 10^{-2} - X \text{ M}$

$$K_{\text{sp}} = [\text{Ag}^+][\text{Cl}^-]$$

$$1.8 \times 10^{-10} = (2.31481 \times 10^{-4} - X)(9.85915 \times 10^{-2} - X)$$

$$X = 2.31480 \times 10^{-4} \text{ mol/L} \rightarrow \text{Ag}^+ \text{ at equilibrium} = 1.8300 \times 10^{-9} \text{ M or } 0.1986 \text{ } \mu\text{g/L}$$

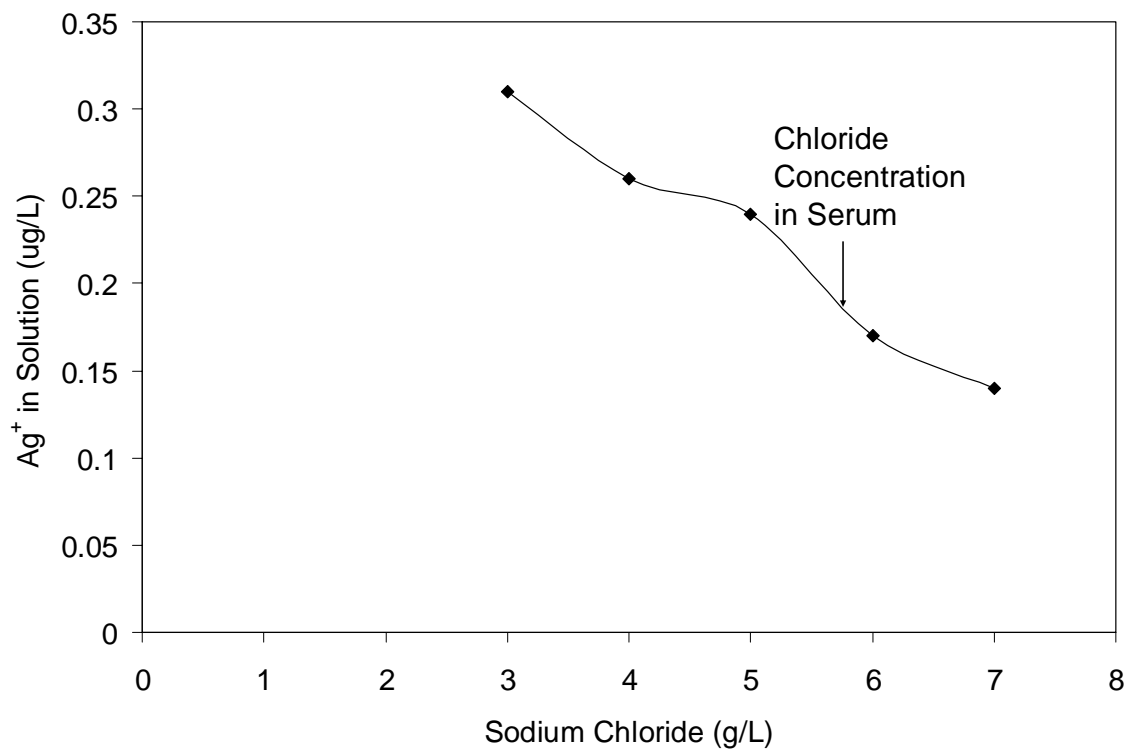


Figure 1-1. The effect of varying chloride concentrations in solution on the free silver (Ag^+) concentrations generated from 40 mg/L silver nitrate. Data extracted from Ricketts *et al.*[28]

Physical and Chemical Properties of Nanocrystalline Silver

Commercial nanocrystalline silver dressings are composed of three layers of material spot welded together. The two outer layers are composed of nanocrystalline silver-coated high-density polyethylene mesh. The inner layer is an absorbent rayon/polyester non-woven gauze. The nanocrystalline silver coated layers are produced by a magnetron sputtering process in which the silver atoms are layered down atom by atom onto the coating, forming poly-nanocrystalline columnar structures. The base (antimicrobial) layer of the film is produced in an argon atmosphere with 4% oxygen, and the upper (optical interference) layer is produced in 4% oxygen at half the power[29]. With the two layers combined, the

total dressing thickness is approximately 900 nm.

Atomic force microscopy (AFM) images of the upper layer show uniformly distributed submicron grainy aggregate structures with the smallest grains being 10-20 nm in size[30]. Scanning electron microscopy (SEM) images demonstrate this same structure[31]. According to AFM, the lower layer has larger grain sizes (50-100 nm)[30]. However, as will be discussed later, other studies using x-ray diffraction (XRD) indicate that the grain size is 11-15 nm[31].

Because of the method by which nanocrystalline silver is produced, the silver is in a highly energized state due to the large number of both point and line defects in the crystal lattice. As well, a high percentage of the total atoms are grain boundary atoms because of the small grain sizes present. These grain boundary atoms, according to Birringer[32], may represent a unique state of solid matter, in addition to amorphous and crystalline matter. Amorphous matter is made up of molecules demonstrating short range order, while molecules in crystalline matter demonstrate long range order due to the lattice structure. Grain boundary atoms, however, are not a part of a crystal lattice structure, but they are affected by the lattice structures of the crystals around them, preventing them from achieving the short range order of amorphous materials. This suggests that grain boundary atoms may behave differently from either amorphous or crystalline materials, and so the high concentration of grain boundary atoms in nanocrystalline silver would be expected to have an impact upon its properties.

From both chemical and biological perspectives, nanocrystalline silver has proven to be unique. Chemical studies have shown that, not surprisingly, Ag^+

dissolution from nanocrystalline silver has been observed via specific ion electrode and scanning electrochemical microscopy (SECM) techniques[12]. Of more interest is that Ag(0) has also been observed to dissolve from nanocrystalline silver, using voltametric electrochemical analysis and SECM[30]. Voltametric studies and x-ray diffraction showed that the lower (antimicrobial) layer contained slightly over 50% Ag(0) and slightly under 50% oxidized silver, while the upper (optical interference) layer contained mostly oxidized silver[30]. These study results also suggested that neither layer appeared likely to contain higher oxidation-state silver species[30]. SECM results indicated that no soluble Ag(0) species were detected leaving the upper layer, but that both soluble Ag(I) (reducible silver) and Ag(0) (oxidizable silver) containing species were detected in the lower layer. As well, the diffusion coefficient for the dissolvable Ag(I)-containing species was lower than that expected for Ag^+ , suggesting that the Ag(I)-containing species might be in a cluster form. The results of studies they performed using electrochemically induced dissolution and SECM further suggested that the dissolution of nanocrystalline silver dressings is facilitated by the coexistence of an Ag(I)/Ag(0) mixed-valence species in a cluster[30]. Since nanosized $\text{Ag}^{(0)}$ particles or clusters are unstable in water, and bare atoms of $\text{Ag}^{(0)}$ are unlikely to be found on their own, they suggested oxide encapsulation might be improving the stability of the soluble $\text{Ag}^{(0)}$ [30]. Furthermore, results from quartz crystal microbalance measurements indicated that perhaps both silver oxide (such as Ag_2O) and silver hydroxide (such as AgOH) species might be dissolving from the nanocrystalline silver films. Overall, these results suggested

that the dissolution products from nanocrystalline silver dressings likely include small clusters containing Ag(0), Ag(I), oxygen, and hydrogen[30]. It is not known whether these clusters are charged, or uncharged, or a mixture of both. In addition, a silver species of higher oxidation state has been observed dissolving from nanocrystalline silver coatings using cyclic voltametry[12]. It is thought that the highly energetic and active surface of nanocrystalline silver, which evidently has silver present in various oxidation states, may produce complex metastable silver hydroxide compounds at the surface of the crystals, which, being metastable, would be able to migrate into the surrounding environment and produce biological interactions which typical silver compounds could not[12].

Recent studies by this group have provided some insight into the physical characteristics necessary to produce these dissolution products, which appear to be responsible for the unique antimicrobial activity observed in nanocrystalline silver. Nanocrystalline silver dressings were heat-treated for 24 hours at temperatures between 23°C and 110°C[31, 33]. For heat treatments at 90°C or above, the dressings were no longer bactericidal, and bacteriostatic longevity was reduced. Soluble silver dropped significantly at the same temperature, indicating nanocrystalline silver is both thermally unstable and necessary for antibacterial activity[33]. There was also evidence of sintering, with a significant increase in crystallite size, and a loss of both silver oxide and total oxygen from the dressings[31]. These results suggested that the decomposition of silver oxide allowed for crystallite growth and sintering, resulting in the observed decrease in silver dissolution and antimicrobial activity. Thus, the silver oxide acts to pin the

nanostructure of the metallic silver-containing nanocrystals, preventing the nanocrystals from growing at room temperature. The results also indicated that dressings with crystallite sizes greater than 32 nm were not effective antimicrobial agents, suggesting that unstable crystallite surfaces and grain boundary atoms may be important in the unique biological properties of nanocrystalline silver dressings[31], since as surface area decreased and crystallite size increased, the percentage of total atoms in grain boundaries would also have decreased, leading to the change in dissolution behavior, and thus antimicrobial activity, observed at high heat-treatment temperatures[31].

Infection and Inflammation in Wound Healing

One of the main uses for nanocrystalline silver dressings is in the treatment of colonized/infected burns and wounds. In these types of clinical situations, both inflammation and infection are often present, and both can slow healing and result in healing via scarring rather than through regeneration. An acute inflammatory response to injury or trauma can be recognized by four cardinal signs. Redness, swelling, and heat are produced by a combination of local vasodilation, fluid leakage into the extravascular space, and blockage of lymph drainage. Pain is produced by distention of tissue spaces from swelling and pressure, or by the irritation of receptors for chemicals[34].

Response to wounding, and subsequent healing of the wound, goes through three overlapping phases: the clotting phase, the inflammatory and proliferative phase, in which inflammation, phagocytosis and deposition of granulation tissue occurs, and the remodeling phase, which involves contraction

and re-epithelialization. The primary function of the clotting phase is to create a temporary plug thereby protecting the host from attack by pathogens, and preventing excessive blood loss due to the injury. The primary function of the inflammatory phase is to attract phagocytes to the injury to remove pathogens and wound debris so that the repair process can begin[34]. The repair and remodeling phase involves re-epithelialization, formation of granulation tissue, angiogenesis, and remodeling in the ECM. The acute inflammatory response usually lasts 24-48h, and should be completed within two weeks. Figure 1-2 shows a timeline of normal wound healing, and indicates where some of the involved cells are active. After the acute response, a subacute phase may last for another two weeks[34].

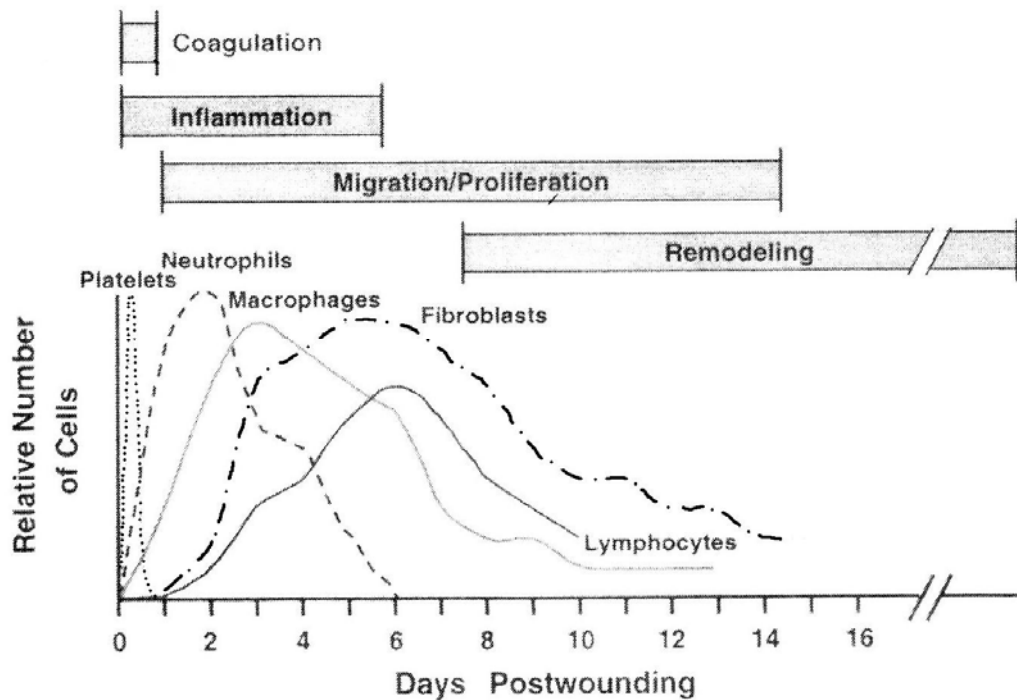


Figure 1-2. Timeline of wound healing and corresponding cell populations in the wounds (Witte *et al.*, 1997, in reference [35]).

Chronic inflammation is an inflammatory response that lasts for more than days or weeks. A chronic wound is one that “deviates from expected sequence of

repair in terms of time, appearance, and response to aggressive and appropriate treatment”[36]. Chronic wounds are characterized by prolonged inflammation, elevated protease activity, a defective wound matrix, and a failure to re-epithelialize[37]. The rate of wound closure is a result of multiple factors, including the wound size (both area and volume), wound location, underlying pathophysiology, presence of infection, and the patient’s medical status, including other medications being taken, and standard of nutrition[36]. Thus, chronic wounding can be the result of a combination of these factors at work. Chronic wounding can also be considered a form of "frustrated repair" – everything needed for repair is present and working, but repair efforts are impeded because the agent causing inflammation is still present[38].

Chronic inflammation can develop in two ways. The first is that acute inflammation can proceed to chronic inflammation if it is not resolved completely[34]. Chronic inflammation can also occur when necrotic tissue seals the wound; excessive edema, eschar, or debris is present; or when the inflammatory response is unable to eliminate initial infection or the agent causing injury[38]. For example, chronic inflammation can occur when phagocytes ingest a microorganism, but the microorganism then resists enzymatic and oxidative killing. Another example is if the microorganism is killed, but its cell wall can't be phagocytized, so it remains in the site of injury, still acting as an antigen. Also, if components of the host cross-react with the bacterial antigen, they may themselves be attacked by the immune system[37].

Many chronic wounds are associated with high levels of colonization by bacteria, which can lead to infection. As well, many pathogens, especially anaerobic bacteria, can affect cell-mediated responses that would normally occur during wound healing, such as inhibiting keratinocyte migration, fibroblast migration, and re-epithelialization, further hindering wound closure[37]. Thus, there is a close link between inflammation, colonization/infection, and wound healing. The same links are present in other types of inflammatory diseases. This indicates that the antimicrobial activity combined with the potential anti-inflammatory/pro-healing activity of nanocrystalline silver could prove very beneficial in a variety of clinical applications.

Antimicrobial Activity of Silver

Minimum Inhibitory Concentrations Required For Silver Treatments

Ricketts *et al.*[28] found that the minimum inhibitory concentration (MIC) for silver (Ag^+), tested against *P. aeruginosa*, was 20 - 40 mg/L in nutrient broth. They also showed that the presence of organics in the test medium could increase the required amount of silver by greater than 80 times. Carr *et al.*[39] determined silver sulfadiazine MICs for 643 organisms. The MICs for *P. aeruginosa* ranged from 0.8 to 50 mg SSD/L (0.2 – 15 mg Ag^+ /L) in their experiments[39]. These are conservative numbers, since sulfadiazine also has some antimicrobial activity. The MIC_{100} , the concentration required to effectively inhibit all test organisms, ranged from 25 – 100 mg SSD/L (7.5 – 30 mg Ag^+ /L) depending upon the bacterial species tested[39]. Carr *et al.* then tested an additional 14 organisms and found MICs that ranged from <0.8 – 100 mg SSD/L (<0.2 – 30 mg Ag^+ /L)[39].

Ten of the additional 14 organisms had MICs >3.13 mg SSD/L (1 mg Ag⁺/L). Spadaro *et al.*[40] showed that *Staphylococcus aureus* and *Escherichia coli* had MICs of 7 and 4.9-5.8 mg Ag⁺/L, respectively. Berger *et al.*[41] determined MICs for 16 organisms in nutrient broth. They ranged from 0.08 – 1.25 mg Ag⁺/L. Hall *et al.*[42] determined 24 and 48 hour MICs for nine organisms in a tryptone-marmite-glucose medium. The MICs ranged from 3.8 - 45 mg Ag⁺/L with eight of the nine organisms having values greater than 12.5 mg Ag⁺/L at 24 hours. There was little difference between MICs determined at 24 hours versus 48 hours. Maple *et al.*[43] determined 24 hour MICs for 80 strains of MRSA to silver sulphadiazine in Iso-Sensitest agar. MICs ranged from 64 – 128 mg SSD/L (21 – 42 mg Ag⁺/L) with MIC₅₀ and MIC₉₀ values of 85 mg SSD/L (28 mg Ag⁺/L) and 120 mg SSD/L (40 mg Ag⁺/L). Li *et al.*[44] measured silver nitrate and silver sulphadiazine MICs for *Escherichia coli* that were susceptible and resistant to Ag⁺. The parent or susceptible strain had MICs of 8 (5 mg Ag⁺/L) and 16 mg/L (5 mg Ag⁺/L) for silver nitrate and silver sulphadiazine, respectively. The silver resistant *E. coli* had an MIC greater than 1024 mg AgNO₃/L (650 mg Ag⁺/L). They also observed that if Cl⁻ was omitted from their test medium the MIC dropped to 64 mg Ag⁺/L. Yin *et al.*[14] compared MICs for three different silver sources (silver sulphadiazine, AgNO₃ and nanocrystalline silver) and five organisms. The MICs observed ranged from 5 – 12.5 mg Ag/L. Overall, the data for MICs presented above, which was generated over the last 40 years, is remarkably consistent. It shows that bacteria have MICs for silver that are generally greater than 1 mg/L in complex media. In fact, over 80% of the

organisms tested in complex media had MICs that exceeded this value. This suggests that if broad spectrum control is a requirement for a silver-containing medical device, then the silver release should significantly exceed 1 mg/L. In fact, in clinical applications, a range of concentrations should be avoided that extends from the minimum inhibitory concentration (MIC) of most susceptible cells to the MIC of the least susceptible single-step bacterial mutants (this concentration is the mutant prevention concentration (MPC) which is approximately the minimum bactericidal concentration (MBC)), as concentrations within this range will select for resistant organisms[45]. Such a selection process would have a serious negative impact on wound care, particularly in burn units where silver is often the first line of defense against wound infections. Thus, silver must be delivered at a concentration greater than the MBC of the least susceptible cells, not merely at the MIC of a species or strain of choice.

Minimum Bactericidal Concentrations Required for Silver Treatments

MBC tests were used as part of the process in determining protocols for silver usage in the early 1960s. As a result, silver nitrate was used at a concentration of 0.5% (3176 mg Ag⁺/L) and silver sulfadiazine was formulated as a 1% cream (3025 mg Ag⁺/kg). Ricketts *et al.*[28] found that the supernatant of an AgCl solution had no bactericidal efficacy. Berger *et al.*[41] determined MBCs for 16 organisms. They found that they ranged from 0.73 – 10.05 mg Ag⁺/L. 12 of the 16 organisms had MBCs greater than 2 mg Ag⁺/L. They noted that the MBCs were about a factor of 10 greater than the MICs for their test organisms. Hall *et al.*[42] measured MBCs (which ranged from 3.8 to >50 mg

Ag⁺/L) for nine organisms. They found eight organisms had MBCs greater than 12.5 mg Ag⁺/L and 5 were greater than 40 mg Ag⁺/L. Contrary to Berger *et al.*'s[41] observations, Hall *et al.*[42] found that the MICs and MBCs were of the same order of magnitude. Maple *et al.*[43] determined MBCs for silver sulfadiazine with 80 strains of MRSA. The range of MBCs measured was from 64 – 256 mg SSD/L (21 – 84 mg Ag⁺/L). The MBC₅₀ and MBC₉₀ were 100 and 200 mg SSD/L (33 and 66 mg Ag⁺/L), respectively. Yin *et al.*[14] measured MBCs for five organisms in Mueller Hinton Agar which ranged from 5 – 12.5 mg Ag⁺/L. These values were identical to their measured MIC values, which was in agreement with Hall *et al.*[42]

Based upon the MBC values reported in the literature over the last 40 years in complex media (such as serum, or growth media), broad spectrum bactericidal control, including control of MRSA, will only be guaranteed if silver is supplied at a minimum of 40 - 50 mg Ag⁺/L.

Bactericidal Activity of Various Silver-Containing Dressings

Spadaro *et al.*[40], Deitch *et al.*[10], Simonetti *et al.*[46], Wright *et al.*[20], Richard *et al.*[47], and Yin *et al.*[14] have all shown that log reduction testing in a complex medium containing organics and chloride is a sensitive way to differentiate the bactericidal activity of various forms of silver. It is difficult to compare literature values for log reductions because of different incubation times, media, and so on. However, the following authors have reported on silver-based microbial log reductions in complex media at various exposure times ranging from 0.5 hours to 48 hours: Spadaro *et al.*[40] (one, two, three, and four hours),

Marino *et al.*[48] (seven and 23 hours), Deitch *et al.*[10] (four, seven, and 23 hours), Hall *et al.*[42] (24 and 48 hours), Wright *et al.*[20] (0.5 and two hours), Yin *et al.*[14] (0.5, one, two, four, and six hours), Spacciapoli *et al.*[49] (one and 24 hours), Taylor *et al.*[33] (0.5 hours), Fraser *et al.*[50] (0, 0.5, two, four, six, eight, and 24 hours) and Ip *et al.*[51] (0, 0.5, two, four, six, and 24 hours). To compare the data from all of the above papers, log reductions were calculated from all data points provided. As a result, there is a broad range of incubation times in the data, but they are still instructive. The data were split into two groups based upon silver concentrations (<36 mg Ag⁺/L and >36 mg Ag⁺/L). When silver concentrations were <36 mg/L, 16 percent of the data showed log reductions great than three (bactericidal[52]), while the remaining 84 percent of the data had log reductions less than three (not bactericidal). When silver concentrations were >36 mg/L, 67.9 percent of the test points were for log reductions greater than three. If the latter data is stratified into nanocrystalline-derived silver and all other forms of silver (which only release Ag⁺), 100% (14/14) of the nanocrystalline-derived silver (which releases 70-100 mg Ag/L) treated organisms had log reductions greater than three in 0.5 to two hours. With all other forms of silver (36 – 3176 mg Ag⁺/L), 58% had log reductions greater than three.

Bactericidal Activity of Nanocrystalline Silver

As indicated in the previous section, *in vitro* studies have shown that nanocrystalline silver has exceptional antimicrobial activity. This includes being active against a variety of bacteria, including many common wound pathogens

such as *Staphylococcus aureus*, *Pseudomonas aeruginosa*, *Bacteroides fragilis*, *Staphylococcus epidermidis*, *Escherichia coli*, and *Klebsiella pneumoniae*[14, 16, 20]. These studies show that nanocrystalline silver has excellent bactericidal efficacy against a broad spectrum of bacteria, as indicated by log reduction assays which showed that nanocrystalline silver produced a log reduction of greater than five in all species tested in less than half an hour. In addition, these studies have shown that nanocrystalline silver has bacteriostatic longevity, as determined by plate-to-plate corrected zone of inhibition assays. Studies have also shown that nanocrystalline silver can greatly decrease bacterial counts in delayed healing porcine models and human chronic wounds[16, 18, 19], as will be discussed further below.

Nanocrystalline silver is also able to kill antibiotic-resistant bacteria. In one study, nanocrystalline silver, silver nitrate, and silver sulphadiazine were tested for bactericidal efficacy against eleven different clinical isolates which demonstrated resistance to multiple antibiotics, using log reduction assays[15]. The results of the study showed that while silver nitrate and silver sulfadiazine were only active against certain species, nanocrystalline silver was bactericidal against all of the antibiotic-resistant bacteria, and had very rapid kill rates[15]. This was true whether the bacteria were inoculated in water, physiological saline, or 50% calf serum, indicating that the bactericidal activity of the nanocrystalline silver was not negatively impacted by either chloride or proteins which would be found in the wound environment[15]. The authors of the study suggested that the combination of speed, efficacy, and broad spectrum activity in the antimicrobial

efficacy of nanocrystalline silver would limit the ability of bacterial cells to develop resistance to nanocrystalline silver as well[15]. In another study, nanocrystalline silver dressings and film dressings, which included a silver salt incorporated into a furnace-fused complex of calcium and sodium phosphates, were tested for bactericidal activity using log reductions against a multiply resistant *Staphylococcus aureus* and a multiply resistant *Alcaligenes sp.*[20] While the film dressing was not bactericidal against these organisms after 30 minutes of exposure, the nanocrystalline silver dressing was, producing log reductions greater than five[20]. In a third study, nanocrystalline silver dressings were tested against five species of multiply antibiotic resistant bacteria for both bactericidal efficacy and bacteriostatic longevity[16]. As with the above studies, the nanocrystalline silver dressings showed excellent bactericidal activity, with log reductions of greater than five produced in less than half an hour for all species tested and bacteriostatic activity lasting at least three days[16].

Nanocrystalline silver has also demonstrated excellent anti-fungal activity. In an *in vitro* study, nanocrystalline silver, silver nitrate, mafenide acetate, and silver sulfadiazine were tested for their ability to kill various fungi and their spores, including *Candida albicans*, *Candida glabrata*, *Candida tropicalis*, *Saccharomyces cerevisiae*, *Aspergillus fumigatus*, and a *Mucor sp.* isolate[13]. The results of the study indicated that the nanocrystalline silver was highly effective in killing all fungi and some types of spores, while other agents were less effective, and that the time to kill for nanocrystalline silver was much more rapid than the other agents[13].

The above studies all indicate that nanocrystalline silver has excellent antimicrobial properties, and that it is significantly more active than traditional silver-containing treatments such as 0.5% silver nitrate or 1% silver sulphadiazine cream, despite the fact that the aqueous concentration of silver ions released from nanocrystalline silver is about 3% of that released from either of the traditional dressings[12]. Studies have also shown that nanocrystalline silver is much more active than the various other commercial silver-containing dressings which have appeared on the market after the development of nanocrystalline silver, all of which release only Ag^+ (see, for example, [16, 20, 52]). This suggests that nanocrystalline silver releases antimicrobial species in addition to Ag^+ . The kill kinetics of nanocrystalline silver also suggest that silver species in addition to Ag^+ are released[12], since nanocrystalline silver has broad spectrum activity with higher rates of kill than Ag^+ only-containing treatments, as described earlier. It has been speculated that an increased variety of oxidized silver species would be expected to cause an increased solubility and higher overall activity, such as that observed with nanocrystalline silver[12]. Thus, the higher oxidation state silver species observed in nanocrystalline silver coatings via cyclic voltametry may be the source of its exceptional antimicrobial activity[12]. Demling and Burrell[12] have speculated that the highly active surface of nanocrystalline silver, with silver present in various oxidation states, may produce unusual metastable silver hydroxide compounds which would have the ability to migrate into, and interact with, the surrounding environment. The rapid kill of bacteria and fungi by nanocrystalline silver suggests a speedy uptake of the active silver species. It is

believed that these metastable silver hydroxide compounds may be taken into the cell via the orthophosphate uptake route, since orthophosphate uptake into cells is quick, and it is possible that other metal oxides with a similar configuration, such as an $\text{Ag}_x(\text{OH})_y$ configuration, could be taken up accidentally by bacteria via this route[12]. This mechanism of action could explain the rapid uptake and kill of a broad spectrum of microorganisms, which has been observed both *in vitro* and *in vivo*.

In Vivo and Clinical Outcomes Related to the Antimicrobial Activity of Nanocrystalline Silver

A thermal injury study in rats performed by Burrell *et al.*[53] compared the efficacy of control dressings, silver nitrate-containing dressings, and nanocrystalline silver dressings as barriers to bacterial infection. The burn injury was not lethal, as 100% of the burn control animals survived. However, only 5% of the infection control group survived, and none of the group treated with silver nitrate survived[53]. Eighty-five percent of the rats treated with nanocrystalline silver dressings survived, however[53]. Weight loss was also significantly less in the animals treated with nanocrystalline silver, demonstrating that the nanocrystalline silver dressings reduced morbidity and mortality by acting as bacterial barriers[53].

Another thermal injury study using a modified Walker-Mason model in rats by Heggens *et al.*[54] compared the antimicrobial activity of a nanocrystalline silver dressing, a metallic silver dressing created through an autocatalytic deposition on nylon, and a silver chloride dressing, on debrided infected wounds.

They found that the nanocrystalline silver dressing was the most active and effective antimicrobial agent[54].

Two studies from this same group used another modified Walker-Mason model in rats[55, 56]. In both of these studies, rats received 15% TBSA full thickness dorsal scald burns, followed by seeding with 0.5 mL broth containing 10^8 CFU of MRSA[55] or *P. aeruginosa*[56]. 24 hours later, the rats began various treatments which lasted seven days, after which weight loss was measured and various specimens were cultured. One study compared nanocrystalline silver dressings, chlorhexidine acetate dressings, and fusidic acid cream[55], while the other compared nanocrystalline silver dressings, chlorhexidine acetate dressings, and silver sulfadiazine 1% cream[56]. Both studies showed that all treatments were a significant improvement over controls, preventing the systemic spread of the organisms.

Wright *et al.*[18] used a contaminated porcine wound model to compare the antimicrobial activity of nanocrystalline silver dressings to silver nitrate soaked dressings, and found that animals treated with nanocrystalline silver dressings appeared to have little or no bacteria at Day 7, whereas the other dressings had an abundance of bacteria. Wright *et al.*[16] used the same model to compare a nanocrystalline silver dressing to a polyhexamethylene biguanide (PHMB)-containing dressing. In the porcine model, the PHMB effectively reduced the bacterial population initially, but could not keep it in check to the same degree as the nanocrystalline silver dressing[16].

Tredget *et al.*[57] compared a nanocrystalline silver dressing to silver

nitrate soaks in the treatment of clinical burn wounds. In this randomized matched pair study, 50 biopsies were taken from 34 wounds over the course of treatment. Half were taken from each dressing treatment. They reported 16 bacteremias from the silver nitrate treatments and five from the nanocrystalline silver treatments[57].

A clinical study examined the use of various dressings post-operatively in 160 bone-anchored hearing aid implantations, and found that compared to Triad Cortyl, Mepitel, and Allevyn, treatment with nanocrystalline silver dressings with Allevyn resulted in a significantly lower infection rate[58].

Another clinical study demonstrated the ability of nanocrystalline silver dressings to prevent infection and allow re-epithelialization of primary burn injuries in premature neonates, despite the sensitivity of their skin[59]. Interestingly, serum silver levels in these neonates were very low, except for one infant who had received treatment with silver sulfadiazine prior to treatment with nanocrystalline silver[59]. In contrast, conventional silver based topical agents caused irritation, did not penetrate eschar well, formed pseudoeschars, caused wound maceration, and slowed epithelialization[60, 61].

Anti-Inflammatory/Pro-Healing Activity of Nanocrystalline Silver

Although anecdotes from clinical cases have suggested that nanocrystalline silver, but not ionic silver, may have anti-inflammatory activity in addition to its antimicrobial activity, there is very little on this subject in the published literature. One of the first such studies was performed in a porcine contaminated wound model[18]. In that study, swine were given 2 cm full-

thickness wounds which were contaminated by covering them with sponges soaked with bacterial inoculum for 15 minutes. The wounds were then bandaged with various dressings, including nanocrystalline silver burn dressings. Skin grafting experiments were then performed, in which 0.5 mm skin grafts were obtained and sutured over fresh wounds, over wounds which had been dressed for four days with nanocrystalline silver burn dressings, or over control dressings. Dressing treatments were continued for the next seven days[18]. Wounds treated with nanocrystalline silver showed enhanced development of granulation tissue over controls, with decreased erythema and edema. Grafts over the granulation tissue from nanocrystalline silver treated wounds were healthy and integrated well, indicating that the granulation tissue was healthy, while grafts over controls became necrotic[18]. In this study, matrix metalloproteinase (MMP) activity was examined. MMPs are required for tissue healing after injury, as they are involved in the removal of dead tissue and extracellular matrix, and in keratinocyte migration and angiogenesis. However, excessively high MMP levels may result in damage to healthy tissue, and may prevent wound closure[62, 63]. On examination of MMP levels, the authors found that in wounds treated with silver nitrate or control dressings, the MMP levels spiked after two days and remained high throughout the experiment. However, in wounds treated with nanocrystalline silver, the MMP levels remained low throughout the experiment, with active MMP-9 levels decreasing over time, suggesting that nanocrystalline silver was effective in modulating overall MMP activity[18]. In addition, controls and silver nitrate-treated wounds showed large numbers of polymorphonuclear

leukocytes (PMNs) and bacterial cells, while nanocrystalline silver treated wounds showed larger numbers of fibroblasts and monocytes, with increased angiogenesis and an absence of bacterial cells[18]. Increased apoptosis was also observed in wounds treated with nanocrystalline silver as compared to wounds treated with silver nitrate or controls, particularly in PMNs. Apoptosis is a process by which cells go through a specific set of steps leading to their death and removal in such a way that the contents of the cells are not released to their external environment. Thus, apoptosis prevents the inflammation which would result if the cells were to die by necrosis, the process in which dying cells swell and disintegrate, releasing their contents[64, 65]. The increased level of apoptosis observed when using nanocrystalline silver thus was at least a partial explanation for the lower levels of PMNs observed, the reduced inflammatory response, and the modulation of MMPs via nanocrystalline silver, which resulted in accelerated wound healing[18].

Another study using a swine model compared the rates of healing of donor sites treated with nanocrystalline silver dressings to petrolatum-impregnated absorbent gauze. The study demonstrated significantly increased rates of re-epithelialization and decreased times to complete re-epithelialization with the use of nanocrystalline silver dressings[66].

More recently, Bhol *et al.*[21] performed a study in which guinea pigs were sensitized to 5% 2,4-dinitrochlorobenzene (DNCB), and then allergic contact dermatitis was elicited nine days later with 5% DNCB. Some guinea pigs were left untreated, while in other guinea pigs the dermatitis was treated with

nanocrystalline silver in an emollient cream vehicle, steroids, or an immunosuppressant[21]. 0.5% and 1% nanocrystalline silver creams significantly reduced erythema and edema scores within one day of treatment as compared to vehicle-treated and untreated guinea pigs, and completely abolished both erythema and edema within five days. Histopathological inflammatory scoring indicated a significant reduction in inflammation with 0.5% and 1% nanocrystalline silver treatments as compared to the vehicles and untreated guinea pigs after five days of treatment[21]. They concluded that nanocrystalline silver was as active as the steroids and immunosuppressants, but that its effect appeared to be more rapid[21].

This study was followed up by a study in which mice were sensitized to 0.5% dinitrofluorobenzene (DNFB) in 4:1 acetone:olive oil[22]. After five and seven days, allergic contact dermatitis was induced on their ears by painting with 0.2% DNFB. The mice were then treated with a high potency steroid, 1% nanocrystalline silver cream, an immunosuppressant, or a vehicle. The study found that the nanocrystalline silver cream significantly reduced ear thickness and erythema, and the number of inflammatory cells present in the skin[22]. As well, the nanocrystalline silver significantly reduced expression of IL-12 and TNF- α (both mRNA and protein levels). IL-12 is a cytokine which is capable of mounting an inflammatory response, and which promotes neutrophil activation, acts as a growth factor for preactivated T and natural killer cells, induces cytokine production, enhances the activity of cytotoxic T lymphocytes, and promotes differentiation of Th1 cells[38, 67]. TNF- α is also a pro-inflammatory cytokine.

Some of its functions include activation of neutrophils, coagulation, and NF- κ B; and the promotion of the expression of various other pro-inflammatory molecules[67, 68]. Thus, downregulation of expression of these two cytokines would be expected to have an anti-inflammatory effect. Nanocrystalline silver also increased the number of inflammatory cells (but not keratinocytes) undergoing apoptosis. The latter was not observed in any other treatment group. These results suggest that nanocrystalline silver may have an anti-inflammatory effect in skin, and that downregulation of TNF- α and IL-12, and the induction of apoptosis may be partly responsible for this effect[22]. However, these studies both used rodent skin models, which heal very differently from human skin[69], so it was not clear whether the results applied to human healing. As well, in these studies, the nanocrystalline silver was incorporated into an emollient cream, which may actually inhibit the nanocrystalline silver from entering the rash, since emollient creams are hydrophobic barriers to the skin surface, thus reducing the efficacy of the nanocrystalline silver. More impressive results could perhaps have been achieved using nanocrystalline silver burn dressings. Interestingly, the same authors have demonstrated, in a rat model, that nanosilver preparations may be effective in the treatment of inflammatory bowel disorder[23].

A study in which guinea pigs were given infected or non-infected grafts over split-thickness wounds and treated with either control mesh dressings or nanocrystalline silver dressings showed that nanocrystalline silver dressings did not alter the cell-mediated immune response, but did increase parameters of innate immunity[70].

Another recent study found that, compared to controls and silver sulfadiazine-treated animals, treatment of thermal injuries in mice with silver nanoparticles increased the rate of healing and decreased scarring[71]. This was accompanied by an increased expression of cytokines including IL-10 (an anti-inflammatory molecule with roles including reduction of TNF- α activity, induction of apoptosis in neutrophils and macrophages, and reduction of IL-6 and IL-8 production([67, 72]), VEGF (which promotes angiogenesis), and IFN- γ (which can cause activation of macrophages, endothelial cells, and natural killer cells, can induce production of IL-2, -12, and -18, and can reduce apoptosis in neutrophils and macrophages[67]); a reduced expression of IL-6 (a pro-inflammatory signaling molecule, with roles including promotion of activated T and B cell maturation, inhibition of the growth of fibroblasts, induction of neutrophil activation, inhibition of phagocytosis of senescent/dysfunctional neutrophils, induction of monocyte chemotactic protein-1 (MCP-1), activation of macrophages, stimulation of keratinocyte migration and proliferation, and stimulation of angiogenesis[67, 73]); and a higher TGF- β 1 expression initially, followed by significantly lower TGF- β 1 expression later on[71]. TGF- β is a pleiotropic growth factor which regulates many biological events, including cell proliferation and differentiation, angiogenesis, and the inflammatory/immune response, where it plays a dual role[74]. TGF- β is a strong chemoattractant for leukocytes and mast cells, and thus is able to initiate an inflammatory response[75], but later in the healing process, TGF- β contributes to the resolution of inflammation[74]. Thus, the pattern of TGF- β expression observed by Tian *et*

al.[71] would not be expected to enhance wound healing. However, the increased expression of IL-10 and VEGF, with decreased expression of IL-6 suggests an anti-inflammatory effect of the silver nanoparticles. Again, this study was performed in an infected rodent model, so it was unclear whether the results were clinically relevant and whether the wound healing observed was the result of anything more than antimicrobial activity.

A clinical study was performed in which patients with various chronic wounds were evaluated before and during application of nanocrystalline silver, using the Pressure Sore Status Tool, photography, and measurements of protease levels[19]. MMP activity decreased dramatically during the first few days of treatment, and remained low until the wounds healed[19]. This reduction in MMPs could have been due to the silver inhibiting bacterial proteases directly through its antimicrobial activity, or it could have been due to the fact that reducing the bacterial population would decrease the level of neutrophils attracted to the wounds, thereby lowering the MMPs produced by neutrophils[19]. Another possible explanation was that nanocrystalline silver directly affected pro-inflammatory cytokines such as IL-1 and TNF- α , and through them impacted the MMP levels, which would indicate a direct anti-inflammatory effect.

Another clinical study examined the use of nanocrystalline silver dressings in chronic wounds and found that suppression of MMP-9 and TNF- α levels approached significance over 21 days of treatment, suggesting that the alterations in MMP-9 and TNF- α levels could be responsible for the improved wound healing observed with these dressings[76].

In a clinical study of re-epithelialization of meshed skin grafts on excised burn wounds, nanocrystalline silver dressings were shown to significantly increase re-epithelization rates (>40%) relative to xeroform and 8-ply gauze dressings moistened with neomycin and polymyxin[77].

A multi-center randomized experiment with blinding and positive parallel control also demonstrated increased healing rates with nanocrystalline silver[78]. In this study, nanocrystalline silver dressings were compared to silver sulfadiazine treatments for the management of post-burn residual wounds, and, in addition to significantly increased rates of bacterial clearance, the time to heal was significantly lower with nanocrystalline silver treatments[78].

Based on the above studies, Demling *et al.*[79, 80] created a theoretical model to explain the differences in healing between nanocrystalline silver and other common topical antibiotics used to treat deep partial thickness burns. In these injuries, excessive inflammation occurs with increased presence of neutrophils and increased protease activity, which can impair wound healing and cause the wounds to convert to deeper injuries. Under typical antimicrobial dressings, Demling *et al.* suggested that burn conversion is caused by excessive inflammation, uncontrolled bacterial colonization, excessive exudate, and increased protease activity causing tissue breakdown to exceed its synthesis[79, 80]. They postulated that with nanocrystalline silver treatment, inflammation is decreased as a result of decreased bacterial presence, suppression of protease activity, and decreased exudate, preventing the wound from deepening and enhancing the rate of healing[79, 80].

Overall, these studies indicate that nanocrystalline silver may have an anti-inflammatory effect in addition to its antimicrobial activity, although this was not clearly proven in the published literature. It is believed that the soluble $\text{Ag}^{(0)}$, likely present in $\text{Ag}^{(0)}$ -containing clusters as discussed earlier, may be the species responsible for the anti-inflammatory activity of nanocrystalline silver[12]. One reason for this is that the other species released from nanocrystalline silver are unlikely to have anti-inflammatory properties. Ag^+ , which is a potent oxidizer, may, in fact, be pro-inflammatory[81-83], and therefore any higher oxidation states of silver would likely be pro-inflammatory as well. In addition, there is evidence to suggest that other noble metals, such as gold, platinum, and palladium, may have anti-inflammatory activity, and that this activity may result from their reduced form. Platinum is used in the treatment of certain forms of cancer, originally in the form of *cis*-platin (and more recently in various other salts due to the side effects caused by *cis*-platin). Its anti-cancer activity is believed to be due, at least in part, to its ability to induce apoptosis in cancer cells by binding to DNA, which prevents the repair of the bound DNA, prevents some DNA repair mechanisms from binding to their natural targets, inhibits DNA transcription and cell cycle progression, and damages telomeres[84]. It may also induce apoptosis by damaging phospholipids in the cell membrane, or by binding to glutathione and other thiol-containing proteins, blocking their natural functions[84]. As mentioned earlier, apoptosis induction of inflammatory cells is one mechanism for anti-inflammatory activity, linking platinum to anti-inflammatory properties. Furthermore, a study showed that platinum reduced

erythema in a guinea pig rheumatoid arthritis (RA) model and inhibited various inflammatory substances present in the RA fluid[85]. The same study indicated that gold also produced inhibition of biologically active substances in the RA fluid, and the authors suggested that this inhibition might be explained by a reaction of gold and platinum with –SH radicals[85]. Gold, like platinum, has demonstrated good antitumor activity both *in vitro* and *in vivo*, due to induction of apoptosis in cancer cells, possibly due to DNA binding or anti-mitochondrial activity[86, 87]. Another study, using a rat adjuvant-induced arthritis model, showed that a mixture of copper, gold, and silver salts had an anti-rheumatic effect with decreases in clinical and biochemical signs of illness, including decreased haptoglobin, ceruloplasmin, and PGE₂ levels[88]. In the past, gold chloride has been used to decrease inflammation in rheumatoid arthritis. However, a large number of side effects has led to a decrease in its use. Gold, like platinum, has been shown to induce apoptosis by binding to DNA, thus inhibiting DNA synthesis and mitosis[89], and by interacting with thiols and selenols[90]. Gold thiolates in particular have been shown to inhibit NF-κB, an important transcription factor in the inflammation process[90]. As well, gold sodium thiomalate has been demonstrated to inhibit IL-5 from preventing eosinophil apoptosis, which led to speculation that the gold may influence intracytoplasmic signal transduction for protein synthesis in eosinophils[91]. Gold salts may also inhibit the release of histamine and reduce serum IgE levels in asthma patients[91], and appear to have immunomodulatory effects on T cells, B cells and macrophages[92]. As well, gold salts inhibit the ability of IL-2 to

stimulate T-cell proliferation[91], which appears to occur by suppression of IL-2 and IL-2 receptor mRNA accumulation in T-cells. Other studies have shown that in monocytes, gold and palladium cause TNF- α and IL-1 β suppression at high concentrations, and that gold also decreases IL-6 expression at high concentrations, which led to speculation that the gold and palladium acted by binding to NF-kB subtypes[93]. Together, these results suggest that gold (and palladium) may have anti-inflammatory effects by direct modulation of cell signaling. Furthermore, *in vitro* and *in vivo* studies have indicated that formation of Au⁽⁰⁾ appears to occur during oxidation of Au⁺ (the form gold treatments are provided in) to Au³⁺ (which is generally considered to be the active species in RA treatment)[94]. These studies have also shown that Au⁽⁰⁾ appears to suppress the activity of inflammatory cytokines such as IL-6 and TNF- α ; immune complexes such as IgG and IgM; and rheumatoid factor in RA patients[94]. In addition, patients treated with colloidal gold lacked the side effects of other gold treatments, but did have decreased RA symptoms[94]. This has led some researchers to speculate that the active ingredient for anti-inflammatory activity is Au⁽⁰⁾, and that the side effects with traditional gold treatments may be caused by Au³⁺, contaminants, or the salts with which the gold is delivered[92, 94, 95]. As with silver, it is unlikely that bare gold atoms will exist in solution, and therefore, these Au⁽⁰⁾ species may also be in a cluster form. Furthermore, the crystal structure (face-centred cubic) and Pauling covalent radii for silver and gold are essentially equal, since their “metallic radius” in close-packed cubic lattices is almost the same[96]. The lattice constants are 4.0862 Å for silver, and 4.07824

Å for gold[97]; the nearest-neighbor interatomic distances are 2.889 Å (Ag-Ag) and 2.884 Å (Au-Au) for coordination number 12[98]; and for a two-coordinate M(I) compound the atomic radii are 1.33 Å for silver, and 1.25 Å for gold[96]. The result of these physical similarities is that silver and gold can replace each other one-to-one in a crystal lattice with very little strain on the lattice, suggesting that Au⁽⁰⁾ and Ag⁽⁰⁾-containing clusters should be nearly identical physically, and therefore may have similar biological activity. This gives further evidence that the anti-inflammatory activity of nanocrystalline silver (and potentially platinum or palladium which also induce apoptosis and have anti-inflammatory activity) may be due to a reduced form, such as Ag⁽⁰⁾-containing clusters. Much has yet to be discovered regarding these clusters and their mechanisms of action.

Purpose

This thesis continues exploration of medical applications for nanocrystalline silver. Its aim is to improve understanding of the antimicrobial activity, and to prove the existence of the anti-inflammatory activity of nanocrystalline silver, and to use this knowledge to develop appropriate silver-containing agents for use in the treatment of infectious and inflammatory conditions which are not easily treated with nanocrystalline silver thin film dressings, such as lung conditions. In Chapters 2-3, the anti-inflammatory effect of nanocrystalline silver in dressing form is proven, and then examined in terms of mechanisms of action and systemic effects. In Chapter 4, the antimicrobial effect of nanocrystalline silver in dressing form is examined in comparison to other dressings, in terms of silver resistance development, and in comparison to

single silver nanoparticles. In Chapters 5-7, nanocrystalline silver-derived solutions are developed and analyzed in terms of their physical, chemical, optical, antimicrobial, and anti-inflammatory activity. In Chapter 8, the effect of modifying sputtering conditions on the resulting physical, chemical and antimicrobial properties of nanocrystalline silver thin films is examined, while in Chapter 9, the kinetics of post-sputter heat treatment on the resulting properties of nanocrystalline silver thin films is examined, in order to better understand the mechanisms of action of nanocrystalline silver, the properties necessary for its unique activity, and the conditions which could negate that activity, such as heat. A study flow guide for the thesis is shown in Figure 1-3.

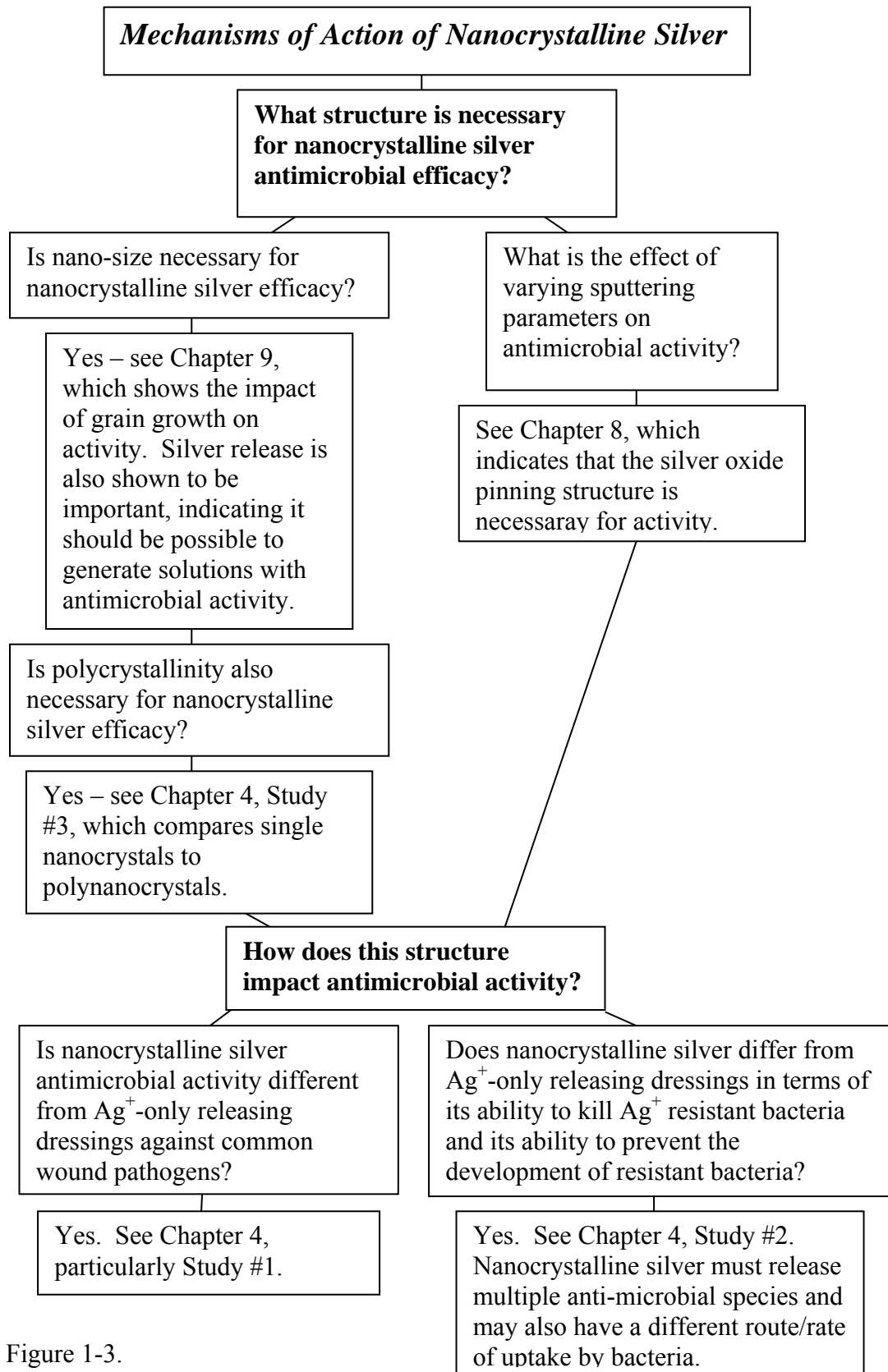
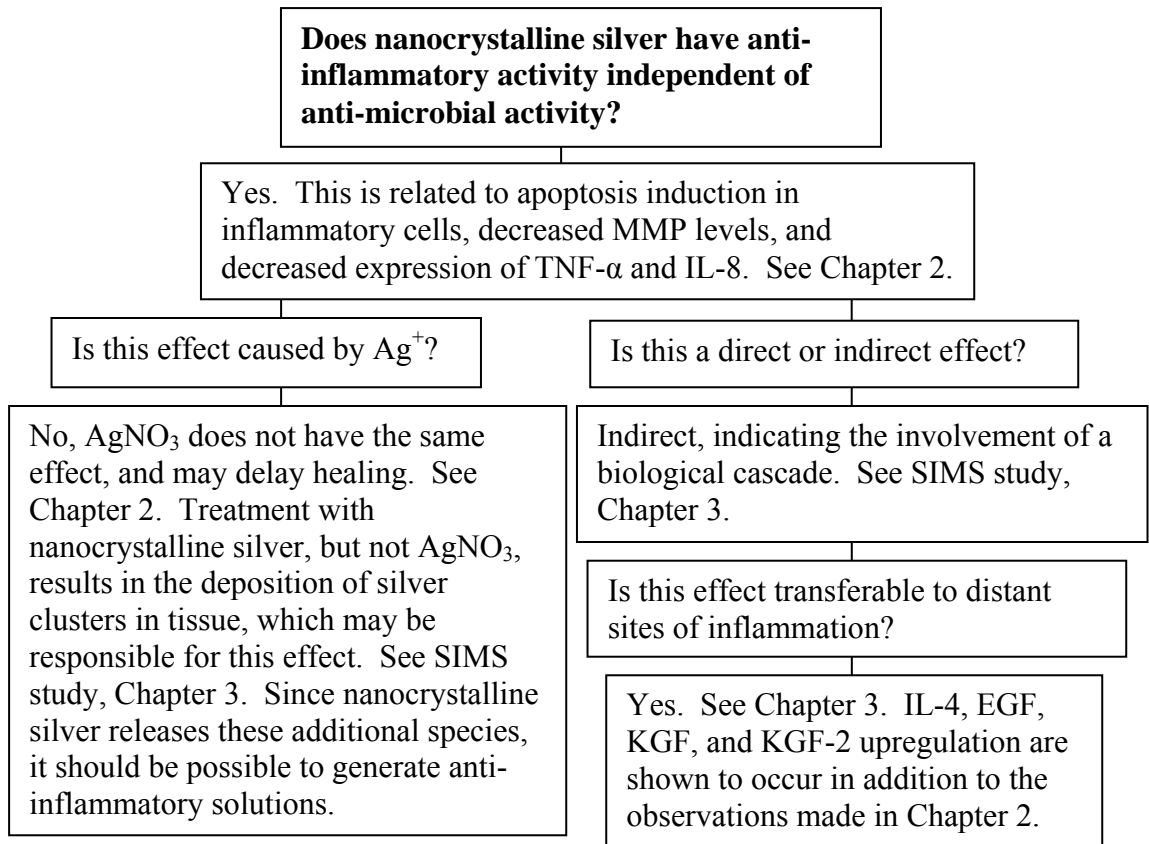


Figure 1-3.



Solution Development

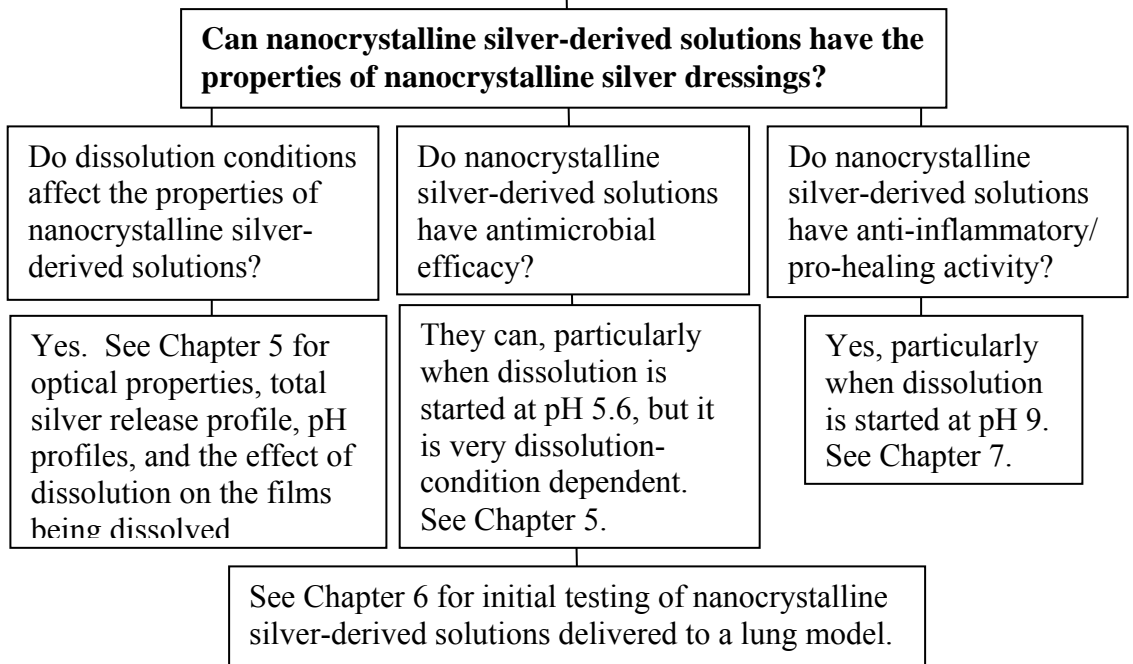


Figure 1-3, cont'd. Study flow diagram for the thesis.

Bibliography

1. Klasen HJ: **Historical review of the use of silver in the treatment of burns. I. Early uses.** *Burns* 2000, **26**:117-130.
2. Sollman T: *A Manual of Pharmacology and its applications to therapeutics and toxicology*, 6th edition. Philadelphia: W.B. Saunders Company; 1942: 1102-1109.
3. Grier N: **Silver and its compounds.** In: *Disinfection, Sterilization and Preservation*. Edited by Block S, 3rd edition. Philadelphia: Lea & Febiger; 1983: 375-389.
4. Halsted WS: **The operative treatment of hernia.** *Am J Med Sci* 1895, **10**:13-17.
5. Moyer CA, Brentano L, Gravens DL, Margraf HW, Monafó WW: **Treatment of large human burns with 0.5% silver nitrate solution.** *Arch Surg* 1965, **90**:812-867.
6. Fox CL: **Silver sulphadiazine, addendum to local therapy.** In: *Modern treatment*. New York: Hoeber Medical Division, Harper and Row; 1967: 1259.
7. Monafó WW, West MA: **Current treatment recommendations for topical burn therapy.** *Drugs* 1990, **40**:364-373.
8. Klasen HJ: **A historical review of the use of silver in the treatment of burns. II. Renewed interest for silver.** *Burns* 2000, **26**:131-138.
9. Monafó WW, Ayvazian VH, Skinner AM: **Control of infection in major burn wounds by cerium nitrate/silver sulphadiazine.** *Burns* 1976, **3**:104-107.
10. Deitch EA, Marino AA, Malakanok V, Albright JA: **Silver nylon cloth: *in vitro* and *in vivo* evaluation of antimicrobial activity.** *J Trauma* 1987, **27**:301-304.
11. Deitch EA, Marino AA, Gillespie TE, Albright JA: **Silver-nylon: a new antimicrobial agent.** *Antimicrob Agents Chemother* 1983, **23**:356-359.
12. Demling R, Burrell RE: **The beneficial effects of nanocrystalline silver as a topical antimicrobial agent.** *Leadership Medica* 2002, **16**:10 pages.
13. Wright JB, Lam K, Hansen D, Burrell RE: **Efficacy of topical silver against fungal burn wound pathogens.** *American Journal of Infection Control* 1999, **27**:344-350.
14. Yin HQ, Langford R, Burrell RE: **Comparative evaluation of the antimicrobial activity of ACTICOAT antimicrobial barrier dressing.** *Journal of Burn Care & Rehabilitation* 1999, **20**:195-200.
15. Wright JB, Lam K, Burrell RE: **Wound management in an era of increasing bacterial antibiotic resistance: a role for topical silver treatment.** *American Journal of Infection Control* 1998, **26**:572-577.
16. Wright JB, Lam K, Olson ME, Burrell RE: **Is Antimicrobial Efficacy Sufficient? A Question Concerning the Benefits of New Dressings.** *Wounds: A Compendium of Clinical Research and Practice* 2003, **15**:133-141.

17. Olson ME, Wright JB, Lam K, Burrell RE: **Healing of porcine donor sites covered with silver-coated dressings.** *Eur J Surg* 2000, **166**:486-489.
18. Wright JB, Lam K, Buret AG, Olson ME, Burrell RE: **Early healing events in a porcine model of contaminated wounds: effects of nanocrystalline silver on matrix metalloproteinases, cell apoptosis, and healing.** *Wound Repair Regen* 2002, **10**:141-151.
19. Kirsner R, Orsted H, Wright, JB: **Matrix Metalloproteinases in Normal and Impaired Wound Healing: A Potential Role of Nanocrystalline Silver.** *Wounds: A Compendium of Clinical Research and Practice* 2002, **13**:4-12.
20. Wright JB, Hansen DL, Burrell RE: **The Comparative Efficacy of Two Antimicrobial Barrier Dressings: *In-vitro* Examination of Two Controlled Release Silver Dressings.** *Wounds: A Compendium of Clinical Research and Practice* 1998, **10**:179-188.
21. Bhol KC, Alroy J, Schechter PJ: **Anti-inflammatory effect of topical nanocrystalline silver cream on allergic contact dermatitis in a guinea pig model.** *Clin Exp Dermatol* 2004, **29**:282-287.
22. Bhol KC, Schechter PJ: **Topical nanocrystalline silver cream suppresses inflammatory cytokines and induces apoptosis of inflammatory cells in a murine model of allergic contact dermatitis.** *Br J Dermatol* 2005, **152**:1235-1242.
23. Bhol KC, Schechter PJ: **Effects of Nanocrystalline Silver (NPI 32101) in a Rat Model of Ulcerative Colitis.** *Dig Dis Sci* 2007:11 pages.
24. **Silver Ionisation Energies.** In: *WebElements Periodic Tables of the Elements* 2009. Ed.: Winter M.
<http://www.webelements.com/silver/atoms/html>. Viewed October 17, 2009.
25. *WebElements Periodic Tables of the Elements* 2009. Ed: Winter M.
<http://www.webelements.com>. Viewed October 17, 2009.
26. **Selected Solubility Products and Formation Constants at 25°C.**
<http://www.csudh.edu/oliver/chemdata/data-ksp/htm>. Viewed October 17, 2009.
27. Trengove NJ, Langton SR, Stacey MC: **Biochemical analysis of wound fluid from non-healing and healing chronic leg ulcers.** *Wound Repair Regen* 1996, **4**:234-239.
28. Ricketts CR, Lowbury EJ, Lawrence JC, Hall M, Wilkins MD: **Mechanism of prophylaxis by silver compounds against infection of burns.** *Br Med J* 1970, **2**:444-446.
29. Burrell RE, Morris LR: **Anti-microbial coating for medical device.** ©1998, US Patent No. 5753251.
30. Fan F, Bard AJ: **Chemical, Electrochemical, Gravimetric, and Microscopic Studies on Antimicrobial Silver Films.** *Journal of Physical Chemistry B* 2002, **106**:279-287.

31. Taylor PL, Omotoso O, Wiskel JB, Mitlin D, Burrell RE: **Impact of heat on nanocrystalline silver dressings Part II: Physical properties.** *Biomaterials* 2005, **26**:7230-7240.
32. Birringer R: **Nanocrystalline Materials.** *Material Science and Engineering* 1989, **A117**:33-43.
33. Taylor PL, Ussher AL, Burrell RE: **Impact of heat on nanocrystalline silver dressings. Part I: Chemical and biological properties.** *Biomaterials* 2005, **26**:7221-7229.
34. Kloth LC, McCulloch JM: **The Inflammatory Response to Wounding.** In: *Wound Healing Alternatives in Management.* Edited by McCulloch JM, Kloth LC, Feedar JA, 2nd edition. Philadelphia: F. A. Davis Company; 1995: 3-14.
35. Park JE, Barbul A: **Understanding the role of immune regulation in wound healing.** *Am J Surg* 2004, **187**:11S-16S.
36. Mulder GF, Brazinsky BA, Seeley JE: **Factors complicating wound repair.** In: *Wound Healing Alternatives in Management.* Edited by McCulloch JM, Kloth LC, Feedar JA, 2nd edition. Philadelphia: F. A. Davis Company; 1995: 47-57.
37. Davies CE, Wilson MJ, Hill KE, Stephens P, Hill CM, Harding KG, Thomas DW: **Use of molecular techniques to study microbial diversity in the skin: Chronic wounds reevaluated.** *Wound Repair Regen* 2001, **9**:332-340.
38. Trowbridge H, Emling RC: *Inflammation: A Review of the Process*, 5th edition. USA: Quintessence Publishing Co., Inc.; 1997.
39. Carr HS, Wlodkowski TJ, Rosenkranz HS: **Silver Sulfadiazine: In Vitro Antibacterial Activity.** *Antimicrob Agents Chemother* 1973, **4**:585-587.
40. Spadaro JA, Berger TJ, Barranco SD, Chapin SE, Becker RO: **Antibacterial Effects of Silver Electrodes with Weak Direct Current.** *Antimicrob Agents Chemother* 1974, **6**:637-642.
41. Berger TJ, Spadaro JA, Bierman R, Chapin SE, Becker RO: **Antifungal Properties of Electrically Generated Metallic Ions.** *Antimicrob Agents Chemother* 1976, **10**:856-860.
42. Hall RE, Bender G, Marquis RE: **Inhibitory and cidal antimicrobial actions of electrically generated silver ions.** *J Oral Maxillofac Surg* 1987, **45**:779-784.
43. Maple PAC, Hamilton-Miller JMT, Brumfitt W: **Comparison of the in-vitro activities of the topical antimicrobials azelaic acid, nitrofurazone, silver sulphadiazine and mupirocin against methicillin-resistant *Staphylococcus aureus*.** *Journal of Antimicrobial Chemotherapy* 1992, **29**:661-668.
44. Li X-Z, Nikaido H, Williams KE: **Silver-Resistant Mutants of *Escherichia coli* Display Active Efflux of Ag⁺ and Are Deficient in Porins.** *Journal of Bacteriology* 1997, **179**:6127-6132.
45. Zhao X, Drlica K: **Restricting the Selection of Antibiotic-Resistant Mutant Bacteria: Measurement and Potential Use of the Mutant**

- Selection Window.** *The Journal of Infectious Diseases* 2002, **185**:561-565.
46. Simonetti N, Simonetti G, Bougnol F, Scalzo M: **Electrochemical Ag⁺ for preservative use.** *Appl Environ Microbiol* 1992, **58**:3834-3836.
 47. Richard JW, Spencer BA, McCoy L, Carino E, Washington J, Edgar P, Rosenblatt J, Goodheart RE, Hegggers J: **ActicoatTM versus Silverlon[®]: The truth.** *J Burns & Surg Wound Care* 2002, **1**:11-19.
 48. Marino AA, Deitch EA, Malakanok V, Albright JA, Specian RD: **Electrical Augmentation of the Antimicrobial Activity of Silver-Nylon Fabrics.** *Journal of Biological Physics* 1984, **12**:93-98.
 49. Spacciapoli P, Buxton D, Rothstein D, Friden P: **Antimicrobial activity of silver nitrate against periodontal pathogens.** *J Periodontal Res* 2001, **36**:108-113.
 50. Fraser JF, Bodman J, Sturgess R, Faoagali J, Kimble RM: **An *in vitro* study of the antimicrobial efficacy of a 1% silver sulphadiazine and 0.2% chlorhexidine digluconate cream, 1% silver sulphadiazine cream and a silver coated dressing.** *Burns* 2004, **30**:35-41.
 51. Ip M, Lui SL, Poon VK, Lung I, Burd A: **Antimicrobial activities of silver dressings: an *in vitro* comparison.** *Journal of Medical Microbiology* 2006, **55**:59-63.
 52. Gallant-Behm CL, Yin HQ, Liu SJ, Hegggers JP, Langford RE, Olson ME, Hart DA, Burrell RE: **Comparison of *in vitro* disc diffusion and time kill-kinetic assays for the evaluation of antimicrobial wound dressing efficacy.** *Wound Repair and Regeneration* 2005, **13**:412-421.
 53. Burrell RE, Hegggers JP, Davis GJ, Wright JB: **Efficacy of Silver-Coated Dressings as Bacterial Barriers in a Rodent Burn Sepsis Model.** *Wounds: A Compendium of Clinical Research and Practice* 1999, **11**:64-71.
 54. Hegggers J, Goodheart RE, Washington J, McCoy L, Carino E, Dang T, Edgar P, Maness C, Chinkes D: **Therapeutic efficacy of three silver dressings in an infected animal model.** *J Burn Care Rehabil* 2005, **26**:53-56.
 55. Ulkur E, Oncul O, Karagoz H, Yeniz E, Celikoz B: **Comparison of silver-coated dressing (ActicoatTM), chlorhexidine acetate 0.5% (Bactigrass[®]), and fusidic acid 2% (Fucidin[®]) for topical antibacterial effect in methicillin-resistant Staphylococci-contaminated, full-skin thickness rat burn wounds.** *Burns* 2005, **31**:874-877.
 56. Ulkur E, Oncul O, Karagoz H, Celikoz B, Cavuslu S: **Comparison of Silver-Coated Dressing (ActicoatTM), Chlorhexidine Acetate 0.5% (Bactigrass[®]), and Silver Sulfadiazine 1% (Silverdin[®]) for Topical Antibacterial Effect in *Pseudomonas aeruginosa*-Contaminated, Full-Skin Thickness Burn Wounds in Rats.** *J Burn Care Rehabil* 2005, **26**:430-433.
 57. Tredget EE, Shankowsky HA, Groeneveld A, Burrell RE: **A matched-pair, randomized study evaluating the efficacy and safety of Acticoat**

- silver-coated dressing for the treatment of burn wounds.** *J Burn Care Rehabil* 1998, **19**:531-537.
58. Doshi J, Karagama Y, Buckley D, Johnson I: **Observational study of bone-anchored hearing aid infection rates using different post-operative dressings.** *J Laryngol Otol* 2006, **120**:842-844.
 59. Rustogi R, Mill J, Fraser JF, Kimble RM: **The use of Acticoat in neonatal burns.** *Burns* 2005, **31**:878-882.
 60. Klein DG, Fritsch DE, Amin SG: **Wound infection following trauma and burn injuries.** *Crit Care Nurs Clin North Am* 1995, **7**:627-642.
 61. Isenberg SJ, Apt L, Yoshimori R, Leake RD, Rich R: **Povidone-iodine for ophthalmia neonatorum prophylaxis.** *Am J Ophthalmol* 1994, **118**:701-706.
 62. Saarialho-Kere UK: **Patterns of matrix metalloproteinase and TIMP expression in chronic ulcers.** *Arch Dermatol Res* 1998, **290 Suppl**:S47-54.
 63. Kahari VM, Saarialho-Kere U: **Matrix metalloproteinases in skin.** *Exp Dermatol* 1997, **6**:199-213.
 64. Stewart B: **Apoptosis.** In: *Mechanisms in Carcinogenesis and Cancer Prevention.* Edited by Vainio H, Hietanen EK, vol. 156. Springer-Verlag; 2003: 83-106.
 65. Lawen A: **Apoptosis-an introduction.** *Bioessays* 2003, **25**:888-896.
 66. Olson ME, Wright JB, Lam K, Burrell RE: **Healing of porcine donor sites covered with silver-coated dressings.** *Eur J Surg* 2000, **166**:486-489.
 67. Lin E, Calvano SE, Lowry SF: **Inflammatory cytokines and cell response in surgery.** *Surgery* 2000, **127**:117-126.
 68. Daly T: **Contraction and Re-epithelialization.** In: *Wound Healing: Alternatives in Management.* Edited by McCulloch J, Kloth LC, Feedar JA, 2nd edition. Philadelphia: F.A. Davis Company; 1995: 32-46.
 69. Meyer W, Schwarz R, Neurand K: **The skin of domestic mammals as a model for the human skin, with special reference to the domestic pig.** *Curr Probl Dermatol* 1978, **7**:39-52.
 70. Mazurak VC, Burrell RE, Tredget EE, Clandinin MT, Field CJ: **The effect of treating infected skin grafts with Acticoat on immune cells.** *Burns* 2007, **33**:52-58.
 71. Tian J, Wong KK, Ho CM, Lok CN, Yu WY, Che CM, Chiu JF, Tam PK: **Topical delivery of silver nanoparticles promotes wound healing.** *ChemMedChem* 2007, **2**:129-136.
 72. Liechty KW, Kim HB, Adzick NS, Crombleholme TM: **Fetal wound repair results in scar formation in interleukin-10-deficient mice in a syngeneic murine model of scarless fetal wound repair.** *J Pediatr Surg* 2000, **35**:866-872.
 73. Liechty KW, Adzick NS, Crombleholme TM: **Diminished interleukin 6 (IL-6) production during scarless human fetal wound repair.** *Cytokine* 2000, **12**:671-676.

74. Wahl SM: **Transforming growth factor-beta: innately bipolar.** *Curr Opin Immunol* 2007, **19**:55-62.
75. Li AG, Lu SL, Han G, Hoot KE, Wang XJ: **Role of TGFbeta in skin inflammation and carcinogenesis.** *Mol Carcinog* 2006, **45**:389-396.
76. Paddock HN, Schultz GS, Perrin KJ, *et al.*: **Clinical assessment of silver-coated antimicrobial dressings on MMPs and cytokine levels in non-healing wounds.** In: *Annual Meeting of the Wound Healing Society*; 2002; Baltimore.
77. Demling RH, DeSanti L: **The rate of re-epithelialization across meshed skin grafts is increased with exposure to silver.** *Burns* 2002, **28**:264-266.
78. Huang Y, Li X, Liao Z, Zhang G, Liu Q, Tang J, Peng Y, Liu X, Luo Q: **A randomized comparative trial between Acticoat and SD-Ag in the treatment of residual burn wounds, including safety analysis.** *Burns* 2007, **33**:161-166.
79. Demling RH, DeSanti L, Orgill DP: **Applications of Silver.** <http://www.burnsurgery.org/Modules/silver/> ©2000. Viewed July 18, 2008.
80. Demling RH, DeSanti L: **Effects of Silver on Wound Management.** *Wounds: A Compendium of Clinical Research and Practice* 2001, **13**:4-15.
81. Teixeira LR, Vargas FS, Acencio MM, Paz PF, Antonangelo L, Vaz MA, Marchi E: **Influence of antiinflammatory drugs (methylprednisolone and diclofenac sodium) on experimental pleurodesis induced by silver nitrate or talc.** *Chest* 2005, **128**:4041-4045.
82. Fyfe MC, Chahl LA: **The effect of single or repeated applications of "therapeutic" ultrasound on plasma extravasation during silver nitrate induced inflammation of the rat hindpaw ankle joint in vivo.** *Ultrasound Med Biol* 1985, **11**:273-283.
83. Chahl JS, Chahl LA: **The role of prostaglandins in chemically induced inflammation.** *Br J Exp Pathol* 1976, **57**:689-695.
84. Fuertes M, Castilla J, Alonso C, Perez JM: **Cisplatin biochemical mechanism of action: from cytotoxicity to induction of cell death through interconnections between apoptotic and necrotic pathways.** *Current Medicinal Chemistry* 2003, **10**:257-266.
85. Mizushima Y, Okumura H, Kasukawa R: **Effects of gold and platinum on necrotizing factor, skin sensitizing antibody, and complement.** *Jpn J Pharmacol* 1965, **15**:131-134.
86. Che CM, Sun RW, Yu WY, Ko C, Zhu N, Sun H: **Gold (III) porphyrins as a new class of anticancer drugs: cytotoxicity, DNA binding and induction of apoptosis in human cervix epitheloid cancer cells.** *Chem Commun* 2003:1718-1719.
87. McKeage MJ: **Gold opens mitochondrial pathways to apoptosis.** *Br J Pharmacol* 2002, **136**:1081-1082.

88. Thunus L, Dauphin JF, Moïny G, Deby C, Deby-Dupont G: **Anti-inflammatory properties of copper, gold, and silver, individually and as mixtures.** *Analyst* 1995, **120**:967-973.
89. Glennas A, Rugstad HE: **Ploidy and cell cycle progression during treatment with gold chloride, auranofin and sodium aurothiomalate. Studies on a human epithelial cell line and its sub-strains made resistant to the antiproliferative effects of these gold compounds.** *Virchows Arch B Cell Pathol Incl Mol Pathol* 1985, **49**:385-393.
90. Handel ML, Nguyen LQ, Lehmann TP: **Inhibition of transcription factors by anti-inflammatory and anti-rheumatic drugs: can variability in response be overcome?** *Clin Exp Pharmacol Physiol* 2000, **27**:139-144.
91. Suzuki S, Okubo M, Kaise S, Ohara M, Kasukawa R: **Gold sodium thiomalate selectivity inhibits interleukin-5-mediated eosinophil survival.** *J Allergy Clin Immunol* 1995, **96**:251-256.
92. Eisler R: **Chrysotherapy: a synoptic review.** *Inflamm Res* 2003, **52**:487-501.
93. Wahata J, Lewis JB, Volkmann KR, Lockwood PE, Messer RLW, Bouillaguet S: **Sublethal concentrations of Au(III), Pd(II), and Ni(II) differentially alter inflammatory cytokine secretion from activated monocytes.** *J Biomed Mater Res Part B: Appl Biomater* 2004, **69B**:11-17.
94. Abraham G, Himmel PB: **Management of Rheumatoid Arthritis: Rationale for the Use of Colloidal Metallic Gold.** *Journal of Nutritional and Environmental Medicine* 1997, **7**:295-305.
95. Zou J, Guo Z, Parkinson JA, Chen Y, Sadler PJ: **Gold(III)-induced oxidation of glycine: relevance to the toxic side-effects of gold drugs.** *Journal of Inorganic Biochemistry* 1999, **74**:352.
96. Bayler A, Schier A, Bowmaker GA, Schmidbaur H: **Gold is smaller than silver, crystal structures of [bis(trimesitylphosphine)gold(I)] and [bis(trimesitylphosphine)silver(I)] tetrafluoroborate.** *Journal of the American Chemical Society* 1996, **118**:7006-7007.
97. Wyckhoff RG: *Crystal Structures*, 2nd edition. New York: Interscience Publishers; 1958: 10.
98. Pauling L: *The Nature of the Chemical Bond.*, 3rd edition. Ithaca, NY: Cornell University Press; 1980: 410.

Chapter 2 – Testing Nanocrystalline Silver Dressings For Anti-inflammatory Activity¹

Introduction

Nanocrystalline silver dressings were originally designed to be, and introduced commercially as, equilibrating antimicrobial burn dressings. However, animal and clinical studies using nanocrystalline silver dressings have also demonstrated improved wound healing[1-3]. This unusual biological response may result from anti-inflammatory activity[4-6]. The unique activity of nanocrystalline silver may be due to the small (~11-15 nm) grain sizes present, which result in a high percentage of the grain boundary silver atoms. As described in Chapter 1, these grain boundary atoms may represent a unique state of solid matter[7].

One of the unique physicochemical properties of nanocrystalline silver, which may be of interest in terms of potential anti-inflammatory activity, is its dissolution behavior: in addition to Ag^+ , Ag^0 dissolves into solution, possibly in clusters of a few atoms[6, 8]. These Ag^0 clusters could be anti-inflammatory, as there is evidence that other noble metals, including gold and platinum, have anti-inflammatory activity which may result from their reduced form[9-14]. Au^+ is the gold species delivered in some treatments for rheumatoid arthritis (RA). In the body, it reacts to form Au^{3+} , which has generally been considered the active agent. However, *in vitro* and *in vivo* studies indicate that Au^0 is formed during this reaction[15]. Au^0 nanoparticles have also been shown to suppress the activity

¹ A version of this chapter has been published. Nadworny, Wang, Tredget, and Burrell, 2008. Nanomedicine: Nanotechnology, Biology, and Medicine. 4:241-258

of inflammatory cytokines such as IL-6 and TNF- α while reducing RA symptoms[15], suggesting that Au⁰ may be the anti-inflammatory agent resulting from gold treatments, while Au³⁺ may actually cause some of the side effects observed with gold treatment[13, 15, 16]. Similar to silver, individual Au⁰ atoms would not exist stably in solution, indicating that the anti-inflammatory activity of Au⁰ may be due to a reduced cluster form. Furthermore, the Pauling covalent radii for silver and gold are essentially equal, since their “metallic radii” in close-packed cubic lattices are almost the same[17]. The lattice constants are 4.0862 Å for silver, and 4.07824 Å for gold[18]; the nearest-neighbor interatomic distances are 2.889 Å (Ag-Ag) and 2.884 Å (Au-Au) for coordination number 12[19]; and for a two-coordinate M(I) compound the atomic radii are 1.33 Å for silver, and 1.25 Å for gold[17]. Silver and gold also both form face centered cubic crystal lattices. The result of these physical similarities is that silver and gold can be replaced one-to-one in a crystal lattice with very little strain on the lattice, suggesting that small Au⁰ and Ag⁰ containing clusters should be nearly identical physically, and thus may have similar activity. This is further evidence that the anti-inflammatory activity of nanocrystalline silver may be due to a reduced form, such as Ag⁰ containing clusters.

A recent study found that, compared to controls and silver sulfadiazine-treated animals, treatment of thermal injuries in mice with silver nanoparticles increased the rate of healing and decreased scarring[20]. This was accompanied by an increased expression of cytokines including IL-10, VEGF, and IFN- γ ; a reduced expression of IL-6; and a higher TGF- β 1 expression initially, followed by

significantly lower TGF- β 1 expression later on[20].

In a porcine contaminated wound model, nanocrystalline silver-treated wounds showed enhanced development of healthy granulation tissue, which was able to support a graft at four days. At the same time, these wounds demonstrated decreased erythema, edema, and inflammatory cells compared to controls and silver nitrate treated wounds[2]. An increase in PMN apoptosis was also observed in nanocrystalline silver treated wounds. In addition, MMP levels remained low in nanocrystalline silver treated wounds, while they rose in other groups[2]. This impact on MMP levels was confirmed in a clinical study performed on patients with various chronic wounds[3]. Taken together, these data indicate that nanocrystalline silver may have an anti-inflammatory effect. However, in these studies, the wounds were infected, and thus it was not possible to distinguish whether the apparent anti-inflammatory activity of the nanocrystalline silver was independent of its antimicrobial activity[3].

Direct evidence for an anti-inflammatory effect of nanocrystalline silver appeared in studies by Bhol *et al.*[4, 5, 21] In their first study, guinea pigs were sensitized to 5% 2,4-dinitrochlorobenzene (DNCB) in acetone. Allergic contact dermatitis was elicited 9 days later with 5% DNCB. Some guinea pigs were left untreated, while the dermatitis of other guinea pigs was treated with various concentrations of nanocrystalline silver cream, steroids, immunosuppressants, or their vehicles[4]. They found that 0.5 and 1% nanocrystalline silver creams significantly reduced erythema and edema scores within 24h. Histopathological inflammation scores were significantly reduced with 0.5 and 1% nanocrystalline

silver treatments as compared to controls after 5 days, and the nanocrystalline silver appeared to be equally active as, but more rapid than, the steroids and immunosuppressants[4].

This study was followed up by a study in which mice were sensitized to 0.5% dinitrofluorobenzene (DNFB) in 4:1 acetone:olive oil[5]. After 5 and 7 days, allergic contact dermatitis was induced on their ears using 0.2% DNFB. The mice were then treated with a high potency steroid, 1% nanocrystalline silver cream, an immunosuppressant, or a vehicle. Nanocrystalline silver cream significantly reduced ear thickness and erythema, and the number of inflammatory cells present[5]. It also significantly reduced expression of the pro-inflammatory molecules IL-12 and TNF- α . In addition, nanocrystalline silver increased the number of inflammatory cells undergoing apoptosis, while keratinocyte apoptosis was not induced. This was not observed in other treatment groups. These results suggest that nanocrystalline silver may have an anti-inflammatory effect in skin[5]. However, these studies both used rodent skin models, which heal very differently from human skin[22], in that they heal mostly by contraction, while human skin heals more by re-epithelialization, and have significant differences in physiology, including the relative thickness of the epidermis and dermis, and the number of dermal appendages present. Furthermore, rodents do not develop hypertrophic scar or intra-abdominal adhesions, indicating further differences between rodent and human healing[22]. Thus, it is not clear whether the results are clinically relevant. As well, in this study, the nanocrystalline silver is incorporated into a hydrophobic emollient

cream, which may have inhibited the nanocrystalline silver from entering the rash, reducing its efficacy.

More recently, the same group performed a study using a rat ulcerative colitis model[21]. Colitis was induced via an intracolonic injection of dinitrobenzenesulfonic acid in ethanol. Nanocrystalline silver was delivered as nanodispersions in 5.7% polyvinyl alcohol, either orally or by intracolonic dosing. The nanocrystalline silver treated rats were compared to untreated rats, vehicle controls and sulfasalazine treated rats[21]. They found that both local and oral nanocrystalline silver treatments, at different doses, were able to significantly reduce total IBD scores (colonic ulcer score + colonic thickness score + stool consistency score) and histopathological scores, while improving body weight[21]. Nanocrystalline silver treatments also suppressed the expression of MMP-9, TNF- α , IL-12, and IL-1 β , as measured by immunohistochemistry; and of gelatinases as measured by zymography[21]. Although the study was not performed in the skin, this suggests that nanocrystalline silver may have anti-inflammatory activity in the skin, since the colonic tissue is also epithelial.

In this study, treatment of dinitrochlorobenzene-induced rashes with nanocrystalline silver, silver nitrate, or saline was examined. The purpose of this study was to determine if nanocrystalline silver has anti-inflammatory activity in the skin independent of its antimicrobial activity. To produce data which could readily be extrapolated to clinical situations, a porcine model was chosen. Pig skin is an excellent model for human skin because of the similarities between them[23, 24], including relative thickness of the epidermis and dermis; presence

of a similar density of dermal appendages[25]; and similarities in healing[23, 24]. Figure 2-1 compares control animal data from two excisional mouse models of re-epithelialization[26, 27], a partial thickness porcine wound model of re-epithelialization[1], and a clinical study of meshed skin graft re-epithelialization[28]. Figure 2-2 compares the effect of treatment with nanocrystalline silver dressings on an excisional mouse model of re-epithelialization[26], a partial thickness porcine wound model of re-epithelialization[1], and a clinical study of meshed skin graft re-epithelialization[28]. Both figures show that while results of mouse models may not be clinically relevant, the data generated using porcine models agreed closely with clinical results. As well, the juvenile pig is an excellent model for studies on skin because the pigs are small and relatively easy to handle and house, have a reproducible pattern of gene expression during healing, do not have significant differences in RNA and mRNA yields between pigs or between locations on a single pig, and have closely correlated total RNA and DNA values, which, in turn, parallel fluctuations of cellularity in the skin[23, 24].

A DNCB-induced contact dermatitis model was chosen in order to distinguish antimicrobial from anti-inflammatory activity. In this model, animals are gradually sensitized to DNCB until they develop a severe skin rash. This model has no introduction of bacteria and no open wounds. DNCB is a type IV hapten, and DNCB-induced contact dermatitis is considered the prototype of T-cell mediated delayed-type hypersensitivity reactions[4, 5, 29]. This type of contact dermatitis occurs in two phases. In the sub-clinical sensitization phase,

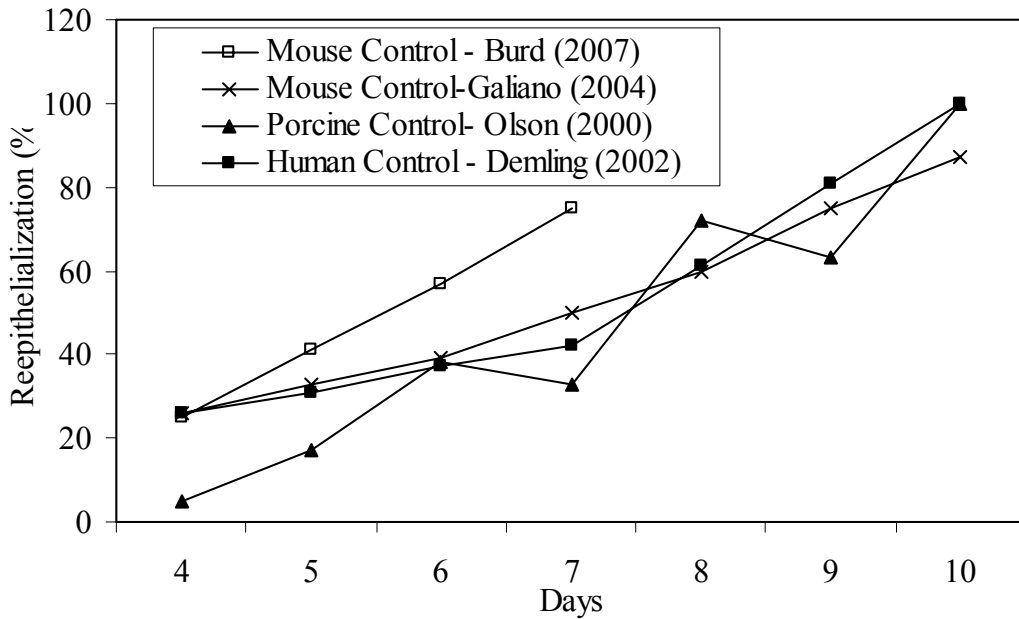


Figure 2-1. Comparison of control animal data from two excisional mouse models of re-epithelialization[26, 27], a partial thickness porcine wound model of re-epithelialization[1], and a clinical study of meshed skin graft re-epithelialization[28].

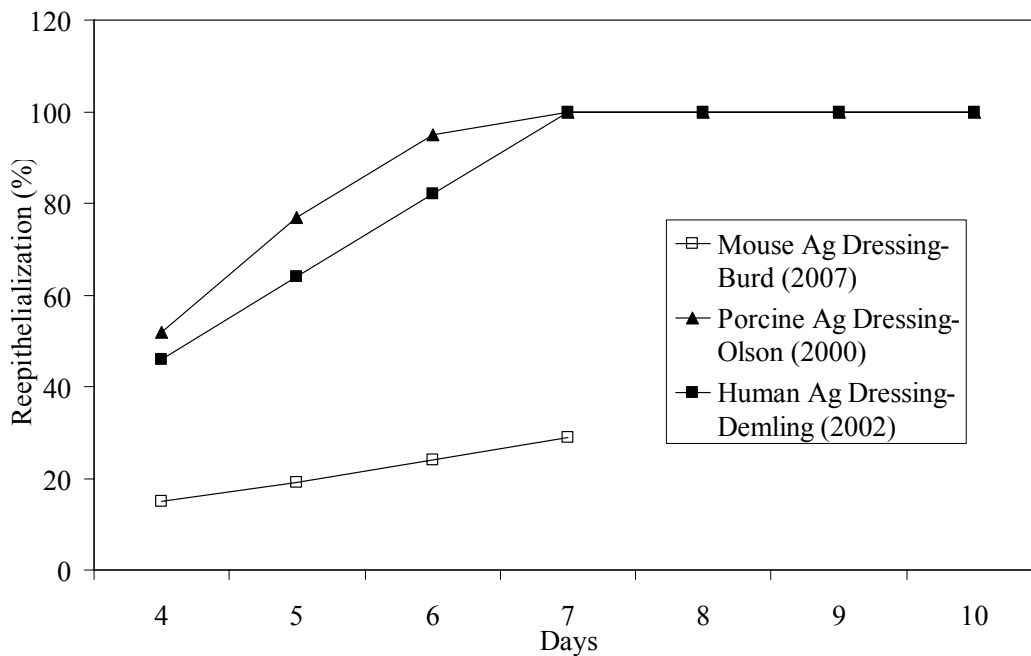


Figure 2-2. Comparison of the effect of treatment with nanocrystalline silver dressings on an excisional mouse model of re-epithelialization[26], a partial thickness porcine wound model of re-epithelialization[1], and a clinical study of meshed skin graft re-epithelialization[28].

hapten which contacts the skin is taken up and processed by epidermal Langerhans cells, which go from a resting state to an active state due to direct effects of the hapten, and also due to keratinocyte secretion of inflammatory cytokines[4, 5, 29, 30]. The Langerhans cells then travel to lymph nodes, where the hapten is presented to naïve T-cells (mainly CD8+ effector T cells) which become active hapten-specific effector T cells[4, 5, 29, 30]. In the elicitation phase, when hapten contacts the skin, antigen presenting cells, including Langerhans cells, present the hapten to the hapten- specific T-cells, which are recruited to the skin. The activated T-cells then release pro-inflammatory cytokines and attract other inflammatory cells. These actions lead to mast cell degranulation; vasodilatation; and an influx of neutrophils, mononuclear cells and other T cells, resulting in severe dermal inflammation[4, 5, 29, 30]. In this study, nanocrystalline silver treatments reduced erythema and edema, increased inflammatory cell apoptosis, and decreased levels of gelatinases, TGF- β , TNF- α , and IL-8, suggesting that nanocrystalline silver is anti-inflammatory independent of its antimicrobial activity.

Materials and Methods

Materials

Unless otherwise mentioned, reagents were purchased from Fisher Scientific Inc. (Ottawa, Ontario, Canada).

Animals

12 young domestic, commercially produced, Large White/Landrace swine (20-25 kg) were used in this study. The animals selected were healthy and

without significant wounds or scars on their backs. The animals were kept in individual pens at the Swine Research and Technology Centre (Edmonton, AB) with a 12 hour light/dark cycle, where they were allowed to acclimatize seven days prior to starting experiments. Three animals were used in all experimental groups, except as noted below. The animals received antibiotic-free water and hog ration *ad libitum* during the first three weeks of the experiment. Rations were limited prior to procedures on Day 0 through 3. The study was approved by the University of Alberta Health Sciences Animal Policy and Welfare Committee (HSAPWC) and was conducted with humane care of the animals in accordance with guidelines established by the Canadian Council of Animal Care (CCAC).

Sensitization to DNCB and Elicitation of Inflammatory Reaction

Inflammation was induced using DNCB, similar to procedures described in the literature[4, 30-32]. On Day -14, the hair on the left side of the backs of 12 pigs was shaved using electric clippers. 10% DNCB (in 4:1 acetone:olive oil) was painted over an area of approximately 15 cm x 25 cm on the shaved portion of the back, which was caudal to the scapula running over the rib cage and five centimetres off the dorsal median line. The total body surface area painted was about 5%, as determined by the equation of Kelley *et al.*[33]. The volume of DNCB painted per pig was 7 mL on average. This procedure was repeated on Days -7, -3, and 0. On Day -1, pigs were given fentanyl patches (Duragesic, Ortho-McNeil-Janssen Pharmaceuticals, Inc., Titusville, NJ, USA) on shaved skin away from the rash, to avoid discomfort to the pigs during the final application and treatment. The remaining 3 pigs, which were used as negative controls, were

left unexposed to DNCB, but also received fentanyl patches on Day -1. The pigs were weighed after their final DNCB application.

Treatment

Four hours after the final application of DNCB, treatment of the pigs was commenced with the pigs being placed under general anesthetic. On Day 0, visual observations were made, blood samples were taken from the anterior vena cava, and six 4 mm biopsies were obtained from the rash. Biopsies were obtained towards the front of the rash but well within the border of the rash, to ensure that the biopsies were taken from areas which had received full DNCB sensitization and elicitation. On subsequent days, biopsies were taken in a line towards the rear of the pig, spaced sufficiently far apart that the results from the new biopsies would not be affected by the previous biopsies, and still well within the border of the rash. Biopsies taken on each day were randomly assigned for different analyses. One biopsy was placed in 4% paraformaldehyde and kept at room temperature. One biopsy was placed in 0.9% saline, and later frozen in liquid nitrogen, covered with Shandon Cryomatrix™, and placed in a freezer at -80°C for long term storage. The other four biopsies were snap-frozen in liquid nitrogen and then kept at -80°C until use. Calcium alginate dressings (Seasorb®, Convatec, R. Squibb & Sons, L.L.C., Princeton, NJ, USA) were used to reach hemostasis. The pigs were then treated. Nanocrystalline silver burn dressings (Acticoat™, Smith and Nephew, PLC, London, UK) soaked in sterile reverse osmosis water was used to treat three pigs with rashes. Three pigs with rashes were treated with a sterile dressing composed of two layers of HDPE (Delnet,

Applied Extrusion Technologies, Inc., Middletown, Del., USA) with a rayon/polyester core (Sontara Style 8411, DuPont, Mississauga, Ontario, Canada) (the same composition as the nanocrystalline silver dressings) and saturated with 0.5% silver nitrate in sterile reverse osmosis water. 0.5% silver nitrate was chosen because this concentration is used clinically in burn treatments[34]. At a concentration of 0.5% AgNO₃ is bacteriostatic, but is considered not to be harmful to healing epithelium[34]. At 1%, AgNO₃ kills epidermis, while at 0.1% it is no longer bacteriostatic[34]. Three positive controls (referred to as saline treated pigs) and three negative controls were treated with a sterile dressing of the same composition, but saturated with 0.9% sodium chloride in sterile reverse osmosis water. New fentanyl patches were applied, if they had come loose. Surgical drape was placed over each dressing to provide moisture control (see Figure 2-3), and elastic adhesive dressing was wrapped around the pigs' rash area to hold the dressings in place.

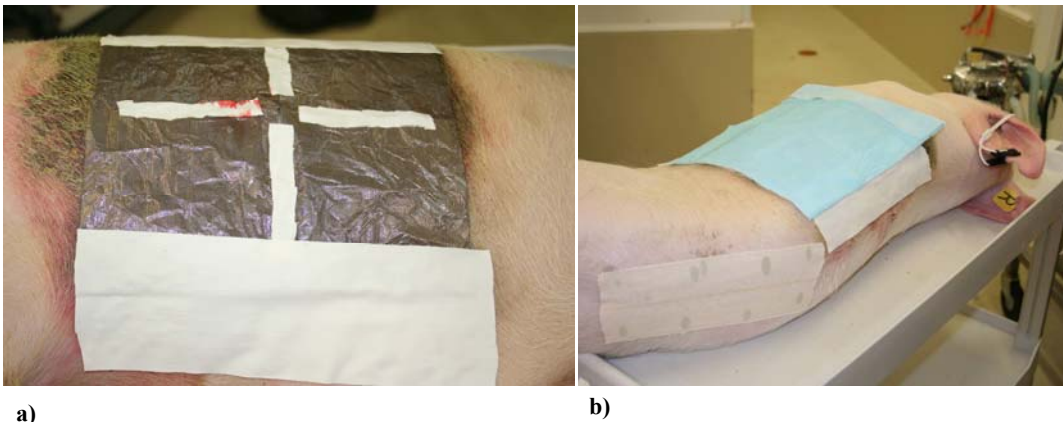


Figure 2-3. Images of application of a nanocrystalline silver dressing over a DNCB-induced rash. a) The moistened nanocrystalline silver dressing was placed over the entire rash and secured. b) Surgical tape was placed over the dressing for moisture control. Elastoplast was then used to secure the dressings in place. Over the rump, elastoplast and crazy glue were used to help secure the Fentanyl patch, which was placed on skin with the hair removed. On the right, the pig's pulse and oxygen levels are monitored via the clip on the ear.

The procedure of Day 0 was repeated on Day 1 and Day 2, except that no blood samples or weights were taken, and all fentanyl patches were replaced on Day 1. On Day 2, pigs received fentanyl patches as necessary. On Day 3, blood samples and weights were again taken, as were biopsies. There was visual inspection, but rather than being re-bandaged, the pigs were then euthanized using euthansol (>150 mg/kg) while they were still under anesthesia. The weight change of each pig during treatment was calculated as the final weight minus the initial weight for each pig, and then the weight change was averaged for each group.

Visual Observations

Pictures were taken of the rash areas regularly during the sensitization period and on each treatment day. Scales were included in the pictures on treatment days with the use of wound rulers (Johnson & Johnson, New Brunswick, NJ, US). Erythema was graded on a scale of 0-4 on Day 0 through 3. A score of 0 represented no redness as compared to a negative control on Day 0, a score of 1 represented barely visible redness, a score of 2 represented moderate redness, a score of 3 represented severe bright red erythema, and a score of 4 represented dark red/purple coloration over the entire rash area. Edema was also graded on a scale of 0-4 on Day 0 through 3. A score of 0 represented no swelling as compared to a negative control on Day 0, a score of 1 represented mildly raised tissue covering parts of the rash, a score of 2 represented moderately raised and firm tissue covering parts of the rash, a score of 3 represented obvious swelling and hardness of tissue over most of the rash, and a score of 4 represented

hard raised tissue over the entire rash area. The pigs were also scored on the level of bleeding at biopsy sites on Day 2 and Day 3, with -1 indicating minimal bleeding, 0 indicating moderate bleeding, and +1 indicating considerable bleeding. The scores were the result of observation by three people. The weight change from Day 0 to Day 3 was also recorded.

Histopathology

All samples to be paraffinized were placed in 4% neutral buffered paraformaldehyde. They were then rinsed with PBS three times before being placed in 70% ethanol and stored at 4°C. The samples were then dehydrated in alcohol and xylene; oriented and embedded in paraffin; and sectioned (5 µm). For histopathological analysis, sections were stained with hematoxylin and eosin following standard procedures[35]. Images were taken of the slides at 20x and 100x magnification at various depths using an optical microscope with an attached digital camera (Nikon Optiphot I, with Nikon Coolpics 950, Nikon Canada, Mississauga, Ontario, Canada). It was determined that the most representative images were those taken at 100x magnification which showed the epidermal-dermal junction, and for which the epidermis took up no more than half of the image.

Epidermal, dermal, and total skin thicknesses were measured in samples stained with hematoxylin and eosin from all pigs using the ruler present in the microscope at 20x and 100x magnification. Thicknesses were measured at two different places in each sample and averaged.

Gelatinase Zymography

To extract protein, snap-frozen tissue samples were powdered using a Mikro-Dismembrator (B. Braun Biotech International, Allentown, PA, USA). Prior to use, the chambers and metal balls for the dismembrator were soaked in detergent overnight, scrubbed, rinsed with distilled water, and allowed to air dry. Tissue samples were taken from -80°C and snap-cooled in liquid nitrogen for 5 minutes. They were then sliced thinly using a scalpel, placed into a dismembrator chamber with 2 metal balls, and the chambers were clamped shut and placed back in the liquid nitrogen for at least five minutes. The samples were powdered in the dismembrator for 45s at 2600 rpm. The freezing and powdering steps were repeated as necessary for sufficient homogenization of the tissues. 400 µL aliquots of lysis buffer (1% Triton-X 100, and 20% glycerol in 10 mmol/L PBS) were added to powdered samples to extract the protein. The buffer was then collected, and centrifuged at 13 000 rpm for 30 min at 4°C to remove debris. The supernatants were collected. To quantify the total proteins extracted, a BCA protein assay reagent kit (Pierce Biotechnology, Inc., Rockford, IL, US) was used. 1µL of samples were added to 799 µL aliquots of distilled water and 200 µL of Bio-Rad protein assay dye, and the optical densities were measured at 595 nm using a spectrophotometer. BSA standards of 0, 1, 2, 4, 8, 16 and 32 µg/mL were made starting from a 10 mg/mL standard. The 0 µg/mL sample was used to zero the spectrophotometer, and the optical densities of BSA standards were used to make a standard curve of protein concentration versus optical density. A best fit line of the three closest BSA standard data points was calculated in Excel and

used to calculate the protein concentrations present in the experimental samples.

Protease activity was run on gelatin zymographs[36]. To run the zymogram, a 0.75 mm thick 12% polyacrylamide separating gel with 0.15% gelatin (gelatin contained 0.1% NaN₃ to prevent bacterial contamination) was made (3 mL double distilled water, 1 mL 1% gelatin, 2.5 mL 1.5 M Tris-HCl pH 8.8, 100 µL 10% SDS, 3.3 mL 30% acrylamide/bis, 50 µL 10% APS, 5 µL TEMED). The gel was allowed to solidify for half an hour under a cover of isopropyl alcohol to prevent oxidation. A stacking gel was made (6.1 mL double distilled water, 2.5 mL 0.5M Tris-HCl, 100 µL 10% SDS, 1.3 mL 30% acrylamide/bis, 50 µL 10% APS) and poured over the separating gel, a comb was placed in it, and it was allowed to set for about half an hour. 3X loading buffer (2.4 mL 0.5M Tris-HCl pH 6.8 , 4.6 mL 10% SDS, 3 mL glycerol, 0.006 g bromophenol blue) and 10X running buffer (25 mM Tris Cl, 100 mM glycine, 0.1% SDS) were made. The gel was placed in the electrophoresis chamber, which was filled with 1X running buffer. Samples were applied to the gels under non-reducing conditions without heating. 20 µL of protein ladder (SDS-PAGE) was placed in the first well. In subsequent well, samples were loaded containing 75 µg of protein in 1x loading buffer plus the amount of extraction buffer (same recipe as lysis buffer) required to produce a total volume of 20 µL. This was added to subsequent wells, except in the case of negative controls, which contained 37.5 µg per well because of the low protein content in those samples. One sample was run twice to be used as a control for the experiment, as will be described subsequently. In any empty wells, 20 µL of 1X loading buffer was

added. Trypsin standards were also run, using concentrations of 100, 50, 25, 10, 1, 0.1 and 0 µg per well. The gel was run at 50V for approximately 20 minutes, and then increased to 150V for another half an hour. The stacking gel was removed from the separating gel, and the control well was cut away from the rest of the separating gel. The gel, including the control well, was then placed in 2% Triton-X 100 and shaken for 20 minutes to wash off the SDS. Next, the main portion of the separating gel was placed in incubation buffer (50 mM Tris pH 8.0, 0.1 mM CaCl₂). The control sample was placed in 50 mM Tris with 0.5 mM EDTA. Both parts of the gel were then incubated overnight at 37°C. The gel was rinsed with distilled water and stained by being placed in 100 mL of coomassie blue (0.25% coomassie brilliant blue, 10% acetic acid, 40% methanol, 50% double distilled water) on the shaker for half an hour. Excess stain was then removed by placing the gel in a destaining solution (50 mL acetic acid, 200 mL methanol, 250 mL double distilled water) for half an hour on the shaker. The gel was rinsed with distilled water, and images were then taken of the gel. The gels were then preserved using a Promega Gel Drying Kit (Promega Corporation, Madison, WI, USA. © 2005). The gels were soaked in a destaining solution (40% methanol, 10% glycerol, 7.5% acetic acid) for about five minutes. A sheet of gel drying film was moistened in the above solution for less than one minute. The gel drying film was placed smoothly on the gel drying frame, and the gels were placed on the film, such that there were no bubbles. A second film was moistened with the above solution and placed on top of the gel (again with no wrinkles or bubbles), and then the top of the frame was placed over the film and the film was

clamped in. The frame was set up vertically and the gels were allowed to air dry in the films. Gelatinase activity appears as a clear band (indicative of cleavage of the gelatine substrate) on a blue background. For quantitative analysis, photographs of the gels were loaded into AlphaImager software (AlphaEase, FC Software Version 4.1.0, Alpha Innotech Corporation, San Leandro, CA, USA © 1993-2004). The integrated density values (IDV) of each band was measured, holding the band area constant. Each IDV was then divided by the IDV of a portion of the gel background of the same area, to correct for differences in gel densities.

Apoptosis Detection

Detection of the presence of apoptotic cells in tissue samples was determined using the In Situ Cell Death Detection Kit (Roche Applied Sciences, Basel, Switzerland), which allows for immunohistochemical detection of apoptosis. During apoptosis, cleavage of genomic DNA occurs, resulting in double-stranded, low molecular weight DNA fragments and single strand breaks in high molecular weight DNA. This test, using TUNEL (Terminal deoxynucleotidyl Transferase mediated Biotin-dUTP Nick End Labeling) technology, allows these DNA strand breaks to be identified by labeling free 3'-OH termini with modified nucleotides via an enzymatic reaction[37]. Testing was performed on paraffinized tissue samples following the manual provided with the kit[37]. Dewaxing and rehydration was performed as follows. Paraffinized tissue samples were placed in an oven at 60°C for half an hour. They were then placed in 100% xylene for five minutes, and then transferred to fresh 100% xylene for an

additional five minutes. Following this, they were placed in 100% ethanol for 5 minutes, and then transferred to fresh 100% ethanol for an additional 5 minutes. After this, they spent five minutes each in the following solutions: 95% ethanol, 80% ethanol, 70% ethanol, and PBS. All solutions were made using double distilled water. After rehydration, the samples were treated with proteinase K. A 2.5 mg/mL proteinase K stock solution in Tris-HCl (pH 7.4-7.8) was made and stored at -20°C. From this 1:100 dilutions were made just prior to use, to create the working concentration of approximately 25 µg/mL. The working solution was stored on ice until used. 100 µL of the proteinase K working solution was added to each tissue, and then the tissues were placed in a moist dark chamber and incubated for half an hour at 37°C. The slides were then rinsed three times for five minutes each in 1xPBS. Positive controls were treated with a 1:200 dilution of DNase (in PBS) and incubated at room temperature for 15 minutes.

The sections were then incubated overnight with a FITC-labeled dNTP and terminal deoxynucleotidyl transferase (TdT) enzyme working solution at 4°C. The enzyme solution used contained TdT from calf thymus, recombinant in *E. coli*, in storage buffer. The label solution used contained a nucleotide mixture in reaction buffer. 50 µL of the enzyme solution was added to 450 µL of the label solution to create the TUNEL reaction mixture. These solutions were kept on ice until use, and unused solution was stored at -20°C. In the dark, 40 µL of the TUNEL reaction mixture was added to all samples except negative controls. 40 µL of the labeling solution only was added to the negative controls. During this step, the DNA strand breaks are labeled via TdT, which catalyzes polymerization

of labeled nucleotides to free 3'-OH DNA ends in a template independent manner[37].

After overnight incubation, the cells were rinsed in PBS for half an hour. Cell nuclei were then counterstained with DRAQ5TM (Alexis Biochemicals, San Diego, CA, USA), and rinsed in PBS for another half hour. The tissue samples were mounted with coverslips using 50% PBS/50% glycerol containing 4 mg/mL *n*-propyl gallate (Sigma, Oakville, ON, Canada). Sections were then examined, and images obtained, using a Zeiss LSM510 multi-channel laser scanning confocal microscope (Carl Zeiss MicroImaging GmbH, Oberkochen, Germany). Multiple images were taken of the epidermal-dermal junction of samples from each pig. Quantitative analysis was performed using ImageJ software (Rasband, W., v1.37, NIH, Rockville, MD, USA. © 2007). First, the epidermis or dermis was manually selected. A set threshold was used for all samples processed on the same day, since they were stained and imaged under identical conditions. Total numbers of green (apoptotic stained) and red (nuclear stained) pixels were counted. A ratio of green to red pixels was calculated to obtain a relative concentration of cells undergoing apoptosis. Images in which apoptotic staining did not coincide with nuclear staining were excluded from this analysis.

First attempts at staining for apoptosis were performed as follows: The tissues were dewaxed and rehydrated as described earlier. They were then treated with proteinase K as above. The FITC-labeled dNTP and terminal deoxynucleotidyl transferase (TdT) enzyme working solution was applied and the slides were incubated at 37°C for one hour. Negative controls for the experiment

received the labeling solution only for this step. The slides were rinsed three times, for five minutes each, using PBS. The slides were then incubated with 50 μ L of Converter AP (alkaline phosphatase), and the samples were incubated in the dark at 37°C for half an hour. This step allows for detection of incorporated fluorescein by anti-fluorescein antibody Fab fragments from sheep, conjugated with alkaline phosphatase. The slides were then rinsed again. Fast Red substrate solution was made by placing a Tris buffer tablet and a Fast Red tablet in double distilled water. This solution was filtered, and the tissue samples were treated with 50 μ L of the solution, incubated for ten minutes at room temperature in the dark. If the slides appeared stained at this point, they were placed in double distilled water to stop the reaction. Crystalmount® mounting solution was used to mount coverslips over the tissue samples. Once the tissues were dried, images were obtained using the microscope with attached camera, as described above. Because of uncertainty as to whether or not the staining was specific, an additional step was added after the proteinase K treatment. The slides were treated with levamisole (1:1 w/v in PBS) for 37°C for 30 minutes in the dark. As well, the slides were incubated with the Fast Red substrate solution for half an hour. After the Fast Red step, the cells were counterstained by incubation for 30 seconds with 100 μ L methyl green (0.5% w/v). The methyl green staining seemed weak, so the concentration was increased to 5% (w/v). Although the staining appeared bright at first, it faded with time. Attempts were made to remove the coverslips and restain the slides with methyl green one day prior to imaging, if the samples were not imaged within 24 hours of the original staining,

but this was not particularly successful either. Staining time with methyl green was increased to 10 minutes at 60°C, but it was found that, again, after the coverslips were placed on, the staining faded. The mounting solution was switched to Permout™ mounting solution. Unfortunately, this mounting solution is not an aqueous solution, and so when it was applied without dehydrating the samples (by taking them through ethanol to xylene) water bubbles were trapped in the mounting solution, obscuring the image. However, dehydration of the samples was not possible, as the Fast Red was removed by the xylene. An attempt was made to dehydrate the samples by drying them carefully with kimwipes and then drying them for 10 minutes at 37°C before mounting them with Permout™ mounting solution. Unfortunately, the Fast Red substrate solution appeared to fade in the Permout™ mounting solution, and it was not possible to obtain clear images of the staining due to the fact that the substrate solution began diffusing through the mounting solution almost immediately. This made it unclear whether the staining was specific for cells undergoing apoptosis. In conclusion, the use of Fast Red substrate solution and methyl green as a counterstain was not found to be an effective way to locate apoptotic activity in these tissues, as the counterstaining faded when Crystalmount®, an aqueous mounting solution was used, but the apoptotic staining faded when Permout™, a non-aqueous mounting solution was used, so it was hard to obtain clear images. This is why staining with the fluorescent labels appeared more effective.

Mast Cell Staining and Counts

Mast cell staining was performed using toluidine blue[38], which turns the heparin present in mast cell granules violet, and turns cell nuclei blue. A stock solution of toluidine blue was made up by adding 1.0 g of toluidine blue to 100 mL of 70% ethanol and was stored at 4°C in the dark. Toluidine blue working solution was made fresh by adding 5 mL of the toluidine blue stock solution to 45 mL of 1% NaCl (in distilled water). Paraffinized tissue samples were dewaxed and rehydrated to distilled water following the method described in the histopathology section. 100 µL of the toluidine blue working solution was placed on the tissue samples for three minutes and then rinsed off with distilled water. Cell counts in ten different fields were immediately performed under the microscope at 300x magnification, and images were taken. The slides were then dried carefully and coverslips were placed over the tissue samples using Crystalmount® mounting solution. The staining appeared to fade over time.

An attempt was made to confirm that cells stained by the toluidine blue (particularly clumps in silver nitrate treated samples, see Results) were, in fact, mast cells. This was done by immunohistochemical staining for histamine, which, if it co-localized with the toluidine blue staining, would provide confirmation that the cells were indeed mast cells. For histamine staining, paraffinized samples were dewaxed and rehydrated to PBS as described earlier. No antigen retrieval step was used. The samples were then treated with 3% H₂O₂ (in PBS) for half an hour in the dark at room temperature. This was followed by a five minute wash in PBS. The samples were then blocked in 10% goat serum in

PBST (PBS with 0.05% Tween 20) for 1 hour at room temperature. Next, the tissues were incubated overnight at 4°C in a 1:100 dilution of rabbit-anti-histamine (Sigma, Product H 7403), the primary antibody. Negative controls were incubated with rabbit IgG (1:120 dilution from 1 mg/mL). The slides were then washed in PBST three times for five minutes each. The secondary antibody, goat-anti-rabbit-HRP (horse radish peroxidase, Endogen, Thermo Fisher Scientific, Inc.) diluted 1:400 in PBST with 1% pig serum, was added to the slides and they were incubated at room temperature for one hour. Next, the slides were washed in PBST and stained with DAB (diaminobenzoate – 25 mg DAB, 50 µL H₂O₂ in 50 mL PBS) for 5 minutes. The slides were then counterstained with hematoxylin, dehydrated and mounted as described in the Immunohistochemistry section (see below). Staining was weak and non-specific (data not shown), suggesting that the antibody purchased was not capable of specifically staining for histamine in paraffinized porcine skin.

mRNA Signal Detection

Tissue powdering. To extract RNA, tissues were powdered using a Mikro-Dismembrator, similar to the procedure above. Prior to use, dismembrator chambers and metal balls were washed with detergent, rinsed with distilled water, soaked with 0.1% DEPC water, and then allowed to air dry. Tissue samples were removed from -80°C and placed in liquid nitrogen for 10 minutes. They were then cut into vertical slices with a scalpel, and placed in dismembrator chambers which were clamped shut and placed in liquid nitrogen for 5 minutes. Chambers were then placed in the dismembrator and the samples were powdered. The

freezing and powdering was repeated if necessary. 1 mL of Trizol was added to the powdered samples and then collected into 1.5 mL tubes.

RNA extraction. RNA extraction and purification was performed using a Qiagen RNeasy® Mini Kit by following the manual provided (Qiagen, Inc., Mississauga, Ontario, Canada). The tubes were centrifuged for 30 minutes at 12 000 rpm. Next, 300 µL of chloroform was added to each tube. The tubes were vortexed for 15 seconds, and then allowed to stand at room temperature for 5 minutes. The samples were then spun at 12 000 rpm for 15 minutes. The aqueous phase, which was about 600 µL, was transferred to new tubes and the organic phase was discarded. Next, 600 µL of 70% ethanol was added to each tube, and the tubes were mixed by inversion. 600 µL of the samples were loaded into spin columns and then spun at 12 000 rpm for 15 seconds. The collection tubes were emptied and then placed back under the columns. The remainder of the sample was placed into the columns and spun (12 000 rpm, 15 s). Again the collection tubes were emptied and replaced. 350 µL of RW1 wash buffer was added to the spin columns and the columns were spun (12 000 rpm, 15 s). New collection tubes were placed under the columns, and 10 µL of Qiagen DNase in 70 µL of DNase buffer was added onto the spin column membranes. The columns were spun again (12 000 rpm, 15 s), and the spin thru was pipetted back onto the columns which were then allowed to sit at 37°C for one hour to break down any DNA in the samples. The columns were then spun (12 000 rpm, 15 s). 350 µL of RW1 wash buffer was then loaded onto each column and the columns were again spun (12 000 rpm, 15 s). The collection tubes were emptied and replaced on the

columns. 500 μL of RPE wash buffer was added to each column and the columns were spun again (12 000 rpm, 15 s). The collection tubes were emptied and then this step was repeated. The spin columns were transferred to 1.5 mL tubes and loaded with 40 μL of RNase free water. The columns were then incubated at room temperature for 15 minutes, and then spun at 12 000 rpm for one minute. The spin columns were then discarded and the tubes were stored at -80°C until use.

RNA quantification. 400 μL of double distilled water was placed into a 1.5 mL tube, and 2 μL of an RNA sample was added. A spectrophotometer (Unicam, Helios, Thermo Fisher Scientific, Inc.), which was zeroed using double distilled water, was used to measure optical densities of the RNA-containing samples at 260 nm. Some samples' optical densities were also measured at 280 nm to check that the samples were uncontaminated. The optical density of the samples as measured at 280 nm should be about half that of the optical density measured at 260 nm, if the samples are not contaminated. Results showed that the samples did not appear to be contaminated. The concentration of RNA in each sample was calculated as:

$$\frac{(\text{OD at 260 nm} * \text{Dilution} * (40 \mu\text{g/mL RNA per OD unit at 260 nm}))}{(1000 \mu\text{L/mL})} \quad (2-1)$$

Reverse transcription (creation of cDNA). Reverse transcription was performed using an Enhanced Avian RT First Strand Synthesis Kit (Sigma) following the manual provided. 1 μL of dNTP, 1 μL of random nonamers, 0.5 μg of RNA as calculated above, and enough distilled water to bring the volume to 10 μL were added to a thin-walled PCR microcentrifuge tube. The contents were

mixed and centrifuged (15 s, 12 000 rpm). The tubes were then placed at 70°C for 10 minutes, followed by centrifugation (15 s, 12 000 rpm). Next 2 µL of 10x buffer for eAMV-RT, 1 µL of enhanced avian RT, 1 µL of RNase inhibitor, and 6 µL of distilled water were added. The tubes were incubated at 25°C for 15 minutes, and then incubated at 50°C for 50 minutes. cDNA was kept on ice if it was going to be used immediately, or stored at -20°C for longer wait times.

Primers. Primers were designed using Real Time PCR Primer Design software (© 2008, GenScript Corporation, Piscataway, NJ, USA), and were synthesized by Operon Biotechnologies, Inc. (Huntsville, Alabama, USA):

Porcine HPRT forward primer: AATGCAAACCTTGCTTTCCT

Porcine HPRT reverse primer: GGTCTATAGCCAACACTTCGAG

Porcine HPRT probe: [6-FAM]TCACCAGCAAGCTTGCAACCTTG[Tamra-Q]

Porcine IL-1β forward primer: GACTGCAAACCTCCAGGACAA

Porcine IL-1β reverse primer: AAGCTCATGCAGAACACCAC

Porcine IL-1β forward primer (1): ACCTGGACCTTGGTTCTCTG

Porcine IL-1β reverse primer (1): CATCTGCCTGATGCTCTTGT

Porcine IL-1β forward primer (2): GGCAGATGGTGTCTGTCATC

Porcine IL-1β reverse primer (2): TCATTGCACGTTTCAAGGAT

Porcine IL-1β forward primer (3): GTGGTGTCTGTCATGAGCTT

Porcine IL-1β reverse primer (3): GGCGTGTCATCTTTCATCAC

Porcine IL-1β probe (3):

[6-FAM]TGTCATCGCTGTCATCTCCTTGCA[Tamra-Q]

Porcine IL-8 forward primer: GACCAGAGCCAGGAAGAGAC

Porcine IL-8 reverse primer: ACAGAGAGCTGCAGAAAGCA

Porcine IL-8 probe: [6-FAM]CTGCCAAGAAGGCAACAGCCAG[Tamra-Q]

Porcine IL-10 forward primer: CCAAGCCTTGTCAGAGATGA

Porcine IL-10 reverse primer: TGAGGGTCTTCAGCTTCTCC

Porcine IL-12 forward primer: TCAACAGTGAGACTGTGCCA

Porcine IL-12 reverse primer: GCTCATCATTCTGTGCGATGG

Porcine IL-12 forward primer (1): CACTTCAGAAGGCCAAACAA

Porcine IL-12 reverse primer (1): GCAACTCTCATTCGTGGCTA

Porcine IL-12 forward primer (2): ACCACCTGGACCATCTCAGT

Porcine IL-12 reverse primer (2): TGGTTGAGGCATTTGAACAT

Porcine IL-12 probe (2): [6-FAM]CAACCACAGCAGGCCCCAGGA[Tamra-Q]

Porcine TNF- α forward primer: GACAGATGGGCTGTACCTCA

Porcine TNF- α reverse primer: GAGGTTGACCTTGGTCTGGT

Porcine TNF- α probe: [6-FAM]TCACACCATCAGCCGCATCG[Tamra-Q]

Porcine TGF- β forward primer: GCACGTGGAGCTATAACCAGA

Porcine TGF- β reverse primer: ACAACTCCGGTGACATCAAA

Porcine TGF- β forward primer (1): CACTCTCAGCCTCTCTGCTG

Porcine TGF- β reverse primer (1): GTACCAGAGGTGGGTGGTCT

Porcine TGF- β forward primer (2): GTGGTAACCTACCCGACTGG

Porcine TGF- β reverse primer (2): CACAGCCGGACCTTTAACTT

Porcine TGF- β forward primer (3): AAAGCGGCAACCAAATCTAT

Porcine TGF- β reverse primer (3): CCCGAGAGAGCAATACAGGT

DNAse/RNAse free water (BioRad, Mississauga, Ontario, Canada) was added to

the lyophilized primers for a primer concentration 100 μM .

Traditional RT-PCR amplification. This was performed with four samples (one from each treatment group on Day 3), or two samples (one from a nanocrystalline silver treated pig, and one from a saline treated pig on Day 3) and each pair of primers, to ensure that the cDNA synthesis was successful and that the primers worked. This was done using iQ Supermix (Bio-Rad), and following the instructions provided with it. 12.5 μL of iQ Supermix, 1 μL of the forward primer to be tested, 1 μL of the reverse primer to be tested, 1 μL of the cDNA sample, and 9.5 μL of PCR water were combined in a 200 μL thin-walled PCR tube. The PCR reaction was run under the following conditions for 40 to 45 cycles: Denature: 95°C for 30s; Anneal and extend: 60°C for 1 minute; Final extension: 60°C for 7 minutes. Hold at 4°C.

Electrophoresis. Electrophoresis was performed on these samples using a 1.5% agarose gel containing 1 $\mu\text{g}/\text{mL}$ ethidium bromide. To make this gel, 5x TBE was made using 54g Trizma base, 27.5 g boric acid, 20 mL of 0.5 M EDTA (pH 8.0) and double distilled water to bring the total volume to 1 L. A 1.5% agarose solution was made in 1xTBE, followed by heating the solution to dissolve the agarose. 1 $\mu\text{g}/\text{mL}$ ethidium bromide was then added, and the gel was allowed to set for half an hour with a 20 well comb in it. The gel was then placed into an electrophoresis chamber and covered with 1xTBE. 2.5 μL of 10x DNA loading buffer (6.25 mL H_2O , 0.025 g xylene cymol, 0.025 g bromophenol blue, 1.25 mL 10% SDS, 12.5 mL glycerol) was added to the PCR product, and 15 μL of the product was loaded per well. DNA standards were run as well. The gel was run

at 100 V for about 45 minutes, and then imaged using a Gel Doc system (Bio-Rad).

Real time RT-PCR. Real time RT-PCR was performed on cDNA samples created as described above. The first attempt was performed using HPRT primers. A master mix was made, consisting of 350 μL iQ Supermix (Bio-Rad), 28 μL forward primer, 28 μL reverse primer, 238 μL PCR H₂O, and 28 μL Sybr Green (Bio-Rad). 24 μL of the master mix was placed in each real time RT-PCR tube, and then 1 μL of each sample was added to each well. One well contained PCR grade H₂O as a control for the experiment. The RT-PCR tubes were placed into two Supercyclers (Bio-Rad) set to measure Sybr green. This procedure was repeated using the IL-8, TNF- α , IL-10, IL-1 β (3), IL-12 (2), and TGF- β (2) primers, which were selected as described above. Analysis of the results was performed in Excel using the formulas:

$$\Delta\text{CT}_{\text{gene}} = \text{CT}_{\text{gene}} - \text{CT}_{\text{HPRT}} \quad (2-2)$$

$$\Delta\Delta\text{CT}_{\text{gene}} = \Delta\text{CT}_{\text{gene}} - \Delta\text{CT}_{\text{average negative control pig gene}} \quad (2-3)$$

$$\text{Fold difference} = 2^{-\Delta\Delta\text{CT}} \quad (2-4)$$

where CT is cycle threshold, and HPRT (hypoxanthine phosphoribosyltransferase) is the chosen housekeeping gene. As the results were unclear (see Results section), the real time RT-PCR was performed for all samples using HPRT and IL-1 β (3) primers using an Applied Biosystems 7300 Real Time PCR System using Applied Biosystems Sequence Detection Software Version 1.3.1 with the 7300 System SDS Software RQ Study Application and the SDS Relative Quantification Study Plug In (© 2005 Applied Biosystems, Ltd.,

Foster City, CA, USA) with the same procedures as before, so that the samples were not having to be run on two machines. The runs were performed using the standard 7300 run mode with the following settings: The volume was set to 25 μL , Stage 1 had one repetition at 50°C for 2 minutes, Stage 2 had one repetition at 95°C for 10 minutes, Stage 3 had 40 repetitions at 95°C for 15 seconds, each followed by a hold at 60°C for 1 minute, when data collection occurred. As the cDNA appeared to have degraded by this time, and the correct reagents for this machine were not used, this experiment was repeated with freshly made cDNA (which was diluted by adding 20 μL PCR water). The master mix used consisted of 350 μL Power Sybr Green master mix (ABI, Foster City, CA, USA), 238 μL PCR H₂O, 28 μL forward primer, and 28 μL reverse primer. 24 μL of the master mix was added per well of a 96 well plate (ABI PRISM™, ABI) and then 2 μL of cDNA sample (or PCR H₂O for negative controls) was added per well. The wells were covered and run in the Applied Biosystems 7300 Real Time PCR System. After testing HPRT and IL-1 β (3) this way, the procedure was repeated for IL-12 (2), TNF- α , and TGF- β (2). As the results were not clearer (see Results section), probes were used, along with ten times less primer, for HPRT and IL-8. The new master mix used was 175 μL ABI mix, 1.4 μL forward primer, 1.4 μL reverse primer, 0.7 μL probe, 143.5 μL PCR H₂O. 23 μL of this master mix was added to each well, and 2 μL of cDNA (or DNase/RNase free H₂O for negative controls) was added per well. At this point, it appeared that the cDNA had broken down again, and so fresh cDNA was made via the procedure described above. The real time RT-PCR still did not work, and so a traditional RT-PCR was run as

described above using negative control and saline treated pig cDNA samples with the primers for HPRT and IL-8. This test indicated that the purified RNA used to create the above sets of cDNA had broken down, as the primer dimers were much stronger than cDNA signals (image not shown). Therefore, fresh tissues were used to collect and purify RNA, the quantity of RNA was measured again, a reverse transcription of the RNA to make cDNA was performed, and a real time RT-PCR was performed, using probes, with HPRT, IL-8, IL-12 (2), and TNF- α primers. Reasonable results still were not achieved (see Results Section).

Immunohistochemistry

Tissue samples after 24h and 72h of treatment were analyzed for the presence of TGF- β . Tissue samples after 72h of treatment were also analyzed for the presence of TNF- α and IL-8. Paraffinized samples were deparaffinized and rehydrated as described for apoptosis detection. For antigen retrieval, the samples were incubated in 25 μ g/mL proteinase K at 37°C for 20 minutes. They were next treated with 3% H₂O₂ for 30 minutes at room temperature to quench endogenous peroxidase activity, and then blocked for one hour at room temperature with the sera from the species that the secondary antibody was raised in (rabbit for TGF- β 1 analysis; goat for TNF- α or IL-8 analysis). For TGF- β analysis, sections were then incubated for one hour at room temperature with a chicken anti-hTGF- β 1 (10 μ g/mL, AF-101-NA, R&D Systems, Minneapolis, MN, USA). The sections were subsequently incubated with rabbit-anti-chicken antibody conjugated with horseradish peroxidase (Sigma, Product A 9046, 1:400 dilution plus 2% pig serum) for an hour. For TNF- α and IL-8 analysis, sections were incubated

overnight at 4°C with a mouse-anti-pTNF- α (5 μ g/mL, MP390, Endogen), or mouse-anti-pIL-8 antibody (5 μ g/mL, MP800, Endogen), respectively. Sections incubated with anti-TNF- α or anti-IL-8 primary antibodies were subsequently incubated with a biotinylated goat-anti-mouse antibody (R&D Systems) for 45 minutes at room temperature, followed by treatment with streptavidin-HRP (R&D Systems) for 30 minutes at room temperature. Cytokines in the tissues were then stained using 3,3'-diaminobenzidine and H₂O₂ (25 mg DAB, 50 μ L H₂O₂ in 50 mL PBS). The samples were then washed in double distilled water, and counterstained with hematoxylin (30 seconds), followed by washing in double distilled water. To preserve the stain, the cells were placed successively in 70%, 90%, and 3 rounds of 100% ethanol for 1 minute each, followed by two rounds of 100% xylene for 5 minutes each. Coverslips were then mounted using Permount™ mounting solution. Images of the samples were taken as described for histology images. All samples stained for one cytokine were run at the same time under identical conditions, including exposure time, temperatures, and dilutions, and, therefore, the intensity of staining can be used as a qualitative indication of the relative quantity of cytokines present in the tissues. Image analysis was attempted using ImageJ software, but because the software was unable to clearly distinguish brown (the cytokine staining) from purple (the nuclear counterstaining) and the two colors were of similar intensity, it was not possible to obtain reliable quantitative results. Changing the contrast, inverting the images, changing the gamma, and eliminating red, green, or blue from the images were all attempted, with each image having the same adjustments made,

but none of these attempts to separate the brown from purple staining worked consistently for all images.

Statistics

During testing, one of the pigs from the group being treated with nanocrystalline silver died on Day 1, apparently from complications due to the anesthetic. Therefore, another 3 pigs were run through the protocol and treated with nanocrystalline silver. The pig from this second set of three which had baseline data (Day 0 histology) most similar to all pigs with rashes in the first time running the experiment was chosen to be used as a replacement for the pig which died at Day 1 for Day 2 and Day 3 data. Tests were performed on all three pigs from each group (since each group contains 3 pigs for all data points) to confirm result repeatability, except for the zymograms, in which the first two pigs from each group were used. For numerical results, one-way ANOVA with the Tukey-Kramer Multiple Comparisons post test was performed using GraphPad InStat version 3.06 (GraphPad Software, San Diego, California, USA, www.graphpad.com, © 2003). Standard deviations are plotted as error bars for all data points on all figures. For some data points, the experimental error was very small.

Results

Visual Assessment

Figure 2-4 shows representative pictures of pigs during sensitization to DNCB. Over two weeks, the pigs progressed from mild erythema in the painted area, to yellow-red scabbing on some portions of the skin, to severe erythema,

edema, and a full scab by Day 0.



Figure 2-4. Images of porcine DNCB-induced rashes at various time points during elicitation of the rash. a) A representative image of the DNCB-painted skin on Day -7, just prior to the second application of DNCB. b) A representative image of the DNCB-painted skin on Day -3, just prior to the third application of DNCB. c) A representative image of DNCB-painted skin on Day -1, between the third and fourth application of DNCB. d) A representative image of the DNCB-induced rash four hours after the final DNCB application (Day 0).

Figures 2-5 to 2-7 show representative pictures of pigs after one (Fig. 2-5), two (Fig. 2-6), and three (Fig. 2-7) days of various treatments. The saline and silver nitrate treated pigs did not show much visual improvement over the course of treatment. The negative controls appeared normal throughout the study, and did not demonstrate any negative consequences from going through the study. The nanocrystalline silver treated pigs showed visual improvement with decreased redness and swelling. Some pigs' scabs began to peel off, revealing near-normal tissue underneath.



a) Negative control



b) Saline treated



c) Silver nitrate treated



d) Nanocrystalline silver treated

Figure 2-5. Representative images of porcine DNCB-induced rashes after one day of treatment. Treatment was done using: b) saline, c) silver nitrate, or d) nanocrystalline silver. A negative control, treated with saline, is shown in a). Wound rulers are included to indicate the image scale in centimetres.



a) Negative control



b) Saline treated



c) Silver nitrate treated



d) Nanocrystalline silver treated

Figure 2-6. Representative images of porcine DNCB-induced rashes after two days of treatment. Treatment was done with: b) saline, c) silver nitrate, or d) nanocrystalline silver. A negative control, treated with saline, is shown in a). Wound rulers are included to indicate the image scale in centimetres.

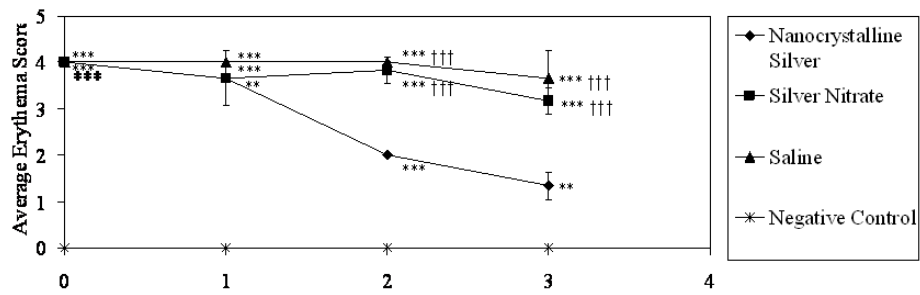


Figure 2-7. Representative images of porcine DNCB-induced rashes after three days of treatment. Treatment was done with: b) saline, c) silver nitrate, or d) nanocrystalline silver. A negative control, treated with saline, is shown in a). Wound rulers are included to indicate the image scale in centimetres.

Erythema scores over the three days of treatment are shown in Figure 2-8a. Pigs treated with nanocrystalline silver had significantly lower erythema scores after two days of treatment as compared to the pigs treated with silver nitrate or saline.

Figure 2-8b, which shows edema scores over three days of treatment, indicates that pigs treated with nanocrystalline silver had significantly lower edema scores than the pigs treated with silver nitrate or saline by Day 1, and they were not significantly different from the negative controls by Day 3.

a) Erythema



b) Edema

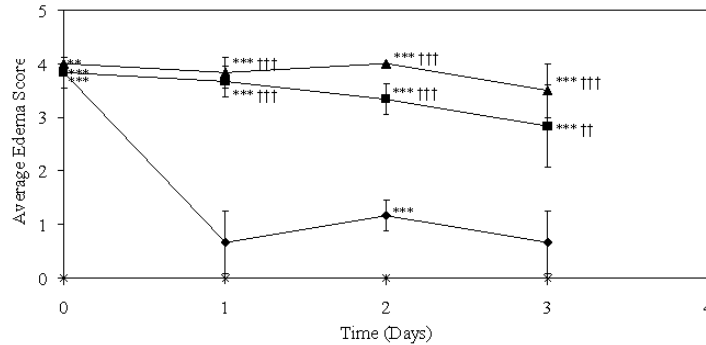


Figure 2-8. Erythema and edema scores for pigs with DNCB-induced contact dermatitis treated for three days with nanocrystalline silver, silver nitrate, or saline. a) Daily average erythema scores and b) daily average edema scores (mean \pm S.D., $n=3$ for all data points) for pigs with DNCB-induced contact dermatitis treated for three days with nanocrystalline silver, silver nitrate, or saline. Negative controls were treated with saline. Statistical analyses were performed using one-way ANOVAs with Tukey-Kramer post tests. The one-way ANOVA tests indicated that the differences between groups were extremely significant ($p<0.0001$ for erythema scores on all days, and $p<0.0001$ for edema scores on Day 0-2, $p=0.0001$ for edema scores on Day 3). Results from the post tests are displayed on the figures as follows: *** or ** indicates significantly different from the negative control ($p<0.001$, and $p<0.01$ respectively). ††† or †† indicates significantly different from nanocrystalline silver treated pigs ($p<0.001$, and $p<0.01$ respectively). Error bars represent standard deviations.

Biopsy Bleeding

Figure 2-9, which shows biopsy bleeding scores on the second and third days of treatment, indicates that the nanocrystalline silver treated animals demonstrated significantly lower biopsy bleeding than silver nitrate treated tissues.

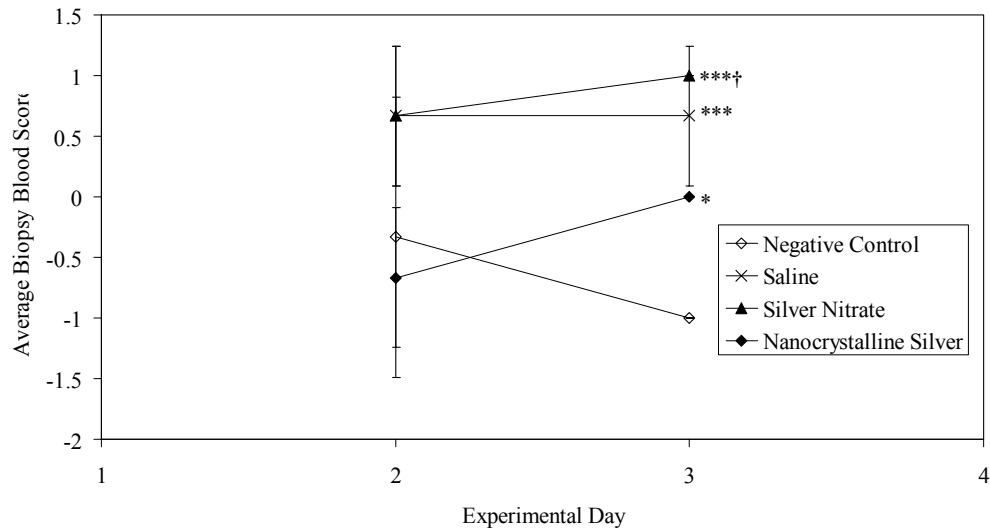


Figure 2-9. Biopsy bleeding scores for pigs with DNCB-induced contact dermatitis treated for three days with nanocrystalline silver, silver nitrate, or saline. Negative controls were treated with saline. A score of -1 indicated minimal bleeding, while a score of 1 indicated considerable bleeding. Statistical analyses were performed using one-way ANOVAs with Tukey-Kramer post tests. The one-way ANOVA tests indicated that the differences between groups were not significant on Day 2 ($p=0.1404$), but that on Day 3, they were extremely significantly different ($p=0.0001$). Results from the post tests are displayed on the figure as follows: *** or * indicates significantly different from the negative control ($p<0.001$, and $p<0.05$ respectively). † indicates significantly different from nanocrystalline silver treated pigs ($p<0.05$). Error bars represent standard deviations ($n=3$ for all data points).

Weight

Figure 2-10 shows the average weight change and standard deviation for each group. There were no significant differences in weight changes between groups. On average, there was weight loss in all groups, including the negative controls. This suggests that the pigs responded poorly to the set of procedures they went through each day, or that they were not getting sufficient time to recover and eat between procedures. However, in each group, one pig gained weight, leading to the large standard deviation.

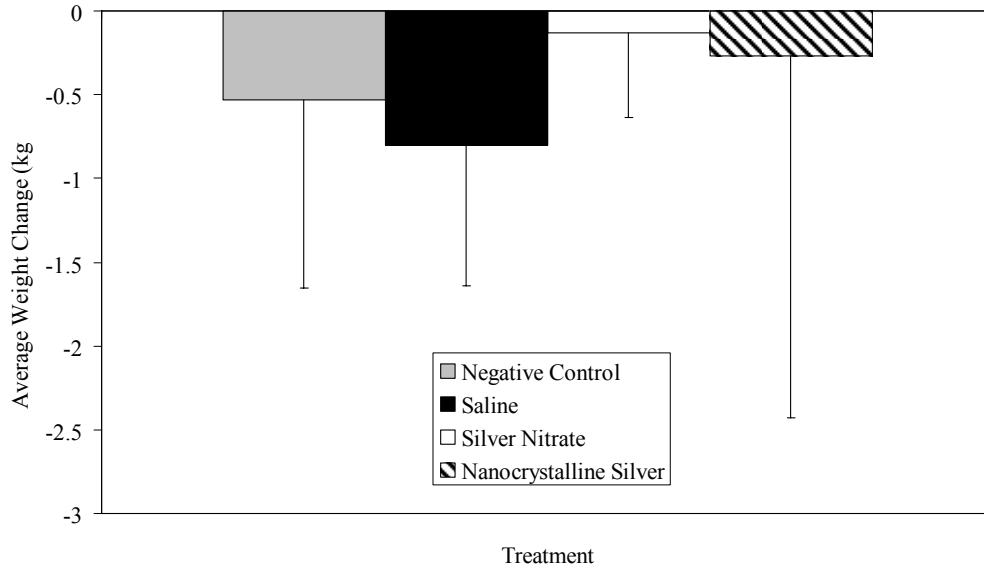


Figure 2-10. Weight change over three days for pigs with DNCB-induced contact dermatitis treated with nanocrystalline silver, silver nitrate, or saline. Negative controls were treated with saline. Statistical analyses were performed using a one-way ANOVA with a Tukey-Kramer post test. The one-way ANOVA tests indicated that the differences between groups were not significant ($p=0.9251$). Error bars represent standard deviations ($n=3$ for all data points).

Histology

Representative histological images for each group are shown over a series of days in Figure 2-11. Figure 2-11a shows the negative control on Day 0. The negative controls appeared to have normal skin, with well-defined intact epidermis and dermis, and low cellularity. Some flaking of the keratinized layer was observed, which is common in healthy pigs. The negative control histological samples did not show any significant changes over the test period (Fig. 2-11b to 2-11d), suggesting that the saline-soaked dressings had minimal impact on skin morphology.

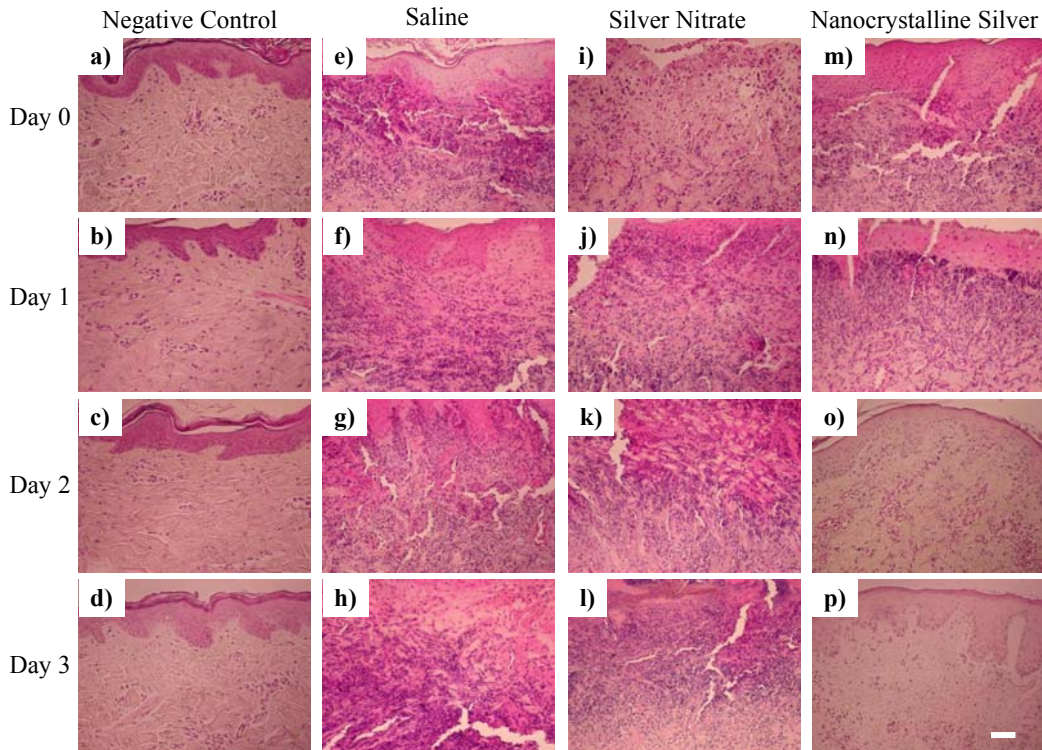


Figure 2-11. Representative images of tissue sections stained with hematoxylin and eosin for pigs with DNCB-induced contact dermatitis treated with saline, silver nitrate, or nanocrystalline silver. Negative controls are also shown. Images were taken showing a portion of the epidermis and a portion of the dermis. Tissue samples from negative controls treated with saline are shown before treatment (a), and after one day (b), two days (c), and three days (d) of treatment. Tissue samples from pigs treated with saline are shown before treatment (e), and after one day (f), two days (g), and three days (h) of treatment. Tissue samples from pigs treated with silver nitrate are shown before treatment (i), and after one day (j), two days (k), and three days (l) of treatment. Tissue samples from pigs treated with nanocrystalline silver are shown before treatment (m), and after one day (n), two days (o), and three days (p) of treatment. Cell nuclei are stained purple with hematoxylin, while cytoplasm was stained pink with eosin. The scale bar represents 50 μm .

Prior to the start of treatment, all animals sensitized and exposed to DNCB demonstrated massive inflammatory responses (Fig. 2-11 e, i, m). Large quantities of red blood cells and inflammatory cells had infiltrated the epidermis and upper dermis. Biopsies also showed tissue damage, with delaminated epidermis due to excessive edema.

The saline treated tissues (Figure 2-11 e through h) showed little improvement over the course of the experiment. This indicates that the inflammation induced by DNCB would not have returned to normal on its own within the experimental time period.

Silver nitrate treated tissues (Figure 2-11 i through l) appeared similar to saline treated pigs throughout the experiment - after three days of treatment, there was minimal histological improvement. Epidermal and dermal tissues both remained damaged, with extensive edema and strong infiltration by inflammatory and red blood cells.

After one day of treatment with nanocrystalline silver (Fig. 2-11n), there were no significant changes. By Day 2 (Fig. 2-11o), however, the old epidermis was gone from many areas, and a new epidermis was forming. Some red blood cells and inflammatory cells were still present near tissue surfaces, but did not extend deep into the dermis. By Day 3 (Fig. 2-11p), some portions of the skin were near-normal, and could only be distinguished from negative controls by the epidermis, which was not fully developed. Inflammatory cells were present only at very low levels.

Skin Thickness

Figure 2-12 shows measurements of total skin thickness of biopsies over 72h after various treatments. On Day 0, there were significant differences between the groups ($p=0.0339$), with the samples to be saline treated being significantly thicker than the negative controls ($p<0.05$). On Day 3, there were also significant differences between the groups ($p=0.0467$). Over time, there was

a trend towards decreasing overall skin thickness in nanocrystalline silver treated groups relative to saline and silver nitrate treated groups. This did not reach statistical significance, but suggests that there was decreased edema, tissue damage and infiltrating cells, leading to decreases in tissue thickness. Statistical significance was likely not reached due to the large variation in tissue sample thickness. This may be partly due to stretching or compressing of the tissue while the biopsy was taken and the samples were processed, partly due to natural differences in the skin tissue thickness in growing pigs, and partly due to the disruption of the epidermis present in some samples, and lack of epidermis in others due to tissue damage.

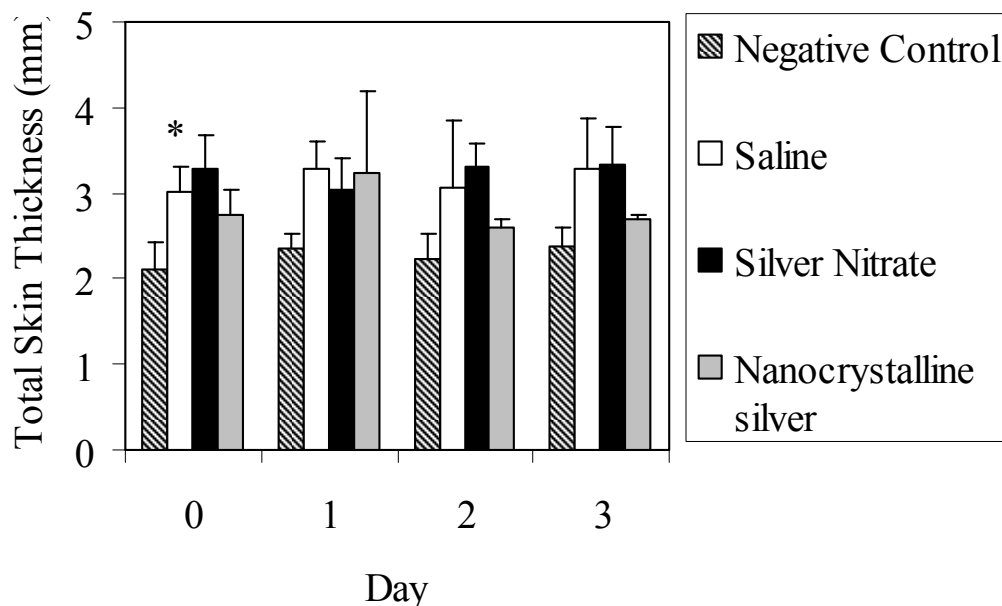


Figure 2-12. Total skin thickness in millimetres measured over time for DNCB-induced rashes treated with saline, silver nitrate, and nanocrystalline silver. Negative controls are also shown. Statistical analyses were performed using one-way ANOVAs with Tukey-Kramer post tests. The one-way ANOVA tests indicated that the differences between groups were significant on Day 0 ($p=0.0339$) and Day 3 ($p=0.0467$), but not on Day 1 ($p=0.1998$) or Day 2 ($p=0.2253$). Results from the post tests are displayed on the figure as follows: * indicates significantly different from the negative control ($p<0.05$). Error bars represent standard deviations ($n=3$ for all data points).

In an attempt to eliminate some of this variability, the thickness of the epidermis only (where present) was measured, as shown in Figure 2-13. Again, there were significant differences between groups on Day 0 ($p=0.0184$), with the animals to be treated with saline having significantly thicker epidermis than the negative controls ($p<0.05$). On Day 3, there were also significant differences between groups ($p=0.0496$). On Day 2 and 3, the nanocrystalline silver treated groups had lower average epidermal thicknesses than the silver nitrate and saline treated animals, but this did not reach statistical significance, likely due to the above stated reasons. Measuring epidermal thickness only, therefore, did not improve the results.

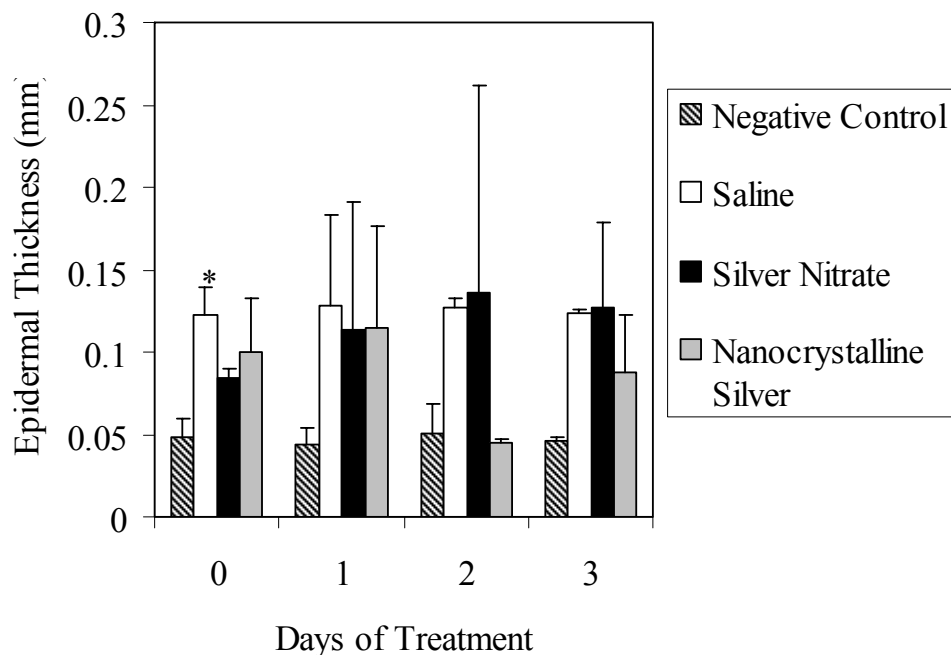


Figure 2-13. Epidermal thickness in millimetres measured over time for DNCB-induced porcine rashes treated with saline, silver nitrate, and nanocrystalline silver. Negative controls are also shown. Statistical analyses were performed using one-way ANOVAs with Tukey-Kramer post tests. The one-way ANOVA tests indicated that the differences between groups were significant on Day 0 ($p=0.0184$) and Day 3 ($p=0.0496$), but not on Day 1 ($p=0.3366$) or Day 2 ($p=0.4202$). Results from the post tests are displayed on the figure as follows: * indicates significantly different from the negative control ($p<0.05$). Error bars represent standard deviations ($n=3$ for all data points).

Gelatinase Zymography

Figure 2-14 shows the protein concentration standard curve created using the BSA standards. The linear best fit line for the region the tissue sample ODs occurred in is shown, along with the corresponding equation and R^2 value. The R^2 value indicates a good linear fit in the selected region, although the overall curve was nonlinear. Figure 2-15 shows the total protein in each sample as calculated from their ODs using the above-mentioned equation. No statistical analysis was performed, due to the fact that the total protein recovered was generally much higher from the tissues of the second group of pigs than the first group, due to the fact that the second recovery of protein was performed on a different day. However, it is interesting to note that the total protein decreased from Day 1 to Day 3 in both nanocrystalline silver treated samples, whereas there was no clear trends in any of the other treatment groups. Figure 2-16a demonstrates the sensitivity of the zymogram assay using known concentrations of trypsin – 1 ng of trypsin can be detected and different concentrations between 1 ng and 50 ng can be distinguished. Figure 2-16b shows a representative zymogram of tissues from different groups at various time points.

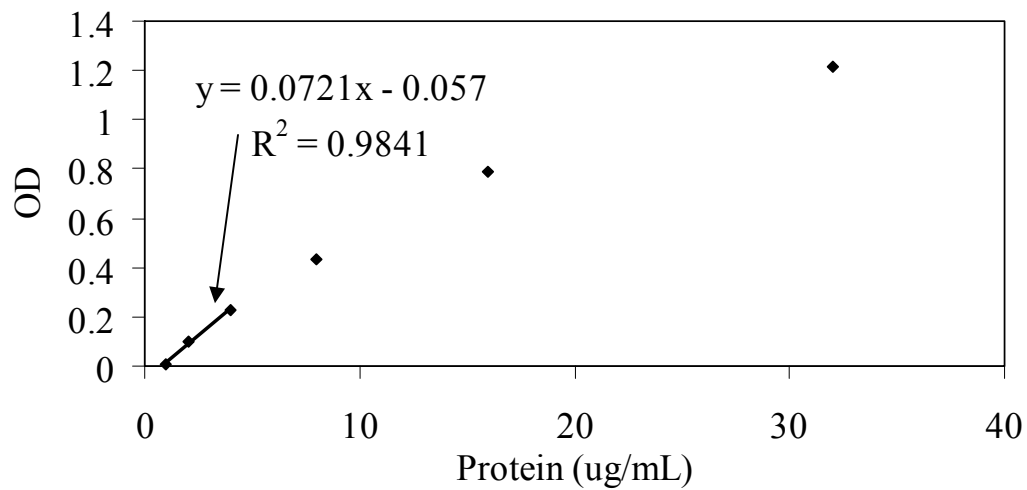


Figure 2-14. Standard curve of optical density versus protein concentration created using BSA standards. A linear fit was performed in Excel for the region shown on the left, and the resulting equation and R^2 value are shown on the figure.

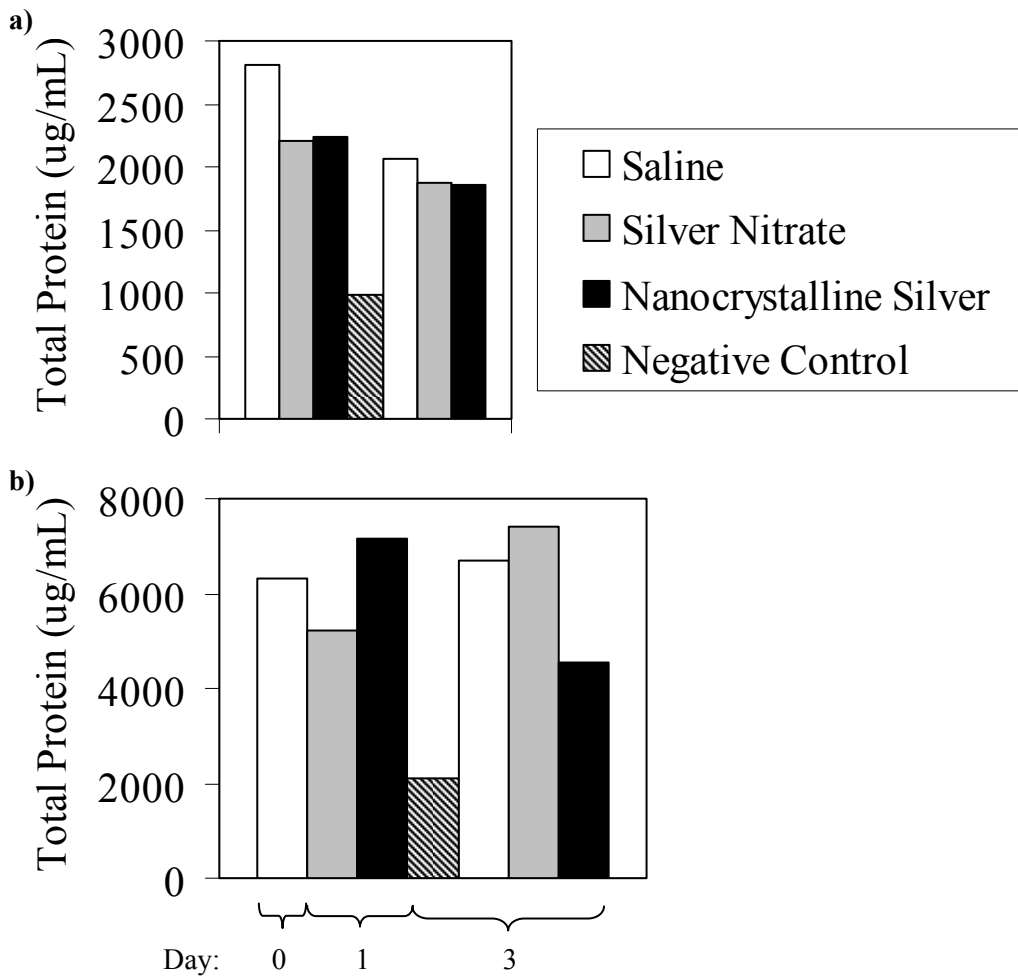


Figure 2-15. Total protein ($\mu\text{g/mL}$) in biopsies from DNCB-induced rashes treated with saline, silver nitrate, or nanocrystalline silver at different time points. Total protein in biopsies from negative controls are shown as well. The total protein from the biopsies of the first pig in each group is shown in a). The total protein from the biopsies of the second pig in each group is shown in b).

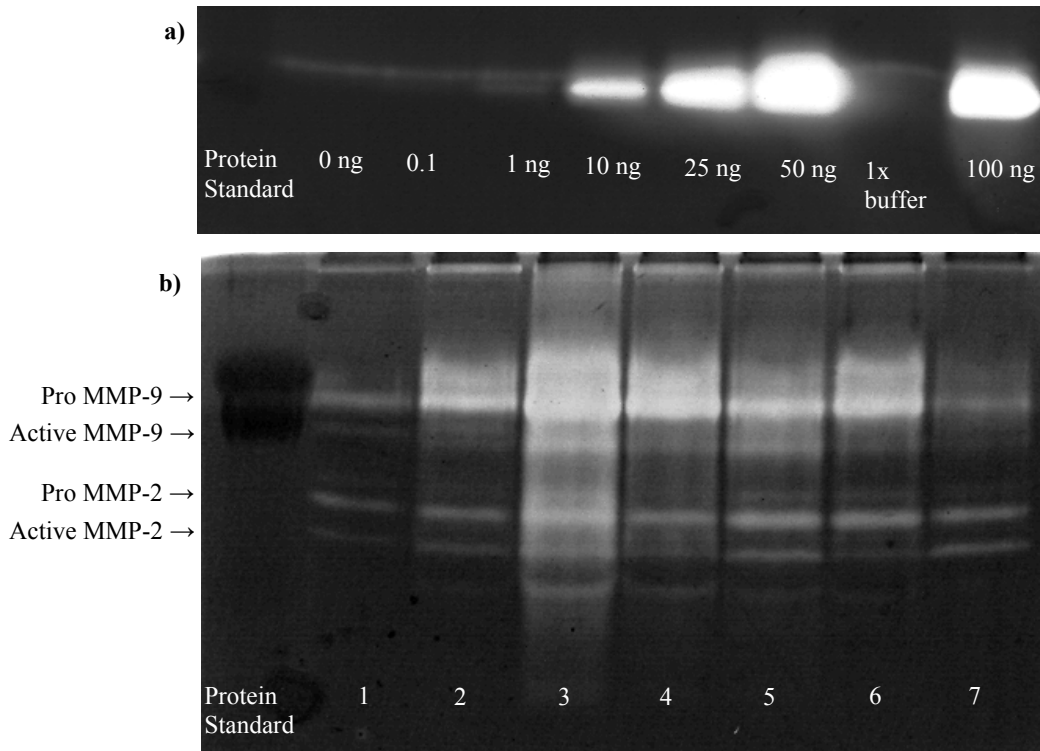


Figure 2-16. Gelatinase activity of tissue samples from DNCB-induced rashes treated with saline, silver nitrate, or nanocrystalline silver, along with negative controls. a) A representative zymogram showing trypsin standard gelatinase activity. The protein standard is shown on the left, and 0 ng, 0.1 ng, 1 ng, 10 ng, 25 ng, 50 ng, and 100 ng standards are shown from left to right, indicating the specificity of the assay. b) A representative zymogram of porcine gelatinase activity. The protein ladder is in the first lane (labeled Protein Standard), followed by a negative control after three days of saline treatment (1); then a Day 0 rash before treatment (2); a saline treated pig after three days of treatment (3); a silver nitrate treated pig after one day of treatment (4), and after three days of treatment (5); and a nanocrystalline silver treated pig after one day of treatment (6), and after three days of treatment (7). A lane was run with the same saline treated pig tissue sample after three days of treatment as above, except that it was incubated with EDTA overnight instead of with calcium. The bands in that lane were very weak (data not shown), indicating that the bands shown in this image are due to gelatinase activity.

Figure 2-17a contains quantitative analysis of pro MMP-9 (pMMP-9) levels, which showed very significant differences between groups ($p=0.0070$). On Day 0, pigs exposed to DNCB had significantly higher pMMP-9 than negative controls. After 72h, the amount of pMMP-9 decreased in saline-treated animals,

and was not significantly different from negative controls. pMMP-9 in AgNO₃-treated pigs increased over time, and at both 24h and 72h was significantly higher than negative controls. After 24h, nanocrystalline silver-treated tissues did not have significantly different pMMP-9 levels from negative controls. By 72h, in nanocrystalline silver-treated pigs, pMMP-9 levels had dropped further, and were significantly lower than levels in AgNO₃-treated pigs or pre-treatment levels.

Panel b shows quantitative analysis of active MMP-9 (aMMP-9) levels, which showed very significant differences between groups ($p=0.0087$). While negative control, Day 0, saline-treated, and nanocrystalline silver-treated animals did not have statistically different aMMP-9 levels, aMMP-9 increased over time with AgNO₃ treatment, so that by 72h, AgNO₃ treated samples had significantly higher aMMP-9 levels than negative controls and nanocrystalline silver treatments after 24h or 72h. It is interesting to note that both nanocrystalline silver- and saline-treated samples had decreases in aMMP-9 over time.

Panel c shows quantitative analysis of pMMP-2, which demonstrated very significant differences between groups ($p=0.0017$). pMMP-2 levels of DNCB-exposed samples at Day 0 were not significantly different from levels in negative controls. pMMP-2 levels increased over time in saline-treated animals, and at 72h were significantly higher than negative controls, and than the animals treated with nanocrystalline silver for 72h. Similarly, pMMP-2 levels increased over time with AgNO₃ treatment, and, by 72h, were significantly higher than negative controls, Day 0 levels, or nanocrystalline silver treated samples at 24 or 72h. In nanocrystalline silver-treated animals, pMMP-2 levels decreased over time. By

72h, they had significantly less pMMP-2 present than saline- or AgNO₃-treated pigs, and were not significantly different from negative controls.

Panel d shows quantitative analysis of aMMP-2, which demonstrated very significant differences between groups (p=0.0038). aMMP-2 levels increased over time in saline-treated animals – by 72h, their levels were significantly higher than negative controls, Day 0 levels, AgNO₃-treated pigs after 24h, and nanocrystalline silver-treated pigs after 24h or 72h. aMMP-2 levels in AgNO₃-treated pigs also increased over time. There was no significant difference between aMMP-2 levels in AgNO₃- and saline-treated pigs at 72h. Nanocrystalline silver-treated pigs showed a much smaller increase in aMMP-2 levels, which was not statistically significant.

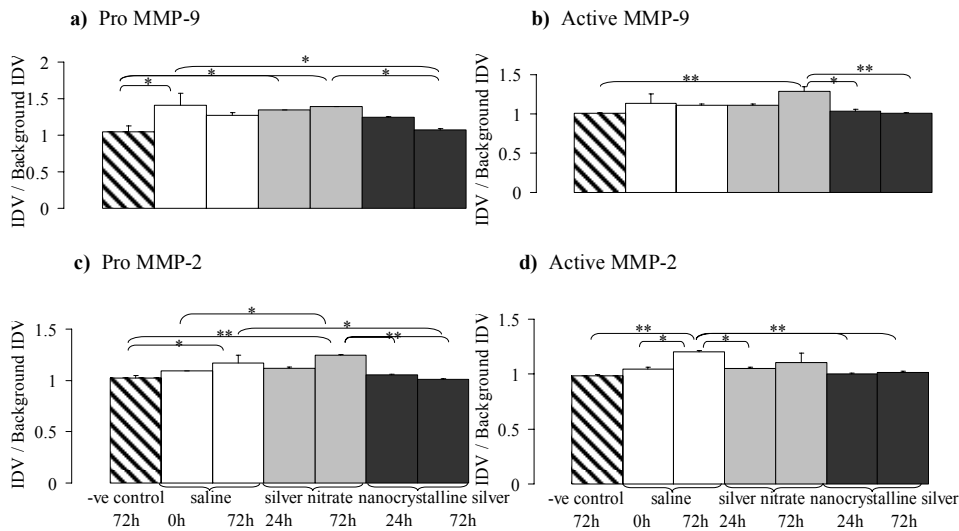


Figure 2-17. Semi-quantitative analysis of gelatinase activity in DNCB-induced porcine rashes treated with saline, silver nitrate, or nanocrystalline silver, as well as in negative controls. Integrated density values (IDV) are shown relative to the gel background IDV for the bands pro MMP-9 (a), active MMP-9 (b), pro MMP-2 (c), and active MMP-2 (d). ANOVA tests indicated that there were very significant differences between groups for all four bands (p=0.0070, p=0.0087, p=0.0017, and p=0.0038, respectively). Statistical analyses were performed using one-way ANOVAs with Tukey-Kramer post tests. * or ** indicates significantly different (p<0.05, and p<0.01 respectively). Error bars represent standard deviations (n=2 for all data points).

Apoptosis Detection

Figure 2-18 shows representative images of negative controls (a) and positive controls (b) for the In-Situ Cell Death Detection kit. Negative controls, which were not exposed to the enzyme solution, show no apoptotic staining, while the positive controls, which were incubated with DNase before testing, show apoptotic staining of nearly all cells. This indicates that the assay was working correctly.

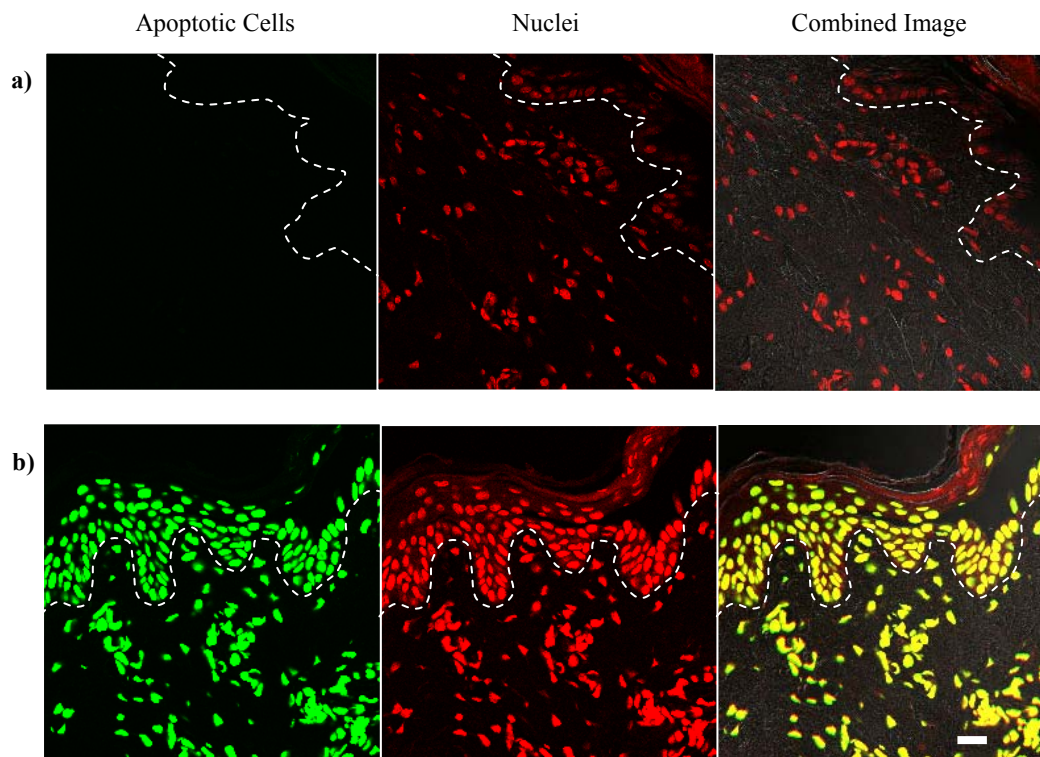


Figure 2-18. Representative fluorescence images for immunohistochemical detection of apoptotic cells in positive and negative controls for the experiment. Delineation between the epidermis and dermis is shown as a dashed white line. The first column shows staining for apoptotic cells (green). The second column shows counterstaining for nuclei (red). The third column shows the combined images of the apoptotic cell and the nuclear imaging. Overlapping staining for apoptosis and nuclei appears yellow. a) A negative control for the experiment, in which samples were not exposed to the enzyme solution. b) A positive control for the experiment, which was treated with DNase. The scale bar (lower right) represents 20 μm .

Figure 2-19 shows representative images of staining for apoptotic cells after 24h of treatment. There were very few apoptotic cells in the negative controls (Figure 2-19 a through c). Saline-treated pigs (Figure 2-19 d through f) demonstrated some apoptosis in the epidermis and upper dermis. AgNO₃-treated pigs (Figure 2-19 g through i) showed high levels of apoptosis near tissue surfaces. Keratinocytes, as well as some inflammatory cells and fibroblasts, show apoptotic staining, suggesting that AgNO₃ induced cell death in all cell types it contacted. In contrast, animals treated with nanocrystalline silver (Figure 2-19 j through l) demonstrated increased inflammatory cell apoptosis compared to all other groups. This apoptosis was in the dermis, and did not target the keratinocytes in the epidermis. Figure 2-20a shows semi-quantitative analysis of the apoptotic staining in the epidermis, which confirmed that AgNO₃ treatment resulted in significantly more apoptosis in the epidermis, which is largely composed of keratinocytes, than in all the other treatments. Figure 2-20b shows semi-quantitative analysis of the apoptotic staining in the dermis. Relative to the other groups, nanocrystalline silver-treated tissues had significantly higher apoptosis in the dermis, which was highly infiltrated with inflammatory cells. AgNO₃ induced apoptosis in the dermis to a certain depth, below which no apoptosis was induced, while nanocrystalline silver induced apoptosis in inflammatory cells throughout the dermis (see Figure 2-21a, b). Thus, had the analysis been performed deeper in the dermis, the difference would have been even more significant.

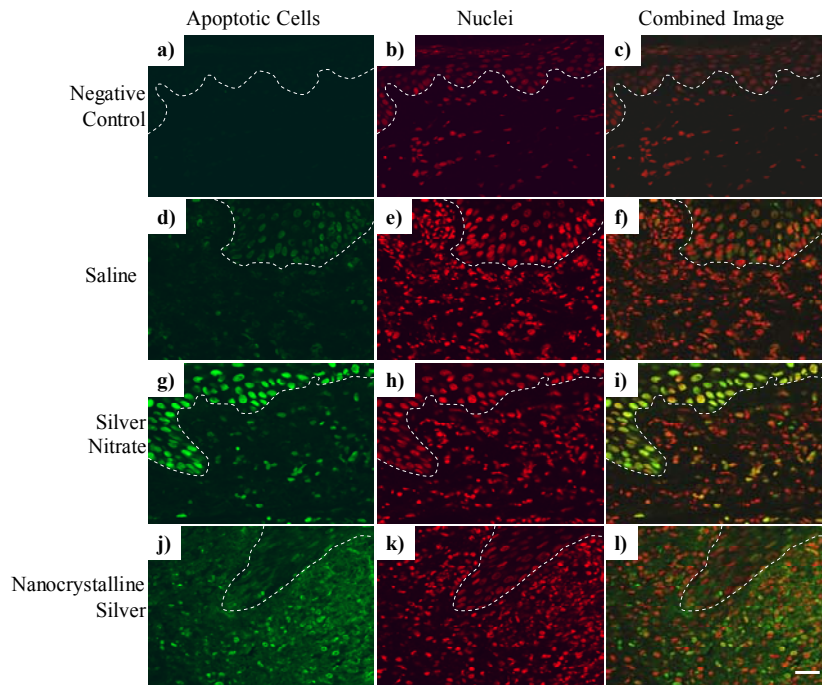


Figure 2-19. Representative fluorescence images for immunohistochemical detection of apoptotic cells in the epidermis and upper dermis of DNCB-induced porcine rashes treated with saline, silver nitrate, or nanocrystalline silver, as well as negative controls. Delineation between the epidermis and dermis is shown as a dashed white line. The first column shows staining for apoptotic cells (green). The second column shows counterstaining for nuclei (red). The third column shows the combined images of the apoptotic cell and the nuclear imaging. Overlapping staining for apoptosis and nuclei appears yellow. Images a) to c) are a negative control pig. Images d) to f) are a saline treated pig. Images g) to i) are a silver nitrate treated pig. Images j) to l) are a nanocrystalline silver treated pig. The scale bar, shown in l), represents 20 μm .

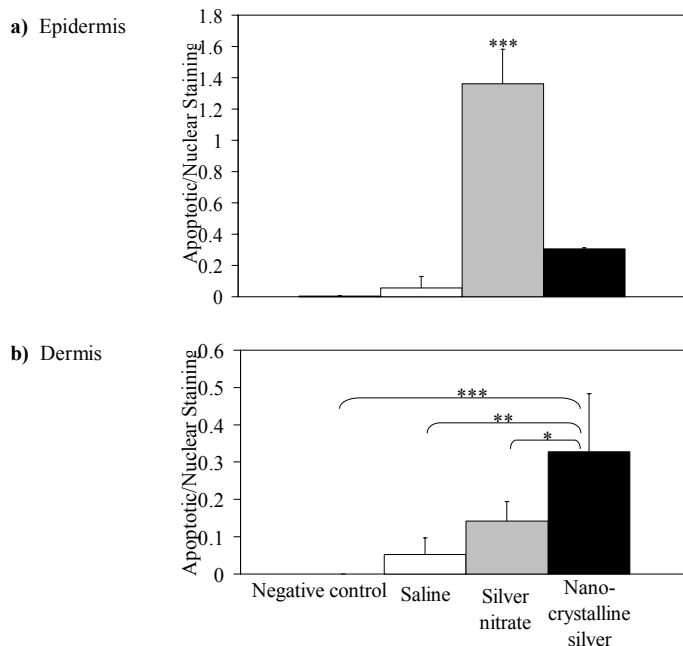
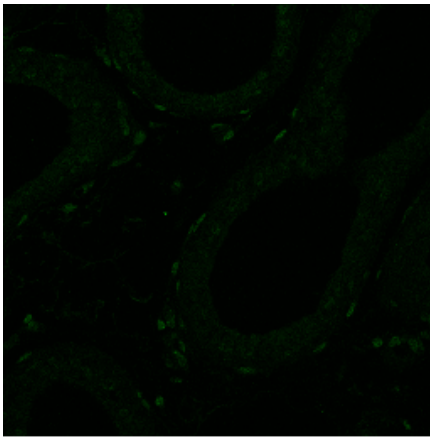
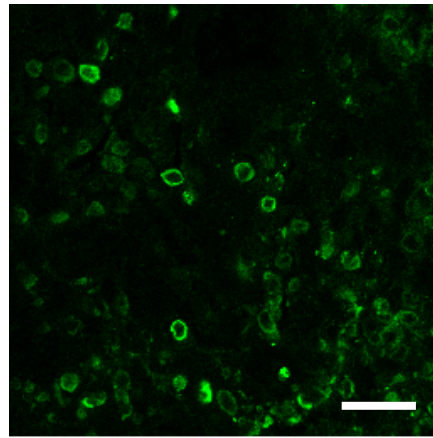


Figure 2-20. Semi-quantitative analysis of apoptotic staining after treatment of DNCB-induced rashes with saline, silver nitrate, or nanocrystalline silver. Results for negative controls are also shown. Panels a) and b) show the ratio of green (staining for apoptosis) to red (staining for nuclei) pixels in the epidermis and dermis, respectively. In the epidermis, a one-way ANOVA indicated there were extremely significant differences between groups ($p < 0.0001$). Tukey-Kramer Multiple Comparisons post testing indicated that the silver nitrate treated group was extremely significantly different from all other groups ($p < 0.001$), and no other groups were significantly different from one another. In the dermis, a one-way ANOVA indicated that there were extremely significant differences between groups ($p = 0.0003$, ***). Tukey-Kramer Multiple Comparisons post tests indicated that the nanocrystalline silver was significantly different from the silver nitrate treated group ($p < 0.5$, *), very significantly different from the saline treated group ($p < 0.01$, **), and extremely significantly different from the negative control ($p < 0.001$, ***), while no other groups were significantly different from one another. Error bars represent standard deviations.



a) Silver nitrate treated



b) Nanocrystalline silver treated

Figure 2-21. Representative fluorescence images for immunohistochemical detection of apoptotic cells in the deep dermis of DNCB-induced rashes treated with a) silver nitrate or b) nanocrystalline silver. Cells undergoing apoptosis are stained green. The scale bar, shown in b), represents 20 μm .

Mast Cell Counts

Images of staining for mast cells are shown for saline treated tissues (Figure 2-22a) and silver nitrate (Figure 2-22b) treated tissues at three days of treatments. With the exception of the silver nitrate treated samples at three days of treatment, the image of the saline treated tissue (a) is representative of the tissues from all the groups at all time points. Average mast cell counts are shown for each treatment group over the course of the study in Figure 2-23. There were no significant differences between negative controls, pigs treated with saline, and pigs treated with nanocrystalline silver on any days of treatment – they all contained low levels of mast cells. However, by Day 3 there were extremely significant differences between the groups ($p=0.0002$). In pigs treated with silver nitrate, significantly higher numbers of mast cells had accumulated in clusters in the epidermis and upper dermis than were present in any other group.

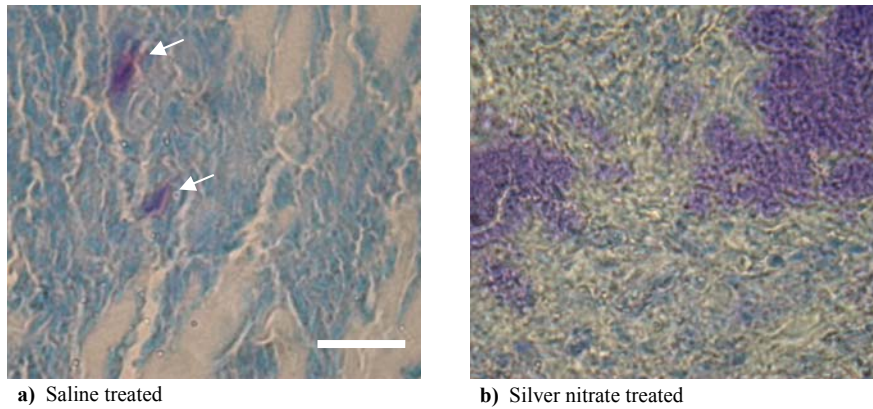


Figure 2-22. Mast cell detection in DNCB-induced rashes after treatment with saline or silver nitrate. Panel a) shows typical staining for mast cells, in which the mast cells appear purple (arrows point to mast cells) and other cells stain blue. The image was taken from a tissue treated 72h with saline. Images of negative controls and tissues treated with nanocrystalline silver appeared similar, as did tissues treated with silver nitrate at early timepoints (images not shown). Panel b) shows a representative image of the clusters of mast cells that appeared in silver nitrate treated tissues by 72h of treatment. The scale bar in a) is 50 μ m.

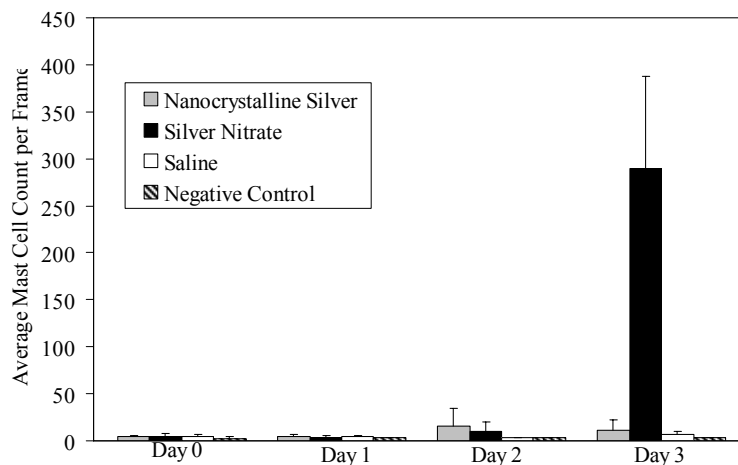


Figure 2-23. Mast cell quantification in DNCB-induced rashes after treatment with saline, silver nitrate, or nanocrystalline silver. Quantification for negative controls is also shown. The average number of mast cells was counted under high magnification (200x) over three days of treatment for DNCB-induced rashes treated with saline, nanocrystalline silver, or silver nitrate. Counts were also performed for negative controls. Statistical analyses were performed using one-way ANOVAs with Tukey-Kramer post tests. The one-way ANOVA tests indicated that the differences between groups were not significant on Day 0, Day 1, and Day 2 ($p=0.6533$, 0.3449 , and 0.4831 , respectively). Differences between groups were extremely significant on Day 3 ($p=0.0002$). Tukey-Kramer Multiple Comparisons post tests indicated that silver nitrate was significantly different from all other groups tested ($p<0.001=***$). Error bars represent standard deviations ($n=3$ for all data points).

Primer Testing

Images from traditional PCR reactions, testing cDNA synthesis and the designed primers, are shown in Figure 2-24. From Figure 2-24a, it appears that the HPRT primer and IL-10 primer worked well (and therefore were selected for real time RT-PCR experiments), while the TNF- α primer had extra bands that may be extra primer dimers or TNF- α isoforms. The TGF- β primer did not work at all. cDNA synthesis was successful in all samples tested. In Figure 2-24b, the IL-8 primer worked (and therefore was selected for real time RT-PCR experiments), but the IL-12 primer had a very strong primer dimer signal. The TGF- β (mouse) primer did not work, and the IL-1 β primer signal was weak, and it appears that in the IL-1 β runs, some heavier DNA strands, possibly contaminant genomic DNA, were amplified. Figure 2-24c indicates that the IL-1 β primer (1) signal was weak, and the IL-1 β primer (2) was weak, with primer dimers stronger than the actual signal. The IL-1 β primer (3) signal was strong and no other bands were present, so this primer set was selected for real time RT-PCR experiments. The TGF- β primer (1) had many bands, and the TGF- β primer (3) didn't work at all, so the TGF- β primer (2) set was selected for further experiments, as it had the strongest signal bands, although it has an extra high molecular weight band present in the saline treated sample. The IL-12 primer (1) set didn't work, but the IL-12 primer (2) set did, so although it was a weak signal, and somewhat smeared for the nanocrystalline silver treated sample, it was selected for experimentation with real time RT-PCR.

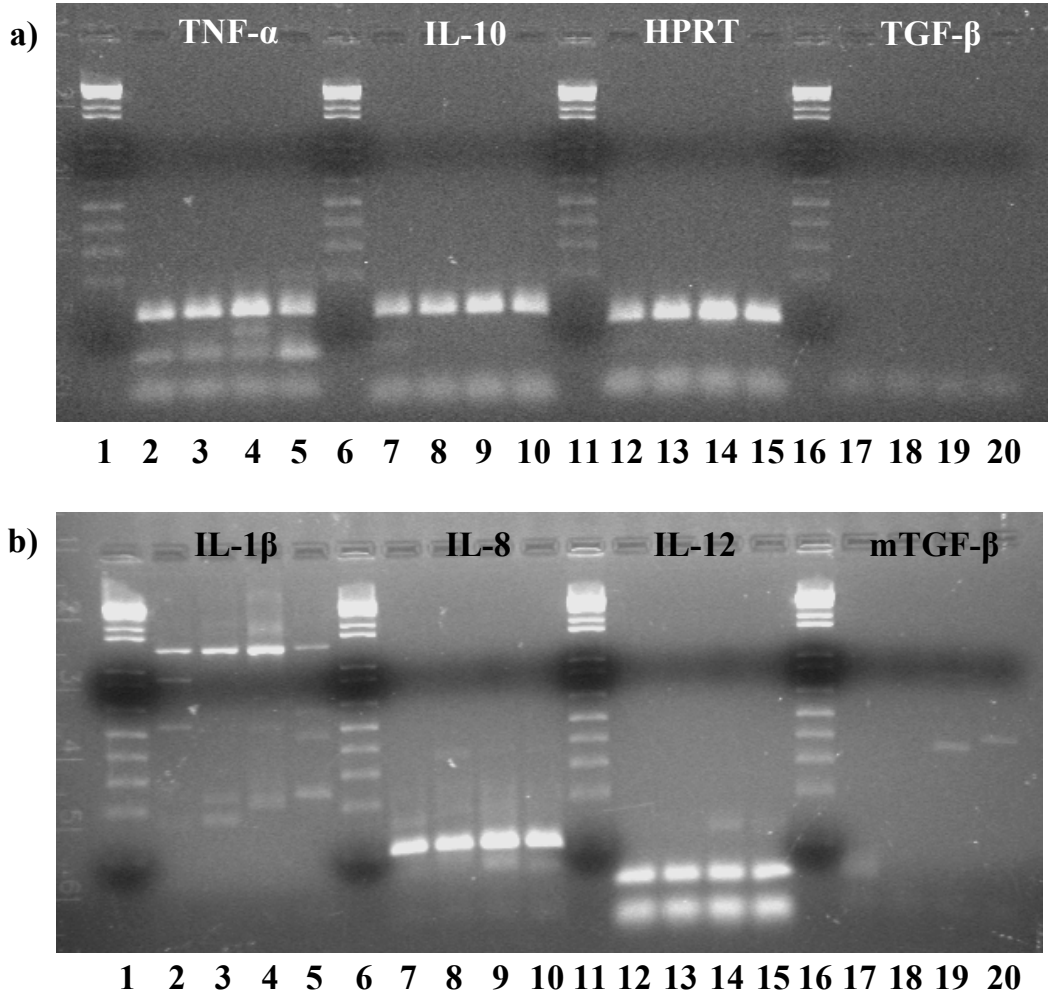


Figure 2-24

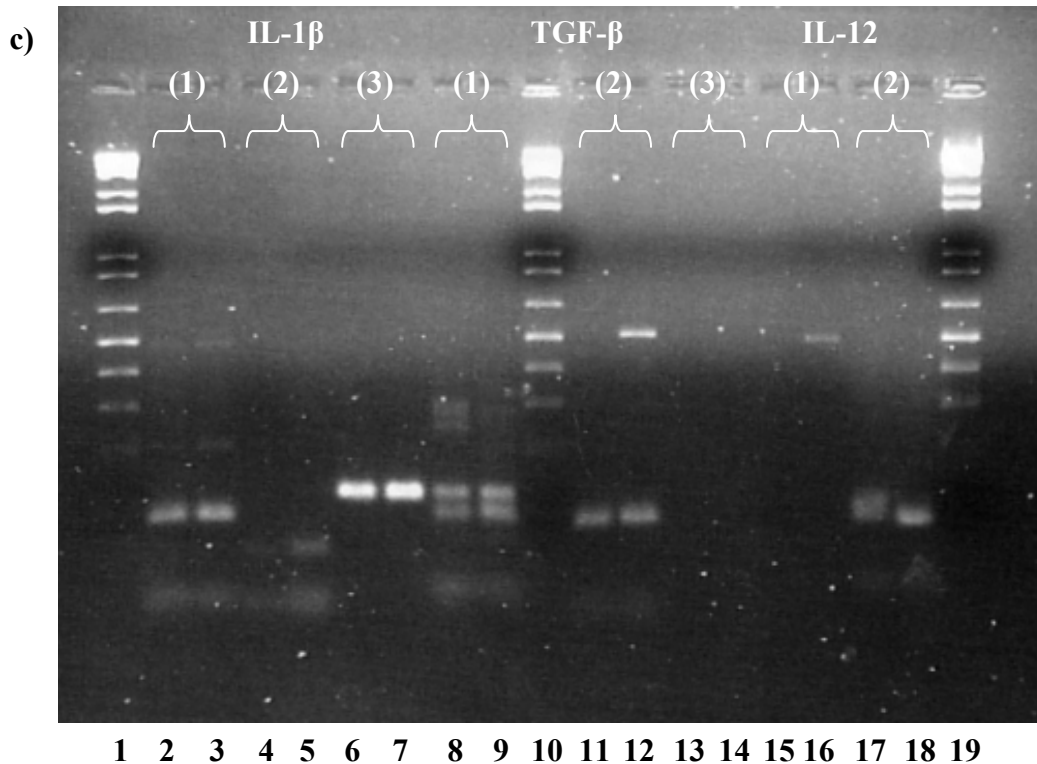


Figure 2-24, continued. Testing for successful primer design and cDNA synthesis. In both a) and b), well 1, 6, 11, and 16 are DNA standards, while the wells in between the standard wells are as follows: negative controls are in wells 2, 7, 12, and 16; nanocrystalline silver treated samples are in wells 3, 8, 13 and 17; silver nitrate treated sample are in wells 4, 9, 14, and 18; and saline treated samples are in wells 5, 10, 14, and 20. All samples are from the third day of treatment. In a), wells 2-5 were run with the TNF- α primers, wells 7-10 were run with the IL-10 primers, wells 12-14 were run with the HPRT primers, and wells 16-20 were run with the TGF- β primers. In b), wells 2-5 were run with IL-1 β primers, wells 7-10 were run with IL-8 primers, wells 12-14 were run with IL-12 primers, and wells 16-20 were run with TGF- β (mouse) primers. In c), wells 1, 10, and 19 are DNA standards. Wells 2, 4, 6, 8, 11, 13, 15, and 17 contain a nanocrystalline silver treated sample after three days of treatment, and wells 3, 5, 7, 9, 12, 14, 16, and 18 contain a saline treated sample after three days of treatment. Wells 2-3 were run with IL-1 β (1) primers, wells 4-5 were run with IL-1 β (2) primers, wells 6-7 were run with IL-1 β (3) primers, wells 8-9 were run with TGF- β (1) primers, wells 11-12 were run with TGF- β (2) primers, wells 13-14 were run with TGF- β (3) primers, wells 15-16 were run with IL-12 (1) primers, and wells 17-18 were run with IL-12 (2) primers.

Semi-quantitative analysis of mRNA expression

All mRNA expression shown in this section was calculated relative to negative control tissue samples. Figure 2-25 shows the expression of IL-1 β mRNA for treatments at various timepoints. mRNA levels for Figures 2-25 to 2-30 were measured using Supercyclers (Bio-Rad). Statistical analysis indicated that there were significant differences between groups ($p=0.0120$) and that pigs treated with nanocrystalline silver for 24h had significantly higher IL-1 β mRNA levels than their 72h levels, Day 0 rashes, pigs treated for 24h with silver nitrate, or saline treated animals at 72h. Most of the other tissue samples appeared to have similar IL-1 β expression levels to the negative controls. Figure 2-26 shows the expression of IL-8 mRNA for treatments after various amounts of time. Day 0 levels appeared higher than any of the treatment groups. On Day 1, the nanocrystalline silver treatments appeared to have higher IL-8 mRNA expression, with silver nitrate treated samples having the lowest expression. By Day 3, however, the saline and silver nitrate treated samples had similar IL-8 expression levels, and the nanocrystalline silver had the lowest IL-8 expression, which was near that of the negative controls. However, these patterns were not statistically significant ($p=0.2202$). Figure 2-27 shows the IL-10 mRNA expression for treatments at various time points. The Day 0 IL-10 mRNA levels were lower than those of the negative controls. Saline treated and silver nitrate treated tissue IL-10 levels were relatively constant over time, with the IL-10 levels being lower for the silver nitrate treated pigs than for the saline treated pigs. IL-10 levels were highest of any group for nanocrystalline silver treated pigs on Day 0, but they

dropped by Day 3, so that the IL-10 mRNA expression was lower than any other group, and lower than the negative controls as well. However, none of these trends reached statistical significance ($p=0.0913$). In Figure 2-28, IL-12 mRNA expression for treatments at various time points is displayed. The Day 0 rash tissues, saline treated tissues on Day 1 and 3, and nanocrystalline silver treated tissues on Day 1 all showed similar IL-12 mRNA expression to that of the negative controls. Silver nitrate treated samples were quite low on Day 1, increasing slightly by Day 3. Nanocrystalline silver treated samples show a large decrease in IL-12 mRNA expression by Day 3. A one-way ANOVA test indicated that there were significant differences between groups ($p=0.0138$), but post tests did not indicate any significant differences between individual groups. Expression of TNF- α mRNA with various treatments over time is shown in Figure 2-29. There were significant differences in measured TNF- α mRNA expression between groups ($p=0.0043$). TNF- α mRNA expression was similar in Day 0 rashes and saline treated animals at 24h. The mRNA expression was lower in silver nitrate treated samples at Day 1. Saline treated and silver nitrate treated animals showed increased TNF- α expression over time, but this expression was not higher than that of the negative controls. Nanocrystalline silver treated tissues at 24h showed significantly higher TNF- α expression than silver nitrate treated samples at 24h. However, TNF- α expression by nanocrystalline silver treated samples dropped significantly by 72h. Figure 2-30 displays TGF- β mRNA expression with various treatments over time. There were significant differences between groups ($p=0.0425$), and post testing indicated that nanocrystalline silver

and silver nitrate treated tissues expressed significantly lower TGF- β at 72h than nanocrystalline silver treated tissues did at 24h. It is interesting to note that TGF- β mRNA levels also decreased over time with both saline and silver nitrate treatment, but these trends did not reach significance.

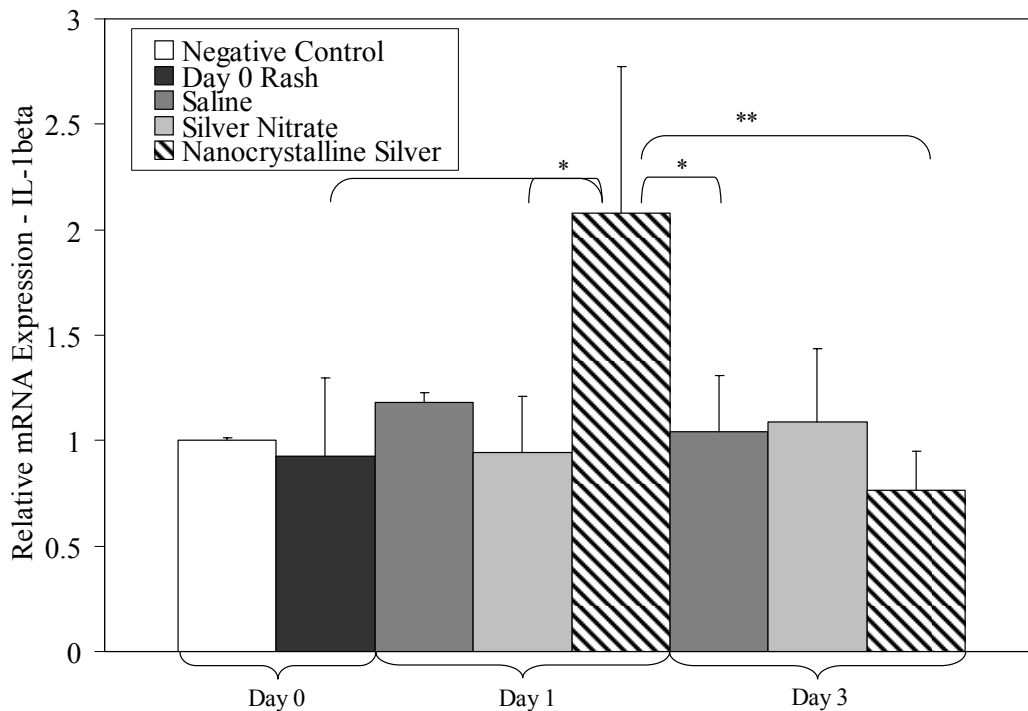


Figure 2-25. Relative expression of IL-1 β mRNA in negative controls and DNCB-induced porcine rashes treated with saline, silver nitrate, or nanocrystalline silver. IL-1 β mRNA levels were measured using the IL-1 β (3) primer set via real time RT-PCR using Supercyclers (Bio-Rad). mRNA expression of IL-1 β in Day 0 Rash samples, and samples treated with saline, silver nitrate, or nanocrystalline silver at Day 1 or 3 was calculated relative to the mRNA expression by negative controls. Statistical analyses were performed using one-way ANOVAs with Tukey-Kramer post tests. The one-way ANOVA tests indicated that the differences between groups were significant ($p=0.0118$). Results of the Tukey-Kramer Multiple Comparisons post tests are indicated on the figure as follows: $p<0.5 = *$, and $p<0.01 = **$. Error bars represent standard deviations ($n=3$ for all data points).

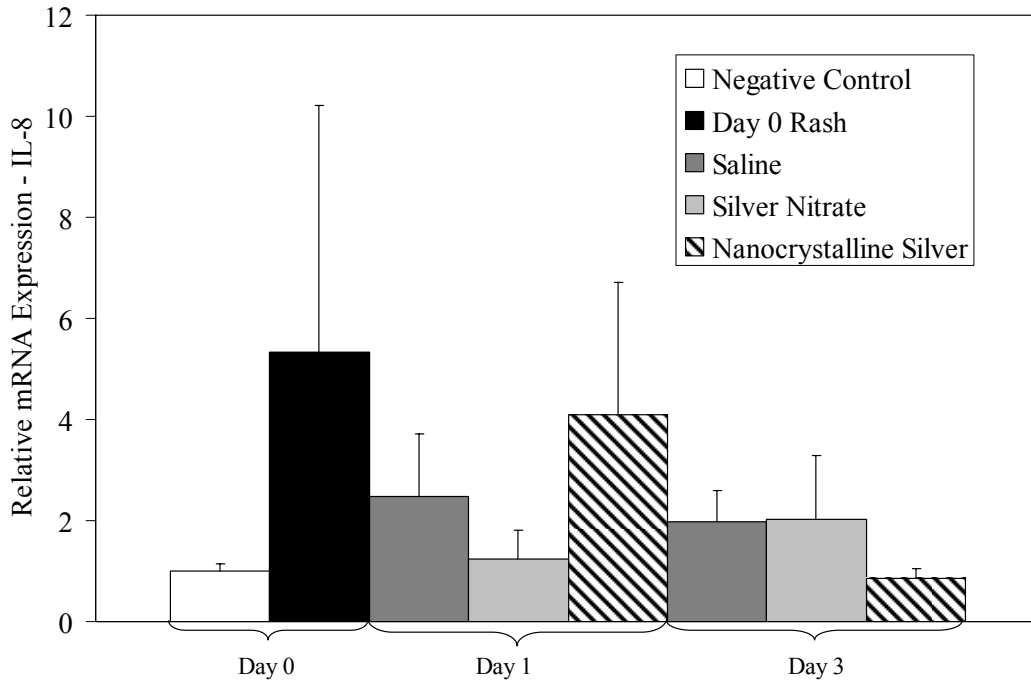


Figure 2-26. Relative expression of IL-8 mRNA in negative controls and DNCB-induced porcine rashes treated with saline, silver nitrate, or nanocrystalline silver. IL-8 mRNA levels were measured via real time RT-PCR using Supercyclers (Bio-Rad). mRNA expression of IL-8 in Day 0 Rash samples, and samples treated with saline, silver nitrate, or nanocrystalline silver at Day 1 or 3 was calculated relative to the mRNA expression by negative controls. Statistical analyses were performed using one-way ANOVAs with Tukey-Kramer post tests. The one-way ANOVA tests indicated that the differences between groups were not significant ($p=0.2323$). Error bars represent standard deviations ($n=3$ for all data points).

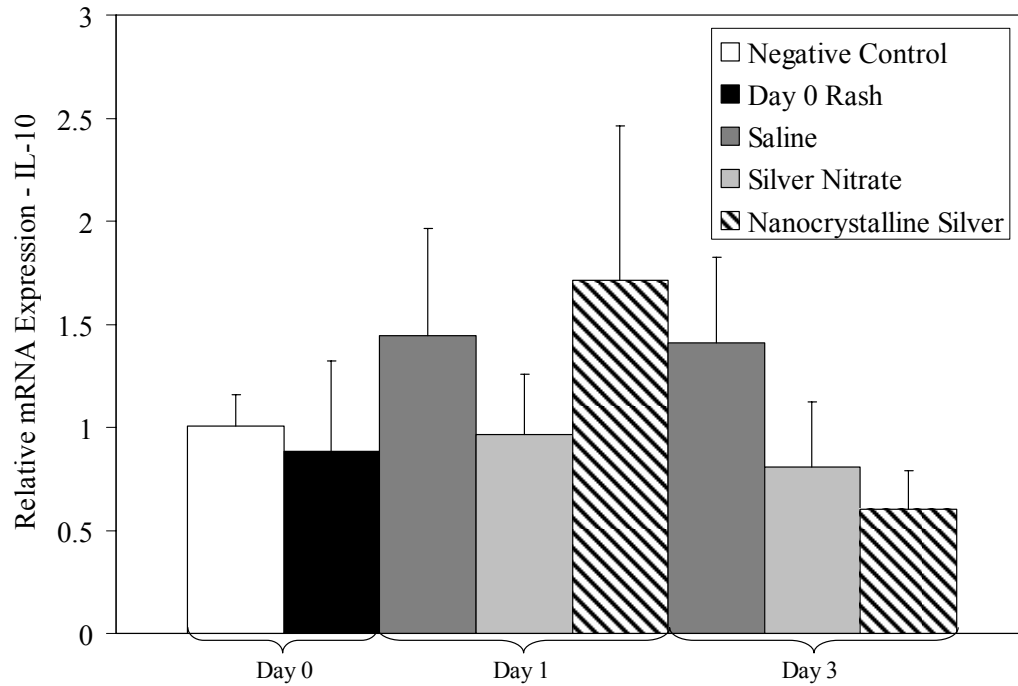


Figure 2-27. Relative expression of IL-10 mRNA in negative controls and DNCB-induced porcine rashes treated with saline, silver nitrate, or nanocrystalline silver. IL-10 mRNA levels were measured via real time RT-PCR using Supercyclers (Bio-Rad). mRNA expression of IL-10 in Day 0 Rash samples, and samples treated with saline, silver nitrate, or nanocrystalline silver at Day 1 or 3 was calculated relative to the mRNA expression by negative controls. Statistical analyses were performed using one-way ANOVAs with Tukey-Kramer post tests. The one-way ANOVA tests indicated that the differences between groups were not significant ($p=0.0805$). Error bars represent standard deviations ($n=3$ for all data points).

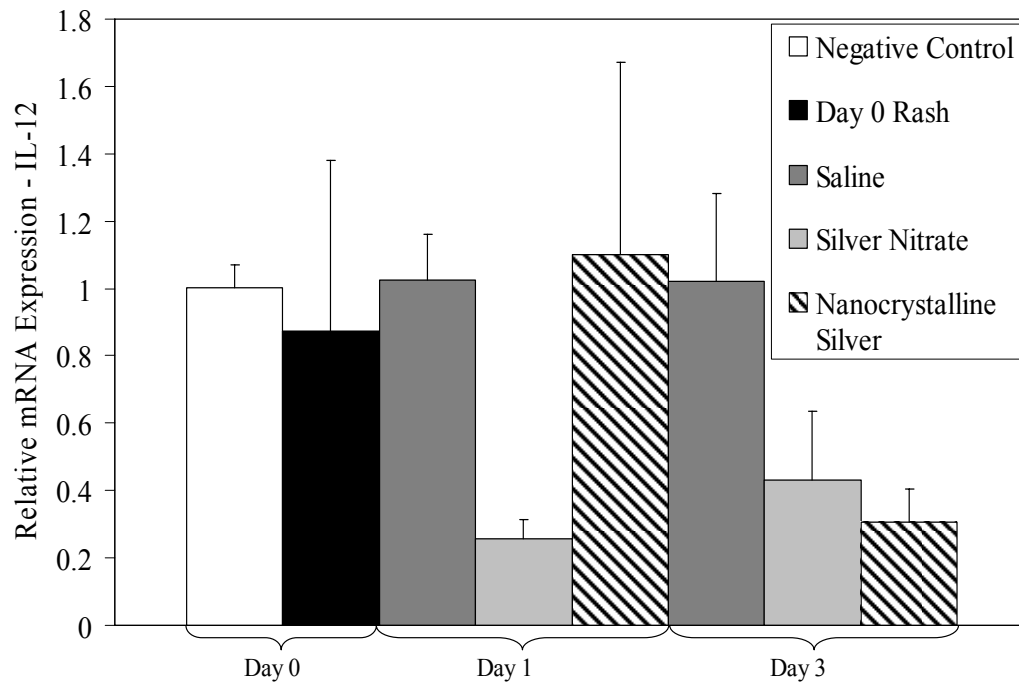


Figure 2-28. Relative expression of IL-12 mRNA in negative controls and DNCB-induced porcine rashes treated with saline, silver nitrate, or nanocrystalline silver. IL-12 mRNA levels were measured using the IL-12 (2) primer set via real time RT-PCR using Supercyclers (Bio-Rad). mRNA expression of IL-12 in Day 0 Rash samples, and samples treated with saline, silver nitrate, or nanocrystalline silver at Day 1 or 3 was calculated relative to the mRNA expression by negative controls. Statistical analyses were performed using one-way ANOVAs with Tukey-Kramer post tests. The one-way ANOVA tests indicated that the differences between groups were significant ($p=0.0161$), but the post tests did not indicate any significant differences between individual groups. Error bars represent standard deviations ($n=3$ for all data points).

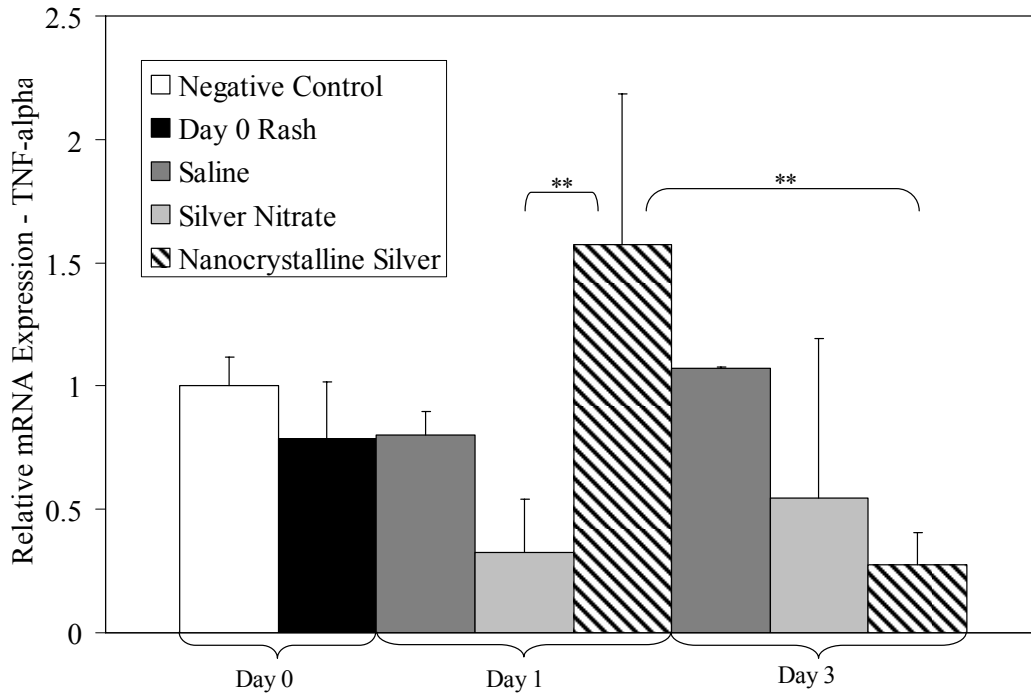


Figure 2-29. Relative expression of TNF- α mRNA in negative controls and DNCB-induced porcine rashes treated with saline, silver nitrate, or nanocrystalline silver. TNF- α mRNA levels were measured via real time RT-PCR using Supercyclers (Bio-Rad). mRNA expression of TNF- α in Day 0 Rash samples, and samples treated with saline, silver nitrate, or nanocrystalline silver at Day 1 or 3 was calculated relative to the mRNA expression by negative controls. Statistical analyses were performed using one-way ANOVAs with Tukey-Kramer post tests. The one-way ANOVA tests indicated that the differences between groups were significant ($p=0.0048$). Results of the Tukey-Kramer Multiple Comparisons post tests are indicated on the figure as follows: $p<0.01 = **$. Error bars represent standard deviations ($n=3$ for all data points).

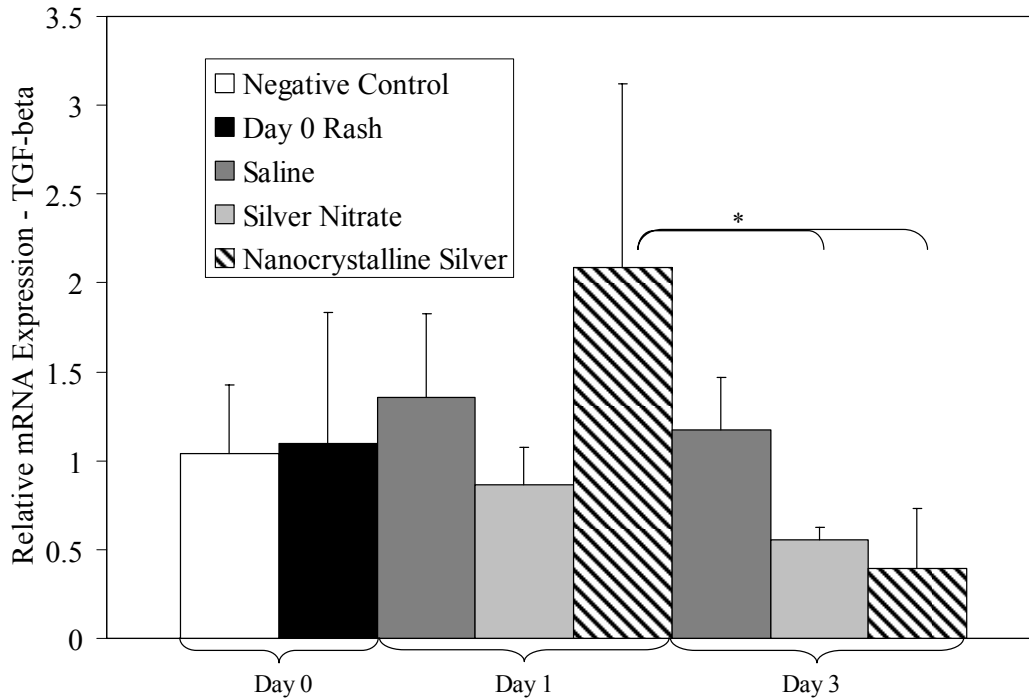


Figure 2-30. Relative expression of TGF- β mRNA in negative controls and DNCB-induced porcine rashes treated with saline, silver nitrate, or nanocrystalline silver (n=3 for each). TGF- β mRNA levels were measured using the TGF- β (2) primer set via real time RT-PCR using Supercyclers (Bio-Rad). mRNA expression of TGF- β in Day 0 Rash samples, and samples treated with saline, silver nitrate, or nanocrystalline silver at Day 1 or 3 was calculated relative to the mRNA expression by negative controls. Statistical analyses were performed using one-way ANOVAs with Tukey-Kramer post tests. The one-way ANOVA tests indicated that the differences between groups were significant (p=0.0341). Results of the Tukey-Kramer Multiple Comparisons post tests are indicated on the figure as follows: p<0.5 = *. Error bars = standard deviations.

However, there were some significant concerns with the data presented in Figures 2-26 to 2-30. Firstly, the mRNA expression measured for all the molecules tested was barely stronger than the negative controls, and was often lower than the negative controls, no matter what treatment group or time point was considered. This seems unlikely as, for example, Day 0 rashes should have exhibited much higher expression for pro-inflammatory molecules such as TNF- α and IL-1 β . Another concern was the high variability in expression within groups.

As well, there seemed to be similar relative mRNA expression patterns between groups no matter what molecule was tested, whether it be pro-inflammatory (eg TNF- α), anti-inflammatory (e.g. IL-10), or pleotropic (e.g. TGF- β). Furthermore, although the real time RT-PCR was run simultaneously for all samples, they were run in two machines as they did not all fit into one, and there seemed to be a pattern in which samples tested in one machine had lower expression levels on average than those samples run in the other machine. Therefore the above results, while interesting, are considered to be unreliable.

In order to eliminate the problem of differences in measurements between the two machines, an Applied Biosystems 7300 Real Time PCR System was used, which could fit all the samples at once. Fresh cDNA was made from the RNA as well, in case the cDNA used to generate the previous figures had begun to degrade. Figures 2-31 to 2-35 show analysis of relative mRNA expression using this equipment. In Figure 2-31, measurements of the relative expression of IL-1 β mRNA are shown over time for various treatments. IL-1 β mRNA expression appeared low in Day 0 rashes, and Day 1 rashes treated with saline. IL-1 β expression was slightly higher on Day 1 for nanocrystalline silver treated samples, and decreased by Day 3. Saline treated samples showed increased IL-1 β expression by Day 3. Silver nitrate treated samples had much higher IL-1 β expression, which was relatively constant from Day 1 to Day 3. None of these trends reached statistical significance ($p=0.0657$). Figure 2-32 shows IL-8 mRNA expression over time for various treatments. The pattern seen in this figure is nearly identical to that of Figure 2-31, and again, the trends observed did

not reach statistical significance ($p=0.4546$). Figure 2-33 shows relative expression of IL-12 mRNA for various treatment groups over time. Day 0 rash samples and Day 1 samples treated with saline showed similar levels of IL-12 mRNA expression, which were slightly elevated relative to the negative controls. Silver nitrate treated samples showed stronger IL-12 mRNA expression on Day 1, while nanocrystalline silver treated samples showed a much lower expression on Day 1. However, saline and silver nitrate treated samples showed decreases in expression over time, while the nanocrystalline silver treated samples showed an increased expression at Day 3. Again, these trends were not statistically significant ($p=0.2390$). The same pattern is again observed in Figure 2-34, which shows the measured relative expression of TNF- α mRNA. However, the trends are less pronounced than in the previous figure, and again, the trends are not significant ($p=0.2976$). Figure 2-35, which displays the expression of TGF- β mRNA, shows a nearly identical pattern to Figure 2-34. Day 0 rashes and saline treated samples at Day 1 show similar expression levels, which are slightly elevated relative to the negative controls. Silver nitrate treated tissues show higher TGF- β expression on Day 1, which decreases by Day 3. Saline treated tissues also show decreased expression at Day 3. Nanocrystalline silver treated samples showed lower TGF- β expression than the other groups on Day 1, but higher expression on Day 3. The trends observed were not statistically significant ($p=0.1830$).

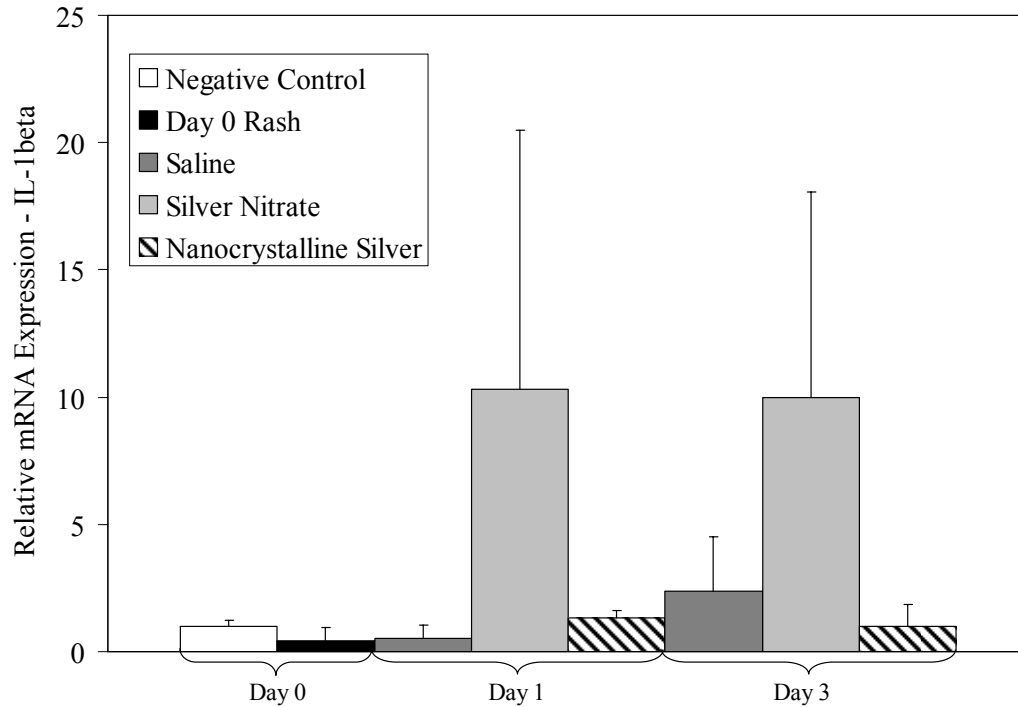


Figure 2-31. Relative expression of IL-1 β mRNA in negative controls and DNCB-induced porcine rashes treated with saline, silver nitrate, or nanocrystalline silver. IL-1 β mRNA levels were measured using the IL-1 β (3) primer set via real time RT-PCR using an Applied Biosystems 7300 Real Time PCR System. mRNA expression of IL-1 β in Day 0 Rash samples, and samples treated with saline, silver nitrate, or nanocrystalline silver at Day 1 or 3 was calculated relative to the mRNA expression by negative controls. Statistical analyses were performed using one-way ANOVAs with Tukey-Kramer post tests. The one-way ANOVA tests indicated that the differences between groups were not quite significant ($p=0.0861$). Error bars represent standard deviations ($n=3$ for all data points).

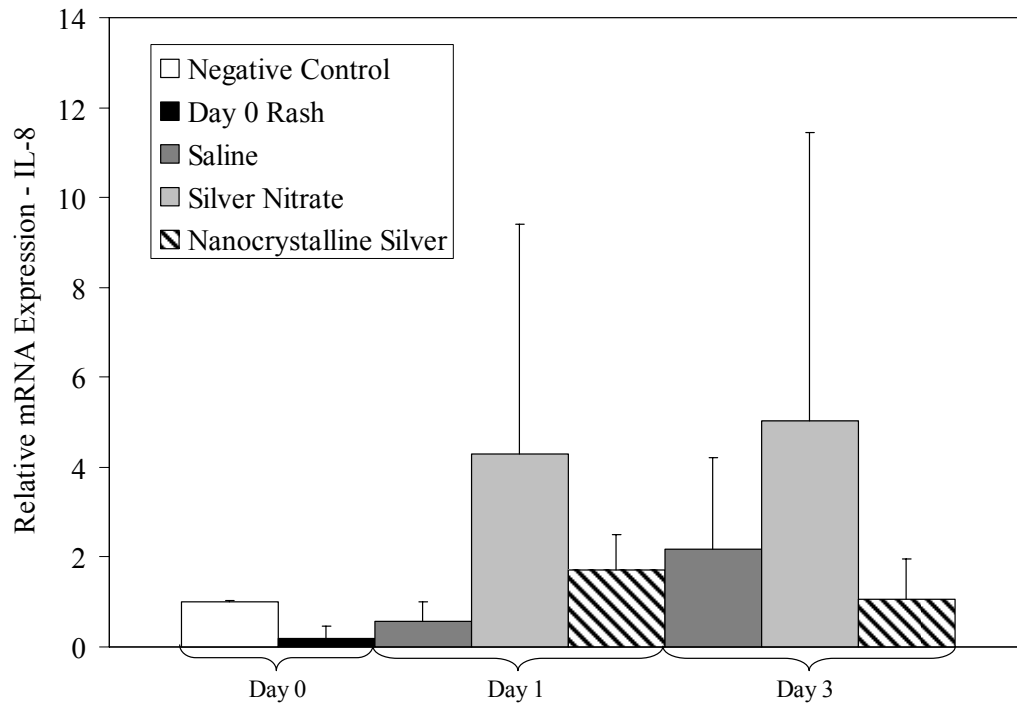


Figure 2-32. Relative expression of IL-8 mRNA in negative controls and DNCB-induced porcine rashes treated with saline, silver nitrate, or nanocrystalline silver. IL-8 mRNA levels were measured via real time RT-PCR using an Applied Biosystems 7300 Real Time PCR System. mRNA expression of IL-8 in Day 0 Rash samples, and samples treated with saline, silver nitrate, or nanocrystalline silver at Day 1 or 3 was calculated relative to the mRNA expression by negative controls. Statistical analyses were performed using one-way ANOVAs with Tukey-Kramer post tests. The one-way ANOVA tests indicated that the differences between groups were not significant ($p=0.4709$). Error bars represent standard deviations ($n=3$ for all data points).

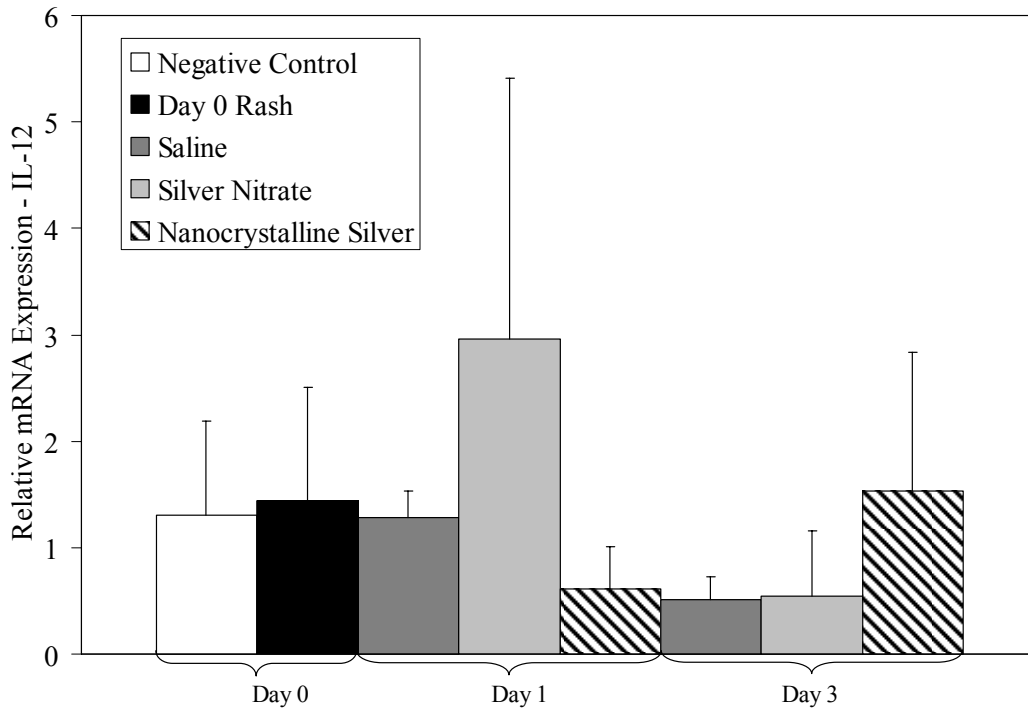


Figure 2-33. Relative expression of IL-12 mRNA in negative controls and DNCB-induced porcine rashes treated with saline, silver nitrate, or nanocrystalline silver. IL-12 mRNA levels were measured using the IL-12 (2) primer set via real time RT-PCR using an Applied Biosystems 7300 Real Time PCR System. mRNA expression of IL-12 in Day 0 Rash samples, and samples treated with saline, silver nitrate, or nanocrystalline silver at Day 1 or 3 was calculated relative to the mRNA expression by negative controls. Statistical analyses were performed using one-way ANOVAs with Tukey-Kramer post tests. The one-way ANOVA tests indicated that the differences between groups were not significant ($p=0.2596$). Error bars represent standard deviations ($n=3$ for all data points).

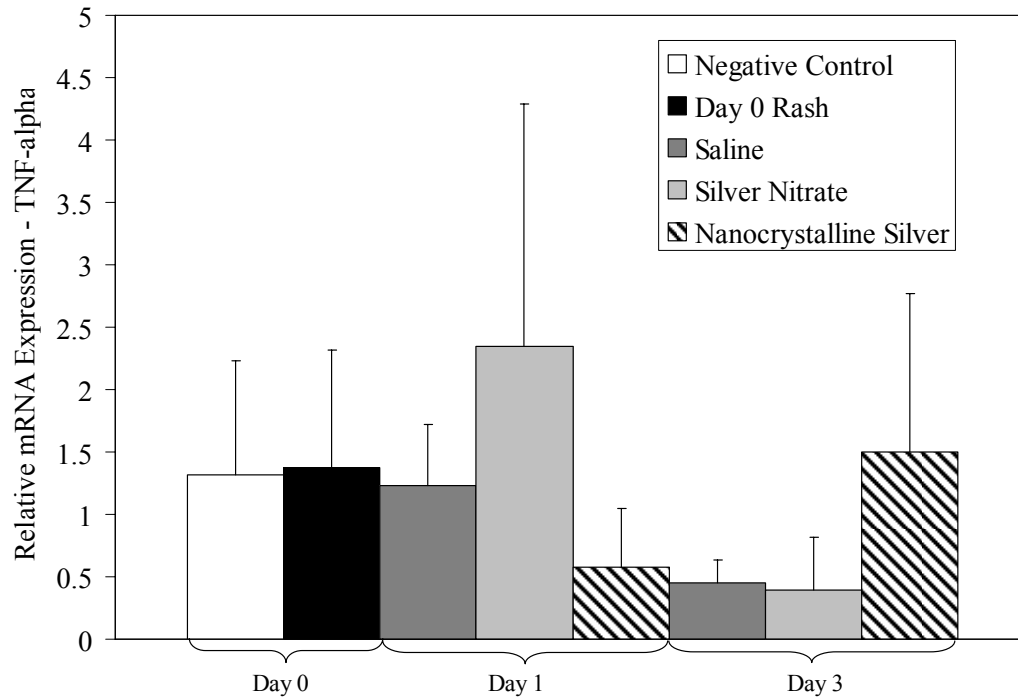


Figure 2-34. Relative expression of TNF- α mRNA in negative controls and DNCB-induced porcine rashes treated with saline, silver nitrate, or nanocrystalline silver. TNF- α mRNA levels were measured via real time RT-PCR using an Applied Biosystems 7300 Real Time PCR System. mRNA expression of TNF- α in Day 0 Rash samples, and samples treated with saline, silver nitrate, or nanocrystalline silver at Day 1 or 3 was calculated relative to the mRNA expression by negative controls. Statistical analyses were performed using one-way ANOVAs with Tukey-Kramer post tests. The one-way ANOVA tests indicated that the differences between groups were not significant ($p=0.2041$). Error bars represent standard deviations ($n=3$ for all data points).

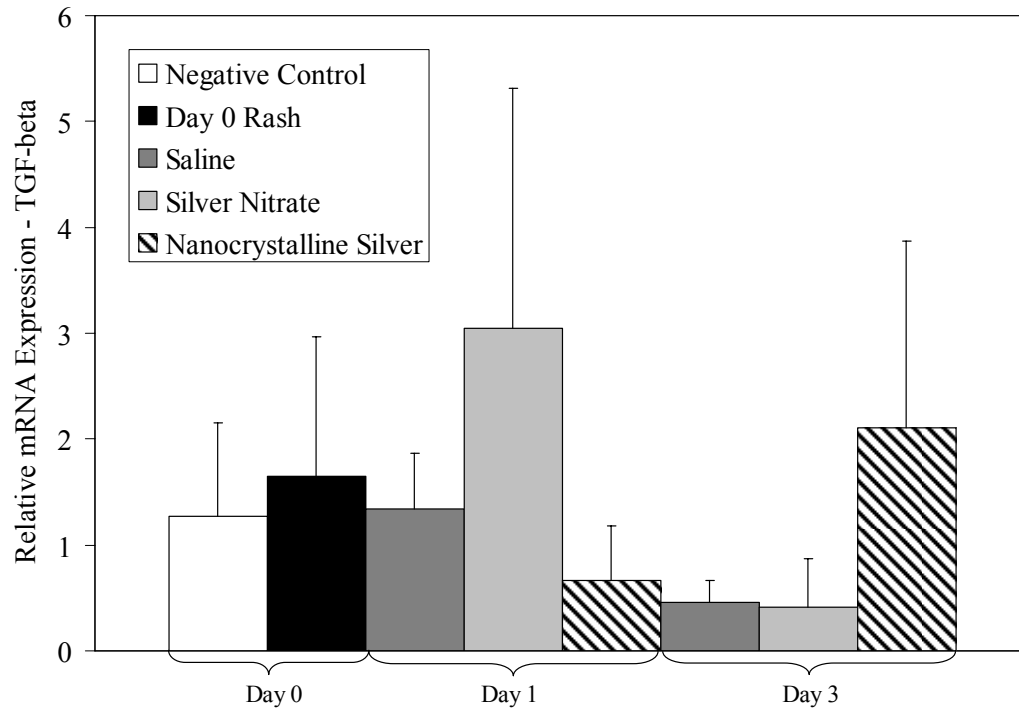


Figure 2-35. Relative expression of TGF- β mRNA in negative controls and DNCB-induced porcine rashes treated with saline, silver nitrate, or nanocrystalline silver (n=3 for each). TGF- β mRNA levels were measured using the TGF- β (2) primer set via real time RT-PCR using an Applied Biosystems 7300 Real Time PCR System. mRNA expression of TGF- β in Day 0 Rash samples, and samples treated with saline, silver nitrate, or nanocrystalline silver at Day 1 or 3 was calculated relative to the mRNA expression by negative controls. Statistical analyses were performed using one-way ANOVAs with Tukey-Kramer post tests. The one-way ANOVA tests indicated that the differences between groups were not significant (p=0.1853). Error bars represent standard deviations.

Despite eliminating the potential problem of performing measurements on two machines, there were still concerns about the data presented in Figures 2-31 through 2-35. One concern was that the pattern of expression between groups remained similar no matter what molecule was tested for. Another was that for many of the molecules tested, their mRNA expression by Day 0 rashes was lower or similar to the expression by negative controls, even though the pro-inflammatory molecule mRNA expression would be expected to be upregulated

four hours after the last application of dinitrochlorobenzene. Cytokine mRNA expression after treatment for various time points was also surprisingly low. Another concern was the large variability between samples within a group, and the lack of statistically significant data.

Because of the above concerns, experiments were run in which probes were used along with the primer sets in the Applied Biosystems 7300 Real Time PCR System in order to improve specificity of the assay, with hopes that this would also eliminate some of the variability observed. For this test, RNA was purified from a second set of snap-cooled tissue samples, and cDNA was made from this fresh RNA. The results of this testing are shown in Figures 2-36 to 2-38. The relative expression of IL-8 mRNA measured using probes is shown in Figure 2-36. IL-8 expression was highest in Day 0 rash samples. IL-8 expression decreased over time with all treatments. Saline treatment showed the highest IL-8 expression at any given time point, with nanocrystalline silver treatment showing the lowest IL-8 expression on Day 1, and silver nitrate treatment showing the lowest IL-8 expression on Day 3. Statistical analysis indicated that the differences between groups were significant ($p=0.0014$), and that silver nitrate and nanocrystalline silver treated groups at Day 3 had significantly lower IL-8 mRNA expression than Day 0 rash levels. Silver nitrate treated samples also had significantly lower IL-8 mRNA expression on Day 3, relative to saline treated samples on Day 1. However, all mRNA levels measured were equal to or lower than negative control levels, with all Day 3 treatment levels being significantly lower. Figure 2-37 shows the relative expression of IL-12 mRNA measured using

probes. Again, the negative controls showed the strongest mRNA expression, followed by the Day 0 rash samples. On Day 1, the saline treated samples had the strongest IL-12 mRNA expression, with the silver nitrate treated samples having the second highest expression on Day 1 and the lowest expression on Day 3. Samples treated with nanocrystalline silver had very similar levels on Day 1 and Day 3, making it the strongest signal on day 3. There were statistically significant differences between groups ($p < 0.0001$). Post tests indicated that all groups except the Day 1 saline treatment group had significantly lower IL-12 mRNA expression than Day 0 rash levels. Silver nitrate and nanocrystalline silver treated samples at Day 3 expressed significantly less IL-12 mRNA than the saline treated group at Day 1. However, all groups at all time points except the Day 0 Rash showed significantly lower IL-12 mRNA expression than negative controls. TNF- α mRNA expression for the various treatment groups, measured with probes, are shown over time in Figure 2-38. A similar pattern of expression was measured for this cytokine as was measured for IL-12. Again, there were significant differences between groups ($p = 0.0005$), and the Day 0 rash samples had significantly higher expression of TNF- α mRNA than any other group except the saline treated animals on Day 1. However, silver nitrate and saline treated animals on Day 3 had significantly lower levels measured compared to negative controls, and only the Day 0 rash tissues showed increased TNF- α mRNA expression relative to negative controls.

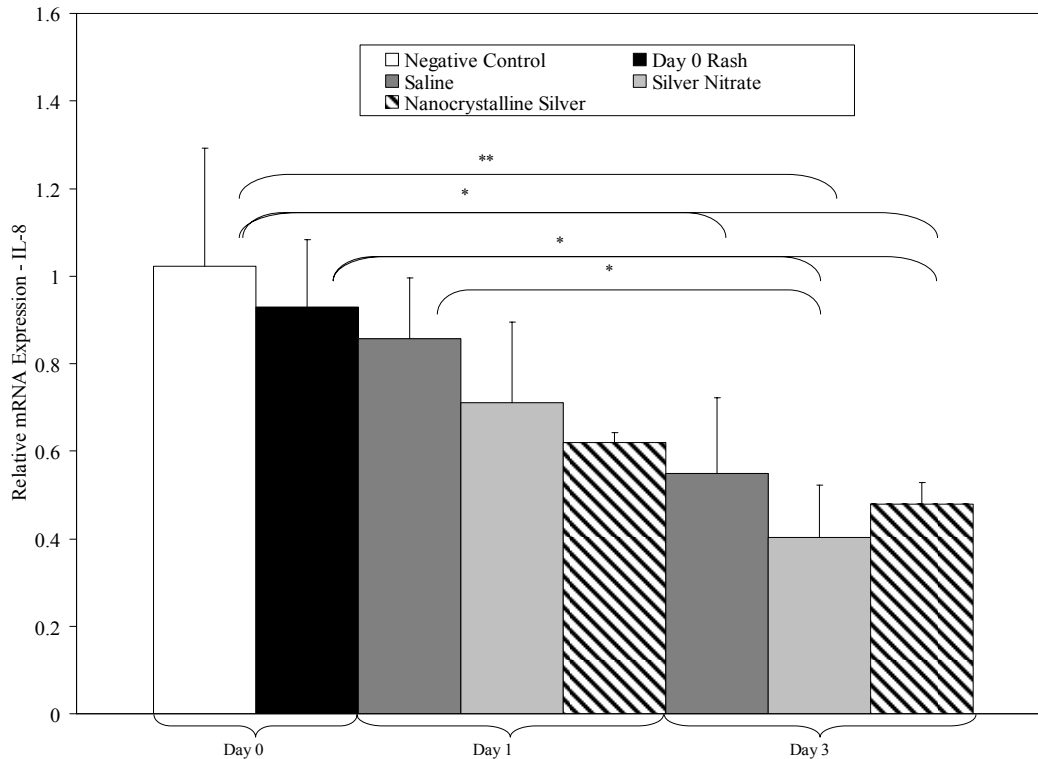


Figure 2-36. Relative expression of IL-8 mRNA in negative controls and DNCB-induced porcine rashes treated with saline, silver nitrate, or nanocrystalline silver. IL-8 mRNA levels were measured using the probe accompanying the primer set via real time RT-PCR using an Applied Biosystems 7300 Real Time PCR System. mRNA expression of IL-8 in Day 0 Rash samples, and samples treated with saline, silver nitrate, or nanocrystalline silver at Day 1 or 3 was calculated relative to the mRNA expression by negative controls. Statistical analyses were performed using one-way ANOVAs with Tukey-Kramer post tests. The one-way ANOVA tests indicated that the differences between groups were significant ($p=0.0021$). Results of the Tukey-Kramer Multiple Comparisons post tests are indicated on the figure as follows: $p<0.5 = *$, and $p<0.01 = **$. Error bars indicate standard deviations ($n=3$ for all data points).

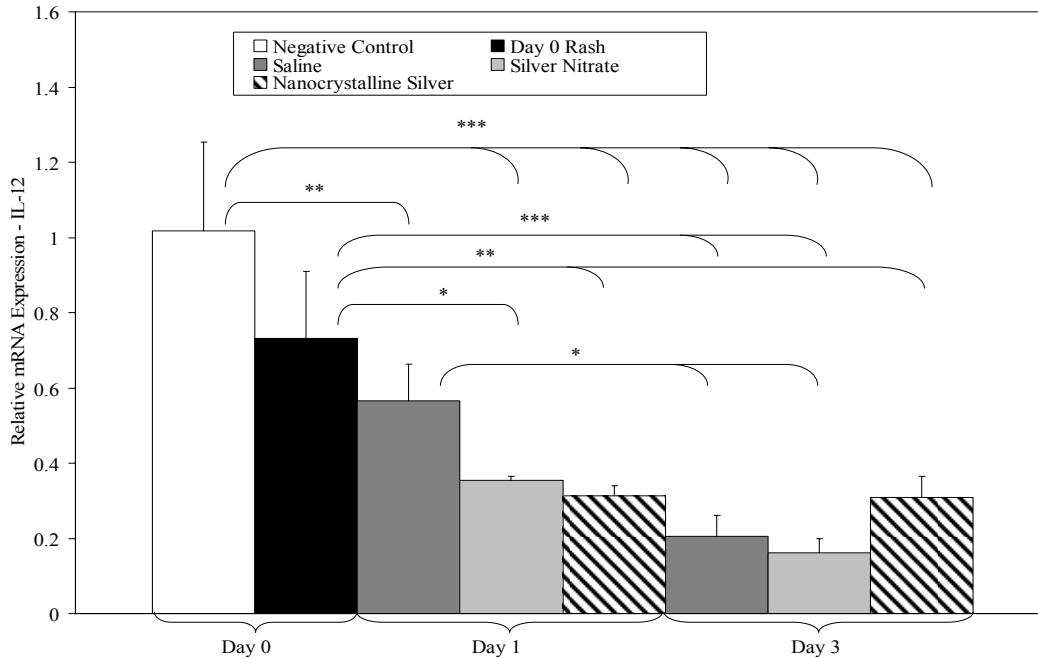


Figure 2-37. Relative expression of IL-12 mRNA in negative controls and DNCB-induced porcine rashes treated with saline, silver nitrate, or nanocrystalline silver. IL-12 mRNA levels were measured using the IL-12 (2) primers and probe set via real time RT-PCR using an Applied Biosystems 7300 Real Time PCR System. mRNA expression of IL-12 in Day 0 Rash samples, and samples treated with saline, silver nitrate, or nanocrystalline silver at Day 1 or 3 was calculated relative to the mRNA expression by negative controls. Statistical analyses were performed using one-way ANOVAs with Tukey-Kramer post tests. The one-way ANOVA tests indicated that the differences between groups were extremely significant ($p < 0.0001$). Results of the Tukey-Kramer Multiple Comparisons post tests are indicated on the figure as follows: $p < 0.5 = *$, $p < 0.01 = **$, and $p < 0.001 = ***$. Error bars represent standard deviations ($n=3$ for all data points).

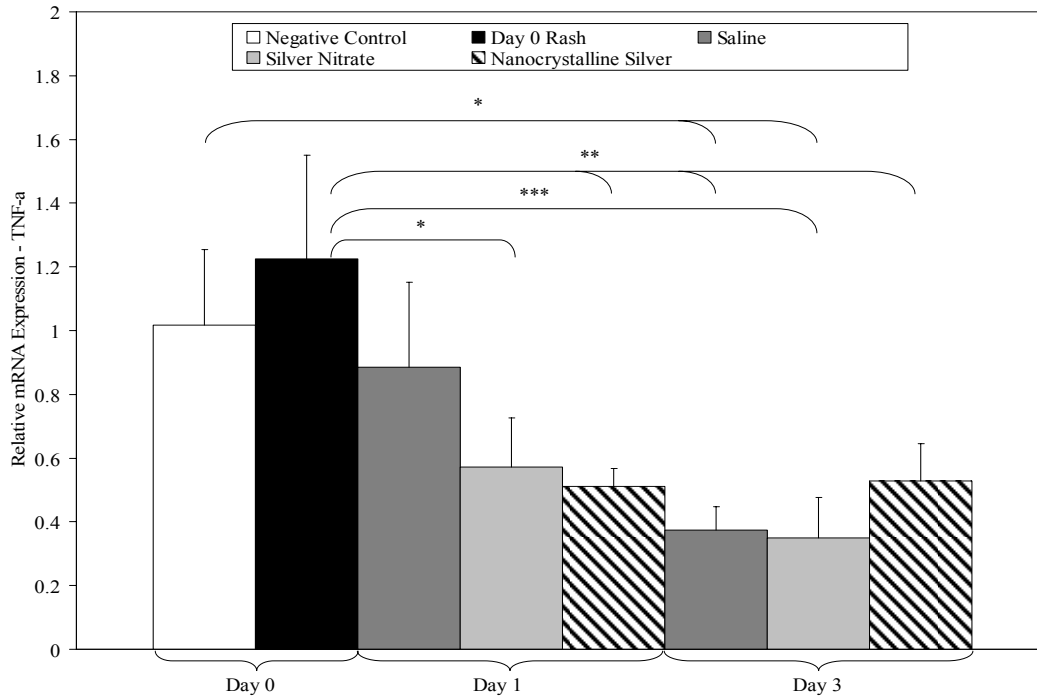


Figure 2-38. Relative expression of TNF- α mRNA in negative controls and DNCB-induced porcine rashes treated with saline, silver nitrate, or nanocrystalline silver. TNF- α mRNA levels were measured including a probe via real time RT-PCR using an Applied Biosystems 7300 Real Time PCR System. mRNA expression of TNF- α in Day 0 Rash samples, and samples treated with saline, silver nitrate, or nanocrystalline silver at Day 1 or 3 was calculated relative to the mRNA expression by negative controls. Statistical analyses were performed using one-way ANOVAs with Tukey-Kramer post tests. The one-way ANOVA tests indicated that the differences between groups were extremely significant ($p=0.0005$). Results of the Tukey-Kramer Multiple Comparisons post tests are indicated on the figure as follows: $p<0.5 = *$, $p<0.01 = **$, and $p<0.001 = ***$. Error bars represent standard deviations ($n=3$ for all data points).

Immunohistochemistry

Figure 2-39 shows representative images of immunohistochemical staining for TGF- β , TNF- α , and IL-8 for each group of pigs at 72h. Negative controls showed little TGF- β staining, with some staining localized in the epidermis (Figure 2-39a). Saline-treated and AgNO₃-treated tissues (Figure 2-39b, c) demonstrated intense staining for TGF- β . The staining appeared most widespread in AgNO₃-treated tissues, while in saline-treated tissues it was

concentrated around inflammatory cells. Nanocrystalline silver-treated pigs (Figure 2-39d) showed similar levels of TGF- β staining to negative controls.

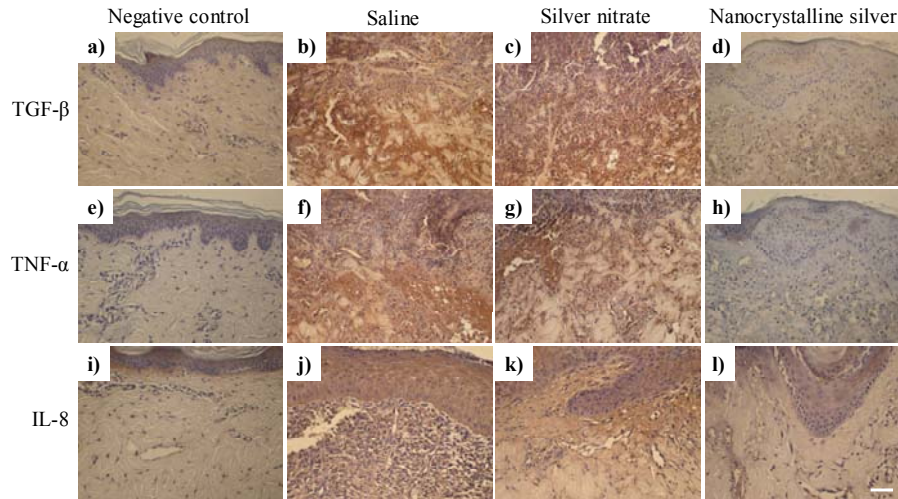


Figure 2-39. Representative images for immunohistochemical detection of cytokines after 72h of treatment of DNCB-induced porcine rashes with saline, silver nitrate, or nanocrystalline silver, as well as negative controls. The scale bar represents 50 μ m. a)-d) show staining for TGF- β , e)-h) show staining for TNF- α , and i)-l) show staining for IL-8. a), e), and i) contain images of negative control pigs; b), f), and j) contain images of saline treated pigs; c), g), and k) contain images of silver nitrate-treated pigs; and d), h), and l) contain images of nanocrystalline silver-treated pigs. Staining of TGF- β , TNF- α and IL-8 is brown, while the cell nuclei are counterstained purple using hematoxylin.

Negative controls (Figure 2-39e) showed minimal staining for TNF- α , as did nanocrystalline silver-treated pigs (Figure 2-39h). Saline-treated pigs showed widespread intense staining (Figure 2-39f) which was primarily localized to cells. AgNO₃-treated pigs had less widespread but similarly intense staining (Figure 2-39g).

Although staining was generally less intense for IL-8, a similar pattern emerged to that of TNF- α and TGF- β . There was minimal staining, with some present in the epidermis, for negative controls and nanocrystalline silver-treated pigs (Figure 2-39i, l). Saline- and AgNO₃-treated pigs (Figure 2-39j, k)

demonstrated stronger cell-associated staining.

Since there were differences in staining at 72h, immunohistochemistry was performed at 24h for TGF- β . Figure 40 shows representative images of staining in a saline treated animal (a), a silver nitrate treated animal (b), and a nanocrystalline silver treated animal (c). Although the differences are less pronounced at 24h, the same pattern is observed as that seen at 72h – the staining is clearly weaker and less diffuse in nanocrystalline silver treated animals than in silver nitrate or saline treated animals.

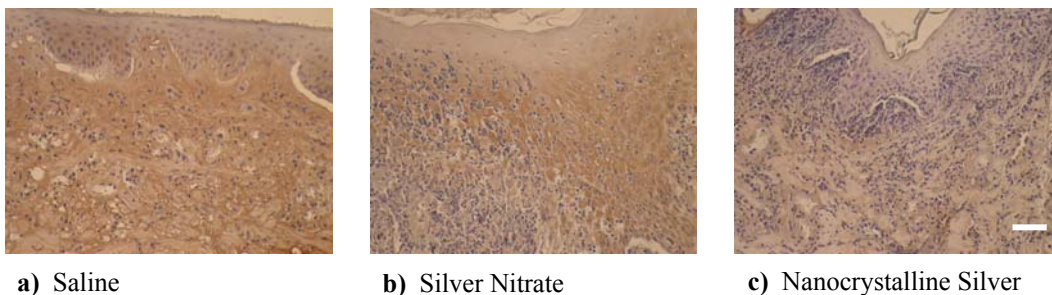


Figure 2-40. Representative images for immunohistochemical detection of TGF- β after 24h of treatment with a) saline, b) silver nitrate, or c) nanocrystalline silver. The scale bar represents 50 μ m. Staining for TGF- β appears brown, while the cell nuclei are counterstained purple using hematoxylin.

Discussion

Studies have suggested that nanocrystalline silver may have an anti-inflammatory effect[1-6], but its molecular and cellular mechanisms of action have not been fully elucidated. In this study, contact dermatitis was induced using DNCB in a porcine model. DNCB-induced dermatitis is the prototype of T-cell mediated delayed-type hypersensitivity reactions[4, 5, 29], which occur in two phases. In the sensitization phase, Langerhans cells take up haptens and present them to naïve T-cells which become active hapten-specific effector T-

cells[4, 5, 29, 30]. During the elicitation phase, reapplication of the hapten results in recruitment of these cells, which release pro-inflammatory cytokines and attract other inflammatory cells. This leads to mast cell degranulation, vasodilatation and an influx of T cells, neutrophils, and mononuclear cells, resulting in dermal inflammation[4, 5, 29, 30]. DNCB applications resulted in a consistent rash by Day 0 in this study.

Nanocrystalline silver treatments decreased DNCB-induced erythema and edema, increased apoptosis in inflammatory cells, and decreased MMP and pro-inflammatory cytokine expression compared to AgNO₃ and saline treatments. This study is believed to be the first to report a direct anti-inflammatory effect of nanocrystalline silver in a DNCB-induced porcine contact dermatitis model.

Apoptosis is a form of cell death with unique morphologic and biochemical hallmarks. It is involved in eliminating inflammatory cells from inflamed tissues[39]. Hence, compounds which induce apoptosis, such as noble metals, may be beneficial in the treatment of inflammatory diseases. Various gold-containing compounds, used as anti-inflammatory agents in the treatment of rheumatoid arthritis, induce apoptosis in cells including T-cells and macrophages through multiple mechanisms[10-13, 15, 40, 41]. The observed significant induction of apoptosis in inflammatory cells by nanocrystalline silver is consistent with the literature. For example, Bhol *et al.*[5] found that nanocrystalline silver promoted apoptosis in inflammatory cells, and Wright *et al.*[2] observed an increase in apoptosis in PMNs in wounds treated with nanocrystalline silver, but not in controls. The significant induction of apoptosis in dermal inflammatory

cells by nanocrystalline silver observed in this study suggests a highly discriminatory process, related to the unique silver species released (e.g. Ag^0), that is different from the indiscriminate activity of Ag^+ . Silver ions can interfere with the respiratory chain at the cytochromes[42] and can interact with the electron transport chain[43] to activate the intrinsic signalling pathway to apoptosis through the activation of downstream procaspases[44]. In this study nanostructured silver apoptotic activity was discriminatory (dermal cells) and AgNO_3 apoptotic activity was indiscriminate – apoptosis was induced in all cell types at the tissue surface, including keratinocytes. This has important implications for the treatment of burns and other wounds as induction of apoptosis in keratinocytes and fibroblasts would be expected to retard wound healing. This induction may be due to the release of a toxic bolus[34] of Ag^+ , resulting in indiscriminate induction of apoptosis and potentially necrosis[39]. Addition of AgNO_3 to rat mitochondria *in vitro* caused accelerated respiration and mitochondrial swelling, leading to the release of cytochrome *c*[45], which triggers events leading to apoptosis, confirming that AgNO_3 can induce apoptosis. These results contradict Moyer *et al.*[34], who indicated that 0.5% AgNO_3 treatments did not harm epithelial tissue, but that a concentration of 1% would cause necrosis. It is unlikely that the concentration of AgNO_3 would have increased to 1% in this model, as the dressings were still moist when removed and the large quantities of proteins and chlorides in the scabs likely reacted with Ag^+ , decreasing its concentration. It is also possible that the nitrate component may have a negative impact on cells[46]. In nanocrystalline silver treatments, Ag^0

clusters may induce apoptosis via cellular interactions causing the production of pro-apoptotic signal molecules which act specifically on inflammatory cells. By inducing inflammatory cells to undergo apoptosis, the cells are prevented from releasing inflammatory chemicals and attracting further inflammatory cells. They are also prevented from undergoing necrosis, in which cells burst, releasing cytotoxic inflammatory compounds including proteases, oxygen radicals, and acids[2, 12]. By undergoing apoptosis instead, these compounds are contained until they are broken down by macrophages. Thus, it appears that the increase in apoptosis of inflammatory cells observed with nanocrystalline silver treatments provides at least a partial explanation for the lower levels of inflammatory cells and the reduced inflammatory response observed[2].

In DNCB-induced contact dermatitis, pro-inflammatory cytokines including TNF- α , IL-1, and IFN- γ are upregulated due to cellular contact with haptens[47]. In this model, the primary source of TNF- α , a major inflammatory response mediator[48], was likely inflammatory cells such as T lymphocytes, PMNs, and macrophages. In nanocrystalline silver-treated animals, decreased TNF- α , as indicated by immunohistochemistry, likely resulted from the elimination of inflammatory cells by apoptosis. It should be noted that the immunohistochemical data from tissue samples taken at 72h indicates that TNF- α protein levels were much higher in saline and silver nitrate treated animals relative to negative controls. This indicates that prior to Day 3, TNF- α mRNA expression must have been increased in these animals relative to the negative controls, and therefore the data presented in Figure 2-38 is not reliable, as all

groups show lower TNF- α mRNA expression than negative controls.

IL-8 is another major mediator of inflammatory responses. Secreted by several cell types in response to inflammatory stimuli, it acts as a chemoattractant for neutrophils, basophils, and T-cells[39]. The staining pattern of IL-8 in this study resembled that of TNF- α . Decreased IL-8 in nanocrystalline silver-treated pigs may have resulted from the elimination of inflammatory cells via apoptosis. Again, the immunohistochemical data indicates an increase in the presence of IL-8 protein expression in saline and silver nitrate treated samples by 72h, relative to negative controls. This indicates that the IL-8 mRNA expression must have been increased in these tissues relative to negative controls at some point prior to this time, and therefore, as suspected, the data presented in Figure 2-36 is not reliable, as it indicates the IL-8 mRNA expression in all groups at all times was equal to or lower than that of negative controls. This indicates that the PCR experiments were flawed. One possibility is that samples were not taken soon enough to measure increased cytokine expression relative to negative controls. Another possibility is that something was wrong with the negative controls themselves, or that something went wrong during the processing of the tissues. This is suggested by the fact that the total RNA levels were similar in Day 0 rashes and negative controls, which should not have been the case, considering the cellularity present in the Day 0 rashes as indicated by the histology. Another possibility is that using HPRT as the house keeping gene (see Equation 2-2) was a poor choice, as there is some suggestion in the literature that HPRT expression can be modified during wound healing[49]. HPRT is an enzyme involved in the salvage pathway, and

can be found in high levels in healing skin wounds, particularly in keratinocytes at the hyperproliferative epithelium at wound edges[49]. While in this study, there were no open wounds, it is possible that HPRT would be upregulated while new epidermal tissues were being formed, which would impact the results, as the house keeping gene should be one whose expression is not changed during the course of the experiment. Perhaps if a larger number of pigs had been used in each group, outliers would have been evident, in which case, they could have been removed. With only three pigs per group, this was not possible. In any case, the immunohistochemical data confirms that the mRNA expression data should not be used to make any definite conclusions.

Increased TGF- β was observed after AgNO₃ and saline treatment as measured via immunohistochemistry, while nanocrystalline silver treatment decreased TGF- β staining by Day 3. TGF- β is a pleiotropic growth factor regulating many biological events including cell proliferation and differentiation, angiogenesis, and the inflammatory/immune response, where it plays a dual role[50]. TGF- β is a strong chemoattractant for leukocytes and mast cells, and thus is able to initiate an inflammatory response[51]. Later in the healing process, TGF- β contributes to the resolution of inflammation[50]. The increased TGF- β staining in the saline- and AgNO₃-treated groups likely was a measure of its role as a chemoattractant for inflammatory cells, since the tissue samples were taken early in the healing process, as indicated by the histology of saline-treated animals. Immunohistochemical data after 24h of treatment indicates that decreases in TGF- β protein expression began to occur very early with

nanocrystalline silver treatment, during the time that TGF- β plays a pro-inflammatory signalling role. Decreased TGF- β staining in nanocrystalline silver-treated tissues may, again, be due to the elimination of inflammatory cells by apoptosis.

Overexpression of matrix metalloproteinases including MMP-2 and MMP-9 contributes to tissue injury and inflammation[51]. Therefore, MMP inhibition has been suggested as a therapeutic approach to controlling inflammation[36]. In this study, MMP levels remained high throughout saline and AgNO₃ treatments with increased levels of the active forms over time. However, both pMMP-9 and aMMP-9 decreased over time with nanocrystalline silver treatment, and at 72h, levels for both were significantly lower than levels present in AgNO₃-treated tissues. A similar pattern was observed for pMMP-2, while in aMMP-2, the nanocrystalline silver-treated animals had significantly lower levels than saline-treated animals at 72h, but were not significantly different from AgNO₃-treated animals. These results showing decreased gelatinase expression and activity after nanocrystalline silver treatment corroborate the literature[2, 3], which indicates that MMP levels drop and/or remain low within the first few days of treatment with nanocrystalline silver, but are not completely eliminated. Together, these results suggest that nanocrystalline silver is capable of modulation of overall MMP presence and activity such that inflammation is decreased and healing is promoted in a variety of tissue injury models[2, 3]. It is important to note that in this study, as well as previous studies, MMP activity was never completely eliminated by treatment with nanocrystalline silver. This is

critical because, although elevated MMP levels may lead to excessive breakdown of tissues and thus to slowed healing, MMPs break down extracellular matrix and damaged cellular components, as well as creating pathways for cell migration and angiogenesis, and therefore a complete shutdown of MMP activity would prevent healing[52, 53]. Kirsner *et al.*[3] postulated that MMP modulation in nanocrystalline silver treatments could be the result of its antimicrobial activity. However, in the current study, the rashes were not infected, and so Kirsner's theory cannot explain these results. As an alternative, Kirsner *et al.*[3] also suggested that nanocrystalline silver could directly affect cytokines such as IL-1 and TNF- α , and through them impact MMP levels. This remains a possible explanation, as the current study demonstrated that treatment with nanocrystalline silver decreased the expression of pro-inflammatory molecules TNF- α , IL-8, and TGF- β , via apoptosis of inflammatory cells. Wright *et al.*[2] also suggested that the mechanism for MMP modulation by nanocrystalline silver could be partly through the induction of apoptosis in PMNs, because they produce MMPs. Thus, the decreased overall MMP expression after nanocrystalline silver treatment likely resulted from the reduction of inflammatory cells via apoptosis, since these cells contain high MMP levels[54], and produce pro-inflammatory molecules which also regulate MMP expression. The decrease in active MMPs suggests there may also be a direct or indirect suppression of MMP activity.

Consistent with the above results, the histology demonstrated that nanocrystalline silver treatment decreased inflammation. By 48h, there was decreased inflammatory cells and evidence of a new epidermis forming. By 72h,

nanocrystalline silver-treated tissues appeared similar to negative controls. In contrast, AgNO₃ and saline treatments did not demonstrate decreased inflammation over 72h. Visual observations, biopsy bleeding scores, and erythema and edema scores demonstrated a significant improvement in the rate of resolution of inflammation with the nanocrystalline silver treatments as compared to AgNO₃ or saline treatments. This is supported by observations from rodent DNCB models treated with nanocrystalline silver cream[4, 5]. Animal weights and skin thicknesses did not appear to be good measures of the pigs' response to different treatments due to high inter-animal variability, or (for the latter) treatment of tissue during collection and processing.

Overall, the results indicate that AgNO₃ is not anti-inflammatory, and may irritate the inflamed area and slow healing by inducing apoptosis of keratinocytes and fibroblasts. Other studies have demonstrated that AgNO₃ has pro-inflammatory properties in the lungs and joints[3, 55-57], confirming this outcome. Silver nitrate treatments also resulted in significantly increased mast cell counts in the epidermis and upper dermis over 72h, relative to all other treatment groups. Mast cells play a key role in allergic responses, by releasing granules containing histamine; proteoglycans such as heparin, serine proteases, prostaglandins and leukotrienes; and cytokines after contact with an allergen. They also are involved in the recruitment of inflammatory cells to the skin when activated by antibodies and complement compounds, and they are integral to the innate immune response[58]. This suggests that silver nitrate treatment in this

model may have resulted in the development of an allergic sensitivity or other immune response.

Since silver nitrate treatment, which releases only Ag^+ , did not have the same anti-inflammatory effect observed with nanocrystalline silver treatments, a species other than Ag^+ , such as soluble Ag^0 clusters[8], must be responsible for the anti-inflammatory activity of nanocrystalline silver. This suggests that the species responsible for the anti-inflammatory activity of other noble metals, such as gold, may be in a reduced cluster form. Developing a form of silver with a higher Ag^0 cluster concentration could therefore prove valuable in the treatment of anti-inflammatory diseases.

It appears that nanocrystalline silver has anti-inflammatory activity independent of its antimicrobial activity in the DNCB-induced porcine contact dermatitis model. This activity may be due in part to the induction of apoptosis in inflammatory cells, and suppression of MMP activity. Nanocrystalline silver may also suppress the production of pro-inflammatory cytokines $\text{TNF-}\alpha$, IL-8 and $\text{TGF-}\beta$, as well as others, including IL-12[5]. Due to the similarities between human and pig skin[23, 24], nanocrystalline silver may have a similar impact on the treatment of human skin inflammatory conditions, such as contact dermatitis and psoriasis.

Bibliography

1. Olson ME, Wright JB, Lam K, Burrell RE: **Healing of porcine donor sites covered with silver-coated dressings.** *Eur J Surg* 2000, **166**:486-489.
2. Wright JB, Lam K, Buret AG, Olson ME, Burrell RE: **Early healing events in a porcine model of contaminated wounds: effects of nanocrystalline silver on matrix metalloproteinases, cell apoptosis, and healing.** *Wound Repair Regen* 2002, **10**:141-151.
3. Kirsner RS, Orsted H, Wright JB: **Matrix metalloproteinases in normal and impaired wound healing: a potential role of nanocrystalline silver.** *Wounds* 2002, **13**:4-12.
4. Bhol KC, Alroy J, Schechter PJ: **Anti-inflammatory effect of topical nanocrystalline silver cream on allergic contact dermatitis in a guinea pig model.** *Clin Exp Dermatol* 2004, **29**:282-287.
5. Bhol KC, Schechter PJ: **Topical nanocrystalline silver cream suppresses inflammatory cytokines and induces apoptosis of inflammatory cells in a murine model of allergic contact dermatitis.** *Br J Dermatol* 2005, **152**:1235-1242.
6. Demling RH, Burrell RE: **The beneficial effects of nanocrystalline silver as a topical antimicrobial agent.** *Leadership Medica* 2002, **16**:10 pages.
7. Birringer R: **Nanocrystalline Materials.** *Mater Sci Eng* 1989, **A117**:33-43.
8. Fan FF, Bard AJ: **Chemical, electrochemical, gravimetric, and microscopic studies on antimicrobial silver films.** *J Phys Chem B* 2002, **106**:279-287.
9. Fuertes MA, Castilla J, Alonso C, Perez JM: **Cisplatin biochemical mechanism of action: from cytotoxicity to induction of cell death through interconnections between apoptotic and necrotic pathways.** *Curr Med Chem* 2003, **10**:257-266.
10. Mizushima Y, Okumura H, Kasukawa R: **Effects of gold and platinum on necrotizing factor, skin sensitizing antibody, and complement.** *Jpn J Pharmacol* 1965, **15**:131-134.
11. Handel ML, Nguyen LQ, Lehmann TP: **Inhibition of transcription factors by anti-inflammatory and anti-rheumatic drugs: can variability in response be overcome?** *Clin Exp Pharmacol Physiol* 2000, **27**:139-144.
12. Suzuki S, Okubo M, Kaise S, Ohara M, Kasukawa R: **Gold sodium thiomalate selectivity inhibits interleukin-5-mediated eosinophil survival.** *J Allergy Clin Immunol* 1995, **96**:251-256.
13. Eisler R: **Chrysotherapy: a synoptic review.** *Inflamm Res* 2003, **52**:487-501.
14. Wahata JC, Lewis JB, Volkmann KR, Lockwood PE, Messer RLW, Bouillaguet S: **Sublethal concentrations of Au(III), Pd(II) and Ni(II) differentially alter inflammatory cytokine secretion from activated monocytes.** *J Biomed Mater Res Part B: Appl Biomater* 2004, **69B**:11-17.

15. Abraham GE, Himmel PB: **Management of Rheumatoid Arthritis: Rationale for the Use of Colloidal Metallic Gold.** *J Nutr Env Med* 1997, **7**:295-305.
16. Zou J, Guo Z, Parkinson JA, Chen Y, Sadler PJ: **Gold(III)-induced oxidation of glycine: relevance to the toxic side-effects of gold drugs.** *J Inorg Biochem* 1999, **74**:352.
17. Bayler A, Schier A, Bowmaker GA, Schmidbaur H: **Gold is smaller than silver, crystal structures of [bis(trimesitylphosphine)gold(I)] and [bis(trimesitylphosphine)silver(I)] tetrafluoroborate.** *J Am Chem Soc* 1996, **118**:7006-7007.
18. Wyckhoff RG: *Crystal Structures*, 2nd edition. New York: Interscience Publishers; 1958: 10.
19. Pauling L: *The Nature of the Chemical Bond.*, 3rd edition. Ithaca, NY: Cornell University Press; 1980: 410.
20. Tian J, Wong KK, Ho CM, Lok CN, Yu WY, Che CM, Chiu JF, Tam PK: **Topical delivery of silver nanoparticles promotes wound healing.** *ChemMedChem* 2007, **2**:129-136.
21. Bhol KC, Schechter PJ: **Effects of Nanocrystalline Silver (NPI 32101) in a Rat Model of Ulcerative Colitis.** *Dig Dis Sci* 2007:11 pages.
22. Mast B: **Skin.** In: *Wound healing: biochemical and clinical aspects.* Ed. Cohen I, Diegelmann RF, Lindblad WJ. Philadelphia: W.B. Saunders Co.; 1992.
23. Wang JF, Olson ME, Reno CR, Kulyk W, Wright JB, Hart DA: **Molecular and cell biology of skin wound healing in a pig model.** *Connect Tissue Res* 2000, **41**:195-211.
24. Wang JF, Olson ME, Reno CR, Wright JB, Hart DA: **The pig as a model for excisional skin wound healing: characterization of the molecular and cellular biology, and bacteriology of the healing process.** *Comp Med* 2001, **51**:341-348.
25. Meyer W, Schwarz R, Neurand K: **The skin of domestic mammals as a model for the human skin, with special reference to the domestic pig.** *Curr Probl Dermatol* 1978, **7**:39-52.
26. Burd A, Kwok CH, Hung SC, Chan HS, Gu H, Lam WK, Huang L: **A comparative study of the cytotoxicity of silver-based dressings in monolayer cell, tissue explant, and animal models.** *Wound Repair Regen* 2007, **15**:94-104.
27. Galiano RD, Michaels J, Dobryansky M, Levine JP, Gurtner GC: **Quantitative and reproducible murine model of excisional wound healing.** *Wound Repair Regen* 2004, **12**:485-492.
28. Demling RH, DeSanti L: **The rate of re-epithelialization across meshed skin grafts is increased with exposure to silver.** *Burns* 2002, **28**:264-266.
29. Grabbe S, Schwarz T: **Immunoregulatory mechanisms involved in elicitation of allergic contact hypersensitivity.** *Immunol Today* 1998, **19**:37-44.

30. Scott AE, Kashon ML, Yucesoy B, Luster MI, Tinkle SS: **Insights into the quantitative relationship between sensitization and challenge for allergic contact dermatitis reactions.** *Toxicol Appl Pharmacol* 2002, **183**:66-70.
31. Laidlaw A, Flecknell P, Rees JL: **Production of acute and chronic itch with histamine and contact sensitizers in the mouse and guinea pig.** *Exp Dermatol* 2002, **11**:285-291.
32. Groth O, Skoog ML: **Measurement and differentiation of the cellular infiltrate in experimental allergic contact dermatitis.** *Acta Derm Venereol* 1979, **59**:129-134.
33. Kelley KW, Curtis SE, Marzan GT, Karara HM, Anderson CR: **Body surface area of female swine.** *J Anim Sci* 1973, **36**:927-930.
34. Moyer CA, Brentano L, Gravens DL, Margraf HW, Monafó WW: **Treatment of large human burns with 0.5% silver nitrate solution.** *Arch Surg* 1965, **90**:812-867.
35. Woods A: **Hematoxylyn and Counterstains.** In: *Laboratory Histopathology: A Complete Reference.* Eds. Woods A, Ellis R. Livingstone: Churchill Livingstone; 1994.
36. Korostoff JM, Wang JF, Sarment DP, Stewart JC, Feldman RS, Billings PC: **Analysis of *in situ* protease activity in chronic adult periodontitis patients: expression of activated MMP-2 and a 40 kDa serine protease.** *J Periodontol* 2000, **71**:353-360.
37. ***In situ* Cell Death Detection Kit, AP, Instruction Manual.** ©Roche Diagnostics Corporation. www.roche-applied-science.com/pack-insert/11684809910a.pdf. Viewed September 21, 2006.
38. **Surgical Pathology - Histology Staining Manual - Special Cells and Tissues: Mast Cells - Toluidine Blue.** In: *The Internet Pathology Laboratory for Medical Education.* ©Florida State University College of Medicine. <http://www-medlib.med.utah.edu/WebPath/HISTHTML/MANUALS/TOLUID.PDF> Viewed September 21, 2006.
39. Serhan CN, Savill J: **Resolution of inflammation: the beginning programs the end.** *Nat Immunol* 2005, **6**:1191-1197.
40. Rigobello MP, Scutari G, Boscolo R, Bindoli A: **Induction of mitochondrial permeability transition by auranofin, a gold(I)-phosphine derivative.** *Br J Pharmacol* 2002, **136**:1162-1168.
41. Glennas A, Rugstad HE: **Ploidity and cell cycle progression during treatment with gold chloride, auranofin and sodium aurothiomalate. Studies on a human epithelial cell line and its sub-strains made resistant to the antiproliferative effects of these gold compounds.** *Virchows Arch B Cell Pathol Incl Mol Pathol* 1985, **49**:385-393.
42. Bragg PD, Rainnie DJ: **The effect of silver ions on the respiratory chain of *Escherichia coli*.** *Can J Microbiol* 1974, **20**:883-889.
43. Dunn K, Edwards-Jones V: **The role of Acticoat with nanocrystalline silver in the management of burns.** *Burns* 2004, **30 Suppl 1**:S1-9.

44. Denecker G, Vercammen D, Declercq W, Vandenabeele P: **Apoptotic and necrotic cell death induced by death domain receptors.** *Cell Mol Life Sci* 2001, **58**:356-370.
45. Almofti MR, Ichikawa T, Yamashita K, Terada H, Shinohara Y: **Silver ion induces a cyclosporine a-insensitive permeability transition in rat liver mitochondria and release of apoptogenic cytochrome C.** *J Biochem (Tokyo)* 2003, **134**:43-49.
46. Demling RH, DeSanti L: **Effects of Silver on Wound Management.** *Wounds: A Compendium of Clinical Research and Practice* 2001, **13**:4-15.
47. Effendy I, Loffler H, Maibach HI: **Epidermal cytokines in murine cutaneous irritant responses.** *J Appl Toxicol* 2000, **20**:335-341.
48. Girolomoni G, Pastore S, Albanesi C, Cavani A: **Targeting tumor necrosis factor-alpha as a potential therapy in inflammatory skin diseases.** *Curr Opin Investig Drugs* 2002, **3**:1590-1595.
49. Beer HD, Gassmann MG, Munz B, Steiling H, Engelhardt F, Bleuel K, Werner S: **Expression and function of keratinocyte growth factor and activin in skin morphogenesis and cutaneous wound repair.** *J Investig Dermatol Symp Proc* 2000, **5**:34-39.
50. Wahl SM: **Transforming growth factor-beta: innately bipolar.** *Curr Opin Immunol* 2007, **19**:55-62.
51. Li AG, Lu SL, Han G, Hoot KE, Wang XJ: **Role of TGFbeta in skin inflammation and carcinogenesis.** *Mol Carcinog* 2006, **45**:389-396.
52. Saarialho-Kere UK: **Patterns of matrix metalloproteinase and TIMP expression in chronic ulcers.** *Arch Dermatol Res* 1998, **290 Suppl**:S47-54.
53. Kahari VM, Saarialho-Kere U: **Matrix metalloproteinases in skin.** *Exp Dermatol* 1997, **6**:199-213.
54. Stockley RA: **Neutrophils and protease/antiprotease imbalance.** *Am J Respir Crit Care Med* 1999, **160**:S49-52.
55. Teixeira LR, Vargas FS, Acencio MM, Paz PF, Antonangelo L, Vaz MA, Marchi E: **Influence of antiinflammatory drugs (methylprednisolone and diclofenac sodium) on experimental pleurodesis induced by silver nitrate or talc.** *Chest* 2005, **128**:4041-4045.
56. Fyfe MC, Chahl LA: **The effect of single or repeated applications of "therapeutic" ultrasound on plasma extravasation during silver nitrate induced inflammation of the rat hindpaw ankle joint *in vivo*.** *Ultrasound Med Biol* 1985, **11**:273-283.
57. Chahl JS, Chahl LA: **The role of prostaglandins in chemically induced inflammation.** *Br J Exp Pathol* 1976, **57**:689-695.
58. Prussin C, Metcalfe DD: **4. IgE, mast cells, basophils, and eosinophils.** *J Allergy Clin Immunol* 2003, **111**:S486-494.

Chapter 3 – Systemic Effect of Nanocrystalline Silver Dressings¹

Introduction

Studies have demonstrated that nanocrystalline silver has pro-healing and anti-inflammatory activity in infected wounds, rashes, and meshed skin grafts[1-4]. In Chapter 2, it was shown that nanocrystalline silver had an anti-inflammatory effect independent of its antimicrobial activity[5]. However, the study did not elucidate the mechanisms of action for this effect. One possible mechanism was that silver molecules traveled to, and directly interacted with, individual inflammatory cells, causing their apoptosis. This then led to reduced inflammation via reduced production and activation of MMPs, and reduced production of pro-inflammatory signaling molecules. Another possibility was that nanocrystalline silver interacted with native cell types near tissue boundaries, causing them to release biological signals which modified the inflammatory cascade, resulting in the anti-inflammatory effects described in Chapter 2. If the latter was the primary mechanism of action, then nanocrystalline silver could have an impact on inflammation distant from the site of treatment. Interestingly, clinical observations have suggested that nanocrystalline silver may have anti-inflammatory/pro-healing effects on tissues in locations distant from the treatment site (personal communications, Dr. Burrell). In addition, a study of adjuvant arthritis in rat paws showed that when a solution containing silver proteinate, gold thioglucose, and copper gluconate was injected intraperitoneally, the paws had improved healing relative to controls[6].

¹ A version of this chapter has been submitted for publication. Nadworny, Landry, Wang, Tredget, and Burrell, 2009. Wound Repair and Regeneration.

The purpose of this study was to determine whether the anti-inflammatory effect of nanocrystalline silver occurs solely through direct action on cells such as inflammatory cells, or whether it works by triggering a biological cascade resulting in indirect anti-inflammatory effects. A second goal of this study was to determine whether or not nanocrystalline silver treatments could result in anti-inflammatory/pro-healing effects on tissues distant from the site of application of nanocrystalline silver, and if so, to determine some of the signaling molecules involved in this effect.

Materials and Methods

Materials

Unless otherwise mentioned, all reagents were purchased from Fisher Scientific Inc.

Samples

Tissue samples and blood samples from animals used in the study performed in Chapter 2 were used in this chapter as indicated. Please see Chapter 2 for the procedures performed on these animals. Positive controls from the experiment in Chapter 2 were also used as positive controls for the animal study performed in this chapter, since this study was performed in parallel to the study in Chapter 2.

Testing for Silver Deposition in Tissues

XPS and SIMS

X-ray photoelectron spectroscopy (XPS) and Time-of-Flight secondary ion mass spectrometry (ToF-SIMS) were used to detect the presence, depth, and

concentration of various silver species in paraffinized porcine tissue samples from Chapter 2 which were treated directly with nanocrystalline silver, silver nitrate, or saline. Tissues of the negative controls were also analyzed. Prior to analysis, samples were deparaffinized as follows: Tissue samples were incubated at 60°C for half an hour. They were then placed in 100% xylene for five minutes, transferred to fresh 100% xylene for another five minutes, and then placed in 100% ethanol for 10 minutes to remove the xylene. They were then allowed to air dry.

XPS was completed using an Axis Ultra spectrometer (Kratos Analytical, Shimadzu Corp., Kyoto, Japan) with a base pressure of 5×10^{-10} Torr, at the Alberta Center for Surface Engineering and Science (ACSES). The x-rays were generated using an Al Mono ($K\alpha$) source operated at 210 W. Spectra were collected at normal (90°) take-off angle, with an analyzer pass energy of 160 eV. The analysis was performed in the mid-dermis and in the subcutaneous fat layer.

ToF-SIMS was performed using an ION-TOF IV (ION-TOF GmbH, Munster Germany) in the imaging operational mode, at ACSES. Scans were performed at the tissue surfaces to obtain mass spectra and mass-selective images for tissues after 24 and 72 hours of treatment. Optical images were taken parallel to the ToF-SIMS images to locate tissue morphology in the SIMS images. Gallium ions were used as an analytical beam, and the Ga^+ gun was operated at 25 keV in a static mode. Burst alignment mode was used for the mapping. The size of the area mapped is shown on each image. Both positive and negative secondary ions were collected. Metallic silver, silver nitrate, silver chloride,

silver oxide, and silver cluster species weights were analyzed (see weights tested in Table 3-1), using instrument software to generate the mass-selective images. The images generated show the summed intensities for all weights tested for each silver species. The total counts (tc) and maximum intensities (mc) were measured for each image to compare the levels of silver in the different tissues. mcs from multiple images for each tissue were averaged and tested for statistically significant differences. Each image was scaled from 0 to its mc.

Table 3-1. Weights used in SIMS analysis.

Species	Isotopes	Atomic Weights Analyzed
Ag	Ag: 107, 109	107, 109
AgO	Ag: 107, 109; O: 16	123, 125
AgCl	Ag: 107, 109; Cl: 35, 37	142, 144, 146
AgNO ₃	Ag: 107, 109; N: 14, 15; O: 16	169, 170, 171, 172
Ag ₂	Ag: 107, 109	214, 216, 218
Ag ₂ O	Ag: 107, 109; O: 16	230, 232, 234
Ag ₃	Ag: 107, 109	321, 323, 325, 327
Ag ₄	Ag: 107, 109	428, 430, 432, 434, 436
Ag ₅	Ag: 107, 109	535, 537, 539, 541, 543, 545
Ag ₆	Ag: 107, 109	642, 644, 646, 648, 650, 652, 654
Ag ₇	Ag: 107, 109	749, 751, 753, 755, 757, 759, 761, 763

Testing for Remote Anti-inflammatory/Pro-healing Effects

Animals

Three young domestic, commercially produced, Large White/Landrace swine (20-25 kg) were used in this study, which was performed in parallel to the study of Chapter 2. The animals selected were healthy and without significant wounds or scars on their backs. The animals were kept at the SRTC under the same conditions as those described in Chapter 2 (individual pens, 12 hour light/dark cycle, seven day acclimatization period, *ad libitum* antibiotic-free water

and hog ration). Rations were limited prior to procedures on Day 0 through 3.

The study was approved by the HSAPWC and was conducted with humane care of the animals in accordance with guidelines established by the CCAC.

Sensitization to DNCB and Elicitation of Inflammatory Reaction

Inflammation was induced as described in Chapter 2. Briefly, on Day -14, the hair on the left side of the three pigs' backs was shaved, and 10% DNCB (in 4:1 acetone:olive oil) was painted over the shaved area as described in Chapter 2 (25 cm x 15 cm, caudal to the scapula running over the rib cage and five centimeters off the dorsal median line, for a total body surface area of approximately 5%[7]). The volume of DNCB painted per pig was 7 mL on average, as before. This procedure was repeated on Days -7, -3, and 0. On Day -1, the pigs were given transdermal fentanyl patches on shaved skin away from the rash and the future location of the treatment area (between their shoulder blades) to mitigate potential discomfort during the final application and treatment period without impacting the inflammation in the skin or the treatment. Animals were weighed on Day 0 before commencing treatment.

Treatment

Four hours after the final application of DNCB, treatment of the pigs was commenced with the pigs being placed under general anesthetic. On Day 0, visual observations were made (see procedure below), and blood samples were taken from the anterior vena cava. Six 4 mm biopsies were obtained from the rash and randomly assigned for different analyses as described in Chapter 2. On Day 0, skin samples were obtained near the front of the rash, but well within its

borders. On subsequent days, biopsies were taken in a line caudally, spaced such that newly biopsied tissues would not be influenced by previous biopsies. Calcium alginate dressings were used to achieve hemostasis. The pigs' rashes were then treated with a sterile dressing composed of two layers of HDPE with a rayon/polyester core (same composition as the nanocrystalline silver dressings) moistened with sterile 0.9% saline. On the right side of the pigs' backs, the hair was shaved from an area of the same size as the rash (15 cm x 25 cm), and nanocrystalline silver dressings moistened with sterile reverse osmosis water were placed over the shaved area. These animals, which received nanocrystalline silver on the opposite side of their back from the rash, and had saline placed directly on the rash, will herein be referred to as receiving "remote" nanocrystalline silver. Surgical drape was placed over both dressings on each pig to provide moisture control, and Elastoplast adhesive dressing was wrapped around the pigs to hold their dressings in place. New fentanyl transdermal patches were applied as needed.

The procedure of Day 0 was repeated on Day 1 and Day 2, except that no blood samples were taken. On Day 3, blood samples and weights were again taken, and biopsies and visual inspections were performed, and then the pigs were euthanized using Euthansol (>150 mg/kg) while still under anesthesia.

Visual Observations

Pictures were taken of the rash areas on each treatment day. Erythema and edema scores were graded on a scale of 0-4 on Day 0 through 3, with the scoring system described in Chapter 2. The pigs were also scored on the level of bleeding

at biopsy sites on Day 2 and Day 3, with -1 indicating minimal bleeding, 0 indicating moderate bleeding, and +1 indicating considerable bleeding. The scores were the result of observation by three people.

Storage of Blood Samples

Blood samples for serum analysis were collected into heparin-free tubes for the groups of pigs described in Chapter 2, as well as for this group of pigs. The samples were kept at room temperature, and then centrifuged for 15 minutes at 1500 rpm. The supernatant was then collected (3-4 mL) and stored at -20°C.

Histopathology

All samples to be paraffinized were placed in 4% neutral buffered paraformaldehyde. They were then rinsed with PBS three times before being placed in 70% ethanol and stored at 4°C. The samples were then dehydrated in alcohol and xylene; oriented and embedded in paraffin; and sectioned (5 µm). For histopathological analysis, sections were stained with hematoxylin and eosin following standard procedures[8]. Representative images (100x magnification, showing the epidermal-dermal junction, with no more than half the image taken up by the epidermis) were taken of the slides using an optical microscope with an attached digital camera (Nikon Optiphot I, with Nikon Coolpics 950).

Apoptosis Detection and Quantification

Detection of the presence of apoptotic cells in tissue samples of positive controls and animals treated indirectly with nanocrystalline silver was performed using the In Situ Cell Death Detection Kit (Roche Applied Sciences, Basel, Switzerland), as described in Chapter 2, with a few modifications. Briefly, testing

was performed on paraffinized tissue samples following the manual provided with the kit[9]. Dewaxing and rehydration was performed as described in Chapter 2. After rehydration, the samples were treated with 100 μ L proteinase K at a working concentration of 25 μ g/mL, and incubated for half an hour at 37°C. The slides were then rinsed three times for five minutes each in 1xPBS. Positive controls for the apoptosis assay were treated with a 1:200 dilution of a 151 units/ μ L DNase stock solution (in PBS), and incubated at room temperature for 15 minutes.

All tissues were then incubated overnight with a FITC-labeled dNTP and TdT working solution at 4°C. Labeling solution only was added to the negative controls for the apoptosis assay. After overnight incubation, the cells were rinsed in PBS three times for 10 minutes each. The tissue samples were mounted using a polyvinyl alcohol based mounting medium containing 1:1000 DAPI (4',6-diamidino-2-phenylindole, provided by the Department of Oncology Cell Imaging Facility, University of Alberta) for nuclear counterstain. Sections were then examined, and images obtained, using a Zeiss LSM510 multi-channel laser scanning confocal microscope (Carl Zeiss MicroImaging GmbH, Oberkochen, Germany) at the Department of Oncology Cell Imaging Facility, University of Alberta. Images were taken of the epidermal-dermal junction of samples from each pig using the following settings: objective: 40x 1.3; laser for DAPI: 364 nm, 1% power, 477 μ m pinhole; and laser for FITC: 488 nm, 10% power, 66 μ m pinhole. Quantitative analysis was performed using ImageJ software (Rasband, W., v1.37, NIH, Rockville, MD, USA. © 2007). Images were excluded when

apoptotic and nuclear staining did not coincide. The epidermis or dermis was manually selected. A set threshold was used for all samples, since they were processed on the same day, and stained and imaged under identical conditions. Total numbers of green (apoptotic stained) and blue (nuclear stained) pixels were counted. A ratio of green to blue pixels was calculated to obtain a relative concentration of cells undergoing apoptosis.

Immunohistochemistry

Paraffinized tissue sections from rash biopsies after treatment for 24h and 72h (remote nanocrystalline silver, direct nanocrystalline silver, or saline only) were analyzed for the presence of TNF- α , IL-8, IL-4, IL-10, TGF- β , EGF, KGF (FGF-7), and KGF-2 (FGF-10). Paraffinized samples were deparaffinized and rehydrated (see Chapter 2). To improve antigen retrieval, samples used to test for TNF- α , IL-8, and KGF were incubated in 25 μ g/mL proteinase K at 37°C for 20 minutes. All samples were then treated with 3% H₂O₂ for 30 minutes at room temperature to quench endogenous peroxidase activity, and then blocked for one hour at room temperature with the sera from the species that the secondary antibody was raised in (rabbit for TGF- β 1, KGF, KGF-2, or IL-4 analysis; goat for TNF- α , IL-8, IL-10, or EGF analysis). For TGF- β analysis, sections were then incubated for one hour at room temperature with a chicken-anti-hTGF- β 1 (10 μ g/mL, AF-101-NA, R&D Systems, Minneapolis, MN, USA). Control tissues were incubated with chicken IgG (10 μ g/mL). The sections were subsequently incubated with rabbit-anti-chicken antibody conjugated with horseradish peroxidase (Sigma, Product A 9046, 1:400 plus 2% pig serum) for an

hour. For all other analyses, sections were incubated overnight at 4°C with 5 µg/mL of the appropriate antibody: mouse-anti-pTNF-α (MP390, Endogen), mouse-anti-pIL-8 antibody (MP800, Endogen), goat-anti-pIL-4 (AF654, R&D Systems), mouse-anti-hEGF (MAB236, R&D Systems), mouse-anti-pIL-10 (MAB6932, R&D Systems), goat-anti-hFGF-7 (KGF, AF-251-NA, R&D Systems), or goat-anti-hFGF-10 (KGF-2, AF345, R&D Systems). For sections incubated with primary antibodies produced in mouse, negative control tissues were incubated with 5 µg/mL mouse IgG during the primary antibody incubation step. These sections were subsequently incubated with a goat-anti-mouse-HRP solution (R&D Systems, 1:400 plus 2% pig serum) for one hour at room temperature. For sections incubated with primary antibodies produced in goat, negative control tissues were incubated with PBS during the primary antibody incubation step (using a 1:50 dilution of goat serum invariably resulted in dark staining of the negative controls). These sections were subsequently incubated with a rabbit-anti-goat-HRP solution (R&D Systems, 1:400 plus 2% pig serum). All tissues were then stained using DAB and H₂O₂ (25 mg DAB, 50 µL H₂O₂ in 50 mL PBS). The samples were then washed in double distilled water, and counterstained with hematoxylin (30 seconds), followed by washing in double distilled water. To preserve the tissues, the cells were dehydrated by successive placement in 70%, 90%, and three rounds of 100% ethanol for one minute each, followed by two rounds of 100% xylene for five minutes each. Coverslips were then mounted using Permount™ mounting solution. Images of the samples were taken as described for histology images. Samples stained for one cytokine were

all run at the same time under identical conditions, including exposure time, temperatures, and dilutions. Therefore, the intensity of staining can be used as a qualitative indication of the relative quantity of cytokines present in the tissues. Negative controls for the experiment, which were performed in parallel to each test tissue, were stain-free.

Testing for Systemic Effect Via the Blood

IL-10 Detection (Tissue) and Quantification (Serum)

IL-10 detection in tissues from Chapter 2 was performed using a polyclonal antibody before the IL-10 monoclonal antibody was developed which was used above. The techniques and results are provided for comparison purposes. Paraffinized samples were deparaffinized and rehydrated. For antigen retrieval, the samples were incubated in 25 µg/mL proteinase K at 37°C for 20 minutes. They were next treated with 3% H₂O₂ for 30 minutes at room temperature to quench endogenous peroxidase activity, and then blocked for one hour at room temperature with rabbit serum. Sections were then incubated with the primary antibody, goat-anti-pIL-10 (15 µg/mL, AF693, R&D Systems), overnight at 4°C in a dark moist chamber. Negative controls were incubated in goat serum diluted 1:50 in PBS. The sections were subsequently incubated with rabbit-anti-goat-HRP (1:200 dilution in PBS with 2% pig serum, Sigma, Product A 5420) for an hour. Cytokines in the tissues were then stained using DAB and H₂O₂ (25 mg DAB, 50 µL H₂O₂ in 50 mL PBS). The samples were then washed in double distilled water, and counterstained with haematoxylin (30 seconds), followed by washing in double distilled water. To preserve the stained tissues,

the cells were dehydrated as described above, and then mounted using PermountTM mounting solution. All samples stained for one cytokine were run at the same time under identical conditions, including exposure time, temperatures, and dilutions. Using this method, there was non-specific staining, including on negative controls. To try to improve specificity of stain, a citrate buffer (0.01M citric acid in PBS) treatment for antigen retrieval was used. The slides were placed in citrate buffer, covered and microwaved until the buffer boiled (approximately 40s). After five minutes, it was microwaved for another five seconds, and then allowed to cool for an hour. Other slides were treated with a proteinase K antigen retrieval step. The tissues were added to 0.5 mg/mL proteinase K and incubated at 37°C for 20 minutes. Lower concentrations of the primary antibody were also used (5 µg/mL). Incubations were tried where the primary antibody and the negative controls (goat serum) were made up in 10% rabbit serum in PBS. The secondary antibody was also diluted 1:400. However after all these changes, the negative controls still stained strongly, although there seemed to be some improvement in the specificity of the staining of the samples. Samples were tried in which the negative controls were incubated overnight in PBS without goat serum. As well, the primary antibody was pre-incubated with 1% pig serum in an attempt to block non-specific staining. While these modifications decreased the staining present on the negative control tissues, there still appeared to be non-specific staining on the tissues treated with the primary antibody, such as staining of the collagen, where IL-10 is unlikely to be present. This suggests that the primary antibody obtained from R&D Systems (AF693)

may not be truly specific for immunohistochemical analysis of paraffinized pig skin, which may perhaps be due to the fact that it is a polyclonal antibody. This is why subsequent experiments described above, and in Chapter 7, used the monoclonal antibody described earlier in this chapter.

Serum IL-10 levels were analyzed using a Quantikine Porcine IL-10 immunoassay kit (P1000, R&D Systems). This analysis was also performed before the monoclonal antibody for IL-10 immunohistochemistry was available. All solutions were allowed to reach room temperature before starting the experiment. The kit control was reconstituted with 1 mL distilled water. The kit control contains lyophilized recombinant porcine IL-10, and the concentration measured when this sample is reconstituted can be used to check the accuracy of the assay. 1 mL of conjugate concentrate was added to 22 mL of conjugate diluent in the dark. The conjugate concentrate contains a polyclonal antibody against porcine IL-10 conjugated to horseradish peroxidase. 25 mL of wash buffer concentrate was added to 600 mL of double distilled water. The lyophilized pIL-10 standard was reconstituted with 2.0 mL of calibrator diluent RD6-33 (a buffered protein solution) to produce a stock solution of 2000 pg/mL, which was gently mixed for five minutes. 2-fold dilutions of this stock solution down to 31.25 pg/mL were made by adding 300 μ L of the solution to 300 μ L of the calibrator diluent RD6-33. The calibrator diluent RD6-33 alone was used as a 0 pg/mL standard. 120 μ L of each serum sample was diluted 2-fold in Calibrator Diluent RD6-33 for a total volume of 240 μ L. 100 μ L of assay diluent RD1W (a buffered protein solution) was added to the wells of the porcine IL-10 microplate,

which is coated with a mouse monoclonal antibody specific for porcine IL-10. 100 μ L of sample, control, or standard was added to each well. The microplate was then placed in a moist dark chamber and incubated at room temperature on a shaker for two hours. The wells were then decanted and washed by filling each well with wash buffer (approximately 400 μ L). The wells were decanted and tapped dry, and this procedure was repeated four times. Next, 200 μ L of the dilute pIL-10 conjugate was added to each well, and the wells were again placed in a moist, dark chamber and incubated for two hours at room temperature on a shaker. The wells were decanted and washed, as above. Color reagents A and B were mixed 1:1 within 15 minutes of use. Color reagent A is stabilized hydrogen peroxide, and color reagent B is stabilized tetramethylbenzidine (a chromogen). 120 μ L of this substrate solution was added to each well. The wells were then incubated for 30 minutes at room temperature in a dark moist chamber (not on a shaker). As there was limited color development, the wells were incubated for an additional 10 minutes at room temperature, followed by a 20 minute incubation at 37°C. At this point, 120 μ L of the stop solution (dilute hydrochloric acid) was added to each well and the wells were tapped to ensure good mixing. The optical density of each well was measured within 30 minutes, using a microplate reader (Thermomax Microplate Reader, Molecular Devices, Inc., Sunnyvale, CA, USA) at 450 nm, with wavelength correction at 540 nm. The absorbance of the standards was plotted against the concentration of each standard, with the background absorbance (read using the 0 pg/mL sample) subtracted from each sample. A best fit log curve was drawn using the data from the standards which

covered the range of the sample optical densities (see Figure 3-1). However, when the concentrations of the test samples were then calculated by interpolating from the curve, the optical density of many of the samples was below that of the lowest standard, and thus, the best fit logarithmic equation produced large negative numbers for these samples. Therefore, a linear best fit was performed instead, which appeared to be a good fit for the optical densities over the entire range of standards (see Figure 3-2). The background absorbance was subtracted from the sample optical densities, and the concentration of IL-10 in serum sample was calculated by interpolating from the linear best fit curve and multiplying the interpolated value by the appropriate dilution factor. A few samples had negative optical densities after the background absorbance was subtracted from the sample optical density, and the IL-10 concentration in these samples was set to zero.

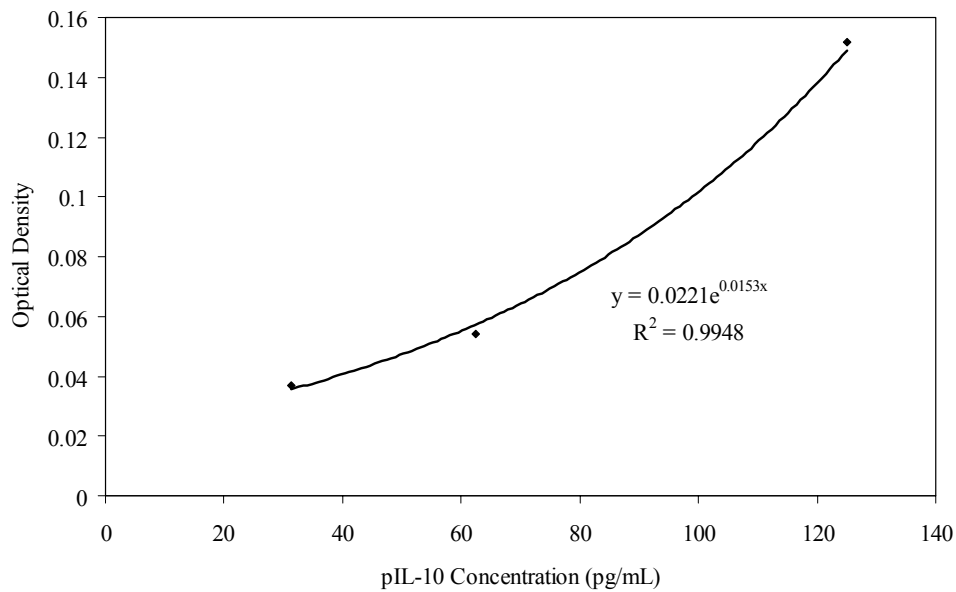


Figure 3-1. Standard curve for the optical densities of the lowest concentration standards versus pIL-10 concentration (pg/mL). Standards were created by dilution of a pIL-10 standard which came with the Quantikine Porcine IL-10 immunoassay kit. A logarithmic fit was performed in Excel for the region shown, and the resulting equation and R^2 value are displayed on the figure.

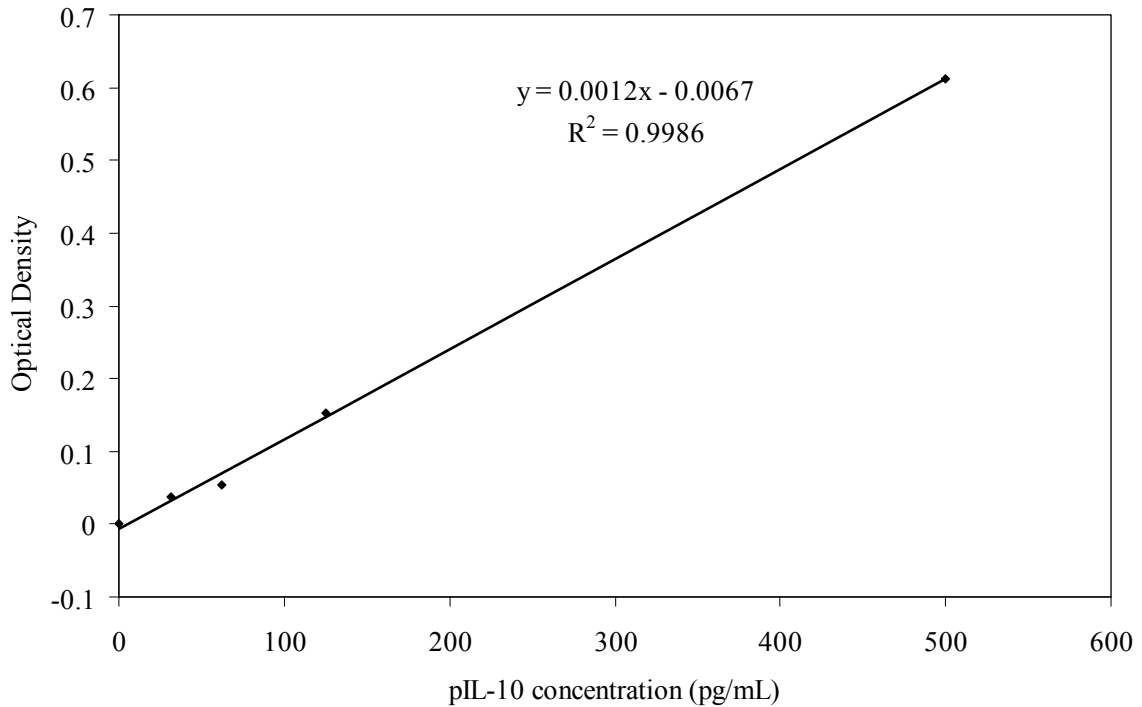


Figure 3-2. Standard curve for the optical densities of all standards versus pIL-10 concentration (pg/mL). Standards were created by dilution of a pIL-10 standard which came with the Quantikine Porcine IL-10 immunoassay kit. A linear fit was performed in Excel over the entire concentration region as shown, and the resulting equation and R^2 value are displayed on the figure.

Serum c-Reactive Protein Quantification

CRP serum concentrations were quantified using a “PHASE” CRP-Porcine Species Specific Acute Phase Protein Assay kit (Tridelta Development, Ltd., Bray County, Wicklow, Ireland). Concentrated diluent and wash buffer from the kit were diluted 1:10 and 1:20 with distilled water, respectively. Serum samples were diluted 1:100 in sample dilution buffer prior to the start of the procedure. A 1:10 dilution was also tried on one sample from each group. A 1500 ng/mL standard was provided with the kit and two fold dilutions in the diluent buffer were used to make standards down to 46.9 ng/mL. Diluent buffer alone was used for the 0 ng/mL standard. 100 μ L of diluted sample or standard

was added to each well of the microplate, which was coated with an antibody specific for porcine CRP. The wells were incubated in a dark, moist chamber at 37°C for 15 minutes. The plates were then decanted and washed four times with diluted wash buffer, as described above for the IL-10 quantification procedure. Next, 100 µL of anti-porcine CRP conjugate was added to each well, and the wells were again incubated in a dark, moist chamber for 15 minutes at 37°C. The wells were again decanted and washed four times as described above. Next, 100 µL of TMB substrate solution was added to each well, which were then incubated in a dark, moist chamber for 15 minutes at room temperature. 100 µL of stop solution was then added to each well, and the absorbance of each well was read at 450 nm. A standard log curve was made as described above, with the background absorbance subtracted from the optical densities of the standard solutions (see Figure 3-3). The background absorbance was also subtracted from the optical densities of the samples, and then the concentrations of CRP in test samples were determined from the standard curve by interpolating and multiplying that value by the appropriate dilution factor. With a 1:100 dilution, the optical densities in the samples were all higher than the most concentrated standard, therefore an additional 3-fold dilution was performed, for a final dilution of 1:300, and the test was repeated.

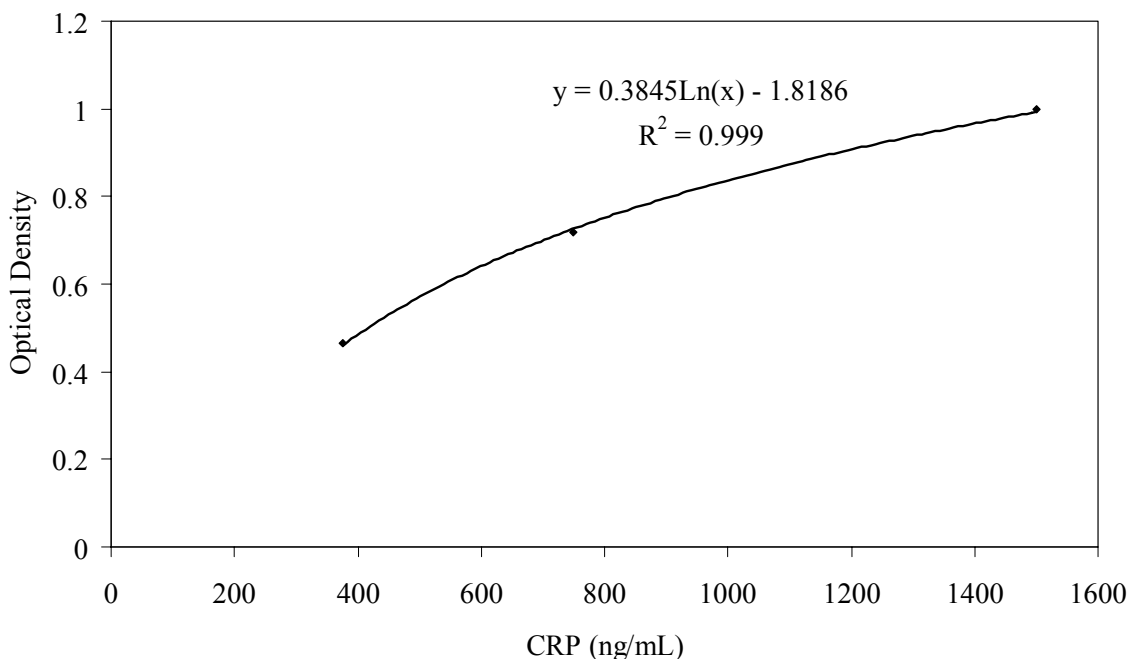


Figure 3-3. Standard curve for the optical densities of the highest concentration standards versus CRP concentration (ng/mL). Standards were created by dilution of a CRP standard which came with the PHASE Porcine CRP kit. A logarithmic fit was performed in Excel for the region shown, and the resulting equation and R^2 value are displayed on the figure.

Statistics

Results of treatments with remote nanocrystalline silver were compared to results for positive control animals treated with saline only. Tests were performed on all pigs in each group to confirm result repeatability. When selecting images for inclusion, all images were viewed together, and the median image in terms of tissue structure and staining intensity was selected. For numerical results, one-way ANOVAs with the Tukey-Kramer Multiple Comparisons post test were performed using GraphPad InStat version 3.06 for data with a normal distribution. For data which was not normally distributed (mcs), statistical analyses were performed using Kruskal-Wallis Tests (non-parametric ANOVAs), with Dunn's Multiple Comparisons post tests. When only two groups were compared,

unpaired t-tests were performed with the Welch correction, again using GraphPad InStat version 3.06. Standard deviations are plotted as error bars for all data points on all figures. For some data points, the standard deviations were very small.

Results

Testing for Silver Deposition in Tissues

XPS and SIMS

XPS analysis performed in the mid-dermis and in the subcutaneous fat layer of tissues treated directly with nanocrystalline silver, silver nitrate, or saline did not indicate the presence of silver in any of the animals tested. An example of the compositional data for an animal treated directly with nanocrystalline silver for 24 hours is shown in Table 3-2. No silver was detected, and the silicon detected is likely from the slides that the tissues were mounted on.

Table 3-2. XPS analysis of tissue composition after direct nanocrystalline silver treatment (24h).

Atom & Orbital Measured	Mid-Dermis Atomic Concentration (%) (Average \pm Standard Deviation)	Subcutaneous Fat Layer Atomic Concentration (%) (Average \pm Standard Deviation)
Na 1s	0.97 \pm 0.26	0.62 \pm 0.35
Zn 2p	0.24 \pm 0.02	0.35 \pm 0.04
O 1s	25.15 \pm 1.82	21.77 \pm 5.47
N 1s	7.98 \pm 1.74	9.20 \pm 3.04
Ca 2p	0.17 \pm 0.04	0.20 \pm 0.10
C 1s	58.63 \pm 2.25	63.24 \pm 6.94
Si 2p	6.88 \pm 1.89	4.62 \pm 4.12

Because silver was not detected in the mid-dermis by XPS, a SIMS analysis in the imaging mode was performed, in which the epidermis and upper dermis were scanned (approximately the top 300 to 500 μm of the tissues). SIMS

is a very sensitive surface science technique, and therefore more likely to detect the trace levels of silver expected to be present in the tissue. Representative SIMS images for negative controls (Figure 3-4a), and DNCB-induced rashes treated for 24 and 72 hours with saline (Figure 3-4 b to c), silver nitrate (Figure 3-4 d to e), or nanocrystalline silver (Figure 3-4 f to g) are shown. Optical images are provided corresponding to each SIMS image, to indicate the orientation of the tissues. Summed weights corresponding to all the isotopes of Ag, AgO, AgCl, and AgNO₃ (top row); Ag₂, Ag₂O, Ag₃, Ag₄ (second row); and Ag₅, Ag₆, Ag₇ and the sum of all silver weights analyzed (third row) are shown for each image. In all samples, the intensity of the image should be compared to the intensity of the slide (background) to determine where there is staining for silver. In addition, each image is scaled from zero (black) to the maximum count (mc) present in that image (white), so images cannot be compared directly to each other based on color intensity. The negative control tissues (a), and positive control tissues (b and c) either appeared darker than the background (the slide), or were indistinguishable from the slide, for all the silver species tested, indicating that there was no silver present in the tissues, as expected. Silver nitrate treated tissues (d-e) showed deposition of species in the epidermis, with some penetration into the dermis, for weights corresponding to silver species analyzed in the top row of the image (metallic silver, silver oxide, silver chloride, and silver nitrate). This penetration into the dermis did not exceed a few hundred micrometers into the skin, and in some samples, silver species were not observed deposited in the dermis at all. For silver species measured in the second and third rows (excepting

the image showing the sum of all silver weights, and possibly the Ag₂ image at 72 hours), the tissue appears darker than the background, indicating that those species were not present in the tissue. In nanocrystalline silver treated samples (f-g), the majority of the species imaged were deposited in a thin layer at the surface of the epidermis. The only species demonstrating penetration into the dermis at 24 hours appeared to be weights corresponding to silver chloride and the silver oxides, and these did not appear to penetrate more than 150 μm into the tissue. At 72 hours, other silver species also demonstrated some penetration into the dermis, but again, this was minimal. Unlike silver nitrate treatment, weights corresponding to all the silver species tested, including silver clusters, were detected in the epidermis of the nanocrystalline silver-treated tissues. This is particularly clear from the 24 hour image shown (f). The mcs detected for the summed weights corresponding to each silver species were averaged from multiple images of each tissue, and are displayed in Figure 3-5. The nanocrystalline silver-treated tissues showed significantly higher mcs for weights corresponding to all silver species tested relative to the negative and positive controls, except Ag₇ at 24 hours. The silver nitrate-treated tissues only showed significantly higher mcs for the weights corresponding to Ag₅ relative to the negative and positive controls. At 72 hours, mc trends were less clear. However, nanocrystalline silver treated animals showed significantly higher total silver and Ag⁽⁰⁾ deposition relative to positive controls, while silver nitrate treated animals showed significantly higher deposition of AgO and AgCl relative to positive controls. The fact that mcs showed fewer significant differences at 72 hours

despite similar visual observations could be due to the unusual shadowing effect observed with most of the nanocrystalline silver treated samples at 72 hours (see Panel g). This could be due to the tissue lifting away from the surface of the slide, or it could be an artifact of ToF-SIMS, and may explain the increased variability and lack of significance observed. Another possibility is that comparing mcs may not be an ideal way to compare silver deposition in tissues, since it only indicates the maximum deposition in one location, rather than the total silver in the tissues. While tcs appeared to be the obvious choice, it is clear from the images of the negative controls (a) that the brightest parts of the images are sometimes the background, and so for tcs to be a useful measure, the counts from the background would need to be eliminated. This was not possible with the current software available, and would be difficult even if it were possible, as tissue processing caused various small cracks in the tissues, which reveal the background, and therefore would also need to be eliminated from the analyses.

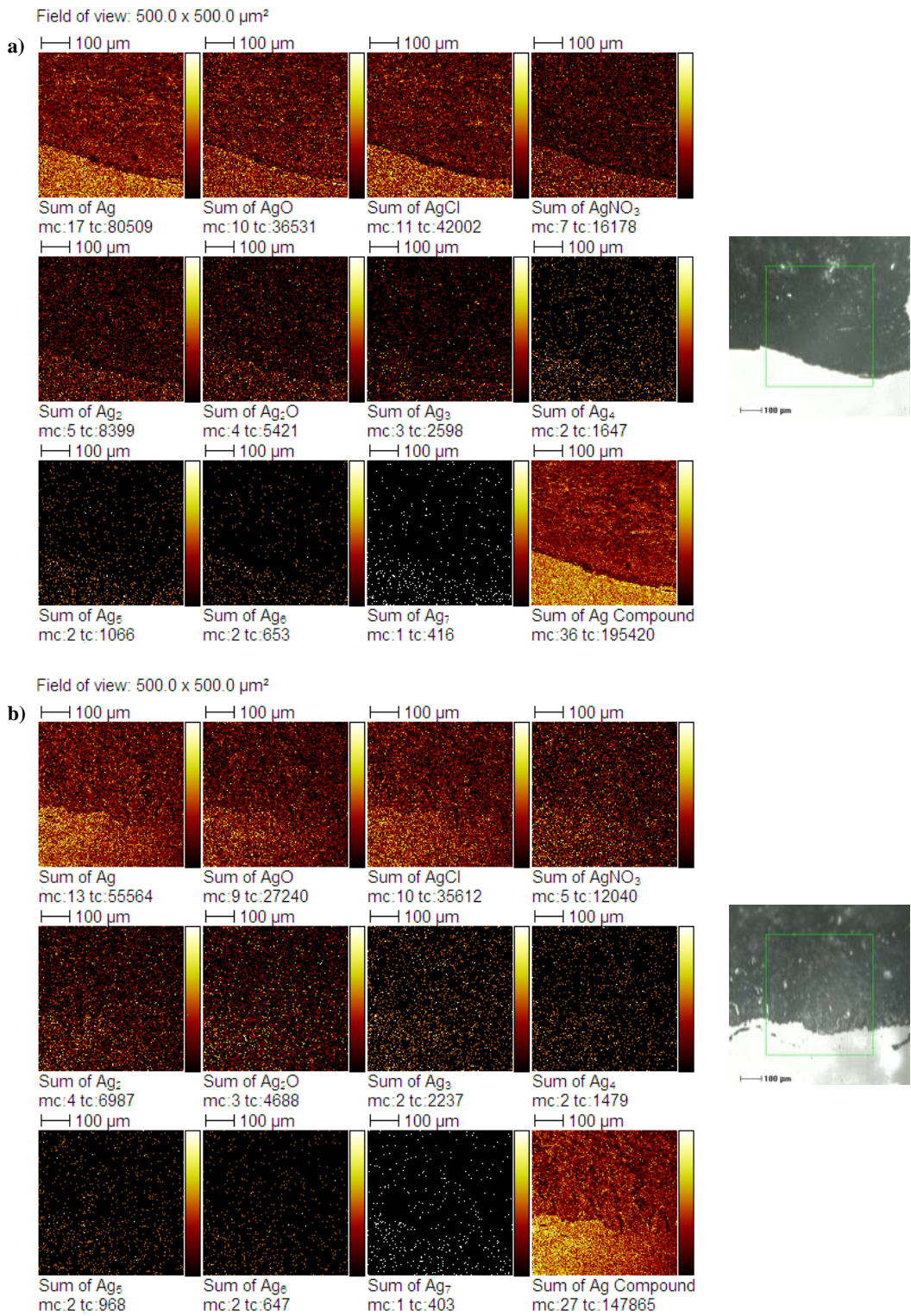


Figure 3-4

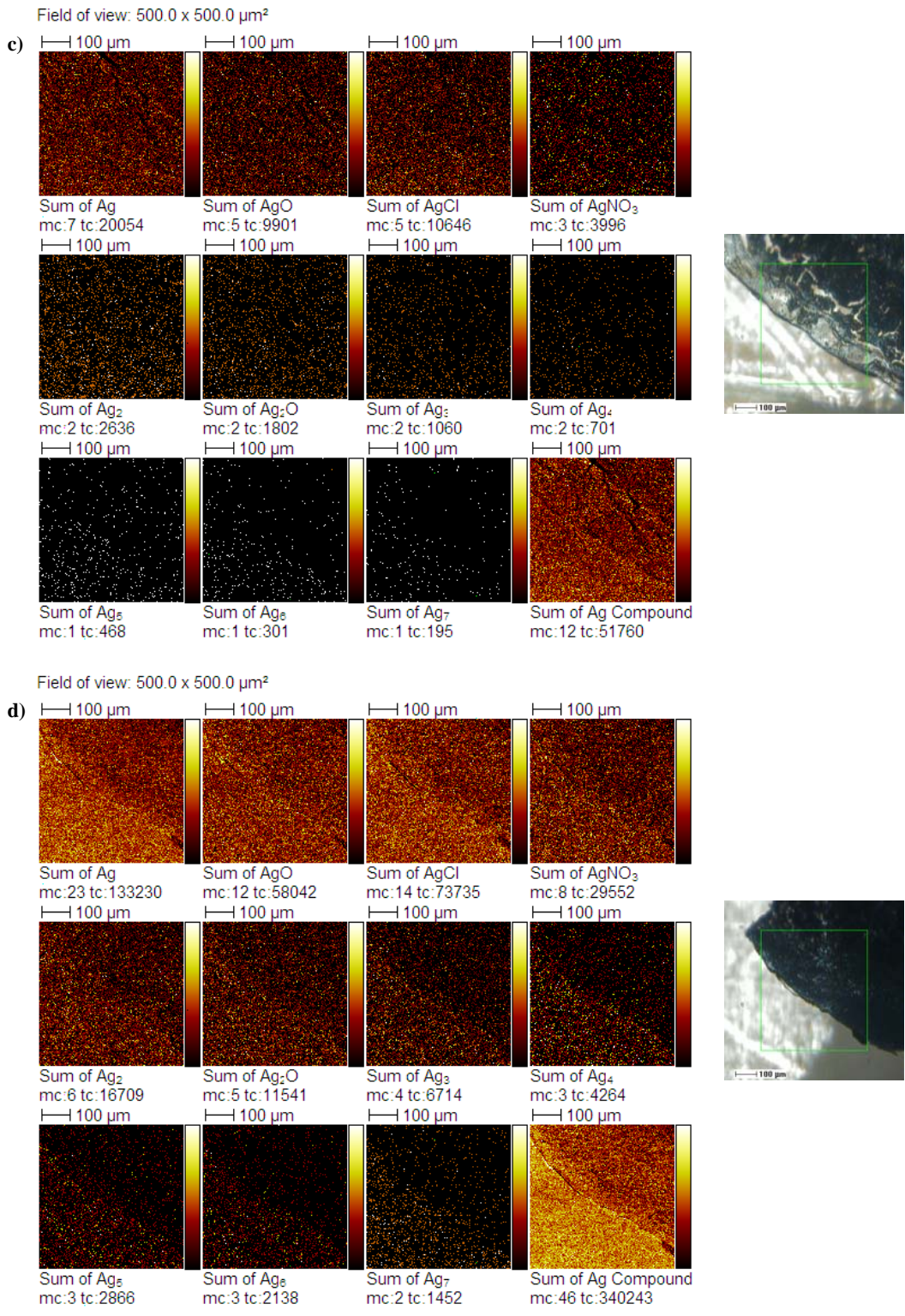


Figure 3-4, continued.

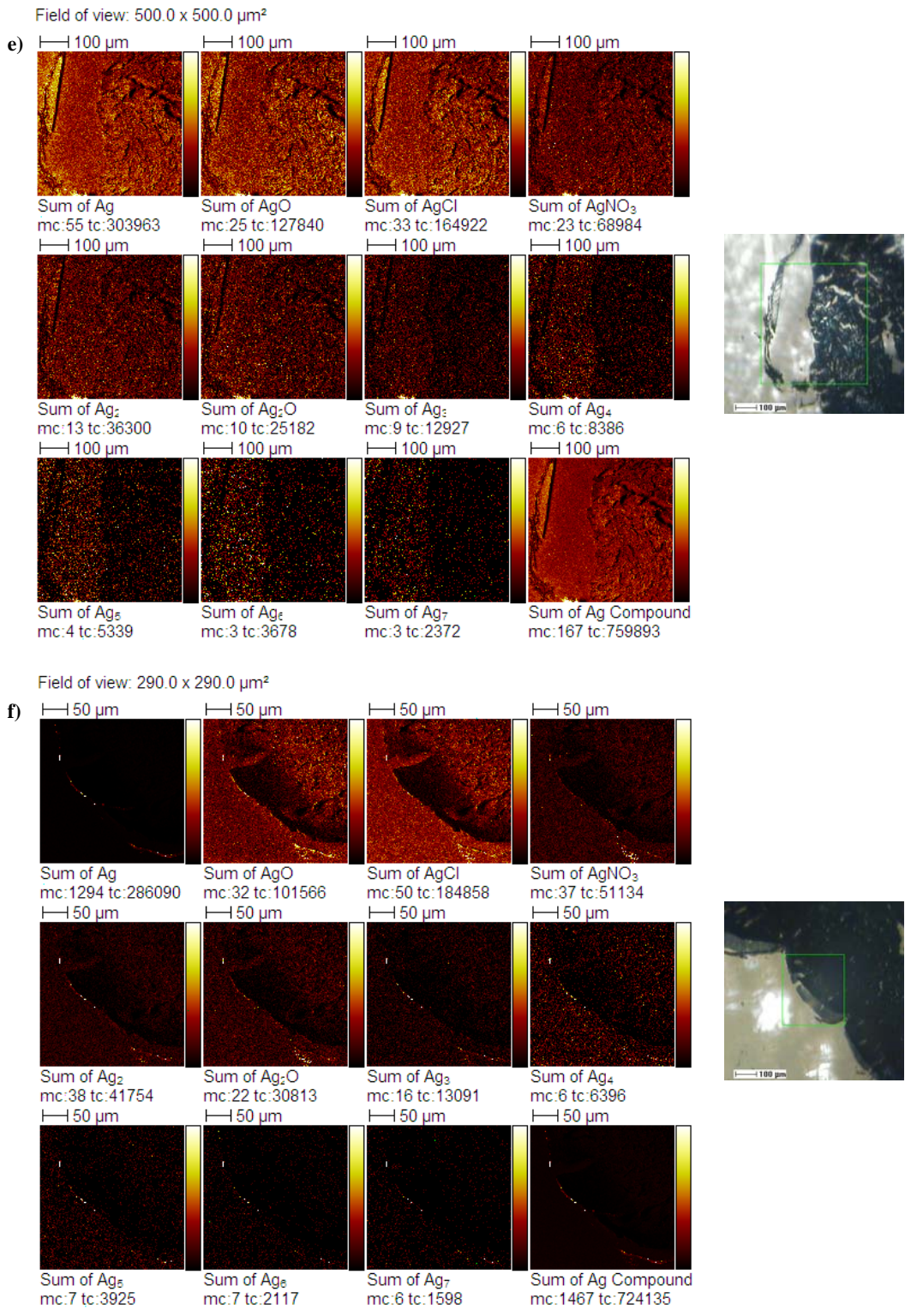


Figure 3-4, continued.

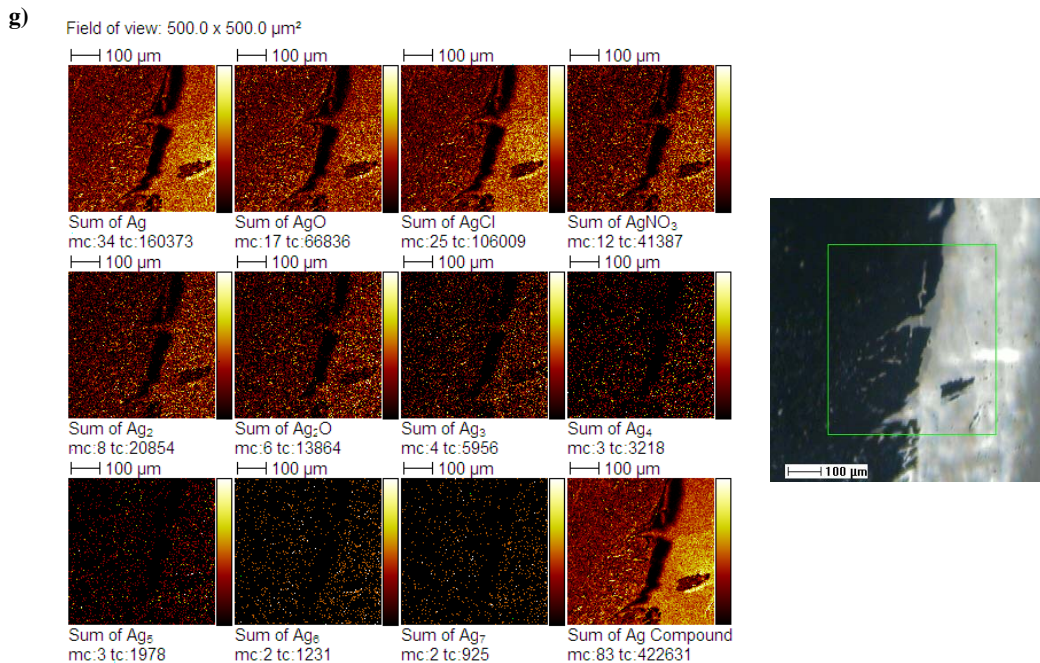


Figure 3-4, continued. Representative images of SIMS analysis of summed weights of various silver species deposited in porcine epidermis and upper dermis. Top row of each image: Ag, AgO, AgCl, AgNO₃; second row of each image: Ag₂, Ag₂O, Ag₃, Ag₄; third row of each image: Ag₅, Ag₆, Ag₇, and sum of all Ag compounds, with silver species/weights tested as indicated in Table 3-1. Images are shown for negative control animals treated with saline at a) 24h. Images are also shown for direct treatment of DNCB-induced porcine rashes with saline at b) 24 and c) 72h; silver nitrate at d) 24h and e) 72h; and nanocrystalline silver at f) 24h and g) 72h. Optical images are also provided, with the area in green being the area scanned for SIMS analysis. mc = maximum count, tc = total count. The coloration of each image is scaled from 0 (black) to the mc for that image (white). Each intensity scale is different, and image intensities should not be compared to one another directly.

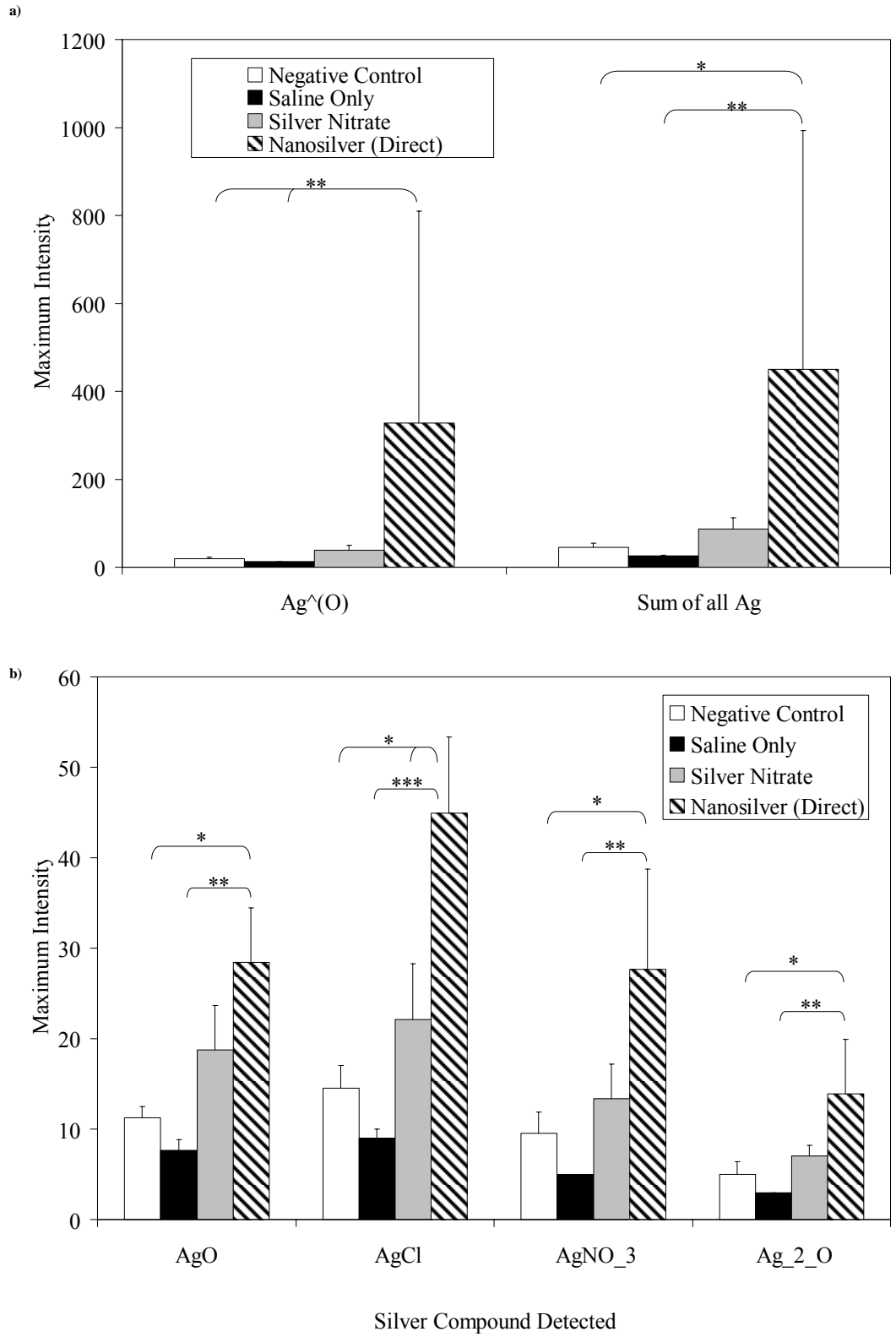


Figure 3-5.

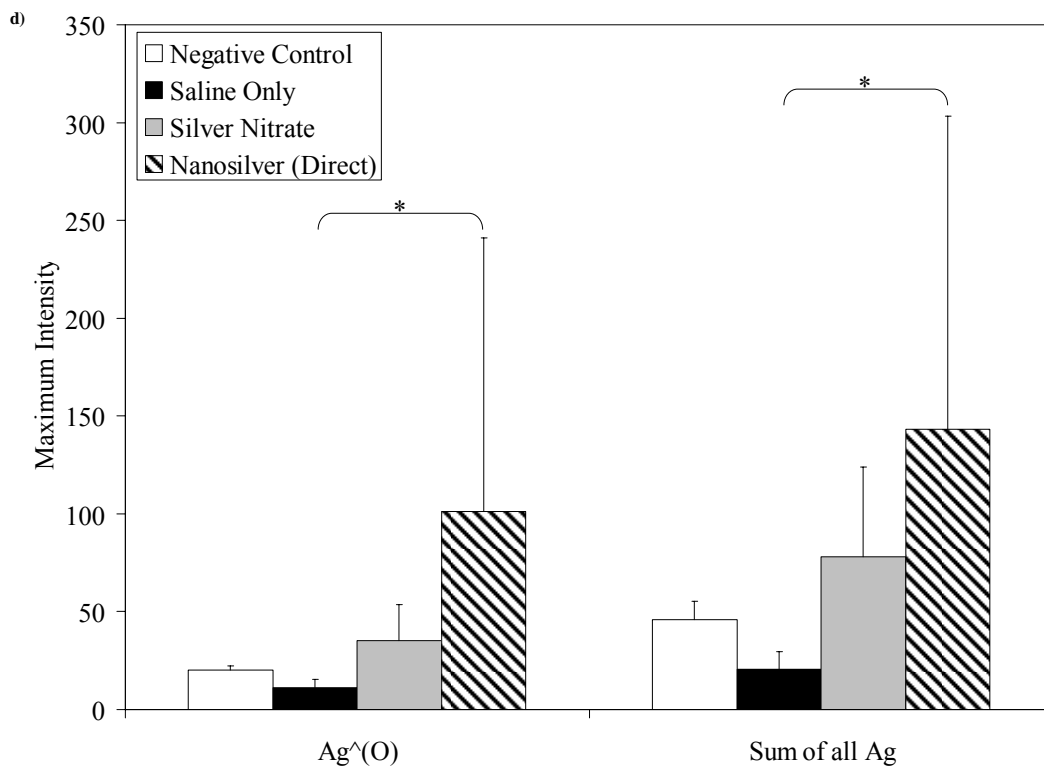
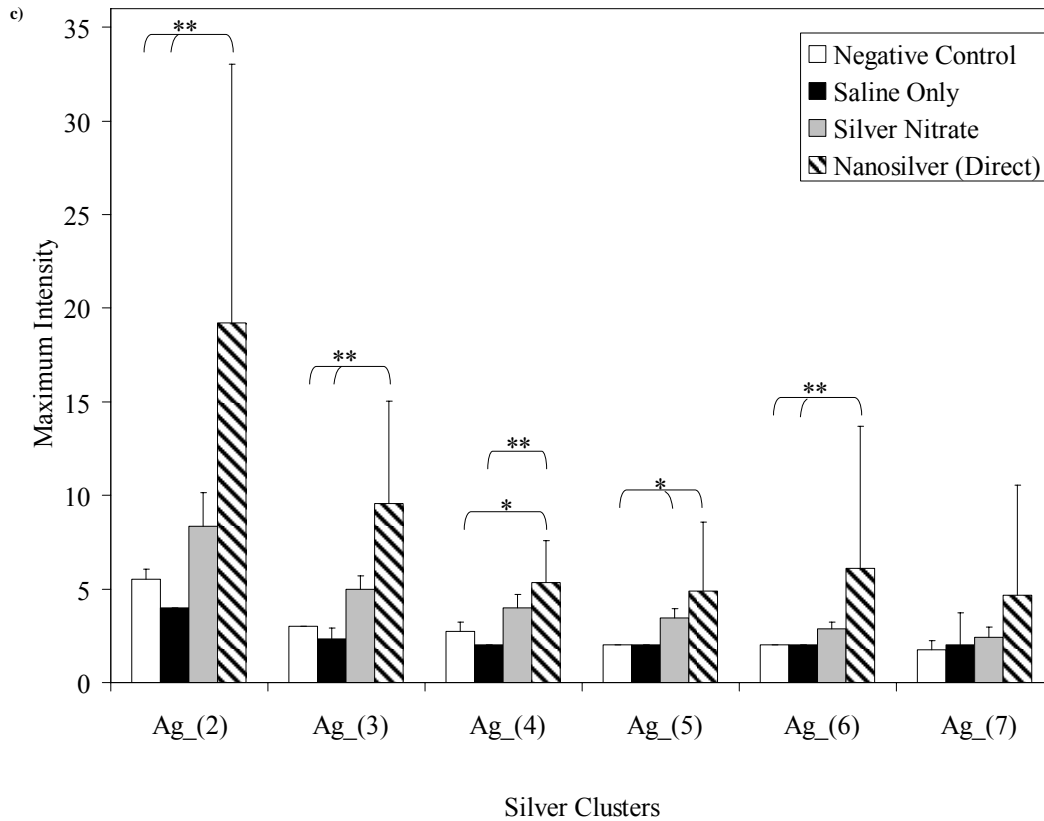


Figure 3-5, continued.

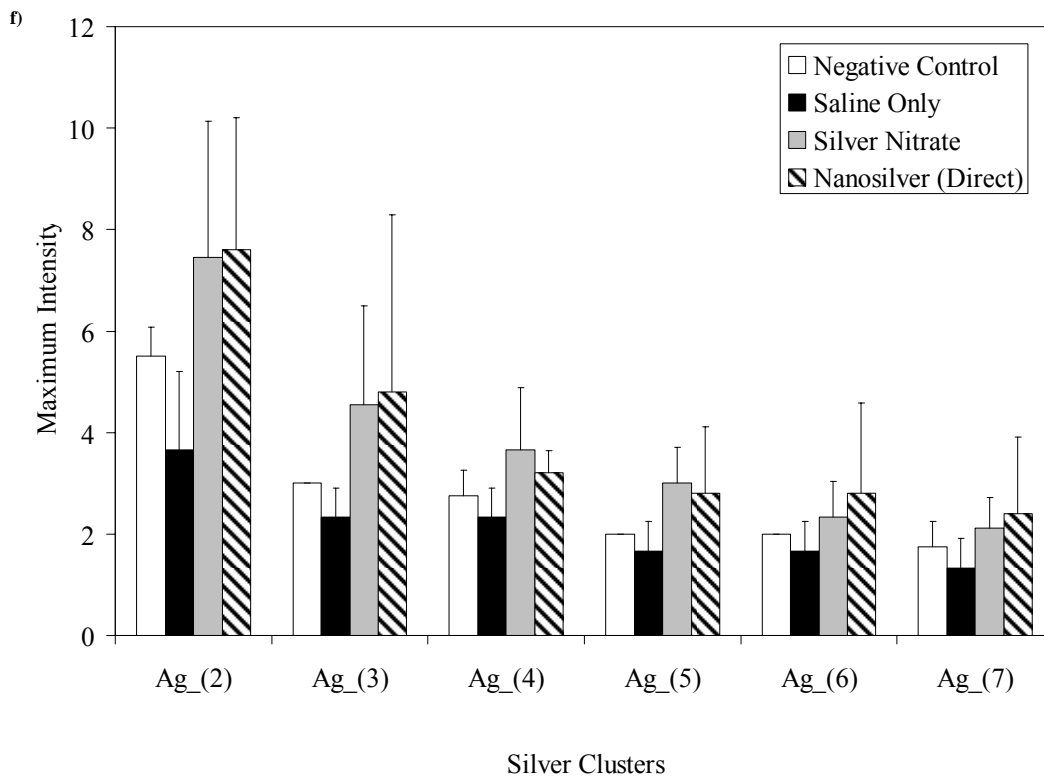
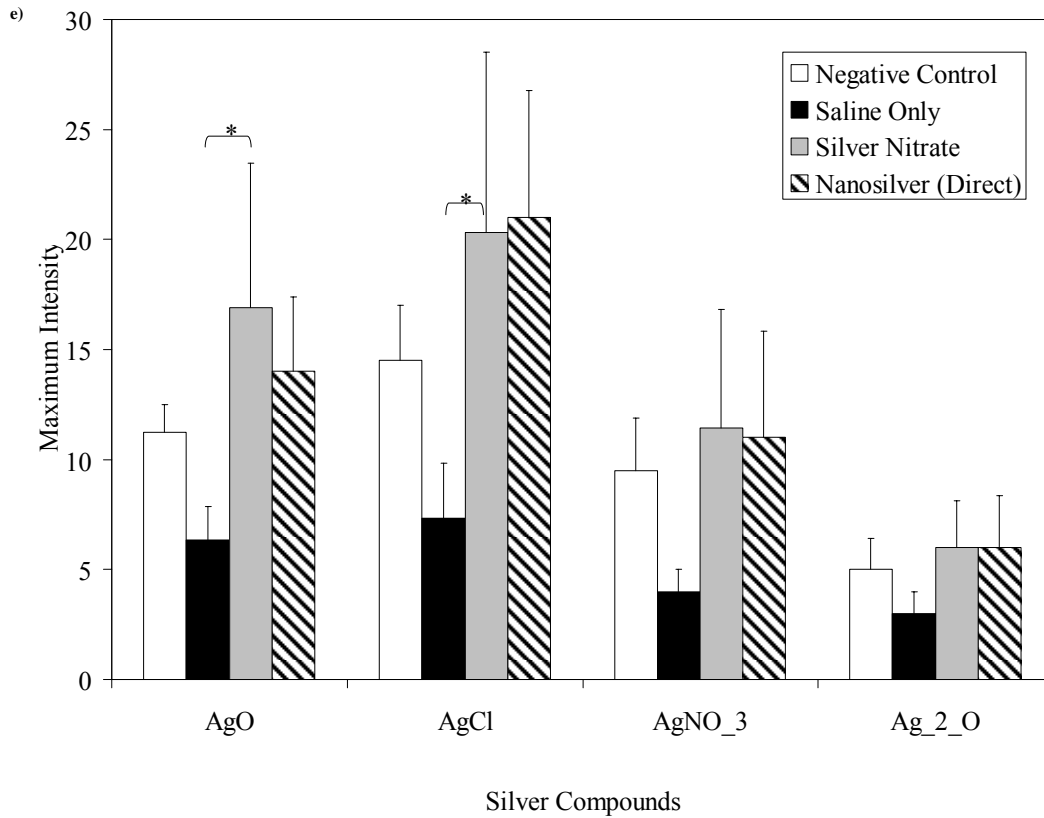


Figure 3-5, continued. Comparison of maximum count measurements for silver species deposited in the upper dermis and epidermis of pigs receiving various

treatments for DNCB-induced rashes. Average maximum counts found via SIMS analyses are shown for the summed weights of $\text{Ag}^{(0)}$ and all silver species summed at a) 24h and d) 72h; silver compounds AgO , AgCl , AgNO_3 , and Ag_2O at b) 24h and e) 72h; and silver clusters Ag_2 , Ag_3 , Ag_4 , Ag_5 , Ag_6 , and Ag_7 at c) 24h and f) 72h. Statistical analyses were performed using Kruskal-Wallis Tests (non-parametric ANOVAs), since the data were not normally distributed, with Dunn's Multiple Comparisons post tests. The results of the Kruskal-Wallis Tests were as follows: 24 hours: $\text{Ag}^{(0)}$ – $p=0.0002$, sum of all silver species – $p=0.0003$, AgO – $p=0.0003$, AgCl – $p=0.0002$, AgNO_3 – $p=0.0004$, Ag_2O – $p=0.0004$, Ag_2 – $p=0.0004$, Ag_3 – $p=0.0002$, Ag_4 – $p=0.0009$, Ag_5 – $p=0.0026$, Ag_6 – $p=0.0004$, Ag_7 – $p=0.2307$; 72 hours: $\text{Ag}^{(0)}$ – $p=0.0203$, sum of all silver species – $p=0.0238$, AgO – $p=0.0309$, AgCl – $p=0.0226$, AgNO_3 – $p=0.0610$, Ag_2O – $p=0.0929$, Ag_2 – $p=0.0375$, Ag_3 – $p=0.0479$, Ag_4 – $p=0.1080$, Ag_5 – $p=0.0316$, Ag_6 – $p=0.3527$, Ag_7 – $p=0.2778$. Results of the post tests are shown on the figure as follows: *, **, or *** indicates significantly different ($p<0.05$), very significantly different ($p<0.01$), or extremely significantly different ($p<0.001$), respectively. Error bars represent standard deviations.

Testing for Remote Anti-inflammatory/Pro-healing Effects

Visual Observations

Figure 3-6 shows the images over time of the rashes for pigs treated with remote nanocrystalline silver. Images a-d are from the first pig, images e-h are from the second pig, and images i-l are from the third pig. The rashes at Day 0 were similar to those observed in Chapter 2, although the third pig appears to have been the most strongly affected. Over the three days of treatment, some improvements were observed in pigs receiving remote nanocrystalline treatments, including some loss of scabbing (j), with decreased redness around the scabbing, and a decrease in the overall size of the rash area. However, these effects are not as great as those seen with direct nanocrystalline silver treatment (see Figure 2-5).

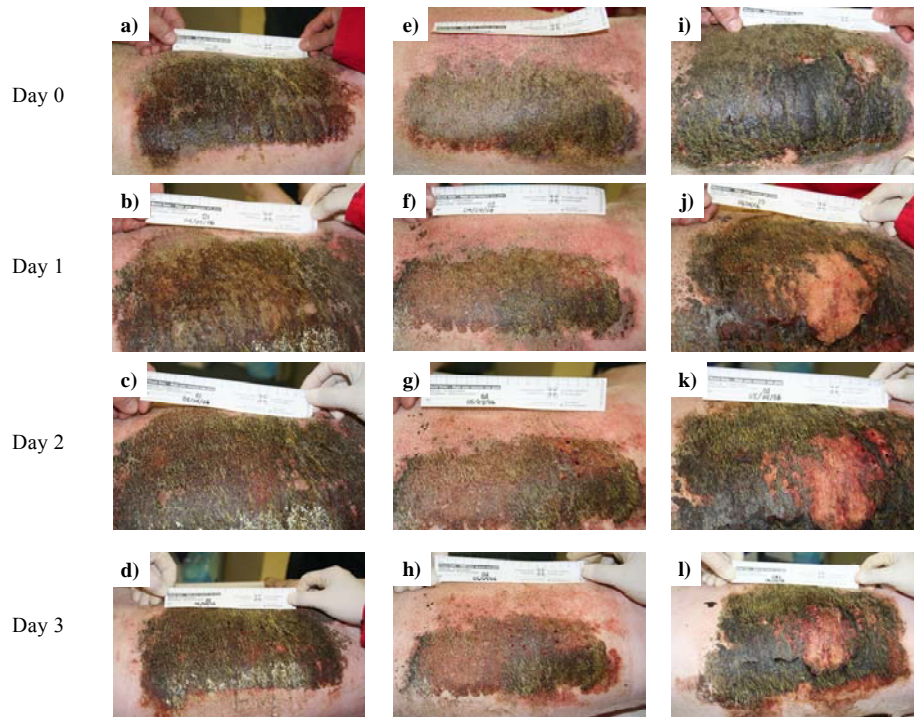


Figure 3-6. Representative images of porcine DNCB-induced rashes over three days of treatment with remote nanocrystalline silver. Images a)-d) are from the first pig treated this way. Images e)-h) are from the second pig treated this way. Images i)-l) are from the third pig treated this way. Day 0 images – a), e) and i) – are in the first row. Day 1 images – b), f) and j) – are in the second row. Day 2 images – c), g) and k) – are in the third row. Day 3 images – d), h) and l) – are in the fourth row. Wound rulers are included to indicate the image scale in centimetres.

Figure 3-7 shows the average erythema scores for the pigs treated with remote nanocrystalline silver. For comparison, the erythema scores for pigs treated with saline only are also shown. Relative to pigs treated with saline only, the pigs treated with remote nanocrystalline silver showed significantly decreased redness on Day 2 only ($p=0.0377$).

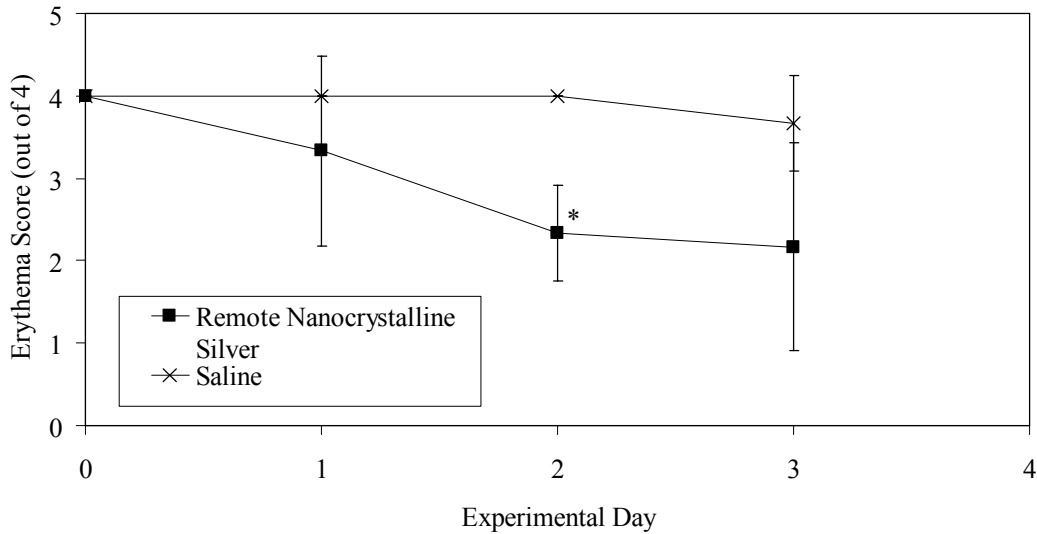


Figure 3-7. Erythema scores with remote treatment. Daily average erythema scores for pigs with DNCB-induced contact dermatitis treated for three days with remote nanocrystalline silver, or saline only on the rash. The statistical analyses were performed using unpaired t-tests with Welch corrections. The t-tests indicated that the differences between groups were not significant on Day 0, Day 1 and Day 3 ($p > 0.05$), but were significant ($p = 0.0377$) on Day 2. * indicates significantly different from the pigs treated with saline only ($p < 0.05$). Error bars represent standard deviations ($n = 3$ for each data point).

The edema scores for pigs treated with remote nanocrystalline silver are shown in Figure 3-8, in comparison to scores for pigs treated with saline only. On Day 1, pigs treated with remote nanocrystalline silver had significantly lower edema scores than pigs treated with saline only ($p = 0.0132$). At Day 2, scores for pigs treated with remote nanocrystalline silver were extremely significantly lower ($p < 0.0001$) than scores for pigs treated with saline only. By Day 3, however, the scores were not quite significantly different ($p = 0.0572$).

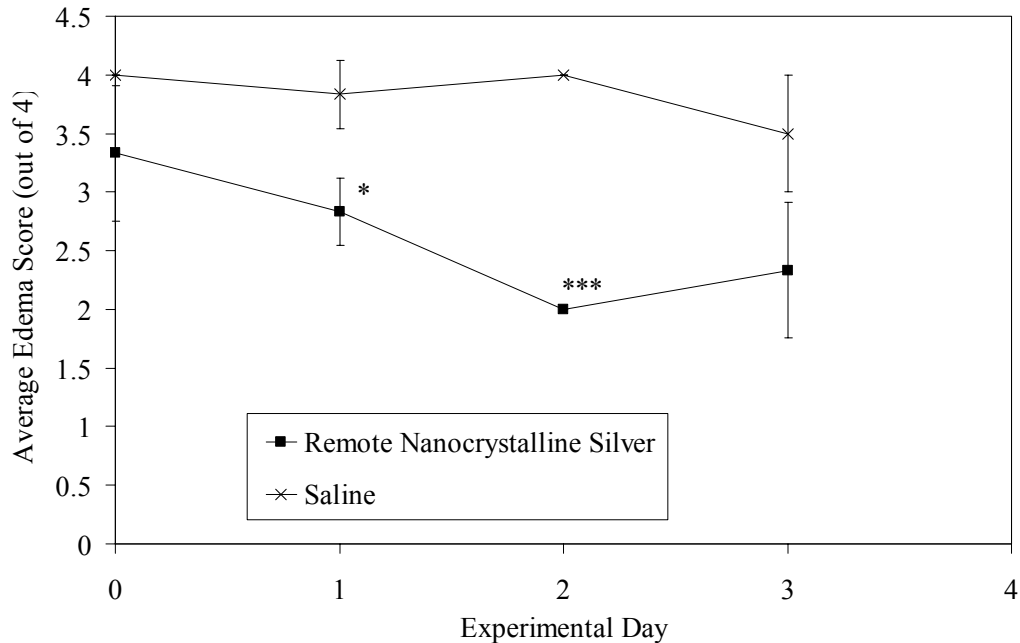


Figure 3-8. Edema scores with remote treatment. Daily average edema scores for pigs with DNCB-induced contact dermatitis treated for three days with remote nanocrystalline silver, or saline only. The statistical analyses were performed using unpaired t-tests with the Welch correction. The t-tests indicated that the differences between groups were not significant on Day 0 ($p=0.1161$), significant ($p=0.0132$) on Day 1, extremely significant on Day 2 ($p<0.0001$), and not quite significant on Day 3 ($p=0.0572$). *** and * indicates significantly different from the pigs treated with saline only ($p<0.0001$ and $p<0.05$, respectively). Error bars represent standard deviations ($n=3$ for each data point).

Biopsy Bleeding

Figure 3-9 shows the biopsy bleeding scores on Day 2 and 3 for the pigs treated with remote nanocrystalline silver, and for pigs treated with saline only.

There was a large variability in biopsy bleeding scores, and there were no significant differences between the two groups.

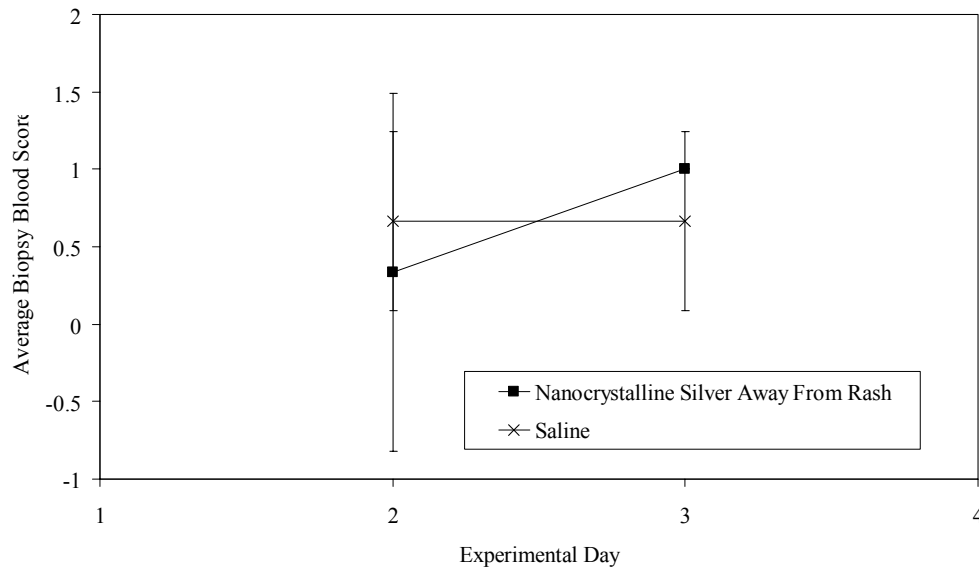


Figure 3-9. Biopsy bleeding scores for pigs with DNCB-induced contact dermatitis treated for three days with remote nanocrystalline silver, or saline only. A score of -1 indicated minimal bleeding, while a score of 1 indicated considerable bleeding. Statistical analyses were performed using unpaired t-tests with the Welch correction. The t-tests indicated that the differences between groups were not significant on Day 2 or 3 ($p>0.05$). Error bars represent standard deviations ($n=3$ for each data point).

Weight Change

The average weight change for the pigs treated with remote nanocrystalline silver was -2.33 kg (± 0.92 kg S.D.). Pigs treated with saline only had an average weight change of -0.8 kg (± 0.84 kg S.D.). The weight changes were not significantly different between these two groups. However, it should be noted that one pig treated with nanocrystalline silver away from the rash injured a toe on the first day of treatment, and that he lost nearly twice as much weight as the other two pigs in the group. Thus his toe injury may have been a compounding factor affecting his weight change, and therefore the average weight change of this group.

Histopathology

Representative histological images over the course of treatment are shown for the pigs treated with remote nanocrystalline silver in Figure 3-10. For comparison, images of pigs treated with saline only are also shown (Figure 3-10 a through d). Pig 1 (Figure 3-10e) and Pig 3 (Figure 3-10m) appear to have very highly inflamed tissues on Day 0, with severe tissue damage due to edema, and infiltration of a large number of red blood cells and inflammatory cells. However, Pig 2 (Figure 3-10i) appears to have started somewhat less inflamed. After one day of treatment (Figure 3-10f, j, n), the pigs treated with remote nanocrystalline silver did not show significant improvements relative to the saline-only treated animals (Figure 3-10b). The third pig appeared to have shed the epidermis over the biopsy area (Figure 3-10n). The first pig receiving remote nanocrystalline silver showed a decrease in red blood cells by Day 2 (Figure 3-10g), and a new epidermis appeared to be forming by Day 3 (Figure 3-10h). There were still fairly high levels of inflammatory cells present, although the levels were lower than those present in the saline-only treated pigs. As well, some tissue damage was still present in the dermis, indicating continued edema. In the second pig, a trend of decreasing inflammatory cell and red blood cell presence was observed on Day 2 and 3 (Figure 3-10k, l). In the third pig, while there was a clear decrease in the number of red blood cells and inflammatory cells present in the tissues over time, the tissue morphology on Day 2 was somewhat unusual (Figure 3-10o). The epidermis appeared to be developing very deep ridges. However at Day 3, the tissue did not show this type of organization. This may be due to differences in

tissue morphology dependent on the location that the biopsy was taken from. Overall, although some improvements were observed relative to the saline-only treated pigs, the changes were not as marked as those observed when the tissues were treated directly with nanocrystalline silver (see Figure 2-9).

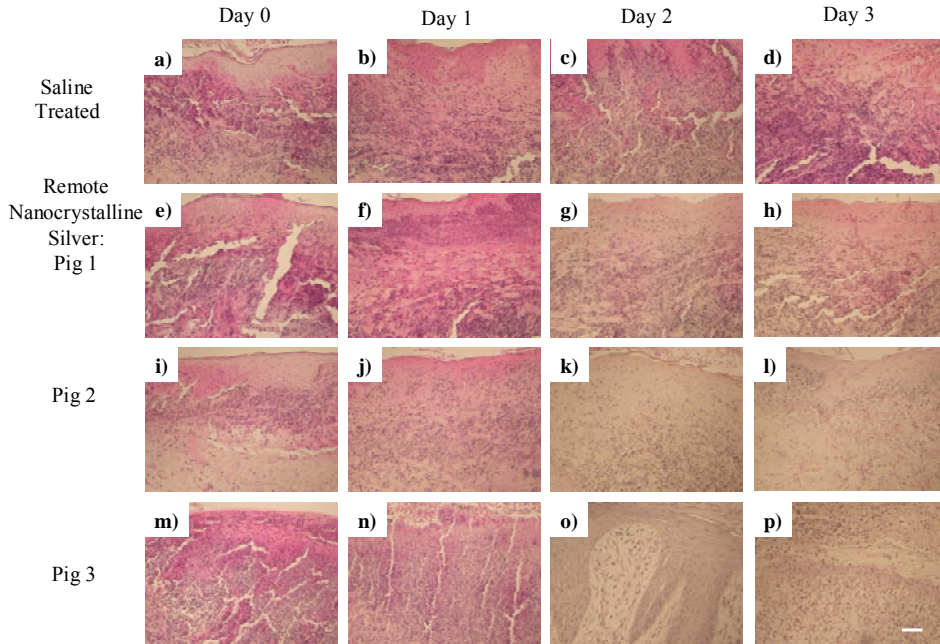


Figure 3-10. Representative histological images of remotely-treated tissue. Sections were stained with hematoxylin and eosin. Images were taken showing a portion of the epidermis and a portion of the dermis. Tissue samples from pigs treated with saline are shown before treatment (a), and after one day (b), two days (c), and three days (d) of treatment. Tissue samples from the first pig treated with remote nanocrystalline silver are shown before treatment (e), and after one day (f), two days (g), and three days (h) of treatment. Tissue samples from the second pig treated with remote nanocrystalline silver are shown before treatment (i), and after one day (j), two days (k), and three days (l) of treatment. Tissue samples from the third pig treated with remote nanocrystalline silver are shown before treatment (m), and after one day (n), two days (o), and three days (p) of treatment. Cell nuclei are stained purple with hematoxylin, while cytoplasm was stained pink with eosin. The scale bar represents 50 μm .

Apoptosis Detection and Quantification

Representative images of apoptotic staining after 24 hours of treatment are

shown in Figure 3-11. Animals treated with saline only (a-c) showed some small amounts of apoptotic staining in the epidermis, but none in the dermis. This is similar to results observed in Chapter 2. Animals treated with remote nanocrystalline silver (3-11 d to f) showed similar levels of apoptotic staining in the epidermis to that of the positive controls, but also demonstrated a high level of apoptotic staining in the dermis, where inflammatory cell infiltration was highest. Quantitative analysis showed that in the epidermis, there were no significant differences in the ratio of apoptotic to nuclear staining between animals treated with remote nanocrystalline silver and those treated with saline only ($p=0.4568$). However, in the dermis, animals treated with remote nanocrystalline silver had significantly higher ratios relative to animals receiving saline only ($p=0.0217$).

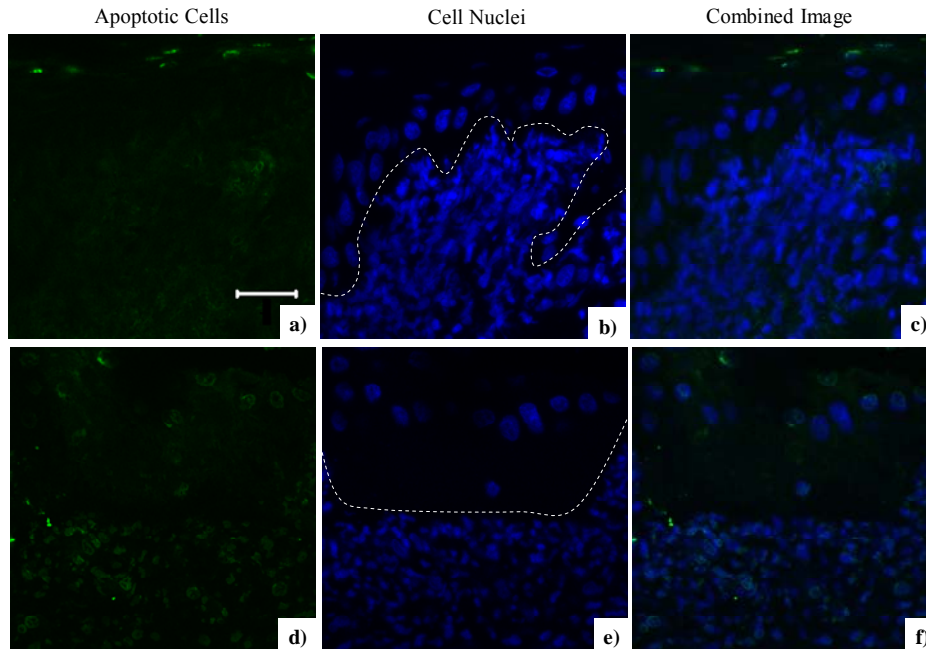


Figure 3-11. Representative fluorescence images obtained via confocal microscopy for immunohistochemical detection of apoptotic cells in the epidermis and upper dermis of pigs with contact dermatitis undergoing remote treatments. Delineation between the epidermis and dermis is shown as a dashed white line in the second column. The first column shows staining by FITC for apoptotic cells (green). The second column shows counterstaining by DAPI for nuclei (blue). The third column shows the combination of apoptotic and nuclear staining. Images in panels a-c) are from a DNCB-induced porcine contact dermatitis rash treated directly with saline only for 24h. Images in panels d-f) are from a DNCB-induced porcine rash treated with remote nanocrystalline silver for 24h. The scale bar (upper left) represents 20 μm .

Immunohistochemical Detection of Cytokines and Growth Factors

Representative images of immunohistochemical staining for TNF- α are shown in Figure 3-12 for animals treated with saline only (a-b), and animals treated with remote nanocrystalline silver (c-d), after 24 hours and 72 hours of treatment. At 24 hours, the animals treated with saline only showed stronger staining for TNF- α than those which also received remote nanocrystalline silver. At 72 hours, the staining increased in animals receiving saline only, while it

further decreased in animals receiving remote nanocrystalline silver.

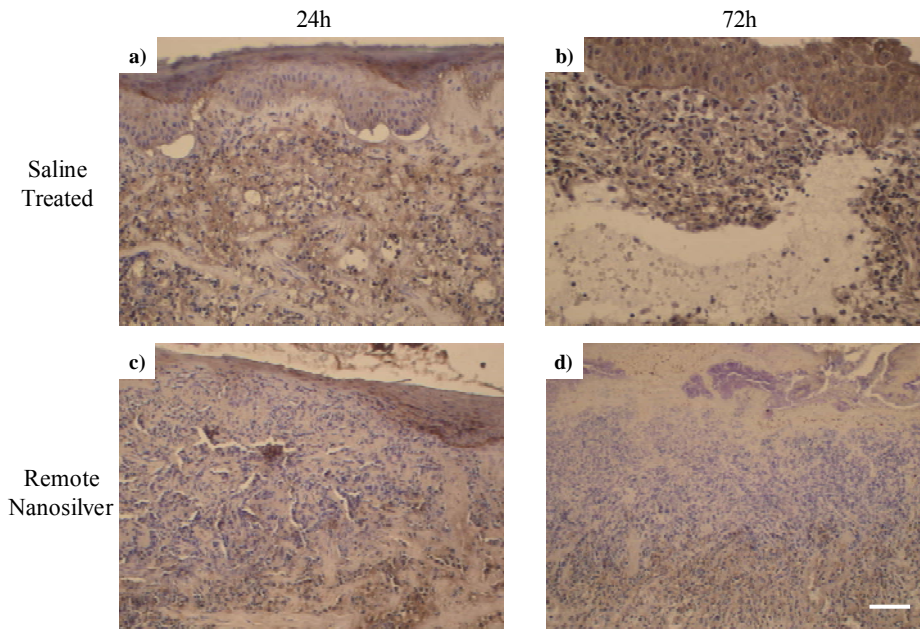


Figure 3-12. Representative images for immunohistochemical detection of TNF- α after 24h (column 1) and 72h (column 2) treatment of DNCB-induced porcine contact dermatitis rashes with saline (a,b), or remote nanocrystalline silver (c, d). The scale bar in d) represents 50 μ m. Staining for TNF- α appears brown, while the cell nuclei are counterstained purple using hematoxylin.

Representative images of immunohistochemical staining for IL-8 are shown in Figure 3-13 for animals treated with saline only (a-b), and animals also treated with remote nanocrystalline silver (c-d), after 24 and 72 hours of treatment. At 24 hours, the two groups show similar levels of staining. However, at 72 hours, the staining increased strongly in animals receiving saline only, while it did not increase in animals receiving remote nanocrystalline silver.

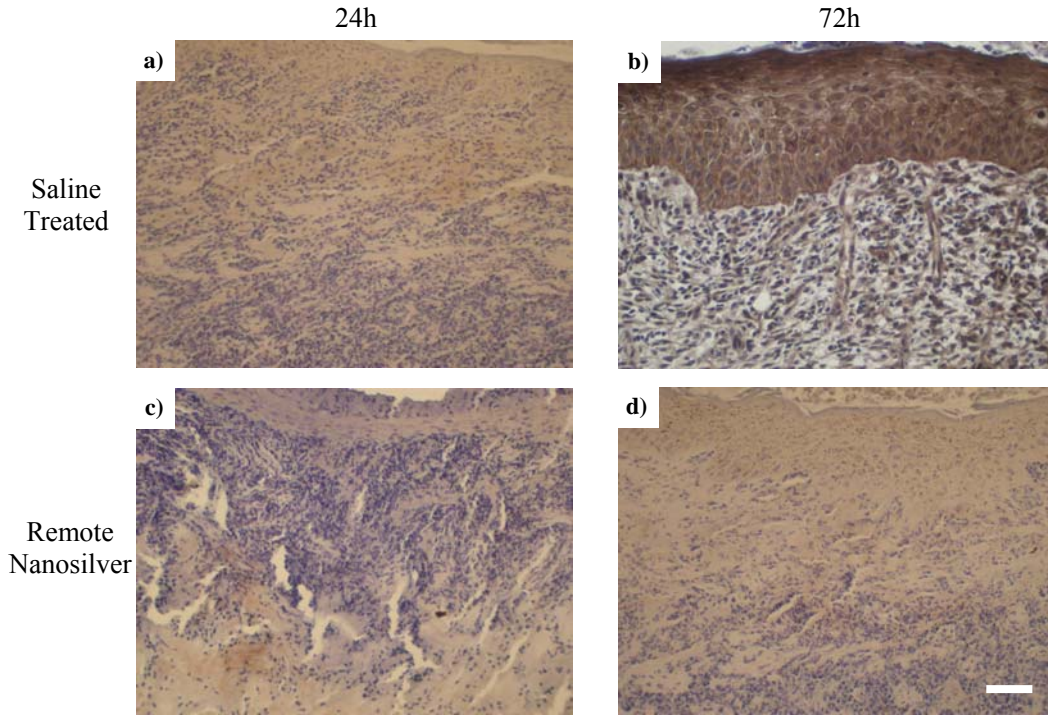


Figure 3-13. Representative images for immunohistochemical detection of IL-8 after 24h (column 1) and 72h (column 2) treatment of DNCB-induced porcine contact dermatitis rashes with saline (a,b), or remote nanocrystalline silver (c, d). The scale bar in d) represents 50 μ m. Staining for IL-8 appears brown, while the cell nuclei are counterstained purple using hematoxylin.

Representative images of immunohistochemical staining for IL-4 are shown in Figure 3-14 for animals treated with saline only (a-b), animals also treated with remote nanocrystalline silver (c-d), and animals treated directly with nanocrystalline silver (e-f), after 24 and 72 hours of treatment. At 24 hours, animals treated with saline only showed light diffuse staining for IL-4, while those which also received remote nanocrystalline silver showed staining specific to the depth at which re-epithelization occurred at later time points. Animals treated directly with nanocrystalline silver showed this same staining pattern. At 72h, staining was only mildly increased in animals receiving saline only, while the staining was very strong and cell specific in animals receiving remote

nanocrystalline silver. While primarily located in keratinocytes in the newly forming epidermis, staining was also present in cells in the upper dermis, such as fibroblasts. With direct nanocrystalline silver treatment, cell specific staining was also observed, particularly in the epidermis. However, the staining was not as strong. This, in combination with the better tissue morphology present with direct treatment, suggests that IL-4 expression peaked between 24 and 72 hours with direct nanocrystalline silver treatment.

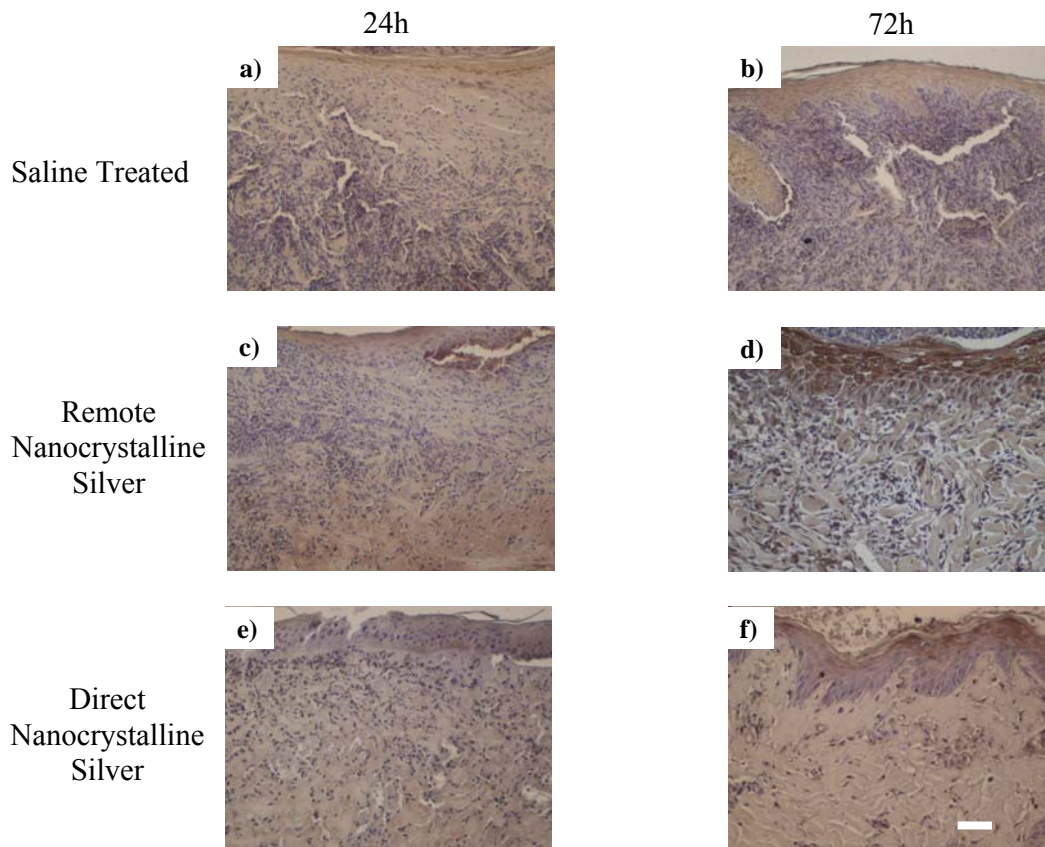


Figure 3-14. Representative images for immunohistochemical detection of IL-4 after 24h (column 1) and 72h (column 2) treatment of DNCB-induced porcine contact dermatitis rashes with saline (a,b), remote nanocrystalline silver (c, d), or direct nanocrystalline silver (e,f). The scale bar in f) represents 50 μ m. Staining for IL-4 appears brown, while the cell nuclei are counterstained purple using hematoxylin.

Representative images of immunohistochemical staining for IL-10 are shown in Figure 3-15. Staining for IL-10 was minimal at all time points for both treatment groups (c-f), and showed only a very mild increase in staining at 72 hours near the tissue surfaces of saline-treated animals (b). Staining was, however, present around blood vessels (data not shown).

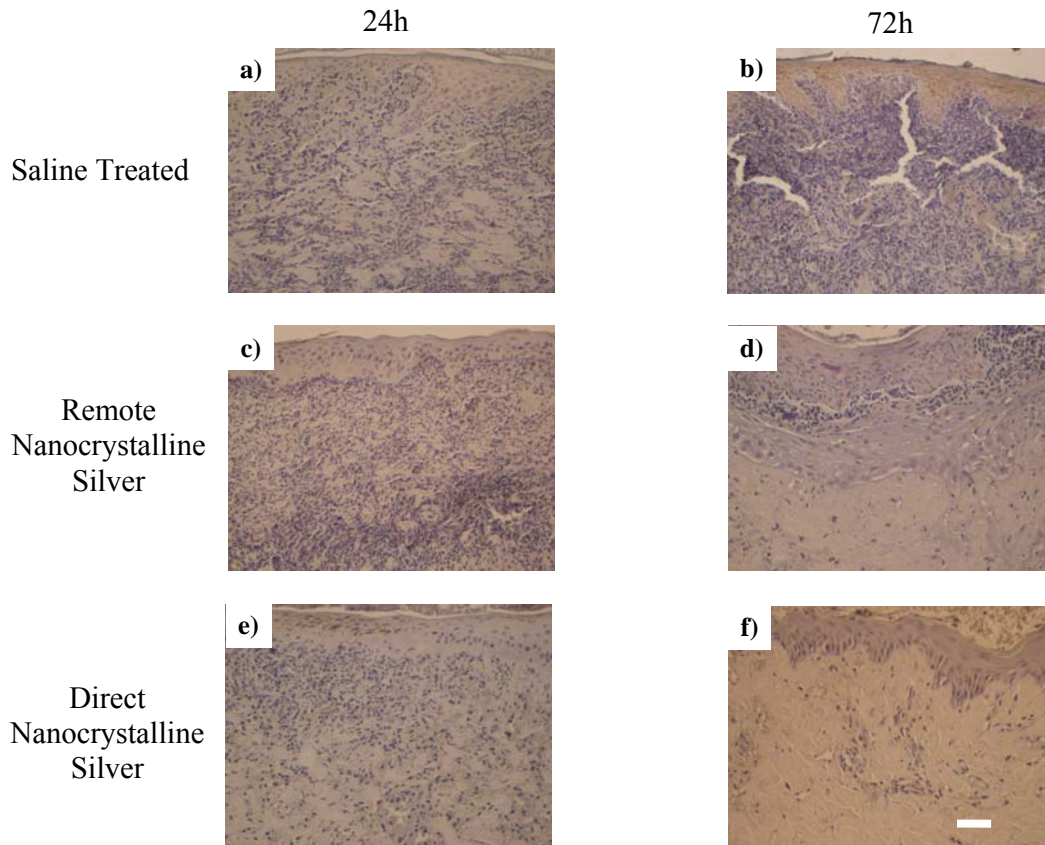


Figure 3-15. Representative images for immunohistochemical detection of IL-10 (using a monoclonal antibody) after 24h (column 1) and 72h (column 2) treatment of DNCB-induced porcine contact dermatitis rashes with saline (a,b), remote nanocrystalline silver (c, d), or direct nanocrystalline silver (e,f). The scale bar in f) represents 50 μm . Staining for IL-10 appears brown, while the cell nuclei are counterstained purple using hematoxylin.

Representative images of immunohistochemical staining for TGF- β are shown in Figure 3-16. Staining was low in both the saline treated animals (a-b) and the animals treated with remote nanocrystalline silver (c-d) at both 24 and 72

hours. Although there is some staining right at the surface with the remote nanocrystalline silver treatment at 24 hours (c), and the saline treatment at 72 hours (b), this may just be an edge effect.

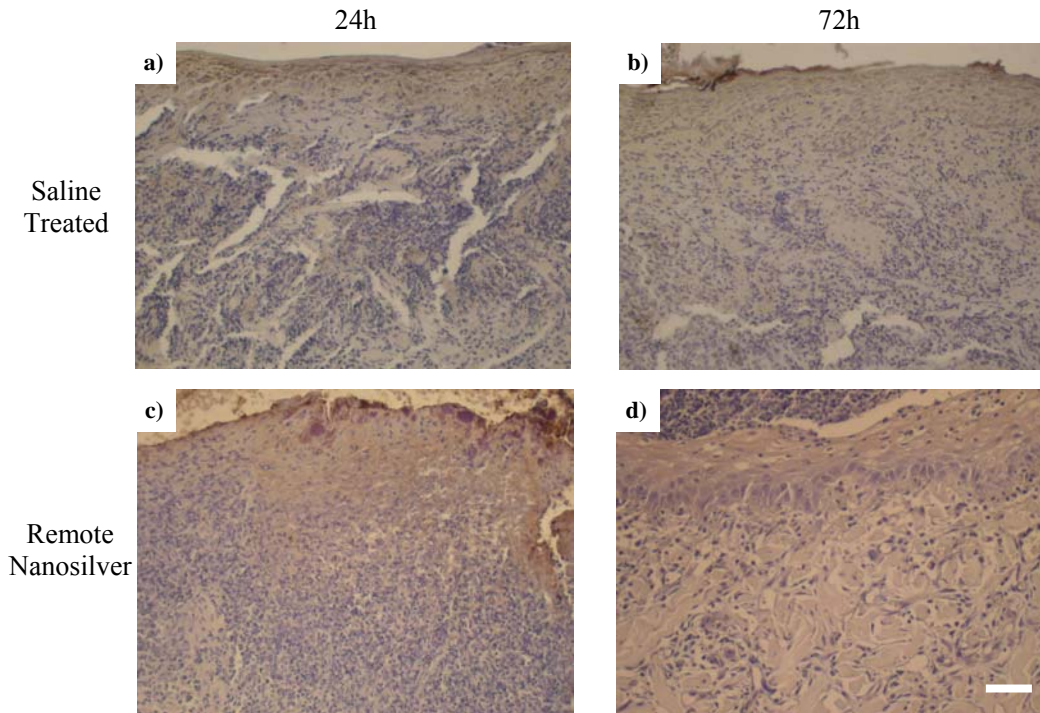


Figure 3-16. Representative images for immunohistochemical detection of TGF- β after 24h (column 1) and 72h (column 2) treatment of DNCB-induced porcine contact dermatitis rashes with saline (a,b), or remote nanocrystalline silver (c, d). The scale bar in d) represents 50 μ m. Staining for TGF- β appears brown, while the cell nuclei are counterstained purple using hematoxylin.

Representative images of immunohistochemical staining for EGF are shown in Figure 3-17 for animals treated with saline only (a-b), animals treated with remote nanocrystalline silver (c-d), and animals treated directly with nanocrystalline silver (e-f), after 24 and 72 hours of treatment, respectively. The staining pattern was very similar to that seen for IL-4. However, the staining was stronger at 24 hours in animals treated with remote nanocrystalline silver. It was also much stronger and more diffuse for animals treated directly with nanocrystalline silver.

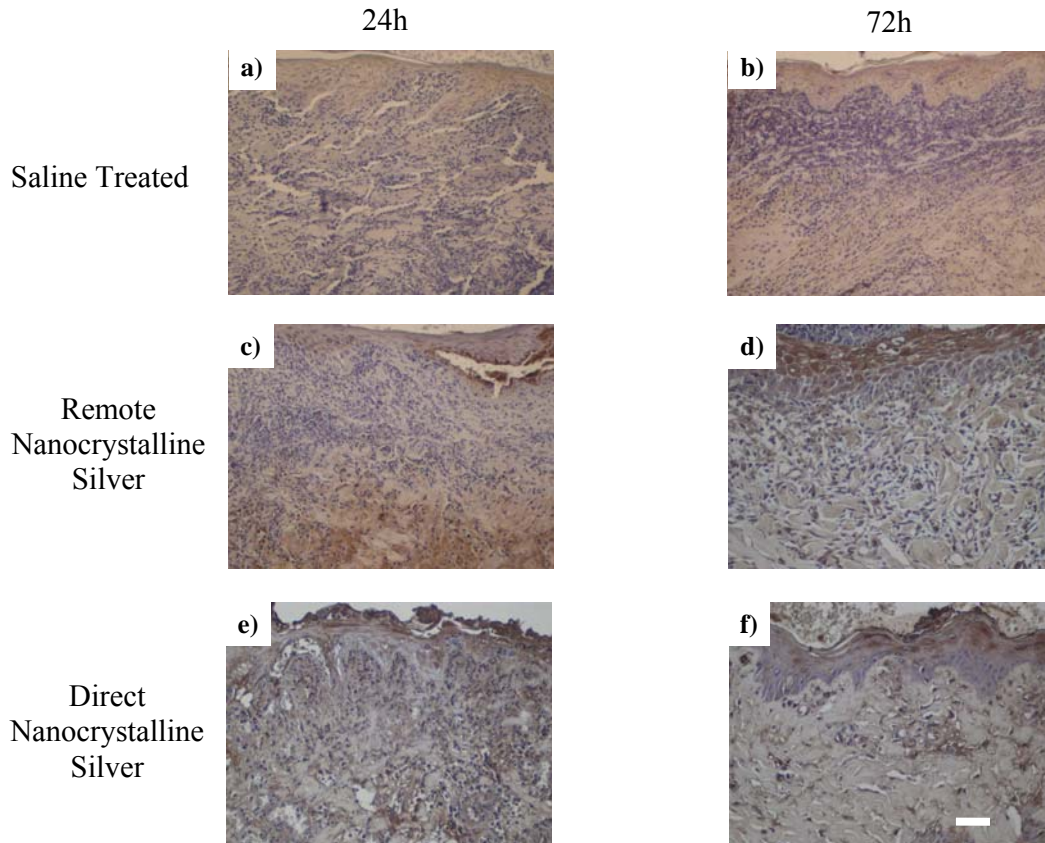


Figure 3-17. Representative images for immunohistochemical detection of EGF after 24h (column 1) and 72h (column 2) treatment of DNCB-induced porcine contact dermatitis rashes with saline (a,b), remote nanocrystalline silver (c, d), or direct nanocrystalline silver (e,f). The scale bar in f) represents 50 μm . Staining for EGF appears brown, while the cell nuclei are counterstained purple using hematoxylin.

Representative images of immunohistochemical staining for KGF are shown in Figure 3-18 for animals treated with saline only (a-b), animals treated with remote nanocrystalline silver (c-d), and animals treated directly with nanocrystalline silver (e-f) after 24 and 72 hours of treatment, respectively. At 24 hours, animals treated with saline show minimal staining for KGF. Animals that received remote nanocrystalline silver showed strong staining specific to the depth at which re-epithelization occurred at later time points. Animals treated directly with nanocrystalline silver also showed increased staining at 24 hours, but

it appeared to be more cell associated than that observed with the indirect treatments. At 72 hours, staining had increased slightly in animals receiving saline only, while the staining in animals receiving remote nanocrystalline silver decreased in strength relative to 24 hours, but was clearly cell specific, being primarily located in keratinocytes of the newly forming epidermis, but also present in cells remaining in the upper dermis. Interestingly, staining for KGF was increased at 72 hours with direct nanocrystalline silver treatment, and appeared to be more diffuse.

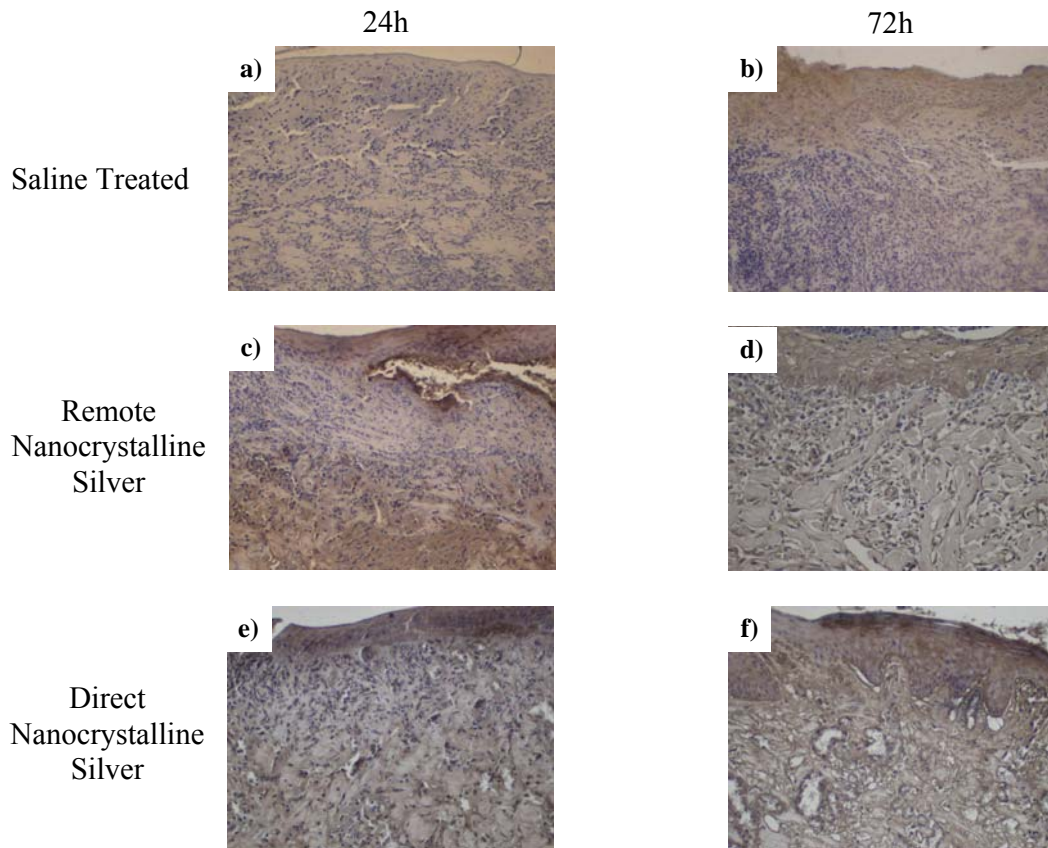


Figure 3-18. Representative images for immunohistochemical detection of KGF after 24h (column 1) and 72h (column 2) treatment of DNCB-induced porcine contact dermatitis rashes with saline (a,b), remote nanocrystalline silver (c, d), or direct nanocrystalline silver (e,f). The scale bar in f) represents 50 μ m. Staining for KGF appears brown, while the cell nuclei are counterstained purple using hematoxylin.

Representative images of immunohistochemical staining for KGF-2 are shown in Figure 3-19 for animals treated with saline only (a-b), animals treated with remote nanocrystalline silver (c-d), and animals treated directly with nanocrystalline silver (e-f), after 24 and 72 hours of treatment. Animals treated with saline only showed light diffuse staining at both time points. However, at 24 hours, animals that also received remote nanocrystalline silver showed stronger staining specific to depths where re-epithelization occurred at later time points, while at 72h, staining was strong and cell specific, showing a similar pattern to IL-4 and EGF. Animals treated directly with nanocrystalline silver did not show much staining for KGF-2 at 24 hours, but did show strong cell specific staining for KGF-2 at 72 hours in both the epidermis and the dermis. The epidermal staining, however, was not as widespread as that seen in the animals treated remotely with nanocrystalline silver, suggesting that the peak expression of KGF-2 occurred earlier with direct nanocrystalline silver treatment.

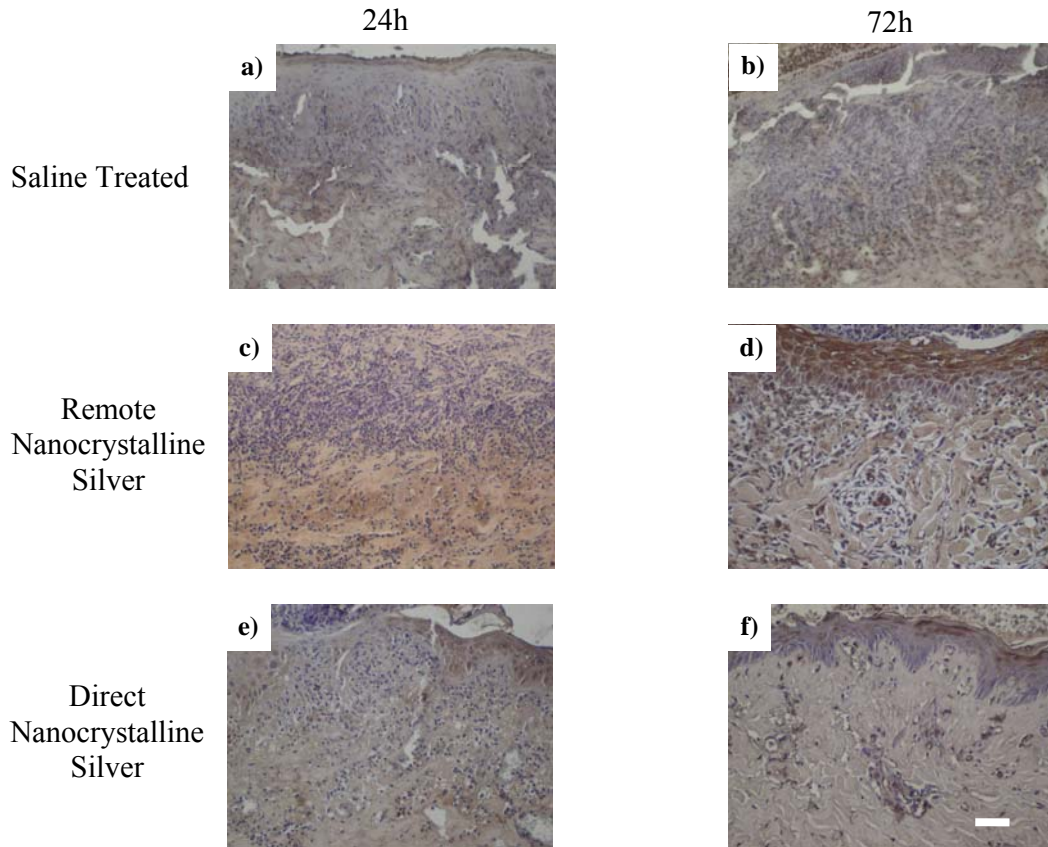


Figure 3-19. Representative images for immunohistochemical detection of KGF-2 after 24h (column 1) and 72h (column 2) treatment of DNCB-induced porcine contact dermatitis rashes with saline (a,b), remote nanocrystalline silver (c, d), or direct nanocrystalline silver (e,f). The scale bar in f) represents 50 μm . Staining for KGF-2 appears brown, while the cell nuclei are counterstained purple using hematoxylin.

Testing for Systemic Effects Via the Blood

IL-10 Tissue and Serum Levels

Figure 3-20 shows representative images of immunohistochemical staining for IL-10, using a polyclonal antibody, in tissues from animals treated for 72h directly with saline (Figure 3-20b, f, j), silver nitrate (Figure 3-20c, g, k), and nanocrystalline silver (Figure 3-20d, h, l). Representative images of negative controls are also shown (Figure 3-20a, e, i). Negative controls showed low levels

of cell-specific staining for IL-10, with most of the staining occurring in the upper layers of the epidermis. However, there was staining of some pockets of cells in the dermis, including blood vessels. Saline treated samples showed staining of only small pockets of cells on Day 1, with a somewhat increased, but more diffuse, staining present by Day 3 in the dermis. Silver nitrate treated samples showed strong diffuse staining for IL-10 on Day 1, particularly in the epidermis. Some of the staining may be nonspecific, as some areas of collagen are highly stained, where IL-10 is unlikely to be present, as it is normally cell-associated. On Day 2, in contrast, there was very little staining for IL-10 in silver nitrate treated tissues, and at Day 3, levels and patterns of staining were similar to that observed with the saline treated animals. Nanocrystalline silver treated samples showed the strongest staining for IL-10 early in the treatment, particularly in the epidermis. However, the staining intensity decreased with time so that by Day 3, only pockets of cells in the dermis appeared to be stained. Again, there was some concern about the specificity of the technique, due to the widespread nature of the staining on Days 1 and 2.

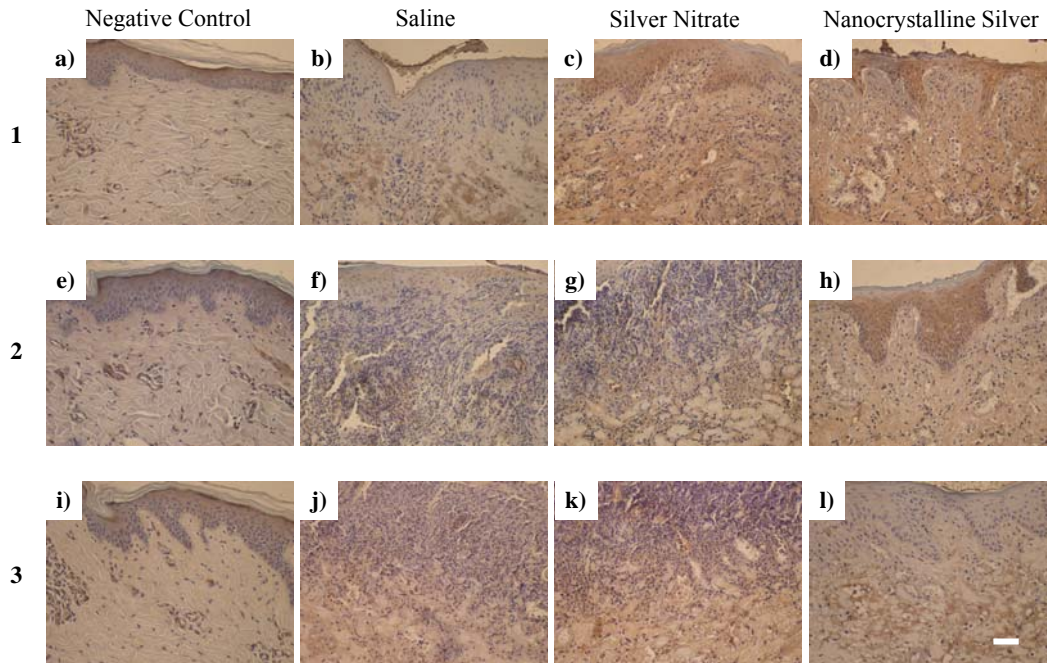


Figure 3-20. Representative images for immunohistochemical detection of IL-10 (using a polyclonal antibody) after 24h (row 1, a-d), 48 h (row 2, e-h), or 72h (row 3, i-l) of treatment with saline (b, f, j), silver nitrate (c, g, k), or direct nanocrystalline silver (d, h, l). Negative controls are also shown (a, e, i). The scale bar in l) represents 50 μm . Staining for IL-10 appears brown, while the cell nuclei are counterstained purple using hematoxylin.

Figure 3-21 shows IL-10 serum levels for pigs with rashes before treatment, and negative controls and pigs with rashes treated with saline, silver nitrate, or direct or remote nanocrystalline silver after three days of treatment. The serum concentration from highest to lowest was: negative control > Day 0 rash > saline treated > silver nitrate treated > direct nanocrystalline silver treated > remote nanocrystalline silver treated. However, there were no significant differences between groups ($p=0.4468$). It should be noted that all the samples, with the exception of some of the negative controls, had IL-10 levels below lowest concentration standard, meaning that they were below the detection limit of the assay.

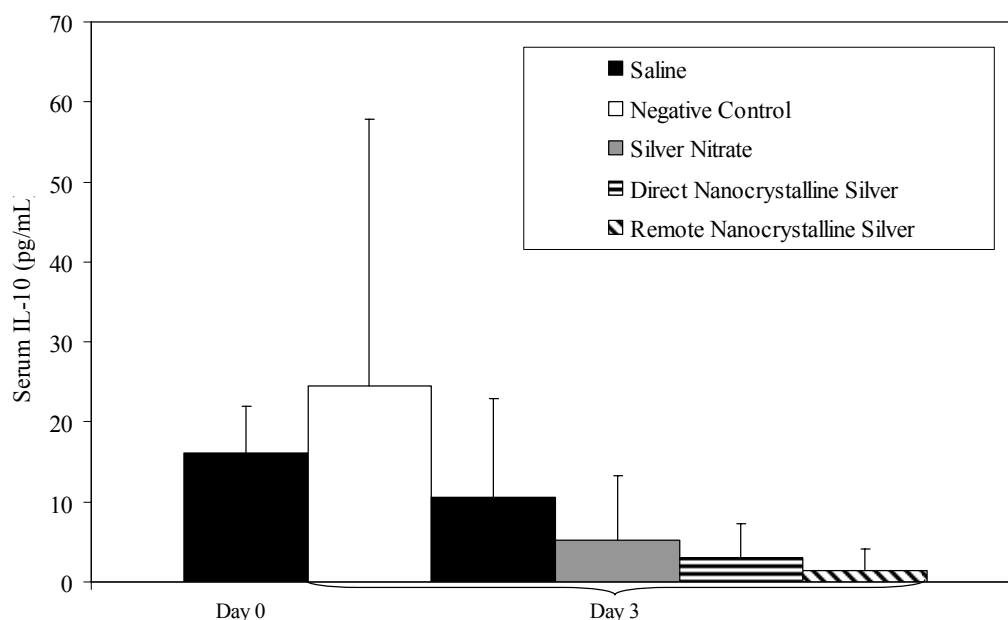


Figure 3-21. Serum IL-10 levels measured from pigs with DNCB-induced rashes before treatment, and treated for three days with saline, silver nitrate, direct nanocrystalline silver, or remote nanocrystalline silver. Serum IL-10 levels were also measured for negative controls treated for three days with saline. Statistical analyses were performed using one-way ANOVAs with Tukey-Kramer post tests. The one-way ANOVA tests indicated that the differences between groups were not significant ($p=0.4468$). Error bars = standard deviations ($n=3$ for each point).

CRP Serum Levels

Figure 3-22 shows the serum levels of c-reactive protein for pigs with rashes before treatment, and negative controls and pigs with rashes treated with saline, silver nitrate, direct or remote nanocrystalline silver after three days of treatment. There were no significant differences between groups ($p=0.5714$). Three groups appeared to have one high outlier each, which still had much higher optical densities than the strongest standard after a 1:500 dilution, and which were very different than the other two values from the same group. Therefore, one outlier was removed from the negative control group, the saline treated group, and

the direct nanocrystalline silver treated group, and the statistics were repeated. Figure 3-23 shows the data with these three outliers removed. The CRP levels are higher in the pigs with rashes at Day 0 than in negative controls at Day 3. By Day 3, CRP serum levels decreased in saline treated animals, and decreased further in direct nanocrystalline silver treated animals. However, in animals treated with silver nitrate or with remote nanocrystalline silver, the CRP serum levels remained near Day 0 levels. These trends were not statistically significant ($p=0.3624$), which may have been due to the large variations between animals, even with the three outliers removed.

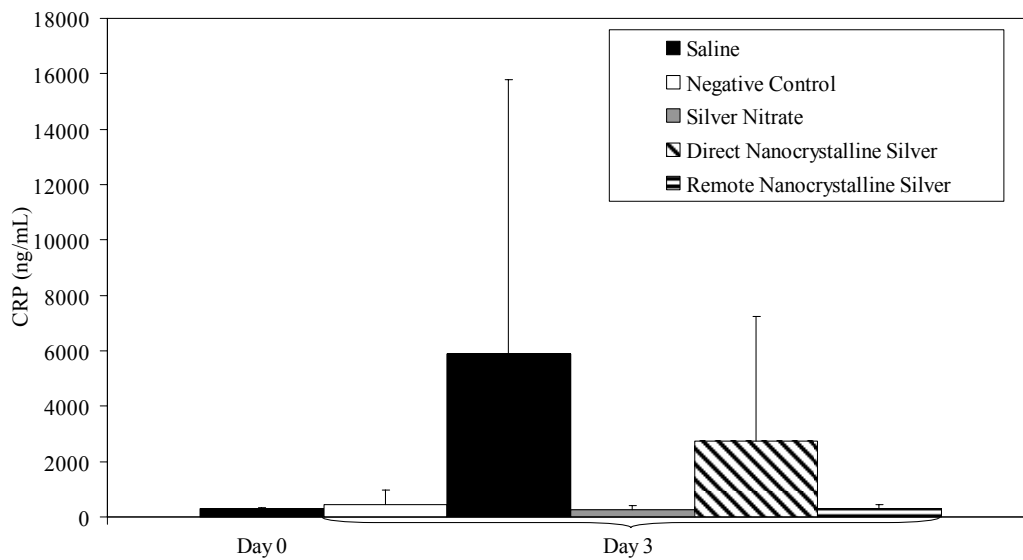


Figure 3-22. Serum CRP levels measured for pigs with DNCB-induced rashes before treatment, and treated for three days with saline, silver nitrate, direct nanocrystalline silver, or remote nanocrystalline silver. Serum CRP levels were also measured for negative controls treated for three days with saline. Statistical analyses were performed using one-way ANOVAs with Tukey-Kramer post tests. The one-way ANOVA tests indicated that the differences between groups were not significant ($p=0.5714$). Error bars represent standard deviations ($n=3$ for all data points).

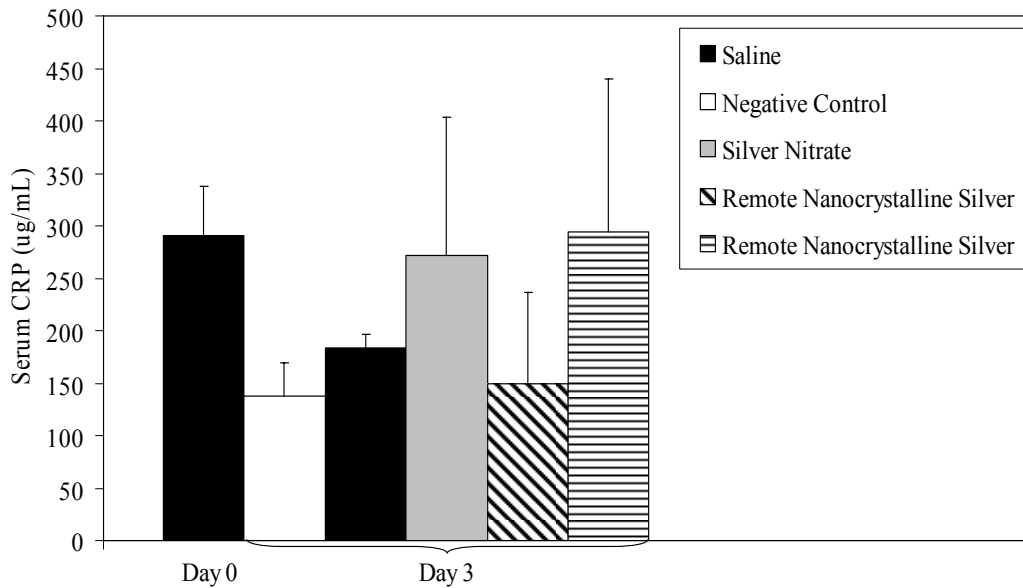


Figure 3-23. Serum CRP levels with outliers removed. Three outliers, one from the saline treated group after three days of treatment, one from the negative control group, and one from the group treated with nanocrystalline silver for three days, were removed from the data set analyzed in Figure 13, and the statistical analysis was repeated as above. The one-way ANOVA tests indicated that the differences between groups were still not significant ($p=0.3624$). Error bars represent standard deviations.

Discussion

Nanocrystalline silver has been used as an antimicrobial for about a decade, but since its clinical introduction, studies have demonstrated that in addition to antimicrobial activity, it has pro-healing/anti-inflammatory activity [1-5, 10]. However, the mechanism of action for this activity is not yet fully understood. Previous studies have not clarified whether nanocrystalline silver acts through direct contact with inflammatory cells, or whether the action is indirect. An indirect action could perhaps be via interaction with cells near treated tissue surfaces, which causes a modification of the behavior of the cells, such that they release signals resulting in anti-inflammatory/pro-healing activity.

If this were the case, then it might be possible for nanocrystalline silver treatment to impact healing remote from the location of application, especially if the biological signals were able to travel systemically. This study suggests that nanocrystalline silver does not produce its anti-inflammatory activity solely by direct interaction with inflammatory cells, and that it can have an impact on healing remote from the location of application.

XPS analysis did not detect silver in the mid-dermis or subcutaneous fat layer for DNCB-induced porcine rashes treated directly with nanocrystalline silver or silver nitrate. SIMS analysis indicated that all forms of silver detected were largely deposited in the epidermis for both direct nanocrystalline silver and silver nitrate treatments, and neither treatment penetrated more than a few hundred micrometers. As the silver did not penetrate more than 100 μm in samples treated with nanocrystalline silver, and the XPS analysis indicated the same, the biopsies from pigs treated with nanocrystalline silver on the opposite side of the back and saline on the rash were not examined for silver, as there appeared to be no possibility that the nanocrystalline silver could have traveled so far. Comparing the XPS and SIMS data to the apoptotic staining data reported for direct silver nitrate treatment in Chapter 2, the strongest apoptotic staining occurred in the same locations where silver nitrate was primarily deposited – in the epidermis and upper dermis. It appears that apoptotic staining decreased with decreasing silver concentration in silver nitrate treated samples through the epidermis and upper dermal layers, and was not present in the deep dermis (see Figures 2-17 and 2-19) where silver nitrate did not contact the tissue. This

suggests that the silver nitrate induced apoptosis only by direct contact with cells, again suggesting that the silver nitrate may be toxic to cells that are in direct contact with it in sufficient concentration[5]. However, apoptotic staining was minimal in the epidermis following direct nanocrystalline silver treatment, despite this study indicating that the nanocrystalline silver was heavily deposited there. Rather, apoptotic staining was strong throughout the dermis (see Figures 2-17 and 2-19) - much deeper than the nanocrystalline silver appears to have been able to penetrate. This suggests that, unlike silver nitrate, the activity of nanocrystalline silver cannot be solely through direct interaction with inflammatory cells, but must be through activation of cells it contacts near the skin surface which then produce biological signals altering the inflammatory cascade, which causes a reduced inflammatory response. It is also interesting to note that this study showed significant levels of weights corresponding to silver clusters Ag_{2-6} in tissues receiving direct nanocrystalline silver treatment. As already discussed in Chapter 2, previous studies have shown that $\text{Ag}^{(0)}$ dissolves off of nanocrystalline silver in aqueous solutions, most likely in a cluster form containing two to eight atoms[11]. It has been hypothesized that these clusters may be the silver species responsible for the anti-inflammatory activity of nanocrystalline silver, because other noble metals believed to be in cluster form have anti-inflammatory activity[12-18]. This study lends weight to this hypothesis, since it shows significant deposition of weights corresponding to silver clusters specifically with nanocrystalline silver treatment.

Since the SIMS and XPS data suggested that the anti-inflammatory

activity of nanocrystalline silver was indirect, as it appears to extend farther into tissues than the nanocrystalline silver itself penetrates, tissues were examined from pigs treated with nanocrystalline silver placed on the opposite side of the back from the DNCB-induced rash. This was to determine whether any indirect effects of nanocrystalline silver were systemic, or only local.

Visual observations suggested that when pigs were treated with remote nanocrystalline silver, there was some repair of the tissues observed over three days of treatment. Pigs treated with saline only did not demonstrate any improvement over the same time period (see Figure 2-5), suggesting that the nanocrystalline silver placed on remote healthy tissue may have had an anti-inflammatory/pro-healing effect.

This was confirmed by erythema and edema scores, which were significantly decreased in pigs treated with remote nanocrystalline silver, relative to pigs treated with saline only. The visual improvements, as well as the impact on erythema and edema scores, observed with remote nanocrystalline silver treatments, were not as pronounced as the effect of directly placing nanocrystalline silver on the rash (see Figures 2-5 and 2-6). This suggests that treatment with remote nanocrystalline silver delays and/or weakens its impact relative to direct treatment.

The histological images corroborate the visual observations, in that clear improvements in tissue morphology occurred in all three pigs treated with remote nanocrystalline silver after two days of treatment. Decreases in tissue damage due to edema, inflammatory cells, and red blood cells were observed in all three

pigs. During this time, pigs treated with saline only showed no improvement, indicating that the remote nanocrystalline silver did have an impact on healing. However, the histological changes were not as marked as those observed when the tissues were treated directly with nanocrystalline silver (see Figure 2-9), where the tissues were nearly indistinguishable from normal skin histologically after three days of treatment. At 72 hours, tissues treated with remote nanocrystalline silver still showed signs of tissue damage (Fig 1), inflammatory cell presence (all three pigs), pockets of red blood cells (Fig 2), and poor tissue morphology (Fig 3). Again, this suggests a delay or weakening of the impact of the nanocrystalline silver with remote treatment. However, as clear reductions in inflammation were observed at Day 2 both for animals treated directly and remotely with nanocrystalline silver, this suggests a weakening of the anti-inflammatory effect, rather than a delayed impact. In contrast, near-normal tissue morphology was not obtained within the three days of indirect treatment, but was obtained with direct treatment, suggesting perhaps a delayed pro-healing effect with indirect treatment.

As with direct treatments, remote nanocrystalline silver treatments significantly upregulated apoptosis in the dermis, which was highly infiltrated with inflammatory cells, relative to positive controls at 24 hours. Thus, both remote and direct treatments appear to induce apoptosis in inflammatory cells by the same mechanism and within the same timeframe. This corroborates the theory of a biological cascade effect, rather than a direct silver interaction with inflammatory cells, as a delayed effect would be expected if the active silver had

to travel in sufficient quantities to the remote tissues to exert its apoptotic effect. A diluted, but not delayed, response would be more likely if silver induced changes to biological signals being produced at the site of silver application, causing the observed remote anti-inflammatory effect. The amplified biological signal should be stronger and more capable of long distance travel in the body, since silver would be expected to bind to chlorides and proteins, and therefore a biological signal could generate a remote impact more quickly. Studies have demonstrated that apoptosis is involved in the elimination of inflammatory cells from inflamed tissues[19], and have shown that nanocrystalline silver treatments are capable of apoptosis induction specifically in inflammatory cells.

Nanocrystalline silver treatment of porcine contaminated wounds resulted in apoptosis induction in inflammatory cells at 48 hours[3]. As well, apoptosis induction specific to inflammatory cells in a mouse ear rash model was observed with a nanocrystalline silver cream treatment, although the timeframe for this effect was not noted[2].

Immunohistochemical analysis confirmed that an anti-inflammatory effect was observed with remote nanocrystalline silver treatments, with reduced expression of pro-inflammatory cytokines TNF- α and IL-8, which are both major mediators of the inflammatory response[19, 20]. This may have been due to induction of apoptosis in inflammatory cells producing these signals. In Chapter 2, the same type of testing showed that direct nanocrystalline silver treatments also resulted in reduced TNF- α and IL-8 expression by 72 hours. In addition, other studies have demonstrated that direct nanocrystalline silver treatments result

in reduced expression of IL-12[2] and IL-6[21], as well as TNF- α [2].

Surprisingly, neither the positive controls nor the animals treated with remote nanocrystalline silver showed upregulation of TGF- β in this study, despite the fact that the positive controls showed strong staining for TGF- β in Chapter 2. This may be due to the fact that a new lot of the primary antibody had to be purchased for this study, which may have been weaker than the previous lot.

IL-10 is an important anti-inflammatory cytokine produced by T cells, B cells, macrophages, keratinocytes, and others[22]. It reduces TNF- α activity, induces apoptosis in neutrophils and macrophages, and decreases IL-6 and IL-8 production[22]. Since treatment of inflamed tissue by nanocrystalline silver increased apoptosis in inflammatory cells, and decreased the expression of TNF- α and IL-8, it seemed likely that IL-10 upregulation would explain many effects observed with nanocrystalline silver treatments. Immunohistochemical data using the polyclonal IL-10 antibody suggested that direct treatment of the DNCB-induced rashes with nanocrystalline silver resulted in increased IL-10 protein levels relative to animals treated with saline or negative controls. As well, since most of the nanocrystalline silver was deposited in the epidermis, and this was where the strongest staining for IL-10 occurred, it seemed possible that nanocrystalline silver directly interacts with cells in the epidermis, causing them to produce IL-10, which could then regulate some of the anti-inflammatory effects observed. However, when a monoclonal antibody was used, IL-10 did not appear to be upregulated with either direct or remote nanocrystalline silver treatments, suggesting that the polyclonal antibody did not provide specific staining.

Interestingly, a study in which murine thermal injuries were treated with silver nanoparticles showed IL-10 upregulation[21]. While this may be due to differences in models or techniques used, it suggests that silver nanoparticles may impact wound healing by different mechanisms than poly-nanocrystalline silver thin films. IL-4 (produced primarily by T cells, but also by macrophages, B cells, and others[22]) is another anti-inflammatory cytokine. It induces apoptosis of neutrophils and macrophages, and downregulates the effects of IL-1, TNF- α , IL-6, and IL-8 on macrophages[22-25]. IL-4 was upregulated with both direct and remote nanocrystalline silver treatments, particularly in areas of re-epithelialization, suggesting that IL-4 may have enhanced apoptosis of inflammatory cells, allowing for re-epithelialization. IL-4 expression may have peaked earlier with direct nanocrystalline silver treatment, suggesting a prolonged anti-inflammatory response with the remote treatments relative to the direct treatments. Since apoptosis induction was observed at 24 hours of treatment with both direct and remote treatments, but some inflammatory cells were still observed at 72 hours with the indirect treatments, this suggests a weakened response with the remote treatment.

In addition to anti-inflammatory effects, the histological data suggested that nanocrystalline silver treatments appeared to have a pro-healing effect, including enhanced rates of tissue repair and re-epithelialization. Thus, growth factors involved in these processes were examined via immunohistochemistry. EGF (secreted by platelets, macrophages, and fibroblasts) acts as a mitogen for keratinocytes and promotes their migration, thus enhancing reepithelialization[26-

28]. It also enhances formation of granulation tissue and stimulates fibroblast motility[29]. KGF and KGF-2 are produced by a variety of cells, including fibroblasts[30, 31], and act on keratinocytes in paracrine fashion[32]. They both stimulate proliferation and migration of keratinocytes, and increase transcription of factors involved in detoxification of reactive oxygen species (ROS), protecting keratinocytes from ROS-induced apoptosis[28, 32]. Thus, the upregulation of EGF, KGF, and KGF-2 observed with both direct and remote nanocrystalline silver treatments may have enhanced the rate of re-epithelialization while protecting the keratinocytes from apoptosis, accounting, at least in part, for the pro-healing effects observed. Since EGF is directly involved in granulation tissue formation[29], and KGF[32] and KGF-2[33] are also involved indirectly, their upregulation may help explain previous observations that nanocrystalline silver treatments resulted in enhanced granulation tissue formation in a porcine contaminated wound model[3]. Additionally, since KGF indirectly promotes angiogenesis via upregulating VEGF[32, 34], the increased expression of KGF with nanocrystalline silver treatment may partially explain the increased VEGF levels observed when mouse thermal injuries were treated with silver nanoparticles[21]. It is noteworthy that KGF expression was enhanced earlier than KGF-2 expression, and that by the time KGF-2 expression was enhanced, KGF levels had dropped. This is particularly clear with the remote treatments. This same sequence of events occurs during normal wound healing, suggesting that rather than rapidly increasing the expression of a few pro-healing molecules simultaneously, nanocrystalline silver treatment appears to have sped up the entire

healing process. Additionally, treating rashes directly with nanocrystalline silver appeared to result in earlier peak expression of IL-4, EGF, and KGF-2 relative to remote treatments. This suggests that with indirect treatment there was a delay in the expression of certain growth factors, and may explain why histological improvements in tissue morphology were not as marked at the end of the experiment with the remote treatments relative to the direct treatments, despite the fact that there was decreased inflammation at Day 2 due to apoptosis induction for both the direct and remote treatments.

Since the above analyses indicated that treatment with nanocrystalline silver away from the DNCB-induced rashes improved wound healing relative to positive controls, this suggests that nanocrystalline silver has a systemic effect. To examine this potential systemic impact on inflammation, c-reactive protein (CRP) serum levels were examined for the groups of pigs described in Chapter 2, as well as for pigs treated with remote nanocrystalline silver. CRP is an acute phase protein synthesized by hepatocytes. Its plasma concentration is increased during infection and inflammation caused by tissue injuries such as immunological responses, allergic responses, infections, thermal injuries[35], and other conditions in which tissue necrosis occurs, making it a useful measure of the systemic events that accompany inflammation. Plasma CRP levels begin to increase within four to six hours after the initial injury and increase exponentially (several hundred fold) within the first two days[35]. CRP levels remain elevated throughout the acute-phase response, and return to normal as tissue structure and function is restored[35]. It has a half-life of less than 24 hours[36]. Thus, its

levels would be expected to increase with the induction of rashes using DNCB, and to decrease as the inflammation caused by the DNCB subsided. From Figure 3-23, it is clear that serum CRP levels were increased with rash induction relative to negative controls. In addition, these levels decreased somewhat after three days of treatment with saline only, suggesting that systemic measures of inflammation were beginning to subside by this time with only the maintenance of a moist protected environment. Average CRP levels were even lower in the group of pigs receiving direct nanocrystalline silver treatments, suggesting that nanocrystalline silver further decreased the systemic acute response, indicating a decreased inflammation relative to the saline treated pigs. After three days of treatment, silver nitrate treated pigs still have CRP levels near those of Day 0, suggesting that the acute response to inflammation was enhanced by this treatment relative to the saline treated animals. This suggests that the treatment may be associated with increased inflammation and/or tissue necrosis. In contrast to the results for direct nanocrystalline silver treatment, CRP levels after 72 hours of treatment were also near Day 0 levels for pigs treated with remote nanocrystalline silver. However, none of these trends reached statistical significance. A larger study would be needed to clarify the impact of nanocrystalline silver treatments, applied either directly or remotely, on systemic markers of the acute-phase response to DNCB-induced inflammation, as there was large intra-group variability.

As there were indications that nanocrystalline silver treatments resulted in a decrease of the systemic acute-phase response to the epidermal inflammation

induced by DNCB, systemic levels for IL-10 were examined. This was performed before the monoclonal IL-10 primary antibody was obtained, which showed limited IL-10 expression at tissue surfaces during treatment with nanocrystalline silver. Since, despite specificity issues, there appeared to be an increased expression of IL-10 in nanocrystalline silver treated tissues using the polyclonal primary antibody, IL-10 serum levels were examined to determine whether or not it might play a role in the anti-inflammatory/pro-healing effect of remote nanocrystalline silver treatment. In the assay used, all pigs exposed to DNCB had lower serum IL-10 levels than the negative controls, and most had lower concentrations than the lowest standard provided with the assay. As well, there were no statistically significant findings, with large variability between pigs in each group. Thus, the results of the assay were not conclusive. However, the serum from pigs treated with nanocrystalline silver (either directly or remotely) had the lowest serum IL-10 levels of any group. This, combined with the immunohistochemical data using the monoclonal IL-10 primary antibody, suggests that IL-10 is not involved in systemic anti-inflammatory/pro-healing effects caused by nanocrystalline silver.

Overall, this study suggests that the anti-inflammatory/pro-healing effects of nanocrystalline silver in a DNCB-induced porcine contact dermatitis model are not caused by direct contact with inflammatory cells, as the nanocrystalline silver had minimal penetration into the tissue. Therefore, the anti-inflammatory effects of nanocrystalline silver appear to have been induced by interactions with cells in the epidermis and upper dermis, which then release biological signals resulting in

anti-inflammatory activity throughout the dermis, and even to tissue remote from the site of nanocrystalline silver application, as indicated by observations with pigs treated with remote nanocrystalline silver. These traits of nanocrystalline silver could prove very useful clinically. Nanocrystalline silver placed on uninjured tissues, or only on certain portions of an injury, could potentially reduce inflammation throughout the injured area.² This may result in improved treatment of wounds with uneven surfaces, such as tunneling wounds. Furthermore, it is possible that nanocrystalline silver could indirectly reduce inflammation of internal epithelial tissues, such as linings of the lungs and gastrointestinal tract.

² It is important to note that nanocrystalline silver's antimicrobial activity would not extend to tissue distant from the site of application, as the bacteria are likely killed directly via the uptake of Ag^+ , and potentially higher oxidation state silver species, from the dressing[37], and the SIMS and XPS data indicates that the silver species themselves are not penetrating the tissues or traveling through the body. Furthermore, these species would be deactivated very quickly by proteins, even if they were able to enter the bloodstream. Therefore, in situations where infection is a concern, the dressings should still be applied directly to the injured tissues whenever possible.

Bibliography

1. Bhol KC, Alroy J, Schechter PJ: **Anti-inflammatory effect of topical nanocrystalline silver cream on allergic contact dermatitis in a guinea pig model.** *Clin Exp Dermatol* 2004, **29**:282-287.
2. Bhol KC, Schechter PJ: **Topical nanocrystalline silver cream suppresses inflammatory cytokines and induces apoptosis of inflammatory cells in a murine model of allergic contact dermatitis.** *Br J Dermatol* 2005, **152**:1235-1242.
3. Wright JB, Lam K, Buret AG, Olson ME, Burrell RE: **Early healing events in a porcine model of contaminated wounds: effects of nanocrystalline silver on matrix metalloproteinases, cell apoptosis, and healing.** *Wound Repair Regen* 2002, **10**:141-151.
4. Demling RH, DeSanti L: **The rate of re-epithelialization across meshed skin grafts is increased with exposure to silver.** *Burns* 2002, **28**:264-266.
5. Nadworny PL, Wang JF, Tredget EE, Burrell RE: **Anti-inflammatory activity of nanocrystalline silver in a porcine contact dermatitis model.** *Nanomed: NBM* 2008, **4**:241-251.
6. Thunus L, Dauphin JF, Moyny G, Deby C, Deby-Dupont G: **Anti-inflammatory properties of copper, gold and silver, individually and as mixtures.** *Analyst* 1995, **120**:967-973.
7. Kelley KW, Curtis SE, Marzan GT, Karara HM, Anderson CR: **Body surface area of female swine.** *J Anim Sci* 1973, **36**:927-930.
8. Woods A: **Hematoxylyn and Counterstains.** In: *Laboratory Histopathology: A Complete Reference.* Eds. Woods A, Ellis R. Livingstone: Churchill Livingstone; 1994.
9. **In situ Cell Death Detection Kit, AP, Instruction Manual.** ©Roche Diagnostics Corporation. www.roche-applied-science.com/pack-insert/11684809910a.pdf. Viewed September 21, 2006.
10. Kirsner RS, Orsted H, Wright JB: **Matrix metalloproteinases in normal and impaired wound healing: a potential role of nanocrystalline silver.** *Wounds* 2002, **13**:4-12.
11. Fan FF, Bard AJ: **Chemical, electrochemical, gravimetric, and microscopic studies on antimicrobial silver films.** *J Phys Chem B* 2002, **106**:279-287.
12. Fuertes MA, Castilla J, Alonso C, Perez JM: **Cisplatin biochemical mechanism of action: from cytotoxicity to induction of cell death through interconnections between apoptotic and necrotic pathways.** *Curr Med Chem* 2003, **10**:257-266.
13. Mizushima Y, Okumura H, Kasukawa R: **Effects of gold and platinum on necrotizing factor, skin sensitizing antibody, and complement.** *Jpn J Pharmacol* 1965, **15**:131-134.
14. Handel ML, Nguyen LQ, Lehmann TP: **Inhibition of transcription factors by anti-inflammatory and anti-rheumatic drugs: can**

- variability in response be overcome?** *Clin Exp Pharmacol Physiol* 2000, **27**:139-144.
15. Suzuki S, Okubo M, Kaise S, Ohara M, Kasukawa R: **Gold sodium thiomalate selectivity inhibits interleukin-5-mediated eosinophil survival.** *J Allergy Clin Immunol* 1995, **96**:251-256.
 16. Eisler R: **Chrysotherapy: a synoptic review.** *Inflamm Res* 2003, **52**:487-501.
 17. Abraham GE, Himmel PB: **Management of Rheumatoid Arthritis: Rationale for the Use of Colloidal Metallic Gold.** *J Nutr Env Med* 1997, **7**:295-305.
 18. Zou J, Guo Z, Parkinson JA, Chen Y, Sadler PJ: **Gold(III)-induced oxidation of glycine: relevance to the toxic side-effects of gold drugs.** *J Inorg Biochem* 1999, **74**:352.
 19. Serhan CN, Savill J: **Resolution of inflammation: the beginning programs the end.** *Nat Immunol* 2005, **6**:1191-1197.
 20. Girolomoni G, Pastore S, Albanesi C, Cavani A: **Targeting tumor necrosis factor-alpha as a potential therapy in inflammatory skin diseases.** *Curr Opin Investig Drugs* 2002, **3**:1590-1595.
 21. Tian J, Wong KK, Ho CM, Lok CN, Yu WY, Che CM, Chiu JF, Tam PK: **Topical delivery of silver nanoparticles promotes wound healing.** *ChemMedChem* 2007, **2**:129-136.
 22. Lin E, Calvano SE, Lowry SF: **Inflammatory cytokines and cell response in surgery.** *Surgery* 2000, **127**:117-126.
 23. Donnelly RP, Fenton MJ, Finbloom DS, Gerrard TL: **Differential regulation of IL-1 production in human monocytes by IFN-gamma and IL-4.** *J Immunol* 1990, **145**:569-575.
 24. Essner R, Rhoades K, McBride WH, Morton DL, Economou JS: **IL-4 down-regulates IL-1 and TNF gene expression in human monocytes.** *J Immunol* 1989, **142**:3857-3861.
 25. Szabo G, Kodys K, Miller-Graziano CL: **Elevated monocyte interleukin-6 (IL-6) production in immunosuppressed trauma patients. II. Downregulation by IL-4.** *J Clin Immunol* 1991, **11**:336-344.
 26. Schultz G, Rotatori DS, Clark W: **EGF and TGF-alpha in wound healing and repair.** *J Cell Biochem* 1991, **45**:346-352.
 27. Brown GL, Curtsinger L, 3rd, Brightwell JR, Ackerman DM, Tobin GR, Polk HC, Jr., George-Nascimento C, Valenzuela P, Schultz GS: **Enhancement of epidermal regeneration by biosynthetic epidermal growth factor.** *J Exp Med* 1986, **163**:1319-1324.
 28. Barrientos S, Stojadinovic O, Golinko MS, Brem H, Tomic-Canic M: **Growth factors and cytokines in wound healing.** *Wound Repair Regen* 2008, **16**:585-601.
 29. Hardwicke J, Schmaljohann D, Boyce D, Thomas D: **Epidermal growth factor therapy and wound healing--past, present and future perspectives.** *Surgeon* 2008, **6**:172-177.

30. Braun S, auf dem Keller U, Steiling H, Werner S: **Fibroblast growth factors in epithelial repair and cytoprotection.** *Philos Trans R Soc Lond B Biol Sci* 2004, **359**:753-757.
31. Beer HD, Florence C, Dammeier J, McGuire L, Werner S, Duan DR: **Mouse fibroblast growth factor 10: cDNA cloning, protein characterization, and regulation of mRNA expression.** *Oncogene* 1997, **15**:2211-2218.
32. Beer HD, Gassmann MG, Munz B, Steiling H, Engelhardt F, Bleuel K, Werner S: **Expression and function of keratinocyte growth factor and activin in skin morphogenesis and cutaneous wound repair.** *J Invest Dermatol Symp Proc* 2000, **5**:34-39.
33. Jimenez PA, Rampy MA: **Keratinocyte growth factor-2 accelerates wound healing in incisional wounds.** *J Surg Res* 1999, **81**:238-242.
34. Frank S, Hubner G, Breier G, Longaker MT, Greenhalgh DG, Werner S: **Regulation of vascular endothelial growth factor expression in cultured keratinocytes. Implications for normal and impaired wound healing.** *J Biol Chem* 1995, **270**:12607-12613.
35. Husain TM, Kim DH: **C-Reactive Protein and Erythrocyte Sedimentation Rate in Orthopaedics.** *University of Pennsylvania Orthopaedic Journal* 2002, **15**:13-16.
36. Foglar C, Lindsey RW: **C-reactive protein in orthopedics.** *Orthopedics* 1998, **21**:687-691.
37. Demling RH, Burrell RE: **The beneficial effects of nanocrystalline silver as a topical antimicrobial agent.** *Leadership Medica* 2002, **16**:10 pages.

Chapter 4 – Understanding Nanocrystalline Silver Antimicrobial Mechanisms of Action via Comparison to Other Silver Products¹

Introduction

Although nanocrystalline silver dressings clearly have more beneficial properties than do dressings which release only Ag^+ , the mechanisms of action behind the activity of nanocrystalline silver are not well understood. In order to make the best use of nanocrystalline silver dressings and to create other silver-containing products with optimal activity, a better understanding of how nanocrystalline silver functions is necessary. By comparing the similarities and differences between the activity of nanocrystalline silver dressings and other silver-containing dressings or treatments, new knowledge about the mechanisms of action of nanocrystalline silver can be obtained.

The purpose of the studies presented in this chapter was to compare nanocrystalline silver to various other silver-containing products in terms of their biological activity and their physicochemical properties in order to determine what properties were necessary for biological activity. The first study compares nanocrystalline silver to a variety of recently released silver-containing commercial products in terms of their antimicrobial activity, silver release, and other dressing properties. The second study compares the activity of nanocrystalline silver dressings against Ag^+ -resistant bacteria to that of other silver-containing dressings, as well as the ability of the various silver-containing treatments to prevent or promote the development of silver resistant bacteria. The

¹ A version of the first study in this chapter has been submitted for publication. Cavanagh, Burrell, and Nadworny, 2009. International Wound Journal.

third study compares the activity of nanocrystalline silver thin film dressings (which are polycrystalline) to nanocrystalline silver composed of single nanocrystals, to determine if size alone is important for antimicrobial activity, or if polycrystallinity is also necessary.

Study #1: Comparison of Antimicrobial Efficacy of New Commercially Available Silver Dressings Relative to Nanocrystalline Silver Dressings

Background

Chronic and acute wounds are often heavily colonized or infected by bacteria[1] which interfere with wound healing processes by inducing an inflammatory host response[2, 3]. This makes prevention and treatment of bacterial colonization a critical part of wound care. Traditional methods of controlling bacterial colonization involve the use of topical antimicrobial agents such as silver nitrate and silver sulphadiazine. However, over the past decade, a large number of advanced silver-containing dressings have become commercially available. The majority of these dressings are marketed as effective against a broad range of bacteria over multiple days, and are indicated for a variety of serious conditions including partial thickness burns, ulcers of various etiologies, donor and graft sites, traumatic and surgical wounds, dermatologic disorders, and skin tears. However, there is little data available in the peer-reviewed literature regarding these dressings, particularly those which have been released recently.

Nanocrystalline silver dressings have been commercially available for about a decade, and have been recognized for excellent antimicrobial activity in

the peer-reviewed literature. Gallant-Behm *et al.*[4] performed a study comparing corrected zones of inhibition to log reduction assays in the testing of eight advanced silver-containing dressings. Of the dressings tested, they found that only nanocrystalline silver dressings produced bactericidal activity, which was related to its rapid and sustained release of active silver[4]. They also indicated that log reduction assays were the most reliable way to assess the antimicrobial activity of silver containing dressings, while corrected zone of inhibition assays should only be used to test dressing longevity in plate-to-plate transfer assays, and should be performed in conjunction with other tests, such as log reduction or active agent release assays[4].

Thomas and McCubbin[5, 6] tested ten advanced silver-containing wound products for antimicrobial activity using corrected zones of inhibition, challenge tests (using the same methods as those used for log reduction assays), and microbial transmission tests, which they correlated with total extractable silver content. They then gave the dressings a total performance score. A nanocrystalline silver dressing and a silver alginate dressing tied for top score, with their antimicrobial activity being attributed to the rapid release of active silver[5, 6].

A study by Wright *et al.*[7] compared the efficacy of nanocrystalline silver dressings, silver nitrate, silver sulphadiazine, and mafenide acetate against various fungal inocula via kill kinetic (log reduction) assays. They found that the nanocrystalline silver dressing provided the fastest and broadest spectrum fungicidal activity[7]. Yin *et al.*[8] also performed a study comparing

nanocrystalline silver dressings to silver nitrate, silver sulphadiazine, and mafenide acetate, using minimum inhibitory concentration, minimum bactericidal concentrations, zones of inhibition, and killing curve (log reduction) assays against five common wound pathogens. They concluded that the nanocrystalline silver dressing had better antimicrobial properties than the other products tested, with a much faster rate of kill. They also found that a combination of assays was desirable in the testing of these types of antimicrobial materials[8]. Another study by Wright *et al.*[9] compared the efficacy of the nanocrystalline silver dressing to that of a controlled release silver film dressing against a wide variety of wound pathogens, including gram positive (of which *S. aureus* was one) and gram negative bacteria, fungi, and yeast[9]. The assays used were day-to-day transfer corrected zone of inhibition assays, log reduction assays, and silver release assays. Of the two dressings, the nanocrystalline silver dressing demonstrated a much more rapid bactericidal activity against a broader spectrum of organisms[9]. The antimicrobial efficacy of nanocrystalline silver dressings demonstrated *in vitro* in these studies has been corroborated by *in vivo* and clinical studies[10-13].

These studies show that comparison of different silver-containing treatments can provide valuable information about how the dressings behave and why some dressings are more effective than others. Studies such as these also provide useful data regarding which assays, or combinations of assays, provide the most useful information for comparison of different silver-containing products.

The purpose of this study was to compare the activity of some more

recently available silver-containing dressings to nanocrystalline silver dressings, to provide additional knowledge on the following:

1. How nanocrystalline silver dressings work.
2. What can be learned about the efficacy of silver in general from new products.
3. Why some silver-containing products work better than others.
4. What assays provide the most information about silver containing product efficacy.

Five dressings were compared to nanocrystalline silver dressings – a silver sulphate dressing, a silver alginate dressing, a silver collagen matrix dressing, and two ionic silver foam dressings.

There are no known studies concerning the silver sulphate dressing in the peer-reviewed literature. There are, however, a handful of case studies[14-18] and one open non-comparative multicentre investigation[19] which have been presented as posters, but which do not show any direct measures of antimicrobial activity. One open non-comparative single centre study, also presented as a poster, did include microbiological culture swabs, and concluded that the dressing showed antimicrobial efficacy. However, their tabulated data actually shows that 6 out of 11 patients who were initially colonized with *S. aureus*, and 9 out of 11 patients who were initially colonized with *P. aeruginosa*, had little or no reduction (“low” to “none”) of bacterial burden of these species after 30 days of treatment with the dressing[20]. One *in vitro* study by Taherinejad *et al.*[21] also presented as a poster, indicated that the dressing was bactericidal against a variety

of common wound pathogens within three hours, and even within thirty minutes for some organisms[21]. They also showed that the dressings could be challenged daily for seven days with these organisms and retain their activity[21]. However, in their methods, they indicate that for all tests, they put one gram of dressing in 50 mL of media plus bacteria. Based on measurements performed for the current study, one gram of this dressing is 5.9 cm² of material, and thus, in their assay, the dressing was instantly exposed to 8.5 mL/cm² of fluid (approximately 8.5 g/cm²). Since wound exudate can be classified by quantity as mild (0.25 g/cm²/24 hours), moderate (0.5 g/cm²/24 hours), and heavy (1.0 g/cm²/24 hours)[22], the method used by Taherinejad *et al.*[21] would instantly expose the dressings to 8.5 times and 34 times the 24 hour fluid volume of highly and mildly exudative wounds, respectively. This suggests that the results of their study may not be indicative of the clinical efficacy of the dressings[23].

There are no known studies concerning the silver collagen matrix dressing in the peer-reviewed literature. Again, there are a handful of case studies which have been presented as posters[24-28]. These case studies do not focus on the antimicrobial activity of the dressing, but rather on other features.

There are no known studies concerning the silver alginate dressing, either in the peer reviewed literature or presented as posters. Their product claims are based on data the company has on file.

There are a variety of case studies concerning the ionic silver foam dressings which have been presented as posters[29-37]. There are also two *in vitro* studies in the peer reviewed literature[38, 39] that tested one of the ionic

silver foam dressings, along with a variety of other silver containing dressings, for antimicrobial activity using methods similar to that of Taherinejad *et al.*[21] (described above). Both studies concluded that the ionic silver foam dressing was ineffective against *P. aeruginosa* and only marginally effective against *S. aureus*[38, 39]. One of the above studies also tested the nanocrystalline silver dressing and concluded that it had a broad spectrum of bactericidal activity[38]. The clinical relevance of the antimicrobial testing performed in these studies, however, remains uncertain due to the methods used[23].

Materials and Methods

Materials

All dressings used were obtained free from the companies which produced them. All dressings were stored as indicated on the packaging and tested within their expiry dates. Unless mentioned, all other materials were purchased through Fisher Scientific Canada, Inc.

Dressings tested in this study were as follows:

- A silver sulphate (Ag_2SO_4) dressing (Mepilex® Ag Antimicrobial Soft Silicone Foam Dressing, Molnlycke Health Care LLC, Sweden). Product information indicates that this dressing inactivates a wide range of bacteria, including *S. aureus*, within thirty minutes; that the dressing provides a rapid sustained silver release; that the dressing can be worn for seven days; and that the dressing does not stain. The dressing is indicated for low to moderately exuding wounds such as partial thickness burns, leg ulcers, foot ulcers, and pressure ulcers[40].

- A silver alginate dressing (Algicell™ Ag, Derma Sciences, Inc., Ontario, Canada). Product information indicates that this dressing contains 1.4% ionic silver; has a kill rate of 99.99, 99.91, and 97.46% at Days 1, 3, and 5 of challenge, respectively, for *S. aureus*; and behaves as a bacterial barrier with controlled sustained silver release. The dressing is indicated for diabetic foot ulcers, leg ulcers, pressure ulcers, donor sites, and traumatic and surgical wounds[41].
- Two ionic silver foam dressings (PolyMem® Silver Non-Adhesive Pads, and PolyMem® Silver Shapes, Ferris Mfg. Corp., Illinois, USA). Product information indicates that both of these dressings kill 99.9% of bacteria tested (including *S. aureus*), won't stain skin, and can be worn for three days. These dressings are indicated for first and second degree burns, leg ulcers, pressure ulcers, diabetic ulcers, venous ulcers, donor and graft sites, traumatic and acute wounds, surgical wounds, dermatologic disorders, and skin tears[42].
- A silver collagen matrix dressing with calcium alginate and EDTA (Biostep™ Ag, Smith and Nephew, Inc., Largo, FL). The silver is provided as silver chloride. Product information for this dressing indicates that it has antibacterial activity, targets and deactivates excess matrix metalloproteinases (MMPs), and has a six day wear. The silver in the dressing is intended to prevent colonization of the dressing[43]. The dressing is indicated for management of full-thickness and partial thickness acute and chronic wounds including pressure ulcers, diabetic ulcers, mixed vascular etiology ulcers, venous ulcers, first and second degree burns, donor or graft sites, abrasions,

dehiscid surgical wounds, and traumatic wounds[43].

- A nanocrystalline silver dressing (Acticoat™, Smith and Nephew, Inc., Largo, FL). Product information for this dressing indicates that it kills bacteria *in vitro* in thirty minutes, acts as an antibacterial barrier for up to three days, provides sustained silver release, and is effective against over 150 microorganisms including gram positive and gram negative bacteria (including *S. aureus*), antibiotic-resistant bacteria, yeast, and mold. The product is indicated for reducing infection in partial and full-thickness wounds including pressure ulcers, venous ulcers, diabetic ulcers, surgical wounds, first and second degree burns, and graft and dermal substitute recipient sites[44].

Bactericidal Efficacy - Log Reduction Assay

Log reductions were used to determine the ability of commercial silver dressings to kill bacteria in 30 minutes. Methods used were similar to those presented in Gallant-Behm *et al.*[4] All tests were performed in triplicate. *Staphylococcus aureus* (3 colonies off a Mueller Hinton Agar (MHA) plate or 1 mL of a 4-5 hour growth culture grown as described below) was used to inoculate 100 mL of tryptic soy broth (TSB) and was grown overnight at 37°C and 120 rpm. One milliliter of this culture was used to inoculate another flask of TSB (100 mL) and was grown under the same conditions for 4-5 hours to ensure the bacteria were in log phase growth. Using aseptic technique, dressings were cut into various sizes, with dressings that expand considerably upon saturation being cut to smaller sizes than those that do not. The nanocrystalline silver and silver alginate dressings were cut into 2.54 x 2.54 cm pieces. Silver collagen matrix

dressings were cut into 2.54 x 1.27 cm pieces. Silver sulphate dressings and both ionic silver foam dressings were cut into 1.27 x 1.27 cm squares. The dressing pieces were placed on thin sheets of plastic (aseptically cut into 3.8 x 3.8 square cm pieces) in the inverted lid of a sterile Petri dish. Experimental dressing pieces were then moistened with the required moistening volume of sterile distilled water. To determine the moistening volume, the saturation volume of each dressing was determined by a simple water holding test (see Table 4-1), and then the inoculum volume was subtracted from 90% of the saturation volume to obtain the moistening volume. Control dressing pieces were moistened with the moistening volume of SPS, a detergent which inactivates silver (6.0% w/v NaCl, 1% v/v polysorbate 20, and 0.1% w/v sodium thioglycolate for *S. aureus*[45]). Both control and experimental dressing pieces were then inoculated with 75 μ L of inoculum per 1.27 cm square. A second sheet of plastic was then laid on top of the dressings to contain the inoculum, followed by the Petri dish base placed upright to ensure good contact between the bacteria and the dressings. The inoculated dressings were then incubated at 37°C for 30 minutes. After removal of the dressings from the incubator, they were placed in SPS in order to achieve a 1:10 dilution of the original inoculum. The dressings in SPS were then vigorously vortexed and the resulting solutions containing the recovered bacteria were serially diluted in phosphate-buffered saline (PBS, pH 7.0, containing 8.5 g/L NaCl, 0.61g/L KH₂PO₄, and 0.96 g/L K₂HPO₄). Three 20 μ L drops from each dilution were plated on MHA. The plates were then incubated at 37°C, and after 24 and 48 hours the numbers of bacterial colonies were counted. The counts

generated from the experimental pieces of dressings were used to calculate the surviving number of colony forming units while the counts generated from the control pieces of dressings were used to calculate the numbers of bacterial colony forming units in the original inoculants that were not trapped in the dressings. The \log_{10} of the starting numbers and surviving numbers of bacteria were then determined. Log reductions were then calculated as the difference between the log of the initial number of bacteria and the log of the final surviving number of bacteria.

Silver Dissolution Assay

The release of silver from each dressing was determined with static dissolution tests using methods similar to those of Wright *et al.*[9] One 2.54 x 2.54 cm piece of dressing per 5 mL of sterile distilled water plus the dressing saturation volume was placed in a sealed vial wrapped in aluminum foil to prevent silver precipitation. The submerged dressings were then incubated at 37°C for 24h. Afterwards, the dressings were aseptically removed from the vials, allowed to drip into the vials for 10 seconds, and then disposed of. The remaining solutions were immediately filtered with a 70 μm filter if pieces of the dressings had broken off in solution (which was the case for both of the ionic silver foam dressings, for the silver collagen matrix dressings, and for the silver alginate dressings). Filtering was done on these samples in order to prevent further leaching of silver from the pieces after the 24h time point, and to facilitate atomic absorption spectroscopy (AAS). The solutions were then acidified in 9% nitric acid/0.9% tartaric acid to ensure that all silver released over the 24h period

remained in solution. The solutions were then submitted for total silver analysis by AAS. For AAS, a Varian 220 FS double beam Atomic Absorption Spectrophotometer was used, with the following instrument parameters: a silver hollow cathode lamp with a wavelength of 328.1 nm, and a lean air-acetylene flame. A calibration plot was generated using silver standards of 0.5, 1.0, 3.0, and 5.0 ppm, prepared from a silver standard stock solution of 1000 ppm. If dressings had released more than 5 ppm into solution (as was the case for the nanocrystalline silver dressings and the silver sulphate dressings), the solutions were diluted as necessary with distilled water until they were in the linear range for silver analysis (0.1 ppm to 5 ppm), and the results were corrected for the dilution factor.

Bacteriostatic Longevity – Day-To-Day Corrected Zone of Inhibition (CZOI) Assay

The bacteriostatic longevity of the dressings was assessed using day-to-day transfer corrected zone of inhibition assays. The method used for this procedure, a modified form of the Kirby-Bauer assay, is similar to that of Wright *et al.*[9] 100 µL of *S. aureus* taken from an overnight culture grown up as described above was spread onto MHA plates, and silver dressing pieces pre-moistened with their saturation volume of distilled water were then placed onto the center of the plates. The original dressing placement was traced onto the bottom of the Petri plate to correct for dressings which shrank over time (as with the silver collagen matrix dressing). The plates were incubated overnight at 37°C and then the zones of bacterial inhibition and dressing widths (or tracings as

appropriate) were measured in two perpendicular directions. The CZOI was calculated by subtracting the dressing width from the zone width, and the results for the two directions were averaged.

After zone measurement, the dressings were transferred to new MHA plates seeded with bacteria, as described above, and again incubated overnight. CZOIs were determined and this procedure was repeated for seven more days, for a total of nine days. During this period, if all three dressing pieces of an experimental group ceased to produce any zone of inhibition, they were eliminated from the procedure. The shaped ionic silver foam dressing was not tested in this protocol (see discussion section).

Statistics

One way ANOVA tests with Tukey-Kramer Multiple Comparisons post tests were performed for all assays in which more than two dressings were compared (log reductions, absorptive capacity, silver release, and corrected zone of inhibition assays up to Day 6). For Days 7 through 9 in the CZOI assays, where only the nanocrystalline silver dressing and the silver collagen matrix dressing were still active, the two dressings were compared using unpaired t-tests with Welch corrections. All statistical analyses were performed using Graphpad InStat Version 3.06 (GraphPad Software, San Diego, California, © 2003, www.graphpad.com).

Results

Table 4-1 shows the dressing saturation volumes for each commercially available silver dressing tested. One way ANOVA testing indicated that there

were extremely significant differences in absorptive capacity between dressings ($p < 0.0001$). The silver sulphate dressing had a significantly higher absorptive capacity than all other dressings tested ($p < 0.001$), while the non-adhesive ionic silver foam dressing had a significantly higher absorptive capacity than all the remaining dressings ($p < 0.001$). The only other significant differences were that the silver collagen matrix dressing and the shaped ionic silver foam dressing had significantly higher absorptive capacities than the nanocrystalline silver dressing ($p < 0.05$).

Table 4-1. Dressing saturation volumes.

Dressing Description	Average Saturation Volume ($\mu\text{L}/\text{cm}^2$ \pm S.D., n=3)
Silver sulphate dressing	808 \pm 43
Non-adhesive ionic silver foam dressing	594 \pm 43
Shaped ionic silver foam dressing	172 \pm 66
Silver alginate dressing	151 \pm 11
Silver collagen matrix dressing	176 \pm 5
Nanocrystalline silver dressing	53 \pm 1

Table 4-2 shows the log reductions measured for each commercially available silver dressing tested. One way ANOVA testing indicated extremely significant differences in the activity of the various silver-containing dressings ($p < 0.0001$). The nanocrystalline silver dressing produced very significantly higher log reductions than all other dressings tested ($p < 0.001$). It was also the only dressing to produce a total kill, and the only dressing that was bactericidal, where the definition of bactericidal is a dressing capable of producing a log reduction greater than three[4]. The silver collagen matrix dressing produced very significantly higher log reductions than the remaining four dressings ($p < 0.001$). The remaining four dressings showed no significant differences from

one another, and all produced no positive log reductions.

Table 4-2. Bactericidal efficacy.

Dressing Description	Average Log Reduction (\pm S.D., n=3)
Silver sulphate dressing	-0.61 \pm 0.08
Non-adhesive ionic silver foam dressing	-0.03 \pm 0.01
Shaped ionic silver foam dressing	-0.33 \pm 0.08
Silver alginate dressing	-0.08 \pm 0.30
Silver collagen matrix dressing	1.18 \pm 0.29
Nanocrystalline Silver dressing	>3.46 \pm 0.00

Table 4-3 shows the silver release from the commercially available silver-containing dressings into distilled water after a 24 hour period. There were extremely significant differences between groups, as indicated by one-way ANOVA testing ($p < 0.0001$). The silver sulphate dressing released significantly more silver than all other dressings ($p < 0.001$), and the nanocrystalline silver dressing released significantly more silver than the remaining dressings ($p < 0.001$). The other dressings were not significantly different from one another. Overall, in terms of silver release from highest to lowest, the dressings ranked as follows: silver sulphate > nanocrystalline silver > silver alginate > silver collagen matrix > non-adhesive ionic silver foam > shaped silver foam.

Table 4-3. 24 hour silver release.

Dressing Description	Average Silver Release (mg/cm ² \pm S.D.)
Silver sulphate dressing	0.69808 \pm 0.03124 (n=3)
Non-adhesive ionic silver foam dressing	0.00014 \pm 0.00004 (n=3)
Shaped ionic silver foam dressing	0.00009 \pm 0.00007 (n=2)
Silver alginate dressing	0.00401 \pm 0.00245 (n=2)
Silver collagen matrix dressing	0.00040 \pm 0.00018 (n=2)
Nanocrystalline Silver dressing	0.14398 \pm 0.00911 (n=3)

The corrected zones of inhibition over a nine day period are shown in Figure 4-1 for the nanocrystalline silver dressing (n=3), the silver collagen matrix dressing (n=2), and the silver alginate dressing (n=3). The silver sulphate

dressing (n=3) and non-adhesive ionic silver foam dressing (n=2) did not generate any zones of inhibition on the first day of testing, and in fact had *S. aureus* growing under the dressings. Therefore, no transfers were performed for these dressings. The nanocrystalline silver dressing generated consistent zone sizes until the experiment was terminated after nine days. The silver collagen matrix dressing zone sizes began to decrease after Day 7 ($p<0.05$) but were still present out to Day 9. The silver alginate dressing zone sizes decreased significantly after Day 1 ($p<0.001$). Smaller zones were generated by the silver alginate dressings out to Day 6, at which point the dressing completely liquefied, making further transfers impossible. There were significant differences ($p<0.05$) in zone sizes between dressings on all days up to Day 6, with the silver alginate dressing having the largest zone on the first day, and the smallest zone on all subsequent days. On all days but Day 4 and 5, the silver collagen dressing produced smaller zones than the nanocrystalline silver dressing, but these differences were not significant except on Day 1.

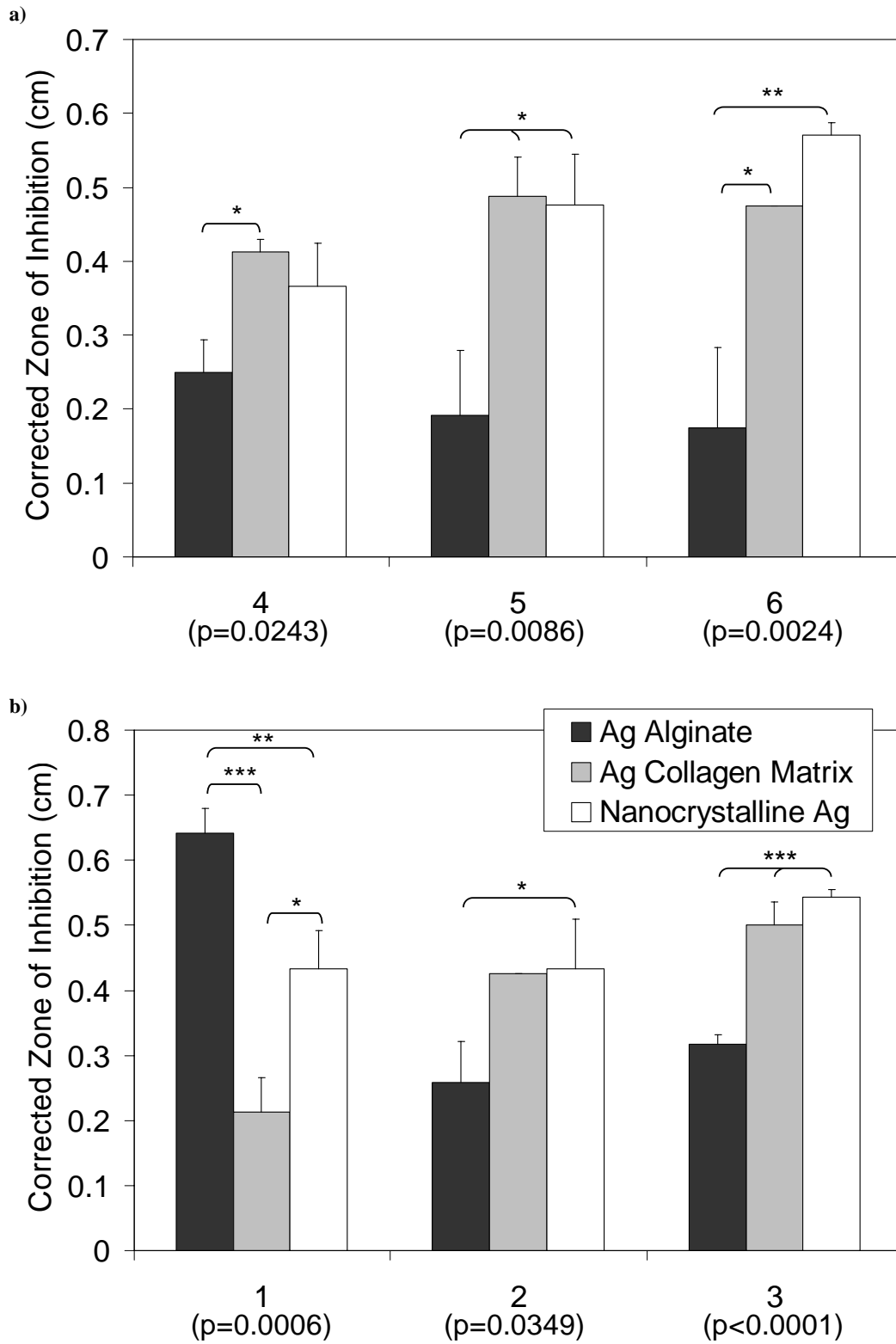


Figure 4-1.

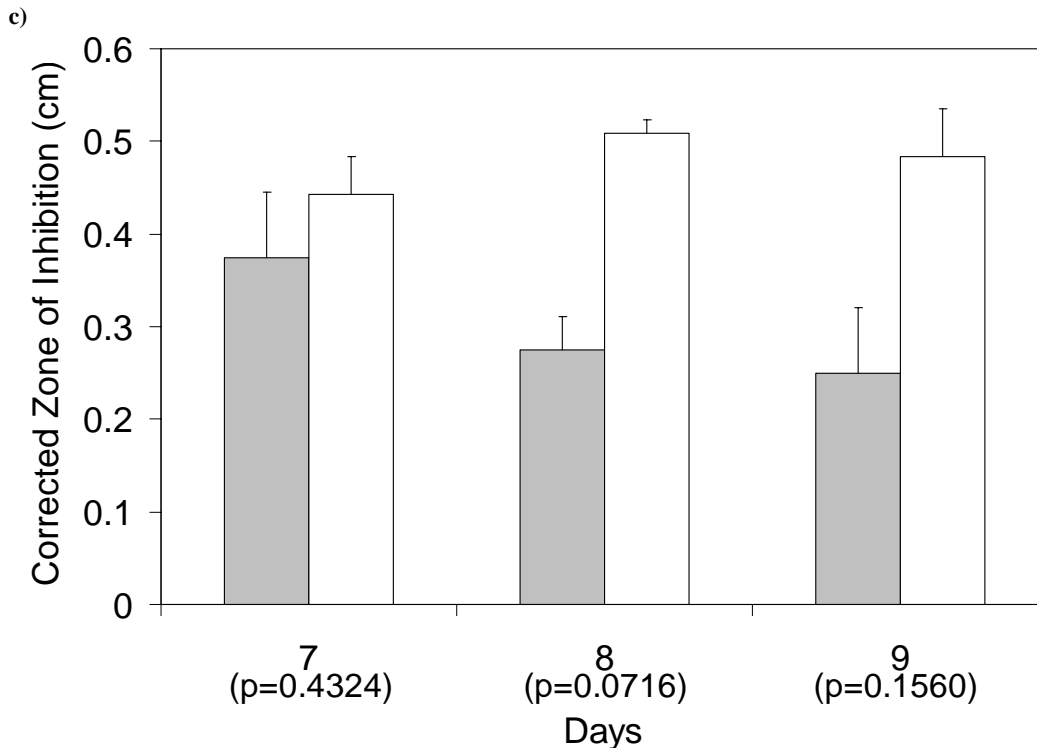


Figure 4-1, continued. Corrected zone of inhibition (CZOI) of *S. aureus* over a series of days for nanocrystalline silver dressings (n=3), silver collagen matrix dressings (n=2), and silver alginate dressings (n=3). Days 1-3 are shown in panel (a), Days 4-6 are shown in panel (b), and Days 7-9 are shown in panel (c). Error bars show standard deviation. P-values from one-way ANOVA testing are written below each day on the x-axis. When there were significant differences between groups ($p < 0.05$), Tukey-Kramer Multiple Comparisons post-testing is indicated on the graph, where * indicates $p < 0.05$, ** indicates $p < 0.01$, and *** indicates $p < 0.001$.

Discussion

In a thirty minute time-period, only the nanocrystalline silver dressing was bactericidal against *S. aureus*, contrary to the product information for some of the other dressings. This corresponded to a rapid release of greater concentrations of active silver compared to most of the other dressings tested. Interestingly, the level of silver released by the nanocrystalline silver was about six percent of traditional silver treatments which release Ag^+ only: Silver nitrate is provided at 2.95-5.91 $\text{mg}/\text{cm}^2/\text{day}$, while silver sulphadiazine is provided at 1.21 $\text{mg}/\text{cm}^2/\text{day}$

in burn treatment[46, 47]. The nanocrystalline silver dressing also demonstrated an inhibitory effect for over nine days of *in vitro* challenges with *S. aureus*, indicating that the release of active silver was sustained over this time period. These results are in good agreement with those of previous studies.[4-9, 38] The species of silver released, as well as the total silver release, is believed to be an important factor in the activity of the dressing, since the dressing demonstrated good antimicrobial activity despite releasing one tenth the amount of silver provided by traditional silver treatments. Based on the product information provided for the dressings, nanocrystalline silver dressings are the only silver-containing dressings tested in this study which release species other than ionic silver (Ag^+). Other studies have shown that nanocrystalline silver releases multiple species, including metallic silver ($\text{Ag}^{(0)}$, likely in cluster form), and a higher oxidation state species, into solution[48]. The release of these species from high energy grain boundaries, which are present in large quantities in nanocrystalline silver, may contribute to the enhanced activity of the dressing. This dressing, which is designed to be a porous moisture wicking wound interface, has a fairly low absorptive capacity – significantly lower than all the other dressings tested except the silver alginate dressing, and requires a secondary dressing for clinical use, but it did not shed pieces during any of the assays.

The silver sulphate dressing released high quantities of silver into distilled water in a 24 hour period compared to the other dressings tested (about 30% of the amount provided by traditional silver-containing burn treatments). However, unlike the nanocrystalline silver dressing, it was not able to generate any log

reduction against *S. aureus* in half an hour. In addition, the dressing was unable to generate any zone of inhibition, with bacteria growing under the wound-contacting surface of the dressing, suggesting it had no bacteriostatic activity. However, it was determined that both the top surface and the wound-contacting surface of the dressing were hydrophobic, which could prevent fluid from entering the dressing or silver from being released from the dressing through these surfaces. Interestingly, it was found that silver could be released by the dressing edges. Thus, during the log reduction assay, when the bacteria were placed on the wound-contacting surface of the dressing, it appears that the bacteria were prevented from contacting the silver within the dressing. In addition, in order to pre-moisten the dressings, the water had to be fed into the dressings through the dressing edges, as otherwise the water formed drops on the both the top surface and the wound-contacting surface and was not absorbed into the dressing. Thus, when the wound-contacting surface of the dressing was placed down onto the agar seeded with *S. aureus*, no liquid transfer could occur between the plate and the dressing, and therefore no silver could be released onto the plate, preventing any zone of inhibition from occurring. The silver released into solution during the total silver assay therefore was released through the edges of the dressing - the only portion of the dressing which allowed for fluid exchange. This was confirmed by cutting a silver sulphate dressing into three strips, moistening the strips to their saturation volume, and placing the strips onto plates seeded with *S. aureus* such that the dressings contacted the plate edge down. The plates were then incubated overnight at 37°C, and in this orientation, the dressings were able

to produce zones of inhibition. Unfortunately, this orientation is not clinically relevant, as the edges of the dressing would not be in contact with the wound, and therefore no silver would be released into the wound and no bacteria would be taken into the dressing, preventing any contact between the bacteria and the silver. It should also be noted that the saturation volume, which was measured by submerging the dressing in water and was shown to be significantly higher than all the other dressings tested, is not clinically relevant either. The absorption capacity in a wound environment for this dressing configuration would be essentially zero – that is, there would be no fluid exchange from the wound surface to the dressing. Thus, although the dressing contains a large quantity of silver that can be solubilized, in its current configuration it has neither any wound fluid absorption capacity nor any antimicrobial properties *in vitro*. Product information for the dressing confirms that its wound-contacting surface is hydrophobic, despite its claims of absorbency, as it indicates that “The [wound-contacting] layer seals the wound edges, preventing the exudate to [sic] leak onto the surrounding skin, thus minimizing the risk of maceration.”[40] The study by Taherinejad *et al.*[21] was performed with the dressings submerged (rather than placing fluids on the wound-contacting surface of the dressings) thus allowing contact between bacteria and silver through the absorbent edges of the dressing. This likely explains the discrepancy between their results regarding the efficacy of the dressing against *S. aureus* and the results of this study.

The silver collagen matrix dressing produced a log reduction of 1.2, indicating that this dressing did not have a bactericidal effect against *S. aureus* in

half an hour. The dressing was bacteriostatic against *S. aureus* for nine days, although the zone size decreased over the last two transfers. However, the dressing shrank substantially over the course of nine days, and left behind material at the edges of the dressings from the fifth transfer on. The dressing also left material behind in solution during the total silver assay. This suggests that material would also be left behind in the wound bed if the dressing was left on for extended periods of time, which may or may not be a problem for generation of a foreign body response, depending on dressing bioabsorbability. The absorptive capacity of the silver collagen matrix dressing was similar to that of the silver alginate dressing and the shaped silver ionic foam dressing, which were mid-range compared to the other dressings tested. The silver release from the silver collagen matrix dressing in 24h, which releases only Ag^+ , was significantly lower than that of the nanocrystalline silver dressing, as it only released 0.02% of the Ag^+ provided by gold standard silver-containing burn treatments. This suggests at least a partial explanation for its lack of bactericidal efficacy. However, the silver release from this dressing was higher than that of the ionic silver foam dressings, which had no bacteriostatic activity. Overall, although the silver collagen matrix dressing did demonstrate bacteriostatic longevity, and was capable of producing a small log reduction against *S. aureus*, it did not appear to be the best product examined in this study in terms of its antimicrobial activity, its absorptive capacity (which was significantly lower than that of some of the other dressings tested), or its ease of use.

The only other dressing which demonstrated any antimicrobial activity *in*

vitro was the silver alginate dressing. Although the dressing was unable to generate any log reduction in 30 minutes against *S. aureus*, it was able to generate zones of inhibition for six days. The zone size was much higher on the first day than on subsequent days, suggesting an initial dump of silver, followed by a lower sustained release over time. Thus, the dressing did not demonstrate bactericidal properties in this study, but did demonstrate bacteriostatic properties. This may have serious consequences, as studies have indicated that when an antimicrobial agent is provided in concentrations such that bacterial inhibition occurs but the bacteria are not actually killed, selection for resistant organisms occurs[49, 50]. The antimicrobial activity of this dressing appears to be related to its silver release in 24 hours, which was significantly lower than that of the only bactericidal dressing (the nanocrystalline silver dressing), but was higher than some dressings which were unable to generate bacteriostatic activity (the ionic silver foam dressings). This dressing, which releases only Ag^+ , released approximately 0.2% of the Ag^+ released by traditional silver-containing burn treatments. Its absorptive capacity is not significantly different from those of the shaped ionic silver foam dressing, the silver collagen matrix dressing, or the nanocrystalline silver dressing, and appears to be highly variable. It should also be noted that portions of the dressing flaked off into solution during the total silver assay, and fibers were left behind on the Petri plates after each transfer in the CZOI assay. Furthermore, the dressings became difficult to lift off the plates from the third transfer on because they were not holding together well, and after the fifth transfer, the dressings liquefied completely. This suggests that fibers from the

dressings would likely be left in the wound when the dressings are removed, potentially causing a foreign body response and/or delayed wound healing, contrary to claims in the product information indicating that the dressing does not leave any silver coated nylon thread residue in the wound and remains intact, facilitating ease of removal[41]. Furthermore, the dressings may become more difficult to remove if they are left on for an extended period of time as they may start to break apart and liquefy. It is anticipated that this process of liquefaction could occur much more quickly in a wound environment than it did on the Petri plates, since the wound environment is a harsh and dynamic environment, containing enzymes which could help to break down the dressing, as well as being moister than a Petri plate. As the dressing properties appeared to change completely, it is uncertain what the wound environment would subsequently be exposed to in terms of liquefaction products.

The product information for the shaped ionic silver foam dressing and the non-adhesive ionic silver foam dressing indicates that the dressings have the same silver technology, releasing ionic silver (Ag^+) only[42], and therefore they would be expected to have equal performance. This was confirmed in this study, where the shaped ionic silver foam dressing performed as poorly in the log reduction assays as the non-adhesive ionic silver foam dressing, with log reductions of zero. As well, the shaped ionic silver foam dressing released about the same level of silver into solution during a 24 hour period, at approximately 0.005% of the Ag^+ released by traditional silver-containing burn treatments, but had a significantly lower absorptive capacity than the non-adhesive silver foam, possibly due to

differences during manufacturing of the shaped dressings, which are adhesive, unlike the other ionic silver foam dressing tested. The non-adhesive ionic silver foam dressing was not able to generate zones of inhibition for even one day, and in fact had bacteria growing under the wound-contacting surface of the dressing, and therefore, the shaped ionic silver foam dressing was not expected to generate zones of inhibition either. Thus, neither of the ionic silver foam dressings demonstrated bactericidal or bacteriostatic activity against *S. aureus*. This corroborates the results of previous studies[38, 39]. This lack of activity appears to correspond to the low quantity of silver released from these products into distilled water over a 24 hour period, with the silver released into solution being barely detectable using AAS. As well, although these dressings have a fairly high absorptive capacity, the dressings appeared to shed pieces into solution during the total silver assay, and onto plates during the CZOI assays, suggesting that upon removal of the dressings in a clinical situation, pieces would be left in the wound. Thus, the ionic silver foam dressings demonstrated the worst performance overall, with the shaped dressing being inferior to the non-adhesive dressing.

This study did not examine the benefits or disadvantages related to other components of the dressings (for example, the glycerol and cleansing agents present in the ionic foam dressings or the EDTA and carboxymethylcellulose present in the silver collagen matrix dressing), but these components should also be taken into consideration when deciding on the acceptability of a dressing for use in the treatment of a wound.

Although caution must be exercised when extrapolating the results of *in*

in vitro studies to the clinical environment[6], important differences were detected in the antimicrobial activity of the dressings tested, with the nanocrystalline silver dressing producing much stronger antimicrobial activity than any of the other dressings tested. This appears to be related to the rapid release of multiple active silver species into solution[48]. While dressings such as the silver alginate dressing and silver collagen matrix dressing have some bacteriostatic activity, this activity may not be sufficient support for the immunocompromised patient population likely to be treated with these dressings. Furthermore, exposure of bacteria to silver concentrations at which bacteriostatic but not bactericidal activity occurs creates a high-risk situation in terms of development of silver-resistant bacteria[49, 50]. The silver sulphate dressing appears to have no clinically relevant antimicrobial activity in its current configuration due to the hydrophobicity of the wound-contacting surface, while the ionic silver foam dressings do not appear to contain sufficient silver for antimicrobial activity. The latter three dressings, which were the only dressings in the study described as non-staining, were the dressings that demonstrated neither bactericidal nor bacteriostatic activity, suggesting that clinicians should question the antimicrobial activity of non-staining silver products, since it may be indicative of silver release below that of antimicrobial levels.

The results of this study emphasize the importance of confirming the claims made in product information through simple *in vitro* efficacy tests. If a dressing does not demonstrate efficacy in the relatively benign environment of a Petri plate, it is unlikely that it will provide antimicrobial activity in the severe

and dynamic environment of a wound. Finally, this study corroborates the conclusions of Gallant-Behm *et al.*[4] that silver release, log reduction, and day-to-day transfer corrected zone of inhibition assays should be used in conjunction to analyze silver-containing dressings. Sufficient information about the antimicrobial activity of the dressings examined in this study, and more specifically why certain dressings were active while others were not, could not have been gained from running only one of the above assays. It also suggests that methods such as those used by Taherinejad *et al.*[21] and others, in which dressing pieces are placed in large volumes of bacteria-containing fluids, do not provide clinically relevant data regarding dressing efficacy, since a dressing can contain a large quantity of silver, but may not release it in a wound environment.

Overall, this study shows that the activity of nanocrystalline silver must be due, at least in part, to the release of silver species at relatively high concentrations compared to other silver-containing dressings available commercially. However, the concentration of these species was low relative to the levels provided via traditional silver treatments such as silver nitrate and silver sulphadiazine. This suggests that nanocrystalline silver must act via release of multiple species, some of which are more active antimicrobial agents than Ag^+ , thus delivering a stronger bactericidal effect than gold standard treatments[8] at a lower dose. In general, it is clear from this study that silver must be released from dressings in relatively large quantities in order to provide bactericidal activity, and that, while bacteriostatic activity can be achieved with lower silver release, decreasing silver release resulted in decreased bacteriostatic longevity as well. It

is clear that nanocrystalline silver is more active than the Ag^+ provided via silver chloride, silver alginate, and other forms of ionic silver, which again is due to a combination of total soluble silver and the particular silver species released.

Study #2: Development of Silver Resistance and Ability to Kill Ag^+ -Resistant Bacteria: Comparison of Nanocrystalline Silver to Other Silver Treatments

Background

Due to increasing numbers of antibiotic-resistant bacteria, alternative methods for treating bacterial infections in acute and chronic wounds are being sought. Bacterial infection is the leading cause of mortality from extensive burn injury, despite many advances in wound therapy[51], making the proper prevention and treatment of infection a major focus of burn and wound care. The long-known antimicrobial properties of silver have regained attention of late, due in part to the search for alternatives to antibiotics. The inhibitory action of ionic silver can be attributed in part to its interference with the respiratory chain[52], which is due at least partially to its strong interaction with thiol groups present in bacterial respiratory enzymes[53] and other electron transport chain components[54]. Silver also interacts with structural proteins, enzymes, and various components of the cell membranes of the bacteria, as well as preferentially binding with DNA bases, thus inhibiting replication[55]. Thus, silver appears to be a good alternative treatment to antibiotics.

However, the potential for silver resistance development in bacteria is a significant concern for wound healing, due to the large number of commercial

wound dressings containing silver which have recently become available as alternative therapies to antibiotics. It has been suggested that the development of silver resistance could occur in the clinical environment in a manner analogous to that of antibiotic resistance development[56], rendering the antiseptic properties of silver useless against wound pathogens. As the bactericidal activity of silver is key to a wide range of other technologies[56, 57], including the control of microbes in water distribution systems[56], the threat of silver resistant bacteria has implications beyond the wound care setting, should silver resistance become widespread.

Development of resistance to any antimicrobial agent, including silver, may be maximized when the organisms are exposed to relatively low levels of the agent. The minimum inhibitory concentration (MIC) is defined as the lowest concentration of an active agent that prevents bacterial growth. It does not measure the viability of the bacteria. The mutant prevention concentration (MPC) is defined as the concentration at which multiple mutations must occur for resistance to develop, or the concentration which blocks the growth of the least susceptible single-step mutant. This concentration often coincides with the minimum bactericidal concentration (MBC), which is defined as the concentration at which all cells are killed by the active agent. Mutants may have a growth advantage at concentrations between the MIC for the most susceptible cells and the MPC, making this range of concentrations the mutant selection window[58]. The mutant selection window is both organism and active agent dependent. Repeated exposure to antimicrobials in this concentration window could

selectively enrich silver-resistant mutant populations over time, optimizing resistance development. Such treatment regimes could lead to the selection and development of multiple silver-resistance mutations[58]. Li *et al.*[50] were able to confirm this theory experimentally with silver by exposing *Escherichia coli* to silver nitrate and silver sulphadiazine. With stepwise-increasing exposures to silver starting at $\frac{1}{2}$ the MIC (well below the MBC), they were able to increase the MIC of originally silver-susceptible strains by 128-fold for silver nitrate and 64-fold for silver sulfadiazine without the use of mutagens[50]. They were unable to develop these mutants in a one-step exposure protocol. The resulting mutants showed decreased susceptibilities to antibiotics, but not to other heavy metals[50]. The mutants were deficient in major membrane porins, and had much lower outer membrane permeability than the silver-sensitive parent strains[50]. As well, less silver was accumulated in silver-resistant strains², and silver was determined to be pumped out of the silver-resistant cells by active efflux[50]. The genes for this resistance were believed to be chromosomal, rather than carried on a plasmid[50]. In a similar study, *Klebsiella pneumoniae*, which was originally sensitive to 10 $\mu\text{g/mL}$ silver, was adapted to increasing concentrations of silver nitrate over time and, within 10-11 transfers, became resistant to 70 $\mu\text{g/mL}$ silver[59]. Silver resistance was retained after growth for more than 50 generations in the absence of silver nitrate[59]. In the *K. pneumoniae*, silver uptake in resistant cells was much lower than in sensitive cells, suggesting altered cell permeability or cell-surface associated changes, so that binding of silver to the cells was decreased.

² At low concentrations. At higher concentrations, the active efflux appeared to be overwhelmed and silver levels inside the resistant cells were about the same as in the external environment.

Higher lipid quantities in the cell walls were thought to be responsible for this[59]. As well, prevention of respiration inhibition by silver was observed, suggesting a structural alteration to, or change in the enzyme environment of, succinate dehydrogenase, rendering it less susceptible to silver[59]. A study examining the development of resistance with the use of antimicrobial catheters found that 20 passages of *S. epidermidis* through chlorhexidine acetate combined with silver sulphadiazine at subinhibitory concentrations did not result in significantly increased MICs or MBCs[60], although the MICs had doubled. To the author's knowledge, silver resistance has never been developed in a laboratory setting using commercial silver-containing wound dressings. However, theoretically, the application of silver-containing dressings multiple times to a wound could cause a stepwise increase in exposure to low-level silver, potentially at levels falling into the mutant selection window. Due to the chloride and protein levels present in wounds, the active silver in wounds delivered from some silver-containing dressings can be quite low (see Chapter 1), enhancing the likelihood that the silver concentrations contacted by microbes could be in the mutant selection window. As there are a large number of relatively new silver-containing dressings containing and releasing low concentrations of silver (even below the MICs of clinically relevant bacteria, which can range between 5-40 µg/mL in complex organic media[8, 61]), it is probable that treatment with some of these dressings could prove to be mutation-prone regimens. Thus, despite reports indicating that silver resistance is unlikely to occur[56, 62-64], this may not be the case.

Silver nitrate (0.5%) and silver sulfadiazine (1%), which have been used in wound care for over forty years[46, 47, 65, 66] and are considered the gold standards in burn care, are dosed based on the assumption that the active antimicrobial moiety is Ag^+ , as demonstrated by Ricketts[61]. They contain 3176 and 3025 mg Ag^+ /L and are delivered at approximately 38 000 and 16 000 $\mu\text{g Ag}^+/\text{in}^2/\text{day}$, respectively. These large doses were required to maintain effective concentrations of available silver, offsetting losses due to the reactivity of the Ag^+ ion in the wound environment, and inactivation due to exposure to light. By maintaining doses of silver which exceed the MBC of common pathogens, bacterial growth is controlled and silver resistance is rare using these treatments. However, numerous silver containing dressings have been introduced to the wound care market over the last ten years that release less than 0.1% of the silver in silver nitrate and silver sulfadiazine (see Table 4-4).

Table 4-4. Comparison of various commercial silver dressings.

Dressing	Silver Form – In Dressing	Silver Form – In Solution	Silver Contained ($\mu\text{g}/\text{cm}^2$)	Water Concentration ($\mu\text{g}/\text{mL}$)	Log Reduction (30 min, <i>P. aeruginosa</i>)
Acticoat™ (Smith and Nephew LLC)	Nanocrystalline	Ag^+ , Ag^0/Ag^+ clusters, AgX (Fan&Bard)[48]	465 (Wright <i>et al.</i>)[9]	50-100 (Burrell)[67] (~800 $\mu\text{g}/\text{in}^2/\text{day}^{**}$)	>5 (Taylor <i>et al.</i>)[68]
Aquacel Ag® (ConvaTec, Inc.)	Silver carboxymethylcellulose	Ag^+	116	0.8-1 mg/L (Burrell, Bowler)[67, 69] (6-8 $\mu\text{g}/\text{in}^2/\text{day}^{**}$)	<1
Arglaes (Medline)	Silver/calcium phosphate	Ag^+	20	130 (Burrell)[67] (130 $\mu\text{g}/\text{in}^2/\text{day}^{**}$)	<1 (Gallant-Behm)[4]
Silverlon® (Argentum Medical LLC)	Metallic	Ag^+		<1-5 mg/L (Burrell)[67] (16 $\mu\text{g}/\text{in}^2/\text{day}^{**}$)	<1 (Gallant-Behm)[4]
Actisorb® Silver 220 (Johnson & Johnson)	Silver charcoal	Ag^+		<1 (Burrell)[67]	<1 (Gallant-Behm)[4]
Contreet H® (Coloplast US)	Silver sodium hydrogen zirconium phosphate	Ag^+			
Silvasorb (Acrymed, Medline)	Silver chloride	Ag^+	0.00015 – 1.3 mg/L***	<1 (Burrell)[67] (10 $\mu\text{g}/\text{in}^2/\text{day}^{**}$, 0.0012 $\mu\text{g}/\text{in}^2/\text{day}$)	
Acryderm (Acrymed, Medline)	Silver halide	Ag^+		<1	<1

Actisorb® Plus (Johnson & Johnson) Oligon® (Implemed, Inc.)	Silver carbon	Ag ⁺		<1	<1
1% silver sulfadiazine	Silver/platinum metal	Ag ⁺		<1	ND
0.5% AgNO ₃	Ag ⁺	Ag ⁺	3025 mg/L	300* (15700 µg/in ² /day)	1 (Gallant-Behm)[4]
	Ag ⁺	Ag ⁺	3176 mg/L	320* (38000 µg/in ² /day)	1 (Gallant-Behm)[4]
Avance (SSL International)	Silver hydropolymer	Ag ⁺		<1	ND (Gallant- Behm)[4]

Note: Unless indicated, data in this table is from personal communications with Dr. Burrell.

*Estimated based on dilution of initial concentration.

**Estimated based on the release of 8 mL exudate/in²/day, which is very heavy[22].

***Estimated based on the solubility product of AgCl, which is 1.8×10^{-10} M.

ND=not detected

These low silver concentrations may be within (or even below) the mutant selection window of many bacteria. This concern would be amplified if physicians started treatments with dressings releasing very low silver quantities and switched to dressings releasing higher quantities of silver as the low-silver releasing dressings proved inactive due to bacterial resistance buildup. The frequency of a successful mutation to a single mechanism of action compound is about 1 in every 10^8 cell divisions (personal communication, Burrell). If an active agent such as silver has five mechanisms of action that are concentration dependent, and a dose greater than the highest concentration was applied, the probability of resistance developing would be 1 in 10^{40} cell divisions, which is a very rare event. However, if the concentrations of active agent applied in succession were less than the concentration of each mechanism of action and were gradually built up over time, then the probability of developing a fully resistant organism would be about 1 in 5×10^8 cell divisions, which is a far more likely event. Thus, the development of resistance would be favored by successive exposures to an active agent at concentrations in the mutant selection window.

In fact, silver resistance development in bacteria has been demonstrated in the literature, and two different forms of resistance have been well described – intracellular complexation and active efflux. In intracellular complexation, silver reacts with non-essential cellular components and is effectively sequestered. For example, some resistant *Pseudomonas stutzeri* produce H_2S , which then removes silver from solution[55], since Ag_2S has a K_{sp} of 6.68×10^{-50} . Sources do not agree on whether the reaction of Ag^+ to metallic silver is one of the mechanisms

for silver inactivation[70-72]. In active efflux, efflux systems are developed which pump the silver out of the cell. Gram negative and gram positive bacteria can both develop efflux systems, which are similar, although not identical. An efflux system in *E. coli* was described by Li *et al.*[50], who developed their resistant organisms in the lab using a multiple step exposure protocol, as described above.

Silver resistant bacterial strains have been isolated from silver mines and photographic film waste effluent. For example, a *Pseudomonas stutzeri* isolate from a silver mine was found to have a silver-resistance encoding plasmid which appeared to be associated with intracellular complexation[73]. *Ralstonia metallidurans*, which is typically found colonizing industrial sediments, soils, or wastes (all of which have a high content of heavy metals), has coding for silver resistance mechanisms, including active efflux pumps, in its genomic DNA[74].

To date, occurrences of silver resistance are relatively rare in a clinical setting, but they have been documented. One of the earliest clinical reports of silver resistance was published in 1974. In this study, two silver sulfadiazine-resistant isolates of *Enterobacter cloacae* were obtained from burn units[75]. The isolates were able to grow in 400 µg/mL silver sulfadiazine, with the resistance appearing to relate to the cell wall[75]. The species were cross-resistant to silver benzoate, but not silver nitrate, and were also resistant to antibiotics, but not organic mercurials[75]. The resistance did not appear to be transferable[75].

In 1975, *Salmonella typhimurium* isolated from burn patients receiving 0.5% silver nitrate treatments were found to be resistant to silver nitrate, mercuric

chloride, and various antibiotics. This resistance was transferrable to sensitive bacteria of the same species, and also to *E. coli*[76]. This resistance resulted in septicemia killing three patients and requiring the closure of the burn unit[77]. Later study of this isolate indicated that the resistance was encoded on a plasmid which contained genes for both periplasmic metal-binding proteins and two parallel efflux pumps (a P-type ATPase and a three-component cation/proton antiporter)[57, 77]. These genes might be regulated by the presence of silver[78]. Closely related genes were identified in bacteria isolated from the environment and from the clinic in diverse geographic locations[57].

Pseudomonas aeruginosa strains collected from burn patients in 1977-1978 demonstrated both silver and gentamycin resistance, although the silver resistance was unstable[79]. In 1998-1999, 19 patients in a burn unit were infected with a silver sulfadiazine resistant *Pseudomonas aeruginosa* that was antibiotic sensitive and mostly present in the burn wounds, although various body sites on multiple patients were colonized for long periods of time[80]. During the same time period in this hospital, a multi-drug resistant *Pseudomonas aeruginosa* was prevalent which was silver sulfadiazine sensitive[80]. In comparing the two, they found that the time between admission and isolation of the bacteria was shorter and the mean colonization length was longer with the silver-resistant organism, which resulted in severe infection and the death of one patient due to lethal burn sepsis[80]. This led the authors to conclude that the silver-resistant *P. aeruginosa* could pose problems comparable to those caused by antibiotic-resistant strains[80].

Silver-resistant *Enterobacteriaceae* were recovered from in-hospital patients receiving silver sulfadiazine for burn wound prophylaxis in the late 1970s, with some wounds being colonized by silver- and sulfonamide-resistant bacteria within just two weeks of treatment[81]. In another study of 39 clinical *Acinetobacter* isolates, 10 species grew in >10 mM/mLⁱⁱⁱ silver nitrate, 12 species could grow in up to 1 mM/mLⁱⁱⁱ silver nitrate, 13 species could grow in up to 0.1 mM/mLⁱⁱⁱ silver nitrate, and 4 species could only grow in up to 0.01 mM/mLⁱⁱⁱ silver nitrate[82]. This indicates that some of the isolates had 1000-fold higher resistance to silver compared to others. The resistant species frequently showed other heavy metal resistances as well as β -lactam resistance, via production of β -lactamase, which protects the cell by non-specifically binding the β -lactam antibiotic, preventing it from reaching its target site on the cytoplasmic membrane[83]. The authors hypothesized that this impermeability-type resistance mechanism resulting from exopolysaccharide produced by the isolates might have a role in imparting dual resistance to β -lactam and metals, and that the β -lactamase genes may be on a plasmid associated with metal resistance similar to observations with *S. aureus*[82, 84]. The same group studied an environmental isolate of *A. baumannii* which had an MIC of 1 mM silver nitrate, and found that the isolate was a β -lactamase producer which was resistant to at least ten antibiotics and 13 other heavy metals[85]. Only the silver resistance was transferable to a susceptible *E. coli* strain during conjugation, indicating the silver resistance gene was carried on a plasmid[85]. The resultant resistant *E. coli* had a slower growth rate than the parent strain, suggesting a metabolic burden was

ⁱⁱⁱ These are the units used in the reference. It seems likely that they meant millimolar.

posed by the maintenance of the plasmid in the cells[85]. The growth rate was further lowered in the presence of Ag^+ , suggesting the silver resistance was an inducible property[85]. In the *A. baumannii* isolate, the plasmid was 76% stable and 9.6% stable respectively in the presence and absence of selective pressure (addition of silver nitrate)[85], which was considered evidence of its plasmid-encoded nature. Interestingly, the *A. baumannii* isolate accumulated and retained the silver, while the *E. coli* effluxed 63% of the accumulated silver ions. The authors of the study suggested that the silver accumulation occurred via surface chelation, rather than intracellular deposition, and that the *Acinetobacter* serves as a reservoir for naturally occurring metal resistant plasmids[85].

A study using a clinical isolate of silver-resistant *E. coli* found that silver accumulation by the resistant strain was five-fold lower than by the sensitive strain; that the resistant strain produced more H_2S and intracellular acid labile SH groups than the sensitive strain, which may be secreted to react with silver around the cell; and that the resistant strain was more hydrophobic than the sensitive strain, likely due to surface exposure of hydrophobic outer membrane components such as phospholipids and proteins, suggesting decreased accumulation of silver may have been due to absent or diminished outer membrane proteins[86, 87]. However, the authors of the study were unable to transfer the resistance to silver-sensitive *E. coli* strains or other species[86].

A study examining 95 clinical strains of gram-negative bacteria showed that 21% of the strains were silver resistant, with 10 strains showing plasmid-mediated silver resistance[88].

Another study tested the prevalence of silver-resistance genes in MRSA (33 samples) and methicillin-resistant coagulase-negative Staphylococci (MR-CNS, 8 samples) isolated from wounds and nasal passages in animals and humans[89]. They found that of the silver genes tested for (*silE*, *silP*, and *silS*), *silP* and *silS* genes were not detected, but *silE* was detected in two MRSA isolates and one MR-CNS isolate[89]. They subsequently tested the susceptibility of these strains to a silver-containing hydrofiber (Aquacel[®] Ag), and concluded that the silver resistance genes did not protect the strains from the silver-containing dressing[89]. Based on these results, this may indicate that the *silE* gene was not being expressed, or was not sufficient on its own to provide silver resistance against the dressing[89]. However, the testing methods used were single zone of inhibition assays and confocal microscopy with live/dead fluorescent staining[89]. Studies have shown that these methods are not adequate to determine whether or not an agent is bactericidal[4, 23], suggesting that the strains may have been growth-inhibited but not killed. In addition, the confocal microscopy results indicated that the MRSA *sil*-negative bacteria were killed within three hours, while the *sil*-positive strains took 24-48 hours to kill, suggesting that the *sil*-positive bacteria did demonstrate some resistance to the dressing[89]. Furthermore, their method of calculating zone of inhibition was incorrect, as they subtracted the dressing width after contraction[89], rather than as the initial size as placed on the petri plate, indicating that the actual zones of inhibition were much smaller than reported. Additionally, the dressing used for the assay is not considered bactericidal against silver-sensitive bacterial strains[6], making it a

poor dressing choice for determination of silver resistance development. Testing would have been more accurate using silver nitrate in combination with MICs/MBCs and log reduction assays.

In a study on *Enterobacter cloacae*, two isolates from burn wounds were determined to be resistant to high levels of silver nitrate, but the resistance was unstable. One strain was linked to rapid lactose fermentation and mucoid colony structure, while the other was not[90].

A study of a silver-resistant *Pseudomonas stutzeri* showed that they accumulated more silver than silver-sensitive strains, which appeared to be deposited as silver sulfide in an energy dependent or enzyme-linked manner inside the cells[55]. This silver-resistant *P. stutzeri* was further studied, and it was found that the silver resistance was not due to silver complexation to intracellular polyphosphate, nor to the presence of low molecular weight metal binding proteins[91]. It was also determined that, surprisingly, the silver-resistant strain produced less H₂S than the silver-sensitive strain, but it contained higher levels of intracellular acid-labile sulfides[91]. The silver-resistant strain was found to accumulate silver in large quantities in the periplasm, where the silver was deposited as particles in vacuole-like granules, some as silver sulfide but most as elemental silver[55, 71].

These examples indicate that silver resistances have developed in clinical bacterial populations, and that there appears to be a variety of different mechanisms of resistance which can develop, some of which occur simultaneously with resistance to a variety of other heavy metals and antibiotics.

If silver resistance becomes a global clinical issue, it will develop in the populations that are most at risk – pressure ulcer, burn, and other chronic wound patients. It is possible that dressings which release multiple active silver species may prevent development of resistance because if such dressings can kill microbial populations with multiple resistance mechanisms to silver ions, via the release of other silver species to which the bacteria remain sensitive, they should minimize the risk of development of fully silver-resistant organisms.

There is some controversy regarding the mechanism(s) of action (MOA) of silver wound dressings. Some researchers suggest that the only active ingredient of all silver dressings is Ag^+ (ionic silver)[92], and therefore the ability of a dressing to sustain a controlled release of silver ions is its most important feature for efficacy. However, having a single active agent, such as these researchers suggest, may make the dressings highly susceptible to microbial resistance development despite its multiple mechanisms of action, since the research described above has indicated that bacteria are capable of developing a variety of mechanisms of resistance to ionic silver. However, as discussed in previous chapters, there is evidence that nanocrystalline silver releases unique species of silver in addition to Ag^+ , including $\text{Ag}^{(0)}$ in a possible cluster form, and a higher oxidation state species[48]. The anti-inflammatory studies of Chapters 2 and 3 demonstrated that nanocrystalline silver dressings released an anti-inflammatory species which was not Ag^+ , as silver nitrate treatments did not generate the same anti-inflammatory effect. Studies have also shown that nanocrystalline silver appears to be a much more active antimicrobial agent than

Ag^+ , with a faster rate of kill, suggesting that it contains unique antimicrobial species as well. If there are, in fact, unique antimicrobial species released by nanocrystalline silver in addition to Ag^+ , this could prove very important in the battle against the development of antimicrobial resistance to silver, as these unique species would provide additional mechanisms of action, requiring the bacteria to develop multiple resistance mechanisms simultaneously.

The purposes of this study were:

1. To try to develop bacteria resistant to various silver-containing treatments in order to determine which treatments resulted in a mutant-selective regimen. This would help to determine whether bacterial resistance to silver could become a clinically relevant problem, and specifically to determine whether this is likely to pose a problem with nanocrystalline silver dressing treatments.
2. To test the ability of various commercial silver-containing dressings to kill parent and Ag^+ -resistant strains of bacteria, in order to better understand the mechanisms of action of nanocrystalline silver relative to other silver-containing dressings and to clarify whether or not nanocrystalline silver dressings release unique antimicrobial silver species (in addition to Ag^+) which cause it to differ from other silver-containing dressings in relation to silver-resistant bacteria.

Materials and Methods

Materials

All reagents, unless otherwise specified, were obtained from Fisher Scientific. Materials and solutions were sterilized at 41 kPa and 121°C. Standard ionic silver solutions were prepared using silver nitrate. 1.574 g of AgNO₃ was dissolved in 10 mL of reverse osmosis water to make a 0.1 g Ag⁺/mL solution. This solution was serially diluted to make 10 and 1 mg Ag⁺/mL solutions. Ag⁺-containing Mueller-Hinton Broth (MHB) solutions were generated using different proportions of the stock solutions. For example, to make a 10 µg Ag⁺/mL solution in MHB, 100 µL of the 1000 µg Ag⁺/mL solution was added to 10 mL of MHB. Stock solutions were covered in foil and stored at room temperature. New stock solutions were made every six days.

Bacteria were tested for their ability to develop resistance over time to seven silver-containing dressings:

- A nanocrystalline silver dressing (Acticoat™) described in Study #1, referred to as “nanocrystalline silver dressing” throughout this study.
- A silver nylon dressing (Silverlon®, Argentum Medical, LLC, Chicago, IL, USA) which contains electroplated pure metallic silver, and will be referred to as “silver nylon dressing” throughout this study. Product information indicates that this dressing releases ionic silver, does not stain, can be left on for several days, and kills bacteria including MRSA and superbugs. The dressings are also reported to serve as antimicrobial barriers to fungi and bacteria. The dressings are indicated for first and

second degree burns, incisions, skin grafts, donor sites, lacerations, abrasions, pressure ulcers, chronic wounds, and chronic, dermal, vascular, and diabetic ulcers[93].

- A silver sodium carboxymethylcellulose (NaCMC) Hydrofibre® dressing (Aquacel Ag®, ConvaTec, Inc., ER Squibb and Sons LLC, Dorval, Quebec, Canada) , which contains 1.2% w/w silver in an ionic form, known to be silver chloride[94] (see Figure 4-2, which contains an XRD of Aquacel Ag®, and shows that the silver is present as AgCl), and will be referred to as “silver NaCMC dressing” throughout this study. Product information for this dressing indicates that it gels to trap bacteria, and releases silver ions which exert a sustained antimicrobial effect for over seven days against a wide range of organisms including *Pseudomonas aeruginosa*, *Staphylococcus aureus*, MRSA and VRE, preventing colonization of the dressing and providing an antimicrobial barrier to protect the wound. The dressings are indicated for leg ulcers, superficial pressure ulcers, partial-thickness burns, and granulating wounds. The dressings can be left on for up to 14 days and do not stain[95].
- An ionic silver foam dressing (PolyMem®) described in Study #1, referred to as “ionic silver foam dressing” throughout this study.
- A dressing containing hydrocolloidal silver (silver sodium hydrogen zirconium phosphate) and a semi-permeable polyurethane film (Contreet®, Coloplast US, Minneapolis, Minnesota, USA), which will be referred to as “hydrocolloidal silver dressing” throughout this study.

Product information for this dressing indicates that it provides sustained silver release at 1 ppm and has *in vitro* antibacterial activity for up to seven days in some bacterial strains detrimental to wound healing. The dressings are indicated for moderately to highly exudative wounds, wounds that are colonized or where risk of infection exists, chronic wounds (specifically leg ulcers and all stages of pressure ulcers), partial thickness wounds, donor sites, postoperative wounds, skin abrasions, and diabetic foot ulcers. These dressings do stain wounds[96].

- A dressing consisting of an absorbent polyacrylate matrix containing silver chloride (SilvaSorb, AcryMed, Medline Industries, Inc., Mundelein, Illinois, USA), which will be referred to as “silver chloride dressing” throughout this study. Product information for this dressing indicates that it provides antimicrobial protection against a broad spectrum of bacteria (including MRSA, VRE, *E. coli*, and *Pseudomonas*) and fungi via controlled release of antimicrobial silver at 1.5 ppm, is effective for up to seven days, and does not stain skin. The dressings are indicated for pressure ulcers (all stages), partial and full thickness wounds, leg ulcers, diabetic foot ulcers, grafted wounds and donor sites, skin tears, surgical wounds, lacerations and abrasions, and first and second degree burns[97].
- A dressing composed of alginate, CMC, and silver coated nylon fibers, containing 8% elemental silver (SilvercelTM, Systagenix Wound Management, Inc., North Yorkshire, UK), which will be referred to as “silver alginate dressing” throughout this study. Product information

indicates that this dressing is an effective barrier to bacterial penetration with antimicrobial activity against over 150 clinically relevant strains including MRSA, MRSE, VRE, viruses, and fungi *in vitro*, producing a log reduction greater than 5 for *E. coli*, *Streptococcus pyogenes*, and *Pseudomonas aeruginosa*, but not *Staphylococcus aureus*, within an hour. The dressings are indicated to help reduce infection in moderately to heavily exuding partial and full thickness wounds including pressure ulcers, venous ulcers, diabetic ulcers, donor sites, and traumatic and surgical wounds[98].

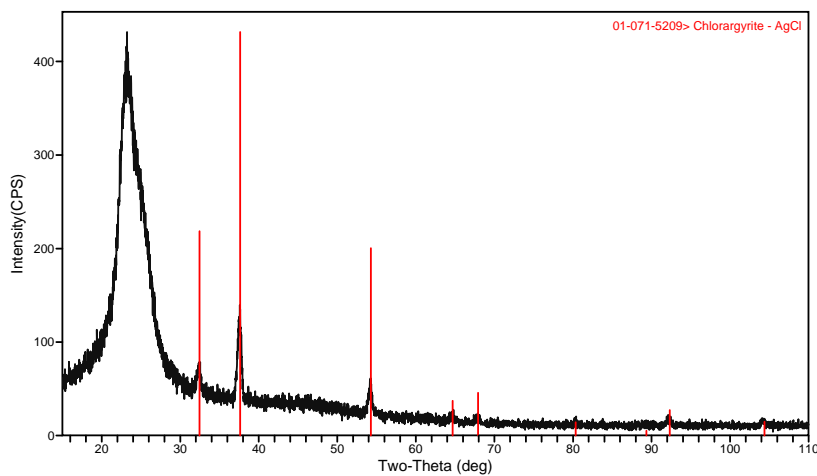


Figure 4-2. Diffraction pattern of Aquacel Ag®. XRD was performed using a Rigaku Geigerflex Powder Diffractometer (Rigaku Americas Corp., The Woodlands, Texas, USA) with a Co tube and a graphite monochromator. The silver-containing peaks were identified using an online computer which performs routine search/match procedures of diffraction patterns using the Joint Committee on Powder Diffraction Standards (JCPDS) database.

Based on results of the tests for development of silver resistance to dressings, four silver-containing dressings were selected and tested for their ability to kill Ag⁺ resistant *P. aeruginosa*:

- A nanocrystalline silver dressing (Acticoat™)
- A silver nylon dressing (Silverlon®)

- A silver NaCMC dressing (Aquacel Ag®)
- A silver alginate dressing (Silvercel™)

All dressings were stored according to the instructions on their packaging and were used prior to their expiration dates.

Micro-organisms

The bacterial strains used were *Pseudomonas aeruginosa* (ATCC 27317), *Escherichia coli* (ATCC 11393 and B/5), *Enterobacter aerogenes* (62-1), *Proteus vulgaris*, *Staphylococcus aureus* (ATCC 25923), and *Staphylococcus epidermidis* (ATCC e15J). The organisms were obtained from the University of Alberta's Department of Biology.

MIC Testing

Minimum inhibitory concentrations (MICs) were determined in triplicate using methods similar to those presented in the literature[8, 50]. Briefly, doubling dilutions of silver nitrate solutions in 10 mL of MHB were inoculated with 100 µL of bacteria in log phase growth (grown overnight followed by transfer and growth for an additional four hours), resulting in final silver concentrations of 2, 4, 8, 16, 32, etc. ppm silver. The tubes were vortexed and incubated at 37°C overnight, at which point, the MIC was determined (the lowest concentration that prevented visual growth of the bacteria). This procedure was then repeated for a narrower range of concentrations if the MIC needed to be determined more accurately.

MBC Testing

To determine the minimum bactericidal concentration (MBC), 100 µL of

solution was taken from each test tube from the MIC testing which showed no growth and was spread-plated onto MHA, similar to techniques presented in the literature[8, 50]. The plates were incubated overnight at 37°C and examined for growth. The MBC was defined as the lowest concentration at which no bacteria grew once they were removed from the silver-containing solution (the concentration at which the bacteria are killed).

Development of Ag⁺ Resistant Bacteria using Silver Nitrate

Development of silver resistance to silver nitrate was performed using stepwise techniques similar to those used in the literature[50]. Bacteria were grown up overnight in 100 mL TSB (37°C, 200 rpm) and then 1 mL of this culture was transferred to fresh TSB and grown up for four hours under the same conditions to produce log phase bacteria. The original MIC and MBC of each culture was determined as described above. Attempts to develop resistance were begun by exposing the bacteria to half their MIC. To do this, 10 mL of MHB, containing the appropriate quantity of silver nitrate solution, was inoculated with 100 µL of bacteria in log phase growth. The tubes were vortexed and then incubated at 37°C overnight. If growth was observed, then 100 µL of the cultures were added to 10 mL of MHB containing an incrementally larger quantity of silver nitrate solution. These tubes were then incubated again as described. This procedure was repeated daily unless growth flagged.

The increase in silver concentration was determined based on the apparent health of the bacteria. If the growth was strong, a relatively large step in silver concentration was made, but if it was weak, a small increase was made, or in the

case of very weak growth, the concentration was held constant. If no growth was observed, then the cultures from the previous day's tubes were exposed to the same concentration again, or to a small increase in concentration. If no growth was observed for three consecutive days, the experiment was terminated or restarted. The decision tree for this process is shown in Figure 4-3. MICs were determined periodically throughout the experimentation to determine the organisms' susceptibility to silver nitrate.

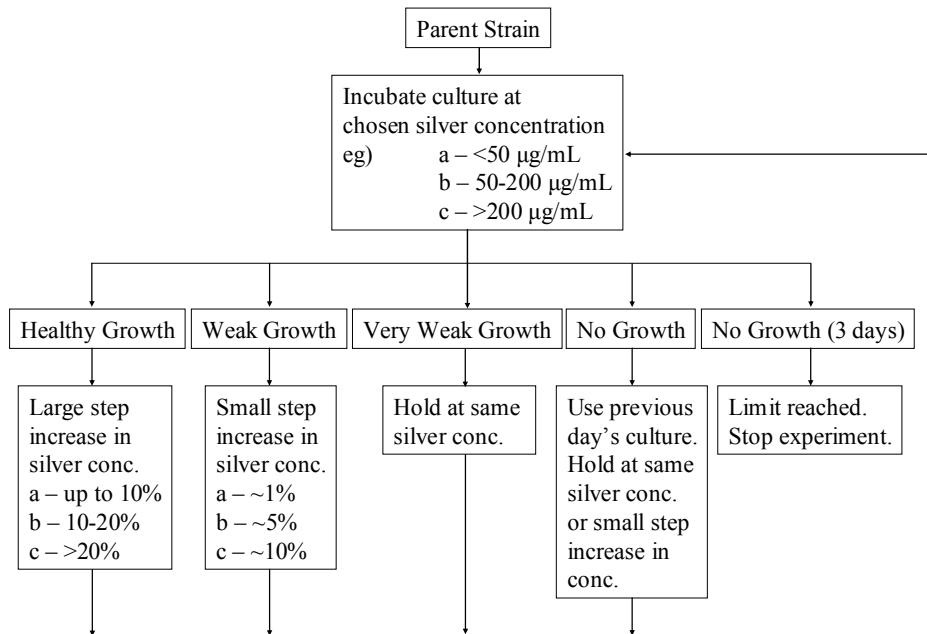


Figure 4-3. Decision tree for the incremental development of silver-resistant organisms.

Development of Silver-Dressing Resistant Bacteria

For this study, the dressings tested were cut into 1 cm x 8 cm strips using sterile techniques. Bacteria (*P. aeruginosa* or *S. aureus*) were grown in 100 mL of TSB overnight (37°C, 200 rpm). Then 1 mL of this inoculum was transferred

to fresh TSB and grown up for four hours under the same conditions to generate log phase bacteria. 100 μ L of this culture was spread on MHA plates in triplicate. Strips of the dressings were then placed on the center of each plate and moistened according to their water holding capacity with reverse osmosis water (see Table 4-5). The plates were incubated at 37°C overnight, and then the corrected zone of inhibition was determined by measuring the dressing and the zone along its narrower dimension and then subtracting the dressing width from the zone width. Any organisms present within the zone (growth inhibited or not) were deemed likely to be the least sensitive organisms to the dressing, and therefore were harvested by removing the dressing and aseptically cutting the agar out of the zone of inhibition and placing it in 9 mL of PBS. This was then shaken vigorously and the solution was decanted and used to harvest the microorganisms from within the zones of the remaining two plates, in order to obtain sufficient organisms. 100 μ L of this solution was then spread onto MHA plates, and fresh dressing strips were placed on the surface as described above. The process was repeated daily until the dressings no longer created zones of inhibition. Exposure to the dressing was continued past this point in some cases to see if additional resistance could be developed with continued exposures to the ineffective dressing. Periodically throughout testing, MICs were determined using silver nitrate to test the susceptibility of the cells to Ag^+ . When MICs no longer changed for a substantial period of time after the dressings ceased to produce zones of inhibition, the experiment was terminated.

Table 4-5. Water holding capacities of various silver containing dressings.

Dressing Description	Average Water Holding Capacity ($\mu\text{L}/\text{cm}^2$, \pm S.D., n=3 unless indicated)
Silver NaCMC dressing	443 \pm 6
Ionic silver foam dressing	333 \pm 28
Silver alginate dressing	208 \pm 14
Silver chloride dressing	46 \pm 3
Silver nylon dressing	25 \pm 4 (n=2)
Silver hydrocolloid dressing	4 \pm 6

In one run where the bacteria were exposed to nanocrystalline silver, after the zone size had decreased, a log reduction assay was performed to test the bactericidal efficacy of nanocrystalline silver against these organisms that appeared to have developed resistance. The procedure for this was as described in the next section.

Testing for Ability of Silver Dressings to Kill Ag⁺ Resistant Bacteria

The ability of four commercial silver-containing dressings to kill bacteria which were resistant to Ag⁺ in the form of silver nitrate was tested using log reductions using similar techniques to the literature[4, 9]. The organisms selected for this test were the silver resistant *Pseudomonas aeruginosa* (SRPA) and the silver resistant *Staphylococcus aureus* (SRSA). Results with both mutant strains were compared to results obtained using their parent strains. Both mutants and their parent strains were grown overnight in TSB (37°C, 200 rpm). 1 mL of each culture was added to 100 mL of TSB and incubated under the same conditions for four hours to generate bacteria in log phase growth. For each test, a piece of plastic just over one square inch in size was placed in the top portion of a Petri dish. A one inch square piece of the dressing to be tested was then laid on the

plastic sheet, and inoculated with 300 μL of one of the cultures grown up for four hours. A second piece of plastic was placed on top of the inoculated dressing and weighed down with the bottom portion of the Petri dish to ensure good contact between the dressing and the bacteria. This was then incubated at 37°C for half an hour, and then the plastic-dressing sandwich was placed in 2.7 mL of SPS (0.85% w/v NaCl, 1% v/v polysorbate 20, and 0.1% w/v sodium thioglycolate for *P. aeruginosa*. See Study #1 for *S. aureus* recipe). This was vortexed vigorously to inactivate the silver and recover the bacteria. The resulting solutions were then serially diluted out to 10^{-6} in PBS. From each dilution, 20 μL was drop-plated in triplicate onto MHA plates, which were then incubated at 37°C overnight. A similar procedure was performed for the inoculum, and plate counts were performed to determine the log of the original CFUs and the surviving CFUs. The log reductions were then calculated as the difference between the two. All procedures were performed in triplicate.

Growth Rates of Silver Resistant Strains

The growth rates of silver resistant strains SRPA and SRSA were compared to the growth rates of their parent strains via optical density measurements and viable cell counts.

Freeze-dried SRPA and SRSA, as well as their parent strains, were cultured on MHA, MICs were measured to ensure that the SRPA and SRSA were still silver resistant, and then cultures were grown overnight in 100 mL TSB (37°C, 200 rpm). 1 mL of the overnight culture was transferred into 100 mL TSB, and incubated (37°C, 200 rpm). After 0.5, 1, 2, 4, and 6 hours, 1 mL of the

solution was transferred into 9 mL of PBS, vortexed, and the optical density was measured at 650 nm using a spectrophotometer with distilled water as the standard. The same procedure was used to measure viable cell counts, except that at the above time points after inoculation, 1 mL of culture was transferred into 9 mL PBS, vortexed, and serially diluted out to 10^{-7} . Using the drop plate technique, three drops were plated per dilution. Both procedures were performed in triplicate.

Testing for Stability of Mutation

The stability of silver resistant organisms is a measure of a pathogen's potential clinical impact. If a pathogen is able to develop silver resistance, but the mutation is not stable, it is a less serious clinical threat than if it demonstrates relatively permanent resistance.

Stability of the mutation produced in SRPA was tested in two ways. In the first test, the SRPA was transferred daily in TSB containing 5000 ppm Ag^+ (silver nitrate) following procedures described above. MICs were performed periodically to test for the organisms' ability to maintain resistance to Ag^+ in the presence of a high concentration of silver nitrate.

In the second test, the SRPA was transferred daily in silver-free TSB following procedures described above. MICs were performed periodically to test for the organisms' ability to maintain resistance to Ag^+ in the absence of silver nitrate.

Antibiotic Sensitivity Testing in Ag^+ Resistant Pseudomonas aeruginosa

Antibiotic sensitivity testing was performed using a modified Kirby-Bauer

assay[99-101]. Briefly, 3-5 colonies of the parent strain of *Pseudomonas aeruginosa* (ATCC 27317) or SRPA were used to inoculate 4-5 mL of TSB. The bacteria were incubated at 35°C for four to six hours until their optical density was higher than 0.1 (turbidity equivalent to a 0.5 McFarland turbidity standard, which is $1-2 \times 10^8$ CFU/mL). At this point, they were diluted with TSB, as necessary, to obtain the correct optical density. Within 15 minutes, a cotton swab was dipped into the adjusted inoculum, and rotated firmly a few times against the inside wall of the tube to eliminate excess fluid. The entire surface of an MHA plate was streaked three times, rotating the plate 60° between streakings to create an even layer of inoculum. The lid was left ajar for about three minutes to let surface moisture absorb. Tobramycin discs (6 mm BD BBL™ Sensi-Disc™ Susceptibility Test Discs) were then carefully placed on the MHA plates with their centers at least 10 mm from the edge of the plate, and at least 24 mm from each other. Six discs were placed on each plate and pressed down. Within 15 minutes, the plates were placed agar side up in an incubator at 35°C, where they were incubated overnight. After 16-18 hours of incubation, zones of inhibition around each disc were measured to the nearest millimeter in two perpendicular directions and averaged. This strain was tested for Ag⁺ resistance just prior to the antibiotic sensitivity assay, and was shown to have a minimum inhibitory concentration (MIC) of greater than 5000 ppm Ag⁺ at the time, as tested with silver nitrate. *Pseudomonas aeruginosa* is considered resistant to tobramycin if the zones created are less than 12 millimeters, intermediate if the zones created are 13-14 millimeters, and susceptible if the zones are greater than 15 millimeters.

The parent strain of *Pseudomonas aeruginosa* would be expected to produce zones between 19 and 25 millimeters[99-101].

Statistical Analyses

One way ANOVA tests with Tukey-Kramer Multiple Comparisons post tests were performed for all assays in which more than two groups were compared. When only two groups were compared, this was done using unpaired t-tests with Welch corrections. All statistical analyses were performed using Graphpad InStat Version 3.06 (GraphPad Software, San Diego, California, © 2003, www.graphpad.com). Error bars on figures represent standard deviations.

Results

Original MICs

The original MICs measured for each bacterial species used to develop silver resistance are shown in Table 4-6, from the naturally most sensitive (*P. aeruginosa*), to the naturally most resistant (*S. aureus*).

Table 4-6. Minimum inhibitory concentrations for micro-organisms tested for the development of resistance to Ag⁺.

Microorganism	Silver Nitrate MIC (µg/mL)
<i>Pseudomonas aeruginosa</i>	<2 to 2.5*
<i>Escherichia coli</i> ATCC 11303	3
<i>Escherichia coli</i> B/5	3
<i>Enterobacter aerogenes</i>	8**,4***
<i>Staphylococcus epidermidis</i>	8
<i>Proteus vulgaris</i>	10
<i>Staphylococcus aureus</i>	10-14*

*Minor variations occurred with different trials. **MIC determined prior to first and second trial.

***MIC determined prior to third trial.

Development of Ag⁺ Resistant Bacteria

Each organism was first exposed to half their MIC as determined from

Table 4-6. The results of step-wise exposure of *P. aeruginosa* to increasing amounts of silver nitrate, proceeding via the decision tree in Figure 4-3, are shown in Table 4-7. A plot of the silver concentration the bacteria were grown in versus the exposure day is shown in Figure 4-4. Earlier trials were performed which are not shown because they would not be visible due to the scale of the figure, and to limit the length of the table.

Table 4-7. Results of Ag⁺ resistance development assay in *P. aeruginosa*.

Day	Silver Concentration (µg/mL)	Growth	Decision	% Increase
1	1.25	healthy	large increase	50%
2	1.875	healthy	large increase	17%
3	2.1875	healthy	large increase	3%
4	2.25	healthy	large increase	2%
5	2.3	very weak	same concentration	0%
6	2.3	healthy	large increase	4%
7	2.4	healthy	large increase	2%
8	2.45	weak	small increase	1%
9	2.475	weak	small increase	1%
10	2.5	very weak	same concentration	0%
11	2.5	healthy	large increase	2%
12	2.55	healthy	large increase	2%
13	2.6	healthy	large increase	2%
14	2.65	healthy	large increase	2%
15	2.7	healthy	large increase	4%
16	2.8	healthy	large increase	4%
17	2.9	healthy	large increase	3%
18	3	healthy	large increase	17%
19	3.5	weak	small increase	3%
20	3.6	healthy	large increase	3%
21	3.7	healthy	large increase	8%
22	4	healthy	large increase	5%
23	4.2	healthy	large increase	5%
24	4.4	healthy	large increase	5%
25	4.6	none	back to 24, large increase	2%
25	4.5	weak	small increase	1%
26	4.55	weak	small increase	1%
27	4.6	weak	small increase	1%
28	4.65	weak	small increase	1%
29	4.7	weak	small increase	1%

30	4.75	weak	small increase	1%
31	4.8	healthy	large increase	2%
32	4.9	healthy	large increase	2%
33	5	healthy	large increase	4%
34	5.2	healthy	large increase	4%
35	5.4	healthy	large increase	7%
36	5.8	healthy	large increase	7%
37	6.2	healthy	large increase	6%
38	6.6	healthy	large increase	6%
39	7	healthy	large increase	4%
40	7.25	healthy	large increase	2%
41	7.4	weak	small increase	1%
42	7.5	weak	small increase	1%
43	7.6	healthy	large increase	2%
44	7.75	healthy	large increase	3%
45	8	healthy	large increase	3%
46	8.25	healthy	large increase	3%
47	8.5	healthy	large increase	6%
48	9	healthy	large increase	6%
49	9.5	healthy	large increase	5%
50	10	healthy	large increase	5%
51	10.5	healthy	large increase	5%
52	11	healthy	large increase	5%
53	11.5	healthy	large increase	2%
54	11.75	healthy	large increase	2%
55	12	healthy	large increase	3%
56	12.3	healthy	large increase	6%
57	13	healthy	large increase	4%
58	13.5	healthy	large increase	4%
59	14	healthy	large increase	4%
60	14.5	very weak	back to 58, same conc.	0%
59	14	very weak	same concentration	0%
60	14	healthy	large increase	4%
61	14.5	healthy	large increase	3%
62	15	healthy	large increase	7%
63	16	healthy	large increase	6%
64	17	healthy	large increase	6%
65	18	very weak	same concentration again	0%
66	18	healthy	large increase	6%
67	19	healthy	large increase	5%
68	20	healthy	large increase	10%
69	22	none	back to 68, large increase	10%
69	22	healthy	large increase	14%
70	25	healthy	miscommunication ^{iv}	-8%

^{iv} Miscommunication between week day and weekend staff regarding health of organism and procedure to follow.

71	23	healthy	large increase	4%
72	24	healthy	large increase	4%
73	25	healthy	large increase	12%
74	28	healthy	large increase	15%
75	32.3	healthy	large increase	8%
76	35	healthy	large increase	9%
77	38	healthy	large increase	8%
78	41	healthy	large increase	12%
79	46	healthy	large increase	11%
80	51	healthy	large increase	12%
81	57	healthy	large increase	12%
82	64	healthy	large increase	13%
83	72	healthy	large increase	11%
84	80	healthy	large increase	10%
85	88	healthy	large increase	9%
86	96	healthy	large increase	9%
87	105	healthy	large increase	10%
88	115	healthy	large increase	13%
89	130	healthy	large increase	19%
90	155	healthy	large increase	29%
91	200	healthy	large increase	25%
92	250	healthy	large increase	30%
93	325	healthy	large increase	23%
94	400	healthy	large increase	25%
95	500	healthy	large increase	20%
96	600	healthy	large increase	25%
97	750	healthy	large increase	27%
98	950	healthy	large increase	26%
99	1200	healthy	large increase	25%
100	1500	healthy	large increase	27%
101	1900	healthy	large increase	32%
102	2500	healthy	large increase	32%
103	3300	healthy	large increase	30%
104	4300	healthy	large increase	28%
105	5500	healthy	large increase	27%
106	7000	healthy	large increase	14%
107	8000	healthy	large increase	19%
108	9500	healthy	large increase	37%
109	13000	healthy	large increase	15%
110	15000	healthy	large increase	7%
111	16000	no growth	mistake - revert to 108	-41%
112	9500	healthy	small increase	5%
113	10000	healthy	large increase	10%
114	11000	v weak	same concentration	0%
115	11000	healthy	large increase	9%
116	12000	healthy	end of experiment	N/A

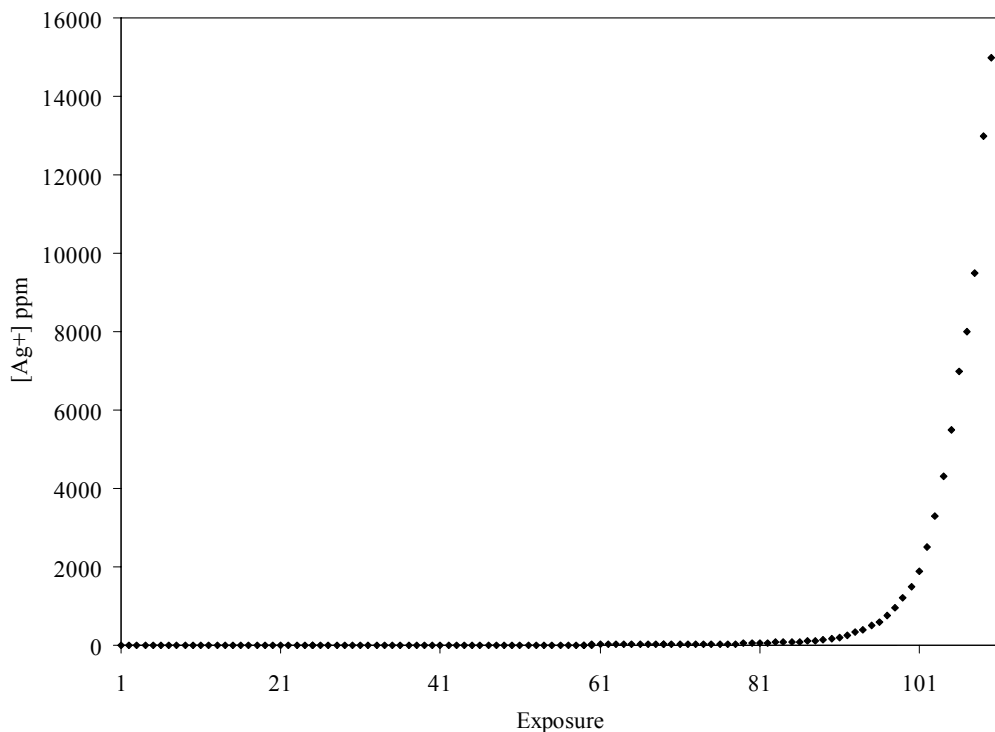


Figure 4-4. The Ag^+ (silver nitrate) concentration that *Pseudomonas aeruginosa* (ATCC 27317) was exposed to during silver-resistance development experiments is plotted over time. The original *P. aeruginosa* MIC is plotted as a dashed horizontal line, but cannot be seen clearly because of the scale on the y-axis.

In one of the initial trials with *P. aeruginosa*, the silver concentration that the organism was exposed to was 2.25, 3.38, and 4.5 $\mu\text{g}/\text{mL}$ Ag^+ for the first three exposures, and the organism had corresponding MICs of between 4.5-9 $\mu\text{g}/\text{mL}$ Ag^+ for the first two exposures, but had an MIC of >13.5 $\mu\text{g}/\text{mL}$ Ag^+ after the third exposure, indicating a >300% increase in MIC with three exposures. For the trial shown in Table 4-7, *Pseudomonas aeruginosa* was able to grow at its original MIC within 10 exposures to silver nitrate, and was able to grow at a concentration 2200 times the original MIC (5500 $\mu\text{g}/\text{mL}$ Ag^+) within 105 exposures. The results of the periodic MIC determinations for *P. aeruginosa* for this trial are

shown in Table 4-8.

Table 4-8. Periodically measured MICs for *P. aeruginosa* during step-wise exposure to Ag⁺.

Exposure #	MIC (µg/mL)
17	>4.5
34	>7.5
43	>10
56	>15
84	>256
90	>1024
105	>16384

The MIC for *P. aeruginosa* increased by over two times by the 17th day, and by over 410 times by the 90th day. During the course of the experiment, the growth stalled at concentrations of 2.3 µg/mL, 2.5 µg/mL, 4.6 µg/mL, 14.5 µg/mL, and 18 µg/mL Ag⁺. The appearance of the bacteria in broth culture changed during the course of the experiment – growth appeared green until 13.5 µg/mL Ag⁺, brown between 13.5 and 23 µg/mL Ag⁺, green again between 23 and 35 µg/mL Ag⁺, and dark amber for concentrations above 38 µg/mL Ag⁺. The daily incremental increase in silver was chosen to be relatively small for the first 30 exposures but was increased rapidly after that point. The Ag⁺ resistant *P. aeruginosa* developed as described here will be called SRPA below.

The results of step-wise exposure of *E. coli* ATCC 11303 and *E. coli* B/5 to increasing amounts of silver nitrate, proceeding via the decision tree in Figure 4-3, are shown in Tables 4-9 and 4-10, respectively. Plots of the silver concentrations that the bacteria were grown in versus the exposure day are shown in Figures 4-5 and 4-6 for *E. coli* ATCC 11303 and B/5, respectively.

Table 4-9. Results of Ag⁺ resistance development assay in *E. coli* (11303).

Day	Silver Concentration (µg/mL)	Growth	Decision	% Increase
1	1.5	healthy	large increase	50%
2	2.25	healthy	large increase	11%
3	2.5	healthy	large increase	10%
4	2.75	healthy	large increase	9%
5	3	healthy	large increase	8%
6	3.25	healthy	large increase	8%
7	3.5	healthy	large increase	7%
8	3.75	healthy	large increase	7%
9	4	healthy	large increase	6%
10	4.25	healthy	large increase	2%
11	4.35	healthy	large increase	3%
12	4.5	very weak	back to 11, same conc.	0%
12	4.4	very weak	same concentration	0%
13	4.4	weak	small increase	1%
14	4.45	weak	small increase	1%
15	4.5	weak	small increase	1%
16	4.55	weak	small increase	1%
17	4.6	weak	small increase	2%
18	4.7	mistake	back to 16, small increase	2%
18	4.7	healthy	large increase	2%
19	4.8	healthy	large increase	2%
20	4.9	healthy	large increase	2%
21	5	healthy	large increase	2%
22	5.1	healthy	large increase	2%
23	5.2	healthy	large increase	4%
24	5.4	healthy	large increase	4%
25	5.6	healthy	large increase	4%
26	5.8	healthy	large increase	2%
27	5.9	healthy	large increase	2%
28	6	healthy	large increase	3%
29	6.15	very weak	same concentration	0%
30	6.15	weak	small increase	1%
31	6.2	very weak	back to 30, same conc.	0%
31	6.15	very weak	same concentration	0%
32	6.15	very weak	same concentration	0%
33	6.15	weak	small increase	1%
34	6.2	weak	small increase	1%
35	6.25	healthy	large increase	2%
36	6.35	healthy	large increase	2%
37	6.45	healthy	large increase	2%
38	6.6	healthy	large increase	3%
39	6.8	healthy	large increase	3%

40	7	healthy	large increase	4%
41	7.25	healthy	large increase	3%
42	7.5	healthy	large increase	4%
43	7.8	healthy	large increase	4%
44	8.1	healthy	large increase	4%
45	8.4	healthy	large increase	4%
46	8.7	healthy	large increase	5%
47	9.1	healthy	large increase	10%
48	10	healthy	large increase	9%
49	10.9	healthy	large increase	9%
50	11.9	healthy	large increase	9%
51	13	healthy	large increase	4%
52	13.5	healthy	large increase	8%
53	14.6	healthy	large increase	3%
54	15	healthy	large increase	3%
55	15.5	healthy	large increase	5%
56	16.2	weak	small increase	2%
57	16.5	weak	small increase	2%
58	16.8	healthy	large increase	3%
59	17.3	healthy	large increase	4%
60	18	healthy	large increase	6%
61	19	healthy	large increase	5%
62	20	healthy	large increase	5%
63	21	healthy	large increase	14%
64	24	healthy	large increase	25%
65	30	healthy	large increase	17%
66	35	healthy	large increase	14%
67	40	weak	small increase	5%
68	42	weak	small increase	5%
69	44	weak	small increase	5%
70	46	healthy	large increase	9%
71	50	healthy	large increase	10%
72	55	healthy	large increase	13%
73	62	healthy	large increase	13%
74	70	healthy	large increase	14%
75	80	healthy	large increase	13%
76	90	healthy	large increase	28%
77	115	healthy	large increase	26%
78	145	healthy	large increase	24%
79	180	weak	same concentration	0%
80	180	healthy	mild increase	6%
81	190	healthy	large increase	58%
82	300	healthy	large increase	17%
83	350	healthy	large increase	14%
84	400	healthy	large increase	13%
85	450	healthy	large increase	11%

86	500	healthy	large increase	10%
87	550	healthy	large increase	9%
88	600	healthy	large increase	3%
89	620	healthy	large increase	5%
90	650	healthy	large increase	8%
91	700	healthy	large increase	4%
92	730	weak	same concentration	0%
93	730	healthy	mild increase	3%
94	750	healthy	mild increase	3%
95	770	healthy	large increase	4%
96	800	healthy	large increase	6%
97	850	healthy	end of experiment	N/A

Table 4-10. Results of Ag⁺ resistance development assay in *E. coli* (B/5).

Day	Silver Concentration (µg/mL)	Growth	Decision	% Increase
1	1.5	healthy	large increase	50%
2	2.25	healthy	large increase	11%
3	2.5	healthy	large increase	10%
4	2.75	healthy	large increase	9%
5	3	none	back to 4, small increase	2%
5	2.8	very weak	same concentration	0%
6	2.8	healthy	large increase	4%
7	2.9	healthy	large increase	3%
8	3	healthy	large increase	10%
9	3.3	healthy	large increase	6%
10	3.5	healthy	large increase	7%
11	3.75	healthy	large increase	7%
12	4	healthy	large increase	2%
13	4.1	very weak	same concentration	0%
14	4.1	weak	small increase	1%
15	4.15	weak	small increase	1%
16	4.2	weak	small increase	1%
17	4.25	weak	small increase	1%
18	4.3	very weak	same concentration	0%
19	4.3	very weak	same concentration	0%
20	4.3	weak	small increase	1%
21	4.35	weak	small increase	1%
22	4.4	healthy	large increase	2%
23	4.5	healthy	large increase	2%
24	4.6	healthy	large increase	4%
25	4.8	healthy	large increase	4%
26	5	healthy	large increase	4%
27	5.2	healthy	large increase	2%

28	5.3	healthy	large increase	2%
29	5.4	weak	small increase	2%
30	5.5	healthy	large increase	4%
31	5.7	very weak	back to 30, small increase	4%
31	5.7	very weak	same concentration	0%
32	5.7	very weak	same concentration	0%
33	5.7	very weak	same concentration	0%
34	5.7	weak	small increase	1%
35	5.75	weak	small increase	1%
36	5.8	healthy	large increase	2%
37	5.9	healthy	large increase	2%
38	6	healthy	large increase	2%
39	6.1	healthy	large increase	2%
40	6.25	healthy	large increase	3%
41	6.45	healthy	large increase	4%
42	6.7	healthy	large increase	4%
43	6.95	healthy	large increase	4%
44	7.25	healthy	large increase	3%
45	7.5	healthy	large increase	3%
46	7.75	healthy	large increase	3%
47	8	healthy	large increase	6%
48	8.5	healthy	large increase	12%
49	9.5	healthy	large increase	11%
50	10.5	healthy	large increase	10%
51	11.5	healthy	large increase	9%
52	12.5	healthy	large increase	12%
53	14	healthy	large increase	11%
54	15.5	weak	small increase	3%
55	16	weak	small increase	3%
56	16.5	healthy	large increase	4%
57	17.2	weak	small increase	2%
58	17.5	weak	small increase	2%
59	17.8	healthy	large increase	3%
60	18.3	healthy	large increase	4%
61	19	healthy	large increase	5%
62	20	healthy	large increase	5%
63	21	healthy	large increase	5%
64	22	healthy	large increase	14%
65	25	healthy	large increase	20%
66	30	healthy	large increase	17%
67	35	healthy	large increase	14%
68	40	weak	small increase	5%
69	42	weak	small increase	5%
70	44	weak	small increase	5%
71	46	healthy	large increase	9%
72	50	healthy	large increase	10%

73	55	healthy	large increase	13%
74	62	healthy	large increase	13%
75	70	healthy	large increase	14%
76	80	healthy	large increase	13%
77	90	healthy	large increase	28%
78	115	healthy	large increase	26%
79	145	healthy	large increase	24%
80	180	weak	same concentration	0%
81	180	healthy	mild increase	6%
82	190	healthy	large increase	58%
83	300	healthy	large increase	17%
84	350	healthy	large increase	14%
85	400	healthy	large increase	13%
86	450	healthy	large increase	11%
87	500	healthy	large increase	10%
88	550	healthy	large increase	9%
89	600	weak	mild increase	8%
90	650	healthy	mild increase	8%
91	700	healthy	mild increase	7%
92	750	healthy	mild increase	4%
93	780	weak	same concentration	0%
94	780	healthy	mild increase	3%
95	800	healthy	mild increase	3%
96	820	healthy	large increase	4%
97	850	healthy	large increase	6%
98	900	healthy	end of experiment	N/A

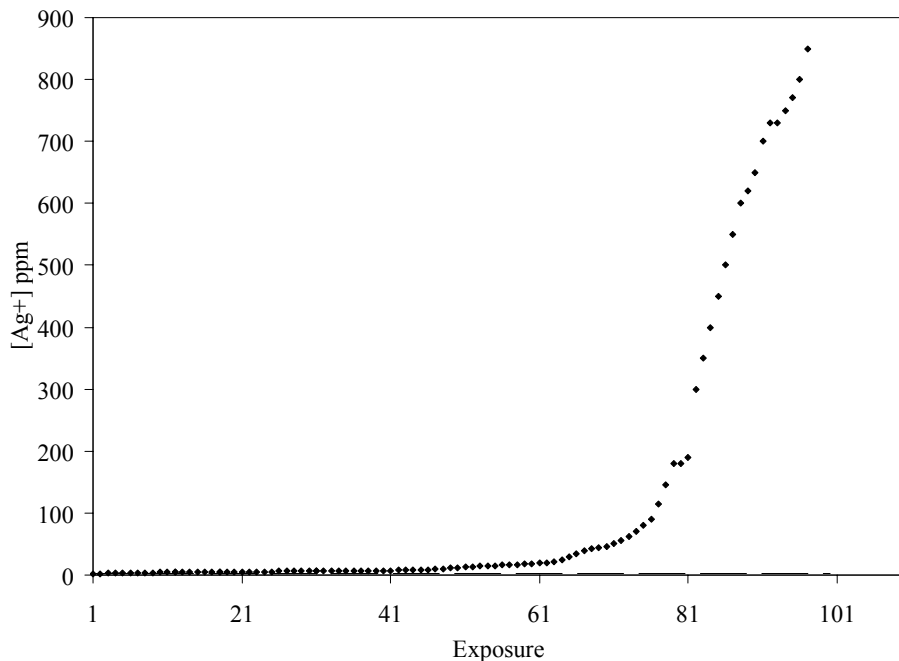


Figure 4-5. The Ag^+ (silver nitrate) concentration that *Escherichia coli* (ATCC 11393) was exposed to during silver-resistance development experiments is plotted over time. The original *E. coli* (ATCC 11393) MIC is plotted as a dashed horizontal line, but is difficult to see clearly because of the scale on the y-axis.

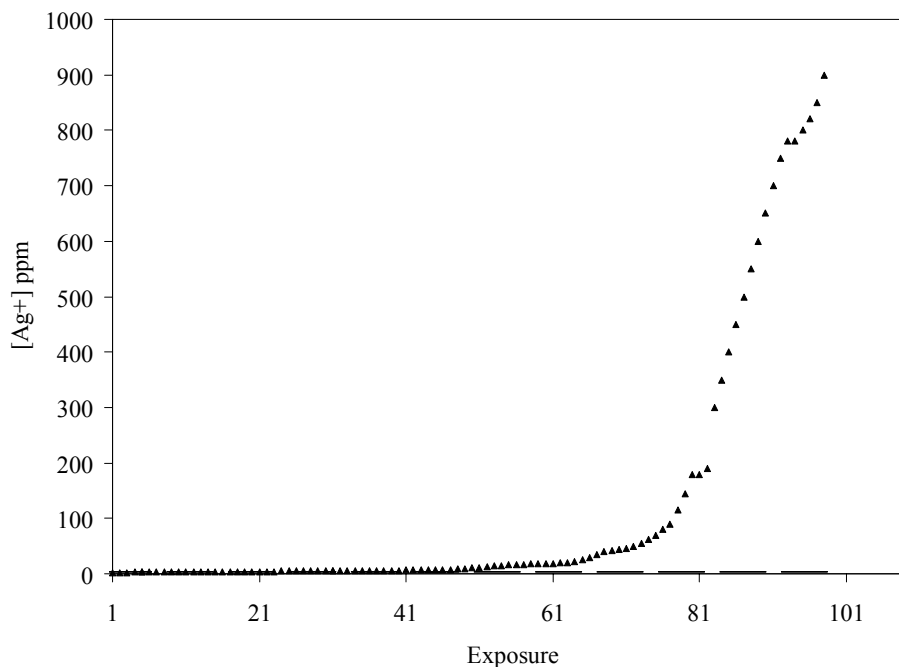


Figure 4-6. The Ag^+ (silver nitrate) concentration that *Escherichia coli* (B/5) was exposed to during silver-resistance development experiments is plotted over time. The original *E. coli* (B/5) MIC is plotted as a dashed horizontal line, but is difficult to see clearly because of the scale on the y-axis.

As shown in Tables 4-9 and 4-10, *E. coli* ATCC 11303 and *E. coli* B/5 grew at their original MICs within five and eight days, respectively. The results of the periodic MIC determinations for both *E. coli* strains are shown in Table 4-11. At the end of the experiment, the MICs for both *E. coli* strains were >2000 µg/mL Ag⁺.

Table 4-11. Periodically measured MICs for *E. coli* 11303 and *E. coli* B/5 during step-wise exposure to silver nitrate (Ag⁺).

Strain	Day	MIC (µg/mL)
11303	46	>12
B/5	47	>12
11303 and B/5	76	>250
11303 and B/5	78	>1024

The MICs for both *E. coli* strains increased by over four times by the 47th day, and by over 83 times by the 76th day. During the course of the experiment, growth stalled for the ATCC 11303 strain at concentrations of 4.5, 6.15, 16, 180, and 730 µg/mL Ag⁺. Growth stalled for the B/5 strain at concentrations of 2.8, 4.1, 5.7, 16, 180, 600, and 780 µg/mL Ag⁺. The daily incremental increase in silver was selected to be relatively small for the first 63 exposures, but was increased rapidly after that point for both strains. The only exception to this was when the rate of increase was decreased for a few days due to a change in the appearance of the bacteria grown in broth to a clearer solution with dark deposits, which occurred at 40 µg/mL Ag⁺. The rate of increase was slowed to ensure the organisms were still healthy despite the change in physical appearance.

The results of step-wise exposure of *E. aerogenes* to increasing amounts of silver nitrate are shown in Table 4-12. Plots of the silver concentrations grown in versus the exposure day for the various trials are shown in Figure 4-7.

Table 4-12. Results of Ag⁺ resistance development assay in *E. aerogenes*.

Day	Silver Concentration (µg/mL)	Growth	Decision	% Increase
Trial 1:				
1	4			50%
2	6	none	back to 1, large increase	25%
2	5	healthy	large increase	10%
3	5.5	healthy	large increase	9%
4	6	healthy	large increase	8%
5	6.5	healthy	large increase	8%
6	7	healthy	large increase	7%
7	7.5	healthy	large increase	7%
8	8	healthy	large increase	6%
9	8.5	healthy	large increase	6%
10	9	healthy	large increase	6%
11	9.5	healthy	large increase	5%
12	10	healthy	large increase	5%
13	10.5	healthy	large increase	5%
14	11	none	back to 13, small increase	2%
14	10.75	none	back to 13, small increase	1%
14	10.6	none	limit reached, stop experiment	N/A
Trial 2:				
1	4	healthy	large increase	13%
2	4.5	none	back to 1, large increase	6%
2	4.25	none	back to 1, same conc. again	0%
2	4	very weak	same concentration again	0%
3	4	none	back to 3rd 2, small decrease	-13%
3	3.5	healthy	large increase	14%
4	4	none	limit reached, stop experiment	N/A
Trial 3:				
1	2	healthy	large increase	25%
2	2.5	healthy	large increase	20%
3	3	healthy	large increase	7%
4	3.2	healthy	large increase	9%
5	3.5	healthy	large increase	11%
6	3.9	healthy	large increase	13%
7	4.4	healthy	large increase	14%
8	5	healthy	large increase	16%
9	5.8	very weak	small increase	2%
10	5.9	none	back to 8, large increase	5%
9	5.25	very weak	back to 1st 9, same conc.	0%
10	5.8	none	back to 2nd 9, same conc.	0%
10	5.25	none	back to 2nd 9, small decrease	-5%
10	5	none	limit reached, stop experiment	N/A

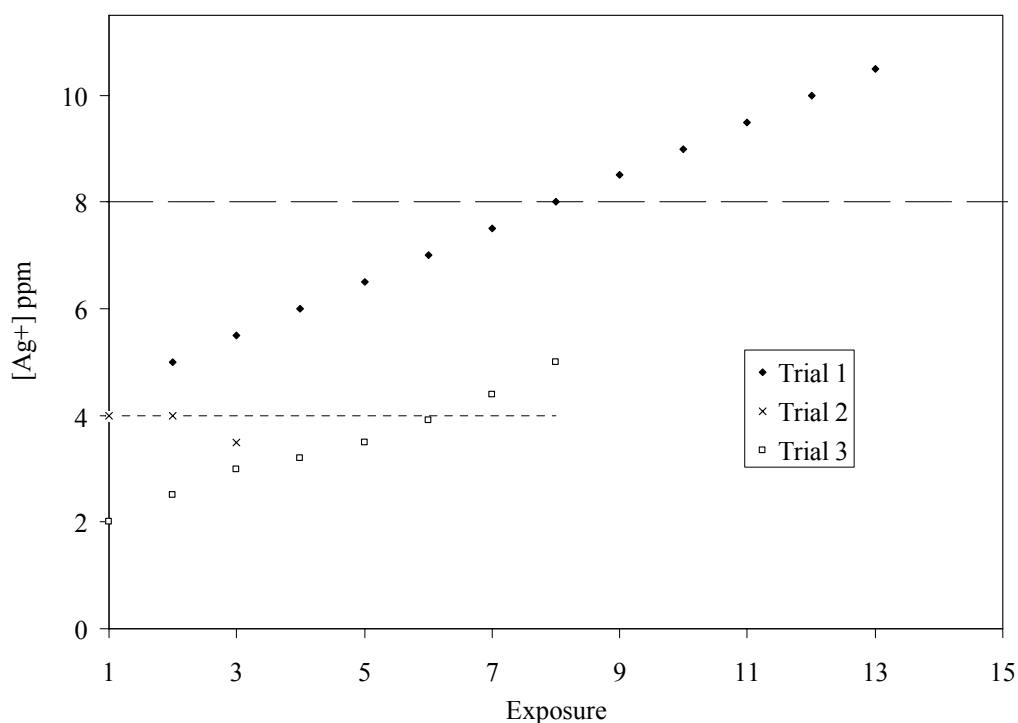


Figure 4-7. The Ag^+ (silver nitrate) concentration that *Enterobacter aerogenes* (62-1) was exposed to during three silver-resistance development experiments is plotted over time. The original *E. aerogenes* MICs are plotted as dashed horizontal lines (see note in Table 4-6).

Three attempts were made to develop *E. aerogenes* which were resistant to Ag^+ . During the first trial, it grew at its original MIC within eight days. It continued to grow to up to a concentration of $10.5 \mu\text{g/mL Ag}^+$ at Day 13, after which point the bacteria died. During the second trial, the bacteria died after only three days, at a concentration of $3.5 \mu\text{g/mL Ag}^+$. Prior to the third trial, the original MIC for *E. aerogenes* was re-evaluated, and found to be $4 \mu\text{g/mL Ag}^+$. During the third trial, the bacteria grew at a concentration of $3.9 \mu\text{g/mL Ag}^+$ on the sixth day; however, the organisms were no longer alive by Day 8, when a concentration of $5 \mu\text{g/mL Ag}^+$ was used. Periodic MICs were not determined for *E. aerogenes* during the three trials.

The results of step-wise exposure of *P. vulgaris* to increasing amounts of silver nitrate, proceeding via the decision tree in Figure 4-3, are shown in Table 4-13. Plots of the silver concentrations that the bacteria were grown in versus the exposure day are shown in Figure 4-8.

Table 4-13. Results of Ag⁺ resistance development assay in *P. vulgaris*.

Day	Silver Concentration (mg/mL)	Growth	Decision	% Increase
Trial 1:				
1	5			50%
2	7.5	none	back to 1, large increase	20%
2	6	none	back to 1, large increase	10%
2	5.5	healthy	large increase	9%
3	6	healthy	large increase	8%
4	6.5	healthy	large increase	8%
5	7	healthy	large increase	7%
6	7.5	healthy	large increase	7%
7	8	healthy	large increase	6%
8	8.5	healthy	large increase	6%
9	9	healthy	large increase	6%
10	9.5	healthy	large increase	5%
11	10	healthy	large increase	5%
12	10.5	healthy	large increase	5%
13	11	none	back to 12, small increase	2%
13	10.75	none	back to 12, small increase	1%
13	10.6	none	limit reached, stop experiment	N/A
Trial 2:				
1	5	healthy	large increase	10%
2	5.5	very weak	back to 1, same conc	0%
2	5	none	back to 1 st 2, large decrease	-9%
3	5	none	back to 1 st 2, large decrease	-18%
3	4.5	very weak	same concentration	0%
4	4.5	none	back to 3, same conc	0%
4	4.5	none	limit reached, stop experiment	N/A

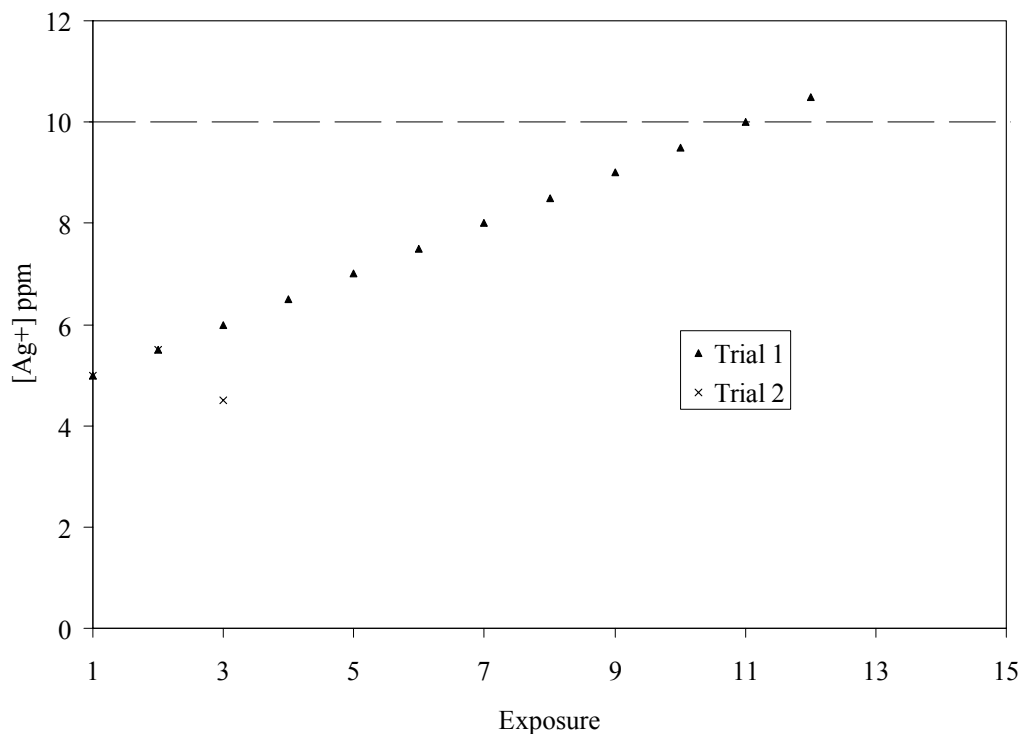


Figure 4-8. The Ag^+ (silver nitrate) concentration that *Proteus vulgaris* was exposed to during two silver-resistance development experiments is plotted over time. The original *P. vulgaris* MIC is plotted as a dashed horizontal line.

Resistance-development experiments were conducted two times for *P. vulgaris*. During the first trial, the bacteria grew at its original MIC within 11 days. It continued to grow up to a concentration of $10.5 \mu\text{g/mL Ag}^+$ at Day 12, after which point it died. During the second trial, it died after only three days, at a concentration of $4.5 \mu\text{g/mL Ag}^+$. Periodic MICs were not determined for *Proteus vulgaris* during the two trials.

The results of step-wise exposure of *S. aureus* to increasing amounts of silver nitrate, proceeding via the decision tree in Figure 4-3, are shown in Table 4-14. Plots of the silver concentrations that the bacteria were grown in versus the exposure day are shown in Figure 4-9.

Table 4-14. Results of Ag⁺ resistance development assay in *S. aureus*.

Day	Silver Concentration (mg/mL)	Growth	Decision	% Increase
Trial 1				
1	4	healthy	large increase	25%
2	5	healthy	large increase	20%
3	6	healthy	large increase	8%
4	6.5	healthy	large increase	23%
5	8	none	back to 4, large increase	15%
5	7.5	weak	small increase	1%
6	7.6	none	back to 5, small increase	1%
6	7.55	very weak	same concentration	0%
7	7.55	weak	small increase	1%
8	7.6	weak	small increase	1%
9	7.7	weak	small increase	1%
10	7.8	weak	small increase	1%
11	7.85	very weak	back to 10, same concentration	0%
11	7.8	none	back to 1st 11, same concentration	0%
12	7.85	none	back to 2nd 11, same conc.	0%
12	7.8	none	limit reached, stop experiment	N/A
Trial 2				
1	5	healthy	large increase	20%
2	6	very weak	same concentration	0%
3	6	very weak	same concentration	0%
4	6	weak	small increase	2%
5	6.1	weak	small increase	2%
6	6.2	healthy	large increase	3%
7	6.4	healthy	large increase	3%
8	6.6	healthy	large increase	3%
9	6.8	healthy	large increase	3%
10	7	very weak	same concentration	0%
11	7	healthy	large increase	3%
12	7.2	healthy	large increase	3%
13	7.4	very weak	same concentration	0%
14	7.4	very weak	same concentration	0%
15	7.4	weak	small increase	1%
16	7.5	very weak	same concentration	0%
17	7.5	weak	small increase	1%
18	7.6	weak	small increase	2%
19	7.75	healthy	large increase	3%
20	8	healthy	large increase	3%
21	8.25	healthy	large increase	3%
22	8.5	healthy	large increase	3%
23	8.75	healthy	large increase	3%

24	9	healthy	large increase	3%
25	9.25	healthy	large increase	3%
26	9.5	healthy	large increase	3%
27	9.75	healthy	large increase	3%
28	10	healthy	large increase	3%
29	10.25	healthy	large increase	3%
30	10.6	healthy	large increase	4%
31	11	healthy	large increase	5%
32	11.5	none	back to 31, small increase	2%
32	11.25	none	back to 31, small increase	1%
32	11.1	very weak	back to 30, same concentration	0%
31	10.6	none	limit reached, stop experiment	N/A
Trial 3				
1	5	healthy	large increase	10%
2	5.5	very weak	same concentration	0%
3	5.5	weak	small increase	2%
4	5.6	very weak	same concentration	0%
5	5.6	weak	small increase	1%
6	5.65	very weak	same concentration	0%
7	5.65	weak	small increase	1%
8	5.7	very weak	same concentration	0%
9	5.7	very weak	back to 8, same concentration	0%
9	5.7	weak	small increase	1%
10	5.75	weak	small increase	1%
11	5.8	weak	small increase	1%
12	5.85	healthy	large increase	2%
13	5.95	healthy	large increase	3%
14	6.1	healthy	large increase	2%
15	6.25	healthy	large increase	3%
16	6.45	healthy	large increase	3%
17	6.65	healthy	large increase	4%
18	6.9	healthy	large increase	4%
19	7.2	healthy	large increase	3%
20	7.4	healthy	large increase	4%
21	7.7	healthy	large increase	5%
22	8.1	healthy	large increase	6%
23	8.6	healthy	large increase	6%
24	9.1	healthy	large increase	5%
25	9.6	healthy	large increase	7%
26	10.3	healthy	large increase	9%
27	11.2	healthy	large increase	7%
28	12	healthy	large increase	7%
29	12.8	healthy	large increase	8%
30	13.8	healthy	large increase	9%
31	15	healthy	large increase	9%
32	16.4	healthy	large increase	9%

33	17.8	healthy	large increase	8%
34	19.3	healthy	large increase	9%
35	21	healthy	large increase	10%
36	23	healthy	large increase	13%
37	26	healthy	large increase	15%
38	30	healthy	large increase	17%
39	35	none	mistake, back to 38, large increase	17%
39	35	healthy	large increase	17%
40	41	healthy	large increase	17%
41	48	healthy	large increase	21%
42	58	healthy	large increase	21%
43	70	healthy	large increase	21%
44	85	healthy	large increase	18%
45	100	healthy	large increase	15%
46	115	healthy	large increase	17%
47	135	healthy	large increase	11%
48	150	healthy	large increase	17%
49	175	healthy	large increase	9%
50	190	healthy	large increase	11%
51	210	healthy	large increase	10%
52	230	healthy	large increase	9%
53	250	healthy	large increase	12%
54	280	healthy	large increase	11%
55	310	healthy	large increase	10%
56	340	healthy	large increase	18%
57	400	healthy	large increase	13%
58	450	healthy	large increase	11%
59	500	healthy	large increase	10%
60	550	healthy	large increase	9%
61	600	healthy	large increase	8%
62	650	healthy	large increase	8%
63	700	healthy	end of experiment	N/A

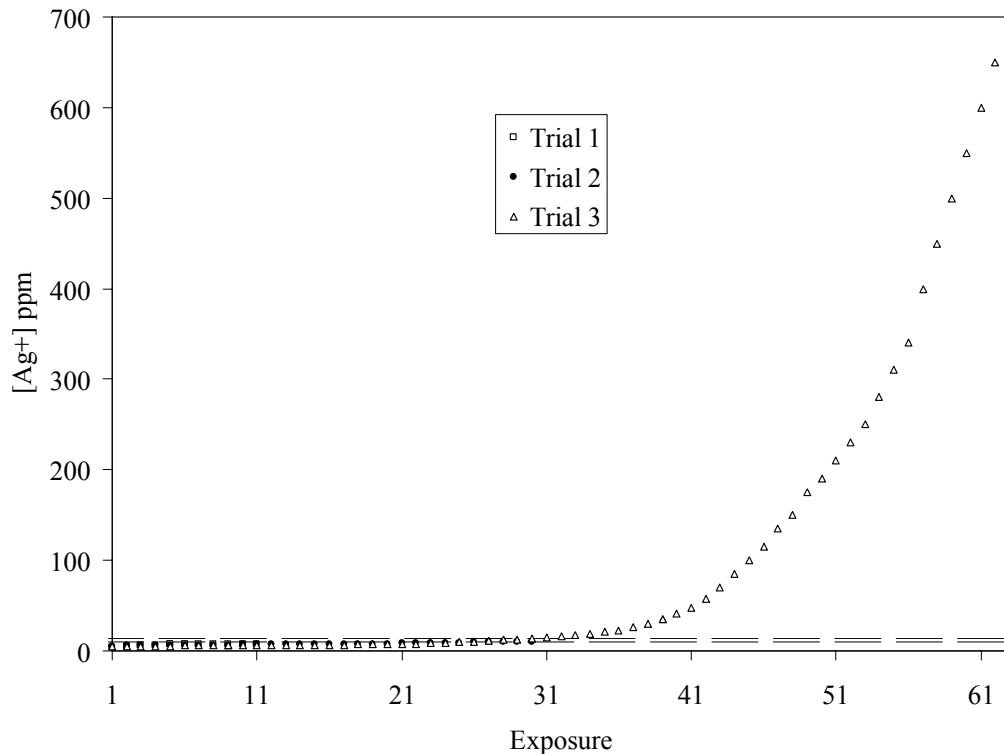


Figure 4-9. The Ag^+ (silver nitrate) concentration that *Staphylococcus aureus* (ATCC 25923) was exposed to during four silver-resistance development experiments is plotted over time. The original *S. aureus* MICs are plotted as dashed horizontal lines (see note in Table 4-6).

Resistance development trials were conducted three times for *S. aureus*. During the first trial, bacteria grew to a maximum concentration of 7.85 $\mu\text{g}/\text{mL}$ Ag^+ at Day 11. During the second trial, it grew at its original MIC within 28 days; however, it hit a maximum concentration of 11 $\mu\text{g}/\text{mL}$ Ag^+ by Day 31. Despite a slower start during the third trial, it grew at its original MIC within 26 days. The organisms grew at a concentration of 4.8 times the original MIC by Day 41. The new MIC was determined only once during the third trial: the MIC was greater than 200 $\mu\text{g}/\text{mL}$ Ag^+ , over 20 times the original MIC, on the 41st day. At the end of the third trial, the MIC was >4000 $\mu\text{g}/\text{mL}$ Ag^+ . The Ag^+ resistant *S. aureus* will be referred to as SRSA herein.

The results of step-wise exposure of *S. epidermidis* to increasing amounts of silver nitrate, proceeding via the decision tree in Figure 4-3, are shown in Table 4-15. Plots of the silver concentrations that the bacteria were grown in versus the exposure day are shown in Figure 4-10.

Table 4-15. Results of the Ag⁺ resistance development assay in *S. epidermidis*.

Day	Silver Concentration (mg/mL)	Growth	Decision	% Increase
1	4	healthy	large increase	50%
2	6	healthy	large increase	17%
3	7	none	back to 2, large increase	8%
3	6.5	none	back to 2, large increase	4%
3	6.25	very weak	same concentration	0%
4	6.25	none	back to 3rd 3, small decrease	-4%
4	6	none	back to 4, same concentration	0%
5	6.25	weak	small increase	1%
6	6.3	weak	small increase	2%
7	6.4	weak	small increase	2%
8	6.5	very weak	same concentration	0%
9	6.5	none	back to 8, same concentration	0%
9	6.5	none	back to 1st 9, same conc.	0%
10	6.5	very weak	same concentration	0%
11	6.5	weak	small increase	2%
12	6.6	very weak	same concentration	0%
13	6.6	weak	small increase	2%
14	6.7	weak	small increase	1%
15	6.8	none	back to 14, small increase	1%
15	6.75	none	back to 14, same concentration	0%
15	6.7	very weak	same concentration	0%
16	6.7	weak	small increase	1%
17	6.75	weak	small increase	1%
18	6.8	weak	small increase	1%
19	6.85	weak	small increase	1%
20	6.9	weak	small increase	1%
21	7	weak	small increase	1%
22	7.1	healthy	large increase	3%
23	7.3	healthy	large increase	16%
24	8.5	healthy	large increase	6%
25	9	healthy	large increase	6%
26	9.5	healthy	large increase	11%
27	10.5	healthy	large increase	14%
28	12	healthy	large increase	13%

29	13.5	healthy	large increase	11%
30	15	healthy	large increase	13%
31	17	healthy	large increase	12%
32	19	healthy	large increase	11%
33	21	healthy	large increase	10%
34	23	healthy	large increase	9%
35	25	healthy	large increase	8%
36	27	healthy	large increase	11%
37	30	healthy	large increase	17%
38	35	healthy	large increase	14%
39	40	healthy	large increase	13%
40	45	healthy	large increase	11%
41	50	healthy	large increase	10%
42	55	weak	same concentration	0%
43	55	weak	same concentration	0%
44	55	healthy		

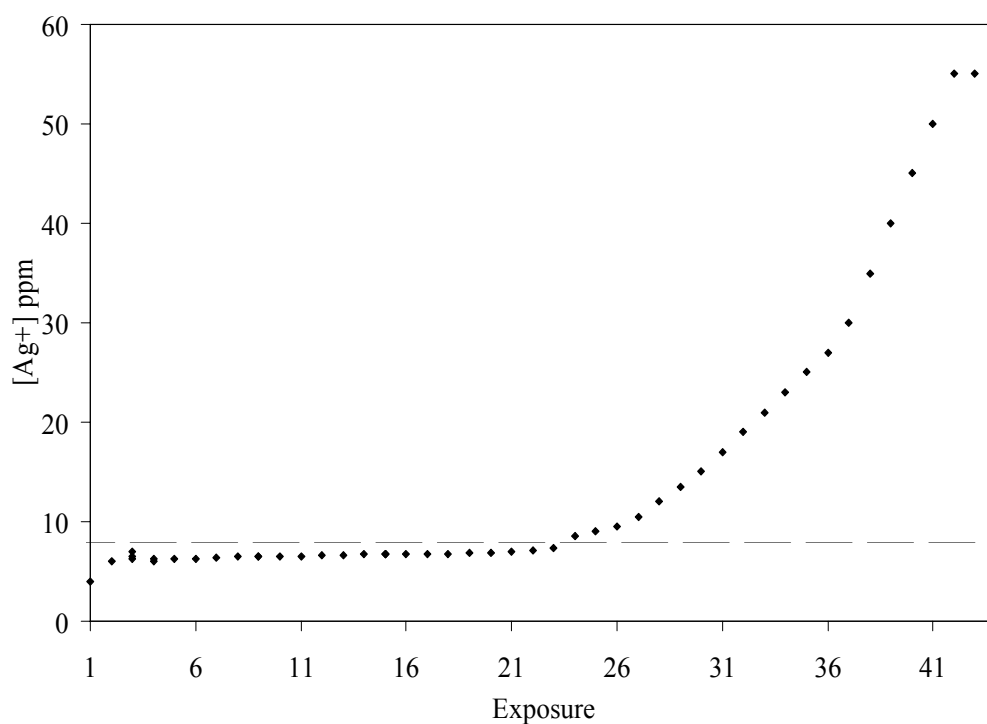


Figure 4-10. The Ag^+ (silver nitrate) concentration that *Staphylococcus epidermidis* (ATCC e15J) was exposed to during silver-resistance development experiments is plotted over time. The original *S. epidermidis* MIC is plotted as a dashed horizontal line.

The daily incremental increases were kept fairly constant for the first 23 days, after which point, the growth became healthier and larger increases were possible. *S. epidermidis* grew to a concentration of 7.3 $\mu\text{g/mL Ag}^+$ by Day 23, after stalled growth around a concentration of 6.5 $\mu\text{g/mL Ag}^+$. The final MIC at the end of the experiment was $>400 \mu\text{g/mL Ag}^+$, despite an apparent stalling of growth just before the end of the experiment at 55 $\mu\text{g/mL}$.

Development of Silver-Dressing Resistant Bacteria

The results of daily exposure of parent strain *P. aeruginosa* to nanocrystalline silver dressings are shown in Figure 4-11. The experiment was repeated six times, and the zone of inhibition decreased in size over the course of each trial, with some suggestion of a stepwise behavior. The MIC of the harvested cells was not measured during the first trial. It was only determined once during the second trial, and it was found to be greater than 5 $\mu\text{g/mL Ag}^+$ (tested using silver nitrate) after the fourth day. A log reduction was performed on the organisms collected near the end of this trial, when the zone of inhibition had clearly decreased, however, the nanocrystalline silver dressings still produced a total kill against the organisms within half an hour. MICs were not determined during the fourth trial. During the fifth trial, the nanocrystalline silver dressings ceased to produce zones of inhibition after the 11th day. However, after the 14th day, the bacteria still had MICs less than 2 $\mu\text{g/mL Ag}^+$. In the sixth trial, after the ninth exposure, the MIC was between 2 and 4 $\mu\text{g/mL Ag}^+$. After the 14th and 21st exposures, the MIC was between 4-6 $\mu\text{g/mL Ag}^+$. The dressings ceased to produce zones of inhibition after the 28th exposure, at which point the MIC was

found to be greater than 8 $\mu\text{g/mL Ag}^+$. However, when exposures were continued (despite the dressings producing no zone of inhibition), after the 36th exposure, the MIC was back to being less than 2 $\mu\text{g/mL Ag}^+$, and after the 39th, 42nd, and 47th exposures, the MIC remained constant between 2 and 4 $\mu\text{g/mL Ag}^+$.

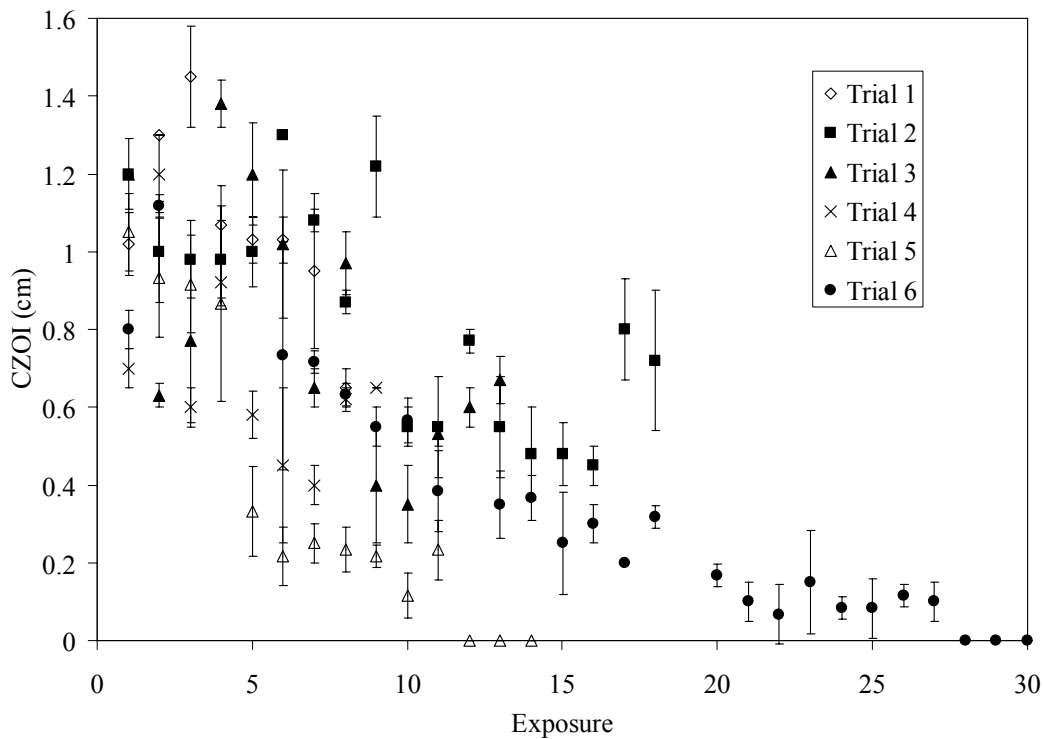


Figure 4-11. Corrected zones of inhibition are plotted over time for six attempts to develop *P. aeruginosa* which were resistant to a nanocrystalline silver dressing. Each day, lawns of bacteria were generated from bacteria collected within zones of inhibition created by nanocrystalline silver dressings, and these lawns were exposed to fresh pieces of nanocrystalline silver dressings for an overnight incubation, the zone of inhibition created was measured, and the process was repeated. Error bars indicate standard deviations (n=3 for all data points).

The results of daily exposure of parent strain *P. aeruginosa* to silver alginate dressings are shown in Figure 4-12. Two trials were run. In both trials, the zone sizes decreased with number of exposures in a roughly exponential manner. During the first trial, the dressings ceased to produce zones of inhibition against *P. aeruginosa* by the 6th exposure. After the 8th exposure, there was no

change in MIC – it was still less than 2 $\mu\text{g/mL Ag}^+$. During the second trial, the dressings first produced no zone after the 6th exposure, but produced a zone after the 7th exposure. The dressings produced no zone from the 8th exposure on. After the 5th exposure, 12th exposure, and 20th exposure, the MIC was constant at between 4 and 6 $\mu\text{g/mL Ag}^+$.

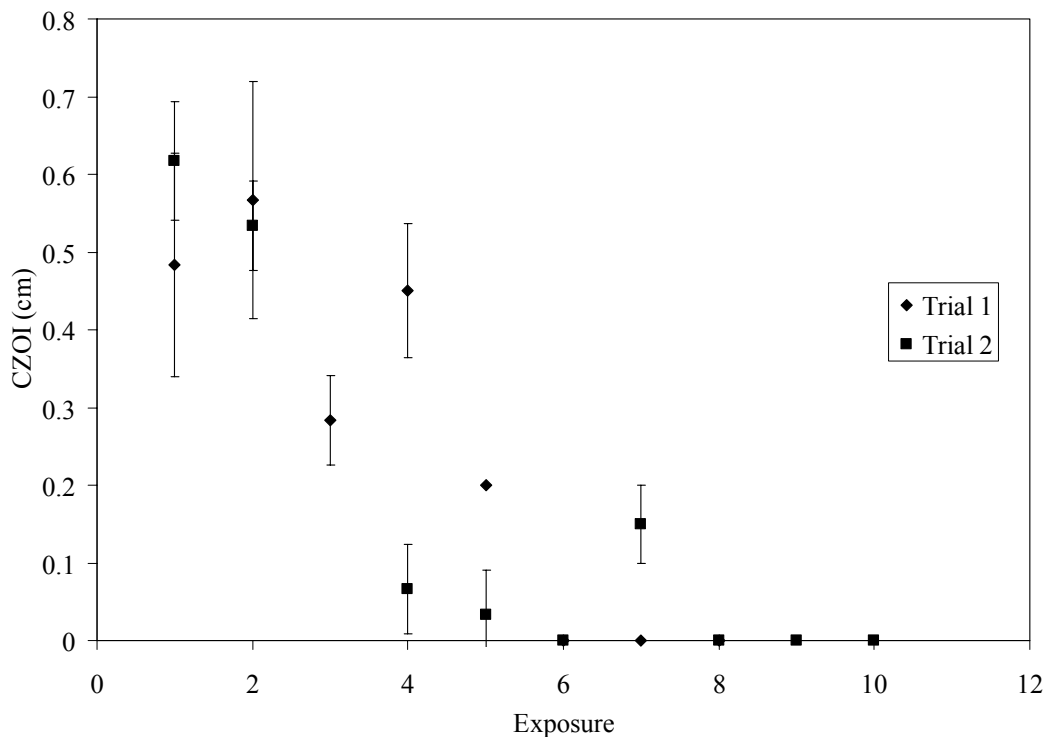


Figure 4-12. Corrected zones of inhibition are plotted over time for two attempts to develop *P. aeruginosa* which were resistant to a silver alginate dressing. Each day, lawns of bacteria were generated from bacteria collected within zones of inhibition created by silver alginate dressings, and these lawns were exposed to fresh pieces of silver alginate dressings for an overnight incubation, the zone of inhibition created was measured, and the process was repeated. Error bars indicate standard deviations (n=3 for all data points).

The results of daily exposure of *P. aeruginosa* to silver chloride dressings are shown in Figure 4-13. Only one trial was run. In it, the dressings ceased to produce zones of inhibition against *P. aeruginosa* after the 3rd exposure in a single

step. With continued exposure of the bacteria to the dressings, the MIC was found to be between 3 and 4 $\mu\text{g/mL Ag}^+$ after the 9th exposure, greater than 5 $\mu\text{g/mL Ag}^+$ after the 15th exposure, and between 8 and 10 $\mu\text{g/mL Ag}^+$ after the 21st exposure.

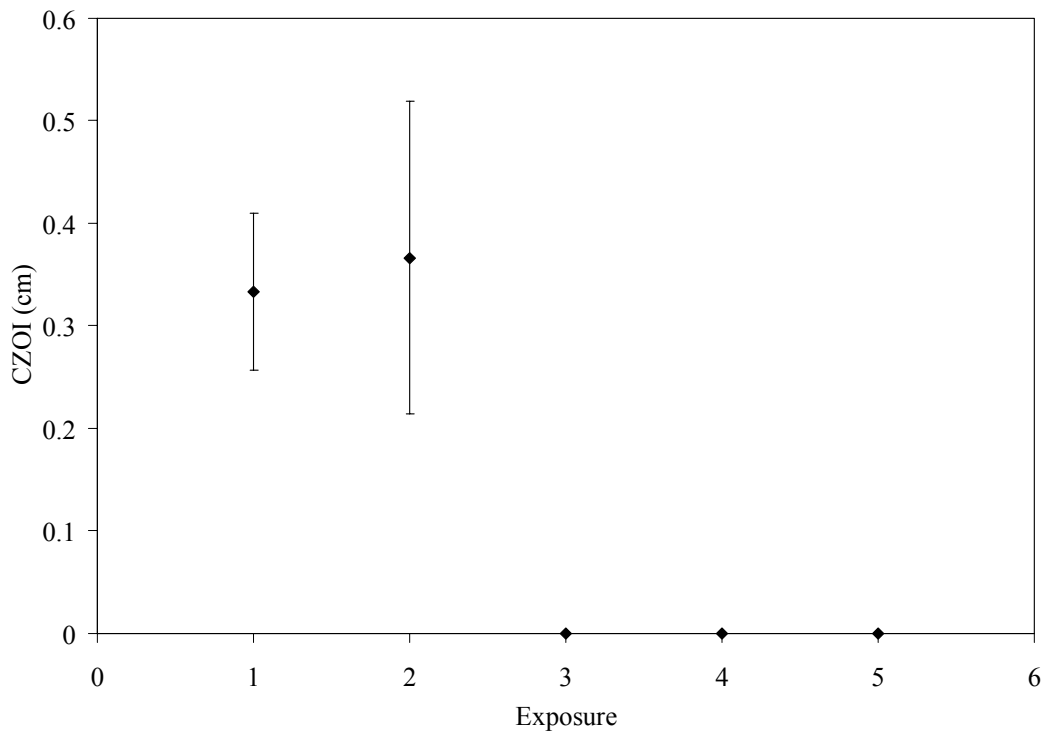


Figure 4-13. Corrected zones of inhibition are plotted over time for an attempt to develop *P. aeruginosa* which were resistant to a silver chloride dressing. Each day, lawns of bacteria were generated from bacteria collected within zones of inhibition created by silver chloride dressings, and these lawns were exposed to fresh pieces of silver chloride dressings for an overnight incubation, the zone of inhibition created was measured, and the process was repeated. Error bars indicate standard deviations ($n=3$ for all data points).

The results of daily exposure of *P. aeruginosa* to silver NaCMC dressings are shown in Figure 4-14. Three trials were run, all of which showed decreases in zone size with increasing number of exposures, which appeared to be step-wise. During the first trial, the dressings were unable to produce zones against the

organisms after 22 exposures. The only MIC measured during this trial was after the 11th exposure, at which point the MIC had not changed – it was still less than 2 $\mu\text{g/mL Ag}^+$. During the second trial, the dressings ceased to create zones by the 13th exposure. After the 8th exposure, the MIC had increased to between 4 and 6 $\mu\text{g/mL Ag}^+$, and after the 14th exposure, the MIC was found to be between 6 to 8 $\mu\text{g/mL Ag}^+$, where it remained out to the 22nd exposure. During the third trial, the MIC was between 2 and 4 $\mu\text{g/mL Ag}^+$ after the 7th exposure, between 4 and 6 $\mu\text{g/mL Ag}^+$ after the 12th exposure, and between 6 and 8 $\mu\text{g/mL Ag}^+$ after the 18th exposure.

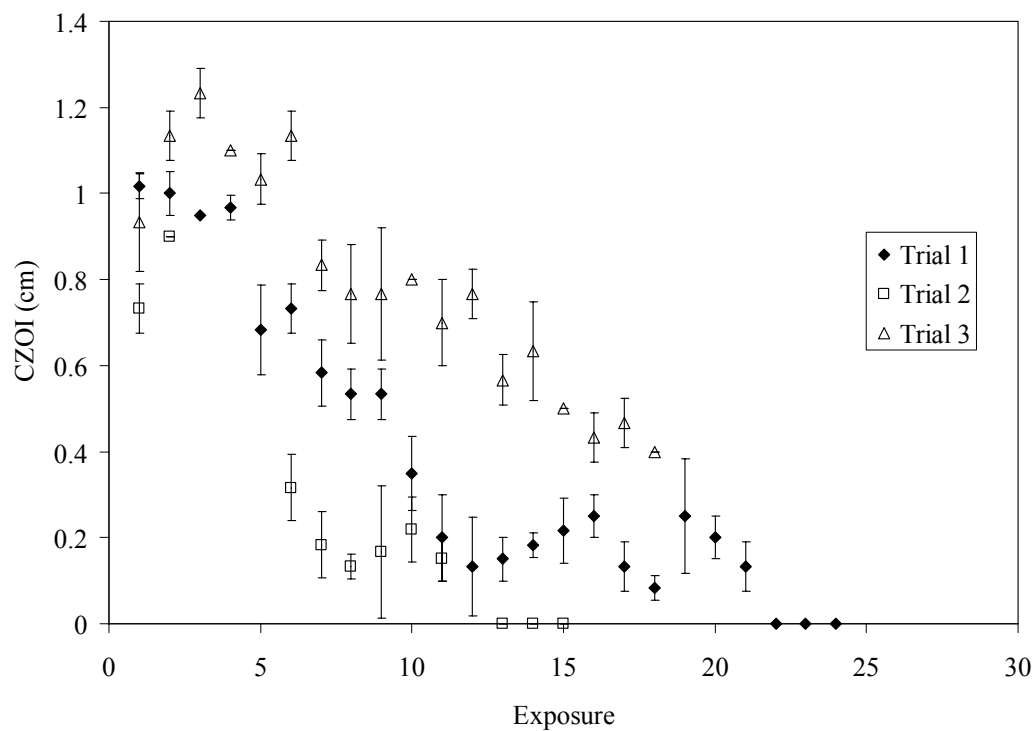


Figure 4-14. Corrected zones of inhibition are plotted over time for three attempts to develop *P. aeruginosa* which were resistant to a silver NaCMC dressing. Each day, lawns of bacteria were generated from bacteria collected within zones of inhibition created by silver NaCMC dressings, and these lawns were exposed to fresh pieces of silver NaCMC dressings for an overnight incubation, the zone of inhibition created was measured, and the process was repeated. Error bars indicate standard deviations (n=3 for all data points).

The results of daily exposure of *P. aeruginosa* to silver hydrocolloid dressings are shown in Figure 4-15. During the first trial, the dressings were unable to produce zones of inhibition against the bacteria after nine exposures. During the second trial, the dressings were unable to produce zones of inhibition after the 11th exposure. MIC measurements for both trials are shown in Table 4-16.

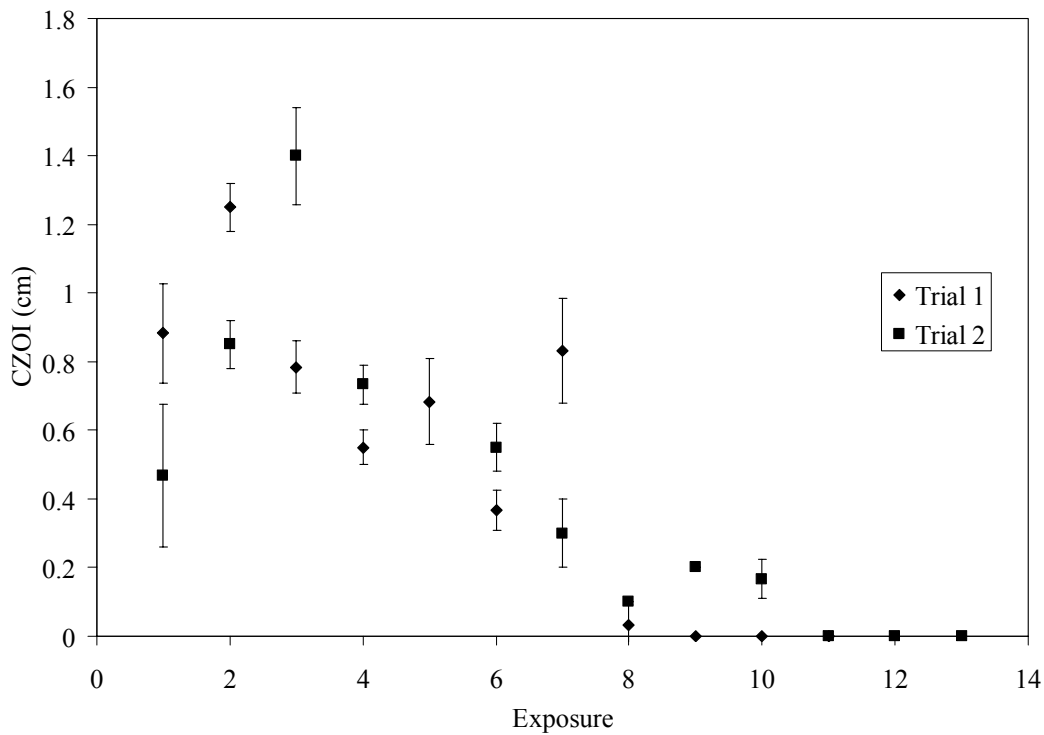


Figure 4-15. Corrected zones of inhibition are plotted over time for two attempts to develop *P. aeruginosa* which were resistant to a silver hydrocolloid dressing. Each day, lawns of bacteria were generated from bacteria collected within zones of inhibition created by silver hydrocolloid dressings, and these lawns were exposed to fresh pieces of silver hydrocolloid dressings for an overnight incubation, the zone of inhibition created was measured, and the process was repeated. Error bars indicate standard deviations (n=3 for all data points).

Table 4-16. MICs during attempts to develop resistance to silver hydrocolloid dressings.

Trial 1		Trial 2	
Exposure Number	MIC	Exposure Number	MIC ($\mu\text{g/mL Ag}^+$)
9	>4	9	>8
15	>6	20	>12
21	>10	27	>18
29	>15	28	>28
32	>25	32	>50
		35	>60
		39	80-100

The results of daily exposure of *P. aeruginosa* to silver nylon dressings are shown in Figure 4-16. One trial was performed, in which a fairly exponential decrease in zone size occurred with increasing number of exposures, followed by a final step drop. Two exposures earlier on had much lower zone sizes, but the zone size increased again to follow the more exponential shaped curve. The dressings were unable to create zones of inhibition against the bacteria after the 25th exposure. The MIC increased to between 4 and 8 $\mu\text{g/mL Ag}^+$ after the 15th exposure. It was between 5 and 7 $\mu\text{g/mL Ag}^+$ after the 21st exposure, between 8 and 10 $\mu\text{g/mL Ag}^+$ after the 23rd exposure, and remained $>8 \mu\text{g/mL Ag}^+$ after the 29th exposure.

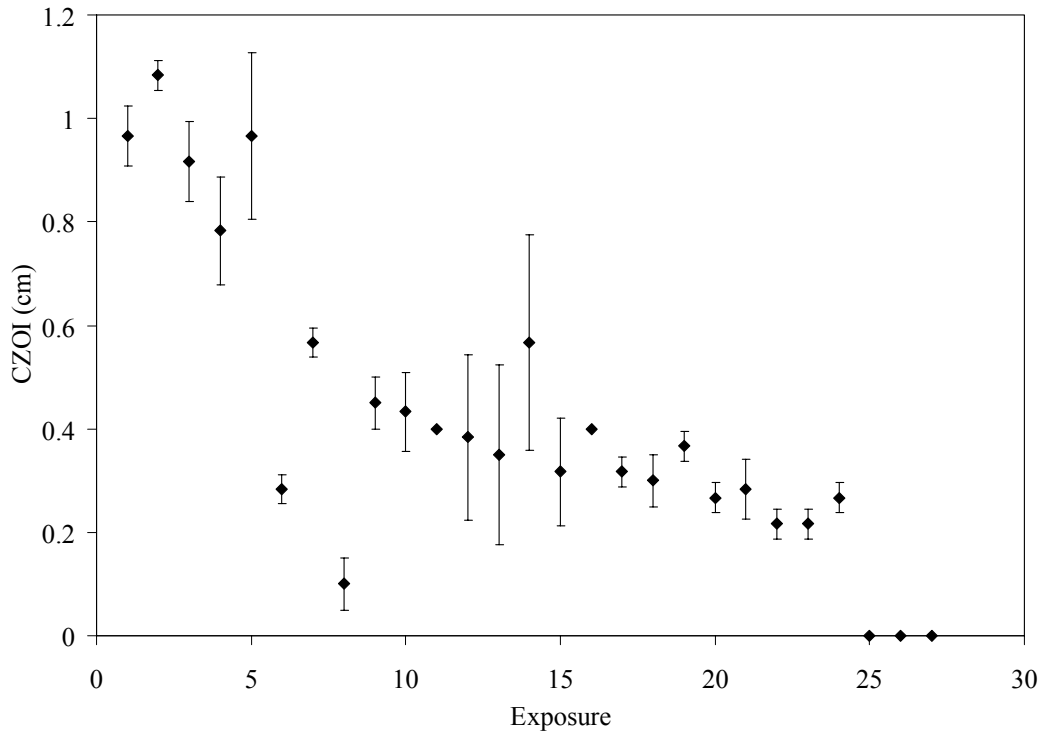


Figure 4-16. Corrected zones of inhibition are plotted over time for an attempt to develop *P. aeruginosa* which were resistant to a silver nylon dressing. Each day, lawns of bacteria were generated from bacteria collected within zones of inhibition created by silver nylon dressings, and these lawns were exposed to fresh pieces of silver nylon dressings for an overnight incubation, the zone of inhibition created was measured, and the process was repeated. Error bars indicate standard deviations (n=3 for all data points).

The results of daily exposure of *P. aeruginosa* to ionic silver foam dressings are shown in Figure 4-17. One trial was performed, in which the zone size decreased exponentially, resulting in the dressings being unable to create zones of inhibition after the third exposure. After the 6th and 13th exposures, the bacteria had MICs of approximately 6 µg/mL Ag⁺.

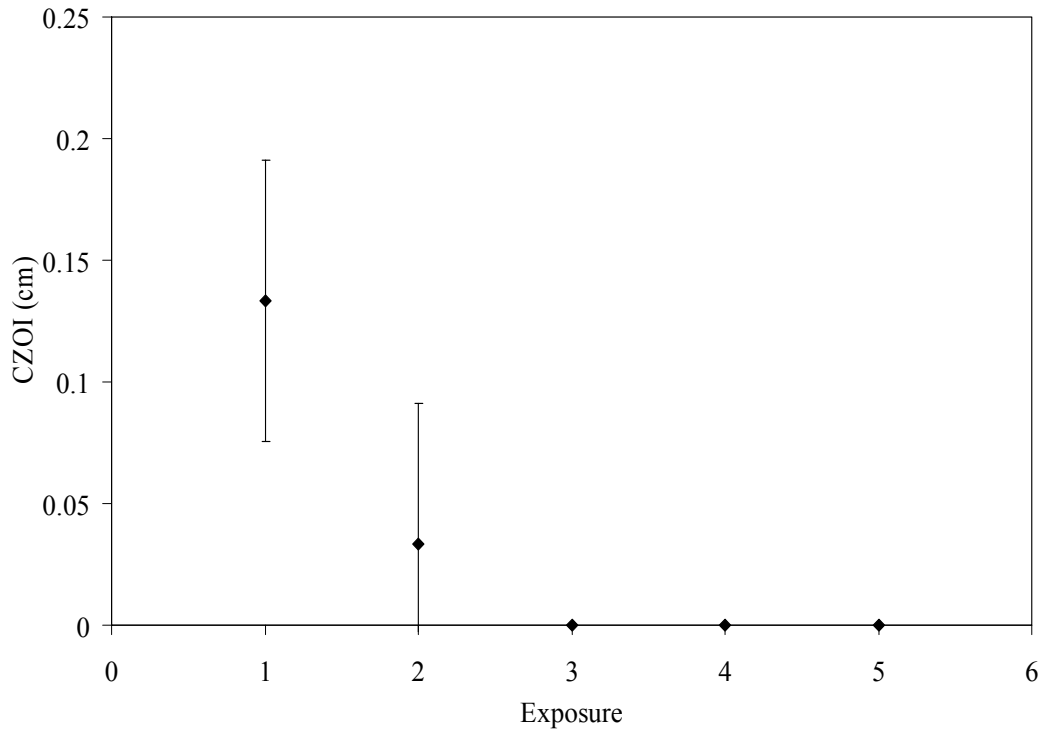


Figure 4-17. Corrected zones of inhibition are plotted over time for an attempt to develop *P. aeruginosa* which were resistant to an ionic silver foam dressing. Each day, lawns of bacteria were generated from bacteria collected within zones of inhibition created by ionic silver foam dressings, and these lawns were exposed to fresh pieces of ionic silver foam dressings for an overnight incubation, the zone of inhibition created was measured, and the process was repeated. Error bars indicate standard deviations (n=3 for all data points).

The results of daily exposure of *S. aureus* to nanocrystalline silver dressings are shown in Figure 4-18. Four trials were performed. None of the trials demonstrated any definite decreases in zone size with increasing exposure time. MICs were not determined during the trials.

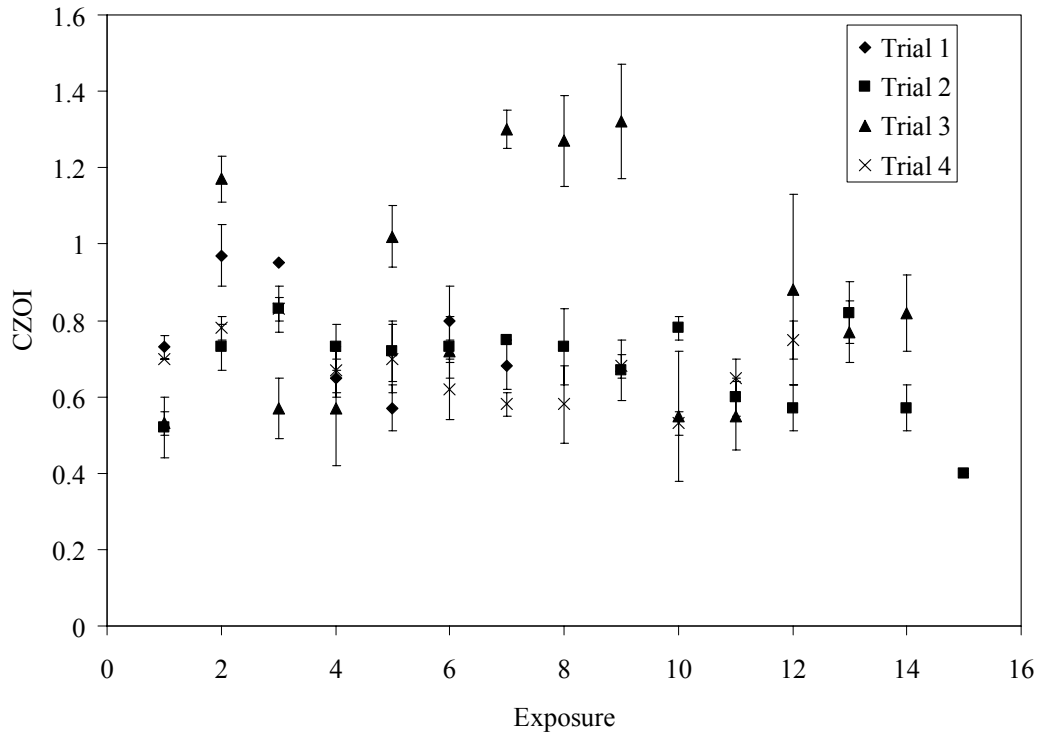


Figure 4-18. Corrected zones of inhibition are plotted over time for four attempts to develop *S. aureus* which were resistant to a nanocrystalline silver dressing. Each day, lawns of bacteria were generated from bacteria collected within zones of inhibition created by nanocrystalline silver dressings, and these lawns were exposed to fresh pieces of nanocrystalline silver dressings for an overnight incubation, the zone of inhibition created was measured, and the process was repeated. Error bars indicate standard deviations (n=3 for all data points).

Testing for Ability of Silver Dressings to Kill Ag⁺ Resistant Bacteria

Nanocrystalline silver dressings, silver nylon dressings, silver NaCMC dressings, and silver alginate dressings were tested for their ability to kill SRPA and SRSA, as well as the parent strains. The results for the SRPA and its parent strain are shown in Table 4-17. For both strains, there were extremely significant differences between groups ($p < 0.0001$), with the nanocrystalline silver dressing producing significantly higher log reductions than the other three treatment groups ($p < 0.001$). For the parent strain, the silver nylon dressing had a significantly higher log reduction than the silver NaCMC dressing ($p < 0.01$) and

the silver alginate dressing ($p < 0.001$), which were not significantly different from one another ($p > 0.05$), and which were unable to kill the parent strain. However, the silver nylon dressing also was not bactericidal against the parent strain of *P. aeruginosa*, as it produced a log reduction less than three[4]. There were no significant differences in the ability of the silver nylon dressing, the silver NaCMC dressing, and the silver alginate dressing to kill SRPA ($p < 0.05$) – they all had virtually no effect on it. The nanocrystalline silver dressing produced total kill on both strains within the limit of detection of the experiment.

Table 4-17. Bactericidal efficacy of silver dressings against SRPA and its parent strain.

Dressing Description	Average Log Reduction Against <i>P. aeruginosa</i> Parent Strain (\pm S.D., n=3)	Average Log Reduction Against SRPA (\pm S.D., n=3)
Silver NaCMC	0.8 \pm 0.4	0.3 \pm 0.1
Silver nylon	2.6 \pm 0.8	0.2 \pm 0.1
Nanocrystalline Silver	>6.3 \pm 0.0	>6.0 \pm 0.0
Silver alginate	0.1 \pm 0.1	0.3 \pm 0.0

The results of the ability of selected dressing to kill SRSA and its parent strain are shown in Table 4-18. For both strains, there were extremely significant differences between groups ($p < 0.0001$), with the nanocrystalline silver dressing producing significantly higher log reductions than the other three dressings ($p < 0.001$). Both the silver NaCMC and silver nylon dressings were able to produce significantly higher log reductions than the silver alginate dressing ($p < 0.05$ and $p < 0.01$, respectively) against the *S. aureus* parent strain, but there were no significant differences among the three dressings against the SRSA strain. The silver NaCMC, silver nylon, and silver alginate dressings were not

bactericidal against either the parent or resistant strain, while the nanocrystalline silver produced a total kill of the parent strain (within the limit of detection of the experiment), and produced a log reduction of 5.5 against the resistant strain, indicating that it was bactericidal against both strains within 30 minutes.

Table 4-18. Bactericidal efficacy of silver dressings against SRSA and its parent strain.

Dressing Description	Average Log Reduction Against <i>S. aureus</i> Parent Strain (\pm S.D., n=3)	Average Log Reduction Against SRSA (\pm S.D., n=3)
Silver NaCMC	0.3 \pm 0.2	-0.1 \pm 0.2
Silver nylon	0.6 \pm 0.3	-0.1 \pm 0.4
Nanocrystalline Silver	6.8 \pm 0.0	5.5 \pm 0.0
Silver alginate	-0.2 \pm 0.0	-0.1 \pm 0.1

Growth Rates of Silver Resistant Strains

The growth rates of the parent and silver resistant strains of *P. aeruginosa* as measured by optical density and viable cell counts are shown in Figures 4-19 and 4-20, respectively. Due to the poor sensitivity of the spectrophotometer at low densities, a high degree of error is anticipated at the earlier time points (0.5 and 1 hour), which may explain the lag in Figure 4-19 and the corresponding figure produced for *S. aureus* (Figure 4-21), relative to the measurements obtained using the viable cell counts. The optical densities of the two strains (Figure 4-19) were not significantly different at 0.5 or one hour ($p=0.5799$ and $p=0.7306$, respectively). The SRPA had a significantly higher optical density at two hours ($p=0.0095$), while the parent strain had a significantly higher optical density at four and six hours ($p=0.0025$ and $p=0.0002$, respectively). The viable cell counts (Figure 4-20) were not significantly different at 0.5 hours ($p=0.4491$), but at one hour, the SRPA had a significantly higher viable cell count than the

parent strain ($p=0.0077$). At two hours and six hours, the viable cell counts were not significantly different for the parent and resistant strains ($p=0.6309$ and $p=0.4077$, respectively), but at 4 hours, the parent strain had a significantly higher viable cell count than the SRPA ($p=0.0203$). Overall, the growth appeared quite similar between the two strains, with no apparent trends.

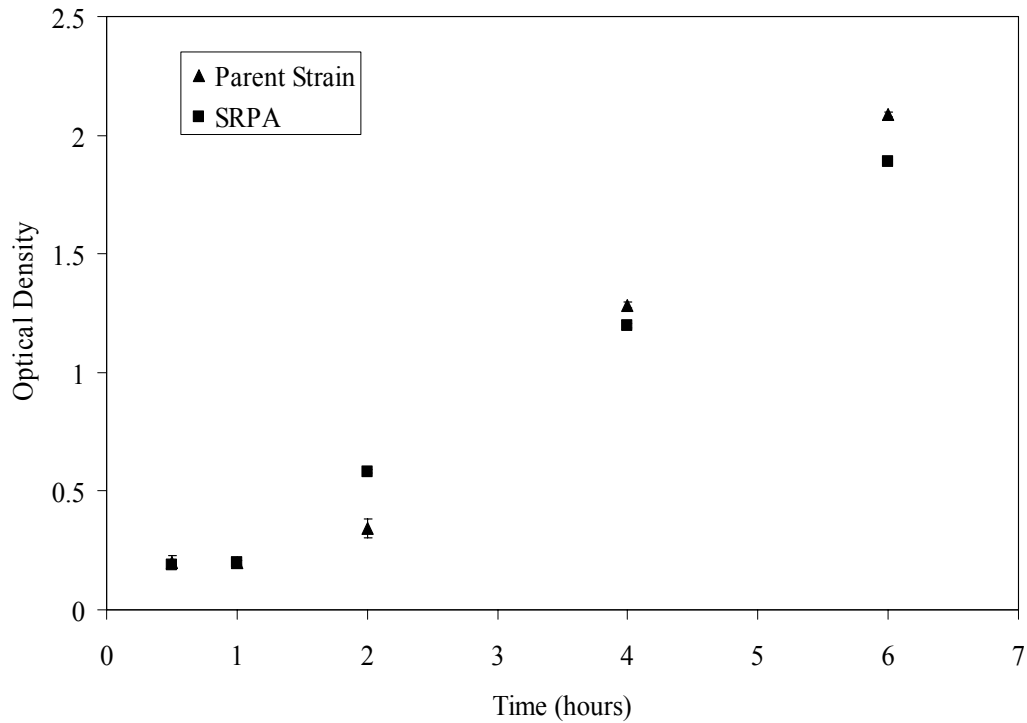


Figure 4-19. Optical densities are shown over time for SRPA and its parent strain grown up in TSB. Error bars represent standard deviations ($n=3$ for all data points).

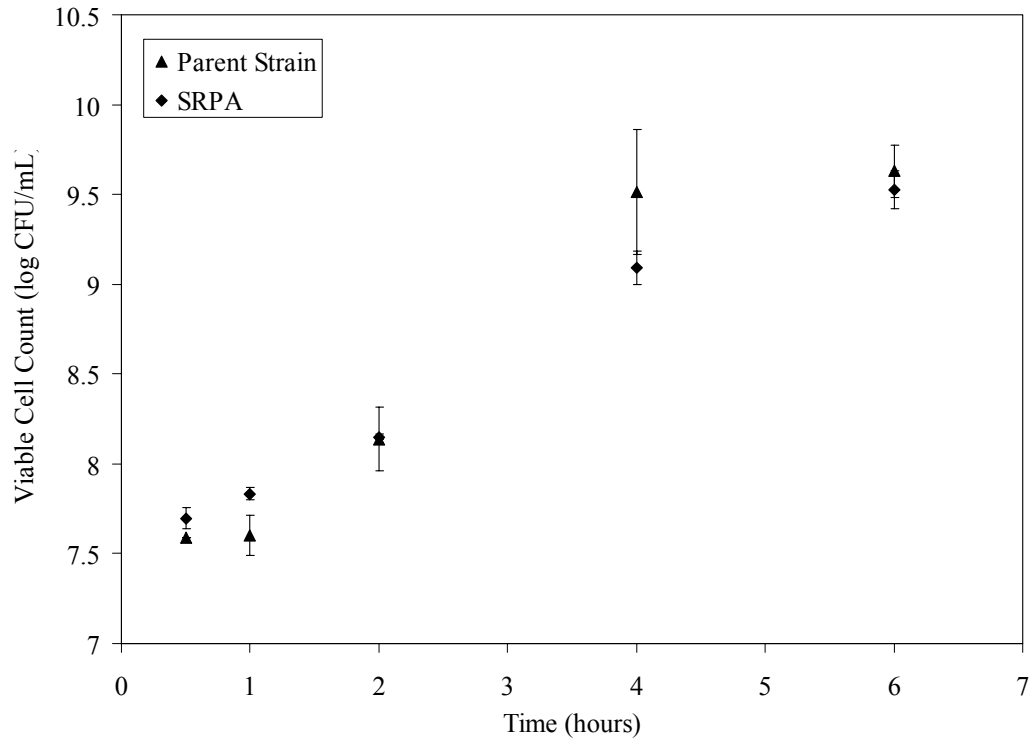


Figure 4-20. Viable cell counts are shown over time for SRPA and its parent strain grown up in TSB. Error bars = standard deviations (n=3 for all points).

The growth rates of the parent and silver resistant strains of *S. aureus* as measured by optical density and viable cell counts are shown in Figures 4-21 and 4-22, respectively. The optical densities of the two strains (Figure 4-21) were not significantly different at 0 hours, 0.5 hours, one hour, two hours, or six hours of growth ($p > 0.9999$, $p = 0.2897$, $p = 0.7995$, $p = 0.3971$, and $p = 0.2127$, respectively). At four hours, the optical density of the parent strain was significantly higher than that of the SRSA ($p = 0.0460$). The viable cell counts of the two strains (Figure 4-22) at 0 hours, 0.5 hours, and one hour were not significantly different ($p = 0.0795$, $p = 0.1637$, and $p = 0.2890$, respectively). The viable cell counts of the parent strain were significantly higher than the viable cell counts of the SRSA at two, four, and six hours of growth ($p = 0.0044$, $p = 0.0121$, and $p = 0.1607$, respectively). The

viable cell counts suggested that the parent *S. aureus* strain grew at a faster rate than the SRSA.

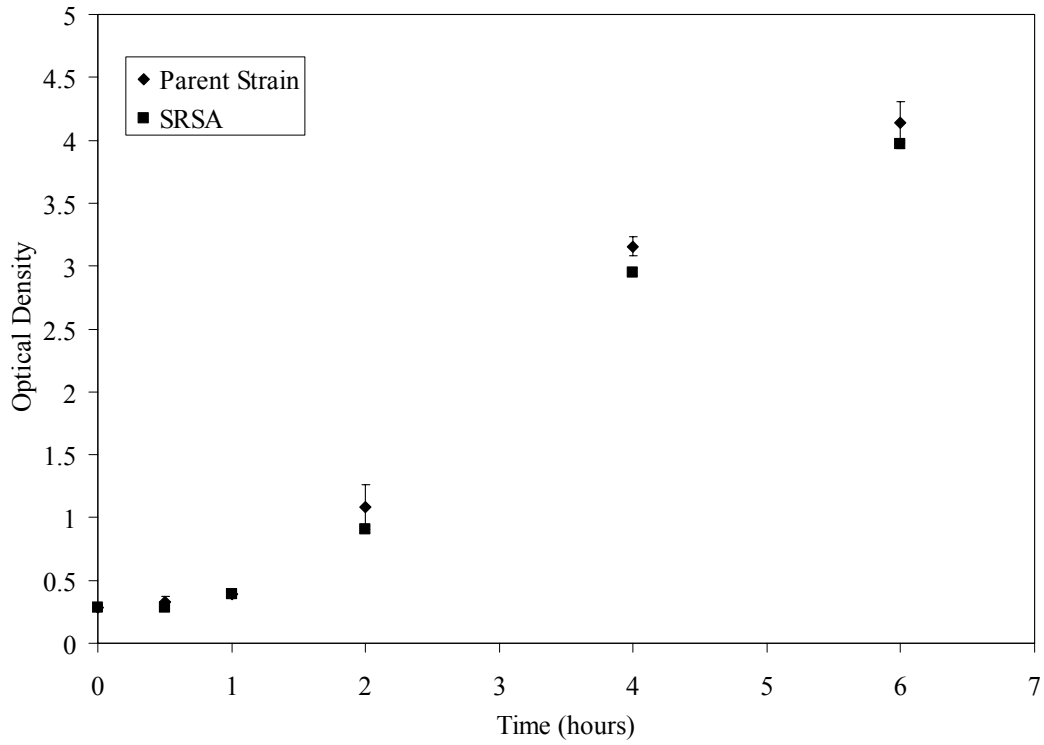


Figure 4-21. Optical densities are shown over time for SRSA and its parent strain grown up in TSB. Error bars represent standard deviations (n=3 for all data points).

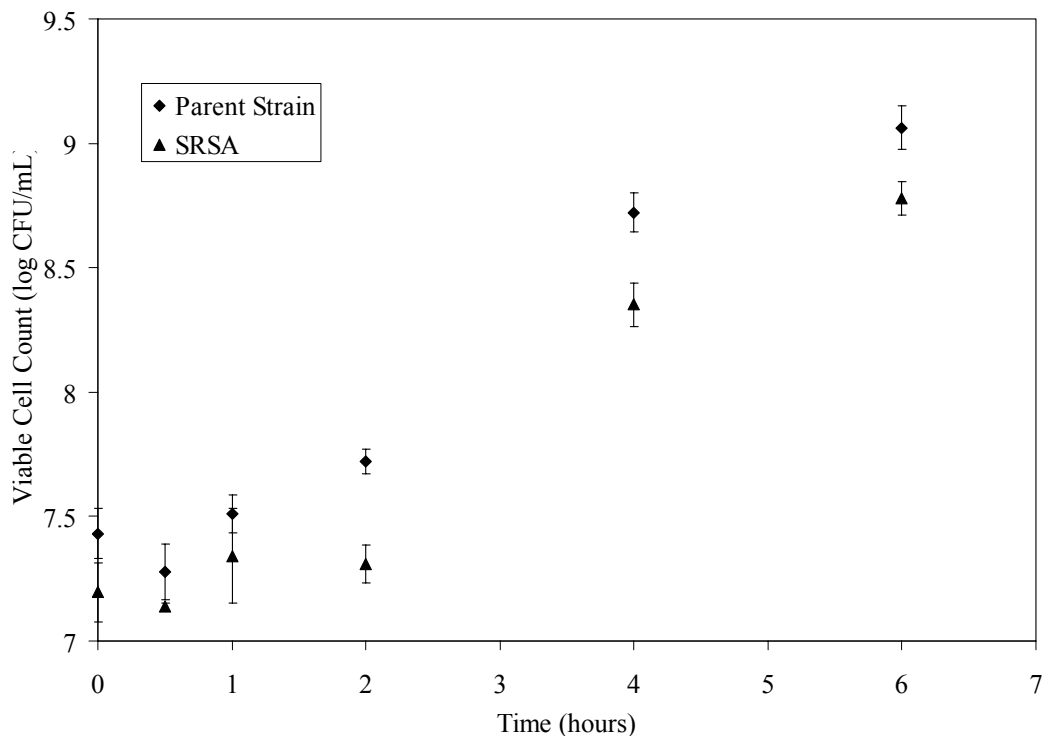


Figure 4-22. Viable cell counts are shown over time for SRSA and its parent strain grown up in TSB. Error bars = standard deviation (n=3 for all data points).

Testing for Stability of SRPA Mutation

One trial was performed to test the stability of SRPA in the presence of 5000 ppm Ag^+ (silver nitrate). The SRPA was transferred daily to fresh silver-containing media for 42 days, and MICs were tested weekly. The MICs remained $>5000 \mu\text{g/mL Ag}^+$ throughout this time period.

Three trials were performed to test the stability of the SRPA mutation in the absence of Ag^+ (silver nitrate). In the first 97 day trial, at the start of the experiment and after 5, 11, 19, and 23 transfers, the MIC and MBC were both $>9000 \mu\text{g/mL Ag}^+$. After the 41st transfer, the MIC and MBC were approximately $3000 \mu\text{g/mL Ag}^+$. After 51 transfers, the MBC was between 2000 and 3000 $\mu\text{g/mL Ag}^+$. After the 58th transfer, however, the MBC was back to being greater

than 3000 $\mu\text{g/mL Ag}^+$, and after the 63rd transfer, the MBC was greater than 4000 $\mu\text{g/mL Ag}^+$. After the 65th transfer, the MBC was greater than 6000 $\mu\text{g/mL Ag}^+$. After the 77th transfer, the MIC was between 7000 and 8000 $\mu\text{g/mL Ag}^+$. After the 82nd transfer, the MBC dropped again, to between 3000 and 5000 $\mu\text{g/mL Ag}^+$, and after the 90th transfer, the MIC was less than 1000 $\mu\text{g/mL Ag}^+$, and the MBC was between 3000 and 5000 $\mu\text{g/mL Ag}^+$. Regular purity checks were performed throughout the trial. In a second trial involving 57 transfers both in tubes and on plates, the MIC and MBC remained greater than 6000 $\mu\text{g/mL Ag}^+$ throughout the trial, with regular purity tests. Of note, testing of the 39th transfer showed that it grew at 10 000 $\mu\text{g/mL Ag}^+$. In the third trial, the MIC of the SRPA did decrease over time when transferred in silver-free media, as shown in Figure 4-23. The MIC remained constant out to the 26th transfer, but then dropped dramatically to about 2500 $\mu\text{g/mL Ag}^+$ by the 34th transfer, 500 $\mu\text{g/mL Ag}^+$ by the 41st transfer, 100 $\mu\text{g/mL Ag}^+$ by the 46th transfer, 10 $\mu\text{g/mL Ag}^+$ by the 51st transfer, and 5 $\mu\text{g/mL Ag}^+$ by the 61st transfer.

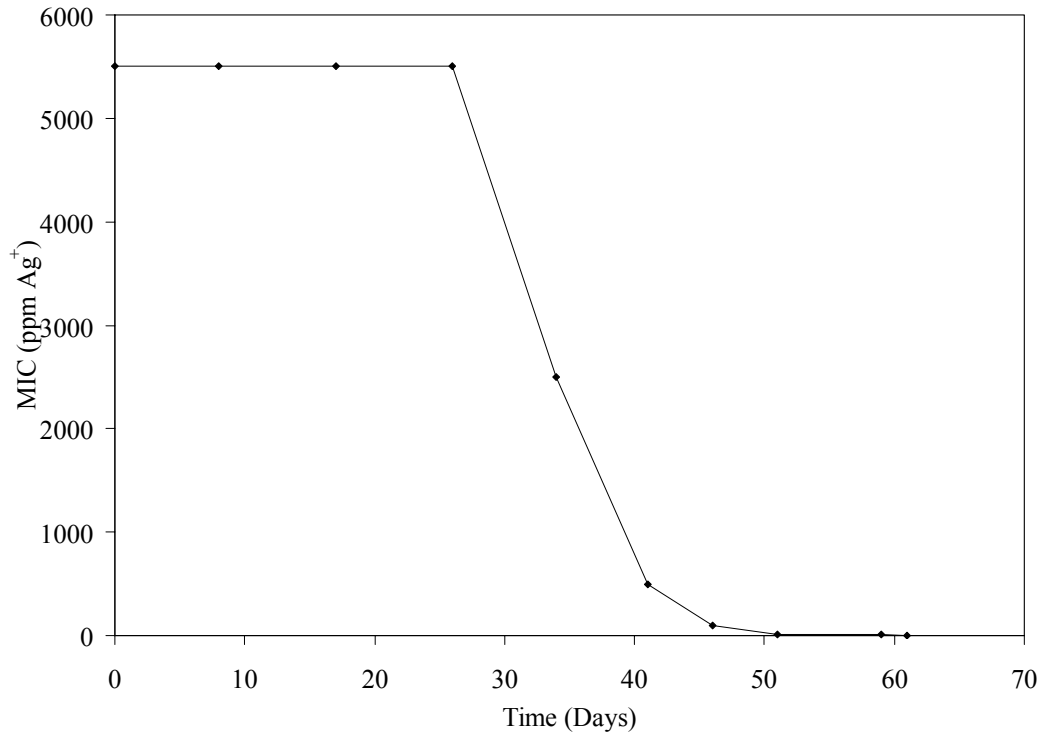


Figure 4-23. MICs to Ag⁺ (silver nitrate) are shown over time for SRPA grown up daily in TSB (with no exposure to Ag⁺).

Antibiotic Sensitivity Testing in SRPA

When challenged with tobramycin, the parent strain of *Pseudomonas aeruginosa* produced an average zone size of 21.8±0.1 mm. The SRPA produced an average zone size of 22.7±0.2 mm. This was significantly larger than the zone size produced by the parent strain (p=0.0064). Both the parent and silver resistant strains of *P. aeruginosa* were classified as sensitive to tobramycin.

Discussion

The *P. aeruginosa*, and both *E. coli* strains easily developed resistance to silver. Resistance to silver was also developed with the *S. aureus* and *S. epidermidis* strains. The susceptibility of *P. aeruginosa* to silver decreased by over 8000 times during the course of the experiment. Both *E. coli* strains were

quick to grow at concentrations above their initial MIC, and the susceptibility of both strains to silver decreased by over 650 times during the experiment. The *S. aureus* had a 285 fold increase in MIC over the course of the experiment, while the *S. epidermidis* had a 50 fold increase in MIC. The results suggest that the *P. aeruginosa*, and *E. coli* are quick to mutate under the selective pressure of increasing concentrations of silver. The *S. epidermidis* demonstrated a similar but slower effect, while the *S. aureus* required multiple trials to generate a successful mutation. This suggests that gram negative bacteria more readily develop high levels of silver resistance than gram positive bacteria, which corroborates the literature discussed in the background section of this study, where more often gram negative bacteria appear to be reported as silver resistant than gram positive. However, the *E. aerogenes* and the *P. vulgaris*, which are also gram negative, appeared only to grow in the silver up to or sometimes slightly exceeding their MICs, and then to die. In some trials, they were not even able to grow at their original MICs after a few exposures to silver, suggesting that they may have become sensitized to silver, rather than resistant to it with successive exposures to increasing (but low) silver concentrations. Interestingly, the organisms which did not develop silver resistance easily were those which had higher natural resistance to silver, while the organisms which were originally most sensitive (see Table 4-6) were the organisms that most readily developed a strong resistance to Ag^+ .

The ability of the species to grow in increasing concentrations of silver stalled at multiple points during the assay for development of Ag^+ resistance. As well, some of the species (*P. aeruginosa* and both *E. coli*) changed in appearance

during the course of the experiment. These observations suggest that the organisms developed different mechanisms of resistance at different concentrations of silver, and that a new mechanism of resistance was required above the concentrations at which the organisms stalled. Since most of the organisms reached a point where increasingly larger increments of silver did not hinder their growth, this suggests that the resistant organisms are no longer sensitive to Ag^+ at any concentration. Overall, these results show that resistant organisms will readily develop in response to step-wise exposure of bacteria to a silver source such as silver nitrate, if the silver concentration is initially at a sublethal concentration. The resulting organisms would be very dangerous in a clinical environment relying on silver-containing treatments, particularly those which release only Ag^+ , since many of the resistant organisms had MICs above the silver concentrations released by all the silver dressing shown in Table 4-4, and some even grew at concentrations well above that of 0.5% silver nitrate or 1% silver sulfadiazine treatments.

In order to test the health of the resistant organisms, and thus obtain a better understanding of their clinical significance, growth rates of the SRPA and SRSA were tested. The growth rate of SRPA in the absence of silver was very similar to the growth rate of its parent strain, indicating that the SRPA was healthy, and the silver resistance mechanisms developed did not represent a metabolic burden. This suggests that the mutations may be regulated such that they are expressed only in the presence of silver. This would be corroborated if future tests showed that the bacteria grew more slowly in the presence of

silver[85]. It also, in combination with the stability of the bacteria (discussed below) suggests that the mutations may be present on the genomic DNA, rather than in a plasmid which would require extra maintenance in the cell[85]. This indicates that the SRPA would not be out-competed by parent strains, making it a more dangerous organism clinically. The SRPA remained stable both growing in high concentrations of silver nitrate and in the absence of silver nitrate. The shortest time for the loss of the SRPA mutation was a month, and in other trials, the silver resistance remained high after two and even three months. The stability of this mutation would make it very difficult to eliminate clinically. Interestingly, the SRPA remained sensitive to tobramycin, despite developing resistance to silver (Ag^+). This suggests that the mechanisms for silver resistance that were developed are different than the mechanisms by which antibiotic resistances are developed, although no definite conclusions can be made without testing the SRPA against many more antibiotics.

The SRSA grew more slowly in log phase than its parent strain, suggesting that the resistance mechanisms developed by this strain may have been different from those developed by the SRPA, as the mutations did appear to result in a metabolic burden, suggesting that they may have been present on a plasmid[85], and that it might be outcompeted by its parent strain.

Although not all the organisms used in this study developed stable silver resistances that could compete with the parent strains in the absence of silver, they all had MICs that exceeded the silver released into water by most of the silver dressings mentioned in Table 4-4. This implies that many of these dressings are

not only ineffective against the pathogens, but may provide an ideal environment for resistance to develop, with silver levels below or within the mutant selection window of the organisms – a very similar environment to that which was generated in this study using low levels of silver nitrate. Therefore, development of silver resistance to a variety of different silver dressing formulations was attempted *in vitro*.

Zone of inhibition measurement suggested that *P. aeruginosa* developed silver resistance via daily exposure to nanocrystalline silver. The consistently decreasing zones of inhibition with each trial, resulting in some cases in a complete failure to generate zones within two-four weeks, suggested decreasing susceptibility of the organisms to Acticoat, as did intermediate MIC measurements showing decreasing susceptibility to Ag^+ . The stepwise appearance of decreased zone size suggested the development of resistances to the increasing concentrations of silver in the agar at smaller distances from the dressing. However, the log reduction procedure done at the end of one trial resulted in a total kill of all the seemingly resistant organisms within 30 minutes, and when the bacteria which grew right up to the dressing were continually exposed to it, their MICs to Ag^+ actually decreased back to original levels rather than continuing to increase as seen with some other dressings. These unexpected results can be explained partially if some of the different forms of silver released by nanocrystalline silver dressings[48] in addition to Ag^+ contribute to the dressings' antimicrobial activity. These different forms of silver may have different diffusion rates in agar, and therefore, although the dressings failed to

create zones of inhibition, the organisms may not have been able to develop resistance to all the antimicrobial moieties released by nanocrystalline silver dressings. They may also not have been able to develop full resistance to Ag^+ due to the multiple species present, which might require multiple resistances to develop simultaneously at a particular total silver concentration. These results, in combination with the fact that the *S. aureus* zone sizes never decreased with multiple exposures of the in-zone bacteria to nanocrystalline silver dressings, suggests that nanocrystalline silver dressings may limit bacterial resistance development clinically.

Using the silver alginate dressing, the zone size produced by the dressing decreased exponentially in both trials, and within a week, no zone sizes were produced against *P. aeruginosa*. Continued exposure of these bacteria to fresh dressings resulted in a tripling of the Ag^+ MIC within five exposures, but no further increases were observed over the next two weeks. This suggests that the silver alginate dressings released enough silver for the bacteria to develop at least one mechanism of resistance, but not enough silver for the bacteria to become fully resistant.

The silver chloride dressing ceased to produce any zone of inhibition against the bacteria within three exposures in a single step change in zone size. With continued exposure of the bacteria to the dressing, the Ag^+ MIC continued to increase over a three week period, resulting in a five fold increase in resistance to Ag^+ in that time period. This dressing appears to release quantities of silver within the mutant selection window, resulting in the gradual development of

multiple resistances to Ag^+ over time. However it does not appear to have released sufficient silver for the bacteria to become fully resistant to Ag^+ .

Using the silver NaCMC dressing, stepwise decreases in zone size were observed over time, and the dressings were unable to generate zones of inhibition against the bacteria within two to three weeks (a shorter time period than that observed with the nanocrystalline silver dressings and the silver nylon dressings, but a longer time period than any of the other dressings tested). Ag^+ MICs began to increase before the dressings ceased to generate zones against the bacteria, increasing four fold over the original MIC. However, with continued exposure of the *P. aeruginosa* to the dressings after zones were no longer generated, the MICs did not continue to increase, suggesting that, as with the silver chloride dressing, the silver NaCMC dressing (which also contains silver chloride) can generate multiple silver resistance mutations over time, as suggested by both the step-wise decrease in zone size and the increased MICs, but did not generate a fully Ag^+ resistant *P. aeruginosa*.

The silver hydrocolloid dressings had exponential decreases in zone size, and were unable to generate zones within two weeks of exposing *P. aeruginosa* to fresh dressings daily. With continued exposure to the dressings past this time point, the Ag^+ MICs steadily increased, with a 50 fold increase occurring in just over a month in one trial, suggesting that with this dressing not only were multiple silver resistance mechanisms developed, but perhaps the bacteria could become fully Ag^+ resistant. Thus, this dressing may present sufficient

concentrations of silver over time within the mutant selection window to make it clinically a very dangerous dressing to use.

Exposure of *P. aeruginosa* to the silver nylon dressing resulted in a fairly exponential decrease in zone size, with no zone being produced within four weeks. The presence of certain days with much lower zone sizes suggests that on the previous day both sensitive and resistant bacteria were collected, but that the resistant mutation was unstable or had a growth disadvantage which resulted in its being overtaken by sensitive bacteria over the next couple of days. The MIC for Ag⁺ increased by four fold as the zone sizes decreased, and remained at that level with continued exposures after no zone size was produced. This suggested that this dressing, similar to the silver chloride dressings, released silver concentrations in the mutant selection window, but did not release silver concentrations sufficiently high to generate a fully Ag⁺-resistant organism.

Exposure of *P. aeruginosa* to the ionic silver foam dressing resulted in a rapid decrease in zone size, with no zones being produced after the second exposure to the dressing. With continued exposure to the dressing after no zones were produced, the MIC to Ag⁺ increased three-fold and remained there, suggesting that this dressing releases a lower quantity of silver, resulting in, perhaps, the development of one fewer silver resistance mechanisms than those developed by the silver chloride, silver NaCMC, and silver nylon dressings. Overall, all of the dressings which released low quantities of Ag⁺ only resulted in the development of some silver resistance mechanisms with continued exposure. The rate at which silver resistance mechanisms developed and the number of

silver resistance mechanisms which developed was likely related to the total silver released by the dressings (a combination of the solubility of the silver compound incorporated into the dressing, the total silver incorporated into the dressing, the silver species released by the dressing, and any other possible slow- or sustained-release mechanisms). The silver hydrocolloid dressing, which rapidly releases more silver than most of the other dressings tested[6] (excepting the nanocrystalline silver dressing) appeared to release optimal quantities of silver for development of completely Ag⁺-resistant bacteria over time.

In the future, it would be interesting to determine whether Ag⁺ resistant *S. aureus* or other species of bacteria could also be generated using silver-containing dressings. It seems likely that this would be the case, considering the ease with which *P. aeruginosa* became silver resistant using these dressings. These results suggest that if low concentrations of silver are used in a clinical environment, either in the form of a silver solution such as silver nitrate or in the form of a silver containing dressing, silver resistance will occur, and may develop quite rapidly, well within a patient's treatment period. This corroborates the clinical study indicating that some patients presented silver-resistant bacteria within two weeks of entry into the hospital[81]. The data presented here calls into question the efficacy of most current silver-containing dressings used to treat and prevent infection in wounds, and is at variance with the assumption made by many that clinically-relevant silver resistance will not develop.

If an Ag⁺-resistant bacterial strain develops in a clinical setting, it appears that very few silver-containing dressings would be able to combat them, as the

Ag⁺-only releasing dressings tested in this study were not bactericidal against SRPA or SRSA. It should be noted that they were not bactericidal against the parent strains either. Only the nanocrystalline silver dressing was bactericidal against these two Ag⁺-resistant bacterial strains, despite releasing much lower total silver into solution than the Ag⁺ MICs of these strains. This is conclusive proof that the nanocrystalline silver dressings release additional antimicrobial silver species to which Ag⁺-resistant bacteria are still sensitive. These antimicrobial species are likely higher oxidation state species, which would be potent oxidizers and thus more effective antimicrobials than Ag⁺. Hence, they would be active at a lower total soluble silver than Ag⁺ treatments such as silver nitrate or silver sulfadiazine. These species may have a different mechanism of action than Ag⁺, or may have a different rate or mechanism of uptake into the cell. For example, these species may interact with bacteria via a well conserved and necessary portion of the bacterial cell, such as orthophosphate uptake channels (personal communication, Dr. Burrell), making it very difficult for the bacteria to develop resistances to these species while remaining viable competitive strains. The presence of these additional antimicrobial species in nanocrystalline silver dressings may be critical in the fight against silver resistance development. However, there is no reason to believe that bacteria *cannot* develop resistances to these species, and therefore these dressings should be used with the same caution which is recommended for the use of any antimicrobial to avoid resistance development.

Study #3: Improving Understanding of Nanocrystalline Silver Mechanisms of Action: Structure Versus Size

Background

Although nanocrystalline silver, which is commercially used as a wound and burn dressing, is known to demonstrate excellent antimicrobial, antifungal, and anti-inflammatory activity[7-9, 45, 102, 103], its mechanisms of action have not yet been fully elucidated. While many commercial silver-containing products used for wound healing release only Ag^+ , nanocrystalline silver releases other unique silver species, including Ag^0 (likely in cluster form as indicated in Chapter 3) and a higher oxidation state species[48] (see Chapter 1). These species, although not yet fully characterized, appear to provide additional properties that result in nanocrystalline silver having superior activity to commercial products that release Ag^+ only[4]. These species are released into the wound environment due to unique physical and chemical properties of the nanocrystalline silver thin films. Previous work has indicated that when the average crystallite size of nanocrystalline silver was increased beyond approximately 30 nm via heat treatment, the dissolution of silver from the thin films and the antimicrobial efficacy of the dressings decreased, indicating an inactivation of the dressings[68, 104]. (More details on the kinetics of this inactivation due to heat treatment are described in Chapter 9.) This inactivation was accompanied by a decrease in silver-oxygen bonds. Silver oxide is thought to stabilize the nanostructure of the material by acting as pinning structures that limit adatom diffusion, so that the dressings retain their functional structure. It was unclear from these studies

whether the inactivation caused by heat treatment was due simply to an increase in the size of the crystals, or whether it was also due to a shift in the crystalline structure of the silver from polycrystals (which have many defects and high energy grain boundary atoms) to single crystals, with a resulting decreased defect concentration and decreased percentage of grain boundary atoms. Grain boundaries may represent a third state of solid matter, separate from crystalline and amorphous states, according to Birringer[105]. While amorphous materials are made up of atoms or molecules that demonstrate short range order, interacting with their nearest neighbors, crystals demonstrate long range order due to lattice structures. Grain boundary atoms, however, are not part of a crystal lattice structure, but they are still affected by the lattice structures of the crystals around them, preventing them from the free interaction with their neighbors exhibited by amorphous materials. This suggests that grain boundary atoms demonstrate neither short nor long range order, meaning they may behave differently from either amorphous or crystalline solids. This behavior would affect the properties of nanocrystalline silver, and is a possible explanation for its unique dissolution products. Since, in previous studies[68, 104], both smaller grains and grain boundary atoms were lost with heat treatment, resulting in both a decrease in the defect concentration and an increase in grain size, it could not be concluded whether the unique biological activity of the dressing was due only to the nanosized crystals, or if it was due also to the defect concentration in the polynanocrystalline structure of the silver.

The purpose of this study was to determine if the antimicrobial efficacy of

nanocrystalline silver dressings was due solely to the crystallite size or was due also to its polycrystallinity, via the assessment of the bactericidal activity of several nanosilver materials with varying degrees of polycrystallinity.

Materials and Methods

Materials

Silver was deposited on zeolite structures to form nanosilver-containing powders. The zeolites used were sodium aluminum silicates. 5 wt% and 20 wt% silver exchanged zeolites were used. As well, a 20 wt% silver exchanged zeolite was modified via chemical reduction to produce metallic silver micro-ensembles, and the silver was thermally reduced in another 20 wt% silver exchanged zeolite, to create 2-4 nm metallic silver nanoclusters. These materials thus contained metallic silver spheres which were previously characterized using XRD, and found to have average crystallite sizes ranging from 2-12 nm. These materials were described by the supplier as being single crystals of silver deposited on the zeolites. Thus, they had no or a limited number of grain boundaries and represented a negligibly or minimally polycrystalline structure. These silver-exchanged zeolites were compared to nanocrystalline silver dressings (ActicoatTM), which had an average grain size of 14 nm[104] aggregated in a coarse columnar structure 900 nm thick, to create a highly polycrystalline material.

Microorganism

Pseudomonas aeruginosa (ATCC 27317) was used for bactericidal efficacy testing. The inoculum was prepared by adding three colonies of *P.*

aeruginosa to TSB, and incubating the TSB overnight at 37°C. 1 mL of this culture was added to 100 mL of TSB, which was incubated for an additional four hours at 37°C to ensure the bacteria were in log phase growth.

Log Reduction Assay

The bactericidal efficacy of the various silver-containing materials was determined using log reduction assays, with methods similar to those of Gallant-Behm, *et al.*[4] The silver content used for each test was held the same, at 3 mg.

For the 20 wt% silver powders, 15 mg of powder was placed in a test tube and 300 µL of the inoculum was then added to the test tube for a ratio 1 mg Ag/100 µL inocula. The test tubes were incubated for 30 minutes at 37°C. Next, 2.7 mL of SPS (0.85% w/v NaCl, 1% v/v polysorbate 20, and 0.1% w/v sodium thioglycolate for *P. aeruginosa*) was added to inactivate the silver via complexation. These solutions were then serially diluted in PBS, drop-plated on MHA, and incubated overnight at 37°C. The resulting cultures were used to calculate the log number of surviving CFUs. The log number of CFUs in the original inoculum was determined via the same method. The log reduction was then calculated as the difference between the log number of CFUs in the original inoculum and the log number of CFUs in the inoculum challenged by the silver powder. This was performed in triplicate for each silver powder. For the 5 wt% silver powder, the same procedure was performed as above, except that 60 mg of powder was used in order to obtain 3 mg of silver.

The bactericidal activity of the nanocrystalline silver dressing was determined similarly. A one square inch piece of the silver thin film was placed

on a sheet of plastic and inoculated with 300 μL of inocula. A second sheet of plastic was placed on the dressing to contain the bacteria. A weight was placed on the plastic to ensure good contact between the inocula and the thin film. This was then incubated for 30 minutes at 37°C, and then the plastic pieces containing the thin film were transferred to 2.7 mL of SPS to inactivate the silver and recover the bacteria. The resulting solution was vigorously vortexed, serially diluted in PBS, drop-plated on MHA, and incubated overnight at 37°C. Log reductions were calculated as above. This test was performed in triplicate.

Scanning Electron Microscopy (SEM)

Scanning electron microscopy was used to “visualize” the samples. SEM imaging was performed using a Hitachi S-4880 cold tip field emission SEM. Zeolites were mounted using carbon tape, while nanocrystalline silver dressings were mounted using an isopropanol based graphite paste. Samples were not cleaned prior to imaging, as such a process could alter the nanostructure. An accelerating voltage of 5 kV was used for imaging the zeolites, and 10 kV was used for imaging the nanocrystalline silver dressings. These low voltages were required to prevent sample charging. Images were taken at magnifications from 1000-600 000x. The working distance was approximately 4 mm, and the condenser lens was set in high mode.

X-ray Photoelectron Spectroscopy (XPS)

X-ray photoelectron spectroscopy was used for elemental identification and oxidation state determination in the samples. XPS was performed using an Axis Ultra Spectrometer (Kratos Analytical) with a base pressure of 5×10^{-10} Torr.

X-rays were generated using an Al Mono ($K\alpha$) source operated at 210W. Spectra were collected at normal (90°) take-off angle. The analyzer pass energy was 160 eV for survey spectra, and 20 eV for high-resolution spectra. Linear background and Gauss component approximations were used for data processing, which was performed using instrument software. No charge corrections to the binding energy values were introduced.

Statistics

A one way ANOVA test with a Tukey-Kramer Multiple Comparisons post test was performed to analyze the log reduction data, using Graphpad InStat Version 3.06 (GraphPad Software, San Diego, California, © 2003, www.graphpad.com).

Results

Bactericidal Efficacy

The results of the log reduction assays are shown in Table 4-19. None of the silver exchanged zeolites demonstrated bactericidal efficacy, while the nanocrystalline silver dressings generated log reductions greater than 5.9, classifying the dressings as bactericidal. Statistical analysis indicated that there were significant differences between groups ($p < 0.0001$), with the nanocrystalline silver dressing producing significantly higher log reductions than any of the silver exchanged zeolites ($p < 0.001$). There were no significant differences in the log reductions produced by any of the silver exchanged zeolites ($p > 0.05$).

Table 4-19. Comparison of the bactericidal efficacy of various silver nanostructured materials.

Material	Log Reduction in 30 minutes
5% Silver Exchanged Zeolite	-0.6±0.2
20% Silver Exchanged Zeolite	-0.4±0.1
20% Silver Supported on Zeolite - chemically reduced metal nanoclusters	-0.5±0.1
20% Silver Supported on zeolite - thermally reduced metal nanoclusters (2-4 nm grain size)	-0.2±0.4
Nanocrystalline silver dressing	>5.9±0.0

*Note: > indicates that there were no bacteria detected within the limit of detection of the experiment.

SEM

Representative SEM images of the various silver exchanged zeolites are shown in Figure 4-24. The samples all had small isolated structures deposited on their surfaces which appeared to be on the order of 10-20 nm in the x- and y- directions. The structures appeared to be very thin in the z-direction, since they were in focus with the plane behind them, suggesting that they were on the order of 2-4 nm in the z-direction. This suggests these may be the single silver nanocrystals described by the supplier. The nanocrystalline silver dressing (Figure 4-25) had small equi-axed features on the order of 10-20 nm, but these were not isolated from one another, demonstrating the dressings' nanopolycrystallinity.

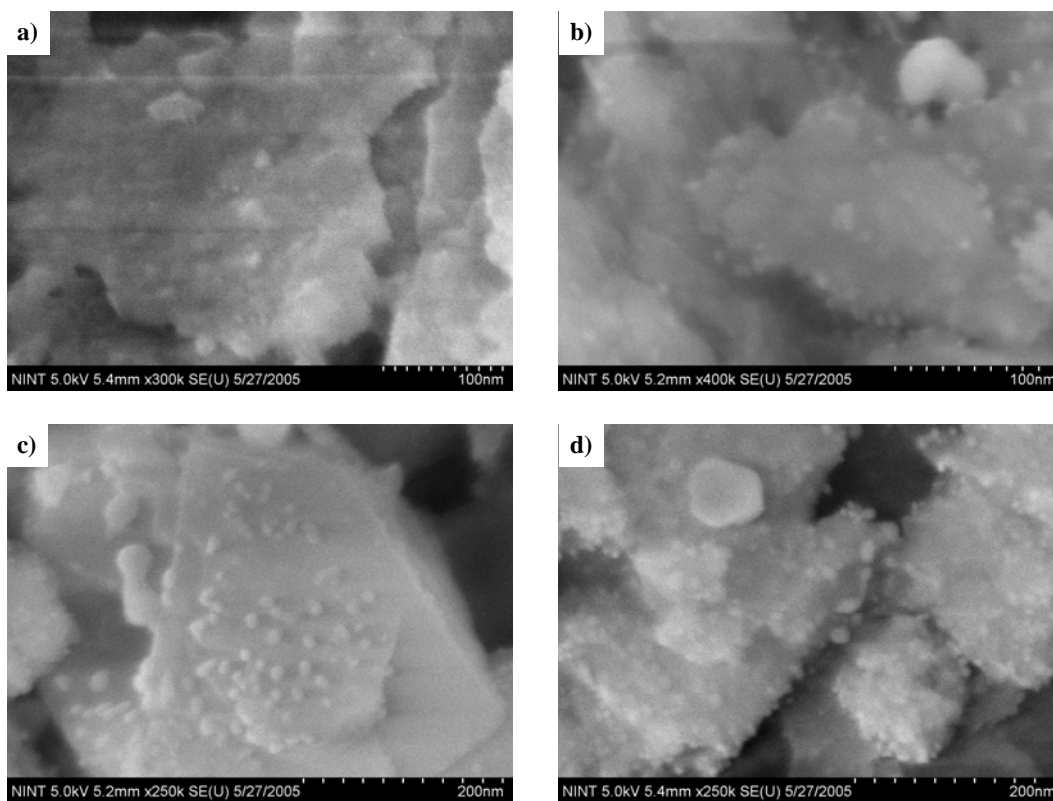


Figure 4-24. Scanning electron microscopy (SEM) images of silver exchanged zeolites. Representative SEM images are shown for (a) 5 wt% silver exchanged zeolite, (b) 20 wt% silver exchanged zeolite, (c) 20 wt% chemically reduced silver supported on zeolite, and (d) 20 wt% thermally reduced silver supported on zeolite. Note that the images do not all have the same scale.

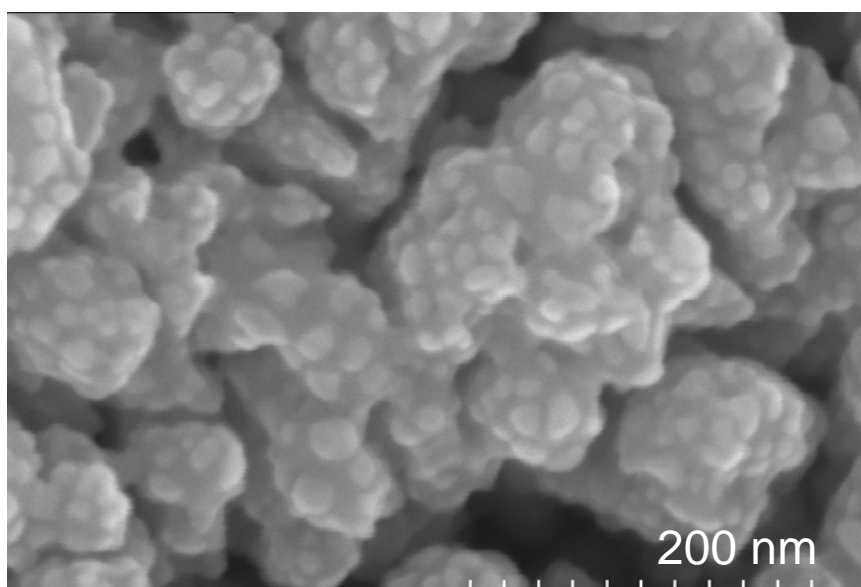


Figure 4-25. Representative SEM image of a nanocrystalline silver dressing.

XPS

Figure 4-26 contains representative XPS deconvolutions for the O1s and Ag3d peaks of nanocrystalline silver dressings (a-b), and of the thermally reduced silver exchanged zeolite (c-d). Other silver exchanged zeolites showed similar patterns to the thermally reduced zeolites. The silver exchanged zeolites appeared to have a higher silver oxide to silver metal ratio and to have more adsorbed oxygen relative to the nanocrystalline silver dressings. They also had a much higher silver carbonate content. The nanocrystalline silver dressings had approximately equal amounts of silver oxide and metallic silver.

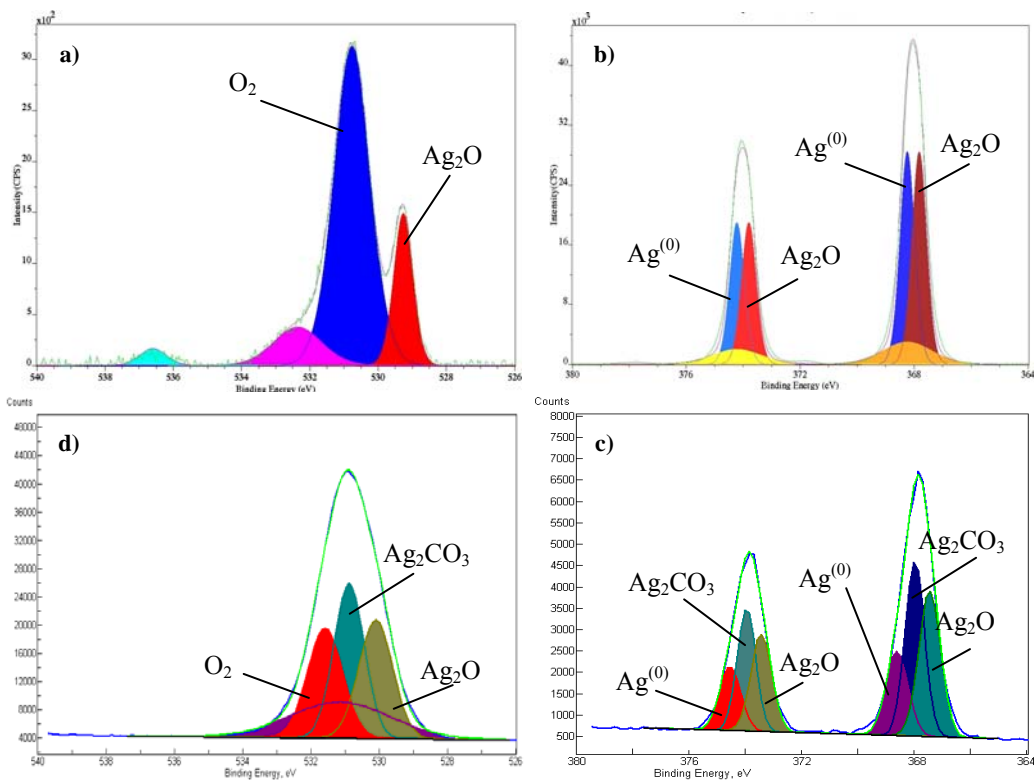


Figure 4-26. Representative XPS spectra for silver exchanged zeolites and nanocrystalline silver dressings. The deconvolution of the XPS spectra is shown for the O 1s peaks in panels (a) and (c), and for the Ag 3d peaks in (b) and (d). Panels (a) and (b) show the deconvolution for a nanocrystalline silver dressing. Panels (c) and (d) show the deconvolution for thermally reduced silver supported on zeolite. Different identified silver species are labeled on the figures, which are plotted as counts per second (CPS) versus binding energy.

Discussion

The silver nanoparticles on zeolite supports were unable to produce log reductions against *P. aeruginosa*. Comparison of this result to log reductions produced by various silver products in the literature indicates that these silver powders had less bactericidal efficacy than silver salts such as silver nitrate and silver sulfadiazine, which produce a log reduction of ~1 with somewhat lower silver quantities than used in this study[8]. However, the silver powders had about the same efficacy as some commercially available silver dressings[4]. The silver on zeolites, which were described as single nanocrystals, all had a much lower antimicrobial efficacy than the poly-nanocrystalline silver dressings, which produced a log reduction of 6 in this study. Thus, although the species released from the reduced silver zeolites have not been determined, their level of activity corresponds to that of the various silver products that release only Ag^+ , and not to that of nanocrystalline silver dressings which release additional species, suggesting that Ag^+ is all that the silver supported on zeolites released as well.

Assuming the small structures in the SEMS of the silver exchanged zeolites are silver, then the zeolite powders do in fact contain single nanocrystals of silver, and this, combined with the log reduction data, suggests that single nanocrystals of silver are not effective antimicrobial agents, while poly-nanocrystalline silver is. The XPS data demonstrated that, although both samples contained the same silver species, there were differences in the relative quantities of different oxidation states of silver in the single silver nanocrystals relative to the poly-nanocrystalline silver, despite the crystals in each being approximately

the same size. This may partially account for the differences observed in antimicrobial activity. Dissimilarities in the chemistry of single and poly-nanocrystalline silver due to their different crystal structures or the different processes used to make them may result in differences in soluble species. The higher silver carbonate content present in the silver supported on zeolites is the clearest difference, but it may not in itself explain the differences in activity, since higher quantities of silver carbonate have been observed in poly-nanocrystalline silver samples made in-house (data not shown), without affecting the activity of the films. However, the silver carbonate observed on the poly-nanocrystalline silver films may just be a surface phenomenon (personal communication, Dr. Robert Burrell), and since the film is 900 nm thick, the silver carbonate would then have minimal effect on the activity of the layers below, while in the silver supported on the zeolites, a silver carbonate surface phenomenon would have a much bigger impact, since the silver is only deposited as a single layer.

Overall, these results suggest that the efficacy of nanocrystalline silver thin films used in dressings is not due solely to the small crystallite size present, since, based on the SEMs, the single crystals of silver supported on zeolites were at least as small as the poly-nanocrystals but were not able to produce the same antimicrobial effects. Thus, nanocrystalline silver activity appears to be related to its poly-nanocrystalline nature. The large percentage of defect structures present in the dressing and the high concentration of grain boundary atoms present, due to the dressing's combination of nanocrystalline size and polycrystallinity, appear to be important contributors to its antimicrobial efficacy.

Conclusions

Overall, the comparison of nanocrystalline silver dressings to various other silver-containing products as demonstrated in these studies has shown that:

1. Nanocrystalline silver behaves differently from various dressings that release only ionic silver. It has much stronger antimicrobial activity, which is attributed partially to the rapid release of a relatively high concentration of silver species. This indicates the importance of silver release for dressing activity.

2. As well as being more active than the ionic silver provided by dressings containing silver chloride, silver alginate, and other forms of ionic silver, nanocrystalline silver is more active than traditional silver treatments which are provided at higher concentrations of ionic silver. This indicates that nanocrystalline silver must release additional active silver species. Thus, the combination of total silver released and the type of silver released appears to be important for its activity.

3. Nanocrystalline silver dressings are able to kill Ag^+ -resistance bacteria, providing definitive evidence that they release additional antimicrobial species which kill bacteria by another mechanism of action, or have a different rate/mechanism of uptake into the bacteria.

4. While it was easy to develop bacterial resistance to Ag^+ using a variety of silver-containing dressings, the methods used in this study did not result in the generation of Ag^+ -resistant bacteria or nanocrystalline silver-resistant bacteria using nanocrystalline silver dressings. This indicates that the multiple antimicrobial silver species released at relatively high concentrations by the

dressing may help prevent the development of silver-resistant bacteria by requiring the development of multiple simultaneous mutations to occur, some of which may be deleterious to the overall health of the organism. The shrinking size of CZOIs observed with the repeated exposures of bacteria to nanocrystalline silver dressings suggests a differing response of the bacteria to at least the farthest diffusing active agent over time. However, this response did not result in a change of the response of the bacteria to other active species in the dressing, as indicated by a lack of change in MIC to Ag^+ , and the continued ability of the dressing to kill the bacteria upon direct contact.

5. The antimicrobial activity of nanocrystalline silver appears to be due to the combination of small crystallite size and poly-crystallinity, which results in a large concentration of defect structures and grain boundary atoms, from which multiple unique silver species can dissolve into aqueous solutions, resulting in its unique antimicrobial activity, as well as its unique anti-inflammatory activity.

Bibliography

1. Bowler PG: **The anaerobic and aerobic microbiology of wounds: a review.** *Wounds* 1998, **10**:170-178.
2. Robson MC: **Wound infection. A failure of wound healing caused by an imbalance of bacteria.** *Surg Clin North Am* 1997, **77**:637-650.
3. Heggers JP, Haydon S, Ko F, Hayward PG, Carp S, Robson MC: ***Pseudomonas aeruginosa* exotoxin A: its role in retardation of wound healing: the 1992 Lindberg Award.** *J Burn Care Rehabil* 1992, **13**:512-518.
4. Gallant-Behm CL, Yin HQ, Liu SJ, Heggers JP, Langford RE, Olson ME, Hart DA, Burrell RE: **Comparison of in vitro disc diffusion and time kill-kinetic assays for the evaluation of antimicrobial wound dressing efficacy.** *Wound Repair and Regeneration* 2005, **13**:412-421.
5. Thomas S, McCubbin P: **A comparison of the antimicrobial effects of four silver-containing dressings on three organisms.** *J Wound Care* 2003, **12**:101-107.
6. Thomas S, McCubbin P: **An in vitro analysis of the antimicrobial properties of 10 silver-containing dressings.** *Journal of Wound Care* 2003, **12**:305-308.
7. Wright JB, Lam K, Hansen D, Burrell RE: **Efficacy of topical silver against fungal burn wound pathogens.** *American Journal of Infection Control* 1999, **27**:344-350.
8. Yin HQ, Langford R, Burrell RE: **Comparative evaluation of the antimicrobial activity of ACTICOAT antimicrobial barrier dressing.** *Journal of Burn Care & Rehabilitation* 1999, **20**:195-200.
9. Wright JB, Hansen DL, Burrell RE: **The Comparative Efficacy of Two Antimicrobial Barrier Dressings: In-vitro Examination of Two Controlled Release Silver Dressings.** *Wounds: A Compendium of Clinical Research and Practice* 1998, **10**:179-188.
10. Burrell RE, Heggers JP, Davis GJ, Wright JB: **Efficacy of Silver-Coated Dressings as Bacterial Barriers in a Rodent Burn Sepsis Model.** *Wounds: A Compendium of Clinical Research and Practice* 1999, **11**:64-71.
11. Tredget EE, Shankowsky HA, Groeneveld A, Burrell RE: **A matched-pair, randomized study evaluating the efficacy and safety of Acticoat silver-coated dressing for the treatment of burn wounds.** *J Burn Care Rehabil* 1998, **19**:531-537.
12. Doshi J, Karagama Y, Buckley D, Johnson I: **Observational study of bone-anchored hearing aid infection rates using different post-operative dressings.** *J Laryngol Otol* 2006, **120**:842-844.
13. Rustogi R, Mill J, Fraser JF, Kimble RM: **The use of Acticoat in neonatal burns.** *Burns* 2005, **31**:878-882.
14. Blakely M, Weir D: **The innovative use of Safetac soft silicone in conjunction with negative pressure wound therapy: three case**

- studies.** In: *20th Annual Symposium on Advanced Wound Care and the Wound Healing Society Meeting*; 2007; Tampa, Florida, USA.
15. Meites H, Jett M, Gauthier S, *et al.*: **The examination of antimicrobial soft silicone foam with regards to partial thickness burns.** In: *Third Congress of the World Union of Wound Healing Societies*; 2008; Toronto, Ontario, Canada.
 16. Nisbet TAS: **Promoting complex wound healing through the utilization of an antimicrobial soft silicone foam dressing: solving the wound puzzle one piece at a time.** In: *21st Annual Symposium on Advanced Wound Care and the Wound Healing Society Meeting*; 2008; San Diego, California, USA.
 17. Barrows C: **Enhancing patient outcomes - reducing the bottom dollar: the use of antimicrobial soft silicone foam dressings in home health.** In: *21st Annual Symposium on Advanced Wound Care and the Wound Healing Society Meeting*; 2008; San Diego California, USA.
 18. Timmins J: **Management of a large haematoma with a new silver impregnated foam dressing.** In: *European Wound Management Association Conference*; 2008; Lisbon, Portugal.
 19. Schumann H, Apelqvist J, Schmidtchen A, Hansson C: **Open, non-comparative, multicentre investigation exploring the tolerance of an absorbent foam dressing containing silver used in chronic wounds.** In: *European Wound Management Association Conference*; 2007; Glasgow, United Kingdom.
 20. Durante CM: **Chronic wounds and local malpractice: an antimicrobial silver soft silicone foam can help solving the problem.** In: *Third Congress of the World Union of Wound Healing Societies*; 2008; Toronto, Ontario, Canada.
 21. Taherinejad F, Hamberg K: **Antimicrobial effect of a silver-containing foam dressing on a broad range of common wound pathogens.** In: *Third Congress of the World Union of Wound Healing Societies*; 2008; Toronto, Ontario, Canada.
 22. Varma AK, Bal A, Kumar H, Kesav R, Nair S: **Efficacy of Polyurethane Foam Dressing in Debrided Diabetic Lower Limb Wounds.** *WOUNDS* 2006, **18**:300-306.
 23. Nadworny PL, Burrell RE: **A review of assessment techniques for silver technology in wound care. Part 1: *In vitro* methods for assessing antimicrobial activity.** *J Wound Tech* 2008, **1**:6-13.
 24. Allam RC, Partain R, Munson BA: **A prospective, clinical in-market evaluation to assess the performance of a new collagen matrix dressing on facilitating granulation and epidermal migration, in a variety of wound types.** ©2007. http://global.smith-nephew.com/cps/rde/xbcr/smithnephewls/R._Allam_New_Collagen_Dressing_1.2_LOW.pdf. Viewed February 3, 2009.
 25. Williams RL: **Experience with novel porcine collagen matrix and silver used in long-term dressings.** ©2007. <http://global.smith->

- [nephew.com/cps/rde/xbcr/smithnephewls/R_Lewis-Long_Term_Dressings.pdf](http://global.smith-nephew.com/cps/rde/xbcr/smithnephewls/R_Lewis-Long_Term_Dressings.pdf). Viewed February 3, 2009.
26. Williams RL: **Novel porcine collagen matrix used to stimulate wound closure in arrested wounds.** ©2007. http://global.smith-nephew.com/cps/rde/xbcr/smithnephewls/R_Williams_Arrested_Wounds-8x4.pdf. Viewed February 3, 2009.
 27. Williams RL: **Clinical experience with a novel porcine collagen matrix to facilitate final closure of granulating wounds originally treated with negative pressure wound therapy.** ©2007. http://global.smith-nephew.com/cps/rde/xbcr/smithnephewls/R_Williams_Final_Closure-8x4-9_27.pdf. Viewed February 3, 2009.
 28. Davis C, Dalbey C, Hill S: **The successful use of a new adjunct therapy in a [sic] both acute and chronic wounds - a prospective, descriptive case series.** ©2007. http://global.smith-nephew.com/cps/rde/xbcr/smithnephewls/S_Hill-Successful_use_of_adjunct-8x4.pdf. Viewed February 3, 2009.
 29. Agathangelou C: **Huge sacral pressure ulcer closed in four months using PolyMem Silver and PolyMem Wic Silver dressings.** In: *Third Congress of the World Union of Wound Healing Societies*; 2008; Toronto, Ontario, Canada.
 30. Hubbard M: **Dramatic healing of three stalled venous hypertension ulcers in a bariatric patient using PolyMem Silver dressings under an Unna's boot.** In: *The WOCN Society's 39th Annual Conference*; 2007; Salt Lake City, Utah, USA.
 31. Hubbard M: **Pain relief and healing using PolyMem and PolyMem Silver dressings under compression for venous hypertension ulcers.** In: *20th Annual Symposium on Advanced Wound Care*; 2007; Tampa, Florida, USA.
 32. Stamps J: **Polymem Silver dressings successful in bringing quick closure to a chronic venous ulcer with an exposed tendon in a patient with arterial insufficiency.** In: *20th Annual Symposium on Advanced Wound Care*; 2007; Tampa, Florida, USA.
 33. Thurs K: **Chronic venous leg ulcer closed in only seven dressing changes using PolyMem Silver dressings.** In: *The WOCN Society's 39th Annual Conference*; 2007; Salt Lake City, Utah, USA.
 34. Caras J: **Three malleolus wounds of two years' duration closed in four weeks using PolyMem Silver.** In: *19th Annual Symposium on Advances in Skin and Wound Care*; 2006; San Antonio, Texas, USA.
 35. Benskin L: **Maintaining tunnel tissue viability with PolyMem Silver QuadraFoam dressings during osteomyelitis treatment.** In: *19th Annual Symposium on Advances in Skin and Wound Care*; 2006; San Antonio, Texas, USA.
 36. Benskin L: **Dramatic pain relief through the use of PolyMem QuadraFoam dressings on a deep axillary wound for entire course of healing.** In: *Third Congress of the World Union of Wound Healing Societies*; 2008; Toronto, Ontario, Canada.

37. Benskin L: **Activation of a stalled traumatic finger wound with PolyMem Silver QuadraFoam dressings.** In: *19th Annual Symposium on Advances in Skin and Wound Care*; 2006; San Antonio, Texas, USA.
38. Ip M, Lui SL, Poon VK, Lung I, Burd A: **Antimicrobial activities of silver dressings: an *in vitro* comparison.** *Journal of Medical Microbiology* 2006, **55**:59-63.
39. Parsons D, Bowler PG, Myles V, Jones S: **Silver antimicrobial dressings in wound management: a comparison of antibacterial, physical, and chemical characteristics.** *Wounds* 2005, **17**:222-231.
40. Molnlycke Health Care, LLC: **Mepilex Ag The effective antimicrobial absorbent foam dressing.** In: *Mepilex Ag*. ©2009, Sweden. http://www.molnlycke.com/Files/Wound_Care/Productsheets/MepilexAg_PS.pdf. Viewed February 3, 2009.
41. Derma Sciences, Inc.: **ALGICELL™ Ag Silver Alginate Brochure.** In: *Product Literature*. ©2006, Ontario, Canada. http://dermasciencesinc.com/editor/uploads/files/DermaSciences_ALGICELL_Ag.pdf. Viewed February 3, 2009.
42. Ferris Mfg, Corp: **PolyMem® Silver The world's only QuadraFoam® silver dressings.** In: *Brochures and Literature*. ©2008, Illinois, USA. http://www.polymem.com/Silver.pdf?line_id=5. Viewed February 3, 2009.
43. Smith and Nephew, Inc.: **Biostep Ag Product Insert.** In: *Biostep Ag Collagen Matrix Dressing Downloadable Materials*. ©2008, Largo, FL, USA. http://global.smith-nephew.com/cps/rde/xbcr/smithnephewls/Biostep_Ag_Patient_Insert_PI_02273-A.pdf. Viewed February 3, 2009.
44. Smith and Nephew, Inc.: **Acticoat™ product information.** In: *Acticoat Product Range*. ©2008, Largo, FL, USA. http://wound.smith-nephew.com/ca_en/Product.asp?NodeId=2722&Tab=1&Hide=True. Viewed February 3, 2009.
45. Wright JB, Lam K, Burrell RE: **Wound management in an era of increasing bacterial antibiotic resistance: a role for topical silver treatment.** *American Journal of Infection Control* 1998, **26**:572-577.
46. Moyer CA, Brentano L, Gravens DL, Margraf HW, Monafó WW: **Treatment of large human burns with 0.5% silver nitrate solution.** *Arch Surg* 1965, **90**:812-867.
47. Monafó WW, West MA: **Current treatment recommendations for topical burn therapy.** *Drugs* 1990, **40**:364-373.
48. Fan FF, Bard AJ: **Chemical, electrochemical, gravimetric, and microscopic studies on antimicrobial silver films.** *J Phys Chem B* 2002, **106**:279-287.
49. Zhao X, Drlica K: **Restricting the Selection of Antibiotic-Resistant Mutant Bacteria: Measurement and Potential Use of the Mutant Selection Window.** *The Journal of Infectious Diseases* 2002, **185**:561-565.

50. Li X-Z, Nikaido H, Williams KE: **Silver-Resistant Mutants of *Escherichia coli* Display Active Efflux of Ag⁺ and Are Deficient in Porins.** *Journal of Bacteriology* 1997, **179**:6127-6132.
51. Demling RH: **Burns.** *N Engl J Med* 1985, **313**:1389-1398.
52. Bragg PD, Rainnie DJ: **The effect of silver ions on the respiratory chain of *Escherichia coli*.** *Can J Microbiol* 1974, **20**:883-889.
53. Russell AD, Hugo WB: **Antimicrobial activity and action of silver.** *Prog Med Chem* 1994, **31**:351-370.
54. Modak SM, Fox CL, Jr.: **Binding of silver sulfadiazine to the cellular components of *Pseudomonas aeruginosa*.** *Biochem Pharmacol.* 1973, **22**:2391-2404.
55. Slawson RM, Trevors JT, Lee H: **Silver accumulation and resistance in *Pseudomonas stutzeri*.** *Arch Microbiol* 1992, **158**:398-404.
56. Silver S: **Bacterial silver resistance: molecular biology and uses and misuses of silver compounds.** *FEMS Microbiol Rev* 2003, **27**:341-353.
57. Gupta A, Silver S: **Silver as a biocide: Will resistance become a problem?** *Nat Biotechnol* 1998, **16**:888.
58. Drlica K: **The mutant selection window and antimicrobial resistance.** *J Antimicrob Chemother* 2003, **52**:11.
59. Kaur P, Vadehra DV: **Mechanism of resistance to silver ions in *Klebsiella pneumoniae*.** *Antimicrob Agents Chemother* 1986, **29**:165-167.
60. Tambe SM, Sampath L, Modak SM: ***In vitro* evaluation of the risk of developing bacterial resistance to antiseptics and antibiotics used in medical devices.** *J Antimicrob Chemother* 2001, **47**:589-598.
61. Ricketts CR, Lowbury EJ, Lawrence JC, Hall M, Wilkins MD: **Mechanism of prophylaxis by silver compounds against infection of burns.** *Br Med J* 1970, **2**:444-446.
62. Lansdown AB: **Silver. I: Its antibacterial properties and mechanism of action.** *J Wound Care* 2002, **11**:125-130.
63. Hamilton-Miller JM, Shah S, Smith C: **Silver sulphadiazine: a comprehensive *in vitro* reassessment.** *Chemotherapy* 1993, **39**:405-409.
64. Zhao G, Stevens SE, Jr.: **Multiple parameters for the comprehensive evaluation of the susceptibility of *Escherichia coli* to the silver ion.** *Biomaterials* 1998, **11**:27-32.
65. Monafa WW, Ayvazian VH, Skinner AM: **Control of infection in major burn wounds by cerium nitrate/silver sulphadiazine.** *Burns* 1976, **3**:104-107.
66. Fox CL: **Silver sulphadiazine, addendum to local therapy.** In: *Modern treatment.* New York: Hoeber Medical Division, Harper and Row; 1967: 1259.
67. Burrell RE: **A scientific perspective on the use of topical silver preparations.** *Ostomy Wound Manage* 2003, **49**:19.
68. Taylor PL, Ussher AL, Burrell RE: **Impact of heat on nanocrystalline silver dressings. Part I: Chemical and biological properties.** *Biomaterials* 2005, **26**:7221-7229.

69. Bowler PG: In: *Australia New Zealand Burn Association Meeting*; 2002; Auckland.
70. Silver S, Phung LT: **Bacterial heavy metal resistance: new surprises.** *Annu Rev Microbiol* 1996, **50**:753-789.
71. Klaus T, Joerger R, Olsson E, Granqvist CG: **Silver-based crystalline nanoparticles, microbially fabricated.** *Proc Natl Acad Sci U S A* 1999, **96**:13611-13614.
72. Russell AD: **Plasmids and bacterial resistance to biocides.** *J Appl Microbiol* 1997, **83**:155-165.
73. Haefeli C, Franklin C, Hardy K: **Plasmid-determined silver resistance in *Pseudomonas stutzeri* isolated from a silver mine.** *J Bacteriol* 1984, **158**:389-392.
74. Mergeay M, Monchy S, Vallaeyts T, Auquier V, Benotmane A, Bertin P, Taghavi S, Dunn J, van der Lelie D, Wattiez R: ***Ralstonia metallidurans*, a bacterium specifically adapted to toxic metals: towards a catalogue of metal-responsive genes.** *FEMS Microbiol Rev* 2003, **27**:385-410.
75. Rosenkranz HS, Coward JE, Wlodkowski TJ, Carr HS: **Properties of silver sulfadiazine-resistant *Enterobacter cloacae*.** *Antimicrob Agents Chemother* 1974, **5**:199-201.
76. McHugh GL, Moellering RC, Hopkins CC, Swartz MN: ***Salmonella typhimurium* resistant to silver nitrate, chloramphenicol, and ampicillin.** *Lancet* 1975, **1**:235-240.
77. Gupta A, Matsui K, Lo JF, Silver S: **Molecular basis for resistance to silver cations in *Salmonella*.** *Nat Med* 1999, **5**:183-188.
78. Rosen BP: **Bacterial resistance to heavy metals and metalloids.** *JBIC* 1996, **1**:273-277.
79. Bridges K, Kidson A, Lowbury EJ, Wilkins MD: **Gentamicin- and silver-resistant *Pseudomonas* in a burns unit.** *Br Med J* 1979, **1**:446-449.
80. Pirnay JP, De Vos D, Cochez C, Bilocq F, Pirson J, Struelens M, Duinslaeger L, Cornelis P, Zizi M, Vanderkelen A: **Molecular epidemiology of *Pseudomonas aeruginosa* colonization in a burn unit: persistence of a multidrug-resistant clone and a silver sulfadiazine-resistant clone.** *J Clin Microbiol* 2003, **41**:1192-1202.
81. Hendry AT, Stewart IO: **Silver-resistant *Enterobacteriaceae* from hospital patients.** *Can J Microbiol* 1979, **25**:915.
82. Deshpande LM, Kapadnis BP, Chopade BA: **Metal resistance in *Acinetobacter* and its relation to beta-lactamase production.** *Biometals* 1993, **6**:55-59.
83. Sanders CC: **Novel resistance selected by the new expanded spectrum cephalosporins: a concern.** *J Infect Dis* 1983, **147**:585-589.
84. Novick RP, Roth C: **Plasmid-linked resistance to inorganic salts in *Staphylococcus aureus*.** *J Bacteriol* 1968, **95**:1335-1342.
85. Deshpande LM, Chopade BA: **Plasmid mediated silver resistance in *Acinetobacter baumannii*.** *Biometals* 1994, **7**:49-56.

86. Starodub ME, Trevors JT: **Silver accumulation and resistance in *Escherichia coli* R1.** *J Inorg Biochem* 1990, **39**:317-325.
87. Starodub ME, Trevors JT: **Silver resistance in *Escherichia coli* R1.** *J Med Microbiol* 1989, **29**:101-110.
88. Khor SY, Jegathesan M: **Heavy metal and disinfectant resistance in clinical isolates of gram-negative rods.** *Southeast Asian J Trop Med Public Health* 1983, **14**:199-203.
89. Loh JV, Percival SL, Woods EJ, Williams NJ, Cochrane CA: **Silver resistance in MRSA isolated from wound and nasal sources in humans and animals.** *International Wound Journal* 2009, **6**:32-38.
90. Annear DI, Mee BJ, Bailey M: **Instability and linkage of silver resistance, lactose fermentation, and colony structure in *Enterobacter cloacae* from burn wounds.** *J Clin Pathol* 1976, **29**:441-443.
91. Slawson RM, Lohmeier-Vogel EM, Lee H, Trevors JT: **Silver resistance in *Pseudomonas stutzeri*.** *Biometals* 1994, **7**:30-40.
92. Ovington LG: **The truth about silver.** *Ostomy Wound Manage* 2004, **50**:1S-10S.
93. Argentum Medical, LLC: **Silver Coated Wound Care, Burn Care, and Surgical Dressings, Bandages and Gauze.** In: *Silverlon*. ©2009, Chicago. www.silverlon.com. Viewed July 3, 2009.
94. Parsons D, Jacques E, Bowler PG: **Light stabilized antimicrobial materials.** Issued December 30, 2003. U.S. Patent No. 6669981. 3 pages.
95. Convatec, Inc.: **Aquacel® Ag dressing.** ©1999, Dorval. <http://www.convatec.ca/enca/cvtca-aqcagdbpca/cvt-portallev1/0/detail/0/1234/1706/aquacel-ag-dressing.html>. Viewed July 3, 2009.
96. Kirsner RS, Hess CT: **A Practical Approach to Utilizing a State-of-the-Art Silver Dressing to Heal Refractory Wounds.** Eds.: Coloplast Corp. In: *SAWC*, April 29, 2003, Las Vegas, pg. 8.
97. Medline Industries, Inc.: **SilvaSorb® Targeted antimicrobial protection.** ©2008, Mundelein. http://www.medline.com/wound-skin-care/lit/silvasorb/Silvasorb_brochure.pdf. Viewed July 3, 2009.
98. Systagenix Wound Management, Inc.: **Silvercel Product Information.** In: *Products*. ©2003, North Yorkshire. <http://www.systagenix.com/us/products/silvercel/epi.php>. Viewed July 3, 2009.
99. Bauer AW, Kirby WM, Sherris JC, Turck M: **Antibiotic susceptibility testing by a standardized single disk method.** *Am J Clin Pathol* 1966, **45**:493-496.
100. Ryan KJ, Schoenknecht FD, Kirby WMM: **Disk sensitivity testing.** *Hospital Practice* 1970, **5**:91-100.
101. National Committee for Clinical Laboratory Standards, NCCLS: **BD BBL™ Sensi-Disc™ Antimicrobial Susceptibility Test Discs.** In: *Document M100-S13 (M2): Disk Diffusion Supplemental Tables.* Series: *Performance Standards for Antimicrobial Susceptibility Testing.* Mississauga, Ontario, Canada: BD; 2004: 1-5.

102. Wright JB, Lam K, Buret AG, Olson ME, Burrell RE: **Early healing events in a porcine model of contaminated wounds: effects of nanocrystalline silver on matrix metalloproteinases, cell apoptosis, and healing.** *Wound Repair Regen* 2002, **10**:141-151.
103. Nadworny PL, Wang JF, Tredget EE, Burrell RE: **Anti-inflammatory activity of nanocrystalline silver in a porcine contact dermatitis model.** *Nanomed: NBM* 2008, **4**:241-251.
104. Taylor PL, Omotoso O, Wiskel JB, Mitlin D, Burrell RE: **Impact of heat on nanocrystalline silver dressings Part II: Physical properties.** *Biomaterials* 2005, **26**:7230-7240.
105. Birringer R: **Nanocrystalline Materials.** *Mater Sci Eng* 1989, **A117**:33-43.

University of Alberta

Biological Activity of Nanostructured Silver

by

Patricia L. Nadworny

A thesis submitted to the Faculty of Graduate Studies and Research
in partial fulfillment of the requirements for the degree of

Doctor of Philosophy

Department of Chemical and Materials Engineering
Medical Sciences - Biomedical Engineering

©Patricia Nadworny
Spring 2010
Edmonton, Alberta

Permission is hereby granted to the University of Alberta Libraries to reproduce single copies of this thesis and to lend or sell such copies for private, scholarly or scientific research purposes only. Where the thesis is converted to, or otherwise made available in digital form, the University of Alberta will advise potential users of the thesis of these terms.

The author reserves all other publication and other rights in association with the copyright in the thesis and, except as herein before provided, neither the thesis nor any substantial portion thereof may be printed or otherwise reproduced in any material form whatsoever without the author's prior written permission.

Table of Contents

Volume 2

Chapter 5 – Releasing Biologically Active Nanocrystalline Silver

Species – Effect of Dissolution Conditions	333
Introduction.....	333
Materials and Methods.....	338
Materials	338
Setup for Carbonated Water Dissolution Experiments.....	338
Procedure for Dissolutions.....	340
Spectrophotometric Analysis	341
Effect of Sampling	342
Spectrofluorimetry	343
Total Silver Profiles – Atomic Absorption	344
Ag ⁺ Profiles.....	344
Antimicrobial Activity	347
Effect of Dissolution on Nanocrystalline Silver Dressings	350
Scanning Electron Microscopy (SEM)	350
X-ray Photoelectron Spectroscopy (XPS)	350
X-ray Diffraction (XRD)	351
Effect of Storage Under Vacuum.....	351
Statistics	352
Results and Discussion	352
Spectrophotometric Analysis	352

Effect of Sampling	387
Spectrofluorimetry	388
Total Silver Profiles	405
pH Profiles	424
Antimicrobial Activity	441
XPS	448
SEM	462
XRD	473
Conclusions.....	476
Bibliography	479

Chapter 6 – Testing for Anti-inflammatory and Antimicrobial

Activity of Nanocrystalline Silver-Derived Solutions in the Lung	483
Introduction.....	483
Materials and Methods.....	502
Materials	502
Anti-inflammatory Activity Study.....	503
Animals	503
Preparation of Nanocrystalline Silver Solutions.....	504
Induction of Inflammation	504
Treatment	505
Cryopreservation.....	506
Serum Preservation	506
Bacterial Cell Count.....	506

Histopathology	507
Lipopolysaccharide Titration Study	507
Animals	507
Induction of Inflammation	508
Pseudomonas Aeruginosa Titration Study	508
Animals	508
Induction of Infection	509
Bacterial Cell Counts	509
Antimicrobial Activity Study	510
Preparation of Tobramycin Solutions	510
Preparation of Silver Nitrate Solutions	510
Preparation of Nanocrystalline Silver Solutions	510
Animals	511
Induction of Infection	511
Treatment	512
Cryopreservation	513
Bacterial Cell Counts	513
Histopathology	514
Real Time RT-PCR	514
Tissue powdering	514
RNA extraction	514
RNA quantification	515
Reverse transcription (creation of cDNA)	515

Primers	516
Real time RT-PCR	516
Nanocrystalline Silver-Derived Solution Controls	517
Animals	517
Treatment	517
Cryopreservation	518
Histopathology	518
Confirming Solution Properties	518
Bacteriostatic Activity, Silver Content, and Wettability	518
Characterization of Microsprayer Particle Size	519
Statistical Analysis	519
Results and Discussion (By Study)	520
Anti-inflammatory Activity Study	520
Visual observations	520
Total Silver	521
Digital Images	521
Histology	522
Discussion	524
Lipopolysaccharide Titration Study	531
Visual Observations	531
Histology	531
Discussion	534
<i>Pseudomonas Aeruginosa</i> Titration Study	536

Visual Observations	537
Digital Images	537
Bacterial Counts	538
Antimicrobial Activity Study	539
<i>P. aeruginosa</i> dose	539
Visual Observations up to 24 Hours	539
Digital Images at 24 Hours	540
Histological Images at 24 Hours	541
Visual Observations From 24 to 72 Hours	545
Digital Images at 72 Hours	546
Histology at 72 Hours	547
Bacterial Load at 24 and 72 Hours	550
Real Time RT-PCR	551
Total Silver	556
Nanocrystalline Silver Controls	556
Visual Observations	556
Histology	557
Total Silver	558
Analyzing Solution Properties	558
Wetability	558
Bacteriostatic Activity	559
Total Silver	561
Microsprayer Characterization	563

Conclusions.....	563
Bibliography	570
Chapter 7 – Anti-inflammatory Activity of Nanocrystalline Silver-	
Derived Solutions Varies with Dissolution Conditions.....	577
Introduction.....	577
Materials and Methods.....	579
Materials	579
Animals.....	579
Sensitization to DNCB and Elicitation of Inflammatory Reaction....	580
Treatment	580
Total Silver Analysis.....	582
Visual Observations	582
Histopathology	583
mRNA Signal Detection and Quantification	583
Tissue Powdering.....	583
RNA Extraction	584
RNA Quantification	585
Reverse Transcription (creation of cDNA).....	585
Primers	586
Real Time RT-PCR.....	587
Gelatinase Zymography	588
Apoptosis Detection.....	590
Immunohistochemistry	592

Statistics	593
Results.....	594
Visual Assessment	594
Histology.....	605
Semi-quantitative Analysis of mRNA Expression	608
Gelatinase Zymography	631
Apoptosis Detection and Quantification.....	635
Immunohistochemistry	641
Average Solution Volume, Silver, and Calcium Delivered.....	666
Discussion.....	668
Bibliography	683

Chapter 8 – Effect of Sputtering Parameters on Resulting

Nanocrystalline Silver Thin Film Properties.....	686
Introduction.....	686
Materials and Methods.....	689
Generation of Nanocrystalline Silver Thin Films.....	689
Total Silver Digest	691
Ammonia Silver Digest.....	692
X-ray Diffraction (XRD)	692
Bactericidal Efficacy.....	693
Results and Discussion	694
Total and Ammonia Soluble Silver.....	694
XRD	743

Log Reductions	749
Conclusions.....	772
Bibliography	774

Chapter 9 – Using the kinetics of heat treatment to determine critical physicochemical properties for nanocrystalline silver

antimicrobial activity.....	775
Introduction.....	775
Materials and Methods.....	786
Dressing Materials	786
Biological Assays.....	786
Bacterial Preparation.....	786
Log Reduction.....	787
Corrected Zone of Inhibition (CZOI)	788
Physical and Chemical Methods.....	789
Silver Dissolution.....	789
Scanning Electron Microscopy (SEM)	790
X-ray Diffraction (XRD)	791
X-ray Photoelectron Spectroscopy (XPS)	791
Thermal Analysis.....	792
Differential Scanning Calorimetry.....	792
Statistical Analysis.....	796
Results.....	796
Biological Assays.....	796

Log Reduction.....	796
Corrected Zones of Inhibition.....	797
Physical and Chemical Assays.....	799
Silver Dissolution.....	799
SEM Analysis	800
XRD Analysis	806
XPS Analysis	812
Thermal Analysis	815
Differential Scanning Calorimetry (DSC)	815
Discussion.....	819
Bibliography	830
Chapter 10 – Conclusions.....	832
Conclusions.....	832
Future Directions	840
Bibliography	842
Appendix 1 – HSLAS Protocol	843
Health Sciences Laboratory Animal Services Standard Operating Procedure Medical Sciences Building Necropsy M-B74	843
Appendix 2 – Lipopolysaccharide Isolation Protocol.....	847
Collection of Biomass and Lyophilization	847
LPS Extraction with Hot Phenol.....	849
Removal of Phenol from the LPS-Rich Aqueous Layer by Dialysis.....	849
Concentration of the LPS-Rich Aqueous Layer via Centrifugation	850

Reduction of Contaminants via Enzymatic Digestion	850
Final Centrifugation for Purification and Isolation of LPS	850
Assessment of LPS Purity.....	851
Bibliography	852

List of Tables

Volume 2

Table 5-1. Results of statistical analyses of the effect of varying dissolution conditions (the ratio of silver dressing to solution volume, and whether or not the solution was stirred) at starting pHs of 4 or 5.6 on the total silver dissolved.....	407-9
Table 5-2. Results of statistical analyses of the effect of varying the ratio of silver dressing to solution volume, at starting pHs of 7 or 9, on the total silver dissolved in stirred solutions.....	413
Table 5-3. Results of statistical analyses of the effect of starting pH (pH 4 versus pH 5.6) on the total silver dissolved in solutions generated in the absence of stirring	416
Table 5-4. Results of statistical analyses of the effect of starting pH (pH 4, pH 5.6, pH 7, or pH 9) on the total silver dissolved in solutions generated under stirring.....	418-21
Table 5-5. Results of statistical analyses of the effect of dissolution time on the total silver dissolved under various conditions	423
Table 5-6. Results of statistical analyses on the effect of varying dissolution conditions (stirred or unstirred, ratio of nanocrystalline silver dressing to solution) on the pH during dissolution using a starting pH of 4 or 5.6.....	425-7
Table 5-7. Results of statistical analyses on the effect of varying the ratio of nanocrystalline silver dressing to solution on the pH during	

dissolution using a starting pH of 7 or 9.....	430
Table 5-8. Results of statistical analyses of the effect of varying the starting pH (4 or 5.6), during dissolution without stirring, on pH over time	433
Table 5-9. Results of statistical analyses on the effect of varying the starting pH (4, 5.6, 7, or 9) during dissolution, with stirring, on the pH over time	435-8
Table 5-10. Results of the statistical analysis of the effect of dissolution time on the pH of solutions generated under various conditions.....	441
Table 5-11. Results of log reductions generated using nanocrystalline silver-derived solutions generated under a variety of conditions against <i>S. aureus</i>	443
Table 5-12. Results of statistical analyses of the effect of starting pH (pH 4 versus pH 5.6) on the bactericidal efficacy of solutions generated in the absence of stirring	443
Table 5-13. Results of statistical analyses on the effect of starting pH on the bactericidal efficacy of solutions generated under stirring for 24h.....	444
Table 5-14. Results of statistical analyses of the effect of stirring on the bactericidal efficacy of solutions	444
Table 5-15. Results of statistical analyses of the effect of varying the ratio of silver dressing to solution volume on bactericidal efficacy, holding other variables constant	445

Table 5-16. Results of statistical analyses of the effect of dissolution for 1 or 24 hours on bactericidal efficacy, holding other variables constant	446
Table 5-17. Summary of XRD analysis for nanocrystalline silver dressings dissolved at 35°C for 24 hours in various solutions.....	475
Table 5-18. Summary of XRD analysis for nanocrystalline silver dressings dissolved at 35°C for 24 hours in various solutions, followed by storage under vacuum.....	476

Table 6-1. Comparison of the IA-1B® and IA-1C® MicroSprayers by PennCentury™, Inc.....	503
Table 6-2. Bacterial counts from lungs of acute inflammation study at 24 hours.....	526
Table 6-3. Bacterial counts for <i>P. aeruginosa</i> titration study.....	539
Table 6-4. Bacterial counts for the antimicrobial activity study.....	551
Table 6-5. Total silver in solutions under various conditions.....	563
Table 8-1. Effect of substrate location on the total silver deposited when sputtering at 4% O ₂ and 0.75A for various lengths of time	720
Table 8-2. Effect of substrate sample location on the total silver deposited when sputtering for 10 minutes at various currents and oxygen concentrations	723-4
Table 8-3. Effect of oxygen concentration on the total silver deposited when sputtering for 10 minutes at various currents at substrate locations W3 and W4.....	725
Table 8-4. Effect of substrate sample location on the percent ammonia soluble silver deposited when sputtering for 10 minutes at various currents and oxygen concentrations.....	727-8
Table 8-5. Effect of oxygen concentration on the percent ammonia soluble silver deposited when sputtering for 10 minutes at various currents at substrate locations W3 and W4.....	729
Table 8-6. The effect of current on the total silver deposited when sputtering for 10 minutes at various oxygen concentrations at substrate	

locations W3 and W4.....	738
Table 8-7. The effect of current on the ammonia soluble silver deposited when sputtering for 10 minutes at various oxygen concentrations at substrate locations W3 and W4.....	740
Table 8-7. Results of XRD analysis of nanocrystalline silver thin films generated under a variety of sputtering conditions. All samples were sputtered for 10 minutes statically	747
Table 8-8. The effect of substrate location on the resulting log reduction generated against <i>P. aeruginosa</i> for nanocrystalline silver thin films generated at various oxygen concentrations, web speeds, and currents ..	751-3
Table 8-9. The effect of current on the log reductions generated against <i>P. aeruginosa</i> at substrate locations W3 and W4 when sputtering at various oxygen concentrations and web speeds.....	754
Table 8-10. The effect of web speed on log reductions produced against <i>P. aeruginosa</i> for nanocrystalline silver thin films generated at 4% oxygen and various currents	764
Table 8-11. The effect of percent oxygen on log reductions produced against <i>P. aeruginosa</i> for nanocrystalline silver thin films generated at various currents for dynamic runs at 20 mm/min	765
Table 8-12. Effect of substrate location on log reduction against <i>S. aureus</i> for nanocrystalline silver dressings generated using 10 minute static sputtering runs at various oxygen concentrations and currents.....	767

Table 8-13. The effect of 4, 8, 10, and 12% oxygen on log reductions generated against <i>S. aureus</i> for nanocrystalline silver thin films generated using 10 minute static sputtering runs at various currents	768
Table 8-14. The effect of current (0.75, 1, or 1.5 A) on log reductions generated against <i>S. aureus</i> for nanocrystalline silver thin films generated using 10 minute static sputtering runs at various currents	769
Table 9-1. Summary of XRD analysis, including domain size, composition, and microstrain for nanocrystalline silver dressings heat-treated for 24 hours at various temperatures.....	784
Table 9-2. XRD analysis of nanocrystalline silver dressings heat-treated at 90, 100, and 110°C for various times	808

List of Figures or Illustrations

Volume 2

Figure 5-1. Setup for generating and testing nanocrystalline silver-derived solutions	340
Figure 5-2. Initial testing of the antimicrobial activity of nanocrystalline silver-derived solutions	349
Figure 5-3. Example of effect of starting pH on absorbance of nanocrystalline silver-derived solutions	353
Figure 5-4. Relationship between peak height at 210 nm in spectrophotometric scans and total silver in nanocrystalline silver-derived solutions	354
Figure 5-5. Example of spikes generated from a nanocrystalline silver-derived solution started at pH 4 using an Ultrospec 3000	355
Figure 5-6. Example of spikes generated from a nanocrystalline silver-derived solution started at pH 4.5 using an Ultrospec 3000	356
Figure 5-7. Example of spikes generated from a nanocrystalline silver-derived solution started at pH 5.6 using an Ultrospec 3000	357
Figure 5-8. Example of spikes generated in a quartz cuvette after it held a nanocrystalline silver-derived solution started at pH 5.6 using an Ultrospec 3000	359
Figure 5-9. Example of a spectrophotometric scan of a nanocrystalline silver-derived solution using an Ultrospec 2000	361
Figure 5-10. Effect of multiple spectrophotometric scan on a	

nanocrystalline silver-derived solution	361
Figure 5-11. Spectrophotometric analysis of a nanocrystalline-silver derived solution, generated at a starting pH of 4, performed using a diode array	362
Figure 5-12. Spectrophotometric analysis of a nanocrystalline silver- derived solution, generated at a starting pH of 5.6, performed using a diode array	363
Figure 5-13. Spectrophotometric scan of a nanocrystalline silver-derived solution, generated at a starting pH of 4, using an Ultrospec 3000	363
Figure 5-14. Spectrophotometric scan of a nanocrystalline silver-derived solution, generated at a starting pH of 5.6, using an Ultrospec 3000	364
Figure 5-15. Spectrophotometric scan of nanocrystalline silver dissolved in nitric acid for one hour.....	365
Figure 5-16. Spectrophotometric scan of nanocrystalline silver dissolved in nitric acid for 17 hours.....	366
Figure 5-17. Spectrophotometric scan of 0.25% nitric acid	366
Figure 5-18. Spectrophotometric scan of sodium nitrate.....	367
Figure 5-19. Spectrophotometric scans of silver nitrate	367
Figure 5-20. Spectrophotometric scan of silver nitrate in sodium hydroxide	368
Figure 5-21. Spectrophotometric scan of high density polyethylene backing in nitric acid.....	369
Figure 5-22. Spectrophotometric scan of nanocrystalline silver dissolved	

in nitric acid (HDPE reference)	370
Figure 5-23. Spectrophotometric scan of nanocrystalline silver dissolved	
in sodium nitrate	371
Figure 5-24. Spectrophotometric scan of nanocrystalline silver dissolved	
in acetic acid	373
Figure 5-25. Spectrophotometric scan of nanocrystalline silver dissolved	
in carbonic acid	374
Figure 5-26. Spectrophotometric scan of nanocrystalline silver dissolved	
in phosphoric acid	375
Figure 5-27. Spectrophotometric scan of nanocrystalline silver dissolved	
in glacial acetic acid with sodium nitrate for one hour	376
Figure 5-28. Spectrophotometric scan of nanocrystalline silver dissolved	
in glacial acetic acid with sodium nitrate for 24 hours	377
Figure 5-29. Spectrophotometric scan of ammonia	378
Figure 5-30. Spectrophotometric scan of a nanocrystalline silver dissolved	
in ammonia for different periods of time	379
Figure 5-31. Spectrophotometric scan of silver nitrate in nitric acid	380
Figure 5-32. Spectrophotometric scan of silver nitrate in glacial acetic	
acid	381
Figure 5-33. Excitation scans for various nanocrystalline silver-derived	
solutions using a spectrofluorimeter	391
Figure 5-34. Emission scans for various nanocrystalline silver-derived	
solutions using a spectrofluorimeter	392

Figure 5-35. Excitation scans for examination of the effect of allowing a nanocrystalline silver-derived solution to sit in a cuvette for various lengths of time (without exposure to further nanocrystalline silver).....	393
Figure 5-36. Emission scans for examination of the effect of allowing a nanocrystalline silver-derived solution to sit in a cuvette for various lengths of time (without exposure to further nanocrystalline silver).....	394
Figure 5-37. Excitation scans for examination of the effect of rinsing a cuvette with a nanocrystalline silver-derived solution.....	395
Figure 5-38. Emission scans for studying the effect of rinsing a cuvette with a nanocrystalline silver-derived solution	396
Figure 5-39. Excitation scans testing for the presence of adsorbed species on cuvettes after exposure to nanocrystalline silver-derived solutions ...	397
Figure 5-40. Emission scans testing for the presence of adsorbed species on cuvettes after exposure to nanocrystalline silver-derived solutions ...	398
Figure 5-41. Total silver profiles over time for nanocrystalline silver-derived solutions generated at a starting pH of 4 under various conditions.....	407
Figure 5-42. Total silver profiles over time for nanocrystalline silver-derived solutions generated at a starting pH of 5.6 under various conditions.....	411
Figure 5-43. Total silver profiles over time for nanocrystalline silver-derived solutions generated at a starting pH of 7 at different silver:solution ratios.....	412

Figure 5-44. Total silver profiles over time for nanocrystalline silver-derived solutions generated at a starting pH of 9 at different silver:solution ratios.....	414
Figure 5-45. Comparison of total silver profiles over time of nanocrystalline silver-derived solutions generated at starting pHs of 4 (carbonated water) and 5.6 (distilled water), unstirred, at a ratio of 1:5 in ² Ag/mL solution.....	415
Figure 5-46. Comparison of total silver profiles over time of nanocrystalline silver-derived solutions generated at starting pHs of 4 (carbonated water) and 5.6 (distilled water), unstirred, at a ratio of 1:1 in ² Ag/mL solution.....	417
Figure 5-47. Comparison of total silver profiles over time of nanocrystalline silver-derived solutions generated at starting pHs of 4 (carbonated water), 5.6 (distilled water), 7 (adjusted using calcium hydroxide), or 9 (adjusted using calcium hydroxide), stirred, at a ratio of 1:5 in ² Ag/mL solution	418
Figure 5-48. Comparison of total silver profiles over time of nanocrystalline silver-derived solutions generated at starting pHs of 4 (carbonated water), 5.6 (distilled water), 7 (adjusted using calcium hydroxide), or 9 (adjusted using calcium hydroxide), stirred, at a ratio of 1:1 in ² Ag/mL solution	422
Figure 5-49. pH profiles over time for nanocrystalline silver-derived solutions generated at a starting pH of 4 under various conditions	425

Figure 5-50. pH profiles over time for nanocrystalline silver-derived solutions generated at a starting pH of 5.6 under various conditions	428
Figure 5-51. pH profiles over time for nanocrystalline silver-derived solutions generated at a starting pH of 7 at different silver:solution ratios.....	429
Figure 5-52. pH profiles for nanocrystalline silver-derived solutions generated at a starting pH of 9 at different silver:solution ratios.....	431
Figure 5-53. Comparison of pH profiles over time for nanocrystalline silver-derived solutions generated at starting pHs of 4 (carbonated water) and 5.6 (distilled water), unstirred, at a ratio of 1:5 in ² Ag/mL solution.....	432
Figure 5-54. Comparison of pH profiles over time for nanocrystalline silver-derived solutions generated at starting pHs of 4 (carbonated water) and 5.6 (distilled water), unstirred, at a ratio of 1:1 in ² Ag/mL solution.....	434
Figure 5-55. Comparison of pH profiles over time for nanocrystalline silver-derived solutions generated at starting pHs of 4 (carbonated water), 5.6 (distilled water), 7 (adjusted using calcium hydroxide), or 9 (adjusted using calcium hydroxide), stirred, at a ratio of 1:5 in ² Ag/mL solution	435
Figure 5-56. Comparison of pH profiles over time for nanocrystalline silver-derived solutions generated at starting pHs of 4 (carbonated water), 5.6 (distilled water), 7 (adjusted using calcium hydroxide), or	

9 (adjusted using calcium hydroxide), stirred, at a ratio of 1:1 in ² Ag/mL solution	439
Figure 5-57. Unusual growth of <i>P. aeruginosa</i> with the appearance of plaques, suggesting infection of the culture by a bacteriophage	447
Figure 5-58. Summary of XPS intensities of C 1s peaks for nanocrystalline silver dressings after heating dry at 37°C (control dressings), or dissolution at 37°C in solutions at starting pHs of 4 (adjusted using HCl), 5.6 (reverse osmosis water), 9 (adjusted using NaOH), or fetal calf serum.....	449
Figure 5-59. Examples of deconvolution of C 1s XPS spectra for nanocrystalline silver dressings after dissolution under various conditions.....	450-2
Figure 5-60. Summary of XPS intensities of O 1s peaks for nanocrystalline silver dressings after heating dry at 37°C (control dressings), or dissolution at 37°C in solutions at starting pHs of 4 (adjusted using HCl), 5.6 (reverse osmosis water), 9 (adjusted using NaOH), or fetal calf serum.....	453
Figure 5-61. Examples of deconvolution of O 1s XPS spectra for nanocrystalline silver dressings after dissolution under various conditions.....	454-6
Figure 5-62. Summary of XPS intensities of Ag 3d peaks for nanocrystalline silver dressings after heating dry at 37°C (control dressings), or dissolution at 37°C in solutions at starting pHs of 4	

(adjusted using HCl), 5.6 (reverse osmosis water), 9 (adjusted using NaOH), or fetal calf serum.....	457
Figure 5-63. Examples of deconvolution of Ag 3d XPS spectra for nanocrystalline silver dressings after dissolution under various conditions.....	458-60
Figure 5-64. Measurement of total oxygen and silver oxide via XPS	461-2
Figure 5-65. SEM images of nanocrystalline silver dressings heated dry at 37°C (controls).....	463-4
Figure 5-66. SEM images of nanocrystalline silver dressings dissolved at a starting pH of 4 (adjusted using HCl) at 37°C	464-5
Figure 5-67. SEM images of nanocrystalline silver dressings dissolved at a starting pH of 5.6 (reverse osmosis water) at 37°C.....	466-7
Figure 5-68. SEM images of nanocrystalline silver dressings dissolved at a starting pH of 9 (adjusted using sodium hydroxide) at 37°C	468-9
Figure 5-69. SEM image of nanocrystalline silver dressings dissolved in fetal calf serum at 37°C for 2 hours	470
Figure 5-70. SEM images of nanocrystalline silver dressings heated dry at 37°C, followed by placement in a vacuum chamber.....	471-2
Figure 6-1. Images of lungs in the lung cavities of rats after euthanasia at the end of the anti-inflammatory activity study (24 hours)	522
Figure 6-2. Representative histological images of the lungs of each rat 24 hours after treatment in the anti-inflammatory activity study	523-4
Figure 6-3. Images from the literature demonstrating the techniques for	

visualizing the trachea and using microsprayers in rats.....	525
Figure 6-4. Histological images showing the range of inflammation present in the upper left lung lobe of each rat used in the lipopolysaccharide (LPS) titration study	532-34
Figure 6-5. Representative digital images showing the upper left lung lobe of rats used in the <i>Pseudomonas aeruginosa</i> titration study.....	538
Figure 6-6. Representative digital images showing the portions of lung lobes of rats used for bacterial counts in the antimicrobial activity study 24 hours after inoculation of a 1:30 dilution of <i>Pseudomonas aeruginosa</i> incubated at 37°C overnight, followed four hours later by various treatments	541
Figure 6-7. Histological images showing the range of inflammation present in the upper left lung lobe of each rat euthanized 24 hours into the antimicrobial activity study	543-5
Figure 6-8. Representative digital images showing the portions of lung lobes of rats used for bacterial counts in the antimicrobial activity study 72 hours after inoculation of a 1:30 dilution of <i>Pseudomonas aeruginosa</i> incubated at 37°C overnight, followed four hours later by various treatments	547
Figure 6-9. Histological images showing the range of inflammation present in the upper left lung lobe of each rat euthanized at 72 hours in the antimicrobial activity study.....	548-50
Figure 6-10. Real time RT-PCR reaction rates	552

Figure 6-11. Relative expression of TNF- α mRNA in negative controls, <i>P. aeruginosa</i> infected rat lungs treated for 24 hours with 100 μ L of distilled water (positive controls), 2.4 mg/mL tobramycin in 0.9% saline, 0.31 mg/mL silver nitrate in distilled water, or nanocrystalline silver-derived solution (starting pH of 4, 24 hour dissolution time, \sim 100 rpm, 1 in ² /mL).....	553
Figure 6-12. Real time RT-PCR reaction rates.....	554-5
Figure 6-13. Relative expression of TNF- α mRNA in negative controls, <i>P. aeruginosa</i> infected rat lungs treated for 72 hours with 100 μ L of distilled water (positive controls), 2.4 mg/mL tobramycin in 0.9% saline, 0.31 mg/mL silver nitrate in distilled water, or nanocrystalline silver-derived solution (starting pH of 4, 24 hour dissolution time, \sim 100 rpm, 1 in ² /mL)	556
Figure 6-14. Histological images showing the range of inflammation present in the upper left lung lobe of each nanocrystalline silver control rat euthanized after 24 hours	558
Figure 6-15. Solution wettability	559
Figure 6-16. Bacteriostatic activity of nanocrystalline silver-derived solutions	560-1
Figure 7-1. Digital images of rashes exposed to DNCB four times and then treated with various nanocrystalline silver-derived solutions.....	595
Figure 7-2. Digital images of rashes treated with various nanocrystalline silver-derived solutions on skin exposed once to DNCB after	

sensitization of the animal	597-9
Figure 7-3. Erythema scores for porcine skin exposed to DNCB four times over two weeks and then treated with various nanocrystalline silver-derived solutions.....	600
Figure 7-4. Edema scores for porcine skin exposed to DNCB four times over two weeks and then treated with various nanocrystalline silver-derived solutions	601
Figure 7-5. Biopsy bleeding scores for skin exposed to DNCB four times over two weeks and then treated various nanocrystalline silver-derived solutions	602
Figure 7-6. Erythema scores for porcine skin exposed to DNCB once (after sensitization of the animal) and then treated with various nanocrystalline silver-derived solutions	603
Figure 7-7. Edema scores for porcine skin exposed to DNCB once (after sensitization of the animal) and then treated with various nanocrystalline silver-derived solutions	604
Figure 7-8. Biopsy bleeding scores for skin exposed to DNCB once (after sensitization of the animal) and then treated various nanocrystalline silver-derived solutions.....	605
Figure 7-9. Representative histological images for skin exposed to DNCB four times over two weeks and then treated with various nanocrystalline silver-derived solutions	606-7
Figure 7-10. Representative histological images for skin exposed to	

DNCB once (after sensitization of the animal) and then treated with various nanocrystalline silver-derived solutions.....	609
Figure 7-11. Real time RT-PCR reaction rates for 24h samples	610-14
Figure 7-12. Real time RT-PCR reaction rates for 72h samples	614-18
Figure 7-13. Relative expression of TNF- α mRNA in negative controls and DNCB-induced porcine rashes treated for 24 hours with distilled water (positive controls), or nanocrystalline silver-derived solutions generated at starting pHs of 4, 5.6, 7, and 9.....	619
Figure 7-14. Relative expression of IL-1 β mRNA in negative controls and DNCB-induced porcine rashes treated for 24 hours with distilled water (positive controls), or nanocrystalline silver-derived solutions generated at starting pHs of 4, 5.6, 7, and 9	620
Figure 7-15. Relative expression of IL-8 mRNA in negative controls and DNCB-induced porcine rashes treated for 24 hours with distilled water (positive controls), or nanocrystalline silver-derived solutions generated at starting pHs of 4, 5.6, 7, and 9.....	621
Figure 7-16. Relative expression of IL-10 mRNA in negative controls and DNCB-induced porcine rashes treated for 24 hours with distilled water (positive controls), or nanocrystalline silver-derived solutions generated at starting pHs of 4, 5.6, 7, and 9.....	622
Figure 7-17. Relative expression of IL-12 mRNA in negative controls and DNCB-induced porcine rashes treated for 24 hours with distilled water (positive controls), or nanocrystalline silver-derived solutions	

generated at starting pHs of 4, 5.6, 7, and 9.....	623
Figure 7-18. Relative expression of IL-17 mRNA in negative controls and DNCB-induced porcine rashes treated for 24 hours with distilled water (positive controls), or nanocrystalline silver-derived solutions generated at starting pHs of 4, 5.6, 7, and 9.....	624
Figure 7-19. Relative expression of TNF- α mRNA in negative controls and DNCB-induced porcine rashes treated for 72 hours with distilled water (positive controls), or nanocrystalline silver-derived solutions generated at starting pHs of 4, 5.6, 7, and 9.....	625
Figure 7-20. Relative expression of IL-1 β mRNA in negative controls and DNCB-induced porcine rashes treated for 72 hours with distilled water (positive controls), or nanocrystalline silver-derived solutions generated at starting pHs of 4, 5.6, 7, and 9.....	626
Figure 7-21. Relative expression of IL-8 mRNA in negative controls and DNCB-induced porcine rashes treated for 72 hours with distilled water (positive controls), or nanocrystalline silver-derived solutions generated at starting pHs of 4, 5.6, 7, and 9.....	627
Figure 7-22. Relative expression of IL-10 mRNA in negative controls and DNCB-induced porcine rashes treated for 72 hours with distilled water (positive controls), or nanocrystalline silver-derived solutions generated at starting pHs of 4, 5.6, 7, and 9.....	628
Figure 7-23. Relative expression of IL-12 mRNA in negative controls and DNCB-induced porcine rashes treated for 72 hours with distilled water	

(positive controls), or nanocrystalline silver-derived solutions generated at starting pHs of 4, 5.6, 7, and 9.....	629
Figure 7-24. Relative expression of IL-17 mRNA in negative controls and DNCB-induced porcine rashes treated for 72 hours with distilled water (positive controls), or nanocrystalline silver-derived solutions generated at starting pHs of 4, 5.6, 7, and 9.....	630
Figure 7-25. Zymogram showing gelatinase activity in biopsies from DNCB-induced rashes treated with various nanocrystalline silver- derived solutions.....	631
Figure 7-26. Quantitation of MMP band intensities from biopsies of DNCB-induced rashes treated with various nanocrystalline silver- derived solutions.....	633-4
Figure 7-27. Apoptosis detection in biopsies of DNCB-induced rashes treated for 24 hours with various nanocrystalline silver-derived solutions.....	636-40
Figure 7-28. Immunohistochemical detection of TNF- α in biopsies of DNCB-induced rashes treated with various nanocrystalline silver- derived solutions for 24 hours.....	642
Figure 7-29. Immunohistochemical detection of TNF- α in biopsies of DNCB-induced rashes treated with various nanocrystalline silver- derived solutions for 72 hours.....	643
Figure 7-30. Semi-quantitative analyses of immunohistochemical staining for TNF- α in biopsies of DNCB-induced rashes treated with various	

nanocrystalline silver-derived solutions	643-4
Figure 7-31. Immunohistochemical detection of TGF- β in biopsies of DNCB-induced rashes treated with various nanocrystalline silver- derived solutions for 24 hours.....	645
Figure 7-32. Immunohistochemical detection of TGF- β in biopsies of DNCB-induced rashes treated with various nanocrystalline silver- derived solutions for 72 hours.....	646
Figure 7-33. Semi-quantitative analyses of immunohistochemical staining for TGF- β in biopsies of DNCB-induced rashes treated with various nanocrystalline silver-derived solutions	647
Figure 7-34. Immunohistochemical detection of IL-8 in biopsies of DNCB-induced rashes treated with various nanocrystalline silver- derived solutions for 24 hours.....	649
Figure 7-35. Immunohistochemical detection of IL-8 in biopsies of DNCB-induced rashes treated with various nanocrystalline silver- derived solutions for 72 hours.....	650
Figure 7-36. Semi-quantitative analyses of immunohistochemical staining for IL-8 in biopsies of DNCB-induced rashes treated with various nanocrystalline silver-derived solutions	650-1
Figure 7-37. Immunohistochemical detection of IL-4 in biopsies of DNCB-induced rashes treated with various nanocrystalline silver- derived solutions for 24 hours.....	652
Figure 7-38. Immunohistochemical detection of IL-4 in biopsies of	

DNCB-induced rashes treated with various nanocrystalline silver- derived solutions for 72 hours.....	653
Figure 7-39. Semi-quantitative analyses of immunohistochemical staining for IL-4 in biopsies of DNCB-induced rashes treated with various nanocrystalline silver-derived solutions	653-4
Figure 7-40. Immunohistochemical detection of IL-10 in biopsies of DNCB-induced rashes treated with various nanocrystalline silver- derived solutions for 24 hours.....	655
Figure 7-41. Immunohistochemical detection of IL-10 in biopsies of DNCB-induced rashes treated with various nanocrystalline silver- derived solutions for 72 hours.....	656
Figure 7-42. Semi-quantitative analyses of immunohistochemical staining for IL-10 in biopsies of DNCB-induced rashes treated with various nanocrystalline silver-derived solutions	656-7
Figure 7-43. Immunohistochemical detection of EGF in biopsies of DNCB-induced rashes treated with various nanocrystalline silver- derived solutions for 24 hours.....	658
Figure 7-44. Immunohistochemical detection of EGF in biopsies of DNCB-induced rashes treated with various nanocrystalline silver- derived solutions for 72 hours.....	659
Figure 7-45. Semi-quantitative analyses of immunohistochemical staining for EGF in biopsies of DNCB-induced rashes treated with various nanocrystalline silver-derived solutions	659-60

Figure 7-46. Immunohistochemical detection of KGF in biopsies of DNCB-induced rashes treated with various nanocrystalline silver-derived solutions for 24 hours.....	661
Figure 7-47. Immunohistochemical detection of KGF in biopsies of DNCB-induced rashes treated with various nanocrystalline silver-derived solutions for 72 hours.....	662
Figure 7-48. Semi-quantitative analyses of immunohistochemical staining for KGF in biopsies of DNCB-induced rashes treated with various nanocrystalline silver-derived solutions	662-3
Figure 7-49. Immunohistochemical detection of KGF-2 in biopsies of DNCB-induced rashes treated with various nanocrystalline silver-derived solutions for 24 hours.....	664
Figure 7-50. Immunohistochemical detection of KGF-2 in biopsies of DNCB-induced rashes treated with various nanocrystalline silver-derived solutions for 72 hours.....	665
Figure 7-51. Semi-quantitative analyses of immunohistochemical staining for KGF-2 in biopsies of DNCB-induced rashes treated with various nanocrystalline silver-derived solutions	665-6
Figure 7-52. Average volume of solution delivered per day per side for treatment of DNCB-induced rashes	667
Figure 7-53. Average weight of silver delivered per day per side to DNCB-induced rashes via various nanocrystalline silver-derived solutions	668

Figure 8-1. Substrate sampling locations.....	691
Figure 8-2. Preliminary results showing total silver deposited on samples sputtered at 4% O ₂ for a 10 minute static run	695
Figure 8-3. Preliminary results showing ammonia-soluble silver deposited on samples sputtered at 4% O ₂ for a 10 minute static run	696
Figure 8-4. Effect of current on total silver deposited on samples sputtered at 4% O ₂ for a 20 mm/min dynamic run	697
Figure 8-5. Effect of current on ammonia-soluble silver deposited on samples sputtered at 4% O ₂ for a 20 mm/min dynamic run	698
Figure 8-6. Effect of current on total silver deposited on samples sputtered at 4% O ₂ for a 43 mm/min dynamic run	699
Figure 8-7. Effect of current on ammonia-soluble silver deposited on samples sputtered at 4% O ₂ for a 43 mm/min dynamic run	700
Figure 8-8. Effect of current on total silver deposited on samples sputtered at 4% O ₂ for an 80 mm/min dynamic run at 1.5A	701
Figure 8-9. Effect of current on ammonia-soluble silver deposited on samples sputtered at 4% O ₂ for an 80 mm/min dynamic run at 1.5A.....	702
Figure 8-10. Effect of web speed for dynamic runs on total silver deposited on samples sputtered at 4% O ₂	703
Figure 8-11. Effect of web speed for dynamic runs on ammonia-soluble silver deposited on samples sputtered at 4% O ₂	704
Figure 8-12. Effect of current on total silver deposited on samples sputtered at 2% O ₂ for a 20 mm/min dynamic run	705

Figure 8-13. Effect of current on ammonia-soluble silver deposited on samples sputtered at 2% O ₂ for a 20 mm/min dynamic run	706
Figure 8-14. Effect of current on total silver deposited on samples sputtered at 0% O ₂ for a 20 mm/min dynamic run	708
Figure 8-15. Effect of current on ammonia-soluble silver deposited on samples sputtered at 0% O ₂ for a 20 mm/min dynamic run	709
Figure 8-16. Effect of percent oxygen on total silver deposited on samples sputtered for a 20 mm/min dynamic run.....	710
Figure 8-17. Effect of percent oxygen on ammonia-soluble silver deposited on samples sputtered for a 20 mm/min dynamic run.....	711
Figure 8-18. Effect of solid versus meshed substrate on total silver deposited on samples sputtered at 4% O ₂ for a 10 minute static run.....	712
Figure 8-19. Effect of solid versus meshed substrate on ammonia-soluble silver deposited on samples sputtered at 4% O ₂ for a 10 minute static run	713
Figure 8-20. Preliminary study of the effect of percent oxygen on total silver deposited on samples sputtered at 1.5A for a 10 minute static run	714
Figure 8-21. Effect of percent oxygen on ammonia-soluble silver deposited on samples sputtered at 1.5A for a 10 minute static run.....	715
Figure 8-22. Preliminary study of the effect of current and percent oxygen on total silver deposited on samples sputtered in a 10 minute static run.....	716

Figure 8-23. Preliminary study of the effect of current and percent oxygen on ammonia-soluble silver deposited on samples sputtered in a 10 minute static run.....	717
Figure 8-24. The effect of sputtering time on total silver deposited on samples sputtered at 0.75A and 4% oxygen	719
Figure 8-25. Effect of sputtering time on ammonia-soluble silver deposited on samples sputtered at 0.75A and 4% oxygen	721
Figure 8-26. The effect of percent oxygen on total silver deposited on samples sputtered at 0.75A in a 10 minute static run	722
Figure 8-27. Effect of percent oxygen on ammonia-soluble silver deposited on samples sputtered at 0.75A in a 10 minute static run	726
Figure 8-28. The effect of percent oxygen on total silver deposited on samples sputtered at 1A in a 10 minute static run	730
Figure 8-29. Effect of percent oxygen on ammonia-soluble silver deposited on samples sputtered at 0.75A in a 10 minute static run	733
Figure 8-30. The effect of percent oxygen on total silver deposited on samples sputtered at 1.5A in a 10 minute static run	734
Figure 8-31. Effect of percent oxygen on ammonia-soluble silver deposited on samples sputtered at 1.5A in a 10 minute static run	736
Figure 8-32. Total silver deposited on samples sputtered at 0.9A and 4% O ₂ in a 30 minute static run	742
Figure 8-33. Ammonia-soluble silver deposited on samples sputtered at 0.9A and 4% O ₂ in a 30 minute static run.....	743

Figure 8-34. Example of an XRD footprint for a nanocrystalline silver thin film generated in-house	746
Figure 8-35. An XRD footprint for Acticoat™	746
Figure 8-36. Preliminary study of the effect of current on the log reduction of <i>Pseudomonas aeruginosa</i> produced by nanocrystalline silver thin films generated at 4% oxygen during a 10 minute static run	750
Figure 8-37. Log reductions of <i>P. aeruginosa</i> produced by nanocrystalline silver thin films generated at 4% oxygen and 1.5A during an 80 mm/min dynamic run.....	755
Figure 8-38. The effect of current on the log reductions of <i>P. aeruginosa</i> produced by nanocrystalline silver thin films generated at 4% oxygen during a 43 mm/min dynamic run.....	757
Figure 8-39. The effect of current on the log reductions of <i>P. aeruginosa</i> produced by nanocrystalline silver thin films generated at 4% oxygen during a 20 mm/min dynamic run.....	759
Figure 8-40. The effect of current on the log reductions of <i>P. aeruginosa</i> produced by nanocrystalline silver thin films generated at 2% oxygen during a 20 mm/min dynamic run.....	761
Figure 8-41. The effect of current on the log reductions of <i>P. aeruginosa</i> produced by nanocrystalline silver thin films generated at 0% oxygen during a 20 mm/min dynamic run.....	762
Figure 8-42. The effect of percent oxygen on the log reductions of <i>S.</i>	

<i>aureus</i> produced by nanocrystalline silver thin films generated at various currents during a 10 minute static run.....	766
Figure 9-1. Total release of silver in water versus time for nanocrystalline silver dressings heat treated at various temperatures for 24 hours	777
Figure 9-2. Total silver released after 24 hours in water for nanocrystalline silver dressings heat treated at various temperatures for 24 hours	777
Figure 9-3. Log reduction of <i>S. aureus</i> exposed to nanocrystalline silver dressings heated at various temperatures for 24 hours	778
Figure 9-4. Log reduction of <i>P. aeruginosa</i> exposed to nanocrystalline silver dressings heat treated at various temperatures for 24 hours	778
Figure 9-5. Corrected zone of inhibition (CZOI) of <i>S. aureus</i> over a series of days using nanocrystalline dressings heat treated at various temperatures for 24 hours	779
Figure 9-6. Corrected zones of inhibition (CZOI) of <i>P. aeruginosa</i> over a series of days using nanocrystalline silver dressings heat treated at various temperatures for 24 hours.....	779
Figure 9-7. Days of nanocrystalline silver dressing antibacterial activity for dressing heat treatment at various temperatures for 24 hours.....	780
Figure 9-8. SEM images of nanocrystalline silver dressings heat-treated for 24 hours	780-84
Figure 9-9. Comparison of atomic concentration of total oxygen and oxygen bonded to silver (determined via XPS, in percent), to	

crystallite size (determined via XRD, in nm/10, n=3), silver dissolution (in [mg/L]/10, n=3) and biological activity (<i>S. aureus</i> log reduction and days of activity data, n=3) after exposure of the dressing to various temperatures for 24 hours	785
Figure 9-10. Log reductions of <i>P. aeruginosa</i> exposed to nanocrystalline silver dressings heat-treated at 90, 100, or 110°C for various times	797
Figure 9-11. Corrected zones of inhibition for <i>P. aeruginosa</i> over a series of days in response to nanocrystalline silver dressings heat-treated for various times.....	798-9
Figure 9-12. Total release of silver in water after a 24 hour dissolution versus nanocrystalline silver dressing heat treatment time at temperatures of 90, 100, and 110°C	800
Figure 9-13. SEM images of heat-treated nanocrystalline silver dressings.....	802-6
Figure 9-14. Diffraction patterns of nanocrystalline silver dressings after isothermal holds at indicated times and temperatures	807
Figure 9-15. Comparison of the ratio of silver oxide to metallic silver over time and relative to crystallite size	809
Figure 9-16. Grain growth curves and exponents.....	811
Figure 9-17. Raw XPS data of heat-treated dressings	813-14
Figure 9-18. Oxygen percentage in heat-treated nanocrystalline silver dressing samples at 90, 100, and 110°C for various times	815
Figure 9-19. Differential scanning calorimetry of nanocrystalline silver	

oxide sputtered on an aluminum sample cell.....	816
Figure 9-20. Differential scanning calorimetry of nanocrystalline silver sputtered on aluminum foil layered in a nanocrystalline silver- sputtered sample cell.....	817-18
Figure 9-21. Diffraction patterns of nanocrystalline silver thin films sputtered onto aluminum foil for 30 minutes at 4% oxygen, 0.9 A, 40 mTorr pressure, and a working distance of 10 cm.....	819
Figure 10-1. Hypotheses about the mechanisms of action of nanocrystalline silver anti-inflammatory activity	837-9
Figure A2-1. pH, temperature, airflow, and stirring data over time for <i>Pseudomonas aeruginosa</i> growth in a fermentor	848

Volume 2

Chapter 5 – Releasing Biologically Active Nanocrystalline Silver Species – Effect of Dissolution Conditions

Introduction

The dissolution of silver into the wound environment is of key importance to its activity[1]. Charged species must interact with bacteria in order to have an antimicrobial effect, and active species generated by nanocrystalline silver must interact with cells at the skin surface in order to set off the biological cascade necessary for its anti-inflammatory activity (see Chapter 3). For this to occur, the active moieties must be released from the dressing by dissolution. This is why nanocrystalline silver dressings must be pre-moistened with water when used clinically, and why a moist wound environment must be maintained throughout treatment with nanocrystalline silver.

Anecdotal clinical evidence has suggested that dissolved species from nanocrystalline silver dressings may be active for the treatment of lung diseases involving both infection and inflammation (personal communication, Dr. Robert Burrell); however, there are no known published reports on the subject. One study has shown that, in a murine model of ulcerative colitis, proprietary nanocrystalline silver nanodispersions delivered intracolonicly or orally suppressed the expression of matrix metalloproteinase (MMP)-9, TNF- α , IL-1 β , and IL-12[2]. This suggests that nanocrystalline silver has anti-inflammatory activity which could be used to treat internal epithelial tissues, as well as the skin.

Based on these observations, it seemed likely that solutions could be

generated which contained some or all of the active agents, and thus some or all of the antimicrobial and anti-inflammatory/pro-healing properties, of nanocrystalline silver.

The purposes of this chapter's investigations were:

1. To generate nanocrystalline silver-derived solutions under a variety of conditions.

2. To develop an understanding of the dissolution process both from the perspective of changes occurring in the solution during dissolution and from the perspective of changes occurring to the dressings during the dissolution. This could help in the development of appropriate solutions for various therapeutic applications, and in the understanding of processes occurring in the clinical environment during treatment with nanocrystalline silver.

3. To test nanocrystalline silver-derived solutions for antimicrobial activity.

4. If possible, to develop methods to identify the presence of species in solution additional to Ag^+ , possibly leading to the identification of these species, which would then help in identifying the dissolution conditions which generate solutions with the most desirable properties.

In regards to the latter point, currently the total silver dissolved in solution can be measured, which provides a general indicator that silver species are present in solution. However, a measurement of total dissolved silver does not indicate if all of the species which can be made available from nanocrystalline silver are actually present in a solution (or in what ratio they are present), and whether all of

the silver dissolved is active, or if it has reacted with solution components, changing it to an inactive state. Studies have shown that both Ag^+ and metallic silver, possibly in a cluster form, are released from nanocrystalline silver into solution[3], and have indicated that a higher oxidation state species is likely also released. However, there is currently no means of determining how much of each species is released (the species have not even been identified yet), and this is expected to vary with dissolution conditions. It is hypothesized that Ag^0 -containing clusters are released from nanocrystalline silver[3], and that these species are responsible for the anti-inflammatory activity of nanocrystalline silver dressings. The latter part of the hypothesis is based on the fact that other noble metals, including gold and platinum, have anti-inflammatory activity which may result from their reduced form[4-9]. For example, Au^+ , the gold species delivered in some RA treatments, reacts to form Au^0 *in vivo*[10]. Au^0 nanoparticles also suppress the activity of inflammatory cytokines while reducing RA symptoms[10], suggesting that Au^0 may be the anti-inflammatory agent[8, 10, 11]. Since individual Au^0 atoms would not exist stably in solution, this anti-inflammatory activity of metallic gold may be due to a reduced cluster form. Due to the physical similarities between gold and silver[12-14], small Au^0 and Ag^0 containing clusters should be nearly identical physically, and thus would be expected to have similar activity, suggesting that the anti-inflammatory activity of nanocrystalline silver may be due to a reduced form, such as Ag^0 containing clusters.

Therefore, it would be ideal to develop a simple method to determine

whether or not Ag^0 -containing species are present in solution. Fan and Bard have suggested that the Ag^0 species available in solution may be small clusters on the order of 2-8 atoms[3], which suggests that they might fluoresce when photoactivated. This is because the Dickson group was able to produce intermittent fluorescence from silver oxide thin films upon photoactivation[15, 16]. Irradiation of these films at room temperature induces a photochemical transformation such that after subsequent visible light excitation, irradiated areas give rise to strong multi-colored fluorescence[15]. This fluorescence is due to the formation of silver nanoclusters via photodecomposition of the silver oxide[16]. These clusters range from two to eight atoms in size, and the fluorescence is highly dependent on cluster size and geometry[16]. Furthermore, the same group reported that water-soluble, monodisperse, Au_8 nanodots stabilized by PAMAM dendrimers exhibit blue fluorescence[17]. They went on to show that nanogold exhibits size-tunable plasmon absorption widths[18], and that although many gold nanocluster sizes are non-fluorescent, certain cluster sizes consistently fluoresce, with the energy of emission increasing as the size of the cluster decreased: Au_5 emitted UV light, Au_8 emitted blue light, Au_{23} emitted red light, and Au_{31} emitted NIR light[18]. They indicated that their studies in gold were performed because of its better stability in solution, and should serve as a guide to understanding the even brighter emissions they observed with silver nanoclusters, because gold shows similar size scalings and excellent optical properties[19].

Small silver clusters trapped in rare gas matrixes also exhibit fluorescence – specifically, laser-induced fluorescence signals have been observed for Ag_4 [20],

Ag₈[21], and Ag₉[22] in argon matrices. This confirms that the photoactivation and resulting fluorescence of silver oxide films is also due to the formation of small silver particles[23]. As well, silver cluster generation by photoactivation of silver halides may be responsible for image generation in photography[24, 25].

These findings suggest that doing optical analyses of nanocrystalline silver-derived solutions, including spectrophotometry or spectrofluorimetry, might provide an indication as to whether or not Ag⁰-containing clusters were present in solution. If this was the case, this would provide a method of ensuring that these species, which are hypothesized to be involved in the anti-inflammatory activity of nanocrystalline silver, were present in solutions used for future analyses, which could then lead to the confirming or disproving of this hypothesis. Furthermore, if an ion selective electrode were used to determine the quantity of Ag⁺ in solution, this quantity could be subtracted from the total silver in solution to determine what quantity of silver was related to other silver species, and how dissolution conditions affected the quantity of these other species. As an example, it was anticipated that lowering the pH of a solution would increase the total silver dissolved, based on preliminary studies. However, it was uncertain as to whether this would result in the presence of a large quantity of anti-inflammatory species, antimicrobial species, both, or inactivated species in solution. With appropriate tools for species identification, it could be possible to select solutions which mostly provide anti-inflammatory activity, provide a combination of anti-inflammatory and antimicrobial activity, and so on. This would be very useful clinically, as the treatments could then be tailored to

individual conditions.

Materials and Methods

Materials

Commercially produced nanocrystalline silver dressings (Acticoat™, Smith and Nephew, PLC, London UK) were used for all dissolution assays, unless otherwise indicated. For dissolution experiments, the dressings were taken apart and the gauze was removed. The dressings were then cut into 2 inch x 2 inch squares.

Setup for Carbonated Water Dissolution Experiments

The setup for the dissolution experiments using carbonated water is shown in Figure 5-1. A CO₂ (99.998%) tank was connected to a flow meter to control the flow of CO₂ to a 250 mL amber glass bottle. The cap of the bottle had holes drilled in it. Passing through the first hole was the tube connected to the flowmeter (Model 7640T, Matheson Tri-Gas, Inc., Basking Ridge, NJ), through which CO₂ enters the bottle. The tube ended in an aerator (Hagen Elite Aqua Fizzz 1 inch Airstone, Rolf C. Hagen, Inc., Montreal, Quebec, Canada) to disperse the CO₂. Passing through the second hole was a pH probe (pH electrode SenTix 42 probe, read with inoLab Terminal 3 pH meter, Mandel Scientific Company, Inc., Guelph, Ontario, Canada). A third hole was used as a vent. A tube could be passed through it and hooked up to a manometer. Passing through the fourth hole was a thermometer, and the fifth hole contained a well-sealed septum through which samples could be obtained, using a needle and syringe,

without breaking the system's seal. The tubes were all sealed to the cap using silicon (Aquarium Sealant, Perfecto Manufacturing, Inc., Noblesville, IN, USA). The flowmeter was calibrated using a Soap Film Flowmeter (Hewlett-Packard (Canada) Co., Mississauga, Ontario, Canada). A bubble of soap was squeezed into the container, and the time for the bubble to travel from the 10 mL to the 100 mL mark (i.e. a 90 mL volume of CO₂) was recorded at different settings on the flowmeter. This data was then used to convert the markings on the flowmeter to flow rates in litres per minute. A linear best fit was performed in Excel to determine the relationship between the height of the ball in the flowmeter and the flow rate. For the silver ball, the relationship was determined to be:

$$\text{Flow rate (L/min)} = 0.0719 * \text{Flowmeter Reading} - 0.1884 \quad (1)$$

and for the black ball, the relationship was determined to be:

$$\text{Flow rate (L/min)} = 0.0382 * \text{Flowmeter Reading} - 0.1069 \quad (2).$$

Experiments were then performed to determine what flow rates of CO₂ to use in order to bubble the water down to a particular pH with the most ease. It was determined that setting the silver ball at a flowmeter reading of 5-6 (0.17 – 0.24 L/min) produced a good flow rate that reduced the pH quickly, without spraying liquid out of the solutions.

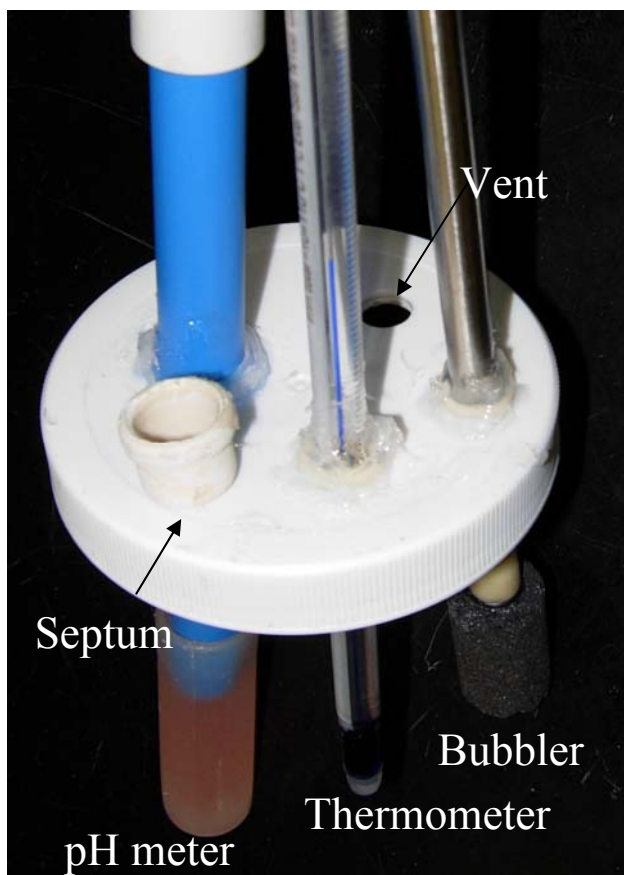


Figure 5-1. Setup for generating and testing nanocrystalline silver-derived solutions. The white cap is sealed onto an amber jar containing distilled water. To generate solutions with a starting pH of 4 or 4.5, CO₂ is bubbled into solution via the bubbler, which is connected via a flowmeter to a CO₂ tank. The vent allows for escape of air and CO₂ during this process. Nanocrystalline silver is added to the solution and the cap is again sealed onto the amber jar. The vent is also sealed off. The pH and temperature can be monitored via the pH meter and thermometer sealed into the system. The septum allows for sampling of the solution during dissolution for obtaining total silver profiles, without breaking the seal.

Procedure for Dissolutions

Dissolutions were performed in distilled water (pH ~5.6), distilled water adjusted to pH 7 or pH 9 using calcium hydroxide, or carbonated water. For pH 7 and pH 9 solutions, a saturated calcium hydroxide solution was added to 200 mL of distilled water drop-wise with stirring, while monitoring the pH. For carbonated water dissolutions, 200 mL of distilled water was added to the amber

glass jar. The CO₂ flow was started at the chosen flow rate (see above). The pH was recorded over time as the CO₂ was bubbled through the water. When the water reached the desired pH (either pH 4.5, or the lowest pH possible attainable, which was ~pH 4 when using CO₂; alternate methods as described were used to generate water at pHs of ~5.6, 7, or 9), the jar was opened and 1 in²/mL (1:1 dissolution) or 1 in²/5 mL (1:5 dissolution) of nanocrystalline silver was added to the jar as quickly as possible. For dissolution under stirring, a magnet was also added at this point and the jar was placed on a magnetic stirrer at 100 rpm. The jar was closed up and the lid was sealed. In initial experiments, the vent tube was hooked up to a manometer, and then the pressure, pH, and/or temperature were recorded over time. However, for most experiments measuring change in pH, the vent was sealed and pH alone was measured. For experiments measuring total silver, a lid with only a septum (sample port) in it was sealed onto the jar.

Spectrophotometric Analysis

Prior to performing any scans, dual beam spectrophotometers' baselines were corrected using paired cuvettes containing identical solutions (typically distilled water). Optical absorbance scans were taken on a UV-1601 (Shimadzu, distributed by Mandel) to scan from high wavelength to low wavelength, and initial scans from low to high wavelength were taken on a Ultrospec 3000 (Pharmacia Biotech, Uppsala, Sweden) at Sherritt Technologies Analytical Laboratory (Fort Saskatchewan, AB). Solutions were made as described above, and 3 mL samples were then taken at select times (e.g. 1 or 24 hours) and scanned immediately. The reference sample used was the solution in which the

nanocrystalline silver was dissolved (e.g. distilled water, or carbonated water at the appropriate starting pH). When concerns arose relative to the performance of the Ultrospec 3000 (Pharmacia) at Sherritt Technologies Analytical Laboratory, tests were performed on a Ultrospec 2000 (Pharmacia), an 8453 UV-Visible Spectrophotometer (diode array, Agilent Technologies, Inc., Santa Clara, CA, USA), and a second Ultrospec 3000 (Pharmacia). Dissolutions of nanocrystalline silver and the resulting optical absorbance scans were also performed using various dilutions of nitric acid, up to 16.25%. As well, dissolutions of nanocrystalline silver were performed as described above for solutions generated in carbonic acid, 5% and 16.25% sodium nitrate, 85% phosphoric acid, glacial acetic acid, glacial acetic acid saturated with sodium nitrate, and 20 g/L ammonium hydroxide. For later scans, high density polyethylene mesh (Delnet, Applied Extrusion Technologies, Inc., Middletown, Del., USA), which is the backing for nanocrystalline silver dressings, was placed in the same quantity as it was present in the nanocrystalline silver dissolutions ($1 \text{ in}^2/\text{mL}$ or $1 \text{ in}^2/5 \text{ mL}$) and left in the solutions for the same amount of time as allowed for the dissolutions (1 hour or 24 hours). This eliminated any peaks due to the high density polyethylene. Scans of 0.1% silver nitrate dissolved in glacial acetic acid and 16.25% nitric acid were also performed.

Effect of Sampling

The effect of taking samples from nanocrystalline silver-derived solution over time was examined. For this, solutions ($1 \text{ in}^2 \text{ Ag}/5 \text{ mL}$) were dissolved in carbonated water (pH 4) or distilled water (pH ~ 5.6) for one or 24 hours without

stirring, as described above. The solutions were then sampled for optical absorbance testing (~ 3 mL) every 10 minutes for 30 minutes, to see if the optical absorbance patterns changed significantly during the time period, which, if true, would suggest that if the solutions were delivered to multiple animals in future tests, the animals might not be receiving the same dose/species of silver. As well, the effect of sampling from different solutions made under identical conditions was tested to see if animals receiving solutions from separate jars, but generated under the same conditions, would be receiving the same treatment.

Spectrofluorimetry

Samples dissolved for one or 24 hours in carbonated water (pH 4) or distilled water (pH ~5.6) (1:5 or 1:1 in² silver:mL solution, unstirred), as above, were taken for analysis using a spectrofluorimeter (PTI Quantamaster fluorescence spectrophotometer, Photon Technology International, Lawrenceville, NJ). For each sample, an excitation scan was performed between 270 nm and 510 nm, followed by an emission scan using an excitation of 300 nm, as selected from the excitation scans. The emission scans were performed from 320 nm to 575 nm. Between samples, cuvettes were either changed or soaked in 25% nitric acid for at least 10 minutes to try to eliminate effects of residual silver. After the samples were scanned, tests were performed to examine the effect of leaving a sample in a cuvette (away from the nanocrystalline silver dressings used to generate the solution) over time. Scans were taken every 10 minutes for half an hour. The effect of rinsing the cuvette with the nanocrystalline silver-containing solutions one time or five times was also tested. Scanning with distilled water after

scanning with nanocrystalline silver solutions was also examined to check for species adsorbed to the cuvette. Scanning was then performed with distilled water after cleaning the cuvette for 10 minutes with dilute nitric acid (25% v/v), followed by scanning with carbonated water only in the cuvette, followed by scanning with distilled water only in the cuvette.

Total Silver Profiles - Atomic Absorption

Total silver profiles were performed on triplicate solutions made as described above (pH 4, 5.6, 7, and 9, stirred or unstirred, 1:5 or 1:1 in² dressing/solution). 1 mL samples were taken via the sample port at 2, 4, 6, 8, 10, 20, 30, 40, 50, 60, 120, 180, 240, 300, 360, and 1440 minutes using fresh needles and syringes for each sample. Samples were stored in sealed plastic containers in the dark until they were taken to Sherritt Technologies Analytical Laboratory (Fort Saskatchewan) for total silver analysis by atomic absorption. There, the samples were diluted in 10% nitric acid (usually a 20 fold dilution was required), and then analyzed using a Varian SpectrAA 200 Atomic Absorption Spectrometer (Palo Alto, CA, USA) with a standard air-acetylene flame and a calibration range of 0-5 mg/L of silver in 10% nitric acid. The results after calculation for the dilution were reported as mg/L total silver in the sample. The triplicate total silver results were averaged.

Ag⁺ Profiles

An Ag⁺ Specific Ion Electrode (SIE, Mandel Scientific, Inc.) was used in preliminary attempts to measure Ag⁺ over time during the dissolution of nanocrystalline silver at different dressing concentrations in water at different

pHs. To do this, dissolutions were performed as described above, and readings (in mV) were taken at 2, 4, 6, 8, 10, 20, 30, 40, 50, and 60 minutes, and at 2, 3, 4, 5, 6, and 24h. The intention was to perform tests in triplicate and average the resulting profiles, measure reference samples with known Ag^+ concentrations in triplicate and used to make a calibration curve, use the calibration curve to convert the mV measurements from experimental solutions to the final Ag^+ profiles, and then subtract the total Ag^+ in solution from the total silver measured in solution by atomic absorption, to provide a measure of the silver in solution which was not in the form of Ag^+ . Unfortunately, the technician performing this assay left the probe in the solution for the entire 24 hour period, resulting in the probe failing after four runs. An Ag^+ Ion Selective Electrode (ISE, Metrohm, distributed by Brinkmann, Canada) was purchased due to reports that it was a more reliable stable probe, with the intention of dipping it in and out of solution for readings, rather than leaving it in continuously. However, the KCl from the reference probe leaked into the solution, causing silver to precipitate and preventing stable readings, even with reference solutions, meaning that the probes could not be calibrated. Sales representatives recommended switching the reference chamber solution to KNO_3 and using an ionic strength adjustment (ISA) solution in both the reference samples and the experimental samples to be measured, at a volume of 3 mL ISA per 50 mL sample/standard (personal communication, Bach Duong, August 20, 2009). While this would be a feasible method of measuring the Ag^+ in solution at a single time point, it could affect the dissolution profile relative to the dissolution occurring when the total silver

profiles were measured, and as the difference between the Ag^+ in solution and the total silver in solution is expected to be small, even minor differences in dissolution pattern could have a significant impact on the results of subtracting the Ag^+ from the total silver to obtain the non- Ag^+ species in solution. Therefore, Ag^+ profiles were not completed as a part of this work. It is possible that if runs were performed in the future in one of the following ways, relevant Ag^+ profiles could be generated:

1. Use an Ag^+ SIE from Mandel, but seal it into the system using a flexible seal such that the probes could be taken in and out of solution during dissolution. Samples should be taken at the same time as the readings are taken in order to keep conditions as close as possible to those used during total silver profiling.
2. Use an Ag^+ ISE from Metrohm, with the KNO_3 solution in the reference probe, and follow the technique of Method 1 (i.e. do not add an ISA to references or samples).
3. Use an Ag^+ ISE from Metrohm, generate a different solution for each time point (sampling at correct times up to that time point to match solutions generated for total silver profiles), add an ISA and make the Ag^+ measurement. This would require far more time and resources than the other two methods, and adding the ISA would cause a slight dilution of the solution which would need to be accounted for.

Antimicrobial Activity

Dissolutions were performed under the conditions described above (carbonated water – pH 4, distilled water, or calcium hydroxide-adjusted water – pH 7 or 9, stirred or unstirred, at one or 24 hours, with in^2 Ag/mL ratios of 1:5 or 1:1), and tests were performed to determine the antimicrobial activity of these solutions. The bacterial strains used were *Staphylococcus aureus* (ATCC 25923) and *Pseudomonas aeruginosa* (ATCC 27317). A log reduction assay was used to determine the ability of the nanocrystalline silver-derived solutions to kill bacteria in 30 min. The method used was similar to that used by Taylor *et al.*[26], with modifications due to the fact that liquids were being tested in this assay, rather than dressings.

For all assays, 1 mL of bacteria, obtained from a culture grown overnight in tryptic soy broth (TSB) at 37°C (created by adding three colonies from a streak plate or 1 mL from a previous culture flask to 100 mL broth), was added to 100 mL of TSB and incubated at 37°C for three to five hours to obtain a bacterial culture in the log phase of growth.

Since there is no standard dilution at which to test silver solutions with bacteria, preliminary testing was performed to determine what dilution should be used for log reduction assays of these solutions. For this assay, nanocrystalline silver solutions were dissolved at a ratio of 1 in^2 per 5 mL carbonated water (pH 4) for one hour without stirring. The test solution was then added to log phase *Pseudomonas aeruginosa* at different dilutions: 1%, 2.5%, 5%, 7.5%, and 10% v/v bacteria. This solution was then incubated for half an hour at 37°C. After

removing the solutions from the incubator, they were vortexed, and immediately 0.2 mL of the solution was added to 1.8 mL of a salt/polysorbate/sodium thioglycollate (SPS, 0.85% [w/v] NaCl, 1% [v/v] polysorbate 20, and 0.1% [w/v] sodium thioglycolate for *P. aeruginosa*) bacterial recovery solution which also inactivates the silver. The solution was then vortexed again and the resulting bacterial recovery solutions (which were 10^{-1} dilutions of the inoculum plus silver solutions) were serially diluted in phosphate-buffered saline (PBS; pH 7.0, containing 8.5 g/L NaCl, 0.61 g/L KH_2PO_4 , and 0.96 g/L K_2HPO_4) out to 10^{-6} . From each of these dilutions, 20 μL was dropped onto Mueller Hinton agar in triplicate using a drop plate technique. The plates were then incubated at 37°C . After 24 and 48 hours, the numbers of bacterial colonies were counted, and these counts were then used to calculate the surviving CFUs. The numbers of bacterial CFUs in the original inoculum were determined using serial dilutions (including an original dilution in the solution used to dissolve the nanocrystalline silver, i.e. 1%, 2.5%, 5%, 7.5%, or 10% bacteria (v/v) in carbonated water (pH 4)), plated on Mueller Hinton agar as above, and grown at 37°C . The log reductions were calculated as the difference between the log of the initial number of bacteria and the log of the final surviving number of bacteria. Based on this test, it was determined that a 99% silver solution (v/v) consistently provided sufficient silver in the test solution to produce a total kill in half an hour (Figure 5-2), which corresponded to a log reduction of 3.5, the highest log reduction measurable within the detection limit of the experiment.

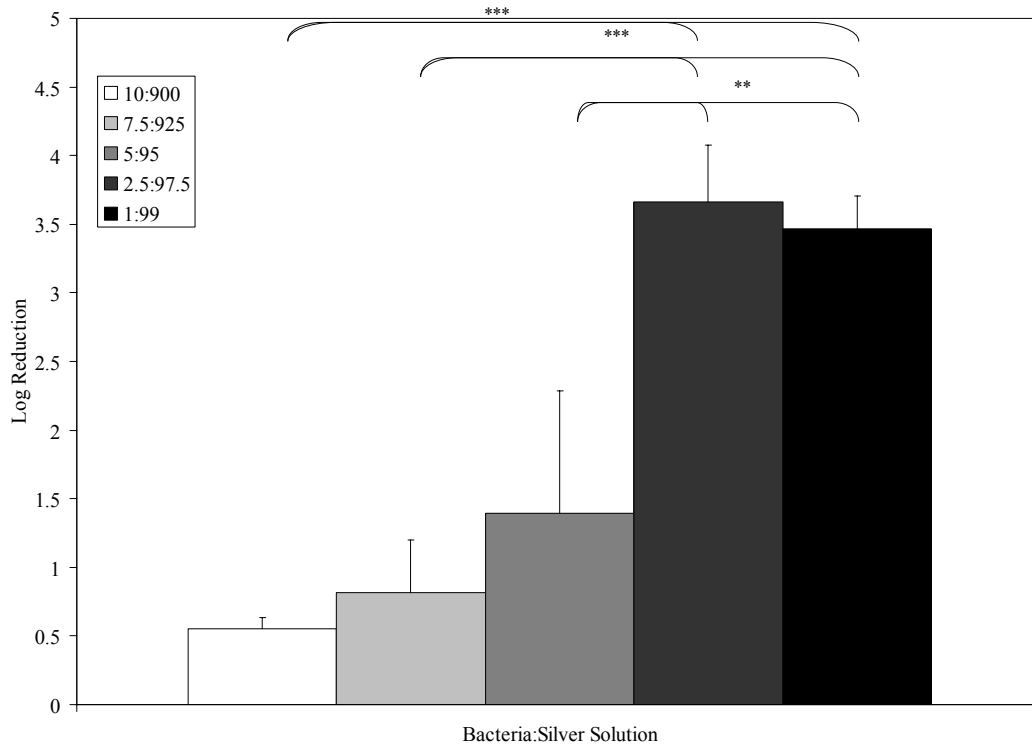


Figure 5-2. Initial testing of the antimicrobial activity of nanocrystalline silver-derived solutions. Solutions were allowed to dissolve for one hour at a starting pH of 4, unstirred, with a ratio of 1 in² nanocrystalline silver dressing per milliliter of solution. Log reductions were then performed using *P. aeruginosa* with bacteria:solution ratios of 10:900, 7.5:925, 5:95, 2.5:97.5, and 1:99. Error bars show standard deviation. The p-value from the one-way ANOVA testing was <0.0001. Significant differences between groups, determined by Tukey-Kramer Multiple Comparisons post-testing, are indicated on the graph, where ** indicates p<0.01, and *** indicates p<0.001. Error bars represent standard deviations (n=3 for all data points).

Based on these results, for all future testing, 4.95 mL of the silver containing solution to be tested was added to 50 µL of the log phase bacteria. The starting CFU varied with the day of the assay, and therefore the highest detectable log reduction within the limit of the assay varied as well. The solution was processed as above, with the only exception being that the salt/polysorbate/sodium thioglycolate solution was changed to 6.0% (w/v) NaCl, 1% (v/v) polysorbate 20, and 0.1% (w/v) sodium thioglycolate when *S. aureus* was used, to provide better recovery of the organisms[27].

Effect of Dissolution on Nanocrystalline Silver Dressings

3 in² of nanocrystalline silver dressing were aseptically placed in sterile polyethylene cups which were wrapped in aluminum foil and contained 15 mL of one of the following solutions:

- Reverse osmosis water (nominal pH 5.6)
- Reverse osmosis water adjusted to a pH of 4 using HCl
- Reverse osmosis water adjusted to a pH of 9 using NaOH
- Fetal calf serum

The cups were sealed and placed at 35°C. Control dressings were placed at 35°C in dry sealed cups, i.e. they were left unexposed to solutions. After 2, 4, 8, 16, or 24 hours, samples were removed from solution, allowed to drip for 10 seconds, and then placed on aluminum foil in the biosafety cabinet and allowed to dry.

The samples were then stored in aluminum foil-wrapped plastic bags at 4°C until they were analyzed further.

Scanning Electron Microscopy (SEM). SEM analysis of the dressings after dissolution was performed using a Hitachi S-4800 field emission SEM (FE-SEM) at CanmetENERGY, NRC, Devon. Samples were attached to a specimen mount using an isopropanol-based graphite paste. Samples were not cleaned prior to imaging, to prevent alteration of the nanostructure. Images were taken at 200 000x magnification, using an accelerating voltage of 5 kV, a working distance of about 2-4 mm, and a low emission current.

X-ray Photoelectron Spectroscopy (XPS). XPS of the dressings after dissolution was completed using an Axis Ultra spectrometer (Kratos Analytical, at

the Alberta Centre for Surface Engineering and Science (ACSES) at the University of Alberta) with a base pressure of 5×10^{-10} Torr. The x-rays were generated by an Al Mono ($K\alpha$) source operated at 210 W. The spectra were collected at normal (90°) take-off angle. For the survey spectra, the analyzer pass energy was 160 eV, and for the high-resolution spectra, the pass energy was 20 eV. A linear background and a Gauss/Lorentz component approximation were used in data processing performed using CasaXPS software (Version 2.3.9, © 1999-2005 Neal Fairley). Atomic concentrations of species were determined from the peak areas. No charge corrections to the binding energy values were introduced.

X-ray Diffraction (XRD). XRD of the dressings after dissolution was performed on a Bruker D8 diffractometer equipped with $CoK\alpha$ and double multilayer mirrors in a parallel beam configuration. Diffraction data were collected between 15 and $101^\circ 2\theta$. Using boron lanthanum (NIST 660) as an instrument standard, the composition, mean microstrain and crystallite size of the crystalline phases were evaluated using TOPASTM, a Rietveld refinement software (Bruker-axs, ©2003). The microstructural analysis implemented in TOPAS entails direct convolution of the instrument and sample contributions to the diffraction profiles followed by the double integral method of Balzar[28] to separate the crystallite size from the mean microstrain effect.

Effect of Storage Under Vacuum. Select nanocrystalline silver dressings which had undergone the dissolution protocol were subsequently left in the S-4800 SEM sample chamber under vacuum for up to 96 hours. The samples were

then re-imaged using the SEM (control samples), or XRD was performed on them (pH 4, pH 9, or serum-dissolved samples), as described above.

Statistics

One-way ANOVAs with Tukey–Kramer Multiple Comparisons post tests were performed using GraphPad InStat version 3.06 (GraphPad Software, San Diego, California, USA, © 2003, www.graphpad.com). Where only two groups were compared, unpaired t-tests with Welch corrections were performed, also using GraphPad InStat version 3.06. Standard deviations were plotted as error bars for all data points on appropriate figures.

Results and Discussion

Spectrophotometric Analysis

Scans performed from high wavelength to low wavelength using the UV-1601 on solutions generated unstirred using a ratio of 1:5 in² Ag/mL at starting pHs of 4, 4.5 and 5.6 and a dissolution time of 24 hours are shown in Figure 5-3. Characteristic peaks at 200-220 nm were observed, which increased with decreasing pH. The peak height showed a logarithmic correlation with the total silver present in solution at the time of sampling (Figure 5-4). This suggests that perhaps in the future, the absorbance at ~210 nm could be used as a measurement of total silver in solution, as a replacement for AAS.

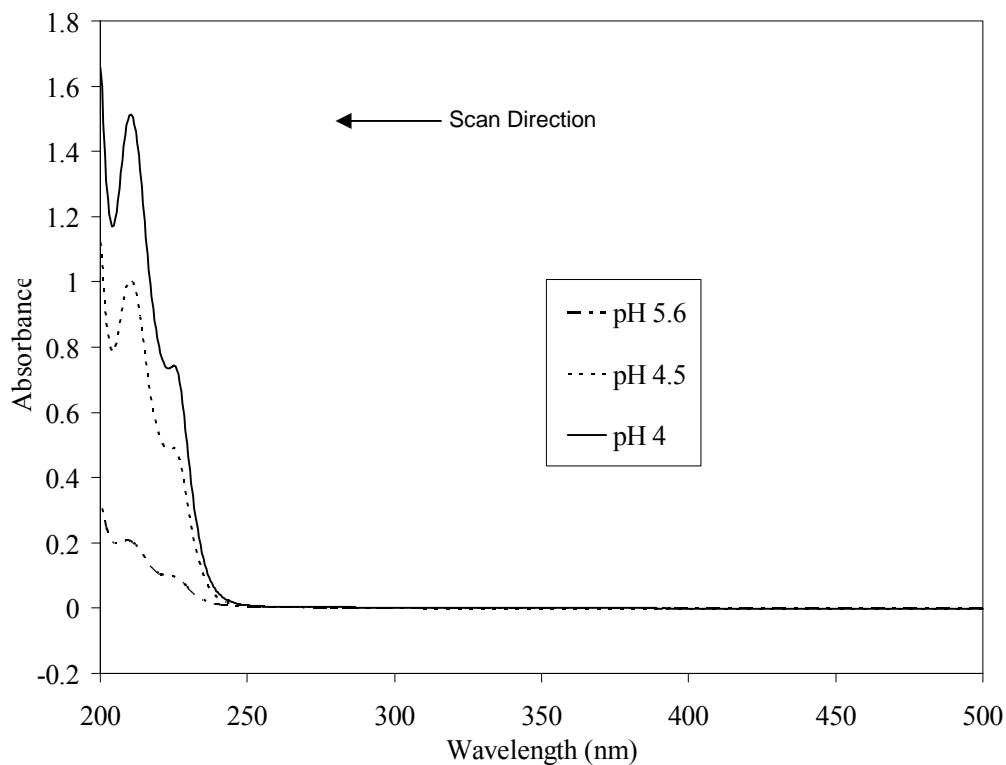


Figure 5-3. Example of effect of starting pH on absorbance of nanocrystalline silver-derived solutions. Nanocrystalline silver ($1 \text{ in}^2 \text{ Ag}/5 \text{ mL}$ solution) was allowed to dissolve in solutions with starting pHs 4 and 4.5 (generated using CO_2) or in distilled water (nominally pH 5.6). Dissolution continued until the pH appeared to stabilize (24 hours at pH 4, 48 hours at pH 4.5, and 72 hours at pH 5.6 – later it was determined that this was not a true equilibration). Solution samples were then scanned spectrophotometrically using a UV-1601, scanning from 500 to 200 nm, with solutions of matching starting pHs in the reference cell.

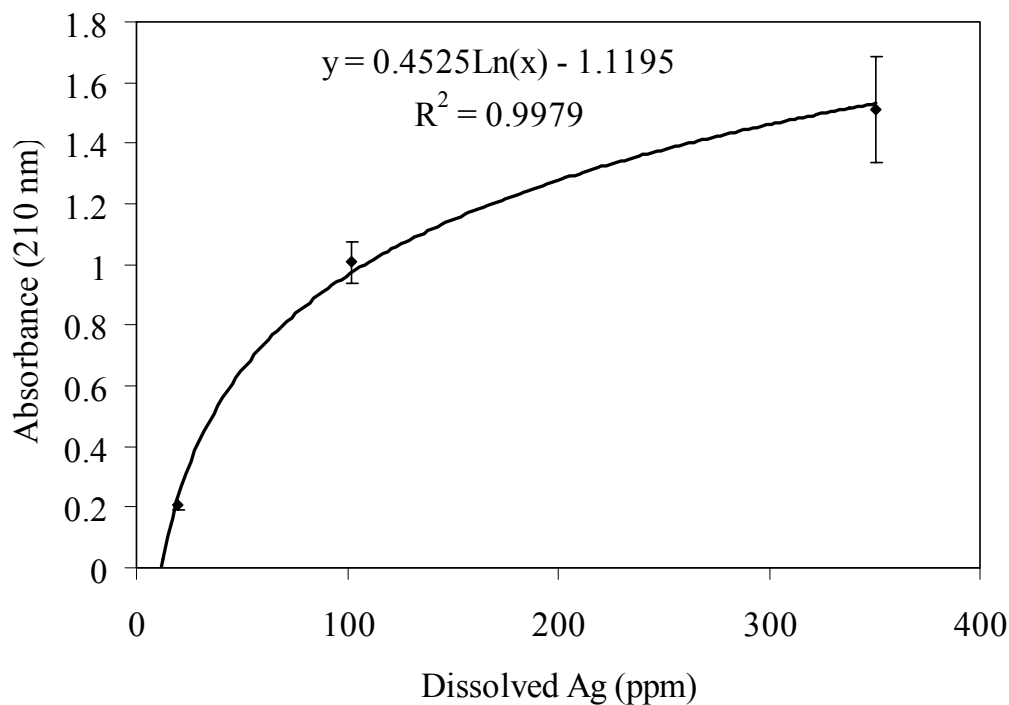


Figure 5-4. Relationship between peak height at 210 nm in spectrophotometric scans and total silver in nanocrystalline silver-derived solutions. Solutions generated at starting pHs of 4, 4.5, and 5.6, unstirred, with a ratio of 1:5 in^2/Ag , were scanned at using a UV-1601, and the absorbance peak height at 210 nm was measured. At the same time, samples of solution were submitted for AAS to determine the total silver in the solutions. The total silver was then compared to the absorbance peak height, and the equation describing the relationship is shown on the figure. Error bars represent standard deviations ($n=3$ for all data points).

When solutions were scanned from low wavelength to high wavelength using the Ultrospec 3000, similar behavior was observed at 210 nm (not shown). However, between 300 and 550 nm, spikes were reproducibly observed in patterns which were different for different dissolution conditions. Spikes observed for solutions generated at a 1:5 ratio $\text{in}^2 \text{Ag/mL}$ and allowed to dissolve unstirred for 24 hours at starting pHs of 4, 4.5, and 5.6 are shown in Figures 5-5 through 5-7, respectively. Since the spikes observed went down as well as up, this suggested an emission of light after absorption of light energy, possibly due to fluorescence. It was hypothesized that the emissions occurring at different

wavelengths corresponded to fluorescence by different sized clusters of silver, as studies in fluorescent noble metal nanoclusters have demonstrated a correlation between size and wavelength of fluorescence[16, 18]. However, it should be noted that in the literature, fluorescence and optical absorbance patterns observed due to gold and silver nanoclusters occurred not as spikes, but rather as broader peaks with widths of over 50 nm[17, 29].

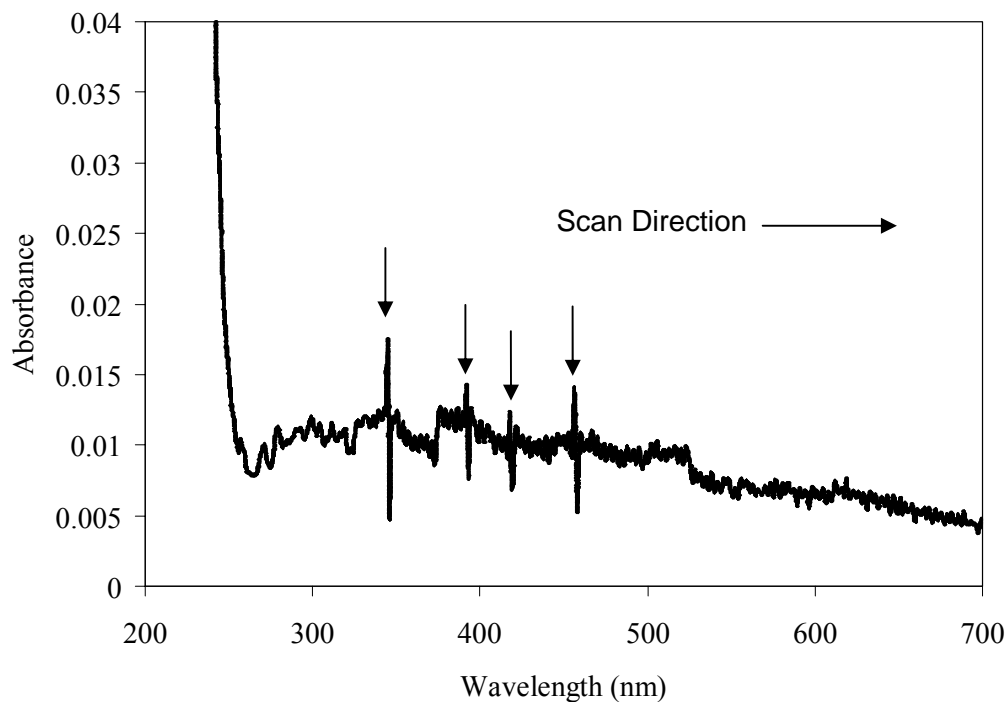


Figure 5-5. Example of spikes generated from a nanocrystalline silver-derived solution started at pH 4 using an Ultrospec 3000. A solution was generated by dissolution of 1:5 nanocrystalline silver:solution (mL) at a starting pH of 4 without stirring for 24 hours. A solution sample was scanned using an Ultrospec 3000 from 200 to 700 nm. Spikes are indicated with arrows. A pH 4 solution generated using CO₂ was used as a reference.

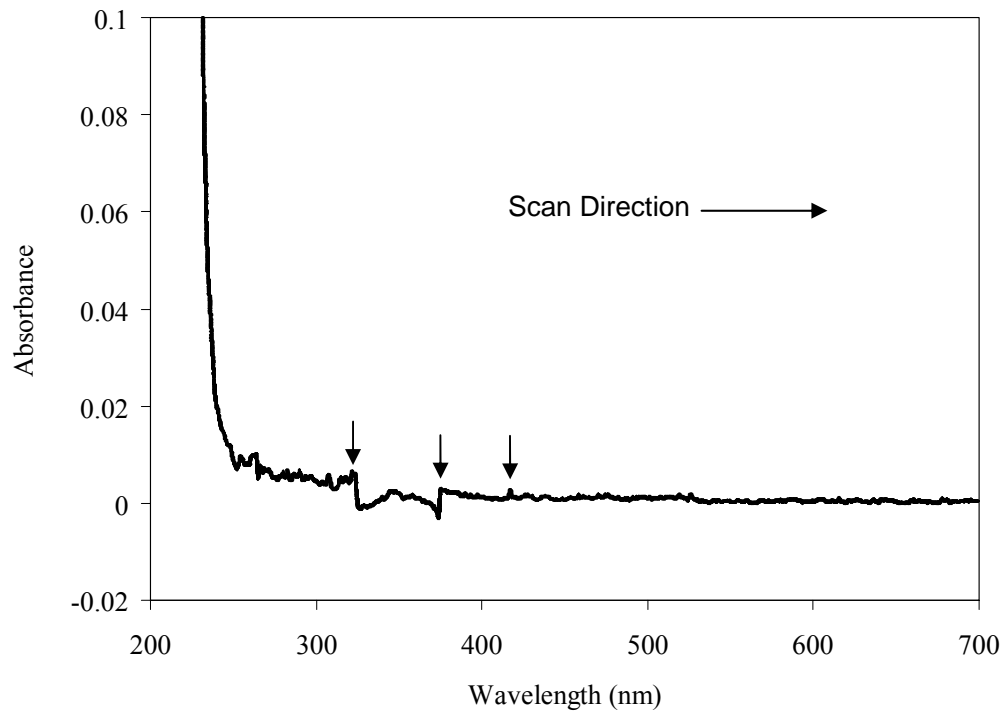


Figure 5-6. Example of spikes generated from a nanocrystalline silver-derived solution started at pH 4.5 using an Ultrospec 3000. A solution was generated by dissolution of 1:5 nanocrystalline silver:solution (mL) at a starting pH of 4.5 without stirring for 24 hours. A solution sample was scanned using an Ultrospec 3000 from 200 to 700 nm. Spikes are indicated with arrows. A pH 4.5 solution generated using CO₂ was used as a reference.

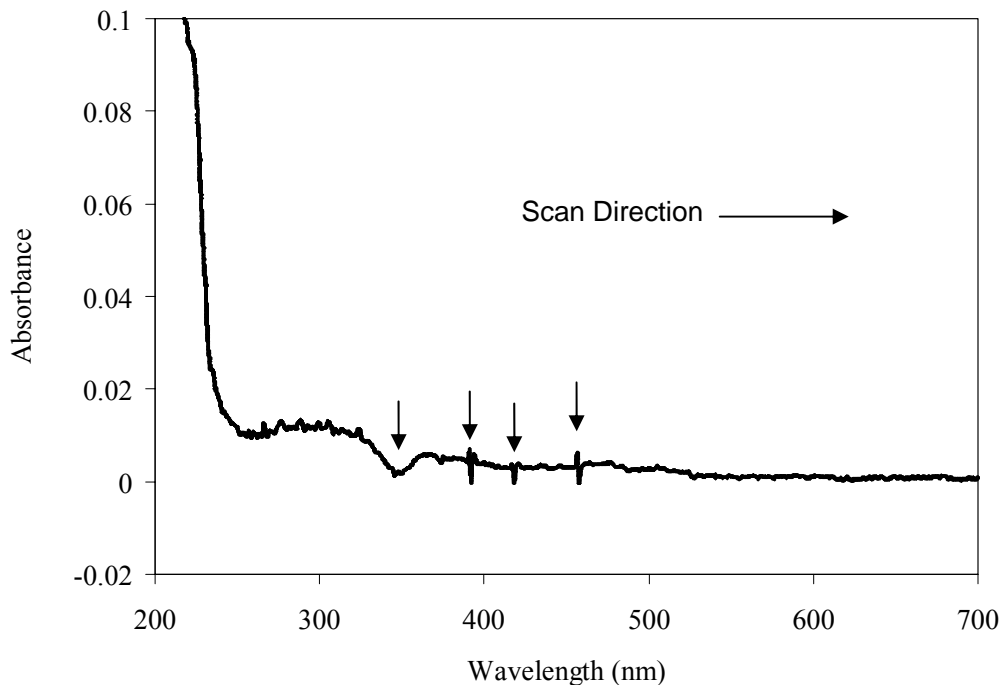


Figure 5-7. Example of spikes generated from a nanocrystalline silver-derived solution started at pH 5.6 using an Ultrospec 3000. A solution was generated by dissolution of 1:5 nanocrystalline silver:solution (mL) at a starting pH of 5.6 without stirring for 24 hours. A solution sample was scanned using an Ultrospec 3000 from 200 to 700 nm. Spikes are indicated with arrows. Distilled water (pH 5.6) was used as a reference.

It was thought that when scanning from high to low, these apparently emissive spikes were overwhelmed as the machine scanned at higher energy wavelengths, explaining why they would appear when scanning one direction on a spectrophotometer, but not the other. Attempts were made to quantify and compare the spikes by spike absorbance height, emission depth, width, spacing, horizontal shifts etc. There appeared to be larger emissions, as well as more emissions, and better consistency of the shape and spacing of the emissions when solutions were generated at a starting pH of 4.0 (statistics not shown). Based on these results, it was hypothesized that more active fluorescent species were dissolved at that pH, since, based on the observations made by the Dickson group

and others[15, 16, 19, 29], the appearance of fluorescence would indicate that small clusters of silver atoms were being dissolved into solution, and particularly so at lower pHs. Thus, from the hypothesis described in the introduction connecting silver clusters to anti-inflammatory activity,[10, 11] this would suggest that more anti-inflammatory species were being made available in solutions generated at lower starting pHs.

As it seemed possible that the strength of the emissions produced would be related to the quantity of anti-inflammatory fluorescent species present in solution, attempts were made to increase the signal strength, focusing on pH 4, due to the stronger signals observed. The ratio of silver to solution was increased to 1:1, and different dissolution times were tried, both shorter (one hour) and longer (up to weeks), but no clear increases in emission strength were observed (data not shown). The strongest signals appeared to be present when solutions were generated at a starting pH of 4, 1:5 in² Ag/mL, unstirred, with a dissolution time of 24 hours. This was part of the reason for the conditions selected for the solution chosen in the anti-inflammatory rat study performed at HSLAS in Chapter 6, before better data was available.

It was observed that when a cuvette had nanocrystalline silver-derived solution in it, and the solution was replaced by plain distilled water and scanned again, or the cuvette was scanned empty, the spikes remained (although the silver absorbance peaks around 210 nm were gone, as expected), suggesting that some of the optically active species had adsorbed to the cuvette walls (for example, see Figure 5-8). Attempts were made to build up these spikes observed when the

cuvettes were scanned empty or with water in them after exposure to nanocrystalline silver-derived solutions, as this would presumably mean the buildup of fluorescing species on the cuvettes. It was hoped that if the signals could be built up, a similar procedure could be used to concentrate the species on a quartz slide which could then be examined under atomic force microscopy, possibly allowing for the identification/sizing of any silver clusters which might be fluorescent and therefore potentially have anti-inflammatory properties. However, neither multiple rinses of the cuvettes in nanocrystalline silver-derived solutions nor extended soaking of the cuvettes in the nanocrystalline silver-derived solutions (for up to 56 hours) resulted in increased spike strength (data not shown).

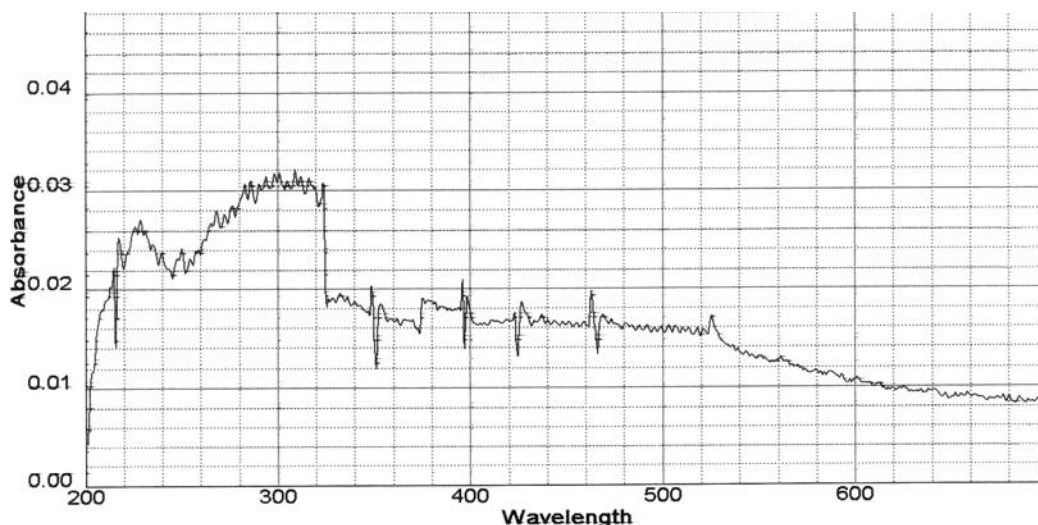


Figure 5-8. Example of spikes generated in a quartz cuvette after it held a nanocrystalline silver-derived solution started at pH 5.6 using an Ultrospec 3000. A solution was generated by dissolution of 1:5 nanocrystalline silver:solution (mL) at a starting pH of 5.6 without stirring for 56 hours. A quartz cuvette was in the solution for the entire dissolution process. A solution sample was scanned using an Ultrospec 3000 from 200 to 700 nm in the quartz cuvette. The quartz cuvette was then emptied, rinsed with distilled water, and scanned empty, from 200 to 700 nm.

By the end of these experiments, the Ultraspec 3000 being used began to demonstrate baseline instability, and there began to be changes in terms of the number of spikes present. Then the baseline for a clean cuvette showed some of the spikes which had only been observed previously with the nanocrystalline-silver derived solutions. At this point, the behavior of the machine was questioned. Scans on an Ultrospec 2000, which also scans from low to high wavelength did not show spikes (see Figure 5-9). 15 scans in a row were performed on solutions using this machine to see if photoactivating the solutions resulted in spikes, but this was not observed (see Figure 5-10). 15 scans were run from high wavelength to low wavelength as well, using the UV-1601, with the same result as Figure 5-10 (data not shown). Solutions generated at pH 4 and pH 5.6 (see Figures 5-11 and 5-12, respectively) were scanned using a diode array, which scans all wavelengths simultaneously, and no spikes were observed. Finally, a second Ultrospec 3000 was found and the same solutions were scanned. Again, no spikes were observed (see Figures 5-13 and 5-14). This indicated that the spikes observed using the Ultrospec 3000 at Sherritt Technologies were specific to that machine. Although they were reproducible, appeared to be specific to solutions derived from nanocrystalline silver (personal communication, Qin Fu, July 5, 2007), and appeared to vary with dissolution conditions in a measurable way, they were not related to absorbance/emission properties of the solutions.

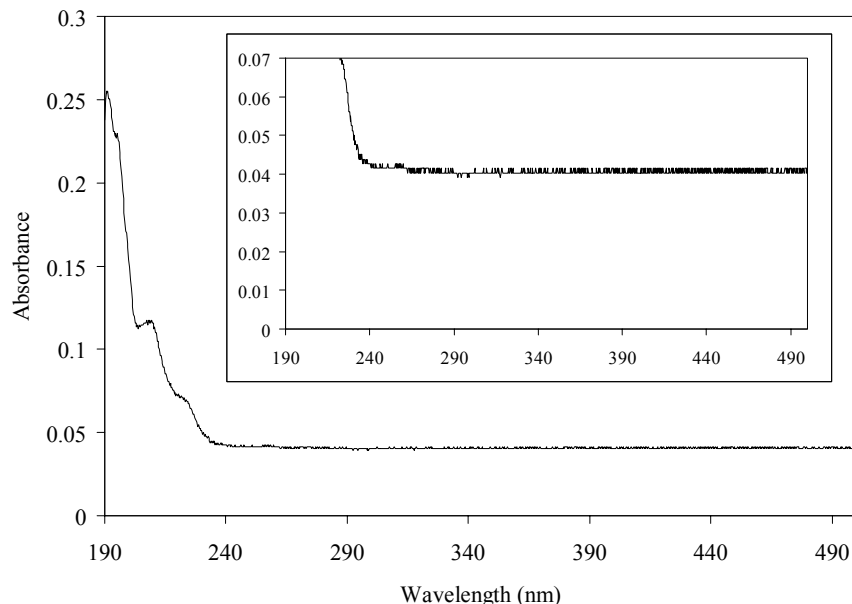


Figure 5-9. Example of a spectrophotometric scan of a nanocrystalline-silver derived solution using an Ultrospec 2000. A solution was generated by dissolution of 1:5 nanocrystalline silver:solution (mL) at a starting pH of 5.6 without stirring for 24 hours. A solution sample was then scanned using an Ultrospec 2000 from 190 to 500 nm, with distilled water as the reference. The inset shows a close-up of the scan. No spikes were observed.

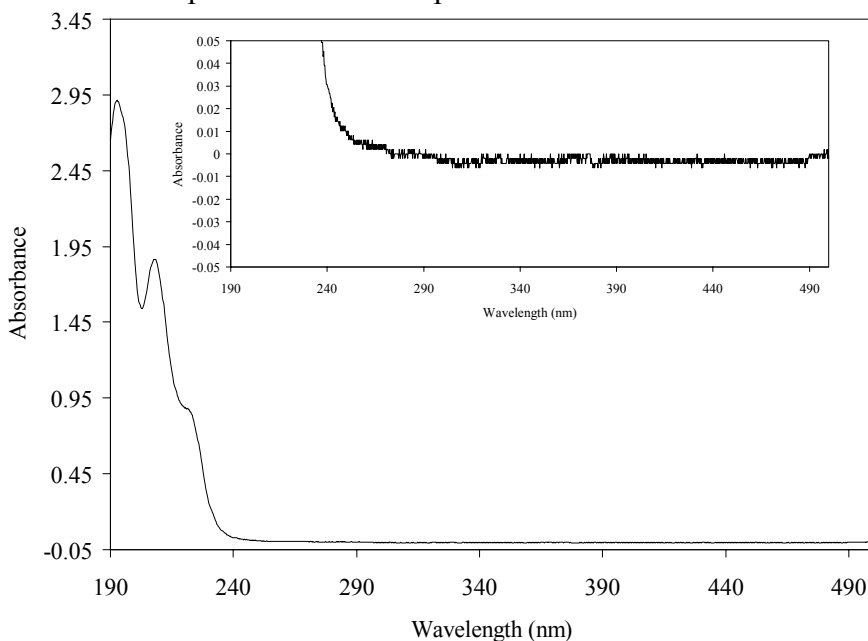


Figure 5-10. Effect of multiple spectrophotometric scan on a nanocrystalline-silver derived solution. A solution was generated by dissolution of 1:1 nanocrystalline silver:solution (mL) at a starting pH of 4 without stirring for 24 hours. A solution sample was then scanned using an Ultrospec 2000 from 190 to 500 nm 15 times, with pH 4 carbonated water as a reference. The 15th time is shown here. The inset shows a close-up of the baseline of the scan. No spikes were observed, nor was there evidence of a photochemical reaction.

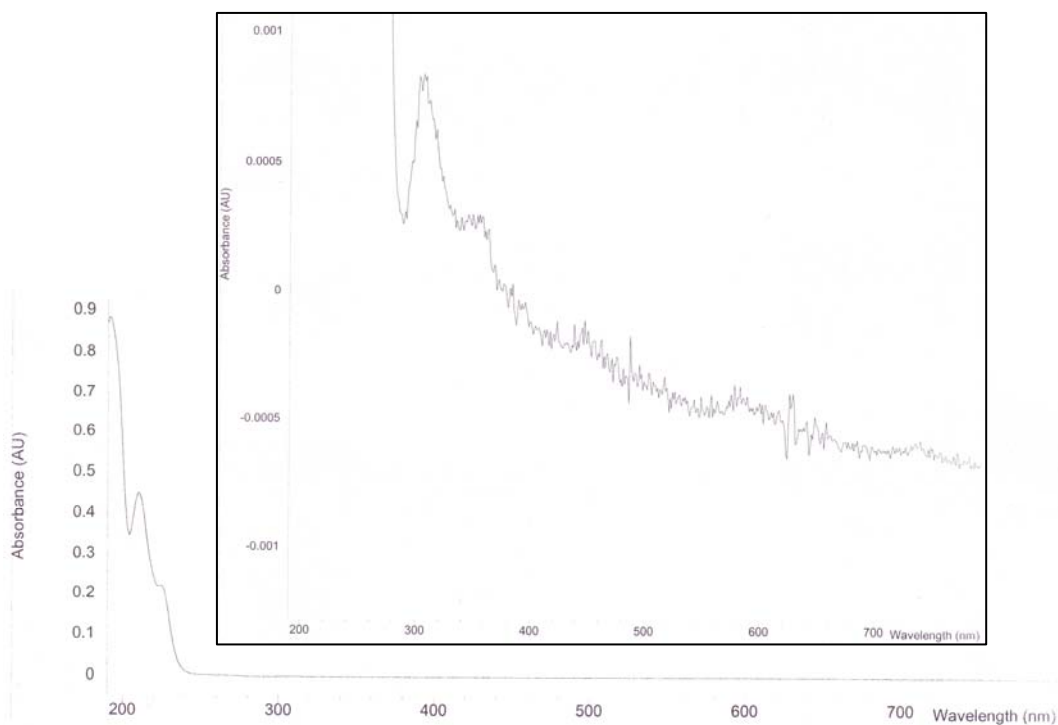


Figure 5-11. Spectrophotometric analysis of a nanocrystalline-silver derived solution, generated at a starting pH of 4, performed using a diode array. A solution was generated by dissolution of 1 in² nanocrystalline silver per milliliter of solution at a starting pH of 4, without stirring, for one hour. A solution sample was then analyzed using an 8453 UV-Visible Spectrophotometer over a range of 200-700 nm, using pH 4 carbonated water as a reference. The inset shows a close-up of the baseline of the scan. No spikes were observed.

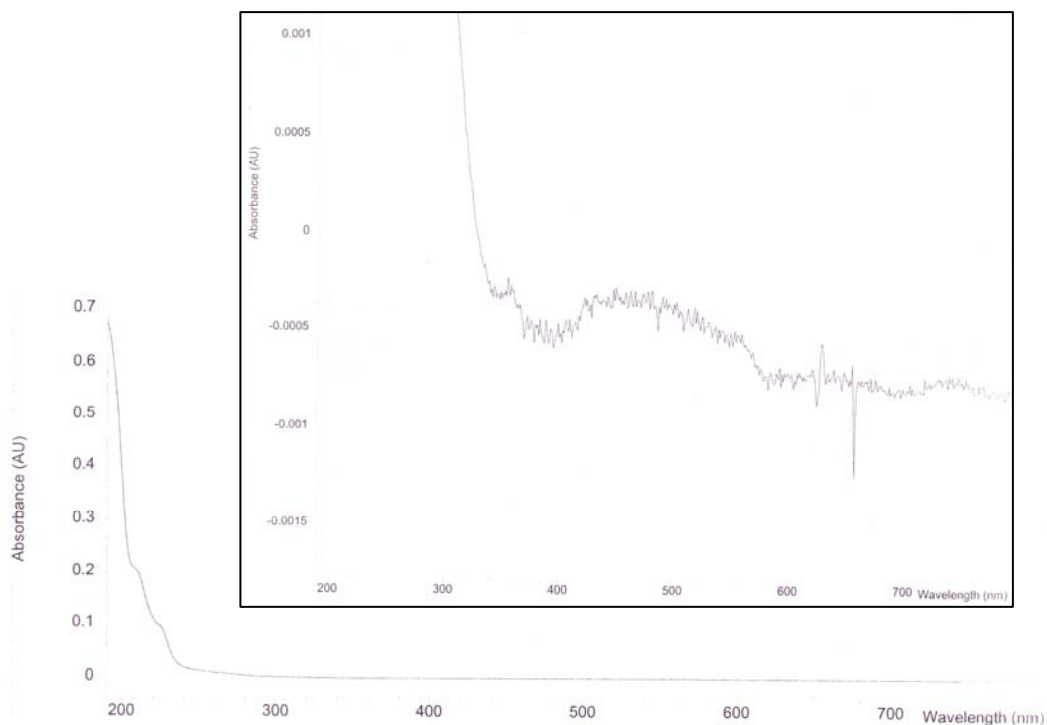


Figure 5-12. Spectrophotometric analysis of a nanocrystalline silver-derived solution, generated at a starting pH of 5.6, performed using a diode array. A solution was generated by dissolution of 1 in² nanocrystalline silver per milliliter of solution at a starting pH of 5.6, without stirring, for 24 hours. A solution samples was then analyzed using an 8453 UV-Visible Spectrophotometer over a range of 200-700 nm, with distilled water as a reference. The inset shows a close-up of the baseline of the scan. No spikes were observed.



Figure 5-13. Spectrophotometric scan of a nanocrystalline silver-derived solution, generated at a starting pH of 4, using an Ultrospec 3000. A solution was generated by dissolution of 1 in² nanocrystalline silver per milliliter of solution at a starting pH of 4, without stirring, for one hour. A solution sample was then analyzed using an Ultrospec 3000 from 190-900 nm, with pH 4 carbonated water as a reference. No spikes were observed. Changes in signal at 330 nm and 800 nm are filter changes.

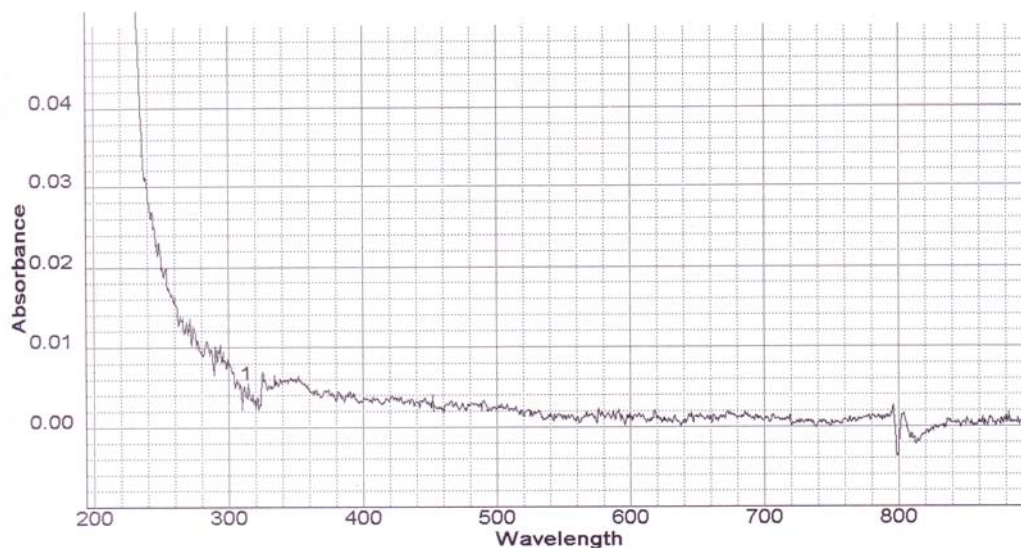


Figure 5-14. Spectrophotometric scan of a nanocrystalline silver-derived solution, generated at a starting pH of 5.6, using an Ultrospec 3000. A solution was generated by dissolution of 1 in² nanocrystalline silver per milliliter of solution at a starting pH of 5.6, without stirring, for 24 hours. A solution sample was then analyzed using an Ultrospec 3000 from 190-900 nm, with distilled water as a reference. No spikes were observed. Changes in signal at 330 nm and 800 nm are filter changes.

During initial examination of the spikes observed using the Ultrospec 3000, a few runs were performed in which nanocrystalline silver was dissolved in various concentrations of nitric acid. A very different set of peaks was observed in this case, obscuring the region where the spikes were originally observed (see Figure 5-15), and this set of peaks seemed to decrease in size with extended dissolution time (Figure 5-16), suggesting that the species causing these peaks reached a maximum level, and then reacted gradually to form species without the same optical activity. Further analyses were performed in order to understand the peaks observed when nitric acid was used for dissolving the nanocrystalline silver instead of carbonated water, since it resulted in very different optical properties. The peaks were not due to nitric acid or nitrates in general, because a nitric acid reference was used for the scan in Figure 5-15, the peaks present in a scan of

nitric acid are very different from those observed in Figure 5-15 (Figure 5-17), and a scan of sodium nitrate produced peaks similar to a scan of nitric acid (Figure 5-18). The signal was not due to the combination of Ag^+ and nitrates, as scans for silver nitrate (Figure 5-19) showed peaks present at the same locations as the scans of nitric acid or sodium nitrate.

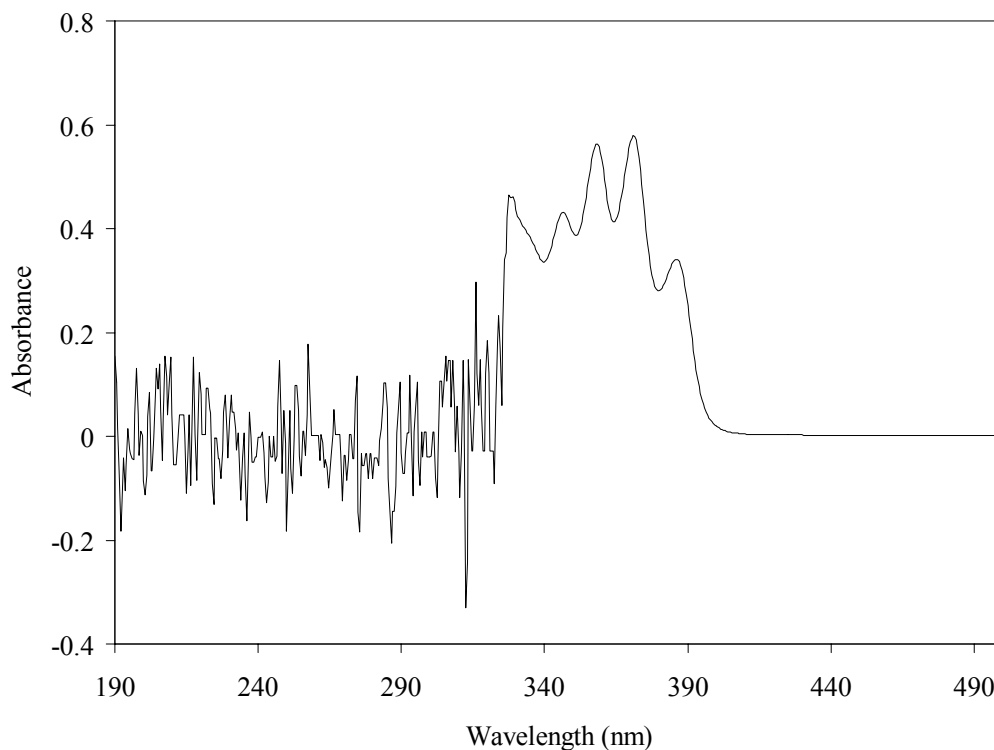


Figure 5-15. Spectrophotometric scan of nanocrystalline silver dissolved in nitric acid for one hour. A solution was created by the dissolution of 1 in² nanocrystalline silver per milliliter of 16.25% nitric acid (diluted in distilled water) for one hour, unstirred. This solution was then analyzed using a UV-1601, with 16.25% nitric acid in the reference cell.

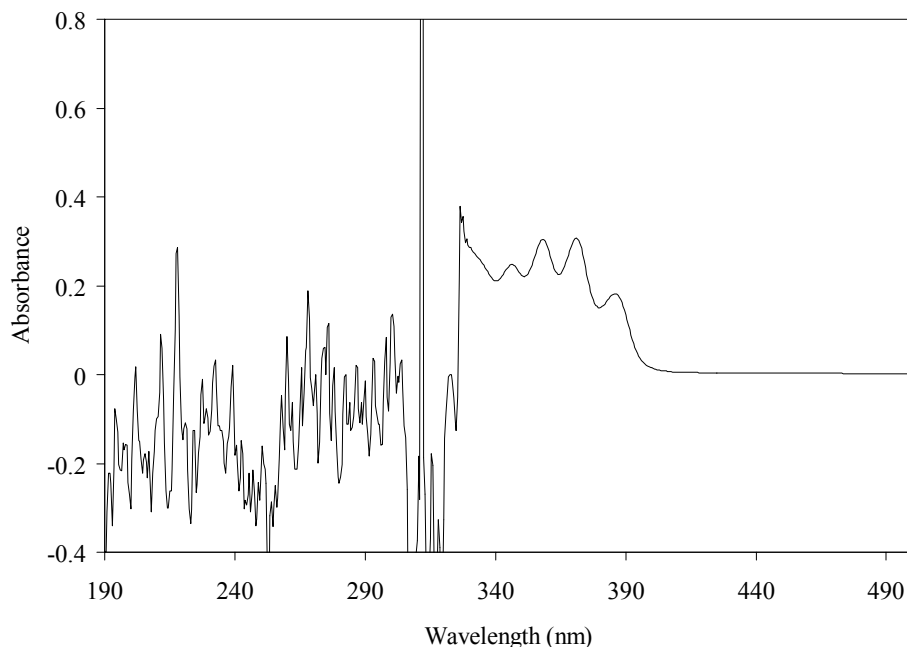


Figure 5-16. Spectrophotometric scan of nanocrystalline silver dissolved in nitric acid for 17 hours. A solution was created by the dissolution of 1 in² nanocrystalline silver per milliliter of 16.25% nitric acid (diluted in distilled water) for 17 hours, unstirred. This solution was then analyzed using a UV-1601, with 16.25% nitric acid in the reference cell.

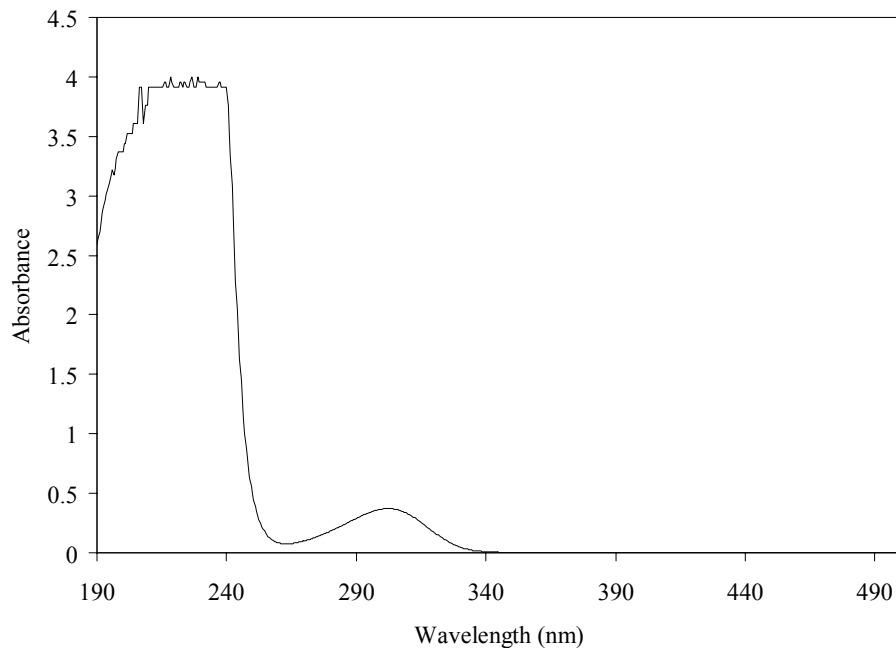


Figure 5-17. Spectrophotometric scan of 0.25% nitric acid. 16.25% nitric acid was diluted 1:1 six times and scanned using a UV-1601, with distilled water in the reference cell.

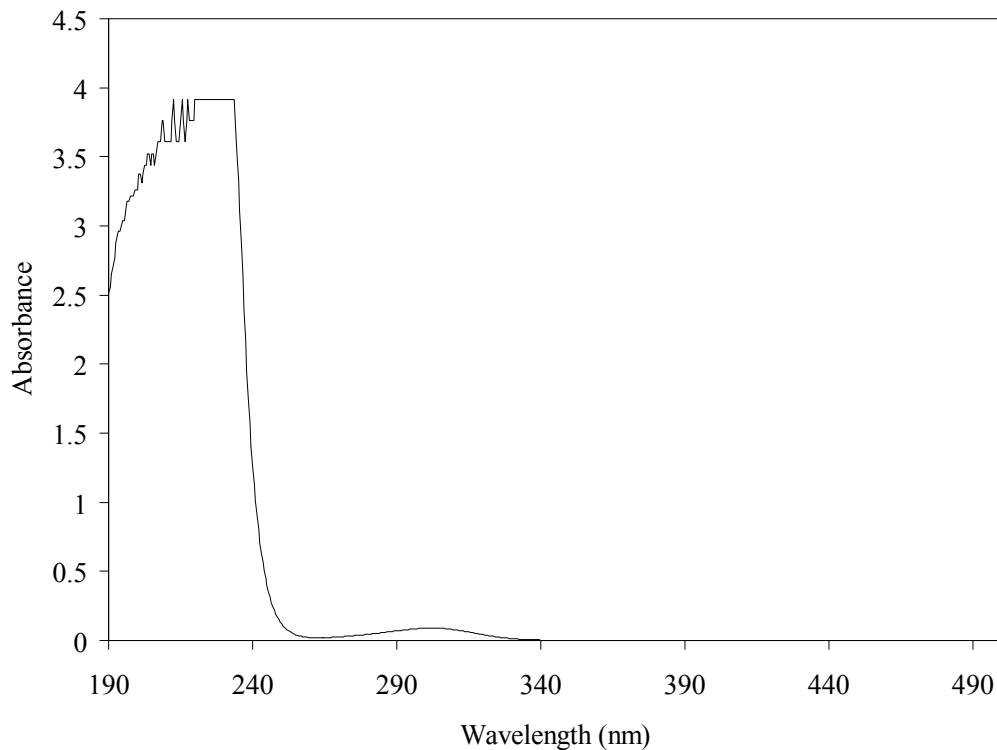


Figure 5-18. Spectrophotometric scan of sodium nitrate. 0.1% sodium nitrate was scanned using a UV-1601, with distilled water in the reference cell.

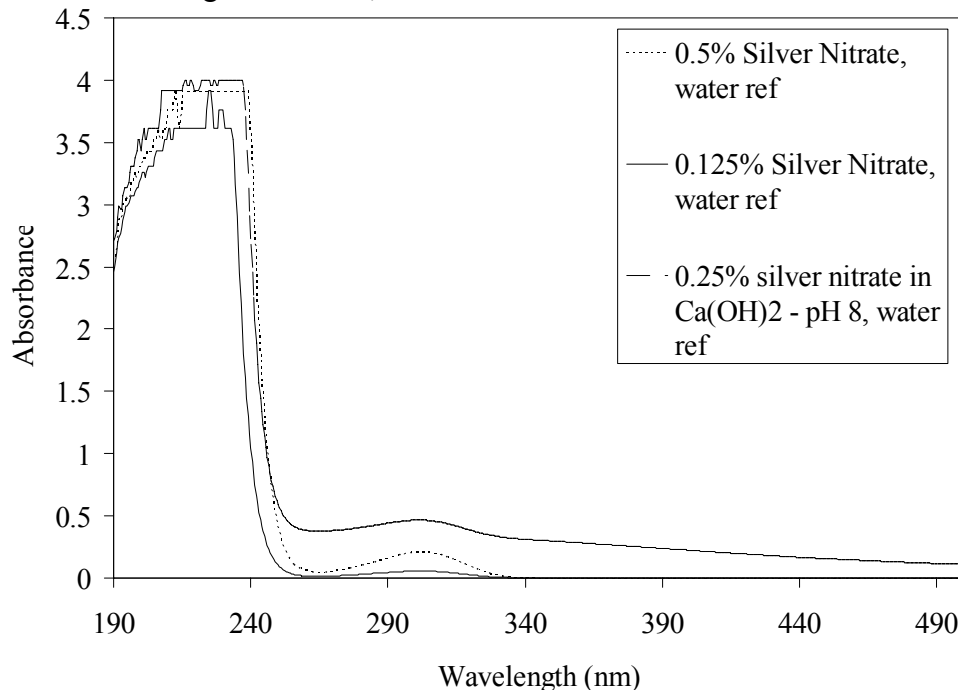


Figure 5-19. Spectrophotometric scans of silver nitrate. 0.5% silver nitrate, 0.125% silver nitrate, and silver nitrate adjusted to pH 8 using calcium hydroxide (resulting in a final concentration of approximately 0.25% silver nitrate), were scanned using a UV-1601, with distilled water in the reference cell.

(As an aside, scans were performed on silver nitrate dissolved in solutions containing calcium hydroxide (see Figure 5-19) or sodium hydroxide (Figure 5-20), as silver nitrate dissolved under basic conditions can sometimes show unusually high antimicrobial activity (personal communication, Dr. Robert Burrell). However, the scans did not show any unusual optical properties.)

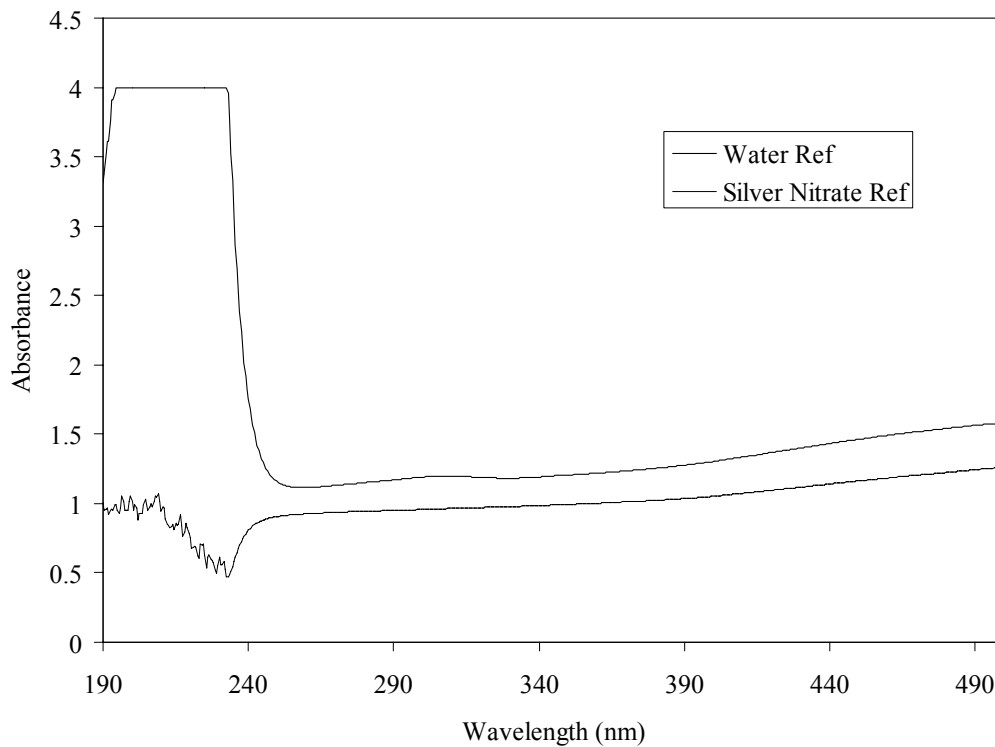


Figure 5-20. Spectrophotometric scan of silver nitrate in sodium hydroxide. Sodium hydroxide was added to 0.1% silver nitrate until the pH reached 9, and the resulting solution was scanned using a UV-1601, first with distilled water in the reference cell, and then with 0.1% silver nitrate in the reference cell. The solution was very cloudy, resulting in the higher baselines for these scans.

One of the peaks observed when nanocrystalline silver dressings were dissolved in nitric acid, occurring at 328 nm, was determined to be due to the high density polyethylene backing (Figure 5-21), and therefore uncoated high density polyethylene was allowed to soak in the reference solution while the

nanocrystalline silver dissolved in the test solution for all optical scans performed after that point. However, this did not account for the remaining peaks occurring at higher wavelengths, as shown in Figure 5-22.

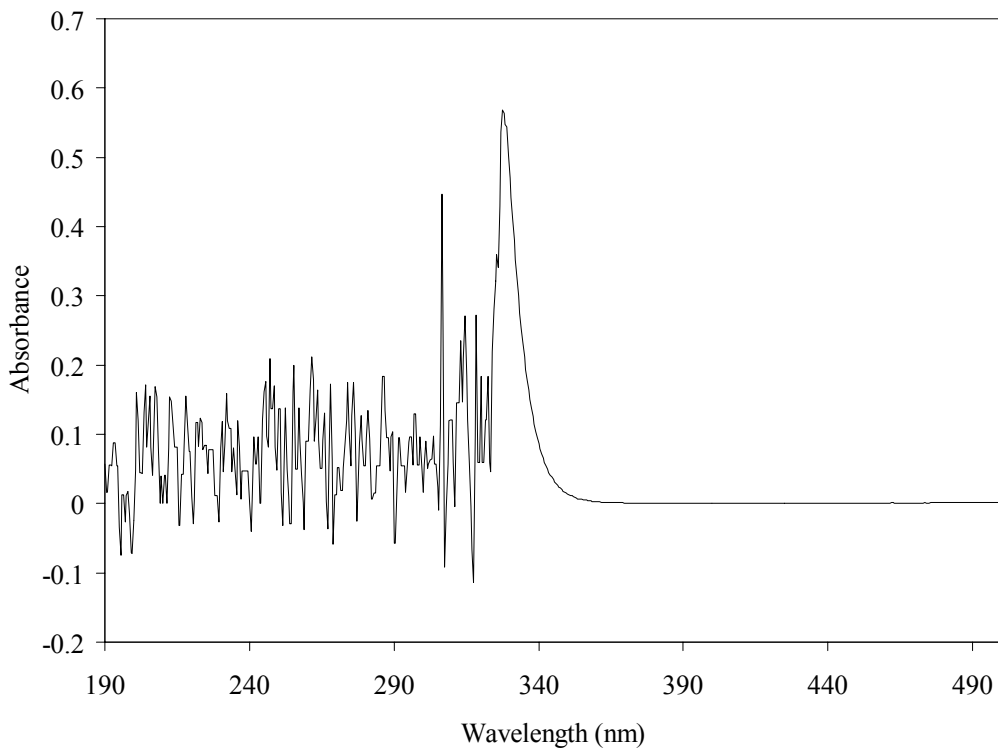


Figure 5-21. Spectrophotometric scan of high density polyethylene backing in nitric acid. The high density polyethylene backing used for nanocrystalline silver dressings was placed in 16.25% nitric acid at a ratio of 1 in²/mL for one hour without stirring, and then the solution was scanned using a UV-1601, with 16.25% nitric acid in the reference cell.

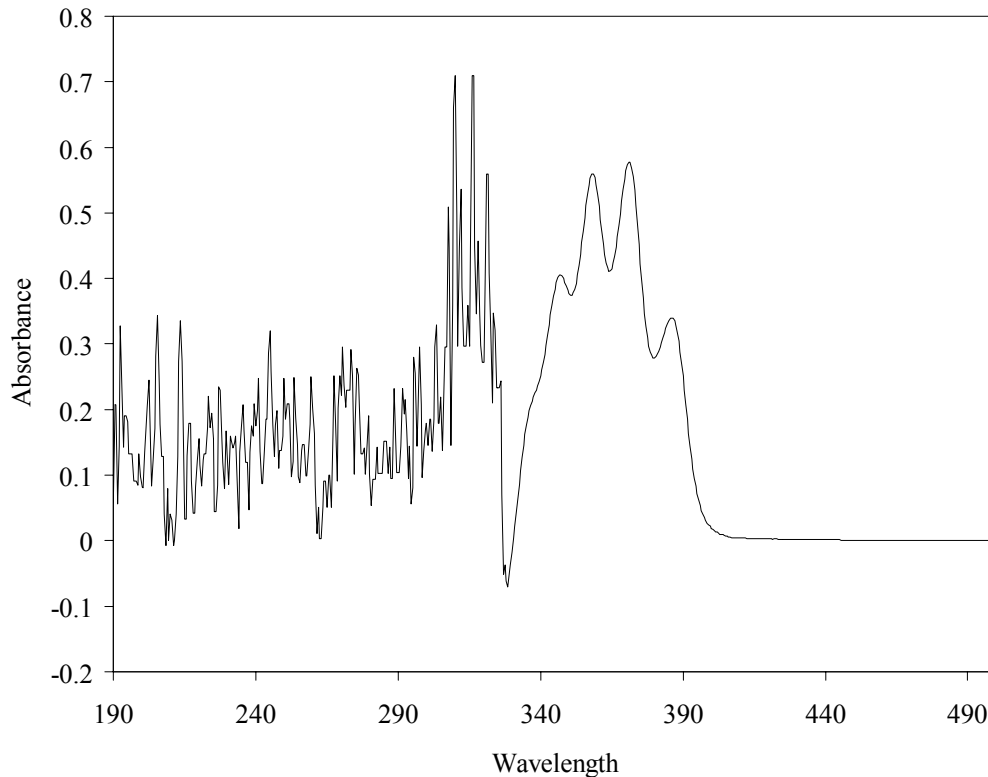


Figure 5-22. Spectrophotometric scan of nanocrystalline silver dissolved in nitric acid (HDPE reference). Nanocrystalline silver dressings were allowed to dissolve in 16.25% nitric acid for one hour at a ratio of 1 in² Ag/mL solution without stirring. At the same time, uncoated high density polyethylene was also soaked in 16.25% nitric acid for one hour at a ratio of 1 in² Ag/mL solution without stirring. A scan of the nanocrystalline-silver derived solution was then obtained using a UV-1601, with solution taken from the 16.25% nitric acid containing HDPE used for the reference cell.

Nanocrystalline silver dressings were dissolved in sodium nitrate to see if the peaks were due to interactions between the nanocrystalline silver and the nitrates. Figure 5-23 shows that the peaks were not due to nanocrystalline silver – nitrate interactions.

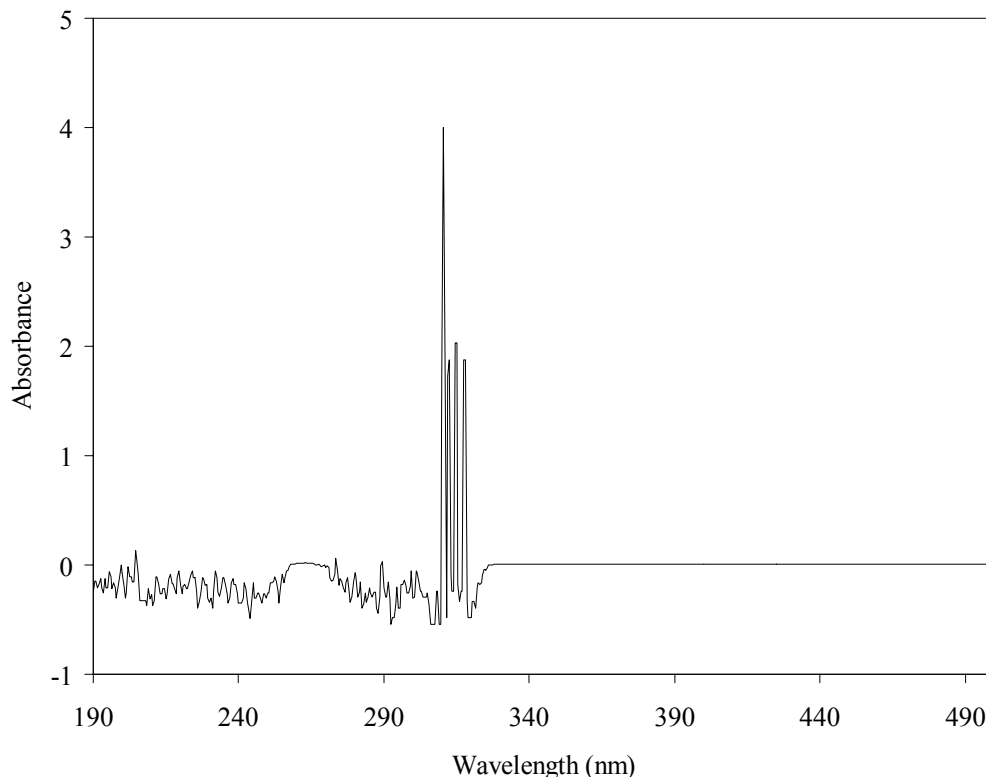


Figure 5-23. Spectrophotometric scan of nanocrystalline silver dissolved in sodium nitrate. A solution was generated by placing nanocrystalline silver dressings in 16.25% sodium nitrate at a ratio of 1 in² Ag/mL solution. The silver was allowed to dissolve for one hour without stirring. At the same time, uncoated HDPE was also soaked in 16.25% sodium nitrate at a ratio of 1 in²/mL solution without stirring for one hour. A scan of the nanocrystalline silver-derived solution was then obtained using a UV-1601, with solution taken from the 16.25% sodium nitrate solution containing HDPE used for the reference cell.

Although it seemed unlikely that the peaks could be due to the interaction of nanocrystalline silver with acids (as if that were the case, the peaks might have been observed when solutions were generated in carbonated water at pH 4), the spectra of nanocrystalline silver dissolved in other acids was examined. Each acid produced a different spectra (see Figures 5-24, 5-25, and 5-26 for nanocrystalline silver dissolved in acetic acid, carbonic acid, and phosphoric acid, respectively), none of which matched the spectra produced when nanocrystalline

silver was dissolved in nitric acid. Next, nanocrystalline silver dressings were dissolved in acetic acid with sodium nitrate added, to see if nanocrystalline silver in combination with nitrates and an acid would produce the peaks observed when nanocrystalline silver was dissolved in nitric acid. Figure 5-27 shows that when both an acid and nitrates were present during dissolution, the peaks could be reproduced, along with the peak generated when nanocrystalline silver was dissolved in acetic acid only (see Figure 5-26), which presumably was associated with a silver reaction to the acetate anion. As with dissolution in nitric acid, the peaks diminished over time, disappearing at 24 hours, so that only the peak associated with the acetate anion remained and increased in size (Figure 5-28, compare with Figure 5-24).

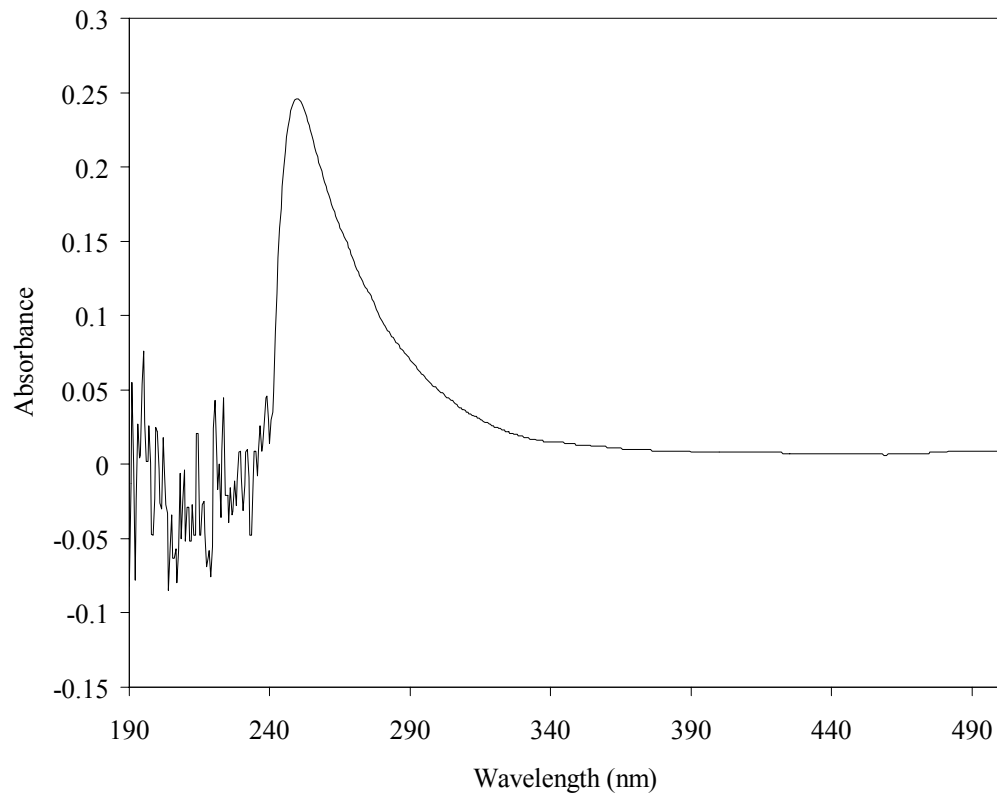


Figure 5-24. Spectrophotometric scan of nanocrystalline silver dissolved in acetic acid. A solution was generated by placing nanocrystalline silver in 25% acetic acid (glacial acetic acid diluted in distilled water) at a ratio of 1 in² Ag/mL solution. The silver was allowed to dissolve for one hour without stirring. A scan of the nanocrystalline silver-derived solution was then performed using a UV-1601, with 25% acetic acid in the reference cell (this scan was performed before it was determined that the HDPE backing of nanocrystalline silver dressings could change the optical absorbance of a solution).

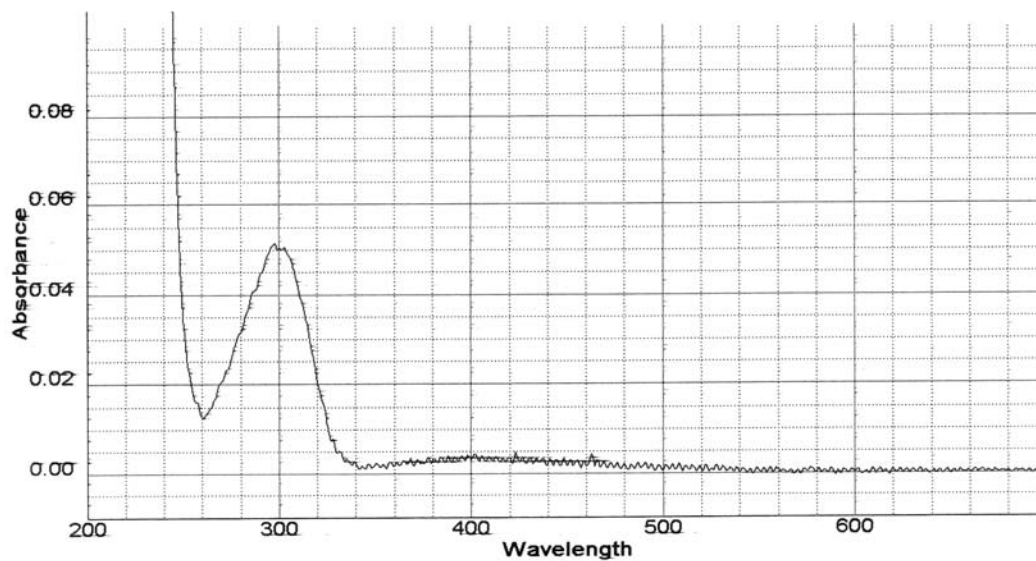


Figure 5-25. Spectrophotometric scan of nanocrystalline silver dissolved in carbonic acid. A solution was generated by placing nanocrystalline silver in purchased carbonic acid at a ratio of 1 in² Ag/5 mL solution. The silver was allowed to dissolve for 24 hours without stirring. A scan of the solution was then performed using an Ultrospec 3000, with carbonic acid in the reference cell (this scan was performed before it was determined that the HDPE backing of nanocrystalline silver dressings could change the optical absorbance of a solution).

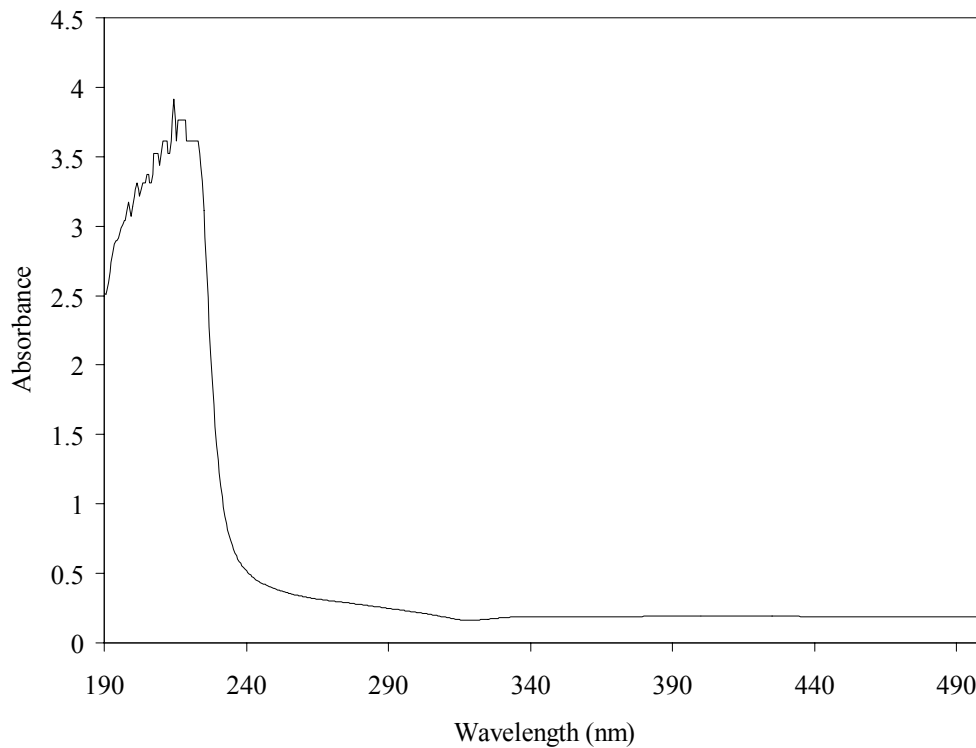


Figure 5-26. Spectrophotometric scan of nanocrystalline silver dissolved in phosphoric acid. A solution was generated by placing nanocrystalline silver in 85% phosphoric acid at a ratio of 1 in² Ag/mL solution. The silver was allowed to dissolve for one hour without stirring. At the same time, HDPE was placed in 85% phosphoric acid at a ratio of 1 in²/mL and allowed to soak without stirring. A scan of the nanocrystalline silver-derived solution was performed using a UV 1601, with the 85% phosphoric acid in which the HDPE had soaked used in the reference cell.

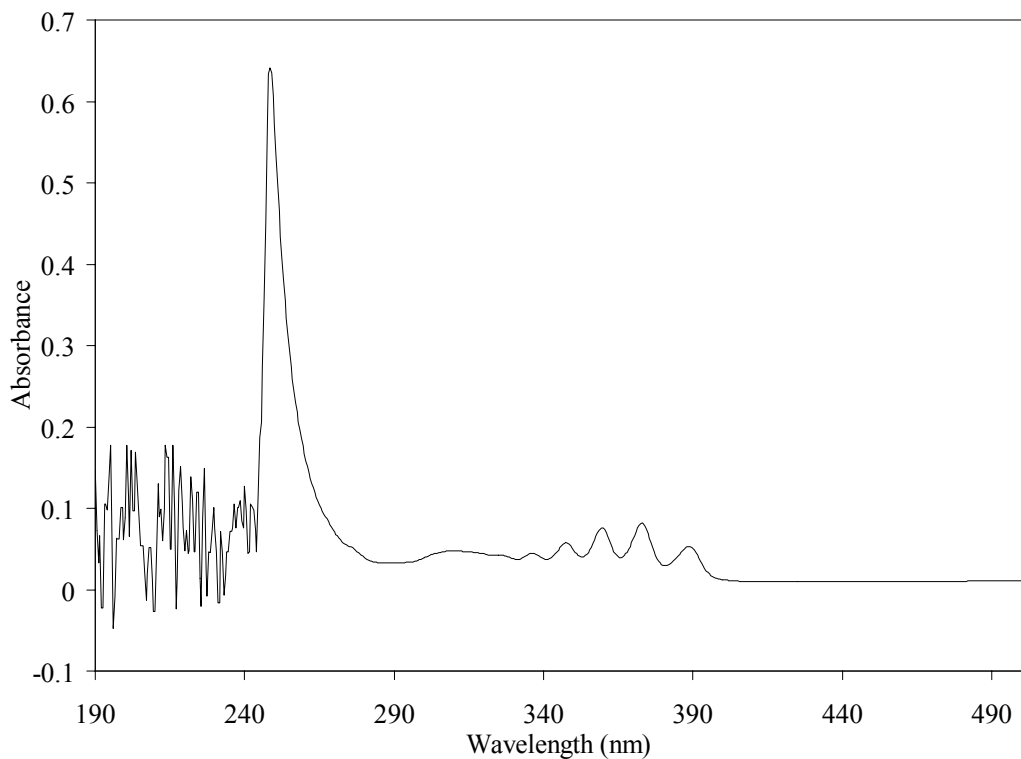


Figure 5-27. Spectrophotometric scan of nanocrystalline silver dissolved in glacial acetic acid with sodium nitrate for one hour. A solution was generated by placing nanocrystalline silver in glacial acetic acid at a ratio of 1 in² Ag/mL solution, along with 5% sodium nitrate. The silver was allowed to dissolve for one hour without stirring. At the same time, HDPE was placed in glacial acetic acid at a ratio of 1 in²/mL, along with 5% sodium nitrate, and allowed to soak without stirring. A scan of the nanocrystalline silver-derived solution was performed using a UV 1601, with the glacial acetic acid/sodium nitrate solution in which the HDPE had soaked used in the reference cell.

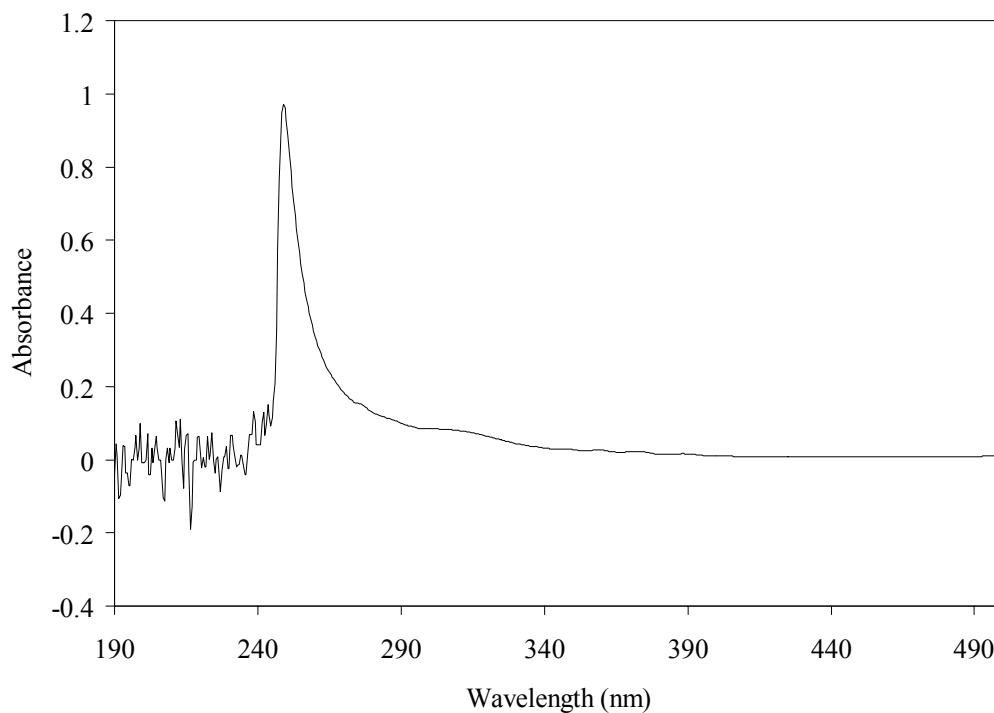


Figure 5-28. Spectrophotometric scan of nanocrystalline silver dissolved in glacial acetic acid with sodium nitrate for 24 hours. A solution was generated by placing nanocrystalline silver in glacial acetic acid at a ratio of 1 in² Ag/mL solution, along with 5% sodium nitrate. The silver was allowed to dissolve for 24 hours without stirring. At the same time, HDPE was placed in glacial acetic acid at a ratio of 1 in²/mL, along with 5% sodium nitrate, and allowed to soak without stirring. A scan of the nanocrystalline silver-derived solution was performed using a UV 1601, with the glacial acetic acid/sodium nitrate solution in which the HDPE had soaked used in the reference cell.

Another group which observed a similar result when dissolving nanocrystalline silver dressings in nitric acid thought that the nanocrystalline silver might be reacting with the nitric acid to form ammonia, suggesting that this was the cause of the peaks observed between 340 and 390 nm (personal communication, M. Kahera). To test this theory, a scan was performed of ammonia, but ammonia only has one broad peak in the region of interest (Figure 5-29), so the optical absorbance pattern observed when nanocrystalline silver is dissolved in nitric acid is not due to the formation of ammonia.

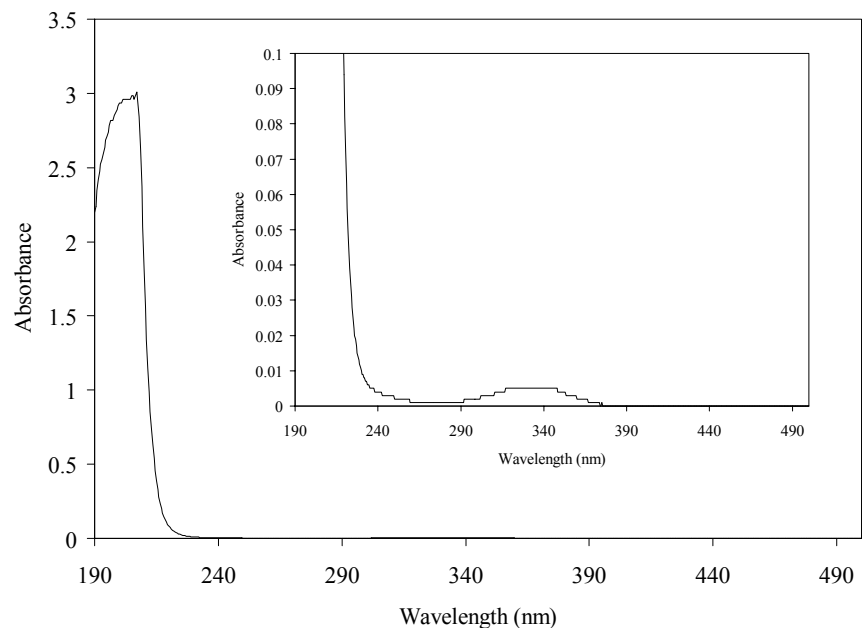


Figure 5-29. Spectrophotometric scan of ammonia. A 20 g/L ammonia solution was scanned using a UV 1601, with distilled water in the reference cell.

(As another aside, ammonia-soluble silver is related to the silver oxide present in the nanocrystalline silver dressings, as well as its antimicrobial activity. Therefore, the solubility of silver films in ammonia is tested as described in Chapter 8, with silver samples being dissolved for three minutes and then submitted for total silver analysis by AAS. The time for dissolution is very important, as with longer dissolution times, eventually all the silver in the dressings will dissolve. Because of this, the effect of dissolution time for nanocrystalline silver dressings in ammonia on the optical properties of the solution was examined. Figure 5-30 shows the effect of dissolution time in ammonia, with a shift to the right and a large increase in absorbance occurring over 24 hours. The peak at 24 hours appears to be a combination of the peak present at three minutes plus a second peak at a higher wavelength, suggesting the dissolution of additional species to those present at three minutes, as anticipated.

The results of this experiment suggest that it might be possible to use the optical absorbance of solutions generated by dissolving silver for three minutes in ammonia as a measure of the ammonia soluble silver present in a sample, with commercial nanocrystalline silver dressings as a reference, for assays such those performed in Chapter 8, rather than submitting the samples for AAS.)

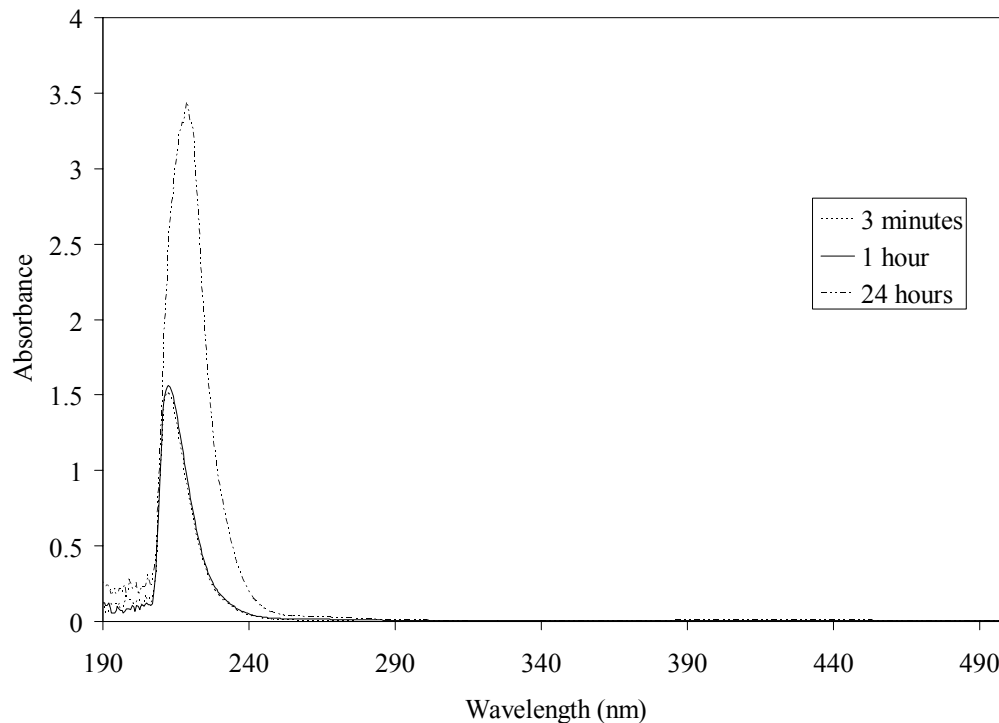


Figure 5-30. Spectrophotometric scan of a nanocrystalline silver dissolved in ammonia for different periods of time. A solution was generated by placing nanocrystalline silver in 20 g/L ammonia at a ratio of 1 in² Ag/mL solution. The silver was allowed to dissolve for 3 minutes, one hour, or 24 hours without stirring. At the same time, HDPE was placed in 20 g/L ammonia at a ratio of 1 in²/mL, and allowed to soak without stirring. Scans of the nanocrystalline silver-derived solution was performed using a UV 1601, with the ammonia solution in which the HDPE soaked used in the reference cell.

As a final check to confirm that the optical absorbance pattern of nanocrystalline silver was unique when dissolved in acid in the presence of nitrate, silver nitrate was dissolved in nitric acid (Figure 5-31) and glacial acetic acid (Figure 5-32). In both scans, the region of interest (340-390 nm) had no

peaks at all (although the acetate peak was present in the acetic acid scan), suggesting that the set of peaks generated when nanocrystalline silver is dissolved in nitric acid is unique and cannot be generated by other forms of silver in the same conditions. The multiple peaks suggest the presence of multiple species in solution.

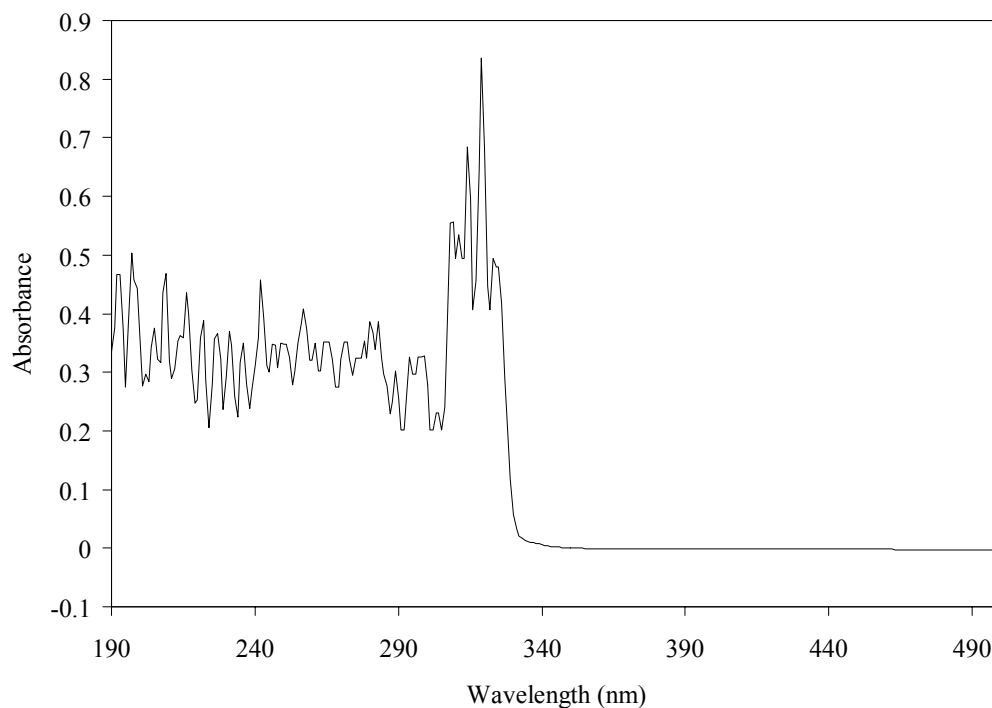


Figure 5-31. Spectrophotometric scan of silver nitrate in nitric acid. 0.1% silver nitrate was dissolved in 16.25% nitric acid, and scanned using a UV 1601, with 16.25% nitric acid in the reference cell.

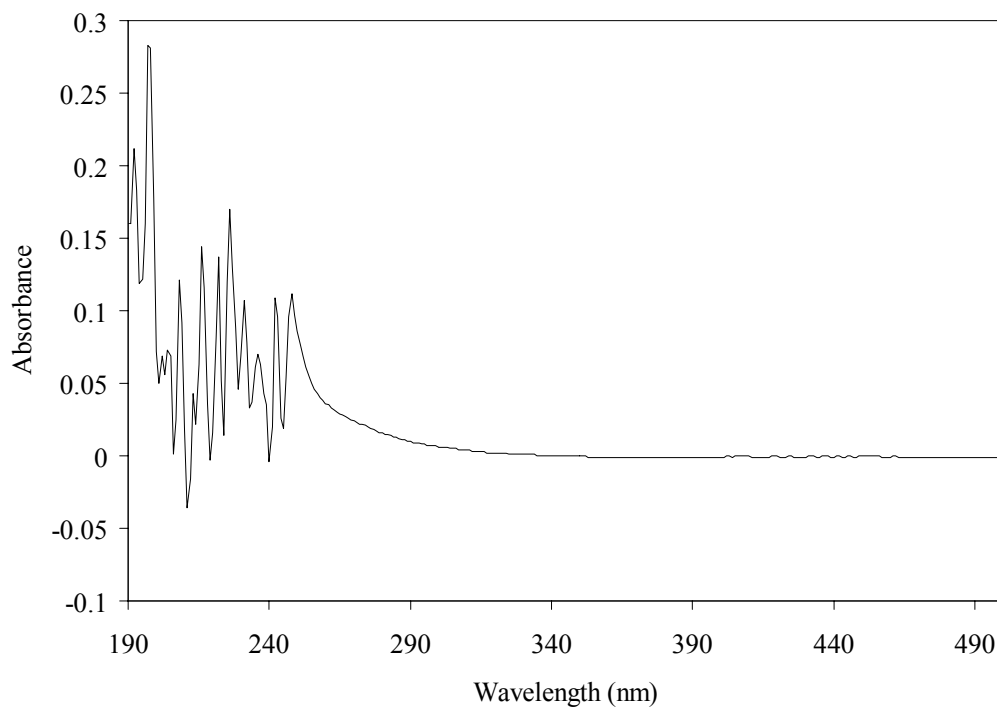


Figure 5-32. Spectrophotometric scan of silver nitrate in glacial acetic acid. 0.1% silver nitrate was dissolved in glacial acetic acid (not all of it dissolved), and scanned using a UV 1601, with glacial acetic acid in the reference cell.

The peaks present may be due to surface plasmon resonance, with the multiple peaks related to various sizes of silver clusters in solution. Previous studies have indicated that unlike bulk materials, the optical absorption of silver nanoparticles (>20 nm) is characterized by a strong absorption band, due to plasmon resonance[30], which has been attributed by some sources to collective oscillation of conduction electrons in response to optical excitation[31]. Recent studies have shown that the surface plasmon resonance (SPR) for silver nanoparticles occurs at approximately 400-420 nm, and shifts with the size of the particles[32]. In particular, in a study of heat treated nanometallic silver in a silica aerogel matrix with starting grain sizes from 6-8 nm up to 25-80 nm, a blue shift followed by a red shift in the SPR was observed with decreasing grain

size[32]. The SPR bands observed in that study were broad and at a higher wavelength than the peaks present in the scan of nanocrystalline silver dissolved in nitric acid shown in this chapter (Figure 5-22). This suggests that if the peaks seen here represent SPR peaks for silver nanoparticles or clusters in solution, they are likely smaller than those observed in the silica aerogel matrix study due to the red shift, and that perhaps the individual peaks represent the presence of five or more different particle sizes (see Figure 5-22).

In studies by the Dickson group, PAMAM dendrimers were used to concentrate, stabilize, and solubilize silver nanoclusters in aqueous solutions. Initially no visible absorption or fluorescence was observed, but after photoactivation with white light, the solution absorption spectra demonstrated two new peaks at 345 and 430 nm due to the SPR of small, photoreduced silver nanodots[33]. These changes in absorbance correlated with increased fluorescence of the solutions[33]. Similarly, when they created water-soluble, monodisperse, blue-emitting Au₈ nanodots stabilized by PAMAM dendrimers, a new absorption band at 384 nm with a bandwidth of 60 nm appeared in the final fluorescent solutions[17].

Aqueous solutions containing spherical silver nanoparticles (20-80 nm) generated via an electro-exploding wire technique had broad SPR peaks centered at a wavelength of 390 nm in its absorption spectrum[34]. Silver colloidal nanospheres (12 nm diameter) synthesized electrochemically showed peaks at 410 (due to non-aggregated nanospheres) and 470 nm (due to aggregated nanospheres) in the absorption spectrum, which were the result of transverse and longitudinal

SPR[35]. An as-prepared silver cluster solution, generated by reduction of silver nitrate using NaBH_4 , showed an intense plasmon absorption band at about 390 nm, signifying that the clusters contained very few silver atoms[36]. They estimated the clusters had an average diameter of about 0.55 nm, as estimated from the half width of the surface plasmon band[36]. Red shifts observed in the SPR band were attributed to cluster agglomeration over time[36]. In a study examining silver nanoclusters generated by first atomizing silver using femtosecond laser induced multiphoton reduction, following by aggregating the silver to form nanoclusters via heat treatment, the authors showed that with laser radiation, absorption peaks appeared at about 350 nm, then shifted to about 430 nm with heat treatment, becoming larger with increasing heat treatment time (i.e. crystal growth)[37]. “Chemically clean” silver nanoparticles generated by the reduction of silver(I) oxide by hydrogen gas in water[38] at different sizes from 29 – 136 nm all showed absorbance peaks around 440 nm, but the peaks got smaller with increasing particle size[39]. Together, these studies suggest that the SPR absorbance band produced by nanosilver is highly dependent on dissolution conditions and particle size. However, there is some discrepancy between papers, as some papers indicate that the SPR bands are due to nanoparticles on the order of nanometers in diameter, while other articles indicate that the SPR bands are due to much smaller silver clusters.

Some clarity on this issue can be gained from an article examining silver nanoparticles synthesized by γ -irradiation in a water-in-oil microemulsion (SDS, n-hexanol, cyclohexane, and aqueous solution)[40]. This study concluded that it

was silver clusters in the emulsion, and not the silver nanoparticles themselves, that caused the luminescence observed when irradiating the silver nanoparticles[40]. They found that their absorption spectra, which contained three main peaks (a broad band between 240 and 260 nm, a band at about 345 nm, and another one at 421 nm) changed with increased irradiation time – the two lower wavelength peaks dropped in size while the latter one got bigger. This was attributed to loss of silver clusters and growth of nanoparticles, and correlated with changes in fluorescent activity (see below)[40]. However, another study showed that during the annealing of silver-polyvinyl films, the absorbance spectrum had a peak at 420 nm due to SPR that grew with annealing time and was attributed to the growth of silver clusters[41]. Further clarification on this topic can be found in the section on spectrofluorimetry.

In addition to size effects on absorption spectra, other studies have shown that silver nanoparticle morphology can impact the absorption peaks. One study showed that silver nanoparticle morphology (nanospheres, triangular nanoplates, circular nanodisks, nanocubes) and structure (hollow versus solid) affected both the position and the number of SPR bands, with the number of SPR peaks increasing as the symmetry of the nanoparticles decreased[42]. Silver nanostructures on glass demonstrated different absorbance peaks dependent on the structure shape, with absorbance peaks at under 400 nm with silver fractals, at 400 and 475 nm for silver islands on glass, and at 450 nm for silver colloids on glass[43]. Another study showed that spectra from solutions, generated by a wet chemistry seed mediated method, containing different quantities of triangular,

spherical, and nano-rod shaped silver nanoparticles had different absorbance peaks from below 400 to about 700 nm[44]. A study of shape-controlled synthesis of complex-shaped silver nanoplates, generated by reducing $\text{Ag}(\text{NH}_3)_2^+$ with ascorbic acid in the presence of silver seed at room temperature, showed that the SPR peak location was related to the silver nanoplate geometric shape, with peaks occurring between 400 and 700 nm[45]. Huge changes in the peaks present in the absorbance spectra were observed with changes in the shape of nanoparticles when big triangular plates, hexagonal plates, triangular plates, long rods, cubes, spheres, and short rods prepared by one-step seedless solvothermal reduction in dimethylformamide with poly(vinyl pyrrolidone) were compared[46].

Although the silver nanoparticles examined in the above shape studies are anticipated to be much larger than anything generated by the dissolution of nanocrystalline silver dressings in solutions, they do demonstrate the impact of the particle shape on optical properties. Interestingly, even differing cluster isomers have been shown to demonstrate different optical properties. A study of Ag_2 and larger clusters isolated in rare gas matrices showed that the clusters were very photosensitive, and that laser radiation could transform the clusters from one isomer to another, resulting in variations in the absorbance spectra[47]. Ag_2 had an absorbance peak at 393 nm, while various Ag_3 absorption peaks (depending on isomers) appeared at 425, 442, and 475 nm, and Ag_4 absorption peaks appeared at 535 and 557 nm in Xe[47]. In a similar study, silver cluster cations, produced by sputtering, were mass selected in a quadrupole mass filter and co-deposited with krypton on sapphire or CaF_2 windows. Absorption bands for Ag_1 were observed

at 309, 313, and 322 nm, while for Ag₂ they were observed at 271, 281, 390, 407, 331, 364, 402, 421, 458, and 514 nm[48]. Similarly, silver nanoclusters in argon matrices had absorption bands as follows: Ag₁ peaks were observed at 298, 304, 314.5, and 326 nm; while Ag₂ peaks were observed at 234, 242.5, 255, 262, 273, 384, and 441 nm; and Ag₃ peaks were observed at 321, 331, 350, 362, 386, 402, 423, 444, and 492 nm[49]. The same group found that for Ag₄ in an argon matrix, absorption bands were observed at 405, 387, 299, 295, 275, 273, 268, 262, 258, 251, and 235 nm[20]. Absorption spectra were shown to vary specifically with different isomers of the silver trimer: Ag₃(I) showed absorbance peaks at 323/326, 388, and 419 nm; while Ag₃(II) showed absorbance peaks at 350/363, 426, and 492 nm; and Ag₃(III) showed absorbance peaks at 385, and 488 nm[50]. The same group has also demonstrated isomer-specific spectroscopy of Ag₉ in an argon matrix[22]. This suggests that the multiple peaks observed during dissolutions such as the one seen in nitric acid could be due to the presence of different cluster isomers.

The concentration of silver nanoparticles or clusters in solution can also impact the optical absorbance spectrum. One study showed that silver nanoparticles (20 nm) in water prepared by microwave synthesis showed an absorbance peak at 455 nm, which had enhanced intensity with increased silver concentration, but no peak shift[51]. However, another study showed that silver nanoparticles (20 nm diameter) adsorbed on a glass substrate could be subsequently dissolved into pure water under white light irradiation, resulting in a decreased peak size at 500 nm in the absorbance spectrum[52]. Thus the effect of

concentration of silver nanoparticles on solution absorbance is not totally clear. It may depend on whether or not the particles fluoresce.

Finally, pH of a solution has been shown to affect the absorbance spectrum of silver cluster or nanoparticle-containing solutions. Silver nanoparticles prepared from silver nitrate by borohydride in a basic medium (3 ± 2 nm) or without the basic medium (8 ± 2 nm particles) resulted in absorbance peaks around 400 nm, while preparing the nanoparticles in citrate (20 ± 5 nm) resulted in absorbance peaks shifted to higher wavelength (~ 420 nm)[53]. Subsequent photofragmentation of the particles with 308 nm light showed that with decreased particle sizes, both the location of maximum absorption and the FWHM decreased[53].

Thus, while the absorbance patterns observed, particularly during dissolution in nitric acid, have not yet been fully explained, they may be due to the effect of a variety of properties of silver clusters and dissolution conditions on SPR.

Effect of Sampling

The effect of solution sampling was examined by measuring the optical absorbance at 210 nm using an Ultrospec 3000 from solutions sampled every 10 minutes. With sampling for up to 30 minutes, no significant differences in peak height were observed. In comparison, if three solutions were generated in pH 4 at the same time under identical conditions, there were significant differences in the peak height ($p=0.0075$). The fact that peak heights did not vary with multiple sampling with single solution, while they did vary when generating multiples of

the solution under identical conditions indicated that for experimentation involving taking solution samples, including for animal experiments such as those of Chapters 6 and 7, there would be less variability in the studies if multiple small samples were taken from a single jar over time, rather than having a separate jar for each sample (e.g. for each animal).

Spectrofluorimetry

Solutions were generated in which nanocrystalline silver dressings were dissolved at a ratio of 1:5 and 1:1 in 2 Ag/mL solution in carbonated (pH 4) or distilled water (pH 5.6) for 1 or 24 hours unstirred. These were taken for analysis by spectrofluorimetry to determine whether or not the solutions fluoresced, as the results of the spectrophotometry were inconclusive. The results shown are for pH 4 solutions, but similar results were obtained using pH 5.6 solutions. The excitation scan for various dissolution conditions are shown in Figure 5-33. The signal was highest for the solution generated with a ratio of 1:1 for 1 hour, followed by the solution generated at a ratio of 1:5 for 1 hour, then the solution generated at a ratio of 1:1 for 24 hours, and finally the solution generated at a ratio of 1:5 for 24 hours, suggesting that the excitation signal strength was stronger with shorter dissolution times, and higher silver:solution ratios. Overall excitation patterns were similar, and based on the patterns, the wavelength of strongest excitation (other than the peak at 444 nm, which the operator could not identify) was selected to be 300 nm, and this wavelength of excitation was used for all emission scans. At 300 nm, emission was higher with 1:1 ratios relative to 1:5 ratios, while dissolution time had no clear impact (Figure 5-34). The initial

peak in Figure 5-34 was attributed to the Raman band for water, and the next peak was considered very weak and not likely to be due to fluorescence (personal communication, Wayne Moffat, December 1, 2007). However, to try to better understand the optical behavior of nanocrystalline silver solutions, a solution generated at pH 4, 1:1 in² Ag/mL, unstirred for 24 hours was placed in a cuvette for 10, 20, and 30 minutes. The signals obtained from both the excitation and emission scans (Figures 5-35 and 5-36, respectively) decreased with increasing time, indicating that when the solution was taken away from the nanocrystalline silver, the species resulting in the emissive signal reacted/were quenched over time. To see if the excitable species could be adsorbed to the cuvette walls and thus built up, cuvettes were rinsed with solution one or five times. While a single rinse showed some increase in the signal for both the excitation and emission scans (Figures 5-37 and 5-38, respectively), an additional four rinses actually resulted in a slight decrease in signal strength, suggesting that if species were being built up on the cuvette walls, the adsorption wasn't very strong and some of the species were being knocked off with subsequent washes. Finally, as a check for species adsorption to the sides of the cuvette, the solution was placed in the cuvette and scanned, and then the cuvette was rinsed with distilled water three times and then scanned with distilled water in it, rinsed another three times and scanned again (with only water in the cuvette), soaked for 10 minutes in nitric acid and then scanned again (with only water in the cuvette), rinsed with water and then scanned with carbonated water in the cuvette (pH 4), rinsed again with water, and then scanned with water in the cuvette (distilled). The excitation and

emission scans are shown in Figures 5-39 and 5-40, respectively. Emptying out the solution, rinsing the cuvette, and scanning with plain distilled water decreased the signal observed, but did not eliminate it. Soaking the cuvette in nitric acid and then scanning it with plain distilled water in it actually brought the signal strength up, suggesting that rather than removing the species from the cuvette, the low pH actually enhanced their optical activity. Furthermore, the scan after the nitric acid soak indicated that the signal was composed of multiple peaks, only one of which was enhanced after the nitric acid soak, perhaps suggesting that the nitric acid acted on one of multiple species adsorbed to the sides of the cuvette. Scanning in carbonated water heavily dampened the signal, and a peak appeared around 530 nm instead. This indicated that the signals observed were not due to the carbonated water. Interestingly, rinsing the cuvette out and scanning it with water again restored the signal, which had been quenched by the carbonated water, to a level slightly higher than that obtained after the initial rinses with distilled water, indicating that the species causing that signal were still adsorbed to the cuvette. Overall, these results suggest that there were species adsorbed to the sides of the cuvette, and that they had pH-modifiable optical activity. It would be interesting in the future to examine the optical activity of higher pH solutions, such as pH 9, in a spectrofluorimeter.

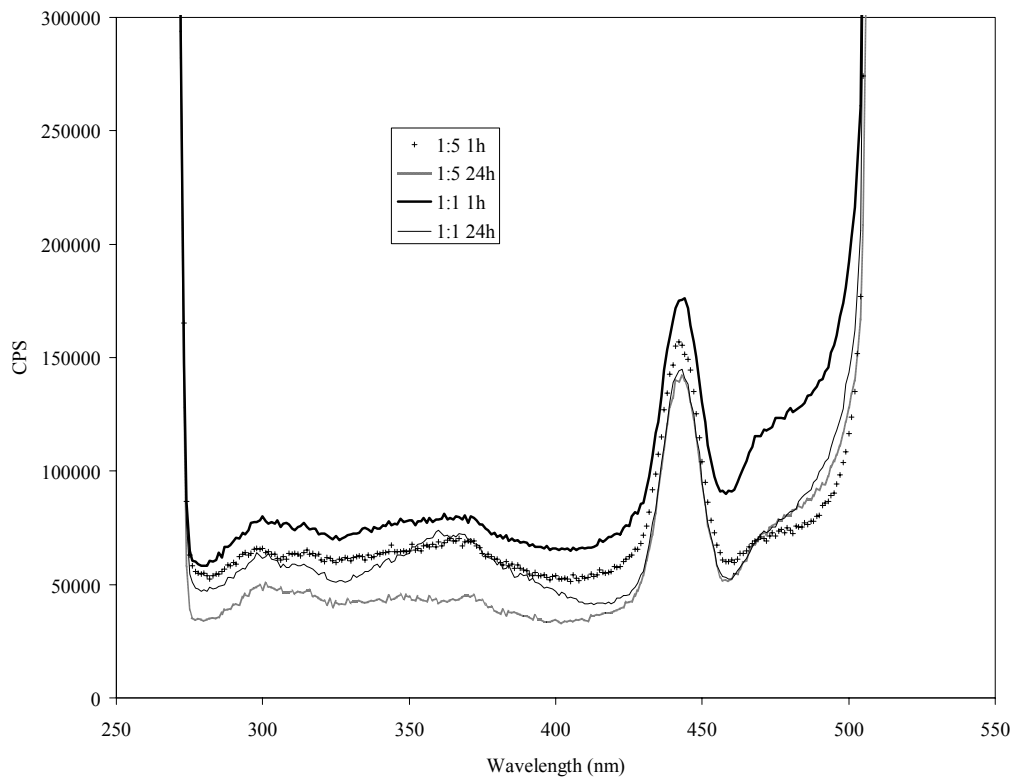


Figure 5-33. Excitation scans for various nanocrystalline silver-derived solutions using a spectrofluorimeter. Nanocrystalline silver-derived solutions were generated by placing nanocrystalline silver at a ratio of either 1:5 in² Ag/mL or 1:1 in² Ag/mL solution at a starting pH of 4, and allowing the silver to dissolve for either one or 24 hours without stirring. Excitation scans were then performed on a spectrofluorimeter to determine the correct wavelength for the subsequent emission scans.

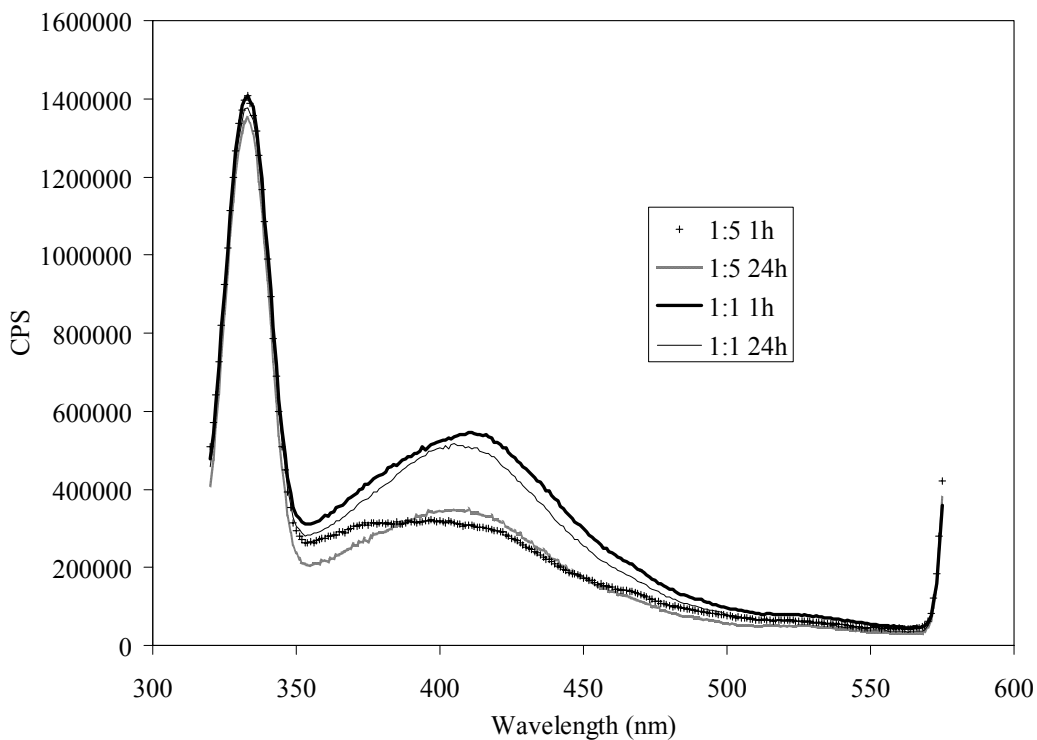


Figure 5-34. Emission scans for various nanocrystalline silver-derived solutions using a spectrofluorimeter. Nanocrystalline silver-derived solutions were generated by placing nanocrystalline silver at a ratio of either 1:5 in² Ag/mL or 1:1 in² Ag/mL solution at a starting pH of 4, and allowing the silver to dissolve for either one or 24 hours without stirring. Emission scans were then performed on a spectrofluorimeter using an excitation wavelength of 300 nm.

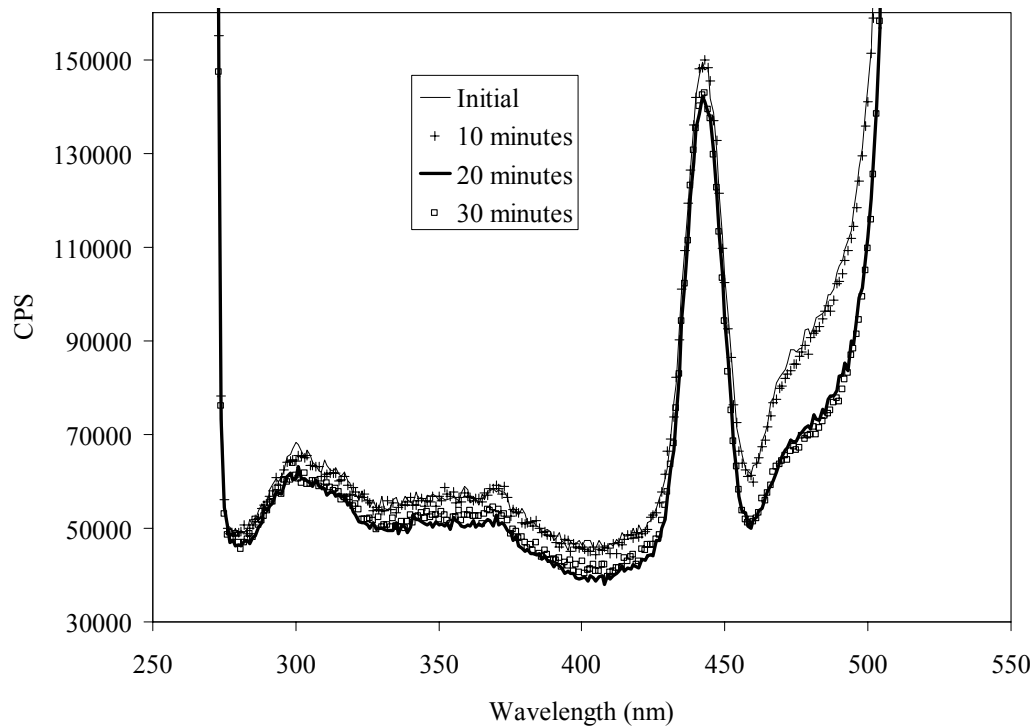


Figure 5-35. Excitation scans for examination of the effect of allowing a nanocrystalline silver-derived solution to sit in a cuvette for various lengths of time (without exposure to further nanocrystalline silver). A nanocrystalline silver-derived solution was generated by placing nanocrystalline silver at a ratio of 1:1 in 2 Ag/mL solution at a starting pH of 4, and allowing the silver to dissolve for 24 hours without stirring. Subsequently, a portion of the solution was allowed to sit in a cuvette for 10, 20, or 30 minutes, and scans were performed on a spectrofluorimeter to examine the resulting signal strength.

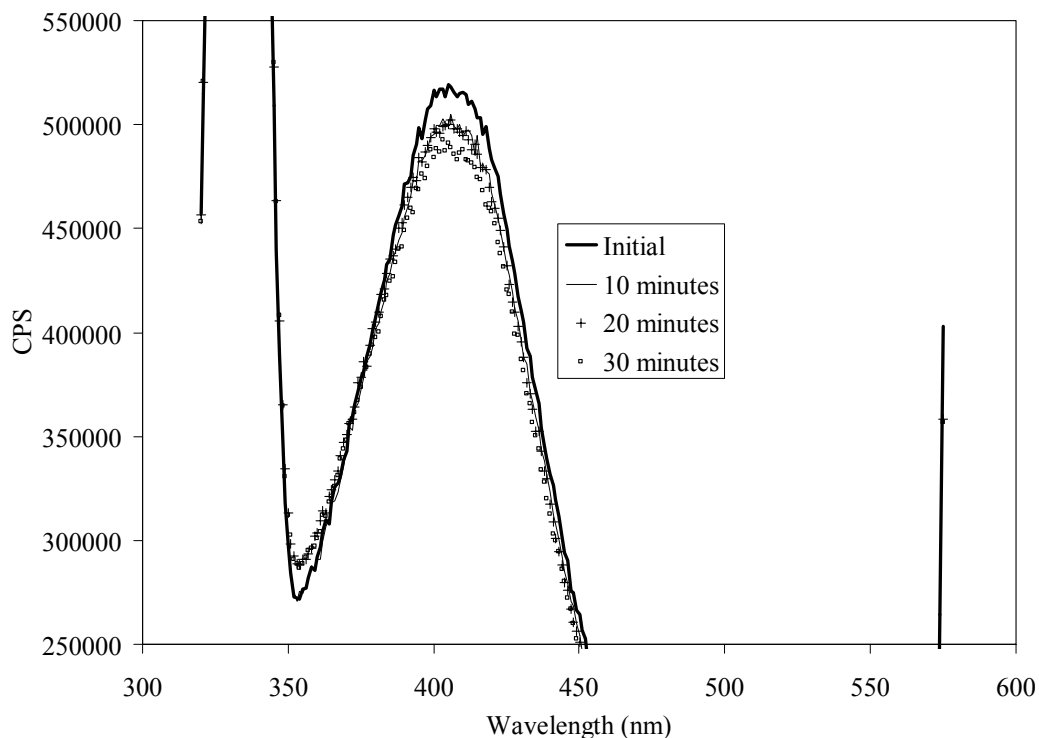


Figure 5-36. Emission scans for examination of the effect of allowing a nanocrystalline silver-derived solution to sit in a cuvette for various lengths of time (without exposure to further nanocrystalline silver). A nanocrystalline silver-derived solution was generated by placing nanocrystalline silver at a ratio of 1:1 in 2 Ag/mL solution at a starting pH of 4, and allowing the silver to dissolve for 24 hours without stirring. Subsequently, a portion of the solution was allowed to sit in a cuvette for 10, 20, or 30 minutes, and scans were performed to examine the resulting signal strength. Emission scans were then performed on a spectrofluorimeter using an excitation wavelength of 300 nm.

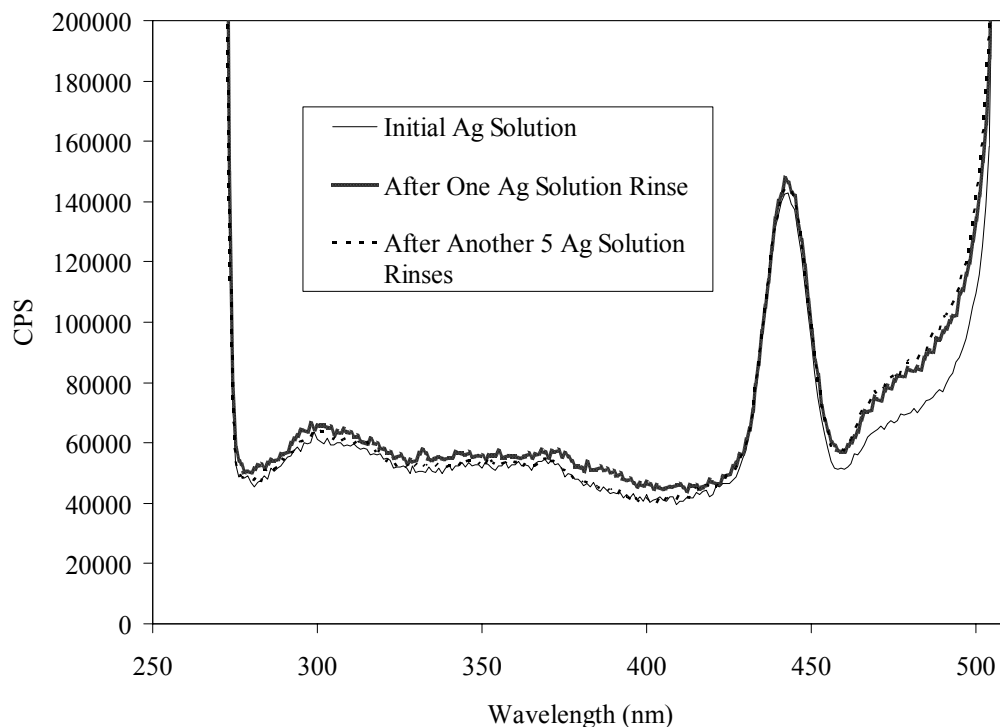


Figure 5-37. Excitation scans for examination of the effect of rinsing a cuvette with a nanocrystalline silver-derived solution. A nanocrystalline silver-derived solution was generated by placing nanocrystalline silver at a ratio of 1:1 in² Ag/mL solution at a starting pH of 4, and allowing the silver to dissolve for 24 hours without stirring. Subsequently, portions of the solution were used to rinse a cuvette one or five times, and scans were performed on a spectrofluorimeter to examine the resulting signal strength.

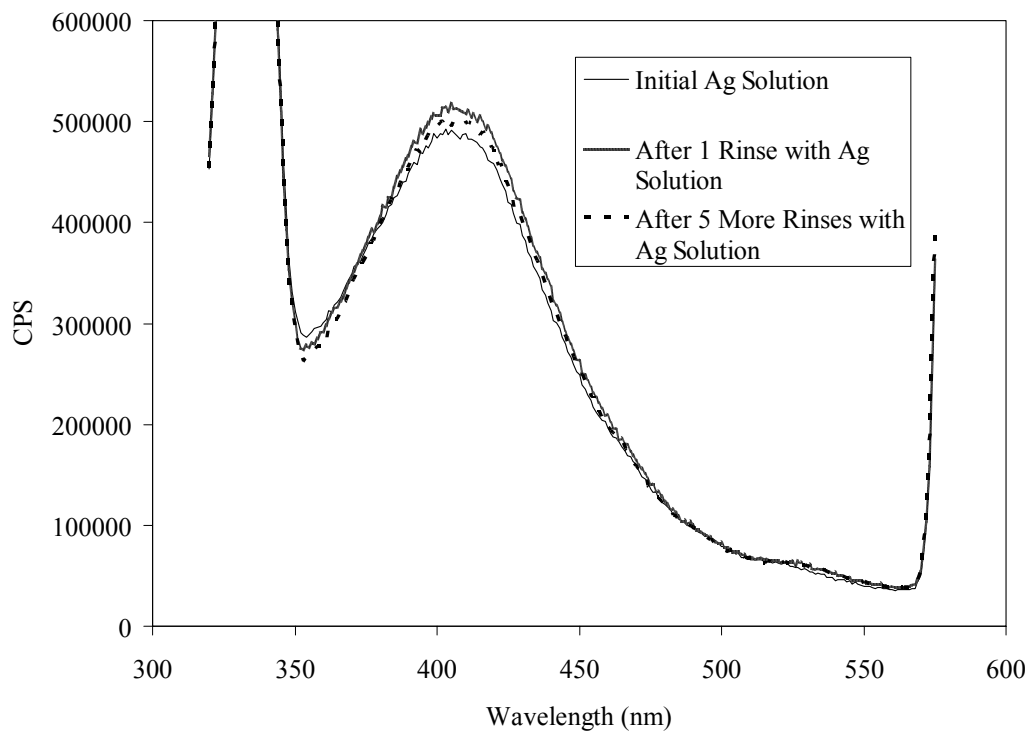


Figure 5-38. Emission scans for studying the effect of rinsing a cuvette with a nanocrystalline silver-derived solution. A nanocrystalline silver-derived solution was generated by placing nanocrystalline silver at a ratio of 1:1 in 10^{-2} Ag/mL solution at a starting pH of 4, and allowing the silver to dissolve for 24 hours without stirring. Subsequently portions of the solution were used to rinse a cuvette one or five times, and emission scans were performed on a spectrofluorimeter, using an excitation wavelength of 300 nm.

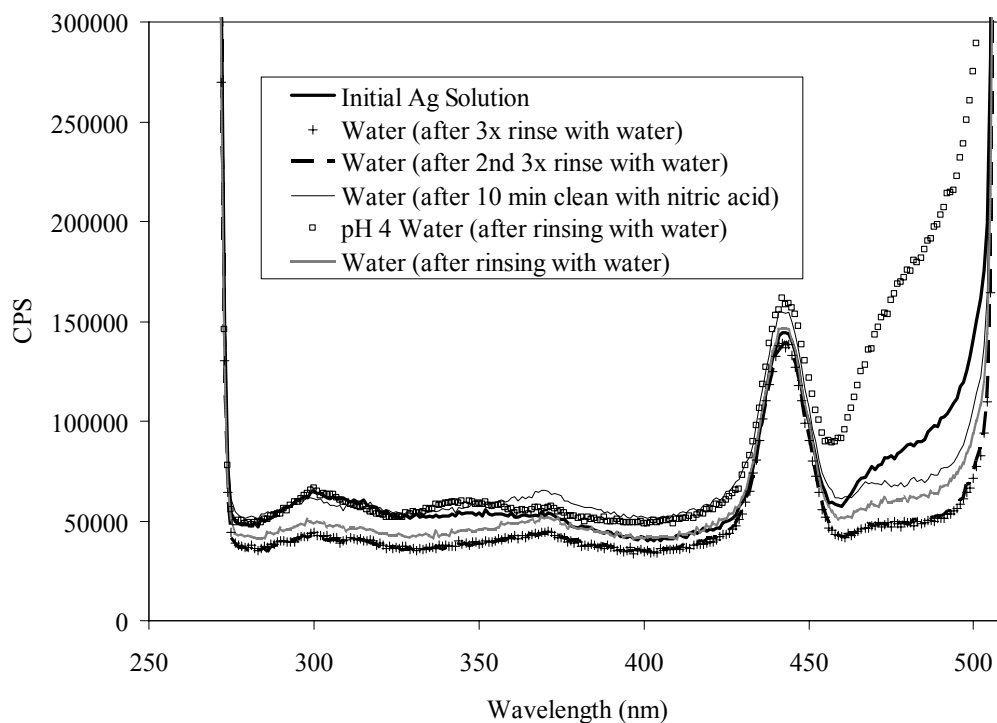


Figure 5-39. Excitation scans testing for the presence of adsorbed species on cuvettes after exposure to nanocrystalline silver-derived solutions. A nanocrystalline silver-derived solution was generated by placing nanocrystalline silver at a ratio of 1:1 in 2 Ag/mL solution at a starting pH of 4, and allowing the silver to dissolve for 24 hours without stirring. An initial scan was performed with the cuvette containing the nanocrystalline silver-derived solution. Following that, the cuvette was rinsed three times with distilled water than then scanned again containing only distilled water. This was repeated a second time. The cuvette was then soaked in 16.25% nitric acid for 10 minutes and then rinsed and scanned again containing only distilled water. The cuvette was rinsed with distilled water again, and then scanned containing pH 4 carbonated water such as was used to generate the nanocrystalline silver-derived solution. Finally, the cuvette was rinsed with water again, and scanned with distilled water in it again.

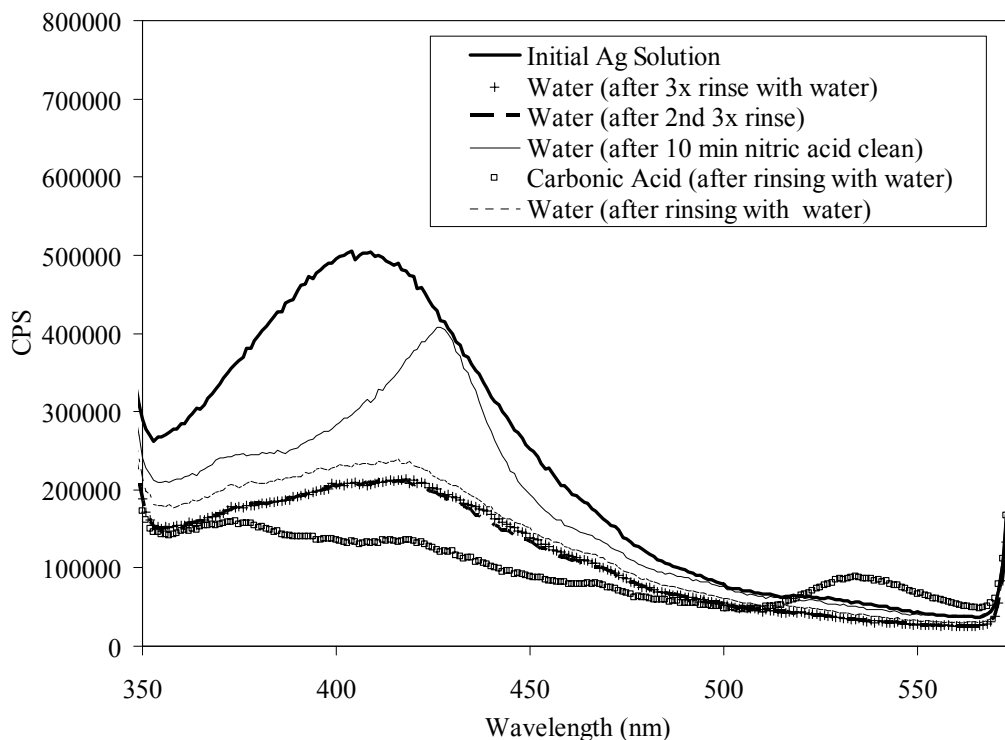


Figure 5-40. Emission scans testing for the presence of adsorbed species on cuvettes after exposure to nanocrystalline silver-derived solutions. A nanocrystalline silver-derived solution was generated by placing nanocrystalline silver at a ratio of 1:1 in² Ag/mL solution at a starting pH of 4, and allowing the silver to dissolve for 24 hours without stirring. An initial scan was performed with the cuvette containing the nanocrystalline silver-derived solution. Following that, the cuvette was rinsed three times with distilled water then scanned again containing only distilled water. This was repeated a second time. The cuvette was then soaked in 16.25% nitric acid for 10 minutes and then rinsed and scanned again containing only distilled water. The cuvette was rinsed with distilled water again, and then scanned containing pH 4 carbonated water such as was used to generate the nanocrystalline silver-derived solution. Finally, the cuvette was rinsed with water again, and scanned with distilled water in it again. All emission scans were performed on a spectrofluorimeter using an excitation wavelength of 300 nm.

To try to clarify these results, nanocrystalline silver dressing samples were submitted to Dr. Robert Dickson, who was the principal investigator for the team discovering the fluorescence of silver and gold nanoclusters as described in the introduction[15-19, 33], along with instructions for generating the solutions in starting pHs of 4 and 5.6. He did not find any fluorescence activity related to the

silver (personal communication, Dr. Robert Dickson, February 13, 2008). He indicated that the HDPE backing did generate fluorescence, after directly analyzing the dressings, but this observation would not explain the features observed in solution, as the solution samples do not contain the HDPE. However, one peak related to the HDPE was observed in the absorbance spectrum, so it is not impossible that an HDPE dissolution product is responsible for some of the optical behavior observed in the spectrofluorimeter, and therefore future studies should include controls with HDPE in them throughout the dissolution period. A direct analysis of the dressings was not expected to reveal fluorescent silver, as the clusters may only be “generated” (i.e. released from the surrounding silver-silver oxide matrix) in solution, and therefore may only be fluorescent in solution. Samples were also submitted for femtosecond pulsed laser mass spectrometry of the solutions, in hopes of identifying individual species generated during dissolution, but no results were returned.

Although the spectrofluorimetry scans did not clearly demonstrate solution fluorescence, this does not mean that that silver nanoclusters are not generated in solution, as cluster size may impact the ability of the clusters to fluoresce, as indicated in the introduction. Furthermore, some studies have demonstrated emissive properties which are due to the fluorescence of silver clusters/nanoparticles, and are similar to the behavior of the solutions tested in this chapter, or which are due to other properties of silver nanoclusters. A brief discussion of some of these studies is provided below to indicate the range of possible explanations for the spectrofluorimetry results observed with

nanocrystalline silver-derived solutions.

It has been shown that similar to the optical absorbance of solution, the luminescence of a solution correlates with dissolution conditions, particle sizes, and SPR. Silver nanoclusters (concentrated, stabilized and solubilized with polyamidoamine (PAMAM) G4-OH and G2-OH dendrimers in aerated and deaerated aqueous solutions) irradiated with blue light (450-480 nm) yielded multicolored fluorescence throughout the visible region due to size and geometry differences in the clusters generated[33]. Five stable distinct fluorescence spectra were obtained with emissions at 533, 553, 589, 611, and 648 nm[33]. NaBH_4 reduction resulted in larger silver nanoparticles (3-7 nm) with strong SPR at 398 nm, but no fluorescence[33], indicating that the small size of the clusters was necessary for their luminescence. The study that showed these results also showed that fluorescence correlated with absorption changes, and that fluorescence grew with increasing irradiation time, due to photoreduction of silver ions to form additional silver clusters[33].

In silver colloidal nanospheres (12 nm) synthesized electrochemically, two kinds of fluorescence emission peaks were observed – one was observed at about 315 nm due to local field enhancement when samples were excited at 230-280 nm, and one longer wavelength peak was observed resulting from electron interband transitions. The longer wavelength peak demonstrated red shift with increasing excitation wavelength (with 380 nm excitation, the peak appeared at 550 nm, while with 440 nm excitation, it appeared at 600 nm)[35].

In a study of silver nanoparticles generated via electro-exploding wires, weak green fluorescence (500-550 nm) was observed when the nanoparticles were excited at wavelengths of 340, 360 and 390 nm[34]. The authors suggested that the fluorescence was due to the excitation of surface plasmon coherent electronic motion with small size effect and surface effect considerations[34].

Another study showed that during annealing of silver-polyvinyl films, excitation at 375 nm resulted in weak emission at about 550 nm, which decreased with annealing time, possibly due to the growth of silver clusters into larger nanoparticles[41].

Further confirmation that silver clusters, rather than silver nanoparticles, are the luminescent species, was found in a study of silver nanoparticles (15 nm) spin-coated on glass[54]. The nanoparticles, when excited at 476 nm, showed emitted light with blinking and spectral fluctuations under continuous excitation, with similar behavior observed on oxidized silver powders. The authors concluded that this indicated that the emissive sites were small silver clusters of a few atoms photoactivated by light illumination of the oxide, with different particles showing emissions at multiple different wavelengths between 540 and 640 nm[54].

In a study on silver nanoparticles prepared from silver nitrate in borohydride, a red shift in fluorescence was observed as particle size increased. All the peaks in this study were very broad, with wavelengths between 500 and 550 nm.[53]

Another study confirming that silver clusters, rather than nanoparticles,

are responsible for its fluorescence, examined silver nanoparticles synthesized by γ -irradiation in a water-in-oil microemulsion (SDS, n-hexanol, cyclohexane, and aqueous solution). These solutions demonstrated three peaks upon excitation at 220 nm - the first was located between 300 and 330 nm, the second between 350 and 420 nm, and last between 450 and 500 nm[40]. The luminescence was observed to decrease with increased radiation time, which was attributed to loss of silver clusters in the emulsion and growth of nanoparticles[40].

Another study confirmed the concept that silver nanoparticle fluorescence is due to silver clusters on particle surfaces[55], but also found a necessity of charged clusters for luminescence. They found that optical properties of silver colloidal particles in solution were observed only with surface deposition of silver ions[55]. A large visible emission under UV or SPR region excitations was observed for $\text{Ag}_n @ \text{Ag}^+$, but no fluorescence emissions were observed for Ag_n or Ag^+ only systems[55]. They found that oligomeric clusters, composed of Ag_{4+x}^{x+} produce emissions in the same visible region, and concluded that the photoemission of their chemically modified silver colloidal particles was due to oligomeric clusters on the silver particle surface[55].

As with the optical absorbance spectra, silver fluorescence appears to be geometry dependent. For silver nanostructures on glass irradiated at 442 nm, the irradiance required to photoactivate the silver structures was dependent on the nature of the nanostructure – silver fractal-like structures were highly emissive, compared to silver island films and spin-coated silver colloids, with luminescence occurring at 600 nm for all three structures[43].

Also similar to the optical absorbance of solutions, the emissive properties of silver clusters vary depending on the isomers present. Silver cluster cations deposited with krypton on sapphire or CaF₂ windows showed emissions corresponding to particular absorption bands, which varied with the silver cluster isomers. The emission peaks for Ag₁ were at 418, 490, and 525 nm; while the emission peaks for Ag₂ were observed at 297, 453, and 506 nm; and the emission peaks for Ag₃ were seen at 381, 560, and 626 nm[48]. Similarly, emission bands corresponding to specific absorption bands for silver nanoclusters in argon matrices were observed as follows: Emissive peaks for Ag₁ were seen at 326, 369, 425, 451, and 458 nm; emissive peaks for Ag₂ were seen at 278, 286, 298, and 479 nm; and emissive peaks for Ag₃ were observed at 374, 616, and 705 nm[49]. The same group found that although Ag₁ and Ag₄ fluoresced at the same wavelength (458 nm) in an argon matrix, the peak width was five times narrower for Ag₄, allowing for separation of the two silver sizes[20]. Ag₄ emission bands were also observed at 481 and 519 nm[20]. Specific fluorescence patterns were demonstrated with different isomers of the silver trimer, and it was shown that different excitation wavelengths could change the trimers from one isomer to another[50]. For Ag₃(I), emission bands were observed at 369, and 608 nm; while for Ag₃(II), emission bands were observed at 373, 420, 625, and 703 nm; and for Ag₃(III), an emission band was observed at 618 nm[50].

Studies have also suggested that the luminescence of silver depends on the concentration of silver in solution. One study demonstrated that silver nanoparticles (20 nm) in water prepared by microwave synthesis had a

fluorescence peak at 465 nm and strong resonance scattering peak at 450 nm[51]. A red shift and decreased luminescence was observed with increased silver concentration in solution[51].

pH of solution has also been shown to affect silver fluorescence.

Reactively sputtered silver oxide layers photoactivated at 488 nm showed fluorescence shifting from 625 to 725 nm with photoactivation time, and also showed fluorescence quenching in 2-propanol, water, ethanol, and methanol, with recovery on addition of benzoic acid[56]. Coupling of other ligands always led to at least partial recovery of the previously quenched fluorescence, with the degree of recovery dependent on strength of the complex formed between the active surface sites and the ligand[56]. At the same time, a strong surface enhanced Ramon scattering (SERS) signal developed from the coupled molecule[56]. Ag⁺-containing silver clusters are necessary to promote this type of SERS behavior[56]. Ag⁺-containing silver clusters are considered soft Lewis acids, so they form stable complexes with soft Lewis bases[56]. SERS inactive water and alcohol molecules only physisorb at the surface of the silver while stronger Lewis acids occupy the active sites by forming stable covalent bonds, preventing the fluorescent silver particles from transferring the excitation energy to quenching molecules in solution[56]. This study also made the observation that a double peak observed between 530 and 540 nm was not fluorescence but a SERS signal from amorphous or nanocrystalline contaminant carbon domains[56]. Another study has indicated that a likely source of luminescence for silver nanoparticles in various solutions spincoated onto glass (with diameters of about 1 nm) is

SERS[57].

The effect of pH on luminescence of silver nanoclusters photoreduced in a microgel has also been studied. Modifying pH resulted in changes in luminescence – stronger peaks at higher wavelengths were observed with increasing pH up to pH 7, and then decreasing luminescence occurring with further increase in pH, such that there was almost no luminescence at pH 9[29].

Although it remains unclear whether or not the solutions generated in this study can fluoresce, they do present interesting optical properties which may be related to some of the dissolution conditions described above, and which should be further analyzed in the future, as this may provide clarity about the species present in solution and how to generate solutions with optimum levels of desirable species.

Total Silver Profiles

Profiles of total silver over time during the dissolution of nanocrystalline silver in solutions generated either with or without stirring, at starting pHs of 4, 5.6, 7, or 9, and with nanocrystalline silver dressing:solution ratios of 1 in²/mL or 1 in²/5 mL (1:1 or 1:5) were generated.

The total silver profiles generated at pH 4 are shown in Figure 5-41. Most of the change in total silver occurred within the first hour, but in all solutions except the unstirred 1:1 solution, the total silver continued to rise gradually out to 24 hours. The solutions generated at a ratio of 1:1 in² Ag/mL had higher total silver through most of the profiling period relative to the solutions generated at a ratio of 1:5 in² Ag/mL. Statistical analyses, shown in Table 5-1, indicated that at

early time points, solutions generated unstirred with a ratio of 1:1 in² Ag/mL had significantly higher total silver than the other three solutions. After 120 minutes, they were no longer significantly higher than the stirred equivalents, and at 24 hours, they were no longer significantly higher than the other solutions. After 30 minutes, the 1:1 stirred solutions had significantly higher total silver than the 1:5 unstirred solutions, and after 50 minutes, they were also higher than the 1:5 stirred solutions. By 120 minutes, the 1:1 stirred solutions were only significantly higher than the 1:5 stirred solutions, and this remained true until the end of the sampling period. Overall, these results showed that, at pH 4, solutions generated at 1 in² Ag/mL typically released more silver into solution than those generated at 1 in² Ag/5 mL solution. A true equilibrium was not reached in 24 hours, and it appears that the semi-equilibrated level reached would depend on the amount of silver available in dressing form for dissolution. As the 1:5 stirred solutions had the lowest silver release at 24 hours, while the 1:1 stirred solutions had the highest release, it does not appear that stirring consistently enhanced the total silver released. There was high variability in the total silver released into solution with a starting pH of 4, which may be due to varying leak of carbon dioxide out of the container at the start of the experiment, or perhaps leaks during the profiling period. While adding a liquid acid would likely result in less variability than bubbling carbon dioxide through water to generate a pH 4 solution, from a practical perspective it would be difficult to find an acid which would have as low an impact in the lung environment as the quantities of carbonic acid present in these solutions would, since the lung is designed to buffer carbonic acid/carbon

dioxide.

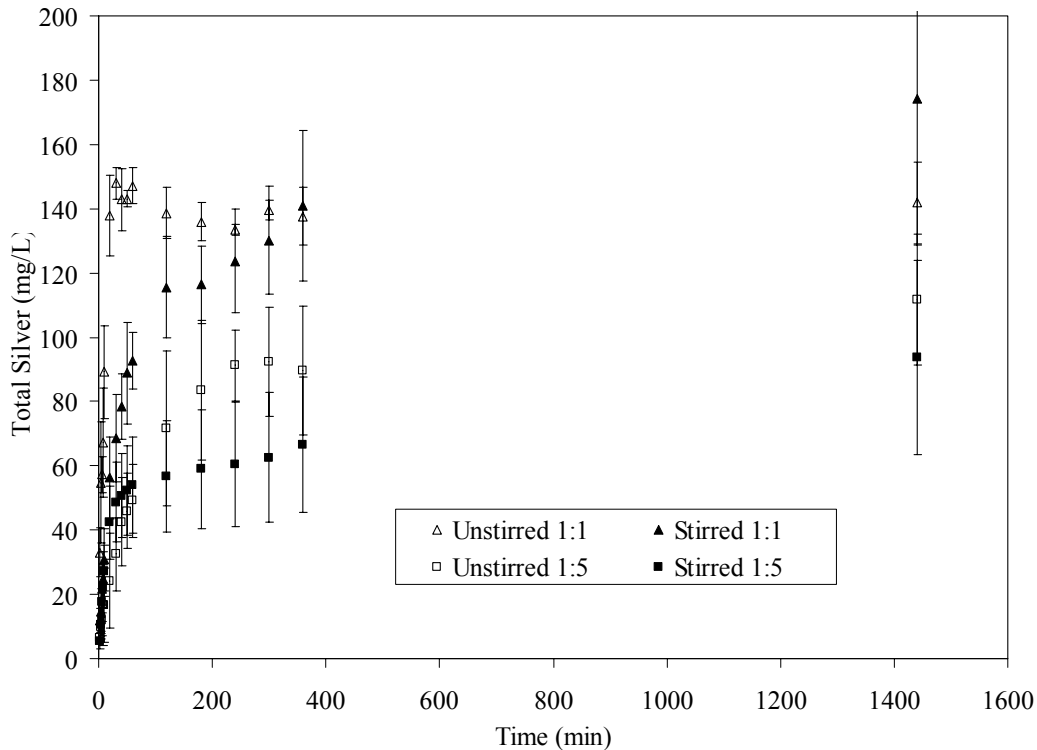


Figure 5-41. Total silver profiles over time for nanocrystalline silver-derived solutions generated at a starting pH of 4 under various conditions. Solutions were generated by adding nanocrystalline silver to water bubbled down to a pH of 4 using carbon dioxide at a ratio of either 1:5 or 1:1 in² Ag/mL. The silver was allowed to dissolve either stirred or unstirred, and samples were collected for total silver analysis by AAS at set times. Error bars = standard deviations (n=3).

Table 5-1. Results of statistical analyses of the effect of varying dissolution conditions (the ratio of silver dressing to solution volume, and whether or not the solution was stirred) at starting pHs of 4 or 5.6 on the total silver dissolved. Statistically significant results are in bold.

pH	Time (min)	ANOVA	Post-Tests
4	2	p=0.0003	p<0.01 1:1u vs 1:1s* (1:1u ↑) p<0.001 1:5u vs. 1:1u (1:1u ↑) 1:5s vs. 1:1u (1:1u ↑)
4	4	p=0.0017	p<0.01 1:5u vs. 1:1u (1:1u ↑) 1:5s vs. 1:1u (1:1u ↑) 1:1u vs. 1:1s (1:1u ↑)
4	6	p<0.0001	p<0.001 1:5u vs. 1:1u (1:1u ↑)

4	8	p=0.0028	1:5s vs. 1:1u (1:1u ↑) 1:1u vs. 1:1s (1:1u ↑) p<0.01 1:5u vs. 1:1u (1:1u ↑) 1:5s vs. 1:1u (1:1u ↑) 1:1u vs. 1:1s (1:1u ↑)
4	10	p=0.0002	p<0.001 1:5u vs. 1:1u (1:1u ↑) 1:5s vs. 1:1u (1:1u ↑) 1:1u vs. 1:1s (1:1u ↑)
4	20	p<0.0001	p<0.001 1:5u vs. 1:1u (1:1u ↑) 1:5s vs. 1:1u (1:1u ↑) 1:1u vs. 1:1s (1:1u ↑)
4	30	p<0.0001	p<0.05 1:5u vs. 1:1s (1:1s ↑) p<0.001 1:5u vs. 1:1u (1:1u ↑) 1:5s vs. 1:1u (1:1u ↑) 1:1u vs. 1:1s (1:1u ↑)
4	40	p<0.0001	p<0.05 1:5u vs. 1:1s (1:1s ↑) p<0.001 1:5u vs. 1:1u (1:1u ↑) 1:5s vs. 1:1u (1:1u ↑) 1:1u vs. 1:1s (1:1u ↑)
4	50	p=0.0003	p<0.05 1:5u vs. 1:1s (1:1s ↑) 1:5s vs. 1:1s (1:1s ↑) 1:1u vs. 1:1s (1:1u ↑) p<0.001 1:5u vs. 1:1u (1:1u ↑) 1:5s vs. 1:1u (1:1u ↑)
4	60	p<0.0001	p<0.01 1:5u vs. 1:1s (1:1s ↑) 1:5s vs. 1:1s (1:1s ↑) 1:1u vs. 1:1s (1:1u ↑) p<0.001 1:5u vs. 1:1u (1:1u ↑) 1:5s vs. 1:1u (1:1u ↑)
4	120	p=0.0013	p<0.05 1:5s vs. 1:1s (1:1s ↑) p<0.01 1:5u vs. 1:1u (1:1u ↑) 1:5s vs. 1:1u (1:1u ↑)
4	180	p=0.0015	p<0.05

4	240	p=0.0007	1:5u vs. 1:1u (1:1u ↑) p<0.01 1:5s vs. 1:1u (1:1u ↑) 1:5s vs. 1:1s (1:1s ↑) p<0.05 1:5u vs. 1:1u (1:1u ↑) p<0.01 1:5s vs. 1:1s (1:1s ↑) p<0.001 1:5s vs. 1:1u (1:1u ↑) p<0.05 1:5u vs. 1:1u (1:1u ↑) p<0.01 1:5s vs. 1:1u (1:1u ↑) 1:5s vs. 1:1s (1:1s ↑) p<0.05 1:5u vs. 1:1s (1:1s ↑) p<0.01 1:5s vs. 1:1u (1:1u ↑) 1:5s vs. 1:1s (1:1s ↑) p<0.05
4	300	p=0.0011	1:5s vs. 1:1s (1:1s ↑) p<0.001 1:5s vs. 1:1u (1:1u ↑) p<0.05 1:5u vs. 1:1u (1:1u ↑) p<0.01 1:5s vs. 1:1u (1:1u ↑) 1:5s vs. 1:1s (1:1s ↑) p<0.05 1:5u vs. 1:1s (1:1s ↑) p<0.01 1:5s vs. 1:1u (1:1u ↑) 1:5s vs. 1:1s (1:1s ↑) p<0.05
4	360	p=0.0034	1:5s vs. 1:1s (1:1s ↑) p<0.05 1:5u vs. 1:1s (1:1s ↑) p<0.01 1:5s vs. 1:1u (1:1u ↑) 1:5s vs. 1:1s (1:1s ↑) p<0.05
4	1440	p=0.0468	1:5s vs. 1:1s (1:1s ↑) p<0.05 1:5s vs. 1:1s (1:1s ↑)
5.6	2	p=0.1171	N/A
5.6	4	p=0.1148	N/A
5.6	6	p=0.2220	N/A
5.6	8	p=0.3419	N/A
5.6	10	p=0.4506	N/A
5.6	20	p=0.1077	N/A
5.6	30	p=0.0380	p<0.05 1:5u vs. 1:5s (1:5s ↑)
5.6	40	p=0.0803	N/A
5.6	50	p=0.2044	N/A
5.6	60	p=0.0059	p<0.05 1:5u vs. 1:1u (1:1u ↑) 1:5u vs. 1:1s (1:1s ↑) p<0.01 1:5u vs. 1:5s (1:5s ↑)
5.6	120	p=0.3073	N/A
5.6	180	p=0.0932	N/A
5.6	240	p=0.1364	N/A
5.6	300	p=0.1624	N/A
5.6	360	p=0.1530	N/A
5.6	1440	p=0.2204	N/A

*u=unstirred, s=stirred

Total silver profiles generated at pH 5.6 are shown in Figure 5-42. The increase in total silver was more gradual at pH 5.6 and the total silver continued to rise at 24 hours, again indicating that a true equilibrium was not reached. There were no clear differences in total silver with varying conditions of dissolution. Statistical analysis, shown in Table 5-1, indicated that the only time points at which there were significant differences in total silver release were 30 minutes and 60 minutes, and the only difference that was present at both time points was that the 1:5 stirred solution had significantly higher total silver than the 1:5 unstirred solution. Variability was high with dissolution at pH 5.6, likely due to the fact that distilled water was used, and the pH of the water may have varied from day to day. The pH was not precisely controlled, as it was anticipated that the simplest method of generating solutions in a hospital setting would be dissolution of the dressings in distilled water, if the solutions demonstrated appropriate properties. Therefore, these results are similar to those which would be obtained in a hospital setting.

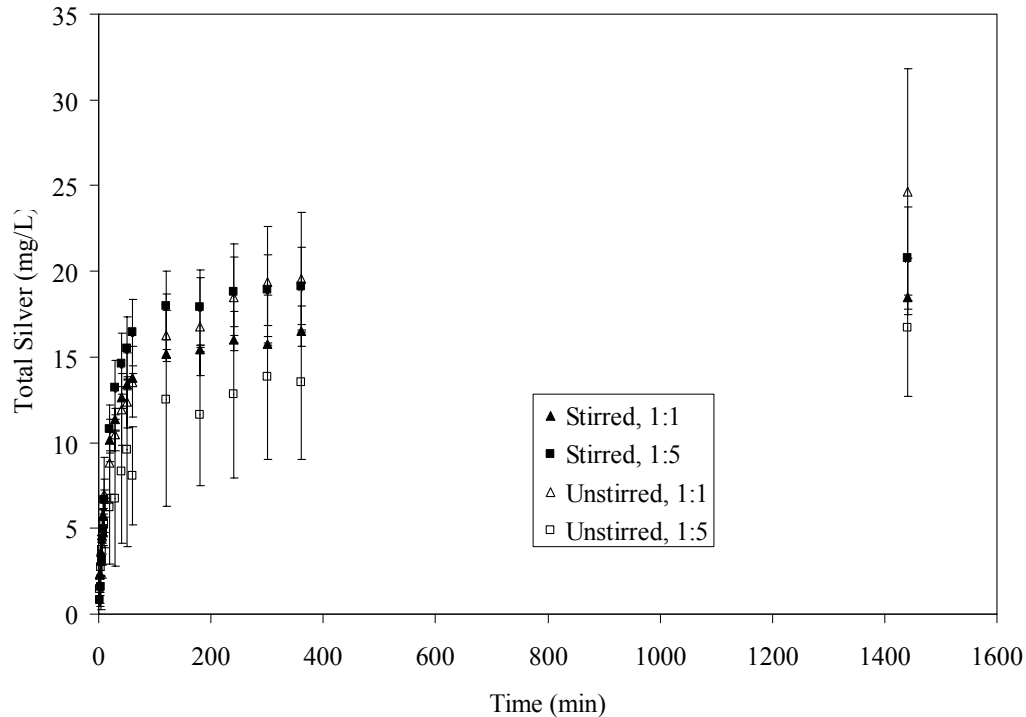


Figure 5-42. Total silver profiles over time for nanocrystalline silver-derived solutions generated at a starting pH of 5.6 under various conditions. Solutions were generated by adding nanocrystalline silver to distilled water at a ratio of either 1:5 or 1:1 in² Ag/mL. The silver was allowed to dissolve either stirred or unstirred, and samples were collected for total silver analysis by AAS at set times. Error bars represent standard deviations (n=3 for all data points).

Figure 5-43 shows total silver profiles generated at pH 7. The pattern of increase in total silver was very similar to that observed with solutions generated at pH 5.6, but the variability was much smaller. This is likely due to the fact that the starting pH was not controlled at pH 5.6, but was precisely controlled using calcium hydroxide at pH 7. At pH 7, a ratio of 1:1 in² Ag/mL resulted in higher total silver in solution throughout the time period studied relative to a ratio of 1:5. Only stirred solutions were analyzed as results with pH 4 and pH 5.6 indicated that there might be less variability, without reduced efficacy, when stirring was applied (see further discussion below). Statistical analyses, shown in Table 5-2, indicated that a ratio of 1:1 in² Ag/mL resulted in significantly higher total silver

than a ratio of 1:5 at four minutes, and at eight minutes through 60 minutes, after which time point, the two were no longer significantly different statistically. This is different from the results of pH 4 dissolutions, and suggests that the starting quantity of silver available for dissolution has less impact on the semi-equilibrated state at neutral pH than in acids.

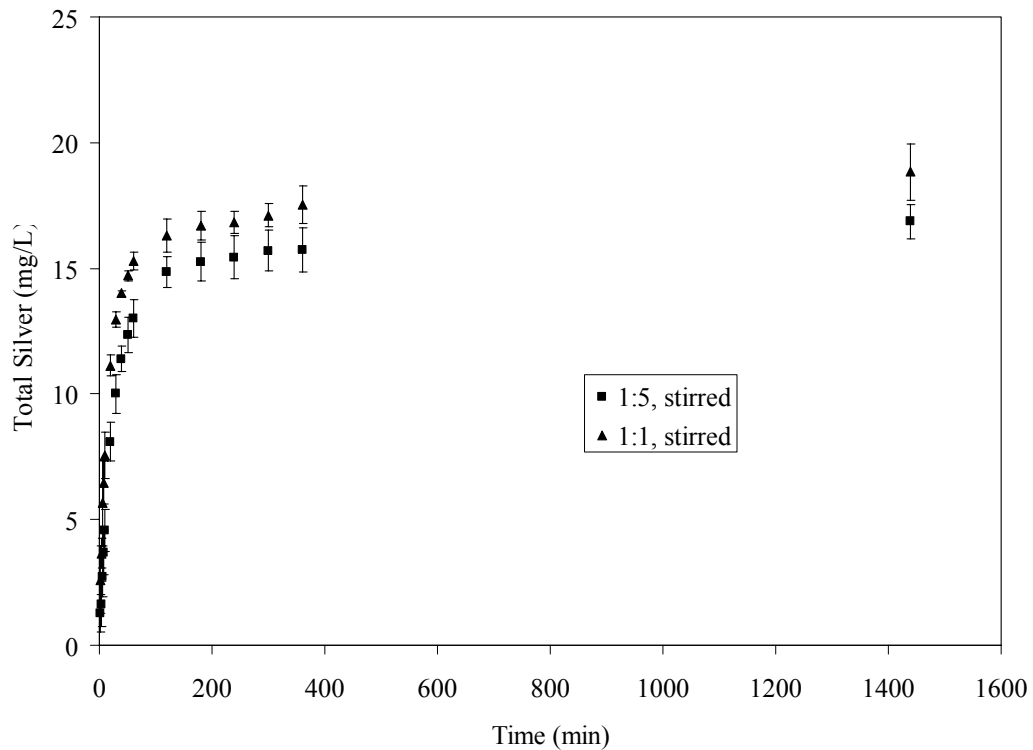


Figure 5-43. Total silver profiles over time for nanocrystalline silver-derived solutions generated at a starting pH of 7 at different silver:solution ratios. Solutions were generated by adding nanocrystalline silver to water, adjusted to a starting pH of 7 using calcium hydroxide, at a ratio of either 1:5 or 1:1 in² Ag/mL. The silver was dissolved under stirring, and samples were collected for total silver analysis by AAS at set times. Error bars represent standard deviations (n=3 for all data points).

Table 5-2. Results of statistical analyses of the effect of varying the ratio of silver dressing to solution volume, at starting pHs of 7 or 9, on the total silver dissolved in stirred solutions. Statistically significant results are in bold.

pH	Time (min)	P Value
7	2	0.2308
7	4	0.0486 (1:1↑)
7	6	0.1146
7	8	0.0298 (1:1↑)
7	10	0.0258 (1:1↑)
7	20	0.0269 (1:1↑)
7	30	0.0242 (1:1↑)
7	40	0.0126 (1:1↑)
7	50	0.0308 (1:1↑)
7	60	0.0408 (1:1↑)
7	120	0.0660
7	180	0.0766
7	240	0.0863
7	300	0.0783
7	360	0.0727
7	1440	0.0809
9	2	0.0220 (1:1↑)
9	4	0.0404 (1:1↑)
9	6	0.0043 (1:1↑)
9	8	0.0037 (1:1↑)
9	10	0.0037 (1:1↑)
9	20	0.0027 (1:1↑)
9	30	0.0064 (1:1↑)
9	40	0.0085 (1:1↑)
9	50	0.0142 (1:1↑)
9	60	0.0649
9	120	0.0547
9	180	0.0653
9	240	0.0263 (1:1↑)
9	300	0.0250 (1:1↑)
9	360	0.0650
9	1440	0.0107 (1:1↑)

Figure 5-44 shows total silver profiles generated at pH 9. The pattern observed was very similar to that of the pH 7 solutions. However, unlike at pH 7, a ratio of 1:1 in² Ag/mL resulted in a significantly higher total silver at most time points relative to a ratio of 1:5 (see Table 5-2). Similar to dissolution in acids,

this suggests that at basic pHs, the total silver dissolved in solution over time, including at a semi-equilibrated state (i.e. 24 hours), is dependent on the initial quantity of silver provided for dissolution. It should be noted that at the end of all experiments, the dressings in solution were examined and they always still had plenty of silver available for dissolution.

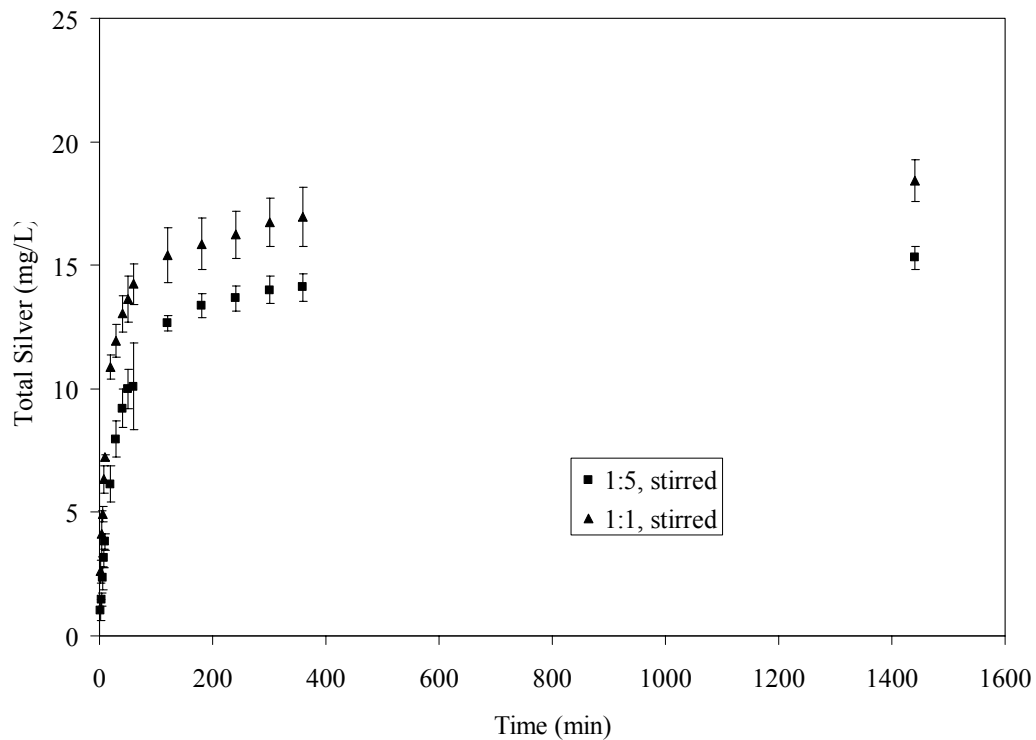


Figure 5-44. Total silver profiles over time for nanocrystalline silver-derived solutions generated at a starting pH of 9 at different silver:solution ratios. Solutions were generated by adding nanocrystalline silver to water, adjusted to a starting pH of 9 using calcium hydroxide, at a ratio of either 1:5 or 1:1 in² Ag/mL. The silver was dissolved under stirring, and samples were collected for total silver analysis by AAS at set times. Error bars represent standard deviations (n=3).

A comparison of solutions generated unstirred at pH 4 and 5.6 is shown in Figure 5-45, where a ratio of 1:5 in² Ag/mL solution was used. Under these conditions, solutions generated at pH 4 had much higher total silver than those generated at pH 5.6. Statistical analyses of the data is shown in Table 5-3, and

indicates that from 50 minutes on, with the exception of 120 minutes, the solutions generated at pH 4 were significantly higher than those generated at pH 5.6. Similar results were observed when solutions with starting pHs of 4 or 5.6 generated unstirred at a ratio of 1:1 in² Ag/mL were compared (Figure 5-46). Table 5-3 indicates that throughout the time period studied, the solutions generated in pH 4 had significantly higher total silver than those generated in pH 5.6. Initial high readings and higher variability associated with some profiles generated in the absence of stirring may be related to the position of the sample port relative to the dressings. The change in volume of solution due to sampling may also have had a bigger impact on variability in unstirred solutions than in stirred solutions, and the sampling itself may have caused minor disturbances resulting in variability in the results.

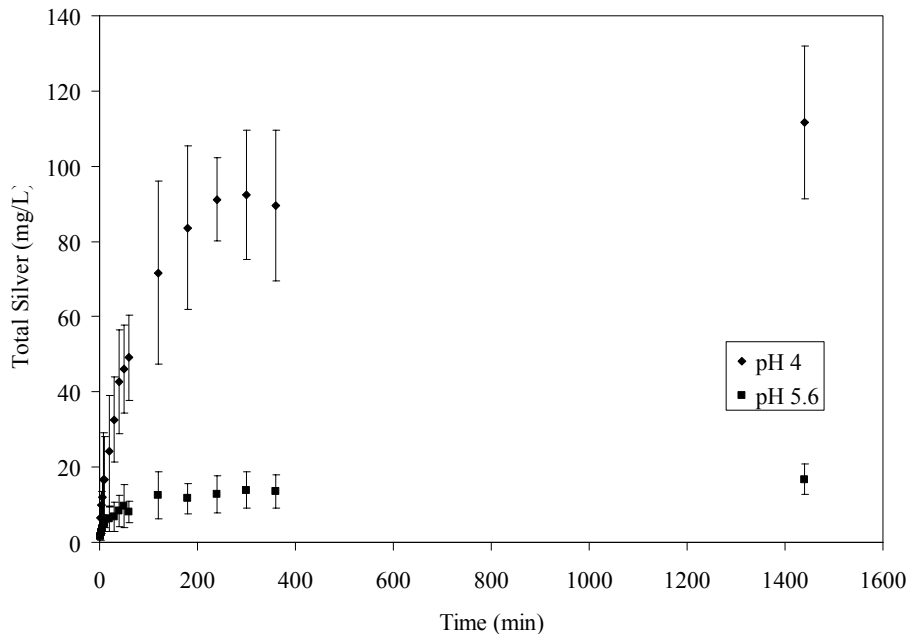


Figure 5-45. Comparison of total silver profiles over time of nanocrystalline silver-derived solutions generated at starting pHs of 4 (carbonated water) and 5.6 (distilled water), unstirred, at a ratio of 1:5 in² Ag/mL solution. Samples were collected at set times during dissolution for total silver analysis by AAS. Error bars represent standard deviations (n=3 for all data points).

Table 5-3. Results of statistical analyses of the effect of starting pH (pH 4 versus pH 5.6) on the total silver dissolved in solutions generated in the absence of stirring. Statistically significant results are in bold.

Ratio	Time (min)	p Value
1:5	2	0.1314
1:5	4	0.0822
1:5	6	0.0952
1:5	8	0.2434
1:5	10	0.2301
1:5	20	0.1745
1:5	30	0.0652
1:5	40	0.0544
1:5	50	0.0401 (pH 4 ↑)
1:5	60	0.0259 (pH 4 ↑)
1:5	120	0.0548
1:5	180	0.0300 (pH 4 ↑)
1:5	240	0.0077 (pH 4 ↑)
1:5	300	0.0166 (pH 4 ↑)
1:5	360	0.0236 (pH 4 ↑)
1:5	1440	0.0155 (pH 4 ↑)
1:1	2	0.0206 (pH 4 ↑)
1:1	4	0.0418 (pH 4 ↑)
1:1	6	0.0039 (pH 4 ↑)
1:1	8	0.0246 (pH 4 ↑)
1:1	10	0.0104 (pH 4 ↑)
1:1	20	0.0032 (pH 4 ↑)
1:1	30	0.0004 (pH 4 ↑)
1:1	40	0.0019 (pH 4 ↑)
1:1	50	0.0093 (pH 4 ↑)
1:1	60	0.0007 (pH 4 ↑)
1:1	120	0.0015 (pH 4 ↑)
1:1	180	0.0010 (pH 4 ↑)
1:1	240	0.0003 (pH 4 ↑)
1:1	300	<0.0001 (pH 4 ↑)
1:1	360	0.0023 (pH 4 ↑)
1:1	1440	0.0008 (pH 4 ↑)

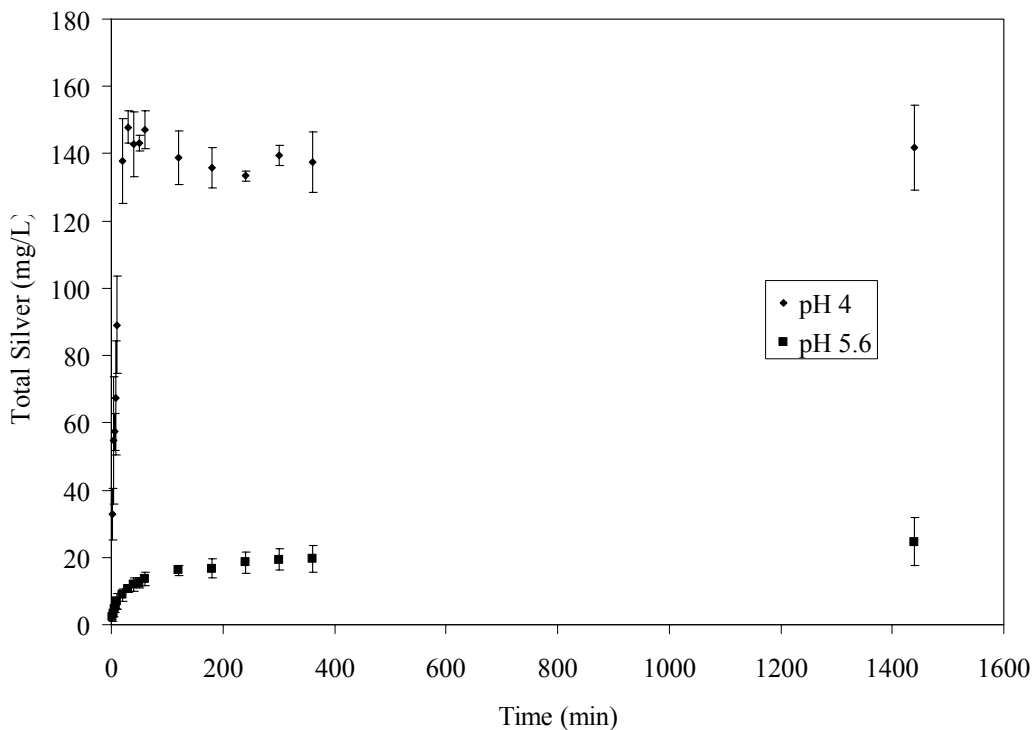


Figure 5-46. Comparison of total silver profiles over time of nanocrystalline silver-derived solutions generated at starting pHs of 4 (carbonated water) and 5.6 (distilled water), unstirred, at a ratio of 1:1 in² Ag/mL solution. Samples were collected at set times during dissolution for total silver analysis by AAS. Error bars represent standard deviations (n=3 for all data points).

A comparison of solutions generated stirred at pHs 4 through 9 is shown in Figure 5-47, where a ratio of 1:5 in² Ag/mL solution was used. Solutions generated at pH 4 had the highest total silver in solution, being statistically significantly higher than the other three solutions at all time points (see Table 5-4), and the total silver in solution decreased at any given time with increasing pH, but there were never statistically significant differences in total silver between solutions generated at pH 5.6, 7, or 9.

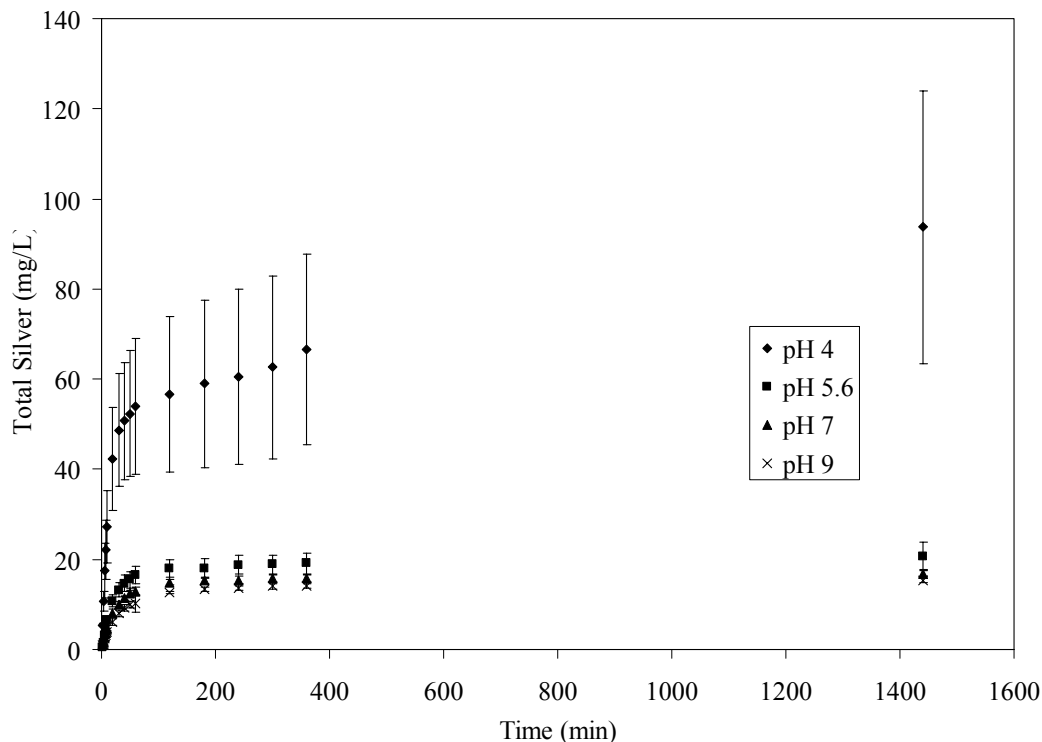


Figure 5-47. Comparison of total silver profiles over time of nanocrystalline silver-derived solutions generated at starting pHs of 4 (carbonated water), 5.6 (distilled water), 7 (adjusted using calcium hydroxide), or 9 (adjusted using calcium hydroxide), stirred, at a ratio of 1:5 in² Ag/mL solution. Samples were collected at set times during dissolution for total silver analysis by AAS. Error bars represent standard deviations (n=3 for all data points).

Table 5-4. Results of statistical analyses of the effect of starting pH (pH 4, pH 5.6, pH 7, or pH 9) on the total silver dissolved in solutions generated under stirring. Statistically significant results are in bold.

Ratio (in ² Ag/mL)	Time (min)	ANOVA	Post Tests
1:5	2	p<0.0001	p<0.001 pH 4 vs. pH 5.6 (pH 4 ↑) pH 4 vs. pH 7 (pH 4 ↑) pH 4 vs. pH 9 (pH 4 ↑)
1:5	4	p<0.0001	p<0.001 pH 4 vs. pH 5.6 (pH 4 ↑) pH 4 vs. pH 7 (pH 4 ↑) pH 4 vs. pH 9 (pH 4 ↑)
1:5	6	p=0.0007	p<0.01 pH 4 vs. pH 5.6 (pH 4 ↑) pH 4 vs. pH 7 (pH 4 ↑) pH 4 vs. pH 9 (pH 4 ↑)
1:5	8	p=0.0003	p<0.01 pH 4 vs. pH 5.6 (pH 4 ↑) p<0.001

1:5	10	p=0.0003	pH 4 vs. pH 7 (pH 4 ↑) pH 4 vs. pH 9 (pH 4 ↑) p<0.01 pH 4 vs. pH 5.6 (pH 4 ↑) p<0.001
1:5	20	p=0.0002	pH 4 vs. pH 7 (pH 4 ↑) pH 4 vs. pH 9 (pH 4 ↑) p<0.001 pH 4 vs. pH 5.6 (pH 4 ↑) pH 4 vs. pH 7 (pH 4 ↑) pH 4 vs. pH 9 (pH 4 ↑)
1:5	30	p=0.0001	p<0.001 pH 4 vs. pH 5.6 (pH 4 ↑) pH 4 vs. pH 7 (pH 4 ↑) pH 4 vs. pH 9 (pH 4 ↑)
1:5	40	p=0.0002	p<0.001 pH 4 vs. pH 5.6 (pH 4 ↑) pH 4 vs. pH 7 (pH 4 ↑) pH 4 vs. pH 9 (pH 4 ↑)
1:5	50	p=0.0002	p<0.001 pH 4 vs. pH 5.6 (pH 4 ↑) pH 4 vs. pH 7 (pH 4 ↑) pH 4 vs. pH 9 (pH 4 ↑)
1:5	60	p=0.0003	p<0.01 pH 4 vs. pH 5.6 (pH 4 ↑) p<0.001 pH 4 vs. pH 7 (pH 4 ↑) pH 4 vs. pH 9 (pH 4 ↑)
1:5	120	p=0.0008	p<0.01 pH 4 vs. pH 5.6 (pH 4 ↑) pH 4 vs. pH 7 (pH 4 ↑) pH 4 vs. pH 9 (pH 4 ↑)
1:5	180	p=0.0009	p<0.01 pH 4 vs. pH 5.6 (pH 4 ↑) pH 4 vs. pH 7 (pH 4 ↑) pH 4 vs. pH 9 (pH 4 ↑)
1:5	240	p=0.0010	p<0.01 pH 4 vs. pH 5.6 (pH 4 ↑) pH 4 vs. pH 7 (pH 4 ↑) pH 4 vs. pH 9 (pH 4 ↑)
1:5	300	p=0.0011	p<0.01 pH 4 vs. pH 5.6 (pH 4 ↑) pH 4 vs. pH 7 (pH 4 ↑) pH 4 vs. pH 9 (pH 4 ↑)
1:5	360	p=0.0008	p<0.01 pH 4 vs. pH 5.6 (pH 4 ↑)

1:5	1440	p=0.0006	pH 4 vs. pH 7 (pH 4 ↑) pH 4 vs. pH 9 (pH 4 ↑) p<0.01 pH 4 vs. pH 5.6 (pH 4 ↑) pH 4 vs. pH 7 (pH 4 ↑) pH 4 vs. pH 9 (pH 4 ↑)
1:1	2	p=0.0010	p<0.01 pH 4 vs. pH 5.6 (pH 4 ↑) pH 4 vs. pH 7 (pH 4 ↑) pH 4 vs. pH 9 (pH 4 ↑)
1:1	4	p=0.0111	p<0.05 pH 4 vs. pH 5.6 (pH 4 ↑) pH 4 vs. pH 7 (pH 4 ↑) pH 4 vs. pH 9 (pH 4 ↑)
1:1	6	p=0.0015	p<0.01 pH 4 vs. pH 5.6 (pH 4 ↑) pH 4 vs. pH 7 (pH 4 ↑) pH 4 vs. pH 9 (pH 4 ↑)
1:1	8	p=0.0018	p<0.01 pH 4 vs. pH 5.6 (pH 4 ↑) pH 4 vs. pH 7 (pH 4 ↑) pH 4 vs. pH 9 (pH 4 ↑)
1:1	10	p=0.0007	p<0.01 pH 4 vs. pH 5.6 (pH 4 ↑) pH 4 vs. pH 7 (pH 4 ↑) pH 4 vs. pH 9 (pH 4 ↑)
1:1	20	p<0.0001	p<0.001 pH 4 vs. pH 5.6 (pH 4 ↑) pH 4 vs. pH 7 (pH 4 ↑) pH 4 vs. pH 9 (pH 4 ↑)
1:1	30	p<0.0001	p<0.001 pH 4 vs. pH 5.6 (pH 4 ↑) pH 4 vs. pH 7 (pH 4 ↑) pH 4 vs. pH 9 (pH 4 ↑)
1:1	40	p<0.0001	p<0.001 pH 4 vs. pH 5.6 (pH 4 ↑) pH 4 vs. pH 7 (pH 4 ↑) pH 4 vs. pH 9 (pH 4 ↑)
1:1	50	p<0.0001	p<0.001 pH 4 vs. pH 5.6 (pH 4 ↑) pH 4 vs. pH 7 (pH 4 ↑) pH 4 vs. pH 9 (pH 4 ↑)
1:1	60	p<0.0001	p<0.001 pH 4 vs. pH 5.6 (pH 4 ↑) pH 4 vs. pH 7 (pH 4 ↑) pH 4 vs. pH 9 (pH 4 ↑)

1:1	120	p<0.0001	p<0.001 pH 4 vs. pH 5.6 (pH 4 ↑) pH 4 vs. pH 7 (pH 4 ↑) pH 4 vs. pH 9 (pH 4 ↑)
1:1	180	p<0.0001	p<0.001 pH 4 vs. pH 5.6 (pH 4 ↑) pH 4 vs. pH 7 (pH 4 ↑) pH 4 vs. pH 9 (pH 4 ↑)
1:1	240	p<0.0001	p<0.001 pH 4 vs. pH 5.6 (pH 4 ↑) pH 4 vs. pH 7 (pH 4 ↑) pH 4 vs. pH 9 (pH 4 ↑)
1:1	300	p<0.0001	p<0.001 pH 4 vs. pH 5.6 (pH 4 ↑) pH 4 vs. pH 7 (pH 4 ↑) pH 4 vs. pH 9 (pH 4 ↑)
1:1	360	p<0.0001	p<0.001 pH 4 vs. pH 5.6 (pH 4 ↑) pH 4 vs. pH 7 (pH 4 ↑) pH 4 vs. pH 9 (pH 4 ↑)
1:1	1440	p<0.0001	p<0.001 pH 4 vs. pH 5.6 (pH 4 ↑) pH 4 vs. pH 7 (pH 4 ↑) pH 4 vs. pH 9 (pH 4 ↑)

A comparison of solutions generated stirred at pHs 4 through 9 is shown in Figure 5-48, where a ratio of 1:1 in² Ag/mL solution was used. As with a ratio of 1:5, the pH 4 solutions resulted in consistently higher total silver in solution than the other pHs. Statistical analyses, which are shown in Table 5-4, again show that the solutions generated at pH 4 had significantly higher total silver at all time points, while the other three solutions were never significantly different. Overall, this indicates that at low pH, the total silver dissolved into solution is much higher (5-10 fold) than at mid-to-high pHs, and that at pHs of distilled water and up the total silver dissolved doesn't change significantly with pH.

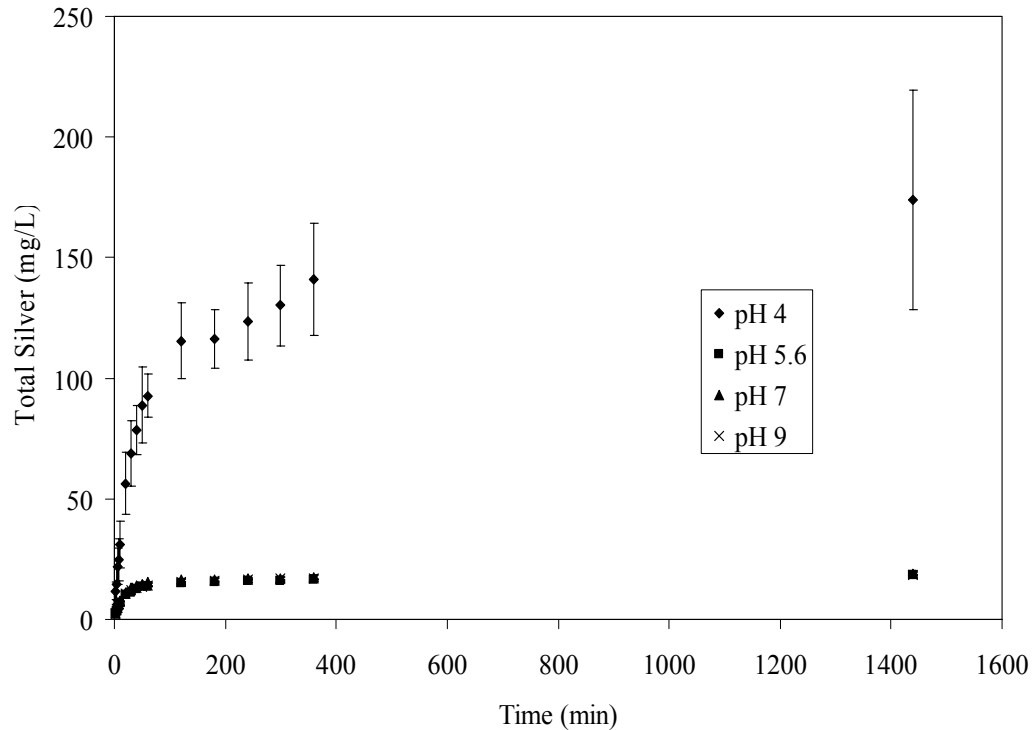


Figure 5-48. Comparison of total silver profiles over time of nanocrystalline silver-derived solutions generated at starting pHs of 4 (carbonated water), 5.6 (distilled water), 7 (adjusted using calcium hydroxide), or 9 (adjusted using calcium hydroxide), stirred, at a ratio of 1:1 in² Ag/mL solution. Samples were collected at set times during dissolution for total silver analysis by AAS. Error bars represent standard deviations (n=3 for all data points).

Table 5-5 analyzes the effect of dissolution time on total silver under various dissolution conditions. With solutions generated at pH 4, there were no clear trends, as there were statistically significant differences between 1 hour and 24 hour dissolutions for solutions generated at a ratio of 1:5 unstirred, or for solutions generated at a ratio of 1:1 stirred, but no significant differences for 1:5 stirred or 1:1 unstirred solutions. What is clear, however, is that there were never significant differences in total silver between 6 and 24 hours. With solutions generated at pH 5.6, there were no significant differences in total silver between 1 and 24 hours for 1:5 unstirred solutions, 1:5 stirred solutions, or 1:1 unstirred

solutions. However, with 1:1 stirred solutions, there were statistically significant differences between all three time points tested. At pH 7, stirred solutions generated at ratios of either 1:1 or 1:5 had statistically significant differences in total silver between 1 and 6 hours, and between 1 and 24 hours, but not between 6 and 24 hours. The same results were obtained for pH 9 solutions. This indicates that the total silver did not change significantly when the solutions were allowed to dissolve overnight, but that there were significant differences occurring within the first few hours of dissolution.

Table 5-5. Results of statistical analyses of the effect of dissolution time on the total silver dissolved under various conditions. Significant results are in bold.

pH	Ratio (in ² Ag/mL)	Stirred?	ANOVA	Post-Tests
4	1:5	No	p=0.0136	P<0.05 1h vs. 24h (24h ↑)
4	1:5	Yes	p=0.1771	N/A
4	1:1	No	p=0.5104	N/A
4	1:1	Yes	p=0.0428	P<0.05 1h vs. 24h (24h ↑)
5.6	1:5	No	p=0.0825	N/A
5.6	1:5	Yes	p=0.1688	N/A
5.6	1:1	No	p=0.0818	N/A
5.6	1:1	Yes	p<0.0001	P<0.001 1h vs. 6h (6h ↑) 1h vs. 24h (24h ↑) 6h vs. 24h (24h ↑)
7	1:5	Yes	p=0.0022	p<0.05 1h vs. 6h (6h ↑) p<0.01 1h vs. 24h (24h ↑)
7	1:1	Yes	p=0.0049	p<0.05 1h vs. 6h (6h ↑) p<0.01 1h vs. 24h (24h ↑)
9	1:5	Yes	p=0.0026	p<0.01 1h vs. 6h (6h ↑) 1h vs. 24h (24h ↑)
9	1:1	Yes	p=0.0049	p<0.05 1h vs. 6h (6h ↑) 1h vs. 24h (24h ↑)

pH Profiles

Profiles of the pH during dissolution were generated over time for a starting pH of 4 under various conditions (different ratios of nanocrystalline silver dressing to solution volume, and whether or not the solution was stirred), and are shown in Figure 5-49. Solutions generated under stirring did not demonstrate pH equilibration in 24 hours, and reached higher pHs than solutions that were left unstirred (pHs of ~7 versus pHs of ~5 at 24 hours). Unstirred solutions generated at a ratio of 1:1 in² Ag/mL reached higher pHs than unstirred solutions generated at a ratio of 1:5 in² Ag/mL. The same result was observed with stirred solutions. Statistical analyses (shown in Table 5-6) indicate that at early time points (8-40 minutes), 1:1 stirred solutions were at significantly higher pHs relative to either 1:5 unstirred solutions or 1:1 unstirred solutions. From 50 minutes to 360 minutes, 1:1 stirred solutions were no longer significantly different from 1:1 unstirred solutions, but they were significantly different again at 24 hours. From 60 minutes on, 1:1 stirred solutions had significantly higher pHs than 1:5 unstirred or stirred solutions. From 50 minutes on, 1:1 unstirred solutions had significantly higher pHs than 1:5 unstirred solutions, and at 24 hours, they were also significantly higher than 1:5 stirred solutions. From 300 minutes on, 1:5 stirred solutions also had significantly higher pHs than 1:5 unstirred solutions.

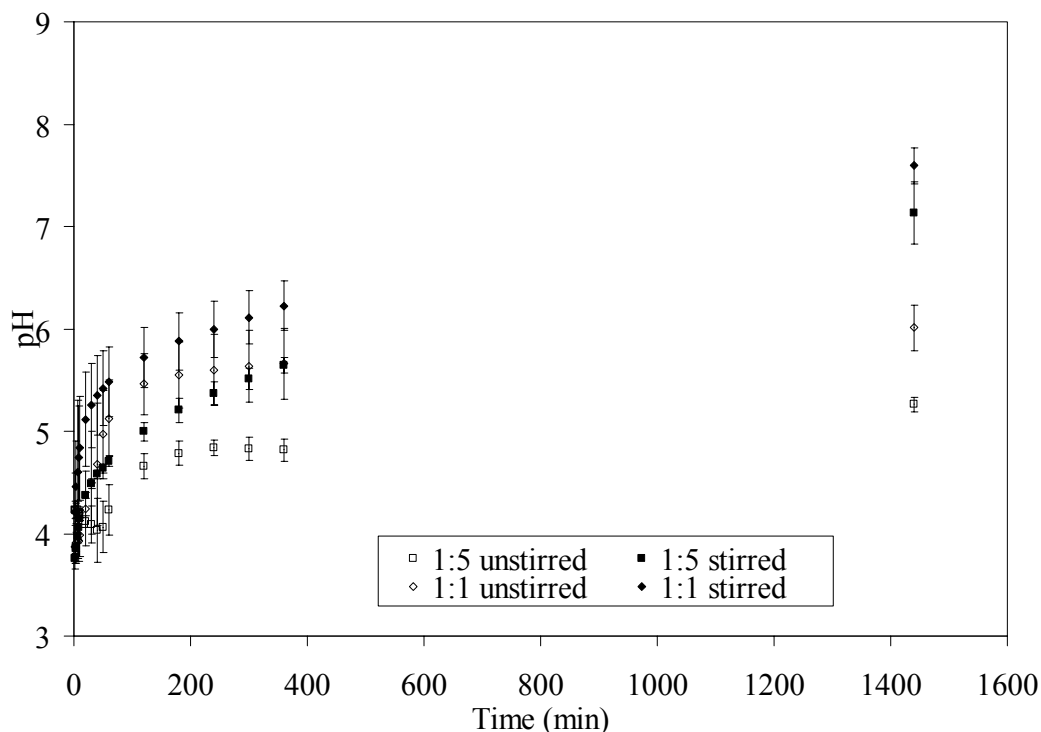


Figure 5-49. pH profiles over time for nanocrystalline silver-derived solutions generated at a starting pH of 4 under various conditions. Solutions were generated by adding nanocrystalline silver to water bubbled down to a pH of 4 using carbon dioxide at a ratio of either 1:5 or 1:1 in² Ag/mL. The silver was allowed to dissolve either stirred or unstirred, and the solution pH was recorded at set times during dissolution. Error bars = standard deviations (n=3 for all points).

Table 5-6. Results of statistical analyses on the effect of varying dissolution conditions (stirred or unstirred, ratio of nanocrystalline silver dressing to solution) on the pH during dissolution using a starting pH of 4 or 5.6. Statistically significant results are in bold.

pH	Time (min)	ANOVA p Value	Post Test
4	2	0.0739	N/A
4	4	0.0547	N/A
4	6	0.1716	N/A
4	8	0.0283	p<0.05 1:1u vs. 1:1s* (1:1s ↑)
4	10	0.0237	p<0.05 1:1u vs. 1:1s (1:1s ↑)
4	20	0.0132	p<0.05 1:5u vs. 1:1s (1:1s ↑) 1:1u vs. 1:1s (1:1s ↑)
4	30	0.0179	p<0.05 1:5u vs. 1:1s (1:1s ↑)
4	40	0.0212	p<0.05 1:5u vs. 1:1s (1:1s ↑)

4	50	0.0042	p<0.05 1:5u vs. 1:1u (1:1u ↑)
4	60	0.0033	p<0.01 1:5u vs. 1:1s (1:1s ↑) p<0.05 1:5u vs. 1:1u (1:1u ↑) 1:5s vs. 1:1s (1:1s ↑)
4	120	0.0016	p<0.01 1:5u vs. 1:1s (1:1s ↑) p<0.05 1:5s vs. 1:1s (1:1s ↑)
4	180	0.0023	p<0.01 1:5u vs. 1:1u (1:1u ↑) 1:5s vs. 1:1s (1:1s ↑) p<0.05 1:5u vs. 1:1s (1:1s ↑)
4	240	0.0018	p<0.01 1:5u vs. 1:1s (1:1s ↑) p<0.05 1:5u vs. 1:1u (1:1u ↑) 1:5s vs. 1:1s (1:1s ↑)
4	300	0.0010	p<0.01 1:5u vs. 1:1s (1:1s ↑) p<0.05 1:5u vs. 1:5s (1:5s ↑) 1:5u vs. 1:1u (1:1u ↑) 1:5s vs. 1:1s (1:1s ↑)
4	360	0.0004	p<0.001 1:5u vs. 1:1s (1:1s ↑) p<0.05 1:5s vs. 1:1s (1:1s ↑) p<0.01 1:5u vs. 1:5s (1:5s ↑) 1:5u vs. 1:1u (1:1u ↑)
4	1440	<0.0001	p<0.001 1:5u vs. 1:1s (1:1s ↑) p<0.01 1:5u vs. 1:1u p<0.001 1:5u vs. 1:5s 1:5u vs. 1:1s 1:5s vs. 1:1u 1:1u vs. 1:1s
5.6	2	0.6066	N/A
5.6	4	0.0828	N/A

5.6	6	0.0098	p<0.05 1:5s vs. 1:5u (1:5s ↑) 1:5u vs. 1:1s (1:1s ↑)
5.6	8	0.0055	p<0.05 1:5s vs. 1:5u (1:5s ↑) p<0.01 1:5u vs. 1:1s (1:1s ↑)
5.6	10	0.0039	p<0.01 1:5s vs. 1:5u (1:5s ↑) 1:5u vs. 1:1s (1:1s ↑)
5.6	20	0.0061	p<0.05 1:5s vs. 1:5u (1:5s ↑) p<0.01 1:5u vs. 1:1s (1:1s ↑)
5.6	30	0.0092	p<0.05 1:5s vs. 1:5u (1:5s ↑) 1:5u vs. 1:1s (1:1s ↑)
5.6	40	0.0102	p<0.05 1:5s vs. 1:5u (1:5s ↑) 1:5u vs. 1:1s (1:1s ↑)
5.6	50	0.0132	p<0.05 1:5s vs. 1:5u (1:5s ↑) 1:5u vs. 1:1s (1:1s ↑)
5.6	60	0.0169	p<0.05 1:5s vs. 1:5u (1:5s ↑) 1:5u vs. 1:1s (1:1s ↑)
5.6	120	0.0219	p<0.05 1:5s vs. 1:5u (1:5s ↑) 1:5u vs. 1:1s (1:1s ↑)
5.6	180	0.0085	p<0.05 1:5s vs. 1:5u (1:5s ↑) 1:5u vs. 1:1s (1:1s ↑)
5.6	240	0.0567	N/A
5.6	300	0.0335	p<0.05 1:5s vs. 1:5u (1:5s ↑)
5.6	360	0.0422	p<0.05 1:5s vs. 1:5u (1:5s ↑)
5.6	1440	0.4355	N/A

*u=unstirred, s=stirred

Figure 5-50 shows pH profiles generated using a starting pH of 5.6 under various conditions. Initial variability was very high, particularly with unstirred solutions, for reasons discussed in the total silver profile section. However, all the

profiles ended up following a similar pattern, resulting in a final pH of approximately 9.5-10, with no significant differences present at 24 hours. From 4-180 minutes, both stirred solutions (1:5 and 1:1) had significantly higher pHs than the 1:5 unstirred solution, while at 300-360 minutes, only the 1:5 stirred solution had a significantly higher pH than the 1:5 unstirred solution (see Table 5-6). The clearest pattern from the data was that, as with pH 4 solutions, stirring resulted in higher pHs than leaving solutions unstirred, irrespective of the ratio of silver to solution.

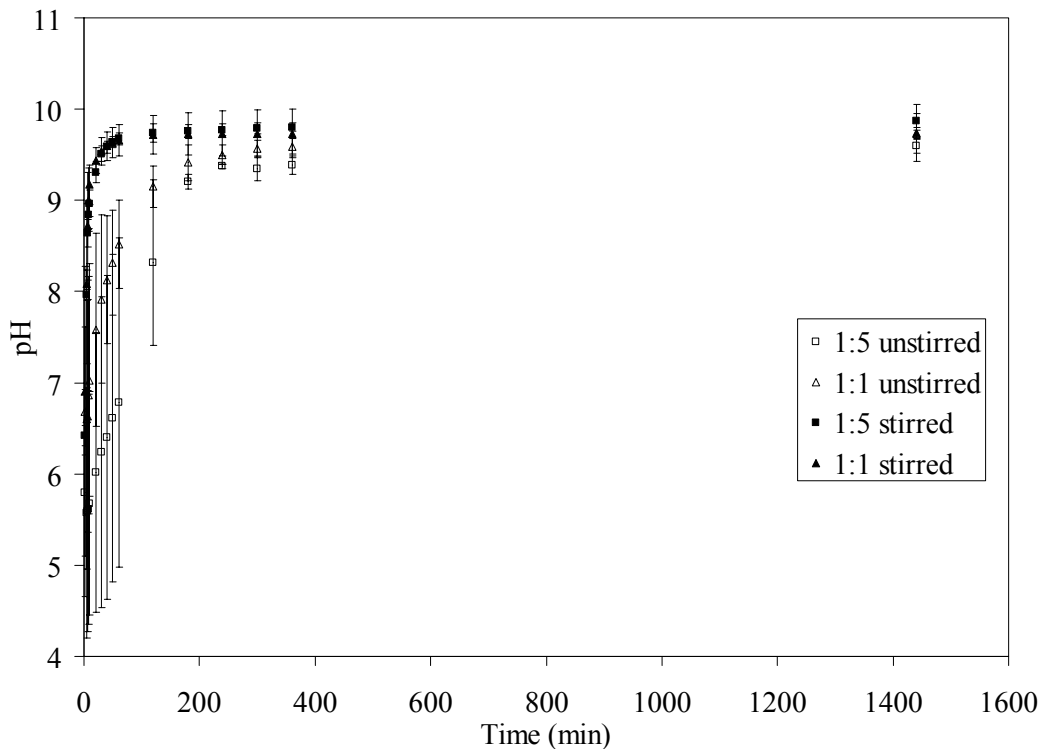


Figure 5-50. pH profiles over time for nanocrystalline silver-derived solutions generated at a starting pH of 5.6 under various conditions. Solutions were generated by adding nanocrystalline silver to distilled water at a ratio of either 1:5 or 1:1 in² Ag/mL. The silver was allowed to dissolve either stirred or unstirred, and the solution pH was recorded at set times during dissolution. Error bars represent standard deviations (n=3 for all data points).

A comparison of pH profiles generated under stirring with a starting pH of 7 and ratios of either 1:1 or 1:5 in² Ag/mL is shown in Figure 5-51. Both ratios of silver to solution showed very similar patterns, and the final pH reached was ~10. Statistical analyses are shown in Table 5-7. The only statistically significant difference between the two solutions occurred at 24 hours, where the 1:5 stirred solution had a higher pH than the 1:1 stirred solution. This suggests again that, unlike total silver measurements, the ratio of nanocrystalline silver dressing to solution volume does not affect the final pH of the solution. This was confirmed as well with the profiles performed at pH 9 (see Figure 5-52), and the statistical analyses (see Table 5-7), which showed that once again, a pH of ~10 was reached, and that there were no significant differences between using a ratio of 1:5 and a ratio of 1:1.

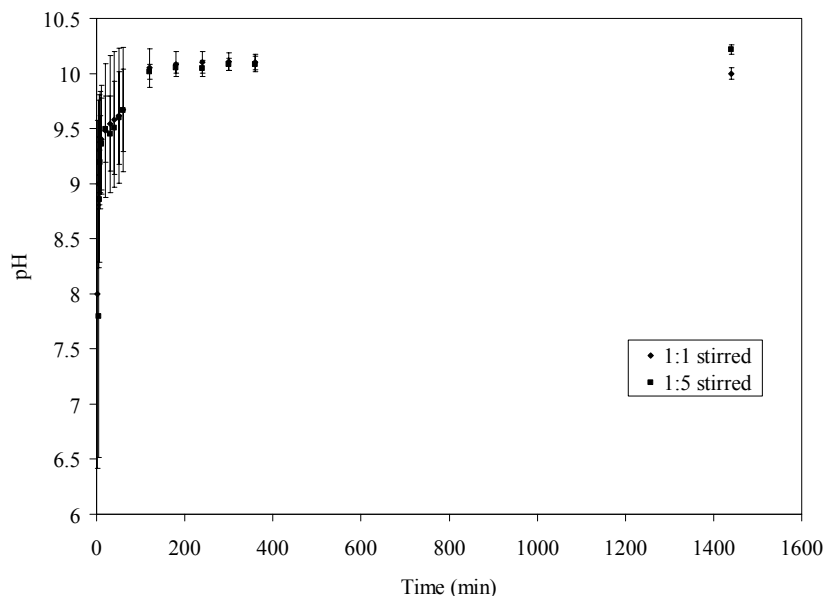


Figure 5-51. pH profiles over time for nanocrystalline silver-derived solutions generated at a starting pH of 7 at different silver:solution ratios. Solutions were generated by adding nanocrystalline silver to water, adjusted to a starting pH of 7 using calcium hydroxide, at a ratio of either 1:5 or 1:1 in² Ag/mL. The silver was dissolved under stirring, and the pH was recorded at set times during dissolution. Error bars represent standard deviations (n=3 for all data points).

Table 5-7. Results of statistical analyses on the effect of varying the ratio of nanocrystalline silver dressing to solution on the pH during dissolution using a starting pH of 7 or 9. Statistically significant results are in bold.

pH	Time (min)	p Value
7	4	0.2566
7	6	0.3767
7	8	0.6419
7	10	0.9156
7	20	0.9729
7	30	0.8458
7	40	0.8712
7	50	0.9656
7	60	0.9837
7	120	0.7868
7	180	0.6550
7	240	0.4691
7	300	0.6686
7	360	0.7771
7	1440	0.0108 (1:5 ↑)
9	2	0.2418
9	4	0.3357
9	6	0.4426
9	8	0.4258
9	10	0.4000
9	20	0.4374
9	30	0.4738
9	40	0.4873
9	50	0.6144
9	60	0.8886
9	120	0.9503
9	180	0.3332
9	240	0.3288
9	300	0.3162
9	360	0.2998
9	1440	0.3106

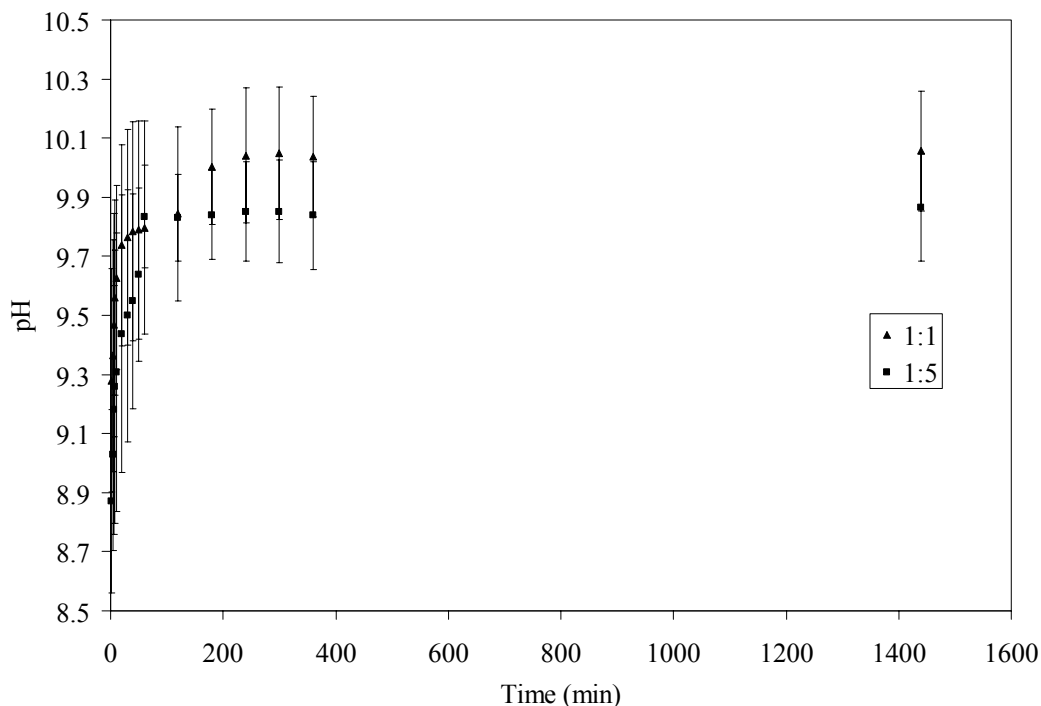


Figure 5-52. pH profiles for nanocrystalline silver-derived solutions generated at a starting pH of 9 at different silver:solution ratios. Solutions were generated by adding nanocrystalline silver to water, adjusted to a starting pH of 9 using calcium hydroxide, at a ratio of either 1:5 or 1:1 in² Ag/mL. The silver was dissolved under stirring, and the solution pH was recorded at set times during dissolution. Error bars represent standard deviations (n=3 for all data points).

A comparison of pH profiles generated from solutions started at pH 4 or 5.6 without stirring, at a ratio of 1:5 in² Ag/mL, is shown in Figure 5-53. The solutions started at pH 5.6 attained a much higher solution pH than the solutions started at pH 4. This was statistically significant from 120 minutes on (see Table 5-8).

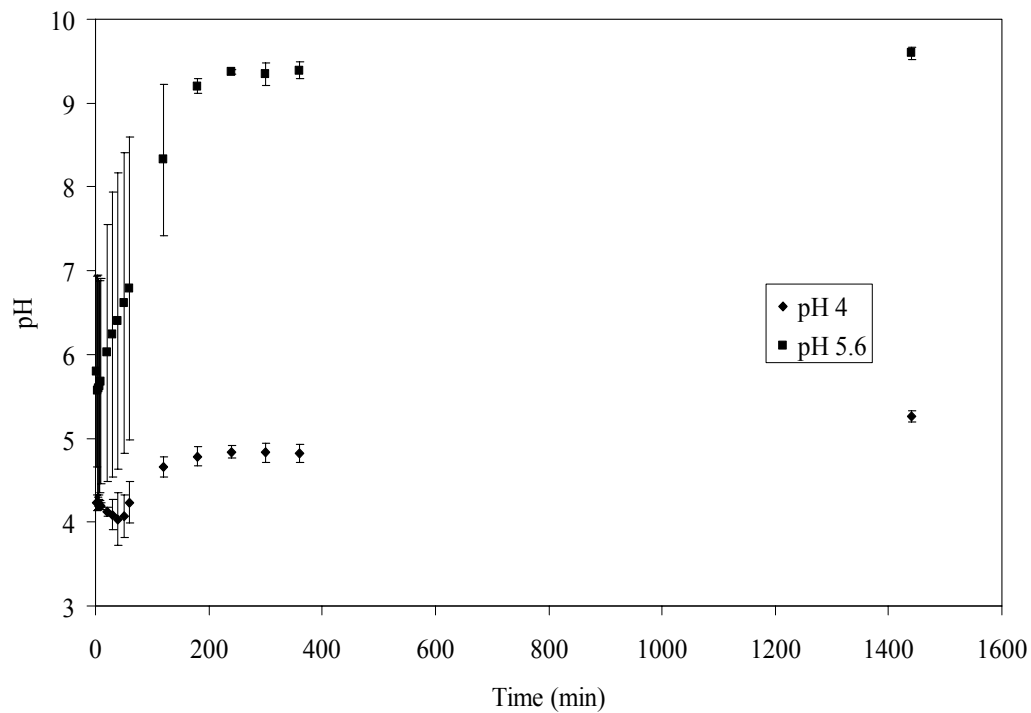


Figure 5-53. Comparison of pH profiles over time for nanocrystalline silver-derived solutions generated at starting pHs of 4 (carbonated water) and 5.6 (distilled water), unstirred, at a ratio of 1:5 in² Ag/mL solution. Solution pHs were recorded at set times during dissolution. Error bars represent standard deviations (n=3 for all data points).

Table 5-8. Results of statistical analyses of the effect of varying the starting pH (4 or 5.6), during dissolution without stirring, on pH over time. Statistically significant results are in bold.

Ratio (in ² Ag/mL)	Time (min)	p Value
1:5	2	0.1412
1:5	4	0.2320
1:5	6	0.2185
1:5	8	0.1924
1:5	10	0.1713
1:5	20	0.1652
1:5	30	0.1616
1:5	40	0.1507
1:5	50	0.1350
1:5	60	0.1361
1:5	120	0.0203 (pH 5.6 ↑)
1:5	180	<0.0001 (pH 5.6 ↑)
1:5	240	0.0001 (pH 5.6 ↑)
1:5	300	<0.0001 (pH 5.6 ↑)
1:5	360	<0.0001 (pH 5.6 ↑)
1:5	1440	0.0002 (pH 5.6 ↑)
1:1	2	0.0929
1:1	4	0.1058
1:1	6	0.0681
1:1	8	0.0609
1:1	10	0.0552
1:1	20	0.0356 (pH 5.6 ↑)
1:1	30	0.0111 (pH 5.6 ↑)
1:1	40	0.0075 (pH 5.6 ↑)
1:1	50	0.0040 (pH 5.6 ↑)
1:1	60	0.0024 (pH 5.6 ↑)
1:1	120	0.0004 (pH 5.6 ↑)
1:1	180	0.0004 (pH 5.6 ↑)
1:1	240	0.0029 (pH 5.6 ↑)
1:1	300	0.0028 (pH 5.6 ↑)
1:1	360	0.0027 (pH 5.6 ↑)
1:1	1440	0.0012 (pH 5.6 ↑)

A comparison of pH profiles generated starting from pHs 4 and 5.6, unstirred with a ratio of 1:1 in² Ag/mL, is shown in Figure 5-54. Again, the pH profile is much higher with the starting pH of 5.6 relative to pH 4. This reached statistical significance from 20 minutes on (see Table 5-8), as the pH changed more quickly at early times relative to the 1:5 unstirred solutions.

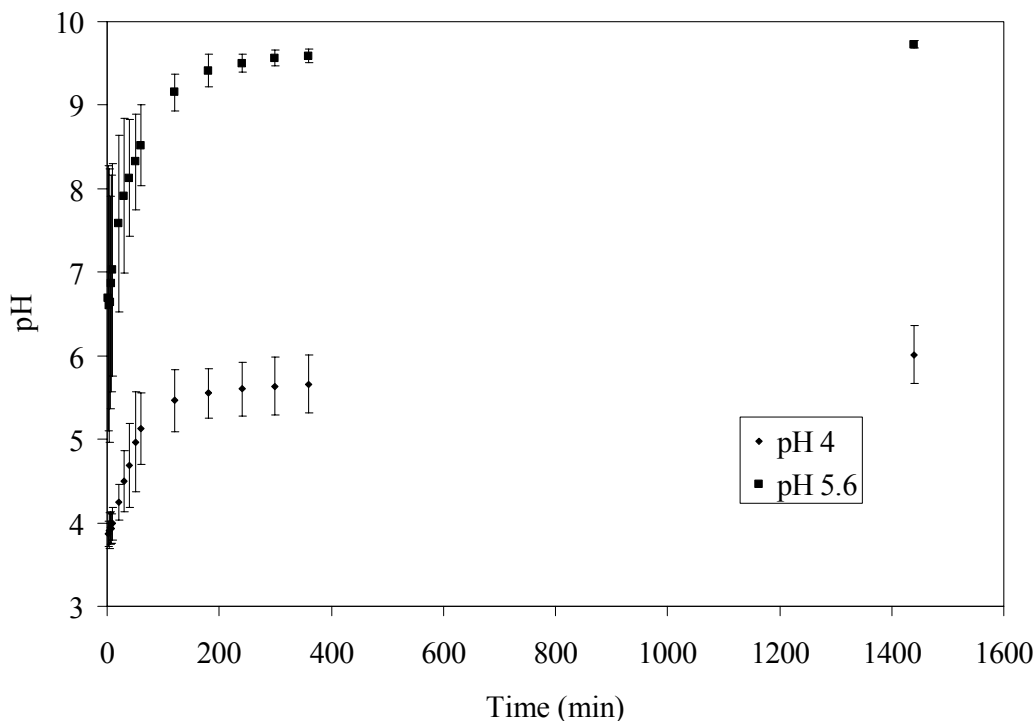


Figure 5-54. Comparison of pH profiles over time for nanocrystalline silver-derived solutions generated at starting pHs of 4 (carbonated water) and 5.6 (distilled water), unstirred, at a ratio of 1:1 in² Ag/mL solution. Solution pHs were recorded at set times during dissolution. Error bars represent standard deviations (n=3 for all data points).

Figure 5-55 shows a comparison of pH profiles generated at starting pHs of 4 through 9, under stirring, with a ratio of 1:5 in² Ag/mL. Starting pHs of 5.6 through 9 had very similar pH profiles, which were much higher than the pH 4 profile. The pH 4 profile had statistically significantly lower pHs than the other three starting pHs throughout the test period (see Table 5-9). At 120, 180, 300, and 360 minutes, solutions started at pH 7 had significantly higher pHs than solutions started at pH 5.6.

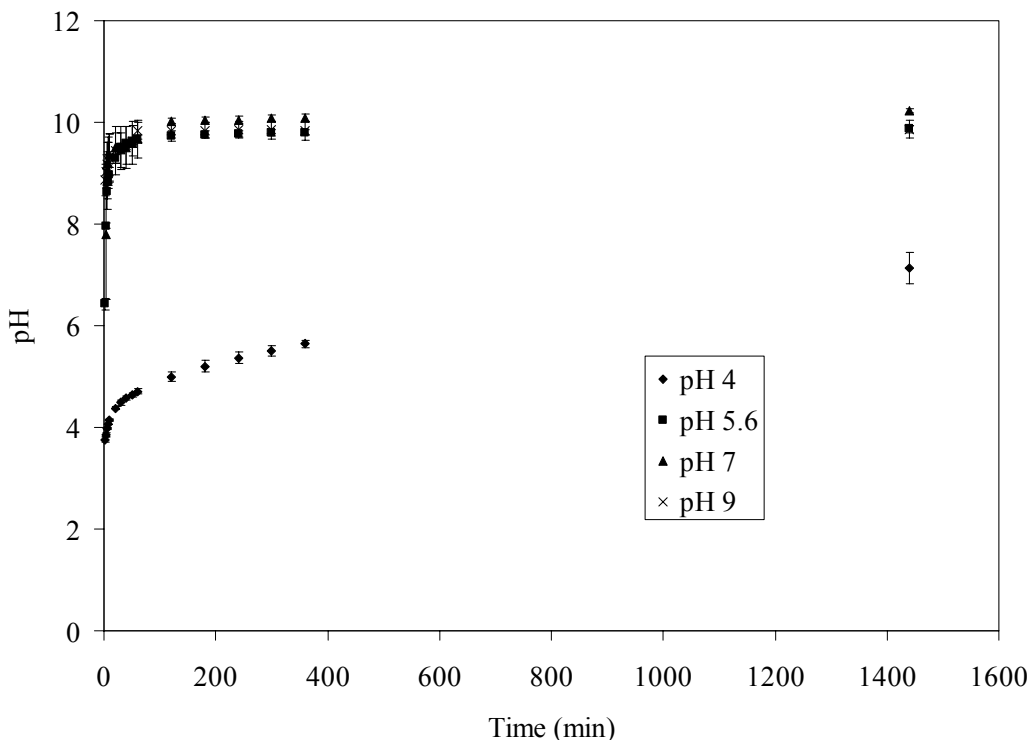


Figure 5-55. Comparison of pH profiles over time for nanocrystalline silver-derived solutions generated at starting pHs of 4 (carbonated water), 5.6 (distilled water), 7 (adjusted using calcium hydroxide), or 9 (adjusted using calcium hydroxide), stirred, at a ratio of 1:5 in² Ag/mL solution. Solution pHs were recorded at set times during dissolution. Error bars = standard deviations (n=3).

Table 5-9. Results of statistical analyses on the effect of varying the starting pH (4, 5.6, 7, or 9) during dissolution, with stirring, on the pH over time. Statistically significant results are in bold.

Ratio (in ² Ag/mL)	Time (min)	ANOVA p Value	Post Tests
1:5	2	<0.0001	p<0.001 pH 4 vs. pH 5.6 (pH 5.6 ↑) pH 4 vs. pH 7 (pH 7 ↑) pH 4 vs. pH 9 (pH 9 ↑)
1:5	4	<0.0001	p<0.001 pH 4 vs. pH 5.6 (pH 5.6 ↑) pH 4 vs. pH 7 (pH 7 ↑) pH 4 vs. pH 9 (pH 9 ↑)
1:5	6	<0.0001	p<0.001 pH 4 vs. pH 5.6 (pH 5.6 ↑) pH 4 vs. pH 7 (pH 7 ↑) pH 4 vs. pH 9 (pH 9 ↑)
1:5	8	<0.0001	p<0.001 pH 4 vs. pH 5.6 (pH 5.6 ↑)

1:5	10	<0.0001	pH 4 vs. pH 7 (pH 7 ↑) pH 4 vs. pH 9 (pH 9 ↑) p<0.001 pH 4 vs. pH 5.6 (pH 5.6 ↑) pH 4 vs. pH 7 (pH 7 ↑) pH 4 vs. pH 9 (pH 9 ↑)
1:5	20	<0.0001	p<0.001 pH 4 vs. pH 5.6 (pH 5.6 ↑) pH 4 vs. pH 7 (pH 7 ↑) pH 4 vs. pH 9 (pH 9 ↑)
1:5	30	<0.0001	p<0.001 pH 4 vs. pH 5.6 (pH 5.6 ↑) pH 4 vs. pH 7 (pH 7 ↑) pH 4 vs. pH 9 (pH 9 ↑)
1:5	40	<0.0001	p<0.001 pH 4 vs. pH 5.6 (pH 5.6 ↑) pH 4 vs. pH 7 (pH 7 ↑) pH 4 vs. pH 9 (pH 9 ↑)
1:5	50	<0.0001	p<0.001 pH 4 vs. pH 5.6 (pH 5.6 ↑) pH 4 vs. pH 7 (pH 7 ↑) pH 4 vs. pH 9 (pH 9 ↑)
1:5	60	<0.0001	p<0.001 pH 4 vs. pH 5.6 (pH 5.6 ↑) pH 4 vs. pH 7 (pH 7 ↑) pH 4 vs. pH 9 (pH 9 ↑)
1:5	120	<0.0001	p<0.05 pH 5.6 vs. pH 7 (pH 7 ↑) p<0.001 pH 4 vs. pH 5.6 (pH 5.6 ↑) pH 4 vs. pH 7 (pH 7 ↑) pH 4 vs. pH 9 (pH 9 ↑)
1:5	180	<0.0001	p<0.05 pH 5.6 vs. pH 7 (pH 7 ↑) p<0.001 pH 4 vs. pH 5.6 (pH 5.6 ↑) pH 4 vs. pH 7 (pH 7 ↑) pH 4 vs. pH 9 (pH 9 ↑)
1:5	240	<0.0001	p<0.001 pH 4 vs. pH 5.6 (pH 5.6 ↑) pH 4 vs. pH 7 (pH 7 ↑) pH 4 vs. pH 9 (pH 9 ↑)
1:5	300	<0.0001	p<0.05 pH 5.6 vs. pH 7 (pH 7 ↑) p<0.001 pH 4 vs. pH 5.6 (pH 5.6 ↑)

1:5	360	<0.0001	pH 4 vs. pH 7 (pH 7 ↑) pH 4 vs. pH 9 (pH 9 ↑) p<0.05 pH 5.6 vs. pH 7 (pH 7 ↑) p<0.001 pH 4 vs. pH 5.6 (pH 5.6 ↑) pH 4 vs. pH 7 (pH 7 ↑) pH 4 vs. pH 9 (pH 9 ↑) p<0.001
1:5	1440	<0.0001	pH 4 vs. pH 5.6 (pH 5.6 ↑) pH 4 vs. pH 7 (pH 7 ↑) pH 4 vs. pH 9 (pH 9 ↑) p<0.001
1:1	2	0.0008	p<0.05 pH 4 vs. pH 5.6 (pH 5.6 ↑) pH 5.6 vs. pH 9 (pH 9 ↑) p<0.01 pH 4 vs. pH 7 (pH 7 ↑) p<0.001 pH 4 vs. pH 9 (pH 9 ↑) p<0.001
1:1	4	<0.0001	pH 4 vs. pH 5.6 (pH 5.6 ↑) pH 4 vs. pH 7 (pH 7 ↑) pH 4 vs. pH 9 (pH 9 ↑) p<0.001
1:1	6	<0.0001	pH 4 vs. pH 5.6 (pH 5.6 ↑) pH 4 vs. pH 7 (pH 7 ↑) pH 4 vs. pH 9 (pH 9 ↑) p<0.001
1:1	8	<0.0001	pH 4 vs. pH 5.6 (pH 5.6 ↑) pH 4 vs. pH 7 (pH 7 ↑) pH 4 vs. pH 9 (pH 9 ↑) p<0.001
1:1	10	<0.0001	pH 4 vs. pH 5.6 (pH 5.6 ↑) pH 4 vs. pH 7 (pH 7 ↑) pH 4 vs. pH 9 (pH 9 ↑) p<0.001
1:1	20	<0.0001	pH 4 vs. pH 5.6 (pH 5.6 ↑) pH 4 vs. pH 7 (pH 7 ↑) pH 4 vs. pH 9 (pH 9 ↑) p<0.001
1:1	30	<0.0001	pH 4 vs. pH 5.6 (pH 5.6 ↑) pH 4 vs. pH 7 (pH 7 ↑) pH 4 vs. pH 9 (pH 9 ↑) p<0.001
1:1	40	<0.0001	pH 4 vs. pH 5.6 (pH 5.6 ↑) pH 4 vs. pH 7 (pH 7 ↑) pH 4 vs. pH 9 (pH 9 ↑) p<0.001

1:1	50	<0.0001	pH 4 vs. pH 9 (pH 9 ↑) p<0.001
1:1	60	<0.0001	pH 4 vs. pH 5.6 (pH 5.6 ↑) pH 4 vs. pH 7 (pH 7 ↑) pH 4 vs. pH 9 (pH 9 ↑) p<0.001
1:1	120	<0.0001	pH 4 vs. pH 5.6 (pH 5.6 ↑) pH 4 vs. pH 7 (pH 7 ↑) pH 4 vs. pH 9 (pH 9 ↑) p<0.001
1:1	180	<0.0001	pH 4 vs. pH 5.6 (pH 5.6 ↑) pH 4 vs. pH 7 (pH 7 ↑) pH 4 vs. pH 9 (pH 9 ↑) p<0.001
1:1	240	<0.0001	pH 4 vs. pH 5.6 (pH 5.6 ↑) pH 4 vs. pH 7 (pH 7 ↑) pH 4 vs. pH 9 (pH 9 ↑) p<0.001
1:1	300	<0.0001	pH 4 vs. pH 5.6 (pH 5.6 ↑) pH 4 vs. pH 7 (pH 7 ↑) pH 4 vs. pH 9 (pH 9 ↑) p<0.001
1:1	360	<0.0001	pH 4 vs. pH 5.6 (pH 5.6 ↑) pH 4 vs. pH 7 (pH 7 ↑) pH 4 vs. pH 9 (pH 9 ↑) p<0.001
1:1	1440	<0.0001	pH 4 vs. pH 5.6 (pH 5.6 ↑) pH 4 vs. pH 7 (pH 7 ↑) pH 4 vs. pH 9 (pH 9 ↑) p<0.001

A comparison of pH profiles generated at starting pHs of 4-9 under stirring with 1:1 in² Ag/mL is shown in Figure 5-56. The results are very similar to those using a ratio of 1:5. Profiles generated at starting pH 4 had significantly lower pHs than the other three profiles throughout the experiment (see Table 5-9). The only other significant difference was that at 2 min, the solutions generated at starting pH 9 had significantly higher pHs than those generated at starting pH 5.6.

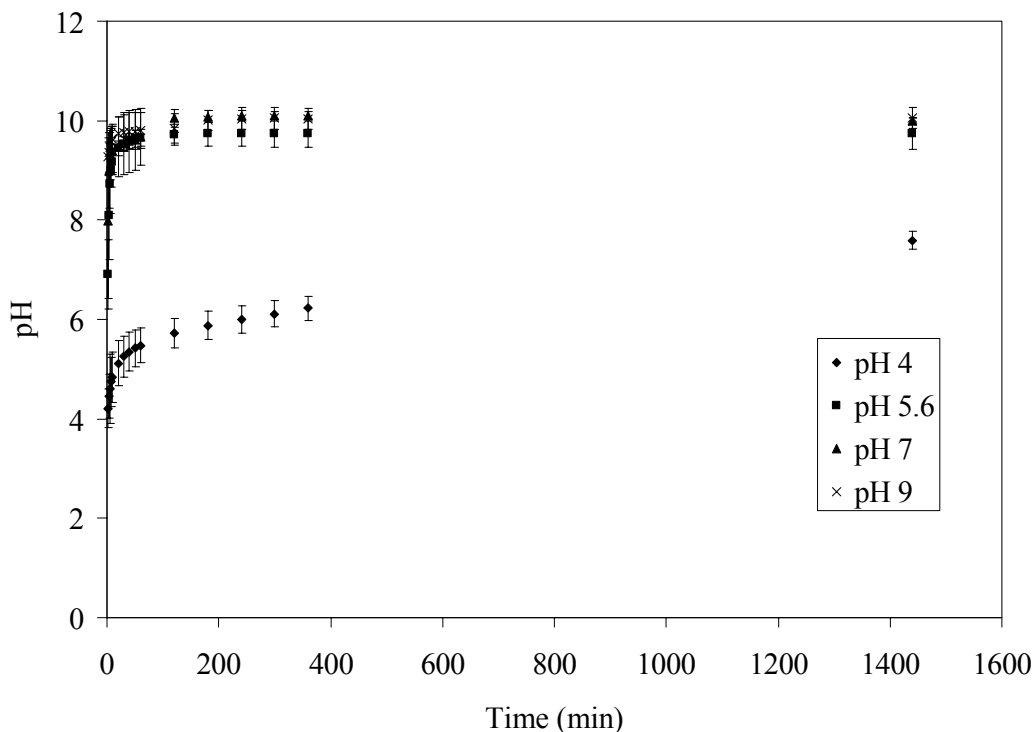


Figure 5-56. Comparison of pH profiles over time for nanocrystalline silver-derived solutions generated at starting pHs of 4 (carbonated water), 5.6 (distilled water), 7 (adjusted using calcium hydroxide), or 9 (adjusted using calcium hydroxide), stirred, at a ratio of 1:1 in² Ag/mL solution. Solution pHs were recorded at set times during dissolution. Error bars = standard deviations (n=3).

These results indicate that the solutions generated at starting pHs of 5.6 and 7 rapidly change pH in the first few minutes so that the solution pH is the same as the solutions generated at pH 9, but that this is not the case for the solution generated at pH 4. The changes in solution pH observed suggest that a reaction with solution components occurred as the nanocrystalline silver dissolved. A different reaction appears to have occurred with pH 4 solutions, as much more silver was dissolved, but the pH did not equilibrate to the same levels observed with other starting pHs, and in some cases did not equilibrate at all. This may be due to the conversion of the silver to an inactive form in the presence of carbonic acid/carbon dioxide. It is also interesting to note that despite the pH

change being smaller in pH 9 solutions relative to pH 5.6 or pH 7 solutions, the same total silver is obtained. This suggests that, relative to pH 5.6 and 7 solutions, a higher percentage of the silver released from the dressing at pH 9 does not contribute to the pH change of the solution. This may be due to the higher dissolution of an uncharged species, such as metallic silver clusters[3], at higher pH.

The effect of dissolution time on the pH profile is analyzed in Table 5-10. At pH 4, when solutions were generated at a ratio of 1:5 in² Ag/mL, with or without stirring, or 1:1 in² with stirring, there were significant differences in pH between 1 and 6 hours, 1 and 24 hours, and 6 and 24 hours, indicating continued reactions throughout the experiment. However, when solutions were generated at a ratio of 1:1 in² Ag/mL without stirring, the only significant difference was between 1 and 24 hours. With a starting pH of 5.6, the only significant differences were observed with solutions generated at a ratio of 1:5 unstirred and 1:1 stirred. In the case of the former, the only significant difference was in comparing 1 hour to 24 hours, while in the latter, the pH was different between 1 and 6 hours, and 1 and 24 hours. With solutions generated at starting pHs of 7 and 9, there were no significant differences in pH over time, due to the small change in pH occurring at higher pHs.

Table 5-10. Results of the statistical analysis of the effect of dissolution time on the pH of solutions generated under various conditions. Statistically significant results are in bold.

pH	Ratio (in ² Ag/mL)	Stirred?	ANOVA p value	Post tests
4	1:5	No	0.0007	p<0.05 1h vs. 6h (6h ↑) 6h vs. 24h (24h ↑)
4	1:5	Yes	<0.0001	p<0.001 1h vs. 24h (24h ↑) p<0.01 1h vs. 6h (6h ↑) p<0.001 1h vs. 24h (24h ↑) 6h vs. 24h (24h ↑)
4	1:1	No	0.0393	p<0.05 1h vs. 24h (24h ↑)
4	1:1	Yes	0.0002	p<0.05 1h vs. 6h (6h ↑) p<0.01 6h vs. 24h (24h ↑) p<0.001 1h vs. 24h (24h ↑)
5.6	1:5	Yes	0.0231	p<0.05 1h vs. 24h (24h ↑)
5.6	1:5	No	0.0360	No sig. differences
5.6	1:1	Yes	0.9056	N/A
5.6	1:1	No	0.0038	p<0.01 1h vs. 6h (6h ↑) 1h vs. 24h (24h ↑)
7	1:5	Yes	0.0507	N/A
7	1:1	Yes	0.3195	N/A
9	1:5	Yes	0.9738	N/A
9	1:1	Yes	0.4632	N/A

Antimicrobial Activity

The results of log reduction testing against *S. aureus* under various conditions are shown in Table 5-11. Of the conditions tested at pH 4, only solutions generated at a silver dressing:solution volume ratio of 1 in²/mL with dissolution for 1 hour resulted in total kill of the bacteria, regardless of whether or

not the solution was stirred. At pH 5.6, these same conditions resulted in total kill. In addition, when 1 in² Ag per 5 mL was used, with dissolution for 24 hours, total kill was achieved if the solution was stirred, but not if it was left unstirred. The conditions tested using pH 7 and 9 solutions did not result in bactericidal activity, but as no dissolutions were performed for only one hour, it is possible that bactericidal activity might have been generated at shorter times, as it was with the pH 4 and pH 5.6 solutions under the correct conditions. Tables 5-12 and 5-13 show the results of statistical analyses comparing the effect of pH on the antimicrobial efficacy, with other conditions held constant. The results indicate that in general, pH 5.6 and pH 7 solutions performed better than pH 4 and pH 9 solutions, with all other variables being held constant. This suggests that at mid-range pHs, more charged species are released into solution than at low or high pHs. At low pH, although the total silver released into solution tended to be more than at higher pHs, the silver released does not appear to be antimicrobial (charged), possibly due to reaction with carbonates in solution. At pH 9, the total silver released is about the same as at pH 5.6 and pH 7, therefore the lowered activity suggests again that the silver species in solution at pH 9 are not antimicrobial, either due to inactivation, or to release of silver species such as metallic silver, which would not be expected to be antimicrobial agents.

Table 5-11. Results of log reductions generated using nanocrystalline silver-derived solutions generated under a variety of conditions against *S. aureus*.

Starting pH	Acticoat : Solution (in ² :mL)	Dissolution Time (hours)	Unstirred or Stirred	Log Reduction (average±S.D.)
4	1:5	1	Unstirred	-0.8±0.1
4	1:5	1	Stirred	-0.9±0.1
4	1:5	24	Unstirred	-0.8±0.1
4	1:5	24	Stirred	0.1±1.2
4	1:1	1	Unstirred	≥2.5±0.6
4	1:1	1	Stirred	≥2.4±0.8
4	1:1	24	Unstirred	-0.2±0.2
4	1:1	24	Stirred	-0.3±0.3
5.6	1:5	1	Unstirred	-0.9±0.2
5.6	1:5	1	Stirred	0.0±0.3
5.6	1:5	24	Unstirred	1.4±0.2
5.6	1:5	24	Stirred	≥2.6±0.8
5.6	1:1	1	Unstirred	≥4.0±0.0
5.6	1:1	1	Stirred	≥3.3±0.6
5.6	1:1	24	Unstirred	0.4±0.2
5.6	1:1	24	Stirred	0.3±0.2
7	1:5	24	Stirred	1.4±0.4
7	1:1	24	Stirred	0.8±0.2
9	1:5	24	Stirred	-0.6±0.1
9	1:1	24	Stirred	-0.7±0.2

Table 5-12. Results of statistical analyses of the effect of starting pH (pH 4 versus pH 5.6) on the bactericidal efficacy of solutions generated in the absence of stirring. Statistically significant results are in bold.

Time (hours)	Ratio (in ² Ag/mL)	Stirred?	p Value
1	1:5	Yes	0.0352 (pH 5.6 ↑)
1	1:5	No	0.6174
1	1:1	Yes	0.2022
1	1:1	No	N/A (no)*
24	1:5	No	0.0027 (pH 5.6 ↑)
24	1:1	No	0.0415 (pH 5.6 ↑)

*One solution had an S.D. of 0, and therefore the analysis could not be run.

Table 5-13. Results of statistical analyses on the effect of starting pH on the bactericidal efficacy of solutions generated under stirring for 24h. Statistically significant results are in bold.

Ratio (in ² Ag/mL)	p Value (ANOVA)	Post Tests
1:5	0.0032	p<0.05: pH 4 vs. pH 5.6 (pH 5.6 ↑) pH 7 vs. pH 9 (pH 7 ↑)
1:1	0.0002	p<0.01: pH 5.6 vs. pH 9 (pH 5.6 ↑) p<0.05: pH 4 vs. pH 5.6 (pH 5.6 ↑) p<0.01: pH 4 vs. pH 7 (pH 7 ↑) pH 5.6 vs. pH 9 (pH 5.6 ↑) p<0.001: pH 7 vs. pH 9 (pH 7 ↑)

A statistical analysis of the effect of stirring on bactericidal efficacy with other variables held constant is shown in Table 5-14. In general, stirring did not appear to make a difference to the bactericidal efficacy of the solutions, except at pH 5.6, 1h dissolution time, and a ratio of 1 in² Ag/5 mL H₂O, where stirring significantly improved the bactericidal efficacy. While generating the solutions under stirring generates more consistent results with lower error (see total silver and pH profiles), there was concern that the additional energy added to the system via stirring could promote the reaction of unstable active species to less active forms. These results suggest, however, that this does not appear to be the case.

Table 5-14. Results of statistical analyses of the effect of stirring on the bactericidal efficacy of solutions. Statistically significant results are in bold.

pH	Time	Ratio	P Value
4	1	1:5	0.8918
4	1	1:1	0.8850
4	24	1:5	0.2940
4	24	1:1	0.6660
5.6	1	1:5	0.0189 (stirred ↑)
5.6	1	1:1	N/A (no)*
5.6	24	1:5	0.1113
5.6	24	1:1	0.6776

*One solution had an S.D. of 0, and therefore the analysis could not be run. However the average for that solution was within the S.D. of the other solution, suggesting there was no significant difference.

A statistical analysis of the effect of varying the ratio of silver dressing to solution volume on bactericidal efficacy, with other variables held constant, is shown in Table 5-15. In general, as would be expected, a higher ratio of silver dressing per millilitre of solution resulted in higher antimicrobial activity. This suggests that when a higher quantity of silver is placed in solution, larger quantities of active species are released into solution. This correlates with the total soluble silver, as total silver profiles (see above) indicated that the total silver in solution also generally increased when a ratio of 1:1 in² nanocrystalline silver dressing per millilitre solution was used, rather than 1:5. The only exception to this, in terms of antimicrobial activity, was when pH 5.6 solutions were allowed to dissolve for 24 hours.

Table 5-15. Results of statistical analyses of the effect of varying the ratio of silver dressing to solution volume on bactericidal efficacy, holding other variables constant. Statistically significant results are in bold.

pH	Time (hours)	Stirred?	p Value
4	1	No	0.0115 (1:1 ↑)
4	1	Yes	0.0185 (1:1 ↑)
4	24	No	0.0373 (1:1 ↑)
4	24	Yes	0.6145
5.6	1	No	N/A (yes) (1:1 ↑)*
5.6	1	Yes	0.0136 (1:1 ↑)
5.6	24	No	0.0089 (1:5 ↑)
5.6	24	Yes	0.0374 (1:5 ↑)
7	24	Yes	0.1286
9	24	Yes	0.2953

*One solution had an S.D. of 0, and therefore the analysis could not be run.

A statistical analysis of the effect of varying the dissolution time on bactericidal efficacy, with other variables held constant, is shown in Table 5-16.

Time points of one hour and 24 hours were examined as the pH profiles and total silver profiles indicated that the most dramatic changes in solution properties occurred within the first hour, with more gradual changes occurring thereafter, and typically few significant differences occurring between six and 24 hours. Interestingly, it appears that when dissolution is done with 1 in² Ag/mL solution, a one hour dissolution results in higher activity than a 24 hour dissolution, while if a dissolution is done with 1 in² Ag/5 mL solution, a 24 hour dissolution results in higher activity than a one hour dissolution, or there is little difference in activity. This suggests that there may be a period of time during which solution activity peaks, which is dependent on the initial quantity of silver placed in solution, thus occurring earlier with a higher silver quantity. After this peak, activity may drop due to silver species in solution interacting with other silver species (likely in combination with other solution components) when concentrations are high enough, resulting in the production of less active/insoluble species.

Table 5-16. Results of statistical analyses of the effect of dissolution for 1 or 24 hours on bactericidal efficacy, holding other variables constant. Statistically significant results are in bold.

pH	Ratio	Stirred?	p Value
4	1:5	No	0.6899
4	1:5	Yes	0.2816
4	1:1	No	0.0196 (1h ↑)
4	1:1	Yes	0.0302 (1h ↑)
5.6	1:5	No	0.0008 (24h ↑)
5.6	1:5	Yes	0.0320 (24h ↑)
5.6	1:1	No	N/A (yes) (1h ↑)*
5.6	1:1	Yes	0.0146 (1h ↑)

*One solution had an S.D. of 0, and therefore the analysis could not be run, however the activity at 1 hour was much higher than at 24 hours (not within the S.D.), suggesting it was significantly different.

Based on the results of Figure 5-2, and the fact that *P. aeruginosa* is generally more silver sensitive than *S. aureus*[58], it is believed that, in general, the solutions would have proved more effective against *P. aeruginosa*. Preliminary studies indicated that when solutions were generated with a ratio of 1:5 in² Ag/mL unstirred for 24 hours, starting pHs of 4.0, 4.5, and 5.6 all resulted in total kill (log reduction $\geq 5.5 \pm 0.0$). Holding all other conditions the same but performing a one hour dissolution resulted in total kill at pH 4.0 (log reduction $\geq 3.6 \pm 0.2$), but not at pH 4.5 (log reduction 1.7 ± 0.3 , which was significantly lower than the log reduction produced at pH 4, $p=0.0036$). However, due to concerns regarding the health of the lab supply of *P. aeruginosa*, and possible infection with a bacteriophage (see Figure 5-57), further tests were not performed with it.



Figure 5-57. Unusual growth of *P. aeruginosa* with the appearance of plaques, suggesting infection of the culture by a bacteriophage.

XPS

The effect of dissolution in various solutions on the dressings used as a silver source was studied. Distilled water and the two extreme starting pHs of 4 and 9 were examined, to assess the behavior of the dressings during dissolution to create solutions such as the ones tested above. Dissolution in fetal calf serum was also examined to improve understanding of the behavior of the dressing in a more physiological setting – when it contacts wound fluid – as studies have shown that fetal calf serum is a good model for human wound fluid[59].

A summary of the C1s peaks for XPS performed on nanocrystalline silver dressings after dissolution for various lengths of time in pH 4, 5.6, or 9 solutions, as well as in serum, is shown in Figure 5-58. The change in appearance of the peaks with dissolution time was most marked with the dissolution of the dressings in serum, with the appearance of an extra peak at lower binding energy, likely due to the interaction of silver with carbon species in the serum and/or deposition of serum components on the dressing during drying post-dissolution. Figure 5-59 shows sample deconvolutions of the C1s peaks in control dressings (a), and dressings dissolved in pH 4 solutions (b), pH 5.6 solutions (c), pH 9 solutions (d), and serum (e) at the 16 hour time point. The carbon peak used to check for peak shifts due to sample charging, etc. (labeled “Contaminant Carbon”) did not appear to shift with dissolution conditions, despite the very different C1s pattern observed with dissolution in serum, and therefore no peak shifts were used in the subsequent analyses.

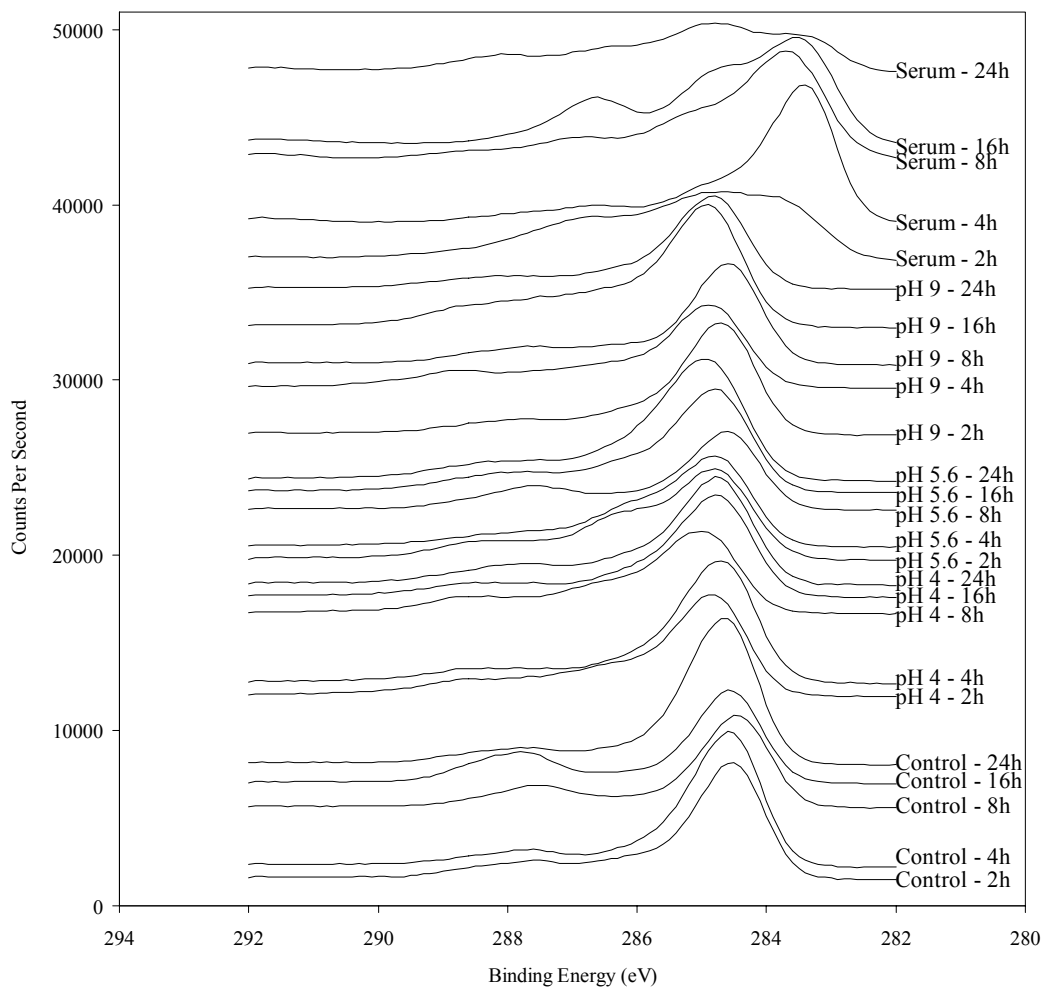


Figure 5-58. Summary of XPS intensities of C 1s peaks for nanocrystalline silver dressings after heating dry at 37°C (control dressings), or dissolution at 37°C in solutions at starting pHs of 4 (adjusted using HCl), 5.6 (reverse osmosis water), 9 (adjusted using NaOH), or fetal calf serum.

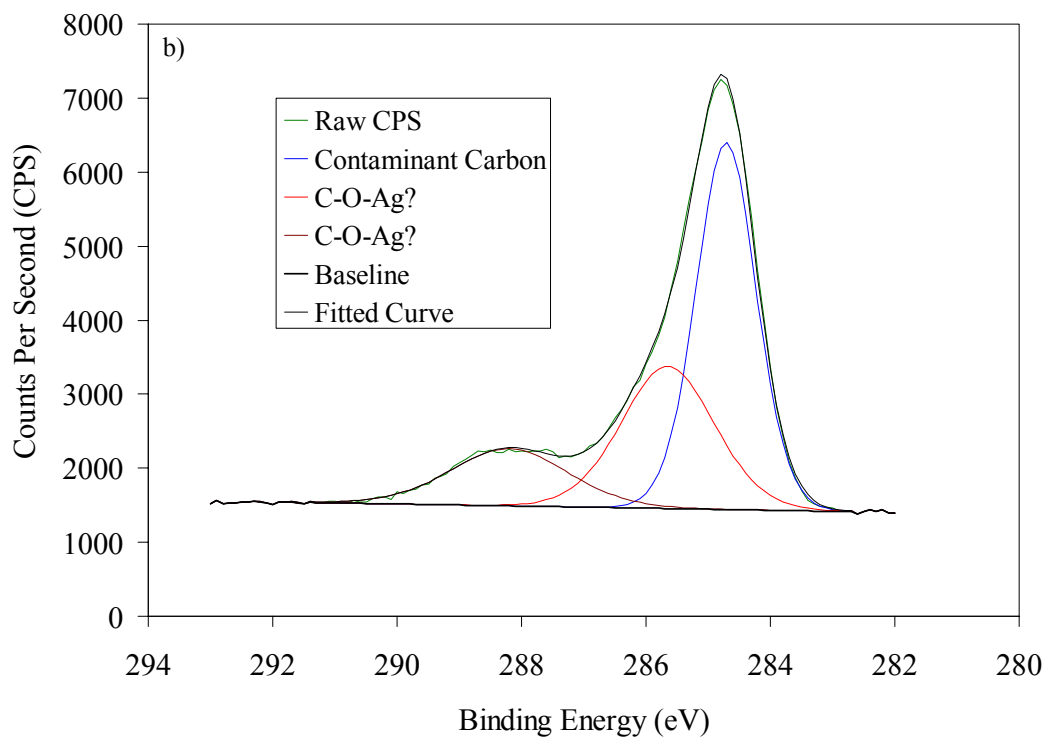
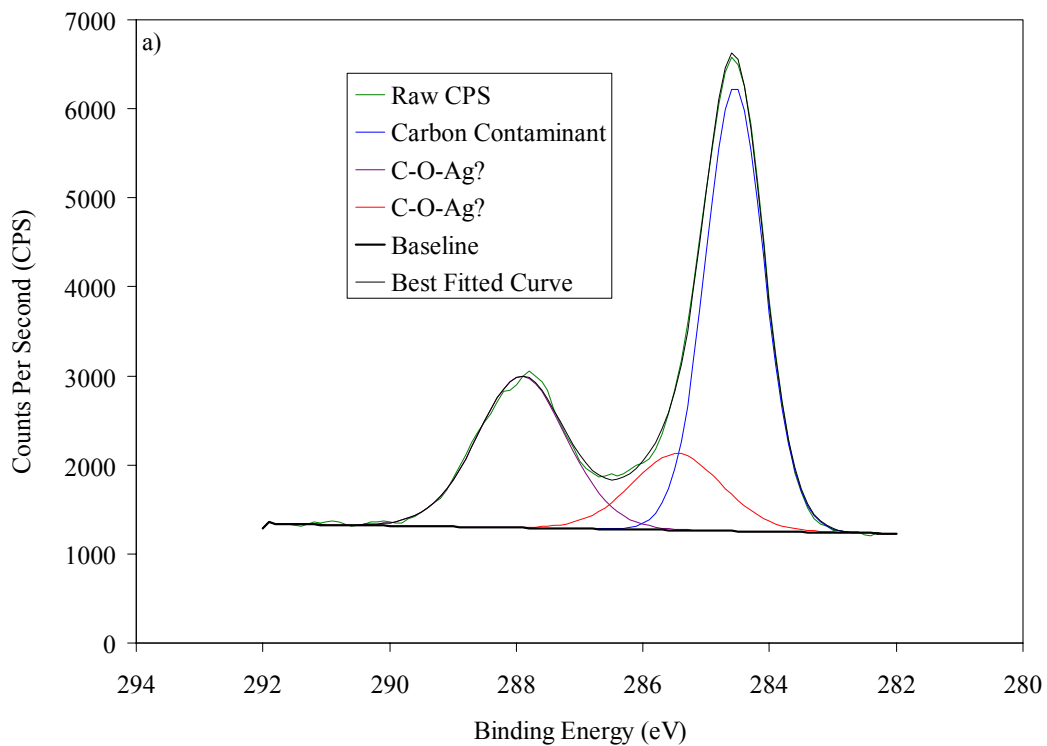


Figure 5-59.

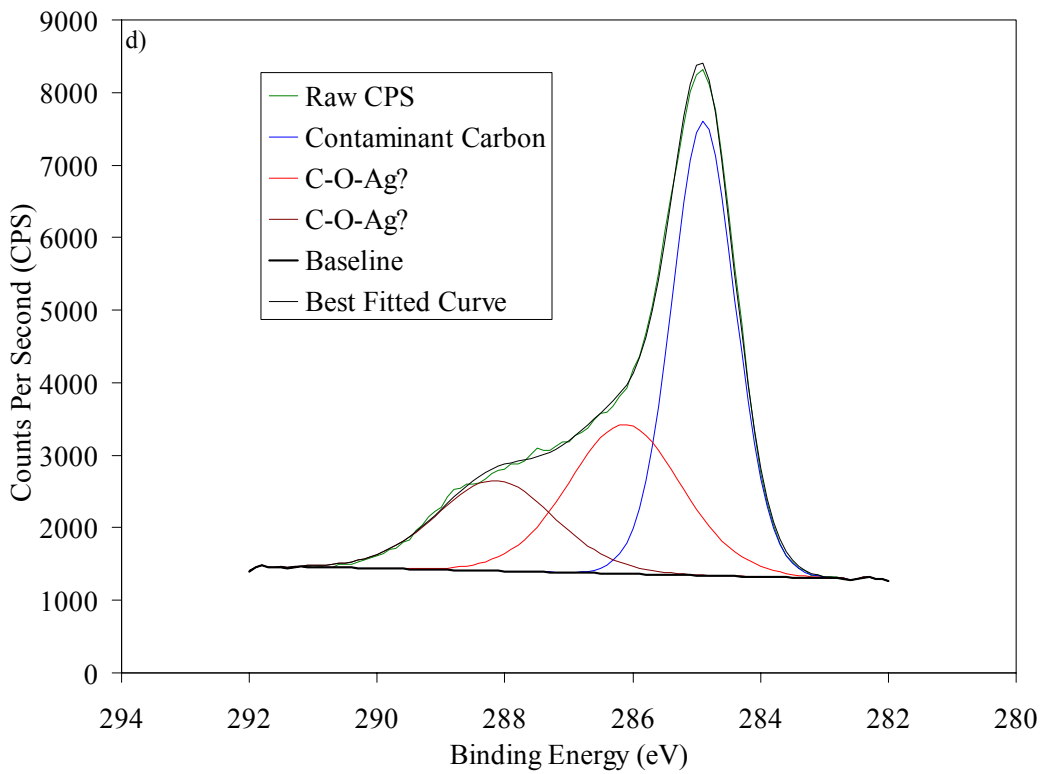
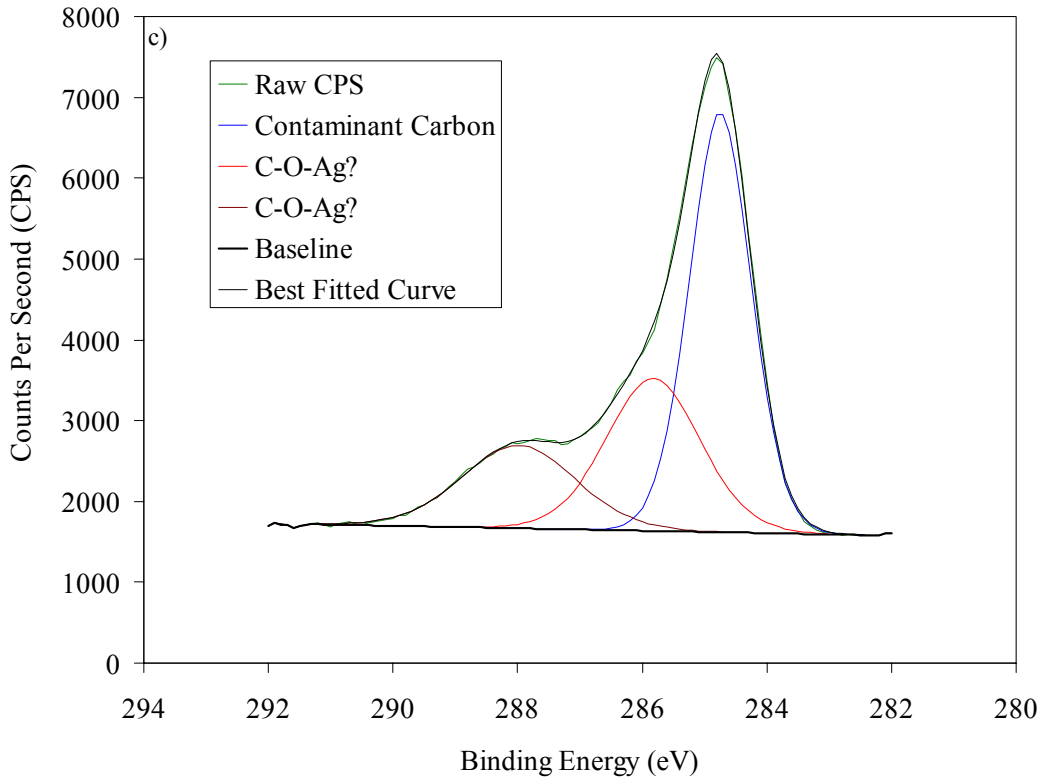


Figure 5-59, continued.

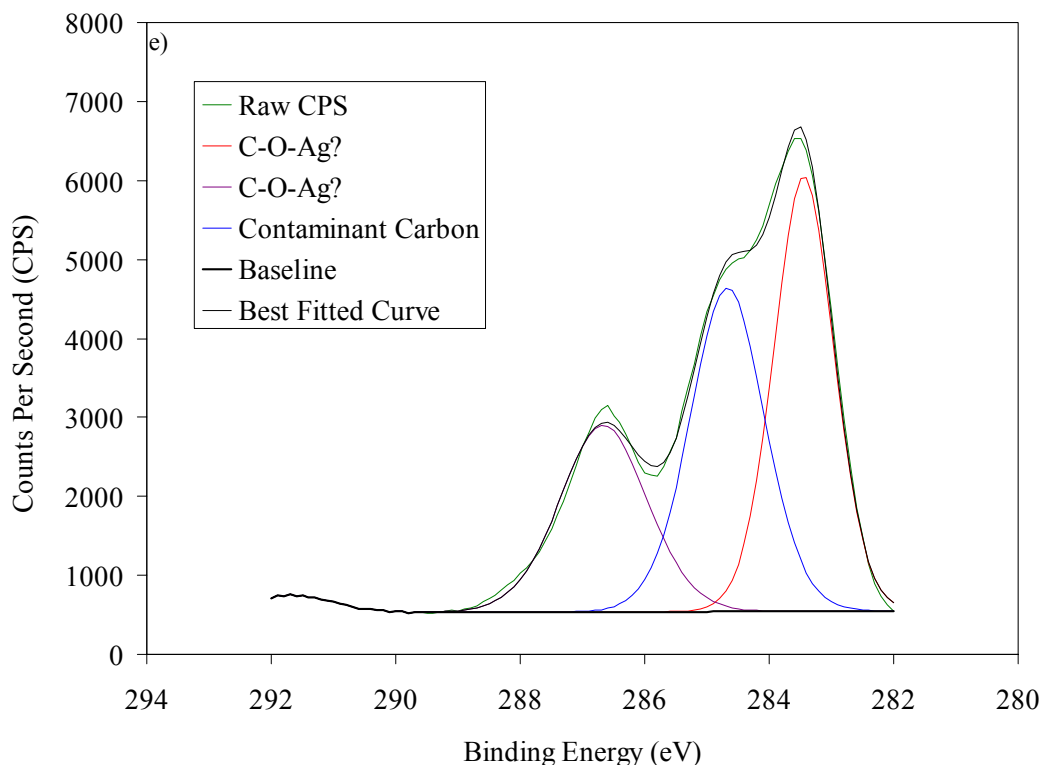


Figure 5-59, continued. Examples of deconvolution of C 1s XPS spectra for nanocrystalline silver dressings after dissolution under various conditions. The deconvolutions of the XPS spectra are shown after 16 hours of dry heat at 37°C (controls) in (a), or after 16 hours of dissolution at 37°C in solutions starting at pH 4 (adjusted using HCl) (b), pH 5.6 (reverse osmosis water) (c), pH 9 (adjusted using NaOH) (d), or fetal calf serum (e).

A summary of the O1s peaks for XPS performed on nanocrystalline silver dressings after dissolution for various lengths of time in pH 4, 5.6, or 9 solutions, as well as in serum, is shown in Figure 5-60. With dissolution at a starting pH of 4, the silver-oxygen bonds appeared to decrease with time (right peak). With a starting pH of 5.6, the silver-oxygen bonds appeared to first increase and then decrease with time. With pH 9, the trend is less clear, while with dissolution in serum, the O1s pattern appears very different, but with no clear evidence of the presence of silver-oxygen bonds. Sample deconvolutions are shown in Figure 5-61 at the 16 hour time point for control dressings (a); dressings dissolved in

solutions at starting pHs of 4 (b), 5.6 (c), and 9 (d); and dressings dissolved in serum (e). In the deconvolution patterns at 16 hours, dissolution at any pH resulted in lower silver oxide levels at the dressing surface relative to control dressings, and there was no silver oxide detected with the serum-dissolved sample. Larger contaminant carbon peaks are observed in dressings after all dissolution conditions, relative to the control dressings. This may have been due in part to carbon interacting with the dressings during the drying process.

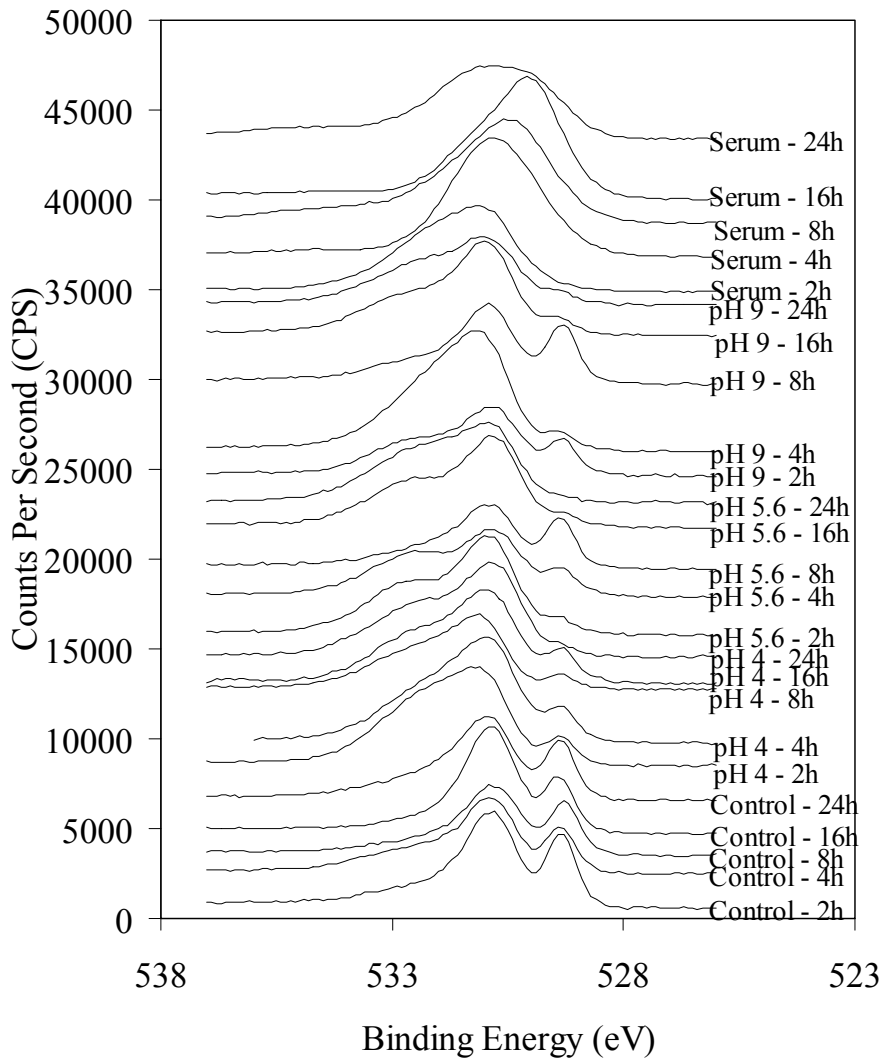


Figure 5-60. Summary of XPS intensities of O 1s peaks for nanocrystalline silver dressings after heating dry at 37°C (control dressings), or dissolution at 37°C in solutions at starting pHs of 4 (adjusted using HCl), 5.6 (reverse osmosis water), 9 (adjusted using NaOH), or fetal calf serum.

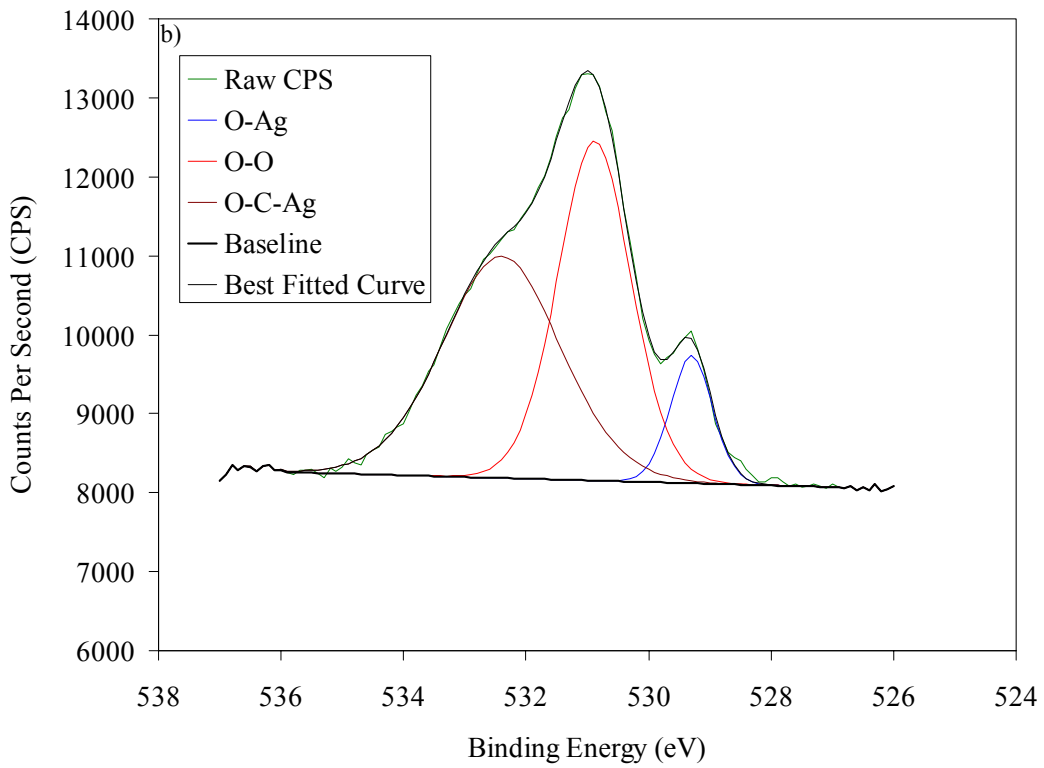
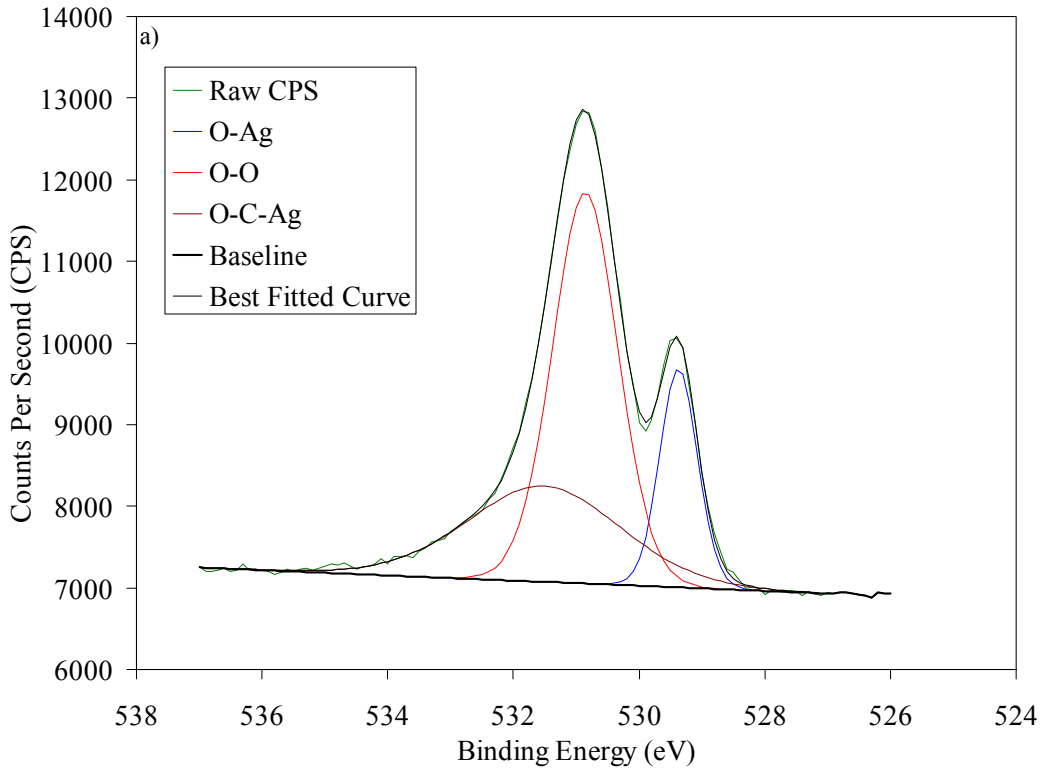


Figure 5-61.

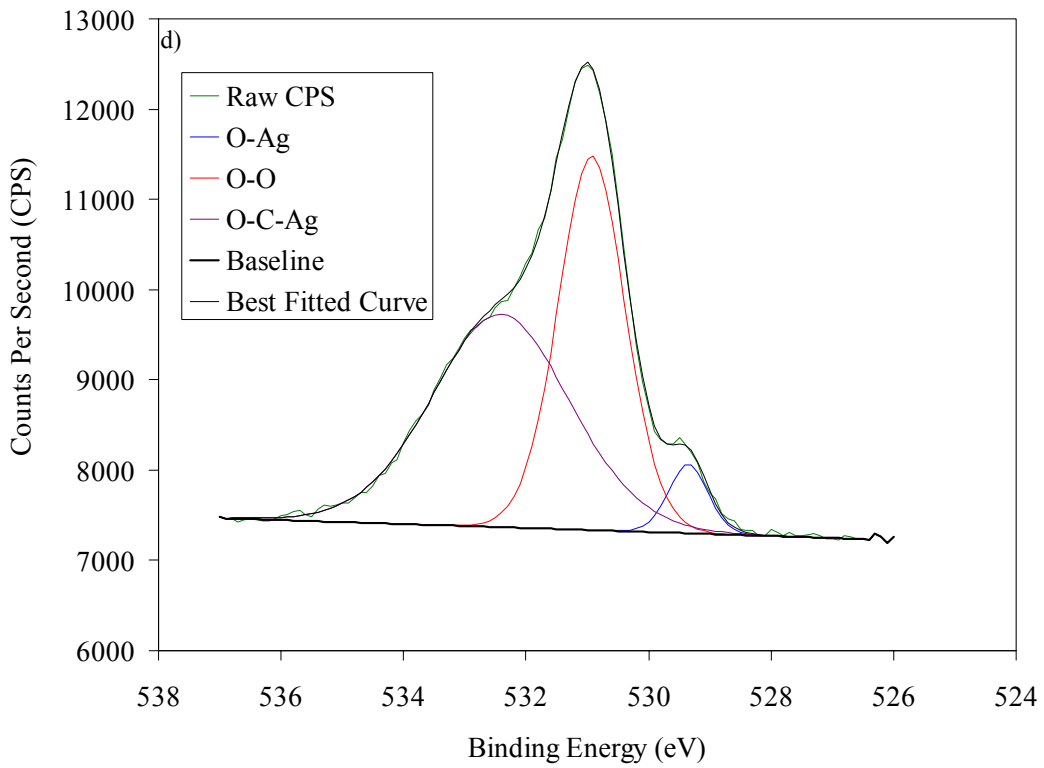
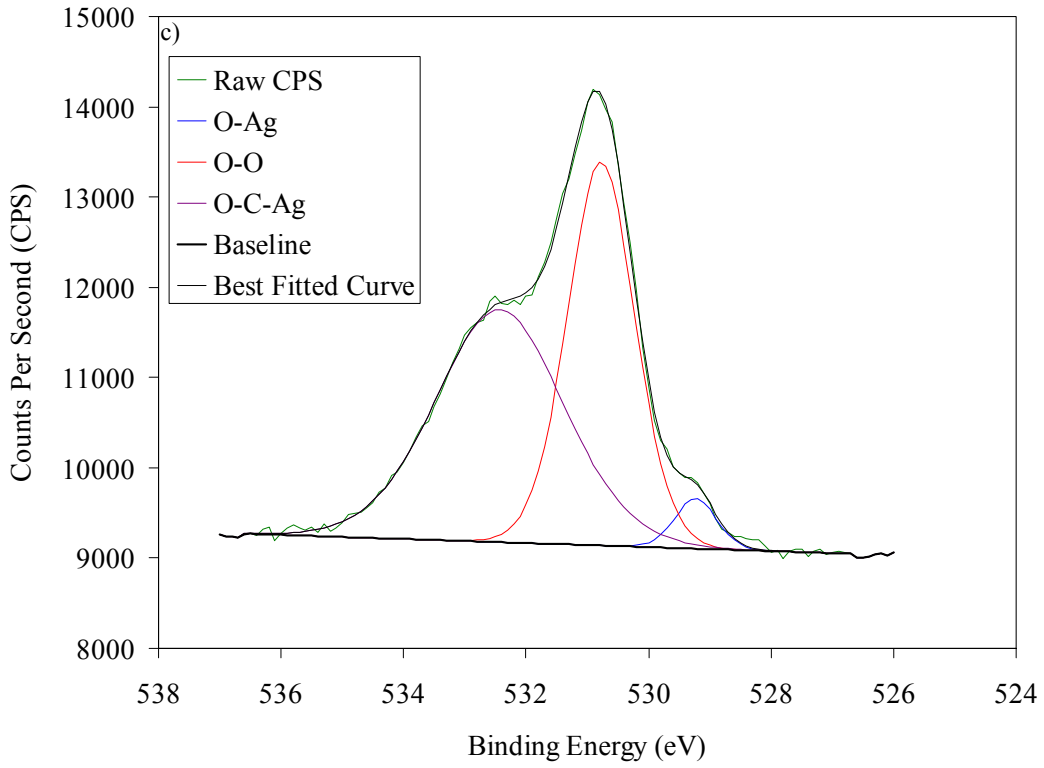


Figure 5-61, continued.

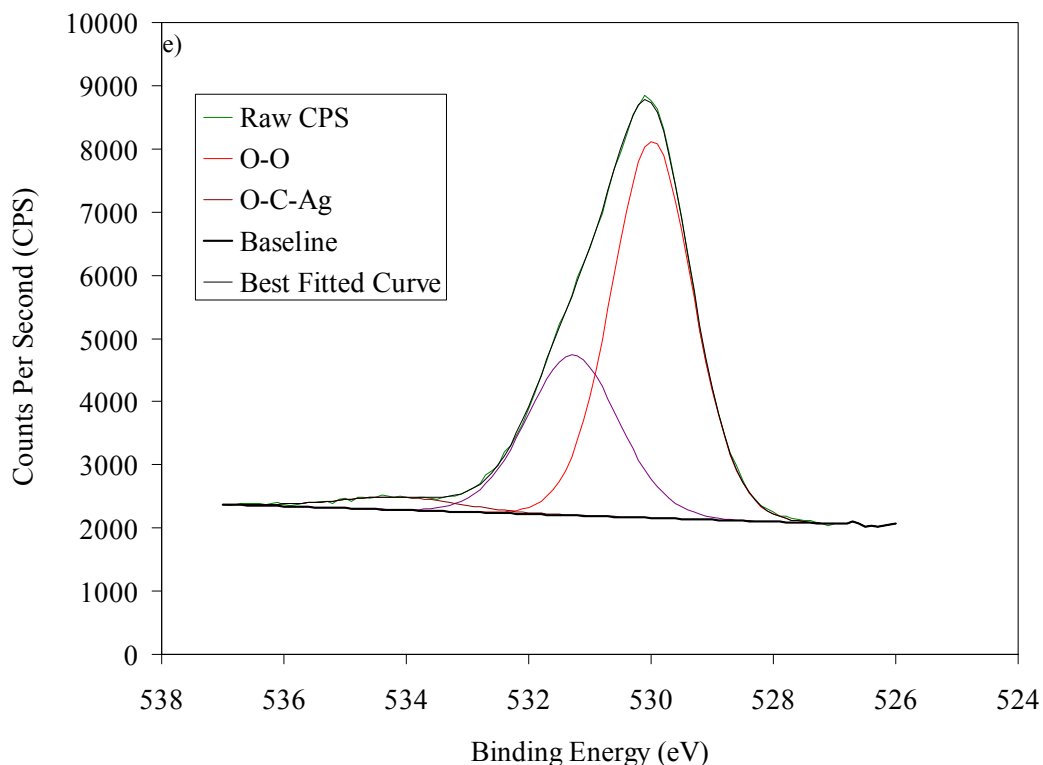


Figure 5-61, continued. Examples of deconvolution of O 1s XPS spectra for nanocrystalline silver dressings after dissolution under various conditions. The deconvolutions of the XPS spectra are shown after 16 hours of dry heat at 37°C (controls) in (a), or after 16 hours of dissolution at 37°C in solutions starting at pH 4 (adjusted using HCl) (b), pH 5.6 (reverse osmosis water) (c), pH 9 (adjusted using NaOH) (d), or fetal calf serum (e).

A summary of the Ag3d peaks for nanocrystalline silver dressings after dissolutions for various lengths of time is shown in Figure 5-62. With pH 4 and 5.6 dissolutions, there is a shift to higher binding energy with increasing dissolution time, suggesting a loss of silver-oxygen bonds. Trends are less clear with dissolution at a starting pH of 9. With dissolution in serum, the silver peaks were very weak, suggesting that the samples were caked with serum components, blocking the detection of the silver. Figure 5-63 shows sample deconvolutions for control dressings (a), or dressings dissolved in pH 4 (b), 5.6 (c), or 9 (d) solutions, or serum (e), all at 16 hours. Control dressings showed nearly equal quantities of

silver oxide (right peak) and metallic silver (left peak), as expected. At 16 hours, samples dissolved in pHs 4 through 9 showed lower silver-oxygen bonds, and higher silver-carbon content, while the samples dissolved in serum show mostly silver-carbon bonds, and no silver-oxygen bonds.

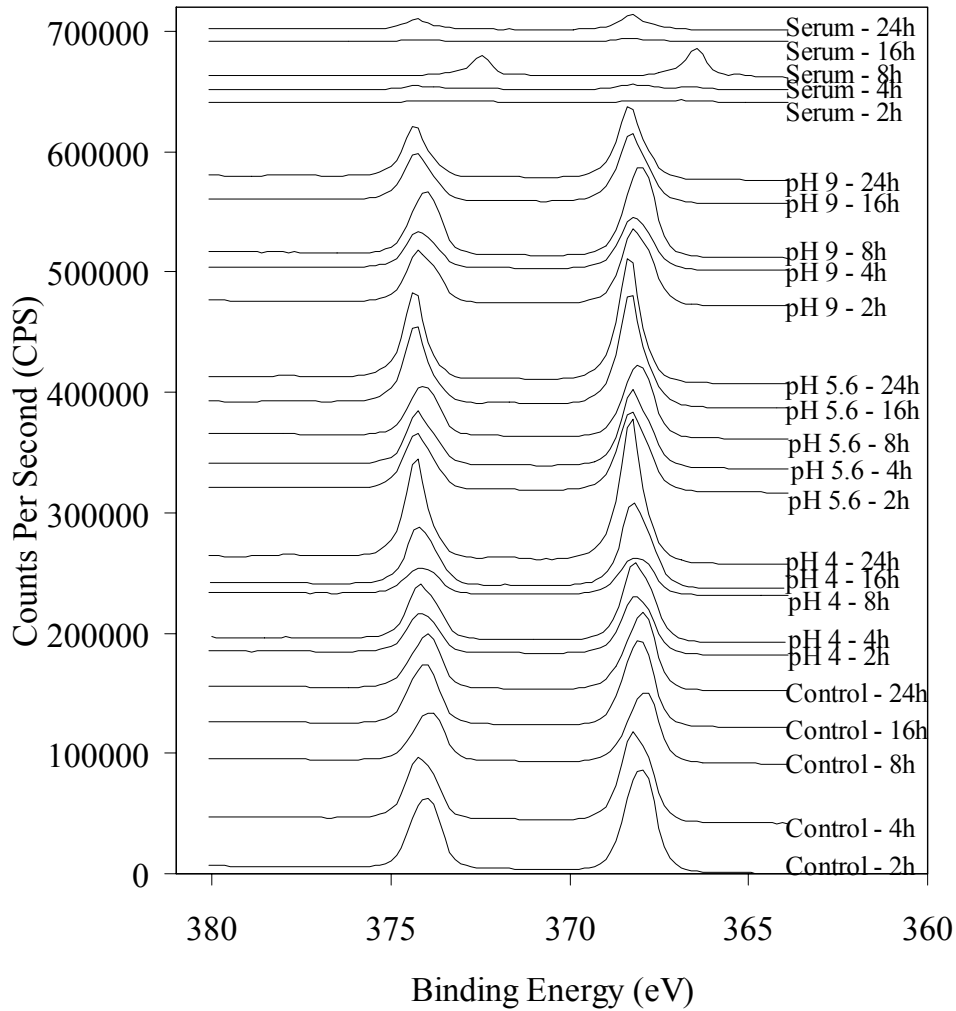


Figure 5-62. Summary of XPS intensities of Ag 3d peaks for nanocrystalline silver dressings after heating dry at 37°C (control dressings), or dissolution at 37°C in solutions at starting pHs of 4 (adjusted using HCl), 5.6 (reverse osmosis water), 9 (adjusted using NaOH), or fetal calf serum.

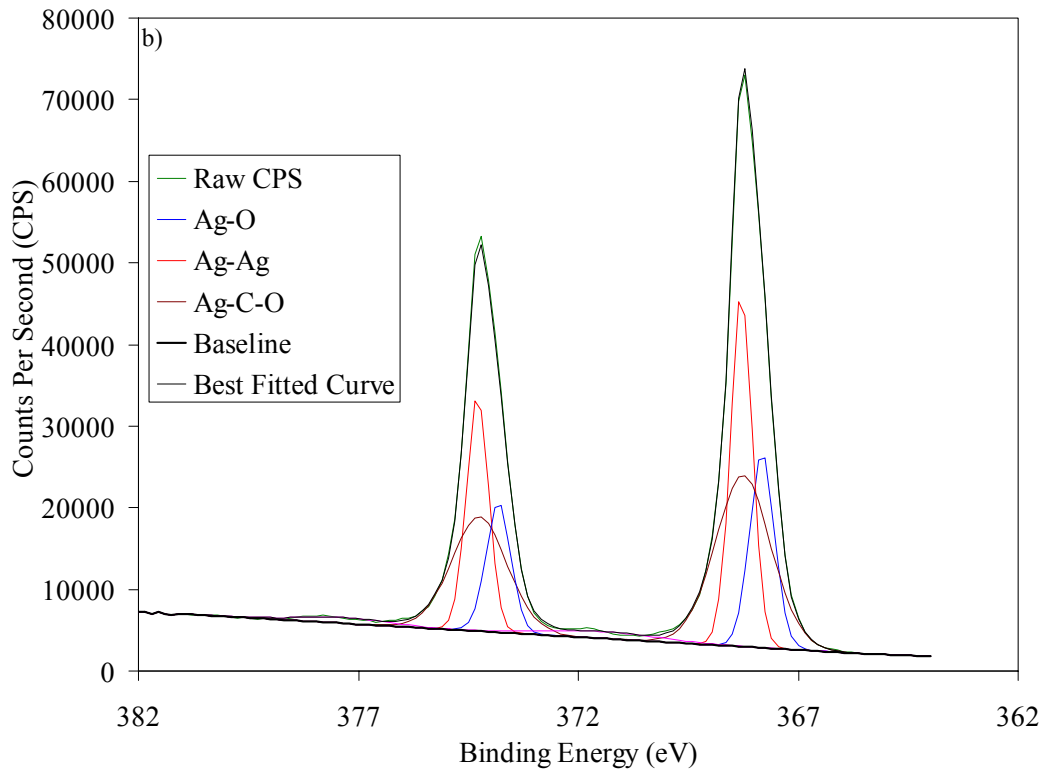
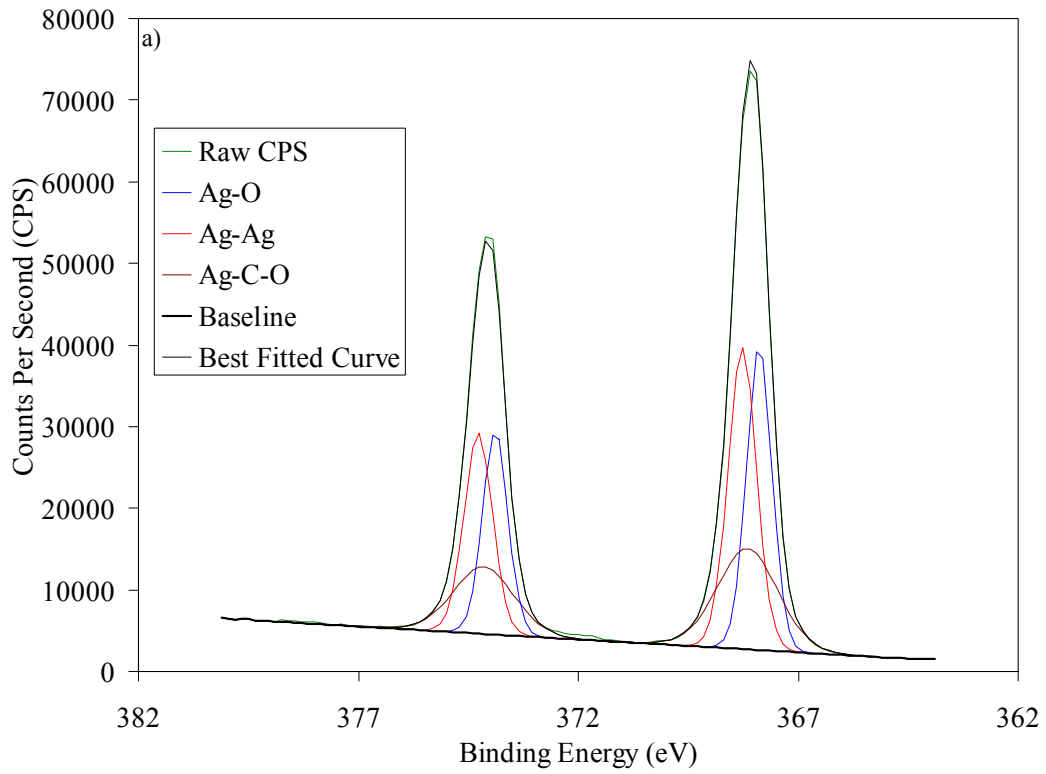


Figure 5-63.

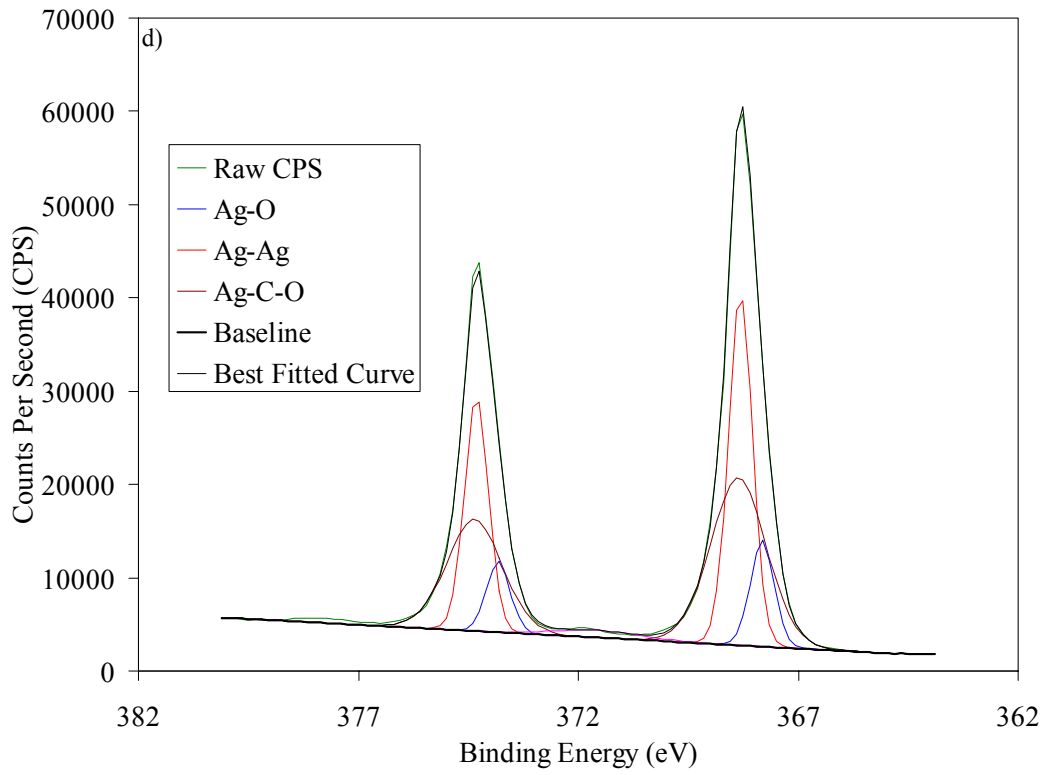
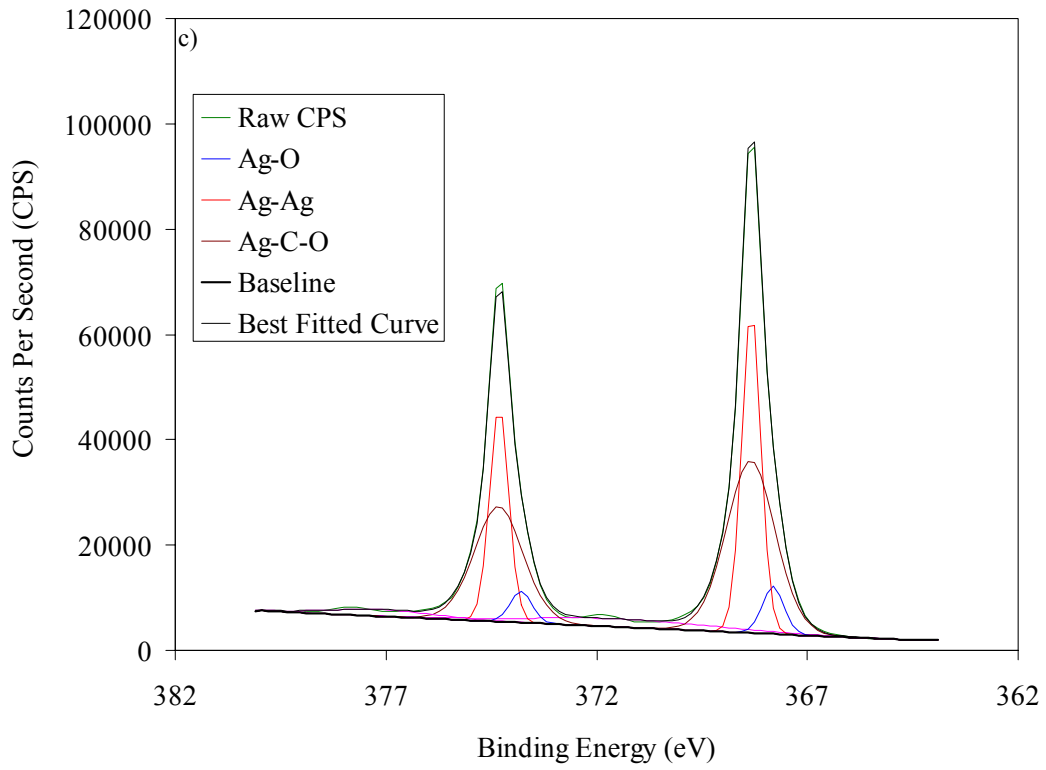


Figure 5-63, continued.

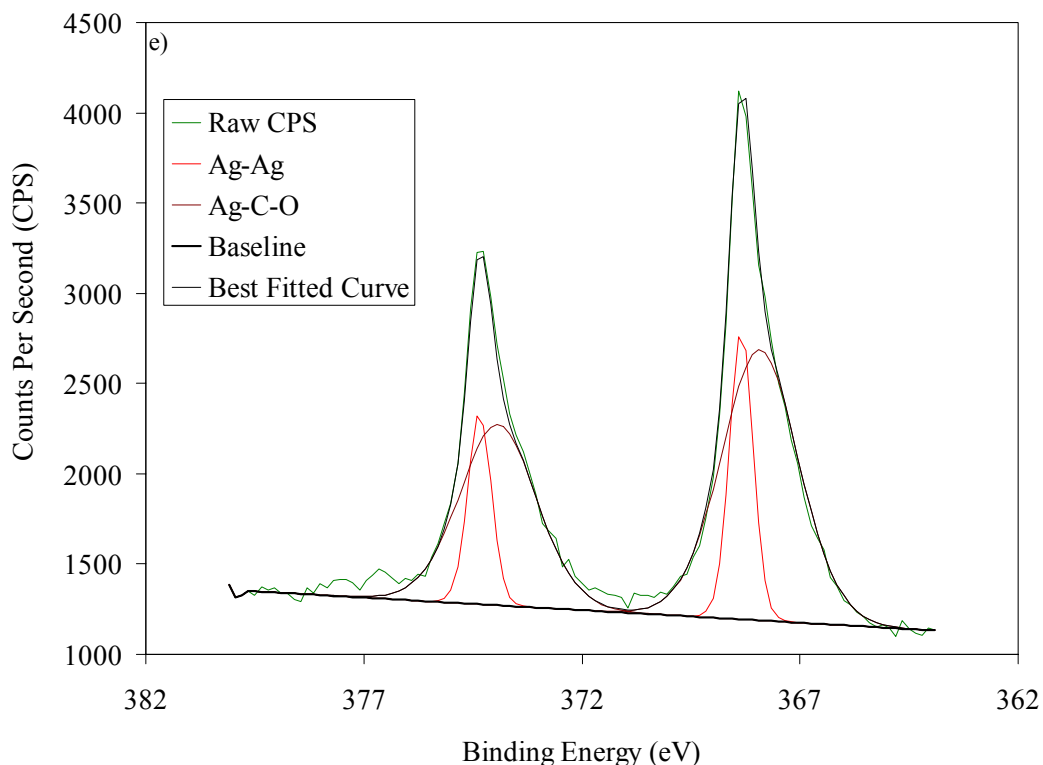


Figure 5-63, continued. Examples of deconvolution of Ag 3d XPS spectra for nanocrystalline silver dressings after dissolution under various conditions. The deconvolutions of the XPS spectra are shown after 16 hours of dry heat at 37°C (controls) in (a), or after 16 hours of dissolution at 37°C in solutions starting at pH 4 (adjusted using HCl) (b), pH 5.6 (reverse osmosis water) (c), pH 9 (adjusted using NaOH) (d), or fetal calf serum (e).

Figure 5-64 shows the results of quantifying the total oxygen and silver oxide content of the dressing surfaces via the O1s spectra (a), and the silver oxide content via the Ag3d spectra (b). Interestingly, there was no clear pattern regarding total oxygen present on the dressing surfaces over time – it appeared to remain relatively consistent independent of dissolution conditions. This suggests that the surface area of dressings did not change significantly during the dissolution period, allowing for levels of adsorbed oxygen to remain constant. The silver oxide content did not change for the control dressings over time. These dressings were in essence heat-treated at 37°C dry. Studies of 24 hours of heat

treatment at this temperature have indicated that mild drops in silver oxide content are possible[60]. Interestingly, in this study, when the first measurement was taken at 2 hours, the silver oxide content was already at the level observed after heat treatment observed in the previous study at 24 hours[60], suggesting that the drop in silver oxide content may have occurred within the first two hours and then remained stable. Dressings dissolved at starting pHs of both 5.6 and 9 showed an initial decrease in silver oxide content, followed by an increase back to control dressing levels at 8 hours, followed by a second drop in silver oxide content. Dressings dissolved at a starting pH of 4 showed an initial drop in silver oxide content prior to 2 hours, and then a second drop between 16 and 24 hours. Dressings dissolved in serum showed no silver oxide content at any time point. The analysis performed using the Ag3d spectra demonstrated the same trends.

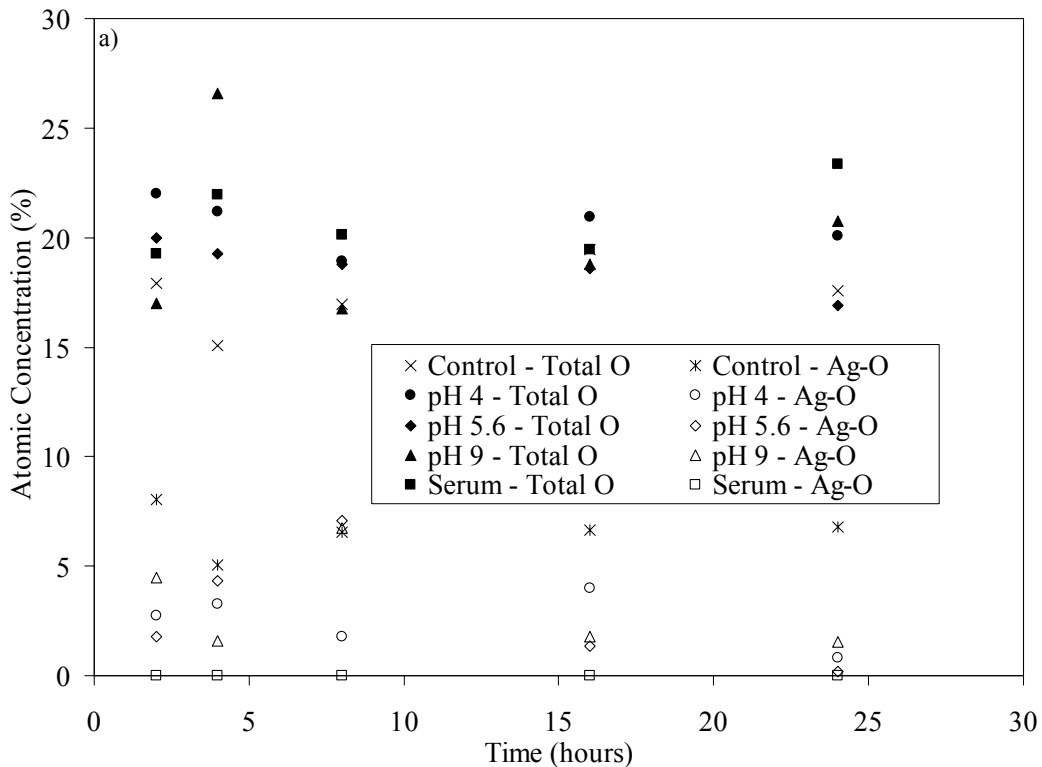


Figure 5-64.

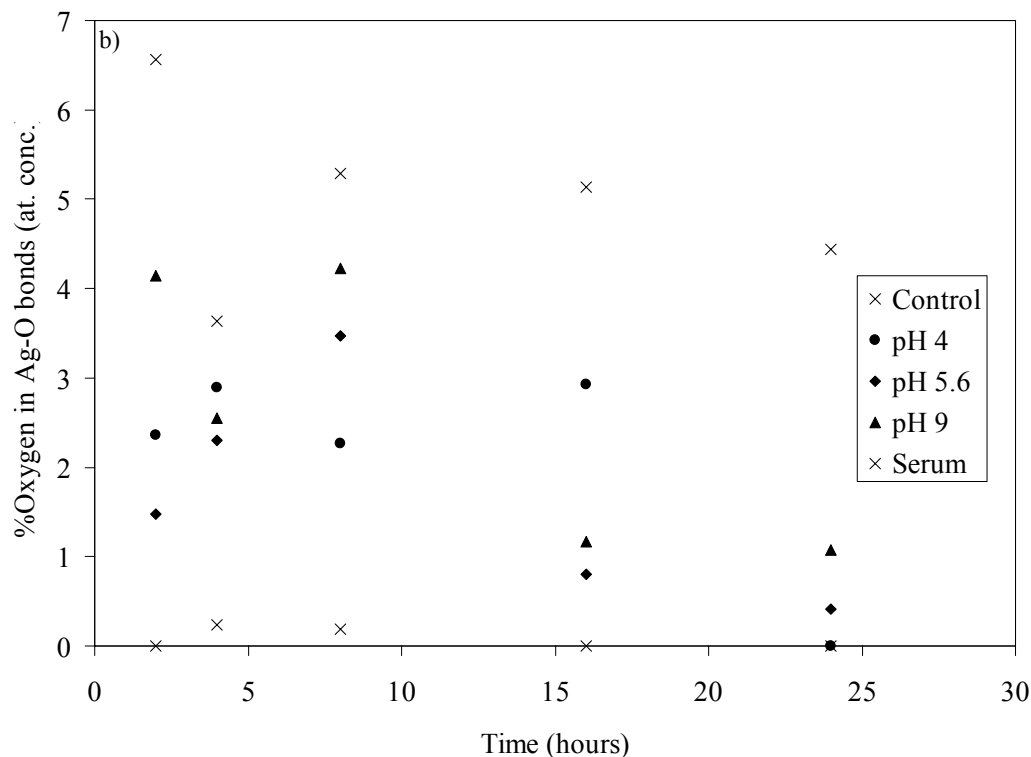


Figure 5-64, continued. Measurement of total oxygen and silver oxide via XPS. (a) Total oxygen percentage and percent silver oxide present in nanocrystalline silver dressings after heating dry at 37°C (control dressings), or dissolution at 37°C in solutions at starting pHs of 4 (adjusted using HCl), 5.6 (reverse osmosis water), 9 (adjusted using NaOH), or fetal calf serum, as determined from the O 1s spectra. (b) Percent silver oxide present in nanocrystalline silver dressings after heating dry at 37°C (control dressings), or dissolution at 37°C in solutions at starting pHs of 4 (adjusted using HCl), 5.6 (reverse osmosis water), 9 (adjusted using NaOH), or fetal calf serum, as determined from the Ag 3d spectra.

SEM

Representative SEM images for control dressings at 2 and 24 hours are shown in Figure 5-65 (a) and (b), respectively. Control dressings demonstrated the presence of fine equi-axed features on the order of 10-15 nm throughout the experiment. Representative SEM images for dressings dissolved at a starting pH of 4 are shown in Figure 5-66, after 4 (a), 8 (b), and 16 (c) hours of dissolution. Clear images were not obtained for samples at 24 hours due to sample charging. This increase in sample charging occurring with higher dissolution times suggests

that changes were occurring at the dressing surface. While the images taken at 4 and 16h suggest a loss of finer features, the images taken at 8h demonstrate the presence of fine features of the same scale and quantity as those present in the control dressings. This indicates that either the features on the dressings were location specific (i.e. some areas had loss of finer features and some did not), or that the images taken at four and 16 hours were not in focus. The former is a possibility, as examination of dressings after dissolution at a starting pH of 4 has shown that sometimes, particularly when dressings are layered in solution, some areas of the dressing pieces change color (to grey) while others remain blue. In particular, the bottom layer of dressing will change color completely, while inner layers change color only at the edges. This suggests that the results discussed in this section in general may show location-related variability.

a)

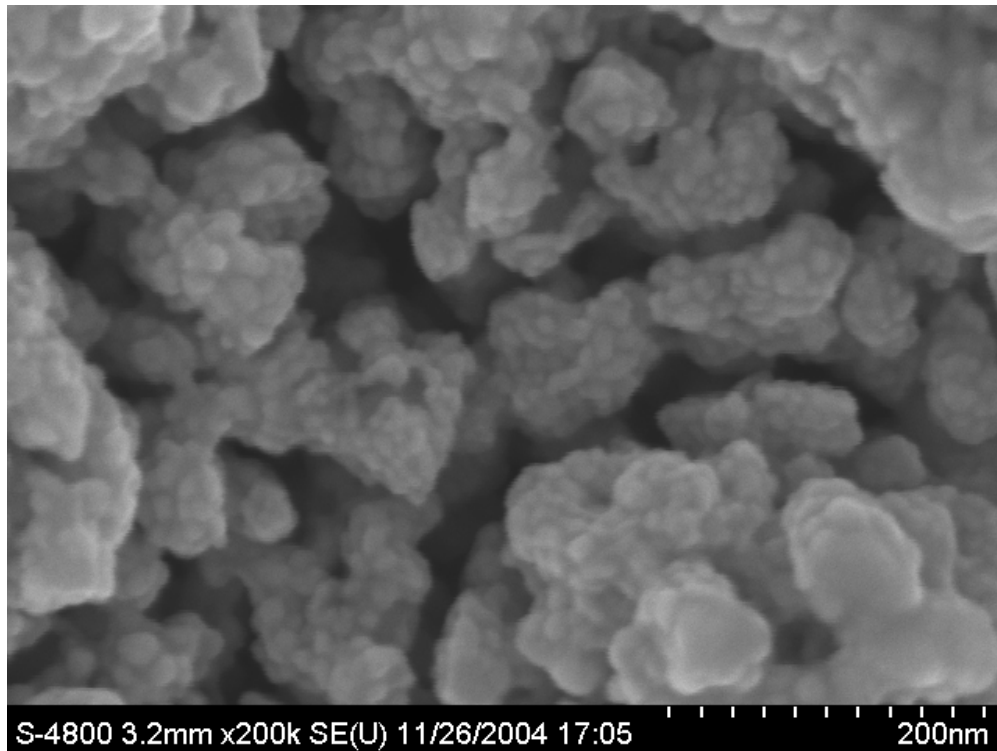


Figure 5-65.

b)

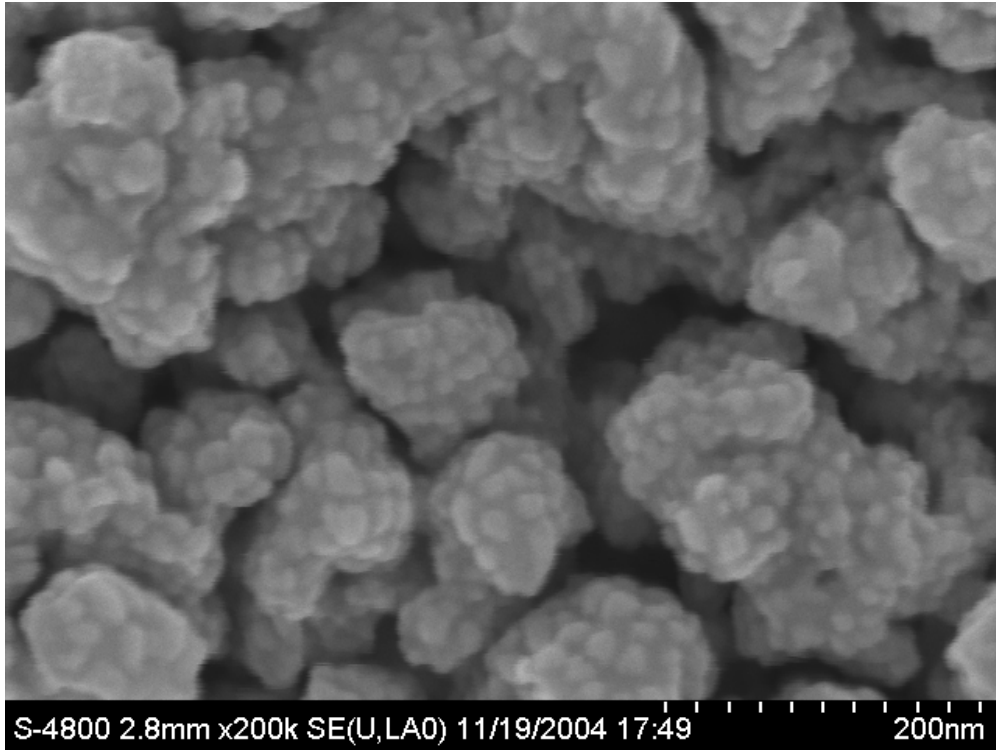


Figure 5-65. SEM images of nanocrystalline silver dressings heated dry at 37°C (controls) for (a) 2, or (b) 24 hours.

a)

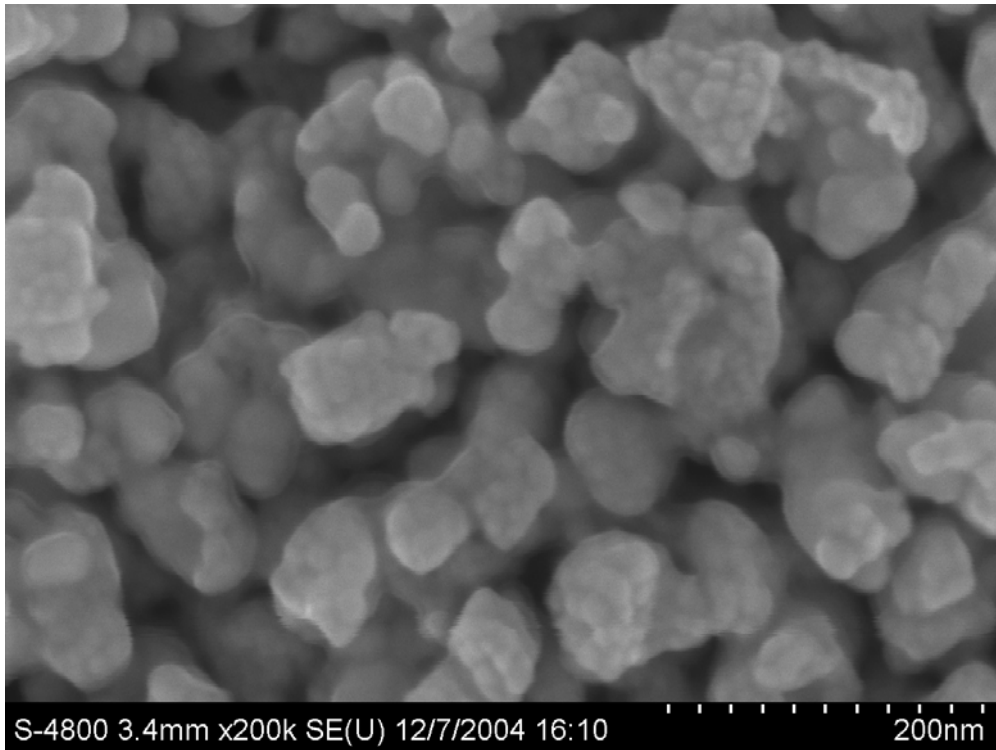
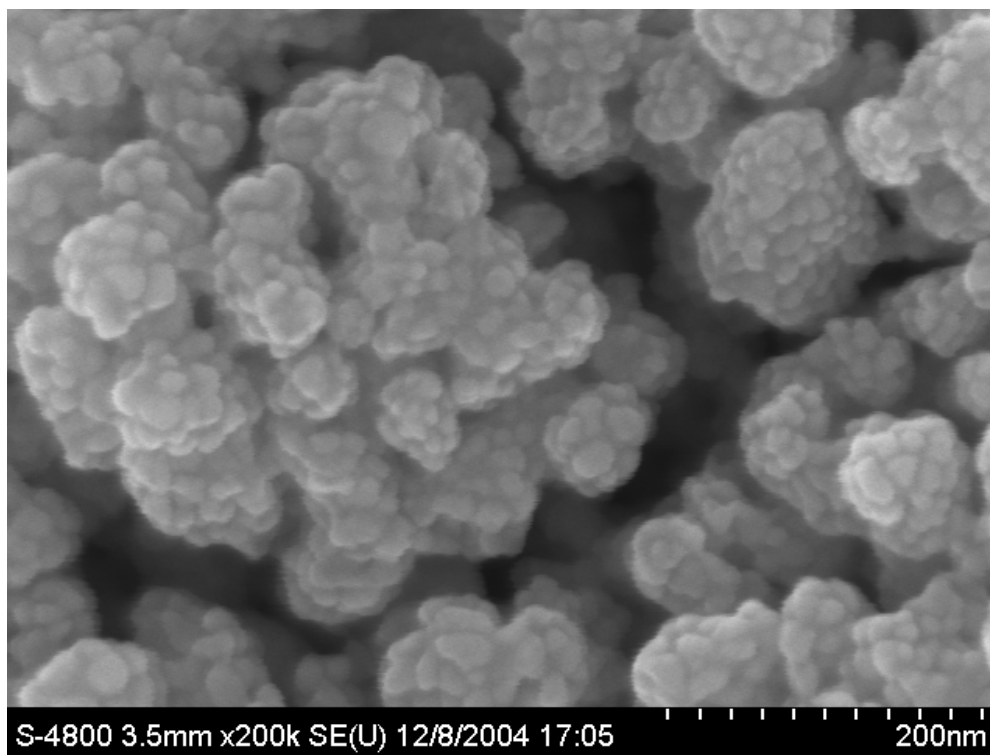


Figure 5-66.

b)



c)

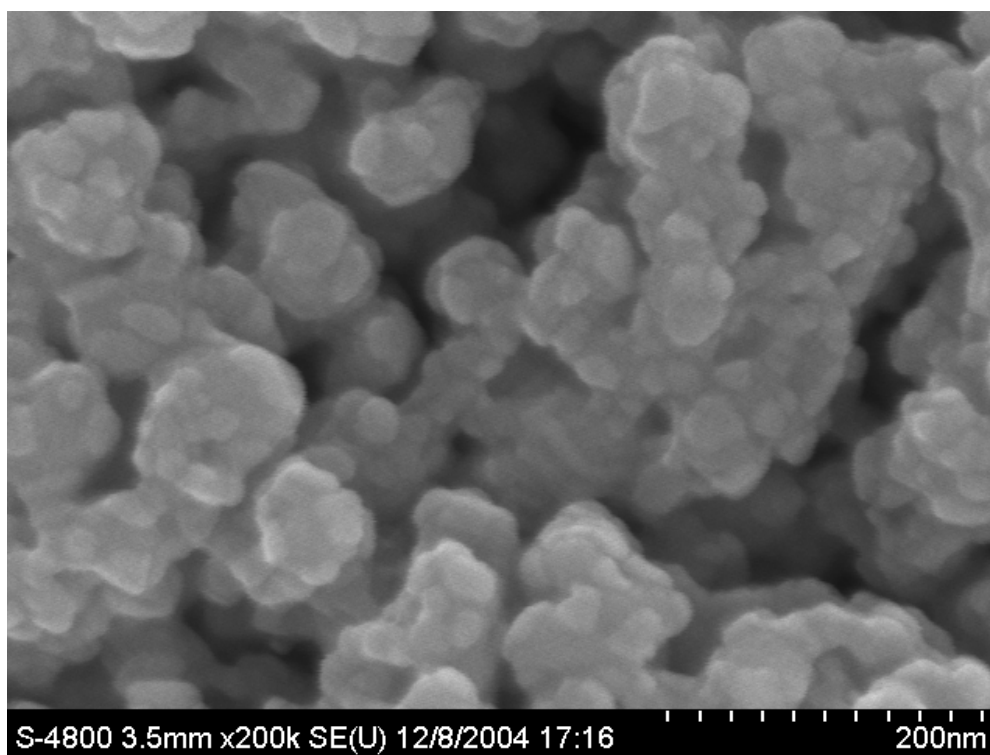


Figure 5-66, continued. SEM images of nanocrystalline silver dressings dissolved at a starting pH of 4 (adjusted using HCl) at 37°C for (a) 4, (b) 8, or (c) 16 hours.

Representative SEMs of nanocrystalline silver dressings after dissolution in distilled water (starting pH 5.6) for 8 (a), 16 (b), and 24 hours (c) are shown in Figure 5-67. These images show that over 24 hours of dissolution, the structure of the dressing did not change, with fine features still prevalent at 24 hours.

a)

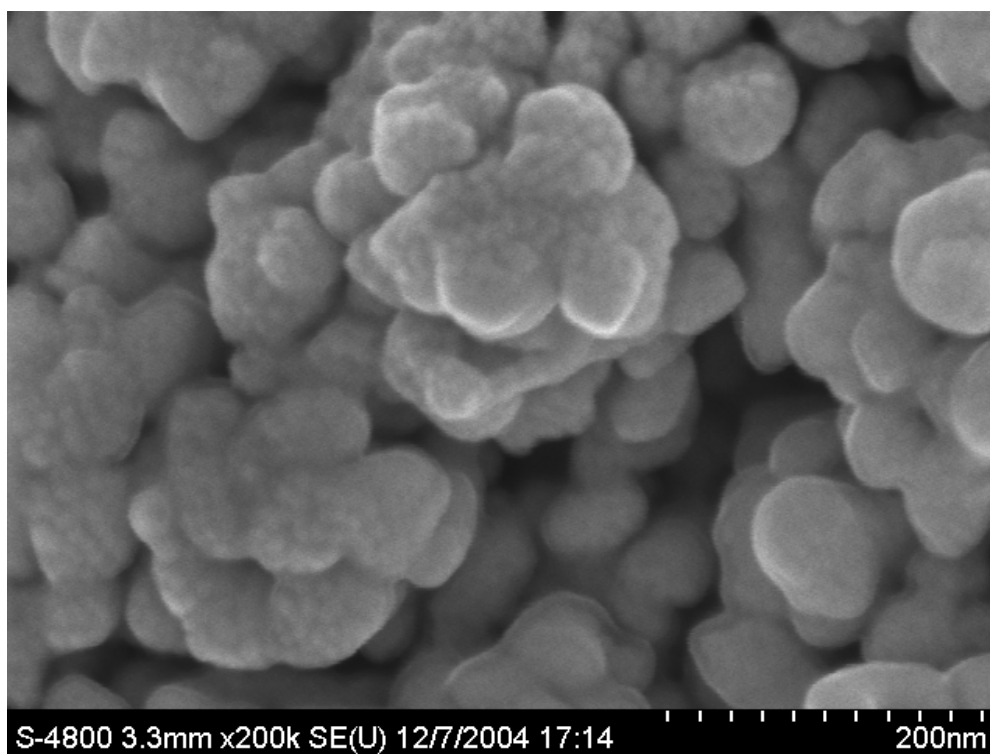
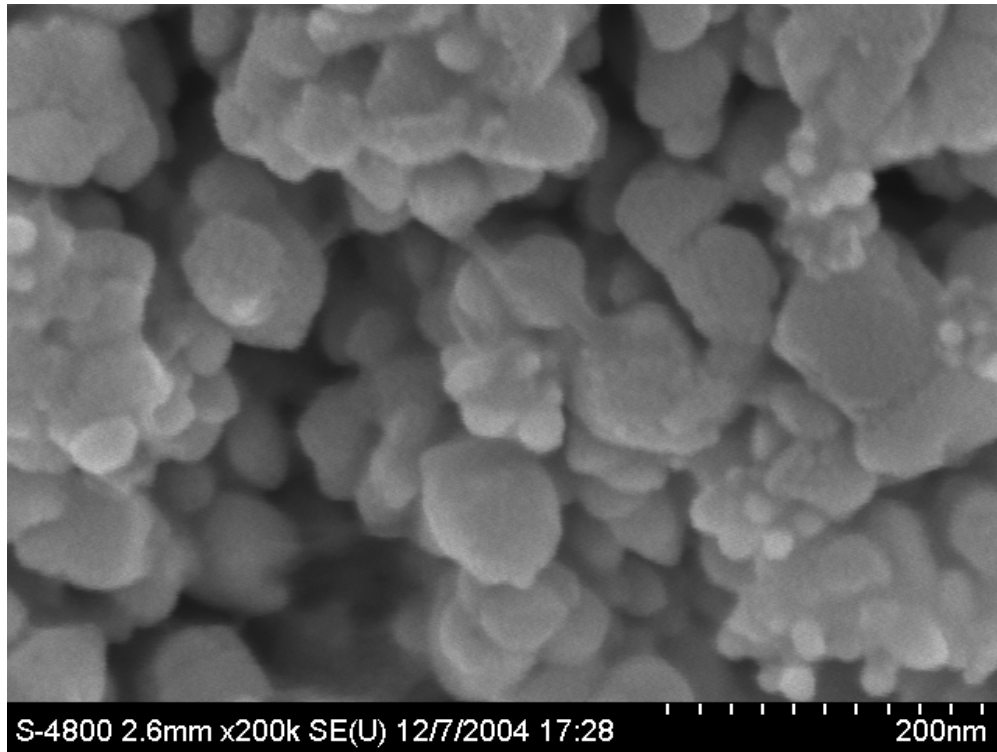


Figure 5-67.

b)



c)

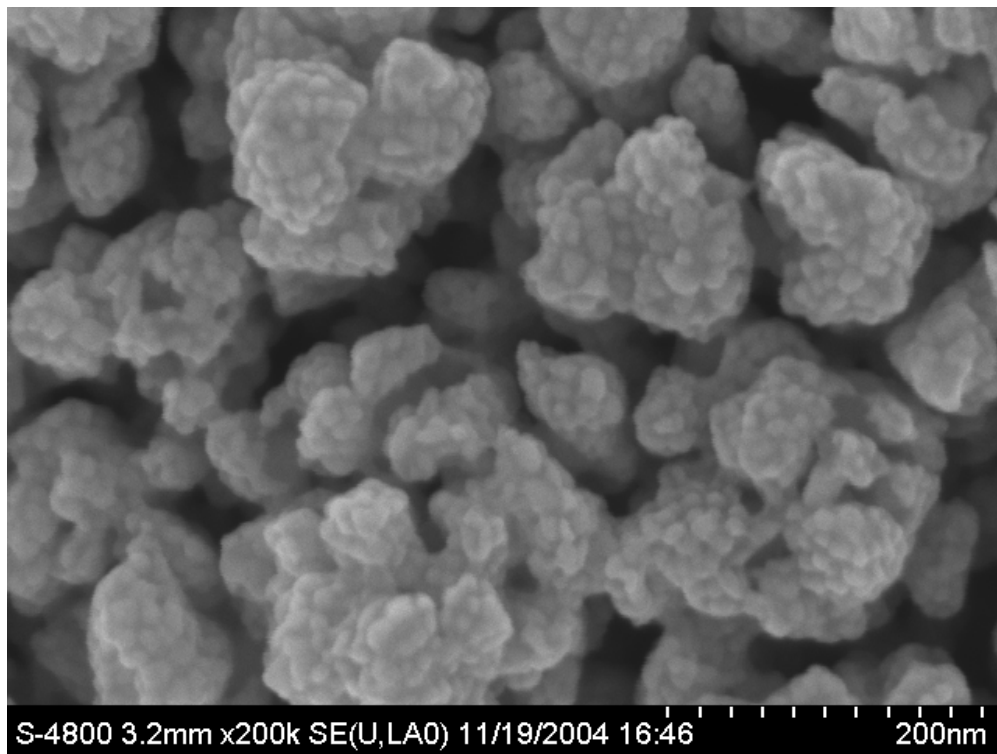


Figure 5-67, continued. SEM images of nanocrystalline silver dressings dissolved at a starting pH of 5.6 (reverse osmosis water) at 37°C for (a) 8, (b) 16, or (c) 24 hours.

Representative SEMs of nanocrystalline silver dressings after dissolution in a solution with a starting pH of 9 for 4 (a), 8 (b), and 16 (c) hours are shown in Figure 5-68. Clear images were not attained at other time points due to sample charging, and the image at 16 hours shows signs of sample charging as well. Although the image at four hours suggests a loss of finer features and grain growth, the images at eight and 16 hours demonstrate fine features and a structure similar to dressing controls. This suggests that, similar to dissolution in the pH 4 solutions, areas of the dressing may undergo loss of fine features while other areas remain unaffected during a 24 hour dissolution period, or the pictures are out of focus.

a)

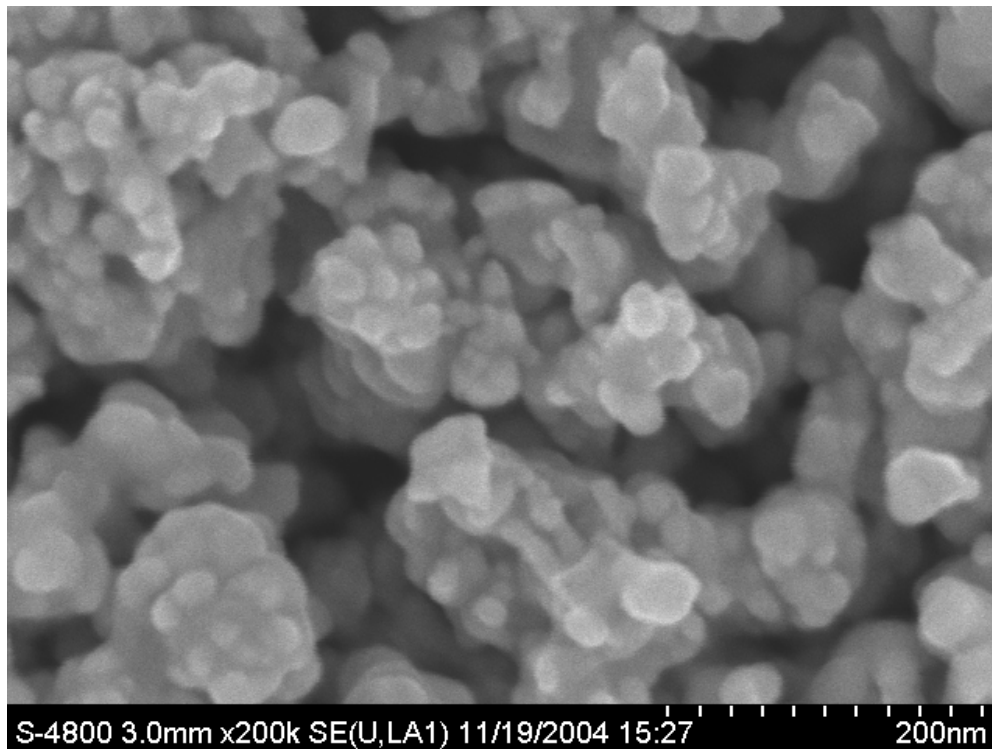
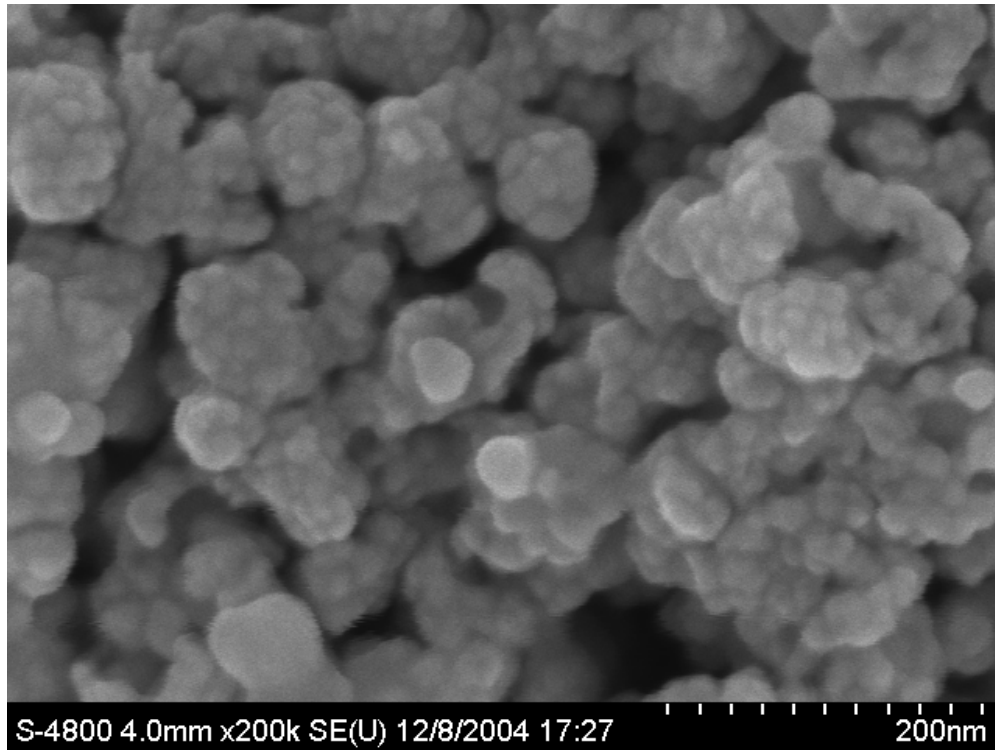


Figure 5-68.

b)



c)

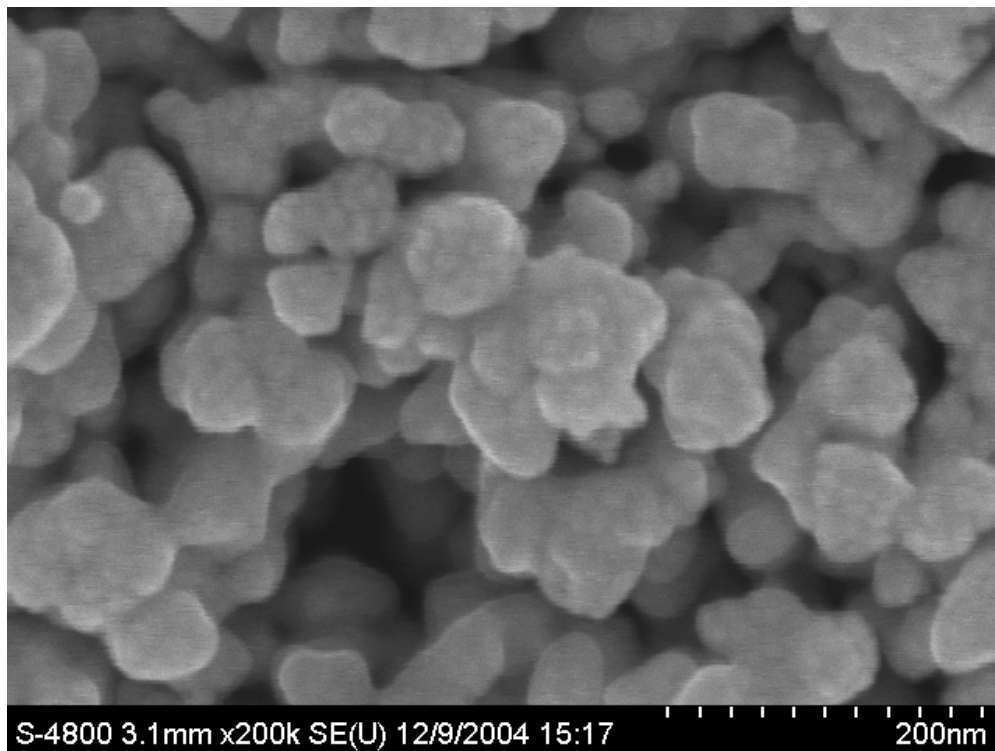


Figure 5-68, continued. SEM images of nanocrystalline silver dressings dissolved at a starting pH of 9 (adjusted using sodium hydroxide) at 37°C for (a) 2, (b) 8, or (c) 16 hours.

SEM imaging of the samples dissolved in serum was not very successful, due to the caking of serum components on the surface of the dressing during drying, resulting in “dirty” samples producing severe charging (see Figure 5-69). Therefore, no firm conclusions can be made regarding the effect of the serum on the physical structure of the dressing, although based on the appearance of the image at two hours dissolution time (Figure 5-69), grain growth may have occurred.

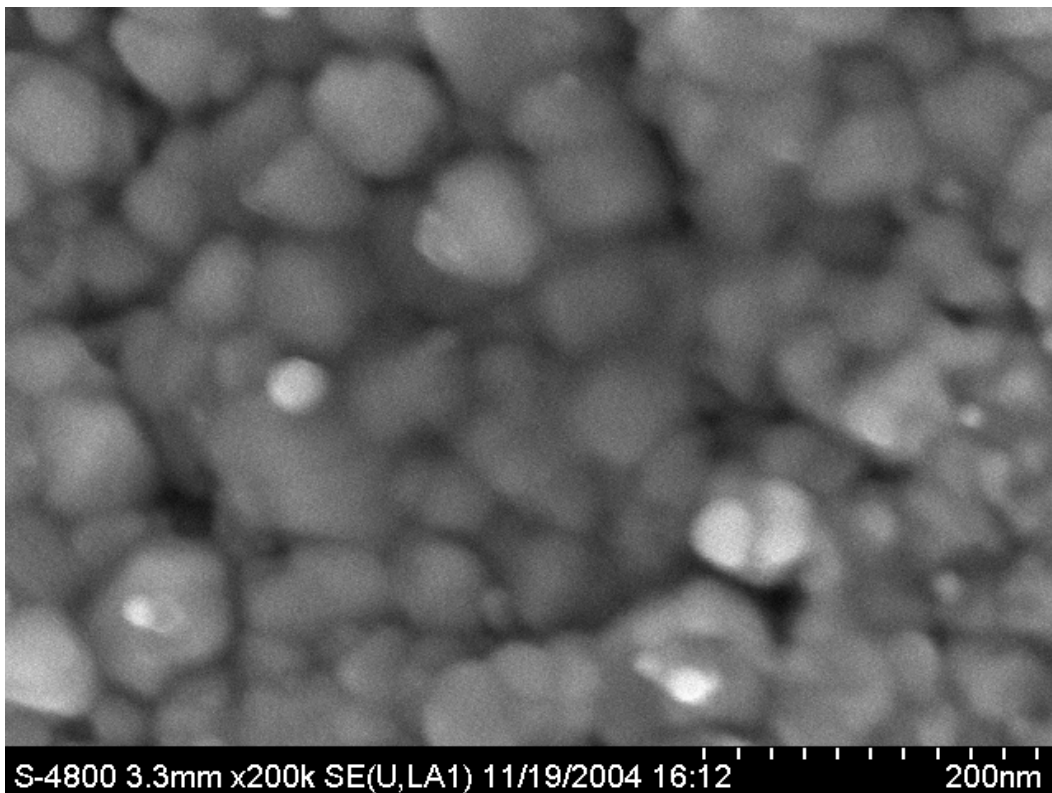


Figure 5-69. SEM image of nanocrystalline silver dressings dissolved in fetal calf serum at 37°C for 2 hours.

As there was some concern regarding the impact of leaving dressings under vacuum for extended periods of time on the structure of the dressings, SEM imaging of control dressings left under vacuum for 72 hours (a and b) and 96 hours (c) were performed, and are shown in Figure 5-70. While the image in

panel (a) suggests that the dressing structure did not change substantially during 72 hours under vacuum, the image in panel (b) suggests that loss of fine features occurred, with grain growth. Panel (c), taken after 96 hours under vacuum also shows signs of a “sintering” behavior.

a)

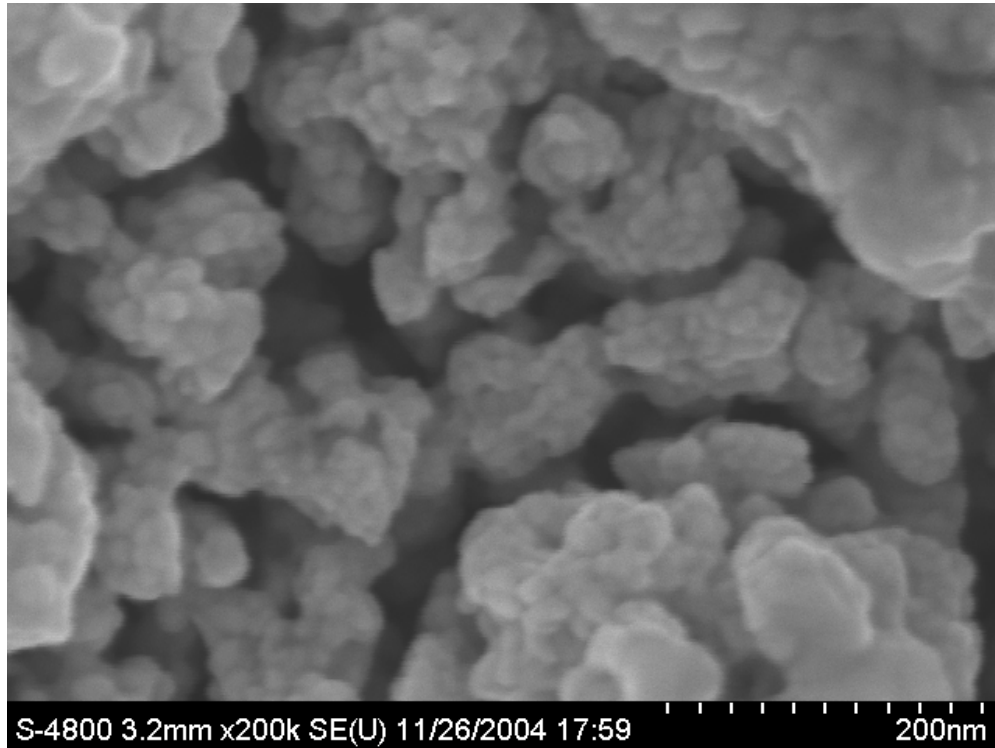
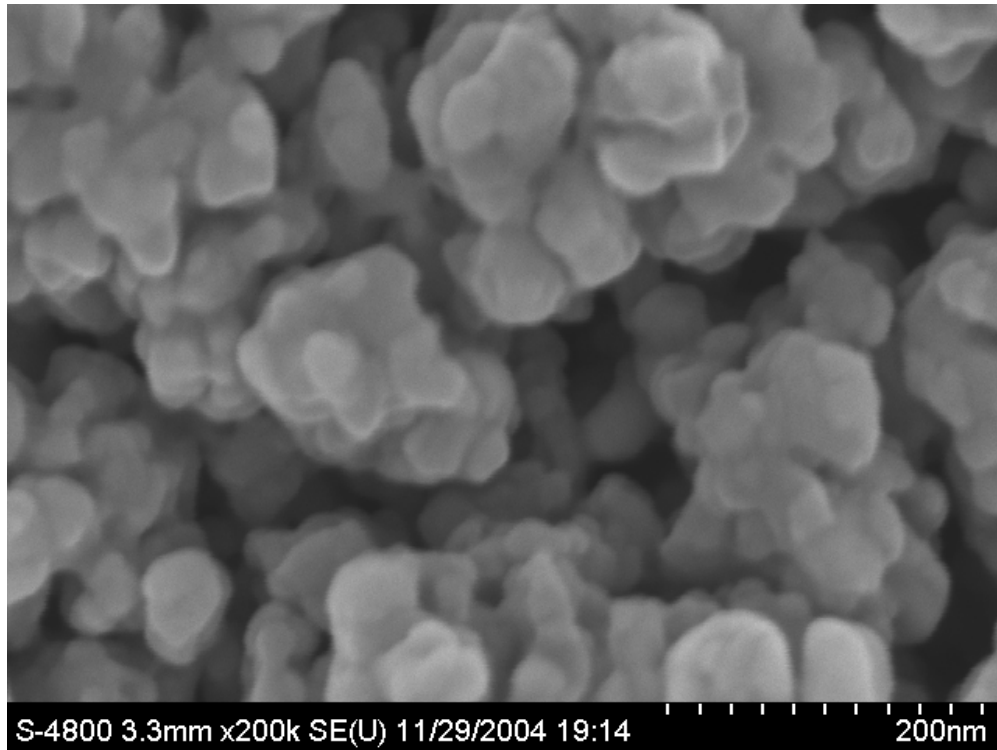


Figure 5-70.

b)



c)

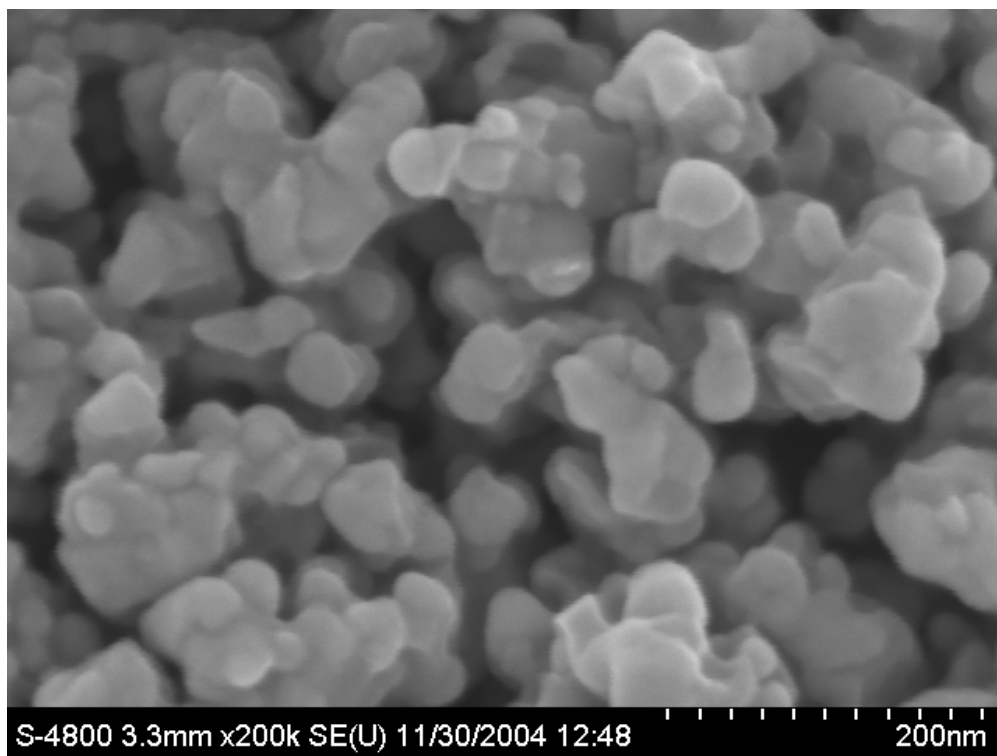


Figure 5-70, continued. SEM images of nanocrystalline silver dressings heated dry at 37°C, followed by placement in a vacuum chamber for 72 hours (a and b), or 96 hours (c).

XRD

Results of the XRD analysis of dressings after various dissolution times in various solutions are shown in Table 5-17. In acidic solutions, the weight percent of silver oxide gradually decreased with increasing dissolution time, suggesting more dissolution of the silver oxide than the metallic silver, or conversion of the silver oxide into metallic silver. In basic solutions, it increased somewhat, suggesting more dissolution of the metallic silver than the silver oxide, or conversion of the metallic silver to silver oxide. The latter seems unlikely, as the metallic silver is likely in a more stable state than the ionic silver. These results differ somewhat from the XPS results, in that with the XPS results, the drop in silver oxide content was more dramatic in the acidic solution, and a drop in silver oxide content was also observed in the basic solution. These differences may be due to the fact that XPS analysis measurements come from the sample surface, whereas with XRD, the sample is penetrated further. Since dissolution would be expected to impact the sample surface the most strongly, some changes observed via XPS may be surface phenomena, while the XRD provides an indication of what changes occur to the dressing below the surface during dissolution, where, as expected, there appears to be less impact. In serum, the silver oxide appeared to be rapidly depleted, with none present after two hours dissolution time. This was observed with the XPS as well. The crystallite size of Ag_2O appeared to decrease with dissolution time in both acidic and basic solutions, suggesting that small amounts of silver oxide were dissolving off of the crystallites, rather than entire crystallites coming off into solution. With dissolution in pH 4 or 9

solutions, the crystallite size of the metallic silver stayed within the normal size range. This confirms the results of most of the SEM images, which indicated that the fine features observed in control dressings were still present after dissolution. These results suggest that the dressings, when dissolved in acidic or basic solutions such as the ones tested here, maintain their structure as the dressing is dissolved, which should result in the release of the same types of species over time. However, the crystallite size increased slightly with dissolution in serum, suggesting that in the absence of the silver oxide pinning structure, the metallic silver began to undergo grain growth. This is similar to observations made during heat treatment of nanocrystalline silver dressings[58, 60] (also see Chapter 9), and indicates that the dressing structure and behavior when in contact with wound fluid may change dramatically over time. The cell constant for metallic silver increased with dissolution time, indicating increased ordering of the metallic silver structure. The cell constant for silver oxide decreased with dissolution time, particularly in the acidic solution, indicating increased disorder of the silver oxide with dissolution time.

Overall, the XRD results suggest that dissolution of the dressing in lower pH solutions will tend to result in the dissolution of the charged (antimicrobial) species, while higher pH solutions will tend to result in the dissolution of metallic silver, which is theorized to be the anti-inflammatory species released by nanocrystalline silver (see discussion in the introduction). This is corroborated by the results above indicating that dissolution of nanocrystalline silver in pH 4 or 5.6 solutions under the correct conditions results in bactericidal activity, and the

results of Chapter 7, which indicates that the pH 9 solution used had the highest anti-inflammatory activity. XPS data suggests that in any solution, silver oxide will be lost from the dressing surface, presumably resulting in the release of charged species and allowing for the dissolution of other species as well.

Table 5-17. Summary of XRD analysis for nanocrystalline silver dressings dissolved at 35°C for 24 hours in various solutions.

Sample Description	Crystallite size (nm)		Wt% (excluding HDPE and gauze)		Weight ratio Ag/Ag ₂ O	Cell constant (Å)	
	Ag	Ag ₂ O	Ag	Ag ₂ O		Ag	Ag ₂ O
Control – 2h	15 (2)	11 (2)	37	63	0.6	4.0855 (4)	4.6935 (8)
pH 4 – 2h	11(2)	11(2)	41	59	0.7	4.0846 (3)	4.6875 (7)
pH 4 – 24h	14(2)	9(1)	57	43	1.3	4.0852 (4)	4.6791 (19)
pH 9 – 2h	10(2)	12(2)	51	49	1.1	4.0851 (4)	4.6913 (8)
pH 9 – 16h	15(2)	10(2)	48	52	0.9	4.0859 (3)	4.6846 (9)
pH 9 – 24h	14(2)	9(1)	46	54	0.9	4.0862 (3)	4.6866 (8)
Serum – 2h	24(4)	N/A	100	0	N/A	4.0839 (2)	N/A
Serum – 24h	18(2)	N/A	100	0	N/A	4.0849 (2)	N/A

*Numbers in brackets represent standard uncertainties.

The effect of storage in the SEM vacuum chamber on the XRD profile of select samples is shown in Table 5-18. No remarkable effect was observed in the samples dissolved in solutions with a starting pH of 4 or in serum (compared to Table 5-17). Small changes in the cell constants were observed, but did not form a clear trend. With the dressing samples dissolved for 2 hours in a solution with a starting pH of 9, vacuum treatment resulted in a decrease in the size of the silver oxide crystallites, and a shift to higher weight percent silver (relative to results of Table 5-17). Overall, these results do not confirm the original observations suggesting that grain growth occurred when the samples were left under vacuum. This suggests that the images taken in the SEM after the control dressings were left under vacuum showing loss of fine features (Figure 69b-c) may not be in focus, or the samples may be charging. Alternately, the samples used for the

XRD analysis may not have been left under vacuum for sufficient time to measure the effect observed in the SEM. The analyses of Chapter 9 indicate that grain growth occurs non-linearly with time and can start after a plateau period during heat treatment. The same may be true for grain growth in a vacuum. Further study would be required to resolve this issue, but it seems clear, based on the XRD data, that leaving dressing samples under vacuum for short periods of time should not affect the results obtained.

Table 5-18. Summary of XRD analysis for nanocrystalline silver dressings dissolved at 35°C for 24 hours in various solutions, followed by storage under vacuum.

Sample Description	Crystallite size (nm)		Wt% (excluding HDPE and gauze)			Cell constant (Å)	
	Ag	Ag ₂ O	Ag	Ag ₂ O	Ag/Ag ₂ O	Ag	Ag ₂ O
pH 4 – 2h dissolution	12 (2)	10 (2)	41	59	0.7	4.0842 (3)	4.6844 (9)
pH 4 – 24h dissolution	14 (2)	8 (1)	56	44	1.3	4.0845 (3)	4.6794 (16)
pH 9 – 2h dissolution	11 (2)	8 (1)	61	39	1.6	4.0873 (3)	4.6711 (25)
Serum – 24h dissolution	15 (2)	N/A	100	0	N/A	4.0854 (3)	N/A

Conclusions

Studying the solutions generated when nanocrystalline silver is allowed to dissolve under various conditions has shown that the dissolution conditions (starting pH, ratio of silver to solution, stirring, and time for dissolution) significantly impact the resulting solutions. Bactericidal activity of the solutions is very dependent on the dissolution conditions. Within its limits, this study showed that near-neutral starting pHs resulted in higher antimicrobial activity than either acidic or basic pHs, that a higher silver:solution ratio resulted in higher

antimicrobial activity, requiring only a short dissolution time, but that with a lower silver:solution ratio, similar activity could be generated over a longer dissolution period. It was also determined that stirring solutions did not negatively impact their antimicrobial activity. It would be interesting to determine whether pH 7 and 9 solutions have bactericidal activity when dissolved for shorter periods of time, and to test the efficacy of the solutions against other microbes. It would also be very useful to generate Ag^+ profiles and subtract these profiles from the total silver profiles, in order to determine what portion of the various solutions is composed of silver species other than Ag^+ , perhaps using one of the methods described above under *Ag⁺ Profiles*. It would be valuable to continue the study examining the effects of dissolution on the dressings with dissolutions in nitric acid, carbonated water (pH 4), and calcium hydroxide (pH 9), to see how the results compare with the solutions used. It would also be helpful to examine the effects of dissolution in serum on the solution, such as performing total silver profiles, Ag^+ profiles, and pH profiles, as well as exploring the optical properties of the solutions, as this would provide more information on the effect of silver dissolution in the wound environment.

While this chapter explored the optical properties of nanocrystalline silver-derived solutions under some conditions, there is much more to be learned in this area. It was not clear at the end of the study whether the optical absorbance patterns observed were related to SPR, and what caused the variations with dissolution conditions. As well, it was not clear if the solutions demonstrated fluorescence, or if they did not, what the emissive peaks observed

were actually related to. To learn more about the optical properties of nanocrystalline silver-derived solutions, and thus the species present in solution, the following might be useful directions:

1. Optical absorbance scans of nanocrystalline silver in neutral and basic solutions.
2. More thorough spectrofluorimetry:
 - a) Different excitation wavelengths could be tried, excitation could be performed over a range of wavelengths, or the excitation time could be extended.
 - b) More solutions could be tested, including neutral and high pH solutions generated under various conditions.
 - c) Emission could be measured up to higher wavelengths.
 - d) Conditions, such as excitation times and wavelengths, used to generate luminescence from silver clusters in the literature could be examined using various nanocrystalline silver-derived solutions.
3. Other optical properties of nanocrystalline silver-derived solutions could be examined directly, using, for example, Raman spectroscopy, SERS, or the simultaneous use of darkfield microscopy, wide-field fluorescence, and Raman spectroscopy, where any emissive features that don't correlate with dark-field scattering must be smaller than 1.8 nm[61].

Bibliography

1. Ricketts CR, Lowbury EJ, Lawrence JC, Hall M, Wilkins MD: **Mechanism of prophylaxis by silver compounds against infection of burns.** *Br Med J* 1970, **2**:444-446.
2. Bhol KC, Schechter PJ: **Effects of Nanocrystalline Silver (NPI 32101) in a Rat Model of Ulcerative Colitis.** *Dig Dis Sci* 2007:11 pages.
3. Fan FF, Bard AJ: **Chemical, electrochemical, gravimetric, and microscopic studies on antimicrobial silver films.** *J Phys Chem B* 2002, **106**:279-287.
4. Fuertes MA, Castilla J, Alonso C, Perez JM: **Cisplatin biochemical mechanism of action: from cytotoxicity to induction of cell death through interconnections between apoptotic and necrotic pathways.** *Curr Med Chem* 2003, **10**:257-266.
5. Mizushima Y, Okumura H, Kasukawa R: **Effects of gold and platinum on necrotizing factor, skin sensitizing antibody, and complement.** *Jpn J Pharmacol* 1965, **15**:131-134.
6. Handel ML, Nguyen LQ, Lehmann TP: **Inhibition of transcription factors by anti-inflammatory and anti-rheumatic drugs: can variability in response be overcome?** *Clin Exp Pharmacol Physiol* 2000, **27**:139-144.
7. Suzuki S, Okubo M, Kaise S, Ohara M, Kasukawa R: **Gold sodium thiomalate selectivity inhibits interleukin-5-mediated eosinophil survival.** *J Allergy Clin Immunol* 1995, **96**:251-256.
8. Eisler R: **Chrysotherapy: a synoptic review.** *Inflamm Res* 2003, **52**:487-501.
9. Wahata JC, Lewis JB, Volkmann KR, Lockwood PE, Messer RLW, Bouillaguet S: **Sublethal concentrations of Au(III), Pd(II) and Ni(II) differentially alter inflammatory cytokine secretion from activated monocytes.** *J Biomed Mater Res Part B: Appl Biomater* 2004, **69B**:11-17.
10. Abraham GE, Himmel PB: **Management of Rheumatoid Arthritis: Rationale for the Use of Colloidal Metallic Gold.** *J Nutr Env Med* 1997, **7**:295-305.
11. Zou J, Guo Z, Parkinson JA, Chen Y, Sadler PJ: **Gold(III)-induced oxidation of glycine: relevance to the toxic side-effects of gold drugs.** *J Inorg Biochem* 1999, **74**:352.
12. Bayler A, Schier A, Bowmaker GA, Schmidbaur H: **Gold is smaller than silver, crystal structures of [bis(trimesitylphosphine)gold(I)] and [bis(trimesitylphosphine)silver(I)] tetrafluoroborate.** *J Am Chem Soc* 1996, **118**:7006-7007.
13. Wyckhoff RG: *Crystal Structures*, 2nd edition. New York: Interscience Publishers; 1958: 10.
14. Pauling L: *The Nature of the Chemical Bond.*, 3rd edition. Ithaca, NY: Cornell University Press; 1980: 410.
15. Peyser LA, Vinson AE, Bartko AP, Dickson RM: **Photoactivated fluorescence from individual silver nanoclusters.** *Abstracts of Papers of the American Chemical Society* 2001, **221**:114.

16. Peyser LA, Lee TH, Dickson RM: **Mechanism of Ag-n nanocluster photoproduction from silver oxide films.** *Journal of Physical Chemistry B* 2002, **106**:7725-7728.
17. Zheng J, Petty JT, Dickson RM: **High quantum yield blue emission from water-soluble Au-8 nanodots.** *Journal of the American Chemical Society* 2003, **125**:7780-7781.
18. Zheng J, Zhang CW, Dickson RM: **Highly fluorescent, water-soluble, size-tunable gold quantum dots.** *Physical Review Letters* 2004, **93**.
19. Zheng J, Nicovich PR, Dickson RM: **Highly fluorescent noble-metal quantum dots.** *Annual Review of Physical Chemistry* 2007, **58**:409-431.
20. Felix C, Sieber C, Harbich W, Buttet J, Rabin I, Schulze W, Ertl G: **Fluorescence and excitation spectra of Ag-4 in an argon matrix.** *Chemical Physics Letters* 1999, **313**:105-109.
21. Felix C, Sieber C, Harbich W, Buttet J, Rabin I, Schulze W, Ertl G: **Ag-8 fluorescence in argon.** *Physical Review Letters* 2001, **86**:2992-2995.
22. Sieber C, Buttet J, Harbich W, Felix C, Mitric R, Bonacic-Koutecky V: **Isomer-specific spectroscopy of metal clusters trapped in a matrix: Ag-9.** *Physical Review A* 2004, **70**:041201:1-4.
23. Burgel C, Mitric R, Bonacic-Koutecky V: **Emissive properties of silver particles at silver oxide surface defects.** *Applied Physics A-Materials Science & Processing* 2006, **82**:117-123.
24. Fayet P, Granzer F, Hegenbart G, Moisar E, Pischel B, Woste L: **Latent-Image Generation by Deposition of Monodisperse Silver Clusters.** *Physical Review Letters* 1985, **55**:3002-3004.
25. Eachus RS, Marchetti AP, Muentner AA: **The photophysics of silver halide imaging materials.** *Annual Review of Physical Chemistry* 1999, **50**:117-144.
26. Taylor PL, Ussher AL, Burrell RE: **Impact of heat on nanocrystalline silver dressings Part I: Chemical and biological properties.** *Biomaterials* 2005, **26**:7221-7229.
27. Wright JB, Lam K, Burrell RE: **Wound management in an era of increasing bacterial antibiotic resistance: a role for topical silver treatment.** *American Journal of Infection Control* 1998, **26**:572-577.
28. Balzar D: **Voigt-function model in diffraction line-broadening analysis.** In: *Microstructure analysis from diffraction.* Ed: Snyder RL. IUCR monograph; ©2001.
29. Zhang J, Xu S, Kumacheva E: **Photogeneration of fluorescent silver nanoclusters in polymer microgels.** *Adv Mater* 2005, **17**:2336-2340.
30. Sonnichsen C, Franzl T, Wilk T, von Plessen G, Feldmann J: **Plasmon resonances in large noble-metal clusters.** *New Journal of Physics* 2002, **4**:93.1-93.8.
31. Bohren CF, Huffman DR: *Absorption and scattering of light by small particles.* New York: Wiley; ©1983. p. 372-4.
32. Ameen KB, Rajasekharan T, Rajasekharan MV: **Grain size dependence of physico-optical properties of nanometallic silver in silica aerogel matrix.** *Journal of Non-Crystalline Solids* 2006, **352**:737-746.

33. Zheng J, Dickson RM: **Individual water-soluble dendrimer-encapsulated silver nanodot fluorescence.** *Journal of the American Chemical Society* 2002, **124**:13982-13983.
34. Abdullah A, Annapoorni S: **Fluorescent silver nanoparticles via exploding wire technique.** *Pramana-Journal of Physics* 2005, **65**:815-819.
35. Zhu J, Zhu X, Wang YC: **Electrochemical synthesis and fluorescence spectrum properties of silver nanospheres.** *Microelectronic Engineering* 2005, **77**:58-62.
36. Pethkar S, Aslam M, Mulla IS, Ganeshan P, Vijayamohanan K: **Preparation and characterisation of silver quantum dot superlattice using self-assembled monolayers of pentanedithiol.** *Journal of Materials Chemistry* 2001, **11**:1710-1714.
37. Dai Y, Hu X, Wang C, Chen DP, Jiang XW, Zhu CS, Yu BK, Qiu JR: **Fluorescent Ag nanoclusters in glass induced by an infrared femtosecond laser.** *Chemical Physics Letters* 2007, **439**:81-84.
38. Evanoff DD, Chumanov G: **Size-controlled synthesis of nanoparticles. 1. "Silver-only" aqueous suspensions via hydrogen reduction.** *Journal of Physical Chemistry B* 2004, **108**:13948-13956.
39. Evanoff DD, Chumanov G: **Size-controlled synthesis of nanoparticles. 2. Measurement of extinction, scattering, and absorption cross sections.** *Journal of Physical Chemistry B* 2004, **108**:13957-13962.
40. He P, Shen XH, Gao HC: **Photoluminescence phenomenon during the formation of silver nanoparticles.** *Acta Physico-Chimica Sinica* 2004, **20**:1200-1203.
41. Karthikeyan B: **Spectroscopic studies on Ag-polyvinyl alcohol nanocomposite films.** *Physica B-Condensed Matter* 2005, **364**:328-332.
42. Sun YG, Xia YN: **Gold and silver nanoparticles: A class of chromophores with colors tunable in the range from 400 to 750 nm.** *Analyst* 2003, **128**:686-691.
43. Geddes CD, Parfenov A, Gryczynski I, Lakowicz JR: **Luminescent blinking from silver nanostructures.** *Journal of Physical Chemistry B* 2003, **107**:9989-9993.
44. Hu M, Petrova H, Wang X, Hartland GV: **Time-resolved and steady state spectroscopy of polydisperse colloidal silver nanoparticle samples.** *Journal of Physical Chemistry B* 2005, **109**:14426-14432.
45. Lu L, Kobayashi A, Tawa K, Ozaki Y: **Silver nanoplates with special shapes: Controlled synthesis and their surface plasmon resonance and surface-enhanced Raman scattering properties.** *Chemistry of Materials* 2006, **18**:4894-4901.
46. Yang Y, Matsubara S, Xiong LM, Hayakawa T, Nogami M: **Solvothermal synthesis of multiple shapes of silver nanoparticles and their SERS properties.** *Journal of Physical Chemistry C* 2007, **111**:9095-9104.
47. Bechthold PS, Kettler U, Schober HR, Krasser W: **Guest-Host Interaction and Photochemical Transformation of Silver Particles**

- Isolated in Rare-Gas Matrices.** *Zeitschrift Fur Physik D-Atoms Molecules and Clusters* 1986, **3**:263-270.
48. Harbich W, Fedrigo S, Meyer F, Lindsay DM, Lignieres J, Rivoal JC, Kreisle D: **Deposition of Mass Selected Silver Clusters in Rare-Gas Matrices.** *Journal of Chemical Physics* 1990, **93**:8535-8543.
 49. Fedrigo S, Harbich W, Buttet J: **Optical-Response of Ag₂, Ag₃, Au₂, and Au₃ in Argon Matrices.** *Journal of Chemical Physics* 1993, **99**:5712-5717.
 50. Rabin I, Schulze W, Ertl G, Felix C, Sieber C, Harbich W, Buttet J: **Absorption and fluorescence spectra of Ar-matrix-isolated Ag-3 clusters.** *Chemical Physics Letters* 2000, **320**:59-64.
 51. Jiang ZL, Yuan WE, Pan HC: **Luminescence effect of silver nanoparticle in water phase.** *Spectrochimica Acta Part a-Molecular and Biomolecular Spectroscopy* 2005, **61**:2488-2494.
 52. Murakoshi K, Tanaka H, Sawai Y, Nakato Y: **Photoinduced structural changes of silver nanoparticles on glass substrate in solution under an electric field.** *Journal of Physical Chemistry B* 2002, **106**:3041-3045.
 53. Badr Y, Abd El Wahed MG, Mahmoud MA: **On 308 nm photofragmentation of the silver nanoparticles.** *Applied Surface Science* 2006, **253**:2502-2507.
 54. Maali A, Cardinal T, Treguer-Delapierre M: **Intrinsic fluorescence from individual silver nanoparticles.** *Physica E-Low-Dimensional Systems & Nanostructures* 2003, **17**:559-560.
 55. Treguer M, Rocco F, Lelong G, Le Nestour A, Cardinal T, Maali A, Lounis B: **Fluorescent silver oligomeric clusters and colloidal particles.** *Solid State Sciences* 2005, **7**:812-818.
 56. Mihalcea C, Buchel D, Atoda N, Tominaga J: **Intrinsic fluorescence and quenching effects in photoactivated reactively sputtered silver oxide layers.** *Journal of the American Chemical Society* 2001, **123**:7172-7173.
 57. Monti OLA, Fourkas JT, Nesbitt DJ: **Diffraction-limited photogeneration and characterization of silver nanoparticles.** *Journal of Physical Chemistry B* 2004, **108**:1604-1612.
 58. Taylor PL, Ussher AL, Burrell RE: **Impact of heat on nanocrystalline silver dressings. Part I: Chemical and biological properties.** *Biomaterials* 2005, **26**:7221-7229.
 59. Burrell RE, Taylor PL, Ussher AL, McCaffrey WC: **Silver release in simulated wound fluids from silver containing dressings.** In: *2nd Congress of the WUWHS*, July 8-13, 2004; Paris, France. 1 page.
 60. Taylor PL, Omotoso O, Wiskel JB, Mitlin D, Burrell RE: **Impact of heat on nanocrystalline silver dressings Part II: Physical properties.** *Biomaterials* 2005, **26**:7230-7240.
 61. Peyser-Capadona L, Zheng J, Gonzalez JI, Lee TH, Patel SA, Dickson RM: **Nanoparticle-free single molecule anti-stokes Raman spectroscopy.** *Physical Review Letters* 2005, **94**.

Chapter 6 – Testing for Anti-inflammatory and Antimicrobial Activity of Nanocrystalline Silver-Derived Solutions in the Lung

Introduction

The lungs, being coated in epithelial tissue which is exposed to the external environment, play a similar role to the skin as a first line of defense against invading pathogens. The lungs are constantly bombarded by infectious agents and potentially harmful particles, and are also more susceptible to these agents than the skin, due to the fact that the warm moist environment which is required for gas exchange also enhances microbial growth. As with the skin, when an infectious agent or harmful substance penetrates the lungs, an inflammatory response is induced by the lungs in order to eliminate the agent or substance. Unfortunately, this inflammatory response can be detrimental because build-up of excessive edema in the lungs makes respiration difficult. In diseases such as pneumonia, adult respiratory distress syndrome (ARDS), acute lung injury (ALI), toxic epidermal necrolysis syndrome (TENS), and septic shock, the cause of patient mortality may not be a direct action of the harmful agent, but rather the over-responsive inflammatory reaction of the lungs.

Pneumonia is an inflammatory illness of the lung, brought on by infection of the lower airways by bacteria, viruses, or fungi[1]. Pneumonia is defined by lung parenchymal/alveolar inflammation and the filling of alveoli with fluid. Although in many cases pneumonia can be treated with antibiotics, antibiotic resistant bacteria have become an increasing threat. The development of methicillin-resistant *Staphylococcus aureus* is a common example[2]. *S. aureus* is

the causative pathogen in 25% of community-acquired pneumonia cases[3]. Both MSSA (methicillin-sensitive *Staphylococcus aureus*) and MRSA strains can produce PVL (Panton-Valentine Leukocidin), although it is more commonly associated with MRSA[2]. PVL-producing *S. aureus* strains cause necrotizing pneumonia that rapidly leads to pleural effusion, shock, and respiratory failure[4], with a mortality rate as high as 56%[5].

Septic shock, ALI, and ARDS are also life-threatening inflammatory lung conditions, having mortality rates of 40-60%[6]. ALI and ARDS, which are distinguished from each other in terms of severity, despite both having mortality rates of 30-50%[7], are caused by direct or indirect insults which lead to pulmonary inflammation, damaged alveolocapillary membranes, and ultimately severe acute respiratory failure. Direct pulmonary causes of ALI and ARDS include viral or bacterial lung infections, gastric aspiration, thoracic trauma or radiation, near-drowning, hyperoxia, or inhalation of smoke or toxicants[7]. Indirect causes of ALI and ARDS include sepsis, burn injuries, hypovolemic shock, trauma, transfusions, and pancreatitis[7]. Lipopolysaccharide (LPS), an antigenic component of gram negative cell walls, activates leukocytes to release inflammatory mediators which contribute to the pathogenesis of both sepsis and ALI/ARDS[8]. The current standard of clinical care for ARDS/ALI patients involves mechanical ventilation (particularly low tidal volume ventilation), fluid management, nutritional support, and treatment of any known underlying causes of injury[7]. Very few pharmacologic advances have been made, although the use of exogenous surfactant therapy may improve patient survival[7].

TENS is a rare disorder, but has a 30% mortality rate[9]. It typically results from drug reactions, and is manifested by widespread epidermal necrosis and mucosal erosions, and can also involve lesions in epithelium of the respiratory and gastrointestinal tracts[9]. The mechanisms resulting in this loss of epithelial tissue, including induction of apoptosis in epithelial cells[9], also enhance inflammatory responses, while widespread loss of epithelial tissue also leaves TENS patients vulnerable to sepsis[9]. When the lungs are involved, bronchial obstruction can occur due to epithelial necrosis, pulmonary infection, or edema caused by the inflammatory response, which can then lead to ARDS[9]. There is currently no consensus about which therapeutic agents should be used to treat TENS[9]. While corticosteroids and other immunosuppressives are sometimes used to treat the inflammation (often via their suppression of TNF- α production or activity), thus reducing epithelial loss, they may increase the risk of the development of sepsis by suppressing the immune system[9].

There are also chronic lung diseases, such as cystic fibrosis (CF) and chronic obstructive pulmonary disease (COPD), which involve chronic inflammation, making the affected lungs more susceptible to chronic infections as well. CF is characterized by thick mucus secretions from epithelia, and is associated with development of progressive bronchiectasis[10]. Initially, the lower respiratory tract of infants with CF gets colonized with organisms such as *S. aureus*, and *H. influenzae*. Over time the incidence of these infections wanes, and chronic infections with mucoid strains of *P. aeruginosa* become a major cause of morbidity and mortality[10]. An exaggerated and persistent, predominantly

neutrophilic, inflammatory response to these *P. aeruginosa* infections is considered a distinguishing feature of lung disease in CF patients[10]. Host factors produced during the chronic inflammation associated with CF play a major role in the etiology of CF. Dysregulated cytokine production by various cell types in the lung may be the underlying basis of excessive inflammatory response in the CF lung, rather than infection directly, and there may be a link between a basic defect in CF and inflammation[10]. The median age of survival for a CF patient is 36.8 years[11]. CF treatments focus on antibiotics and anti-inflammatories.

COPD is characterized by chronic airflow obstruction due to chronic bronchitis and/or emphysema arising from destruction of small airways and septal infrastructure, loss of alveolar wall structures, and mucus plugging because of mucus hypersecretion[12, 13]. (COPD can be generated in animal models via SO₂ and/or elastase inhalation[12, 13]). The presence of inflammation is critical to chronic progression of COPD, with lung damage and remodeling resulting from a possible imbalance between pulmonary proteases and antiproteases released by inflammatory cells[12]. COPD has a mortality rate of 77% within 13 years of patients with COPD applying for pension due to disability[14]. As with CF, treatments for COPD focus on antibiotics, steroids to suppress inflammation, and also bronchodilators.

While it is important to eliminate the cause of the disease where possible, it is equally, and perhaps more immediately, important to control the inflammatory response and promote healing of the lungs of patients with any of

these diseases. Antibiotics can be used to help control the lung infection involved in many of these diseases, but there are limitations for their use. The development of antibiotic-resistant bacteria has become a serious problem over the last few decades, and as more strains become multi-drug resistant, clinicians are being forced to seek alternative means of controlling infection. Additionally, there are many patients who cannot take antibiotics due to allergies or the fact that antibiotics can cause flare-ups of certain diseases, including TENS[9]. In all of these situations, a treatment other than antibiotics is required. In the treatment of skin disorders, scientists and clinicians have shifted towards the use of silver topical treatments as an alternative to antibiotics, although, as was demonstrated in Chapter 4, there is a risk of bacteria developing resistance to Ag^+ just as there is to antibiotics. Ag^+ also was demonstrated in Chapter 2 to be pro-inflammatory. Therefore Ag^+ treatments do not appear to be a good option for the treatment of lung infectious or inflammatory diseases. However, nanocrystalline silver dressings have demonstrated both antimicrobial and anti-inflammatory activity *in vitro*, *in vivo*, and clinically, in the skin[15-26]. Furthermore, the results of Chapter 4 indicated that nanocrystalline silver can kill bacteria resistant to Ag^+ and also that it is difficult for bacteria to build resistance to nanocrystalline silver. Therefore, nanocrystalline silver appears to be a good candidate for treatment both as an antimicrobial agent and an anti-inflammatory/prohealing agent of other epithelial tissues, including those in the lungs. Additionally, a recent study has shown that, in a murine model of ulcerative colitis, proprietary nanocrystalline silver nanodispersions in polyvinyl alcohol/water delivered intracolonicly or

orally (at 10 times the dose) suppressed the expression of matrix metalloproteinase (MMP)-9, TNF- α , IL-1 β , and IL-12[27]. This suggests that nanocrystalline silver has anti-inflammatory activity which could be used to treat internal epithelial tissues, such as those of the lung, in addition to skin tissue.

The study of Chapter 3 indicated that the anti-inflammatory effect of nanocrystalline silver treatments is translocatable from one portion of the skin to another portion of the skin. While this suggests that it might be possible to place nanocrystalline silver on a patients' skin and produce an anti-inflammatory effect in the lung, there is no evidence available currently to indicate that this is the case. Furthermore, a patient being treated for TENS with nanocrystalline silver wrapped all around her body showed improvement in the skin, but not in her lung function. When a doctor took water in which nanocrystalline silver had been soaked and did a bronchoalveolar lavage (BAL), so that the solution had direct contact with the lungs, the woman's lung function improved dramatically (personal communication, Dr. Robert Burrell). Since the antimicrobial activity of nanocrystalline silver can only occur via direct interaction between the active silver species and the microbe, the lack of improvement in lung function when the nanocrystalline silver was only used to treat her skin may have been due to the inability of the treatments to eliminate the lungs' infection. However, it suggests alternatively that the translocatable effect of the nanocrystalline silver anti-inflammatory activity may not extend to the lung. Whether or not this is the case, the fact that antimicrobial activity can only be controlled by direct contact with nanocrystalline silver species indicated that the development of solutions which

had some or all of the properties of nanocrystalline silver – either its antimicrobial activity, anti-inflammatory activity, or both – could be useful for the treatment of a variety of lung diseases.

Since antimicrobial activity of nanocrystalline silver correlates with total silver released in solution when solutions are generated under the same conditions (see Chapter 9) and only silver species released from the nanocrystalline silver dressings would be able to contact human cells in order to initiate the anti-inflammatory events observed in Chapters 2 and 3, this indicated that it might be possible to develop solutions containing the properties of nanocrystalline silver. In Chapter 5, it was shown that some nanocrystalline silver-derived solutions did have antimicrobial activity *in vitro*, but a method was not determined to measure the anti-inflammatory activity of the solutions *in vitro*, and it was not determined whether the solutions would prove anti-inflammatory or antimicrobial *in vivo*.

The purpose of the set of studies presented in this chapter was to test a nanocrystalline silver-derived solution (selected based on data available at the time of the study – only preliminary antimicrobial testing and total silver data had been obtained at that point) for antimicrobial and anti-inflammatory activity independently, in relevant models of lung disease.

The Sprague-Dawley rat was chosen as the animal to be used in these studies because the rat is a commonly used animal model for clinically relevant lung studies. Rats are reasonably priced, easily raised in disease-free environments, genetically homogeneous, and there is plenty of information available in the published literature regarding the study of lung diseases in

rats[28]. In addition, it can be difficult to deliver challenges and treatments to the lungs of larger animals. As well, unlike experiments done in skin models, animals must be terminated any time lung histology, immunohistochemistry, mRNA expression, protein expression, or bacteriological data is required, which can make the use of large animals very costly, even for relatively small experiments. However, animal models smaller than rats, such as mice, present difficulties for lung studies in terms of obtaining sufficiently small equipment, and of using techniques such as intubation, due to their small tracheal diameters.

A model of acute infection was chosen in which rats were exposed to relatively high concentrations of live bacteria. This model was chosen over other related models, such as mucoid models, due to concerns that more chronic models of infection would result in high morbidity and mortality for the animals.

A model of acute inflammation was chosen in which rats were exposed to moderate levels of LPS. LPS is a cell wall surface antigen of gram negative bacteria. It increases lung microvascular permeability, resulting in pulmonary edema with recruitment of leukocytes from the peripheral blood into interstitial pulmonary tissues[29]. It also induces the formation of nitric oxide[30]. While other chemicals, such as oleic acid[31], sulfur mustard[32], sodium dodecyl sulfate[33], or hydrochloric acid[34], can be used to generate similar responses, LPS is a more clinically relevant molecule, since it induces significant inflammation during clinical bacterial infections. Cigarette smoke inhalation models can also be used, but require long exposure times of the animals in order to generate a strong inflammatory response[35, 36]. While delivering whole dead

bacteria is an alternative to using LPS, delivering purified LPS can cause a stronger inflammatory response than whole dead bacteria, making it a better choice to examine lung inflammation in the absence of actual infection by live bacteria.[29] Typically, LPS is administered by intraperitoneal or intravenous injections (where it is anticipated that the lungs will scavenge most of the LPS during the first passage)[30]. Unfortunately, these methods result in sepsis, ALI, or ARDS-like symptoms in rodent models, where mortality in experiments can occur due to failure of organs other than the lungs[29]. However, installation of the LPS more directly into the lungs results in a stronger pulmonary response, with less systemic shock[29]. Other models of inflammation including surfactant depletion via repetitive total lung lavage[37], and models of pulmonary fibrosis[38] were also considered as alternatives to using LPS. However, surfactant depletion is labor intensive, traumatic (as a tracheotomy is required), requires specialized equipment, and results in more severe injury to the lungs (ARDS symptoms) than desired for this study[37]. Also, there isn't a true animal model of idiopathic pulmonary fibrosis, which is the most common form of interstitial pneumonia in man (in which inflammation plays a prominent role early on, followed by continued activity at a lower level)[38]. This is because the natural fibrotic response can differ significantly between animals and humans; the progression of human pulmonary fibrosis is difficult to reproduce in animals; removal of the inciting agent in some animal models can allow the fibrosis to regress (which doesn't occur in human lung fibrosis); and the injuries produced in the animal models are often too severe, precluding meaningful interpretation of

subsequent changes[38]. The most common methods of inducing experimental pulmonary fibrotic reactions include direct pulmonary instillation of a fibrogenic agent or exposure of a susceptible host to thoracic irradiation[38]. Most commonly used chemicals for chemical-induced pulmonary fibrosis are bleomycin[38], which when given in multiple doses can generate a chronic condition, and environmental dusts such as SiO₂, TiO₂, Fe₂O₃, or diesel engine exhaust dust delivered intratracheally[39-42]. Transgenic approaches to develop animals with fibrotic susceptibility have also been used, although genetically engineered animals may have permanent or complex phenotypes that may complicate the accurate assessment of specific interactions in the fibrotic lung[38]. Another problem with using models of lung fibrosis is that it is a chronic and progressive disease that develops over months to years, but in animal models, only individual time points can be analyzed[38]. In acute models this is a less significant concern, as sampling a few time points can provide sufficient information about these models, thus an acute model involving delivery of moderate amounts of LPS directly to the lung was chosen for the inflammation study.

There are a variety of methods which have been developed by which challenges and treatments can be delivered to the lungs of rodents, each of which have their advantages and their drawbacks.

One method is view controlled intratracheal instillation, in which the anesthetized rodent is placed on an oblique plane and the throat is illuminated with a lamp. The tongue is extended from its mouth, and a magnifying glass is

used to help view the trachea, while instillation is performed using a small catheter fixed to a syringe[43]. After instillation of the challenge or treatment, air is blown into the lungs via the catheter to ensure that the whole volume of the fluid has reached the respiratory tract[43]. A relatively high, reproducible[44], quantity (~20%) of the instilled dose is typically found in the lungs after injection[43]. It, along with all other forms of intratracheal instillation (when performed correctly), allows for the material being instilled to be delivered directly to the lungs, regardless of the particle size or viscosity of the material[28, 45], minimizing drug loss in the nose, throat and upper airways. It also has the advantages of allowing for a quantifiable dose, having a short application time, and being a low-cost procedure[45]. It does, however, require specific accessories such as laryngoscopes and illumination equipment[44], it results in poor distribution in the lungs, and only small volumes are tolerated in smaller animals[45]. Also some studies have suggested that the requisite air-bolus after the treatment can cause damage to the animals' lungs[32].

Solutions can also be delivered via tracheotomy, in which a longitudinal median skin incision is made directly over the larynx of the anesthetized animal. The trachea is then laid open and the solution is delivered very slowly into the trachea by a flat inserted needle fixed to a microlitre syringe. After the instillation, the animal is kept oblique (head upwards) to ensure that the whole volume of the solution reaches the respiratory tract[43]. This method has the advantage of delivering a large quantity of the initial dose to the lung (~50%). However, because of the invasiveness of the method, more time is required to

instill solutions in the animals than any other method, and this method is more detrimental to the animals[43]. This method requires more technical expertise than most of the other methods; although the view controlled intratracheal instillation also requires some technical expertise[43].

Solutions can also be applied intranasally, in which case the anesthetized rodent is laid on its side and the solution is applied drop-wise into one nostril, causing it to be inhaled by the animal[43]. This method is not very invasive, and can be performed very quickly. For delivery of bacteria, it is a closer mimic of how clinical infections are obtained compared to intratracheal delivery[46]. However it is highly variable due to the deposition of some of the solution in the nasal cavity[43, 44]. Some improvements to this method have been observed when holding the animals upright for the installation[46].

Blind installation is a method of solution delivery in which the anesthetized animal is fixed in an oblique position and a catheter is pushed forward into the trachea without view controls[43]. This method is not very invasive, can be performed quickly, and reportedly does not result in an adverse reaction from the animals[43]. However it is unreliable, as the correct position of the catheter is difficult to achieve without visualizing the trachea, and the esophagus is cannulated about 95% of the time. In addition, even when the trachea is cannulated, a wide variability in the amount of solution delivered to the lung occurs, and approximately 90% of the solution does not reach the lungs. This method can be improved somewhat by using a blunt curved metal cannula with an IV plastic cannula attached to a syringe[44]. With this setup, the rat is

placed on its back and the metal cannula is introduced into the larynx until resistance is felt as it enters the trachea. The location of the cannula in the trachea is confirmed by feeling with the fingertips – the metal cannula is in the trachea if it can be felt against the rings of cartilage[44]. The plastic cannula is passed through the metal cannula two centimeters past the tip of the metal cannula, and the inoculum is injected. The two cannula are removed immediately and the animal is placed on its stomach[44]. The authors introducing this technique indicated that the technique was not stressful for rats, and that no mortalities resulted when fentanyl fluanisone and diazepam were used for anesthesia/muscle relaxation, preventing laryngeal trauma or respiratory distress/arrest[44]. However, based on the results of this chapter, it is believed that this technique has the potential to cause respiratory distress due to contact with the vocal cords (see discussion at the end of this chapter).

Aerosol inhalation can also be used to deliver solutions to rodents. Rodents are placed in an aerosol dispersal chamber for 15-30 minutes, and a small compressor transfers the solution as an aerosol to the exposure tubes of the inhalation chamber. If animals are pre-trained to the use of the tubes, they will not become stressed and hyperventilate during the experiment, preventing the need for anesthesia[43]. This model, when used for infecting an animal, has the advantage of best mimicking clinical situations, as most respiratory infections are contracted through aerosol inhalation[46]. As well, uniform distribution of the inhaled particles occurs, including good peripheral distribution[45]; the method is non-invasive[45]; and a large number of rodents can be inoculated or treated at

the same time[28]. Disadvantages of this method include that a much higher dose of solution must be delivered using this method than any other method, and even so it is difficult to get sufficient quantities of solutions delivered to the animals' lungs[43]. As well, the time required for the procedures is longer than other methods[45], and variability using this method is high, resulting in poor reproducibility[46]. Other disadvantages are the requirement for costly equipment[44], as well as the time required to train the animals[43]. As well, the physicochemical properties of some types of inoculum make them difficult to aerosolize[28]. For example, bacteria tend not to reach the lung in a viable state after nebulization[43], and the lysis of bacteria during nebulization results in excessive exposure to antigens. As well, both the aerosol and the intranasal methods can result in infection of extrapulmonary tissues if bacteria are delivered via this method[43]. This also occurs with the blind instillation method due to incorrect catheter placement, but is less common with tracheotomies or view controlled intratracheal instillation[43].

Another method of delivering substances to the lung which has been recently developed is the use of microsprayers (PennCenturyTM Inc., Philadelphia, PA, USA). Microsprayers combine instillation with nebulization, as they consist of a sub-miniaturized atomizer or nozzle located in the tip of a stainless steel tube, attached to a hand-operated high pressure syringe[45, 47]. When the syringe plunger is depressed, solution is forced at high pressure into a small mixing chamber on the end of the steel tube, imparting momentum to the solution[48]. The atomizer at the tip of the tube thus allows dispersal of a small volume of

liquid into the lungs without the need for the large volume of air to disperse it as is required when using intratracheal instillation techniques described above[48]. The flow pattern achieves a symmetrical plume of small droplets due to precise placement of the aperture, similar to that achieved via nebulization[48]. For use of the microsprayer in rodents, rodents are typically suspended on a support at an angle of 45° to 60°, hung from an elastic band by their incisors[48, 49]. A small spatula is used to open the rodent's mouth, then blunted forceps are used to move the tongue out to one side of the mouth to improve visualization of the trachea[45, 47, 50, 51], being careful not to impale the tongue on the rodent's lower incisors[52]. Pressing down on the tongue with the spatula improves visualization of the vocal cords[51, 52], which are illuminated by a fibreoptic light source. The microsprayer tip is then inserted into the trachea between the vocal cords up to a bend in the microsprayer, which marks the distance from the mouth to the first bifurcation of the trachea leading to the main bronchi[53]. The solution or suspension is then sprayed into the lungs of the animal from that location, and the tip is left inside the trachea for a few seconds before it is withdrawn from the mouth[45]. The microsprayer is then removed from the trachea and the rodent is removed from the support and allowed to recover[45]. One study suggests insufflating the lungs after the instillation to improve dispersion, resulting in high bioavailability of treatments and reproducibility of the method[47]. They found that the distribution, which was even between the five pulmonary lobes, was not affected by the air bolus used, but that insufflation increased the fraction of solution that was deposited in the peripheral lungs[47]. However, other studies

have indicated that one of the advantages of using microsprayers is that they allow for the dispersion of a small volume of liquid into the lungs without the necessity of using large volumes of air as a vehicle, which could damage the lungs[32].

The microsprayers circumvent the oropharynx, allowing delivery of solutions to the lower airways beyond first bronchial bifurcation[54], however, the nozzle at the tip of the sprayers allows “atomization” of solutions as they leave the microsprayer, creating a similar aerosolizing effect to that seen with a nebulizer, but on a much smaller volume, delivered directly to the lungs and reportedly providing even distribution throughout the lungs[53, 55]. Gamma scintigraphy studies have shown that Tc-labeled lipid-DNA complexes spray-instilled into rat lungs using microsprayers resulted in a uniform distribution of radiolabeled compounds in both central and peripheral regions of the lungs[54]. As well, the distribution of radiolabeled saline solutions aerosolized into upright rhesus macaques was compared using a microsprayer, nebulization through a mouth piece, nebulization through a laryngeal mask airway, and nebulization through an endotracheal tube. It was determined that using the microsprayer, a mass median diameter (MMD) of 22 μm was obtained, while using the nebulizers, an MMD of 4 μm was obtained. MMD is defined such that half of the mass of the aerosol is contained in particles with diameters less than the MMD[56]. However, the average fraction of solution deposited in the lungs was 1.87% or less when the nebulizer was used, depending on the configuration, but was 93% when the aerosols were delivered via the microsprayer, indicating that the

microsprayer was more efficient, delivering a higher dose than the nebulizer, and thus minimizing waste of material, similar to other intratracheal instillation methods[57]. However, this study did note that most of the deposition occurred in the right lung, and that with the microsprayer, the greatest deposition occurred in the central regions of the lungs (12-14%), while only 0.23-7% occurred in the peripheral regions[57]. Deposition occurred more in the smaller airways and alveolar regions when nebulizers were used, due to the smaller MMD produced[57]. In a similar study, the pattern of deposition was inconsistent among animals using the microsprayer. However, the authors found that radioisotopy was detected in all lung regions, and that deposition in the left lung was $30.3 \pm 15.5\%$, while in the right lung, the deposition fraction was $50.1 \pm 9.0\%$ [58]. They also determined that there were no significant differences in deposition between regions within a single lung[58]. They concluded that, although the use of a microsprayer was more invasive than using nebulizers, with the microsprayer they obtained the highest total deposition fraction, and it was more efficient than any nebulization methods of delivery, allowing for delivery of higher doses to the airway surfaces than was possible by nebulization[58]. They also noted that the deposition was more evenly divided between lungs compared to direct instillation methods, and that the method was quick, only taking a few minutes[58]. Another study in rats also concluded that instillation of fluids using microsprayers may be more efficient than intratracheal instillation because the dose after intratracheal instillation is frequently localized[59], covering less than 5% of the lung surface[60], whereas deposition after using the microsprayers

covered the lung surface uniformly[48]. In a study using rhesus macaques, the authors determined that the deposition was 50% in the right lung, and that deposition was achieved throughout the lung, including in the peripheral regions[61]. While they found a difference of a thousand-fold when comparing peripheral deposition to central deposition, when they normalized the deposition to each region of the right lung by weight, they found no significant differences[61]. They also found that a consistent deposition pattern was achieved between animals, and that the animals tolerated repeated treatments, with no acute or chronic inflammation along airways, interstitium, or alveolar spaces[61]. They concluded that the microsprayer produced a uniform and consistent deposition to pulmonary epithelium without the losses associated with nebulization, and permitted a 50-100 fold improvement in treatment delivery[61]. Another study in macaques, involving the delivery of green fluorescent protein (GFP) to the lungs, indicated that the GFP was more commonly observed in proximal regions of the lung near the area of instillation[62].

A study in which radiolabeled lipoplexes were delivered to the lungs of mice using the microsprayer technology concluded that the spray reached the air volume inside the lungs, and had the advantages of achieving aerosolization while allowing the quantity of material reaching the lungs to be accurately determined, and of being a very reproducible technique[63, 64]. Another study in mice also found that a wide distribution of material throughout the lungs occurred, and not just in the larger airways[45]. They were able to obtain a mass median

aerodynamic diameter (MMAD) of $8.01 \pm 0.57 \mu\text{m}$, and a geometric standard deviation (GSD) of 1.1, where MMAD is defined as:

$$\text{MMAD} = \text{MMD} * (\text{specific gravity})^{1/2} \quad (6-1)$$

and GSD is defined as the standard deviation of the logarithm of the particle diameters[56].

A mouse study in which transgenes were delivered to the lungs via a microsprayer found that the transgene was equally distributed throughout all lung lobes[65]. However, another study in mice found that the particles were predominantly deposited in the central lung, with particles lining the bronchial epithelium, using the microsprayer[66], but still concluded that the use of microsprayers offered the opportunity to do multiple administrations of solutions while avoiding surgical procedures, with no associated mortalities[66].

Studies using a canine model reported MMDs of $20 \mu\text{m}$, with close to 100% efficiency, and reproducible deposition in terms of both deposition pattern and mass when the microsprayer was activated during inspiration[67, 68].

Other studies in rodents found homogeneous patterns of deposition, although there was more deposition in the right lung than the left lung, with a total lung deposition of $89\% \pm 10\%$ of dose[69]. They also concluded that microsprayers were a safe and efficacious way to deliver aerosols to rodents, with the advantages of bypassing the upper respiratory tract and avoiding deposition in the nasal passages, thus facilitating intrapulmonary delivery of a coarse aerosol with droplet sizes that would not enter the lungs with the use of a conventional aerosol delivery device[69]. However, in an earlier study by the same group,

there was a 1.3% mortality rate, and they determined the pulmonary deposition was about 70%, which they attributed to mucociliary clearance resulting in some of the delivered solution going to the esophagus and stomach[70].

Although among the studies discussed above, there was some discrepancy regarding the distribution of fluids instilled into lungs via microsprayers, all the studies indicated that the microsprayers were effective and provided a better means of performing inhalation studies than more traditional methods such as intratracheal instillation, tracheotomies, nebulization, or nasal instillation. Most studies also indicated that microsprayers did provide good distribution, which is particularly important for LPS studies, as liquid bolus intratracheal delivery of LPS can produce focal lesions with severe hemorrhage and necrosis in some parts of the lung, while other large portions of lung tissue remain unaffected[48]. Therefore, the microsprayer was selected for use in the studies presented in this chapter.

Materials and Methods

Materials

Unless otherwise mentioned, all reagents were purchased from Fisher Scientific Inc. (Ottawa, Ontario, CA).

Microsprayers come in two configurations for delivering solutions – the IA-1B® and the IA-1C® (PennCentury™ Inc., Philadelphia, PA, USA). Table 6-1 shows a chart comparing the two microsprayers. The IA-1C® was used in the anti-inflammatory study, and the IA-1B® was used in the antimicrobial study,

because the IA-1C® arrived first, in time to do the anti-inflammatory study, while the IA-1B®, which arrived later, was found to be significantly easier to load.

Table 6-1. Comparison of the IA-1B® and IA-1C® MicroSprayers by PennCentury™, Inc.

Specification	IA-1B®	IA-1C®
Diameter	19-gauge (0.042" OD 0.033" ID, 30 gauge tubing at tip of atomizer (0.012" OD, 0.006" ID), 0.0135" aperture[48]	23-gauge (0.025" OD)
MMD	25-30 µm MMD	16-22 µm
Operating Pressure	700 psi	3000 psi
Other	Requires 1cc polycarbonate syringe, not suitable for mice, easier to use	Requires special high- pressure syringe, Model FMJ-250

*Information taken from www.penncentury.com, viewed June 6, 2009, unless indicated. OD = outer diameter, ID = inner diameter.

Anti-inflammatory Activity Study

Animals

16 domestic specific pathogen free (SPF) Sprague-Dawley rats (250 ± 10 g) were used in this study. The animals selected were healthy, with no apparent breathing abnormalities at the start of the experiment. The animals were kept singly in cages at Health Sciences Lab Animal Services (HSLAS) facilities at the University of Alberta, with a 12 hour light/dark cycle, in a room with separate ventilation and controlled temperature. Since the animals were kept singly, they were allowed one week of acclimatization before the start of the experiment. They were also provided with acetaminophen in their water (2.7 g/L[71]) during this time, to acclimatize them to the acetaminophen, which would then provide pain relief during the experimental period. The animals received antibiotic-free water (Petwa Water, with the acetaminophen added) and rat chow *ad libitum*

throughout the experiment. The study was approved by the University of Alberta HSAPWC (now REO) and conducted with humane care of the animals in accordance with guidelines established by the CCAC.

Preparation of Nanocrystalline Silver Solutions

pH 4 carbonated water was prepared as described in Chapter 5. To start the dissolution, one square inch of nanocrystalline silver dressing was added per five milliliters of water. The jar was capped with a lid containing a septum for a sampling port. The lid was sealed using parafilm, and the silver was allowed to dissolve for 24 hours without stirring prior to delivering the solutions to the rats' lungs.

Induction of Inflammation

Procedures were followed under the conditions set by HSLAS (Appendix 1). The rats were placed under 9-27 mg/kg ketamine and 0.09-0.27 mg/kg acepromazine (sterile, in PBS). One at a time, the rats were placed in a fumehood on their stomachs, and their heads were lifted up by suspending their incisor teeth on an elastic in a frame. A microsprayer (IA-1C®), along with an MDS otoscope (000A3748, Hallowell EMC, Pittsfield, MA, USA) modified with a rat specula (200A3588, Hallowell EMC) for use as a laryngoscope, was used to deliver 100 µL of PBS (5 negative controls) or 0.4 mg/kg lipopolysaccharide (Sigma, L9143 – the remaining rats). This dosage was chosen such that the animals would have a consistent inflammatory response in the lungs, but would not be in danger of mortality (see discussion). The rats were allowed to recover and returned to their cages.

Treatment

4 hours after introduction of lipopolysaccharide to the lungs, the rats received treatment. The rats were placed under general anaesthesia for treatments and were delivered the treatments via a microsyringe, as above. All treatments were delivered at a volume of 100 μ L. This was done so that, theoretically, the treatments would be delivered to the same location as the original inoculum. The rats were treated in the same order that they were inoculated. The negative control rats were given distilled water, which, based on the results of Chapter 5, was at approximately the same pH as the treatments described below. Of the rats that received lipopolysaccharide, five, which served as positive controls for the experiment, were given the same treatment as the negative controls. Another five were given nanocrystalline silver-derived solutions prepared as described above. Samples of the silver-containing solutions were taken before and after treatment of the rats and submitted for total silver analysis via atomic absorption spectroscopy (AAS). AAS was performed as described in Chapter 4. The rats were allowed to recover and returned to their cages.

After 24 hours, the rats were anesthetized as above, blood samples were taken from the myocardium and left at room temperature in Eppendorf tubes, and the rats were euthanized using Euthanyl (0.5 mL/rat). The lungs were then removed. Portions of the top right and bottom right lung lobes were snap-cooled in liquid nitrogen for RNA and protein analysis, respectively. These portions were later transferred to -80°C for long-term storage. One portion of the upper lobe of the left lung was placed in 1 mL of 4% PFA and kept at room temperature.

A second portion of the same lobe was placed on ice for subsequent cryopreservation. The middle left lung lobe was placed on ice for bacterial counts.

Cryopreservation

Tissue samples stored on ice were placed on Disposable Base Molds (Richard-Allen Scientific, Kalamazoo, MI) in a methanol/dry ice bath, and covered with Cryomatrix. They were then stored at -80°C.

Serum Preservation

Blood samples were centrifuged for 10 minutes at 5000 rpm and then the supernatant (serum) was collected and stored at -20°C.

Bacterial Cell Counts

Tissue samples stored on ice for bacterial counts were weighed. 0.5 mL of PBS was added to each sample, and then each sample was homogenized by hand using Kontes Pellet Pestles. A ten-fold dilution series was produced by adding 100 µL of the homogenized tissue sample to 900 µL of PBS. This was repeated five times. From each dilution in the series, three 20 µL drops were placed onto MHA plates, using the drop plate method. Once the drops had absorbed, the plates were incubated at 37°C overnight. The resulting CFUs were recorded and used to calculate the bacterial counts per gram of tissue. The plates were left at room temperature for an additional day and checked for new growth. The bacterial counts were calculated by:

$$\text{Bacteria/gram tissue} = \frac{\text{plate count} * 1}{(\text{initial dilution} * \text{subsequent dilutions} * \text{volume plated})} \quad (6-2)$$

where, for tissue samples:

$$\text{Initial Dilution} = \frac{\text{tissue weight}}{\text{tissue weight} + \text{liquid weight for homogenization tissue}} \quad (6-3)$$

Histopathology

All samples placed in 4% PFA were kept at room temperature overnight. They were then rinsed with PBS three times before being placed in 70% ethanol and stored at 4°C. The samples were submitted for further processing to the ABI Histology Core at the University of Alberta, where they were then dehydrated in alcohol and xylene; oriented and embedded in paraffin; and sectioned (5 µm). For histopathological analysis, sections were stained with hematoxylin and eosin following standard procedures[72]. Representative images were taken of the slides at 100x magnification using an optical microscope with an attached digital camera (Nikon Optiphot I, with Nikon Coolpics 950).

Lipopolysaccharide Titration Study

Animals

10 domestic Sprague-Dawley rats (250 ± 10 g) were used in this study. The animals selected were healthy, with no apparent breathing abnormalities at the start of the experiment. The animals were kept in cages of two at the Nagel Veterinary Clinic (Crossfield, AB), with a 12 hour light/dark cycle, in a room with separate ventilation and controlled temperature. Each cage of animals was a separate experimental group. The animals received antibiotic-free water and rat chow *ad libitum* throughout the experiment. The study was conducted with

humane care of the animals in accordance with guidelines established by the CCAC.

Induction of Inflammation

The rats were placed under isoflurane anesthetic. A microsyringe (IA-1B®) was used to deliver 100 µL of various dilutions of LPS (L8643, Sigma) to the lungs (0.1, 0.2, 0.4, 0.8, and 1.6 mg/mL, 2 rats per dilution). The rats were allowed to recover and returned to their cages. The rats were observed during the remainder of the day, and then examined the following morning. They were then euthanized using a CO₂ chamber, and samples of lung from the left top lung lobe were collected for histopathology and cryopreservation. These were processed as described in the “Anti-inflammatory Activity Study” methods section.

Pseudomonas Aeruginosa Titration Study

Animals

10 domestic Sprague-Dawley rats (250 ± 10 g) were used in this study. The animals selected were healthy, with no apparent breathing abnormalities at the start of the experiment. The animals were kept in cages of two at the Nagel Veterinary Clinic (Crossfield, AB), with a 12 hour light/dark cycle, in a room with separate ventilation and controlled temperature. Each cage of animals was a separate experimental group. The animals received antibiotic-free water and rat chow *ad libitum* throughout the experiment. The study was conducted with humane care of the animals in accordance with guidelines established by the CCAC.

Induction of Infection

3-4 colonies of *Pseudomonas aeruginosa* from a streaked MHA plate were transferred to a flask containing 100 mL of sterile TSB. The bacteria were incubated overnight in a shaker incubator (37°C, 120 rpm). Portions of the inoculum were kept at full strength, diluted 1/10, 1/100, or 1/1000 in PBS. The rats were placed under isoflurane anesthetic. The rats were held vertically by a technician, while a veterinarian used a rat laryngoscope (LS-1®, PennCentury™ Inc.) with a fibre optic light source to locate the vocal cords. A microsyringer (IA-1B®, PennCentury™ Inc., with a 1 mm polycarbonate syringe) was inserted between the cords into the trachea, and used to deliver 100 µL of PBS (two negative controls) or the various bacterial dilutions to the lungs (two rats per dilution). The rats were allowed to recover and returned to their cages. The rats were observed during the remainder of the day, and then examined the following morning. They were then euthanized using isoflurane followed by an injection of Euthanyl into the heart, and samples of lung (upper left lobe) and spleen were placed on ice to be used for bacterial counts.

Bacterial Cell Counts

Tissue samples stored on ice for bacterial counts were weighed and imaged. 1 mL of PBS was added to each sample, and then each sample was homogenized using a Polytron Homogenizer. A ten-fold dilution series was produced by adding 100 µL of the homogenized tissue sample to 900 µL of PBS. This was repeated seven times for lung tissue, and four times for spleen tissue. From each dilution in the series, three 20 µL drops were placed onto PIA plates,

using the drop plate method. Once the drops had absorbed, the plates were incubated at 37°C overnight. The resulting CFUs were recorded and used to calculate the bacterial counts per gram of tissue, according to Equations (6-2) and (6-3).

Antimicrobial Activity Study

Preparation of Tobramycin Solutions

Tobramycin solutions were made to create 1 mg/kg[73] solutions when rats were delivered 100 µL doses. Thus, for rats weighing approximately 240 g, the solutions made were at concentrations of 2.4 mg/mL in 0.9% saline[74]. Tobramycin solutions were stored at 4°C until use.

Preparation of Silver Nitrate Solutions

Silver nitrate solutions were made up in distilled water and delivered at 200 ppm Ag⁺ (0.31 mg/mL AgNO₃), which was chosen to be within the range of total silvers obtained from nanocrystalline silver-derived solutions at the time of the study.

Preparation of Nanocrystalline Silver Solutions

pH 4 carbonated water was prepared as described in Chapter 5 and sealed until use (<1 week). Preliminary studies indicated that pH was maintained for over a week in sealed jars. To start the dissolution, 1 in² of nanocrystalline silver dressing was added per milliliter of water, along with a stir bar. The jar was capped with a lid containing a septum for a sampling port. The lid was sealed using parafilm, and the silver was allowed to dissolve for 24 hours with gentle stirring (~100 rpm) prior to delivering it to rat lungs.

Animals

50 domestic Sprague-Dawley rats (200-250 g) were used in this study. The animals selected were healthy, with no apparent breathing abnormalities at the start of the experiment. The animals were kept in cages of five at the Nagel Veterinary Clinic (Crossfield, AB), with a 12 hour light/dark cycle, in a room with separate ventilation and controlled temperature. They were allowed to acclimatize one day prior to the start of the experiments. Five animals were used in each experimental group, and all animals in one cage belonged to the same group. The animals received antibiotic-free water and rat chow *ad libitum* throughout the experiments. The study was approved by the University of Alberta Research Ethics Office (REO), and was conducted with humane care of the animals in accordance with guidelines established by the CCAC.

Induction of Infection

3-4 colonies of *Pseudomonas aeruginosa* from a streaked MHA plate were transferred to a flask containing 100 mL of sterile TSB. The bacteria were incubated overnight in a shaker incubator (37°C, 120 rpm). The inoculum was diluted 1/30 in PBS, based on the results of the titration study (see results below). The rats were placed under isoflurane anesthetic. A microsyringe (IA-1B®) was used to deliver 100 µL of PBS (10 negative controls) or the diluted bacterial inoculum to the lungs (the remaining 40 rats), as described under “*Pseudomonas Aeruginosa* Titration Study”. The rats were allowed to recover and returned to their cages. Prior to beginning treatment, the microsyringes were rinsed thoroughly with 70% ethanol.

Treatment

Four hours after inoculation with *Pseudomonas aeruginosa*, the rats received their first treatment. The rats were placed under general anesthesia (isoflurane) for treatments. The rats were delivered the treatments via a microsprayer, as above. All treatments were delivered at volumes of 100 μ L. This was done so that, theoretically, the treatments would be delivered to the same location as the original inoculum. The rats were treated in the same order that they were inoculated. The ten negative control rats (inoculated with PBS) were given distilled water, which, based on the results of Chapter 5, is at approximately the same pH as the treatments described below. Of the rats that received live bacteria, ten were given the same treatment as the negative controls. These rats serve as positive controls for the experiment. Another ten were given silver nitrate solutions, made as described above. Ten of the rats received tobramycin solutions, made as described above. The last ten received nanocrystalline silver-derived solutions prepared as described above. Samples of the silver-containing solutions were taken before treatment of the rats and submitted for total silver analysis via AAS, which was performed as described in Chapter 4. The rats were allowed to recover and returned to their cages. Between treatment groups, the microsprayers were rinsed thoroughly with distilled water and 70% ethanol.

After 24 hours, half the rats from each group (five) were euthanized using a CO₂ chamber, and blood samples were immediately taken from the myocardium. The lungs were then removed. Portions of the upper lobe of the

right lung were snap-cooled for RNA and protein analysis. One portion of the upper lobe of the left lung was placed in 4% PFA and kept at room temperature. A second portion of the same lobe was placed on ice for later cryopreservation. The remainder of the lung was placed on ice for bacterial counts.

The remaining five rats from each group received additional treatments, as described above, at 24 and 48 hours. At 72 hours, euthanasia, blood sampling, and lung tissue removal and preservation were performed as described above.

It should be noted that at 24 hours, snap-cooling was done by placing the samples in a deep freeze set for the lowest temperature it could generate, as liquid nitrogen was not delivered on time. This was also done for the nanocrystalline silver-derived solution controls described below. At 72 hours, snap-cooling was done in liquid nitrogen.

Cryopreservation

Tissue samples stored on ice were placed on Disposable Base Molds (Richard-Allen Scientific, Kalamazoo, MI) in a -50°C freezer (24h samples) or liquid nitrogen bath (72h samples), and covered with Cryomatrix. They were then stored at -50°C, transported back to Edmonton on dry ice, and then stored at -80°C.

Bacterial Cell Counts

Tissue samples stored on ice for bacterial counts were weighed and imaged. 1 mL of PBS was added to each sample, and then each sample was homogenized using a Polytron Homogenizer. A ten-fold dilution series was produced by adding 100 µL of the homogenized tissue sample to 900 µL of PBS.

This was repeated four times. From each dilution in the series, three 20 μ L drops were placed onto PIA plates, using the drop plate method. Once the drops had absorbed, the plates were incubated at 37°C overnight. The resulting CFUs were recorded and used to calculate the bacterial counts per gram of tissue. The plates were left at room temperature for an additional day and checked for new growth.

Histopathology

Histopathology was performed as described in “Anti-inflammatory Activity Study”, using hematoxylin and eosin staining of paraffinized tissues.

Real Time RT-PCR

Tissue powdering. To extract RNA, tissues were powdered using a Mikro-Dismembrator, similar to the procedure described in Chapter 2, with minor changes described briefly below. Prior to use, dismembrator chambers and metal balls were soaked in bleach for half an hour, washed, rinsed in distilled water, and then allowed to air dry. As well, some of the samples from 72h were cut in half, and half was refrozen at -80°C. The whole sample was used for 24h samples and about half of the 72h samples processed. The samples were then cut into small pieces with a scalpel, and placed in dismembrator chambers, along with two steel balls, in liquid nitrogen for an additional five minutes. The samples were then powdered in the dismembrator. 1 mL of Trizol was added to the powdered samples and then collected into 1.5 mL tubes.

RNA extraction. RNA extraction and purification was performed using a Qiagen RNeasy® Mini Kit by following the manual provided, as described in Chapter 2. For the samples taken at 24h, the entire milliliter of powdered tissue-

containing Trizol was used. However, for samples at 72h, if the entire sample had been powdered, 200 μL of the powdered tissue-containing Trizol was added to 800 μL Trizol and then processed. If only half the sample had been powdered, then 400 μL of the powdered tissue-containing Trizol was added to 600 μL of Trizol. This was done because after measuring the total RNA levels in the 24h samples, there was concern that the amount of RNA, DNA, and other components in the samples may have overwhelmed the spin columns during the RNA purification process, resulting in a less pure product. The spin columns are only designed to handle 100 μg , whereas the total RNA collected from the 24h samples was as high as 355 μg . As in Chapter 2, the RNA was collected in 40 μL of distilled RNase/DNase free water in the final step of the procedure.

RNA quantification. RNA quantification was performed as described in Chapter 2, with minor changes. Briefly, 4 μL of purified RNA solutions were added to 396 μL of distilled RNase/DNase free water. A spectrophotometer (Unicam, Helios, Thermo Fisher Scientific, Inc.), zeroed using double distilled water, was used to measure optical densities of the RNA-containing samples at 260 nm. The concentration of RNA in each sample was calculated via Equation 2-1 in Chapter 2.

Reverse transcription (creation of cDNA). Reverse transcription was performed by mixing 1 μL of dNTP, 1 μL of random nonamers, 1 μg of RNA as calculated via Equation 2-1, and enough distilled water to bring the volume to 10 μL . The mixture was centrifuged (15 s, 12 000 rpm), and then placed at 70°C for 10 minutes. Next 2 μL of 10x buffer for eAMV-RT, 1 μL of enhanced avian RT,

1 μL of RNase inhibitor, and 6 μL of distilled water were added. The tubes were centrifuged, incubated at 25°C for 15 minutes, and then incubated at 42°C for one hour, followed by 75°C for five minutes. cDNA was diluted by the addition of 100 μL of distilled DNase/RNase free water, and kept on ice until real time RT-PCR was performed.

Primers. Primers were designed using Primer Express® Software for Real-Time PCR Version 3.0 (© 2004, Applied Biosystems), and were synthesized by Operon Biotechnologies, Inc.:

Rat TNF- α forward primer: CTGGCCAATGGCATGGAT

Rat TNF- α reverse primer: GGTACAGCCCATCTGCTGGTA

PCR water was added to the lyophilized primers to create a primer concentration of 100 μM .

Real time RT-PCR. Real time RT-PCR was performed on cDNA samples created as described above. A master mixture was made up for rat HPRT, and 20 μL was placed per well of a 96 well plate (ABI PRISM™), resulting in 12.5 μL of SYBR green master mix (ABI), 0.1 μL of forward primer, 0.1 μL of reverse primer, and 7.3 μL of DNase/RNase free water per well. 5 μL of cDNA was added per well. One well contained DNase/RNase free water as a control for the experiment, rather than cDNA. This procedure was repeated using the TNF- α primers shown above. The wells were sealed and run in an Applied Biosystems 7300 Real Time PCR System using Applied Biosystems Sequence Detection Software Version 1.3.1 with the 7300 System SDS Software RQ Study Application and the SDS Relative Quantification Study Plug In (© 2005 Applied

Biosystems, Ltd., Foster City, CA, USA). The runs were performed using the standard 7300 run mode with the following settings: The volume was set to 25 μL , Stage 1 had one repetition at 50°C for 2 minutes, Stage 2 had one repetition at 95°C for 10 minutes, Stage 3 had 40 repetitions at 95°C for 15 seconds, each followed by a hold at 60°C for 1 minute, when data collection occurred. Analysis of the results was performed in Excel using Equations 2-2 through 2-4, where HPRT was the chosen housekeeping gene.

Nanocrystalline Silver-Derived Solution Controls

Animals. 4 domestic Sprague Dawley rats (200-250 g) were used in this study. The animals selected were healthy, with no apparent breathing abnormalities at the start of the experiment. The animals were kept in a single cage at the Nagel Veterinary Clinic (Crossfield, AB), with a 12 hour light/dark cycle, in a room with separate ventilation and controlled temperature. They were allowed to acclimatize one day prior to the start of the experiments. The animals received antibiotic-free water and rat chow *ad libitum* throughout the experiments. The study was conducted with humane care of the animals in accordance with guidelines established by the CCAC. The animals were not exposed to bacteria.

Treatment. The rats were placed under general anesthesia (isoflurane) for treatment. The rats were delivered 100 μL treatments via a microsprayer, as above. Two of the rats received nanocrystalline silver-derived solutions prepared as described above, with the samples taken from the top of the jar. Two of the rats received nanocrystalline silver-derived solutions prepared as described above,

with the samples taken from the bottom of the jar. One rat received nanocrystalline silver-derived solution prepared as described above, with the sample taken from the top of the jar and diluted 1:2. The rats were allowed to recover and returned to their cages. Between treatments, the microsprayers were rinsed thoroughly with distilled water.

After 24 hours, the rats were euthanized using a CO₂ chamber, and blood samples were taken from the myocardium. The lungs were then removed. Portions of the upper lobe of the right lung were snap-cooled for RNA and protein analysis. One portion of the upper lobe of the left lung was placed in 4% PFA and kept at room temperature. A second portion of the same lobe was placed on ice for later cryopreservation.

Cryopreservation. Cryopreservation was performed as described in “Antimicrobial Activity Study”.

Histopathology. Histopathology was performed as described in “Anti-inflammatory Activity Study”, using hematoxylin and eosin staining of paraffinized tissues.

Confirming Solution Properties

Bacteriostatic Activity, Silver Content, and Wettability. 3 colonies of *P. aeruginosa* were added to 100 mL TSB and incubated overnight at 37°C and 120 rpm. 1 mL of this overnight culture was transferred to a fresh flask of TSB and incubated for 3.5 hours. 100 µL drops were spread on PIA plates.

Nanocrystalline silver solutions generated as described above were sprayed onto the plates using both of the two IA-1B® microsprayers for the freshly stirred

solutions, filtered solutions, and solutions that had been allowed to settle (sampled from the top, sampled from the bottom, and sampled from the top followed by a 1:2 dilution in distilled water). Spraying was performed from a consistent height and with as consistent strength as possible, although information from the manufacturer and experiences from characterizing the microsprayer-generated particle size indicate that a variety of strengths will produce the same droplet size and distribution due to the design of the microsprayer. Silver solutions and bacteria were both dropped and sprayed onto glass and Vaseline® (Safeway™, Edmonton, AB, CA)-coated glass to compare their wettability. Samples of the solutions freshly stirred, filtered, and allowed to settle were submitted for atomic absorption spectroscopy, which was performed as described in Chapter 4.

Characterization of Microsprayer Particle Size. Particle sizes generated by an IA-1B microsprayer using a full strength solution of *P. aeruginosa* (heat-killed for >3 hours in a 60°C waterbath) and a full strength nanocrystalline silver-derived solution (generated with a starting pH of 4, 1:1 in² Ag/mL, stirred, allowed to dissolve for 24 hours) were measured using a Malvern SprayTec (Malvern Instruments Ltd., Worcestershire, UK).

Statistical Analysis

Tests were performed on tissues from all rats from each group to confirm result repeatability. For numerical results, one-way ANOVAs with Tukey-Kramer Multiple Comparisons post tests were performed using GraphPad InStat version 3.06[75]. Standard deviations are plotted as error bars for all data points on applicable figures.

Results and Discussion (By Study)

Anti-inflammatory Activity Study

Visual observations. One positive control (originally designated P2) died during the instillation of LPS, and was replaced with a spare rat (designated P6). P2 appeared to have choked – it may have choked on saliva in combination with the microsyringe being held in its throat for a longer-than-desirable time in an attempt to be sure that the microsyringe was placed correctly. One rat designated A3, which had received LPS but had not started treatment, appeared morbid at the time of being returned to the housing room. It never recovered from the anesthesia, as it had not moved and was dead at the time that treatments were started. The rat designated P3, which had received LPS but had not started treatment, was also found dead at the time that treatment was started – it also had not recovered from the anesthetic. These rats may also have choked, suffered from anesthetic stress, or suffered from shock due to the injection of LPS into the lungs. The rat designated P5 died during the treatment procedure. It was a positive control – it had received an injection of LPS and was receiving an injection of distilled water. It is believed that this death was the result of combined LPS stress and anesthetic stress from receiving the two doses of strong injectable anesthetic in a single day, and so the animals receiving treatments after this animal received a 30% decreased dose of anesthetic. All remaining rats survived the treatment procedure and were alive the next morning. Negative controls appeared healthy. Positive controls were unresponsive, had rapid

breathing and ruffled fur, and tended to sit hunched up or hiding in their tubes. Nanocrystalline silver-treated animals were less responsive than negative controls, but were more active and less sick looking than positive controls. They also resisted receiving anesthetic much more strongly than the positive controls. This responsiveness suggested a qualitative improvement in their health relative to positive controls.

Total Silver. Atomic absorption spectroscopy indicated that samples of the nanocrystalline silver-derived solutions taken before the rats were treated contained 0.063 ± 0.002 g/L, while samples taken at the end of the treatment procedure contained 0.076 ± 0.001 g/L, which was significantly higher ($p=0.0029$). This may be due to continued release of silver from the dressing during the length of time required to treat all rats in the group, combined with the decreased volume of solution. This suggests that the first rats treated may have received significantly lower silver than the latter rats, with a range of as much as 6.1 to 7.7 μg per rat.

Digital Images. Representative images of lungs from the three groups of animals are shown in Figure 6-1. The lungs of negative controls (a) appeared normal. The lungs of positive controls were very dark, showing signs of hemorrhage (b). The lungs were also very wet, suggesting excessive edema. The lungs of animals treated with nanocrystalline silver-derived solutions showed dark areas, particularly towards the top of the lungs, but other areas of the lungs appeared normal in color (c). The appearance of the lungs suggested an

improvement over positive controls with nanocrystalline-silver derived treatments.

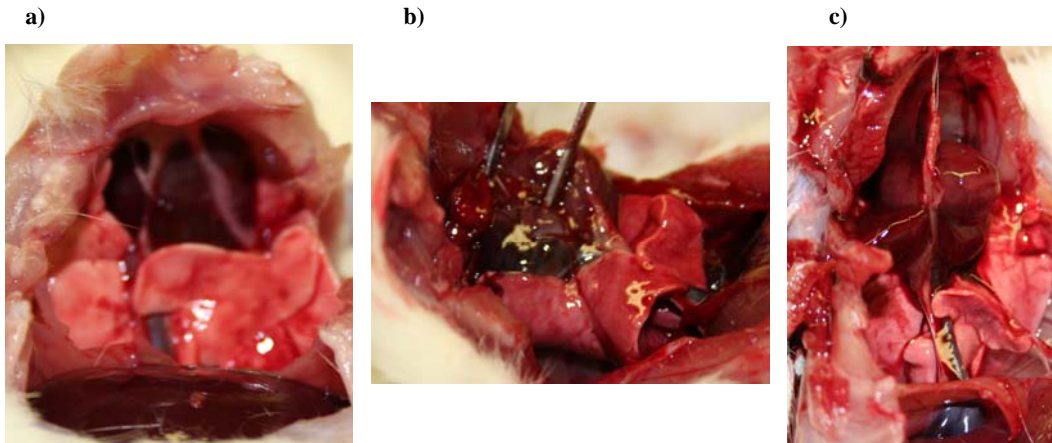


Figure 6-1. Images of lungs in the lung cavities of rats after euthanasia at the end of the anti-inflammatory activity study (24 hours). A representative image of a negative control, which had PBS instilled in the lungs, and then was treated by the same method with distilled water four hours later, are shown in a). Positive controls, which were challenged with lipopolysaccharide (LPS) and then treated with distilled water four hours later, are shown in b) (side view). Animals challenged with LPS and then treated with a nanocrystalline silver-derived solution (starting pH 4, dissolution time 24 hour without stirring, $5\text{in}^2/\text{mL}$) four hours later, are shown in c).

Histology. Figure 6-2 shows the lung histology of each rat which survived to the end of the experiment. Panel (a) shows the histology of the negative controls. While some animals appeared to have normal lung histology, others, particularly animals 4 and 5, showed signs of congestion and cellular infiltration. Panel (b) shows the histology of the positive controls. All animals showed signs of inflammation, which appeared to be fairly consistent between animals, but were not stronger than those observed in animals 4 and 5 of the negative controls. The histology of animals from the experimental group treated with the nanocrystalline silver-derived solution is shown in panel (c). Rats 1 and 2 showed histological improvements relative to positive controls, while Rats 4 and 5 did

not. This is interesting, considering Rats 1 and 2 may have received less total silver than Rats 4 and 5. However, the lung histology of all the animals in this group was within the range of histological results observed in the negative controls, and therefore no definite conclusions could be made.

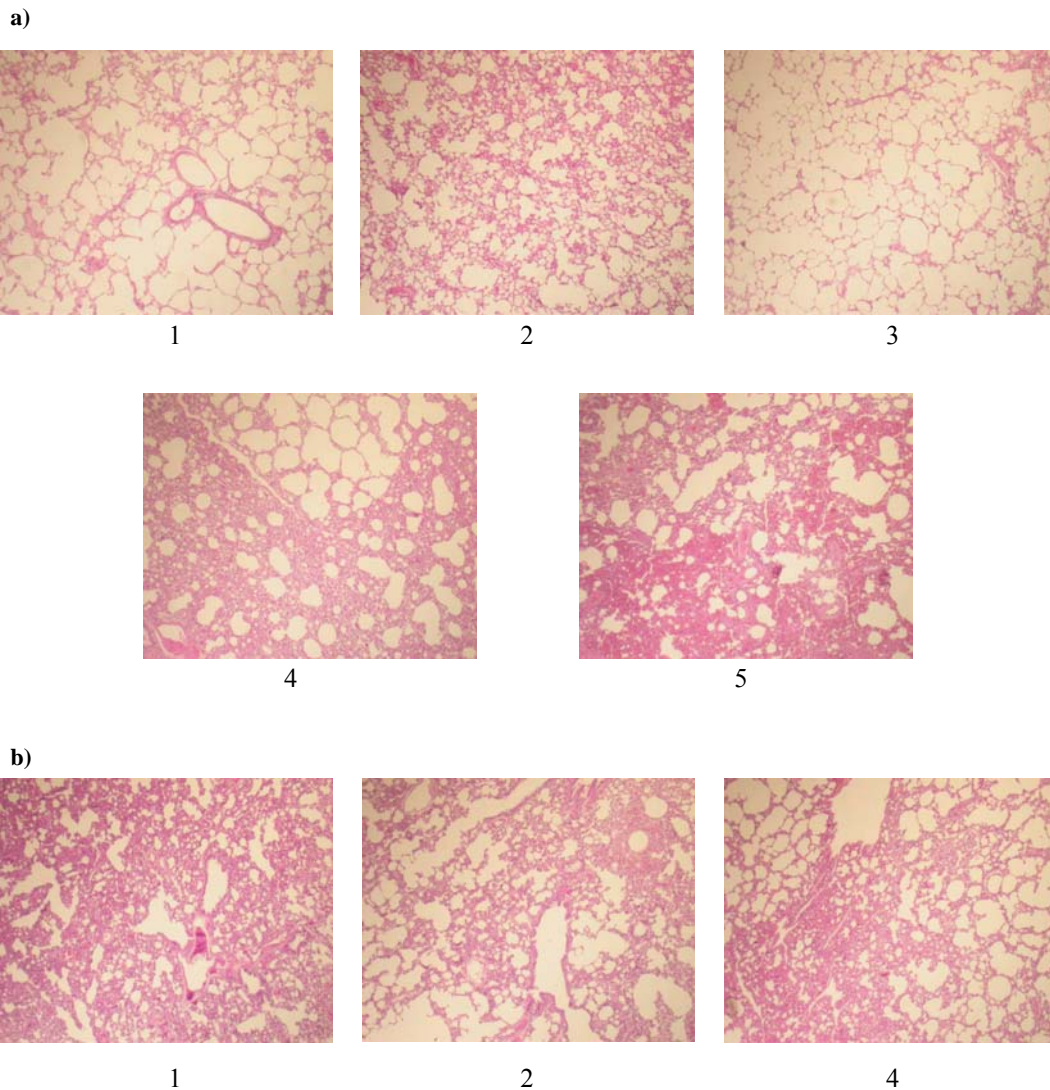


Figure 6-2.

c)

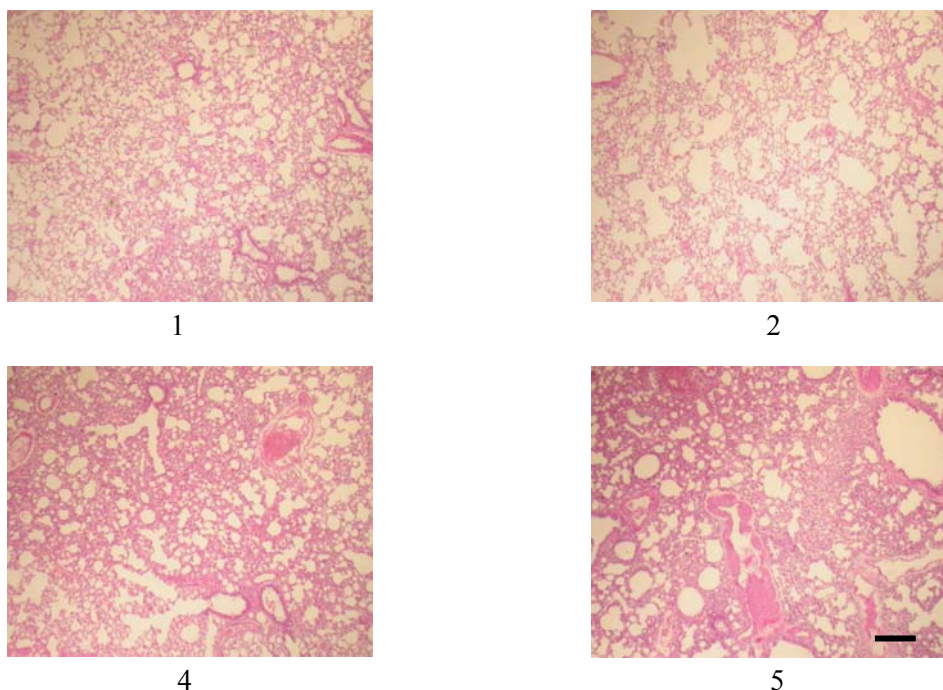


Figure 6-2, continued. Representative histological images of the lungs of each rat 24 hours after treatment in the anti-inflammatory activity study. Each individual animal is identified by a number. Panel a) shows the negative controls, which were challenged with PBS and treated with distilled water four hours later. Panel b) shows the positive controls, which were challenged with lipopolysaccharide (LPS), and treated with distilled water four hours later. Panel c) shows the experimental group, which was challenged with LPS, and treated with a nanocrystalline silver-derived solution (starting pH 4, dissolution time 24 hours without stirring, 5 in²/mL) four hours later. The scale bar in the image of animal 5 of panel (c) is 50 μ m.

Discussion. In examining the methods and results of this experiment, there were a variety of problems associated with this experiment, any of which could have led to the death of animals observed, as well as the variability in results. Animals which died during the initial instillation of LPS may have choked[45]. This possibly resulted from the poor working conditions required by the HSLAS SOP. The microsprayer is designed for vertical delivery, and in preliminary work (practice runs with one or two animals), the rats were suspended by their teeth by an elastic using equipment similar to that shown in Figure 6-3.

However, the apparatus in Figure 6-3 did not fit into the fumehood that HSLAS required the work to be done in, and so the rats had to be placed on their stomachs and their heads were suspended via an elastic across their incisors a few centimeters off of the fumehood benchtop. This resulted in much poorer visualization, which led to much longer times required to intubate the rats and instill the liquids into the animals, which could have resulted in their choking on the tube or their own saliva. To alleviate this possibility, a change of location and setup was required. Approval was received to perform all subsequent experiments at the Nagel Veterinary Clinic (Crossfields, AB), where working in a fumehood was not required, and therefore the whole process could be performed much more quickly.

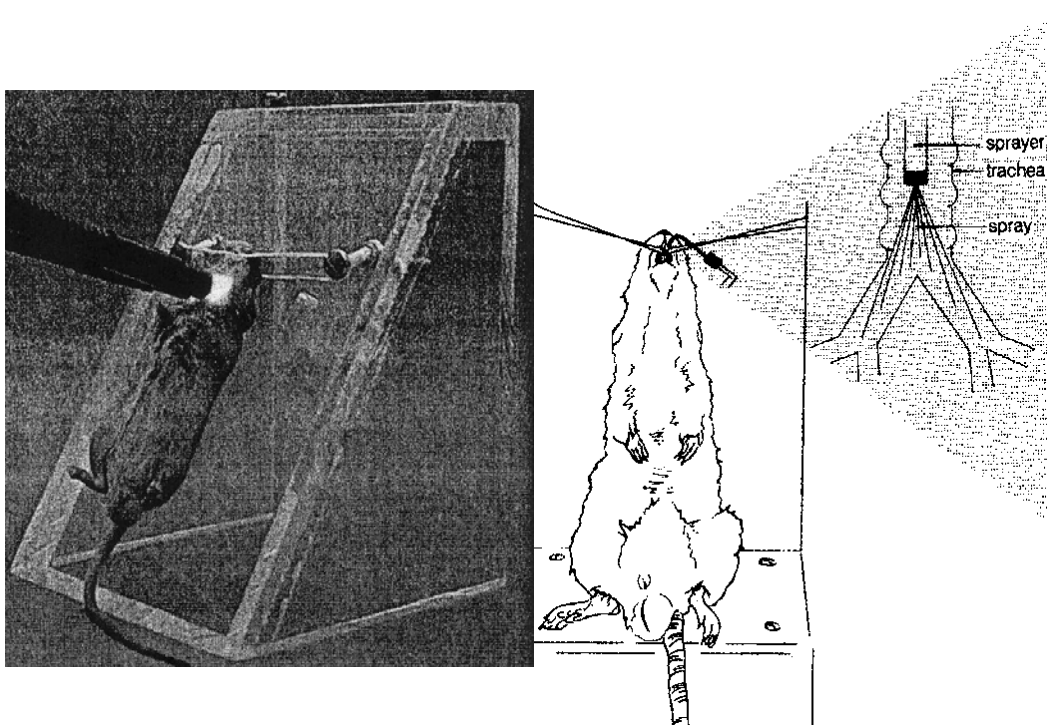


Figure 6-3. Images from the literature [48, 49] demonstrating the techniques for visualizing the trachea and using microsprayers in rats. Rats are suspended by their incisors and their throats are illuminated to help locate the trachea. The microsprayer is inserted into the trachea until it reaches just above the first bifurcation, where the contents of the sprayer are then sprayed into the lungs.

Another possible cause of death for animals which died during the initial instillation of LPS, or before the initiation of treatment, was LPS-induced shock.

This suggested three possible explanations:

- 1) Pre-experimental exposure of the rats to LPS.
- 2) Contamination of the LPS with other materials which caused the rats to go into shock.
- 3) Excessively high dosing of LPS, resulting in shock and ARDS/ALI-like symptoms.

The first possibility appeared unlikely, as there were no bacteria detected in any of the animals within the limit of detection for the experiment (see Table 6-2, and note that standard deviations result only from variations in tissue mass used). However, for future experiments, a different source of rats was used, and none of the rats went into shock during or after LPS delivery (see LPS Titration Study results below).

Table 6-2. Bacterial Counts from Lungs of Acute Inflammation Study at 24 hours.

Group	n	Average Number of Bacteria (Log)	Standard Deviation
Negative Controls	3	<2.68	0.139
Positive Controls	3	<2.55	0.061
Nanocrystalline Ag	4	<2.52	0.107

Note: There were no bacteria present in the -1 dilution for any animal. The log number of bacteria was therefore always less than the detection limit, and variation in the detection limit and standard deviation are the result of varied tissue mass used for the calculations. There were no significant differences in the log number of bacteria (i.e. the detection limit) for the different groups (p=0.2011).

To examine the possibility of contamination, research into the LPS source was performed. It was discovered that the LPS used in this experiment (L9143, Sigma), which was purified by phenol extraction, contained up to 60% RNA (personal communication with Audrey Fleming, Sigma-Aldrich Technical Service representative, December 17, 2007), and had 0.83% protein (specification for lot used). An attempt was made to purify LPS from *Pseudomonas aeruginosa* (ATCC 27317) in the lab following techniques from the literature[76, 77] and procedures provided by Nick Allan (personal communications, September 20–December 13, 2007, see Appendix 2). However, this was halted due to safety issues. Based on a recommendation from Sigma-Aldrich (personal communication with Audrey Fleming, Sigma-Aldrich Technical Service representative, December 17, 2007), LPS purified by gel filtration chromatography (L8643) was purchased for subsequent experiments. It contained less than 20% RNA (personal communication with Audrey Fleming, Sigma-Aldrich Technical Service representative, December 17, 2007) and 0.6% protein (specification for lot used).

To eliminate the third possibility, an LPS titration study was performed (see below).

Another possible cause of animal death during either the initial instillation or the subsequent treatments was anesthetic stress, due to the heavy dose of ketamine and acepromazine required to sedate the animals sufficiently that they would not resist the intubation. This was particularly a problem when the animals were on their stomachs – in this position, they retained a reflex by which they

pushed with their front feet, changing the position of their heads, when the tube was inserted into their mouths. In fact, the trauma to the larynx caused by multiple insertions of the microsyringe resulting from the animals pulling away when it was inserted may have been another cause of shock and death (personal communication, Michael Moxley, March 5, 2008). A fairly deep plane of anesthesia was required to overcome this reflex. This would not have been required when the animals were suspended vertically, since they then had nothing to push against with their front feet, and in fact they did not appear to have the pushing reflex when in that position - they did not move during intubation. Thus, vertical suspension of the animals, allowed for by the working conditions provided by Nagel Veterinary Clinic, lessened the plane of anesthesia required for intubation. In addition, at Nagel Veterinary Clinic, isoflurane was provided rather than injectable anesthetics. The use of isoflurane was not allowed in the room provided by HSLAS, but in any case it would not have been feasible under the conditions required by HSLAS, because the timeframe in which a rat can be intubated after removal from the isoflurane is very short, and it would not have been possible to visualize the trachea quickly enough when working in the fumehood. Working on an open bench at Nagel Veterinary Clinic, which allowed for the use of isoflurane, greatly reduced the anesthetic stress placed on the animals, as the animals woke up immediately after intubation with no apparent side effects.

Another possible cause of animal death during the experiment may have been uneven distribution of the LPS, as suggested by the histology. Uneven

distribution may have led to very strong inflammation in some areas of the lung, particularly at the top of the lungs, which may have cut off major air passages, even though other areas of the lung may not have been significantly inflamed. Even some negative controls showed signs of inflammation, which may have been related to uneven distribution of the solutions into the lungs. One possible cause of uneven distribution was the position of the animals. In order to facilitate working in the fumehood, animals were placed on their stomachs for intubation and instillation of the treatment or control fluids. However, the microsprayers were intended for instillation while the animal is positioned vertically. Thus, the effect of gravity and the position of the animal may have influenced the distribution of the fluids within the lungs. It is also possible that the microsprayer tip was not inserted far enough into the trachea, again due to working conditions – instillation was designed to occur with the tip placed at the bifurcation of the trachea, but if the tip of the microsprayer was located above the bifurcation, then the fluids would likely not be distributed as deeply into the lungs. The transfer of the study to Nagel Veterinary Clinic eliminated these possibilities because the animals could be positioned vertically, allowing intubation and instillation of the fluids into the rats' lungs to be performed much more easily. Another possible reason for the uneven distribution of the fluids was that the microsprayer itself might not produce droplets at a correct size and velocity to penetrate portions of the lungs easily. This was considered unlikely at the time of planning the following experiments, as numerous articles, as well as the manufacturers, claimed that the microsprayer produced consistent, even, deep distribution of fluid

throughout the lungs[45, 48, 53-55, 61, 65, 78]. Other than uneven distribution, inflammation in the negative controls could have been due to exposure to LPS during the treatment. Although the negative controls had the sham challenge before the positive controls and experimental group received the LPS challenge, the negative controls were treated using the same microsyringe that was used to deliver the LPS challenges. The microsyringe was cleaned between uses, but other researchers use separate microsyringes for the controls and LPS instillations, and have indicated that in order to eliminate LPS from the microsyringes, the microsyringes should be treated with dry heat at greater than 200°C for at least 40 minutes (personal communication, Dr. Michael Moxley, March 10, 2008), which was not known at the time that this study was conducted, and therefore was not performed between the challenges and the treatments. One final possible explanation for the histological variation observed within a given group was that if the Euthanyl used to euthanize the animals was accidentally injected into the lungs instead of the heart, the lung histology would be dramatically changed due to hemorrhage. To eliminate this possible source of variability, at the Nagel Veterinary Clinic, the animals were euthanized using CO₂ (with the exception of the *Pseudomonas aeruginosa* Titration Study, for which histology was not performed), which, again, was not a possibility in the room provided at HSLAS, as there was no CO₂ machine available, and the animals were not allowed to leave the fumehood except when they were placed in their HEPA-filtered cages sealed in autoclave bags.

Lipopolysaccharide Titration Study

Visual Observations. During the lipopolysaccharide titration study, no rats showed any immediate response to the LPS instillation, despite the fact that at least some rats from the rat source used by Nagel Veterinary Clinic had previous exposure to bacteria (see negative controls from the Infection Studies below). This indicates that with highly purified LPS, the rats did not go into shock during instillation, and therefore the response observed in the *Anti-inflammatory Activity Study* must either have been due to impurities in the LPS used, choking, or anesthetic shock, rather than an excessively high dose of LPS. 24 hours after LPS instillation, all the rats were still alive, appeared healthy, and were behaving normally.

Histology. Histological images showing the range of inflammation present in each animal in each group are shown in Figure 6-4. Panel (a) shows the histology of lungs of rats receiving 0.1 mg/kg LPS. The first rat showed a range of inflammation, while the second rat showed fairly consistent strong inflammation in the lobe tested, with edema and a massive influx of inflammatory cells, resulting in near-obliteration of the normal alveolar structure. Panel (b) shows the histology of the lungs of rats receiving 0.2 mg/kg LPS. The first rat showed consistent strong inflammation as described above, while the second rat showed some variation across the lobe examined. Panel (c) shows the histology of lungs of rats receiving 0.4 mg/kg LPS. Again, the first rat showed fairly consistent strong inflammation, while the second rat showed some variability in inflammation across the lobe examined. Panels (d) and (e) show the histology of

rats treated with 0.8 and 1.6 mg/kg LPS, respectively. Both rats in each of these groups demonstrated a consistent strong inflammatory response, despite their healthy appearance.

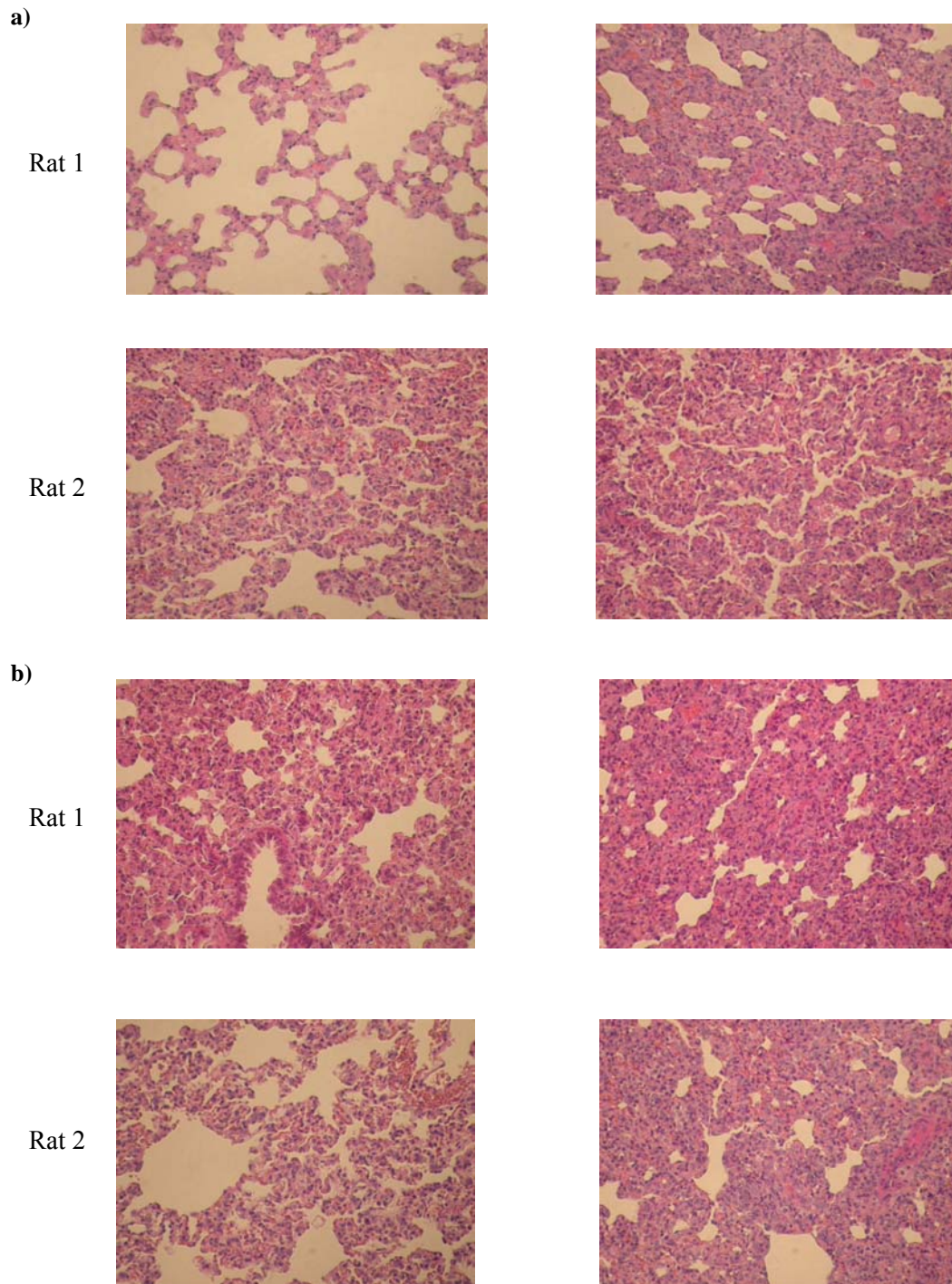
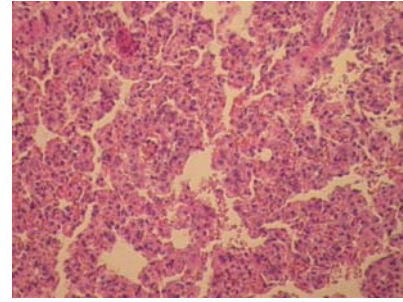
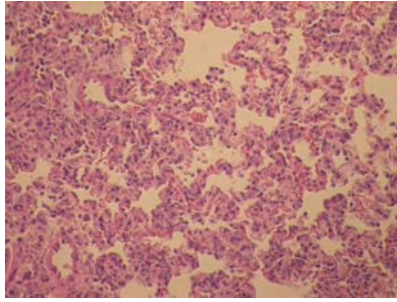


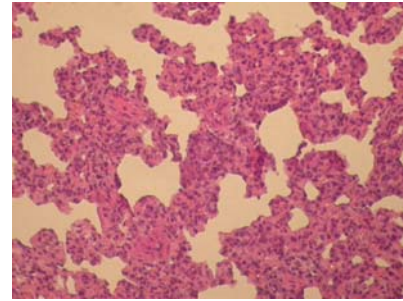
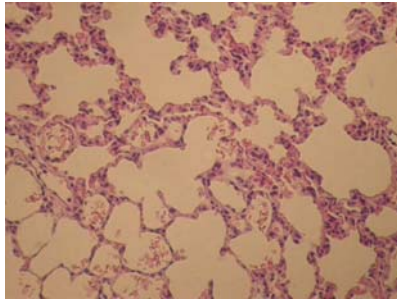
Figure 6-4.

c)

Rat 1

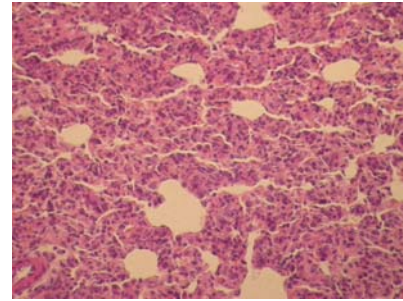
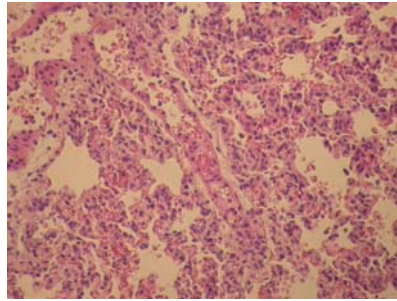


Rat 2



d)

Rat 1



Rat 2

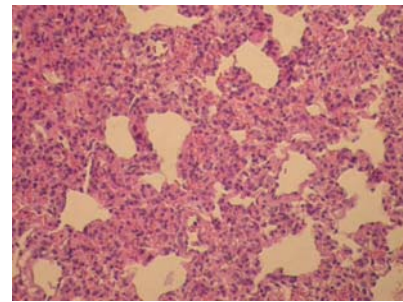
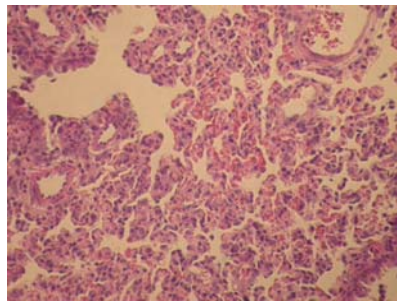


Figure 6-4, continued.

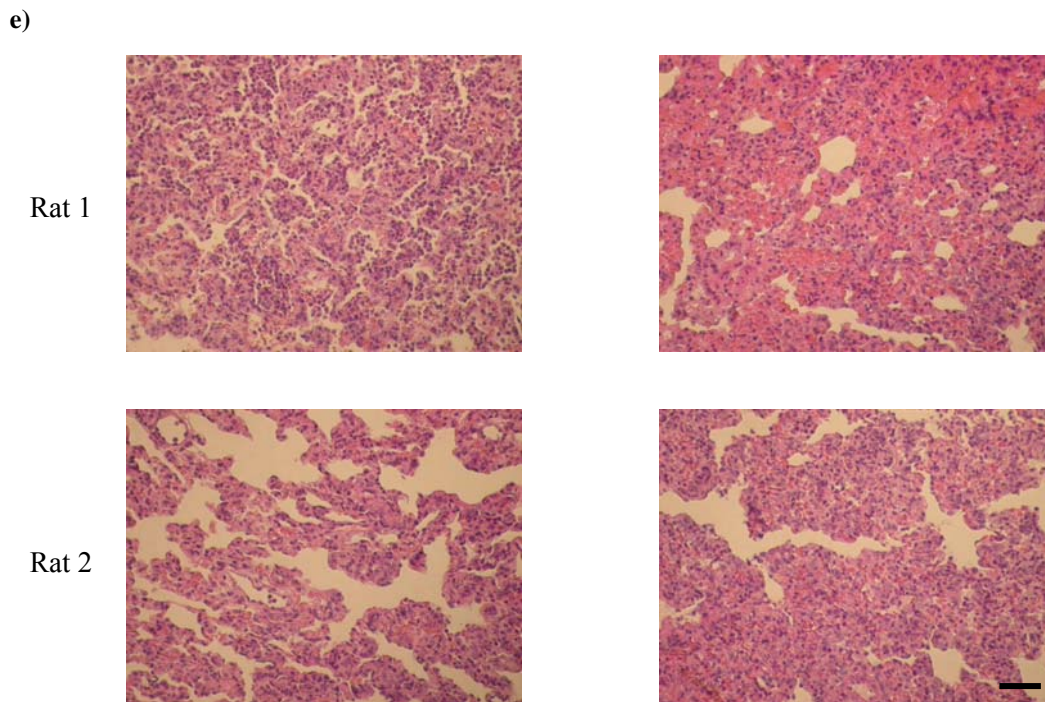


Figure 6-4, continued. Histological images showing the range of inflammation present in the upper left lung lobe of each rat used in the lipopolysaccharide (LPS) titration study. Animals were exposed to 0.1 (a), 0.2 (b), 0.4 (c), 0.8 (d), or 1.6 (e) mg/kg LPS, and then euthanized 24 hours later. Each individual animal is indicated by its assigned number. The scale bar in rat 2 of panel (e) represents 50 μm .

Discussion. This indicates that the dose selected for the Anti-inflammatory Activity Study was not too high, and in fact going to a higher dose such as 0.8 or 1.6 mg/kg could result in more consistent inflammation, without risking the overall health of the animals. The dose of 0.4 mg/kg used in the Anti-inflammatory Activity Study was selected based on literature values. There is a range of LPS doses used in rats in the literature in conjunction with the use of the microsyringe, with three apparent subgroups depending on the goal of the study. Lu *et al.*[34] used 40 mg/kg to generate ARDs in the animals, and in this study 5 of 30 animals died within three hours of instillation. They commented that even at this high dose, the LPS injury model appeared inconsistent, with some rats

showing minimal lung dysfunction, while other animals showed rapid deterioration. Van Rozendaal *et al.*[79] found that 16 mg/kg was sufficient to generate ARDS-like symptoms. This dose was also used by Vreugdenhil *et al.*[80] Moxley *et al.*[81] used 15 mg/kg LPS to mimic ALI. Diemel *et al.*[53] delivered an even smaller dose of 12 mg/kg LPS, generating severe ARDS-like symptoms. Wheeldon *et al.*[48] reported that a dose of 7 mg/kg created a model of ARDS in the rat as well, with decreased lung compliance, and increased pulmonary edema, capillary damage, and leukocyte infiltration. Perng *et al.*[82] used a smaller double dose, where they initially sprayed 2.5 - 2.86 mg/kg, and then provided a second spray 30 minute later, for a total of 5 – 5.72 mg/kg, to generate ALI. In this study, no animals died within the first five hours after instillation, but 11 out of 21 animals died between that time point and Day 5. This range of LPS doses (5 mg/kg – 40 mg/kg) was too high for the scope of this study. This study was designed to induce acute inflammation, but not ARDS or ALI symptoms, and the study was not intended to have animal mortality as an endpoint. Intermediate responses were observed by Lopez *et al.*[83], who used 2.3-5.5 mg/kg LPS, where severe inflammation was observed, which lasted up to seven days but which did not necessarily lead to lung consolidation. This study, however, used intratracheal instillation rather than a microsprayer, unlike the rest of the studies mentioned here. On the other end of the scale, a study by Garcia-Contreras *et al.*[84] used approximately 0.03 µg/kg LPS in a study where the LPS served as a positive control to measure the effect of instilling various substances into the lungs. Hataishi *et al.*[85] used 0.04 – 0.05 mg/kg LPS, and found that the

peak effect occurred at six hours, tapering off by 18 hours after instillation. This range of doses did not appear to induce sufficient inflammation for the current study, as the lungs of positive controls needed to remain inflamed for 72h for this study. Coote *et al.*^[36] selected an LPS dose of 0.5 mg/kg, based on dose-response experiments with the development of a goblet cell metaplasia as the primary read-out. This dose did not result in an ARDS-like condition in the animals.

Furthermore, Spond *et al.*[86] tested doses of 0.04-0.5 mg/kg LPS, and found that the inflammatory response peaked between 8 and 16 hours, and continued out to 48 hours. This was closer to the inflammatory timeline needed for this study, and thus, a dose at the higher end of this range was selected for the Anti-inflammatory Activity Study. In addition, studies have indicated that LPS from *P. aeruginosa* can cause a stronger inflammation relative to other forms of LPS (of which *Escherichia coli* and *Salmonella enteritidis* are the most common and were used in the majority of the above studies), with a later peak in inflammation (closer to 48 hours) and an extended time of inflammation (out to 72 hours) [87], which would be preferable for the current study. It appears, based on the literature values and the results of the LPS titration study, that for future studies it would be possible to increase the LPS dose somewhat, perhaps as high as 1.6 mg/kg, but that it should stay well below 5 mg/kg in order to avoid ARDS/ALI type symptoms and subsequent mortality of the animals.

Pseudomonas Aeruginosa Titration Study

A titration study was performed in order to determine the correct dose of *P. aeruginosa* to deliver to the rats in the “Antimicrobial Activity Study”. The

goal was to select a dose that produced strong inflammation in the animals, but did not result in mortality of the animals during the timeframe of the experiment. Animals were given PBS, full strength bacteria (after overnight grow-up), or dilutions of 1:10, 1:100, and 1:1000 bacteria in PBS (n=2 for each group).

Visual Observations. The animals were examined over the course of the day and on the following morning. One animal receiving the full concentration of *P. aeruginosa* died during the night, and it appeared to have blood and mucus around its nose. The other rat in this group was still alive at 24 hours, but had porphyrin staining around its eyes, blood around its nose, ruffled fur, and heavy breathing. The rats receiving the 1:10 dilution of *P. aeruginosa* did not show the curiosity typical of rats, and had ruffled fur. The rats that received the 1:100 dose of *P. aeruginosa* also did not demonstrate much curiosity, and had somewhat ruffled fur, but showed some normal rat behavior, such as washing. The rats receiving a 1:1000 dilution of the bacteria or PBS were curious and active, with little sign of distress.

Digital Images. Figure 6-5 shows images of the lung lobes used for bacterial counts after instillation with 100 μ L of PBS (a), full strength bacteria (grown up overnight) (b), or bacteria diluted in PBS 1:1000 (c), 1:100 (d), or 1:10 (e). The lungs of animals receiving full doses or 1:10 dilutions of bacteria appeared very similar, with extensive pathology, including dark red hemorrhaging throughout all lobes. It was the impression of the veterinarian that the animals receiving the 1:10 dilution of the bacteria would not have survived out to 48 hours (personal communication, Annabelle Densen, January 18, 2008). The animals

which received the 1:100 dilution of *P. aeruginosa* had less extensive pathology, with some healthy tissue present at the lung peripheries, while the animals treated with a 1:1000 dilution of bacteria or with PBS showed similar patterns in the lungs, which the veterinarian suggested reflected fluid clearance with minimal pathology.

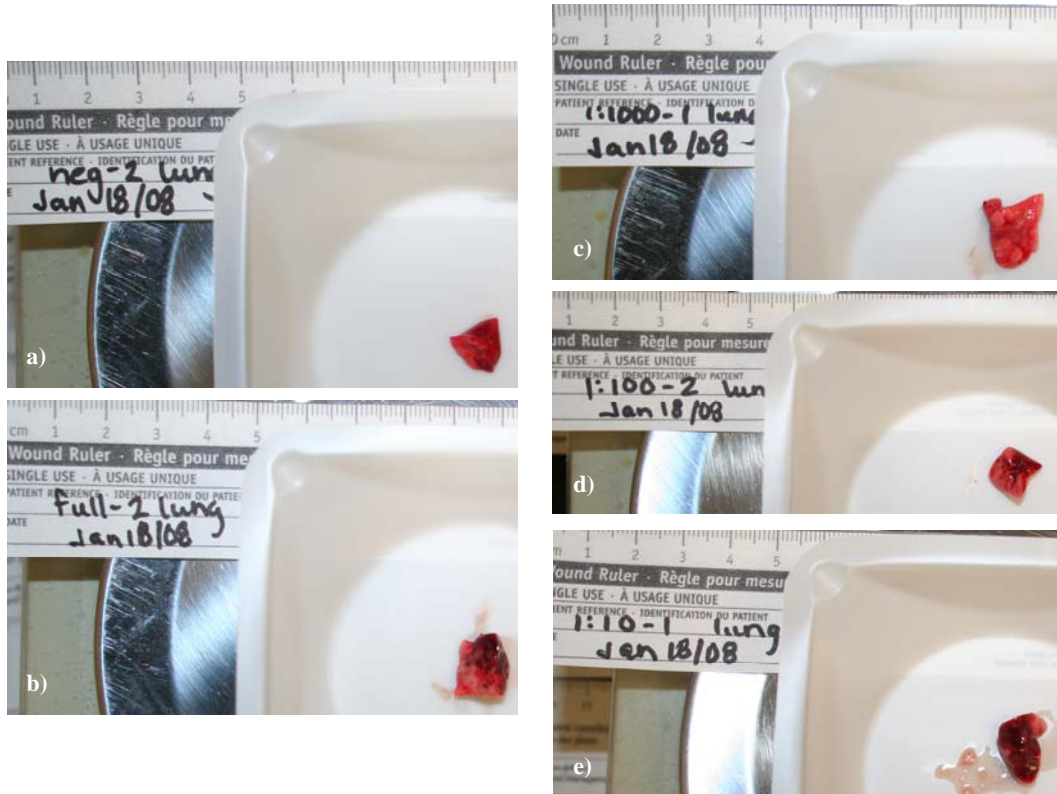


Figure 6-5. Representative digital images showing the upper left lung lobe of rats used in the *Pseudomonas aeruginosa* titration study. Animals were exposed to PBS (a), full strength *P. aeruginosa* (incubated at 37°C overnight) (b), 1:1000 (c), 1:100 (d), or 1:10 (e) dilutions of the original inoculum, and then euthanized 24 hours later.

Bacterial Counts. The results of the bacterial counts in the spleens and lungs of the animals used in the *P. aeruginosa* titration study are shown in Table 6-3. Animals receiving full strength inoculum had significantly higher bacteria counts in the lungs relative to all other groups ($p < 0.001$). Animals receiving 1:10

dilutions of *P. aeruginosa* had significantly higher bacteria counts in the lungs than the remaining groups ($p < 0.01$). There were no significant differences in the bacterial counts present in the spleens of the animals. Animals treated with bacteria diluted 1:100 or 1:1000 had completely cleared the bacteria, within the detection limits of the experiment, within 24 hours. Thus, for the Antimicrobial Activity Study, a bacterial dilution was needed that was between 1:100 (in which all the bacteria were cleared in 24 hours) and 1:10 (in which the animals would not have survived out to 48 hours). Thus, a dilution of 1:30 was selected for the Antimicrobial Activity Study, as this would be approximately half way between the 1:10 and 1:100 on a log scale.

Table 6-3. Bacterial counts for *P. aeruginosa* titration study.

Inoculation Group	Lung (log cells/g)	Spleen (log cells/g)
Full strength	7.2 ± 0.06	3.4 ± 0.52
1:10	3.8 ± 0.17	2.8 ± 0.04
1:100	$<2.8 \pm 0.03$	$<2.8 \pm 0.09$
1:1000	$<2.8 \pm 0.04$	$<2.8 \pm 0.00$
PBS	$<2.8 \pm 0.14$	$<2.9 \pm 0.13$

Note: < indicates that there were no bacteria detected within the detection limit. Variations in such groups were due to the quantity of tissue used for the analysis.

Antimicrobial Activity Study

P. aeruginosa dose. The dose of *Pseudomonas aeruginosa* delivered to the animals was determined to be $10^{7.3 \pm 0.07}$ CFUs, by drop plating a dilution series from the original inoculum.

Visual Observations up to 24 Hours. All rats recovered quickly from instillation of the inoculum and were returned to their cages. Some rats huddled together thereafter, but no other negative consequences were observed. On Day

0, no negative responses were observed with treatment of the negative controls, positive controls, or tobramycin treated animals. One animal receiving silver nitrate died shortly after receiving treatment. The first four rats receiving the nanocrystalline silver-derived solutions were treated with the freshly stirred solution. Three out of four of these rats had severe respiratory distress or arrest. They stopped breathing completely immediately after treatment, although their hearts were still beating. One of them died, but the other two were recovered using cardiopulmonary resuscitation (CPR). It was suggested that silver particles were blocking airways, and therefore the solution was allowed to settle for about half an hour, and sampling was taken from near the top of the solution for the remaining six animals. Although these animals continued to show respiratory distress, none of them required CPR. After 24 hours, one of the positive controls was found dead, but all other animals had survived the night. Visual observation of the rats prior to beginning any procedures indicated that the tobramycin treated rats appeared as active and healthy as negative controls. Positive controls appeared unhealthy, demonstrating huddling behaviors, ruffled fur, and shallow breathing. Silver nitrate and nanocrystalline-silver derived solution treatment groups had similar appearances to the positive controls.

Digital Images at 24 Hours. Figure 6-6 shows images of lung lobes taken 24 hours after the first treatment. Negative controls (a), tobramycin treated animals (c), and nanocrystalline silver-derived solution treated animals (e), all showed patches of normal lung tissue, while other areas showing signs of inflammation with edema, and dark red hemorrhage. Positive controls (b) and

silver nitrate treated animals (d) had virtually no patches of lung that looked normal, and demonstrated extensive pathology with dark red hemorrhaging.

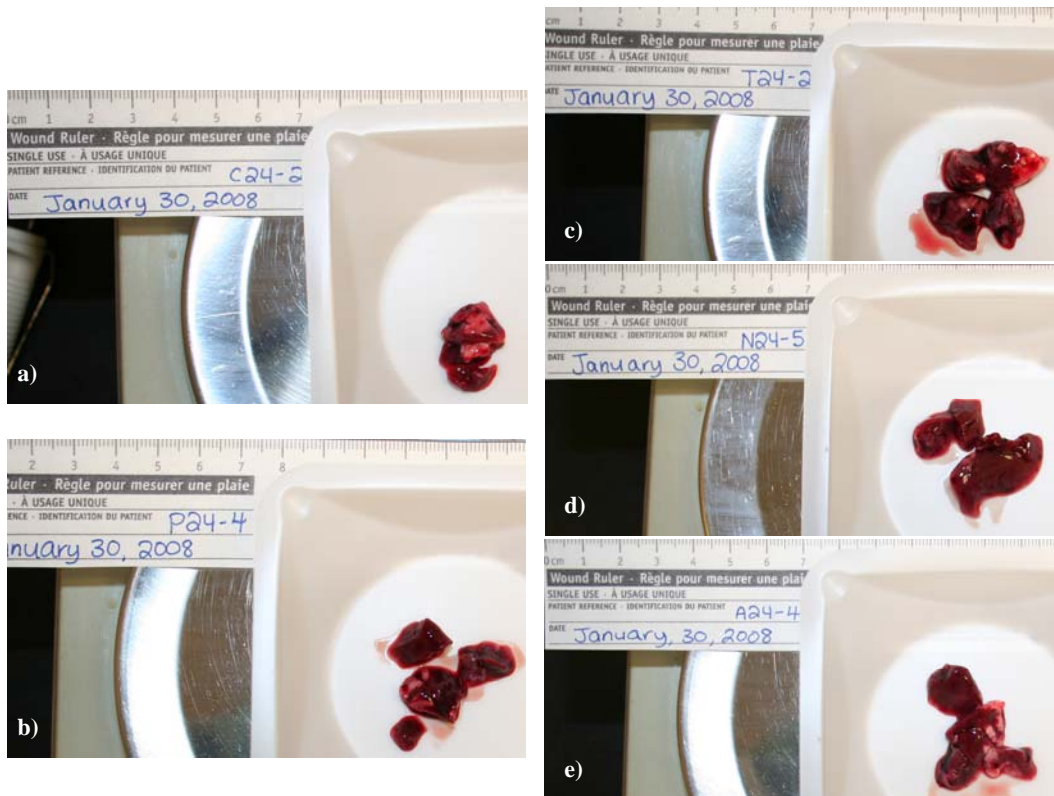


Figure 6-6. Representative digital images showing the portions of lung lobes of rats used for bacterial counts in the antimicrobial activity study 24 hours after inoculation of a 1:30 dilution of *Pseudomonas aeruginosa* incubated at 37°C overnight, followed four hours later by various treatments (n=5 for each group). Negative controls were inoculated with 100 µL of PBS, rather than *P. aeruginosa*, followed by treatment with 100 µL of distilled water (a). Positive controls were also treated with 100 µL of distilled water (b). Other groups were treated with 100 µL of 2.4 mg/mL tobramycin in 0.9% saline (c), 0.31 mg/mL silver nitrate in distilled water (d), or nanocrystalline silver-derived solutions (1 in²/mL, starting pH 4, 24h dissolution under ~100 rpm stirring) (e).

Histological Images at 24 Hours. Figure 6-7 shows histological images of lung lobes taken 24 hours after the first treatment. Images show the range of pathology observed within a single slice taken through the upper left lobe of each animal. Negative controls (a) showed areas of normal tissue, but also areas of

tissue thickening and infiltration by red blood cells and inflammatory cells. Positive controls demonstrated stronger inflammation than negative controls (b), with the normal lung tissue structure being nearly obliterated in many animals. However, some animals showed quite a bit of variability, particularly animal 2, whose histopathology was indistinguishable from the negative controls. Animal 1 was the animal found dead in the morning. Even though tobramycin treated animals demonstrated healthier behavior, their lung histology (c) was similar to positive controls overall, demonstrating a strong inflammatory response including infiltration of leukocytes and red blood cells, and loss of normal tissue structures with tissue thickening. Silver nitrate-treated animals (d) showed less variability in response, with strong inflammation throughout the lobe examined. The only animal that demonstrated significant variation within the lobe was Animal 1, and this was an animal that was provided with a second treatment and died right after receiving that treatment (see below). Animals treated with nanocrystalline silver-derived solutions showed more variability within the lobe examined for each animal treated. Some areas showed the tissue thickening, loss of normal tissue structure, and inflammatory cell infiltration, while other areas showed more normal tissue morphology. This observation was made for all animals in the group. This result suggested mild improvements with the use of this treatment relative to other treatments, particularly silver nitrate and the positive controls, but no definite conclusions could be made, due to the variability present in the negative controls.

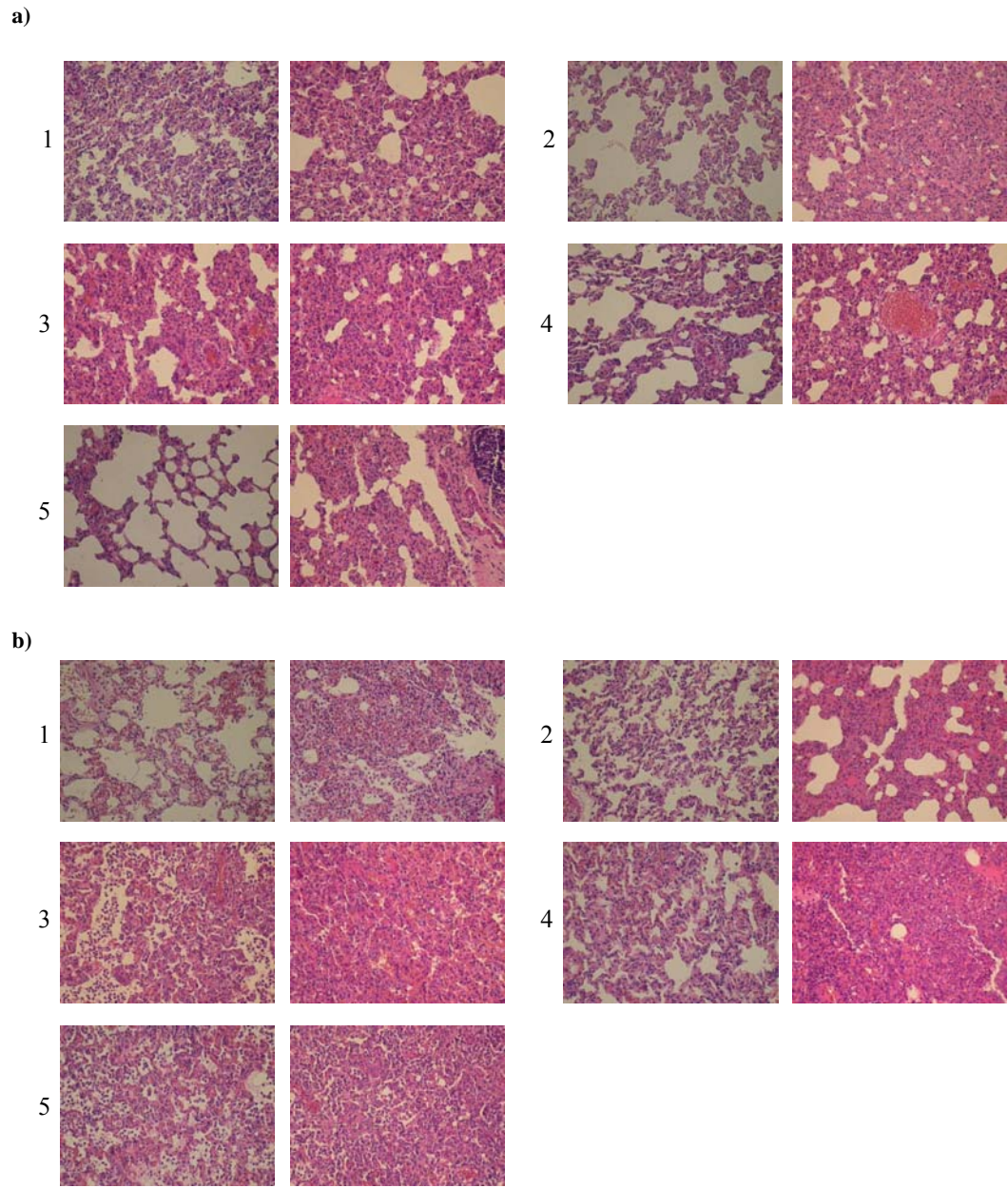


Figure 6-7.

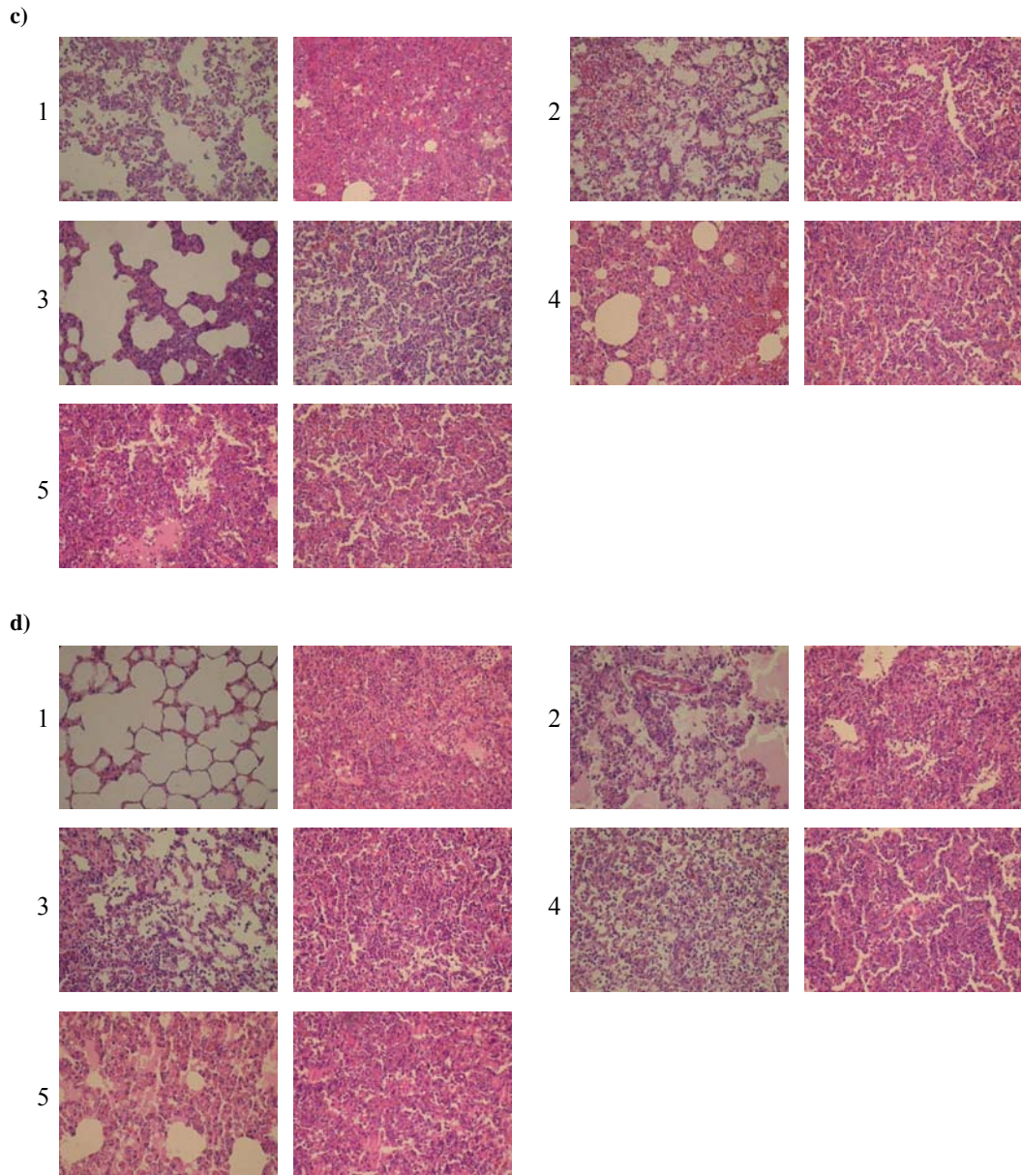


Figure 6-7, continued.

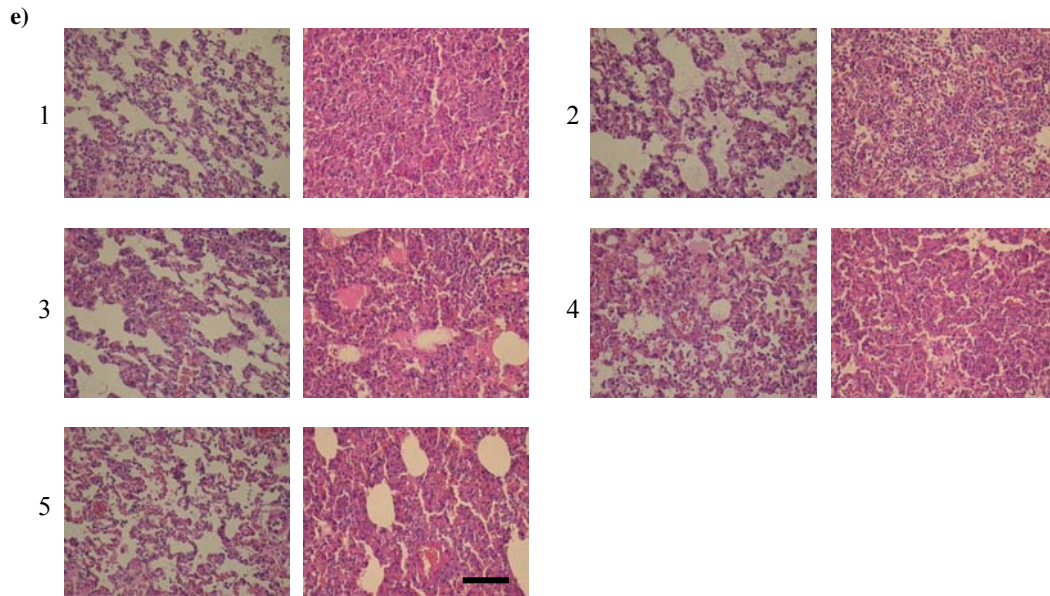


Figure 6-7, continued. Histological images showing the range of inflammation present in the upper left lung lobe of each rat euthanized 24 hours into the antimicrobial activity study. Negative controls were exposed to 100 μ L PBS, followed four hours later by 100 μ L of distilled water (a). All other groups of animals were exposed to 100 μ L of a 1:30 dilution of *P. aeruginosa* in PBS (incubated overnight at 37°C), followed by 100 μ L of distilled water (positive controls) (b), 2.4 mg/mL tobramycin in 0.9% saline (c), 0.31 mg/mL silver nitrate in distilled water (d), or nanocrystalline silver-derived solutions (1 in²/mL, starting pH 4, 24 hours dissolution under \sim 100 rpm stirring) (e). Each individual animal is indicated by its assigned number. Note: Rat 1 in the positive control group (b) died during the night, and Rat 1 in the silver nitrate group (d) was originally assigned to the 72 hour group, but died during the second treatment, so its lungs were sampled at that time (24 hours). Of the nanocrystalline silver treated group, 3 rats received fresh-stirred solutions, while 2 rats received solution taken from the top of the jar after the jar sat unstirred for approximately 30 minutes. The scale bar in the image of animal 5, panel (e), represents 100 μ m.

Visual Observations From 24 to 72 Hours. When the animals continuing on to 72 hours were provided with their second treatment, one animal treated with silver nitrate died right after receiving treatment, and two others demonstrated the respiratory distress observed with nanocrystalline-silver derived solution treated rats on the previous day, requiring CPR. Due to concerns regarding the animals' response to nanocrystalline silver-derived treatments, for the second and third treatments the animals in this group received solution samples taken from the top

of the container after it had time to settle, and these samples were diluted 1:2, in case the response was due to an overdose of the active agent. The rats did not demonstrate any respiratory distress after these changes were made.

No rats were lost overnight, and most rats were active and healthy at 48 hours, although the nanocrystalline silver-derived solution treated animals seemed to have some staining around their eyes and to be mildly less alert. During their final treatment, one negative control died right after receiving the treatment due to respiratory distress. During treatment, some positive controls were noted to have mucus or pus in their throats. No other animals were lost during treatment. All animals survived the night and looked healthy the following morning.

Digital Images at 72 Hours. Figure 6-8 shows representative images of rat lung lobes after 72 hours of treatment. The negative controls (a) had large areas of normal tissue, with some patches of dark red hemorrhaging. The tissues of tobramycin treated animals appeared similar to the negative controls (c). Positive controls (b) and animals treated with silver nitrate (d) showed some areas where tissues looked healthy, but had large areas that demonstrated inflammation. Nanocrystalline silver-derived solution treated animals (e) did not have visible areas of normal tissue, with dark red hemorrhaging covering most of the lobes examined.

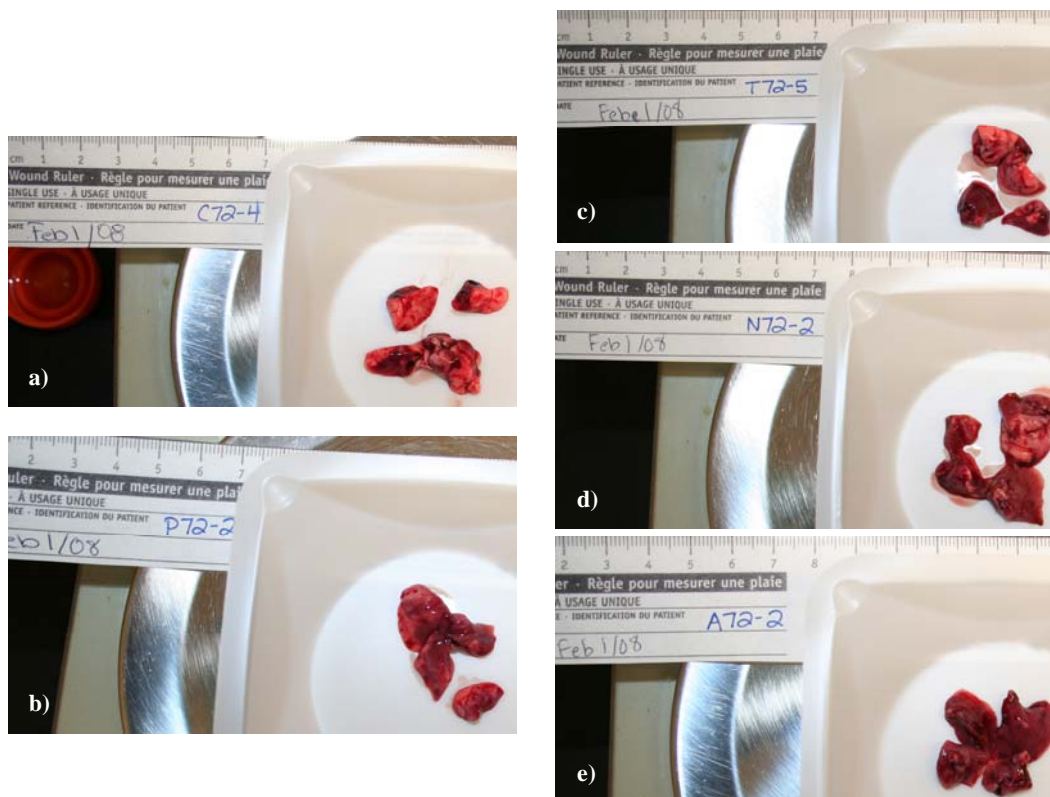


Figure 6-8. Representative digital images showing the portions of lung lobes of rats used for bacterial counts in the antimicrobial activity study 72 hours after inoculation of a 1:30 dilution of *Pseudomonas aeruginosa* incubated at 37°C overnight, followed four hours later by various treatments (n=5 for each group). Subsequent treatments were provided daily. Negative controls were inoculated with 100 µL of PBS, rather than *P. aeruginosa*, followed by treatment with 100 µL of distilled water (a). Positive controls were also treated with 100 µL of distilled water (b). Experimental groups were treated with 100 µL of 2.4 mg/mL tobramycin in 0.9% saline (c), 0.31 mg/mL silver nitrate in distilled water (d), or nanocrystalline silver-derived solutions (1 in²/mL, starting pH 4, 24 hours dissolution under ~100 rpm stirring) (e).

Histology at 72 Hours. Figure 6-9 shows histological images of the animals at 72 hours. Again, the range of tissue morphology observed within one lobe of each animal is shown. Surprisingly, negative controls showed better tissue morphology at 72 hours relative to 24 hours, despite the fact that these animals had received more spray instillations. There was still quite a bit of variability, however, particularly for animal 2. Positive controls also showed

some improvement relative to the histology at 24 hours, with more variability in the tissue structure, meaning less universal inflammation. Four out of five animals treated with tobramycin (c) showed quite a bit of variability, with some areas having near-normal tissue morphology. Animal 4 demonstrated inflammation throughout the lobe when examined after 72 hours of treatment. Animals treated with silver nitrate (d) showed less variability in the lobes examined, with strong inflammation still present throughout the tissues. In animals 2 and 4, the normal alveolar structures were almost completely closed off. With nanocrystalline silver-derived solutions (e), two of the animals (1 and 4) showed some signs of improvement, with areas of near-normal histology, but these animals showed high variability, with other areas still appearing highly inflamed. The remaining two animals (2 and 3), showed no signs of improvement, similar to the silver nitrate treated animals. Again, due to the variability observed, no definite conclusions could be made about any of the treatment groups.

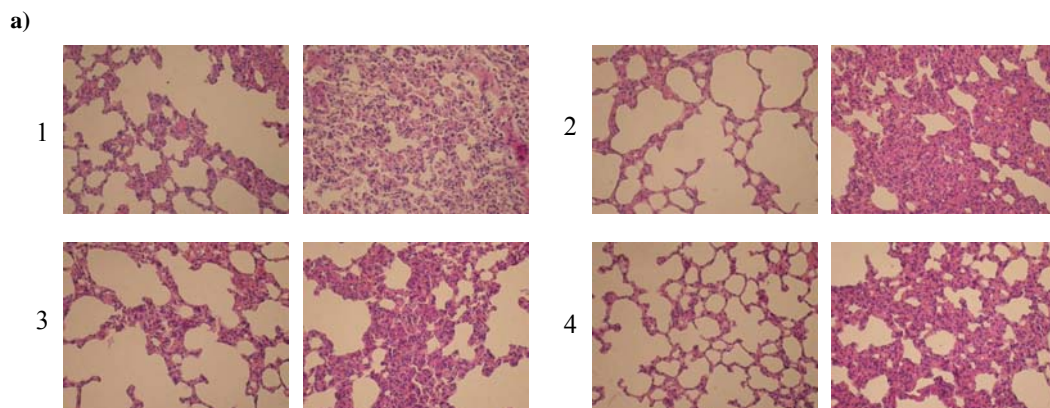


Figure 6-9.

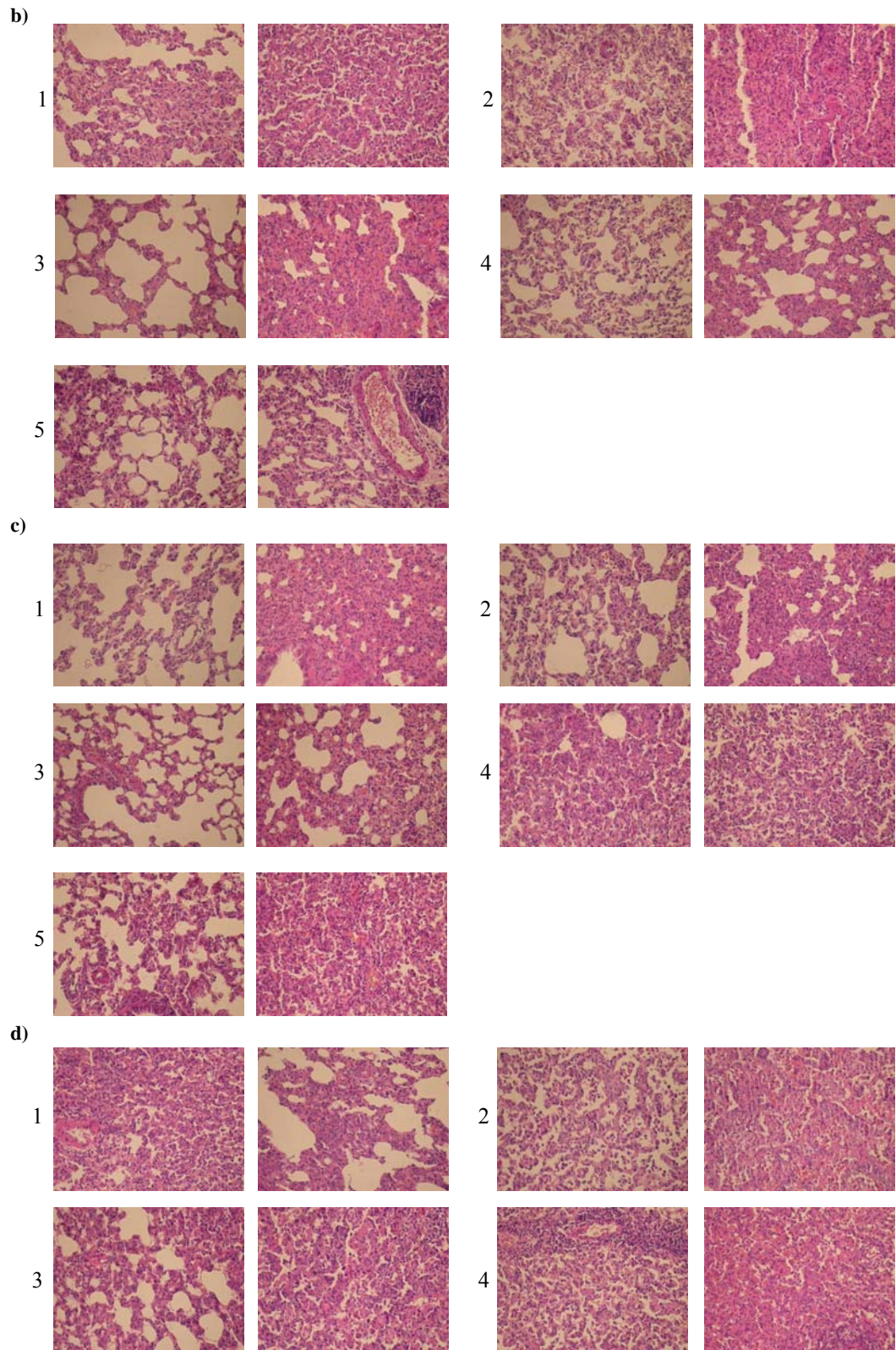


Figure 6-9, continued.

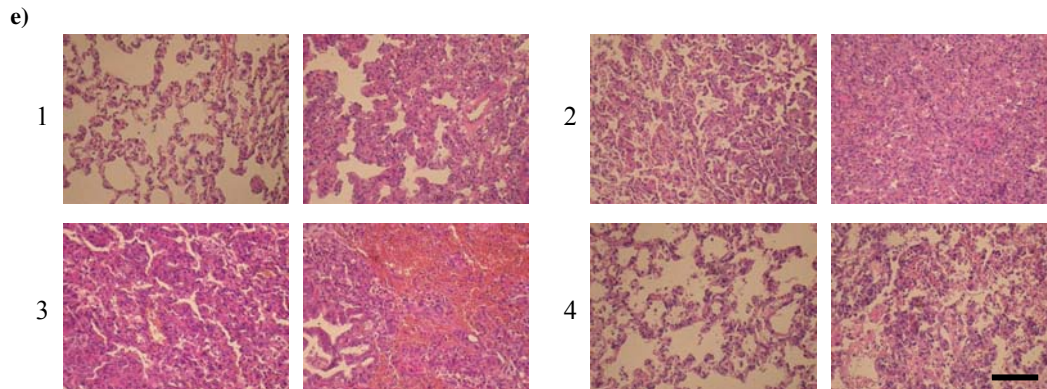


Figure 6-9, continued. Histological images showing the range of inflammation present in the upper left lung lobe of each rat euthanized at 72 hours in the antimicrobial activity study. Negative controls were exposed to 100 μ L PBS, followed four hours later by 100 μ L of distilled water (a). Subsequently, treatments were provided daily. All other groups of animals were exposed to 100 μ L of a 1:30 dilution of *P. aeruginosa* in PBS (incubated overnight at 37°C), followed by treatments with 100 μ L of distilled water (positive controls) (b), 2.4 mg/mL tobramycin in 0.9% saline (c), 0.31 mg/mL silver nitrate in distilled water (d), or nanocrystalline silver-derived solutions (1 in²/mL, starting pH 4, 24 hours dissolution under \sim 100 rpm stirring) (e). Each animal is indicated by its assigned number. The scale bar in the right image of animal 4, panel (e), represents 100 μ m.

Bacterial Load at 24 and 72 Hours. Bacterial counts from lung tissues at 24 and 72 hours are shown in Table 6-4. There were no significant differences in the number of bacteria present in different treatment groups at either time point. There were low levels of bacteria present in the lungs of all animals, no matter what treatment group they belonged to, suggesting the animals were able to clear the bacteria on their own, if they didn't die from exposure to them within the first 24 hours. It is interesting to note that the negative controls were not bacteria free, despite not being instilled with bacteria. As well, it was observed that bacterial cultures were contaminated with bacterial species other than *P. aeruginosa*, particularly with a white gram positive cocci, suggesting that either the rats had been previously exposed to these bacteria, or that the lab space used was

contaminated. Within the constraints of the experiment, it was not possible to determine which was the case.

Table 6-4. Bacterial counts for the antimicrobial activity study.

Treatment Group	24 hours (log cells/g)	# Animals with No Bacteria (24h)	72 hours (log cells/g)	# Animals with No Bacteria (72h)
Negative Controls	<2.8±0.62	1/5	<2.3±0.03	3/4
Positive Controls	<2.5±0.47	0/5	<2.5±0.45	3/5
Tobramycin	<2.3±0.16	0/5	<2.3±0.05	4/5
Silver Nitrate	<2.6±0.24	0/5	<2.2±0.5	1/3
Nanocrystalline Ag	<3.6±0.92	1/5	<2.5±0.6	1/4

Note: < indicates that there were no countable bacteria within the detection limit for some animals in the group.

Real Time RT-PCR. Figure 6-10 shows the Delta Rn (a measure of DNA content) versus cycle number for real time RT-PCR of rat tissues after 24 hours of treatment for (a) HPRT, the housekeeping gene, and (b) TNF- α , an important pro-inflammatory signaling molecule (see Chapter 2). The green line indicates the point at which Cts were read. With HPRT, the data for all treatment groups was very close together, while with TNF- α , the data was well spread apart, suggesting that the procedures were done correctly and that there was variation in TNF- α expression between animals.

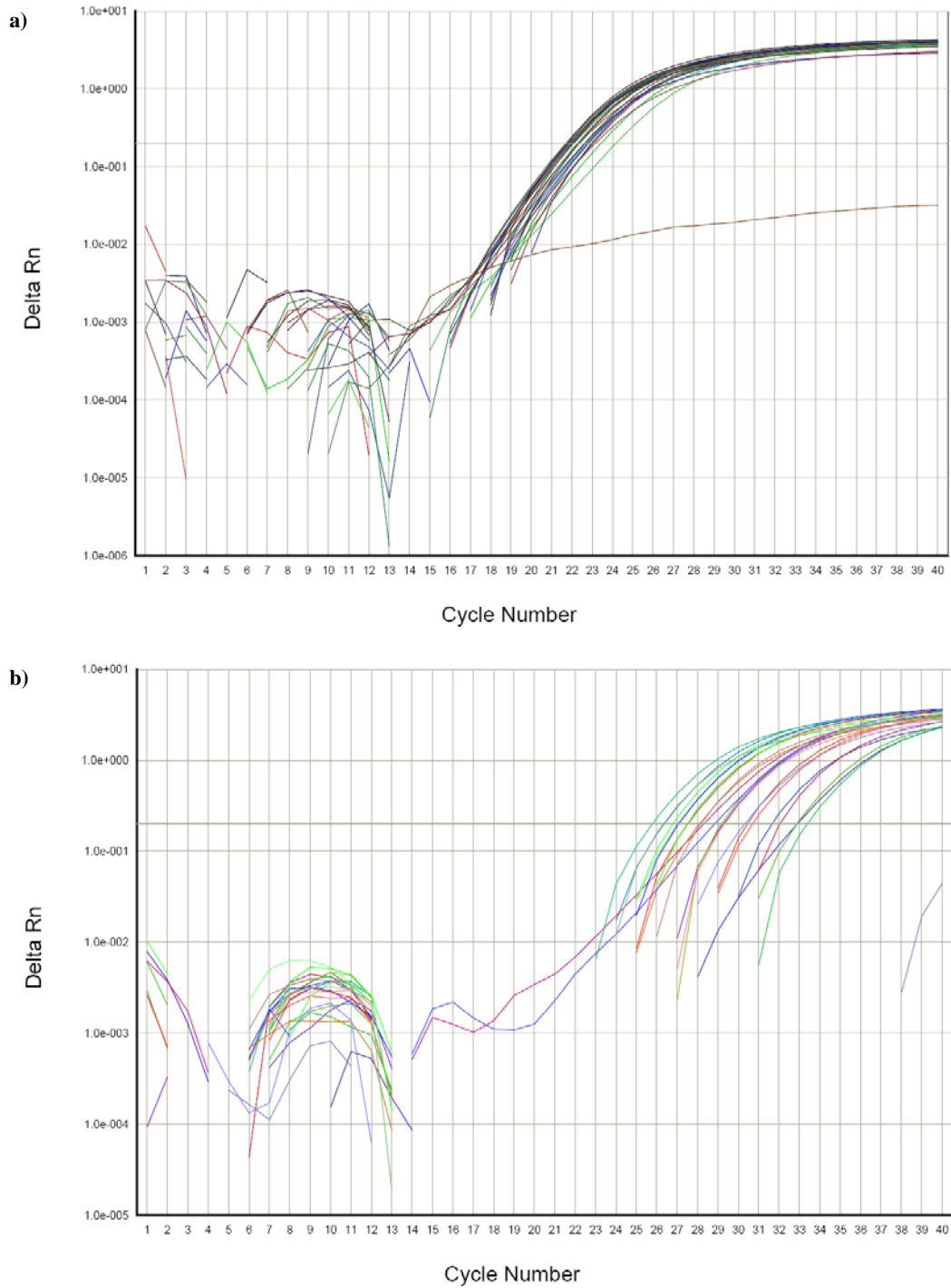


Figure 6-10. Real time RT-PCR reaction rates. Plots of ΔR_n (a measure of the amount of DNA present) over the number of PCR cycles are shown for all rats treated for 24 hours for (a) HPRT, and (b) TNF- α . Green horizontal lines represent the point at which Ct measurements were taken.

Figure 6-11 shows the relative mRNA expression of TNF- α for the different treatment groups at 24 hours. There were significant differences between groups ($p=0.0246$), but the post tests did not indicate any significant differences between individual groups. There appeared to be a trend towards higher expression of TNF- α in the tobramycin treated animals and nanocrystalline silver-derived solution treated animals relative to negative controls, but this trend was not significant due to the high variability of expression within the groups. This may have been due in part to the fact that the tissues were not snap-cooled using liquid nitrogen. However, the high level of variability observed in the histology may also explain this.

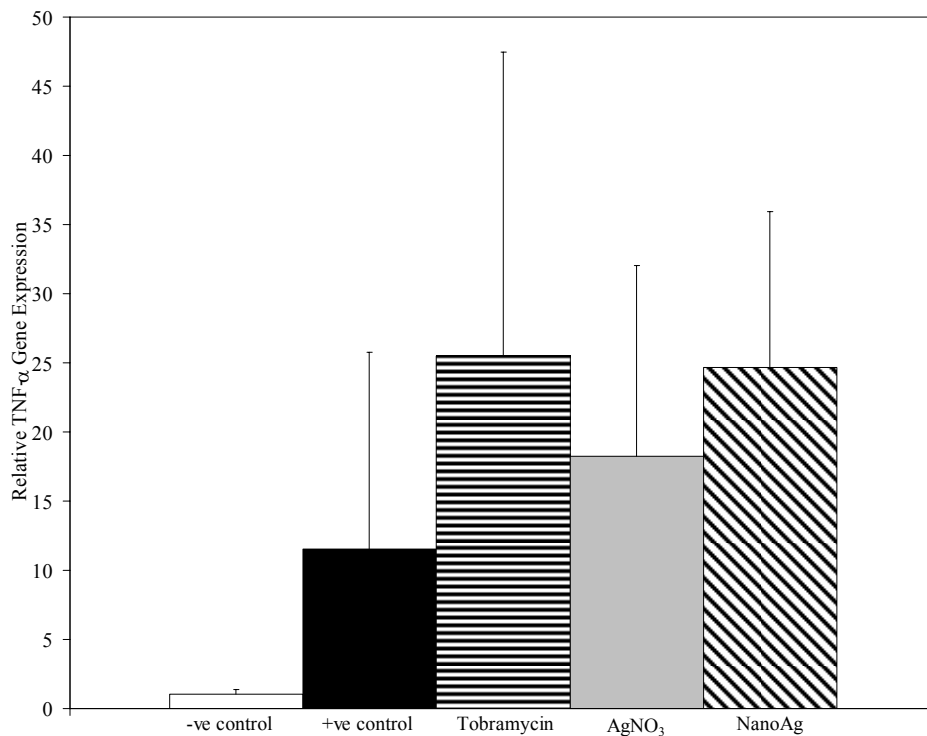


Figure 6-11. Relative expression of TNF- α mRNA in negative controls, *P. aeruginosa* infected rat lungs treated for 24 hours with 100 μ L of distilled water (positive controls), 2.4 mg/mL tobramycin in 0.9% saline, 0.31 mg/mL silver nitrate in distilled water, or nanocrystalline silver-derived solution (starting pH of 4, 24 hour dissolution time, ~ 100 rpm, 1 in²/mL). Error bars represent standard deviations ($n=5$ for each data point).

Figure 6-12 shows the Delta Rn versus cycle number for real time RT-PCR of rat tissues after 72 hours of treatment for (a) HPRT and (b) TNF- α . The green line indicates the point at which Cts were read. With HPRT, the data for most treatment groups was very close together. With TNF- α , the data was somewhat more spread apart, although much less so than at 24 hours, suggesting that perhaps inflammation was resolving and therefore there was less variation, as compared to 24 hours.

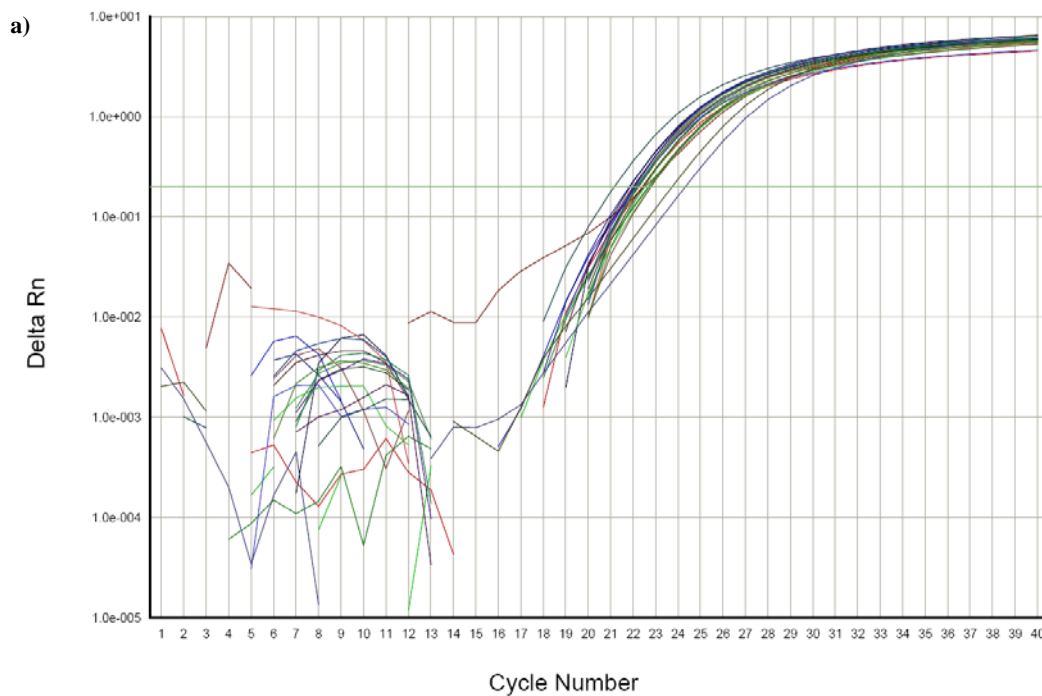


Figure 6-12.

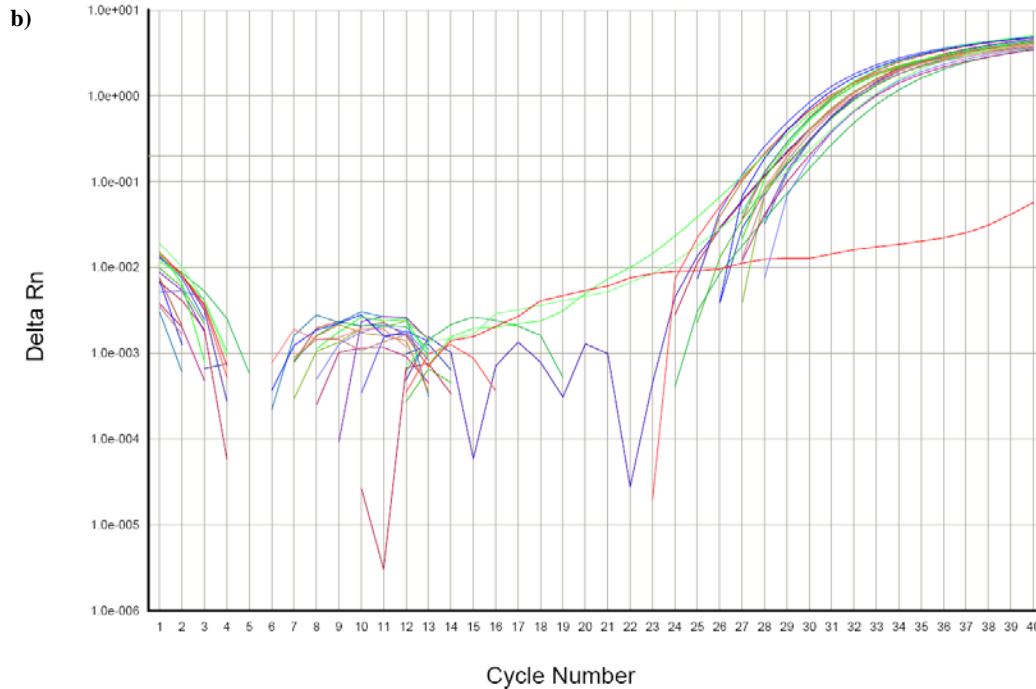


Figure 6-12, continued. Real time RT-PCR reaction rates. Plots of ΔRn (a measure of the amount of DNA present) over the number of PCR cycles are shown for all rats treated for 72 hours for (a) HPRT, and (b) TNF- α . Green horizontal lines represent the point at which Ct measurements were taken.

Figure 6-13 shows the relative mRNA expression of TNF- α for the different treatment groups at 72 hours. There were no significant differences between groups ($p=0.0516$). There appeared to be a trend towards higher expression of TNF- α in the silver nitrate treated animals relative to all other treatment groups, but this trend was not significant due to the high variability of expression within the groups, which again might be explained by the high level of variability observed in the histology.

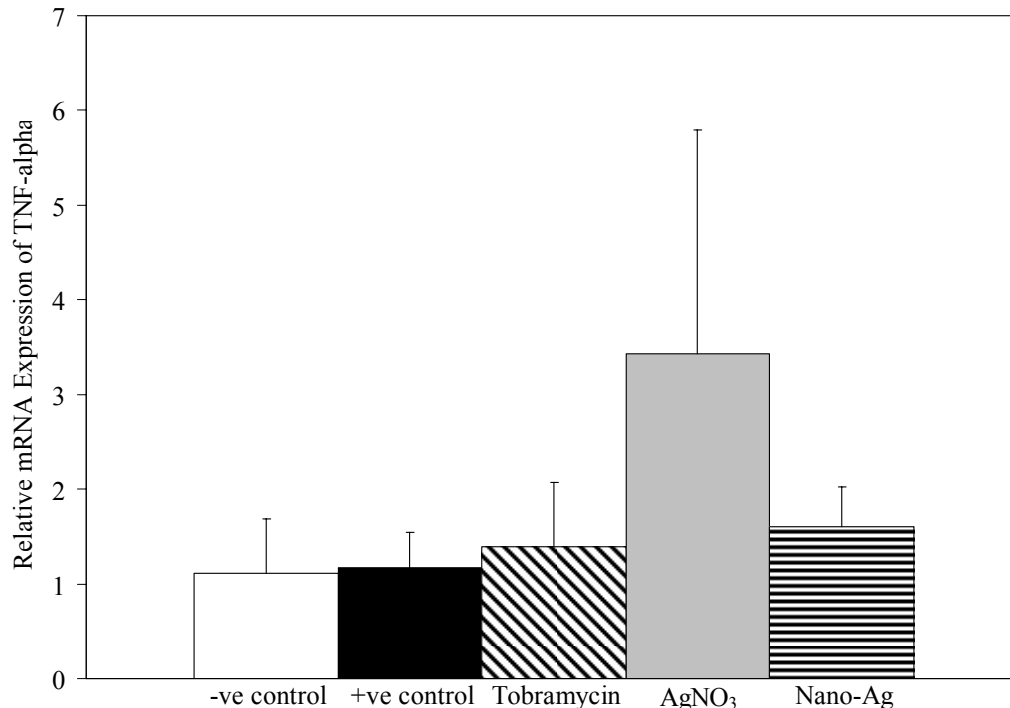


Figure 6-13. Relative expression of TNF- α mRNA in negative controls, *P. aeruginosa* infected rat lungs treated for 72 hours with 100 μ L of distilled water (positive controls), 2.4 mg/mL tobramycin in 0.9% saline, 0.31 mg/mL silver nitrate in distilled water, or nanocrystalline silver-derived solution (starting pH of 4, 24 hour dissolution time, \sim 100 rpm, 1 in²/mL). Error bars = standard deviations (n=5 for each data point).

Total Silver. Samples from the solutions used for the first treatment of animals in the nanocrystalline silver-derived solution treated group contained \sim 124 mg/L total silver, meaning the animals received \sim 12.5 μ g of silver each. For the second treatment, the solutions contained \sim 128 mg/L total silver, so the animals received \sim 4.3 μ g of silver each, since they were receiving 1:2 doses. For the third treatment, the solutions contained \sim 109 mg/L total silver, meaning the animals received \sim 3.6 μ g of silver each.

Nanocrystalline Silver Controls

Visual Observations. Due to concerns about particles in the stirred solutions causing respiratory distress, two rats which had not been exposed to

bacteria were delivered nanocrystalline silver-derived solutions from the top of the container after the solution had sat unstirred for about half an hour, giving enough time for any particles in solution to settle out. Both rats survived out to 24 hours and appeared healthy. Another two rats were treated with solution samples taken from the bottom of the container at this time point. One of the rats receiving the solution from the bottom of the container died immediately (CPR was attempted, but the rat could not be saved), while the remaining rat survived the night, but appeared to have blood on its nose in the morning. Another rat was provided with nanocrystalline silver-derived solution sampled from the top of the container and diluted 1:2 with distilled water. It survived for 24 hours as well and appeared healthy.

Histology. Figure 6-14 shows histological images of the upper left lung lobe of animals treated with nanocrystalline silver only, with no exposure to bacteria. The animals receiving full strength solution sampled from the top of the container after the solution had been allowed to sit for about half an hour are shown in Panels (a) and (b). The range of tissue morphology present is shown for each animal. The animals showed areas of inflammation, but in animal (a), there were areas where the alveolar structure was still well defined, and where leukocyte infiltration was minimal. The tissue morphology observed was within the range seen with the negative controls. Similar results were observed for the animal that was treated once with solution sampled from the top of the container and diluted 1:2 (c). Surprisingly, the animal treated once with solution sampled from the bottom of the container at full strength showed the most normal tissue

morphology (d) – better tissue morphology than that seen with many of the negative controls.

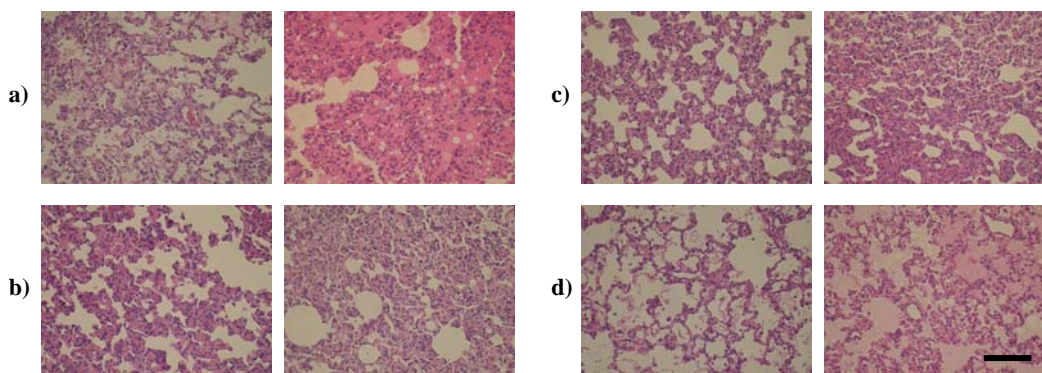


Figure 6-14. Histological images showing the range of inflammation present in the upper left lung lobe of each nanocrystalline silver control rat euthanized after 24 hours. Two rats (a-b) were instilled with full strength nanocrystalline silver-derived solutions (1 in²/mL, 24 hour dissolution, ~100 rpm, starting pH 4) sampled from the top of the solution after 30 minutes settling time. One rat (c) was instilled with the same solution described, but diluted 1:2. One rat (d) was instilled with the same solution, but the sample was taken from the bottom of the container after 30 minutes settling time, rather than the top. The scale bar in panel (d) represents 100 μ m.

Total Silver. The animals in this study received approximately 12.5 μ g of silver each, except for the animal treated with the diluted solution, which received approximately 3.6 μ g of silver.

Analyzing Solution Properties

Due to the uncertainty of the results, tests were performed to ensure that the nanocrystalline silver solutions were behaving as anticipated.

Wetability. First, there were concerns that the nanocrystalline silver-containing solutions were not being delivered to the same parts of the lungs as the bacteria, due to differences in solution wetability. Therefore, drops of nanocrystalline silver solutions and drops of bacteria were placed or sprayed (using the IA-1B® microsprayers) onto a glass (hydrophilic) and a greasy

(hydrophobic) surface. Figure 6-15 shows images of these results. The nanocrystalline silver-containing solutions and the bacteria-containing solutions demonstrated the same behavior on both surfaces, indicating that they have the same wettability and therefore should have been distributed to the same portions of the lungs using the same microsprayers.

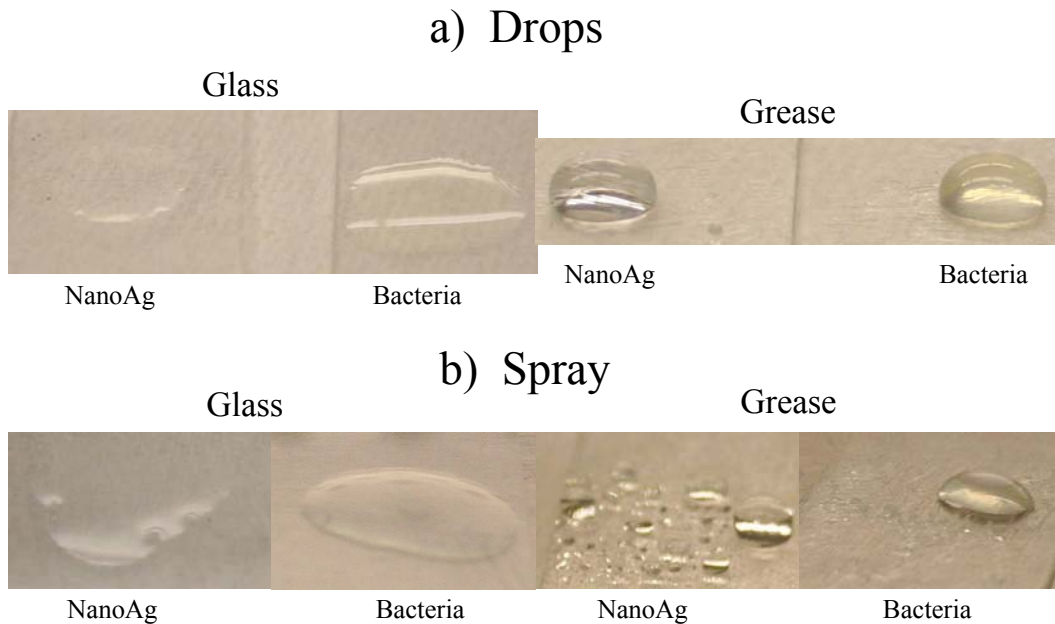


Figure 6-15. Solution wettability. Images demonstrate the wettability of nanocrystalline silver-derived solutions (1 in²/mL, 24 hour dissolution, ~100 rpm, starting pH 4) and bacteria-containing solutions (*P. aeruginosa*) dropped (a) or sprayed using an IA-1B microsprayer (b) onto glass and grease-coated glass.

Bacteriostatic Activity. A test was performed to check that the solutions had bacteriostatic activity under various conditions. Figure 6-16 shows images of the zones created, indicating that the solutions were capable of producing bacteriostatic activity independent of:

1. Whether the solution was freshly stirred or allowed to sit and sampled from the top or bottom.

2. Whether the solution was full strength or diluted 1:2.
3. Which microsyringe was used.
4. Whether the solutions were filtered or not.

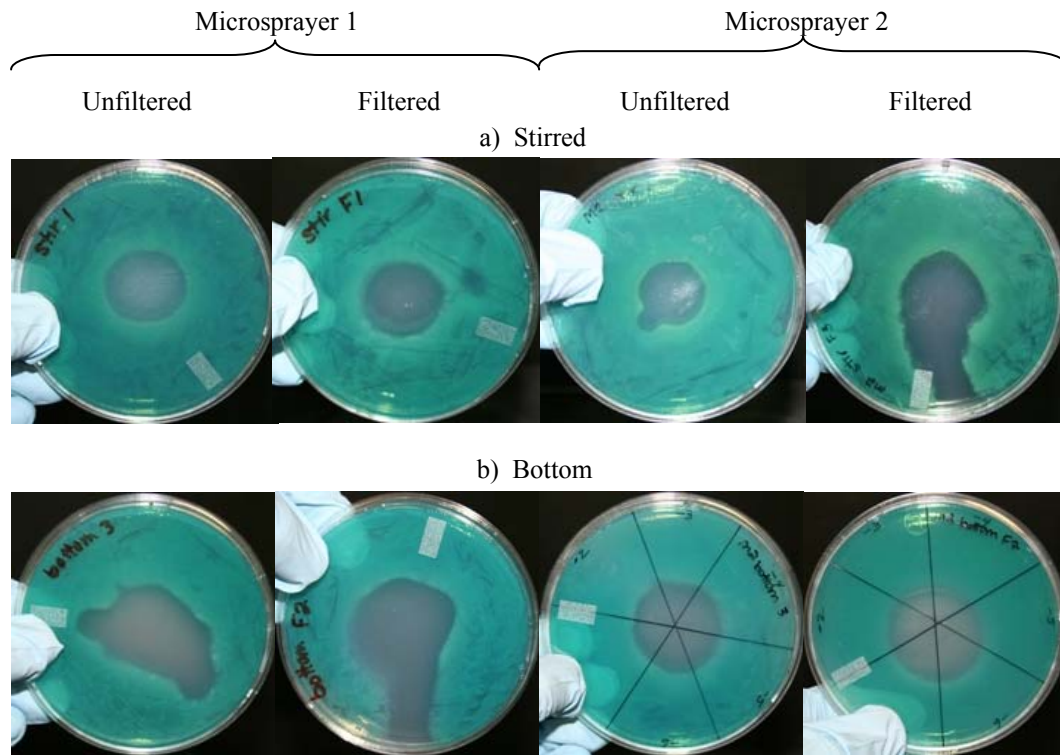


Figure 6-16.

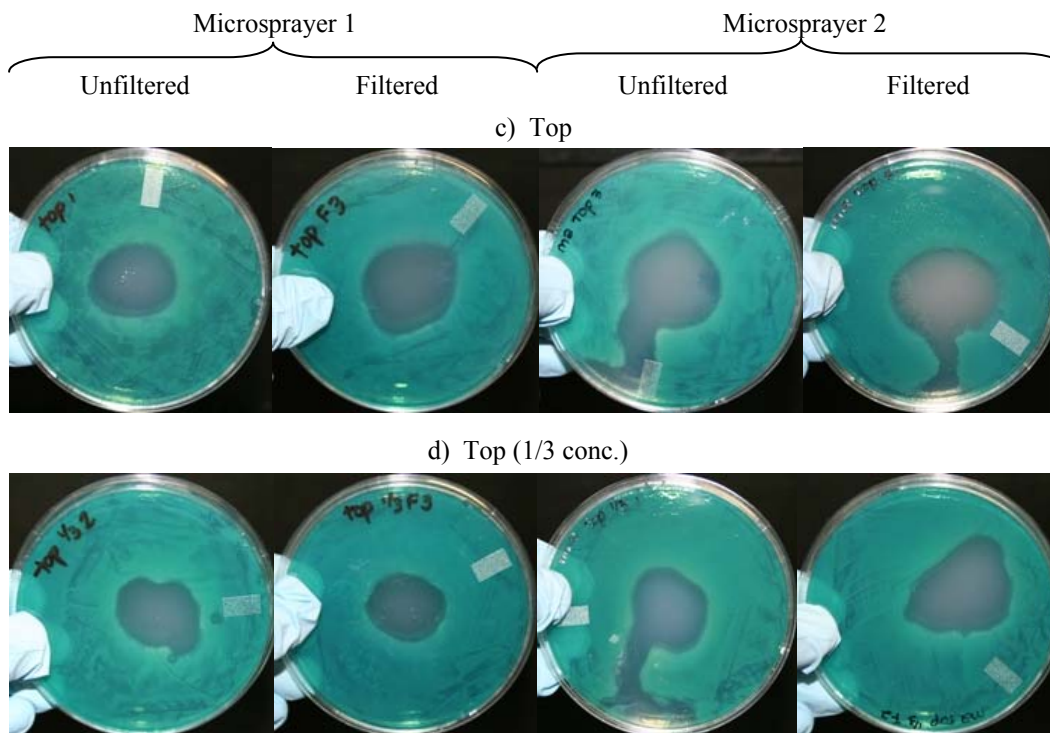


Figure 6-16, continued. Bacteriostatic activity of nanocrystalline silver-derived solutions. Images show areas where bacterial growth was inhibited by nanocrystalline silver-derived solutions (1 in²/mL, 24 hour dissolution, ~100 rpm, starting pH 4) sprayed using either IA-1B microsyrayer (either filtered or unfiltered) onto a lawn of *Pseudomonas aeruginosa* on MHA. Solutions were tested freshly stirred (a), or allowed to sit for half an hour and then sampled from the bottom of the solution (b), the top of the solution at full strength (c), or the top of the solution diluted 1:2 (d).

It is also interesting to note that the fine mist created around the edges of the main spray also was bacteriostatic, creating areas of poor growth around the main zone.

Total Silver. Table 6-5 shows the total silver present in the solutions used for the bacteriostatic activity test. Since these were single readings, no statistics could be done, but it is clear that the silver content was similar in the stirred solution, as well as in the top of the solution or bottom of the solution, if the solution was allowed to sit. As well, filtering with a 0.2 μm filter does not appear

to have removed silver from the solutions, suggesting that if there were particles present in the solutions, they were less than 200 nm in size. In that case, any particles present in the solution were not sufficiently large to block rat terminal branch bronchioles, which at the smallest are on the order of 50-150 μm inner diameter (ID)[88]. If only a few larger particles were present, they could still have resulted in the rat respiratory distress observed on the first day of treatment, however, it seems unlikely that these larger particles could have been filtered out and not have lowered the total silver measured by AAS. However, occasionally silver carbonate formations have been observed in solutions generated at a pH of 4 (this is seen as white particles or cloudy solutions), and black deposits have been observed on the magnets used to stir the solutions. These black deposits were determined by AAS to be silver, and are likely silver oxide. Therefore, an extra safety precaution for future experiments would be to filter the solutions before delivering them to the animals, in order to eliminate the possibility that particles of sufficient size to cause respiratory distress are delivered. This could be done rather than allowing the solutions to settle, which was done because filters were not available at the study location.

Table 6-5. Total silver in solutions under various conditions.

Condition	Filtered?	Before Testing (mg/L)	After Testing (mg/L)
Freshly stirred solution	No	160.5	212.3
	Yes	183.7	208.0
Sampled from top	No	160.9	165.4
	Yes	200.0	190.9
Sampled from bottom	No	99.9	158.3
	Yes	166.2	208.0
Sampled from top (1:2)	No	nss*	nss
	Yes	174.6	nss

*nss indicates that a proper reading was not obtained by AAS.

Microsprayer Characterization

The IA-1B produced MMDs of approximately 50 μm with both the bacteria-containing solution and the nanocrystalline silver-derived solution.

Conclusions

Overall, there were a number of problems related to this study, despite the changes made after the Anti-inflammatory Activity Study. The first problem observed was that the delivery of the full-strength stirred nanocrystalline silver solutions to the animals resulted in respiratory distress to nearly every animal to which it was delivered. While animals in other groups later demonstrated similar respiratory distress (which will be discussed below), the consistency with which the animals treated with nanocrystalline silver-derived solutions experienced respiratory distress on the first day suggested that there may have been an additional problem specific to this treatment. This appeared to be partially allayed by allowing the solution to sit and treating the animals with samples taken from the top of the solution, as animals treated in this way did not require CPR.

This improvement suggested that particles in the solutions, which were heavy enough to settle out, were blocking the animals' airways. Allowing the solutions to sit or filtering the solutions would readily eliminate this problem in future studies. However, animals receiving settled solutions at full strength still demonstrated signs of respiratory distress, which suggested that perhaps the dose they were receiving was too high, as many anti-inflammatory agents have narrow windows in which the treatments are both effective and safe. Thus, the animals were switched to a 1:2 dilution of the solution from the second treatment on, and no further respiratory distress was observed. This suggests that, in the future, a dose-response curve should be generated to determine whether or not there is a limit to the dosage of nanocrystalline silver-derived solutions which can safely be delivered to the lungs.

Later on in experimentation, animals from both the silver nitrate treatment group and the negative control group also began to experience respiratory distress, resulting in the loss of some animals. This suggested that the rats were responding poorly to having any solution sprayed into their lungs using the microsprayers. While there was nothing in the literature which clearly indicated that this was an expected consequence of using the microsprayers, authors of similar studies (personal communication, Michael Moxley, March 5, 2008) indicated that when using the IA-1B microsprayer:

1. Hitting the vocal cords with the microsprayer caused swelling and other reactions, and the resultant severe swelling of the cords led to death in rats.

2. Even with various precautions, such as making sure that everything they were using was LPS free (since LPS also causes swelling), and making sure that visualization was done carefully to avoid hitting the vocal cords, occasionally animals had to be resuscitated with gentle chest compression or oxygen flowing across their noses.

3. Some animals just didn't respond well to having fluid sprayed across most of their alveolar surfaces.

Altogether, this suggested that the rats responded poorly to the spraying effect produced by the microsprayer, and that the use of the microsprayer was the cause of the respiratory distress in at least some of the animals. Another study indicated that in control rats, the instillation of fluid directly into the airways via a microsprayer could influence basal mucociliary clearance as a consequence of irritation or modulation of the physicochemical properties of the animals' mucus, and that the administration procedure could induce an inflammatory response in the lung characterized by an increase in percentage of neutrophils in BAL fluid[36]. They suggested this could be a response to the physical insertion of the microsprayer[36]. The use of microsprayers for rat studies may not be ideal, due to sensitivity to having their lungs sprayed/vocal cords contacted.

Another problem related to the use of the microsprayer was the fact that the negative controls showed signs of inflammation. While mild inflammation might be expected due to the fact that the negative controls were receiving distilled water, which is hypotonic relative to the lung environment, some negative controls in this study had areas of inflammation comparable to the

positive controls. This may be partially explained by the poor tolerance of rats to the microspraying procedure; however, another related problem was the high variability in results, even within a single lobe of an animal. This suggested poor distribution of the fluids within the lung, despite the claims made by the manufacturers of the microsprayers[78]. This in turn appears to have been caused, at least partially, by the droplet sizes produced by the microsprayer, which were much larger than claimed by the manufacturers[78]. In agreement with the work presented in this chapter, another study determined that IA-1B™ microsprayers produced droplet sizes of $45.5 \pm 3.7 \mu\text{m}$ [59]. These droplet sizes were much too large to provide good distribution throughout the rat lungs (personal communication, Dr. Carlos Lange, February 20, 2008). Even the size claimed by the manufacturer would not, in fact, be able to penetrate the rat lung by inhalation (personal communication, Dr. Carlos Lange, February 25, 2008). Overall, the use of microsprayers with rats does not appear to be a good way to generate clear data with low variability, and is a very tricky operation to perform without endangering the rats. For future studies, if a microsprayer is to be used, it is recommended that it be used with a larger animal model. However, if future studies are performed in rats, nebulization studies might be a better method, although the exact dose received cannot be determined, as there is no way to know whether the rats actually inhaled the drug or how much of it, meaning that the variability could be as poor as observed in this study (personal communication, Dr. Carlos Lange, February 25, 2008)[43, 46]. Studies in which treatments are performed by bronchoalveolar lavage (BAL) could be used to

determine the exact dose, as the treatment would be the volume delivered minus the volume sucked back out of the lung cavity. This would prevent damage due to spraying fluids into the lung, and would provide good distribution throughout the lung. This would be more dangerous than nebulization, however, as the BAL would have to be done quickly to avoid rat suffocation, and contacting the rat vocal cords could still be an issue. Also, the use of inhalation anesthetic might not be possible because addition of fluid to the rat lungs tended to wake them up very quickly using the microsprayer, although this may have been due to the spraying action. Using either the nebulizer or BAL methods, the best way to have the challenge and the treatment solutions reach the same portions of the lung would be to provide the challenge by the same method as the treatment. While other studies have used nebulization to deliver bacteria and LPS to rats, the feasibility and safety of this would need to be determined for the specific equipment that was selected.

Another problem encountered in this study was that the rats appeared to be able to clear the bacteria quickly, irrespective of the treatment given. However, a challenge with a higher bacterial count could not be used without introducing animal mortality as an experimental endpoint. This conclusion is based on both the titration study and the fact that one of the positive controls in the Antimicrobial Activity Study died within 24 hours of the initial challenge. Thus, the rats appeared to be sufficiently resistant to the bacteria that if they didn't die from it, they were able to clear it rapidly from their system. If this same strain of rats was to be used in an antimicrobial study in the future, switching from this

acute infection model to a chronic infection model might be necessary. In order to achieve a chronic infection, bacteria must be inoculated within an immobilizing agent such as agar, agarose, or an alginate[10]. This results in a local lung infection lasting over a month, causing CF-like lesions in the rat lungs[10]. Use of a mucoid strain of *P. aeruginosa* (which can be present in chronic infections and CF) in this model could further promote chronic infection[10, 89, 90]. A new titration study would be needed to determine the correct quantity of bacteria to deliver in either of these ways, to ensure that the rats developed significant inflammation in the lungs without causing mortalities. Costa *et al.*[12] indicate that the challenges of all animal studies include detecting a signal above the noise associated with disease, and pin-pointing the appropriate disease severity. Clearly, in the studies presented here, these issues were not completely resolved.

One final concern related to this study was that there was no clear distinction in activity between the nanocrystalline silver-derived treatments and the other groups. Variability due to the use of the microsprayers partially explains this result, as there also was no clear distinction in activity between tobramycin-treated animals and others, despite results of Chapter 4 indicating that the strain used was sensitive to tobramycin. However, it should also be noted that the results from Chapter 5 regarding the bactericidal efficacy of nanocrystalline silver-derived solutions generated under various conditions had not yet been ascertained when this study was run. Only preliminary *in vitro* data had been obtained. The results of Chapter 5 showed that the dissolution time used in this study was likely too long to produce bactericidal activity. Furthermore, the

respiratory distress caused to most of the animals in the nanocrystalline silver-derived solution treated group on the first day of the study may have enhanced the animals' initial lung inflammation, possibly counteracting the effects of the treatment that day. One study has suggested that the supernatant of solutions generated from dissolution of nanocrystalline silver in ammonia or distilled water contains nanoparticles on the order of 15 nm, but which could be agglomerated into much larger particles (as measured by TEM)[91]. This was likely due to re-precipitation of dissolved silver as silver oxide (personal communication, Dr. Robert Burrell). This may explain part of the problem of respiratory arrest specific to nanocrystalline silver-derived solutions and why filtering the solutions or allowing them to settle may have helped. Because of all the issues related to the model used in this set of studies, nanocrystalline silver-derived solutions generated under various conditions were tested more thoroughly *in vitro* for bactericidal activity (see Chapter 5), and were tested for anti-inflammatory activity in the porcine contact dermatitis model studied in Chapter 2, since that was a model from which clear conclusions could be drawn. The results of this dermal study, which are presented in Chapter 7, showed that solutions derived from nanocrystalline silver can have anti-inflammatory activity, but that, again, it was dependent on the dissolution conditions. The conditions used for the antimicrobial and anti-inflammatory studies in this chapter may not have been generated under conditions that would produce the greatest anti-inflammatory activity. Thus future studies in a lung model should examine the effect of varying dissolution condition on anti-inflammatory and antimicrobial activity *in vivo*.

Bibliography

1. Ranganathan SC, Sonnappa S: **Pneumonia and other respiratory infections.** *Pediatr Clin North Am* 2009, **56**:135-156.
2. Ganesan A: **Methicillin-resistant *Staphylococcus aureus* bacteremia and pneumonia.** *Dis Mon* 2008, **54**:787-792.
3. Kollef MH, Shorr A, Tabak YP, Gupta V, Liu LZ, Johannes RS: **Epidemiology and outcomes of health-care-associated pneumonia: results from a large US database of culture-positive pneumonia.** *Chest* 2005, **128**:3854-3862.
4. Francis JS, Doherty MC, Lopatin U, Johnston CP, Sinha G, Ross T, Cai M, Hansel NN, Perl T, Ticehurst JR, Carroll K, Thomas DL, Nuermberger E, Bartlett JG: **Severe community-onset pneumonia in healthy adults caused by methicillin-resistant *Staphylococcus aureus* carrying the Panton-Valentine leukocidin genes.** *Clin Infect Dis* 2005, **40**:100-107.
5. Gillet Y, Vanhems P, Lina G, Bes M, Vandenesch F, Floret D, Etienne J: **Factors predicting mortality in necrotizing community-acquired pneumonia caused by *Staphylococcus aureus* containing Panton-Valentine leukocidin.** *Clin Infect Dis* 2007, **45**:315-321.
6. Nicholas TE, Doyle IR, Bersten AD: **Surfactant replacement therapy in ARDS: white knight or noise in the system?** *Thorax* 1997, **52**:195-197.
7. Raghavendran K, Pryhuber GS, Chess PR, Davidson BA, Knight PR, Notter RH: **Pharmacotherapy of acute lung injury and acute respiratory distress syndrome.** *Curr Med Chem* 2008, **15**:1911-1924.
8. Neuhoef H: **Actions and interactions of mediator systems and mediators in the pathogenesis of ARDS and multiorgan failure.** *Acta Anaesthesiol Scand Suppl* 1991, **95**:7-13.
9. Mukasa Y, Craven N: **Management of toxic epidermal necrolysis and related syndromes.** *Postgrad Med J* 2008, **84**:60-65.
10. Stotland PK, Radzioch D, Stevenson MM: **Mouse models of chronic lung infection with *Pseudomonas aeruginosa*: models for the study of cystic fibrosis.** *Pediatr Pulmonol* 2000, **30**:413-424.
11. Cystic Fibrosis Foundation, USA: **New Statistics Show CF Patients Living Longer.** ©2006 News Archive, Bethesda.
<http://www.cff.org/aboutCFFoundation/NewsEvents/2006NewsArchive/index.cfm?ID=2711&TYPE=1132>. Viewed July 7, 2009.
12. Costa DL, Kodavanti UP: **Toxic responses of the lung to inhaled pollutants: benefits and limitations of lung-disease models.** *Toxicol Lett* 2003, **140-141**:195-203.
13. Xu J, Zhao M, Liao S: **Establishment and pathological study of models of chronic obstructive pulmonary disease by SO₂ inhalation method.** *Chinese Med J* 2000, **113**:213-216.
14. Ringbaek T, Seersholm N, Viskum K: **Standardised mortality rates in females and males with COPD and asthma.** *Eur Respir J* 2005, **25**:891-895.

15. Bhol KC, Schechter PJ: **Topical nanocrystalline silver cream suppresses inflammatory cytokines and induces apoptosis of inflammatory cells in a murine model of allergic contact dermatitis.** *Br J Dermatol* 2005, **152**:1235-1242.
16. Burrell RE, Hegggers JP, Davis GJ, Wright JB: **Efficacy of Silver-Coated Dressings as Bacterial Barriers in a Rodent Burn Sepsis Model.** *Wounds: A Compendium of Clinical Research and Practice* 1999, **11**:64-71.
17. Demling RH, DeSanti L: **The rate of re-epithelialization across meshed skin grafts is increased with exposure to silver.** *Burns* 2002, **28**:264-266.
18. Doshi J, Karagama Y, Buckley D, Johnson I: **Observational study of bone-anchored hearing aid infection rates using different post-operative dressings.** *J Laryngol Otol* 2006, **120**:842-844.
19. Gallant-Behm CL, Yin HQ, Liu SJ, Hegggers JP, Langford RE, Olson ME, Hart DA, Burrell RE: **Comparison of *in vitro* disc diffusion and time kill-kinetic assays for the evaluation of antimicrobial wound dressing efficacy.** *Wound Repair and Regeneration* 2005, **13**:412-421.
20. Kirsner RS, Orsted H, Wright JB: **Matrix metalloproteinases in normal and impaired wound healing: a potential role of nanocrystalline silver.** *Wounds* 2002, **13**:4-12.
21. Nadworny PL, Wang JF, Tredget EE, Burrell RE: **Anti-inflammatory activity of nanocrystalline silver in a porcine contact dermatitis model.** *Nanomed: NBM* 2008, **4**:241-251.
22. Nadworny PL, Landry BK, Wang JF, Tredget EE, Burrell RE: **Does nanocrystalline silver have a systemic effect?** *Wound Repair Regen* 2009, (submitted).
23. Olson ME, Wright JB, Lam K, Burrell RE: **Healing of porcine donor sites covered with silver-coated dressings.** *Eur J Surg* 2000, **166**:486-489.
24. Rustogi R, Mill J, Fraser JF, Kimble RM: **The use of Acticoat in neonatal burns.** *Burns.* 2005, **31**:878-882.
25. Tredget EE, Shankowsky HA, Groeneveld A, Burrell RE: **A matched-pair, randomized study evaluating the efficacy and safety of Acticoat silver-coated dressing for the treatment of burn wounds.** *J Burn Care Rehabil* 1998, **19**:531-537.
26. Wright JB, Lam K, Buret AG, Olson ME, Burrell RE: **Early healing events in a porcine model of contaminated wounds: effects of nanocrystalline silver on matrix metalloproteinases, cell apoptosis, and healing.** *Wound Repair Regen* 2002, **10**:141-151.
27. Bhol KC, Schechter PJ: **Effects of Nanocrystalline Silver (NPI 32101) in a Rat Model of Ulcerative Colitis.** *Dig Dis Sci* 2007:11 pages.
28. Martinez-Burnes J, Lopez A, Lemke K, Dobbin G: **Transoral intratracheal inoculation method for use with neonatal rats.** *Comp Med* 2001, **51**:134-137.

29. Szarka RJ, Wang N, Gordon L, Nation PN, Smith RH: **A murine model of pulmonary damage induced by lipopolysaccharide via intranasal instillation.** *J Immunol Methods* 1997, **202**:49-57.
30. Metcalf K, Berg A, Ericson A-C, Lisander B: **Nitric oxide does not cause extravasation in endotoxemic rats.** *J Trauma Injury Infect & Crit Care* 2003, **58**:1047-1054.
31. Su X, Bai C, Hong Q, Zhu D, He L, Wu J, Ding F, Fang X, Matthay MA: **Effect of continuous hemofiltration on hemodynamics, lung inflammation and pulmonary edema in a canine model of acute lung injury.** *Intensive Care Med* 2003, **29**:2034-2042.
32. van Helden HP, Kuijpers WC, Diemel RV: **Asthma-like symptoms following intratracheal exposure of Guinea pigs to sulfur mustard aerosol: therapeutic efficacy of exogenous lung surfactant curosurf and salbutamol.** *Inhal Toxicol* 2004, **16**:537-548.
33. Hussain A, Ahsan F: **State of insulin self-association does not affect its absorption from the pulmonary route.** *Eur J Pharm Sci* 2005, **25**:289-298.
34. Lu KW, Taeusch HW, Robertson B, Goerke J, Clements JA: **Polyethylene glycol/surfactant mixtures improve lung function after HCl and endotoxin lung injuries.** *Am J Respir Crit Care Med* 2001, **164**:1531-1536.
35. Foronjy RF, Mirochnitchenko O, Propokenko O, Lemaitre V, Jia Y, Inouye M, Okada Y, D'Armiento JM: **Superoxide dismutase expression attenuates cigarette smoke- or elastase-generated emphysema in mice.** *Am J Respir Crit Care Med* 2006, **173**:623-631.
36. Coote K, Nicholls A, Atherton HC, Sugar R, Danahay H: **Mucociliary clearance is enhanced in rat models of cigarette smoke and lipopolysaccharide-induced lung disease.** *Exp Lung Res* 2004, **30**:59-71.
37. Hafner D, Ibrahim M, Wollin L, Germann P-G: **Cyclooxygenase-inhibition enhances the effects of rSP-C surfactant therapy in a rat lavage model of acute respiratory distress syndrome (ARDS).** *Exp & Toxicol Pathol* 2003, **55**:59-68.
38. Chua F, Gauldie J, Larent GJ: **Pulmonary Fibrosis Searching for Model Answers.** *Am J Respir Cell Mol Biol* 2005, **33**:9-13.
39. Warheit DB, Hartsky MA: **Initiating the risk assessment process for inhaled particulate materials: development of short term inhalation bioassays.** *J Exposure Analysis & Env Epid* 1997, **7**:313-325.
40. Zhang Q, Kusaka Y, Zhang Q, He L, Zhang Z, Sato K: **Dynamic changes of constituents in bronchoalveolar lavage fluid in experimental silicotic rats.** *Industrial Health* 1996, **34**.
41. Kobzik L: **Lung macrophage uptake of unopsonized environmental particulates. Role of scavenger-type receptors.** *J Immunol* 1995, **155**:367-376.
42. Yokohira M, Takeuchi H, Yamakawa K, Sao K, Ikeda M, Matsuda Y, Zeng Y, Hosokawa K, Maeta H, Imaida K: **Establishment of a Bioassay System for Detection of Lung Toxicity Due to Fine Particle**

- Instillation: Sequential Histopathological Changes with Acute and Subacute Lung Damage Due to Intratracheal Instillation of Quartz in F344 Male Rats.** *J Toxicol Pathol* 2005, **18**:13-18.
43. Munder A, Krusch S, Tschernig T, Dorsch M, Luhrmann A, van Griensven M, Tummler B, Weiss S, Hedrich HJ: **Pulmonary microbial infection in mice: comparison of different application methods and correlation of bacterial numbers and histopathology.** *Exp Toxicol Pathol* 2002, **54**:127-133.
 44. Smith G: **A simple non-surgical method of intrabronchial instillation for the establishment of respiratory infections in the rat.** *Lab Animals* 1991, **25**:46-49.
 45. Bivas-Benita M, Zwier R, Junginger HE, Borchard G: **Non-invasive pulmonary aerosol delivery in mice by the endotracheal route.** *Eur J Pharm Biopharm* 2005, **61**:214-218.
 46. Yadav V, Sharma S, Harjai K, Mohan H, Chibber S: **Induction & resolution of lobar pneumonia following intranasal instillation with *Klebsiella pneumoniae* in mice.** *Indian J Med Res* 2003, **118**:47-52.
 47. Codrons V, Vanderbist F, Ucakar B, Preat V, Vanbever R: **Impact of formulation and methods of pulmonary delivery on absorption of parathyroid hormone (1-34) from rat lungs.** *J Pharm Sci* 2004, **93**:1241-1252.
 48. Wheeldon EB, Walker ME, Murphy DJ, Turner CR: **Intratracheal aerosolization of endotoxin in the rat: a model of the adult respiratory distress syndrome (ARDS).** *Lab Anim* 1992, **26**:29-37.
 49. Brown RH, Walters DM, Greenberg RS, Mitzner W: **A method of endotracheal intubation and pulmonary functional assessment for repeated studies in mice.** *J Appl Physiol* 1999, **87**:2362-2365.
 50. Bivas-Benita M, van Meijgaarden KE, Franken KL, Junginger HE, Borchard G, Ottenhoff TH, Geluk A: **Pulmonary delivery of chitosan-DNA nanoparticles enhances the immunogenicity of a DNA vaccine encoding HLA-A*0201-restricted T-cell epitopes of *Mycobacterium tuberculosis*.** *Vaccine* 2004, **22**:1609-1615.
 51. Boersma FP, Wieringa RA: **Rat intubation. A method for safe and fast intubation of the rat trachea under direct vision.** *Anaesthetist* 1982, **31**:239-240.
 52. Medd RK, Heywood R: **A technique for intubation and repeated short-duration anaesthesia in the rat.** *Lab Anim* 1970, **4**:75-78.
 53. Diemel RV, Walch M, Haagsman HP, Putz G: **In vitro and in vivo intrapulmonary distribution of fluorescently labeled surfactant.** *Crit Care Med* 2002, **30**:1083-1090.
 54. Suarez S, Garcia-Contreras L, Sarubbi D, Flanders E, O'Toole D, Smart J, Hickey AJ: **Facilitation of pulmonary insulin absorption by H-MAP: pharmacokinetics and pharmacodynamics in rats.** *Pharm Res* 2001, **18**:1677-1684.
 55. Rees DD, Brain JD: **Effects of cystic fibrosis airway secretions on rat lung: role of neutrophil elastase.** *Am J Physiol* 1995, **269**:L195-202.

56. Finlay WH: *The Mechanics of Inhaled Pharmaceutical Agents An Introduction*. London, UK: Academic Press; 2001. p. 306.
57. Beck SE, Laube BL, Adams R, Chesnut KA, Flotte TR, Guggino WB: **Deposition of aerosolized AAV vectors in the lungs of rhesus macaques.** *Pediatr Pulmonol* 1999, **Suppl**:A229.
58. Beck SE, Laube BL, Barberena CI, Fischer AC, Adams RJ, Chesnut K, Flotte TR, Guggino WB: **Deposition and expression of aerosolized rAAV vectors in the lungs of Rhesus macaques.** *Mol Ther* 2002, **6**:546-554.
59. Garcia-Contreras L, Morcol T, Bell SJ, Hickey AJ: **Evaluation of novel particles as pulmonary delivery systems for insulin in rats.** *AAPS PharmSci* 2003, **5**:Article 9, 11 pages.
60. Patton JS, Bukar J, Nagarajan S: **Inhaled insulin.** *Adv Drug Deliv Rev* 1999, **35**:235-247.
61. Fischer AC, Beck SE, Smith CI, Laube BL, Askin FB, Guggino SE, Adams RJ, Flotte TR, Guggino WB: **Successful transgene expression with serial doses of aerosolized rAAV2 vectors in rhesus macaques.** *Mol Ther* 2003, **8**:918-926.
62. Munson K, Tatalick L, Smith CI, Fischer AC, Anklesaria P, Carter B, Guggino WB: **Comparison of AAV2 and AAV2/5 CFTR Vectors in the Lungs of Cynomolgus Macaques.** *Pediatr Pulmonol* 2004, **38**:259.
63. Delepine P, Montier T, Lerondel S, Le Pape A, Ferec C: **Imaging on Small Rodents for Gene Transfer Studies: Interest for Biodistribution and Expression.** *Mol Ther* 2003, **7**:19.
64. Delepine P, Montier T, Guillaume C, Vaysse L, Le Pape A, Ferec C: **Visualization of the transgene distribution according to the administration route allows prediction of the transfection efficacy and validation of the results obtained.** *Gene Ther* 2002, **9**:736-739.
65. Pokreisz P, Fleming I, Kiss L, Barbosa-Sicard E, Fisslthaler B, Falck JR, Hammock BD, Kim IH, Szelid Z, Vermeersch P, Gillijns H, Pellens M, Grimminger F, van Zonneveld AJ, Collen D, Busse R, Janssens S: **Cytochrome P450 epoxygenase gene function in hypoxic pulmonary vasoconstriction and pulmonary vascular remodeling.** *Hypertension* 2006, **47**:762-770.
66. Borchard G, Bivas-Benita M, Junginger HE: **Developing and Testing of Drug Carrier Systems for Pulmonary Drug Delivery.** In: *International Conference on MEMS, NANO, and Smart Systems (ICMENS)* 2004; Banff, Alberta, Canada: IEEE, pg. 5.
67. Chen BT, Yeates DB: **Differentiation of ion-associated and osmotically driven water transport in canine airways.** *Am J Respir Crit Care Med* 2000, **162**:1715-1722.
68. Chen BT, Yeates DB: **Ion transport and regulation of respiratory tract fluid output in dogs.** *J Appl Physiol* 2001, **90**:821-831.
69. Gagnadoux F, Pape AL, Lemarie E, Lerondel S, Valo I, Leblond V, Racineux JL, Urban T: **Aerosol delivery of chemotherapy in an orthotopic model of lung cancer.** *Eur Respir J* 2005, **26**:657-661.

70. Gagnadoux F, Le Pape A, Urban T, Montharu J, Vecellio L, Dubus JC, Leblond V, Diot P, Grimbert D, Racineux JL, Lemarie E: **Safety of pulmonary administration of gemcitabine in rats.** *J Aerosol Med* 2005, **18**:198-206.
71. **Use of Acetaminophen as an Analgesic in Rodents.** In: *Laurentian University: Standard Operating Procedure.* <http://www.laurentian.ca/NR/rdonlyres/588D064E-2873-42F2-A035-59D0F62AE553/11494/acetaminophensop.doc>. Viewed June 7, 2009.
72. Woods A: **Hematoxylyn and Counterstains.** In: *Laboratory Histopathology: A Complete Reference.* Eds. Woods A, Ellis R. Livingstone: Churchill Livingstone; 1994.
73. Beaulac C, Clement-Major S, Hawari J, Lagace J: **Eradication of mucoid *Pseudomonas aeruginosa* with fluid liposome-encapsulated tobramycin in an animal model of chronic pulmonary infection.** *Antimicrob Agents Chemother* 1996, **40**:665-669.
74. Smith AL, Ramsey BW, Montgomery AB: **Aminoglycoside formulation for aerosolization.** © 1996, Pathogenesis Corporation. US Patent No. 5508269, 28 pages.
75. **GraphPad InStat** Version 3.06 for Windows 95 © 2003, GraphPad Software: San Diego, California; <http://www.graphpad.com>.
76. Westphal O, Jann K: **Bacterial lipopolysaccharides.** *Methods Carb Chem* 1965, **5**:83-91.
77. Heckels JE, Virji M: **Separation and purification of cell surface components.** In: *Bacterial Cell Surface Techniques.* Eds. Hancock I, Poxton I. Chichester, UK: John Wiley and Sons; 1988: 91-95.
78. **MicroSprayer® Model IA-1B.** Philadelphia, PA: PennCentury, Inc. http://www.penncentury.com/products/IA_1B.php. Viewed June 7, 2009.
79. van Rozendaal BA, van de Lest CH, van Eijk M, van Golde LM, Voorhout WF, van Helden HP, Haagsman HP: **Aerosolized endotoxin is immediately bound by pulmonary surfactant protein D *in vivo*.** *Biochim Biophys Acta* 1999, **1454**:261-269.
80. Vreugdenhil HA, Haitsma JJ, Jansen KJ, Zijlstra J, Plotz FB, Van Dijk JE, Lachmann B, Van Vught H, Heijnen CJ: **Ventilator-induced heat shock protein 70 and cytokine mRNA expression in a model of lipopolysaccharide-induced lung inflammation.** *Intensive Care Med* 2003, **29**:915-922.
81. Moxley MA, Baird TL, Corbett JA: **Adoptive transfer of acute lung injury.** *Am J Physiol Lung Cell Mol Physiol* 2000, **279**:L985-993.
82. Perng WC, Wu CP, Chu SJ, Kang BH, Huang KL: **Effect of hyperbaric oxygen on endotoxin-induced lung injury in rats.** *Shock* 2004, **21**:370-375.
83. Lopez A, Yong S: **Injury versus inflammatory response in the lungs of rats intratracheally inoculated with bacterial lipopolysaccharide.** *Am J Vet Res* 1986, **47**:1287-1292.
84. Garcia-Contreras L, Sarubbi D, Flanders E, O'Toole D, Smart J, Newcomer C, Hicke AJ: **Immediate and short-term cellular and**

- biochemical responses to pulmonary single-dose studies of insulin and H-MAP.** *Pharm Res* 2001, **18**:1685-1693.
85. Hataishi R, Kobayashi H, Takahashi Y, Hirano S, Zapol WM, Jones RC: **Myeloperoxidase-associated tyrosine nitration after intratracheal administration of lipopolysaccharide in rats.** *Anesthesiology* 2002, **97**:887-895.
86. Spond J, Chapman R, Fine J, Jones H, Kreutner W, Kung TT, Minnicozzi M: **Comparison of PDE 4 inhibitors, rolipram and SB 207499 (ariflo), in a rat model of pulmonary neutrophilia.** *Pulm Pharmacol Ther* 2001, **14**:157-164.
87. Rietschel ET, Schade U, Jensen M, Wollenweber HW, Luderitz O, Greisman SG: **Bacterial endotoxins: chemical structure, biological activity and role in septicemia.** *Scand J Infect Dis Suppl* 1982, **31**:8-21.
88. Sera T, Fujioka H, Yokota H, Makinouchi A, Himeno R, Schroter RC, Tanishita K: **Localized compliance of small airways in excised rat lungs using microfocal X-ray computed tomography.** *J Appl Physiol* 2004, **96**:1665-1673.
89. Amano H, Oishi K, Sonoda F, Senba M, Wada A, Nakagawa H, Nagatake T: **Role of cytokine-induced neutrophil chemoattractant-2 (CINC-2) alpha in a rat model of chronic bronchopulmonary infections with *Pseudomonas aeruginosa*.** *Cytokine* 2000, **12**:1662-1668.
90. Kitazawa H, Sato A, Iwata M: **A study of bronchus-associated lymphoid tissue in a rat model of chronic pulmonary infection with *Pseudomonas aeruginosa*.** *Kansenshogaku Zasshi* 1997, **71**:214-221.
91. Sant SB, Gill KS, Burrell RE: **Nanostructure, dissolution and morphology characteristics of microcidal silver films deposited by magnetron sputtering.** *Acta Biomaterialia 2nd TMS Symposium on biological materials science* 2007, **3**:341-350.

Chapter 7 – Anti-inflammatory Activity of Nanocrystalline Silver-Derived Solutions Varies with Dissolution Conditions¹

Introduction

Although nanocrystalline silver dressings were originally introduced as antimicrobial burn dressings about a decade ago, studies have suggested that these dressings have pro-healing and/or anti-inflammatory activity in infected wounds, rashes, and meshed skin grafts[1-5]. The study of Chapter 2 showed that, unlike solutions that contain only Ag^+ , nanocrystalline silver has anti-inflammatory activity independent of its antimicrobial activity in a porcine contact dermatitis model. The study of Chapter 3 suggested that this effect may be translocatable or systemic, although the effect was weaker with treatment away from the site of injury relative to direct treatment. Another study has shown that, in a murine model of ulcerative colitis, proprietary nanocrystalline silver nanodispersions in polyvinyl alcohol/water delivered intracolonicly or orally (at 10 times the dose) suppressed the expression of matrix metalloproteinase (MMP)-9, $\text{TNF-}\alpha$, $\text{IL-1}\beta$, and IL-12 [6]. This suggests that nanocrystalline silver has anti-inflammatory activity which could be used to treat internal epithelial tissues, as well as the skin.

The anti-inflammatory activity of nanocrystalline silver appears to be due to its dissolution products. Its unique dissolution products may result from its small grain size combined with its polycrystallinity, as indicated in Chapter 4, which together result in a high percentage of high energy grain boundaries and defect structures from which unique silver species can dissolve into aqueous

¹ A version of this chapter has been submitted for publication. Nadworny, Wang, Tredget, and Burrell 2009. Journal of Inflammation.

solutions[7]. One of these unique species released into solution is Ag^0 , which is likely released in a cluster form[7]. Ag^0 is the most likely species to have anti-inflammatory activity, since other noble metals have demonstrated similar activity[8-12], as discussed in Chapters 1 and 2.

While the anti-inflammatory activity of nanocrystalline silver appears to be potent[13], in its current configuration direct nanocrystalline silver dressing applications are limited to treatment of surfaces, and even in surface applications, tissue contact can be problematic. Since nanocrystalline silver is active via its dissolution products, it is possible that silver-containing solutions could be generated which have some or all of the properties of the nanocrystalline silver dressings. Solutions with these properties would be valuable for anti-inflammatory/pro-healing medical applications including treatment of hard-to-dress surfaces, such as tunneling wounds, and inflammatory conditions of internal epithelial tissues including the lungs (for example, acute respiratory distress syndrome – ARDS, and pneumonia) and the gastrointestinal tract (for example, inflammatory bowel disease – IBD). The purpose of this study was to test solutions, derived from nanocrystalline silver under various conditions, for anti-inflammatory activity in a known model of inflammation, since the results of Chapter 6 were inconclusive due to the fact that only one nanocrystalline silver-derived solution was tested and the rat models of infection and inflammation used showed high variability due to the use of the microsprayer.

Materials and Methods

Materials

Unless otherwise mentioned, reagents were purchased from Fisher Scientific Inc.

Silver-containing solutions were generated as follows: Nanocrystalline silver dressings (Acticoat™) were added at a ratio of 1 in²/mL to the following solutions: distilled water (referred to as the pH 5.6 solution), distilled water adjusted to a pH of 4 by bubbling carbon dioxide through the water as described in Chapter 5 (referred to as the pH 4 solution), distilled water adjusted to a pH of 7 by adding calcium hydroxide drop-wise as described in Chapter 5 (referred to as the pH 7 solution), or distilled water adjusted to a pH of 9 by adding calcium hydroxide drop-wise as described in Chapter 5 (referred to as the pH 9 solution). Containers were sealed and dissolution was allowed to proceed for 24h at room temperature under stirring at 100 rpm prior to use.

Animals

18 young domestic, commercially produced, Large White/Landrace swine (15-20 kg) were used in this study. The animals selected were healthy and without significant wounds or scars on their backs. The animals were kept in individual pens at the Swine Research and Technology Centre (Edmonton, AB) with a 12 hour light/dark cycle, where they were allowed to acclimatize seven days prior to starting experiments. Three animals were used in all experimental groups. The animals received antibiotic-free water and hog ration *ad libitum* during the first three weeks of the experiment. Rations were limited prior to

procedures on Days 0 through 3. The study was approved by the University of Alberta Health Sciences Animal Policy and Welfare Committee (HSAPWC, renamed the Animal Policy & Welfare Division of the Research Ethics Office - REO), and was conducted with humane care of the animals in accordance with guidelines established by the CCAC.

Sensitization to DNCB and Elicitation of Inflammatory Reaction

Inflammation was induced using DNCB, similar to procedures described in the literature[1, 14-16]. On Day -14, the hair on the left side of the backs of 15 pigs was shaved using electric clippers. 10% DNCB (in 4:1 acetone:olive oil) was painted over an area of approximately 15 cm x 25 cm on the shaved portion of the back, which was caudal to the scapula running over the rib cage and five centimetres off the dorsal median line. The total body surface area painted was about 5%, as determined by the equation of Kelley *et al.*[17]. The volume of DNCB painted per pig was 3 mL on average. This procedure was repeated on Days -7, -3, and 0. On Day -1, pigs were given fentanyl patches on shaved skin away from the rash, to avoid discomfort to the pigs during the final application and treatment. As well, the same area on the right side of the back was shaved using the procedure described previously, and then on Day 0 this side was painted with DNCB using the same technique as for the left side. The remaining three pigs, which were used as negative controls, were left unexposed to DNCB, but also were shaved and received fentanyl patches on Day -1.

Treatment

Four hours after the final application of DNCB, treatment was commenced

with the pigs being placed under general anesthetic. On Day 0, visual observations were made, blood samples were taken from the anterior vena cava, and five 4 mm biopsies were obtained from the rashes on either side of the animal. Biopsies were obtained towards the front of the rash (cephalic region), but well within the border of the rash, to ensure that the biopsies were taken from areas which had received good DNCB contact. On subsequent days, biopsies were taken in a line towards the rear of the pig, spaced sufficiently far apart that the new biopsies would not be affected by the previous biopsies, and would still be well within the border of the DNCB-painted area. Biopsies taken on each day were randomly assigned for different analyses. From each side of each animal, one biopsy was placed in 4% paraformaldehyde and kept at room temperature; one biopsy was placed in 0.9% saline, and later placed in an OCT card in a liquid nitrogen bath, covered with Shandon Cryomatrix, and placed in a freezer at -80°C for long term storage; and the other three biopsies were snap-frozen in liquid nitrogen and then stored at -80°C . (It should be noted that all the snap-cooled biopsies taken at 24 hours were moved from -80°C to a fridge freezer by an unknown person and remained there until they were discovered over a month later. It is unknown whether biopsies from other time points also spent time in the fridge freezer or not.)

Calcium alginate dressings were used to reach hemostasis after biopsies were taken. The pigs' rashes on both sides of their backs were then treated. Three positive controls (with rashes) and three negative controls were treated with distilled water-soaked rayon/polyester gauze. Three pigs were each treated with

rayon/polyester gauze soaked in pH 4, pH 5.6, pH 7, or pH 9 silver-containing solutions which were generated as described above. New fentanyl patches were applied, if they had come loose. Surgical drape was placed over each dressing to provide moisture control, and elastic adhesive dressing was wrapped around the pigs' rash areas to hold the dressings in place.

The procedure of Day 0 was repeated on Day 1 and Day 2, except that no blood samples were taken. On Day 3, blood samples, visual images and scores, and biopsies were again taken. However, rather than being re-bandaged, the pigs were then euthanized using Euthansol (>150 mg/kg) while they were still under anesthesia.

Total Silver Analysis

Samples of nanocrystalline silver derived solutions were obtained daily at the time of treatment, and submitted for total silver analysis by atomic absorption spectroscopy (AAS). For AAS, a Varian 220 FS double beam Atomic Absorption Spectrophotometer was used, with the following instrument parameters: an Ag hollow cathode lamp with a wavelength of 328.1 nm, and a lean air-acetylene flame. A calibration plot was generated using silver standards of 0.5, 1.0, 3.0, and 5.0 ppm, prepared from a silver standard stock solution of 1000 ppm. If the solutions contained more than 5 ppm silver, they were diluted as necessary with distilled water until they were in the linear range for silver analysis (0.1 ppm to 5 ppm).

Visual Observations

Pictures were taken of the rash areas regularly during the sensitization

period (for the left-hand side) and on each treatment day (both sides). Scales were included in the pictures on treatment days with the use of wound rulers. Erythema and edema on each side of each animal were graded on a scale of 0-4 on Days 0 through 3, using the same scales as in Chapter 2. The pigs were also scored on the level of bleeding at biopsy sites on both sides on Day 2 and Day 3, with -1 indicating minimal bleeding, 0 indicating moderate bleeding, 1 indicating considerable bleeding, and 1.5 indicating strong bleeding.

Histopathology

All samples to be paraffinized were placed in 4% neutral buffered paraformaldehyde as described above. They were then rinsed with PBS three times before being placed in 70% ethanol and stored at 4°C. The samples were then dehydrated in alcohol and xylene; oriented and embedded in paraffin; and sectioned (5 µm). For histopathological analysis, sections were stained with hematoxylin and eosin following standard procedures[18]. Images were taken of the epidermal-dermal junction (or the surface of the tissue if there was no clear junction due to tissue damage caused by the rashes), for each side of each animal at each time point at 100x magnification using an optical microscope with an attached digital camera. Based on the results of visual and histological data, all subsequent analyses were performed only on samples taken from the rashes treated four times with DNCB.

mRNA Signal Detection and Quantification

Tissue Powdering. To extract RNA, tissues were powdered using a Mikro-Dismembrator, similar to the procedure above. Prior to use, dismembrator

chambers and metal balls were placed in 10% bleach for half an hour. They were then washed, rinsed with ddH₂O, and dried. Tissue samples were removed from -80°C and placed in liquid nitrogen for at least five minutes. Half the tissues were then cut into vertical slices with a scalpel, and placed in dismembrator chambers with two metal balls. The chambers were clamped shut and placed in liquid nitrogen for five more minutes. Chambers were then placed in the dismembrator and powdered. 1 mL of Trizol was added to the powdered samples and then collected into 1.5 mL tubes. Tubes were stored at -80°C until extraction and purification were performed.

RNA Extraction. RNA extraction and purification was performed using a Qiagen RNeasy® Mini Kit by following the manual provided (Qiagen, Inc., Mississauga, Ontario, Canada). The tubes were centrifuged for 30 minutes at 12 000 rpm. Next, 300 µL of chloroform was added to each tube. The tubes were vortexed for 15 seconds, and then allowed to stand at room temperature for 5 minutes. The samples were then spun at 12 000 rpm for 15 minutes. The aqueous phase, which was about 600 µL, was transferred to new tubes and the organic phase was discarded. Next, 600 µL of 70% ethanol was added to each tube, and the tubes were mixed by inversion. 600 µL of the samples were loaded into spin columns and then spun at 12 000 rpm for 15 seconds. The collection tubes were emptied and then placed back under the columns. The remainder of the sample was placed into the columns and spun (12 000 rpm, 15 s). Again the collection tubes were emptied and replaced. 350 µL of RW1 wash buffer was added to the spin columns and the columns were spun (12 000 rpm, 15 s). New collection

tubes were placed under the columns, and 10 μL of Qiagen DNase in 70 μL of DNase buffer was added onto the spin column membranes. The columns were spun again (12 000 rpm, 15 s), and the spin through was pipetted back onto the columns which were then allowed to sit at 37°C for one hour to break down any DNA in the samples. The columns were then spun (12 000 rpm, 15 s). 350 μL of RW1 wash buffer was then loaded onto each column and the columns were again spun (12 000 rpm, 15 s). The collection tubes were emptied and replaced on the columns. 500 μL of RPE wash buffer was added to each column and the columns were spun again (12 000 rpm, 15 s). The collection tubes were emptied and then this step was repeated. The spin columns were transferred to 1.5 mL tubes and loaded with 40 μL of RNase free water. The columns were then incubated at room temperature for 15 minutes, and then spun at 12 000 rpm for one minute. The spin columns were then discarded and the tubes were stored at -80°C until use.

RNA Quantification. 396 μL of double distilled water was placed into a 1.5 mL tube, and 4 μL of an RNA sample was added. A spectrophotometer (Unicam, Helios, Thermo Fisher Scientific, Inc.), which was zeroed using double distilled water, was used to measure optical densities of the RNA-containing samples at 260 nm. The concentration of RNA in each sample was calculated using formula (1) of Chapter 2.

Reverse Transcription (creation of cDNA). 1 μL of dNTP, 1 μL of random nonamers, 0.256 μg of RNA as calculated above, and enough distilled water to bring the volume to 10 μL were added to a thin-walled PCR

microcentrifuge tube. The contents were mixed and centrifuged (15 s, 12 000 rpm). The tubes were then placed at 70°C for 10 minutes, followed by centrifugation (15 s, 12 000 rpm). Next 2 µL of 10x buffer for eAMV-RT, 1 µL of enhanced avian RT, 1 µL of RNase inhibitor, and 6 µL of distilled water were added while the samples were on ice. The tubes were incubated at 25°C for 15 minutes, and then incubated at 42°C for one hour, followed by 75°C for five minutes. cDNA was kept on ice for immediate use.

Primers. Primers were designed using Primer Express® Software for Real-Time PCR Version 3.0 (© 2004, Applied Biosystems), and were synthesized by Operon Biotechnologies, Inc. (Huntsville, Alabama, USA):

Porcine HPRT forward primer: CGGCTTGCTCGAGATGTGAT

Porcine HPRT reverse primer: GCACACAGAGGGCTACGATGT

Porcine GAPDH forward primer: TCATCATCTCTGCCCCTTCTG

Porcine GAPDH reverse primer: CATGGTTCACGCCATCAC

Porcine IL-1β forward primer: CACCTCTCAAGCAGAACAAAAGC

Porcine IL-1β reverse primer: ATCTTGGCGGCCTTTGG

Porcine IL-8 forward primer: GCTCTCTGTGAGGCTGCAGTT

Porcine IL-8 reverse primer: TTTATGCACTGGCATCGAAGTT

Porcine IL-10 forward primer: TGGGTTGCCAAGCCTTGT

Porcine IL-10 reverse primer: GCCTTCGGCATTACGTCTTC

Porcine IL-12 forward primer: GCCCAGGAATGTTCAAATGC

Porcine IL-12 reverse primer: TGTTGCTGACGGCCTTCAG

Porcine IL-17 forward primer: CGCCACTGCCCAACTC

Porcine IL-17 reverse primer: TGCAGCCCCTGTCACCAT

Porcine IL-31 forward primer: CCAGCCGCCAAACAACAT

Porcine IL-31 reverse primer: GCTGTCTGATTGTCTTGAGATATGC

Porcine TNF- α forward primer: CGACTCAGTGCCGAGATCAA

Porcine TNF- α reverse primer: CCTGCCAGATTCAGCAAAG

DNase/RNase free water (Bio-Rad) was added to the lyophilized primers for a primer concentration 100 μ M.

Real Time RT-PCR. Real time RT-PCR was performed on cDNA samples created as described above using both HPRT and GAPDH primers as housekeeping genes. Master mixes were made, consisting of 325 μ L SYBR green master mix (ABI), 3 μ L forward primer, 3 μ L reverse primer, and 189.8 μ L DNase/RNase free H₂O. 20 μ L of the master mix was placed in each well of a 96 well plate, and then 5 μ L of each cDNA sample was added to each well. Wells containing PCR grade H₂O, rather than sample cDNA, served as controls for the experiment. The plates were sealed and placed into an Applied Biosystems 7300 Real Time PCR System using Applied Biosystems Sequence Detection Software Version 1.3.1 with the 7300 System SDS Software RQ Study Application and the SDS Relative Quantification Study Plug In (© 2005 Applied Biosystems, Ltd., Foster City, CA, USA). The runs were performed using the standard 7300 run mode with the following settings: The volume was set to 25 μ L, Stage 1 had one repetition at 50°C for two minutes, Stage 2 had one repetition at 95°C for 10 minutes, Stage 3 had 40 repetitions at 95°C for 15 seconds, each followed by a hold at 60°C for one minute, when data collection occurred. Analysis of the

results was performed in Excel using Equations 2-2 to 2-4, where the housekeeping gene was either HPRT or GADPH (glyderaldehyde 3-phosphate dehydrogenase).

Gelatinase Zymography

Gelatinase activity was measured using the methods described in Chapter 2, with some minor modifications. To extract protein, half of a snap-frozen tissue sample from each animal was homogenized using a Mikro-Dismembrator. Prior to use, the chambers and metal balls for the dismembrator were soaked in detergent overnight, scrubbed, rinsed with distilled water, and allowed to air dry. Tissue samples were taken from -80°C and snap-cooled in liquid nitrogen for five minutes. They were then sliced thinly using a scalpel, placed into a dismembrator chamber with two metal balls, and the chambers were clamped shut and placed back in the liquid nitrogen for at least five minutes. The samples were powdered in the dismembrator for 30s at 2600 rpm. All tissues were homogenized on the first try using this procedure. 1 mL aliquots of lysis buffer (1% Triton-X 100, and 20% glycerol in 10 mmol/L PBS) were added to powdered samples to extract the protein. Homogenates were centrifuged at 13 000 rpm for 30 minutes at 4°C to remove debris. The supernatants were collected. To quantify the total protein extracted, a BCA protein assay reagent kit was used. 1 µL of samples were added to 799 µL aliquots of distilled water and 200 µL of Bio-Rad protein assay dye, and the optical densities were measured at 595 nm using a spectrophotometer and compared the BSA standard curve generated in Chapter 2. A 0 µg/mL sample was used to zero the spectrophotometer.

Protease activity was run on gelatin zymographs[19]. The methods used were similar to those of Chapter 2, with modifications. To run the zymogram, 1.5 mm thick 12% polyacrylamide separating gels with 0.15% gelatin were made (6.6 mL double distilled water, 2 mL 1% gelatin, 5 mL 1.5 M Tris-HCl pH 8.8, 200 μ L 10% SDS, 6 mL 40% acrylamide/bis, 100 μ L 10% APS, 10 μ L TEMED). The gels were allowed to solidify for half an hour under a cover of isopropyl alcohol to prevent oxidation. Stacking gels were made (6.4 mL double distilled water, 2.52 mL 0.5M Tris-HCl, 100 μ L 10% SDS, 1 mL 40% acrylamide/bis, 50 μ L 10% APS, 10 μ L TEMED), poured over the separating gel, and allowed to set for about half an hour with a comb in it. 10X loading buffer left over from the experiments of Chapter 2 was thawed and filtered before use. 10X running buffer was made as per Chapter 2. Gels were placed in the electrophoresis chamber, which was filled with 1X running buffer. Samples were applied to the gels under non-reducing conditions without heating. 10 μ L of protein ladder (SDS-PAGE) was placed in the first well. In subsequent wells, samples were loaded containing 50 μ g of protein in 1x loading buffer plus the amount of extraction buffer required to produce a total volume of 50 μ L. The gel was run at 50V for approximately 20 minutes, and then increased to 150V for another hour. The stacking gel was removed from the separating gel, which was then placed in 2% Triton-X 100 and shaken on a gyratory shaker for 20 minutes at room temperature to wash off the SDS. Next, the gel was placed in developing buffer (50 mM Tris pH 8.0, 0.1 mM CaCl_2) and incubated overnight at 37°C. The gel was rinsed with distilled water and stained in 100 mL of coomassie blue (0.25% coomassie brilliant blue, 10%

acetic acid, 40% methanol, 50% double distilled water) on the shaker for 30 minutes. Excess stain was then removed by placing the gel in a destaining solution (50 mL acetic acid, 200 mL methanol, 250 mL double distilled water) for 40 minutes on the shaker. The gel was rinsed with distilled water, and images were then taken of the gel. The gels were then preserved using a Promega Gel Drying Kit as described in Chapter 2. Gelatinase activity appears as a clear band (indicative of cleavage of the gelatine substrate) on a blue background. For quantitative analysis, photographs of the gels were loaded into AlphaImager software. The integrated density value (IDV) of each band was measured, holding the band area constant. Each IDV was then divided by the IDV of a portion of the gel background of the same area, to correct for differences in gel densities between the four gels required to run all the samples.

Apoptosis Detection

Detection of the presence of apoptotic cells in tissue samples after 24 hours of treatment was determined using the In Situ Cell Death Detection Kit, as described in Chapter 3, with a few modifications. Briefly, testing was performed on paraffinized tissue samples following the manual provided with the kit[20]. Dewaxing and rehydration was performed as described in Chapter 2. After rehydration, the samples were treated with 100 μ L proteinase K at a working concentration of approximately 25 μ g/mL, and incubated for half an hour at 37°C. The slides were then rinsed three times for five minutes each in 1xPBS.

Tissues were then incubated overnight with a FITC-labeled dNTP and TdT enzyme working solution at 4°C, as described in Chapter 2. Labeling

solution alone was added to tissues used as the negative controls for the apoptosis assay. After overnight incubation, the cells were rinsed in PBS three times for 10 minutes each. The tissue samples were mounted using a polyvinyl alcohol-based mounting medium containing 1:1000 DAPI (provided by the Cell Imaging Facility) for nuclear counterstain. Sections were then examined, and images obtained, using a Zeiss LSM510 multi-channel laser scanning confocal microscope at the Cell Imaging Facility. Images were taken using the following settings: objective: 40x 1.3; laser for DAPI: 364 nm, 1% power, 444 μ m pinhole; and laser for FITC: 488 nm, 4% power, 91 μ m pinhole. Images were taken of the deep dermis and of the epidermal-dermal junction, which was taken to be either where re-epithelialization was occurring or to be the tissue surface, if no re-epithelialization was observed in the tissue. Images selected to represent each group were median images in terms of their apoptotic staining. Semi-quantitative analysis was performed using ImageJ software (Rasband, W., v1.37, NIH, Rockville, MD, USA. © 2007). First, the epidermis or dermis was manually selected. An AND function was used to select only apoptotic staining which was colocalized with nuclear staining, in order to eliminate any background staining. The same thresholds were used for all samples, since they were stained and imaged under identical conditions. Total numbers of green (apoptotic staining) and blue (nuclear staining) pixels were counted, and a ratio of green to blue pixels was calculated to obtain a relative measure of apoptotic activity. Images in which apoptotic staining did not coincide with nuclear staining were excluded.

Immunohistochemistry

Tissue samples after 24h and 72h of treatment were analyzed for the presence of TNF- α , IL-4, IL-8, IL-10, TGF- β , EGF, KGF (FGF-7), and KGF-2 (FGF-10) using the methods of Chapter 3. Briefly, paraffinized samples were deparaffinized and rehydrated. To improve antigen retrieval, samples tested for TNF- α , IL-8, and KGF were incubated in 25 μ g/mL proteinase K at 37°C for 20 minutes. Samples were treated with 3% H₂O₂ for 30 minutes to quench endogenous peroxidase activity, and then blocked for one hour with the sera from the species that the secondary antibody was raised in (rabbit for TGF- β 1, KGF, KGF-2, and IL-4 analysis; goat for TNF- α , IL-8, IL-10, and EGF analysis). For TGF- β analysis, sections were then incubated for one hour with chicken-anti-hTGF- β 1 (10 μ g/mL, AF-101-NA, R&D Systems). Control tissues were incubated with PBS. The sections were subsequently incubated with rabbit-anti-chicken-HRP (Sigma, A 9046, 1:400 plus 2% pig serum) for an hour. For all other analyses, sections were incubated overnight at 4°C with 5 μ g/mL of the appropriate antibody: mouse-anti-pTNF- α (MP390, Endogen), mouse-anti-pIL-8 antibody (MP800, Endogen), goat-anti-pIL-4 (AF654, R&D Systems), mouse-anti-hEGF (MAB236, R&D Systems), mouse-anti-pIL-10 (MAB6932, R&D Systems), goat-anti-hFGF-7 (KGF, AF-251-NA, R&D Systems), or goat-anti-hFGF-10 (KGF-2, AF345, R&D Systems). For sections incubated with primary antibodies produced in mouse, negative control tissues were incubated with 5 μ g/mL mouse IgG. These sections were subsequently incubated with goat-anti-mouse-HRP (R&D Systems, 1:400 in 2% pig serum) for one hour. For sections

incubated with primary antibodies produced in goat, negative control tissues were incubated with PBS during the primary antibody incubation step. These sections were subsequently incubated with rabbit-anti-goat-HRP (R&D Systems, 1:400 in 2% pig serum). All tissues were then stained using 3,3'-diaminobenzidine and H₂O₂ (25 mg DAB, 50 µL H₂O₂ in 50 mL PBS), and counterstained with hematoxylin (30 seconds). The tissues were dehydrated and mounted using Permount™ mounting solution. Images of the samples were taken as described for histology images. Samples stained for one cytokine were run in three batches of twelve slides under identical conditions, including exposure time, temperatures, and dilutions. Each batch contained samples from all treatment groups. Therefore, the intensity of staining can be used as a semi-quantitative indication of the relative quantity of cytokines present in the tissues. Intensity of staining was scored on a scale from 0 to 4 as follows: 0 – no staining anywhere; 1 – very small areas of staining and/or very light staining; 2 – small areas of dark staining and/or larger areas of light staining; 3 – diffuse light staining and/or larger areas of dark staining, 4 – diffuse dark staining.

Statistics

Tests were performed on all three pigs from each group to confirm result reproducibility. For numerical results, one-way ANOVAs with Tukey-Kramer Multiple Comparisons post tests were performed for normally distributed data using GraphPad InStat version 3.06, unless otherwise indicated. For data which was not normally distributed (apoptotic staining data), Kruskal-Wallis Tests (non-parametric ANOVAs) were performed with Dunn's Multiple Comparisons post-

test, also using GraphPad InStat. Standard deviations are plotted as error bars for all data points on all figures. For some data points, the standard deviations were very small.

Results

Visual Assessment

Figure 7-1 shows representative digital images of rashes exposed four times to DNCB, as well as a negative control. Rash development occurred similar to observations made in Chapter 2, and therefore images of rash development are not shown. Rashes of all animals appeared very similar at Day 0. Images are shown of a negative control (a), a DNCB induced rash just prior to commencing treatment (b), a positive control (rash treated with distilled water) after 72 hours of treatment (c), and animals with rashes treated for 72 hours with pH 4 (d), 5.6 (e), 7 (f), and 9 (g) silver-containing solutions. Animals treated with pH 7 and 9 solutions showed the most improvement during treatment, with decreased redness and swelling around the rash edges, and areas where the scabbing had fallen off, revealing healthy tissue underneath. Animals treated with pH 4 and 5.6 solutions showed some improvement during treatment, with decreased redness around the edges of the rash. However, the scabbing mostly stayed in place for these treatment groups. Positive controls showed little improvement over 72 hours, with a full scab across the rash, and redness and swelling around the scab.

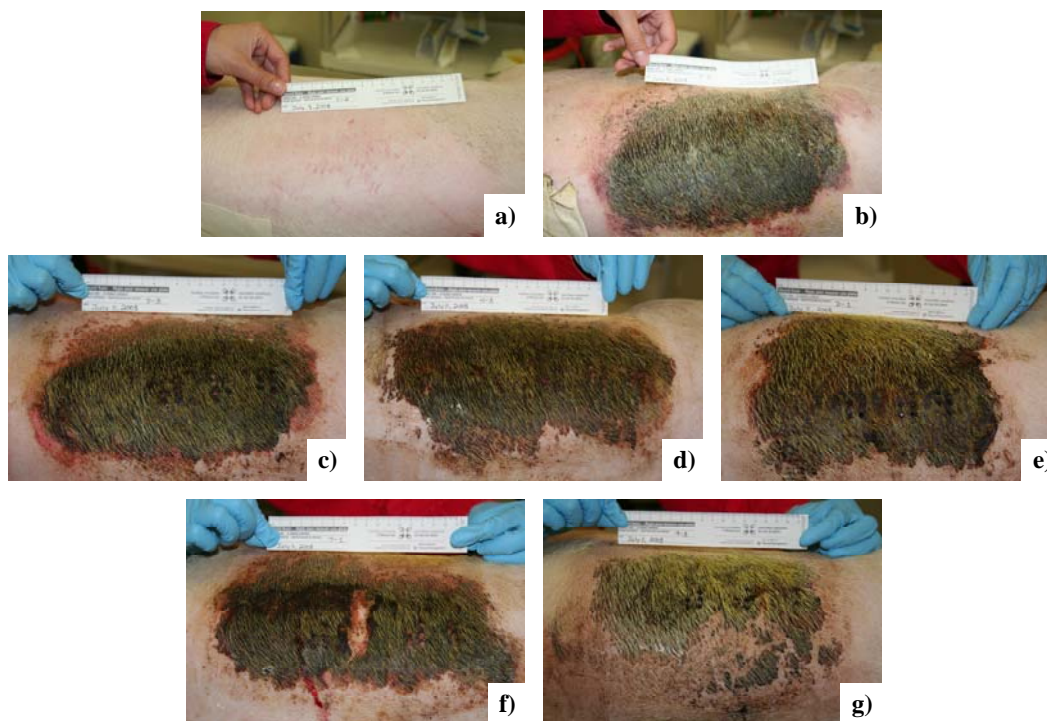


Figure 7-1. Digital images of rashes exposed to DNCB four times and then treated with various nanocrystalline silver-derived solutions. Representative digital images are shown for (a) negative controls (pigs which did not receive a rash, and were treated with distilled water-soaked dressings); (b) DNCB-induced rashes on Day 0 before treatment was commenced; (c) positive controls (pig which had DNCB-induced rashes and were treated with distilled water) after 72 hours of treatment; and animals treated for 72 hours with nanocrystalline silver-derived solutions with starting pHs of (d) 4, (e) 5.6, (f) 7, and (g) 9.

Figure 7-2 shows rash development on the side of the back that was only painted once with DNCB. In (a) and (b) are rashes of two positive controls from Day 0 through 3, showing the variability among animals in this group. The animal shown in (a) had the strongest response to DNCB at Day 1, and this still did not cover the entire rash area. At Day 3, the rash had nearly resolved. The animal shown in (b) had a much darker rash at Day 1, and this rash did not resolve by Day 3, although swelling appeared to be decreased. Figure 7-2c shows representative images of the rashes after one exposure to DNCB followed by

treatment with pH 4 solutions. Animals showed the strongest response to DNCB at Day 1, and had decreased redness and swelling by Day 3, although resolution of the rash was not complete. Figure 7-2d shows representative images of the rashes after one exposure to DNCB followed by treatment with pH 5.6 solutions. A distinct worsening of the rash between Day 0 and Day 1 was observed, with limited changes thereafter. Representative images of rashes after one exposure to DNCB followed by treatment with pH 7 solutions are shown in Figure 7-2e. Again, a distinct worsening of the rash occurred between Day 0 and Day 1, but decreased redness and swelling was observed between Days 2 and 3. Representative images of rashes after one exposure to DNCB followed by treatment with pH 9 solutions are shown in Figure 7-2f. The rash did not appear to worsen between Day 0 and Day 1 to the same extent as that observed in other treatment groups. There appeared to be little change between Day 1 and Day 3.

It is interesting to note that none of the animals showed an even rash over the entire painted area with a single application. A stronger rash appeared towards the backbone of the animal, with less rash appearing ventrally and caudally, despite the fact that care was taken to provide even distribution of the DNCB. A stronger rash can also be seen along the edge of the tape used to hold the fentanyl patch in place. This suggests that the DNCB soaked into the edge of the tape, resulting in a stronger rash there.



Figure 7-2.



Figure 7-2, continued.

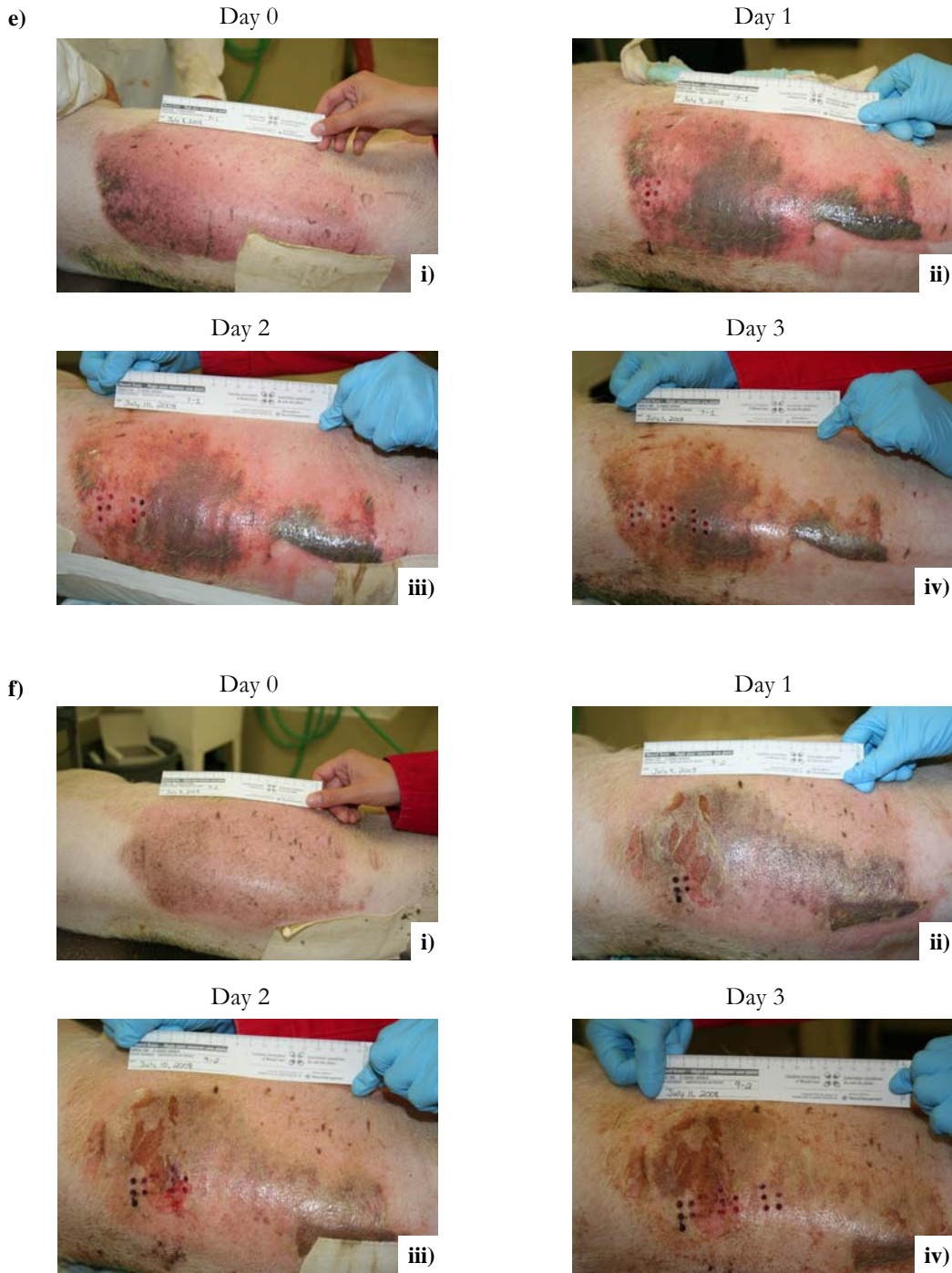


Figure 7-2. Digital images of rashes treated with various nanocrystalline silver-derived solutions on skin exposed once to DNCB after sensitization of the animal. After exposure to DNCB over two weeks on one side of the back, pigs were painted with DNCB once on the other side of their back on Day 0, and then began treatment. Panels (a) and (b) show the rash progression from Day 0 to Day 3 (i-iv) for two positive controls treated with distilled water-soaked gauze. Animals treated for 72 hours with nanocrystalline silver-derived solutions with starting pHs of (c) pH 4, (d) pH 5.6, (e) 7, and (e) 9 are shown on Days 0 through 3 (i-iv).

Figure 7-3 shows the average erythema scores for pigs treated with various nanocrystalline silver-derived solutions after four exposures to DNCB, relative to positive and negative controls. From 48 hours of treatment on, animals treated with pH 9 solutions had significantly lower erythema scores relative to positive controls and animals treated with pH 4 and pH 5.6 solutions.

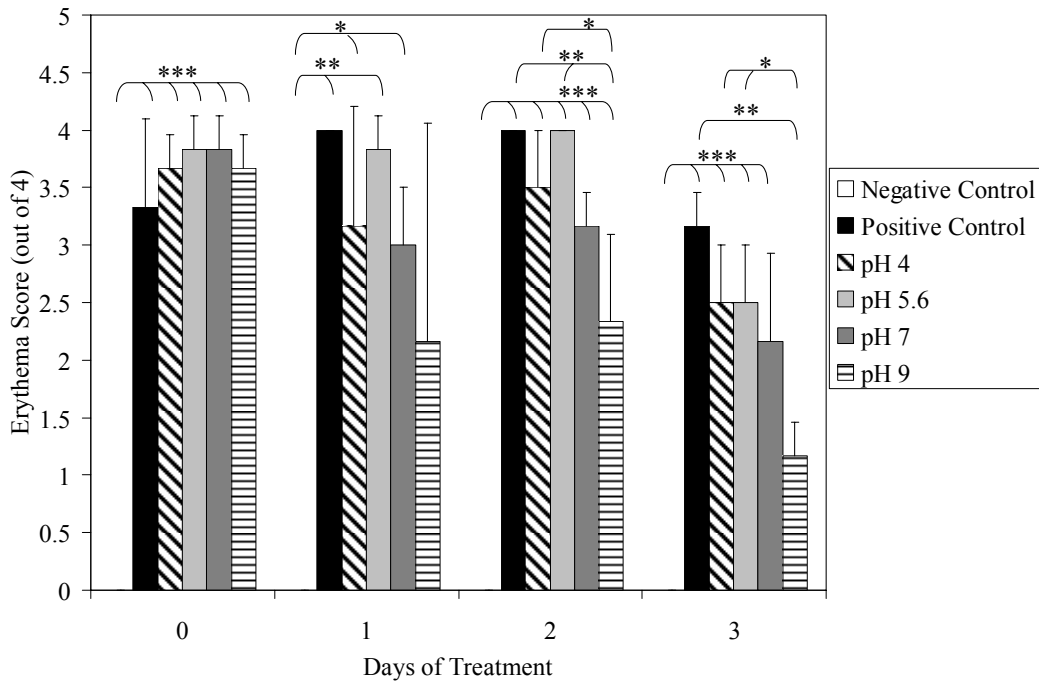


Figure 7-3. Erythema scores for porcine skin exposed to DNCB four times over two weeks and then treated with various nanocrystalline silver-derived solutions. Daily average erythema scores are shown for negative controls (pigs without rashes treated with distilled water-soaked dressings), and for pigs with DNCB-induced contact dermatitis treated for three days with distilled water (positive controls) or nanocrystalline silver-derived solutions with starting pHs of 4, 5.6, 7 or 9. The statistical analysis was performed using one-way ANOVAs with Tukey-Kramer Multiple Comparisons post tests. The overall p values from the one-way ANOVAs were <0.0001, 0.0018, <0.0001, and <0.0001 for Days 0, 1, 2, and 3, respectively. The results of the Tukey-Kramer post tests are indicated on the figure as follows: * indicates significantly different ($p < 0.05$), ** indicates very significantly different ($p < 0.01$), and *** indicates extremely significantly different ($p < 0.001$). Error bars represent standard deviations ($n = 3$ for all data points).

Figure 7-4 shows the average edema scores for pigs treated with various nanocrystalline silver-derived solutions after four exposures to DNCB, again relative to positive and negative controls. After 48 hours of treatment, animals treated with pH 4, 7, or 9 solutions had significantly lower edema scores relative to positive controls or to animals treated with pH 5.6 solutions. After 72 hours of treatment, animals treated with pH 9 solutions had significantly lower edema scores relative to positive controls and to animals treated with pH 4 solutions.

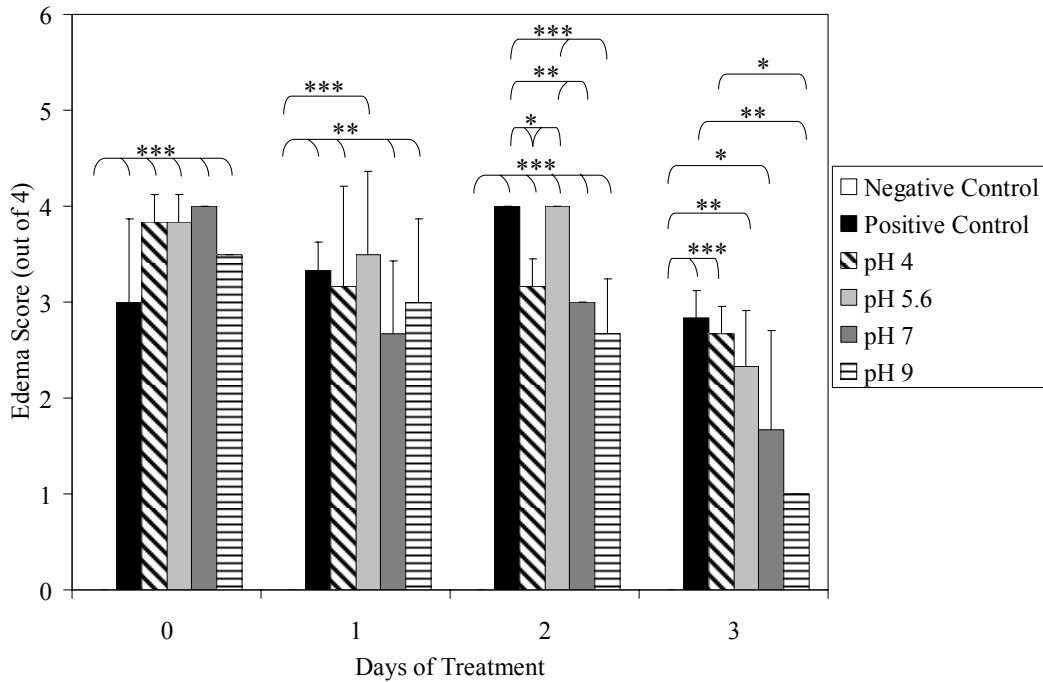


Figure 7-4. Edema scores for porcine skin exposed to DNCB four times over two weeks and then treated with various nanocrystalline silver-derived solutions. Daily average edema scores are shown for negative controls (pigs without rashes treated with distilled water-soaked dressings), and for pigs with DNCB-induced contact dermatitis treated for three days with distilled water (positive controls) or nanocrystalline silver-derived solutions with starting pHs of 4, 5.6, 7 or 9. The statistical analysis was performed using one-way ANOVAs with Tukey-Kramer Multiple Comparisons post tests. The overall p values from the one-way ANOVAs were <0.0001, 0.0007, <0.0001, and 0.0001 for Days 0, 1, 2, and 3, respectively. The results of the Tukey-Kramer post tests are indicated on the figure as follows: * indicates significantly different ($p < 0.05$), ** indicates very significantly different ($p < 0.01$), and *** indicates extremely significantly different ($p < 0.001$). Error bars represent standard deviations ($n = 3$ for all points).

Figure 7-5 shows the average biopsy bleeding scores for pigs treated with various nanocrystalline silver-derived solutions after four exposures to DNCB, relative to negative and positive controls. After 72 hours of treatment, animals treated with pH 9 solutions had significantly lower biopsy bleeding, relative to positive controls and animals treated with pH 4 solutions.

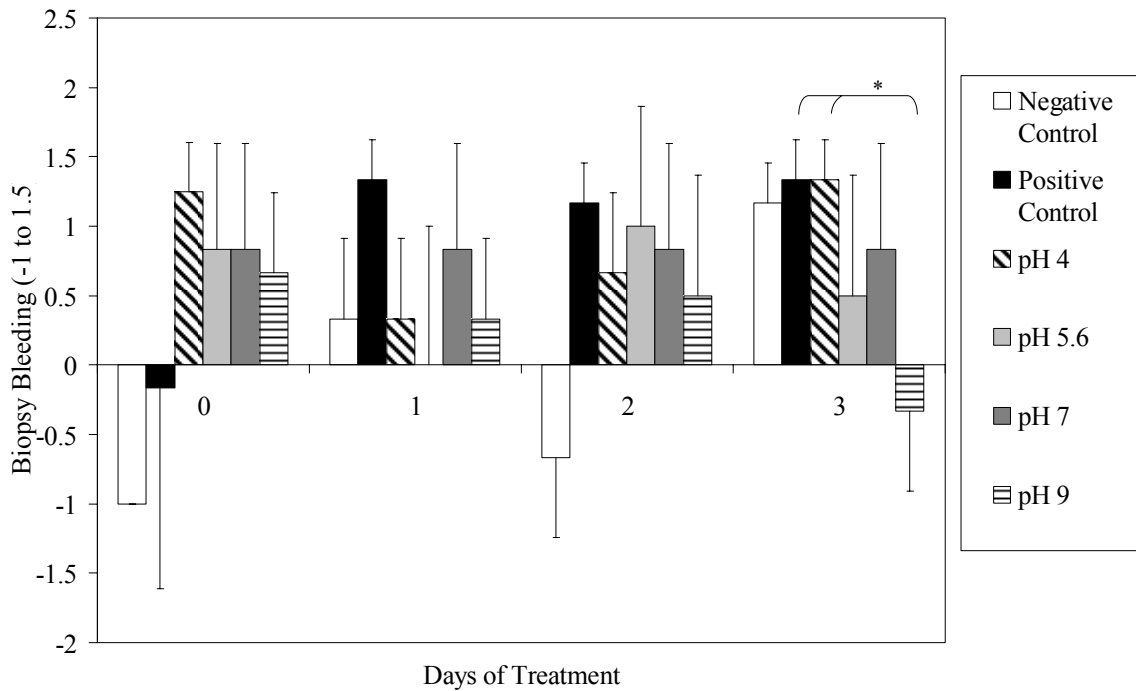


Figure 7-5. Biopsy bleeding scores for skin exposed to DNCB four times over two weeks and then treated various nanocrystalline silver-derived solutions. Daily average biopsy bleeding scores are shown for negative controls (pigs without rashes treated with distilled water-soaked dressings), and for pigs with DNCB-induced contact dermatitis treated for three days with distilled water (positive controls) or nanocrystalline silver-derived solutions with starting pHs of 4, 5.6, 7 or 9. Statistical analyses were performed using one-way ANOVAs with Tukey-Kramer Multiple Comparisons post tests. The overall p values from the one-way ANOVAs were 0.0659, 0.2522, 0.0711, and 0.0247 for Days 0, 1, 2, and 3, respectively. The results of the Tukey-Kramer post tests are indicated on the figure as follows: * indicates significantly different ($p < 0.05$). Error bars represent standard deviations ($n=3$ for all data points).

Figure 7-6 shows the average erythema scores for pigs treated with

various nanocrystalline silver-derived solutions after a single exposure to DNCB, relative to positive and negative controls. After 24 hours of treatment, animals treated with pH 9 solutions had significantly lower erythema scores than positive controls and animals treated with pH 4 and 7 solutions. By 72 hours, however, there were no significant differences between any of the groups.

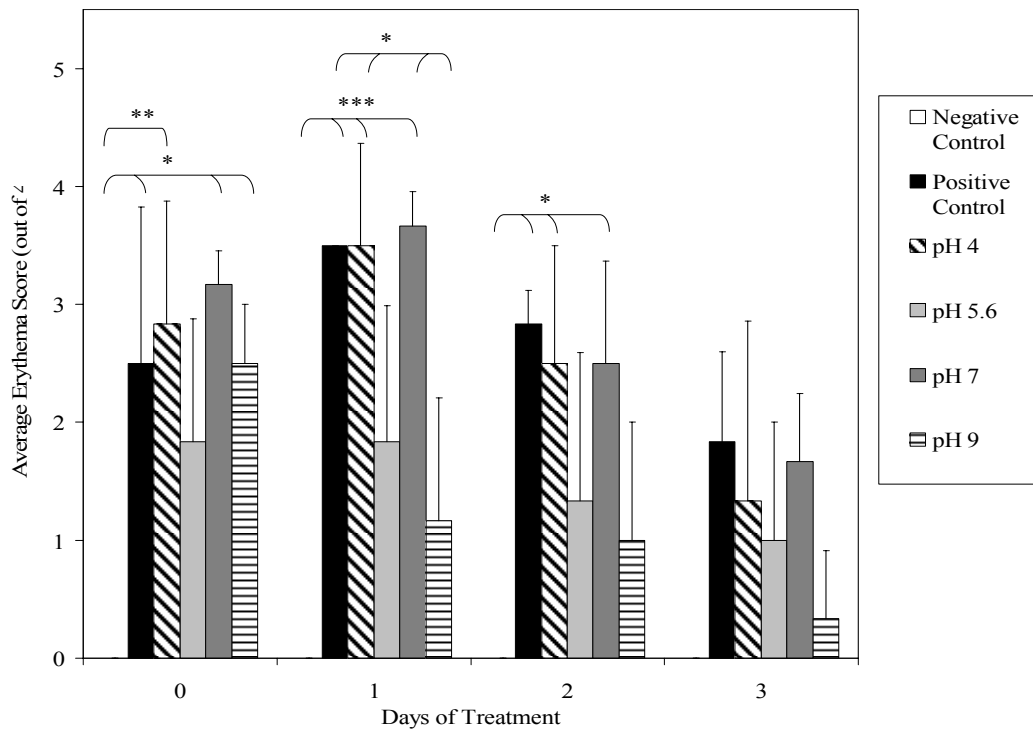


Figure 7-6. Erythema scores for porcine skin exposed to DNCB once (after sensitization of the animal) and then treated with various nanocrystalline silver-derived solutions. Daily average erythema scores are shown for negative controls (pigs without rashes treated with distilled water-soaked dressings), and for pigs with DNCB-induced contact dermatitis treated for three days with distilled water (positive controls) or nanocrystalline silver-derived solutions with starting pHs of 4, 5.6, 7 or 9. The statistical analysis was performed using one-way ANOVAs with Tukey-Kramer Multiple Comparisons post tests. The overall p values from the one-way ANOVAs were 0.0074, 0.0002, 0.0108, and 0.1339 for Days 0, 1, 2, and 3, respectively. The results of the Tukey-Kramer post tests are indicated on the figure as follows: * indicates significantly different ($p < 0.05$), ** indicates very significantly different ($p < 0.01$), and *** indicates extremely significantly different ($p < 0.001$). Error bars represent standard deviations ($n = 3$ for all points).

Figure 7-7 shows the average edema scores for pigs treated with various

nanocrystalline silver-derived solutions after a single exposure to DNCB, again relative to positive and negative controls. After 24 hours of treatment, animals treated with pH 5.6 or 9 solutions had significantly lower edema scores relative to animals treated with pH 7 solutions. After 72 hours of treatment, however, there were no significant differences between any of the groups of animals.

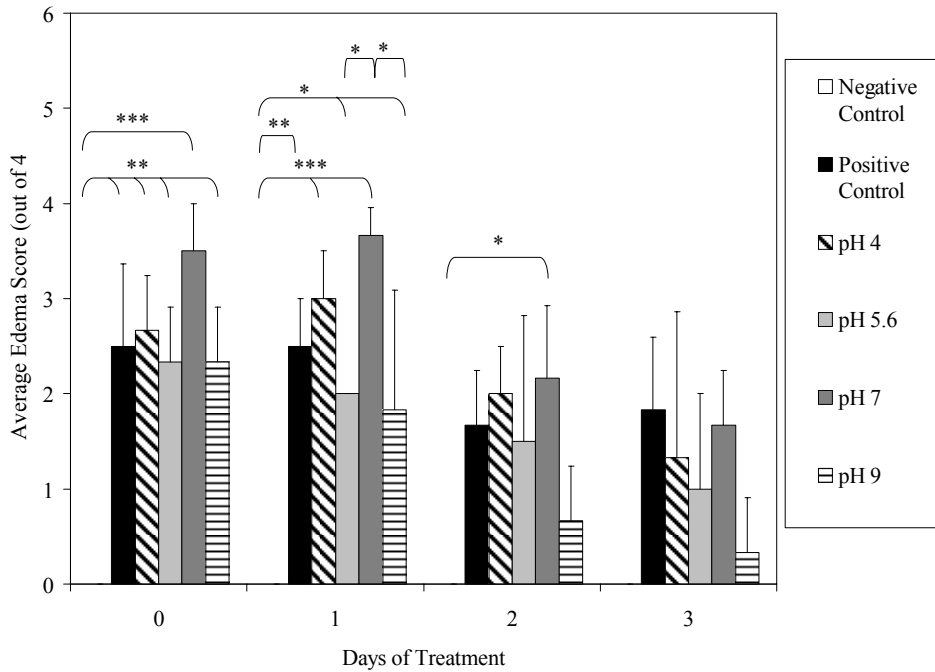


Figure 7-7. Edema scores for porcine skin exposed to DNCB once (after sensitization of the animal) and then treated with various nanocrystalline silver-derived solutions. Daily average edema scores are shown for negative controls (pigs without rashes treated with distilled water-soaked dressings), and for pigs with DNCB-induced contact dermatitis treated for three days with distilled water (positive controls) or nanocrystalline silver-derived solutions with starting pHs of 4, 5.6, 7 or 9. The statistical analysis was performed using one-way ANOVAs with Tukey-Kramer Multiple Comparisons post tests. The overall p values from the one-way ANOVAs were 0.0002, 0.0002, 0.0253, and 0.1339 for Days 0, 1, 2, and 3, respectively. The results of the Tukey-Kramer post tests are indicated on the figure as follows: * indicates significantly different ($p < 0.05$), ** indicates very significantly different ($p < 0.01$), and *** indicates extremely significantly different ($p < 0.001$). Error bars represent standard deviations ($n = 3$ for all data points).

There were no significant differences in the biopsy bleeding scores between the groups of animals on the side which received only one exposure to

DNCB at any time point (Figure 7-8).

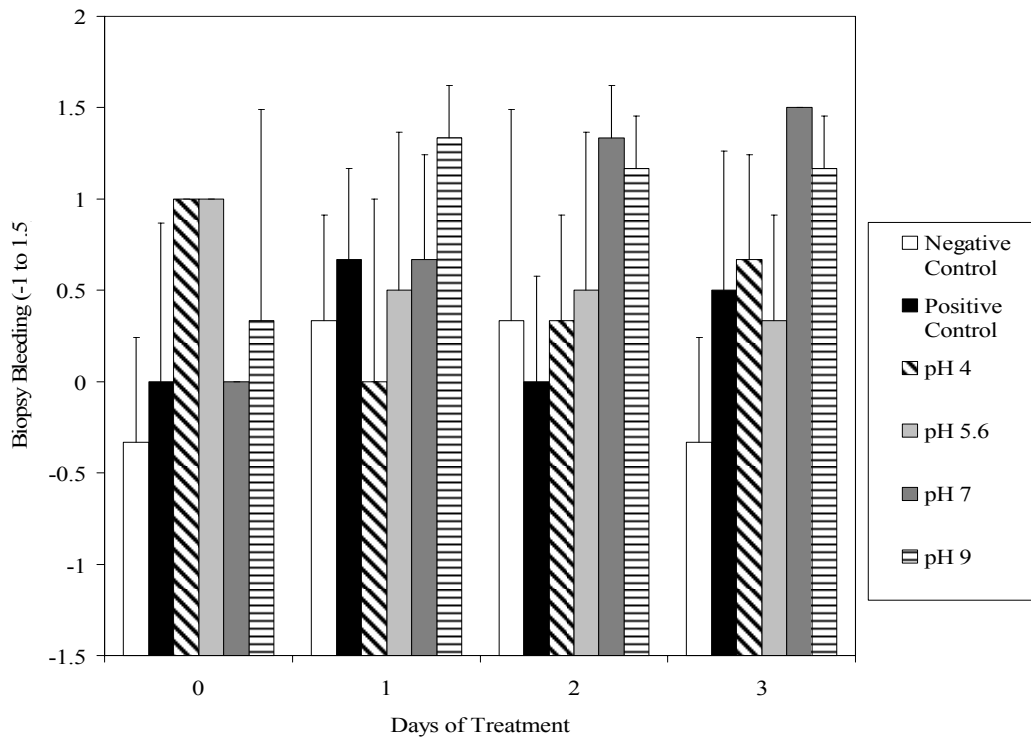


Figure 7-8. Biopsy bleeding scores for skin exposed to DNCB once (after sensitization of the animal) and then treated various nanocrystalline silver-derived solutions. Daily average biopsy bleeding scores are shown for negative controls (pigs without rashes treated with distilled water-soaked dressings), and for pigs with DNCB-induced contact dermatitis treated for three days with distilled water (positive controls) or nanocrystalline silver-derived solutions with starting pHs of 4, 5.6, 7 or 9. Statistical analyses were performed using one-way ANOVAs with Tukey-Kramer Multiple Comparisons post tests. The overall p values from the one-way ANOVAs were 0.1357, 0.3448, 0.1663, and 0.0780 for Days 0, 1, 2, and 3, respectively. The results of the Tukey-Kramer post tests did not identify any significant differences between individual treatment groups. Error bars represent standard deviations (n=3 for all data points).

Histology

Representative histological images over the course of treatment for animals exposed to DNCB four times are shown in Figure 7-9. Before treatment (column 1), tissues from all DNCB-challenged animals demonstrated leukocyte and red blood cell infiltration, with epidermal disruption due to excessive edema. Negative controls (a-d) showed normal tissue morphology throughout the study,

with a well-defined epidermis, and low cellularity in the dermis. Positive controls (e-h) showed no improvement over the course of treatment, with extensive infiltration of inflammatory cells throughout the experiment. Animals treated with pH 4 solutions (i-l) showed a gradual reduction of inflammatory cells over the course of treatment, with re-epithelialization beginning to occur by 48 hours of treatment. Animals treated with pH 5.6 solutions (m-p) did not show histological signs of improvement until 72 hours of treatment, at which point decreased inflammatory cells were present, and re-epithelialization began. Animals treated with pH 7 solutions (q-t) began re-epithelialization at 48 hours, and showed lower leukocyte infiltration at 72 hours than animals treated with pH 4 solutions. However, the re-epithelialization that occurred appeared to be thicker with deeper ridges. Animals treated with pH 9 solutions (u-x) all showed signs of re-epithelialization at 48 hours, with one animal even re-epithelializing at 24 hours (not shown). At 72 hours, the animals treated with pH 9 solutions showed the best overall tissue morphology, including the most well-defined epidermis and dermis, clearest dermal morphology, and lowest leukocyte infiltration.

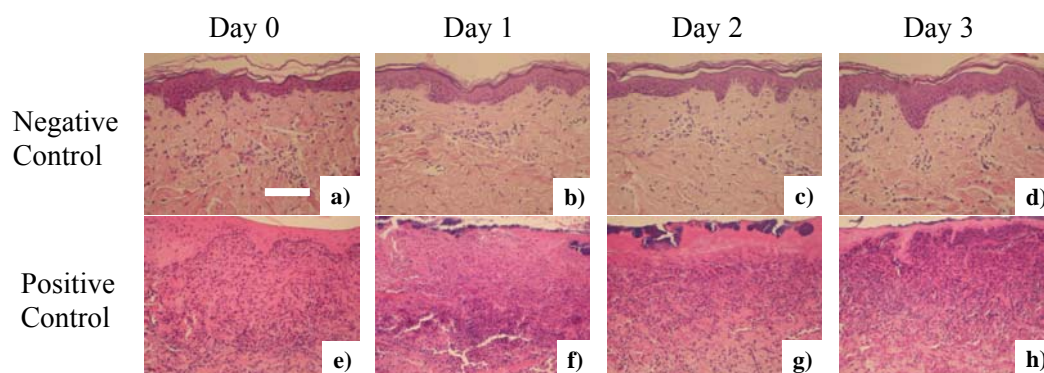


Figure 7-9.

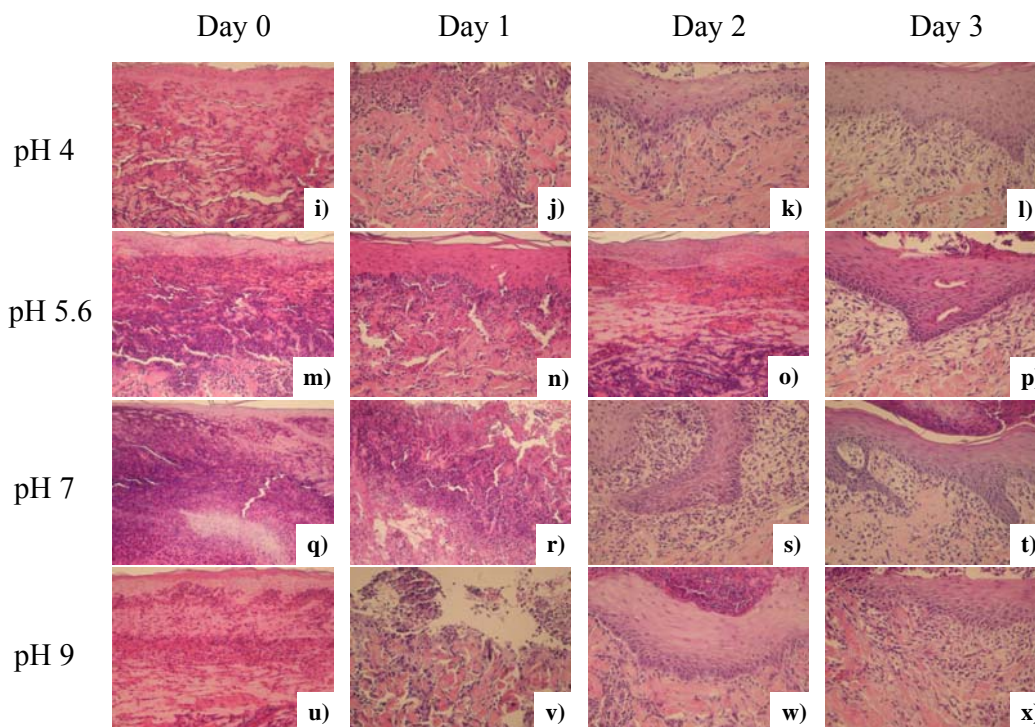


Figure 7-9, continued. Representative histological images for skin exposed to DNCB four times over two weeks and then treated with various nanocrystalline silver-derived solutions. Representative images, including portions of both the epidermis and the dermis, are shown from Days 0 through 3 for negative controls (pigs which did not have rashes and were treated with distilled water-soaked gauze) (a-d), positive controls (pigs which had DNCB-induced rashes which were treated with distilled water-soaked gauze) (e-h), and animals with DNCB-induced rashes treated with nanocrystalline silver-derived solutions generated at starting pHs of 4 (i-l), 5.6 (m-p), 7 (q-t), or 9 (u-x). Cell nuclei were stained purple with hematoxylin, while cytoplasm was stained pink with eosin. The scale bar in A represents 100 μ m.

Representative histological images over the course of treatment are shown in Figure 7-10 for the rashes only exposed to DNCB once. Negative controls showed no effect of treatment (a-d). On Day 0, tissues from DNCB-challenged animals showed variable levels of leukocyte infiltration and tissue damage, with the positive controls (e) having the lowest levels, and the pH 9 treated animals (u) having the highest levels. On Day 1, all animals exposed to DNCB-induced rashes showed increased inflammatory responses, with tissue damage, and

infiltration of leukocytes and red blood cells. One exception to this was that the pH 9 treated group did not appear to worsen from Day 0 to Day 1. Between 48 and 72 hours of treatment, all treatment groups showed improvement histologically, with decreased inflammatory cell infiltration, and re-epithelialization occurring. However, the positive controls also showed these signs of improvement.

Due to the high level of variability between animals within a single treatment group, and the fact that the positive control rashes showed improvement during the treatment period when inflammation was induced this way, subsequent analyses were only performed on biopsies from the rashes which had been exposed to DNCB four times.

Semi-quantitative Analysis of mRNA Expression

Figure 7-11 shows the quantity of DNA generated versus the cycle number measured from biopsies of each animal from each treatment group, for (a) HPRT, (b) GAPDH, (c) TNF- α , (d) IL-1 β , (e) IL-8, (f) IL-10, (g) IL-12, (h) IL-17, and (i) IL-31. For GAPDH, all animals from all groups showed similar quantities of DNA at similar times – there is little spread in the data. With HPRT, the spread in the data is somewhat wider, but the data is still quite closely grouped. With the pro-inflammatory and anti-inflammatory cytokines measured, the data was much more spread out, suggesting differences between animals, and perhaps with treatment group. However, the sequence used for IL-31 was not detected in many of the samples (i). At 72 hours, similar patterns of DNA quantities versus cycle numbers were observed (Figure 7-12).

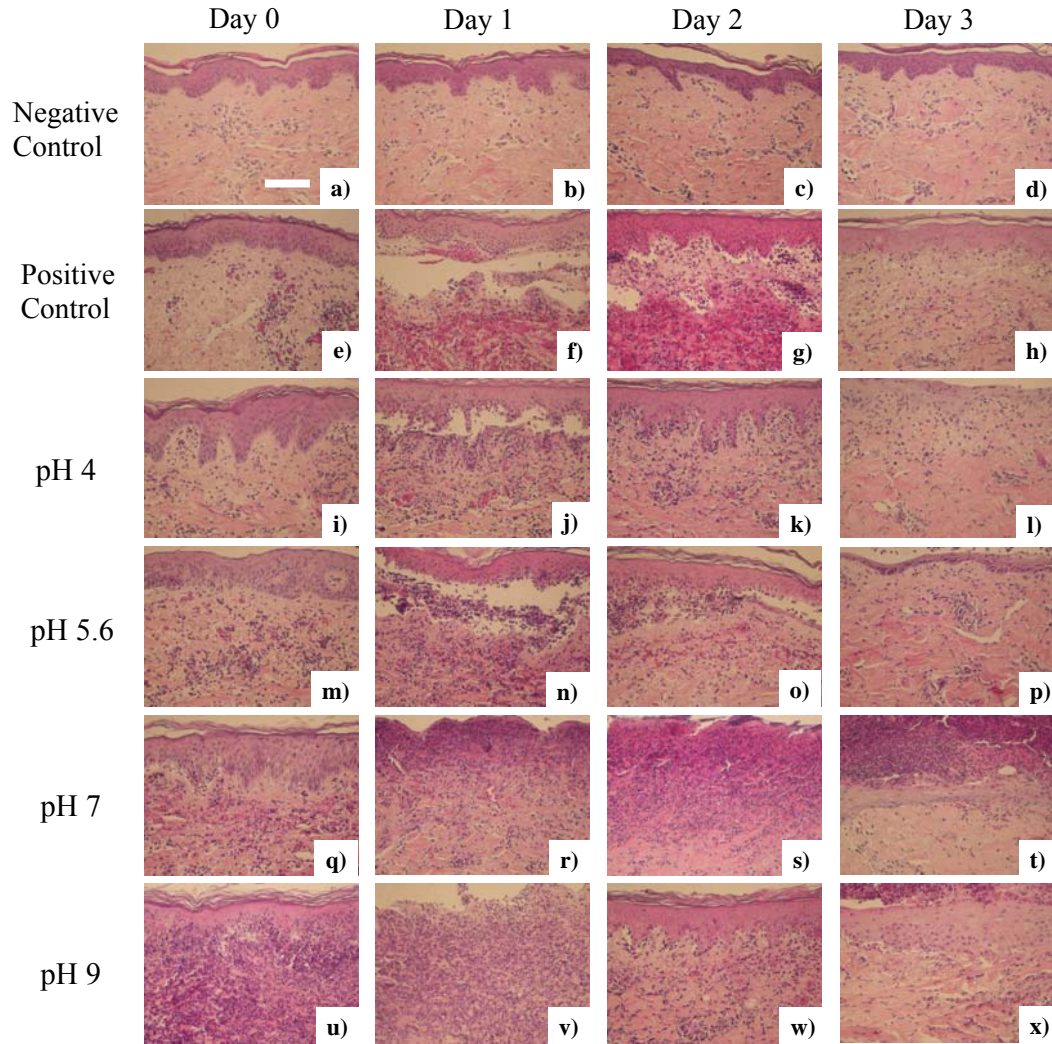


Figure 7-10. Representative histological images for skin exposed to DNCB once (after sensitization of the animal) and then treated with various nanocrystalline silver-derived solutions. Representative images, including portions of both the epidermis and the dermis, are shown from Days 0 through 3 for negative controls (pigs which did not have rashes and were treated with distilled water-soaked gauze) (a-d), positive controls (pigs which had DNCB-induced rashes which were treated with distilled water-soaked gauze) (e-h), and animals with DNCB-induced rashes treated with nanocrystalline silver-derived solutions generated at starting pHs of 4 (i-l), 5.6 (m-p), 7 (q-t), or 9 (u-x). Cell nuclei were stained purple with hematoxylin, while cytoplasm was stained pink with eosin. The scale bar in A represents 100 μm .

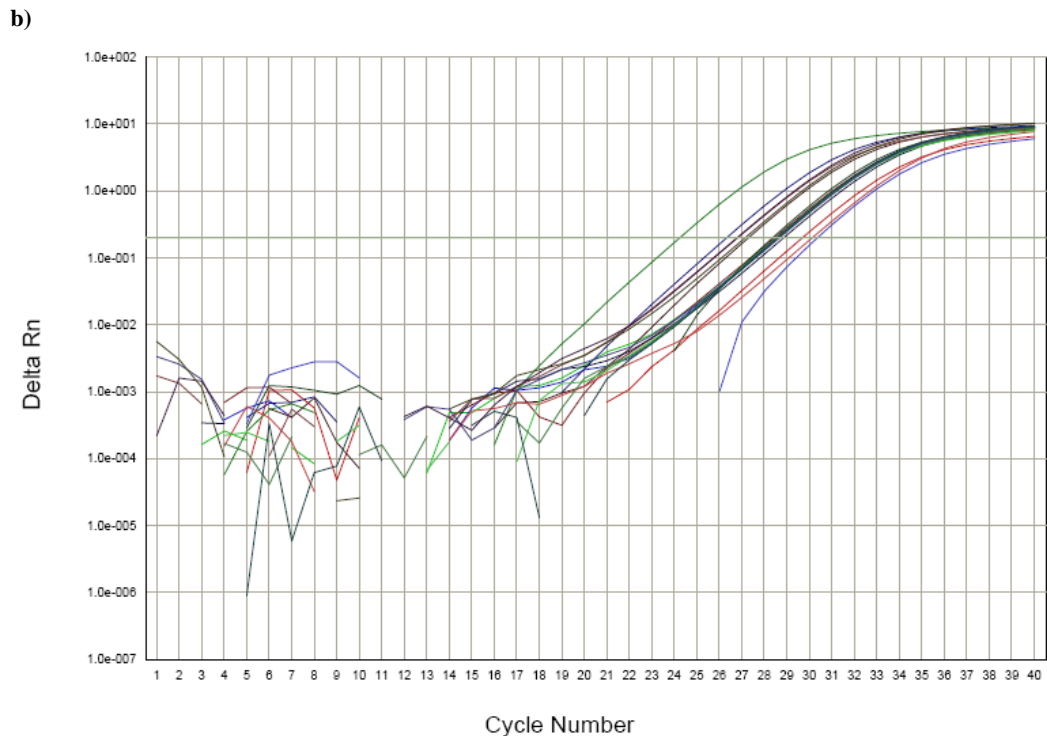
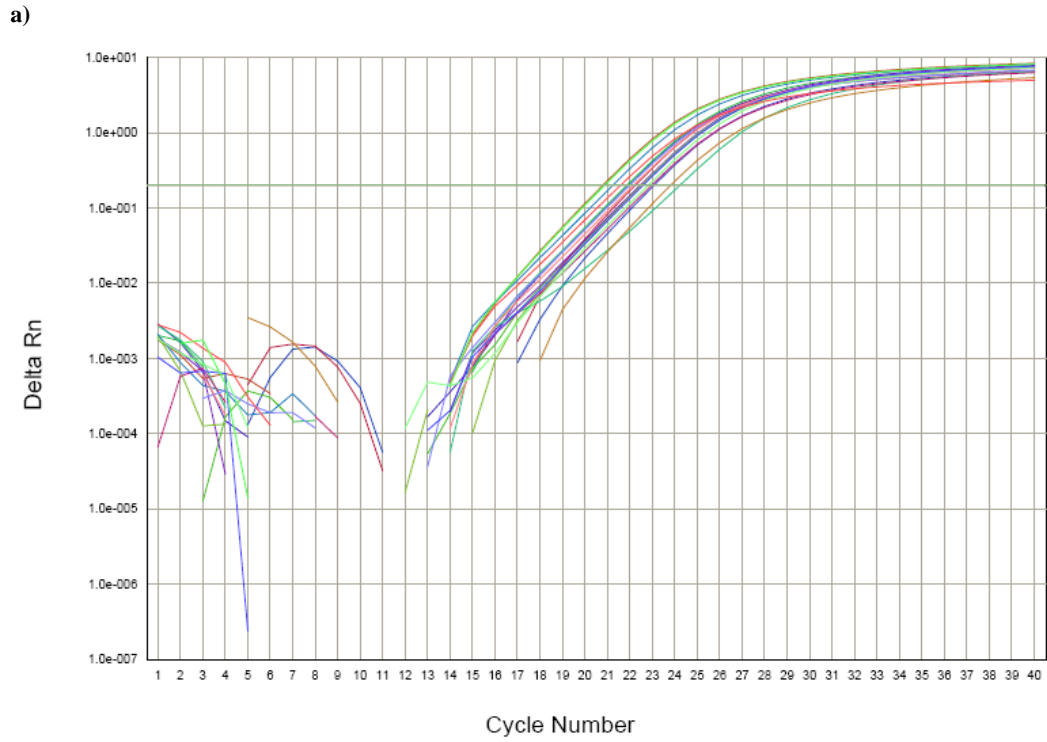
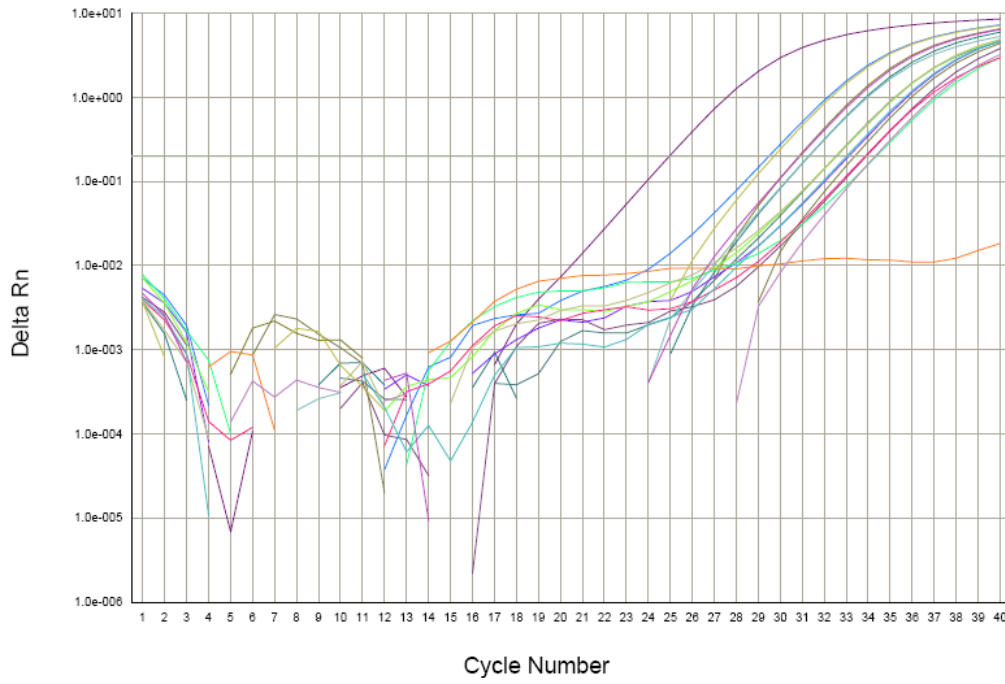


Figure 7-11.

c)



d)

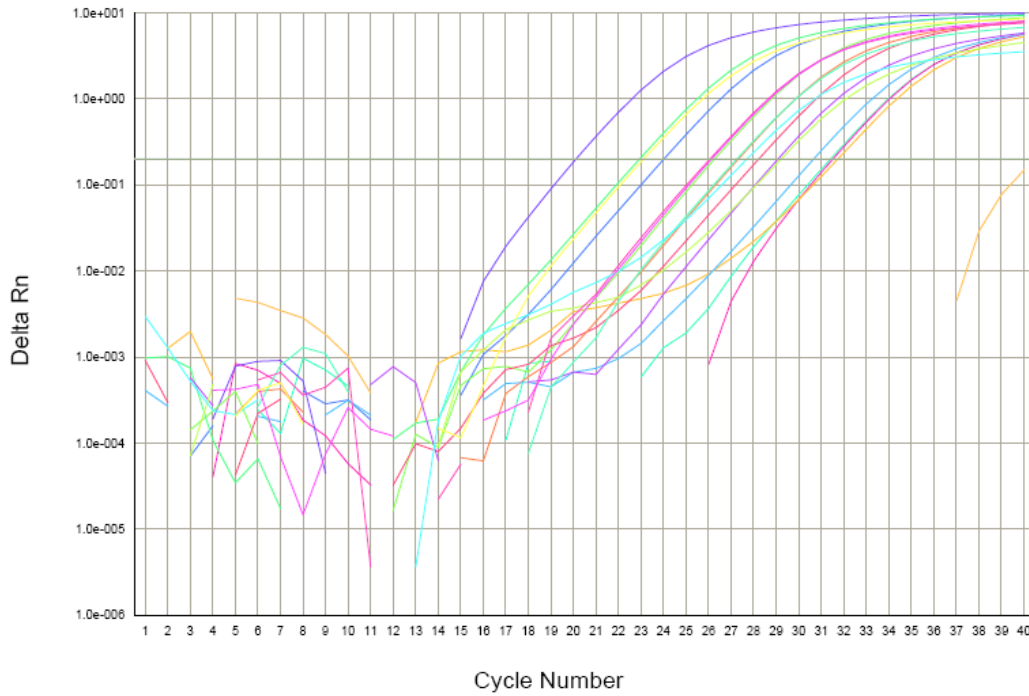
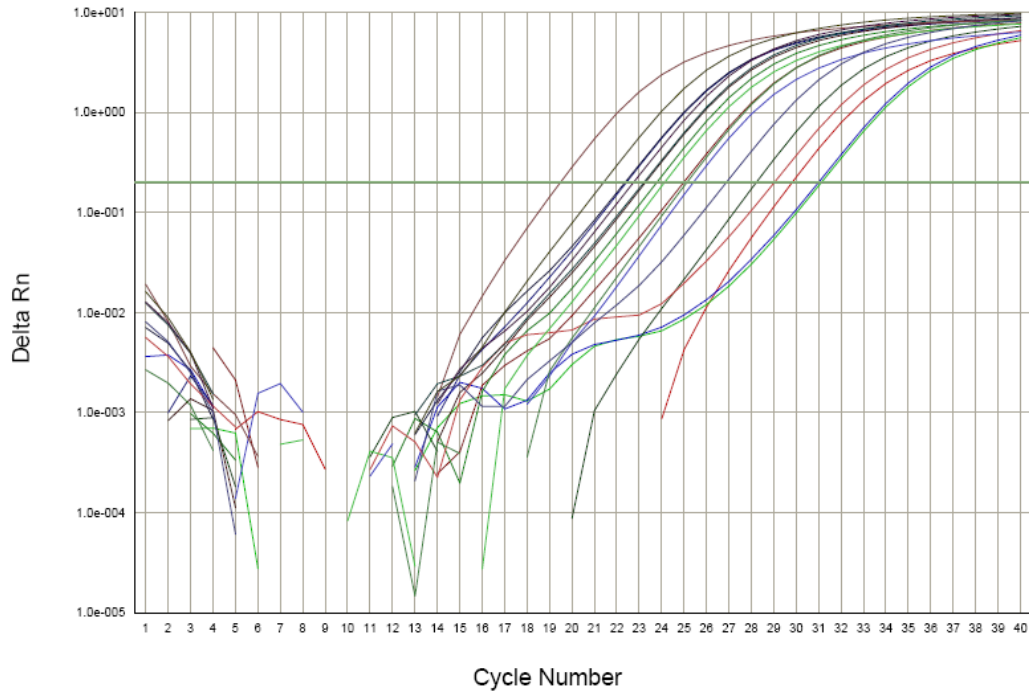


Figure 7-11, continued.

e)



f)

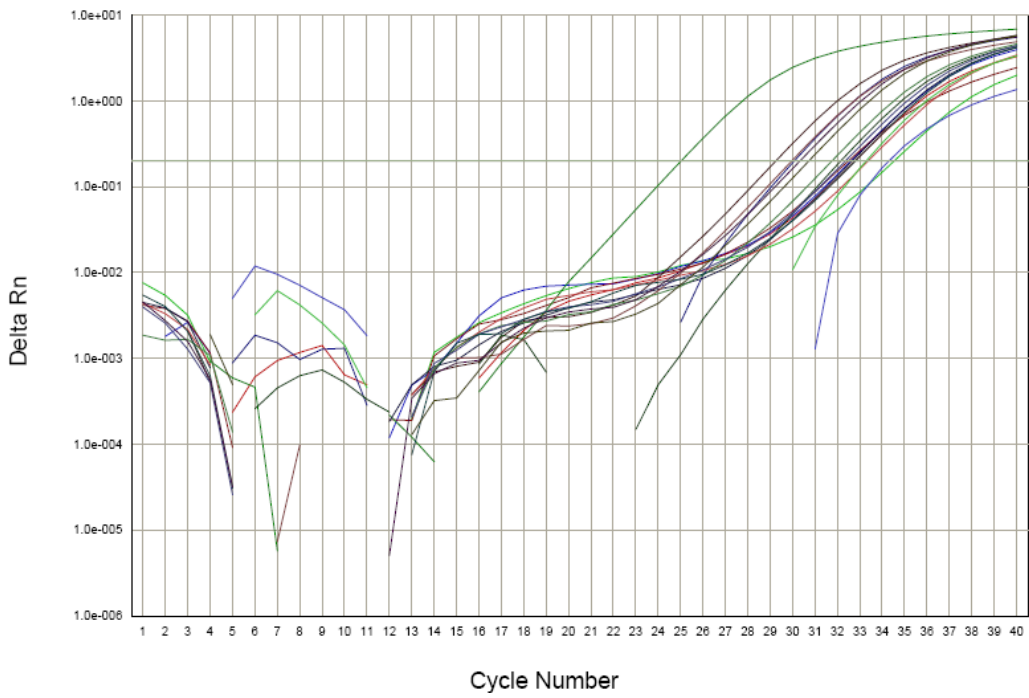
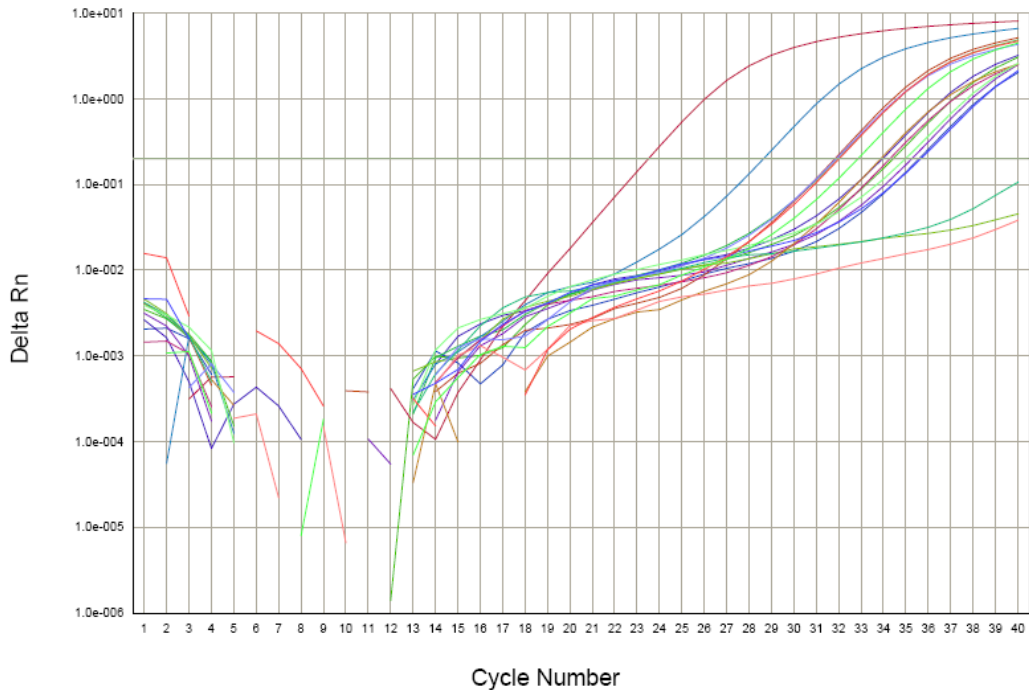


Figure 7-11, continued.

g)



h)

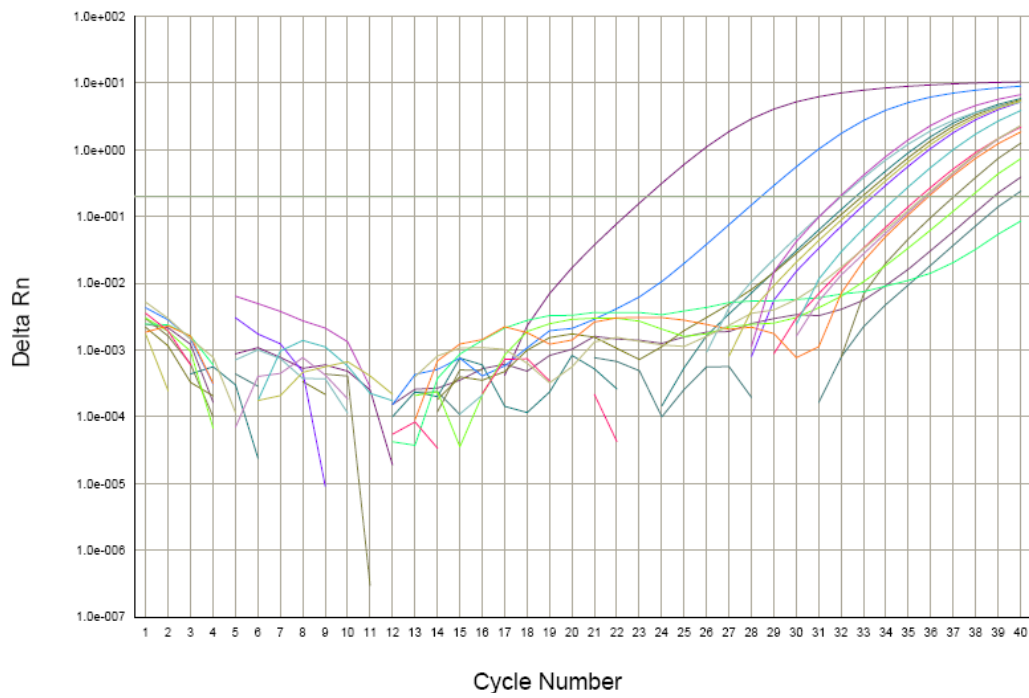


Figure 7-11, continued.

i)

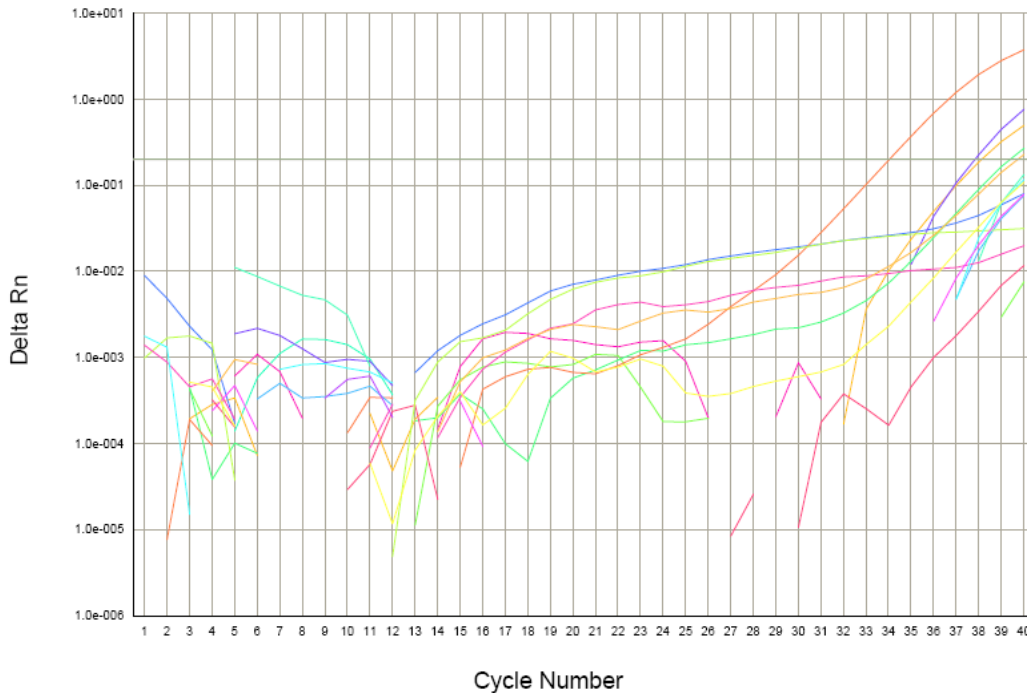


Figure 7-11, continued. Real time RT-PCR reaction rates for 24h samples. Plots of ΔRn (a measure of the amount of DNA present) over the number of PCR cycles are shown for all pigs treated for 24 hours for (a) GAPDH, (b) HPRT, (c) TNF- α , (d) IL-1 β , (e) IL-8, (f), IL-10, (g) IL-12, (h) IL-17, and (i) IL-31. Green horizontal lines represent the point at which Ct measurements were taken.

a)

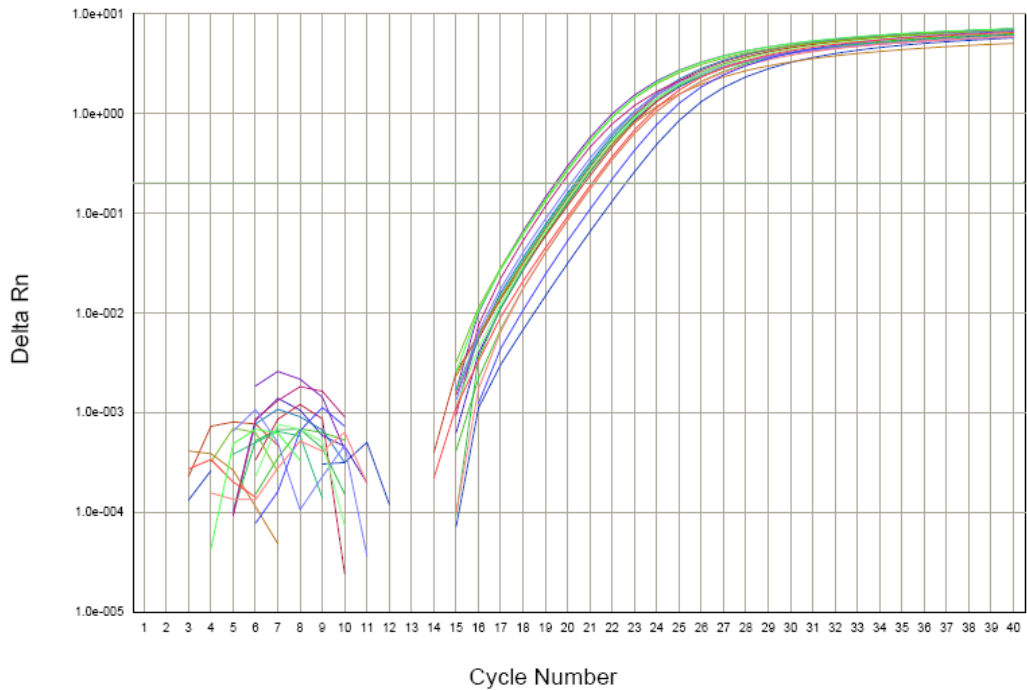


Figure 7-12.

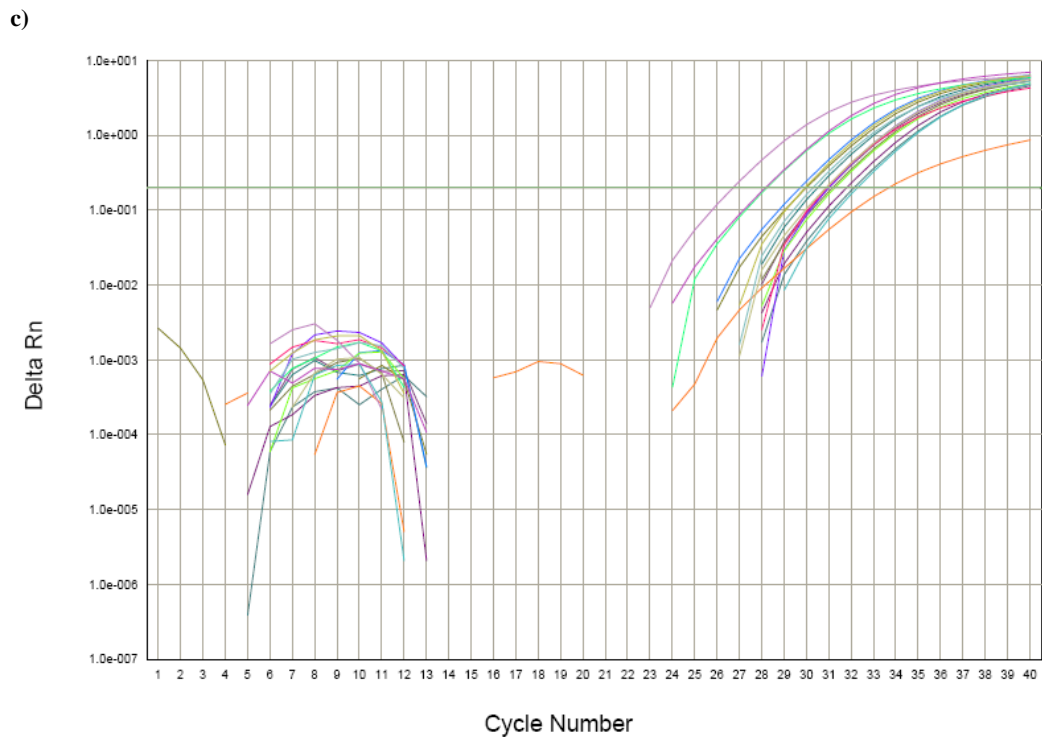
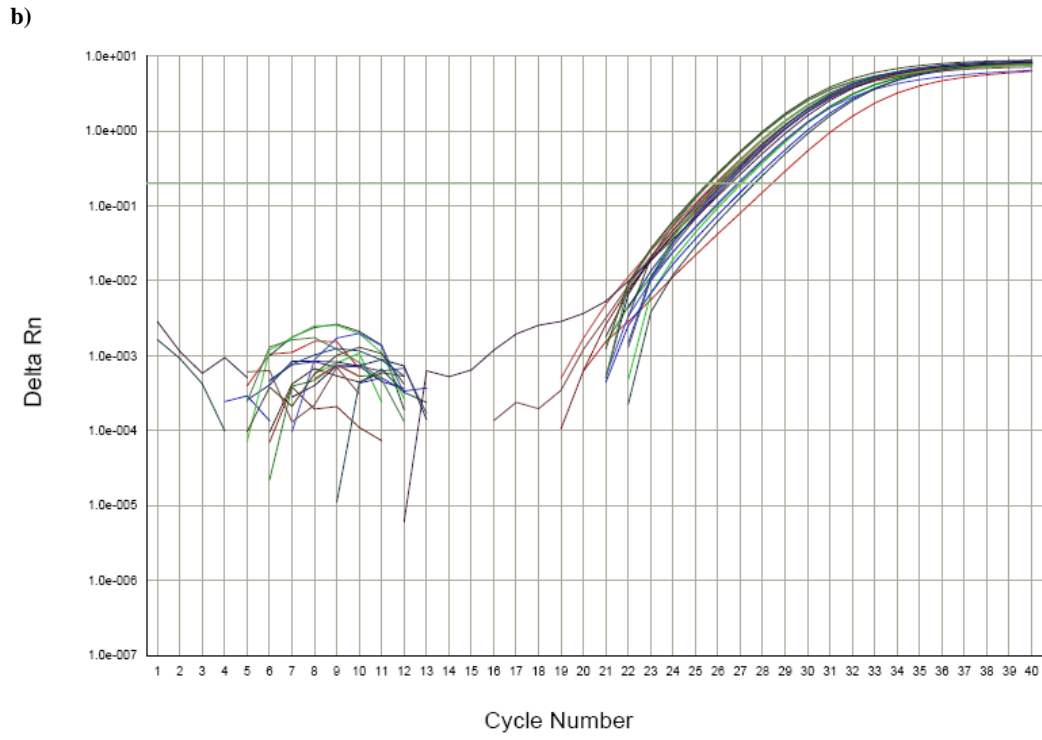


Figure 7-12, continued.

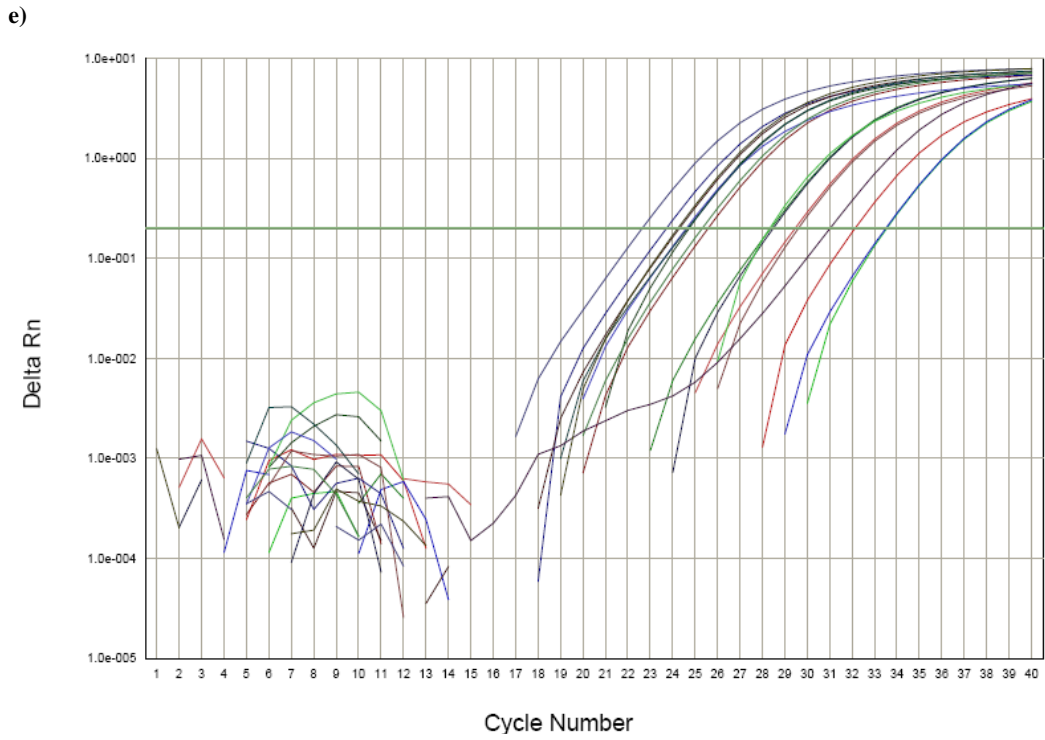
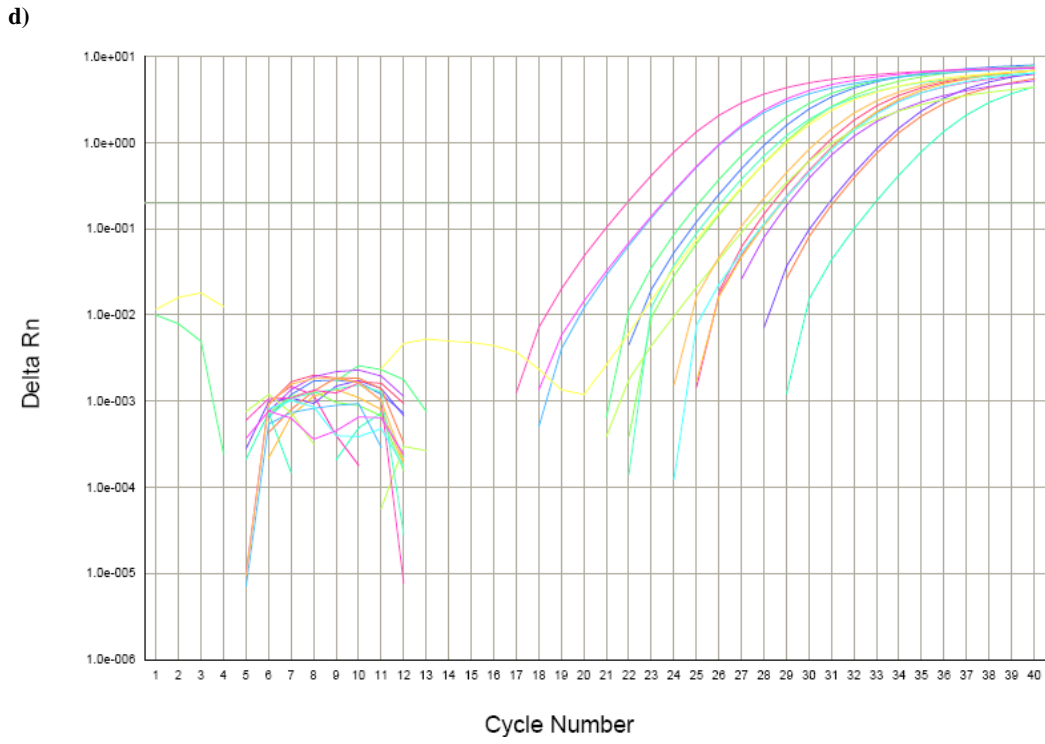
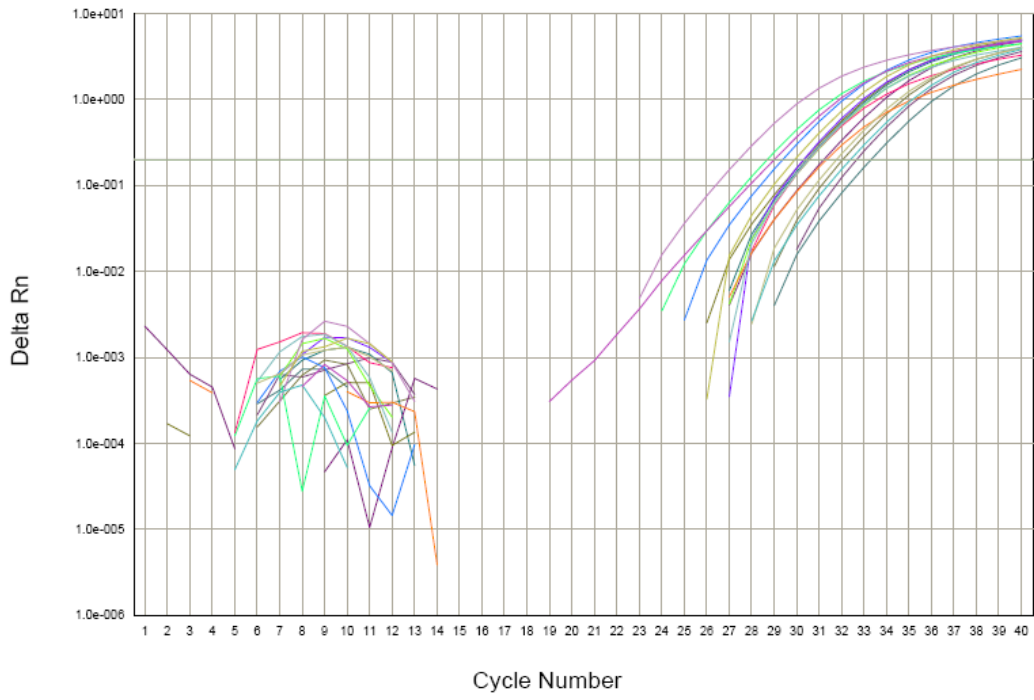


Figure 7-12, continued.

f)



g)

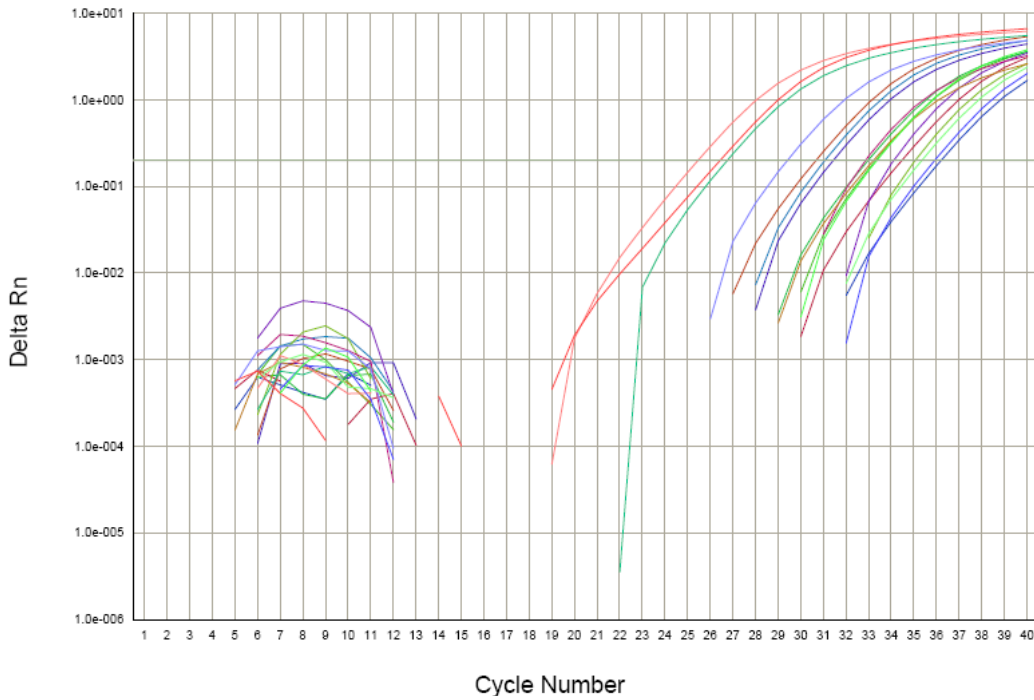


Figure 7-12, continued.

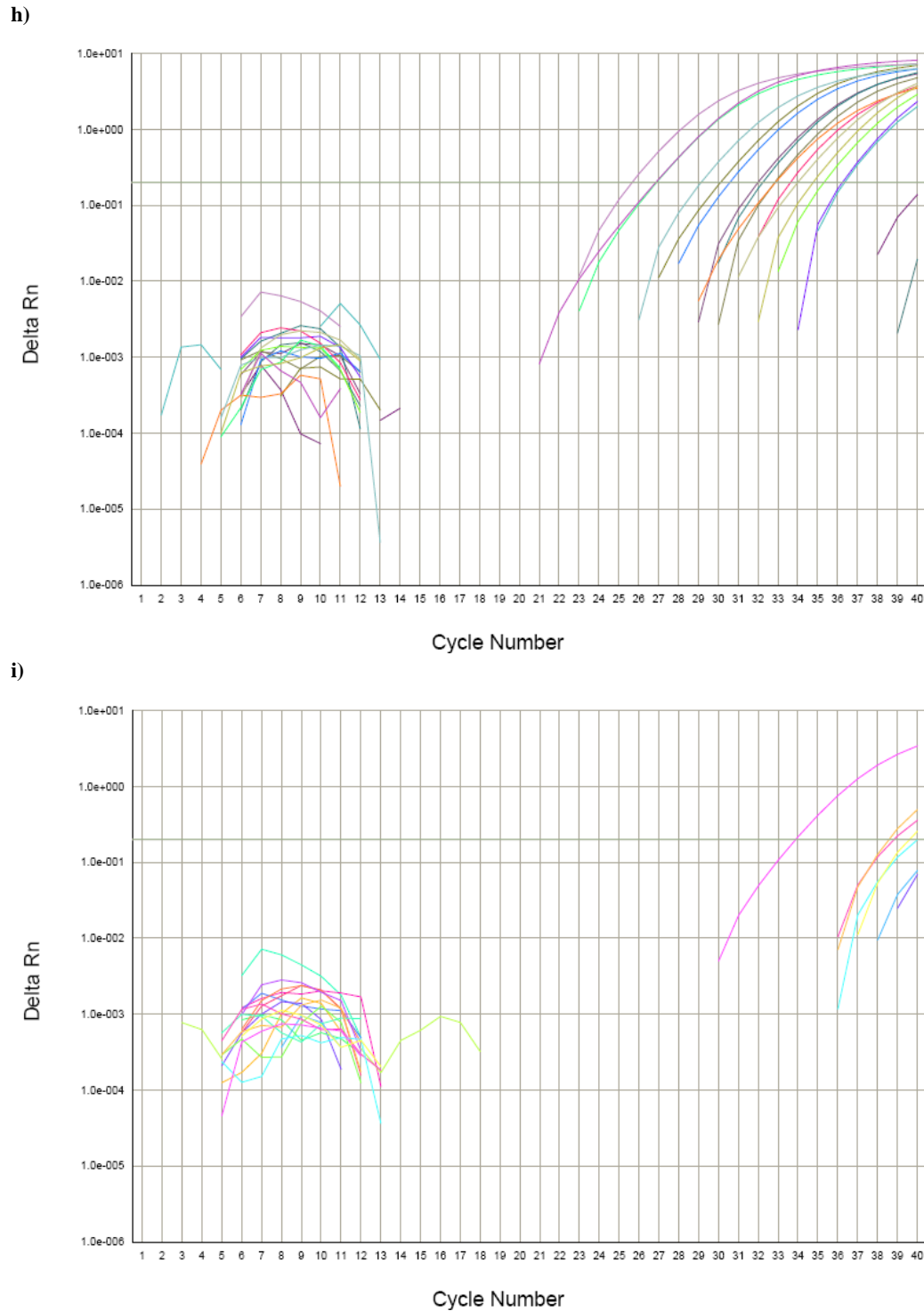


Figure 7-12. Real time RT-PCR reaction rates for 72h samples. Plots of ΔRn (a measure of the amount of DNA present) over the number of PCR cycles are shown for all pigs treated for 72 hours for (a) GAPDH, (b) HPRT, (c) TNF- α , (d) IL-1 β , (e) IL-8, (f) IL-10, (g) IL-12, (h) IL-17, and (i) IL-31. Green horizontal lines represent the point at which Ct measurements were taken.

All mRNA expression shown in this section was calculated relative to negative control tissue samples. Figure 7-13 shows the expression of TNF- α mRNA after 24 hours of treatment with various nanocrystalline silver-derived solutions. Positive and negative controls are shown for comparison. There were no significant differences in the expression of TNF- α calculated using either HPRT (a) or GAPDH (b) as the housekeeping gene, although the positive controls showed a trend towards higher expression of TNF- α relative to the other groups.

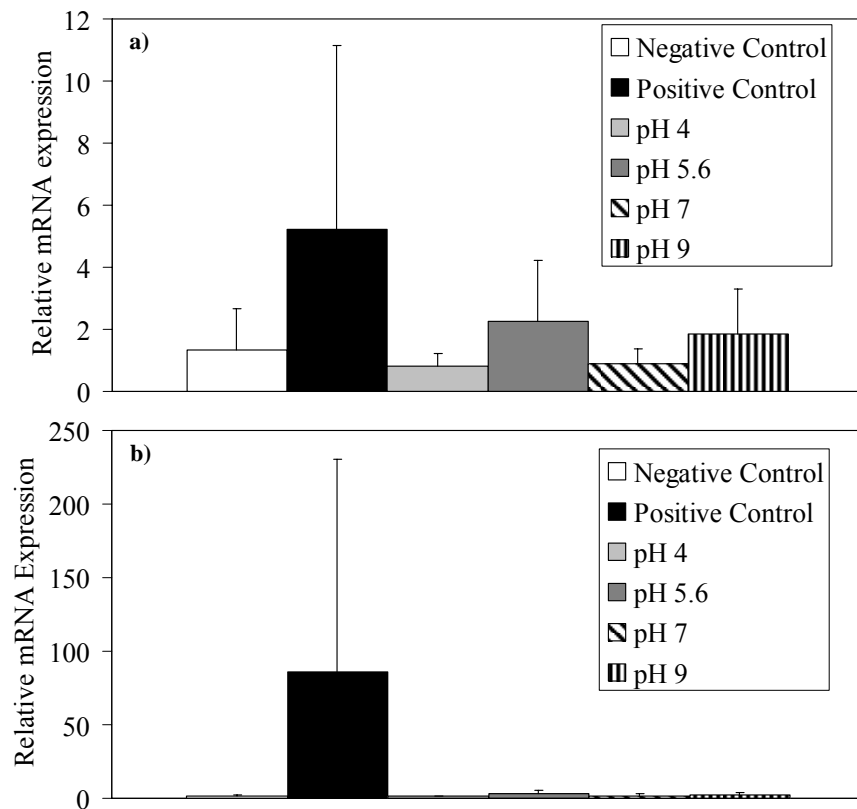


Figure 7-13. Relative expression of TNF- α mRNA in negative controls and DNCB-induced porcine rashes treated for 24 hours with distilled water (positive controls), or nanocrystalline silver-derived solutions generated at starting pHs of 4, 5.6, 7, and 9. Relative mRNA expression of TNF- α was calculated relative to the mRNA expression by negative controls using HPRT (a) or GAPDH (b) as the housekeeping gene. Statistical analyses were performed using one-way ANOVAs with Tukey-Kramer post tests. The one-way ANOVA tests indicated that the differences between groups were not significant ($p=0.4671$ for HPRT, $p=0.5100$ for GAPDH). Error bars represent standard deviations ($n=3$ for all data points).

Figure 7-14 shows the expression of IL-1 β mRNA after 24 hours of treatment with various nanocrystalline silver-derived solutions. There were no significant differences in the expression of IL-1 β calculated using either HPRT (a) or GAPDH (b) as the housekeeping gene, although again the positive controls showed a trend towards higher expression relative to the other groups.

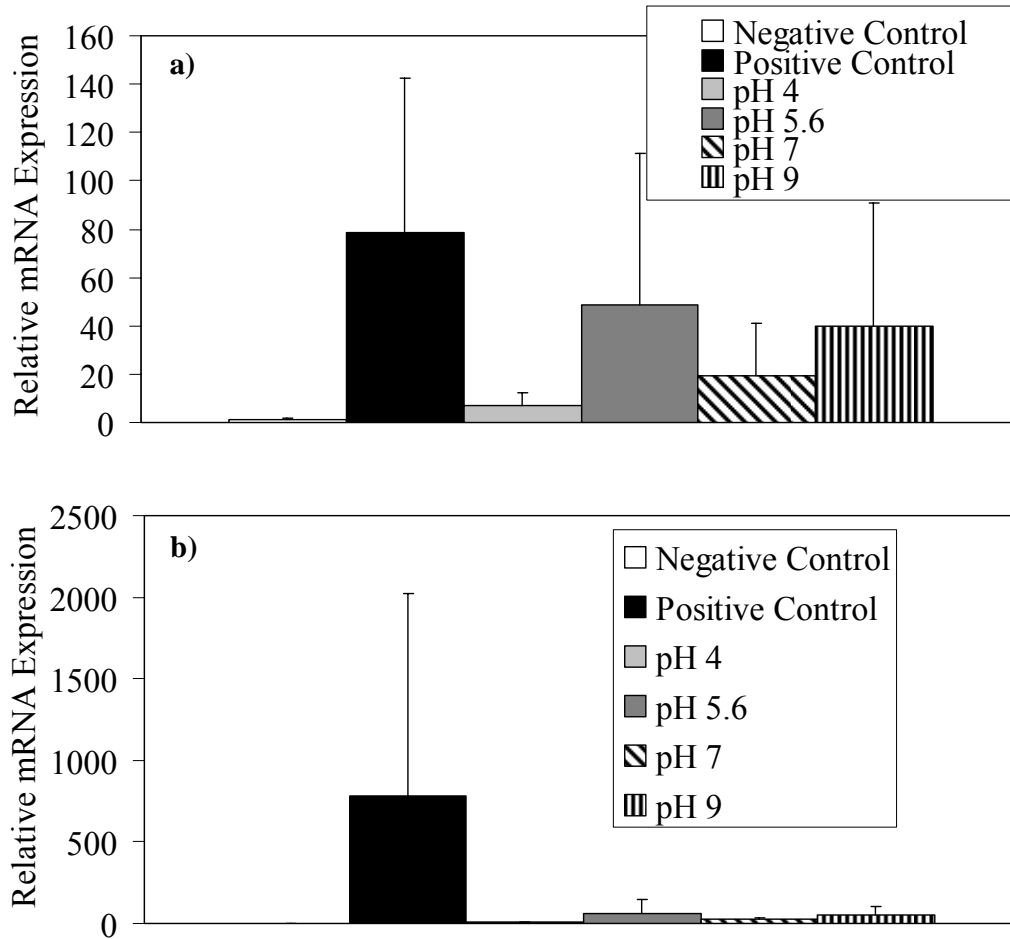


Figure 7-14. Relative expression of IL-1 β mRNA in negative controls and DNCB-induced porcine rashes treated for 24 hours with distilled water (positive controls), or nanocrystalline silver-derived solutions generated at starting pHs of 4, 5.6, 7, and 9. Relative mRNA expression of IL-1 β was calculated relative to the mRNA expression by negative controls using HPRT (a) or GAPDH (b) as the housekeeping gene. Statistical analyses were performed using one-way ANOVAs with Tukey-Kramer post tests. The one-way ANOVA tests indicated that the differences between groups were not significant ($p=0.3435$ for HPRT, $p=0.4660$ for GAPDH). Error bars represent standard deviations ($n=3$ for all data points).

Figure 7-15 shows the expression of IL-8 mRNA after 24 hours of treatment with various nanocrystalline silver-derived solutions. There were no significant differences in the expression of IL-8 calculated using either HPRT (a) or GAPDH (b) as the housekeeping gene. Animals treated with pH 7 solutions showed a trend towards higher expression relative to the other treatment groups and positive controls.

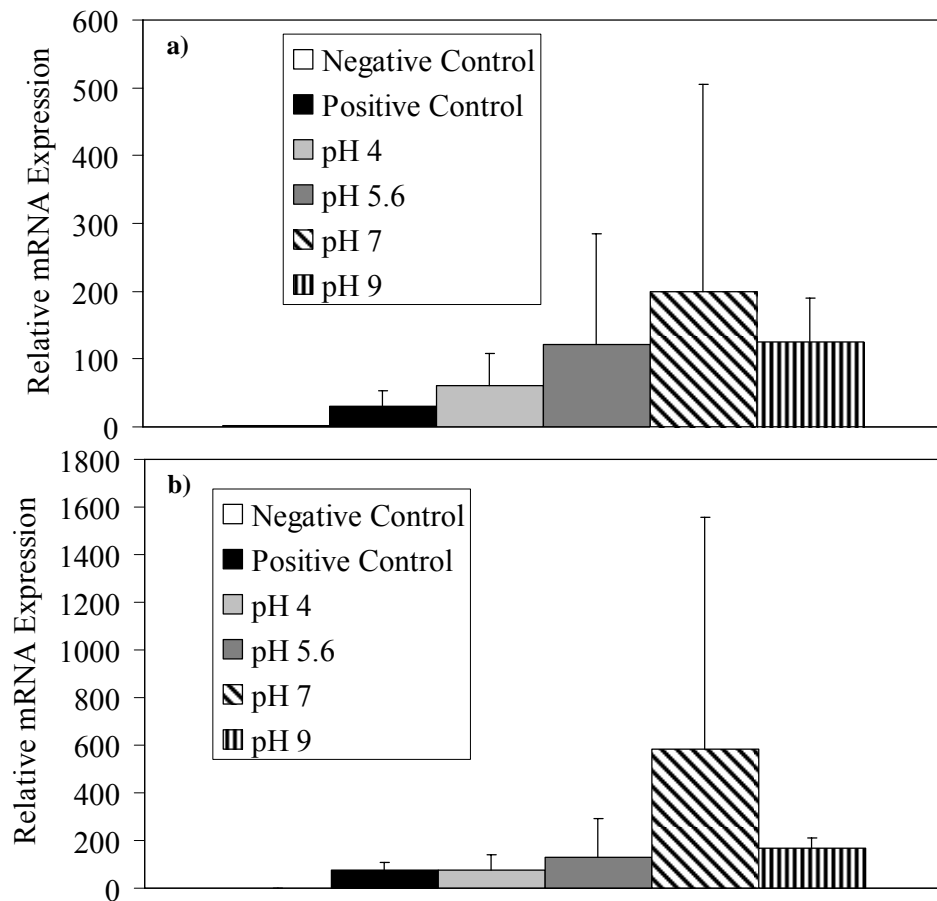


Figure 7-15. Relative expression of IL-8 mRNA in negative controls and DNCB-induced porcine rashes treated for 24 hours with distilled water (positive controls), or nanocrystalline silver-derived solutions generated at starting pHs of 4, 5.6, 7, and 9. Relative mRNA expression of IL-8 was calculated relative to the mRNA expression by negative controls using HPRT (a) or GAPDH (b) as the housekeeping gene. Statistical analyses were performed using one-way ANOVAs with Tukey-Kramer post tests. The one-way ANOVA tests indicated that the differences between groups were not significant ($p=0.5970$ for HPRT, $p=0.5598$ for GAPDH). Error bars represent standard deviations ($n=3$ for all data points).

Figure 7-16 shows the expression of IL-10 mRNA after 24 hours of treatment with various nanocrystalline silver-derived solutions. There were no significant differences in the expression of IL-10 calculated using either HPRT (a) or GAPDH (b) as the housekeeping gene. Positive controls showed a trend towards higher IL-10 expression relative to the treatment groups.

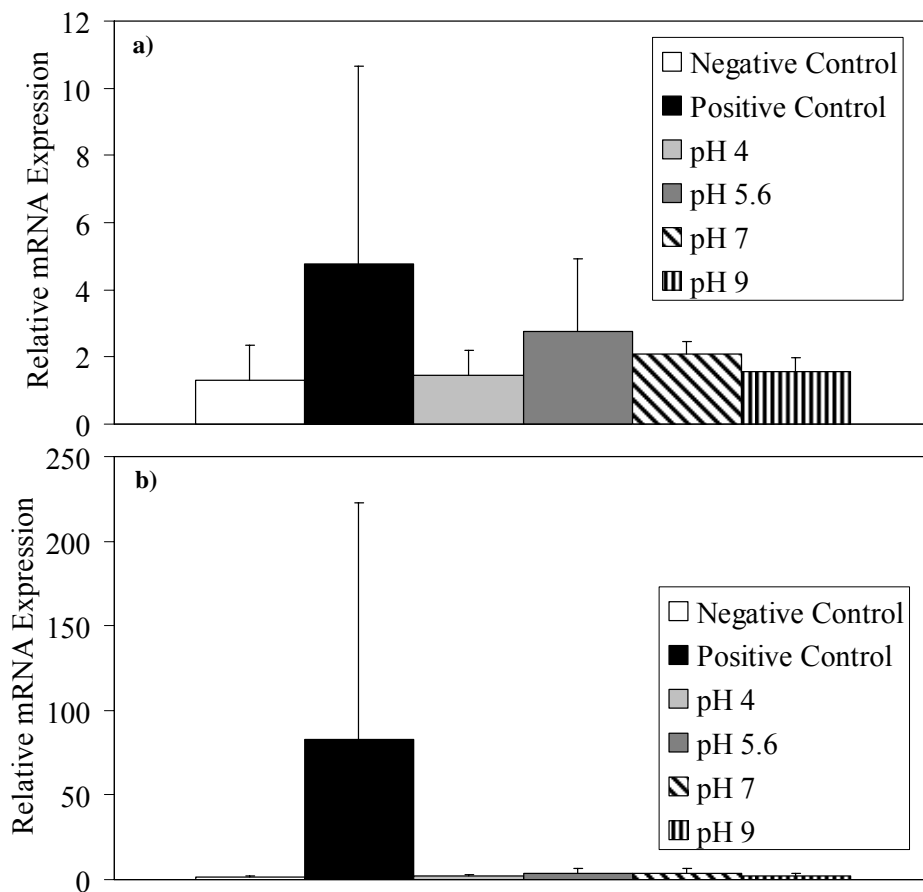


Figure 7-16. Relative expression of IL-10 mRNA in negative controls and DNCB-induced porcine rashes treated for 24 hours with distilled water (positive controls), or nanocrystalline silver-derived solutions generated at starting pHs of 4, 5.6, 7, and 9. Relative mRNA expression of IL-10 was calculated relative to the mRNA expression by negative controls using HPRT (a) or GAPDH (b) as the housekeeping gene. Statistical analyses were performed using one-way ANOVAs with Tukey-Kramer post tests. The one-way ANOVA tests indicated that the differences between groups were not significant ($p=0.6029$ for HPRT, $p=0.4669$ for GAPDH). Error bars represent standard deviations ($n=3$ for all data points).

Figure 7-17 shows the expression of IL-12 mRNA after 24 hours of treatment with various nanocrystalline silver-derived solutions. There were no significant differences in the expression of IL-12 calculated using either HPRT (a) or GAPDH (b) as the housekeeping gene, but again the positive controls showed a trend towards higher expression relative to the treatment groups.

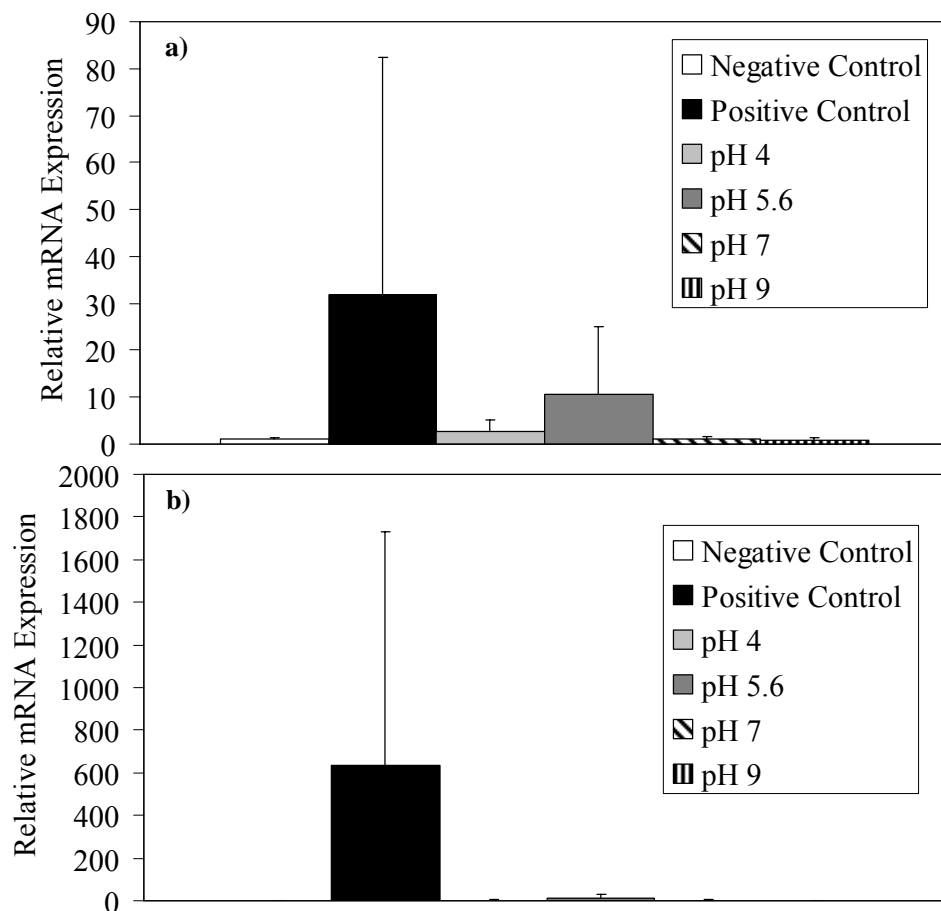


Figure 7-17. Relative expression of IL-12 mRNA in negative controls and DNCB-induced porcine rashes treated for 24 hours with distilled water (positive controls), or nanocrystalline silver-derived solutions generated at starting pHs of 4, 5.6, 7, and 9. Relative mRNA expression of IL-12 was calculated relative to the mRNA expression by negative controls using HPRT (a) or GAPDH (b) as the housekeeping gene. Statistical analyses were performed using one-way ANOVAs with Tukey-Kramer post tests. The one-way ANOVA tests indicated that the differences between groups were not significant ($p=0.6159$ for HPRT, $p=0.6260$ for GAPDH). Error bars represent standard deviations ($n=3$ for all data points).

Figure 7-18 shows the same type of trend for the expression of IL-17 mRNA after 24 hours of treatment with various nanocrystalline silver-derived solutions. Similarly, there were no significant differences in its expression, as calculated using either HPRT (a) or GAPDH (b) as the housekeeping gene.

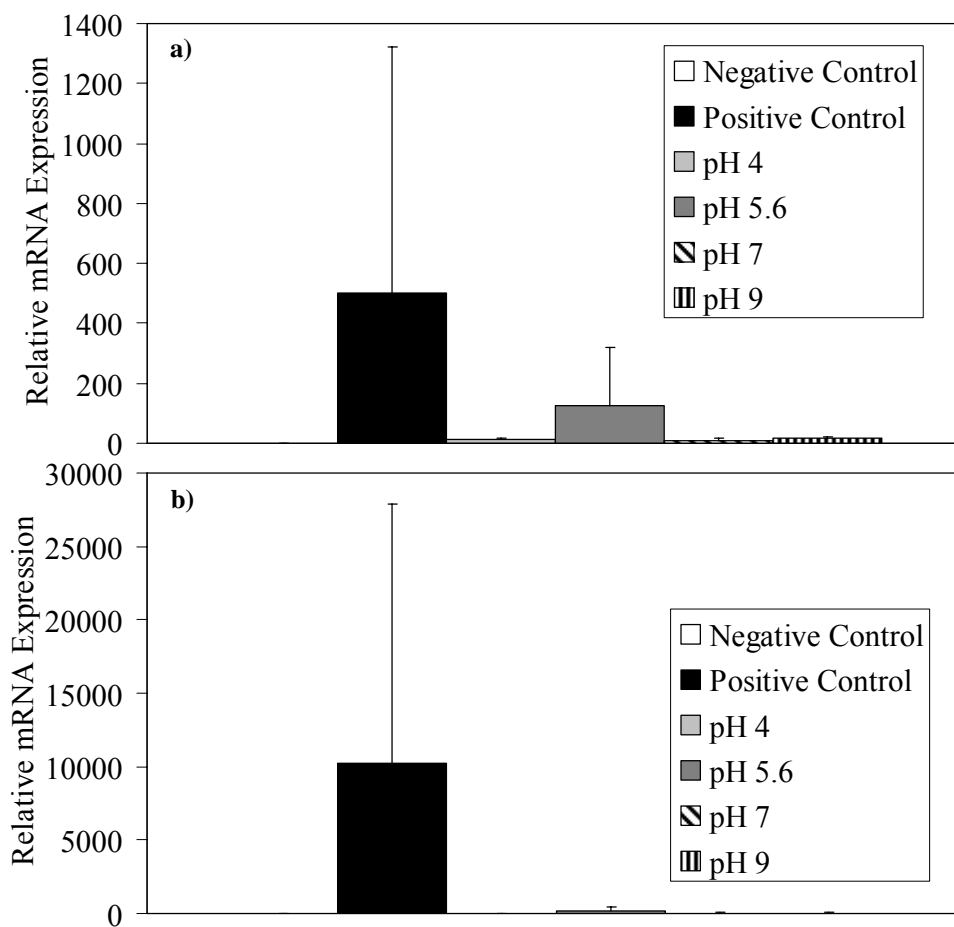


Figure 7-18. Relative expression of IL-17 mRNA in negative controls and DNCB-induced porcine rashes treated for 24 hours with distilled water (positive controls), or nanocrystalline silver-derived solutions generated at starting pHs of 4, 5.6, 7, and 9. Relative mRNA expression of IL-17 was calculated relative to the mRNA expression by negative controls using HPRT (a) or GAPDH (b) as the housekeeping gene. Statistical analyses were performed using one-way ANOVAs with Tukey-Kramer post tests. The one-way ANOVA tests indicated that the differences between groups were not significant ($p=0.5299$ for HPRT, $p=0.5132$ for GAPDH). Error bars represent standard deviations ($n=3$ for all data points).

Figure 7-19 shows the expression of TNF- α mRNA after 72 hours of treatment with various nanocrystalline silver-derived solutions, with positive and negative controls for comparison. There were no significant differences in the expression of TNF- α between groups, as calculated using either HPRT (a) or GAPDH (b) as the housekeeping gene. There were no clear trends in expression with HPRT as the housekeeping gene, but using GAPDH as the housekeeping gene, there is some suggestion that TNF- α expression may have been higher with pH 7 treatments relative to other groups.

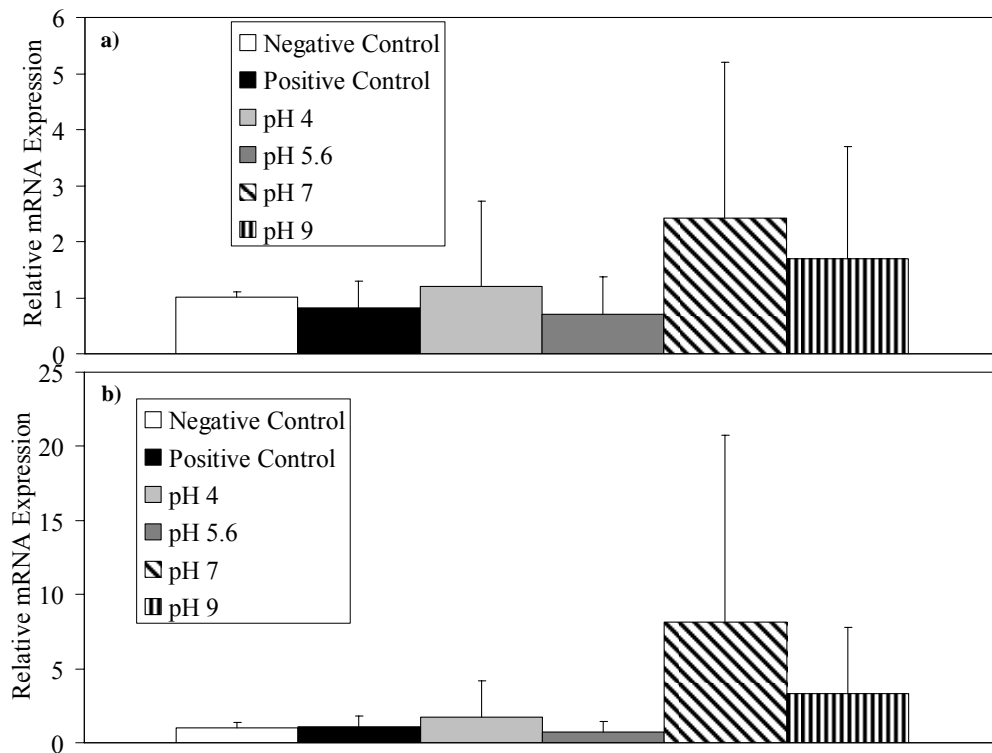


Figure 7-19. Relative expression of TNF- α mRNA in negative controls and DNCB-induced porcine rashes treated for 72 hours with distilled water (positive controls), or nanocrystalline silver-derived solutions generated at starting pHs of 4, 5.6, 7, and 9. Relative mRNA expression of TNF- α was calculated relative to the mRNA expression by negative controls using HPRT (a) or GAPDH (b) as the housekeeping gene. Statistical analyses were performed using one-way ANOVAs with Tukey-Kramer post tests. The one-way ANOVA tests indicated that the differences between groups were not significant ($p=0.7642$ for HPRT, $p=0.5864$ for GAPDH). Error bars represent standard deviations ($n=3$ for all data points).

Very similar results to those seen with TNF- α at 72 hours were observed with IL-1 β mRNA expression after 72 hours of treatment with various nanocrystalline silver-derived solutions (Figure 7-20 – no significant differences).

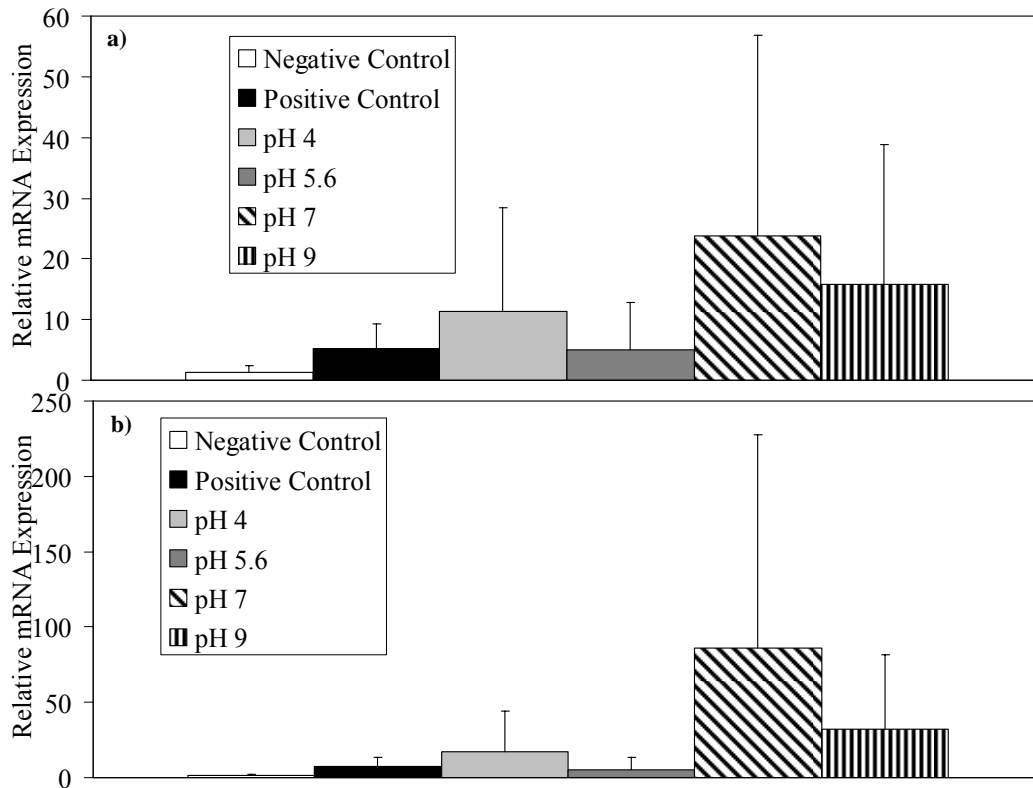


Figure 7-20. Relative expression of IL-1 β mRNA in negative controls and DNCB-induced porcine rashes treated for 72 hours with distilled water (positive controls), or nanocrystalline silver-derived solutions generated at starting pHs of 4, 5.6, 7, and 9. Relative mRNA expression of IL-1 β was calculated relative to the mRNA expression by negative controls using HPRT (a) or GAPDH (b) as the housekeeping gene. Statistical analyses were performed using one-way ANOVAs with Tukey-Kramer post tests. The one-way ANOVA tests indicated that the differences between groups were not significant ($p=0.6846$ for HPRT, $p=0.5735$ for GAPDH). Error bars represent standard deviations ($n=3$ for all data points).

Figure 7-21 shows the relative mRNA expression of IL-8 after 72 hours of treatment with various nanocrystalline silver-derived solutions. There were no significant differences in the expression of IL-8 between groups, using either HPRT (a) or GAPDH (b) as the housekeeping gene, and there were no visible trends in the data.

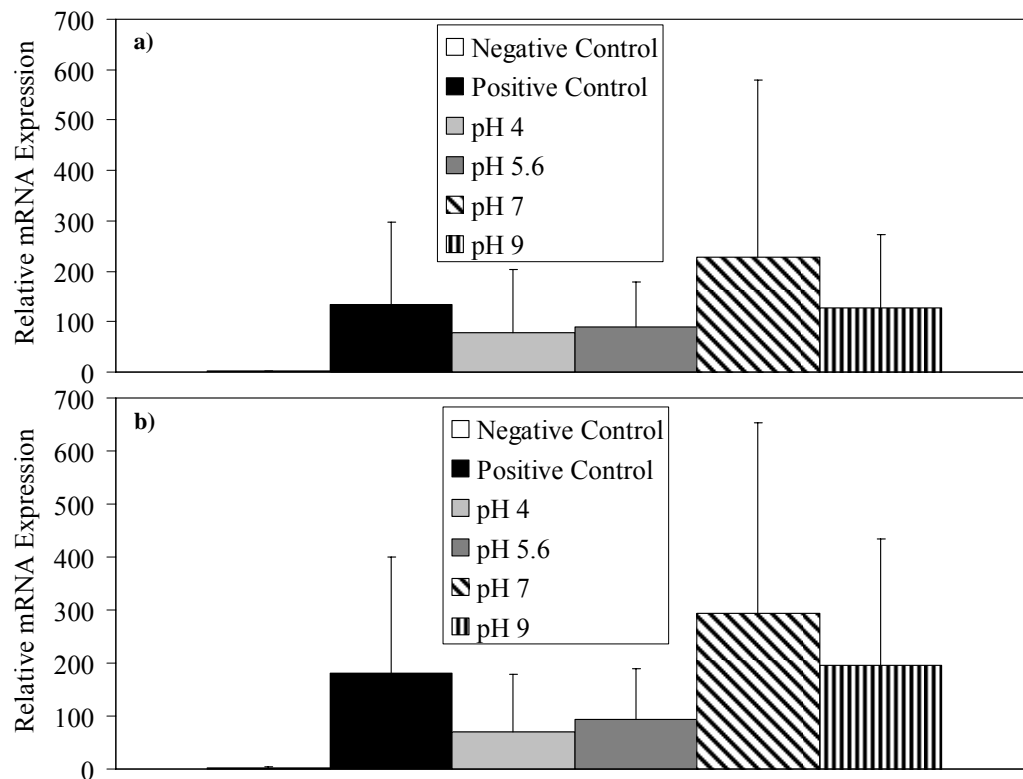


Figure 7-21. Relative expression of IL-8 mRNA in negative controls and DNCB-induced porcine rashes treated for 72 hours with distilled water (positive controls), or nanocrystalline silver-derived solutions generated at starting pHs of 4, 5.6, 7, and 9. Relative mRNA expression of IL-8 was calculated relative to the mRNA expression by negative controls using HPRT (a) or GAPDH (b) as the housekeeping gene. Statistical analyses were performed using one-way ANOVAs with Tukey-Kramer post tests. The one-way ANOVA tests indicated that the differences between groups were not significant ($p=0.7628$ for HPRT, $p=0.5939$ for GAPDH). Error bars represent standard deviations ($n=3$ for all data points).

Figure 7-22 shows the relative mRNA expression of IL-10 after 72 hours of treatment with various nanocrystalline silver-derived solutions, and a similar trend is observed to that of the TNF- α and IL-1 β expression, but there were no significant differences between groups, when calculations were performed using either HPRT (a) or GAPDH (b) as the housekeeping gene.

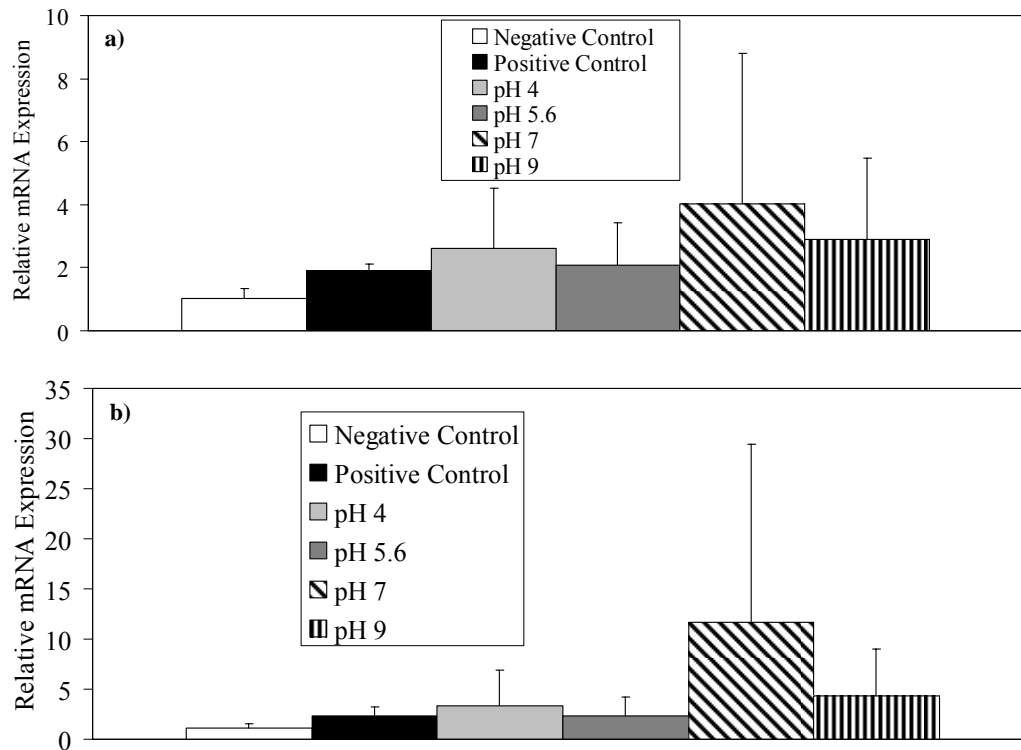


Figure 7-22. Relative expression of IL-10 mRNA in negative controls and DNCB-induced porcine rashes treated for 72 hours with distilled water (positive controls), or nanocrystalline silver-derived solutions generated at starting pHs of 4, 5.6, 7, and 9. Relative mRNA expression of IL-10 was calculated relative to the mRNA expression by negative controls using HPRT (a) or GAPDH (b) as the housekeeping gene. Statistical analyses were performed using one-way ANOVAs with Tukey-Kramer post tests. The one-way ANOVA tests indicated that the differences between groups were not significant ($p=0.7531$ for HPRT, $p=0.6045$ for GAPDH). Error bars represent standard deviations ($n=3$ for all data points).

Figure 7-23 shows the relative mRNA expression of IL-12 after 72 hours of treatment with various nanocrystalline silver-derived solutions. There were no significant differences between groups, using either HPRT (a) or GAPDH (b) as the housekeeping gene during calculations. The data suggests a trend of increased IL-12 mRNA expression in animals treated with pH 4, 7, or 9 solutions relative to the pH 5.6 treated group and positive controls.

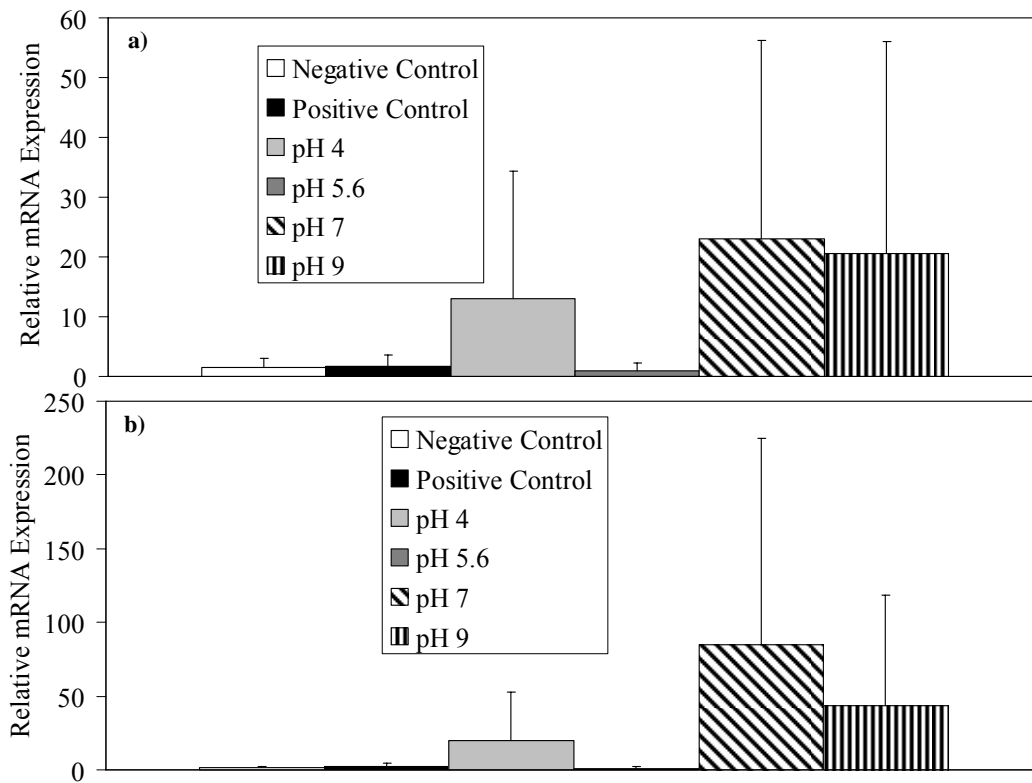


Figure 7-23. Relative expression of IL-12 mRNA in negative controls and DNCB-induced porcine rashes treated for 72 hours with distilled water (positive controls), or nanocrystalline silver-derived solutions generated at starting pHs of 4, 5.6, 7, and 9. Relative mRNA expression of IL-12 was calculated relative to the mRNA expression by negative controls using HPRT (a) or GAPDH (b) as the housekeeping gene. Statistical analyses were performed using one-way ANOVAs with Tukey-Kramer post tests. The one-way ANOVA tests indicated that the differences between groups were not significant ($p=0.6596$ for HPRT, $p=0.5916$ for GAPDH). Error bars represent standard deviations ($n=3$ for all data points).

A similar trend to that observed with IL-12 mRNA expression was observed for IL-17 relative mRNA expression after 72 hours of treatment with various nanocrystalline silver-derived solutions (Figure 7-24). Again, these trends were not significant, when calculations were performed using either HPRT (a) or GAPDH (b) as the housekeeping gene.

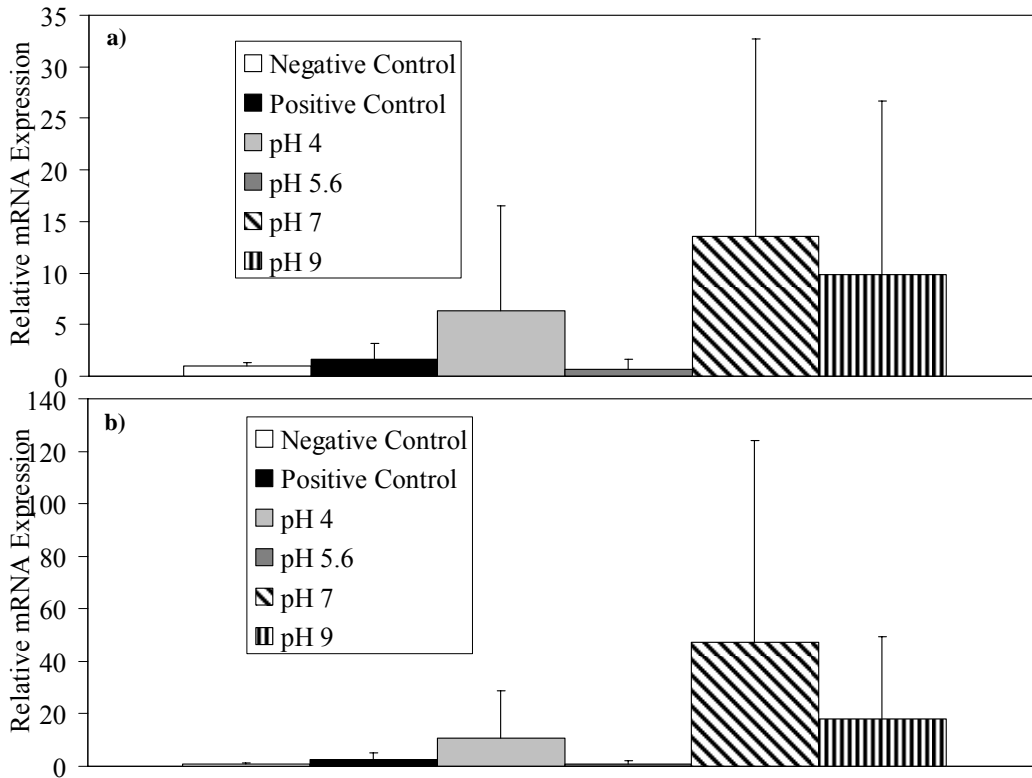


Figure 7-24. Relative expression of IL-17 mRNA in negative controls and DNCB-induced porcine rashes treated for 72 hours with distilled water (positive controls), or nanocrystalline silver-derived solutions generated at starting pHs of 4, 5.6, 7, and 9. Relative mRNA expression of IL-17 was calculated relative to the mRNA expression by negative controls using HPRT (a) or GAPDH (b) as the housekeeping gene. Statistical analyses were performed using one-way ANOVAs with Tukey-Kramer post tests. The one-way ANOVA tests indicated that the differences between groups were not significant ($p=0.7617$ for HPRT, $p=0.6841$ for GAPDH). Error bars represent standard deviations ($n=3$ for all data points).

As most of the samples did not interact with the IL-31 sequence used, it was not possible to calculate the relative mRNA expression of IL-31 in this study.

Gelatinase Zymography

Figure 7-25 shows zymograms for all pigs in each treatment and control group after 24 (a) and 72 (b) hours of treatment. Throughout treatment, negative controls visually showed very low levels of gelatinases. After 72 hours of treatment, positive controls and pH 4 solution-treated animals had two animals out of three showing high gelatinase levels, while animals treated with pH 5.6, 7, and 9 solutions had only one animal out of three showing high gelatinase levels.

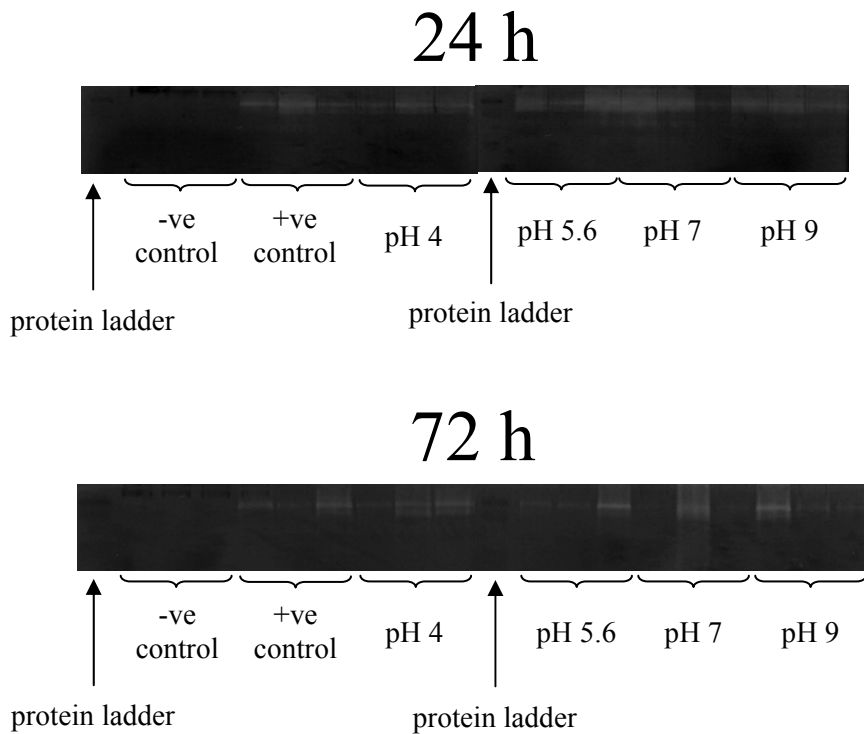


Figure 7-25. Zymogram showing gelatinase activity in biopsies from DNCB-induced rashes treated with various nanocrystalline silver-derived solutions. Zymograms are shown for all three animals of each treatment group at 24 and 72 hours in the follow order for each time period: negative controls (no rash, treated with distilled water), positive controls (had DNCB-induced rash, treated with distilled water), and animals with DNCB-induced rashes that were treated with nanocrystalline silver-derived solutions generated at starting pHs of 4, 5.6, 7, and 9. Protein ladders were run as the first sample on each gel. The gels testing biopsies from 24 hours were run simultaneously, as were the gels testing 72 hour biopsies.

Figure 7-26a shows the semi-quantitative analysis of pMMP-9 levels, which showed a trend towards significant differences between groups ($p=0.0817$), with pMMP-9 levels being lower for pH 5.6, 7, and 9 treatments relative to positive controls and pH 4 treatments. All treatment groups showed similar levels at 72 hours. Figure 7-26b shows the semi-quantitative analysis of active MMP-9 (aMMP-9) levels. Again, there was a trend towards significant differences between groups ($p=0.0944$), with lower expression levels at 24h for silver treated animals relative to positive controls, particularly with treatments at pH 5.6, 7, and 9. Panel 26c shows the semi-quantitative analysis for pMMP-2, which showed significant differences between groups ($p=0.0010$), with pH 5.6 and 9 treated animals having significantly lower pMMP-2 levels relative to positive controls after 24 hours of treatment. Panel 26d shows the semi-quantitative analysis for aMMP-2, which also showed significant differences between groups ($p=0.0019$), with pH 9 solution treated animals showing significantly lower aMMP-2 levels at 24 hours relative to positive controls and pH 4 solution treated animals.

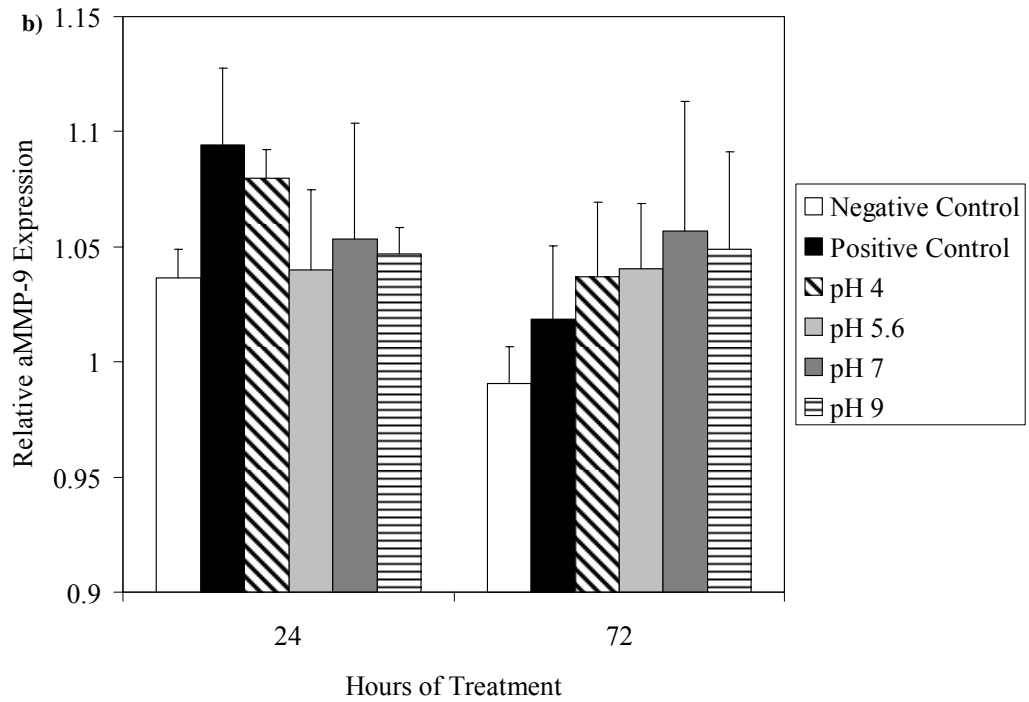
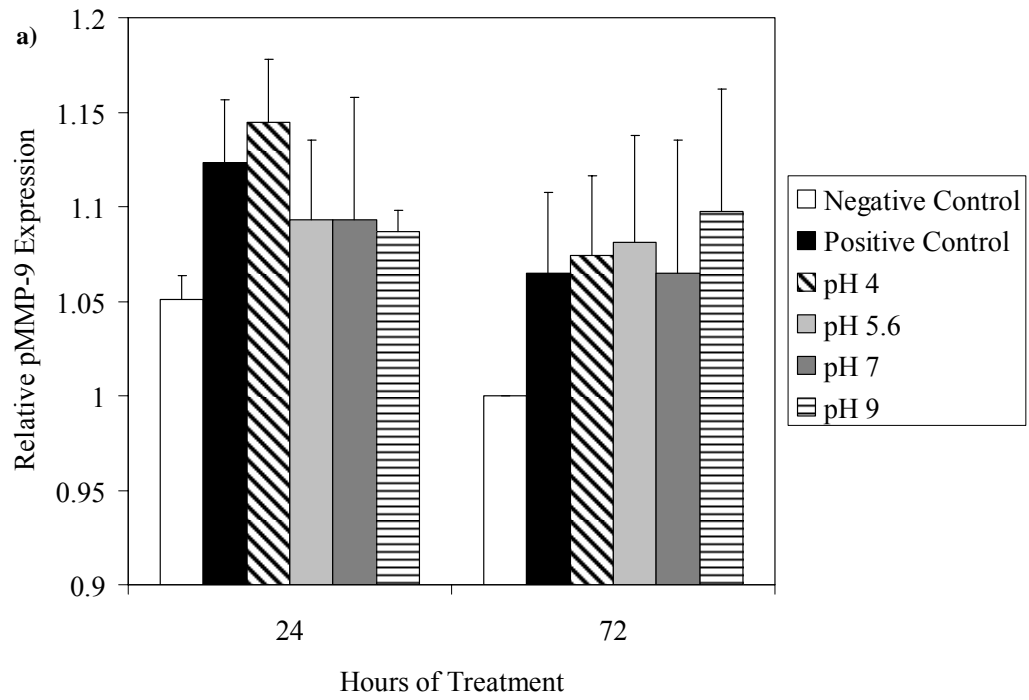


Figure 7-26.

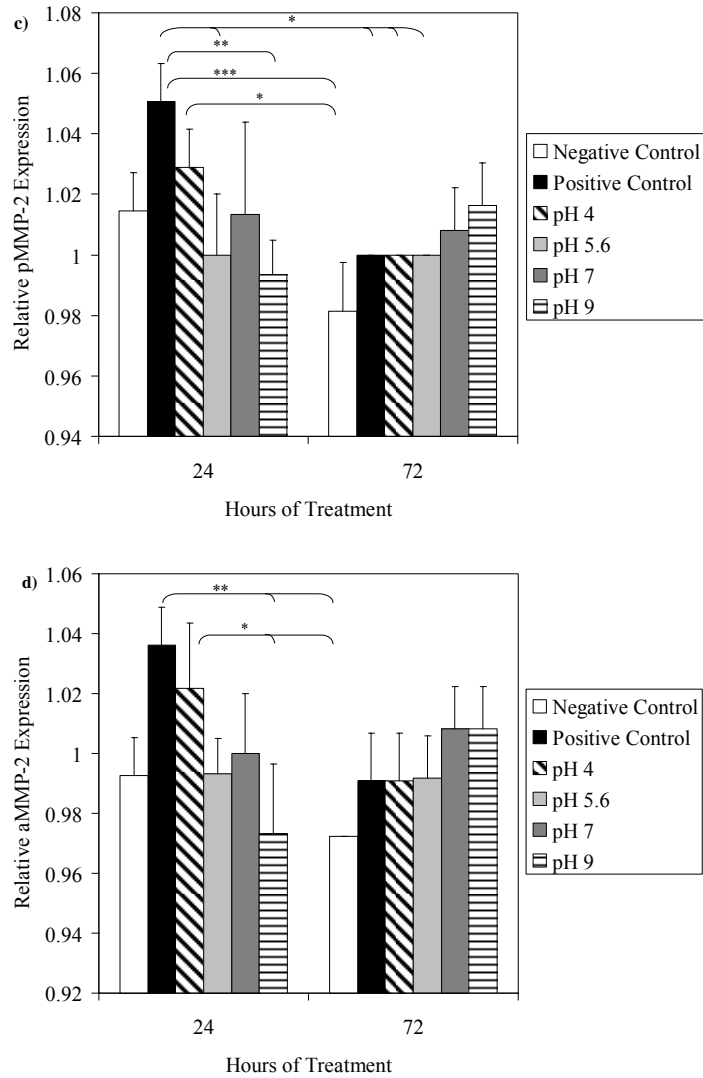


Figure 7-26, continued. Quantitation of MMP band intensities from biopsies of DNCB-induced rashes treated with various nanocrystalline silver-derived solutions. The integrated density values (IDV) relative to the gel background IDV for pMMP-9, aMMP-9, pMMP-2, and aMMP-2 after 24 and 72 hours are shown in Panels (a-d), respectively, for negative controls (no rash, distilled water treatment), positive controls (rash, distilled water treatment), and animals with DNCB-induced rashes treated with nanocrystalline silver-derived solutions generated at starting pHs of 4, 5.6, 7, and 9. The statistical analyses were performed using one-way ANOVAs. The overall p values from the one-way ANOVAs were as follows: 0.0817 (not quite significant) for pMMP-9, 0.0944 (not quite significant) for aMMP-9, 0.0010 for pMMP-2, and 0.0019 for aMMP-2. The results of the Tukey-Kramer multiple comparisons post tests are shown on the figure as follows: * indicates significantly different ($p < 0.05$), ** indicates very significantly different ($p < 0.01$), and *** indicates extremely significantly different ($p < 0.001$). Error bars represent standard deviations ($n=3$ for all data points).

Apoptosis Detection and Quantification

Figure 7-27 panels (a) through (k) show representative images of staining for apoptotic cells after 24 hours of various treatments. Panels (l) through (o) show semi-quantitative analysis of apoptotic staining in the epidermis (l), superficial dermis (m), deep dermis (n), and total dermis (o). Negative controls (a) had very few apoptotic cells. Positive controls showed somewhat higher levels of apoptosis in the epidermis (b), but had decreasing levels of apoptosis with tissue depth, with virtually no cells undergoing apoptosis in the dermis (c, n). Animals treated with pH 4 solutions had somewhat lower levels of apoptosis induction in the epidermis relative to positive controls, with similar levels present in the superficial dermis (d, l, m). However, they demonstrated the highest level of apoptotic cells in the deep dermis (e, n), with levels significantly higher than negative controls. Animals treated with pH 5.6 solutions did not demonstrate apoptosis induction in either the epidermis (f, l) or the dermis (g, m-o). Animals treated with pH 7 solutions showed the highest levels of apoptotic cells in the upper dermis, with significantly higher staining than negative controls (m), and in the epidermis as well (h), although this did not reach statistical significance due to high interanimal variability (l). Apoptotic staining was also present to a lesser extent in the deep dermis (i, n). Animals treated with pH 9 solutions did not show apoptotic staining in the newly forming epidermis (j, l), but did have apoptotic cells in the dermis, although to a lesser extent than present in the pH 4 and 7 treated animals (k, m-n). Combining the superficial and deep dermal semi-

quantitative staining results, animals treated with pH 4 solutions had significantly higher apoptotic staining than negative controls, positive controls, and pH 5.6 solution-treated animals, while animals treated with pH 7 solutions had significantly higher apoptotic staining relative to negative controls and pH 5.6 solution-treated animals (o).

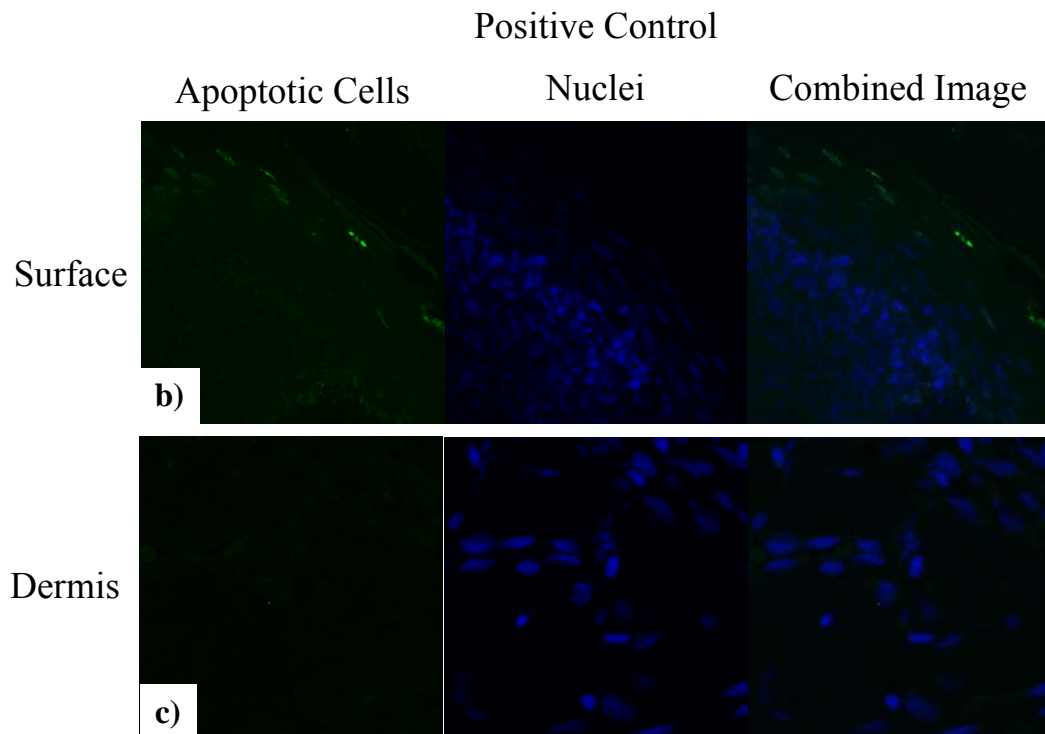
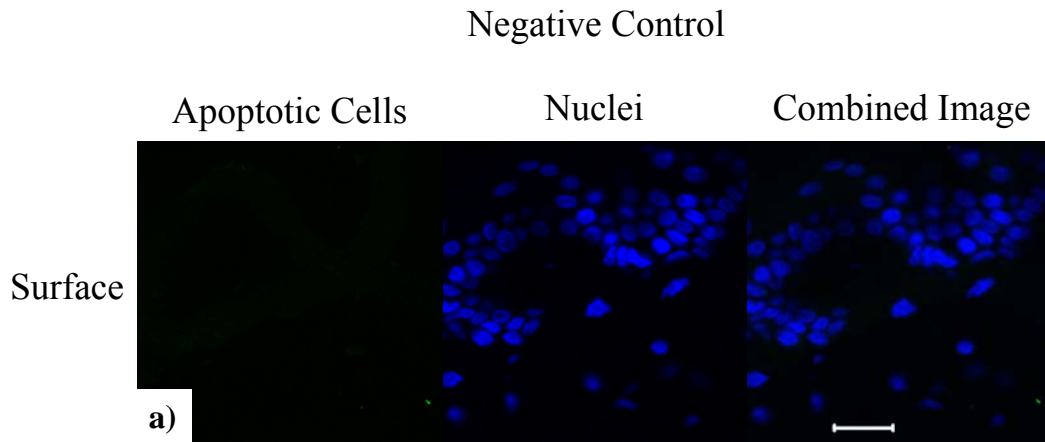


Figure 7-27.

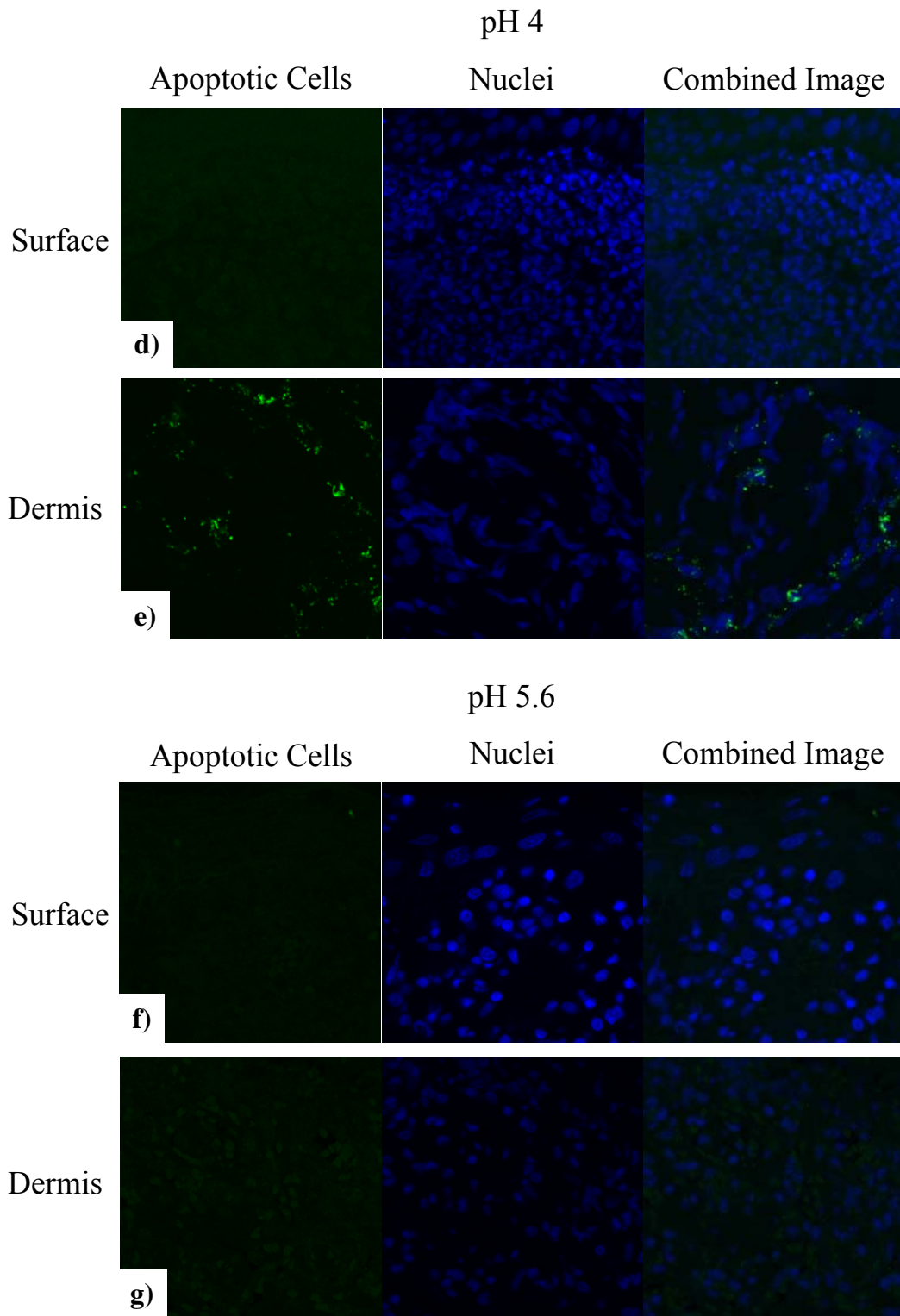


Figure 7-27, continued.

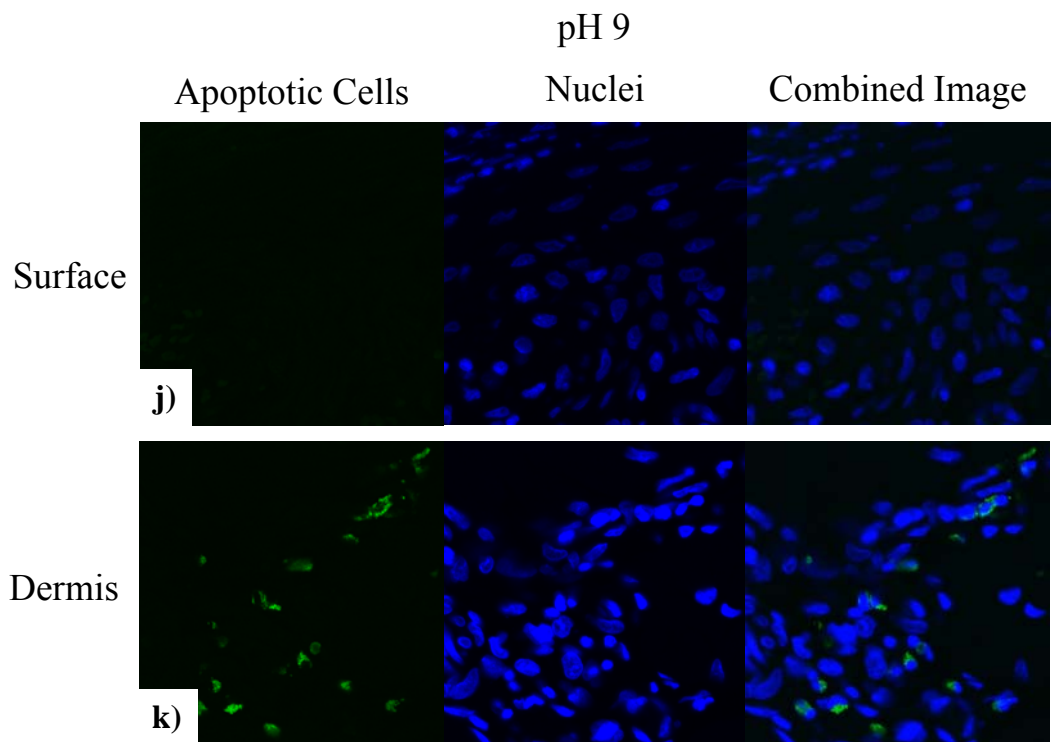
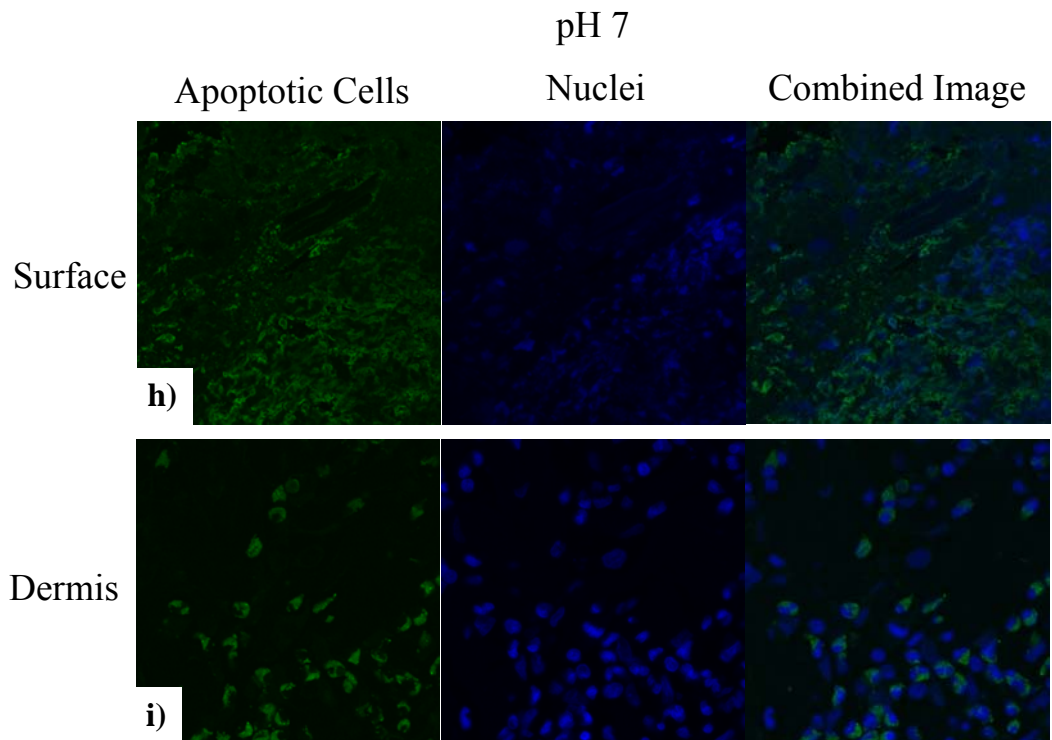


Figure 7-27, continued.

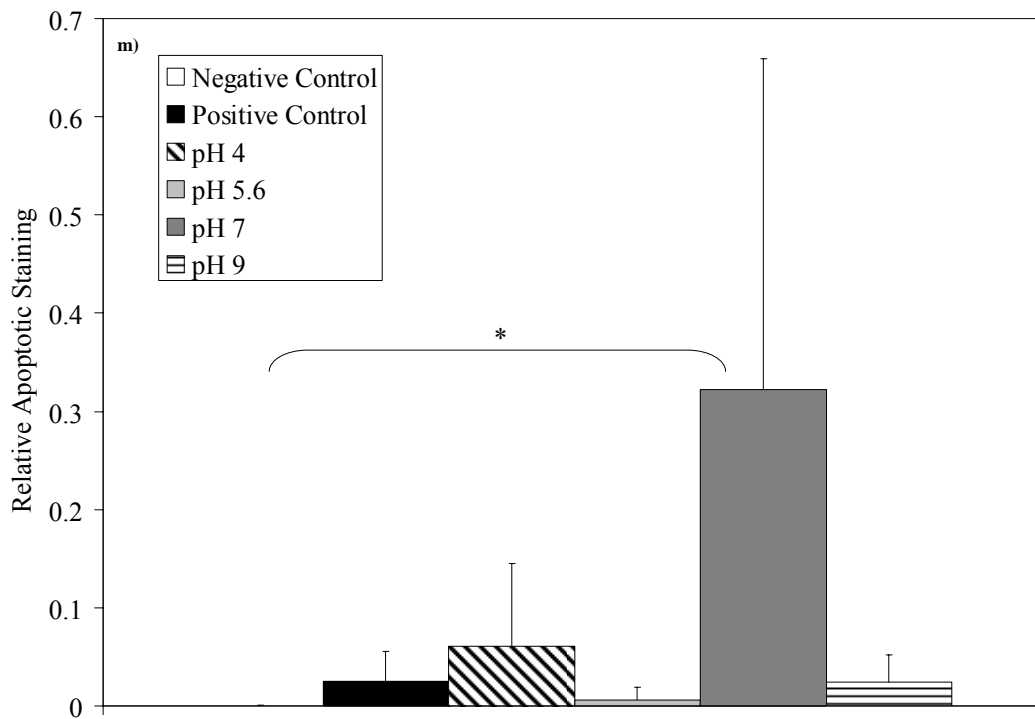
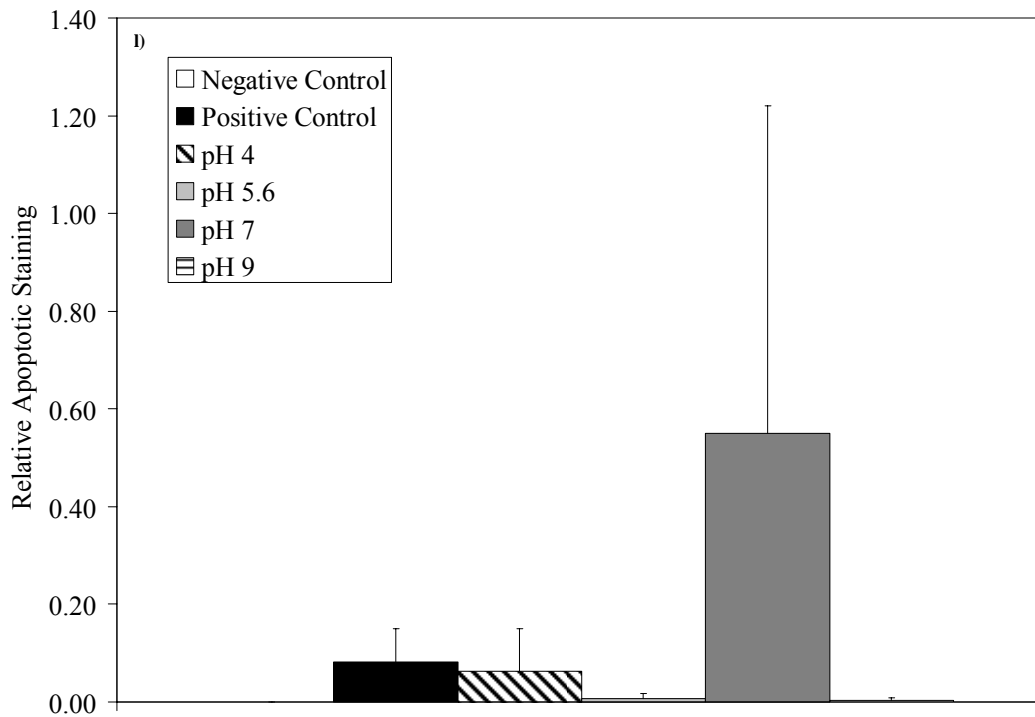


Figure 7-27, continued.

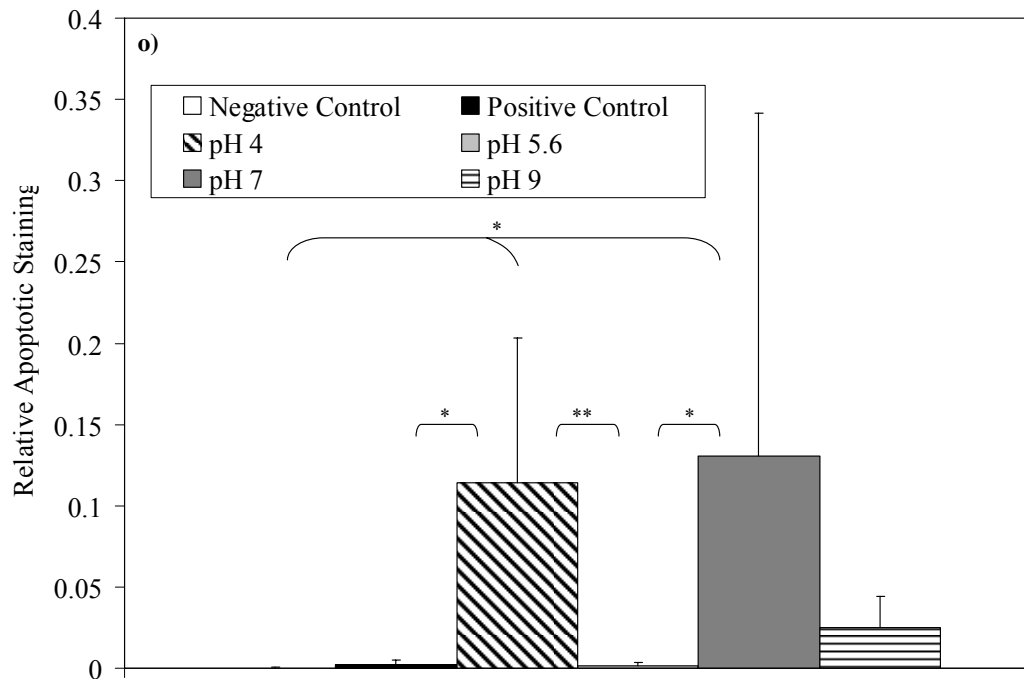
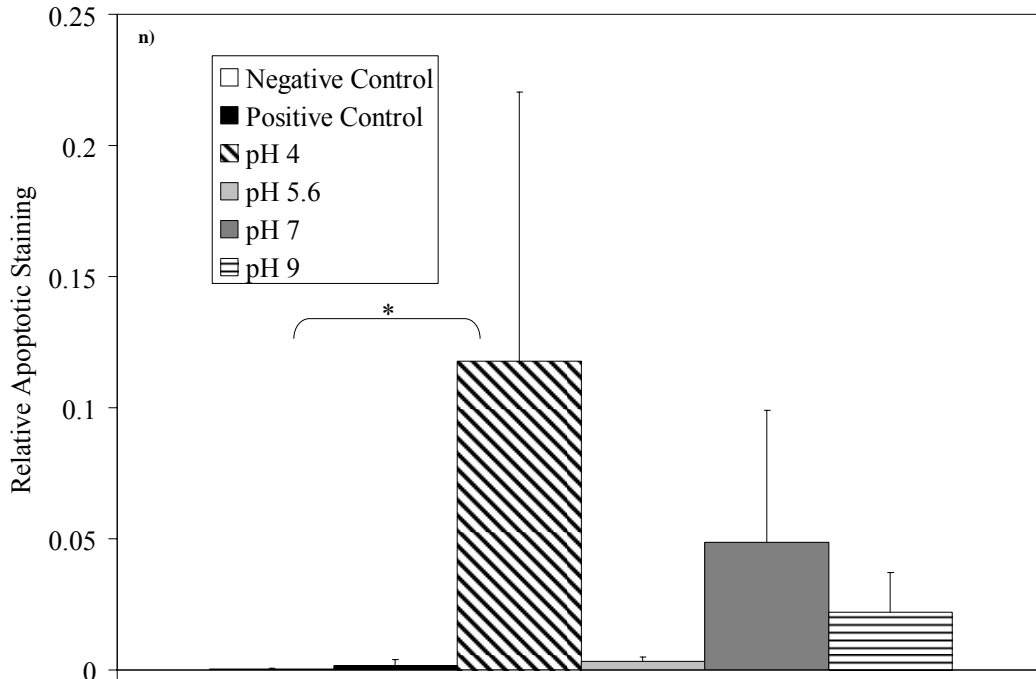


Figure 7-27. Apoptosis detection in biopsies of DNCB-induced rashes treated for 24 hours with various nanocrystalline silver-derived solutions. Representative fluorescence images obtained via confocal microscopy for immunohistochemical detection of apoptotic cells in pigs with DNCB-induced rashes after 24 hours of various treatments are shown. The first column shows staining by FITC for apoptotic cells (green). The second column shows counterstaining by DAPI for

nuclei (blue). The third column shows the combination of apoptotic and nuclear staining. Images in Row (a) are from the surface (epidermis and upper dermis) of a negative control (no rash) treated with distilled water. Images in Rows (b) and (c) are of the skin surface and deep dermis, respectively, of a positive control (rash treated with distilled water). Images in Rows (d) and (e) are of the surface and the deep dermis, respectively, of a DNCB-induced porcine rash treated with a nanocrystalline silver-derived solution with a starting pH of 4. Images in Rows (f) and (g) are of the surface and the deep dermis, respectively, of a DNCB-induced porcine rash treated with a nanocrystalline silver-derived solution with a starting pH of 5.6. Images in Rows (h) and (i) are of the surface and the deep dermis, respectively, of a DNCB-induced porcine rash treated with a nanocrystalline silver-derived solution with a starting pH of 7. Images in Rows (j) and (k) are of the surface and the deep dermis, respectively, of a DNCB-induced porcine rash treated with a nanocrystalline silver-derived solution with a starting pH of 9. The scale bar in the far right image in Row (a) represents 20 μm . Semi-quantitative analysis of apoptotic staining in biopsies from pigs with DNCB-induced rashes after 24h of various treatments is also shown. The relative apoptotic staining level was calculated by taking a ratio of apoptotic staining (where colocalized with nuclear staining) to total nuclear staining in a given image window. Staining in the epidermis, superficial dermis, deep dermis, and all dermal images combined are shown in (l) through (o), respectively. Kruskal Wallis testing indicated that there were no significant differences in staining between groups in the epidermis ($p=0.0673$), but that there were significant differences between groups in the superficial dermis ($p=0.0433$), the deep dermis ($p=0.0055$), and the dermis as a whole ($p<0.0001$). The results of Dunn's multiple comparisons post-tests are shown on the figure as follows: * indicates significantly different ($p<0.05$), and ** indicates very significantly different ($p<0.01$). Error bars represent standard deviations ($n=3$ for all data points).

Immunohistochemistry

Figures 7-28 and 7-29 shows representative images of immunohistochemical staining for TNF- α after 24 and 72 hours of treatment, respectively. Immunohistochemical staining scores are shown in Figure 7-30 after 24 and 72 hours of treatment in panels (a) and (b), respectively. Negative controls showed some staining in the epidermis throughout the experiment, but otherwise had low TNF- α levels. Positive controls showed widespread TNF- α staining, which increased in intensity during the treatment period, having significantly higher staining scores than negative controls at 72 hours ($p<0.05$).

Of the treatment groups, animals treated with pH 7 solutions showed the strongest staining for TNF- α at 24 hours, however this trend did not reach significance. At 72 hours, staining for TNF- α was somewhat increased with pH 4 and pH 5.6 treatments, particularly in the newly forming epidermis, but not to the levels observed in positive controls. In particular, animals treated with pH 5.6 treatments still had significantly lower scores than the positive controls ($p < 0.05$). TNF- α staining appeared to decrease with increasing pH of treatment at 72 hours, with animals treated with pH 7 and 9 solutions having significantly lower staining scores for TNF- α relative to positive controls ($p < 0.01$) and pH 4 treated animals ($p < 0.05$).

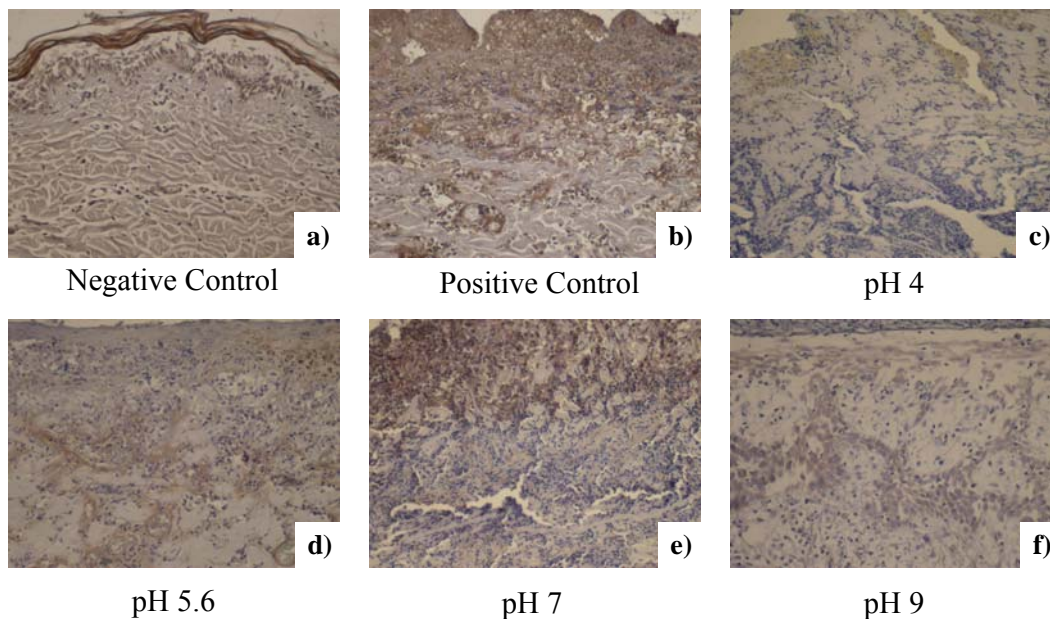


Figure 7-28. Immunohistochemical detection of TNF- α in biopsies of DNCB-induced rashes treated with various nanocrystalline silver-derived solutions for 24 hours. Representative images are shown for immunohistochemical detection of TNF- α after 24 hours treatment of negative controls with distilled water (a), and DNCB-induced porcine contact dermatitis rashes with distilled water (positive control) (b), or nanocrystalline silver-derived solutions generated at starting pHs of 4 (c), 5.6 (d), 7 (e), or 9 (f). The scale bar in A represents 100 μm . Staining for TNF- α appears brown, while the cell nuclei are counterstained purple using hematoxylin.

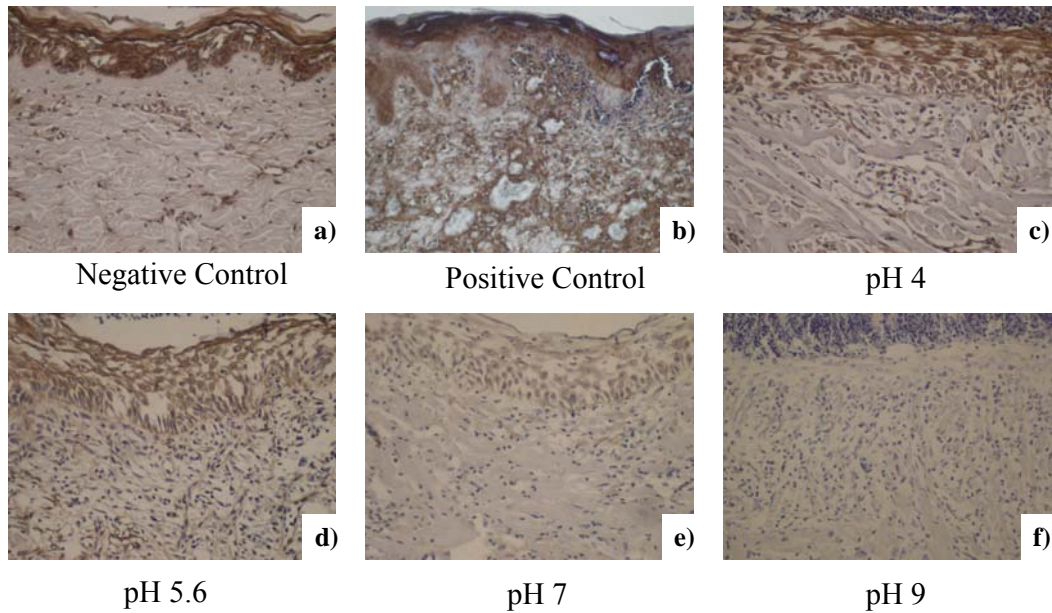


Figure 7-29. Immunohistochemical detection of TNF- α in biopsies of DNCB-induced rashes treated with various nanocrystalline silver-derived solutions for 72 hours. Representative images are shown for immunohistochemical detection of TNF- α after 72 hours treatment of negative controls with distilled water (a), and DNCB-induced porcine contact dermatitis rashes with distilled water (positive control) (b), or nanocrystalline silver-derived solutions generated at starting pHs of 4 (c), 5.6 (d), 7 (e), or 9 (f). The scale bar in A represents 100 μ m. Staining for TNF- α appears brown, while the cell nuclei are counterstained purple using hematoxylin.

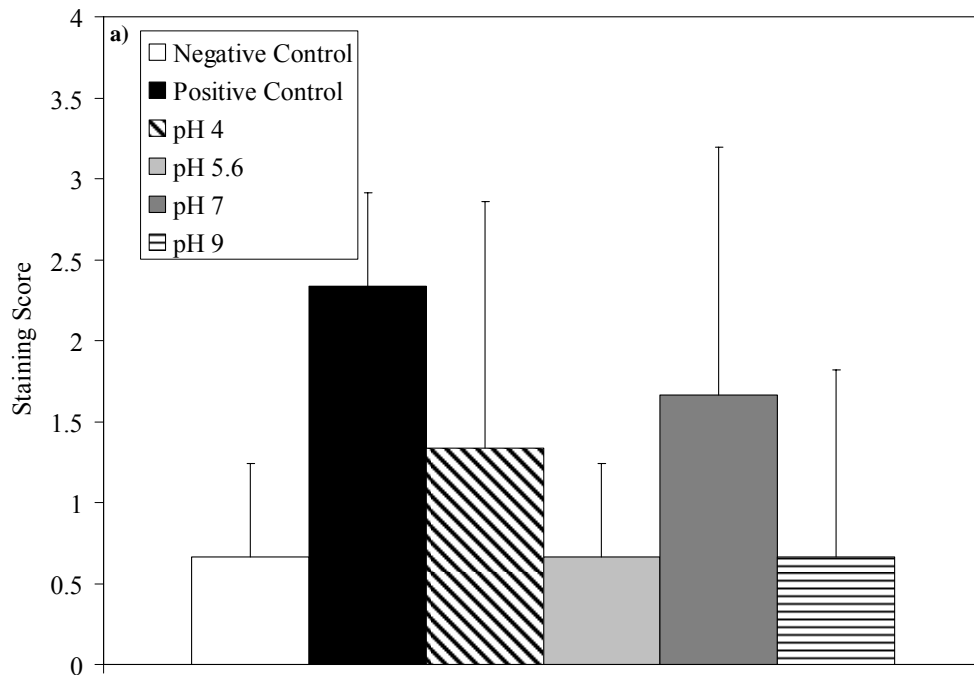


Figure 7-30.

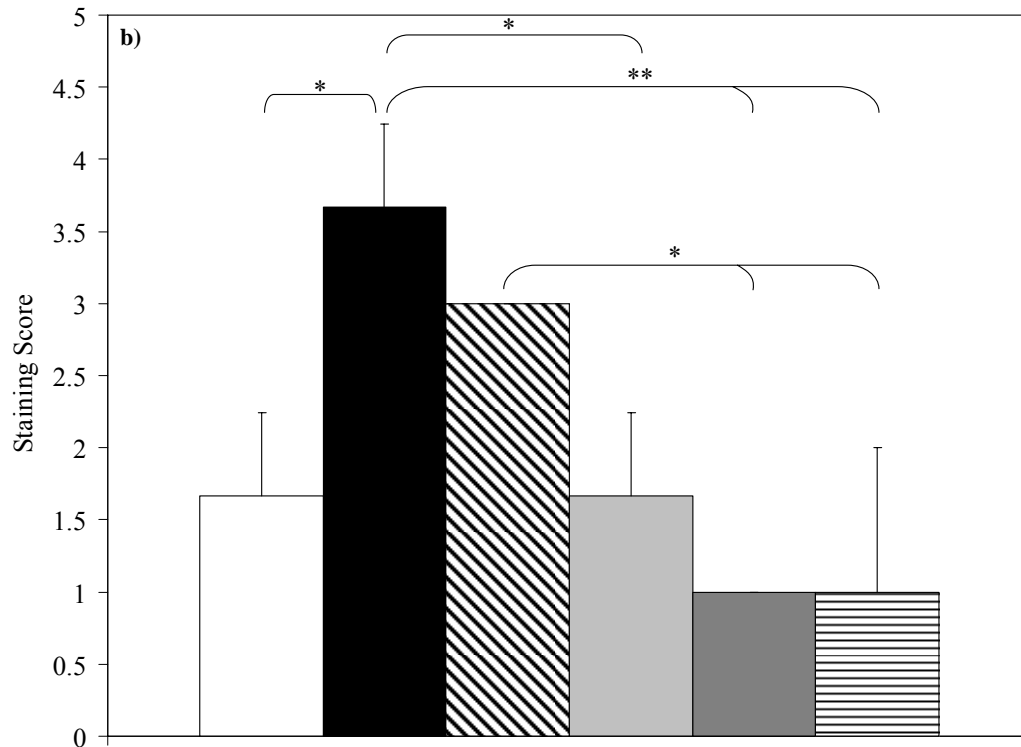


Figure 7-30, continued. Semi-quantitative analyses of immunohistochemical staining for TNF- α in biopsies of DNCB-induced rashes treated with various nanocrystalline silver-derived solutions. Immunohistochemical staining scores for TNF- α are shown after 24 hours (a) and 72 hours (b) of treatment. Statistical analyses were performed using one-way ANOVAs with Tukey-Kramer Multiple Comparisons post tests. Overall p values from the one-way ANOVAs were 0.3582 and 0.0004 after 24 and 72 hours, respectively. The results of the Tukey-Kramer post tests are indicated on the figure as follows: * indicates significantly different ($p < 0.05$), and ** indicates very significantly different ($p < 0.01$). Error bars represent standard deviations ($n=3$ for all data points).

Representative images of immunohistochemical staining for TGF- β are shown in Figures 7-31 and 7-32, for 24 and 72 hours of treatment, respectively, with various nanocrystalline silver-derived solutions. Staining was low in the negative (a) and positive (b) controls, as well as all treatment groups (c-f) at both 24 and 72 hours. Figure 7-33 shows immunohistochemical staining scores for TGF- β after 24 and 72 hours of treatment in panels (a) and (b), respectively. There were no significant differences in staining levels at either time points.

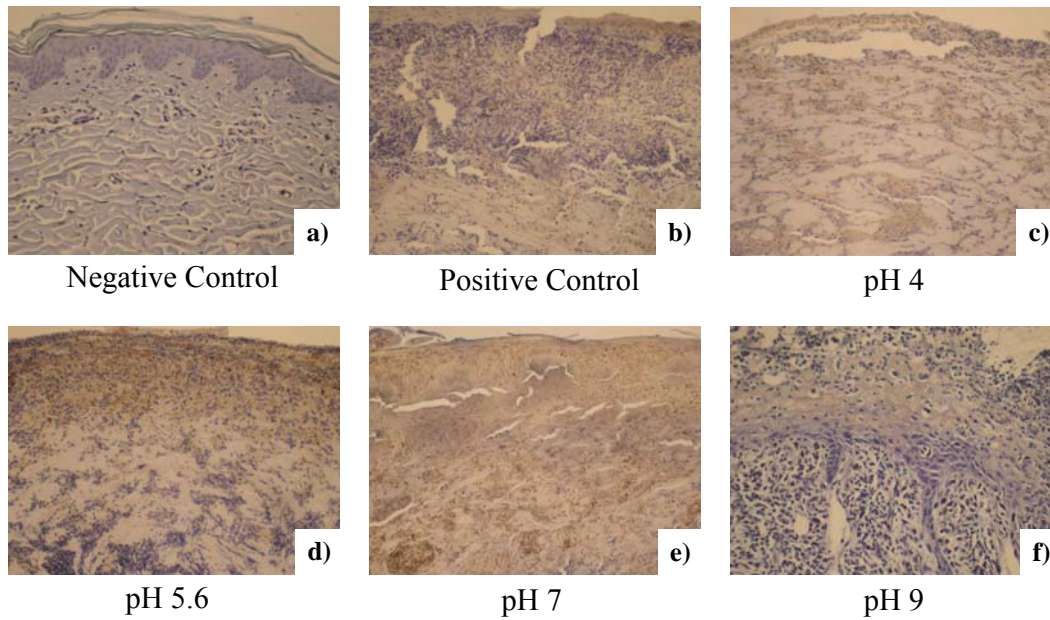


Figure 7-31. Immunohistochemical detection of TGF- β in biopsies of DNCB-induced rashes treated with various nanocrystalline silver-derived solutions for 24 hours. Representative images are shown for immunohistochemical detection of TGF- β after 24 hours treatment of negative controls with distilled water (a), and DNCB-induced porcine contact dermatitis rashes with distilled water (positive control) (b), or nanocrystalline silver-derived solutions generated at starting pHs of 4 (c), 5.6 (d), 7 (e), or 9 (f). The scale bar in A represents 100 μ m. Staining for TGF- β appears brown, while the cell nuclei are counterstained purple using hematoxylin.

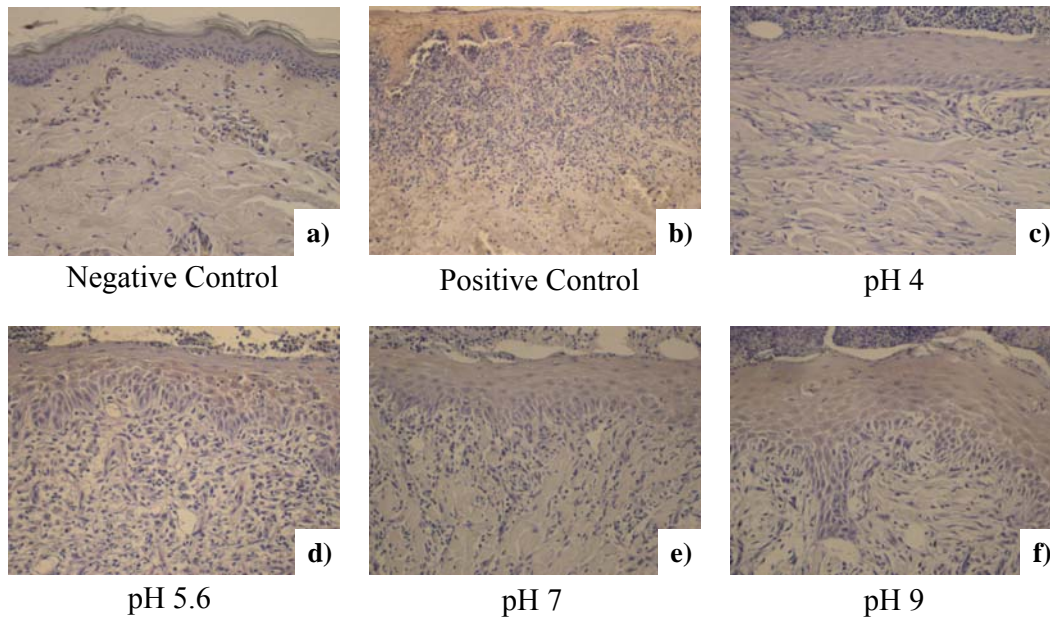


Figure 7-32. Immunohistochemical detection of TGF- β in biopsies of DNCB-induced rashes treated with various nanocrystalline silver-derived solutions for 72 hours. Representative images are shown for immunohistochemical detection of TGF- β after 72 hours treatment of negative controls with distilled water (a), and DNCB-induced porcine contact dermatitis rashes with distilled water (positive control) (b), or nanocrystalline silver-derived solutions generated at starting pHs of 4 (c), 5.6 (d), 7 (e), or 9 (f). The scale bar in A represents 100 μ m. Staining for TGF- β appears brown, while the cell nuclei are counterstained purple using hematoxylin.

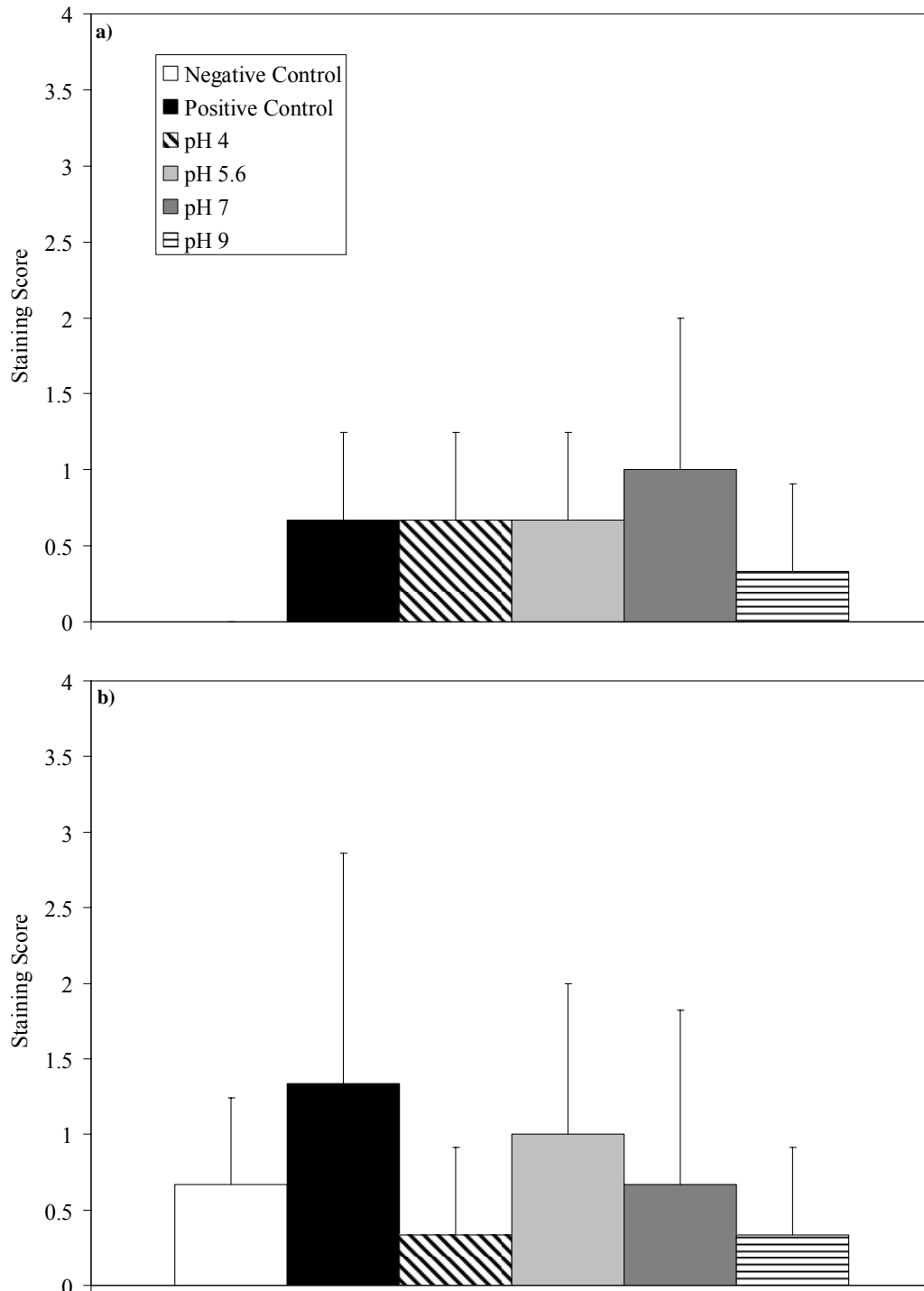


Figure 7-33. Semi-quantitative analyses of immunohistochemical staining for TGF- β in biopsies of DNCB-induced rashes treated with various nanocrystalline silver-derived solutions. Immunohistochemical staining scores for TGF- β are shown after 24 hours (a) and 72 hours (b) of treatment. Statistical analyses were performed using one-way ANOVAs with Tukey-Kramer Multiple Comparisons post tests. Overall p values from the one-way ANOVAs were 0.5038 and 0.7831 after 24 and 72 hours, respectively. Error bars = standard deviations (n=3).

Figures 7-34 and 7-35 show representative images of immunohistochemical staining for IL-8 after 24 and 72 hours of treatment, respectively. Immunohistochemical staining scores for IL-8 after 24 and 72 hours of treatment are shown in panels (a) and (b) of Figure 7-36, respectively. As with staining for TNF- α , negative controls showed some staining for IL-8 in the epidermis, but low levels in the dermis throughout the experiment. Positive controls, and pH 5.6 and 7 solution-treated animals showed mild increases in IL-8 staining relative to negative controls at 24 hours, while pH 4 and 9 treated animals showed lower levels of staining. However, this trend did not reach significance. At 72 hours, positive controls showed strong staining for IL-8 throughout the epidermis and in a cell-associated fashion in the dermis. Animals treated with pH 4, 5.6, and 7 solutions showed low staining for IL-8 at this time point, with the pH 5.6 solution treated animals having significantly lower staining scores relative to the positive controls ($p < 0.05$). Interestingly, animals treated with pH 9 solutions showed strong staining for IL-8 in the epidermis at 72 hours, although this was not as dark as the staining present in the positive controls.

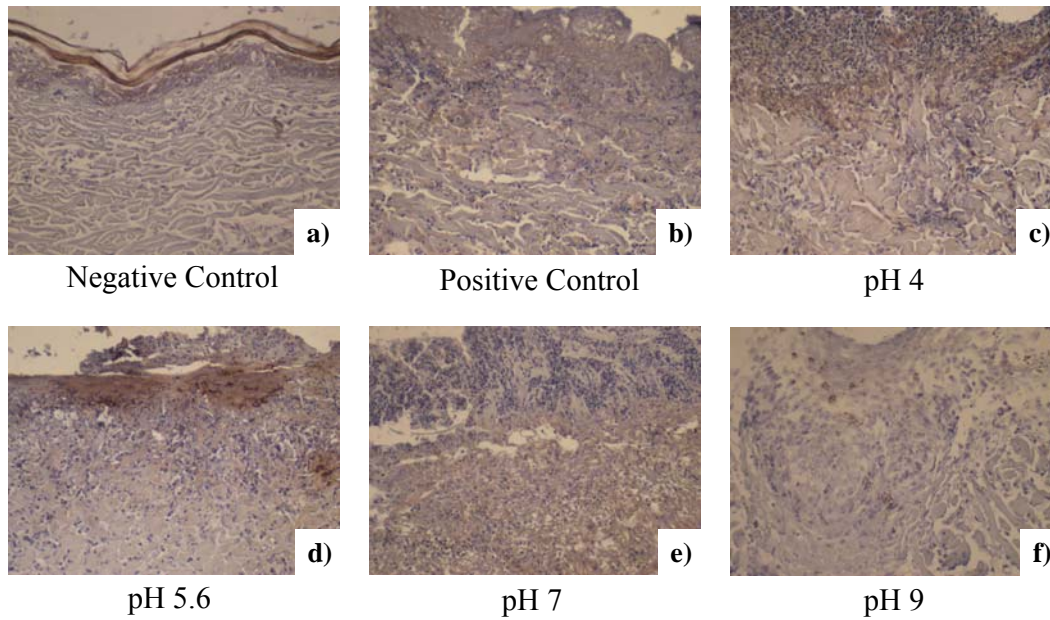


Figure 7-34. Immunohistochemical detection of IL-8 in biopsies of DNCB-induced rashes treated with various nanocrystalline silver-derived solutions for 24 hours. Representative images are shown for immunohistochemical detection of IL-8 after 24 hours treatment of negative controls with distilled water (a), and DNCB-induced porcine contact dermatitis rashes with distilled water (positive control) (b), or nanocrystalline silver-derived solutions generated at starting pHs of 4 (c), 5.6 (d), 7 (e), or 9 (f). The scale bar in A represents 100 μ m. Staining for IL-8 appears brown, while the cell nuclei are counterstained purple using hematoxylin.

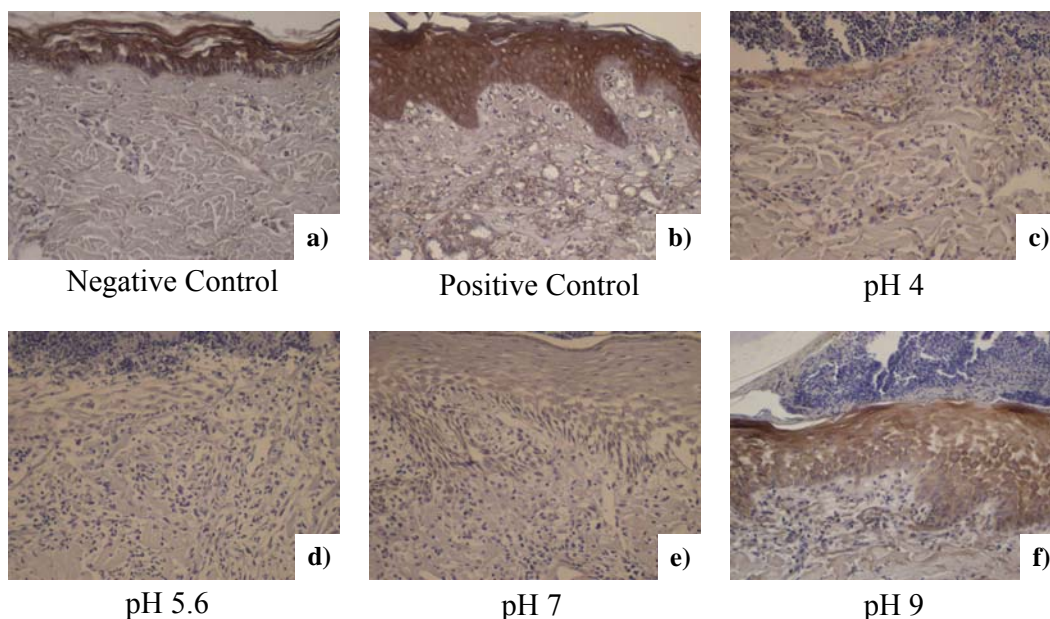


Figure 7-35. Immunohistochemical detection of IL-8 in biopsies of DNCB-induced rashes treated with various nanocrystalline silver-derived solutions for 72 hours. Representative images are shown for immunohistochemical detection of IL-8 after 72 hours treatment of negative controls with distilled water (a), and DNCB-induced porcine contact dermatitis rashes with distilled water (positive control) (b), or nanocrystalline silver-derived solutions generated at starting pHs of 4 (c), 5.6 (d), 7 (e), or 9 (f). The scale bar in A represents 100 μm . Staining for IL-8 appears brown, while the cell nuclei are counterstained purple using hematoxylin.

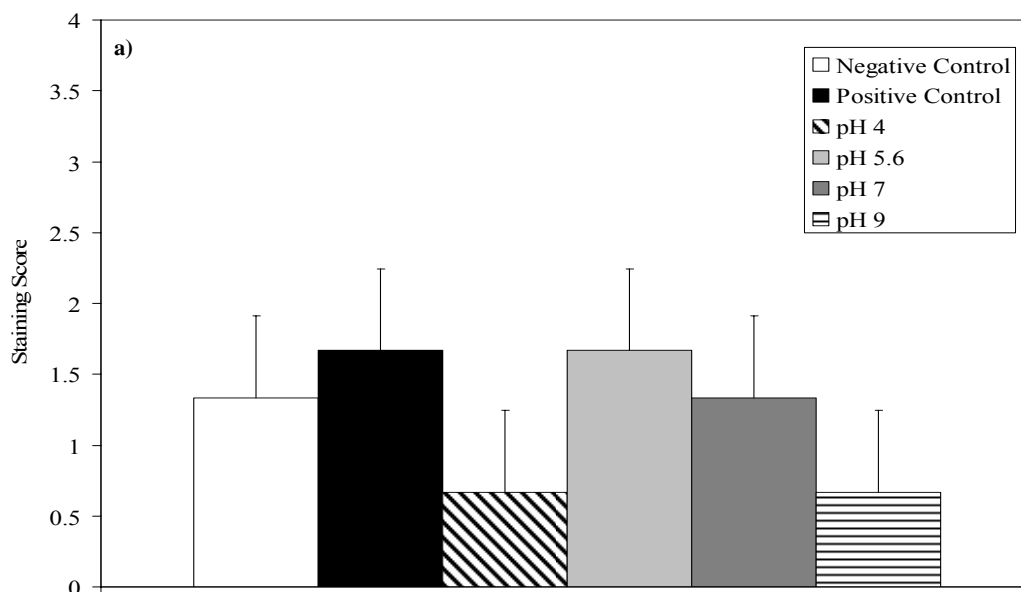


Figure 7-36.

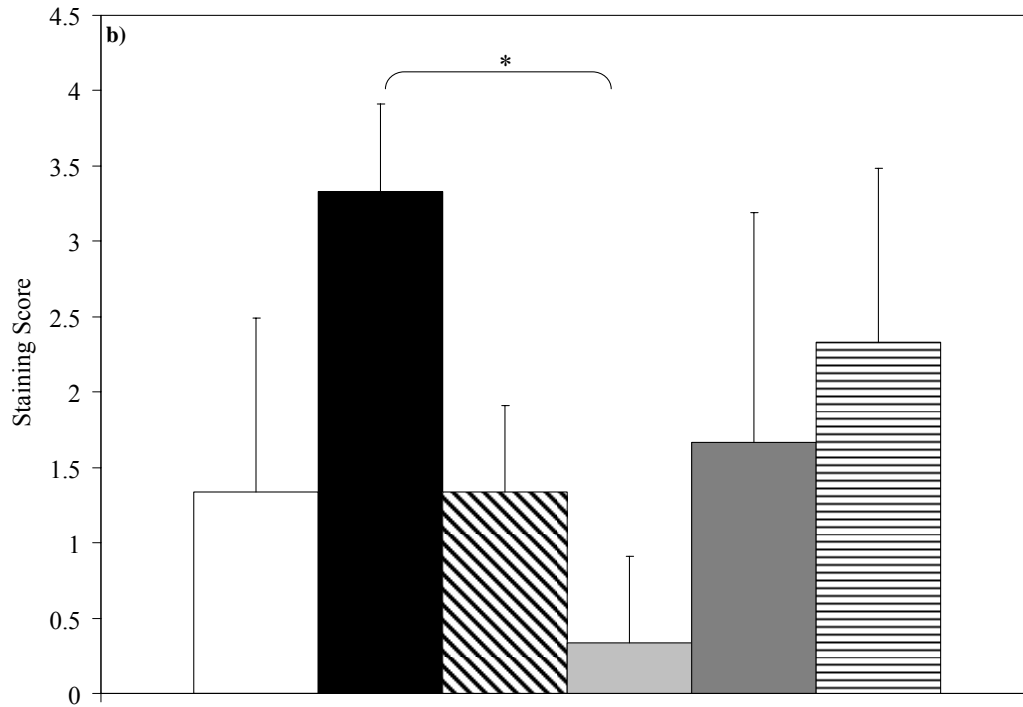


Figure 7-36, continued. Semi-quantitative analyses of immunohistochemical staining for IL-8 in biopsies of DNCB-induced rashes treated with various nanocrystalline silver-derived solutions. Immunohistochemical staining scores for IL-8 are shown after 24 hours (a) and 72 hours (b) of treatment. Statistical analyses were performed using one-way ANOVAs with Tukey-Kramer Multiple Comparisons post tests. Overall p values from the one-way ANOVAs were 0.1742 and 0.0492 after 24h and 72h, respectively. The results of the Tukey-Kramer post tests are indicated on the figure as follows: * indicates significantly different ($p < 0.05$). Error bars represent standard deviations ($n=3$ for all points).

Figures 7-37 and 7-38 show representative images of immunohistochemical staining for IL-4 after 24 and 72 hours of treatment, respectively. Immunohistochemical staining scores for IL-4 after 24 and 72 hours of treatment are shown in Figure 7-39 in panels (a) and (b), respectively. Negative controls showed low levels of staining for IL-4 throughout the study, with only mild cell-specific staining in the dermis. Positive controls and animals treated with pH 4, 5.6, and 7 solutions showed low widespread staining at 24 hours of treatment. However, animals treated with pH 9 solutions showed

stronger staining at 24 hours of treatment. This was the only treatment group to have significantly stronger staining than the negative controls at 24 hours ($p < 0.05$). At 72 hours of treatment, mild increases in IL-4 staining were observed in some keratinocytes of the positive controls and pH 4 treated solutions, with the pH 4 treated solutions having significantly stronger staining than the negative controls ($p < 0.05$). Strong staining was observed in the keratinocytes throughout the newly re-epithelialised tissues which had been treated with pH 5.6, 7, and 9 solutions. In these tissues, cell-associated staining was also observed in the dermis, most likely in fibroblasts. These tissues all had significantly stronger staining than negative controls ($p < 0.01$).

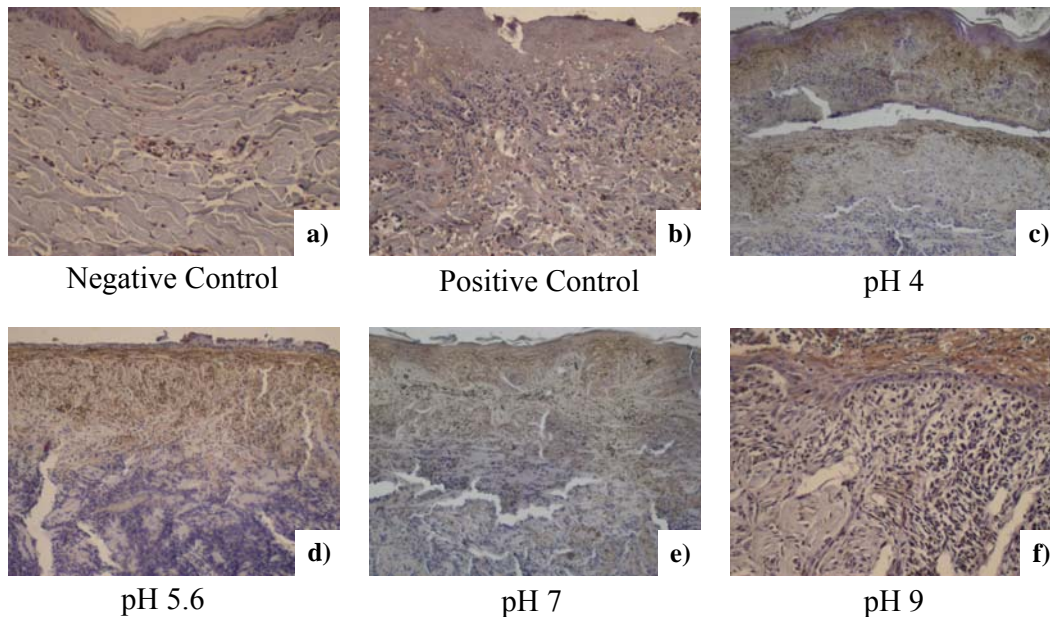


Figure 7-37. Immunohistochemical detection of IL-4 in biopsies of DNCB-induced rashes treated with various nanocrystalline silver-derived solutions for 24 hours. Representative images are shown for immunohistochemical detection of IL-4 after 24 hours treatment of negative controls with distilled water (a), and DNCB-induced porcine contact dermatitis rashes with distilled water (positive control) (b), or nanocrystalline silver-derived solutions generated at starting pHs of 4 (c), 5.6 (d), 7 (e), or 9 (f). The scale bar in A represents 100 μm . Staining for IL-4 appears brown, while the cell nuclei are counterstained purple using hematoxylin.

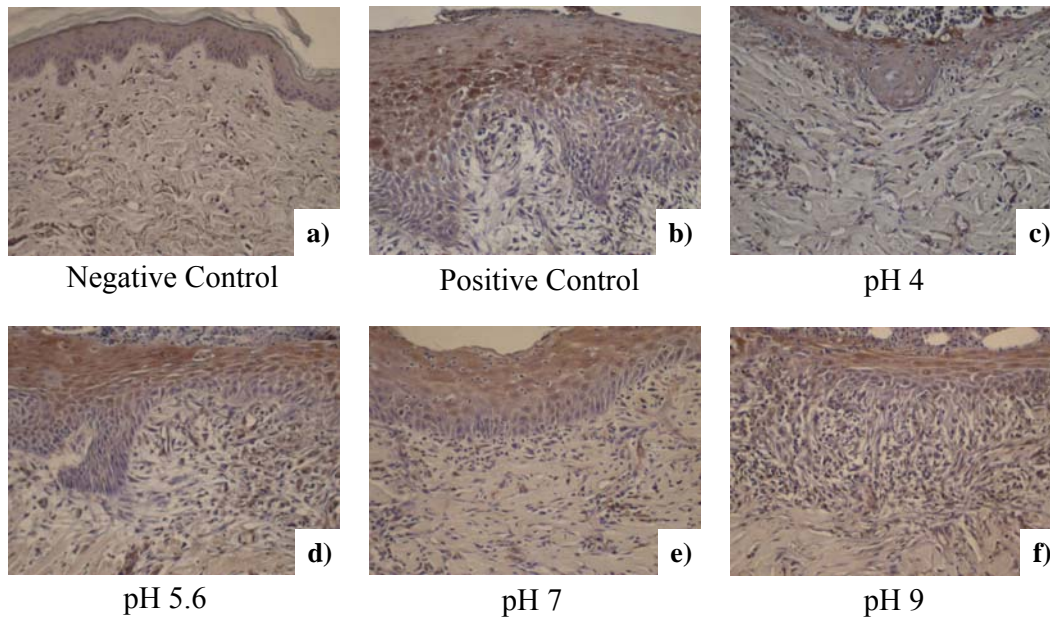


Figure 7-38. Immunohistochemical detection of IL-4 in biopsies of DNCB-induced rashes treated with various nanocrystalline silver-derived solutions for 72 hours. Representative images are shown for immunohistochemical detection of IL-4 after 72 hours treatment of negative controls with distilled water (a), and DNCB-induced porcine contact dermatitis rashes with distilled water (positive control) (b), or nanocrystalline silver-derived solutions generated at starting pHs of 4 (c), 5.6 (d), 7 (e), or 9 (f). The scale bar in A represents 100 μm. Staining for IL-4 appears brown, while the cell nuclei are counterstained purple using hematoxylin.

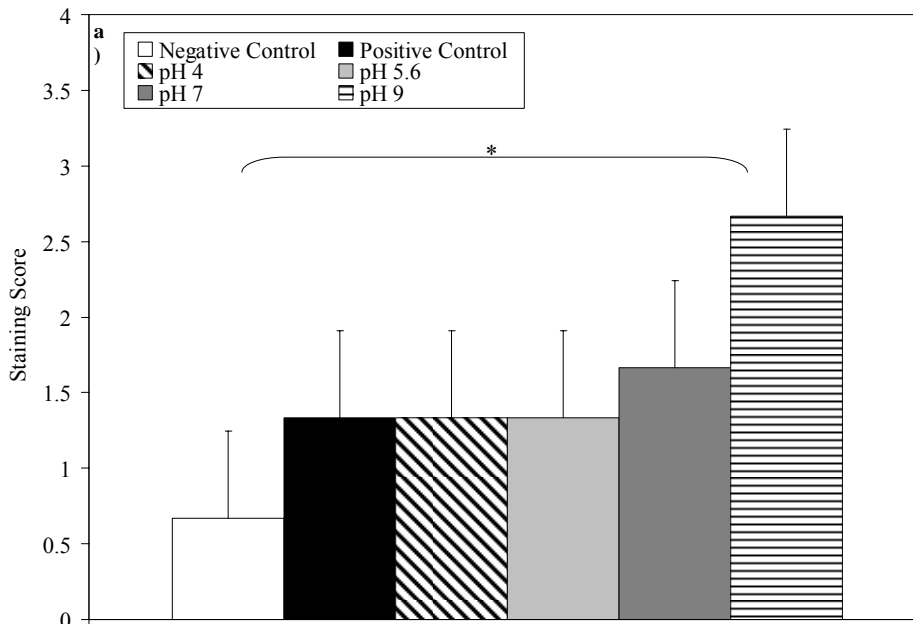


Figure 7-39.

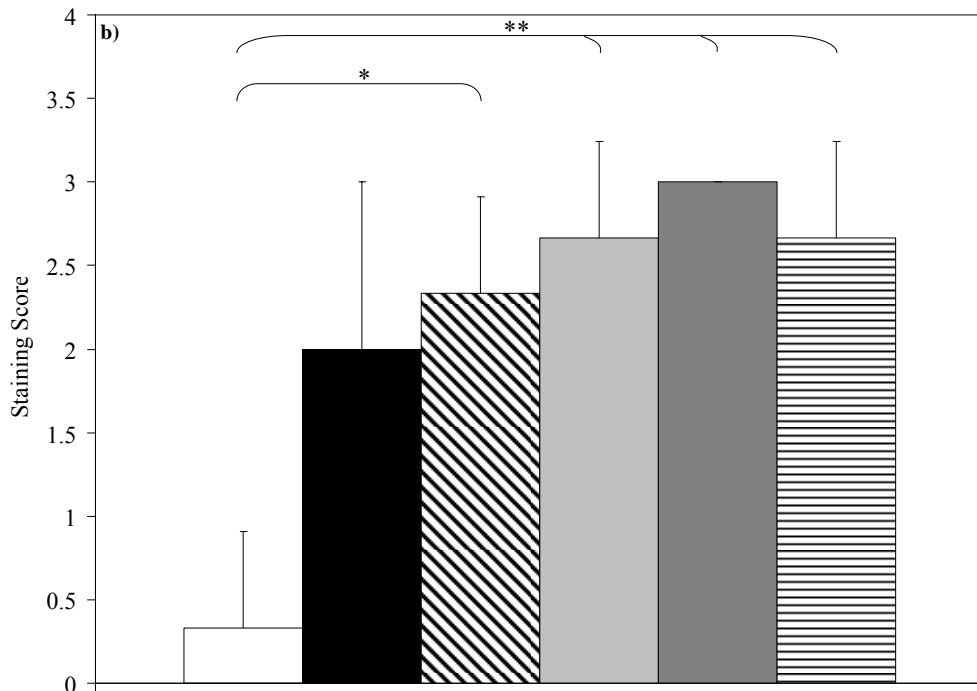


Figure 7-39, continued. Semi-quantitative analyses of immunohistochemical staining for IL-4 in biopsies of DNCB-induced rashes treated with various nanocrystalline silver-derived solutions. Immunohistochemical staining scores for IL-4 are shown after 24 hours (a) and 72 hours (b) of treatment. Statistical analyses were performed using one-way ANOVAs with Tukey-Kramer Multiple Comparisons post tests. Overall p values from the one-way ANOVAs were 0.0248 and 0.0026 after 24h and 72h, respectively. The results of the Tukey-Kramer post tests are indicated on the figure as follows: * indicates significantly different ($p < 0.05$), and ** indicates very significantly different ($p < 0.01$). Error bars represent standard deviations ($n=3$ for all data points).

Immunohistochemical analysis of IL-10 is shown after 24 and 72 hours of treatment in Figures 7-40 and 7-41, respectively. Strong staining for IL-10 was not observed in any of the groups tested at any time point, and there were no clear differences between treatment groups. Staining was present around blood vessels (not shown), and at 72 hours, positive controls showed mild staining in portions of the epidermis. Immunohistochemical staining scores for IL-10 after 24 and 72 hours of treatment are shown in Figure 7-42 panels (a) and (b), respectively. There were no significant differences in the staining scores between the different test groups at either time point.

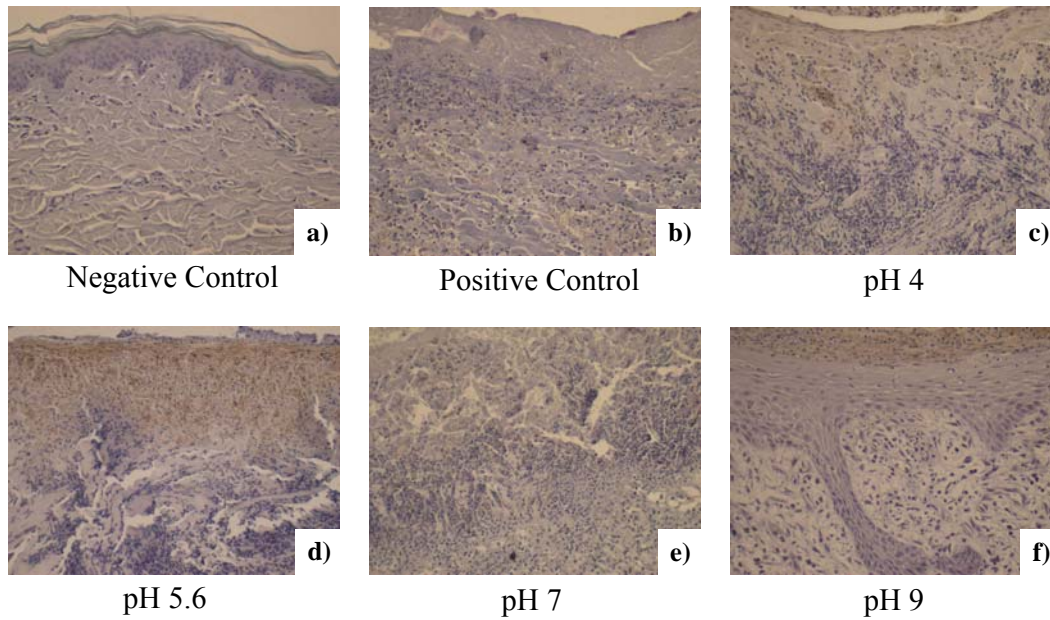


Figure 7-40. Immunohistochemical detection of IL-10 in biopsies of DNCB-induced rashes treated with various nanocrystalline silver-derived solutions for 24 hours. Representative images are shown for immunohistochemical detection of IL-10 after 24 hours treatment of negative controls with distilled water (a), and DNCB-induced porcine contact dermatitis rashes with distilled water (positive control) (b), or nanocrystalline silver-derived solutions generated at starting pHs of 4 (c), 5.6 (d), 7 (e), or 9 (f). The scale bar in A represents 100 μ m. Staining for IL-10 appears brown, while the cell nuclei are counterstained purple using hematoxylin.

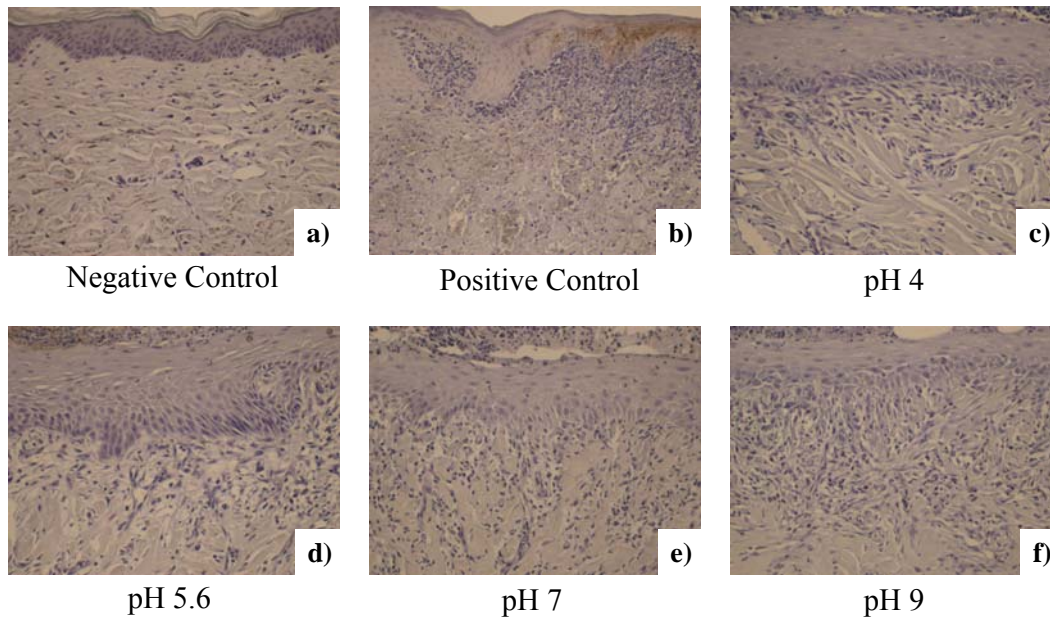


Figure 7-41. Immunohistochemical detection of IL-10 in biopsies of DNCB-induced rashes treated with various nanocrystalline silver-derived solutions for 72 hours. Representative images are shown for immunohistochemical detection of IL-10 after 72 hours treatment of negative controls with distilled water (a), and DNCB-induced porcine contact dermatitis rashes with distilled water (positive control) (b), or nanocrystalline silver-derived solutions generated at starting pHs of 4 (c), 5.6 (d), 7 (e), or 9 (f). The scale bar in A represents 100 μ m. Staining for IL-10 appears brown, while the cell nuclei are counterstained purple using hematoxylin.

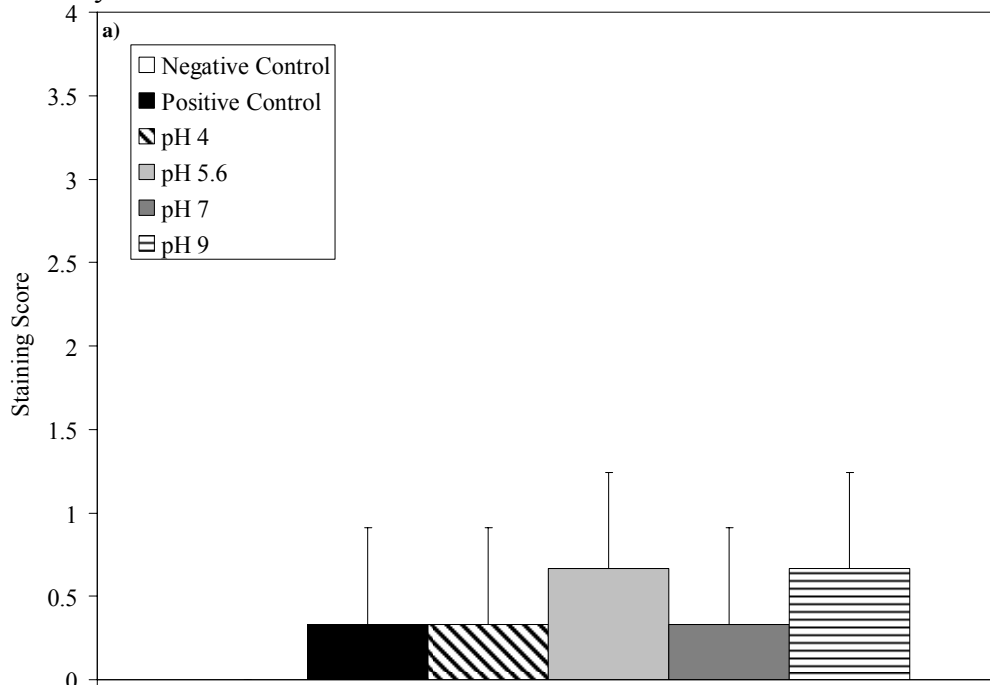


Figure 7-42.

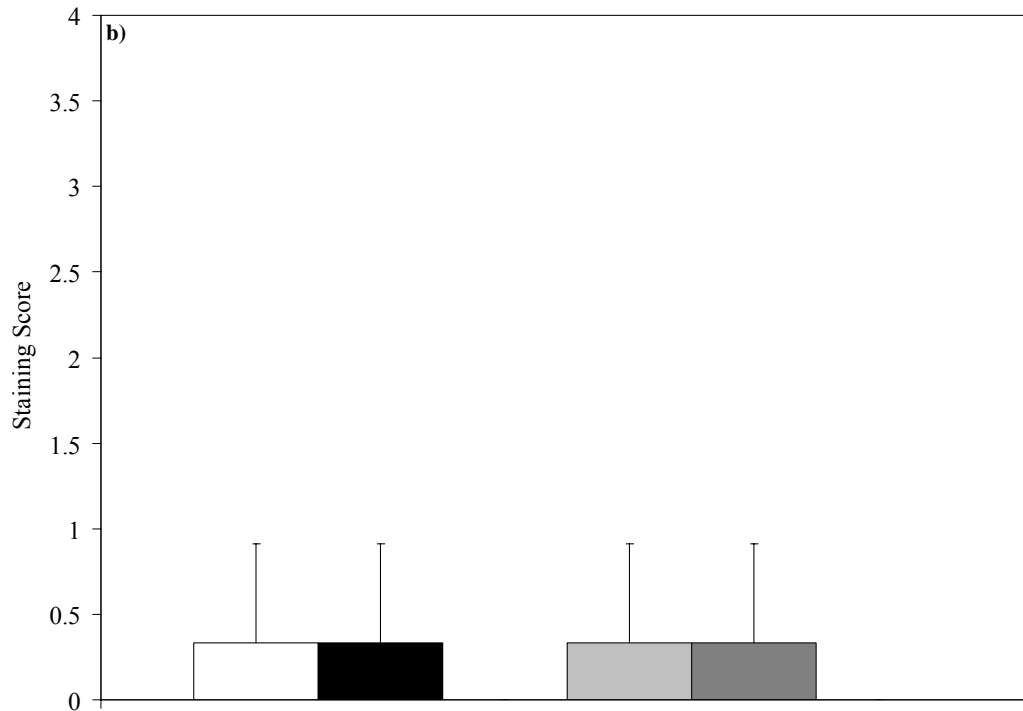


Figure 7-42, continued. Semi-quantitative analyses of immunohistochemical staining for IL-10 in biopsies of DNCB-induced rashes treated with various nanocrystalline silver-derived solutions. Immunohistochemical staining scores for IL-10 are shown after 24 hours (a) and 72 hours (b) of treatment. Statistical analyses were performed using one-way ANOVAs with Tukey-Kramer Multiple Comparisons post tests. Overall p values from the one-way ANOVAs were 0.6472 and 0.8397 after 24h and 72h, respectively. Error bars represent standard deviations (n=3 for all data points).

Figures 7-43 and 7-44 show representative images of immunohistochemical staining for EGF after 24 and 72 hours of treatment, respectively. Immunohistochemical staining scores for EGF after 24 and 72 hours of treatment are shown in Figure 7-45 panels (a) and (b), respectively. Negative controls showed low staining for EGF throughout the experiment, with some cell specific staining present in the dermis. Positive controls showed mild widespread staining for EGF at 24 hours, while pH 4 and pH 7 solution treatments resulted in low levels of staining, which was present in areas of tissue damage. Animals treated with pH 5.6 solutions showed somewhat stronger staining, both in the

damaged epidermis and in the dermis where re-epithelialization would later take place. Animals treated with pH 9 solutions showed staining in the damaged epidermis, but much stronger cell associated staining in the newly forming epidermis. This staining was significantly stronger than all other groups except the pH 5.6 solution treated animals. At 72 hours, all treatment groups, but especially those animals treated with pH 5.6 or higher, showed strong EGF staining in keratinocytes of the newly formed epidermis, as well as some staining in the dermis associated with cells that are most likely fibroblasts. Positive controls continued to show only low levels of widespread staining. While ANOVA testing indicated that there were significant differences between groups, the post tests did not identify differences between individual groups.

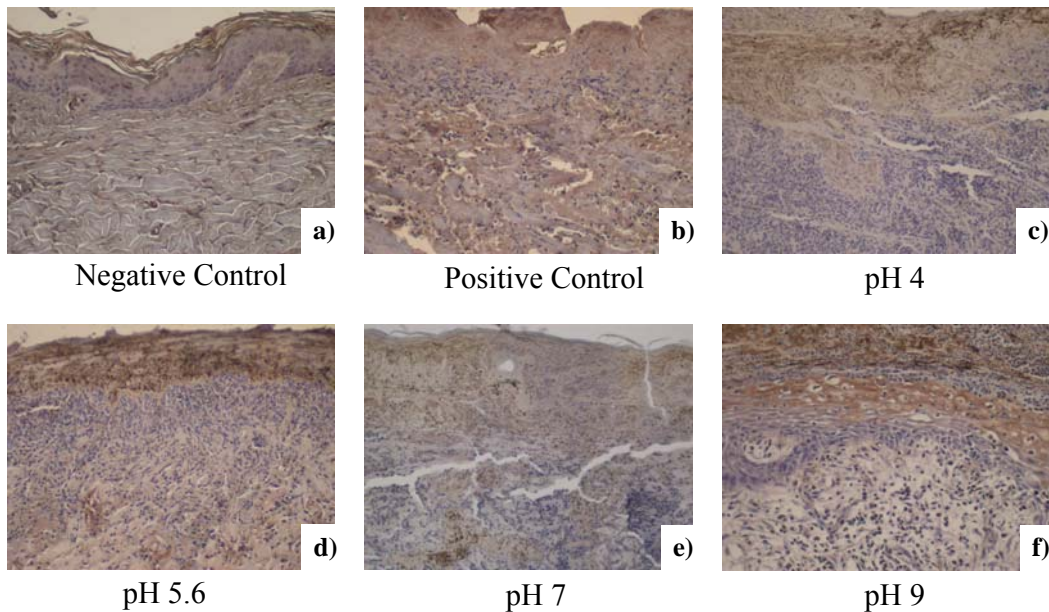


Figure 7-43. Immunohistochemical detection of EGF in biopsies of DNCB-induced rashes treated with various nanocrystalline silver-derived solutions for 24 hours. Representative images are shown for immunohistochemical detection of EGF after 24h treatment of negative controls with distilled water (a), and DNCB-induced porcine contact dermatitis rashes with distilled water (positive control) (b), or nanocrystalline silver-derived solutions generated at starting pHs of 4 (c), 5.6 (d), 7 (e), or 9 (f). The scale bar in A represents 100 μ m. Staining for EGF appears brown, while the cell nuclei are counterstained purple using hematoxylin.

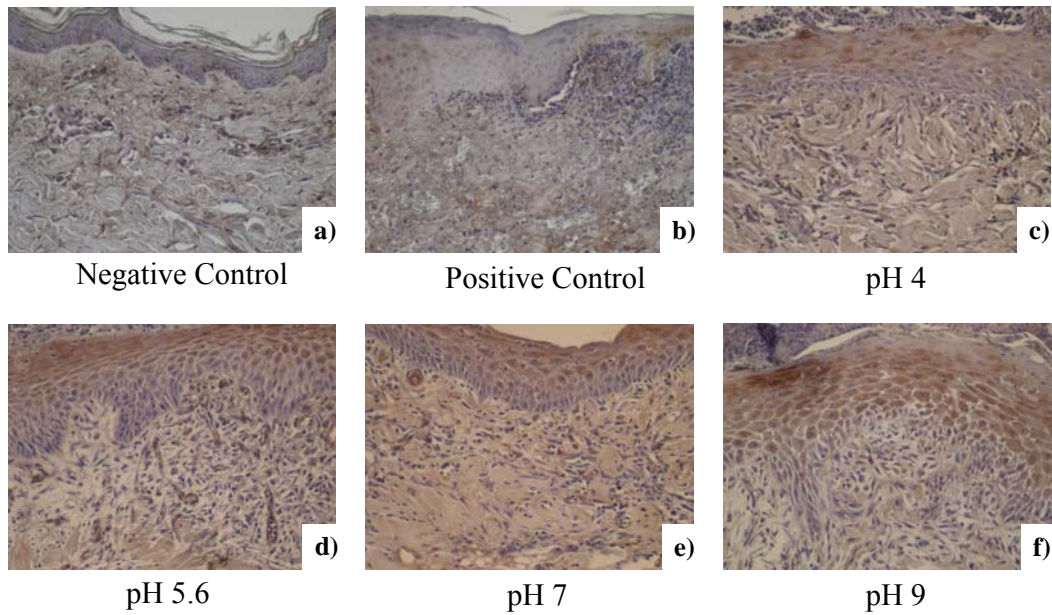


Figure 7-44. Immunohistochemical detection of EGF in biopsies of DNCB-induced rashes treated with various nanocrystalline silver-derived solutions for 72 hours. Representative images are shown for immunohistochemical detection of EGF after 72 hours treatment of negative controls with distilled water (a), and DNCB-induced porcine contact dermatitis rashes with distilled water (positive control) (b), or nanocrystalline silver-derived solutions generated at starting pHs of 4 (c), 5.6 (d), 7 (e), or 9 (f). The scale bar in A represents 100 μ m. Staining for EGF appears brown, while the cell nuclei are counterstained purple using hematoxylin.

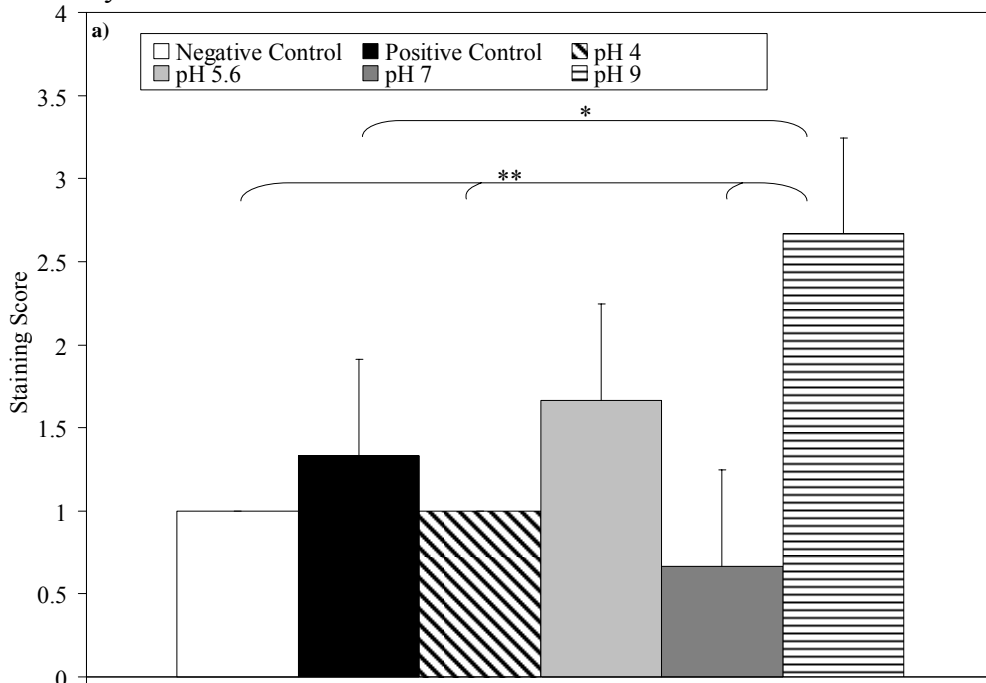


Figure 7-45.

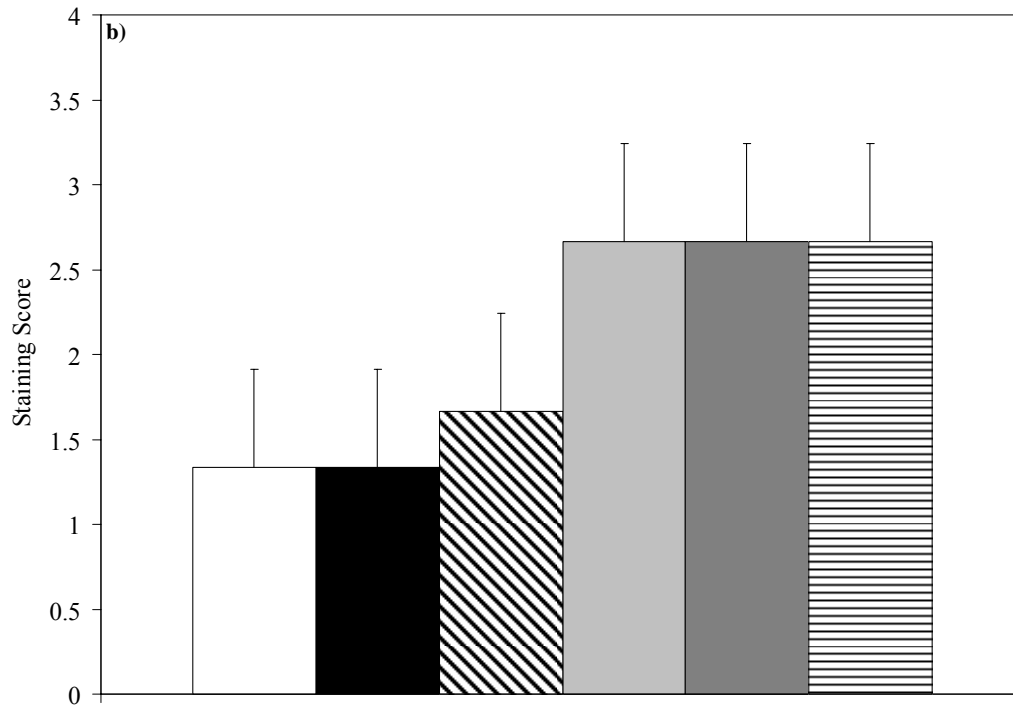


Figure 7-45, continued. Semi-quantitative analyses of immunohistochemical staining for EGF in biopsies of DNCB-induced rashes treated with various nanocrystalline silver-derived solutions. Immunohistochemical staining scores for EGF are shown after 24 hours (a) and 72 hours (b) of treatment. Statistical analyses were performed using one-way ANOVAs with Tukey-Kramer Multiple Comparisons post tests. Overall p values from the one-way ANOVAs were 0.0031 and 0.0199 after 24h and 72h, respectively. The results of the Tukey-Kramer post tests are indicated on the figure as follows: * indicates significantly different ($p < 0.05$), and ** indicates very significantly different ($p < 0.01$). Error bars represent standard deviations ($n=3$ for all data points).

Figures 7-46 and 7-47 show representative images of immunohistochemical staining for KGF after 24 and 72 hours of treatment, respectively. Figure 7-48 shows immunohistochemical staining scores for KGF after 24 and 72 hours of treatment in panels (a) and (b), respectively. Negative controls showed similar levels of staining for KGF in the epidermis throughout the study. Positive controls showed low staining for KGF at 24 hours, as did pH 4 and 7 solution-treated animals. Animals treated with pH 5.6 and 9 solutions showed strongly increased staining, particularly in the epidermis. Animals treated

with pH 5.6 solutions had significantly stronger staining than animals treated with pH 7 solutions ($p < 0.05$), while animals treated with pH 9 solutions had significantly stronger staining than all other groups except animals treated with pH 5.6 solutions ($p < 0.05$). By 72 hours, differences in tissue staining appeared to level out, with medium-strength cell-specific staining occurring in the epidermis of the positive controls and all treatment groups. No significant differences were found at this time point.

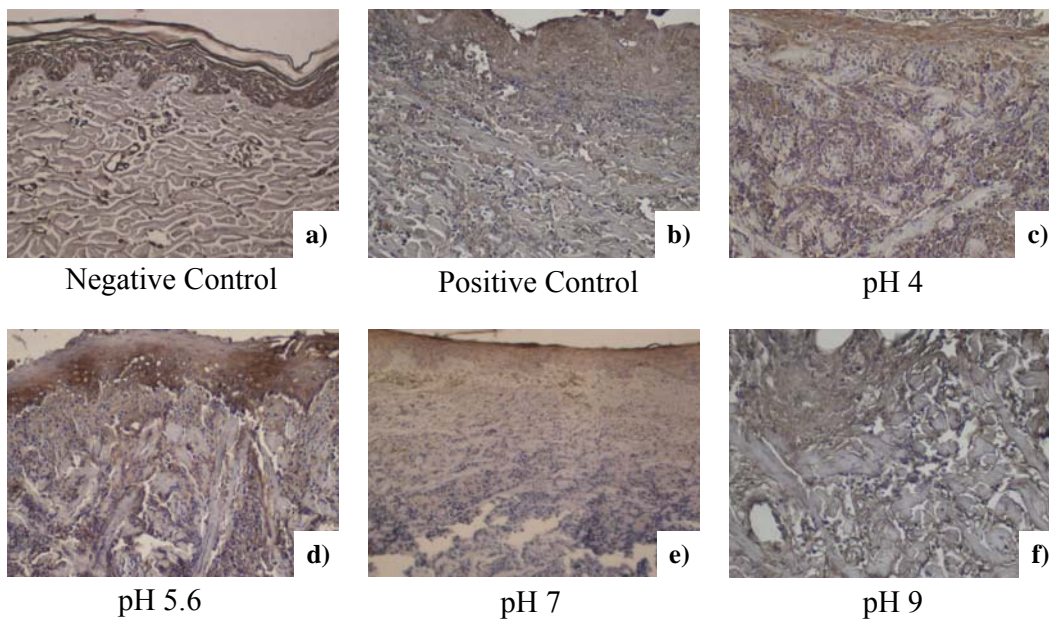


Figure 7-46. Immunohistochemical detection of KGF in biopsies of DNCB-induced rashes treated with various nanocrystalline silver-derived solutions for 24 hours. Representative images are shown for immunohistochemical detection of KGF after 24 hours treatment of negative controls with distilled water (a), and DNCB-induced porcine contact dermatitis rashes with distilled water (positive control) (b), or nanocrystalline silver-derived solutions generated at starting pHs of 4 (c), 5.6 (d), 7 (e), or 9 (f). The scale bar in A represents 100 μm . Staining for KGF appears brown, while the cell nuclei are counterstained purple using hematoxylin.

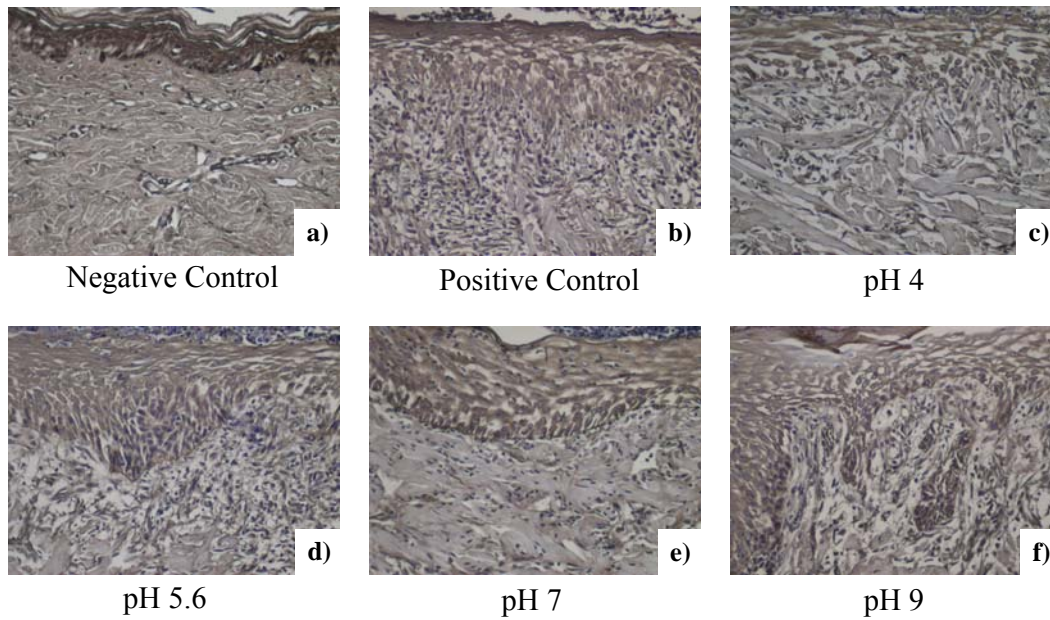


Figure 7-47. Immunohistochemical detection of KGF in biopsies of DNCB-induced rashes treated with various nanocrystalline silver-derived solutions for 72 hours. Representative images are shown for immunohistochemical detection of KGF after 72 hours treatment of negative controls with distilled water (a), and DNCB-induced porcine contact dermatitis rashes with distilled water (positive control) (b), or nanocrystalline silver-derived solutions generated at starting pHs of 4 (c), 5.6 (d), 7 (e), or 9 (f). The scale bar in A represents 100 μm . Staining for KGF appears brown, while the cell nuclei are counterstained purple using hematoxylin.

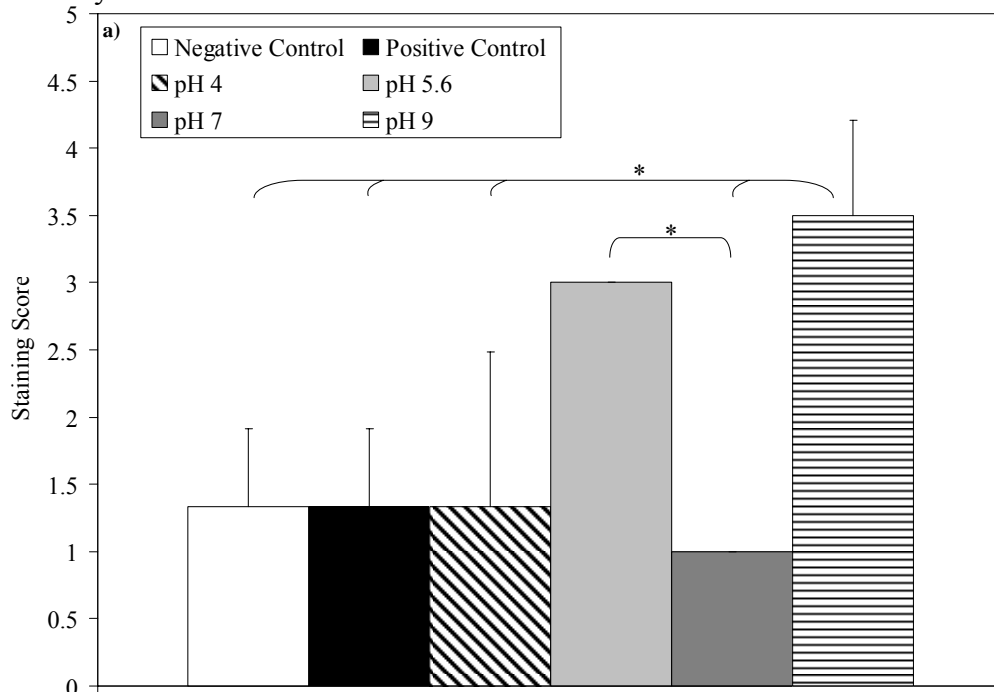


Figure 7-48.

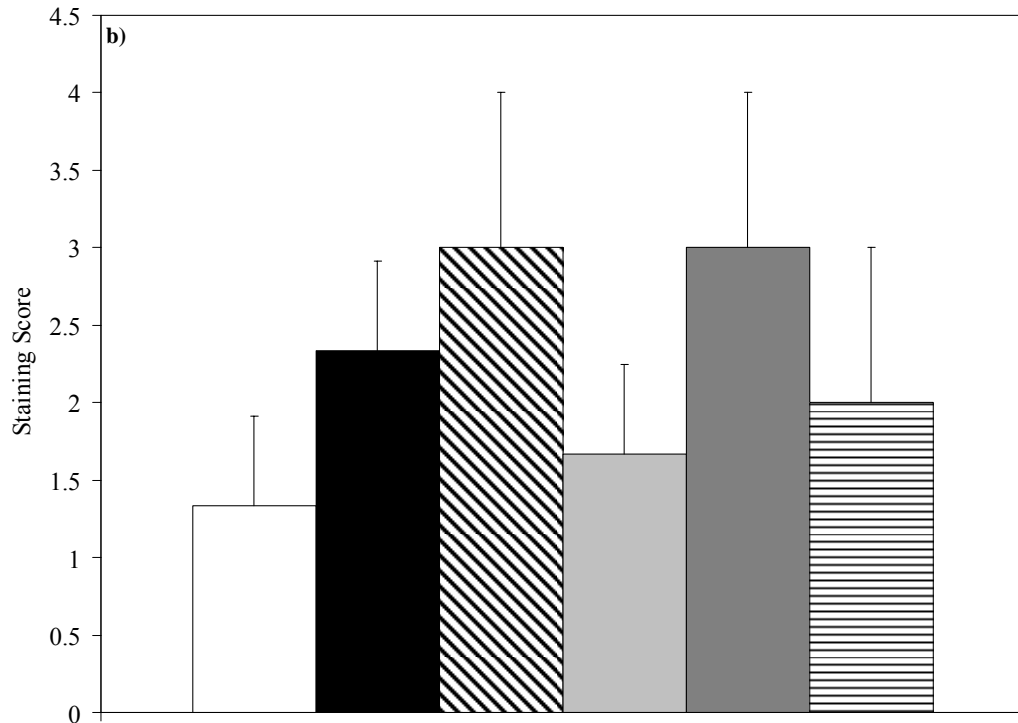


Figure 7-48, continued. Semi-quantitative analyses of immunohistochemical staining for KGF in biopsies of DNCB-induced rashes treated with various nanocrystalline silver-derived solutions. Immunohistochemical staining scores for KGF are shown after 24 hours (a) and 72 hours (b) of treatment. Statistical analyses were performed using one-way ANOVAs with Tukey-Kramer Multiple Comparisons post tests. Overall p values from the one-way ANOVAs were 0.0039 and 0.1310 after 24h and 72h, respectively. The results of the Tukey-Kramer post tests are indicated on the figure as follows: * indicates significantly different ($p < 0.05$). Error bars represent standard deviations ($n=3$ for all points).

Figures 7-49 and 7-50 show representative images of immunohistochemical staining for KGF-2 after 24 and 72 hours of treatment, respectively. Figure 7-51 shows immunohistochemical staining scores for KGF-2 after 24 and 72 hours of treatment in panels (a) and (b), respectively. Negative controls showed some cell-specific staining for KGF-2 in the epidermis and dermis at 24 hours, but minimal staining at 72 hours. Positive controls showed low levels of widespread staining throughout the study. At 24 hours, animals treated with pH 4 and 5.6 solutions showed low levels of staining for KGF-2 near

tissue surfaces, while animals treated with pH 7 solutions showed minimal staining for KGF-2. Animals treated with pH 9 solutions showed strong cell-associated staining for KGF-2, particularly in the keratinocytes of the newly forming epidermis, but also to a lesser extent in the dermis, perhaps in fibroblasts. This staining was significantly higher than that in the negative controls or pH 7 solution treated animals ($p < 0.05$). At 72 hours, all animals receiving silver-containing treatments showed this type of strong cell-associated staining. In animals treated with pH 5.6 or 7 solutions, the staining was significantly stronger than that seen in the negative controls ($p < 0.05$).

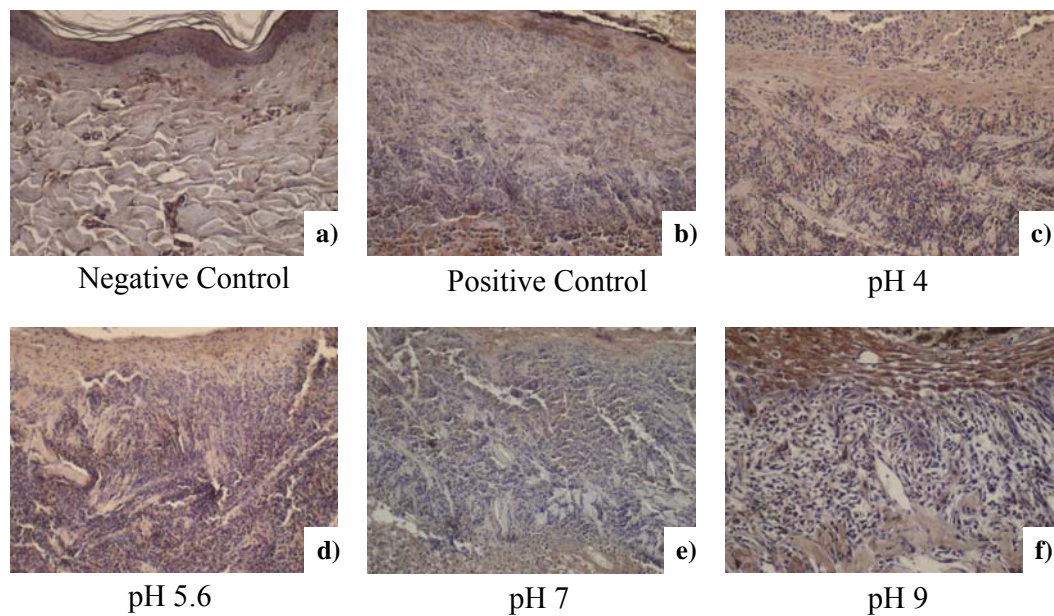


Figure 7-49. Immunohistochemical detection of KGF-2 in biopsies of DNCB-induced rashes treated with various nanocrystalline silver-derived solutions for 24 hours. Representative images are shown for immunohistochemical detection of KGF-2 after 24 hours treatment of negative controls with distilled water (a), and DNCB-induced porcine contact dermatitis rashes with distilled water (positive control) (b), or nanocrystalline silver-derived solutions generated at starting pHs of 4 (c), 5.6 (d), 7 (e), or 9 (f). The scale bar in A represents 100 μm . Staining for KGF-2 appears brown, while the cell nuclei are counterstained purple using hematoxylin.

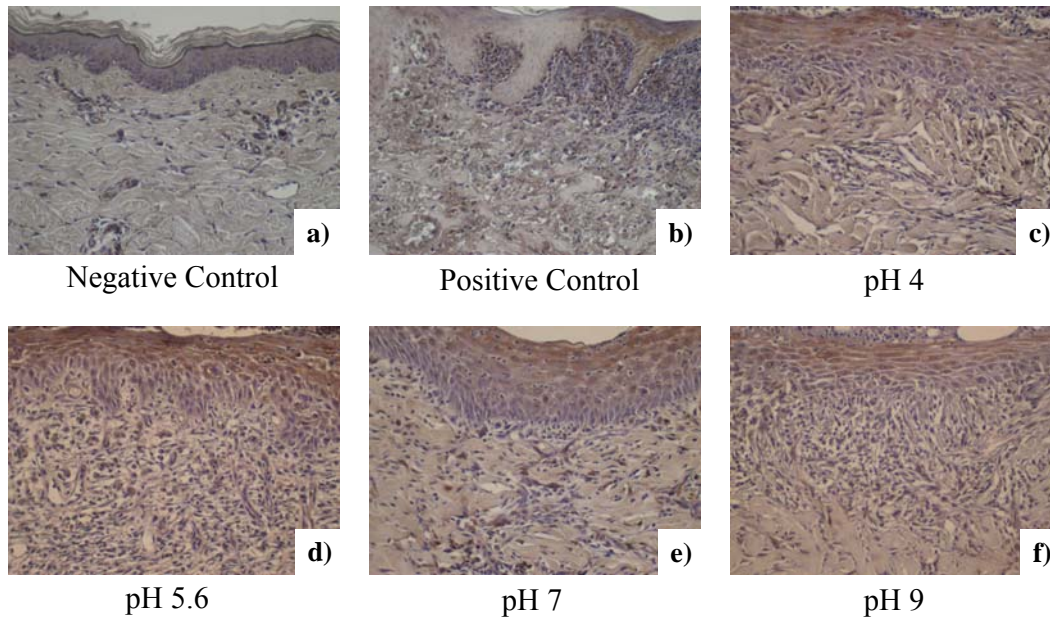


Figure 7-50. Immunohistochemical detection of KGF-2 in biopsies of DNCB-induced rashes treated with various nanocrystalline silver-derived solutions for 72 hours. Representative images are shown for immunohistochemical detection of KGF-2 after 72 hours treatment of negative controls with distilled water (a), and DNCB-induced porcine contact dermatitis rashes with distilled water (positive control) (b), or nanocrystalline silver-derived solutions generated at starting pHs of 4 (c), 5.6 (d), 7 (e), or 9 (f). The scale bar in A represents 100 μ m. Staining for KGF-2 appears brown, while the cell nuclei are counterstained purple using hematoxylin.

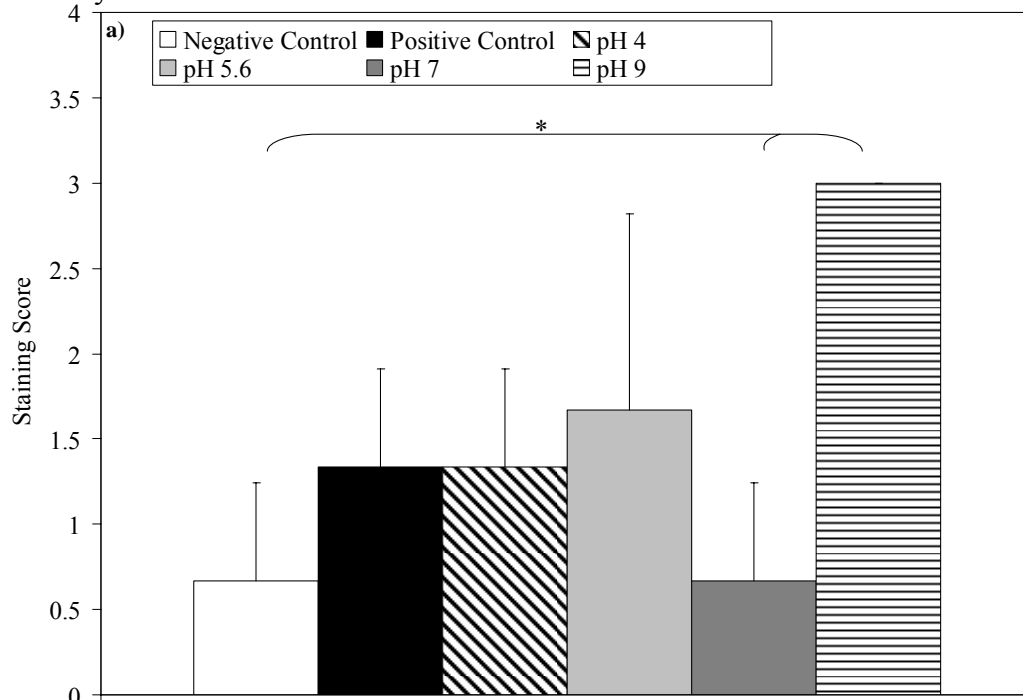


Figure 7-51.

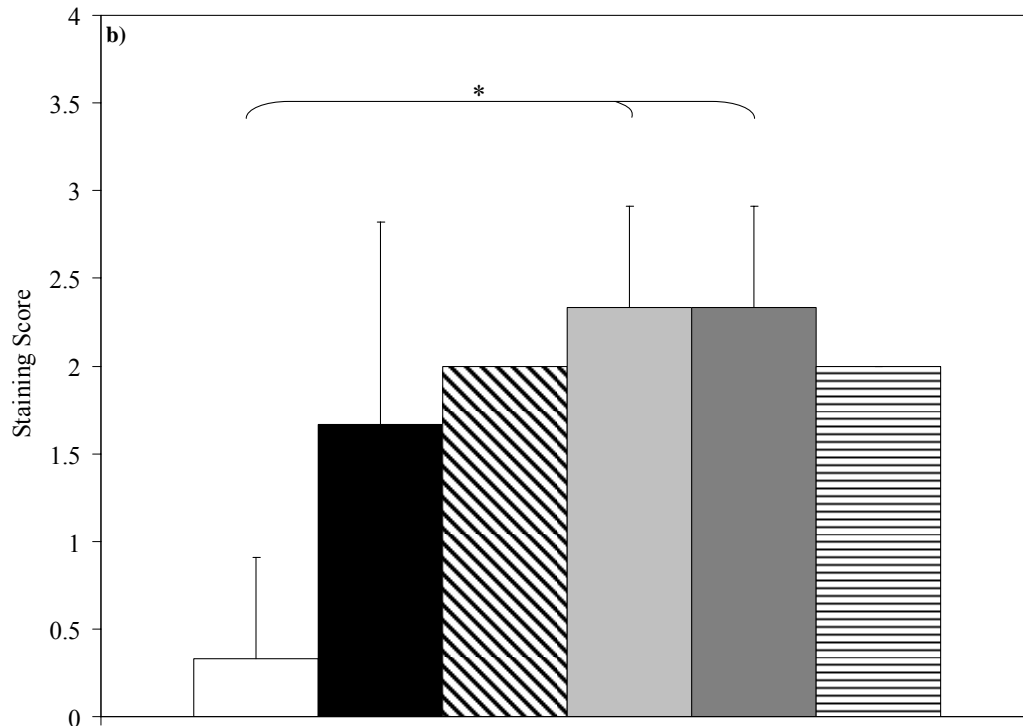


Figure 7-51, continued. Semi-quantitative analyses of immunohistochemical staining for KGF-2 in biopsies of DNCB-induced rashes treated with various nanocrystalline silver-derived solutions. Immunohistochemical staining scores for KGF-2 are shown after 24 hours (a) and 72 hours (b) of treatment. Statistical analyses were performed using one-way ANOVAs with Tukey-Kramer Multiple Comparisons post tests. Overall p values from the one-way ANOVAs were 0.0105 and 0.0173 after 24h and 72h, respectively. The results of the Tukey-Kramer post tests are indicated on the figure as follows: * indicates significantly different ($p < 0.05$). Error bars represent standard deviations ($n=3$ for all points).

Average Solution Volume, Silver, and Calcium Delivered

The average daily total solution volume given to each group of pigs is shown in Figure 7-52. There were no significant differences in the volume received by each group of animals. The average daily total of silver delivered via the nanocrystalline silver-derived solutions to each treatment group is shown in Figure 7-53. Animals in the pH 4 solution treatment group received significantly higher ($p < 0.01$) total silver per day than all other groups. There were no significant differences in silver delivered to the remaining groups. Based on the

quantities of $\text{Ca}(\text{OH})_2$ used to generate solutions, and the volumes delivered per day to the animals, animals in the pH 7 and pH 9 solution groups received approximately 0.004 mg and 0.019 mg Ca^+ per day, respectively.

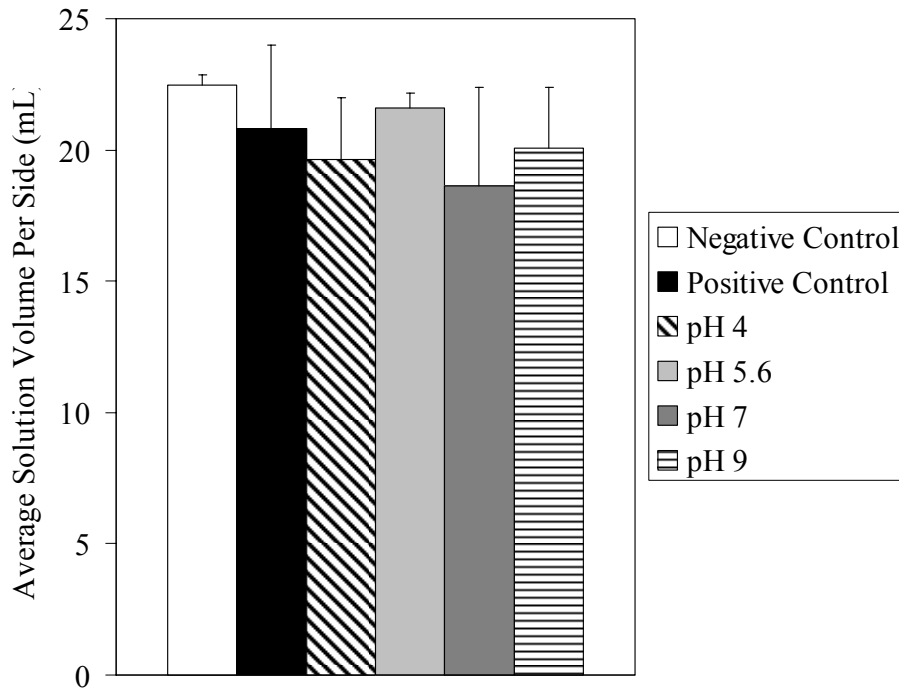


Figure 7-52. Average volume of solution delivered per day per side for treatment of DNCB-induced rashes. Nanocrystalline silver-derived solutions generated at started pHs of 4, 5.6, 7, and 9 were delivered daily to animals with DNCB-induced contact dermatitis rashes. Negative and positive controls received distilled water treatments. Volumes of solution delivered were measured daily and used to calculate the average volume delivered per day to each treatment groups. Statistical analysis, performed using a one way ANOVA, indicated that there were no significant differences in the volume delivered between groups ($p=0.4722$). Error bars represent standard deviations ($n=3$ for all data points).

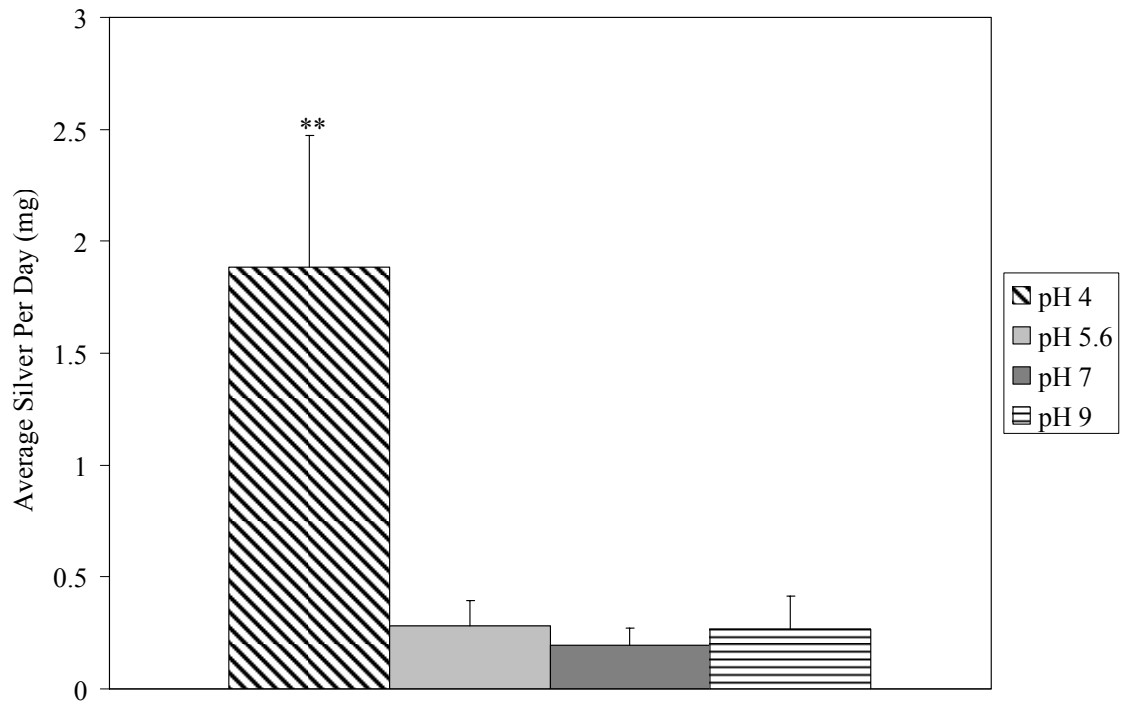


Figure 7-53. Average weight of silver delivered per day per side to DNCB-induced rashes via various nanocrystalline silver-derived solutions. Nanocrystalline silver-derived solutions generated at starting pHs of 4, 5.6, 7, and 9 were delivered daily to animals with DNCB-induced contact dermatitis rash. Volumes of solution delivered were measured daily and samples were taken daily for total silver analysis by AAS. These values were used to calculate the average silver delivered per animal in each treatment group, as shown in the figure. The statistical analysis was performed using a one-way ANOVA. The overall p value was 0.0011. The result of the Tukey-Kramer post test is shown on the figure as ** indicates very significantly different ($p < 0.01$) from all other groups. Error bars represent standard deviations ($n=3$ for all data points).

Discussion

In this study, contact dermatitis was induced via four applications of DNCB over two weeks, causing first sensitization and then elicitation of the rash. During the study of Chapter 2, it was observed that on Day 0, one animal jumped during the final application of DNCB, resulting in the paint brush contacting his back away from the rash. At this location, a bright red swollen spot developed. Thus, it was hypothesized that if animals were sensitized in one location and then

had the last application of DNCB in another location, a strong inflammatory response could be obtained, but without the scabbing. It was thought that this would facilitate visual observations, and also that it would improve treatment-tissue contact. Unfortunately, when this technique was tried, the results were highly variable. Animals within a single group showed highly different responses to a single application of DNCB, despite being clearly sensitized to it, and even the sensitivity within a single animal appeared to vary with the location on the animal's skin, with the rash weakening ventrally. As well, the full effect of the single application of DNCB had not taken place within the four hours before treatment was commenced. Rather, the inflammatory response increased out to 24 hours. In addition, the inflammatory response was not sufficiently strong, as positive controls began to heal within 72 hours. It is interesting to note that an earlier differentiation between treatment groups was observable. In particular, pH 9 solution treated animals demonstrated a preventative effect, as the inflammation did not increase sharply between Day 0 and Day 1 with this treatment group, and significant decreases in erythema and edema scores were observed at 24 hours with this treatment group relative to other treatments. However, due to the above-mentioned concerns related to this technique, it is not recommended for future work, and was not used for analyses beyond the visual and histological data. Consistent strong inflammation was observed at Day 0 when four applications of DNCB were applied to the rash site, consistent with the results of Chapter 2. Negative controls did not appear to be impacted by treatment with distilled water, while positive controls did not show signs of improvement over 72 hours.

Therefore, all subsequent analyses and discussion were based on these results, rather than the results generated with a single application of DNCB to a sensitized animal.

Using the data generated with rashes exposed to DNCB four times, this study shows that solutions derived from nanocrystalline silver have some or all of the anti-inflammatory properties of nanocrystalline silver dressings previously reported[2, 3, 13, 21], depending on dissolution conditions. Nanocrystalline silver-derived solutions were able to reduce visual and histological signs of inflammation. This occurred in conjunction with induction of apoptosis in infiltrating inflammatory cells. Apoptosis of these cells may have led to the observed reduction in expression of TNF- α and IL-8, which are both key mediators of the inflammatory response[22, 23]. Apoptosis is involved with eliminating inflammatory cells from inflamed tissues[22], and compounds which induce apoptosis, including noble metals[9-12, 24-26], are beneficial in the treatment of inflammatory diseases, as discussed in Chapters 1 and 2. Thus, induction of apoptosis in inflammatory cells by nanocrystalline silver-derived solutions appears to be a key factor for their anti-inflammatory activity. Apoptosis induction may have, in part, been regulated by the observed increased expression of IL-4, an anti-inflammatory cytokine which induces apoptosis of neutrophils and macrophages, and downregulates the effects of IL-1, TNF- α , IL-6, and IL-8 on macrophages[27-30]. IL-10 did not appear to be involved in the anti-inflammatory effect seen. This was observed in Chapter 3 as well, but differs from a study using silver nanoparticles to treat murine thermal injuries[31]. As

observed in Chapter 3 using nanocrystalline silver dressings[21], upregulation of EGF, KGF, and KGF-2 was observed with nanocrystalline silver-derived treatments. EGF promotes keratinocyte migration, enhancing re-epithelialization[32-34]; enhances formation of granulation tissue; and stimulates fibroblast motility[35]. KGF and KGF-2 both stimulate proliferation and migration of keratinocytes; promote detoxification of reactive oxygen species (ROS), protecting keratinocytes from ROS-induced apoptosis[34, 36]; and are involved indirectly with granulation tissue formation[36, 37]. Thus, upregulation of these growth factors may partially explain the enhanced re-epithelialization rates and pro-healing activity observed with nanocrystalline silver-derived solutions.

Biospy bleeding in this study was highly variable, and did not appear to be sufficiently discriminatory between groups to provide additional information from that already obtained via other methods of visual observation.

Real-time RT-PCR was used to examine the mRNA expression of pro-inflammatory cytokines (TNF- α , IL-1 β , IL-8, IL-12, IL-17, and IL-31), and the anti-inflammatory cytokine IL-10 (discussed in Chapter 3). TNF- α and IL-8 have been discussed above and in Chapter 2. IL-1 β , which is produced primarily by macrophages and monocytes, performs similar and synergistic functions to TNF- α [29]. IL-12 is also produced largely by macrophages and monocytes, and is capable of mounting an inflammatory response independent of IL-1 β and TNF- α [29]. IL-17, which is overexpressed in a variety of inflammatory diseases, is secreted by Th17 cells, and activates inflammatory dendritic cells, macrophages,

neutrophils, T cells, and epithelial cells[38]. It promotes neutrophil chemotaxis, activation of inflammatory stem cell mediators, and production of inflammatory molecules[38]. IL-31, which is mainly produced by activated Th2 cells, acts on activated monocytes. It is involved in pro-inflammatory responses via its role in the T cell-mediated immune response[39]. The forward and reverse primer sequences used for IL-31 measurement were generated based on human IL-31 sequences. Since these primers did not detect IL-31 in the porcine cDNA samples, this suggests that the homology between porcine IL-31 and the human IL-31 sequence used was poor.

Although the techniques used for the real time RT-PCR appeared to be appropriate and performed correctly, with a close grouping of data for housekeeping genes (particularly GAPDH), and a spread in the data for other genes, statistically significant results were not obtained for any signaling molecule tested at any time point, due to high variability in mRNA expression within each group. Since all the biopsy samples taken at 24 hours were placed in a fridge freezer by an unknown person, this may have partially degraded the RNA in these samples, impacting the results. This appears likely, as RNA content of the samples was highly variable, even within a single group (some purified samples had 4% of the RNA present in the same volume as other samples). In addition, the samples showed visual signs of recrystallization and sublimation (freeze drying), which is a common occurrence in fridge freezers, where the temperature is often above -20°C. As it is unknown whether or not the samples from 72 hours spent time in the fridge freezer as well, this may have been a factor

for these samples. Another possible explanation for the variability within a group is RNA breakdown during handling prior to placing the samples at -80°C . The samples were snap-cooled and left on liquid nitrogen for as much as 12 hours until they were transferred to the -80°C freezer. Due to the large number of biopsies, it is uncertain whether there was good consistent contact between the samples and the liquid nitrogen during this time. Finally, concerns remain about the use of HPRT as a house-keeping gene, as HPRT expression can be modified during wound healing[36]. However, use of GAPDH as the house-keeping gene did not improve the results. Attempts were made to eliminate apparent outliers from the data (not shown), but even when an outlier was removed from each treatment group (the data point most distant from the median data point), very few statistically significant differences were observed, and those that did exist did not coincide well with corresponding immunohistochemical data. Therefore, removal of outliers did not appear to be justified. Due to the high variability within treatment groups, the results of the mRNA expression measurements made via real time RT-PCR were not considered valid results regarding the effect of nanocrystalline silver-derived treatments on DNCB-induced porcine contact dermatitis. Similarly, the snap-cooled biopsies used to measure MMP expression and activation at 24 hours were certainly placed in a fridge freezer for over a month, and it is unknown whether the biopsies taken at 72 hours also spent time in the fridge freezer or not. Although proteins are less susceptible to degradation than RNA, this may explain some of the intragroup variability, which is certainly higher than that seen in Chapter 2, and indicates that the results of the

zymography should not be too highly emphasized.

As discussed in Chapter 3, IL-10 is an important anti-inflammatory cytokine with roles including reduction of TNF- α activity, induction of apoptosis in neutrophils and macrophages, and reduction of IL-6 and IL-8 production[29]. Thus, it appeared that IL-10 upregulation would explain many effects observed with nanocrystalline silver-derived solution treatments. In this study, the monoclonal antibody was used, and IL-10 did not appear to be upregulated with treatment, using any of the nanocrystalline silver-derived solutions. Interestingly, a study in which murine thermal injuries were treated with silver nanoparticles showed IL-10 upregulation[31]. While this may be due to differences in models or techniques used, it suggests that silver nanoparticles may impact wound healing by different mechanisms than nanocrystalline silver-derived solutions.

Similar to results observed in Chapter 3, neither the positive controls nor the animals treated with any nanocrystalline silver-derived solutions showed upregulation of TGF- β in this study, despite the fact that the positive controls showed strong staining for TGF- β in Chapter 2. Again, this may be due to the fact that a new lot of the primary antibody had to be purchased, which was used simultaneously for the results obtained for Chapter 3 and for this study. This lot may have been less active than the previous lot.

Interestingly, this study shows that the activity of nanocrystalline silver-derived solutions varies substantially with dissolution conditions, in terms of both anti-inflammatory and pro-healing effects.

Solutions generated at a starting pH of 4 showed only mild visual

improvements, with the only significant reduction in edema relative to positive controls occurring at Day 2. However, histology showed that re-epithelialization began to occur within two days of treatment, and that there was reduced inflammatory cell infiltration after this time point. There were no significant trends related to MMP expression or activity. At 24 hours, apoptosis did not appear to be induced at tissue surfaces. However, deeper in the dermis (which is normally near-acellular but which had been infiltrated by inflammatory cells) large numbers of apoptotic cells were observed, with visible blebbing. Since apoptosis levels were no higher than those observed in positive controls in the epidermis, this suggests that very little Ag^+ was present in the solutions delivered to the animals, as the results of Chapter 2 indicated that Ag^+ may induce indiscriminate apoptosis induction near tissue surfaces. This suggests that, since there was high total silver in solution, most of the silver being delivered to the animals was inactive. At pH 4, high quantities of Ag^+ may be dissolved into solution initially, which then react with the carbonic acid present to form silver carbonates. This appears to be confirmed by the occasional presence of visible white flakes in solutions during testing performed in Chapter 5, and the fact that dressings contained a lower percentage silver oxide after dissolution in pH 4 solutions (see Chapter 5). Thus, the Ag^+ and any higher oxidation state silver released may be inactivated, creating a gradient for the release of additional silver species, including the anti-inflammatory silver species, which are then able to produce the anti-inflammatory/pro-healing effects observed, including the selective apoptosis of inflammatory cells. Previous studies, as well as those of

Chapters 2 and 3, have demonstrated apoptosis induction selective to inflammatory cells of the dermis[2, 3]. Also, the study of Chapter 3 suggested that this action was via silver interactions with cells close to tissue surfaces which then release signals resulting in an anti-inflammatory series of events including apoptosis induction in inflammatory cells. Treatment with pH 4 solutions resulted in somewhat decreased TNF- α expression relative to positive controls at 72 hours, but this was not as considerable as other treatment groups. However, IL-8 expression was lower than that of positive controls at 72 hours, showing that treatment with pH 4 solutions may be capable of reducing pro-inflammatory cytokine expression. pH 4 treatments did not increase IL-4 expression as strongly as other treatment groups, which may in part explain the weaker anti-inflammatory effect observed. This also suggests that other signaling molecules, not yet identified, were responsible for the apoptosis induction observed in the deep dermis. However, pH 4 treatments did result in mildly increased EGF expression by 72 hours, a mild increase in KGF expression at 24 hours, and increased KGF-2 expression at 24 hours in areas where re-epithelialization would later occur beneath the scab, followed by a mild increase in KGF-2 expression at 72 hours in the newly forming epidermis. The enhanced expression of these growth factors explains, at least in part, the pro-healing activity observed, such as enhanced rate of re-epithelialization and protection of keratinocytes from apoptosis induction.

Animals treated with solutions generated at a starting pH of 5.6 showed similar mild visual improvements to pH 4 treatments. They had no significant

decreases in erythema or edema. Histologically, they were the slowest to begin re-epithelialization and to show signs of decreased leukocyte infiltration, both of which occurred between 48 and 72 hours of treatment. However, this was still enhanced relative to positive controls. pMMP-2 expression was significantly decreased relative to positive controls at 24 hours, and similar trends (not significant) were observed with pMMP-9, aMMP-9, and aMMP-2. Interestingly, apoptosis induction was not observed at 24 hours of treatment, meaning that the reduction of aMMP-2 levels could not have occurred solely through apoptosis of inflammatory cells, and therefore may have occurred via modulation of cellular output and activation of these molecules. Apoptosis induction was examined at 24 hours, since the studies in Chapters 2 and 3 showed apoptosis induction at this time point using nanocrystalline silver dressings. However, it seems likely that with pH 5.6 treatments, apoptosis induction in inflammatory cells occurred later, and could perhaps have been detected at 48 hours, since reduced inflammatory cell presence and re-epithelialization were not observed until 72 hours. In addition, a study of contaminated porcine wounds demonstrated increased apoptosis in inflammatory cells at 48 hours with nanocrystalline silver dressing treatments[3]. The pH 5.6 solution-treated animals showed poor modulation of pro-inflammatory cytokine expression relative to the other treatment groups, with TNF- α expression increased at 72 hours, and IL-8 expression increased at 24 hours. However, the expression of TNF- α and IL-8 in this group was still lower than that of positive controls, with IL-8 expression at 72 hours being significantly lower than positive controls. The expression of anti-inflammatory cytokine IL-4

was increased at 72 hours, which again suggests that apoptosis induction may have occurred between 24 and 72 hours in inflammatory cells. With pH 5.6 treatments, modulation of growth factors related to re-epithelialization was observed: EGF expression was increased at 72 hours; KGF expression was increased at 24 hours, but decreased somewhat at 72 hours; and KGF-2 was expressed at 24 hours in areas where re-epithelialization would later occur, and was expressed at 72 hours in newly formed epidermis. Since growth factor expression was not delayed, the delayed re-epithelialization appears to have been related to the late induction of apoptosis in inflammatory cells of these tissues. The delayed healing in this group relative to other treatment groups may be due to Ag^+ levels in solution. In distilled water, Ag^+ would be less able to react to form inactive/insoluble species than in treatments containing carbonates or hydroxyls, and that, in combination with the low total silver dissolved at pH 5.6, might result in a poor gradient for drawing active silver species, including anti-inflammatory species, into solution, while the Ag^+ present could counteract the pro-healing/anti-inflammatory activity to some degree, delaying healing. The early upregulation of KGF may have protected keratinocytes from Ag^+ -induced apoptosis. Interestingly, solutions generated in distilled water have the highest antimicrobial activity, corroborating the idea that most of the silver present in solution is positively charged (see Chapter 5).

Solutions generated at a starting pH of 7 showed visual improvements during the treatment period, with significant reductions in edema at 48 hours. Histopathology showed that re-epithelialization had begun by 48 hours, with

greatly decreased inflammatory cell infiltration occurring by 72 hours. However, the epidermis was very thick with deep rete ridges. While some researchers have suggested that this tissue morphology is beneficial, as it indicates that the newly forming tissues are better developed[40], being well anchored and less likely to dehisce, others have suggested that this tissue morphology is caused by chronic mechanical shear[41], which, in this case, would be due to animals attempting to scratch their backs or remove their dressings, possibly due to discomfort caused by the treatment. The latter seems unlikely, since animals treated with pH 9 solutions did not demonstrate epidermal thickening or extended rete ridges, although they were exposed to the same quantity of silver and even more calcium hydroxide. If the treatment was irritating, the same effect should have been observed with pH 9 treatments. A third possibility is that the epidermal tissue only appeared to be thicker in this group due to angled slices through the tissue during slide preparation. While a fourth possibility is that hyperkeratinization was occurring, this seems unlikely, considering the low expression of KGF and KGF-2 with pH 7 solution treatments at 24 hours relative to other treatment groups. There was a trend towards decreased MMP expression and activation with pH 7 treatments, but this was not significant. At 72 hours, only one of three animals showed strong MMP expression, while positive controls had two out of three animals showing strong MMP expression. Although strong apoptosis induction was observed in the dermis with pH 7 treatments, some apoptosis induction was also observed in the epidermis, suggesting either a less selective or less protective effect with this treatment. One possible explanation for this is that

there may not have been enough hydroxyls present in the solution to bind to all the Ag^+ released (see further discussion on hydroxyl precipitation below), and thus the Ag^+ caused apoptosis in the epidermis. However, if this was the case, a similar observation would have been expected with the pH 5.6 treatment, where high levels of Ag^+ seem more likely. It also should be noted that the apoptosis induction in the epidermis was not as strong as that observed previously with silver nitrate treatments (which contain Ag^+ only) in Chapter 2, and that the increased expression observed did not reach statistical significance. Expression of pro-inflammatory molecules was modulated via pH 7 treatments, with $\text{TNF-}\alpha$ downregulated by 72 hours, and IL-8 expression low at both 24 and 72 hours. In addition, the expression of anti-inflammatory cytokine IL-4 was increased at 72 hours, along with EGF. Thus pH 7 solutions provide active silver species which generate anti-inflammatory/pro-healing activity. However, expression of KGF and KGF-2 was low at 24 hours compared to other treatment groups. Since these molecules are involved with protection of keratinocytes from apoptosis, this may partially explain why some apoptosis occurred in the epidermis with this treatment.

Solutions generated at a starting pH of 9 showed the most visual improvement, with significant reductions in both erythema and edema scores within two days of treatment. Biopsy bleeding was significantly reduced by 72 hours, relative to other treatment groups as well. Histologically, re-epithelialization occurred the earliest with pH 9 treatments, and the most normal tissue morphology was observed at 72 hours. Apoptosis induction was observed

in the deep dermis at 24 hours, but not in the newly forming epidermis. The induction levels were not as high as those seen with the pH 4 or pH 7 treatments, but since re-epithelialization was already occurring in some of the pH 9 treated animals, it is possible that the peak of apoptosis induction had already passed at 24 hours. TNF- α expression was low throughout the treatment period, but, interestingly, IL-8 expression increased over time, although not to the levels observed with the positive controls. Expression of IL-4 was increased throughout the treatment period, at least partially explaining the anti-inflammatory activity observed. In addition, EGF expression was increased throughout the treatment period, while KGF expression was increased at 24 hours, and KGF-2 expression was increased throughout the experiment, particularly in newly forming epidermis and fibroblasts. This early increased expression of growth factors involved in re-epithelialization and formation of granulation tissue explains, at least in part, the enhanced pro-healing activity observed with the pH 9 treatments. Overall, these results suggest that at higher pHs more of the total silver delivered in solution was active anti-inflammatory species, perhaps Ag⁽⁰⁾ clusters[7]. This is confirmed by the results of Chapter 5 which indicated that dressings contained a lower percentage of metallic silver after dissolution in pH 9 solutions. This suggests that Ag⁺ was dissolved off the dressing, allowing for the dissolution of the anti-inflammatory species as well, but that the Ag⁺ then reacted with hydroxyl ions from the calcium hydroxide in solution, re-precipitating onto the dressings, or in the container. This could provide a gradient for more silver dissolution, resulting in more anti-inflammatory species being released into solution. This is suggested

by the fact that the solubility of silver hydroxide/silver oxide in pure water is about 0.2 mg/kg H₂O, but in a dilute alkali, it drops to about 6 µg/kg water[42]. If this was the case, then the Ag⁺ would not be present in solution to inhibit healing, and a high percentage of the total silver delivered was in the form of anti-inflammatory silver. The levels of Ag⁺ in nanocrystalline silver-containing solutions generated at different pHs will be tested in the future.

It should be noted that serum and wound fluids contain 160-185 mg/L calcium[43]. The daily calcium provided in the pH 7 and 9 treatments was thus <0.0025% and <0.012% of the calcium load per litre of blood, respectively. Therefore, it is unlikely that the calcium provided was a significant contributor to the effects observed.

Overall, nanocrystalline silver-derived solutions appear to have anti-inflammatory/pro-healing activity, particularly when generated at a starting pH of 9. Since this activity does not correlate with total silver, solutions generated under different conditions may have varying concentrations of different silver species, only some of which have anti-inflammatory activity. Future studies will focus on improving understanding of which species have anti-inflammatory activity and what conditions are necessary to generate or dissolve these species. Nanocrystalline silver-derived solutions show promise for a variety of anti-inflammatory treatment applications, including hard-to-treat tissue surfaces, and inflammation of internal epithelial tissues such as the lungs and bowels. Future studies should examine the effect of these solutions in models of ARDS and IBD.

Bibliography

1. Bhol KC, Alroy J, Schechter PJ: **Anti-inflammatory effect of topical nanocrystalline silver cream on allergic contact dermatitis in a guinea pig model.** *Clin Exp Dermatol* 2004, **29**:282-287.
2. Bhol KC, Schechter PJ: **Topical nanocrystalline silver cream suppresses inflammatory cytokines and induces apoptosis of inflammatory cells in a murine model of allergic contact dermatitis.** *Br J Dermatol* 2005, **152**:1235-1242.
3. Wright JB, Lam K, Buret AG, Olson ME, Burrell RE: **Early healing events in a porcine model of contaminated wounds: effects of nanocrystalline silver on matrix metalloproteinases, cell apoptosis, and healing.** *Wound Repair Regen* 2002, **10**:141-151.
4. Demling RH, DeSanti L: **The rate of re-epithelialization across meshed skin grafts is increased with exposure to silver.** *Burns* 2002, **28**:264-266.
5. Bhol KC, Schechter PJ: **Topical nanocrystalline silver cream inhibits expression of MMP-9 in animal models of allergic contact dermatitis.** *J Invest Dermatol* 2005, **124**:A117.
6. Bhol KC, Schechter PJ: **Effects of Nanocrystalline Silver (NPI 32101) in a Rat Model of Ulcerative Colitis.** *Dig Dis Sci* 2007:11 pages.
7. Fan FF, Bard AJ: **Chemical, electrochemical, gravimetric, and microscopic studies on antimicrobial silver films.** *J Phys Chem B* 2002, **106**:279-287.
8. Fuertes MA, Castilla J, Alonso C, Perez JM: **Cisplatin biochemical mechanism of action: from cytotoxicity to induction of cell death through interconnections between apoptotic and necrotic pathways.** *Curr Med Chem* 2003, **10**:257-266.
9. Mizushima Y, Okumura H, Kasukawa R: **Effects of gold and platinum on necrotizing factor, skin sensitizing antibody, and complement.** *Jpn J Pharmacol* 1965, **15**:131-134.
10. Handel ML, Nguyen LQ, Lehmann TP: **Inhibition of transcription factors by anti-inflammatory and anti-rheumatic drugs: can variability in response be overcome?** *Clin Exp Pharmacol Physiol* 2000, **27**:139-144.
11. Suzuki S, Okubo M, Kaise S, Ohara M, Kasukawa R: **Gold sodium thiomalate selectivity inhibits interleukin-5-mediated eosinophil survival.** *J Allergy Clin Immunol* 1995, **96**:251-256.
12. Eisler R: **Chrysotherapy: a synoptic review.** *Inflamm Res* 2003, **52**:487-501.
13. Nadworny PL, Wang JF, Tredget EE, Burrell RE: **Anti-inflammatory activity of nanocrystalline silver in a porcine contact dermatitis model.** *Nanomed: NBM* 2008, **4**:241-251.
14. Scott AE, Kashon ML, Yucesoy B, Luster MI, Tinkle SS: **Insights into the quantitative relationship between sensitization and challenge for**

- allergic contact dermatitis reactions.** *Toxicol Appl Pharmacol* 2002, **183**:66-70.
15. Laidlaw A, Flecknell P, Rees JL: **Production of acute and chronic itch with histamine and contact sensitizers in the mouse and guinea pig.** *Exp Dermatol* 2002, **11**:285-291.
 16. Groth O, Skoog ML: **Measurement and differentiation of the cellular infiltrate in experimental allergic contact dermatitis.** *Acta Derm Venereol* 1979, **59**:129-134.
 17. Kelley KW, Curtis SE, Marzan GT, Karara HM, Anderson CR: **Body surface area of female swine.** *J Anim Sci* 1973, **36**:927-930.
 18. Woods A: **Hematoxylyn and Counterstains.** In: *Laboratory Histopathology: A Complete Reference.* Eds. Woods A, Ellis R. Livingstone: Churchill Livingstone; 1994.
 19. Korostoff JM, Wang JF, Sarment DP, Stewart JC, Feldman RS, Billings PC: **Analysis of in situ protease activity in chronic adult periodontitis patients: expression of activated MMP-2 and a 40 kDa serine protease.** *J Periodontol* 2000, **71**:353-360.
 20. **In situ Cell Death Detection Kit, AP, Instruction Manual.** ©Roche Diagnostics Corporation. www.roche-applied-science.com/pack-insert/11684809910a.pdf. Viewed September 21, 2006.
 21. Nadworny PL, Landry BK, Wang JF, Tredget EE, Burrell RE: **Does nanocrystalline silver have a systemic effect?** *Wound Repair Regen* 2009, (submitted).
 22. Serhan CN, Savill J: **Resolution of inflammation: the beginning programs the end.** *Nat Immunol* 2005, **6**:1191-1197.
 23. Girolomoni G, Pastore S, Albanesi C, Cavani A: **Targeting tumor necrosis factor-alpha as a potential therapy in inflammatory skin diseases.** *Curr Opin Investig Drugs* 2002, **3**:1590-1595.
 24. Abraham GE, Himmel PB: **Management of Rheumatoid Arthritis: Rationale for the Use of Colloidal Metallic Gold.** *J Nutr Env Med* 1997, **7**:295-305.
 25. Glennas A, Rugstad HE: **Ploidity and cell cycle progression during treatment with gold chloride, auranofin and sodium aurothiomalate. Studies on a human epithelial cell line and its sub-strains made resistant to the antiproliferative effects of these gold compounds.** *Virchows Arch B Cell Pathol Incl Mol Pathol* 1985, **49**:385-393.
 26. Rigobello MP, Scutari G, Boscolo R, Bindoli A: **Induction of mitochondrial permeability transition by auranofin, a gold(I)-phosphine derivative.** *Br J Pharmacol* 2002, **136**:1162-1168.
 27. Donnelly RP, Fenton MJ, Finbloom DS, Gerrard TL: **Differential regulation of IL-1 production in human monocytes by IFN-gamma and IL-4.** *J Immunol* 1990, **145**:569-575.
 28. Essner R, Rhoades K, McBride WH, Morton DL, Economou JS: **IL-4 down-regulates IL-1 and TNF gene expression in human monocytes.** *J Immunol* 1989, **142**:3857-3861.

29. Lin E, Calvano SE, Lowry SF: **Inflammatory cytokines and cell response in surgery.** *Surgery* 2000, **127**:117-126.
30. Szabo G, Kodys K, Miller-Graziano CL: **Elevated monocyte interleukin-6 (IL-6) production in immunosuppressed trauma patients. II. Downregulation by IL-4.** *J Clin Immunol* 1991, **11**:336-344.
31. Tian J, Wong KK, Ho CM, Lok CN, Yu WY, Che CM, Chiu JF, Tam PK: **Topical delivery of silver nanoparticles promotes wound healing.** *ChemMedChem* 2007, **2**:129-136.
32. Schultz G, Rotatori DS, Clark W: **EGF and TGF-alpha in wound healing and repair.** *J Cell Biochem* 1991, **45**:346-352.
33. Brown GL, Curtsinger L, 3rd, Brightwell JR, Ackerman DM, Tobin GR, Polk HC, Jr., George-Nascimento C, Valenzuela P, Schultz GS: **Enhancement of epidermal regeneration by biosynthetic epidermal growth factor.** *J Exp Med* 1986, **163**:1319-1324.
34. Barrientos S, Stojadinovic O, Golinko MS, Brem H, Tomic-Canic M: **Growth factors and cytokines in wound healing.** *Wound Repair Regen* 2008, **16**:585-601.
35. Hardwicke J, Schmaljohann D, Boyce D, Thomas D: **Epidermal growth factor therapy and wound healing--past, present and future perspectives.** *Surgeon* 2008, **6**:172-177.
36. Beer HD, Gassmann MG, Munz B, Steiling H, Engelhardt F, Bleuel K, Werner S: **Expression and function of keratinocyte growth factor and activin in skin morphogenesis and cutaneous wound repair.** *J Investig Dermatol Symp Proc.* 2000, **5**:34-39.
37. Jimenez PA, Rampy MA: **Keratinocyte growth factor-2 accelerates wound healing in incisional wounds.** *J Surg Res* 1999, **81**:238-242.
38. Asarch A, Barak O, Loo DS, Gottlieb AB: **Th17 cells: a new paradigm for cutaneous inflammation.** *J Dermatolog Treat* 2008, **19**:259-266.
39. Conti P, Youinou P, Theoharides TC: **Modulation of autoimmunity by the latest interleukins (with special emphasis on IL-32).** *Autoimmun Rev* 2007, **6**:131-137.
40. Barai N, Law M, Perry L, Telgenhoff D, Aust D: **Effect of Collagenase Ointment on Healing of Partial and Full Thickness Porcine Wounds.** In: *Third Congress of the World Union of Wound Healing Societies.* Eds. Sibbald RG, Ayello EA, Orsted HL. Toronto: World Union of Wound Healing Societies; June 4-8, 2008: OR023.
41. Houwing R: **A study of the histopathology of moisture lesions.** In: *Eleventh Annual European Pressure Ulcer Advisory Panel Open Meeting: Bruges.* Ed. Cherry GW. Oxford: Hunts; September 4-6, 2008: p. 83.
42. Johnston HL, Cuta F, Garrett AB: **The solubility of silver oxide in water, in alkali and in alkaline salt solutions. The amphoteric character of silver hydroxide.** *JACS* 1933, **55**:2311-2325.
43. Trengove NJ, Langton SR, Stacey MC: **Biochemical analysis of wound fluid from nonhealing and healing chronic leg ulcers.** *Wound Repair Regen* 1996, **4**:234-239.

Chapter 8 – Effect of Sputtering Parameters on Resulting Nanocrystalline Silver Thin Film Properties

Introduction

Commercially produced nanocrystalline silver dressings (Acticoat™) contain two silver thin films, which are each 900 nm thick, with 3 mg/in² total silver[1], and 40-60% ammonia soluble silver[2]. These dressings are created by magnetron sputtering (physical vapor deposition) onto high density polyethylene (HPDE) in an argon atmosphere with trace oxygen. A variety of parameters affect the resulting sputtered silver, including the percentage of oxygen present in the chamber, the sputtering time, the current applied to the silver target, the target-to-substrate distance, the target geometry, and the total gas pressure present in the system at the time of sputtering.

Previously, Sant *et al.* examined the effect of gas composition, gas pressure, and input power on the nanostructure, antimicrobial activity, and dissolution characteristics of nanocrystalline silver thin films in a series of studies using static dissolution in water, single CZOIs, SEM, TEM, XPS, and resistivity[3]. In their studies, they sputtered silver onto silicon wafers with a 10 cm target-to-substrate distance, using oxygen concentrations of 0, 1, 4, and 20%, total pressures of 10 or 40 mTorr, powers of 0.05, 0.1, 0.15, or 0.3 kW, and final film thicknesses of 90, 300, 900, or 1000 nm (controlled by the sputtering time)[3]. They found that when no oxygen was included in the system, the silver that could be dissolved in water was minimal and the dressings were biologically inactive[3]. These films contained spherical crystallites of about 40 nm, and were

predominantly metallic silver[4-6]. They found that similar results were obtained using a pressure of 10 mTorr with 1% oxygen[4, 5] – the films were inactive and had similar chemical structure, suggesting insufficient oxygen was present. This was confirmed via XPS, which showed that decreasing the chamber pressure from 40 to 10 mTorr resulted in decreased oxygen content in the film[6]. They also found that when 10-20% oxygen was used to make the dressings, the dressings were composed of mostly silver oxide[6], but demonstrated some activity, consistent with the behavior of silver oxide[3]. These films appeared to have faceted particles with a crystallite size of about 50 nm[4]. TEM studies showed that biologically active¹ nanocrystalline silver films, including films generated at 1 and 4% oxygen at 40 mTorr, had grain sizes of about 15 nm with a high density of growth twins whose incoherent twin boundaries intersected grain boundaries[4, 5]. However, the films generated at 1% oxygen contained primarily metallic silver, although some silver was loosely associated with oxygen species; but the films generated at 4% oxygen contained metallic silver, silver that was loosely associated with oxygen, and silver oxide[6]. The films which were biologically active always contained greater than 7% O₂[6], and their XPS analyses suggested that the oxygen species existed in a number of different chemical states, suggesting the presence of multiple silver oxidation states[3, 4]. With increasing oxygen content, Sant *et al.* observed a higher deposition rate[6]. They observed morphological changes with increasing film thickness, including increased

¹ Their definition of “biologically active” was “ability of the film to create a zone size larger than that of silver nitrate” [4]. Other studies have suggested that this would not be a good definition of biological activity, and that log reductions would have provided a clearer definition (see reference 8).

columnar particle sizes and decreasing porosity[4]; however, on the larger columnar grains, small grains on the order of 15 nm were still observed[5]. Increasing the film thickness also resulted in decreased oxygen content of the film, and increased metallic silver in the films, which was attributed to time-dependent variations in the plasma[6]. More spherical particles and more particle agglomerations were observed with increasing power[5]. As well, as power was increased, the oxygen content in the film decreased, as measured by XPS[6]. They concluded that nanocrystallites in association with Ag-O superoxides and twin boundary/grain boundary interactions led to the release of biologically active forms of silver[3]. They found that the unique properties of nanocrystalline silver films were a strong function of grain size and lattice defects which were likely confined to specific grain boundaries. These were suggested to be energetically favorable as segregation points for solute atoms and to contribute to different energy states on the films, providing the driving force for sustained dissolution from the film surface[3, 6]. The grain sizes and lattice defects were, in turn, related strongly to the sputtering conditions used, particularly percent oxygen, power, and gas pressure, in a complex way[6].

The purpose of this study was to examine the effect of varying sputtering conditions on the biological activity and chemical structure of the silver thin films, when created using an in-house sputtering system. This would improve understanding of the conditions necessary to generate biologically active dressings, and therefore would improve understanding of how the dressings work. Another objective of this study was to determine the conditions necessary to

generate films similar to those used in commercially available dressings, using the in-house machine. An overall objective of this and future studies is also to determine conditions which optimize the biological activity of silver thin films.

Materials and Methods

Generation of Nanocrystalline Silver Thin Films

Nanocrystalline silver thin films were generated using an in-house designed and built extreme magnetron sputtering machine (vacuum chamber made by Kurt J. Lesker Co., Toronto, Ontario). The machine was typically allowed to pump down overnight (the pumps are a positive displacement rotary pump – iQDP80, BOC Edwards Ltd., Mississauga, Ontario, which is started at ambient pressure; a turbomolecular pump – TMP-803LM (power supply EL-D1003M), Shimadzu Corp., Burlington, Ontario, which is started at chamber pressures below 1 Torr; and a cryogenic trap – AquaTrap® Cryotiger Cooling System, Brooks Automation, Inc., Chelmsford, MA, which is started once the turbopump is running at full speed) to remove impurities prior to sputtering. A base pressure of $2\text{-}6 \times 10^{-5}$ Torr was achieved. Pressures were measured using a Convection Enhanced Pirani Vacuum Sensor Series 317 (MKS Instruments, Andover, MA) for pressures that were from ambient down to 1.0×10^{-3} Torr; a Baratron Absolute Pressure Transducer (Capacitance Gauge) Type 627B, from 1.0×10^{-1} – 1.0×10^{-4} Torr; and a Cold Cathode Ionization Vacuum Sensor Series 423 I-MAG (MKS) from 1.0×10^{-2} – 1.0×10^{-11} Torr. Leak tests were performed by opening a gate valve and measuring the pressure rise every 15 seconds for a minute. The pressure rise had to be less than 1.0 mTorr/min in order for

sputtering to begin. To begin sputtering, mass flow controllers (MKS 146 control units) were used to turn on the flow of gases to the desired concentration and total pressure. Then the magnetron (powered by an MDX 1.5K Magnetron Drive, Advanced Energy Industries, Inc., Fort Collins, CO) was turned on for the required time at the required current. The sputtering process was monitored via a viewport for arcing or sparking. Parameters varied for sputtering were current (0.5A, 0.75 A, 1 A, 1.5 A, 2A), percent oxygen (0%, 2%, 4%, 8%, 10%, and 12%), and sputtering time (10 min, 30 min) for static runs. For dynamic runs, web speeds of 20 mm/min, 43 mm/min, and 80 mm/min were tested. Parameters held constant were total gas pressure (40 mTorr), target-to-substrate distance (10 cm), target geometry (rectangular, producing an oval race track), and the substrate used (HDPE - Delnet, Applied Extrusion Technologies, Inc., Middletown, Del.).

For dynamic runs (rolling HDPE), or to move the HDPE forward between runs, a re-wind brushless DC motor was used (Faulhaber Motion Controllers, controlled by Faulhaber Motion Manager v. 3.1.1 © Dr. Fritz Faulhaber GmbH and Co., KG, Schoenaich, Germany), with the speed controlled by the voltage to the motor.

Samples were taken from well defined substrate sites under the target, as indicated using the location-labeling system shown in Figure 8-1.

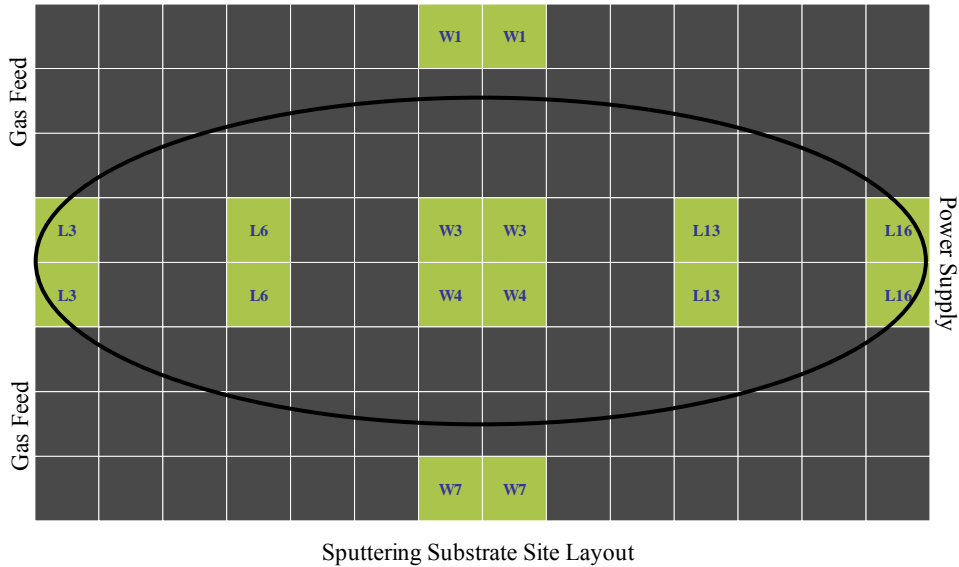


Figure 8-1. Substrate sampling locations. Substrate sampling locations are shown in green along with the codes used in the text for each location. The approximate orientation of the substrate locations under the “racetrack” generated by the magnetron is shown as a black oval. Each square represents 1 in².

Total Silver Digest

To determine the total silver deposited on the substrate, 1 in² of silver film was placed in 20 mL of a 1:2 dilution of 65% w/w nitric acid. The solution was then heated to 105°C±10°C for 20 minutes, after which point the thin film was removed, and the solution was cooled and diluted 1:50 in distilled water, and submitted for atomic absorption spectroscopy (AAS). For AAS, a Varian 220 FS double beam Atomic Absorption Spectrophotometer was used, with the following instrument parameters: a silver hollow cathode lamp with a wavelength of 328.1 nm, and a lean air-acetylene flame. A calibration plot was generated using silver standards of 0.5, 1.0, 3.0, and 5.0 ppm, prepared from a silver standard stock

solution of 1000 ppm. If dressings had released more than 5 ppm into solution, the solutions were diluted as necessary with distilled water until they were in the linear range for silver analysis (0.1 ppm to 5 ppm), and the results were corrected for the dilution factor.

Ammonia Soluble Silver Digest

To determine the percentage ammonia soluble silver (which correlates with silver oxide content), 1 in² samples of silver film were placed in 20 mL of ammonium hydroxide solution (20 g/L). The solutions were then placed on a mixing table (5-7 rev/min) for three minutes. The dressings were then removed, and the solutions were diluted 1:5 in distilled water and submitted for atomic absorption spectroscopy, as described above.

X-ray Diffraction (XRD)

XRD was performed to measure structural differences between dressings generated under different sputtering conditions. 1 in² samples of silver film were submitted to Umicore Canada, Inc. (Fort Saskatchewan) for x-ray diffraction. LaB₆ (NIST 660) was used as an instrument standard. Diffraction data were collected between 15 and 90°2θ. Convolution of the pure diffraction profile and the instrumental profile shape function followed by the integral method was applied to separate scattering domain size (apparent crystallite size) from microstrain effects. The ratio of the Ag₂O to Ag peaks was calculated from the raw data.

Bactericidal Efficacy

Log reduction assays were used to test the ability of the nanocrystalline silver thin films to kill bacteria in 30 minutes, following methods similar to the literature for testing nanocrystalline silver commercial dressings[1]. 1 in² pieces of dressing were constructed that were similar to the commercial nanocrystalline silver dressings by placing rayon/polyester gauze (Sontara Style 8411, DuPont, Mississauga, Ontario, Canada) in between two 1 in² pieces of nanocrystalline silver film (taken from the same substrate location). Plastic squares were cut to a size slightly larger than the dressing samples. A plastic square was placed in the center of a sterile Petri dish lid. Then, a dressing sample was placed on top of the plastic square and inoculated with 300 µL of log phase *P. aeruginosa* or *S. aureus* (see Chapter 4 for a description of the generation of a log phase culture) as indicated, and then covered with a second plastic square. The bottom of the Petri dish was placed on top of the sample, to ensure complete contact of the dressing and the inoculant. The Petri plates containing the inoculated dressings were incubated for 30 minutes at 37°C. Following incubation, the dressings and the plastic squares were placed in 2.7 mL of a salt-polysorbate-sodium thioglycollate (SPS) bacterial recovery solution (see Chapter 4 for recipe) in order to deactivate ionic silver and to recover the bacteria. The dressing sample and plastic squares were vigorously vortexed, and the recovery solution was then serially diluted from 10⁻² to 10⁻⁷ using PBS. 20 µL from each solution was drop-plated in triplicate onto MHA plates that were then incubated at 37°C overnight. The same procedure as described above was done for controls, except that 300 µL of

inoculant was directly added to 2.7 mL of SPS bacterial recovery solution. After 18-24 hours, the bacterial colonies were counted in order to determine the surviving number of CFUs. The controls were used to determine the number of CFUs in the original inoculum. The log reduction was then calculated by subtracting the log of the final CFUs from the log of the CFUs in the original inoculum.

This was performed in triplicate either for all substrate locations labeled in Figure 8-1, or for W3 and W4, as indicated in the results section.

Results and Discussion

Total and Ammonia Soluble Silver

A preliminary study examining the effect of current on total and ammonia soluble silver was performed. Figure 8-2 shows the total silver deposited when nanocrystalline silver thin films were sputtered for a 10 minute static run in a 4% oxygen atmosphere, with currents of 0.75, 1.5, or 2A. The total silver deposited increased with increasing current used, as anticipated, since the higher current results in more energy in the system. Sant *et al.* observed a similar effect[6]. This causes more collisions between ionized argon and the silver target, resulting in the removal of more silver from the target, and thus more silver deposition on the substrate. Some variation in total silver was observed with substrate location. In particular, more variability was observed in the W direction than the L direction, which is likely due to the fact that W1 and W7 are located outside the racetrack. For this 10 minute run, only the highest current used (2A) produced total silver as high as is provided by ActicoatTM (3 mg/in²)[1].

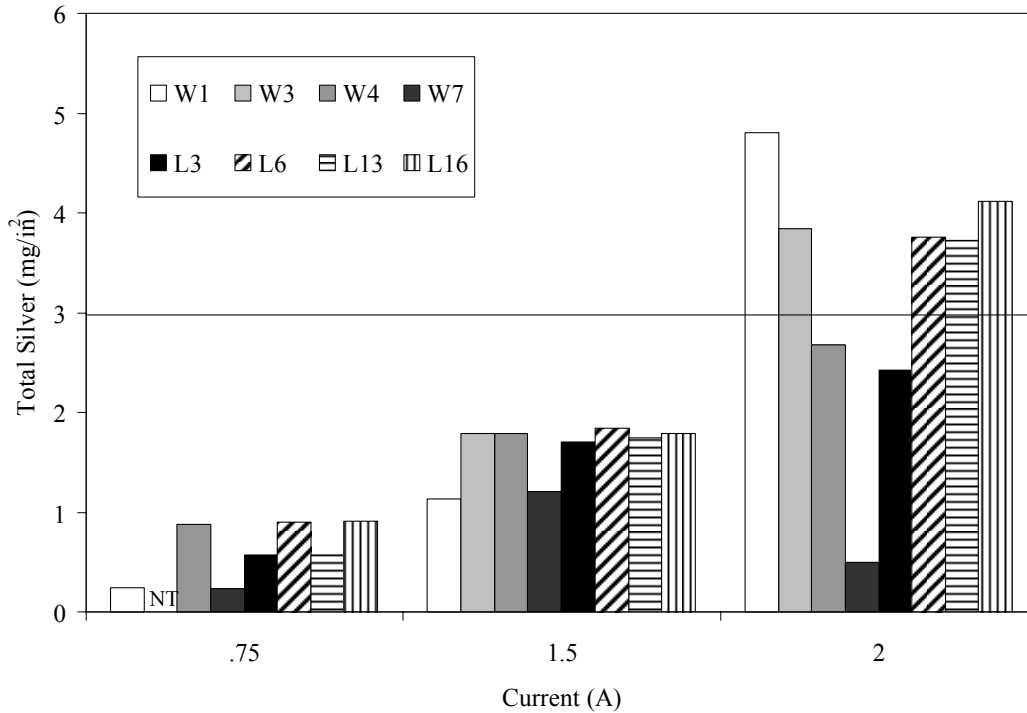


Figure 8-2. Preliminary results showing total silver deposited on samples sputtered at 4% O₂ for a 10 minute static run. Single runs were performed for each data point. Currents of 0.75, 1.5, or 2 A were used, and the total silver deposited at the locations indicated in Figure 8-1 was measured via nitric acid digest. NT= not tested. The total silver present in Acticoat™ (3 mg/in²) is indicated as a horizontal line on the figure.

The ammonia soluble silver measured for thin films generated under the same conditions is shown in Figure 8-3. Ammonia soluble silver was observed to decrease with increasing current, with only the ammonia soluble silver present at 0.75A being within the acceptable range for Acticoat™ (40-60%)[1, 2]. Sant *et al.* also observed a decrease in silver oxide with increasing current used to generate their films[6]. Variability in the ammonia soluble silver with substrate location was observed, but did not demonstrate a clear pattern. The value for W7 for the film generated at 2A is believed to be an outlier, and is likely a result of experimental error. Ammonia soluble silver measurements are highly susceptible to experimental error due to the precise three minute timing required for the

dissolution. In addition, as the ammonia soluble silver is reported as a percentage of the total silver, any experimental error in the measurement of the total silver is also carried over into the calculation of the ammonia soluble silver.

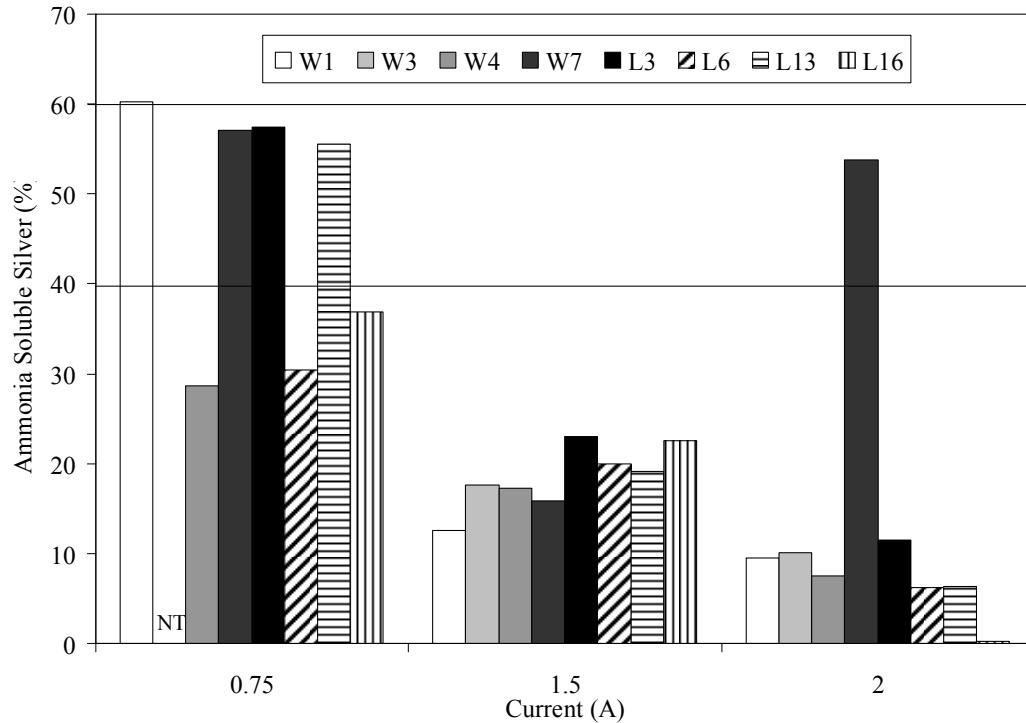


Figure 8-3. Preliminary results showing ammonia-soluble silver deposited on samples sputtered at 4% O₂ for a 10 minute static run. Single runs were performed for each data point. Currents of 0.75, 1.5, or 2 A were used, and the ammonia-soluble silver deposited at the locations indicated in Figure 8-1 was measured. NT= not tested. The range of ammonia soluble silver present in Acticoat™ (40-60%) is indicated as two horizontal lines on the figure.

Next, a study was performed to examine the effect of web speed on the total silver and ammonia soluble silver deposited on in-house sputtered nanocrystalline silver thin films. Figure 8-4 shows the effect of current on the total silver deposited on nanocrystalline silver thin films sputtered in a 4% oxygen atmosphere for a 20 mm/min dynamic run. The results observed are very similar to those of Figure 8-2, with only a current of 2A producing a total silver above the value required for Acticoat™. Little variability with substrate location was

observed in the L direction, but in the W direction, W1 showed consistently lower total silver deposition. This result might not be significant, but it is still surprising, as the web rolled in the W direction, and therefore a dynamic run would be expected to eliminate variability in the W direction, but not to correct variability in the L direction. This suggests that perhaps the motor was not turning at a consistent speed.

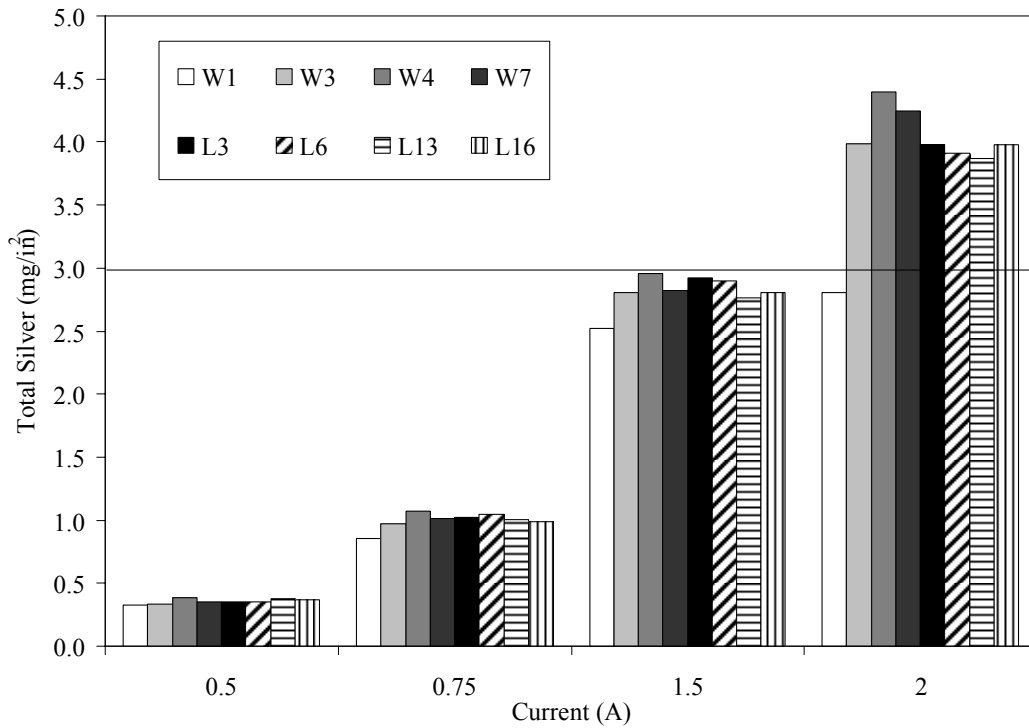


Figure 8-4. Effect of current on total silver deposited on samples sputtered at 4% O₂ for a 20 mm/min dynamic run. Single runs were performed for each data point. Currents of 0.5, 0.75, 1.5, or 2 A were used, and the total silver deposited at the locations indicated in Figure 8-1 was measured via nitric acid digest. The total silver present in Acticoat™ (3 mg/in²) is indicated as a horizontal line on the figure.

Figure 8-5 shows the effect of current on the ammonia soluble silver in nanocrystalline silver thin films sputtered under the same conditions. Again, decreased ammonia soluble silver was observed with increasing current.

Ammonia soluble silver correlates with the percentage of silver oxide in solution, and thus the lower ammonia soluble silver at higher current may be due to the reduction of silver oxide to metallic silver in the higher energy environment. For 4% O₂ 20 mm/min dynamic runs, only a current of 0.5A produced ammonia soluble silver within the range accepted for Acticoat™. This was a lower current than the current which produced an acceptable ammonia soluble silver in the static run shown in Figures 8-2 to 8-3.

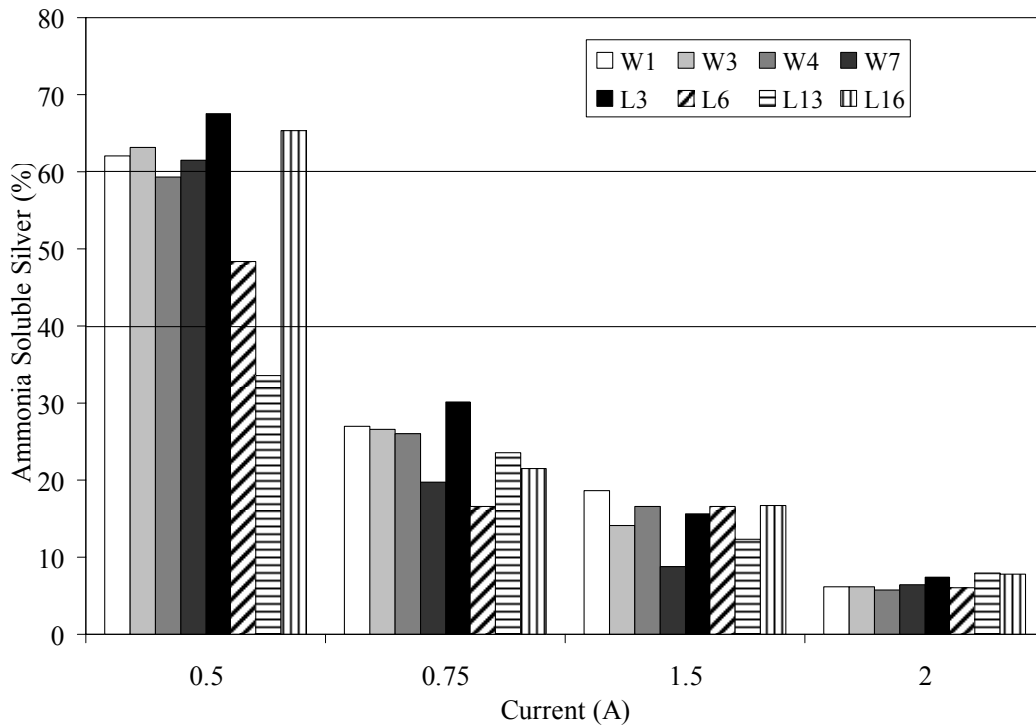


Figure 8-5. Effect of current on ammonia-soluble silver deposited on samples sputtered at 4% O₂ for a 20 mm/min dynamic run. Single runs were performed for each data point. Currents of 0.5, 0.75, 1.5, or 2 A were used, and the ammonia-soluble silver deposited at the locations indicated in Figure 8-1 was measured. The range of ammonia soluble silver present in Acticoat™ (40-60%) is indicated as two horizontal lines on the figure.

At an even higher web speed of 43 mm/min, when sputtering was performed at 4% oxygen, the total silver still increased with increasing current (Figure 8-6), but even at a current of 2A, the total silver was only half the total

silver requirement for Acticoat™. Again, variability in total silver deposited in the W direction was observed. The ammonia soluble silver (Figure 8-7) again decreased with increasing current, and there was no clear trend relative to substrate location. The ammonia soluble silver at 0.5A was lower at a web speed of 43 mm/min relative to a web speed of 20 mm/min, but at higher currents, the web speed did not appear to affect the ammonia soluble silver.

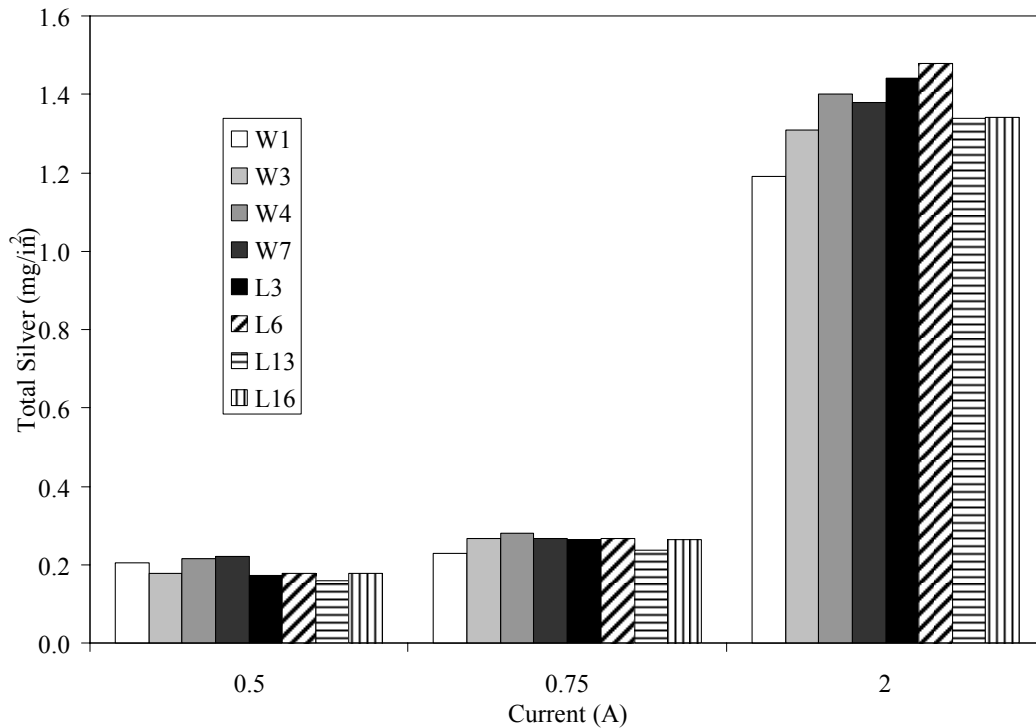


Figure 8-6. Effect of current on total silver deposited on samples sputtered at 4% O₂ for a 43 mm/min dynamic run. Single runs were performed for each data point. Currents of 0.5, 0.75, or 2 A were used, and the total silver deposited at the locations indicated in Figure 8-1 was measured via nitric acid digest.

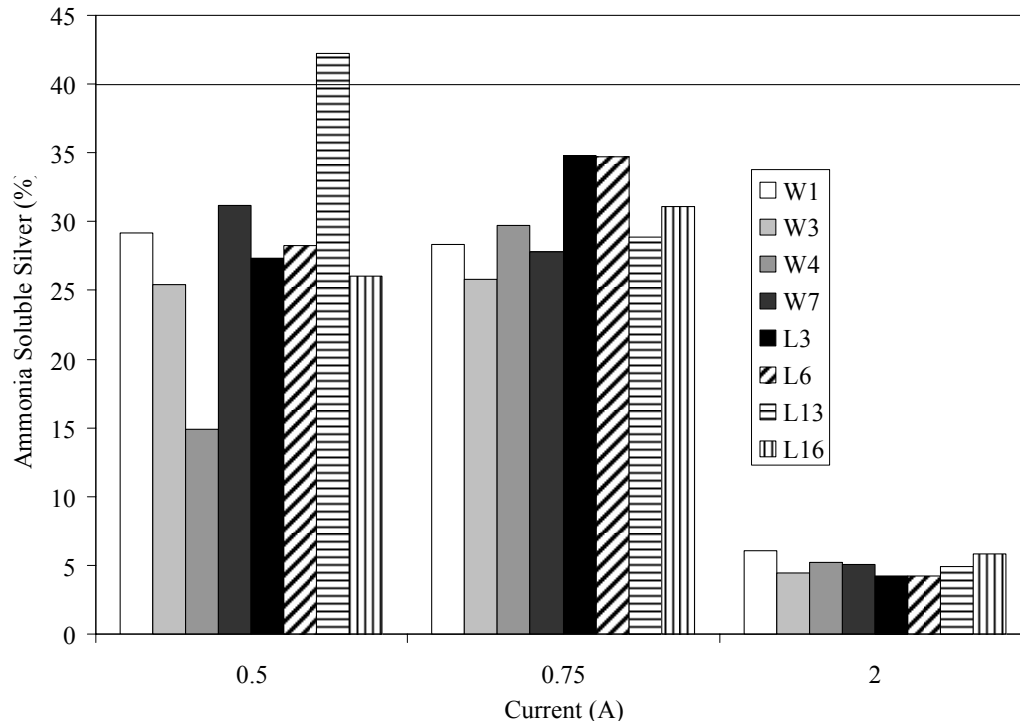


Figure 8-7. Effect of current on ammonia-soluble silver deposited on samples sputtered at 4% O₂ for a 43 mm/min dynamic run. Single runs were performed for each data point. Currents of 0.5, 0.75, or 2 A were used, and the ammonia-soluble silver deposited at the locations indicated in Figure 8-1 was measured. The lower limit for ammonia soluble silver present in Acticoat™ (40%) is indicated as a horizontal line on the figure.

A web speed of 80 mm/min was tested at 1.5A only, and the total silver deposited is shown in Figure 8-8. These results show that when the web speed was tripled (relative to the data shown in Figure 8-4, where the web speed was 20 mm/min), the total silver was reduced by a factor of three. However, in comparing Figure 8-9 (which shows the ammonia soluble silver for the thin films sputtered at a web speed of 80 mm/min and 1.5A) to Figure 8-5, the ammonia soluble silver did not change with web speed. As with previous ammonia soluble silver measurements, the ammonia soluble silver did not show a clear pattern related to substrate location.

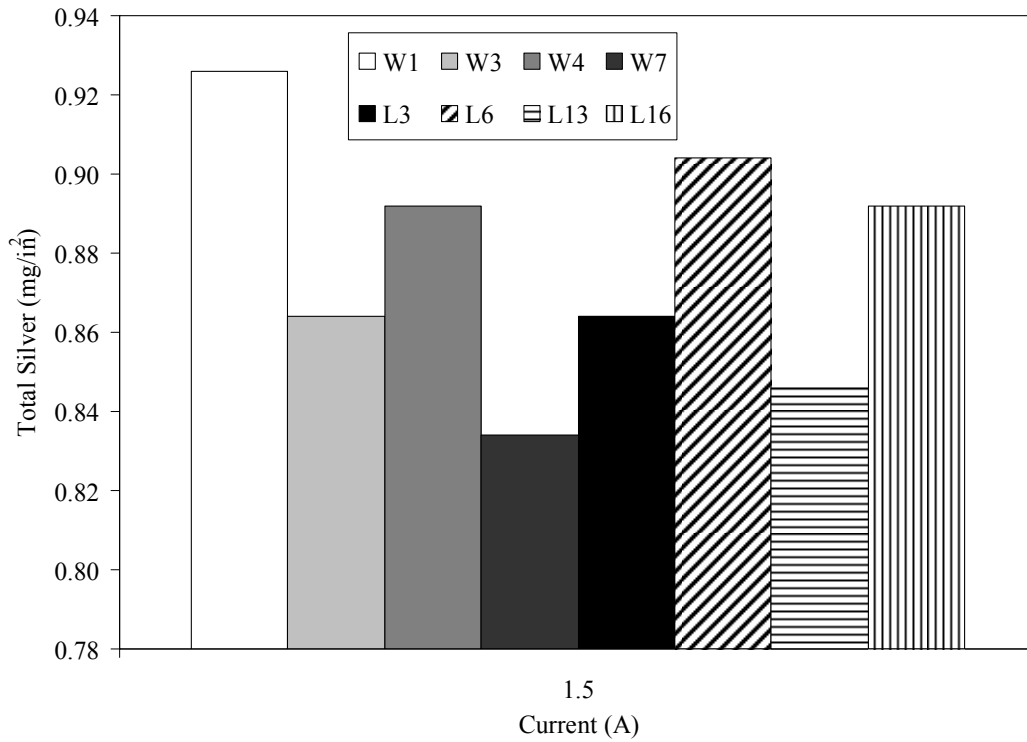


Figure 8-8. Effect of current on total silver deposited on samples sputtered at 4% O₂ for an 80 mm/min dynamic run at 1.5A. Single experiments were performed for each data point. The total silver deposited at the locations indicated in Figure 8-1 was measured via nitric acid digest.

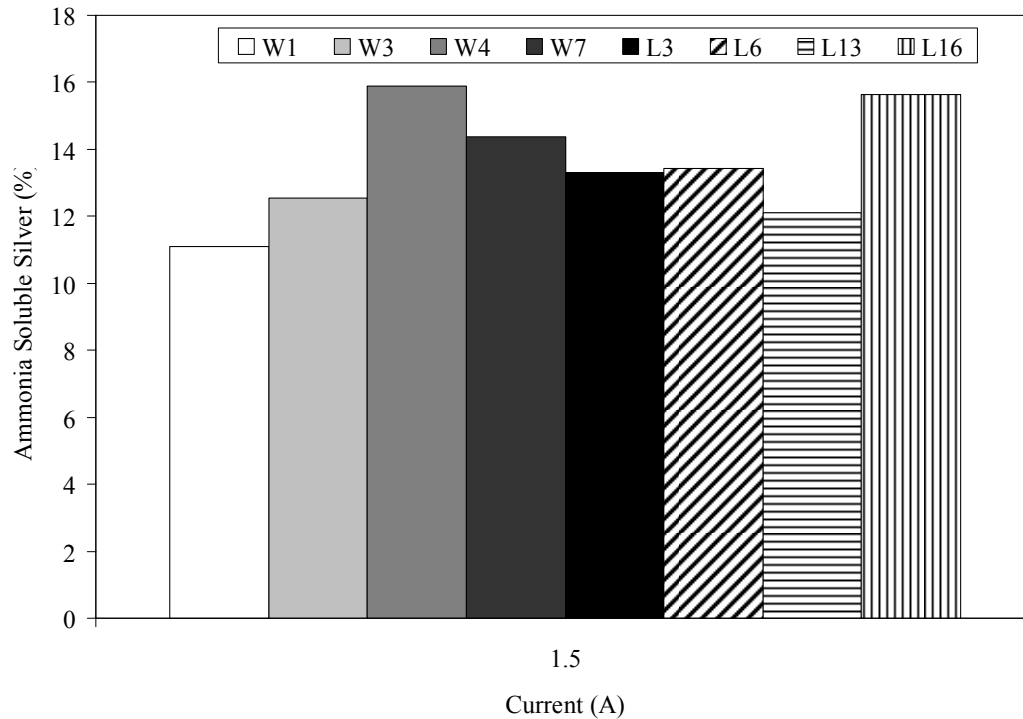


Figure 8-9. Effect of current on ammonia-soluble silver deposited on samples sputtered at 4% O₂ for an 80 mm/min dynamic run at 1.5A. Single experiments were performed for each data point. The ammonia-soluble silver deposited at the locations indicated in Figure 8-1 was measured.

The results of Figures 8-2 through 8-9 for substrate locations W3 and W4 are plotted in comparison to each other for total silver and ammonia soluble silver in Figures 8-10 and 8-11, respectively. The locations W3 and W4 were chosen since they are the central substrate sample locations and most likely represent the “average” or “best” results for each sputtering condition. Figure 8-10 shows that 20 mm/min dynamic runs resulted in higher total silver than 10 minute static runs performed under the same conditions, but that higher speed dynamic runs resulted in progressively lower total silver. For all web speeds, the total silver increased with increasing current. Figure 8-11 shows that in general, either the ammonia soluble silver did not change or decreased slightly with increasing web speed, and clearly decreased with increasing current for all web speeds.

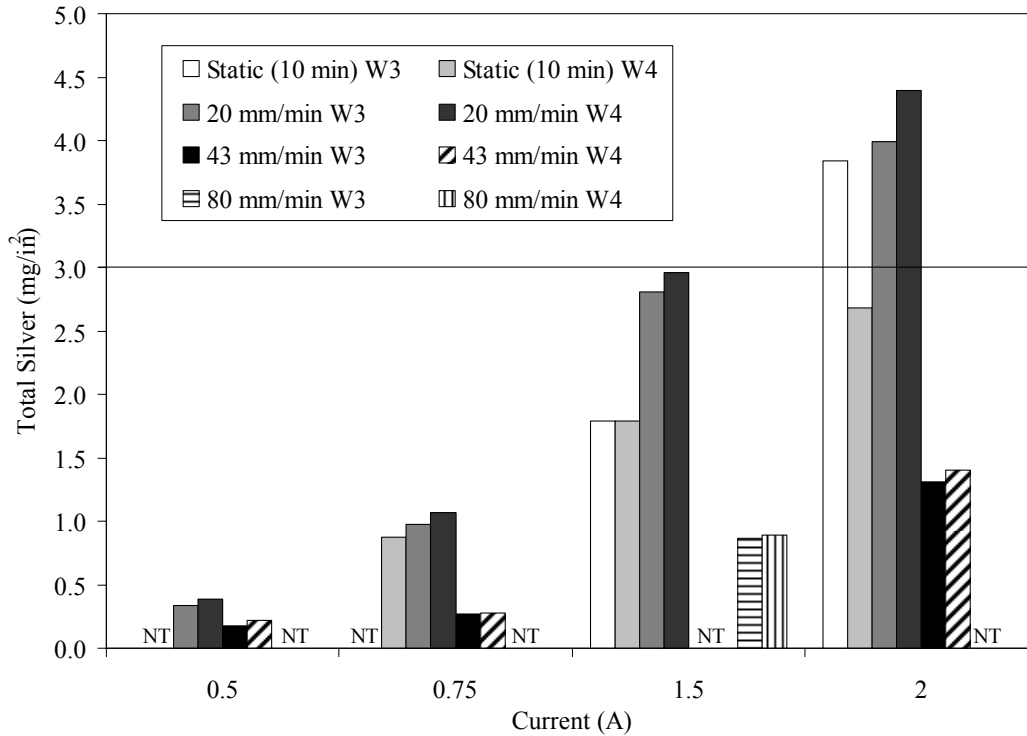


Figure 8-10. Effect of web speed for dynamic runs on total silver deposited on samples sputtered at 4% O₂. Currents used were 0.5, 0.75, 1.5, and 2A. Single experiments were performed for each data point. The total silver deposited at substrate locations W3 and W4 are shown. The total silver present in Acticoat™ (3 mg/in²) is shown as a horizontal line on the figure. NT=not tested.

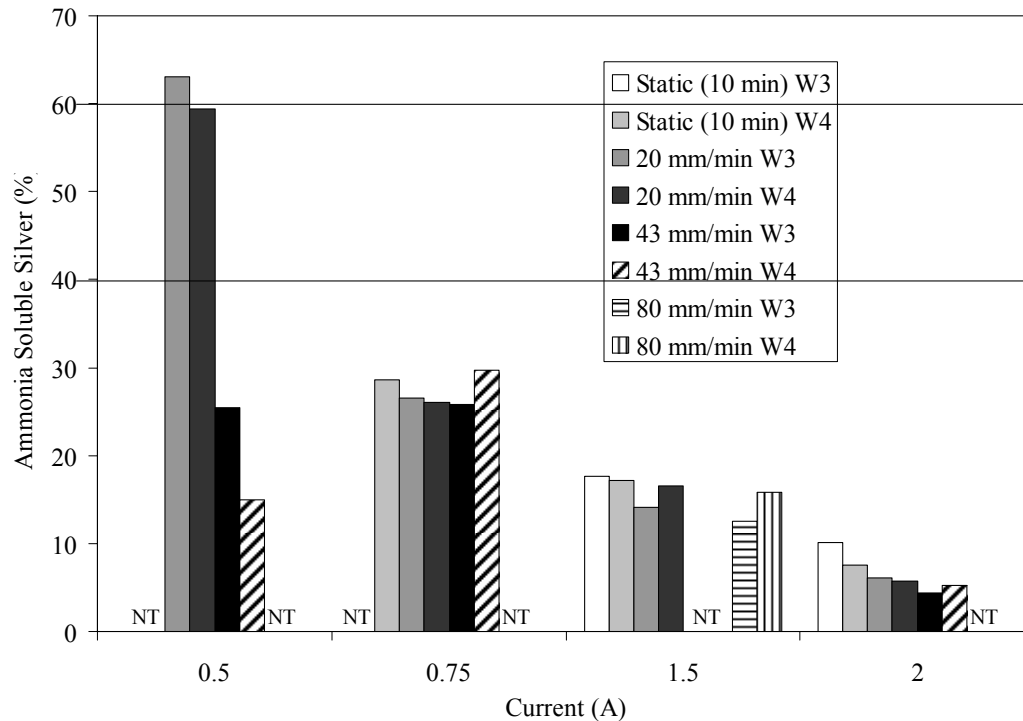


Figure 8-11. Effect of web speed for dynamic runs on ammonia-soluble silver deposited on samples sputtered at 4% O₂. Currents used were 0.5, 0.75, 1.5, and 2A. Single experiments were performed for each data point. The ammonia-soluble silver deposited at substrate locations W3 and W4 are shown. The acceptable range of ammonia-soluble silver in Acticoat™ (40-60%) is shown as two horizontal lines on the figure. NT=not tested.

Overall, these results indicate that there is an approximately linear relationship between increasing web speed and decreasing total silver deposited, with silver deposition being halved as the web speed is doubled. This is due to the fact that if the web is moved more quickly, there is less time for the silver to be deposited on the substrate. The results also indicate that a web speed of 20 mm/min or less is required to produce films with a total silver deposition equal to or greater than the total silver present in Acticoat™. With lower current, a slower web speed is required. The ammonia soluble silver does not appear to be substantially affected by the web speed, indicating that, as might be expected,

having a moving substrate does not affect the composition of the films but simply affects the amount of silver deposited.

Next, the effect of percent oxygen was examined with the web speed held constant. Figure 8-12 shows the total silver deposited for nanocrystalline silver thin films deposited at 2% oxygen, 20 mm/min, and various currents. The results obtained are nearly identical to those of Figure 8-4, where dressings were sputtered under the same conditions except that 4% oxygen was used. This suggests that the oxygen percentage in the atmosphere during sputtering has little effect on the total silver deposited, unlike the observation made by Sant *et al.*[6]

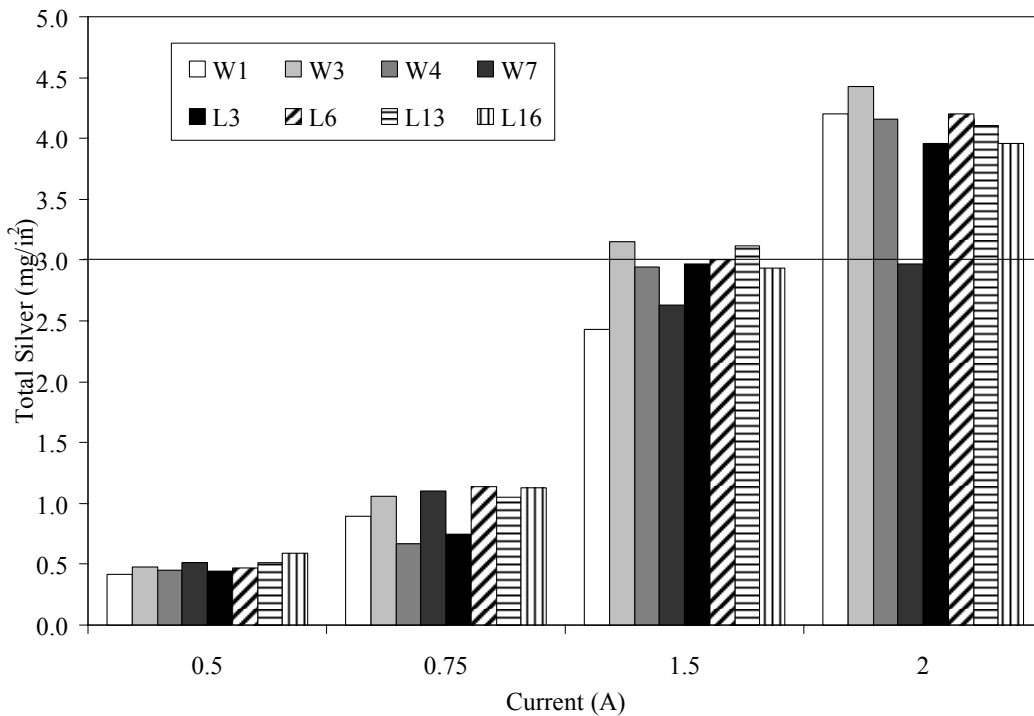


Figure 8-12. Effect of current on total silver deposited on samples sputtered at 2% O₂ for a 20 mm/min dynamic run. Currents used were 0.5, 0.75, 1.5, and 2A. Single experiments were performed for each data point. The total silver deposited at the locations indicated in Figure 8-1 was measured via nitric acid digest. The total silver present in Acticoat™ (3 mg/in²) is shown as a horizontal line on the figure.

Figure 8-13 shows the ammonia soluble silver deposited for the same sputtering conditions as Figure 8-12. As with previous results, the ammonia soluble silver decreased with increasing current and did not vary in any clear trend with substrate location. However, compared to Figure 8-5, which shows the ammonia soluble silver for dressings sputtered under the same conditions but with 4% oxygen rather than 2%, the percentage of ammonia soluble silver at any given current is decreased by one third to one half when using 2% oxygen. Sant *et al.* observed a similar effect of percent oxygen on the silver oxide present in their films[6]. This was anticipated, since less oxygen in the atmosphere should result in fewer collisions between oxygen and silver after the silver is knocked off of the target, and therefore less silver oxide is formed, resulting in less ammonia soluble silver present on the substrate.

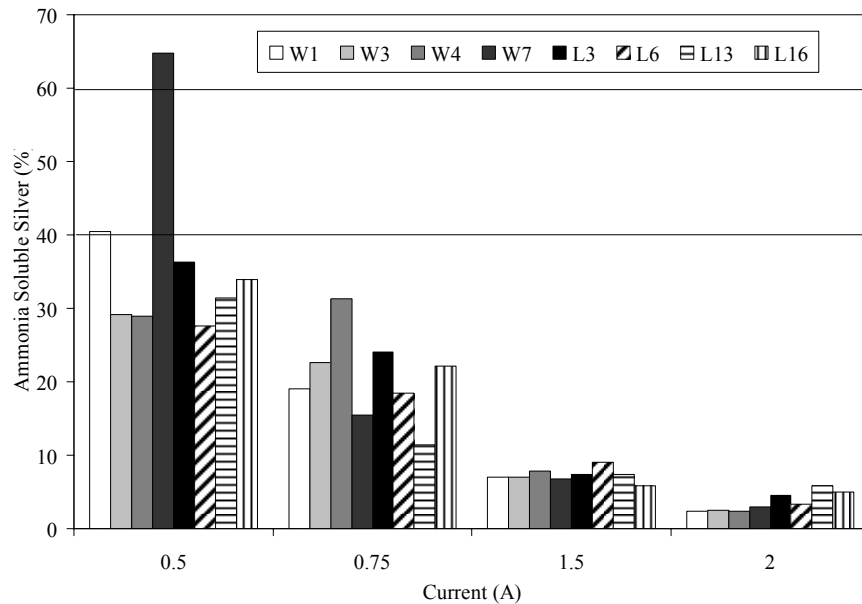


Figure 8-13. Effect of current on ammonia-soluble silver deposited on samples sputtered at 2% O₂ for a 20 mm/min dynamic run. Currents used were 0.5, 0.75, 1.5, and 2A. Single experiments were performed for each data point. The ammonia-soluble silver deposited at the locations indicated in Figure 8-1 was measured. The acceptable range of ammonia-soluble silver in Acticoat™ (40-60%) is shown as two horizontal lines on the figure.

When no oxygen was present in the chamber during sputtering for 20 mm/min dynamic runs, the total silver again did not change substantially (Figure 8-14) relative to runs at 2 and 4% oxygen (Figures 8-12 and 8-4, respectively). The ammonia soluble silver, however, dropped to near-zero (Figure 8-15). Sant *et al.* observed that dressings generated at 0% oxygen *in situ* for XPS analysis contained no silver oxide[6]. Thus, the low ammonia soluble silver levels which were present in the samples from this experiment were likely due to reactions between the dressings and oxygen present in the air post-sputtering. The fact that more ammonia soluble silver was present at lower currents than higher currents suggests that perhaps the dressings generated at lower current had a larger surface area or a more reactive surface, resulting in more silver oxide formation post-sputtering. This is in line with observations made by Sant *et al.*, which indicated that films were more dense, contained more agglomerations, and had larger crystal sizes when sputtered at higher currents[6], as these would all result in a lower surface area, and perhaps a less reactive surface as well.

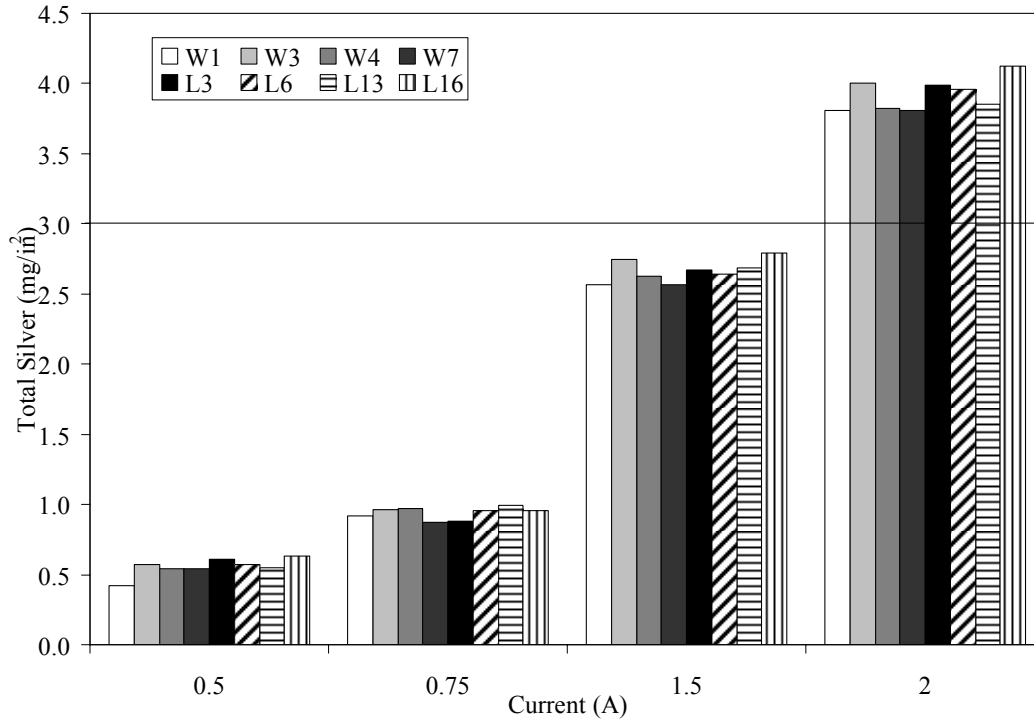


Figure 8-14. Effect of current on total silver deposited on samples sputtered at 0% O₂ for a 20 mm/min dynamic run. Currents used were 0.5, 0.75, 1.5, and 2A. Single experiments were performed for each data point. The total silver deposited at the locations indicated in Figure 8-1 was measured via nitric acid digest. The total silver present in Acticoat™ is shown as a horizontal line on the figure.

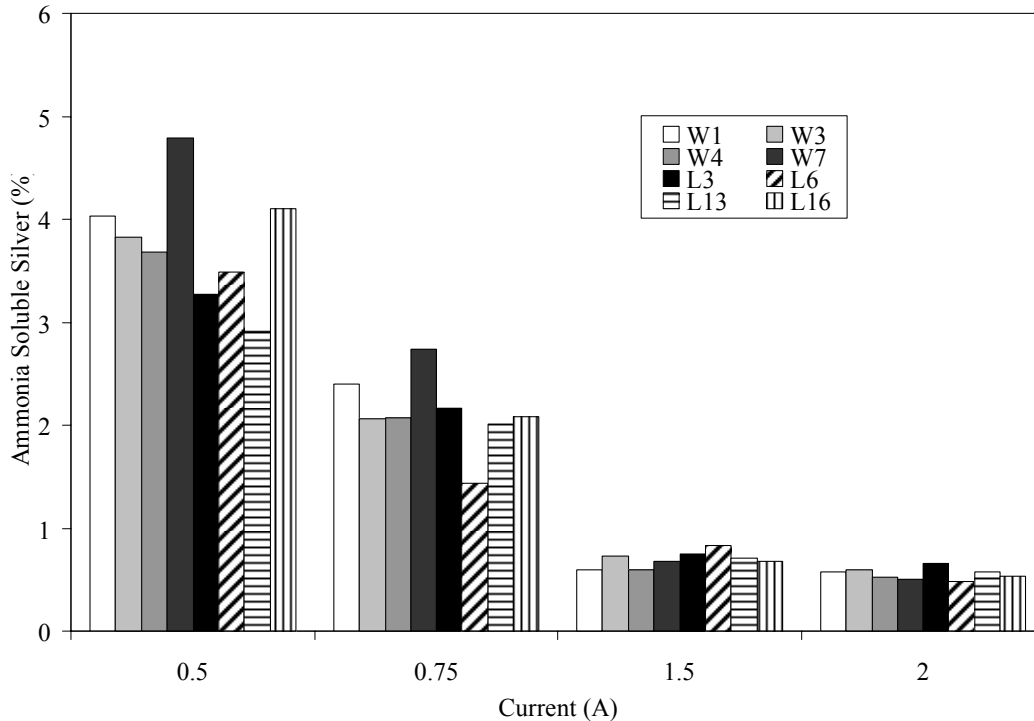


Figure 8-15. Effect of current on ammonia-soluble silver deposited on samples sputtered at 0% O₂ for a 20 mm/min dynamic run. Currents used were 0.5, 0.75, 1.5, and 2A. Single experiments were performed for each data point. The ammonia-soluble silver deposited at the locations indicated in Figure 8-1 was measured.

The results of Figures 8-4, 8-5, and 8-12 through 8-15 for substrate locations W3 and W4 are plotted in comparison to each other for total silver and ammonia soluble silver in Figures 8-16 and 8-17, respectively. Again, the locations W3 and W4 were chosen since they most likely represent the “average” results for each sputtering condition. Figure 8-16 shows that although the total silver increased with total current, there were no clear patterns relating total silver to the percent oxygen present in the system, as seen above. Figure 8-17 shows that the ammonia soluble silver decreased with increasing current at every oxygen concentration, which, again, was similar to earlier results. More importantly, the ammonia soluble silver approximately doubled with an increase from 2% to 4%

oxygen, with the only exception being at 0.75A, where there was no clear difference between the two levels of oxygen.

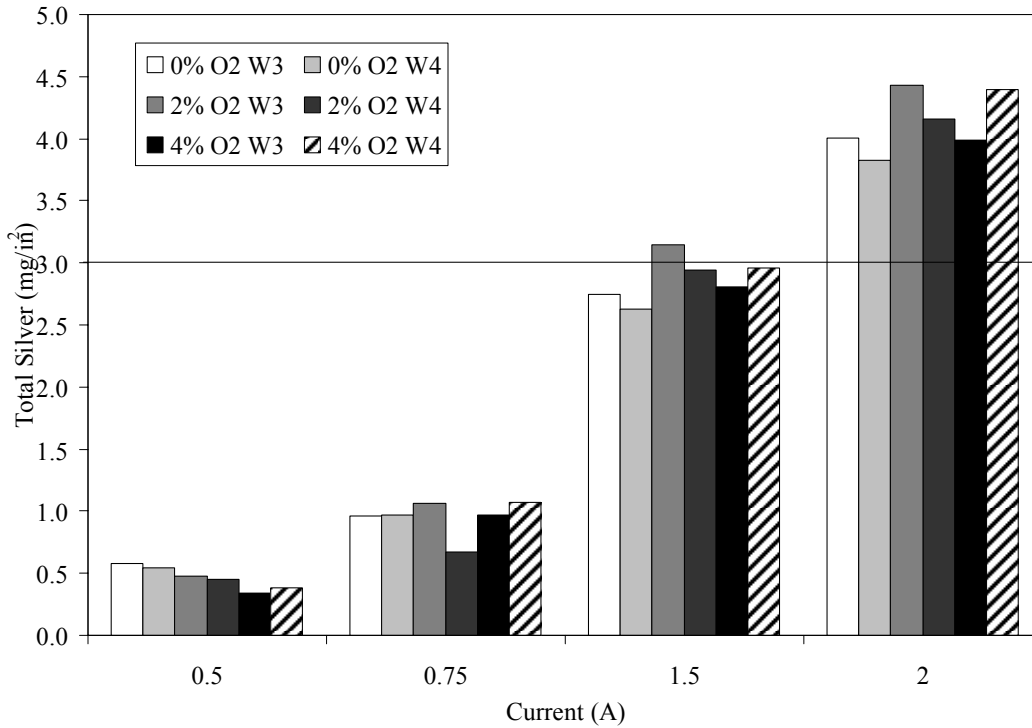


Figure 8-16. Effect of percent oxygen on total silver deposited on samples sputtered for a 20 mm/min dynamic run. Currents used were 0.5, 0.75, 1.5, and 2A. Single experiments were performed for each data point. The total silver deposited at the locations W3 and W4 are shown. The total silver present in Acticoat™ (3 mg/in²) is shown as a horizontal line on the figure.

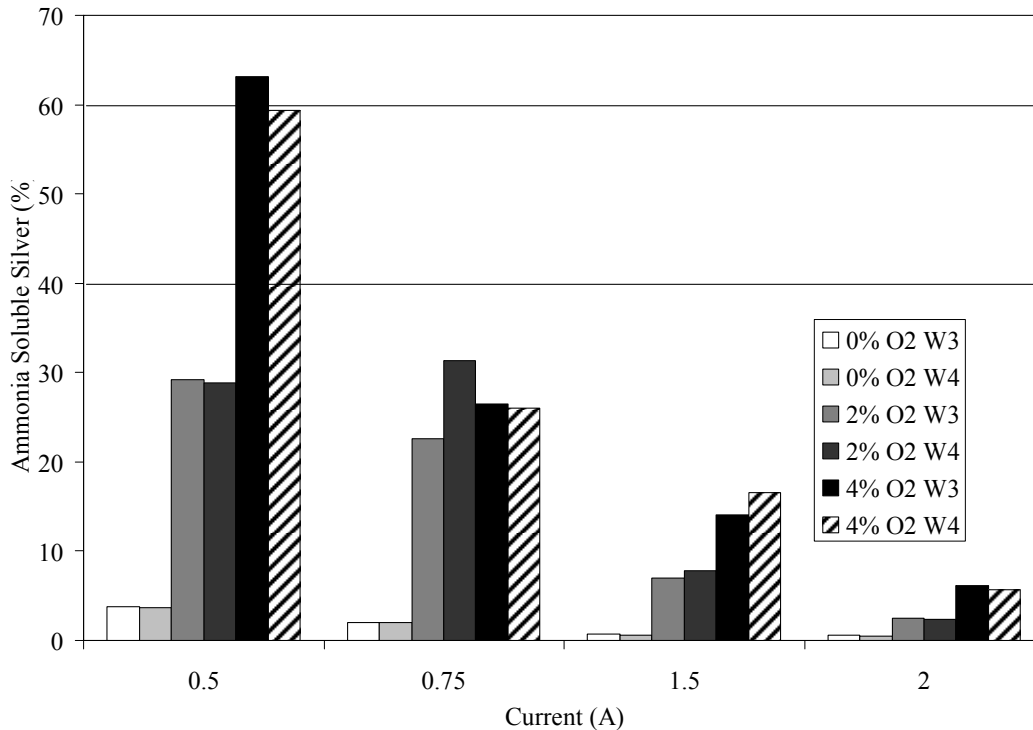


Figure 8-17. Effect of percent oxygen on ammonia-soluble silver deposited on samples sputtered for a 20 mm/min dynamic run. Currents used were 0.5, 0.75, 1.5, and 2A. Single experiments were performed for each data point. The ammonia-soluble silver deposited at substrate locations W3 and W4 are shown. The acceptable range of ammonia-soluble silver in Acticoat™ (40-60%) is shown as two horizontal lines on the figure.

Another experiment was performed to compare films generated on mesh to films generated on a solid substrate. Nanocrystalline silver thin films were generated at 4% oxygen in 10 minute static sputters at 0.75 or 1.5A, and the resultant total silvers deposited are shown in Figure 8-18. While there was no clear pattern to the variation in total silver in the L direction, again less silver appeared to be deposited at W1 in particular relative to other substrate locations. Interestingly, the total silver deposited did not appear to change in switching from mesh to solid. It was anticipated that due to the weave of the mesh, the mesh would have about one third of the total silver deposited on the solid substrate, with the remaining two thirds of the silver being deposited onto the substrate

support, so this result was surprising, and cannot yet be fully explained.

Furthermore, the percent ammonia soluble silver present on the solid surface was consistently lower than that present on the mesh (Figure 8-19). This too was not anticipated, as the substrate was not expected to affect the film composition. This suggests that the solid substrate acted as a reducing agent. Further studies will be needed to examine the impact of the substrate on the resulting film, as these films could potentially be used for a variety of applications other than wound dressings, as long as they can be generated with the same properties that they have on the HPDE mesh, when they are sputtered onto other surfaces. For example, they could be used to coat personal protective equipment, contact lenses, implants, or other medical devices.

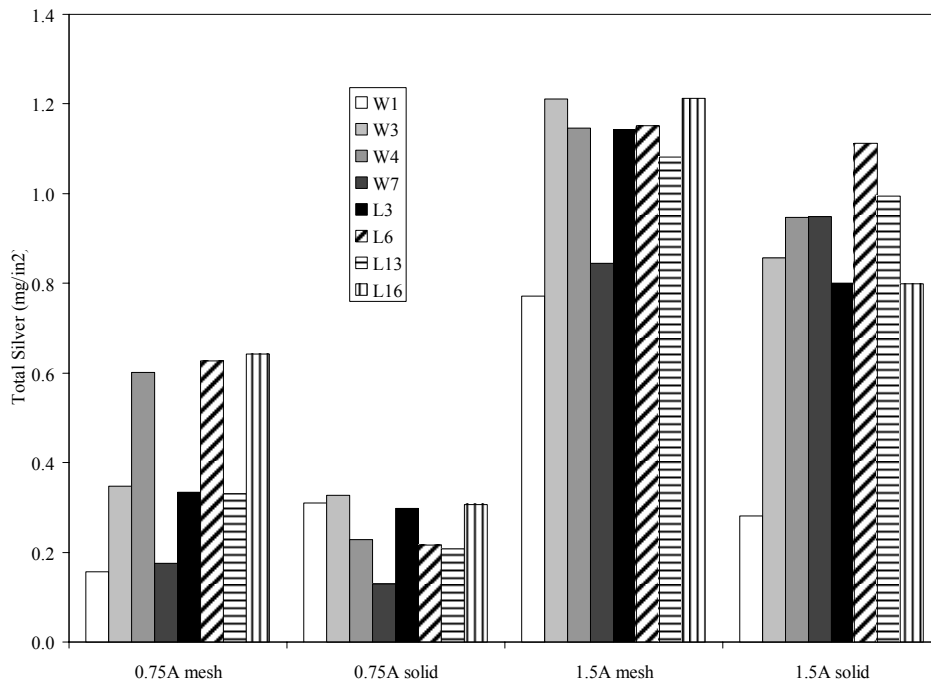


Figure 8-18. Effect of solid versus meshed substrate on total silver deposited on samples sputtered at 4% O₂ for a 10 minute static run. Currents used were 0.75, and 1.5A. Single experiments were performed for each data point. The total silver deposited at the locations indicated in Figure 8-1 was measured via nitric acid digest.

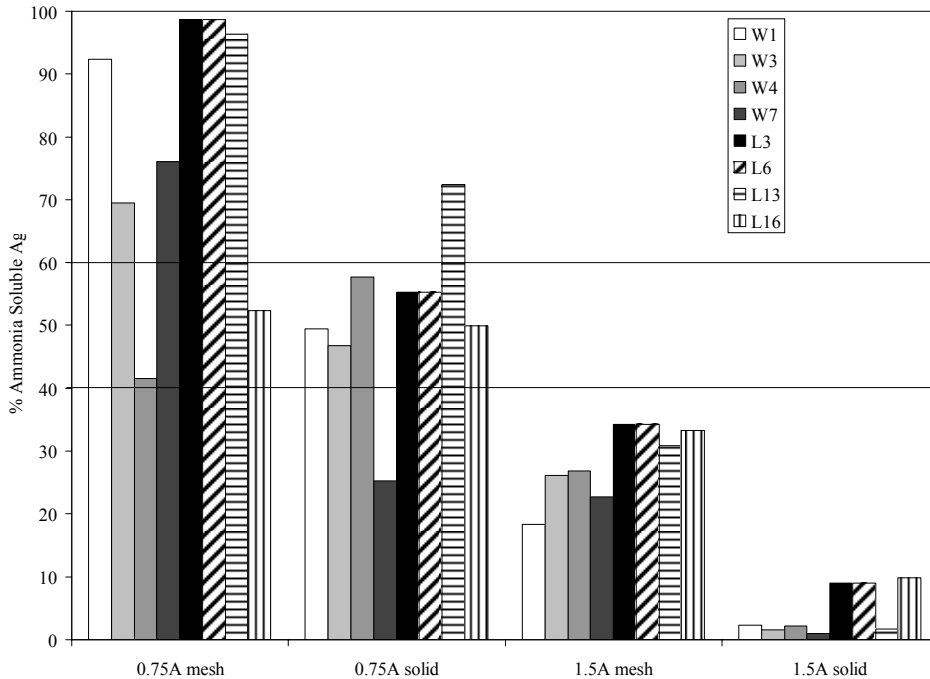


Figure 8-19. Effect of solid versus meshed substrate on ammonia-soluble silver deposited on samples sputtered at 4% O₂ for a 10 minute static run. Currents used were 0.75, and 1.5A. Single experiments were performed for each data point. The ammonia-soluble silver deposited at the locations indicated in Figure 8-1 was measured. The acceptable range of ammonia-soluble silver in Acticoat™ (40-60%) is shown as two horizontal lines on the figure.

An experiment was performed looking at the effect of oxygen concentration on total and ammonia soluble silver deposited in static runs. 10 minute static runs were performed at 1.5A, and 4%, 6% or 8% O₂ was used. The resulting total silver deposited is shown in Figure 8-20. The total silver generated was about the same for all three oxygen levels, and was quite close to that found in Acticoat™. Again, there was no clear pattern in terms of deposition location in the L direction, but there was a very clear pattern of lower deposition at positions W1 and W7, which is likely due to the fact that these positions are outside the racetrack and thus receive silver from only one side of the racetrack, while

positions W3 and W4, as well as all the L positions, would have silver deposition from both sides of the racetrack.

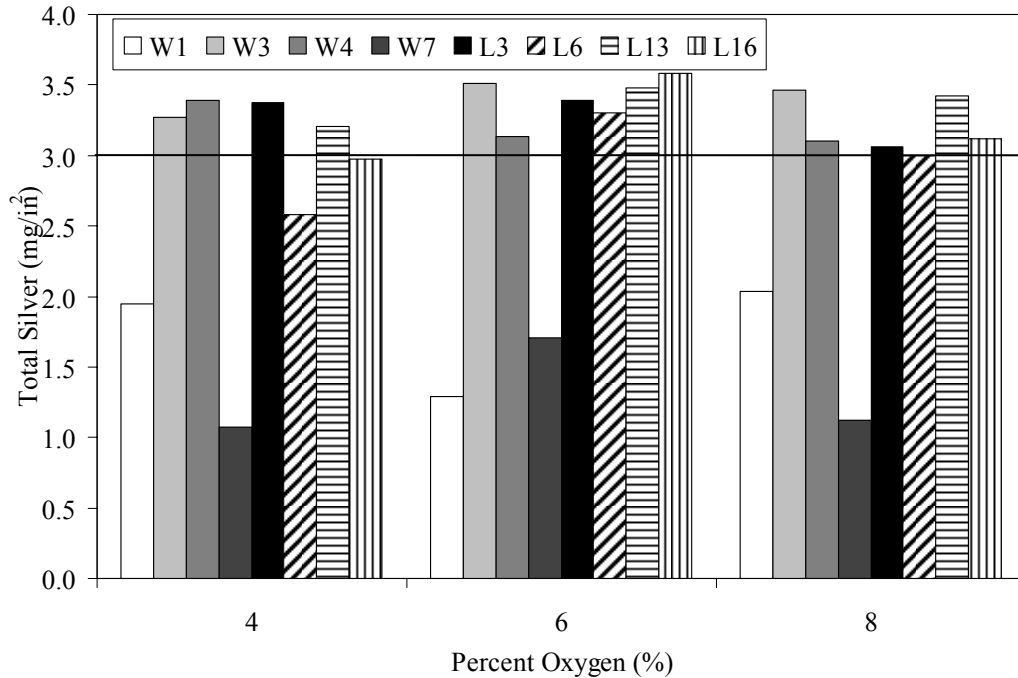


Figure 8-20. Preliminary study of the effect of percent oxygen on total silver deposited on samples sputtered at 1.5A for a 10 minute static run. Single experiments were performed for each data point. The total silver deposited at the locations indicated in Figure 8-1 was measured via nitric acid digest. The total silver present in Acticoat™ (3 mg/in²) is shown on the figure as a horizontal line.

The percentage of ammonia soluble silver is shown in Figure 8-21. At 1.5A current, the ammonia soluble silver increases slightly with each increase in oxygen, but even at 8% oxygen, most locations did not reach the lower limit for ammonia soluble silver in Acticoat™. It is interesting to note that in this particular experiment, the ammonia soluble silver was lower at W1 than the other W locations, and that the ammonia soluble silver increased somewhat with increasing L location. This may be related to gas distribution patterns in the chamber.

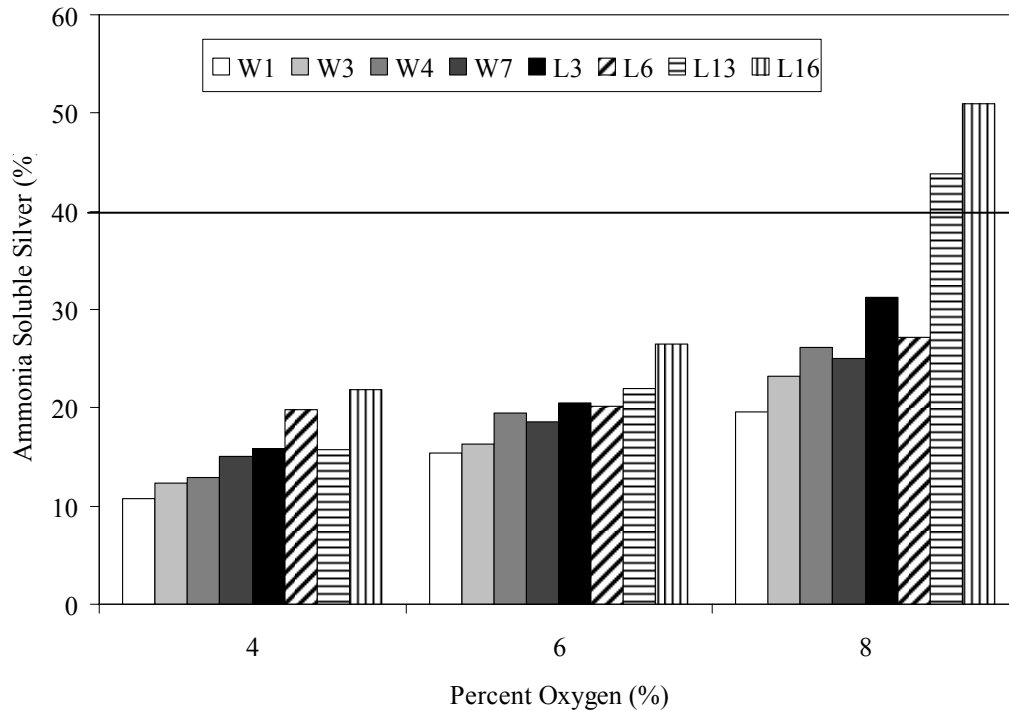


Figure 8-21. Effect of percent oxygen on ammonia-soluble silver deposited on samples sputtered at 1.5A for a 10 minute static run. Single experiments were performed for each data point. The ammonia-soluble silver deposited at the locations indicated in Figure 8-1 was measured. The acceptable range of ammonia-soluble silver in Acticoat™ (40-60%) is shown as horizontal lines on the figure.

Further to this experiment, an experiment was run in which 10 minute static runs were performed at either 0.75A or 1A, and either 8% or 10% oxygen. The total silver deposited under these conditions is shown in Figure 8-22. As seen in previous studies, the total silver increased with current, and did not change with total oxygen. As well, the same substrate location pattern was observed, in which there was little variation in the L direction, but lower total silver deposited at either extremes in the W direction. The total silver deposited never reached the levels present in Acticoat™, indicating that even higher currents would be required to deposit sufficient total silver using a 10 minute sputter. This is similar to the results in Figures 8-2 and 8-18. Interestingly, the ammonia soluble silver

generated under these conditions was very high (see Figure 8-23), well above the acceptable range for Acticoat™, and increased from about 80% to about 100% with a shift from 8% to 10% oxygen. At these oxygen levels, not much change in ammonia soluble silver was observed with increasing current. These ammonia soluble silver levels indicate that the films created were likely mostly silver oxide.

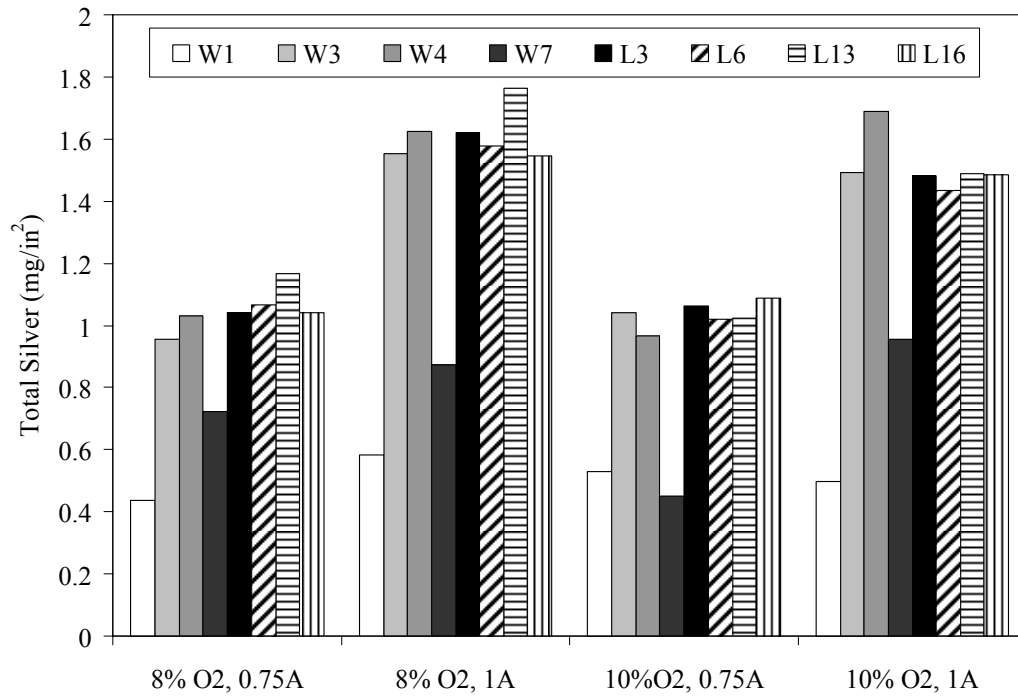


Figure 8-22. Preliminary study of the effect of current and percent oxygen on total silver deposited on samples sputtered in a 10 minute static run. A single experiment was run for each data point. The total silver deposited at the locations indicated in Figure 8-1 was measured via nitric acid digest.

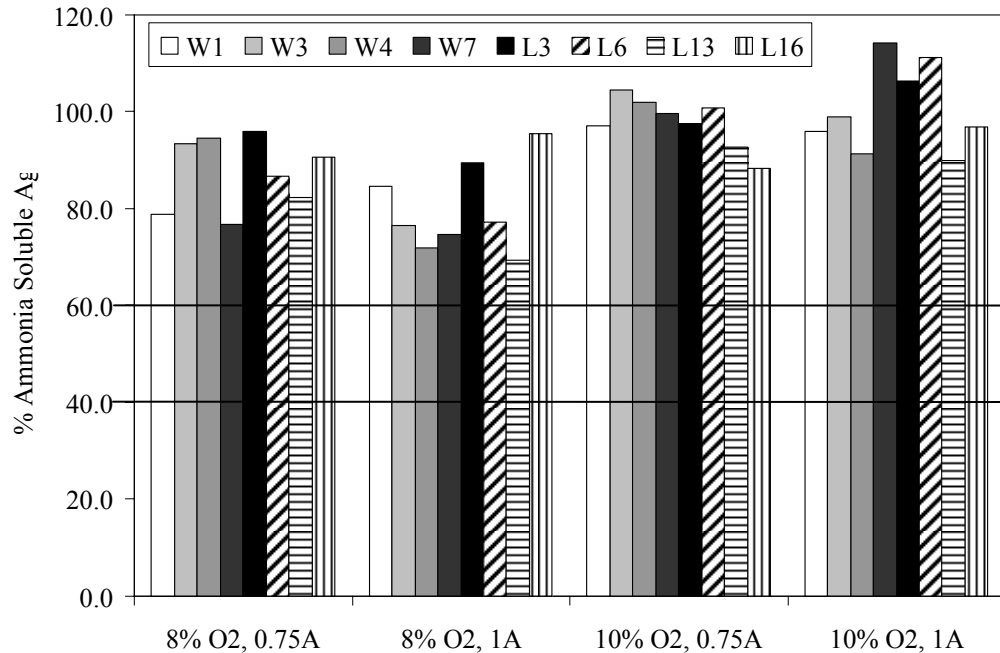


Figure 8-23. Preliminary study of the effect of current and percent oxygen on ammonia-soluble silver deposited on samples sputtered in a 10 minute static run. A single experiment was run for each data point. The ammonia-soluble silver deposited at the locations indicated in Figure 8-1 was measured. The acceptable range of ammonia-soluble silver in Acticoat™ (40-60%) is shown as horizontal lines on the figure.

Next, an experiment was performed examining the effect of time on both the total and ammonia soluble silver. This experiment was done in duplicate, unlike all the previous preliminary experiments. Nanocrystalline silver thin films were sputtered at 4% oxygen and 0.75A, for times of 10, 25, 50, and 80 minutes. The resulting total silver deposited is shown in Figure 8-24. As would be expected, with increasing sputtering time, the total silver deposited increased. Statistical results comparing different locations within a single sputtering time are shown in Table 8-1. With a 10 minute sputtering time, the only significant differences were that W1 and W7 locations had significantly lower silver than L16. However, with increasing sputtering time, differences in total silver deposition were amplified. With a 25 minute deposition time, the W1 location

had significantly less silver than all other locations except W7. W7 had significantly lower silver than L13. With a 50 minute sputter, the same pattern was observed, but W7 also had significantly lower total silver than all other locations except W1. At 80 minutes, there were no significant differences between locations, due to higher experimental error for those runs. Overall, the pattern of low variation in the L direction, but higher variation in the W direction, with lower total silver for W locations outside the race track, was confirmed. In comparing the effect of length of sputtering time at location W3, it was found that there were extremely significant differences between groups ($p=0.0006$), with post tests indicating that 10 minute sputter times resulted in significantly lower total silver than 50 ($p<0.01$) and 80 ($p<0.001$) minutes; 25 minute sputter times had significantly lower total silver than 50 ($p<0.05$) and 80 ($p<0.01$) minutes; and 50 minute sputter times had significantly lower total silver than 80 minutes ($p<0.05$). At location W4, there were very significant differences ($p=0.0023$) with time, with 10 minutes sputtering producing significantly lower total silver than 50 ($p<0.05$) and 80 ($p<0.01$) minutes; and 25 minutes sputtering producing significantly lower total silver than 80 minutes sputtering ($p<0.01$). A total silver correlation was performed using W3 data, and the slope was significantly different from zero ($p<0.0001$), with an equation of:

$$\text{Total Silver (mg/in}^2\text{)} = 0.1125 * \text{Sputtering Time (min)} - 0.05854 \quad (8-1)$$

with an r^2 value of 0.9999. Using the W4 data, the slope was significantly different from zero ($p=0.003$), and the equation fitting the data was:

$$\text{Total Silver (mg/in}^2\text{)} = 0.1091 * \text{Sputtering Time (min)} + 0.1326 \quad (8-2)$$

with an r^2 value of 0.9940.

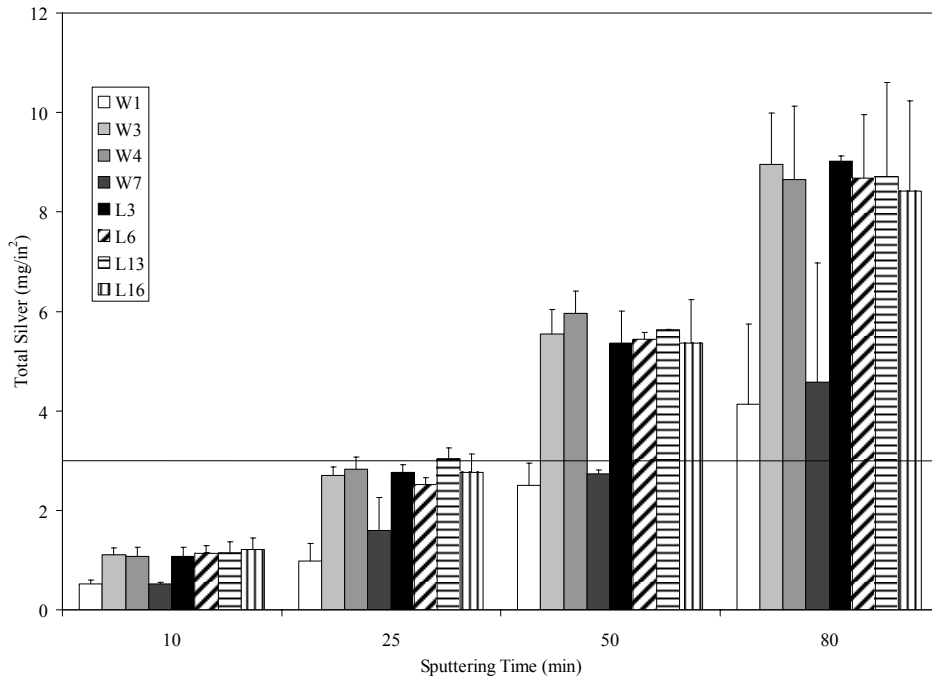


Figure 8-24. The effect of sputtering time on total silver deposited on samples sputtered at 0.75A and 4% oxygen. $n=2$ for each data point. The total silver deposited at the locations indicated in Figure 8-1 was measured via nitric acid digest. The total silver present in ActicoatTM (3 mg/in^2) is shown on the figure as a horizontal line.

Table 8-1. Effect of substrate location on the total silver deposited when sputtering at 4% O₂ and 0.75A for various lengths of time. Statistically significant results are in bold. n=2 for all data points.

Sputtering Time (min)	ANOVA p Value	Post Test Results
10	0.0098	p<0.05 W1 vs. L16 (L16 ↑) W7 vs. L16 (L16 ↑)
25	0.0026	p<0.05 W1 vs. W3 (W3 ↑) W1 vs. L6 (L6 ↑)
50	0.0004	p<0.01 W1 vs. W4 (W4 ↑) W1 vs. L3 (L3 ↑) W1 vs. L13 (L13 ↑) W1 vs. L16 (L16 ↑) W7 vs. L13 (L13 ↑)
80	0.0570	p<0.01 W1 vs. W3 (W3 ↑) W1 vs. W4 (W4 ↑) W1 vs. L3 (L3 ↑) W1 vs. L6 (L6 ↑) W1 vs. L13 (L13 ↑) W1 vs. L16 (L16 ↑) W3 vs. W7 (W3 ↑) W4 vs. W7 (W4 ↑) W7 vs. L3 (L3 ↑) W7 vs. L6 (L6 ↑) W7 vs. L13 (L13 ↑) W7 vs. L16 (L16 ↑)
		N/A

The ammonia soluble silver measured for nanocrystalline silver films sputtered at 4% oxygen and 0.75A for various lengths of time is shown in Figure 8-25. In this particular experiment, the variability was quite high, and so there were no significant differences between substrate locations ($p>0.05$) at any of the times tested. As well, there were no significant differences over time looking at locations W3 or W4 ($p>0.05$). Overall, the dressing composition did not change in increasing sputtering time, which is unlike the results observed by Sant *et al.*,

who observed a decrease in silver oxide with increasing film thickness[6], but the total silver deposited did increase linearly with increasing time, as anticipated.

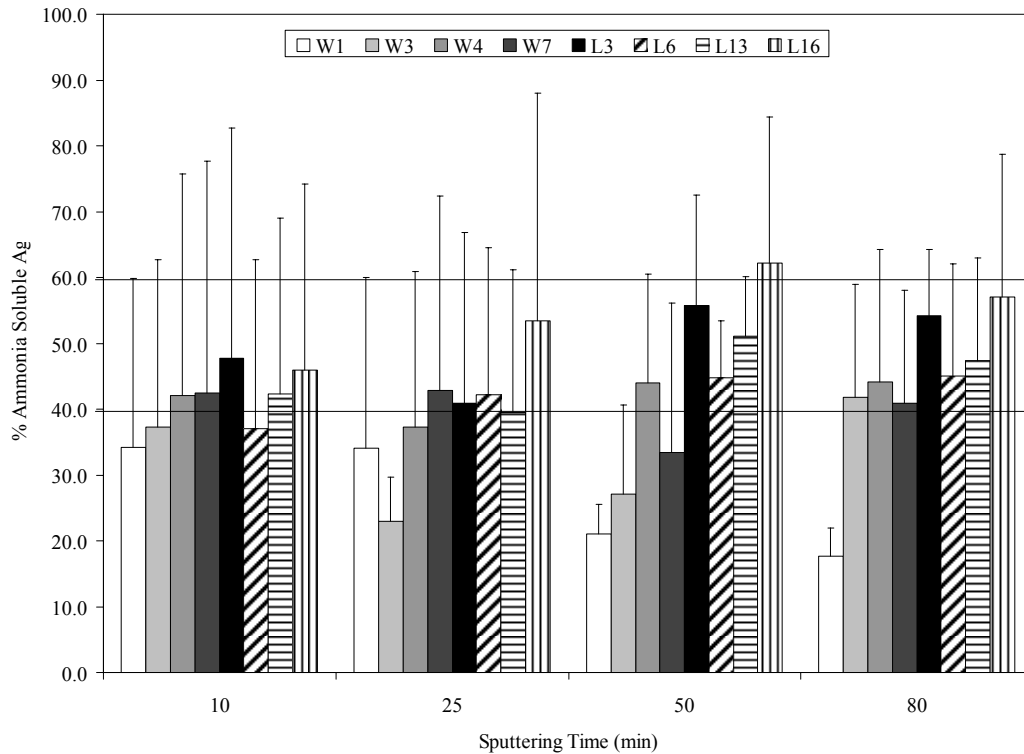


Figure 8-25. Effect of sputtering time on ammonia-soluble silver deposited on samples sputtered at 0.75A and 4% oxygen. n=2 for each data point. The ammonia-soluble silver deposited at the locations indicated in Figure 8-1 was measured. The acceptable range of ammonia-soluble silver in Acticoat™ (40-60%) is shown as horizontal lines on the figure.

The final experiment looking at total and ammonia soluble silver was an in-depth study to verify the relationships between oxygen, current, total silver and ammonia soluble silver, as well as the effect of the above on substrate location. Runs were performed in triplicate unless indicated, and sputtering was performed statically for 10 minutes at 4, 8, 10, or 12% oxygen, and currents of 0.75, 1 or 1.5A. The total silver generated at 0.75A for various concentrations of oxygen is shown in Figure 8-26. The effect of substrate sampling location was analyzed, and the results are shown in Table 8-2. At 4% oxygen, location W1 had

significantly lower total silver than all other substrate locations, and W7 had significantly lower total silver than the remaining locations. The only other significant difference was that W4 had significantly more silver than L3. At 8% oxygen, the same pattern was observed for W1 and W7, and the only other significant difference was that L13 had more silver than L16. At 10% oxygen, there was less variation with location, with W1 having significantly less total silver than W3 and L6, and W7 having significantly less total silver than L6. At 12% oxygen, W1 and W7 again had significantly lower total silver than all other substrate locations, but interestingly, W4 had higher total silver than the remaining substrate locations, including W3, despite the fact that the two locations are very close together. This suggests that with static sputtering, results can be highly location dependent.

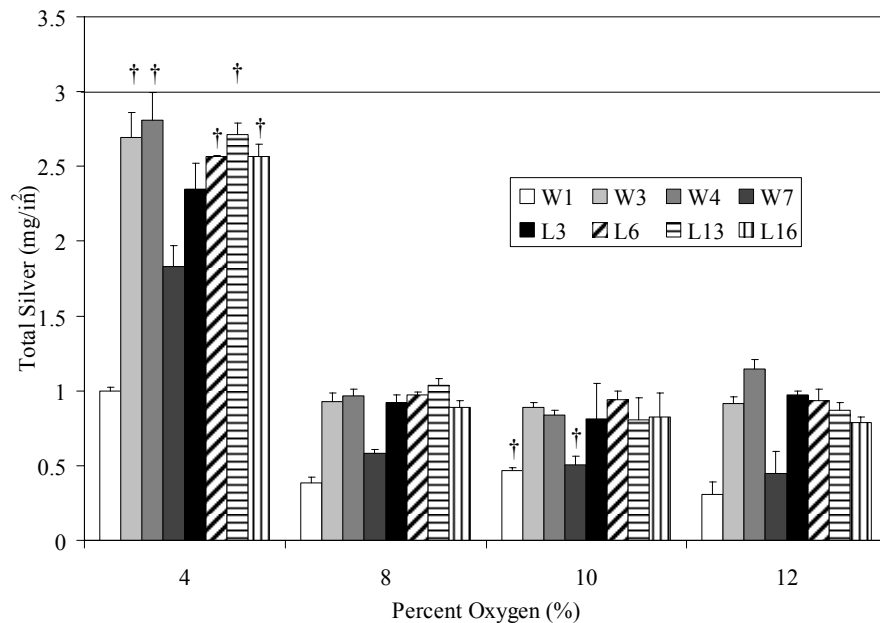


Figure 8-26. The effect of percent oxygen on total silver deposited on samples sputtered at 0.75A in a 10 minute static run. † indicates that n=2. For all other data points, n=3. The total silver deposited at the locations indicated in Figure 8-1 was measured via nitric acid digest. The total silver present in Acticoat™ (3 mg/in²) is shown on the figure as a horizontal line.

Table 8-2. Effect of substrate sample location on the total silver deposited when sputtering for 10 minutes at various currents and oxygen concentrations. Statistically significant results are in bold. n=3 for all data points, unless otherwise indicated on the corresponding figures (Figure 8-26, 8-28, and 8-30).

Current (A)	% O ₂	ANOVA p Value	Post Test Results
0.75	4	<0.0001	p<0.05 W4 vs. L3 (W4 ↑) p<0.01 W7 vs. L3 (W7 ↓) p<0.001 W1 vs. W3, W4, W7, L3, L6, L13, L16 (W1 ↓) W7 vs. W3, W4, L6, L13, L16 (W7 ↓)
0.75	8	<0.0001	p<0.05 L13 vs. L16 (L13 ↑) p<0.001 W1 vs. W3, W4, W7, L3, L6, L13, L16 (W1 ↓) W7 vs. W3, W4, L3, L6, L13, L16 (W7 ↓)
0.75	10	0.0097	p<0.05 W1 vs. W3, L6 (W1 ↓) W7 vs. L6 (W7 ↓)
0.75	12	<0.0001	p<0.05 W3 vs. W4 (W3 ↓) W4 vs. L6 (W4 ↑) p<0.01 W4 vs. L13 (W4 ↑) p<0.001 W1 vs. W3, W4, L3, L6, L13, L16 (W1 ↓) W4 vs. L16 (W4 ↑) W7 vs. W3, W4, L3, L6, L13, L16 (W7 ↓)
1	4	<0.0001	p<0.05 W7 vs. W4, L6 (W7 ↓) p<0.01 W7 vs. L16 (W7 ↓) p<0.001 W1 vs. W3, W4, W7, L3, L6, L13, L16 (W1 ↓)
1	8	<0.0001	p<0.01 W1 vs. L3, L13 (W1 ↓) W7 vs. W3, L3, L13 (W7 ↓) p<0.001 W1 vs. W3, W4, L6, L16 (W1 ↓) W7 vs. W4, L6, L16 (W7 ↓)
1	10	<0.0001	p<0.001 W1 vs. W3, W4, L3, L6, L13, L16 (W1 ↓) W7 vs. W3, W4, L3, L6, L13, L16 (W7 ↓)

1	12	<0.0001	p<0.05 W4 vs. L16 (W4 ↑) p<0.001 W1 vs. W3, W4, W7, L3, L6, L13, L16 (W1 ↓) W7 vs. W3, W4, L3, L6, L13, L16 (W7 ↓)
1.5	4	<0.0001	p<0.01 W7 vs. L3, L6 (W7 ↓) p<0.001 W1 vs. W3, W4, W7, L3, L6, L13, L16 (W1 ↓) W7 vs. W3, W4, L13, L16 (W7 ↓)
1.5	8	<0.0001	p<0.05 W7 vs. W3, L16 (W7 ↓) p<0.01 W7 vs. W4, L6, L13 (W7 ↓) p<0.001 W1 vs. W3, W4, W7, L3, L6, L13, L16 (W1 ↓)
1.5	10	<0.0001	p<0.05 W7 vs. W3, L6, L13, L16 (W7 ↓) p<0.01 W1 vs. W7 (W1 ↓) W7 vs. W4 (W7 ↓) p<0.001 W1 vs. W3, W4, L6, L13, L16 (W1 ↓) L3 vs. W3, W4, L6, L13, L16 (L3 ↓)
1.5	12	0.0074	p<0.05 W1 vs. L13, L16 (W1 ↓) W4 vs. W7 (W7 ↓) p<0.01 W1 vs. W4 (W1 ↓)
0.9 (30 min)	4	<0.0001	p<0.001 W1 vs. W3, W4, L3, L6, L13, L16 (W1 ↓) W7 vs. W3, W4, L3, L6, L13, L16 (W7 ↓)

Table 8-3 shows the statistical analysis of the effect of oxygen on the total silver deposited when the films were sputtered at 0.75A. Surprisingly, at 4% oxygen, the total silver deposited was significantly higher than the total silver deposited at higher concentrations of oxygen, where (from 8% up) the total silver was not significantly different with increasing oxygen. Only the run at 4% oxygen had close to the total silver required for Acticoat™. These results are not

in agreement with the various preliminary studies suggesting that changing the percent oxygen in the chamber did not change the resulting total silver deposited, suggesting that an error may have occurred during the total silver analysis of the 4% oxygen 0.75A runs of this experiment.

Table 8-3. Effect of oxygen concentration on the total silver deposited when sputtering for 10 minutes at various currents at substrate locations W3 and W4. Statistically significant results are in bold. n=3 for all data points, unless otherwise indicated on the corresponding figures (Figure 8-26, 8-28, and 8-30).

Current (A)	Substrate Location	ANOVA p Values	Post Test Results
0.75	W3	<0.0001	p<0.001 4% vs. 8%, 10%, 12% (4% ↑)
0.75	W4	<0.0001	p<0.05 10% vs. 12% (10% ↓)
1	W3	<0.0001	p<0.001 4% vs. 8%, 10%, 12% (4% ↑) p<0.05 10% vs. 12% (10% ↓)
1	W4	0.0009	p<0.001 4% vs. 8%, 10%, 12% (4% ↓) p<0.01 4% vs. 8%, 10% (4% ↓)
1.5	W3	<0.0001	p<0.001 4% vs. 12% (4% ↓)
1.5	W4	<0.0001	p<0.001 12% vs. 4%, 8%, 10% (12% ↓) p<0.001 12% vs. 4%, 8%, 10% (12% ↓)

The ammonia soluble silver measured for nanocrystalline silver thin films sputtered at 0.75A for 10 minutes at various oxygen percentages is shown in Figure 8-27. Table 8-4 shows statistical analyses of the effect of substrate location on the percent ammonia soluble silver for each oxygen concentration at 0.75A. At 4% oxygen, W1 had higher ammonia soluble silver than W3 and W4, and L16 also had higher ammonia soluble silver than W3. At 8% oxygen, W1,

W3 and W4 all had lower ammonia soluble silver than L3, while W1 and W3 had lower ammonia soluble silver than L16. At 10% oxygen, there were no significant differences in percent ammonia soluble silver with substrate location, while at 12% oxygen, W1 had higher ammonia soluble silver than W3, W4, W7, and L6. Overall, although there was some variation in ammonia soluble silver with location, there were no clear trends.

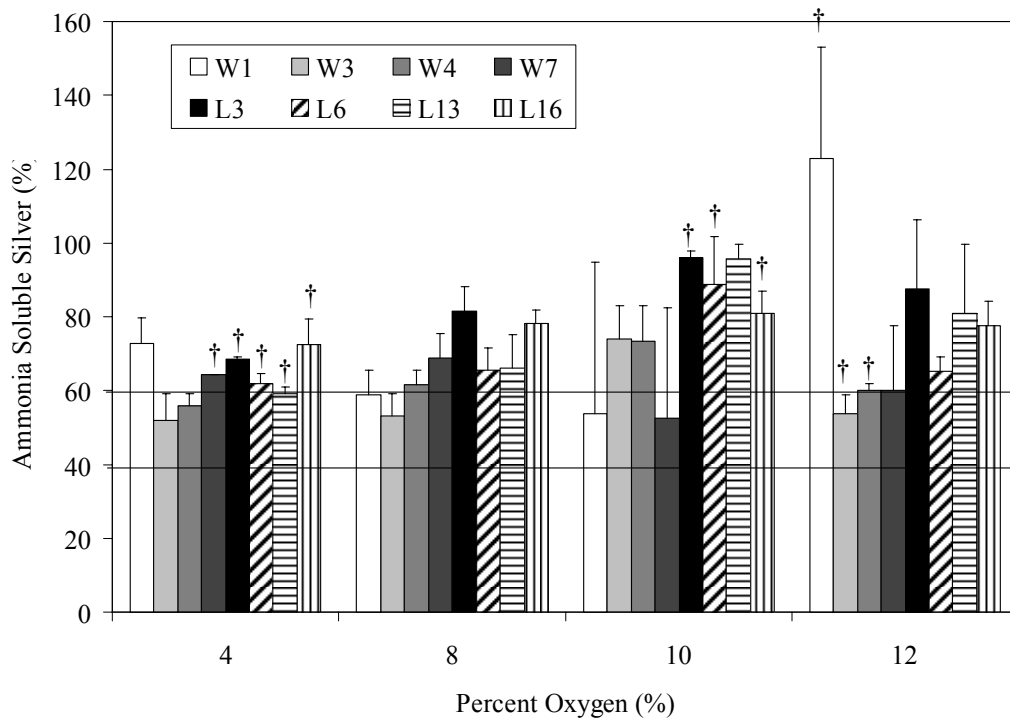


Figure 8-27. Effect of percent oxygen on ammonia-soluble silver deposited on samples sputtered at 0.75A in a 10 minute static run. † indicates that n=2. For all other data points, n=3. The ammonia-soluble silver deposited at the locations indicated in Figure 8-1 was measured. The acceptable range of ammonia-soluble silver in Acticoat™ (40-60%) is shown as horizontal lines on the figure.

Table 8-4. Effect of substrate sample location on the percent ammonia soluble silver deposited when sputtering for 10 minutes at various currents and oxygen concentrations. Statistically significant results are in bold. n=3 for all data points, unless otherwise indicated on the corresponding figures (Figure 8-27, 8-29, and 8-31).

Current (A)	% O ₂	ANOVA p Value	Post Test Results
0.75	4	0.0046	p<0.05 W1 vs. W4 (W1 ↑) W3 vs. L16 (W3 ↓)
0.75	8	0.0007	p<0.01 W1 vs. W3 (W1 ↑) p<0.05 W1 vs. L16 (W1 ↓) W4 vs. L3 (W4 ↓) p<0.01 W1 vs. L3 (W1 ↓) W3 vs. L16 (W3 ↓) p<0.001 W3 vs. L3 (W3 ↓)
0.75	10	0.1743	N/A
0.75	12	0.0100	p<0.05 W1 vs. W3, W7, and L6 (W1 ↑) p<0.01 W1 vs. W4 (W1 ↑)
1	4	0.0089	p<0.05 W1 vs. W3, W4, L13, and L16 (W1 ↑) p<0.01 W1 vs. L6 (W1 ↑)
1	8	<0.0001	p<0.05 L3 vs. W1, W3, and L6 (L3 ↑) W7 vs. L13 and L16 (W7 ↓) p<0.01 W7 vs. W1 and W4 (W7 ↓) L3 vs. W4, L13, and L16 (L3 ↑) p<0.001 W7 vs. W3, L3, and L6 (W7 ↓)
1	10	<0.0001	p<0.01 L3 vs. W4, L6 (L3 ↑) p<0.001 W1 vs. W3, W4, W7, L3, L6, L13, L16 (W1 ↓) W7 vs. W3, W4, L3, L6, L13, L16 (W7 ↑) W3 vs. L13, L16 (W3 ↑) W4 vs. L13, L16 (W4 ↑) L3 vs. W3, L13, L16 (L3 ↑) L6 vs. L13, L16 (L6 ↑)

1	12	0.3081	N/A
1.5	4	0.0119	p<0.05 L13 vs. W1, W4 (L13 ↑)
1.5	8	0.0087	p<0.05 W3 vs. W7, L3, L6 (W3 ↑)
1.5	10	0.0178	p<0.05 L3 vs. W3, W4 (L3↑)
1.5	12	0.2978	N/A
0.9 (30 min)	4	0.5800	N/A

At 0.75A, the ammonia soluble silver appeared to increase with increasing percent oxygen up to 10% oxygen, but at 12% oxygen, it dropped again. Table 8-5 indicates that the total ammonia soluble silver at 10% oxygen was significantly higher than that at 4% and 8% oxygen. The runs at 4% oxygen produced ammonia soluble silver near the top of the acceptable range for Acticoat™, while the other runs were over-range. This suggests that the ammonia soluble silver increases to 100% (i.e. 100% silver oxide) with increasing oxygen concentration, but after 100% silver oxide is reached, other factors become important. It is possible that at very high oxygen concentrations, an oxygen plasma is formed in the machine, resulting in different chemistry of the dressing – different silver species may be formed, and, while at such a high oxygen concentration these species would likely still be oxides, they might not be ammonia soluble oxides. Another possibility is that these species might be very reactive, and post-sputtering they might be reduced to metallic silver, resulting in the lower ammonia soluble percentage at oxygen concentrations above 10%.

Table 8-5. Effect of oxygen concentration on the percent ammonia soluble silver deposited when sputtering for 10 minutes at various currents at substrate locations W3 and W4. Statistically significant results are in bold. n=3 for all data points, unless otherwise indicated on the corresponding figures (Figure 8-27, 29, and 31).

Current (A)	Substrate Location	ANOVA p Values	Post Test Results
0.75	W3	0.0254	p<0.05 10% vs. 4%, 8% (10% ↑)
0.75	W4	0.0229	p<0.05 4% vs. 10% (10% ↑) 10% vs. 12% (10% ↑)
1	W3	<0.0001	p<0.01 4% vs. 8% (4% ↓) 8% vs. 10% (8% ↓) p<0.001 4% vs. 10% (4% ↓) 4% vs. 12% (10% ↓)
1	W4	0.0020	p<0.05 8% vs. 10% (8% ↓) p<0.01 4% vs. 10% (4% ↓)
1.5	W3	0.0066	p<0.05 4% vs. 8%, 10%, 12% (4% ↓)
1.5	W4	0.0027	p<0.05 4% vs. 8% (4% ↓) 10% vs. 12% (10% ↑) p<0.01 4% vs. 10% (4% ↓)

Figure 8-28 shows the impact of percent oxygen on the total silver deposited when nanocrystalline silver thin films were generated for 10 minute static runs at 1A. The effect of substrate location on the total silver deposited under these conditions is analyzed in Table 8-2. At 4% oxygen, W1 had significantly lower silver deposition than all other substrate locations, and W7 also had lower total silver than W4, L6, and L16. At 8% and 10% oxygen, W1 and W7 were not significantly different from one another, but were significantly

lower than all other substrate locations. At 12% oxygen, W1 had significantly lower silver deposition than all other substrate locations, and W7 had significantly lower deposition than the remaining locations. Interestingly, W4 had significantly higher deposition than L16. This was unexpected, as the power supply enters at L16, so if there was uneven current distribution leading to lateral (L direction) variation in power and therefore silver deposition, it would be anticipated that there would be more energy at L16, leading to higher silver deposition there.

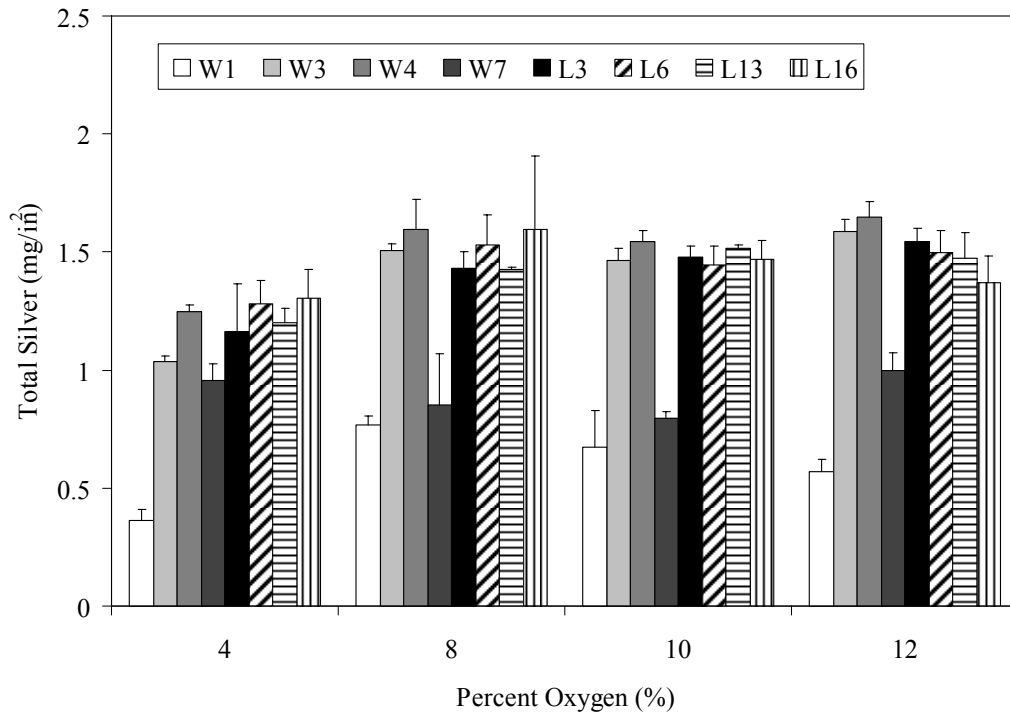


Figure 8-28. The effect of percent oxygen on total silver deposited on samples sputtered at 1A in a 10 minute static run. For all data points, n=3. The total silver deposited at the locations indicated in Figure 8-1 was measured via nitric acid digest.

As was typically the case with the preliminary testing, and unlike the 0.75A run, the total silver deposited did not show a clear pattern of variation with the oxygen percentage in the chamber during sputtering (Figure 8-28), with sputtering at 4% appearing to result in slightly lower silver deposition – the

opposite of what was observed at 0.75A. Table 8-3 shows the statistical analysis of the effect of oxygen on the total silver deposited for films sputtered at 1A at locations W3 and W4. At both locations, there was less total silver deposited at 4% oxygen than at higher oxygen percentages. As well, at W3, there was less total silver deposited at 10% oxygen than 12% oxygen.

Figure 8-29 shows the effect of different oxygen concentrations at 1A on the percent ammonia soluble silver. The statistical analyses of substrate location effect are shown in Table 8-4. At 4% oxygen, W1 had significantly lower ammonia soluble silver than all other substrate locations except W7 and L3. At 8% oxygen, W7 had significantly lower ammonia soluble silver than all other locations, while L3 had significantly higher ammonia soluble silver than all other locations. At 10% oxygen, W1 had significantly lower ammonia soluble silver than all other locations. Surprisingly, W7 had significantly higher ammonia soluble silver than all other locations, but this appears to have been an experimental error. It is possible to get an ammonia soluble silver greater than 100%, due to the fact that samples from different runs must be used to measure the total silver and the ammonia soluble silver, but the ammonia soluble silver is presented as the percentage of the total silver. Slight run-to-run variations or slight variations in the cutting procedure can thus lead to a dressing made of 100% silver oxide being measured to have more than 100% ammonia soluble silver. However, the measurement made at W7 is well over any error that can be accounted for in that way. W3, W4, L3, and L6 all had significantly higher ammonia soluble silver than L13 and L16. L3 also had higher ammonia soluble

silver than W3, W4, and W6. These variations may be due to the fact that the oxygen is fed into the chamber near L3, resulting in slightly higher oxygen-silver interactions and therefore higher silver oxide (ammonia soluble silver) deposition towards that end of the chamber. At 12% oxygen, there were no significant variations in ammonia soluble silver with location. Similar to the effect seen with increasing oxygen at 0.75A, the ammonia soluble silver increased with increasing oxygen at 1A up to 10%, but then dropped again at 12%. At 4% oxygen, the ammonia soluble silver was below the acceptable range for ActicoatTM, and was significantly lower than the ammonia soluble silver present in all higher oxygen percentages at location W3 (Table 8-5), which were all at the high end or over the range acceptable for ActicoatTM. At location W3 with 8% oxygen, the ammonia soluble silver was significantly lower than that at 10% oxygen, but not at 12% oxygen. At W4, both 4% and 8% oxygen resulted in significantly lower ammonia soluble silver than 10% oxygen, but not 12%. This confirms that at very high oxygen levels, the chemistry of sputtering and/or post-sputter reactions changes.

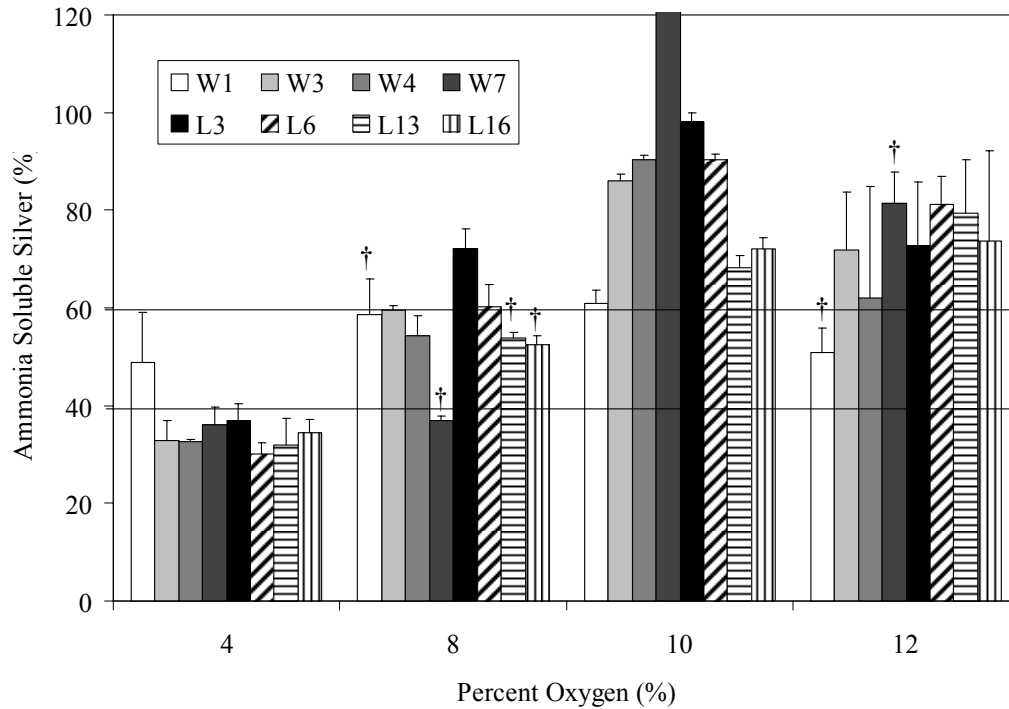


Figure 8-29. Effect of percent oxygen on ammonia-soluble silver deposited on samples sputtered at 0.75A in a 10 minute static run. † indicates that n=2. For all other data points, n=3. The ammonia-soluble silver deposited at the locations indicated in Figure 8-1 was measured. The acceptable range of ammonia-soluble silver in Acticoat™ (40-60%) is shown as horizontal lines on the figure. One data point is cut off – 10% O₂, W7 – so that the other values can be read clearly. The value for this data point is: 190.56±0.89, n=2.

Figure 8-30 shows the effect of percent oxygen on total silver deposited when a current of 1.5A was used for a 10 minute static sputter. The effect of substrate location on the total silver deposited appeared more pronounced at this higher current. Table 8-2 indicates that, similar to other currents, at 4%, 8%, and 10% oxygen, W1 had significantly lower total silver deposited relative to all other substrate locations. W7 had significantly lower total silver as well. Interestingly, at 10% oxygen, the silver deposited at L3 was also significantly lower than all substrate locations except W1 and W7. This appears to be an anomaly rather than

a trend. At 12% oxygen, there were fewer significant differences, with W1 having significantly lower total silver than W4, L13, and L16; and W7 having significantly less total silver than W4. Overall, the effect of substrate location on total silver deposition appears to be primarily related to the location of the racetrack created by the magnetron. Substrate locations outside the racetrack receive much less total silver per unit time than locations inside the racetrack, which means that with increasing sputtering times and increasing energy levels in the system (increasing sputtering current), these differences become more pronounced. There may also be a slight lateral effect (L) due to uneven power distribution, since the electricity enters the magnetron near L16, but this has not been clearly confirmed.

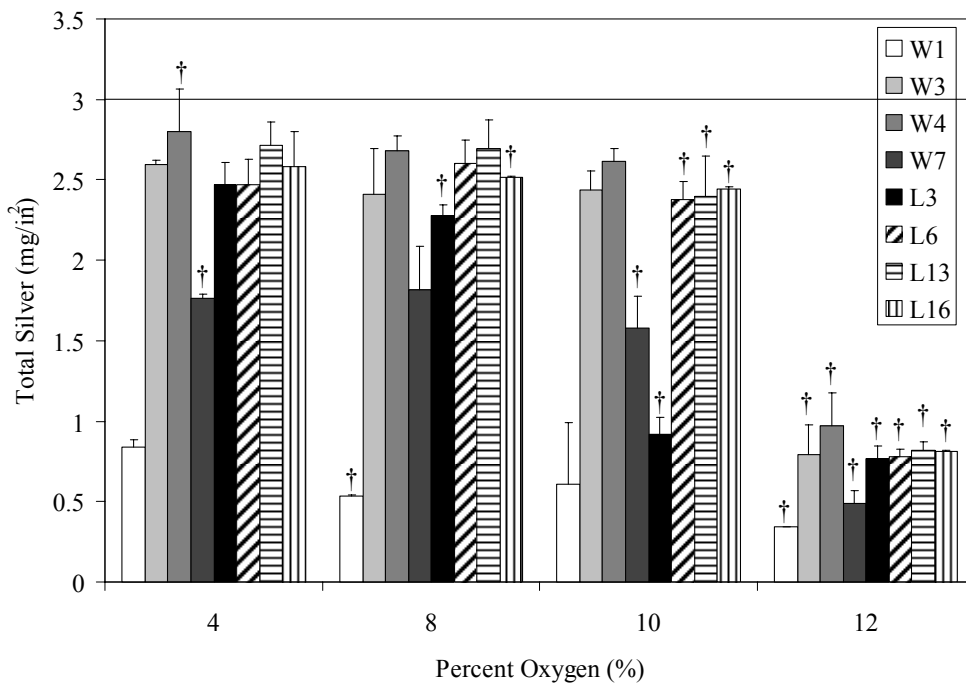


Figure 8-30. The effect of percent oxygen on total silver deposited on samples sputtered at 1.5A in a 10 minute static run. † indicates that n=2. For all other data points, n=3. The total silver deposited at the locations indicated in Figure 8-1 was measured via nitric acid digest. The total silver present in Acticoat™ (3 mg/in²) is shown on the figure as a horizontal line.

In comparing the total silver deposited at different oxygen concentrations and 1.5A (Figure 8-30), the total silver remained about the same up to 10% oxygen, but the total silver deposited at 12% oxygen was much lower. As sputtering at 1.5A current and 12% oxygen was not performed in any of the preliminary studies, it is not known whether these results are due to an experimental error, or if a combination of high current and high oxygen content, with possible generation of an oxygen plasma, leads to less energy being available to dislodge silver from the target, leading to a lower deposition rate despite the higher current. Table 8-3 indicates that at both W3 and W4, samples sputtered at 12% oxygen had significantly lower total silver than the other three oxygen concentrations used, which were not significantly different from one another.

Overall, comparing all twelve combinations of pressure and percent oxygen, there were no consistent trends between the oxygen in the chamber and the total silver deposited, suggesting that the quantity of oxygen in the chamber does not affect the total silver deposited, at least up to the point where there becomes sufficient oxygen in the chamber for an oxygen plasma to form, or for the system chemistry to change in another way.

The effect of oxygen on ammonia soluble silver in 10 minute static sputtering runs performed at 1.5A is shown in Figure 8-31. Table 8-4 examines the effect of substrate location on the percentage ammonia soluble silver. At 1.5A, there were very few significant differences in ammonia soluble silver with substrate location. At 4% oxygen, L13 had significantly higher ammonia soluble silver than W1 and W4; at 8% oxygen, W3 had significantly higher ammonia

soluble silver than W7, L3, and L6; at 10% oxygen, W3 and W4 had significantly less ammonia soluble silver than L3, but the level measured for L3 was likely an experimental error; and at 12% oxygen, there were no significant differences between substrate locations. Overall, for all conditions examined, there did not appear to be a clear trend between substrate location and ammonia soluble silver. It was predicted that there might be higher ammonia soluble silver deposited near the gas feeds, or ammonia soluble silver patterns related to gas dispersion patterns in the chamber, but this does not appear to have been the case.

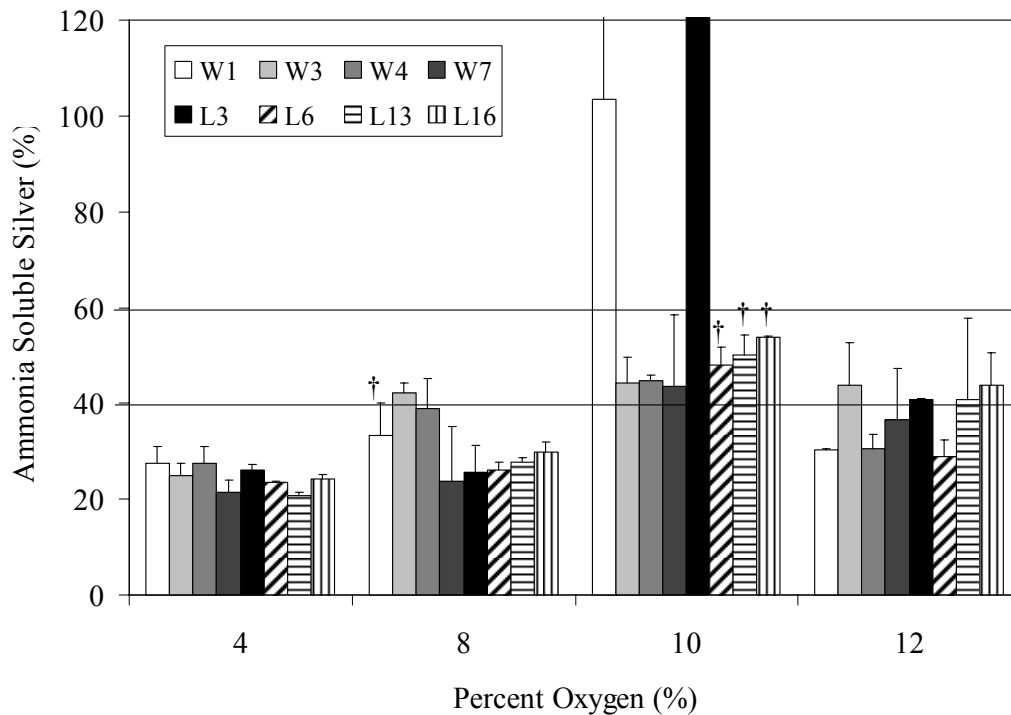


Figure 8-31. Effect of percent oxygen on ammonia-soluble silver deposited on samples sputtered at 1.5A in a 10 minute static run. † indicates that n=2. For all other data points, n=3. The ammonia-soluble silver deposited at the locations indicated in Figure 8-1 was measured. The acceptable range of ammonia-soluble silver in Acticoat™ (40-60%) is shown as horizontal lines on the figure. Two data points at 10% oxygen are cut off in order to better see the remaining data points. The values for these data points are: W1 – 103.41±66.99 %, n=2; and L3 – 125.41±4.05 %, n=2.

As with lower currents examined, the ammonia soluble silver increased with increasing oxygen concentration at 1.5A for concentrations up to 10% oxygen, which was the only concentration which produced ammonia soluble silver levels safely within the range allowable for Acticoat™. At 12% oxygen, the ammonia soluble silver again dropped. Table 8-5 indicates that at W3, sputtering at 4% oxygen led to significantly lower ammonia soluble silver than all higher concentrations of oxygen, while at W4, 4% oxygen led to significantly lower ammonia soluble silver than 8% or 10% oxygen, and 10% oxygen also led to significantly higher ammonia soluble silver than that produced at 12% oxygen. This suggests that at high currents, it is not possible to produce 100% silver oxide dressings of the type produced at 1A and 10% oxygen, since the oxide content peaks at a lower level and then begins to drop. Overall, with all currents used, this confirmed that above a critical oxygen level in the chamber, which appears to be 10%, the physical vapor deposition chemistry changes, possibly due to the formation of an oxygen plasma, resulting in a change in the species deposited towards less ammonia soluble species.

The effect of varying current in the preceding tests on the total silver deposited is shown in Table 8-6. At 4% oxygen, using a current of 0.75A led to a higher total silver deposition at both W3 and W4 compared to 1A, which was also significantly lower than the total silver deposited at 1.5A. As discussed earlier, the higher total silver observed at 0.75A appeared to be atypical of the results obtained using the in-house sputtering machine. At 8% and 10% oxygen, for both W3 and W4, sputtering at 0.75A led to significantly less total silver than

sputtering at 1 or 1.5A, showing a clear trend of increasing total silver with increasing current. However at 12% oxygen, although sputtering at 0.75A still led to less total silver deposition than sputtering at 1 or 1.5A, the total silver deposited at 1A was significantly higher than that at 1.5A. This, as has been suggested above, may be related to the introduction of an oxygen plasma or other form of unusual chemistry at very high chamber oxygen concentrations.

Table 8-6. The effect of current on the total silver deposited when sputtering for 10 minutes at various oxygen concentrations at substrate locations W3 and W4. Statistically significant results are in bold. n=3 for all data points, unless otherwise indicated on the corresponding figures (Figure 8-26, 28, and 30).

% O ₂	Substrate Location	ANOVA p Value	Post Test Results
4	W3	<0.0001	p<0.001 0.75A vs. 1A (0.75A ↑) 1A vs. 1.5A (1A ↓)
4	W4	0.0006	p<0.01 0.75A vs. 1A (0.75A ↑) 1A vs. 1.5A (1A ↓)
8	W3	0.0001	p<0.05 0.75A vs. 1A (0.75A ↓) p<0.01 1A vs. 1.5A (1A ↓) p<0.001 0.75A vs. 1.5A (0.75A ↓)
8	W4	<0.0001	p<0.001 0.75A vs. 1A and 1.5A (0.75A ↓) 1A vs. 1.5A (1A ↓)
10	W3	<0.0001	p<0.001 0.75A vs. 1A and 1.5A (0.75A ↓) 1A vs. 1.5A (1A ↓)
10	W4	<0.0001	p<0.001 0.75A vs. 1A and 1.5A (0.75A ↓) 1A vs. 1.5A (1A ↓)
12	W3	0.0003	p<0.001 0.75A vs. 1A (0.75A ↓) 1A vs. 1.5A (1A ↑)
12	W4	0.0017	p<0.01 0.75A vs. 1A (0.75A ↓) 1A vs. 1.5A (1A ↑)

The effect of current on the ammonia soluble silver in these experiments is analyzed in Table 8-7. When sputtering at 4% oxygen, there was significantly higher ammonia soluble silver deposited at both locations W3 and W4 when 0.75A was used rather than 1 or 1.5A. At 8% oxygen, both currents of 0.75A and 1A resulted in more ammonia soluble silver being deposited than when 1.5A was used, but they were not significantly different from one another. The same trend was observed at 10% oxygen (location W3), but at location W4, sputtering at 0.75A also resulted in significantly higher ammonia soluble silver than sputtering at 1A. At 12% oxygen, the trends were less distinct, with no significant differences present at W4, and only 1A having significantly higher ammonia soluble silver relative to 1.5A at W3. Overall, it appears that with increasing current, i.e. increasing energy in the system, there is a decrease in ammonia soluble silver. This may indicate that when there is higher energy in the system, a reduction of silver oxide to metallic silver occurs after the silver is deposited on the substrate, or that fewer silver-oxygen collisions occur as the silver travels to the substrate. The former seems more likely from a thermodynamic perspective.

Table 8-7. The effect of current on the ammonia soluble silver deposited when sputtering for 10 minutes at various oxygen concentrations at substrate locations W3 and W4. Statistically significant results are in bold. n=3 for all data points, unless otherwise indicated on the corresponding figures (Figure 8-27, 29, and 31).

% O ₂	Substrate Location	ANOVA p Value	Post Test Results
4	W3	0.0015	p<0.01 0.75A vs. 1A, 1.5A (0.75A ↑)
4	W4	<0.0001	p<0.001 0.75A vs. 1A, 1.5A (0.75A ↑)
8	W3	0.0041	p<0.05 0.75A vs. 1.5A (0.75A ↑)
8	W4	0.0036	p<0.01 1A vs. 1.5A (1A ↑) p<0.05 1A vs. 1.5A (1A ↑)
10	W3	0.0004	p<0.01 0.75A vs. 1.5A (0.75A ↑)
10	W4	0.0002	p<0.001 1A vs. 1.5A (1A ↑) p<0.05 0.75A vs. 1A (1A ↑)
12	W3	0.0421	p<0.01 0.75A vs. 1.5A (0.75A ↑) p<0.001 1A vs. 1.5A (1A ↑)
12	W4	0.1015	p<0.05 1A vs. 1.5A (1A ↑) N/A

Based on the results of the preliminary studies and the final study looking at total silver deposition and ammonia soluble silver deposition, conditions were selected for which silver films could be generated in-house to best mimic commercially produced nanocrystalline silver. It was determined that the total silver in the dressings could be increased by increasing the current (at the expense of ammonia soluble silver), and the total ammonia soluble silver could be increased with increasing oxygen content, up to the point at which an oxygen

plasma might be generated. However, it did not appear possible to create dressings with sufficient total silver and ammonia soluble silver by simply increasing both the oxygen and the current. Above a certain current (1A), sufficient ammonia soluble silver could not be obtained by adding more oxygen, as the chemistry of the system changed when sputtering at greater than 10% oxygen (see Figure 8-31) and this change in chemistry occurred before a sufficient total silver could be obtained via increasing current (see Figure 8-30). Therefore, it was determined that increasing the sputtering time would be a better way to produce an appropriate total silver content. An oxygen percentage of 4% was selected, as 8 and 10% oxygen resulted in too much ammonia soluble silver at low currents, while 0 and 2% did not produce enough, and based on the results of Figure 8-24, a 30 minute sputtering time was selected to generate just over 3 mg/in² total silver. In order to produce an ammonia soluble silver percentage in the correct range, according to Figures 8-27 and 8-29, the current needed to be between 0.75 and 1A. Therefore a current of 0.9A was selected. Figure 8-32 shows the total silver deposited at various locations when samples were sputtered for 30 minutes at 0.9A and 4% oxygen. The total silver at all locations, except W1 and W7, was just over 3 mg/in², as desired. Table 8-2 indicates that the only significant differences with location were that W1 and W7 had significantly less total silver deposited than all other locations. Figure 8-33 shows the ammonia soluble silver generated under these conditions. All target locations, except W3 and W4, were safely within the range required for ActicoatTM, and Table 8-4 indicates that there were no significant differences in percent ammonia soluble

silver between substrate locations. Thus, the conditions selected did generate thin films with the same total silver and ammonia soluble silver as commercial nanocrystalline silver dressings.

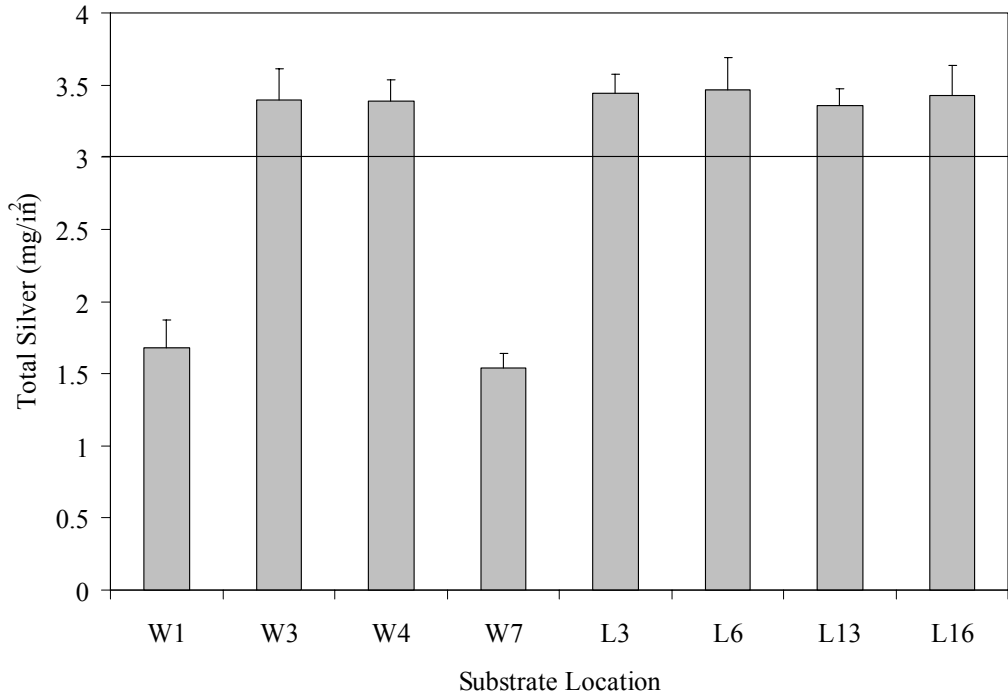


Figure 8-32. Total silver deposited on samples sputtered at 0.9A and 4% O₂ in a 30 minute static run. For all data points, n=3. The total silver deposited at the locations indicated in Figure 8-1 was measured via nitric acid digest. The total silver present in Acticoat™ (3 mg/in²) is shown on the figure as a horizontal line. These conditions were anticipated to generate a film similar to that present in Acticoat™.

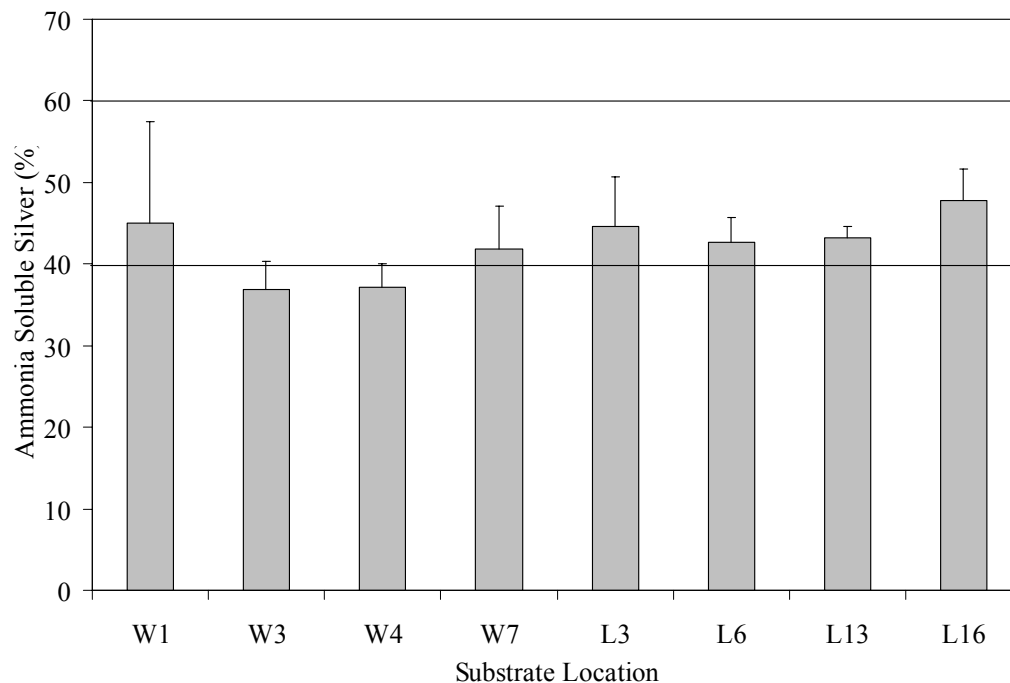


Figure 8-33. Ammonia-soluble silver deposited on samples sputtered at 0.9A and 4% O₂ in a 30 minute static run. For all data points, n=3. The ammonia-soluble silver deposited at the locations indicated in Figure 8-1 was measured. The acceptable range of ammonia-soluble silver in Acticoat™ (40-60%) is shown as horizontal lines on the figure. These conditions were anticipated to generate a film similar to that present in Acticoat™.

XRD

X-ray diffraction was performed to determine the crystallite sizes present in dressings generated during the final study described under the Total and Ammonia Soluble Silver section, where films were sputtered statically for 10 minutes at 4, 8, 10, or 12% oxygen, with currents of 0.75, 1, or 1.5A, as well as under the conditions selected to mimic commercial nanocrystalline silver dressings (0.9A, 4% O₂, 30 min). The sites analyzed were W3 and W4. In addition, relative quantities of silver oxide to metallic silver were determined using the method shown in Figure 8-34, which contains a sample footprint generated from a nanocrystalline silver thin film generated in-house. For

comparison, an XRD footprint of Acticoat™ is shown in Figure 8-35, which has a ratio of about 0.5. A summary of the XRD results is shown in Table 8-7. At 0.75A and various oxygen concentrations, the crystallite sizes were all between 7 and 13 nm, and there was no apparent trend between crystallite size and either the oxygen concentration or the current used. With increasing oxygen concentration, the amount of silver oxide increased, showing the same trend seen with the percent ammonia soluble silver measured in the previous section. At 10 and 12% oxygen, no metallic silver was detected. At 1A, metallic silver could be detected at all concentrations, confirming that with increasing current, less silver oxide/ammonia soluble silver is produced. Again, the silver oxide content increased with increasing current. The crystallite sizes ranged from 6 to 15 nm, and there was a trend towards increasing Ag₂O(111) size, but decreasing Ag(111)+Ag₂O(200) size, with increasing oxygen content. This suggests that with higher oxygen concentrations in the system, larger silver oxide crystallites were formed, and only small crystallites remained metallic. This may partially explain Sant *et al.*'s observation of larger crystallite sizes at higher oxygen contents[6]. At 1.5A, crystallite sizes ranged from 6 to 19 nm, indicating that, overall, larger crystallites could be formed at higher currents, which again concurred with Sant *et al.*[6] This result was anticipated, as more energy in the system might provide enough energy for atoms to move to lower energy locations after deposition on the substrate, and thus allow for crystal growth at the substrate. Interestingly, the ratio of silver oxide to metallic silver increased with oxygen concentration up to 10%, but then decreased at 12%. Similarly, the

Ag(111)+Ag₂O(200) size decreased with increasing oxygen up to 10%, but increased by 12%, and the Ag₂O(111) size decreased at 12% oxygen. These results all correlate with the drop in ammonia soluble silver observed when 12% oxygen was used. Interestingly, the drop in ammonia soluble silver was observed at all three currents, while the drop in silver oxide was only observed at 1.5A via XRD. This suggests that the drop in ammonia soluble silver is due to post-sputtering reactions, such as a photoreduction of the silver, as the XRD analysis was performed prior to the ammonia soluble silver analyses, and therefore the dressings spent more time in storage and had more time to react before the ammonia soluble silver analyses. This may mean that the dressings were the most unstable and reactive when sputtered at the highest current in combination with very high oxygen content, and confirms that the dressing chemistry changed when the oxygen concentration was increased over 10%, since this post-sputtering reaction, resulting in reduction of the silver, only occurred at 12% oxygen.

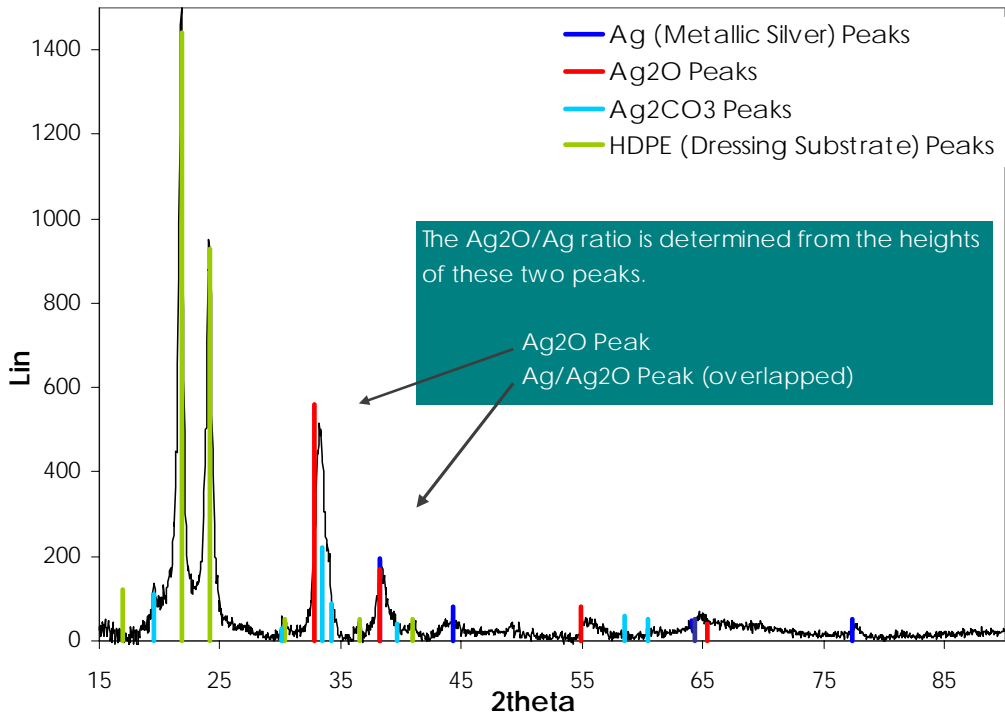


Figure 8-34. Example of an XRD footprint for a nanocrystalline silver thin film generated in-house. The peaks used to calculate the ratio of Ag₂O/Ag in the film are identified.

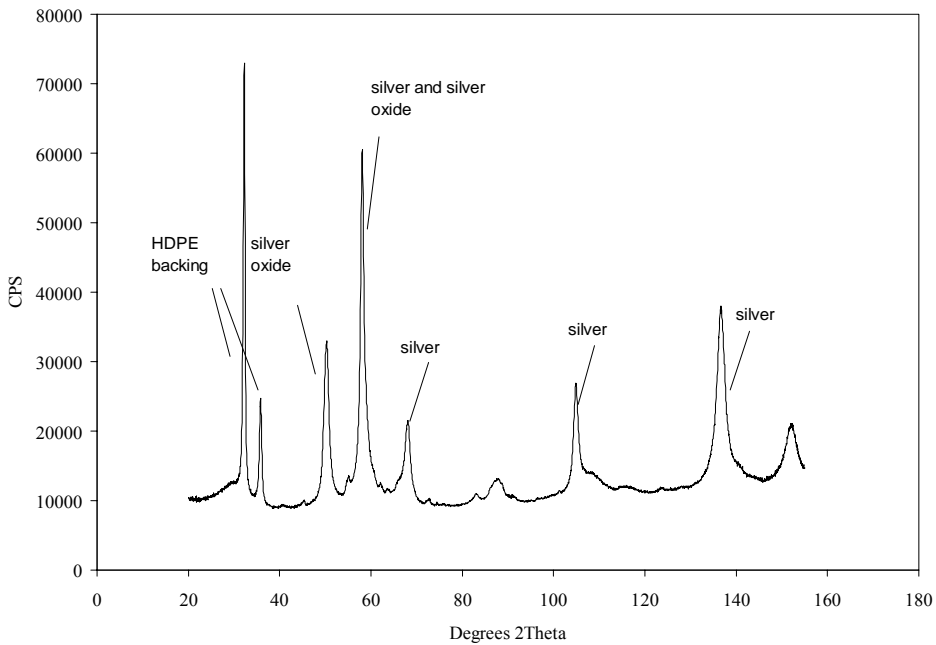


Figure 8-35. An XRD footprint for Acticoat™. Signature peaks are identified.

Table 8-7. Results of XRD analysis of nanocrystalline silver thin films generated under a variety of sputtering conditions. All samples were sputtered for 10 minutes statically. ND=not detected.

Sample	Ag ₂ O (111)			Ag (111) + Ag ₂ O (200)			Ag (200)			Ag ₂ O/Ag
	2θ	FWHM	Size (nm)	2θ	FWHM	Size (nm)	2θ	FWHM	(nm)	
0.75A 4% O ₂ , W3	33.24	0.79	12	38.35	0.91	11	44.13	1.42	7	2.34
0.75A 4% O ₂ , W4	33.28	0.84	11	38.31	1.02	9	44.10	1.34	7	2.69
0.75A 8% O ₂ , W3	33.32	0.85	11	38.30	1.00	10	ND	ND	ND	4.81
0.75A 8% O ₂ , W4	33.38	0.82	12	33.37	1.04	9	ND	ND	ND	5.03
0.75A 10% O ₂ , W3	33.20	0.82	12	ND	ND	ND	ND	ND	ND	All Ag ₂ O
0.75A 10% O ₂ , W4	33.18	0.75	13	ND	ND	ND	ND	ND	ND	All Ag ₂ O
0.75A 12% O ₂ , W3	33.02	0.85	11	ND	ND	ND	ND	ND	ND	All Ag ₂ O
0.75A 12% O ₂ , W4	32.98	0.81	12	ND	ND	ND	ND	ND	ND	All Ag ₂ O
1A 4% O ₂ , W3	33.48	1.13	8	38.43	0.67	15	44.26	1.48	6	0.462
1A 4% O ₂ , W4	33.31	0.86	11	38.40	0.72	14	44.28	1.51	6	0.303
1A 8% O ₂ , W3	33.49	1.00	9	38.40	1.13	8	44.18	1.07	9	2.27
1A 8% O ₂ , W4	33.50	1.03	9	38.44	0.90	11	44.32	1.15	8	2.32
1A 10% O ₂ , W3	33.36	0.81	12	38.42	1.14	8	ND	ND	ND	5.10
1A 10% O ₂ , W4	33.38	0.85	11	38.42	1.16	8	ND	ND	ND	5.08
1A 12% O ₂ , W3	33.31	0.71	14	38.42	1.13	8	ND	ND	ND	10.9
1A 12% O ₂ , W4	33.32	0.72	13	38.35	1.08	9	ND	ND	ND	13.5
1.5A 4% O ₂ , W3	33.31	0.86	11	38.41	0.58	17	44.37	1.47	6	0.252
1.5A 4% O ₂ , W4	33.32	0.83	12	38.40	0.55	19	44.34	1.26	8	0.269
1.5A 8% O ₂ , W3	33.29	0.90	11	38.39	0.71	14	44.28	1.55	6	0.686
1.5A 8% O ₂ , W4	33.24	0.95	10	38.35	0.74	13	44.26	1.42	7	0.569
1.5A 10% O ₂ , W3	33.28	0.89	11	38.35	0.82	12	44.22	1.51	6	1.07
1.5A 10% O ₂ , W4	33.26	0.88	11	38.37	0.81	12	44.26	1.60	6	1.15
1.5A 12% O ₂ , W3	33.49	1.04	9	38.36	0.69	15	44.30	1.28	7	0.740
1.5A 12% O ₂ , W4	33.47	1.03	9	38.37	0.71	14	44.25	1.21	8	0.719

X-ray diffraction was performed on samples generated at 0.9A, 4% oxygen for 30 minutes, which were selected to mimic ActicoatTM. The W3 sample had an Ag₂O(111) crystallite size of 12 nm ($2\theta=33.08$, FWHM=0.82), an Ag(111)+Ag₂O(200) crystallite size of 15 nm ($2\theta=38.21$, FWHM=0.67), and a Ag(200) crystallite size of 5 nm ($2\theta=44.13$, FWHM=1.94). The ratio of Ag₂O(111) to Ag(111)+Ag₂O(200) was 0.587. The W4 sample had an Ag₂O(111) crystallite size of 11 nm ($2\theta=33.09$, FWHM=0.85), an Ag(111)+Ag₂O(200) crystallite size of 13 nm ($2\theta=38.22$, FWHM=0.76), and an Ag(200) crystallite size of 6 nm ($2\theta=44.17$, FWHM=1.55). The ratio of Ag₂O(111) to Ag(111)+Ag₂O(200) was 0.651. The crystallite size of Ag(111)+Ag₂O(200) for ActicoatTM is 10-15 nm[7], so the crystallite sizes produced under these conditions were within the range found in ActicoatTM. The ratio of silver oxide to metallic silver is about 1:1 for ActicoatTM[7] (or about 0.5 for Ag₂O(111) to Ag(111)+Ag₂O(200)), so the ratio in the samples produced at 0.9A, 4% O₂ for 30 minutes was about right for W3 and a little high for W4 as measured by XRD. However, the ammonia soluble silver was measured to be a little low in the W3 and W4 samples, so it is anticipated that on average, the result is in between the measurements made via XRD and via ammonia soluble silver dissolution. Overall, these XRD results confirm that the thin films produced at 0.9A, 4% O₂ for 30 minutes were similar to ActicoatTM both physically and chemically.

Log Reductions

Log reductions were performed for the preliminary study looking at the effect of current, percent oxygen, and web speed on the resulting silver thin films. Figure 8-36 shows the log reductions generated against *P. aeruginosa* for dressings sputtered at 4% O₂ in 10 minute static runs at various currents. For all currents, some locations were bactericidal (log reduction greater than 3[8]), but no total kills were generated. The highest log reductions were generated at 1.5A, suggesting that under these conditions, a current of 1.5A provided the best balance between total silver and ammonia soluble silver. Table 8-8 shows a statistical analysis of the effect of substrate location on the log reductions generated at each current. At 0.5A, W3 and W4 had significantly higher log reductions than most other substrate locations. Location W7 also had higher log reductions than all the L locations, and there was some variation in log reduction produced in the L direction as well, with L6 having significantly higher log reductions than all other L locations. This was followed by L3, then L13, with L16 producing the lowest log reduction. Based on the statistical results, at a current of 1A, W3 and W4 performed well, and W4 actually had a significantly higher log reduction than W3. On the other hand, locations W1 and W7 had significantly lower log reductions than most other substrate locations. In the L direction, L3 had higher activity than L13 and L16, and L13 had higher activity than L16. At 2A, locations W1 and W7 had significantly lower activity relative to most other substrate locations. Surprisingly, so did W3. W4, however, had better antimicrobial activity than all the L direction locations except L16. L3 and L6

had stronger antimicrobial activity than L13, but L16 had the strongest antimicrobial activity of all. The pattern of lower activity at locations W1 and W7 are likely related to the lower total silver deposited at these locations due to their location outside the racetrack. The higher activity generally observed at W3 and W4 is likely related to their central or “average” location, and the higher activity at L16 sometimes observed may be related to its location near the entry point of electricity into the system.

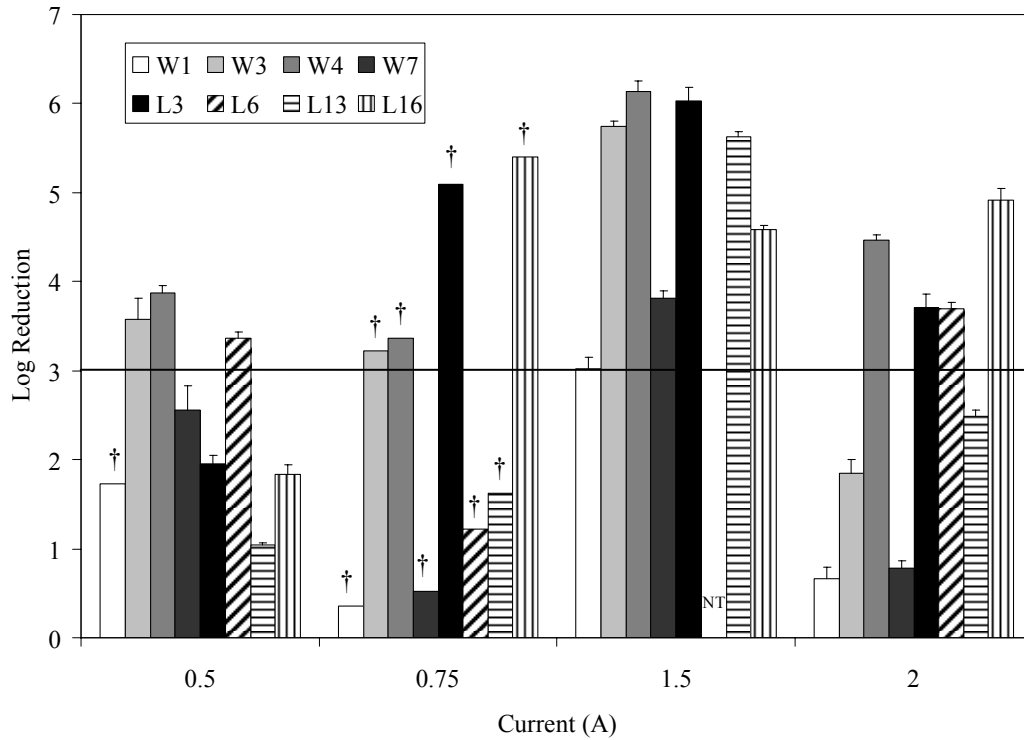


Figure 8-36. Preliminary study of the effect of current on the log reduction of *Pseudomonas aeruginosa* produced by nanocrystalline silver thin films generated at 4% oxygen during a 10 minute static run. Log reductions for silver thin films deposited at the locations indicated in Figure 8-1 were measured. † indicates that n=1. For all other data points, n=3. NT=not tested. A horizontal line is shown at a log reduction of three. Log reductions greater than this value are considered bactericidal.

Table 8-8. The effect of substrate location on the resulting log reduction generated against *P. aeruginosa* for nanocrystalline silver thin films generated at various oxygen concentrations, web speeds, and currents. Statistically significant results are in bold. n=3 for all tests unless otherwise indicated on the corresponding figures (Figures 8-36 through 8-41).

% O ₂	Wind Speed /Length of Static Run	Current (A)	ANOVA p Value	Post Test Results
4	Static, 10 min	0.5	<0.0001	p<0.05 W4 vs. L6 (W4 ↑) p<0.01 W7 vs. L3 (W7 ↑) p<0.001 W3 vs. W7, L3, L13, L16 (W3 ↑) W4 vs. W7, L3, L13, L16 (W4 ↑) W7 vs. L6 (L6 ↑) W7 vs. L13, L16 (W7 ↑) L3 vs. L13 (L3 ↑) L6 vs. L3, L13, L16 (L6 ↑) L13 vs. L16 (L16 ↑)
4	Static, 10 min	1.5A	<0.0001	p<0.01 W3 vs. W4 (W4 ↑) p<0.001 W1 vs. W3, W4, W7, L3, L13, L16 (W1 ↓) W3 vs. L16 (W3 ↑) W4 vs. L13, L16 (W4 ↑) W7 vs. W3, W4, L3, L13, L16 (W7 ↓) L3 vs. L13, L16 (L3 ↑) L13 vs. L16 (L13 ↑)
4	Static, 10 min	2	<0.0001	p<0.01 W4 vs. L16 (L16 ↑) p<0.001 W1 vs. W3, W4, L3, L6, L13, L16 (W1 ↓) W3 vs. W4, L3, L6, L13, L16 (W3 ↓) W4 vs. L3, L6, L13 (W4 ↑) W7 vs. W3, W4, L3, L6, L13, L16 (W7 ↓) L13 vs. L3, L6 (L13 ↓) L16 vs. L3, L6 (L16 ↑) L13 vs. L16 (L16 ↑)
4	80 mm/min	1.5	<0.0001	p<0.01 L16 vs. W4, L3, L6 (L16 ↓) p<0.001

4%	43 mm/min	0.5	<0.0001	W3 vs. W4, W7, L3, L6, L16 (W3 ↓) p<0.05 W3 vs. W1, W4 (W3 ↓) p<0.01 W3 vs. L16 (L16 ↑) p<0.001 L6 vs. W1, W4, L3, L16 (L6 ↓) N/A
4	43 mm/min	0.75	0.2152	
4	43 mm/min	1.5	0.0051	p<0.05 W1 vs. L16 (L16 ↑) W4 vs. L3 (W4 ↑) p<0.01 L3 vs. L16 (L16 ↑) p<0.05 W7 vs. L13 (L13 ↑) p<0.01 W4 vs. W7 (W4 ↑) W4 vs. W3, L3 (W4 ↓) p<0.001 W1 vs. L3 (W1 ↓) W3 vs. W1, W7, L6, L13 (W3 ↑) L3 vs. W7, L6, L13 (L3 ↑) p<0.01 L3 vs. W1, L13 (L3 ↓) p<0.001 L16 vs. W1, W3, W4, W7, L3, L6, L13 (L16 ↑) W7 vs. W3, W4, L3, L6 (W7 ↑) p<0.05 W7 vs. L3 (L3 ↑) W7 vs. L6 (W7 ↑) p<0.01 W1 vs. W7 (W7 ↑) p<0.001 W1 vs. W3, L3, L16 (W1 ↓) W3 vs. W7, L3, L6 (W3 ↑) L16 vs. W3, W7, L3, L6 (L16 ↑) L3 vs. L6 (L3 ↑) p<0.01 W4 vs. L16 (W4 ↑) p<0.001 W1 vs. W4, L16 (W1 ↓) p<0.05 W4 vs. W7 (W4 ↑) L6 vs. L13 (L13 ↑) p<0.01
4	43 mm/min	2	<0.0001	
4	20 mm/min	0.5A	<0.0001	
4	20 mm/min	0.75	<0.0001	
4	20 mm/min	2	<0.0001	
2	20 mm/min	0.5	<0.0001	

				W3 vs. W1, W4, L13, L16 (W3 ↑) L6 vs. W1, W4, L16 (L6 ↓) p<0.001 W1 vs. L3 (W1 ↑) W3 vs. W7, L3, L6 (W3 ↑) L3 vs. W4, L13, L16 (L3 ↓) p<0.05 W1 vs. L6 (L6 ↑) W7 vs. L3 (L3 ↑) p<0.01 W3 vs. W4, L13 (W3 ↑) L3 vs. W4, L13 (L3 ↑) p<0.001 W1 vs. W3, L3 (W1 ↓) p<0.05 W1 vs. W4 (W1 ↑) W1 vs. W7 (W7 ↑) W3 vs. W7 (W3 ↑) W7 vs. L6 (W7 ↑) L6 vs. L13 (L13 ↑) p<0.01 W3 vs. L13 (W3 ↑) W4 vs. L16 (L16 ↑) W7 vs. L3 (W7 ↑) L3 vs. L13 (L13 ↑) p<0.001 W3 vs. W1, W4, L3, L6, L16 (W3 ↑) W4 vs. W7, L13 (W4 ↓) p<0.001 W1 vs. W4, L6, L13, L16 (W1 ↑) W3 vs. W4, L6, L13, L16 (W3 ↑) W7 vs. W1, W3, W4, L3, L6, L13, L16 (W7 ↑) L3 vs. W4, L6, L13, L16 (L3 ↑) L16 vs. W4, L6 (L16 ↓)
2	20 mm/min	0.75	<0.0001	
2	20 mm/min	1.5	<0.0001	
2	20 mm/min	2	<0.0001	
0	20 mm/min	0.5	0.5932	N/A
0	20 mm/min	0.75	0.2256	N/A
0	20 mm/min	1.5	0.0755	N/A
0	20 mm/min	2	0.4017	N/A

Table 8-9 shows a statistical analysis of the effect of current on the log reductions generated at locations W3 and W4 when a 4% oxygen 10 minute static sputter was performed. At location W3, sputtering at 0.5A resulted in a

significantly higher log reduction than sputtering at 2A, while sputtering at 1.5A resulted in a significantly higher log reduction than either 0.5A or 2A. At W4, however, sputtering at 0.5A led to a significantly lower log reduction than at 2A, and again, sputtering at 1.5A led to the highest log reduction of all. As discussed above, the higher log reductions generated at 1.5A may be due to a balance between total silver deposited and percent ammonia soluble silver.

Table 8-9. The effect of current on the log reductions generated against *P. aeruginosa* at substrate locations W3 and W4 when sputtering at various oxygen concentrations and web speeds. Statistically significant results are in bold. n=3 for all analyses unless otherwise indicated on the corresponding figures (Figures 8-36 to 8-41).

%O ₂	Wind Speed/Length of Static Run	Substrate Location	ANOVA p Value*	Post Test Results
4	Static, 10 min	W3	<0.0001	P<0.001 0.5A vs. 2A (0.5A ↑) 1.5A vs. 0.5A, 2A (1.5A ↑)
4	Static, 10 min	W4	<0.0001	P<0.001 0.5A vs. 2A (2A ↑) 1.5A vs. 0.5A, 2A (1.5A ↑)
4	43 mm/min	W3	<0.0001	p<0.05 0.5A vs. 0.75A (0.75A ↑) p<0.001 2A vs. 0.5A, 0.75A (2A ↑)
4	43 mm/min	W4	<0.0001	p<0.001 2A vs. 0.5A, 0.75A, 1.5A (2A ↑)
4	20 mm/min	W4	0.0007	N/A (t-test for 0.5 vs. 2A - 2A ↑)
2	20 mm/min	W3	<0.0001	p<0.01 0.75A vs. 1.5A (0.75A ↑) p<0.001 0.5A vs. 0.75A, 1.5A, 2A (0.5A ↓) 0.75A vs. 2A (0.75A ↑)
2	20 mm/min	W4	<0.0001	p<0.01 0.75A vs. 2A (0.75A ↑) p<0.001 0.75A vs. 0.5A, 1.5A (0.75A ↑)
2	20 mm/min	W3	0.2552	N/A
2	20 mm/min	W4	0.5827	N/A

*Or t-test p value if only two conditions were compared, as indicated under the post tests section.

The log reductions generated when a web speed of 80 mm/min was used for sputtering at 4% oxygen and 1.5A are shown in Figure 8-37. All sputtering locations were bactericidal against *P. aeruginosa*, and locations W4, L3, and L6 produced a total kill. Table 8-8 indicates that locations L16 and W3 produced significantly lower kills than the locations which produced a total kill, and W3 also had a significantly lower kill than W7.

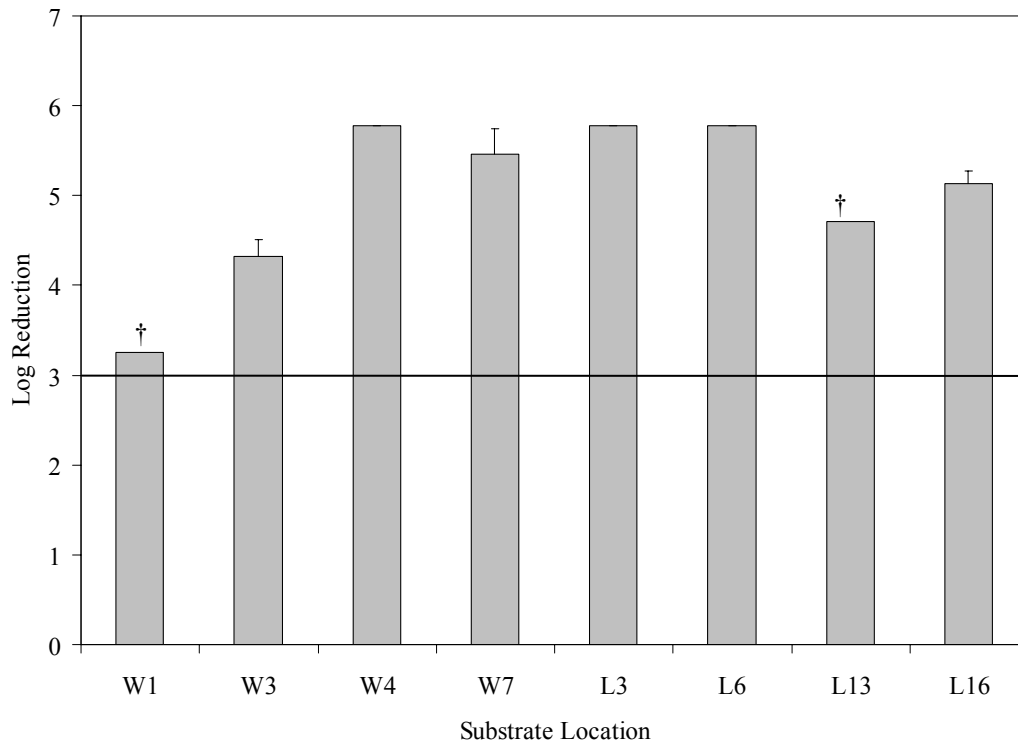


Figure 8-37. Log reductions of *P. aeruginosa* produced by nanocrystalline silver thin films generated at 4% oxygen and 1.5A during an 80 mm/min dynamic run. Log reductions for silver thin films deposited at the locations indicated in Figure 8-1 were measured. † indicates that n=1. For all other data points, n=3. A horizontal line is shown at a log reduction of three. Log reductions greater than this value are considered bactericidal.

Figure 8-38 shows the effect of current on log reductions generated against *P. aeruginosa* for samples sputtered at 4% oxygen, 43 mm/min web

speed, and various currents. None of the conditions tested produced bactericidal activity. Table 8-8 examines the effect of substrate location on the log reductions produced. At 0.5A, W3 and L6 produced significantly lower log reductions than W1, W4, and L16, while L6 also produced significantly lower log reductions than L3. At 0.75A, there were no significant differences with substrate location in terms of the log reductions generated. At 1.5A, L16 produced a significantly higher log reduction than W1 and L3, and location W4 also had a significantly higher log reduction than L3. At 2A, W3 and L3 both generated significantly higher log reductions than W7, L6, and L13. W3 also had a significantly higher log reduction than W1, as did L3. W4 and L13 had significantly higher log reductions than W7, but W4 had a lower log reduction than W3 and L3. There did not appear to be any clear trends in terms of the effect of substrate location on the resulting log reductions at this set of sputtering conditions. A statistical analysis of the effect of current on the resulting log reduction indicated that at the highest current tested (2A), significantly higher log reductions were obtained than at the other currents tested (Table 8-9). As well, for location W3, a current of 0.75A resulted in a higher log reduction than the current of 0.5A. This indicates that the low log reductions seen at 43 mm/min were likely the result of not enough total silver deposition, and makes the results observed at 80 mm/min somewhat surprising, as lower total silver would be expected with the faster web speed, which would be expected to result in a lower log reduction.

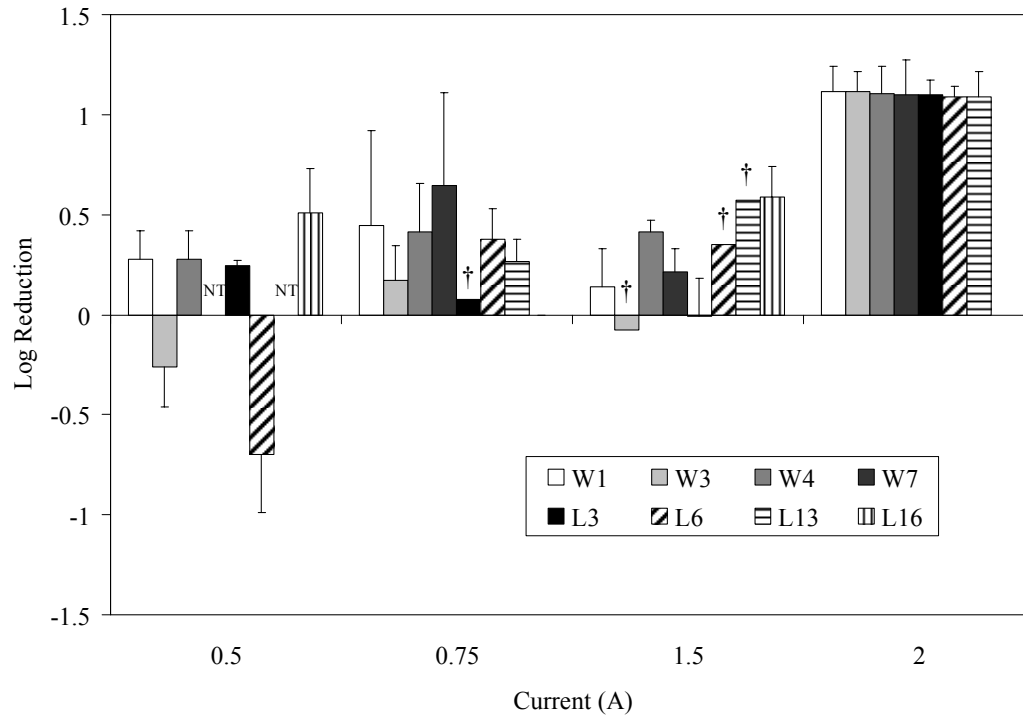


Figure 8-38. The effect of current on the log reductions of *P. aeruginosa* produced by nanocrystalline silver thin films generated at 4% oxygen during a 43 mm/min dynamic run. Log reductions for silver thin films deposited at the locations indicated in Figure 8-1 were measured. † indicates that n=1. For all other data points, n=3. NT=not tested.

Figure 8-39 shows the effect of sputtering current on log reductions against *P. aeruginosa* for nanocrystalline silver thin films sputtered at 4% oxygen and a web speed of 20 mm/min. Although most of the log reductions were below a bactericidal level, they were higher than those obtained at the faster web speed of 43 mm/min, suggesting a more appropriate total silver level was generated at the lower speed. Bactericidal activity was observed at a few substrate locations, particularly using a current of 2A. From Table 8-7, at 0.5A, log reductions were significantly higher at W7 and L16 than most other locations, but were lower at L3. At 0.75A, W1 had a significantly lower log reduction than W3, W7, L3, and L16, while W3 also had significantly higher log reductions than W7, L3, and L6;

L16 had significantly higher log reductions than W3, W7, L3, and L6; L3 had a significantly higher log reduction than L6; and W7 had a significantly higher log reduction than W1 and L6. Thus at 1.5A, there appeared to be more variability in activity with substrate location, with middle locations (W3 and W4), and the location closest to the power supply (L16), being the most active. The amount of variability in the W direction is somewhat surprising theoretically, considering that a dynamic run is intended to smooth out variations in deposition in the W direction, and therefore should even out the activity as well. However, in this study, variations with the W direction were observed in the total silver deposited, which may explain the variation in activity. At 2A, W1 again had a significantly lower log reduction than W4 and L16, and the log reduction produced by L16 was also significantly lower than that produced by W4. From Table 8-9, no significant differences in log reduction were observed with current at 43 mm/min, 4% oxygen. However, very few conditions were analyzed statistically at these conditions.

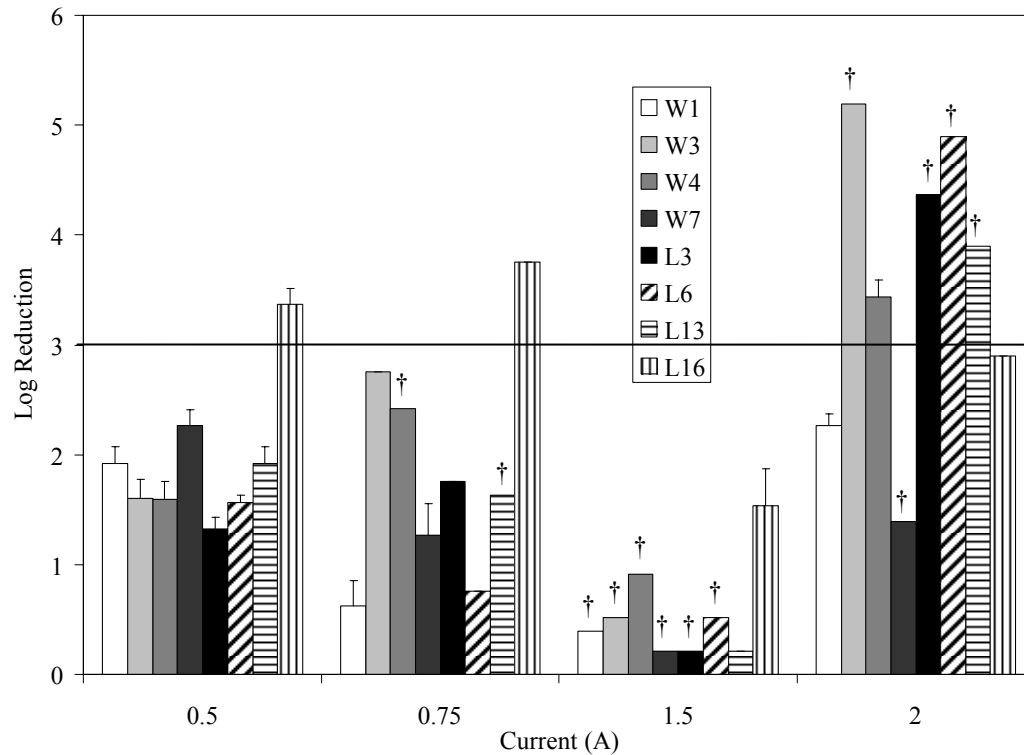


Figure 8-39. The effect of current on the log reductions of *P. aeruginosa* produced by nanocrystalline silver thin films generated at 4% oxygen during a 20 mm/min dynamic run. Log reductions for silver thin films deposited at the locations indicated in Figure 8-1 were measured. † indicates that n=1. For all other data points, n=3. A horizontal line is shown at a log reduction of three. Log reductions greater than this value are considered bactericidal.

Figure 8-40 shows the effect of current on the log reductions against *P. aeruginosa* which were produced using nanocrystalline silver films generated at 2% oxygen, a web speed of 20 mm/min, and various currents. In general, the films produced were not bactericidal, generating lower antimicrobial activity than the films produced at 4% oxygen under the same conditions. From 0.5A to 0.75A, the log reduction increased, but from there it appeared to decrease slightly with increasing current. This suggests that at the lower oxygen percentage, there was not enough ammonia soluble silver present to produce good antimicrobial activity, and that this condition was only worsened by increasing the current.

Table 8-8 shows an analysis of the effect of substrate location on the log reductions generated under each of the conditions tested, and indicates that there was a lot of variability in antimicrobial activity with substrate location. At 0.5A, W3 and W4 in particular showed significantly higher log reductions than various other substrate locations, while L3 and L6 had significantly lower log reductions than many other substrate locations, including W1. At 0.75A, however, L3 produced significantly higher log reductions than all the W locations except W3, and also produced a significantly higher log reduction than L13. W1 produced a significantly lower log reduction than L3, L6, and W3, while W3 had a significantly higher log reduction than W4 and L13. At 1.5A, there was again high variability in log reduction with substrate location. W1 had a significantly higher log reduction than W4 (which had a lower log reduction than most substrate locations) but had a significantly lower log reduction than W7, which also produced a significantly higher log reduction than L3 and L6. L3 and L6 also had significantly lower log reductions than L13. Unlike W4, W3 produced a significantly higher log reduction than most other substrate locations. At 2A, W1, W3, and L3 produced significantly higher log reductions than W4, L6, L13, and L16. W7 produced significantly higher log reductions than all other substrate locations, while L16 had the lowest log reduction, being significantly lower than even W4 and L6. Overall, there were no clear trends relating the log reductions produced with the location examined, despite a surprising level of variability for a dynamic run. Table 8-9 shows the effect of current on the resulting log reductions produced from dressings generated at 2% oxygen during 20 mm/min dynamic

runs. At W3, the run at 0.5A had a significantly lower log reduction than all other currents, while at 0.75A, the log reduction produced was significantly higher than all other currents. At W4, again the current of 0.75A produced the highest log reductions, suggesting that with lower percent oxygen, the effect of going to higher currents on decreasing the resulting ammonia soluble silver is more pronounced, leading to lower activity.

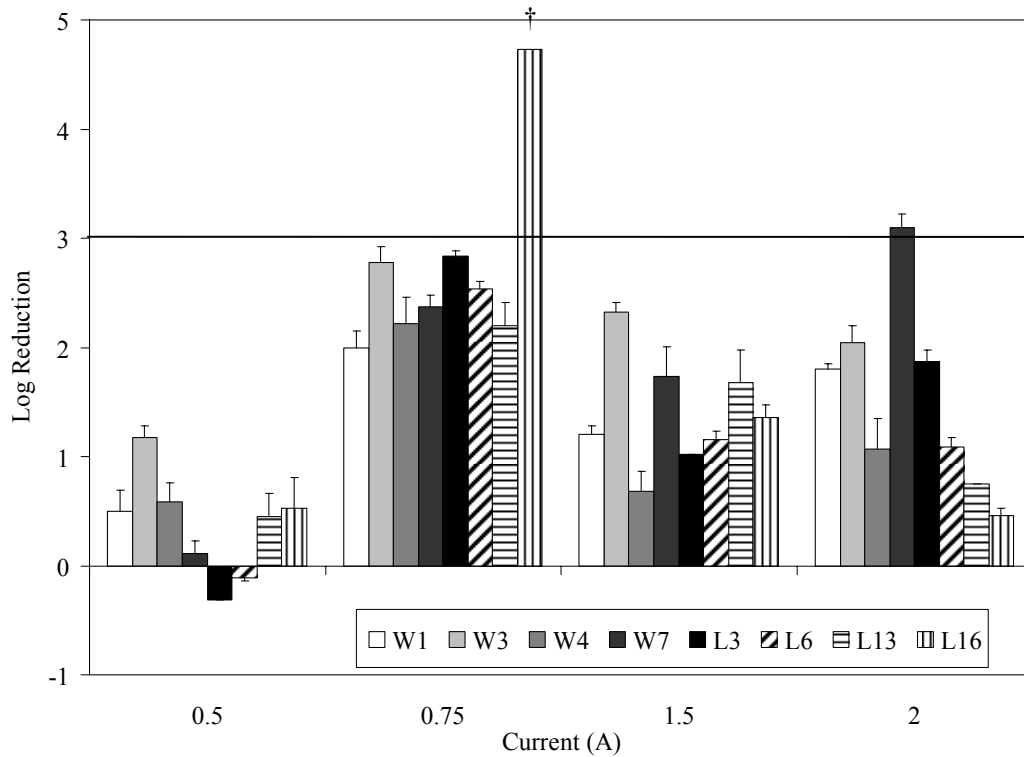


Figure 8-40. The effect of current on the log reductions of *P. aeruginosa* produced by nanocrystalline silver thin films generated at 2% oxygen during a 20 mm/min dynamic run. Log reductions for silver thin films deposited at the locations indicated in Figure 8-1 were measured. † indicates that n=1. For all other data points, n=3. A horizontal line is shown at a log reduction of three. Log reductions greater than this value are considered bactericidal.

Figure 8-41 shows the effect of current on the log reductions produced for nanocrystalline silver thin films generated with no oxygen in the atmosphere for dynamic runs at 20 mm/min. Very little activity was observed at any of the

currents tested, similar to results obtained by Sant *et al.*[6] Table 8-8 indicates that there were no significant differences in the log reductions produced against *P. aeruginosa* with substrate location when no oxygen was included in the atmosphere for any of the currents tested. Likewise, Table 8-9 indicates that there were no significant differences in the log reductions produced with varying current under the above conditions. This confirms the importance of the presence of oxygen for antimicrobial activity.

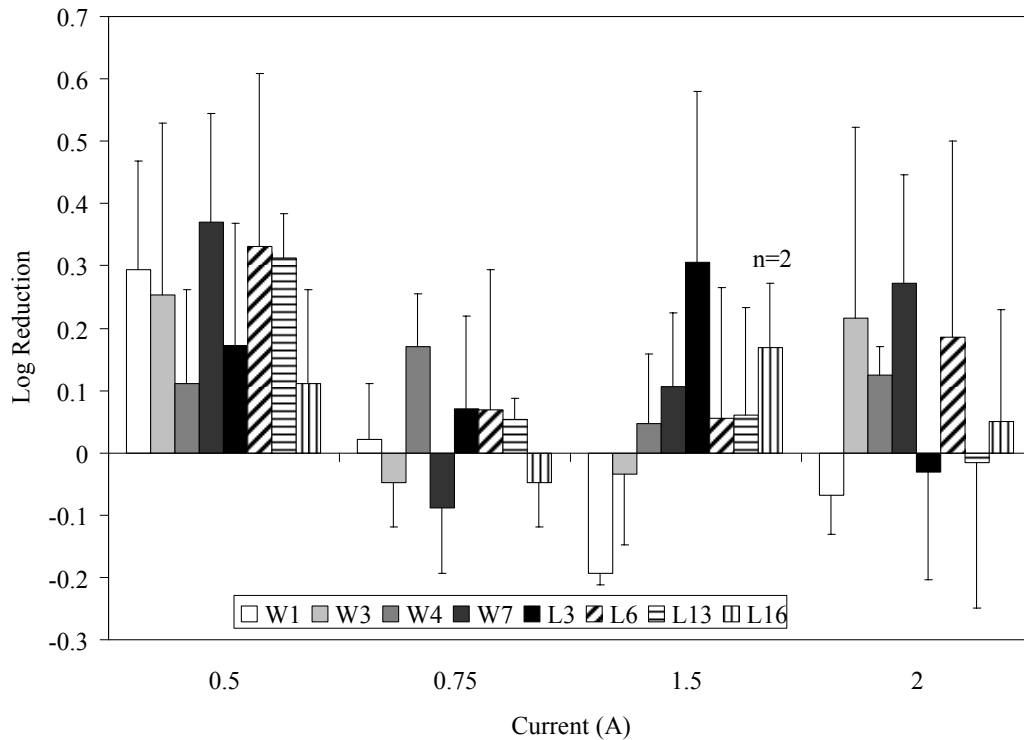


Figure 8-41. The effect of current on the log reductions of *P. aeruginosa* produced by nanocrystalline silver thin films generated at 0% oxygen during a 20 mm/min dynamic run. Log reductions for silver thin films deposited at the locations indicated in Figure 8-1 were measured. For all data points, n=3, except as indicated.

Table 8-10 examines the effect of web speed on the resulting log reductions produced from locations W3 and W4, holding percent oxygen at 4% and comparing runs performed at the same current. At 0.5A, the static 10 minute

run produced a significantly higher log reduction than either the 20 or 43 mm/min run, and (at W3 only) the 20 mm/min run produced a higher log reduction than the 43 mm/min run. At 1.5A, the static 10 minute run produced a significantly higher log reduction than the 80 mm/min run at both W3 and W4. At W4, both the static run and the 80 mm/min run produced significantly higher log reductions than the 43 mm/min run. At 2A, there were no significant differences at W3, while at W4, the static 10 minute run produced a significantly higher log reduction than the 20 or 43 mm/min runs, while the 20 mm/min run also produced a significantly higher log reduction than the 43 mm/min run. Overall, these results indicate that the higher web speeds resulted in lower log reductions, and that a web speed of 20 mm/min or less would be required to generate bactericidal films. This appears to be related to the total silver results which indicated that to have total silver levels at or greater than those present in ActicoatTM, a web speed of 20 mm/min or less would be required.

Table 8-10. The effect of web speed on log reductions produced against *P. aeruginosa* for nanocrystalline silver thin films generated at 4% oxygen and various currents. Statistically significant results are in bold. n=3 for all analyses unless indicated in the corresponding figures (Figures 8-36 to 8-41).

Current (A)	Substrate Location	ANOVA p Value*	Post Test Results
0.5	W3	<0.0001	p<0.001 Static vs. 20 & 43 mm/min (Static ↑) 43 vs. 20 mm/min (20 mm/min ↑)
0.5	W4	<0.0001	p<0.001 Static vs. 43 mm/min (Static ↑) Static vs. 20 mm/min (Static ↑)
1.5	W3	0.0062	N/A (t-test: static vs. 80 mm/min – static ↑)
1.5	W4	<0.0001	p<0.01 Static vs. 80 mm/min (Static ↑) p<0.001 Static vs. 43 mm/min (Static ↑) 43 vs. 80 mm/min (80 mm/min ↑)
2	W3	0.2330	N/A
2	W4	<0.0001	p<0.001 Static vs. 20 and 43 mm/min (Static ↑) 43 vs. 20 mm/min (20 mm/min ↑)

*Or t-test p value if only two conditions were compared, as indicated under the post tests section.

The effect of percent oxygen in the chamber on the resulting log reductions is examined at locations W3 and W4 in Table 8-11 for nanocrystalline silver films generated for dynamic runs of 20 mm/min at various currents. At 0.5A, both 2% and 4% oxygen resulted in significantly higher log reductions than 0% oxygen. At W4, this was also true, and 4% oxygen also resulted in a significantly higher log reduction than 2% oxygen. At 0.75A, using no oxygen led to significantly lower log reductions than 2% (W3 and W4) or 4% oxygen (W3). At 1.5A, using 2% oxygen led to a significantly higher log reduction than using no oxygen at both W3 and W4. This was also true at both locations using a current of 2A, and 4% oxygen also led to a significantly higher log reduction than

either 0% or 2% oxygen (W4). Overall these results confirm that a certain level of oxygen in the chamber is necessary to produce bactericidal activity, with 4% oxygen resulting in higher activity than either 0% or 2% oxygen.

Table 8-11. The effect of percent oxygen on log reductions produced against *P. aeruginosa* for nanocrystalline silver thin films generated at various currents for dynamic runs at 20 mm/min. Statistically significant results are in bold. n=3 for all analyses unless indicated in the corresponding figures (Figures 8-36 to 8-41).

Current (A)	Substrate Location	ANOVA p Value	Post Test Results
0.5	W3	0.0004	p<0.01 2% vs. 0% (2% ↑)
0.5	W4	<0.0001	p<0.001 4% vs. 0% (4% ↑) p<0.05 2% vs. 0% (2% ↑)
0.75	W3	<0.0001	p<0.001 4% vs. 0%, 2% (4% ↑) p<0.001 0% vs. 2%, 4% (0% ↓)
0.75	W4	0.0052	N/A (t-test for 2% vs. 0% - 2% ↑)
1.5	W3	<0.0001	N/A (t-test for 2% vs. 0% - 2% ↑)
1.5	W4	0.0153	N/A (t-test for 2% vs. 0% - 2% ↑)
2	W3	0.0114	N/A (t-test for 2% vs. 0% - 2% ↑)
2	W4	<0.0001	p<0.01 2% vs. 0% (2% ↑) p<0.001 4% vs. 0%, 2% (4% ↑)

The log reductions produced by thin films generated at 4, 8, 10, or 12% oxygen and 0.75, 1, or 1.5A for 10 minute static sputtering runs are shown in Figure 8-42. Many of the conditions used produced bactericidal activity, but the only total kills obtained were from films generated at 8% oxygen and 1.5A current location W4; and 10% oxygen, 1.5A, for both locations. In Table 8-12, a comparison of locations was done, holding all other variables constant, to see if the resulting log reductions varied with substrate locations. In most cases, only

W3 and W4 were compared, but for some conditions other locations were compared as well, as indicated (data for these other locations is not shown in Figure 8-42). At 4%, 8%, and 10% oxygen, there was no difference in the log reductions produced at different locations at any current. This was also true of runs done at 12% O₂ and 0.75A. However, at 1A and 12% O₂, L3 and W3 produced significantly lower log reductions than W4 or L16. At 1.5A, W3 and W4 produced significantly lower log reductions than L3, L6, or L13, while L16 produced a significantly higher log reduction than W3, W4, L3, L6, or L13. Again, this suggests that at higher currents, there may be an increase in bactericidal activity for films taken from substrate locations near the power supply, when total silver may not be sufficient at some locations.

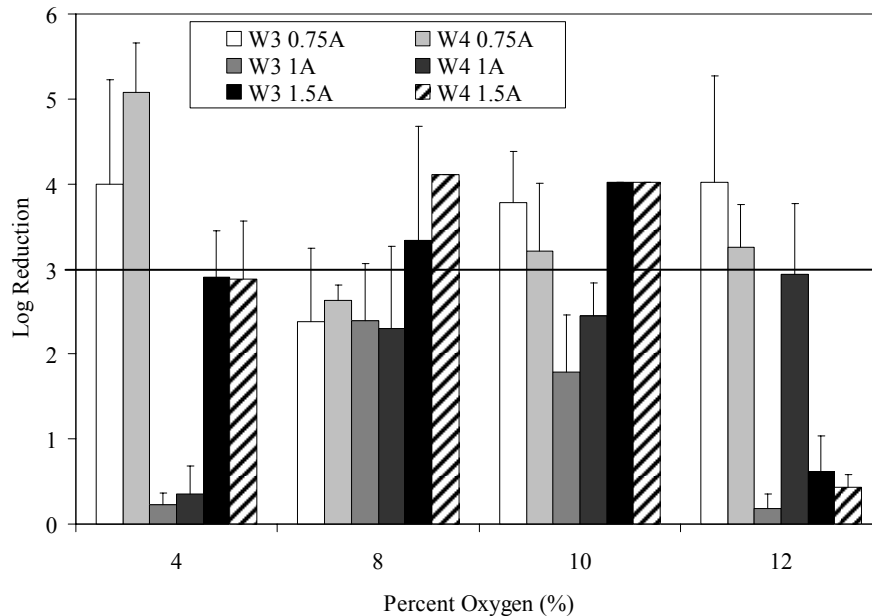


Figure 8-42. The effect of percent oxygen on the log reductions of *S. aureus* produced by nanocrystalline silver thin films generated at various currents during a 10 minute static run. Log reductions for silver thin films deposited at substrate locations W3 and W4 were measured. For all data points, n=3. A horizontal line is shown at a log reduction of three. Log reductions greater than this value are considered bactericidal.

Table 8-12. Effect of substrate location on log reduction against *S. aureus* for nanocrystalline silver dressings generated using 10 minute static sputtering runs at various oxygen concentrations and currents. Statistically significant results are in bold. n=3 for all analyses.

% O ₂	Current (A)	Locations Compared	ANOVA p Value*	Post Test Results
4	0.75	W3, W4	0.3012	N/A
4	1	W3, W4	0.6895	N/A
4	1.5	W3, W4	0.9594	N/A
8	0.75	W3, W4	0.6782	N/A
8	1	W3, W4	0.9000	N/A
8	1.5	W3, W4	not sig. diff.**	N/A
10	0.75	W3, W4	0.3961	N/A
10	1	W3, W4, L13, L16	0.0844	N/A
10	1.5	W3, W4	not sig. diff***	N/A
12	0.75	W3, W4	0.6324	N/A
12	1	W3, W4, L3, L6, L13, L16	0.0015	p<0.05 L3 vs. W4, L16 (L3 ↓) p<0.01 W3 vs. W4, L16 (W3 ↓)
12	1.5	W3, W4, L3, L6, L13, L16	<0.0001	p<0.05 L6 vs. L16 (L16 ↑) p<0.01 W3 vs. L3, L13 (W3 ↓) W4 vs. L3, L13 (W4 ↓) p<0.001 L6 vs. W3, W4 (L6 ↑) L16 vs. W3, W4, L13, L3 (L16 ↑)

*Or t-test p-value if only two locations are compared.

**One group had a standard deviation of zero so the t-test could not be run.

However, the average value for this group was within the standard deviation of the other group, so the results are not significantly different.

***Both groups had identical average values and zero standard deviation, so the t-test could not be run, but the results are not significantly different.

The effect of percent oxygen on the log reductions produced against *S. aureus* are shown in Table 8-13 for 10 minute static runs at various currents, at locations W3 and W4. Using a current of 0.75A, at location W3, there were no significant differences in the log reduction produced with varied percent oxygen.

However, at W4, using 4% oxygen resulted in significantly higher log reductions than all higher percentages of oxygen. At a current of 1A and location W3, using 8% oxygen resulted in a significantly higher log reduction than either 4% or 12% oxygen, while at location W4, log reductions produced at 12% oxygen were significantly higher than those produced at 4% oxygen. At a current of 1.5A, using 12% oxygen resulted in significantly lower log reductions than any of the lower oxygen concentrations at both locations W3 and W4, but 4% oxygen resulted in a lower log reduction than either 8 or 10% oxygen.

Table 8-13. The effect of 4, 8, 10, and 12% oxygen on log reductions generated against *S. aureus* for nanocrystalline silver thin films generated using 10 minute static sputtering runs at various currents. Statistically significant results are in bold. n=3 for all analyses.

Current (A)	Substrate Location	ANOVA p Value	Post Test Results
0.75	W3	0.2416	N/A
0.75	W4	0.0033	p<0.05 4% vs. 10%, 12% (4% ↑)
1	W3	0.0100	p<0.01 4% vs. 8% (4% ↑)
1	W4	0.0292	p<0.05 8% vs. 4%, 12% (8% ↑)
1.5	W3	0.0029	p<0.05 4% vs. 12% (12% ↑)
1.5	W4	<0.0001	p<0.01 4% vs. 12% (4% ↑) 12% vs. 8%, 10% (12% ↓) p<0.05 4% vs. 8%, 10% (4% ↓) p<0.001 12% vs. 4%, 8%, 10% (12% ↓)

Table 8-14 shows the effect of current on the log reductions produced during 10 minute static sputters, holding oxygen constant. At 4% oxygen, at both locations W3 and W4, sputtering at 1A led to a significantly lower log reduction

than sputtering at 0.75 or 1.5A. In addition, at W4, sputtering at 0.75A resulted in a significantly higher log reduction than sputtering at 1.5A. At 8% oxygen, there were no significant differences at W3, but at W4, sputtering at 1.5A led to a significantly higher log reduction than sputtering at 0.75 or 1A. At 10% oxygen, sputtering at 1A led to significantly lower log reductions than at 1.5A (W3 and W4), and even 0.75A (W3). At 12% oxygen, sputtering at 0.75A resulted in a significantly higher log reduction than either 1 or 1.5A at W3, while at W4, sputtering at 1.5A resulted in a significantly lower log reduction than sputtering at either 1 or 0.75A.

Table 8-14. The effect of current (0.75, 1, or 1.5 A) on log reductions generated against *S. aureus* for nanocrystalline silver thin films generated using 10 minute static sputtering runs at various currents. Statistically significant results are in bold. n=3 for all analyses.

% O ₂	Substrate Location	ANOVA p Value	Post Test Results
4	W3	0.0122	p<0.05 1A vs. 0.75A, 1.5A (1A ↓)
4	W4	0.0009	p<0.05 0.75A vs. 1.5A (0.75A ↑) 1A vs. 1.5A (1.5A ↑) p<0.001 0.75A vs. 1A (0.75A ↑)
8	W3	0.4598	N/A
8	W4	0.0178	p<0.05 1.5A vs. 0.75A, 1A (1.5A ↑)
10	W3	0.0035	p<0.01 1A vs. 0.75A, 1.5A (1A ↓)
10	W4	0.0256	p<0.05 1A vs. 1.5A (1.5A ↑)
12	W3	0.0216	p<0.05 0.75A vs. 1A, 1.5A (0.75A ↑)
12	W4	0.0016	p<0.01 1.5A vs. 0.75A, 1A (1.5A ↓)

From these results it appears that the effect of oxygen on the antimicrobial activity is closely tied to the current used. At lower currents, a lower oxygen concentration produces an acceptable ammonia soluble silver fraction, but with increasing current used, increasing amounts of oxygen are required to obtain an effect. However, at very high oxygen levels (12%), the antimicrobial activity dramatically dropped off with increasing current, indicating that the change in the chemistry of the dressings (which was observed as a change in ammonia soluble silver, and in the ratio of silver oxide to metallic silver) resulted in reduced antimicrobial activity. This provides confirmation that the changes observed could be due to a photoreduction reaction post-sputtering, as reduced silver is not expected to have antimicrobial activity, whereas if a different type of silver-oxygen bond was formed that was not ammonia soluble, it might still be antimicrobial, and would possibly show up as a separate peak on the XRD. It is important to note that although some of the conditions in which a high silver oxide content was present in the dressings did result in a bactericidal effect in 30 minutes, silver oxide is not responsible for the unusual antimicrobial activity of nanocrystalline silver. In these dressings, it was observed that all of the silver dissolved off of the dressings into the 300 μL of bacteria within the 30 minute time period. Thus, films generated under these conditions provide an Ag^+ “dump” similar to that seen with silver nitrate and silver sulfadiazine, or dressings such as ContreetTM. These films can generate a bactericidal effect, but they do not have any longevity and would not behave differently from traditional silver treatments.

Thus, CZOIs were not necessary to distinguish some of the variation in levels of activity of dressings generated under different conditions, as the log reduction results did demonstrate differences in activity, but for those sputtering conditions which generated a bactericidal effect, a further examination of the dressings via day-to-day corrected zone of inhibition assays should be performed. This would help to distinguish those conditions which generate sustained-release dressings from those which generate dressings which release all active species within a short time period. As well, future studies for fine-tuning conditions to generate optimal antimicrobial activity could use day-to-day corrected zone of inhibition assays, particularly with a microbial species such as *S. aureus* that shows some natural resistance to silver, to test for changes in dressing longevity, since dressing longevity appears to be more sensitive to changes in dressing chemistry than log reductions (see Chapter 9), and a naturally silver-resistant species would provide an earlier detection of those changes.

Finally, log reductions were performed on the dressings generated at 0.9A and 4% oxygen in a 30 minute static run. Both locations W3 and W4 produced log reductions of $\geq 5.42 \pm 0.0$ (total kill). This indicates that using these sputtering conditions, thin films can be generated in-house that closely mimic Acticoat™, not only in terms of its physical and chemical properties, but also its biological activity.

Conclusions

This chapter has revealed a variety of important relationships between sputtering conditions used to create nanocrystalline silver thin films, their physical and chemical properties, and their antimicrobial activity. It was determined that the total silver deposited was increased with increasing sputtering time or decreasing web speed, but that the ammonia soluble silver fraction was not affected consistently by either. A certain total silver level is necessary but not sufficient to produce antimicrobial activity. The percent oxygen in the chamber increased the ammonia soluble fraction up to a point, as well as increasing the size of silver oxide crystallites, but when very high oxygen levels were used, the film chemistry changed, resulting in a drop in ammonia soluble silver (silver oxide), and a drop in the size of silver oxide crystallites. Increasing current resulted in increased total silver deposition, and caused a slight increase in the crystallite sizes produced, but decreased the ammonia soluble silver fraction. The ammonia soluble silver corresponded to the quantity of silver oxide present in the film. Having some silver oxide in the film was necessary to produce antimicrobial activity, confirming that silver oxide acts as a pinning structure that prevents the silver nanostructure from undergoing crystallite growth. However, above a certain level, the dressings lose their controlled release properties, dumping all the active silver in a short time, which, at very high oxygen concentrations, is likely only Ag^+ from the silver oxide. It was determined that sputtering for a 30 minute static run at 0.9A and 4% oxygen resulted in the production of silver thin films which behaved very similarly to Acticoat™.

Observations specific to the in-house sputtering machine used were also made, including mild effects of the location of the power supply and gas supplies, and the importance of taking samples from within the racetrack. W3 and W4 appear to provide the most uniform results, but sampling in the L direction from L3 to L16 would provide less variation than sampling in the W direction, as W1 and W7 appear to be outside the racetrack and this significantly affects the films deposited at those locations.

In the future, it would be interesting to test various conditions around the ones that were used to mimic Acticoat™ in this study to see if antimicrobial activity can be optimized. As well, in this chapter only *P. aeruginosa* and *S. aureus* were used, and they were used in different experiments. It would be interesting to examine the effect of films generated under various conditions on other bacterial species. Finally, it would be very valuable to test the effect of various sputtering conditions on the anti-inflammatory effect of the thin films. Since the examination of solutions generated in Chapters 5 and 7 indicated that solutions with the highest antimicrobial activity may not have the highest anti-inflammatory activity, it may be possible to generate films with high antimicrobial activity and low anti-inflammatory activity, and vice versa, by changing the conditions under which the dressings are generated. Generating a dressing with higher anti-inflammatory activity might involve finding a method to pin the nanocrystals with something other than an Ag⁺-releaser.

Bibliography

1. Wright JB, Hansen DL, Burrell RE: **The Comparative Efficacy of Two Antimicrobial Barrier Dressings: In-vitro Examination of Two Controlled Release Silver Dressings.** *Wounds: A Compendium of Clinical Research and Practice* 1998, **10**:179-188.
2. Burrell RE, Morris LR: **Anti-microbial coating for medical device.** ©1998, US Patent No. 5753251.
3. Sant SB, Gill KS, Burrell RE: **Nanostructure, dissolution and morphology characteristics of microcidal silver films deposited by magnetron sputtering.** *Acta Biomaterialia 2nd TMS Symposium on biological materials science* 2007, **3**:341-350.
4. Sant SB, Gill KS, Burrell RE: **Morphology of novel antimicrobial silver films deposited by magnetron sputtering.** *Scripta Materialia* 1999, **41**:1333-1339.
5. Sant SB, Gill KS, Burrell RE: **Novel duplex antimicrobial silver films deposited by magnetron sputtering.** *Philosophical Magazine Letters* 2000, **80**:249-256.
6. Sant SB: **The nature of chemical species in novel antimicrobial silver films deposited by magnetron sputtering.** *Philosophical Magazine A-Physics of Condensed Matter Structure Defects and Mechanical Properties* 2002, **82**:1115-1136.
7. Taylor PL, Omotoso O, Wiskel JB, Mitlin D, Burrell RE: **Impact of heat on nanocrystalline silver dressings Part II: Physical properties.** *Biomaterials* 2005, **26**:7230-7240.
8. Gallant-Behm CL, Yin HQ, Liu SJ, Hegggers JP, Langford RE, Olson ME, Hart DA, Burrell RE: **Comparison of *in vitro* disc diffusion and time kill-kinetic assays for the evaluation of antimicrobial wound dressing efficacy.** *Wound Repair and Regeneration* 2005, **13**:412-421.

Chapter 9 Using the kinetics of heat treatment to determine critical physicochemical properties for nanocrystalline silver antimicrobial activity¹

Introduction

Bacterial infection impedes wound and burn healing, and can cause the wounds to convert to a persistent state, such as a chronic ulcer[1]. Silver is important in the treatment of wounds due to its antimicrobial properties, and is therefore commonly used in the treatment of major burn injuries where bacterial infection is a serious concern. A broad range of silver treatments are available, from silver salts (such as 0.5% silver nitrate and 1% silver sulfadiazine) to silver dressings containing various forms of silver. The unique structure present in nanocrystalline silver dressings was specifically developed for use in equilibrating antimicrobial wound dressings that could be left on a wound for multiple days. Nanocrystalline silver has antimicrobial properties, which dramatically improve wound healing[2-5], that are distinct from other silver treatments, as discussed in Chapter 1. Likewise, the physical and chemical properties of nanocrystalline silver differ from micro-/macro-crystalline metallic silver as well as from silver salts, which is likely due in part to the increased percentage of grain boundary atoms and the resultant release of unique silver species, as opposed to other forms of silver which release only Ag^+ (ionic silver)[6, 7]. Atoms along grain boundaries are believed to represent a third state of matter, according to Birringer[8], as grain boundary atoms neither demonstrate the short range order

¹ Introductory material for this chapter has been published in: Taylor, Ussher, and Burrell 2005, *Biomaterials*, 26:7221-7229, and Taylor, Omotoso, Wiskel, Mitlin, and Burrell, *Biomaterials*, 26:7230-7240. A version of this chapter has also been published. Landry, Nadworny, Omotoso, Maham, Burrell, and Burrell 2009, *Biomaterials*, 30:6929-6939.

observed in amorphous materials, nor the long range order observed in crystals, since the grain boundary atoms or molecules are not part of the crystal structure, but their movement is restricted by the crystals surrounding them[8].

The impact of heat on both physical and biological properties of nanocrystalline silver dressings has been previously studied by Taylor *et al.*[9, 10]. Physical, chemical, and biological properties significantly changed after dressings were heat-treated above 75°C for 24 hours[9, 10]. Total silver released over a 24 hour period after heat treatment was decreased with increasing heat treatment temperature (see Figures 9-1 and 9-2). This corresponded to decreases in bactericidal activity of the dressing against *Staphylococcus aureus* and *Pseudomonas aeruginosa*, which are common burn and wound pathogens (see Figures 9-3 and 9-4, respectively). The ability of the dressings to create zones of inhibition against both *S. aureus* and *P. aeruginosa* was decreased with increasing heat treatment temperature above 75°C as well (see Figures 9-5 and 9-6, respectively), resulting in decreased overall days of activity (see Figure 9-7). With increasing heat treatment temperature, loss of fine features and sintering/coarsening behavior was observed via SEM (Figure 9-8). As well, with increasing heat treatment temperature, crystallite size increased, the percentage of silver oxide in the dressing decreased, and the total adsorbed oxygen increased (see Table 9-1 and Figure 9-9), as determined via XRD and XPS. Thus, an inverse relationship between crystallite size and biological activity was observed[9, 10], and the total soluble silver, rather than the total silver present, appeared to affect the dressings' biological efficacy[9, 10].

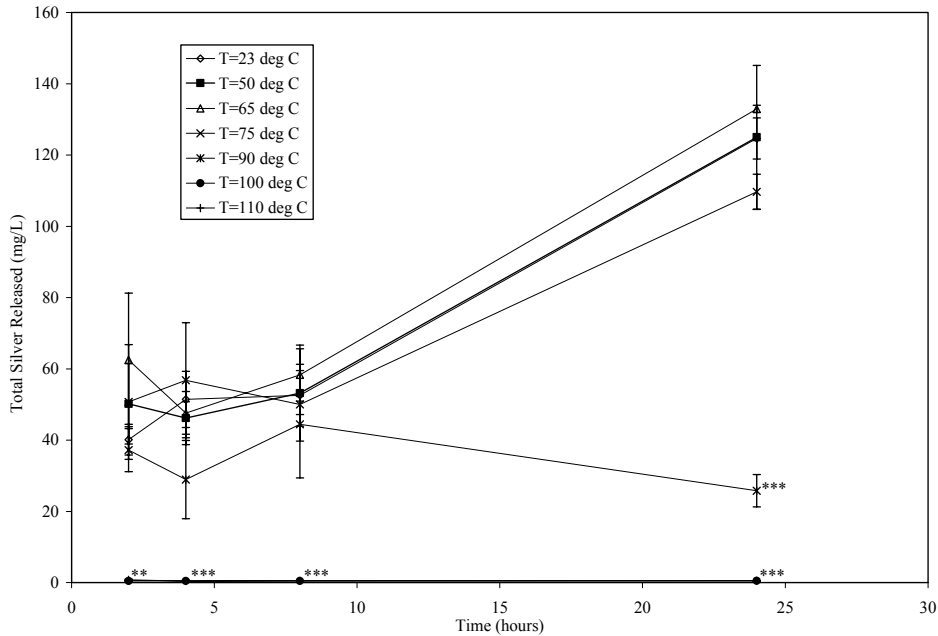


Figure 9-1. Total release of silver in water versus time for nanocrystalline silver dressings heat treated at various temperatures for 24 hours. Error bars show standard deviations. * indicates $P < 0.05$, ** indicates $P < 0.01$, *** indicates $P < 0.001$, as compared to the reference temperature (23°C), using a one-way ANOVA test with a Tukey-Kramer Multiple Comparisons post test ($n = 3$ for each temperature).

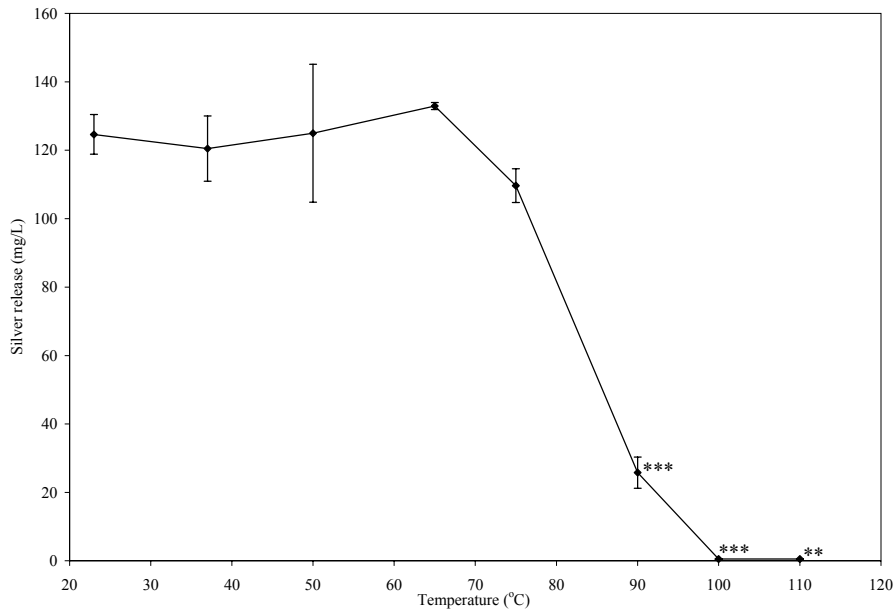


Figure 9-2. Total silver released after 24 hours in water for nanocrystalline silver dressings heat treated at various temperatures for 24 hours. Error bars show standard deviations. * indicates $P < 0.05$, ** indicates $P < 0.01$, *** indicates $P < 0.001$, as compared to the reference temperature (23°C), using a one-way ANOVA test with a Tukey-Kramer Multiple Comparisons post test ($n = 3$ for each temperature).

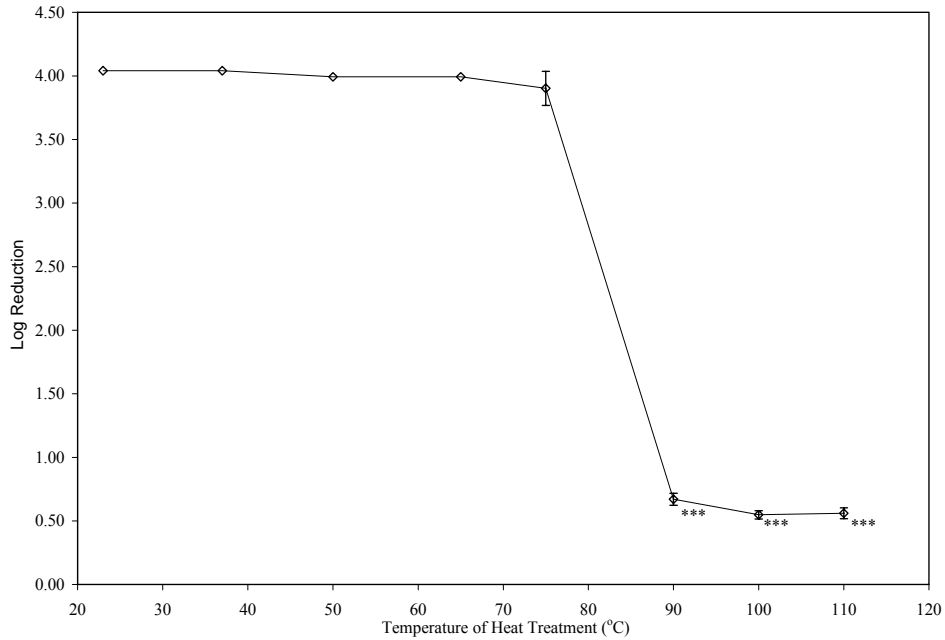


Figure 9-3. Log reduction of *S. aureus* exposed to nanocrystalline silver dressings heated at various temperatures for 24 hours. Error bars show standard deviations. * indicates $P < 0.05$, ** indicates $P < 0.01$, *** indicates $P < 0.001$, as compared to the reference temperature (23°C), using a one-way ANOVA test with a Tukey-Kramer Multiple Comparisons post test ($n = 3$ for each temperature).

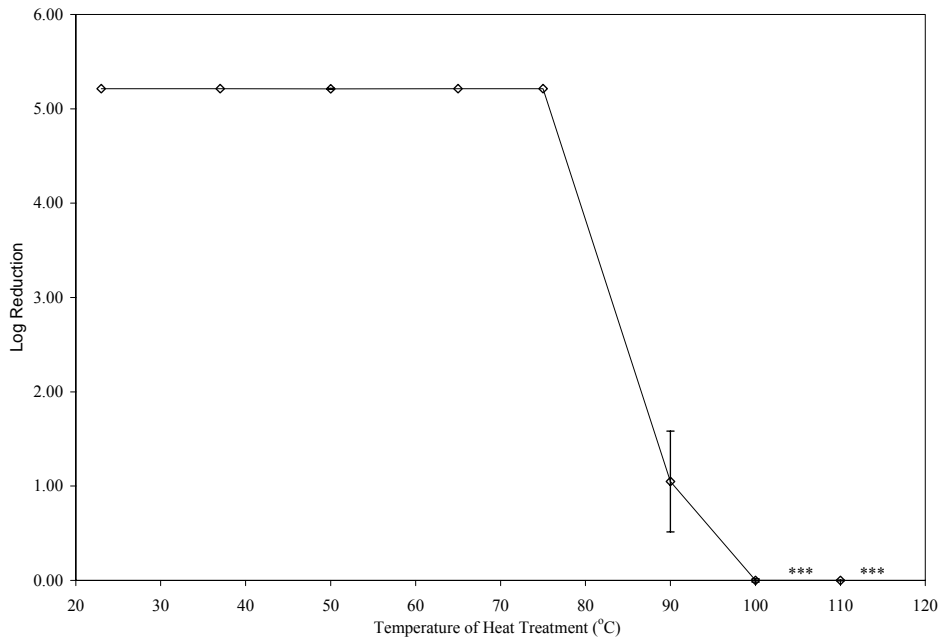


Figure 9-4. Log reduction of *P. aeruginosa* exposed to nanocrystalline silver dressings heat treated at various temperatures for 24 hours. Error bars show standard deviations. * indicates $P < 0.05$, ** indicates $P < 0.01$, *** indicates $P < 0.001$, as compared to the reference temperature (23°C), using a one-way ANOVA test with a Tukey-Kramer Multiple Comparisons post test ($n = 3$ for each temperature).

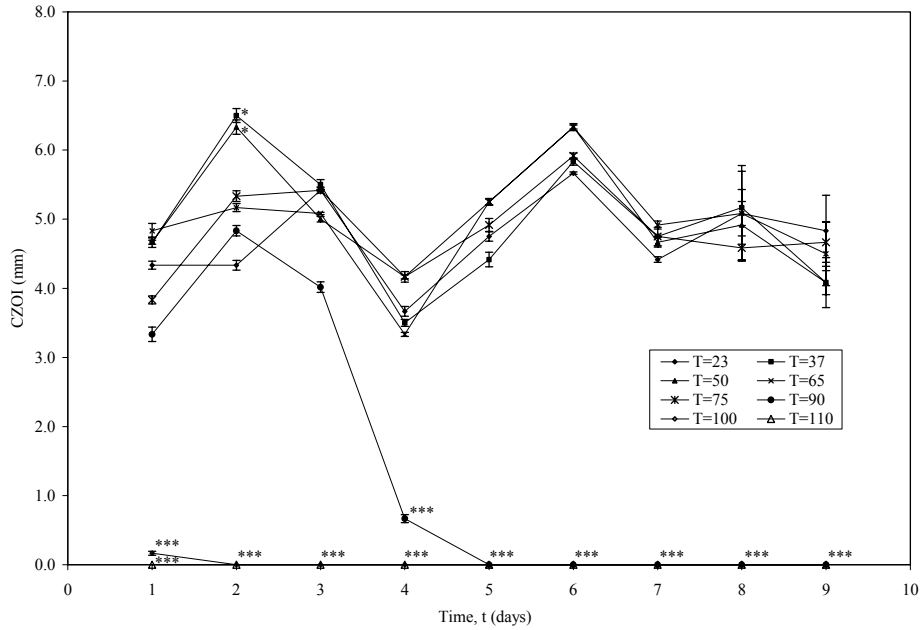


Figure 9-5. Corrected zone of inhibition (CZOI) of *S. aureus* over a series of days using nanocrystalline dressings heat treated at various temperatures for 24 hours. Error bars show standard deviations. * indicates $P < 0.05$, ** indicates $P < 0.01$, *** indicates $P < 0.001$, as compared to the reference temperature (23°C), using a one-way ANOVA test with a Tukey-Kramer Multiple Comparisons post test ($n = 3$ for each temperature).

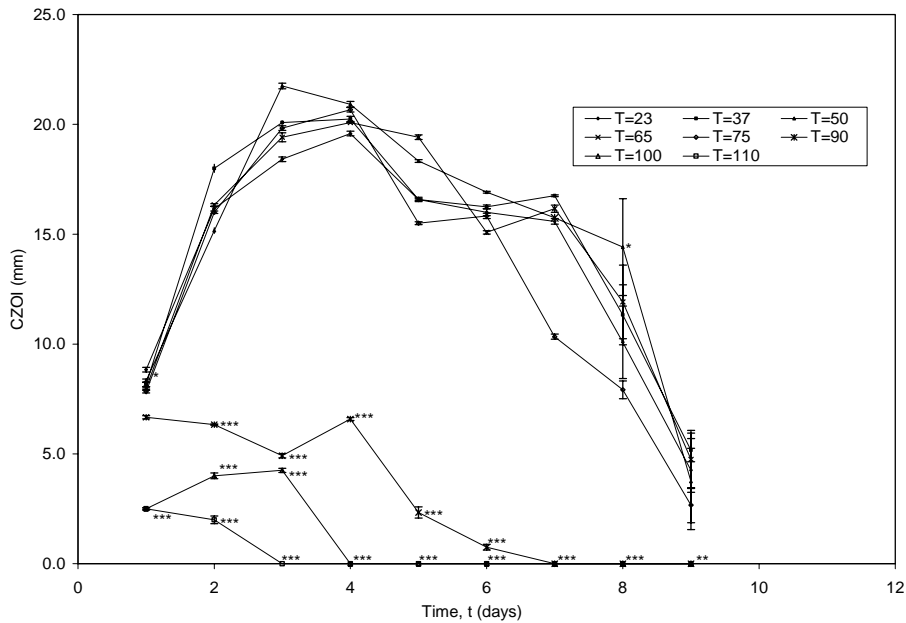


Figure 9-6. Corrected zones of inhibition (CZOI) of *P. aeruginosa* over a series of days using nanocrystalline silver dressings heat treated at various temperatures for 24 hours. Error bars show standard deviations. * indicates $P < 0.05$, ** indicates $P < 0.01$, *** indicates $P < 0.001$, as compared to the reference temperature (23°C), using a one-way ANOVA test with a Tukey-Kramer Multiple Comparisons post test ($n = 3$ for each temperature).

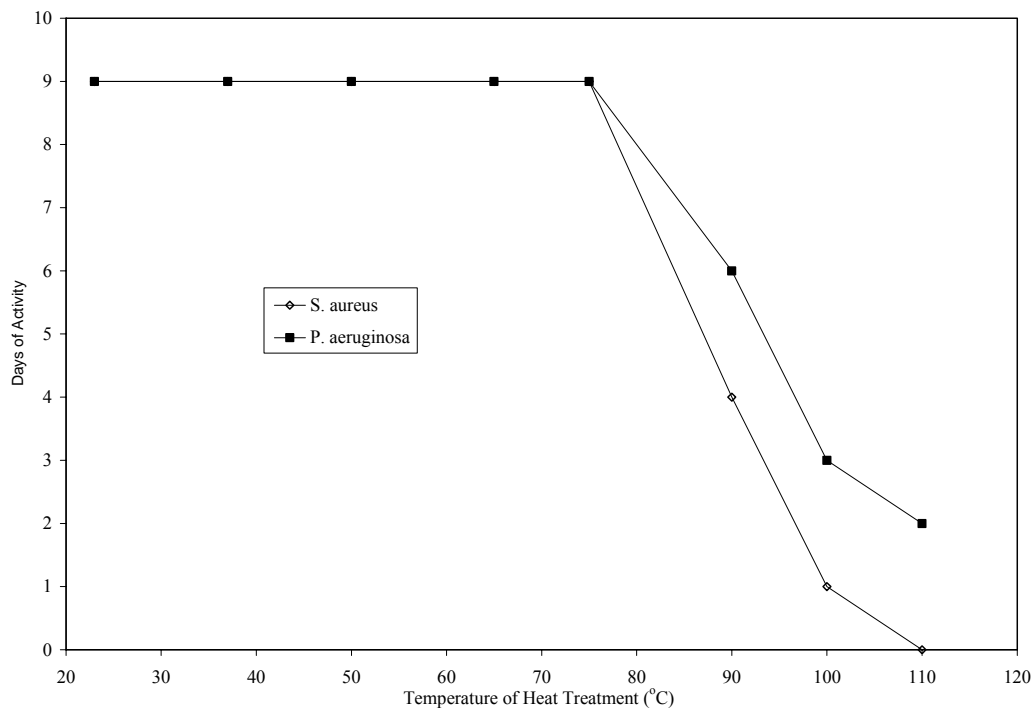


Figure 9-7. Days of nanocrystalline silver dressing antibacterial activity for dressing heat treatment at various temperatures for 24 hours. Error bars show standard deviations. * indicates $P < 0.05$, ** indicates $P < 0.01$, *** indicates $P < 0.001$, as compared to the reference temperature (23°C), using a one-way ANOVA test with a Tukey-Kramer Multiple Comparisons post test ($n = 3$ for each temperature).

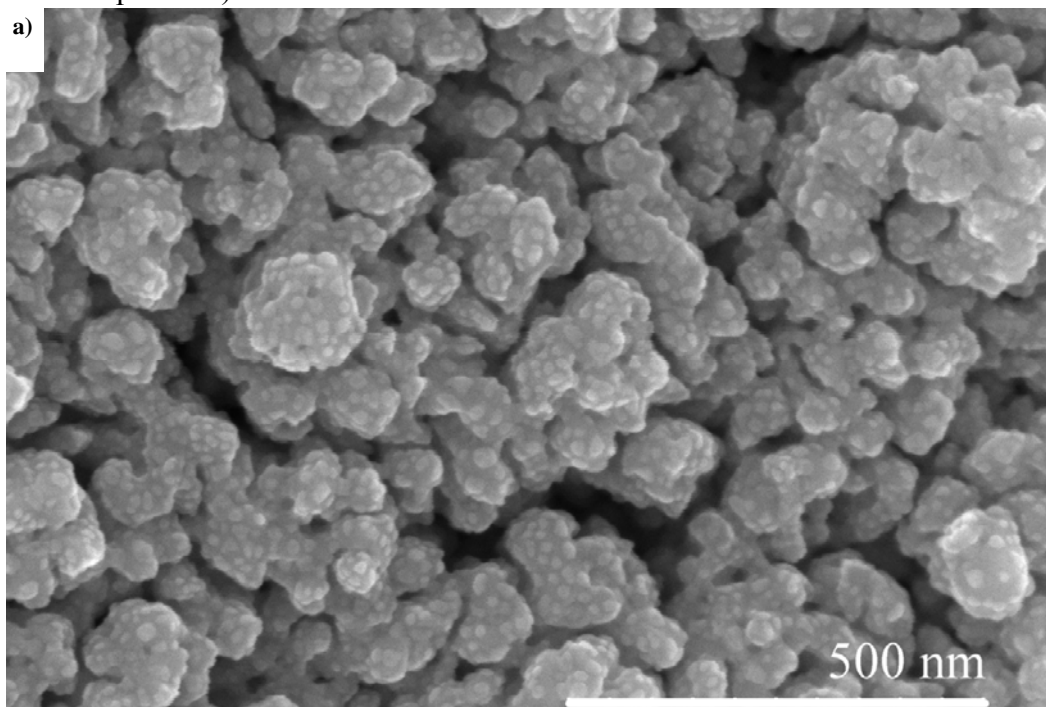


Figure 9-8.

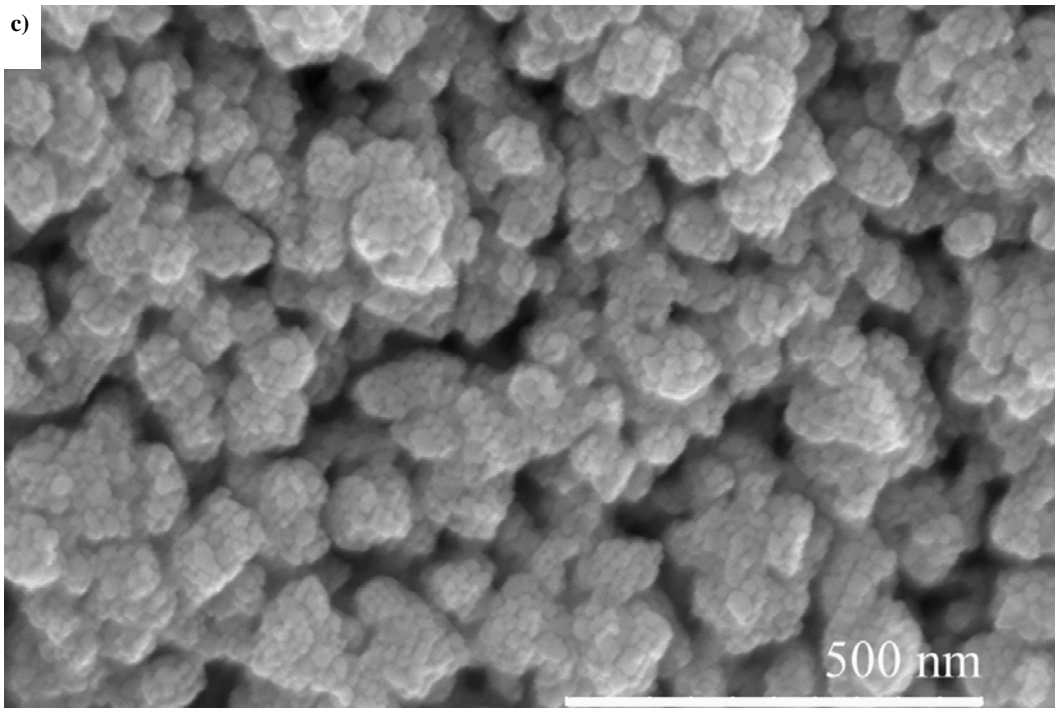
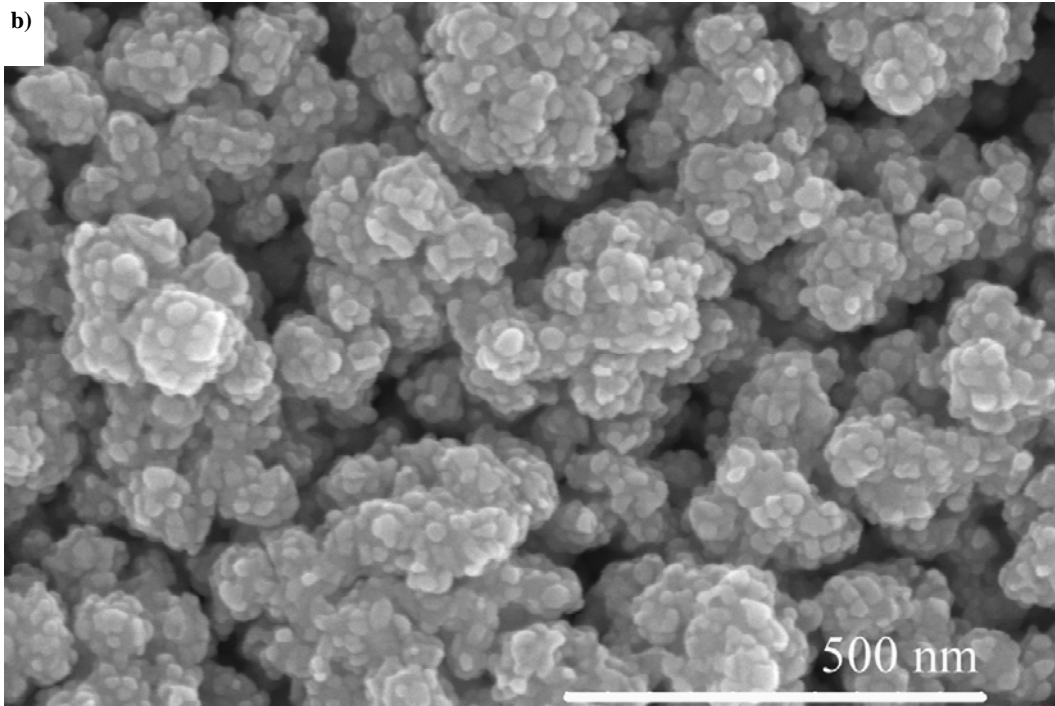


Figure 9-8, continued.

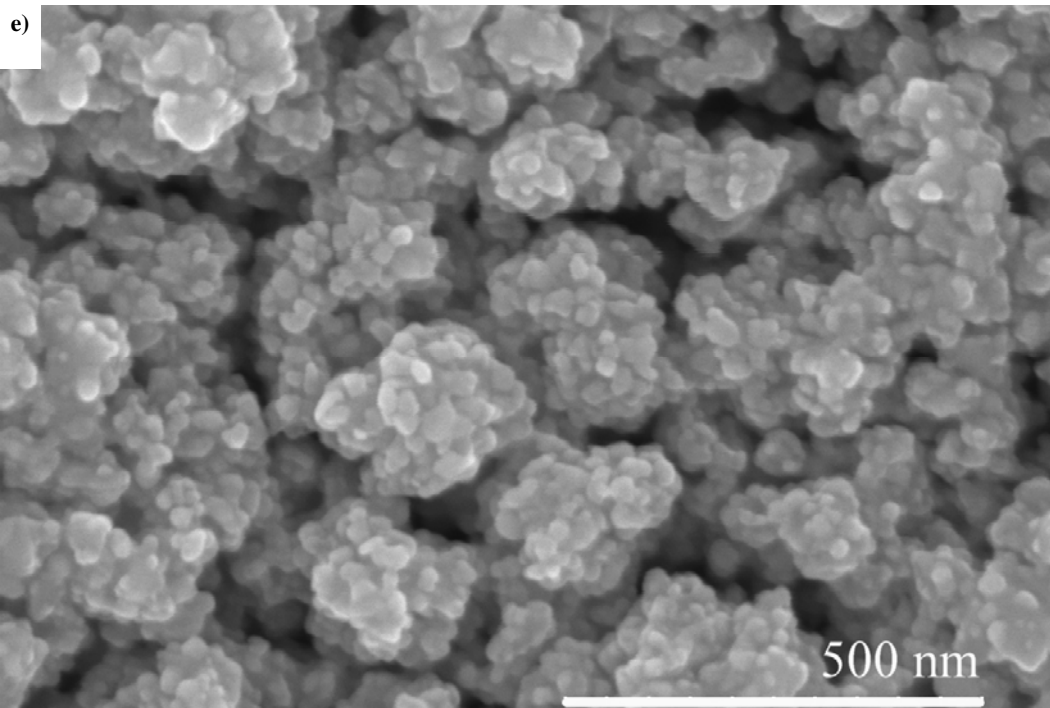
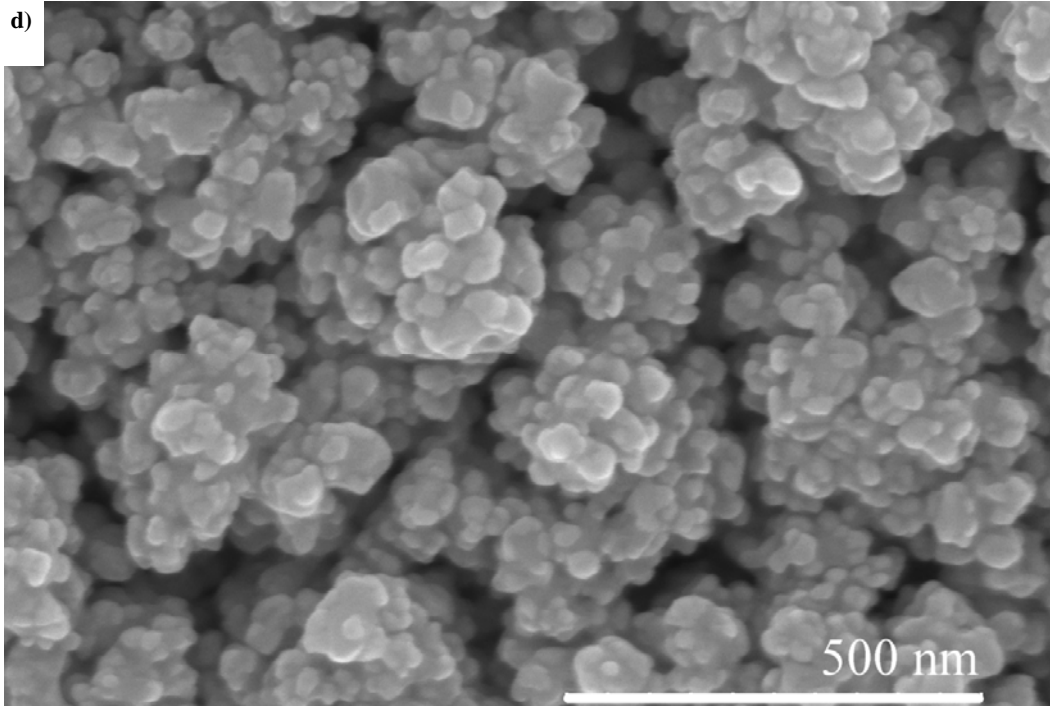


Figure 9-8, continued.

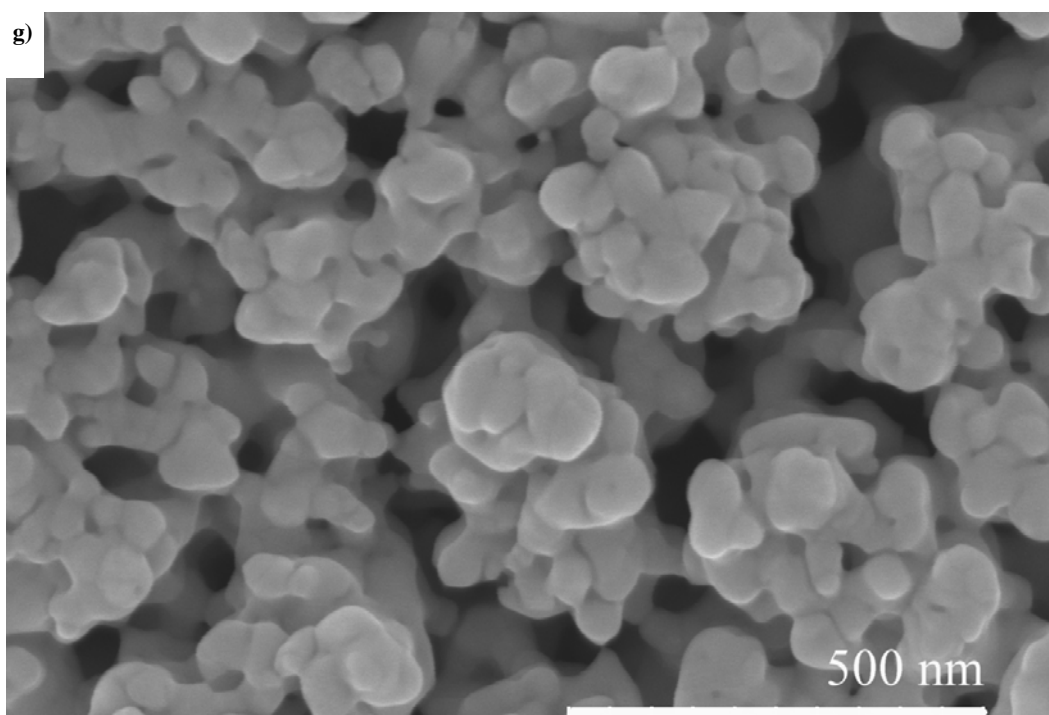
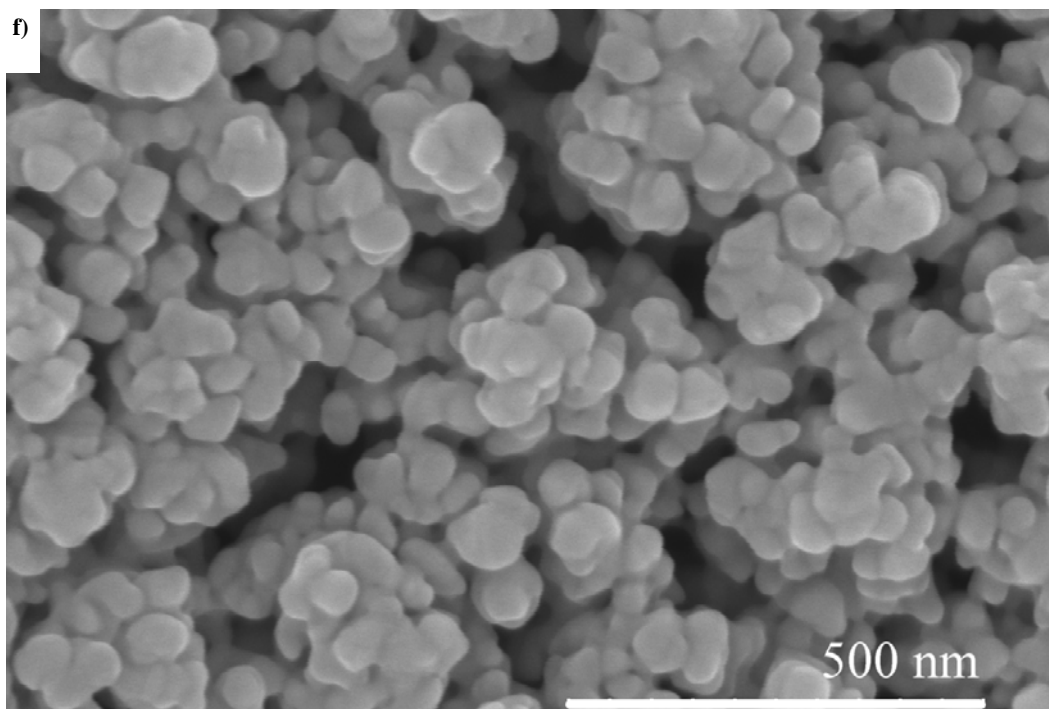


Figure 9-8, continued.

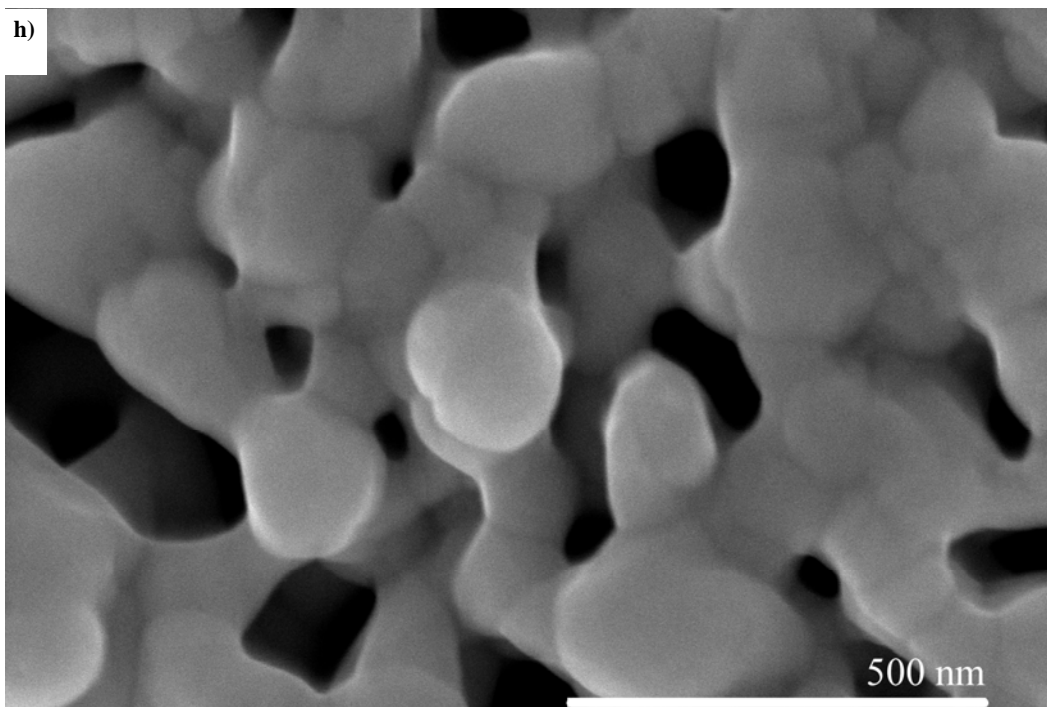


Figure 9-8, continued. SEM images of nanocrystalline silver dressings heat-treated for 24 hours. Samples were heat-treated at: a) 23°C b) 37°C c) 50°C d) 65°C e) 75°C f) 90°C g) 100°C and h) 110°C.

Table 9-1. Summary of XRD analysis, including domain size, composition and microstrain for nanocrystalline silver dressings heat-treated for 24 hours at various temperatures. Standard uncertainties are shown in brackets.

Temperature (°C)	Apparent crystallite size of Ag (nm)	Wt% Ag	Wt% Ag ₂ O	Lattice parameter of Ag ₂ O – <a> (Å)
23	14(2)	51(4)	49(4)	4.6744(6)
37	14(2)	51(4)	49(4)	4.6870(4)
50	13(3)	63(10)	37(10)	4.6956(9)
65	14(2)	59(5)	41(5)	4.7111(4)
75	14(2)	57(5)	43(5)	4.7133(3)
90	32(5)	71(8)	29(8)	4.7043(4)
100	67(8)	100	ND*	ND
110	149(15)	100	ND	ND

* ND = Not detected

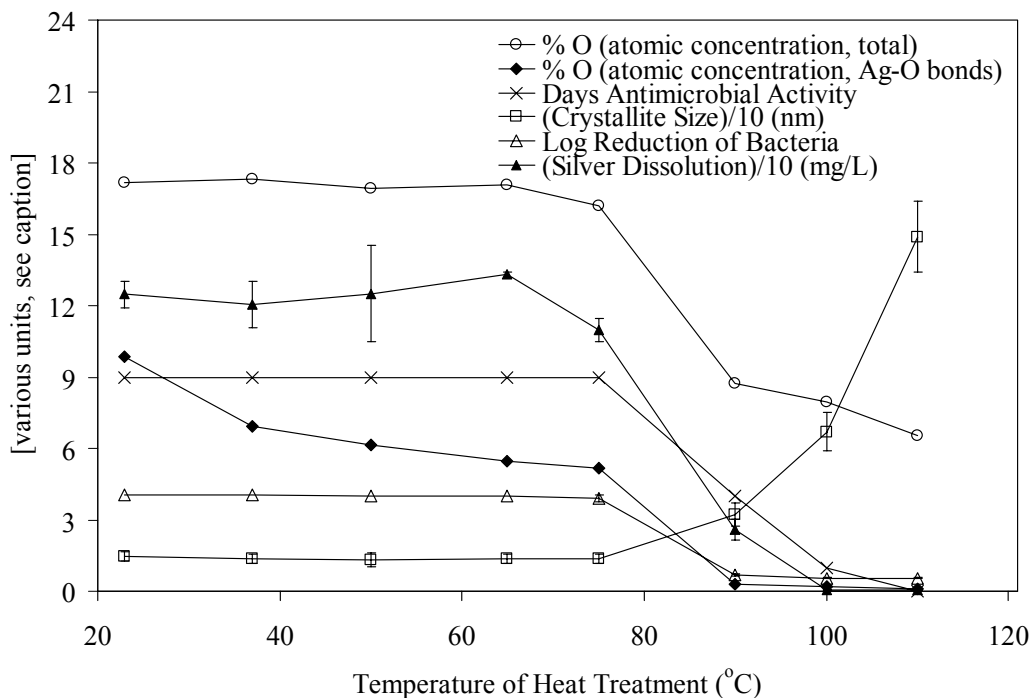


Figure 9-9. Comparison of atomic concentration of total oxygen and oxygen bonded to silver (determined via XPS, in percent), to crystallite size (determined via XRD, in nm/10, n=3), silver dissolution (in [mg/L]/10, n=3) and biological activity (*S. aureus* log reduction and days of activity data, n=3) after exposure of the dressing to various temperatures for 24 hours. The crystallite size and silver dissolution were scaled down by a factor of 10 to fit on the same scale as the other data. Standard deviations are shown as error bars for all data except atomic concentrations. Standard deviation for the biological data was very small.

Although the thermal instability of nanocrystalline silver was thus established, the kinetics of thermally induced physicochemical changes and their impact *in vivo* have not been studied. Understanding the critical properties required for good biological activity, and the impact of altering these properties via exposure to high temperatures, will not only provide insight into the mechanism of action of the material, but also into the practical aspects of working with nanocrystalline silver, such as production, product storage, and product usage. In this study, the impact of the kinetics of heat treatment on the physical and biological properties of nanocrystalline silver thin films was studied at

various temperatures which were previously shown to alter the properties of the dressings at 24 hours of heat treatment, with the purpose of defining critical properties for dressing activity.

Materials and Methods

Dressing Materials

Sterile nanocrystalline silver dressings (Acticoat®, Smith & Nephew Inc., Largo, FL, within expiry date) were used. The dressings were prepared by cutting 2.5 cm² samples aseptically. Samples underwent isothermal heat treatments at 90°C, 100°C, or 110°C for 2, 4, 6, 8, 16, 24, or 40.5 hours in a Fisher Scientific Isotemp oven preheated to the required temperature. During heat treatment, the samples were exposed to air with no humidity control. After heat treatment, the samples were stored in aluminum foil wrapped Petri plates at 4°C. The aluminum foil prevents photoreduction of the silver coating, while the Petri plates prevent contamination and exposure to moisture, and the low temperature prevents further changes to the dressings, such as crystal growth. All reagents, unless otherwise specified, were obtained from Fisher Scientific Inc. (Ottawa, Ontario, Canada). Materials and solutions were sterilized at 41 kPa and 121 °C.

Biological Assays

Bacterial Preparation

The bacterial strain used was *Pseudomonas aeruginosa* (ATCC 27317 Lot:3844749), a common wound and burn pathogen. It was stored on MHA at 4°C. Bacterial cultures were used in the log phase of growth with approximately 1.1×10^9 CFU *P. aeruginosa* per mL, for all tests. To obtain the log phase culture,

a few colonies of *P. aeruginosa* were taken from an agar culture and added to 100 mL TSB and grown overnight in a shaker incubator at 37°C, producing a culture in the stationary phase. Then, 1 mL of the culture was removed and added to 100 mL of TSB and incubated for 3 hours in order to obtain a culture in the log phase.

Log Reduction

In order to test each heat-treated sample for bactericidal efficacy, log reduction analyses, performed in triplicate, were completed following methods similar to those used by Taylor *et al.*[9]. Plastic squares were cut to a size slightly larger than the dressing samples, approximately 3.8 cm². A plastic square was placed in the center of a sterile Petri dish lid. Then, a dressing sample was placed on top of the plastic square and inoculated with 300 µL of the log phase *P. aeruginosa* culture, and then covered with a second plastic square. Finally, the bottom of the Petri dish was placed on top of the sample, to ensure complete contact of the dressing and the inoculant. The Petri plates containing the inoculated dressings were incubated for 30 minutes at 37°C. Following incubation, the dressings and the plastic squares were placed in 2.7 mL of a salt-polysorbate-sodium thioglycollate (SPS) bacterial recovery solution in order to deactivate ionic silver (preventing further antimicrobial activity) and to recover the bacteria. The SPS solution used was 0.85% [w/v] NaCl, 1 % [v/v] polysorbate 20, and 0.1% [w/v] sodium thioglycollate. The dressing samples and plastic squares were then vigorously vortexed to ensure all bacteria was brought into the bacterial recovery solution. The recovery solution was then serially diluted from 10⁻² to 10⁻⁷ using PBS (8.5 g/L NaCl, 0.61 g/L KH₂PO₄ and 0.96 g/L

K₂HPO₄). 20 µL from each solution was drop-plated in triplicate onto MHA plates that were then incubated at 37°C overnight. The same procedure as described above was done for controls, except that 300 µL of inoculant was directly added to 2.7 mL of SPS bacterial recovery solution. After 18-24 hours, the bacterial colonies were counted in order to determine the surviving number of CFUs. The controls were used to determine the number of CFUs in the original inoculum. The log reduction was then calculated by subtracting the log of the final CFUs from the log of the CFUs in the original inoculum.

Corrected Zone of Inhibition (CZOI)

CZOI tests were done to determine the time dependence of the antimicrobial activity of the nanocrystalline silver dressings after heat treatment. The CZOI procedure used was similar to that of Taylor *et al.*[9]. The test was performed in triplicate on samples heat-treated at 2, 4, 8, 16, and 24 hours for 90°C, 100°C, and 110 °C. MHA plates were seeded with 100 µL of *P. aeruginosa* in log phase and then 2.5 cm² silver dressing pieces were placed in the center of the plate with the nanocrystalline silver side down. The dressings were moistened with 350 µL of distilled water and then placed in an incubator at 37°C overnight.

The diameters of the zones of inhibition were measured, as well as the widths of the dressings. The CZOIs were then calculated by subtracting the dressing widths from the zone widths. A second CZOI was calculated for each dressing by measuring the zone of inhibition perpendicular to the first measurement. The two CZOI values were then averaged. Next, the dressing samples were transferred onto new MHA plates seeded with bacteria. If a sample

did not appear moist, 100 μL of distilled water was added. The plates were then incubated overnight.

For weekend storage, each dressing was aseptically removed from the agar plate and placed in a sterile plastic bag. The bags were wrapped in tinfoil and stored at 4°C over the weekend. To resume the experiment, the bacterial culture was first prepared on Day 1. On Day 2, dressings were removed from the refrigerator and allowed to warm to room temperature, in order to prevent thermal shocking of the bacteria and to maintain a consistent usage temperature. The regular procedure, as described above, was then followed.

Physical and Chemical Methods

Silver Dissolution

The amount of silver released into distilled water from heat-treated nanocrystalline silver dressings was measured via a static dissolution test. A procedure similar to that of Taylor *et al.*[9] was followed. Three 2.5 cm^2 samples were added to 15 mL of distilled water, in sterilized polyethylene cups, for a ratio of $2.5\text{ cm}^2/5\text{ mL}$ water. The cups were wrapped in aluminum foil and incubated without agitation for 24 hours at room temperature. After this, the dressings were removed, and the silver solutions were stored in the aluminum foil wrapped cups at 4°C (since samples were unpreserved) until they were analyzed.

Silver standard solutions were also generated, in order to calibrate the results. A 2000 ppm Ag^+ stock solution was made by dissolving 314.8 mg of silver nitrate in 100 mL of distilled water. The stock solution was serially diluted to produce 200, 20, 2, and 0.2 ppm Ag^+ solutions. The standard samples were

stored in the same manner as above.

Silver concentration of the above nanocrystalline silver and standard silver solutions were measured by a commercial laboratory, Sherritt Technologies Analytical, using a Varian SpectraAA 200 Atomic Absorption Spectrometer. The calibration range was 0 to 5 mg/L of silver in 10% nitric acid. A standard air-acetylene flame was used. The silver solutions were diluted with 10% nitric acid in water until a measurable concentration was reached – typically a 20 times dilution. Final values were reported with dilution taken into account.

A correction curve was created based on the difference between the actual and measured concentrations of the standards, which were performed in triplicate and averaged, to correct for machine error. All silver dissolutions were performed in triplicate for each heat treatment time-temperature combination, and the results were averaged and corrected using the correction curve.

Scanning Electron Microscopy (SEM)

SEM analyses of the dressings were done to “visualize” physical changes of the samples as heat treatment time increased at a given heat treatment temperature. SEM of the heat-treated samples was performed using a JAMP 9500F (JEOL) field emission SEM at the Alberta Centre for Surface Engineering and Science (ACES) at the University of Alberta. The SEM has a spatial resolution of 3 nm. Samples were mounted in a spring specimen holder. The samples were not cleaned to ensure that the structure of each sample was unaltered. The images were taken at magnifications of 5,000 to 100,000 times using an accelerating voltage of 25.0kV (15.0kV for 90°C samples), a working

distance of approximately 24 mm, and small-to-medium probe current.

X-ray Diffraction (XRD)

XRD was performed to study the structural changes of the silver. XRD analysis of the heat-treated silver dressing samples was performed on a Bruker D8 Advance diffractometer equipped with $\text{CoK}\alpha$, a monochromating multilayer mirror, and a VANTEC-1TM linear detector. Diffraction data were collected between 15 and $101^\circ 2\theta$. TOPASTM Rietveld refinement software (Bruker-axs, ©2003) was used to evaluate the composition, mean microstrain, and crystallite size of the crystalline phases, using LaB_6 (NIST 660) as an instrument standard. The microstructural analysis implemented in TOPASTM entails direct convolution of the instrument and sample contributions to the diffraction profiles followed by the double integral method of Balzar[11] to separate the crystallite size from the mean microstrain effect.

X-ray Photoelectron Spectroscopy (XPS)

XPS was used for elemental and oxidation state identification of the heat-treated nanocrystalline silver dressings. It was performed using an Axis 165 spectrometer (Kratos Analytical, at Alberta Centre for Surface Engineering and Science (ACSES) at the University of Alberta) with a base pressure of 2×10^{-10} Torr. The x-rays were generated by an Al Mono ($\text{K}\alpha$) source ($h\nu = 1486$ eV) operated at 210 W. The spectra were collected at normal (90°) take-off angle. For the survey spectra, the analyzer pass energy was 160 eV, and for the high-resolution spectra the pass energy was 20 eV. Linear background and Gauss/Lorentz component approximations were used in data processing

performed using CasaXPS software (Version 2.3.9, © 1999-2005 Neal Fairley).

Atomic concentrations of species were determined from the peak areas. No charge corrections to the binding energy values were introduced.

Thermal Analysis

Differential Scanning Calorimetry

Calorimetric studies were performed using a TA Instruments Model Q1000 differential scanning calorimeter (DSC). In order to measure changes in heat flow during grain growth, the samples were heated rapidly (20°C/min) up to isothermal hold temperatures of 90, 100, or 110°C, where they were held constant for 24 hours (100 and 110°C) or 50 hours (90°C), using nitrogen (50 mL/min) as the working gas. The reference cell was kept empty.

In preliminary experiments, it was determined that when pieces of the commercial dressing were placed in the calorimeter, silver was not present in sufficient quantities to provide a detectable signal during heat treatment, and that signals due to the plastic going through a glass transition were overwhelming any silver signal present. Thus, attempts were made to generate silver thin films with no backing. Nanocrystalline silver was sputtered onto silicon wafers at Nucryst™ Pharmaceuticals Corp. (Fort Saskatchewan, Alberta) under conditions used to create nanocrystalline silver dressings, or to create a coating 1.5 times as thick as nanocrystalline silver dressings. Attempts to delaminate the films from the silicon wafers by either scoring the films, doing a tape-lift off the films, breaking the silicon wafers, or snap-cooling the silicon wafers in liquid nitrogen were unsuccessful. Nanocrystalline silver was also sputtered onto Fomblin vacuum

grease-coated wafers at Nucrust. ~10 mg of Fomblin was added to each silicon wafer, which had a 5 centimetre radius, meaning the Fomblin coating was approximately 670 nm thick. Attempts such as those described above were used to try to delaminate the silver coating, but again these attempts were not successful. Similar attempts were made using olive oil, palm oil, flax oil, safflower oil, canola oil, sunflower oil, and lard, either heated (resulting in a thin layer), or unheated (resulting in a thick layer), using the in-house extreme magnetron sputtering machine. None of these coatings resulted in a nanocrystalline silver thin film that would delaminate, as the coatings did not hold together well enough. Attempts were also made to find plastics, such as petri plates, plastic bags, tape, HDPE, sample cup lids, and overhead transparencies, that would dissolve in diethyl ether or acetone, with the idea that the coatings could be dissolved away in a solvent that nanocrystalline silver thin films do not interact with, leaving the nanocrystalline silver film behind. Petri dishes and overhead transparencies appeared to dissolve the best, and therefore coatings were sputtered on to them. However, attempts to delaminate the silver coating were again unsuccessful. The nanocrystalline silver could be removed from plastic easily, but only as a powder, while acetone caused the nanocrystalline silver to flake off in small pieces, and the diethyl ether did not dissolve the plastic as well as in original testing - possibly due to changes to the plastic while under vacuum. Attempts were also made to sputter nanocrystalline silver onto salt and sugar crystals. The crystals were then dissolved in distilled water until the nanocrystalline silver thin films broke off in pieces, often rolling up. However,

large pieces were not obtained, and the effect of the dissolution time on the film was unknown, since nanocrystalline silver is soluble in distilled water. Silver was also sputtered onto nail-polish coated glass slides, in hopes that nail polish remover (acetone) could be used to dissolve the nail polish, releasing the nanocrystalline silver thin film, but again intact pieces were not obtained. Collection of small silver flakes out of the solutions was attempted using vacuum filtration, but the films were too delicate and were destroyed in the process. Samples had to be scooped out of solution (in the case of both water and acetone) and allowed to air dry. Some samples were still destroyed using this technique. Although samples collected from the salt crystal technique and the nail polish technique were submitted for calorimetry, no changes in heat flow were observed (data not shown), suggesting that insufficient sample weight was collected using this method. It should be noted that the samples sputtered onto the various oils, plastics, and crystals were sputtered at 10-12% oxygen for 10 minutes, which were later determined not to be the ideal conditions for generating nanocrystalline silver films with the properties of nanocrystalline silver dressings (see Chapter 8). This may partially explain the poor calorimetric results for samples tested that were obtained by the salt crystal dissolution method or the nail polish removal method, but does not explain the difficulties in delaminating the films, as the films created at NucrystTM did not delaminate either, despite using conditions identical to those used for the nanocrystalline silver dressings. Poor heat flow between the sample flakes and the calorimetry sample holder may have also been an issue.

Finally, flat-bottomed aluminum sample cells were masked and placed at the centre of the racetrack of the in-house extreme magnetron sputtering machine, and pure (99.99%) silver was sputtered directly onto the cells via physical vapor deposition at a total pressure of 40 mTorr, with 4% oxygen (99.993% purity) and 96% argon (99.998% purity), a current of 0.9 A, and a target-to-substrate distance of 10 cm for 30 minutes, as Chapter 8 demonstrated that these conditions resulted in nanocrystalline silver thin films with the properties of the commercial antimicrobial dressing, when using the in-house sputtering system. ~0.3 mg of silver was sputtered onto the masked sample cells. This improved heat transfer between the silver and the sample cell. Similarly, nanocrystalline silver thin films were sputtered onto sheets of aluminum foil (Alcan Inc., Montreal, Quebec, Canada), and portions of the foil were layered into the sample cells, which were then closed up and analyzed promptly to ensure that the samples did not begin to re-crystallize. If there was any delay between sample preparation and analysis, samples were stored at 4°C in dark sealed containers. The layering of silver-sputtered aluminum foil allowed for a larger quantity of silver to be analyzed (~6 mg of silver was added via the addition of aluminum foil), and improved heat transfer relative to layering the commercial dressing with the HDPE backing. In addition, aluminum foil did not undergo any thermal changes during the heat treatment process, since during processing it is thinned at 450-540°C, so no additional changes occur at the temperatures used. This is why aluminum boats are used for DSC.

Statistical Analysis

One-way ANOVAs with Tukey-Kramer Multiple Comparisons post tests were performed using GraphPad InStat version 3.06 (GraphPad Software, San Diego, California, USA, © 2003, www.graphpad.com). Error bars, which represent standard deviations, are present for all data points in Figures 9-10, 9-11, 9-12, and 9-15. Some error bars are very small due to low variability in experimental data.

Results

Biological Assays

Log Reduction

Log reductions of *P. aeruginosa* after various heat treatment times are displayed in Figure 9-10 for heat treatment temperatures of 90, 100, and 110°C. For the entire 90°C heat treatment set, the nanocrystalline silver dressings produced log reductions greater than 5.69. No bacteria were detected at any dilutions for all time points out to 24 hours, and a 5.69 log₁₀ reduction was the maximum measurable log reduction with the original inoculum concentration used and detection limit of this experiment. The 100°C heat treatment set showed decreased bactericidal activity starting between 8 and 14.5 hours. The 110°C heat treatment set showed a decrease in activity between 4 and 8 hours, with statistically significant decreases in activity by 24 hours.

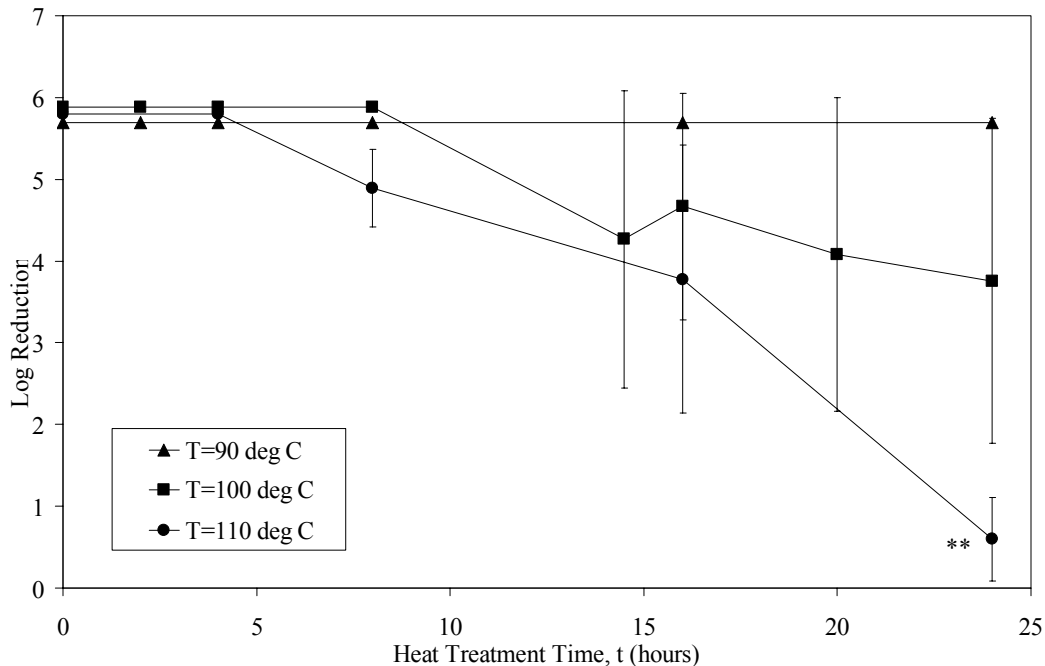


Figure 9-10. Log reductions of *P. aeruginosa* exposed to nanocrystalline silver dressings heat-treated at 90, 100, or 110°C for various times. Error bars show standard deviations. * indicates $p < 0.05$, ** indicates $p < 0.01$, *** indicates $p < 0.001$, as compared to non-heat treated dressings, using one-way ANOVA tests with Tukey-Kramer Multiple Comparisons post tests ($n=3$ for each time point at each temperature).

Corrected Zones of Inhibition

In Figure 9-11, the CZOIs for *P. aeruginosa* are shown for each day that nanocrystalline silver dressings (heat-treated for various times at 90, 100, or 110°C) were exposed to fresh cultures. Loss of longevity was defined as the day the CZOI values were significantly lower than those of the control dressings for that day. Once dressings began to produce CZOI values significantly lower than those of the controls, they continued to do so for the duration of the experiment. For 90°C heat treatments (Figure 9-11a), loss of longevity was observed for dressings heat-treated for 16 hours starting on Day 7, and for the 24h heat-treated dressings starting on Day 5. For 100°C heat treatments (Figure 9-11b), loss of

longevity began at Day 8 for the 8 hour heat treatment, at Day 5 for 16 hour heat treatment, and at Day 1 for the 24 hour heat treatment. The 110°C heat-treated dressings (Figure 9-11c) showed a loss of longevity at Day 5 for the shortest heat treatment time of 4 hours, at Day 2 for the 8 and 16 hour heat treatments, and at Day 1 for the 24 hour heat treatment.

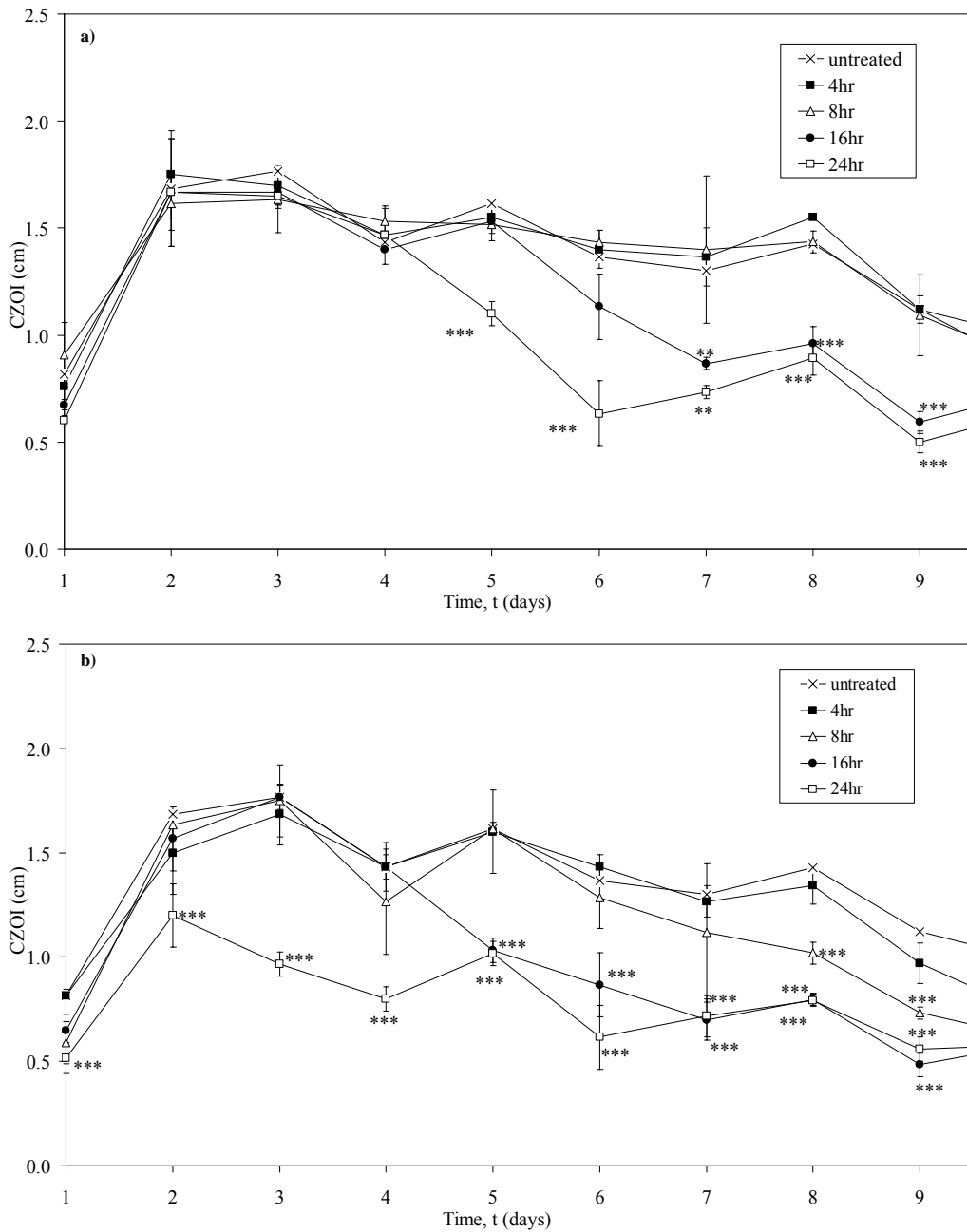


Figure 9-11.

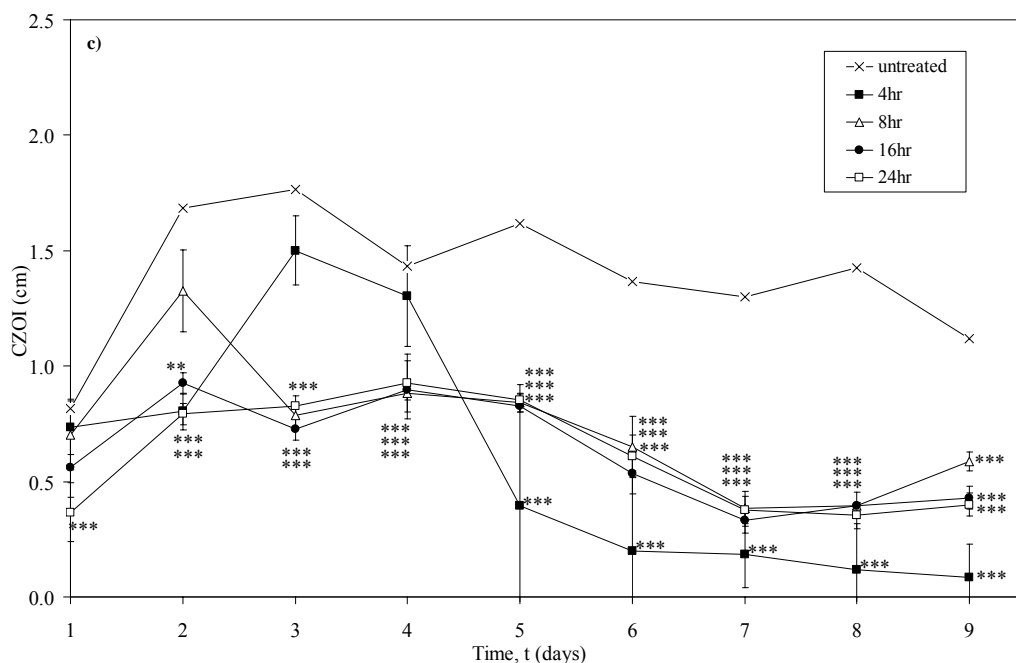


Figure 9-11, continued. Corrected zones of inhibition for *P. aeruginosa* over a series of days in response to nanocrystalline silver dressings heat-treated for various times. Samples were heat-treated at a) 90°C, b) 100°C, and c) 110°C (n=3 for each temperature at each time point). Error bars show standard deviations. * indicates $p < 0.05$, ** indicates $p < 0.01$, and *** indicates $p < 0.001$, as compared to non-heat treated dressings, using one-way ANOVA tests with Tukey-Kramer Multiple Comparisons post tests.

Physical and Chemical Assays

Silver Dissolution

Figure 9-12 shows the total silver released from nanocrystalline silver dressings (which had been heat-treated for various times at 90°C, 100°C, or 110°C) after the dressings were soaked in distilled water at room temperature for 24 hours. The total silver released from the 90°C heat treatment set was not statistically different from control samples (not heat treated) at any heat treatment time. The silver released from nanocrystalline silver dressings heat-treated at 100°C began to decrease at 8 hours of heat treatment, reaching statistical

significance by 20 hours of heat treatment. Lastly, for the 110°C heat treatment set, the total silver released was significantly lower than the untreated control samples after 4 hours of heat treatment, and continued to drop with increasing heat treatment time. By 24 hours of heat treatment, the total soluble silver was less than 1 mg/L.

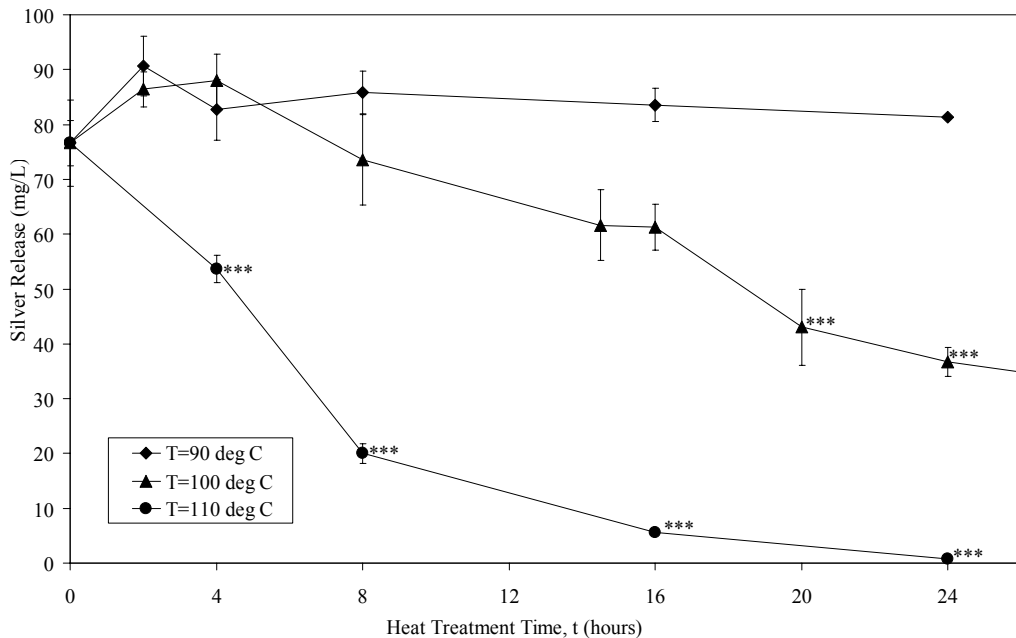


Figure 9-12. Total release of silver in water after a 24 hour dissolution versus nanocrystalline silver dressing heat treatment time at temperatures of 90, 100, and 110°C. Error bars show standard deviations. * indicates $p < 0.05$, ** indicates $p < 0.01$, and *** indicates $p < 0.001$, as compared to non-heat treated dressings, using one-way ANOVA tests with Tukey-Kramer Multiple Comparisons post tests ($n=3$ for each time point at each temperature).

SEM Analysis

SEM images were taken of nanocrystalline silver dressings heat-treated for various times at 90°C, 100°C, and 110°C (Figure 9-13). An image of an untreated sample is shown in Figure 9-8a. In the 90°C image, fine features remained apparent after 24 hours of heat treatment (Figure 9-13a), although some evidence of change was observed. In the images of dressings heat-treated at

100°C, no significant changes in the microstructure were apparent until 8 hours of heat treatment. Between 4 hours (Figure 9-13b) and 8 hours (Figure 9-13c), the 100°C heat-treated samples began to coarsen, as evidenced by the necking and size increase of the agglomerates. The loss of finer features, which were visible in the control and 4 hour heat-treated samples, was apparent in the images after 8 hours of heat treatment (Figure 9-13 c through e). The 110°C heat treatment set began to coarsen immediately, between 0 and 4 hours of heat treatment, which was evident by the significant necking and increase in pore sizes by 4 hours (Figure 9-13f). Coarsening continued, with increased size of agglomerates, as time of heat treatment increased. Between 4-8 hours (Figure 9-13 f through g), most of the finer particles that were present on control samples were no longer visible, and they were completely gone by 16 and 24 hours (Figure 9-13 h to i). Overall, the loss of finer features, coarsening, rounding of edges, and loss of surface area occurred earlier at higher temperatures. As well, loss of finer features was the first change to occur at all heat treatment temperatures when the material began to coarsen.

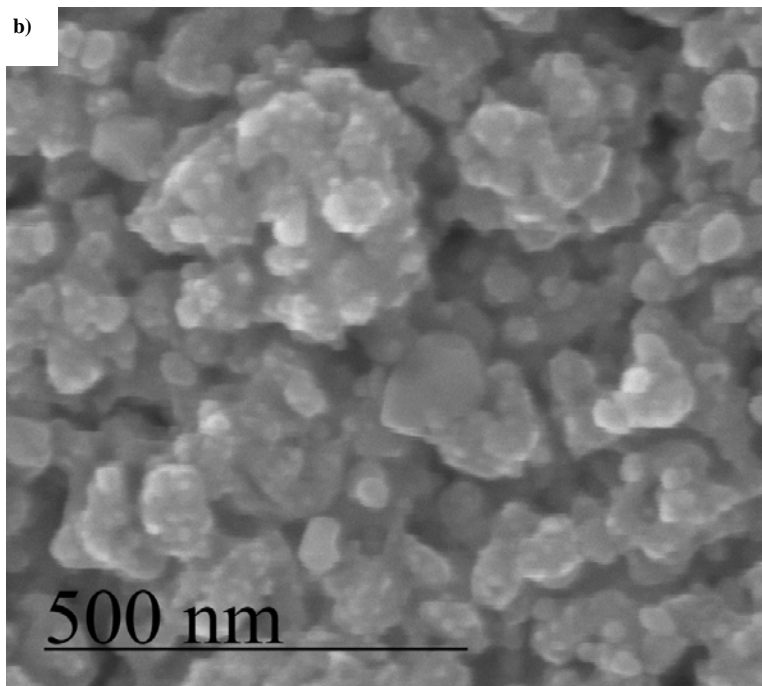
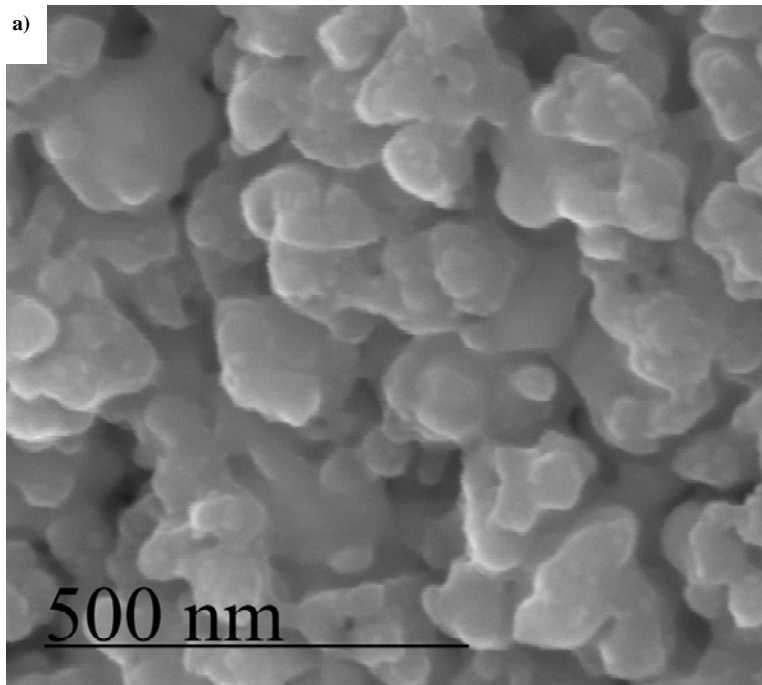


Figure 9-13.

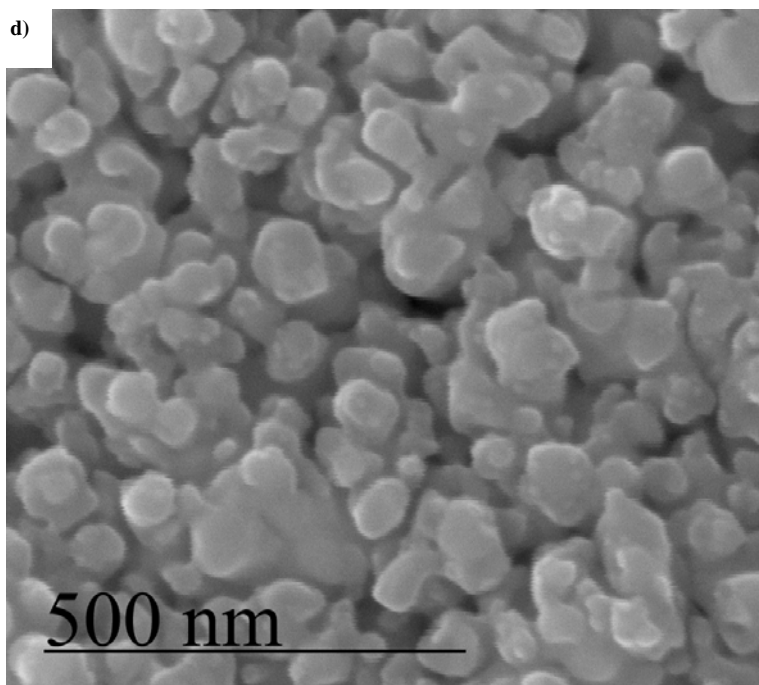
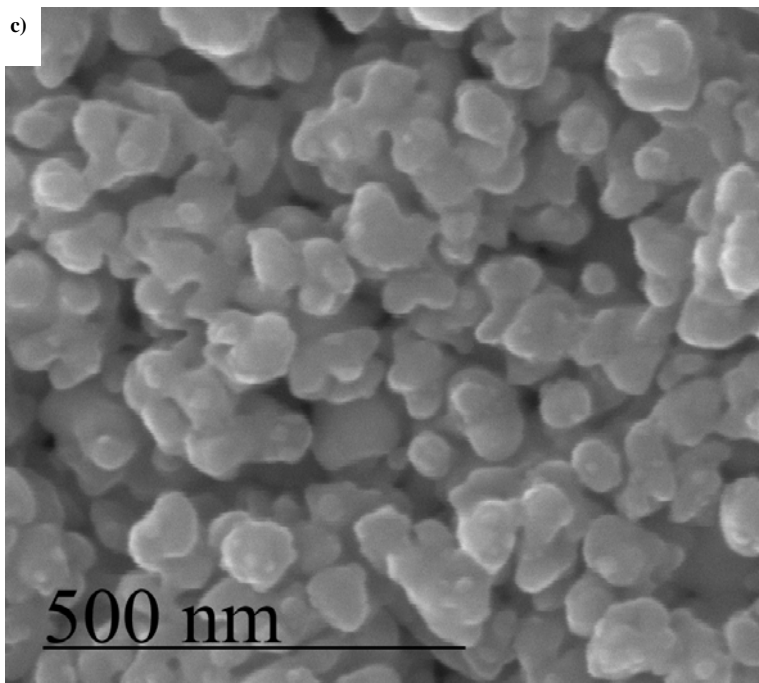


Figure 9-13, continued.

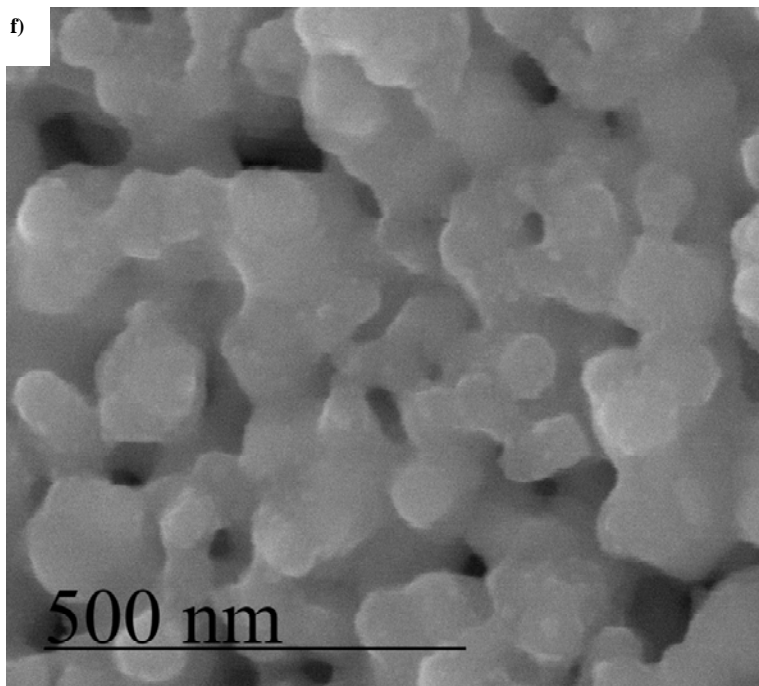
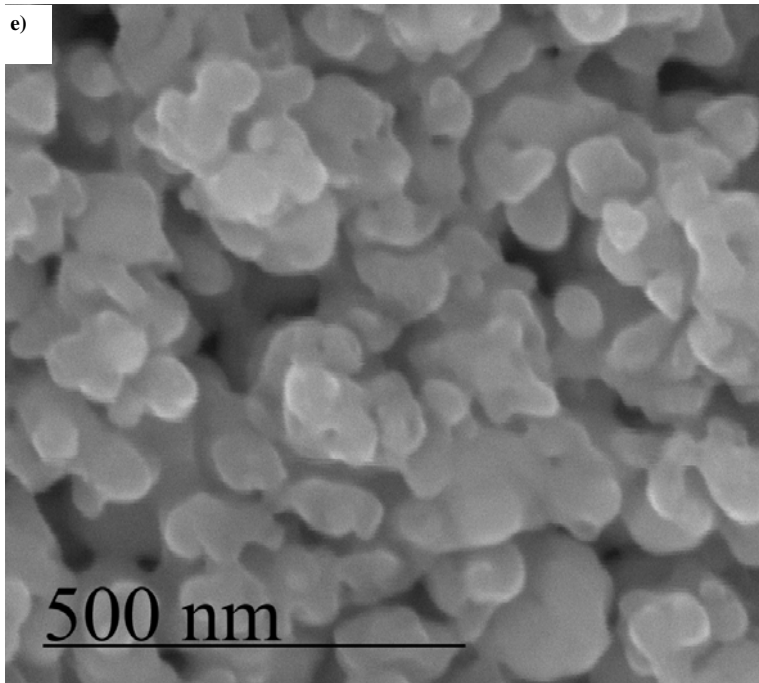


Figure 9-13, continued.

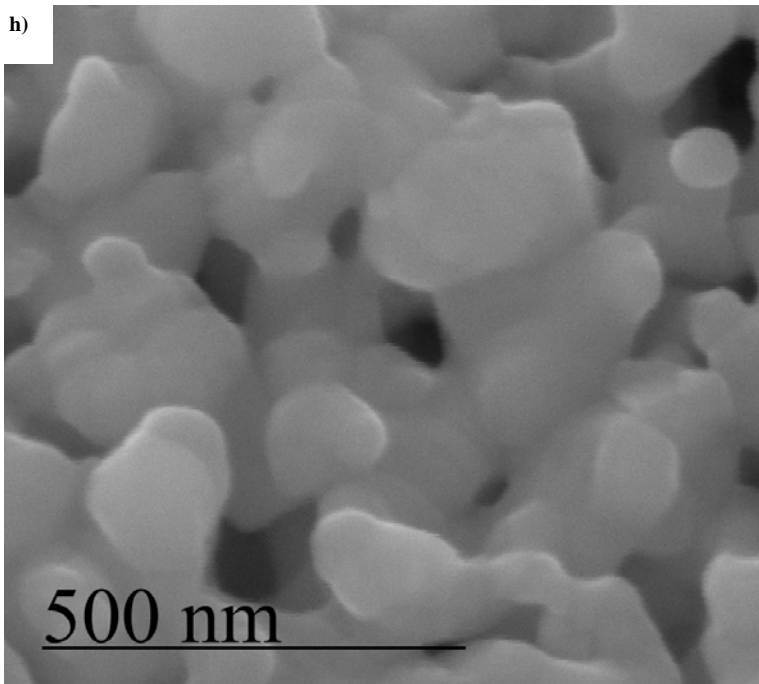
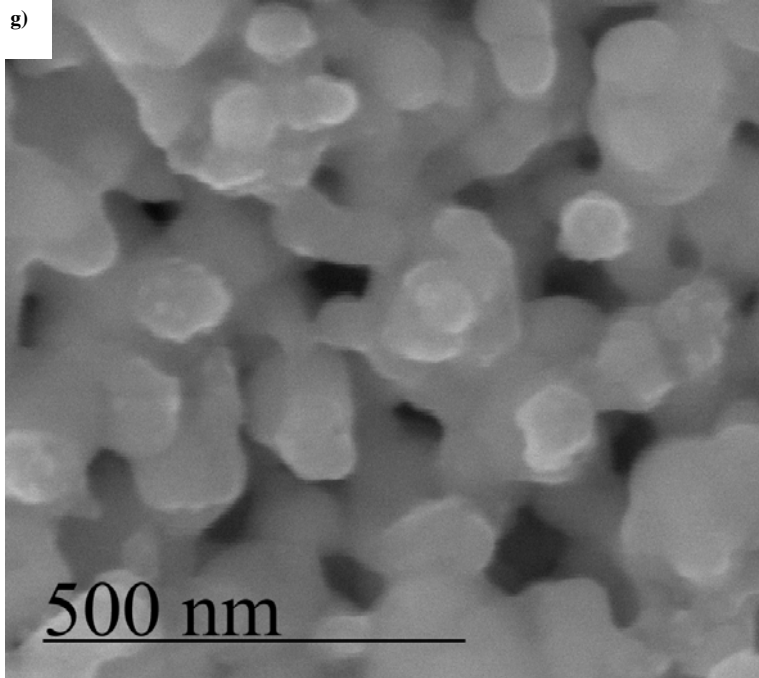


Figure 9-13, continued.

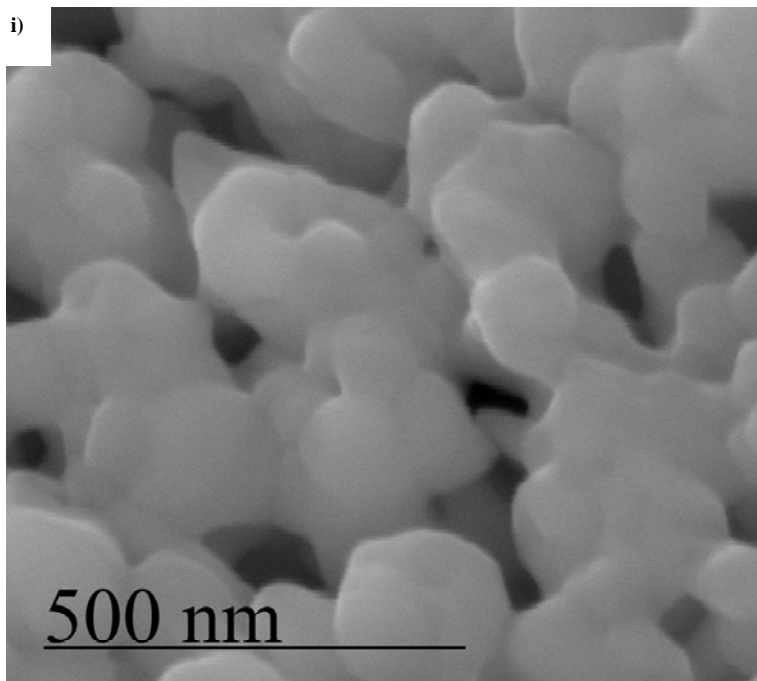


Figure 9-13, continued. SEM images of heat-treated nanocrystalline silver dressings. Samples imaged were heat treated at a) 90°C for 24h, b) 100°C for 4h, c) 100°C for 8h, d) 100°C for 16h, e) 100°C for 24h, f) 110°C for 4h, g) 110°C for 8h, h) 110°C for 16h, and i) 110°C for 24h.

XRD Analysis

Nanocrystalline silver dressings heat-treated at 90, 100, or 110°C for various times were analyzed by XRD to determine the change in structure over time. The starting structures used in the refinement were Ag(*Fm-3m*), Ag₂O (*Pn-3m*), and HDPE (*Pna2₁*). Figure 9-14 displays the diffraction patterns for each heat treatment set. The Delnet pattern shows HDPE without the nanocrystalline silver coating.

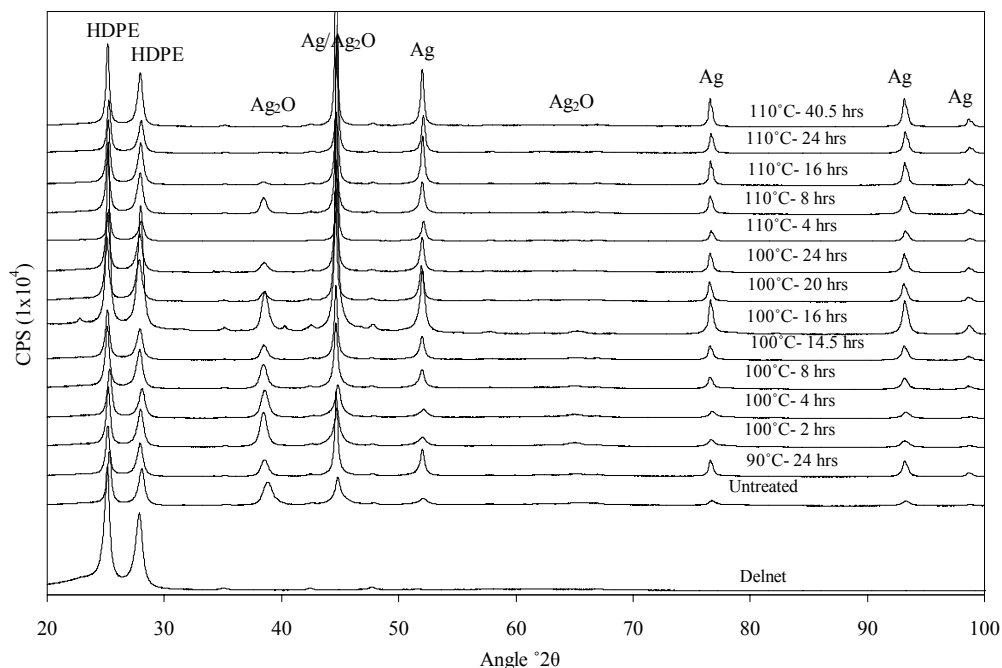


Figure 9-14. Diffraction patterns of nanocrystalline silver dressings after isothermal holds at indicated times and temperatures.

Table 9-2 displays the apparent crystallite size, relative metallic silver and silver oxide content, and lattice parameter for each sample. The XRD-measured crystallite sizes all have small standard deviations. Crystallite growth began within a very short time at elevated temperatures. The crystallite size began to change between 8 and 16 hours with 90°C heat treatment, and had more than doubled by 24 hours. After only 4 hours at 100°C, the average crystallite size increased by 6 nm. Crystallite size steadily increased over time, more than doubling its size in 24 hours. A similar but more rapid growth was seen for the 110°C heat treatment set, with the crystallite size doubling in the first 4 hours (33 nm), and more than tripling at 24 hours (42 nm). A corresponding trend is seen in which the percentage of Ag₂O decreased with time for all heat treatment sets, as the silver oxide was converted to metallic silver.

Table 9-2. XRD analysis of nanocrystalline silver dressings heat-treated at 90, 100, and 110°C for various times.

Temperature (°C)	Time (h)	Apparent Ag crystallite size (nm)	Wt% Ag	Wt% Ag ₂ O	Lattice parameter of Ag ₂ O- <i>a</i> (Å)
Control	0	13 (3) ^a	48 (10)	52 (5)	4.6824(3)
90	2	13 (3)	55	45	4.7043(3)
90	4	12 (3)	58	42	4.7111(3)
90	8	13 (3)	60	40	4.7138(3)
90	16	27 (3)	72	28	4.6947(4)
90	24	31 (3)	83	17	4.7002(4)
100	2	17 (3)	55 (9)	45 (4)	4.7148(2)
100	4	19 (3)	55 (6)	45 (3)	4.7162(2)
100	8	25 (3)	72 (6)	28 (2)	4.7053(3)
100	14.5	31 (3)	83 (8)	17 (2)	4.7024(4)
100	20	35 (3)	90 (8)	10 (1)	4.6987(5)
100	24	36 (3)	90 (8)	10 (1)	4.6972(7)
100	40.5	37 (3)	93 (10)	7 (1)	4.7002(7)
110	4	33 (3)	86 (8)	14 (1)	4.688(4)
110	8	42 (3)	96 (8)	4 (3)	4.7098(4)
110	16	39 (3)	97 (9)	3 (1)	4.715(1)
110	24	42 (3)	100	trace	4.706(3)

^aStandard uncertainties are shown in brackets.

Figure 9-15a shows how the ratio of Ag₂O:Ag dropped exponentially with heat treatment time, calculated based on the x-ray diffraction data. Loss of bactericidal activity occurred after the ratio of Ag₂O:Ag dropped below 0.16.

Figure 9-15b shows that a linear relationship exists between silver crystallite size and the ratio of Ag₂O:Ag, when all x-ray diffraction data is combined, with the silver crystallite size increasing as the ratio of Ag₂O:Ag dropped.

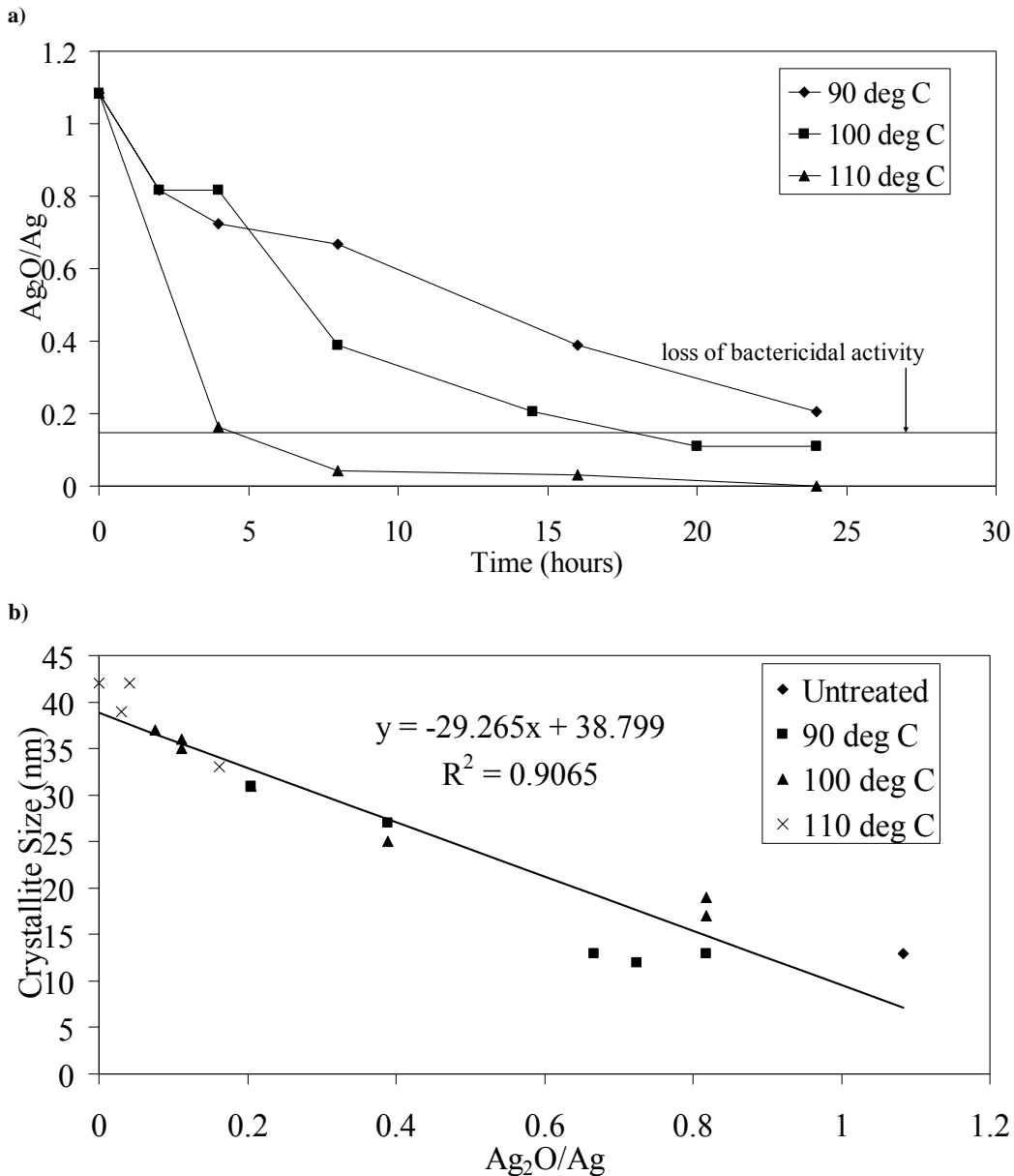


Figure 9-15. Comparison of the ratio of silver oxide to metallic silver over time and relative to crystallite size. a) Comparison of the ratio of silver oxide to metallic silver over time for heat treatments at 90, 100, and 110°C, based on x-ray diffraction data. Loss of bactericidal activity occurs with the loss of a certain percentage of the silver oxide pinning structure (horizontal line). b) Silver crystallite size as a function of the ratio of silver oxide to metallic silver is shown. The best fit line and the equation for it are shown, combining the data of all three heat treatment temperatures (90°C, 100°C, and 110°C).

Grain growth curves for all isothermal hold temperatures were graphed (Figure 9-16a) from the XRD data. Comparing this data to the times at which bactericidal activity dropped, loss of bactericidal activity appeared to correspond to increased crystallite size to a critical value between 30 and 35 nm. Isothermal grain growth kinetics in an ideal system can be described by the following equation:

$$d^n - d_0^n = Kt \quad (1)$$

where d and d_0 are the isothermal holding time grain size and initial grain size, respectively, K is a constant, t is the isothermal hold time, and n is the grain growth exponent[12]. To determine the grain growth exponent, Equation 1 was graphed for a range of n values between 0 and 5. A linear best fit line was plotted for data points that were in the grain growth region. R^2 for the linear best fit line was found to be closest to 1 when $n=2.8$ was used for the isothermal hold temperatures of 100 and 110°C (Figure 9-16b). Following the same method, a grain growth exponent of $n=4.9$ was found for the 90°C isothermal hold grain growth curve.

The activation energy for grain growth (Q) is found using the following equation:

$$K = K_0 \exp\left(\frac{-Q}{RT}\right) \quad (2)$$

where K is the constant from Equation 1, K_0 is a pre-exponential constant, and R is the gas constant[12]. K values for 100 and 110°C were obtained from the slope of Figure 9-16a. In order to determine the activation energy, Equation 2 was linearized and graphed as $1/T$ versus $\ln(K)$. The activation energy required for

grain growth was found to be 177 kJ/mol (1.77 eV). Since only two data points were used, an R^2 value has no significance and therefore is not reported.

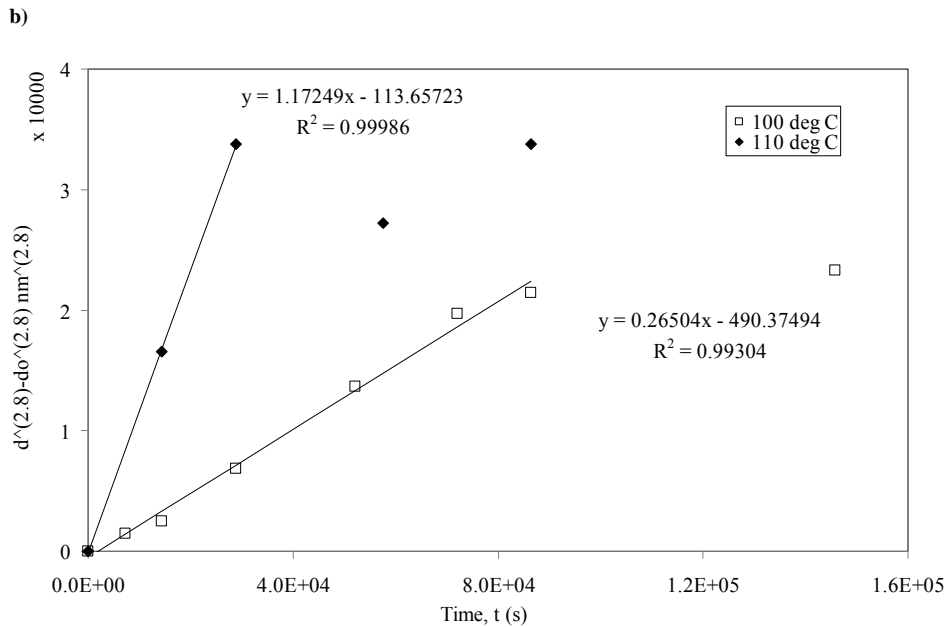
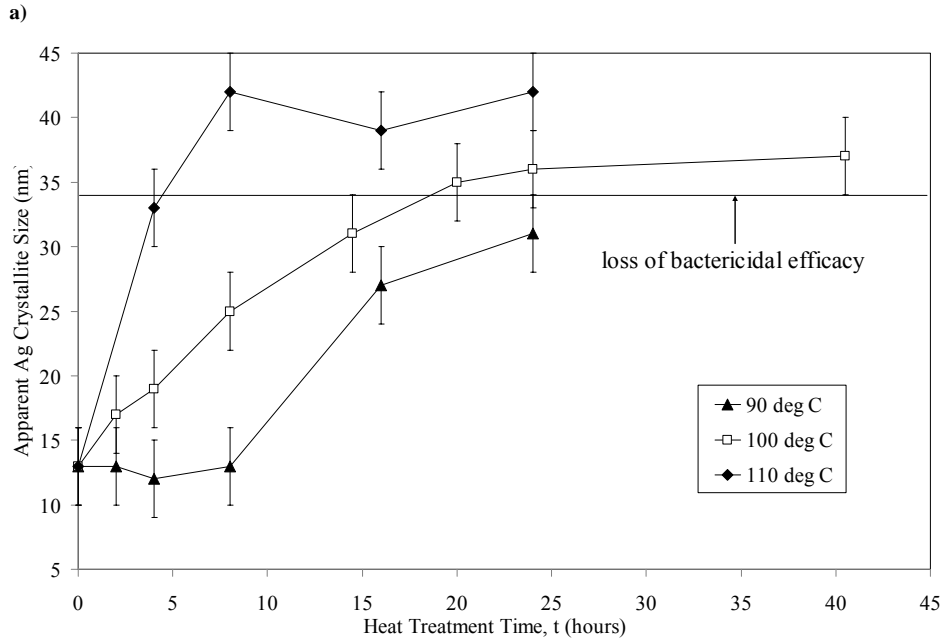


Figure 9-16. Grain growth curves and exponents. a) Grain growth curves for nanocrystalline silver dressings with isothermal holds at 90, 100 and 110°C. Loss of bactericidal activity occurs after a critical crystallite size is reached (horizontal line). b) Determination of grain growth exponents for 100 and 110°C isothermal holds.

XPS Analysis

Figure 9-17 displays the raw XPS spectral data for oxygen (a) and silver (b) bonds. Curve fittings were performed on all XPS spectra obtained (not shown). In the oxygen spectra (Figure 9-17a), two major components related to O-O and O-Ag bonds, positioned at binding energies of 530.7 and 529.2 eV, were observed for untreated samples. With heat treatment at high temperatures, the O-Ag contribution decreased with time, disappearing completely between 24 and 40.5 hours with 100°C heat treatments, and between 8 and 16 hours with 110°C heat treatments. While the O-Ag component also appeared to decrease with 90°C heat treatments, it was still present at 24h and no clear trends were observed. In the silver spectra (Figure 9-17b), the doublet Ag 3d peaks became sharper for 100°C and 110°C heat-treated samples as time increased, but did not change for 90°C heat-treated samples. The doublet Ag 3d peaks shifted to higher binding energies as heat treatment times increased, particularly with heat treatments at 100 and 110°C. In the 90°C heat-treated samples, there was no clear trend in terms of binding energy shift. The width and position of the doublet peaks at lower heat treatment temperatures was due to the overlapping of peaks related to Ag-Ag and Ag-O bonds, with Ag 3d 5/2 peaks positioned at about 368.1 and 367.6 eV, respectively. Thus, the sharpening and shifting of the peaks at higher heat treatment temperatures corresponds to loss of the silver-oxygen bonds. XPS data from 90°C heat-treated samples did not show a clear loss of silver-oxygen bonds while heat treatment at higher temperatures did, with the loss of silver-oxygen bonds beginning before 4 hours with heat treatments at 110°C, and

between 14 and 16 hours with heat treatments at 100°C.

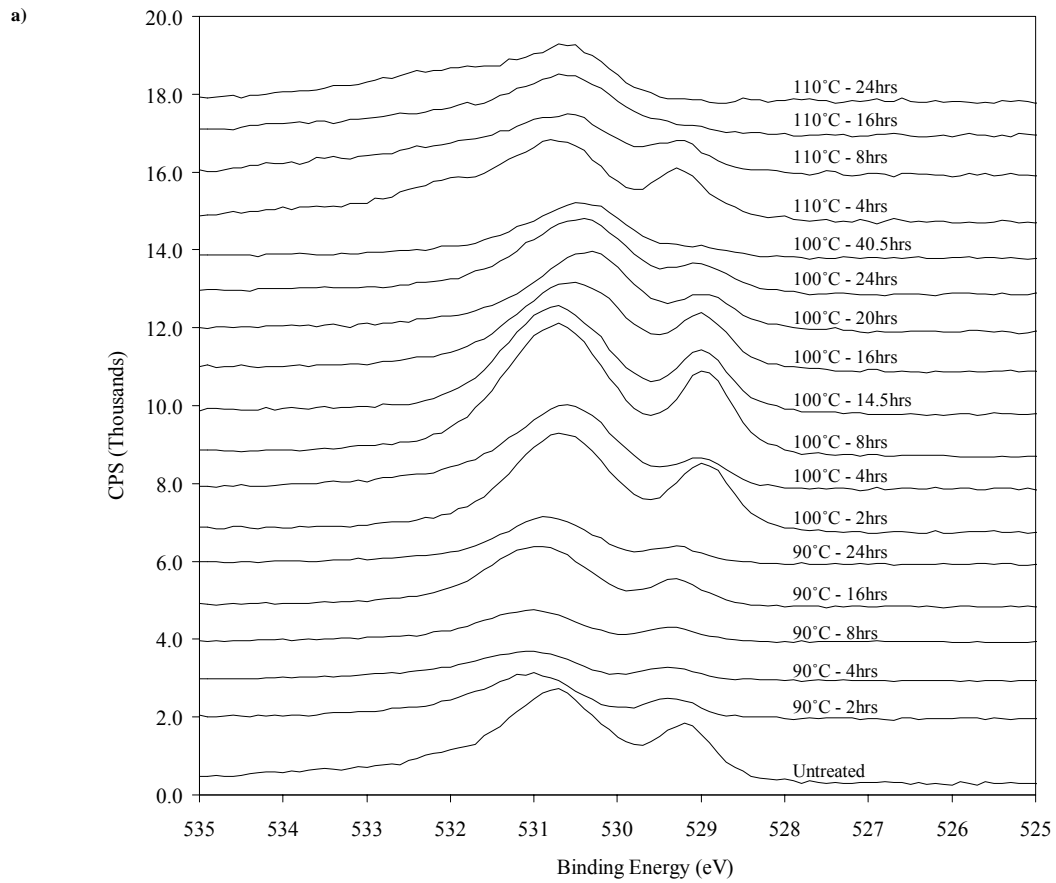


Figure 9-17.

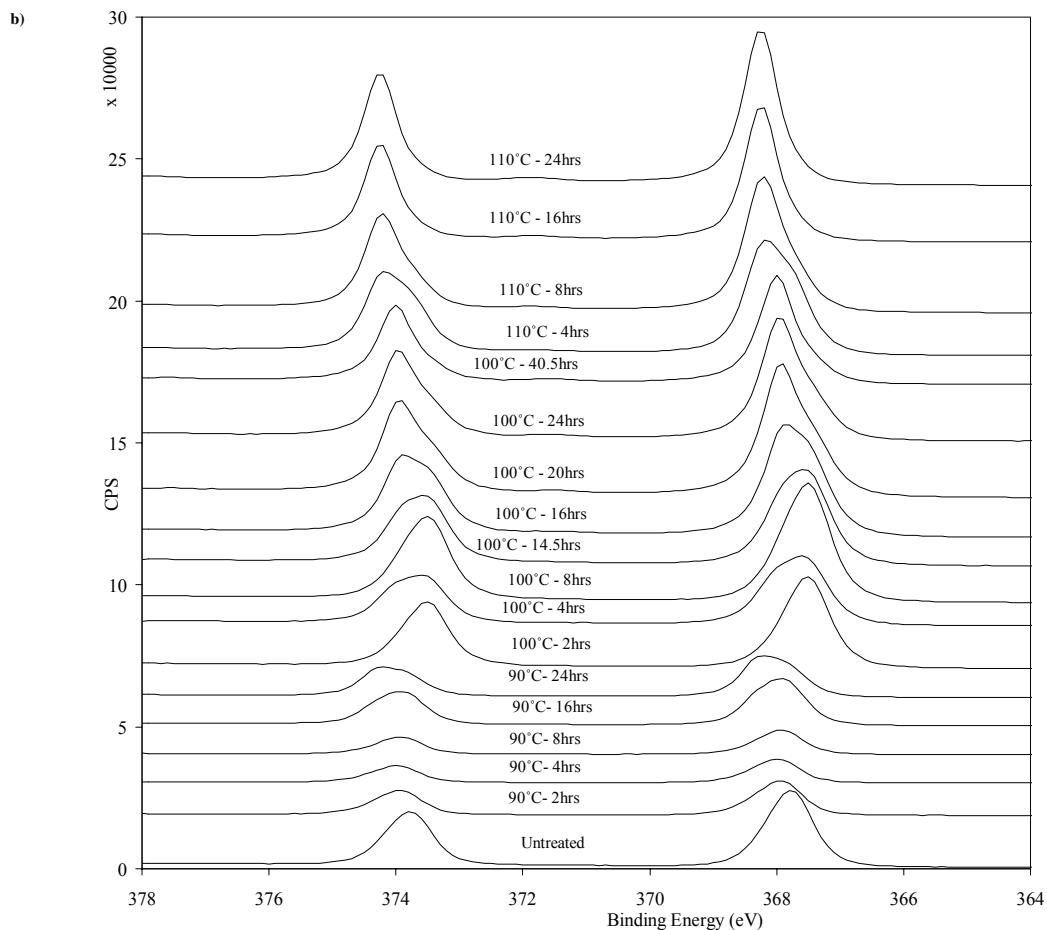


Figure 9-17, continued. Raw XPS data of heat-treated dressings. a) XPS intensities of O 1s peaks for nanocrystalline silver dressings after isothermal holds at indicated times and temperatures. b) XPS intensities of Ag 3d peaks for nanocrystalline silver dressings after isothermal holds at indicated times and temperatures.

The XPS spectra were used to determine the atomic percentage of oxygen in bonds with silver and the total oxygen present in the dressing (Figure 9-18). There were no clear trends in terms of oxygen content with 90°C heat treatment. With 100°C isothermal holds, the total oxygen began to drop by 16 hours, and in the 110°C isothermal hold, it began to drop immediately (prior to 4 hours). A similar pattern was observed for the silver-oxygen bonds.

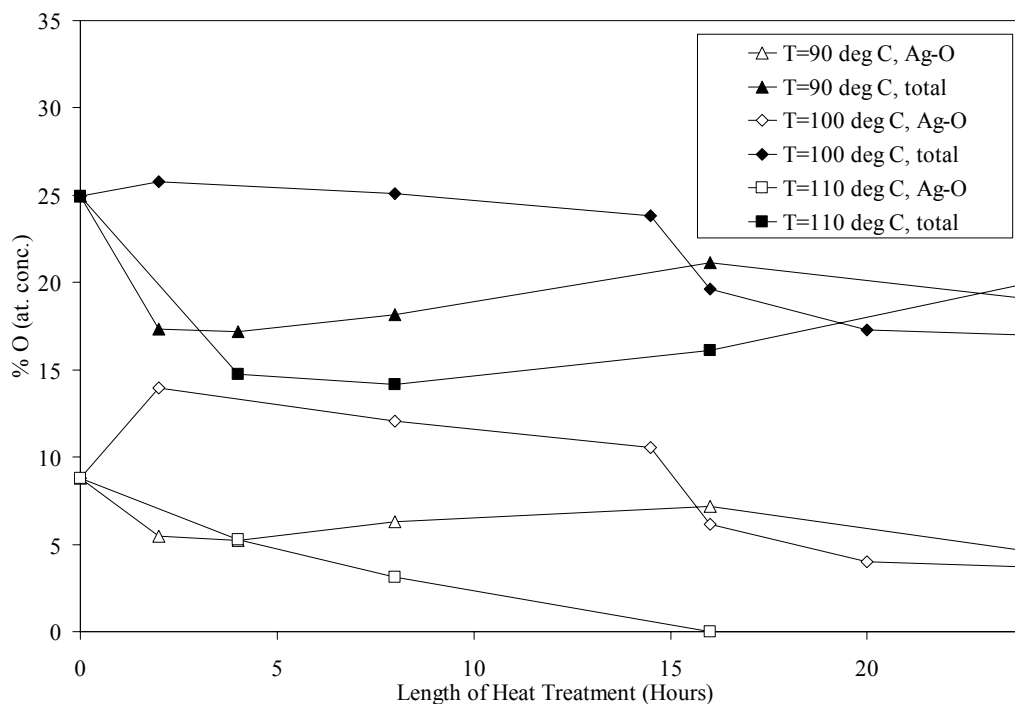


Figure 9-18. Oxygen percentage in heat-treated nanocrystalline silver dressing samples at 90, 100, and 110°C for various times.

Thermal Analysis

Differential Scanning Calorimetry (DSC)

Figure 9-19 shows the heat flow over time for an isothermal hold at 100°C for 20 hours. The sample was a masked aluminum sample cell sputtered under the following conditions: 12% oxygen, 88% argon, 1 A current, for 10 minutes (with other conditions as described in the methods section). The results of Chapter 8 indicate that this was a pure nanocrystalline silver oxide film. Analysis of the x-ray diffraction patterns for samples generated under the same conditions for the analyses of Chapter 8 indicated that the silver oxide was very similar in size and cell constant to the silver oxide present in nanocrystalline silver dressings (personal communication, Dr. Oladipo Omotoso, May 8, 2009). An initial change in heat flow (exothermic) occurs between 250-350 minutes (4.2-5.8 hours). A

larger change in heat flow occurred starting about 860 minutes (14.3 hours) which was not completed at 20 hours.

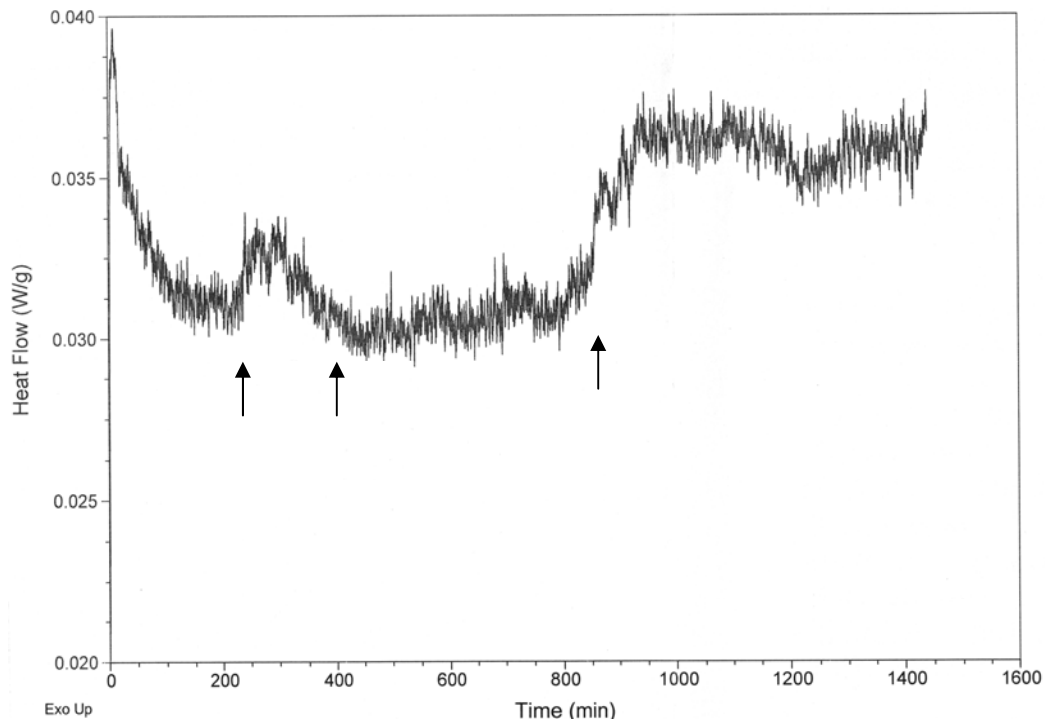


Figure 9-19. Differential scanning calorimetry of nanocrystalline silver oxide sputtered on an aluminum sample cell. Heat flow was measured over 20 hours for an 100°C isothermal hold in a differential scanning calorimeter for a sample cell sputtered with a pure nanocrystalline silver oxide film (12% oxygen, 88% argon, 10 minutes, 1A). Key time points are indicated with arrows.

Figure 9-20 shows the heat flow over time for isothermal holds at 90°C (a), 100°C (b), and 110°C (c) of layers of nanocrystalline silver sputtered aluminum foil in a nanocrystalline silver coated sample cell, measured by a differential scanning calorimeter. At 90°C, the main change in heat flow occurred between 1430 and 1920 minutes (23.8 and 32 hours), lasting 490 minutes (8.2 hours). A smaller and shorter change in heat flow occurred at approximately 950 minutes (15.8 hours). At 100°C, the main change in heat flow occurred between 1040 and 1330 minutes (17.3 and 22.2 hours), lasting 290 minutes (4.8 hours). A smaller and shorter change in heat flow occurred at approximately 375 minutes

(6.3 hours). Isothermal holds at both 90°C and 100°C show a gradual increase in heat flow from the baseline after the initial small change in heat flow up to the main change in heat flow, where a step change occurs. At 110°C, no changes in heat flow were observed after the baseline stabilized. However, it should be noted that the baseline did not stabilize until 120 minutes (2 hours), whereas, it stabilized in 50 minutes with both the 90°C and 100°C runs. The nanocrystalline silver films created on aluminum using the in-house sputtering machine showed the same structure as that typically seen with nanocrystalline silver dressings, as determined using XRD (Figure 9-21).

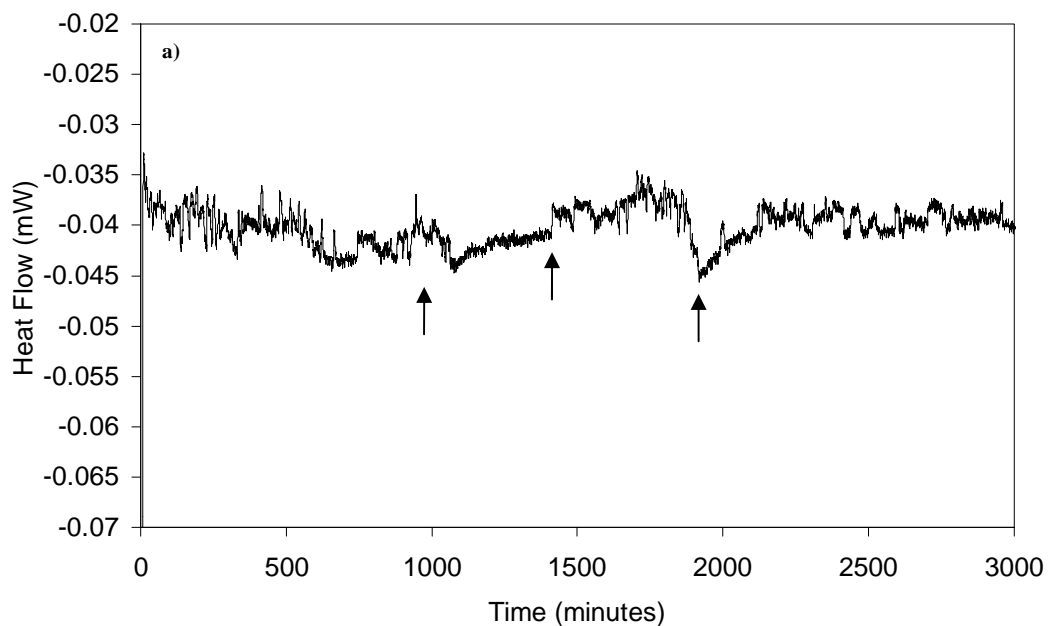


Figure 9-20.

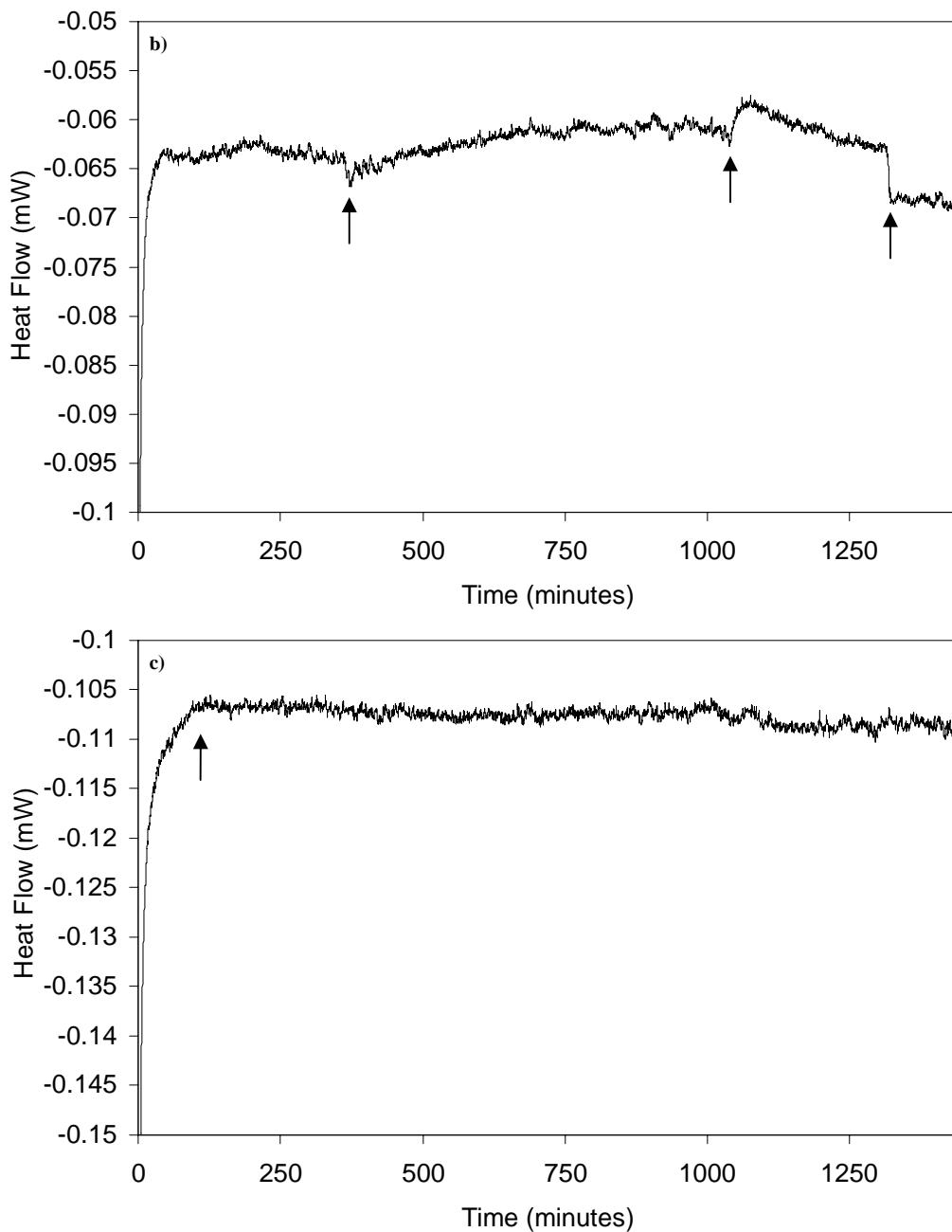


Figure 9-20. Differential scanning calorimetry of nanocrystalline silver sputtered on aluminum foil layered in a nanocrystalline silver-sputtered sample cell. Heat flow was measured over time for isothermal holds at 90°C (a), 100°C (b), and 110°C (c). Key time points are indicated with arrows.

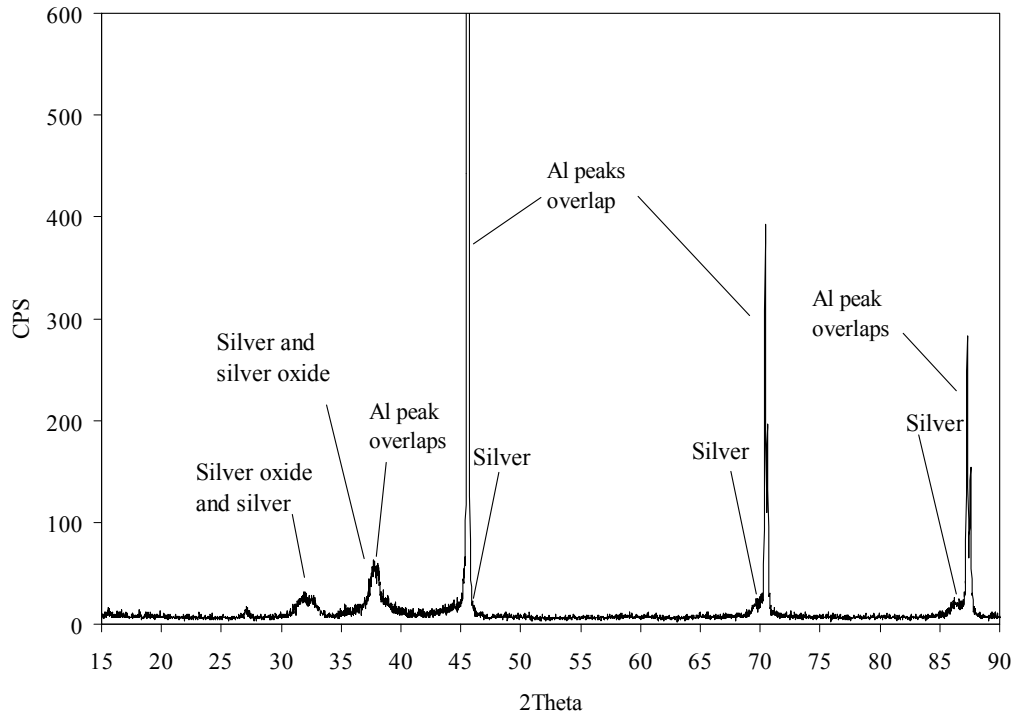


Figure 9-21. Diffraction patterns of nanocrystalline silver thin films sputtered onto aluminum foil for 30 minutes at 4% oxygen, 0.9 A, 40 mTorr pressure, and a working distance of 10 cm.

Discussion

The log reduction data (Figure 9-10) indicated that at short heat treatment times of 4 hours or less, nanocrystalline silver dressings still provided excellent bactericidal efficacy for heat treatment temperatures of 90°C and 100°C. Loss of bactericidal efficacy occurred rapidly with heat treatments of greater than 8 hours at 100°C, and greater than 4 hours at 110°C. Heat treatments at 90°C did not result in any loss of bactericidal efficacy in 24 hours. Since loss of bactericidal efficacy with heat treatment of nanocrystalline silver dressings at 90°C for 24 hours has been previously observed[9], it is expected that a drop in bactericidal efficacy would have been observed if the heat treatment times at 90°C had been extended in this study. Variations in the commercially obtained dressings, as well

as the use of different ovens, may account for the quantitative differences between this study and previously reported results; however, overall trends appear similar. Since at 90°C, critical changes occur right at 24 hours, it is not surprising that more variability in results with this heat treatment temperature was observed within the timeframe studied.

CZOIs were more dramatically impacted by the changes occurring in the dressings during heat treatment than were the log reduction tests. Although the samples heat-treated at 90°C did not show any loss of bactericidal efficacy, a decrease in longevity of the dressings occurred for samples heat-treated for 16 and 24 hours. Earlier onset of decreased zone of inhibition size was observed with heat treatments at 100 and 110°C, where loss of longevity was observed to begin between 4-8 hours and 0-4 hours, respectively.

The loss of bactericidal properties due to heat treatment coincided with the decrease in total soluble silver. The dressings heat-treated at 90°C did not show decreased total silver release or loss of bactericidal efficacy, but still experienced decreased longevity. This suggests that a change in the silver species being released, rather than the total silver released, caused a decrease in the longevity of the dressings with 90°C heat treatments. The decrease in silver release after 4 hours of heat treatment at 100°C with the corresponding loss of bactericidal efficacy and longevity at 8 hours and 4 hours of heat treatment, respectively, suggests that decreased total silver released also negatively impacted the biological activity. The 110°C heat treatment resulted in a very early loss of soluble silver, and a corresponding decrease in bactericidal efficacy and longevity

at shorter heat treatment times, confirming that the total soluble silver impacts the biological activity of the dressings. Thus, the decreased biological activity can be attributed to a change in the silver species being released, as well as the amount of silver being released. These two sources of decreased activity may be related.

During isothermal heat treatments, the crystallite sizes increased (XRD) and the finer features disappeared (SEM). The presence of these finer features (which are about 10-15 nm in diameter) appears to correlate with strong antibacterial efficacy, and the critical crystallite size of the silver, where a decrease in bactericidal activity was first observed at any heat treatment temperature, appears to be between 25-42 nm (~30 nm). The SEM images indicated that normal grain growth was taking place. Normal grain growth is defined as an overall even increase in crystallite size with a small deviation in size between crystallites, whereas in abnormal grain growth, a small number of crystallites increase in size by consuming the neighboring crystallites[13]. The small standard deviations in crystallite size, as measured by XRD, also indicated normal grain growth. The average size of the crystallites after 24 hours of heat treatment at 90°C was comparable to the average crystallite size after heat treatments of 8-14.5 hours at 100°C, and less than 4 hours at 110°C, indicating that grain growth occurred about two to three times more slowly with each 10°C drop in heat treatment temperature.

Grain growth exponents and activation energy help to determine the mechanisms of grain growth. Studies have shown that the grain growth exponent, n , generally varies between 2-10 in nanocrystalline materials[12]. Also, n values

for nanocrystalline materials are higher at lower temperatures[12]. The grain growth exponent for both isothermal heat treatments at 100 and 110°C was calculated to be 2.8, which is comparable to values determined in a grain growth study of silver thin films with initial grain sizes of 40-50 nm, where the grain growth exponent was found to be $n=3$ [14]. The grain growth exponent value for the 90°C isothermal hold of 4.2 may be due to an increase of grain growth exponent values as temperature is decreased. More likely, it could be due to the fact that 90°C grain growth curve did not plateau in the time frame measured, unlike the 100 and 110°C grain growth curves. This is corroborated by the DSC measurements which indicate that the 90°C grain growth mostly occurred between 24 and 32 hours, while XRD analysis was only performed to heat treatment times up to 24 hours.

The calculated activation energy of the nanocrystalline silver on the dressing was 177 kJ/mol (1.77 eV). This is significantly higher than the activation energy found for thin solid films experiencing normal grain growth (53 kJ/mol) with initial grain sizes of 40-50 nm[14], where it was concluded that grain growth was dominated by surface diffusion mass transport. Another study found that the activation energy in silver thin films (with initial grain sizes of approximately 170 nm) was found to be 95 kJ/mol between 225-280°C, suggesting grain growth was dominated by grain boundary diffusion, and 30 kJ/mol between 160-225°C, suggesting surface dominated electrotransport was the main mechanism for grain growth[15]. Hummel and Geier[15] summarized the relationship between silver activation energy and grain growth mechanisms

found in previous studies, where 1.91-1.95 eV was found to correlate with volume diffusion, 0.78-0.95 eV was found to correlate with grain boundary diffusion, and 0.30-0.43 eV was found to correlate with surface diffusion[15]. The activation energy for bulk silver, measured by tracer diffusion at temperatures between 640-955°C, was 189 kJ/mol[16]. Thus, it appears that volume diffusion and/or grain boundary diffusion are the possible dominate forms of diffusion occurring for the nanocrystalline silver dressings. It should be noted, however, that the activation energy calculations performed were based on an ideal system, and significant variations in activation energy are common when small concentrations of a second phase are present.

A decrease in the percentage of Ag₂O in the dressings as time increased for all heat treatment temperatures was observed via both XRD and XPS. Loss of Ag₂O and stabilization of the metallic silver have also been observed via XPS analysis of nanocrystalline silver thin films similar to ActicoatTM which were annealed under vacuum at 250°C for 30 minutes[17]. Thus, as has been previously suggested, Ag₂O is likely pinning the nanostructure of the metallic silver at room temperature, preventing crystallite growth[10]. However, at elevated temperatures, the Ag₂O pinned structure becomes unstable and decomposes over time, thereby allowing for grain growth[10]. The nanocrystalline silver appears to become unstable immediately with heat treatment at 110°C, whereas the breakdown of the nanostructure appears to occur more slowly at lower heat treatment temperatures, as indicated by XRD and XPS.

The cubic lattice structure of Ag₂O (*Pn-3m*) has a lattice parameter of

4.728 Å. Comparing this value to the lattice parameters measured over time with heat treatment at 100°C, the dressings appear to start out highly disordered, but ordering of the structure towards a very highly ordered cubic Ag₂O occurs rapidly with heat treatment (Table 9-2), followed by the breakdown of the Ag₂O.

Comparison of the total oxygen and silver-oxygen atomic concentrations measured during isothermal holds indicates that up to 35% of the oxygen loss is due to the breaking of the silver-oxygen bonds. In previous experiments involving 24 hour heat treatments, Taylor *et al.*[9] found that the total oxygen remained fairly constant until heat treatment temperatures exceeded 75°C. Because oxygen is considered insoluble in silver[18] under the conditions present during this study and that of Taylor *et al.*[9], it appears that the oxygen released by the breakdown of the silver-oxygen bonds (before there was any loss of total oxygen from the dressings) initially adsorbed to the large surface area provided by the nanostructured silver[10]. The total oxygen loss that occurred in heat treatments for 24 hours above 75°C was attributed to oxygen desorption, due to the decreasing surface area as the silver sintered[10]. The desorbed oxygen is therefore made up of oxygen released during silver oxide decomposition, and additional oxygen that adsorbed to the surface of the dressing after manufacturing[10]. The results of this study confirm the above mechanism.

The isothermal DSC results (Figure 9-20) indicate that at 90°C, the majority of the changes in heat flow occurred starting at 24 hours. This may explain the lack of decrease in soluble silver, total oxygen (XPS), or bactericidal activity within 24 hours. It also correlates with the observation of fine features

still present in the SEMs at 24 hours. It is interesting to note that the smaller brief heat flow change that occurred at 15.8 hours correlates in time with significant decreases in bacteriostatic longevity, which appeared with 16 hour heat treatments, but not with 8 hour heat treatments. As well, the first changes in crystallite size were observed at 16 hours, but the critical crystallite size was not reached until 24 hours, after which point the main changes in heat flow began to occur. With 100°C isothermal holds in the calorimeter, the main change in heat flow occurred between 17.5 and 22 hours. This main change in heat flow corresponds to a loss in bactericidal activity (not significant); decreased silver release into solution, which first became significant at 20 hours; the majority of the grain growth and sintering observed via SEM; and the drop in silver oxide and total oxygen observed via XPS. A smaller brief change in heat flow was observed at about 6 hours in the DSC, which appears to correspond to decreased bacteriostatic longevity, which first became significant with 8 hour heat treatments, a loss of some fine features which first became apparent at 8 hours (SEM), and the first clear increases in crystallite size, which occurred at 8 hours (XRD). As with the 90°C heat treatment, the critical crystallite size was reached just prior to the main change in heat flow. All together, these data suggest that the first smaller change in heat flow may correspond to an initial loss of silver oxide pinning structures and defect structures (vacancies followed by some grain boundaries, as crystallite sizes began to change as well), as well as possible changes in the silver species present, resulting in some of the earlier changes detected, while the main change in heat flow was due to normal grain growth. A

gradual increase in heat flow from the baseline between the initial small change in heat flow and the larger step-function change occurring later was observed. This may be due to small changes in crystallite size, small losses of silver oxide, and loss of smaller features occurring up to the critical crystallite size, after which the majority of changes occurred rapidly. It is interesting to note that when a pure nanocrystalline silver oxide film was analysed (Figure 9-19), it showed similar behaviour, likely due to the initial breakdown of unstable silver oxide bonds to form metallic silver, followed by sintering of the metallic silver once most of the silver oxide had converted to metallic silver. This indicates that the lack of signal during early sample analysis (using silver films delaminated from salt/sugar crystals or nail polish) was not due to the structure of the material (as either structure underwent similar changes), but rather to the low sample weights and poor conductivity.

It is also noteworthy that both changes in heat flow observed at 90°C had a starting time point approximately two times greater than at 100°C, and that the main change in heat flow lasted approximately twice as long. This suggests that the reaction times approximately doubled with a 10°C increase in temperature, similar to what was observed for speed of grain growth (XRD) with increased heat treatment temperature. This follows the rule of thumb that reaction rates for many reactions increase by two to three times for every 10°C increase in temperature[19].

When 110°C isothermal holds were performed, no changes in heat flow were observed. However, during these holds, a stable baseline was not reached

until two hours, unlike runs for the other two samples where stable baselines were obtained in less than half the time. Since the critical crystallite size had already been reached by 4 hours and very little silver oxide or total oxygen was remaining at that time, this suggests that the major changes in heat flow, which were observed with 90°C and 100°C isothermal holds, occurred during the first few hours in the DSC, where they went undetected because the baseline had not had a chance to stabilize. This is corroborated by the results showing that bacteriostatic longevity was decreased with only four hours of heat treatment, as was the total soluble silver, and that most of the finer features had disappeared at four hours as well (SEM).

The results of heat treatments at 90°C, 100°C, and 110°C taken together suggest that if the dressings are exposed to lower temperatures than the ones examined in this study over longer periods of time, they may undergo loss of pinning structure followed by grain growth, resulting in loss of activity. The results also suggest that loss of dressing longevity could occur long before the critical crystallite size was reached and any readily detected changes in the dressings (such as dressing color, which changes with the main grain growth) occurred at these lower temperatures. For example, if the trend of an approximately doubling reaction time observed is applicable for other temperatures than those examined, exposure of a dressing to 60°C for five days could result in a loss of bacteriostatic efficacy and a change in dressing structure that would likely make it more susceptible to grain growth.

Overall, exposure of nanocrystalline silver dressing to high temperatures,

in the range of 90-110°C, were found to negatively impact the bactericidal activity and longevity of the dressings. It appears that the dressings remain relatively stable for a period of time during heat treatment, after which they show rapid changes, corresponding to the changes in heat flow observed via DSC. The period of time that they remain stable becomes shorter with higher heat treatment temperature. Loss of bacteriostatic longevity appears to be the earliest biological indicator of changed dressing properties, while loss of silver-oxygen bonds appears to be an early chemical indicator that changes have begun, and loss of fine features appears to be an early physical indicator. Biological activity of nanocrystalline silver is clearly dependent on its specific nanocrystalline structure, which in turn can be easily altered at elevated temperatures over a relatively short interval of time, because even though the crystals are still in a nano-sized range, their antimicrobial properties dramatically decrease. This is corroborated by the fact that 5-12 nm single silver nanocrystals are not antimicrobial (see Chapter 4). Overall, the changes in all the dressing properties over time with heat treatment were non-linear.

Practical applications can be drawn from this study. High temperature exposure may be occurring during transportation and storage of nanosilver products. It is therefore recommended that precautions be undertaken to prevent loss of activity, both by ensuring low temperatures are maintained and by adding a high temperature exposure indicator to packaging. Failure to monitor the heat exposure of dressings may extend a patient's recovery time, which may not only impact the patient's health, but also increase medical costs. Finally, these results

must be taken into account for future development of medical treatments that rely on the healing properties of silver, and also in the analysis of silver products currently available on the market. The activity of dressings should be questioned when the dressings provide silver at crystal/crystallite sizes above 30 nm or provide silver products with low total silver release.

Bibliography

1. Bjarnsholt T, Kirketerp-Moller K, Jensen PO, Madsen KG, Phipps R, Kroghfelt K, Hoiby N, Givskov M: **Why chronic wounds will not heal: a novel hypothesis.** *Wound Repair Regen* 2008, **16**:2-10.
2. Tredget EE, Shankowsky HA, Groeneveld A, Burrell RE: **A matched-pair, randomized study evaluating the efficacy and safety of Acticoat silver-coated dressing for the treatment of burn wounds.** *J Burn Care Rehabil* 1998, **19**:531-537.
3. Burrell RE, Heggors JP, Davis GJ, Wright JB: **Efficacy of Silver-Coated Dressings as Bacterial Barriers in a Rodent Burn Sepsis Model.** *Wounds: A Compendium of Clinical Research and Practice* 1999, **11**:64-71.
4. Doshi J, Karagama Y, Buckley D, Johnson I: **Observational study of bone-anchored hearing aid infection rates using different post-operative dressings.** *J Laryngol Otol* 2006, **120**:842-844.
5. Rustogi R, Mill J, Fraser JF, Kimble RM: **The use of Acticoat in neonatal burns.** *Burns* 2005, **31**:878-882.
6. Fan FF, Bard AJ: **Chemical, electrochemical, gravimetric, and microscopic studies on antimicrobial silver films.** *J Phys Chem B* 2002, **106**:279-287.
7. Nadworny PL, Landry BK, Wang JF, Tredget EE, Burrell RE: **Does nanocrystalline silver have a systemic effect?** *Wound Repair Regen* 2009, (submitted).
8. Birringer R: **Nanocrystalline Materials.** *Mater Sci Eng* 1989, **A117**:33-43.
9. Taylor PL, Ussher AL, Burrell RE: **Impact of heat on nanocrystalline silver dressings. Part I: Chemical and biological properties.** *Biomaterials* 2005, **26**:7221-7229.
10. Taylor PL, Omotoso O, Wiskel JB, Mitlin D, Burrell RE: **Impact of heat on nanocrystalline silver dressings Part II: Physical properties.** *Biomaterials* 2005, **26**:7230-7240.
11. Balzar D: **Voigt-function model in diffraction line-broadening analysis.** In: *Microstructure analysis from diffraction.* Ed: Snyder RL. IUCR monograph; ©2001.
12. Suryanarayana C, Koch C: **Nanocrystalline materials - current research and future directions.** *Hyperfine Interactions* 2000, **130**:5-44.
13. Koch C, Ovid'ko I, Seal S, Veprek S: *Structural nanocrystalline materials: Fundamentals and applications.* Cambridge: Cambridge University Press; 2007. p. 99.
14. Dannenburg R, Stach E, Groza JR, Dresser BJ: **TEM annealing study of normal grain growth in silver thin films.** *Thin Solid Films* 2000, **379**:133-138.
15. Hummel RE, Geier HJ: **Activation energy for electrotransport in thin silver and gold films.** *Thin Solid Films* 1975, **25**:335-342.

16. *CRC handbook of chemistry and physics: a ready-reference book of chemical and physical data*, 88th Edition. Ed. Lide, DR. Boca Raton, Fla: CRC; ©2008.
17. Sant SB: **The nature of chemical species in novel antimicrobial silver films deposited by magnetron sputtering.** *Philosophical Magazine A-Physics of Condensed Matter Structure Defects and Mechanical Properties* 2002, **82**:1115-1136.
18. Niggli P: **Entry 31058 (1977).** In: *Inorganic crystal structure database - ICSD*. Germany: Fiz Karlsruhe; ©2004.
19. Connors KA: **Chemical kinetics: the study of reaction rates in solution.** New York: VCH; (c)1990: p. 14.

Chapter 10 – Conclusions

Conclusions

This work has substantially increased the understanding of the mechanisms of action of nanocrystalline silver, and has also resulted in the development of nanocrystalline silver-derived solutions which, depending on the conditions under which they were generated, were able to produce the biological activity seen with nanocrystalline silver thin films. The following is a list of key conclusions resulting from the work:

1. Nanocrystalline silver has anti-inflammatory activity independent of its antimicrobial activity (Chapter 2). This activity is related to increased apoptosis in inflammatory cells but not keratinocytes, decreased matrix metalloproteinase expression, and decreased expression of pro-inflammatory signaling molecules IL-8, TNF- α , and TGF- β . In contrast, silver nitrate treatments result in apoptosis induction in keratinocytes, increased mast cell presence, and an increased inflammatory response.
2. The apoptosis induction observed in the deep dermis during treatment with nanocrystalline silver is not due to direct contact of silver with inflammatory cells, as nanocrystalline silver has minimal penetration into the skin (Chapter 3). A variety of silver cluster sizes are detectable in skin treated with nanocrystalline silver but not with silver nitrate.
3. Nanocrystalline silver placed over healthy tissue can decrease inflammation present at other locations, indicating a systemic effect (Chapter 3). Due to the observation of point 2 (above), this effect is likely

not due to silver travelling to the site of injury, but rather due to the dissolution products of nanocrystalline silver interacting with nearby cells, setting up an anti-inflammatory biological cascade. Furthermore, nanocrystalline silver treatments result in increased expression of IL-4, EGF, KGF, and KGF-2, indicating that regulation of these molecules may play a part in the anti-inflammatory/pro-healing effect observed.

Surprisingly, IL-10 did not appear to play a role in the process.

4. Nanocrystalline silver has superior bactericidal activity and bacteriostatic longevity relative to a variety of recently developed silver-containing dressings of various formulations which release only Ag^+ (Chapter 4), indicating that nanocrystalline silver must release additional antimicrobial species. This was further confirmed by the fact that nanocrystalline silver was bactericidal against Ag^+ -resistant species of bacteria, which other dressings containing only Ag^+ could not kill. In addition, resistance could be easily developed to a variety of Ag^+ -containing dressings, but was not readily developed to nanocrystalline silver, suggesting multiple antimicrobial mechanisms of action would need to be simultaneously overcome for bacteria to develop resistance to nanocrystalline silver. Nanocrystalline silver dressings should still be used with care in order to prevent the development of bacteria which are resistant to it.
5. The activity of single nanocrystals (or nanoparticles) of silver is minimal relative to nanocrystalline silver, indicating that the polycrystalline

structure, and therefore grain boundaries, of nanocrystalline silver, are important for its activity (Chapter 4).

6. Nanocrystalline silver dissolution products vary significantly with starting pH and solution components, resulting in unique optical properties, pH profiles, and total silver profiles (Chapter 5). Perhaps more importantly, nanocrystalline silver-derived solutions can have excellent antimicrobial activity, particularly when dissolved in distilled water, but this is highly dependent on the dissolution conditions used.
7. Examination of the effect of dissolution on nanocrystalline silver thin films (Chapter 5) showed that dissolution in acidic solutions resulted in decreased silver oxide remaining in the dressings, while dissolution in basic solutions resulted in decreased metallic silver remaining in the dressings. Dissolution did not appear to result in the loss of fine features or increase in crystallite size over time, indicating that new fine features appeared during the dissolution process. An apparent exception to this occurred with dissolution in serum, where no silver oxide remained, and the crystallite size increased slightly, with loss of finer features.
8. Nanocrystalline silver structure does not appear to be impacted by leaving the films under vacuum for 24 hours (Chapter 5).
9. Nanocrystalline silver-derived solutions demonstrate anti-inflammatory/pro-healing properties, particularly at a high starting pH of 9 (Chapter 7). Combined with point 7 (above) this suggests that a metallic silver species is responsible for the anti-inflammatory activity of

nanocrystalline silver. Combined with point 6 (above), it may be possible to generate solutions which have anti-inflammatory activity but not antimicrobial activity, and vice versa. The anti-inflammatory/pro-healing activity observed was very similar to that in the nanocrystalline silver thin films with pH 9 treatments. However, it was weak with pH 4 treatment and delayed with pH 5.6 (distilled water) treatment. At pH 7, apoptosis was induced in both the epidermis and the dermis. This suggests that one of the dissolution products, which was low with dissolution at pH 7, may have a protective effect on keratinocytes, preventing their apoptosis. This could prove very useful in the treatment of diseases such as TENs.

Overall, these results indicate that nanocrystalline silver-derived solutions can have anti-inflammatory activity, and thus may be useful in the treatment of a variety of inflammatory diseases for which treatment with nanocrystalline silver dressings is not a viable option.

10. Conditions to mimic ActicoatTM in an in-house sputtering machine were determined (Chapter 8). As well, the impact of various sputtering conditions on the properties and antimicrobial activity of nanocrystalline silver were examined. Increasing sputtering time increases the total silver deposited but does not affect the dressing chemistry, allowing for sufficient silver to be deposited at a selected chemistry to generate sustained activity. Increasing oxygen results in increased silver oxide up to a point, above which the system chemistry changes, possibly due to generation of an oxygen plasma. A certain level of silver oxide is

necessary for activity, as it is needed to pin the dressing nanostructure, but above that level, activity drops, as mostly silver oxide is deposited.

Increasing current results in increased deposition rate, but decreased ammonia soluble silver, and thus to have a bioactive dressing, an optimum current must balance these two effects.

11. Increasing the crystallite size in nanocrystalline silver thin films by heat treatment results in loss of antimicrobial activity for crystallite sizes above ~30 nm. This corresponds to a loss of soluble silver, silver oxide, total oxygen, and fine features in the dressing. This highlights the importance of grain size for nanocrystalline silver activity, and thus the importance of the silver oxide to pin the nanostructure, preventing its growth. This, in combination with point 5 (above) indicates the importance of having a poly-nanocrystalline silver structure for optimal silver antimicrobial activity. A time-temperature kinetic relationship was developed which indicates that in practical situations such as production, storage, and use of the dressings, the temperature of the dressings should be monitored to prevent their deactivation.

Figure 10-1 provides some hypotheses, based on the results of the studies performed in this work, regarding the mechanisms of action of nanocrystalline silver in a wound healing environment.

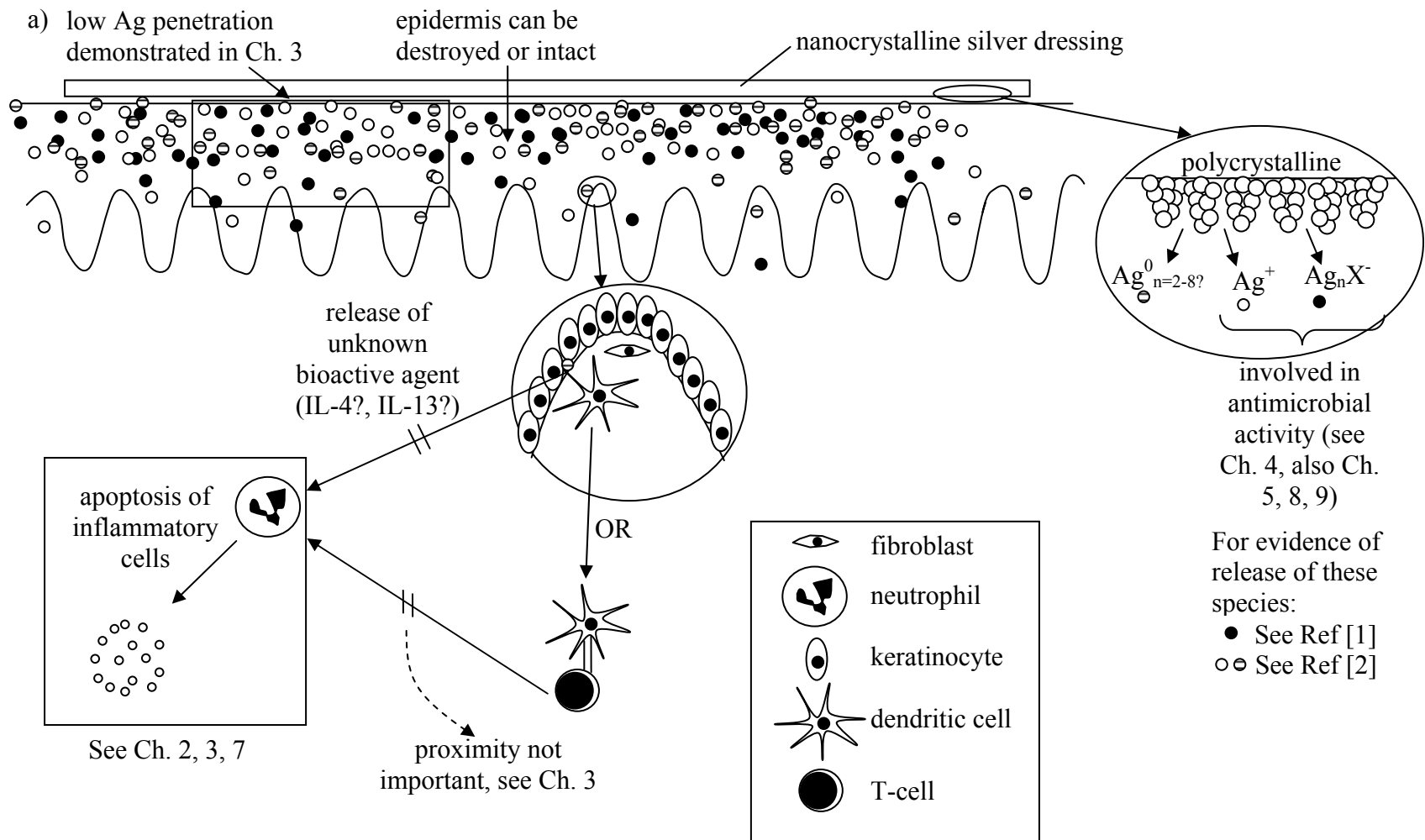


Figure 10-1.

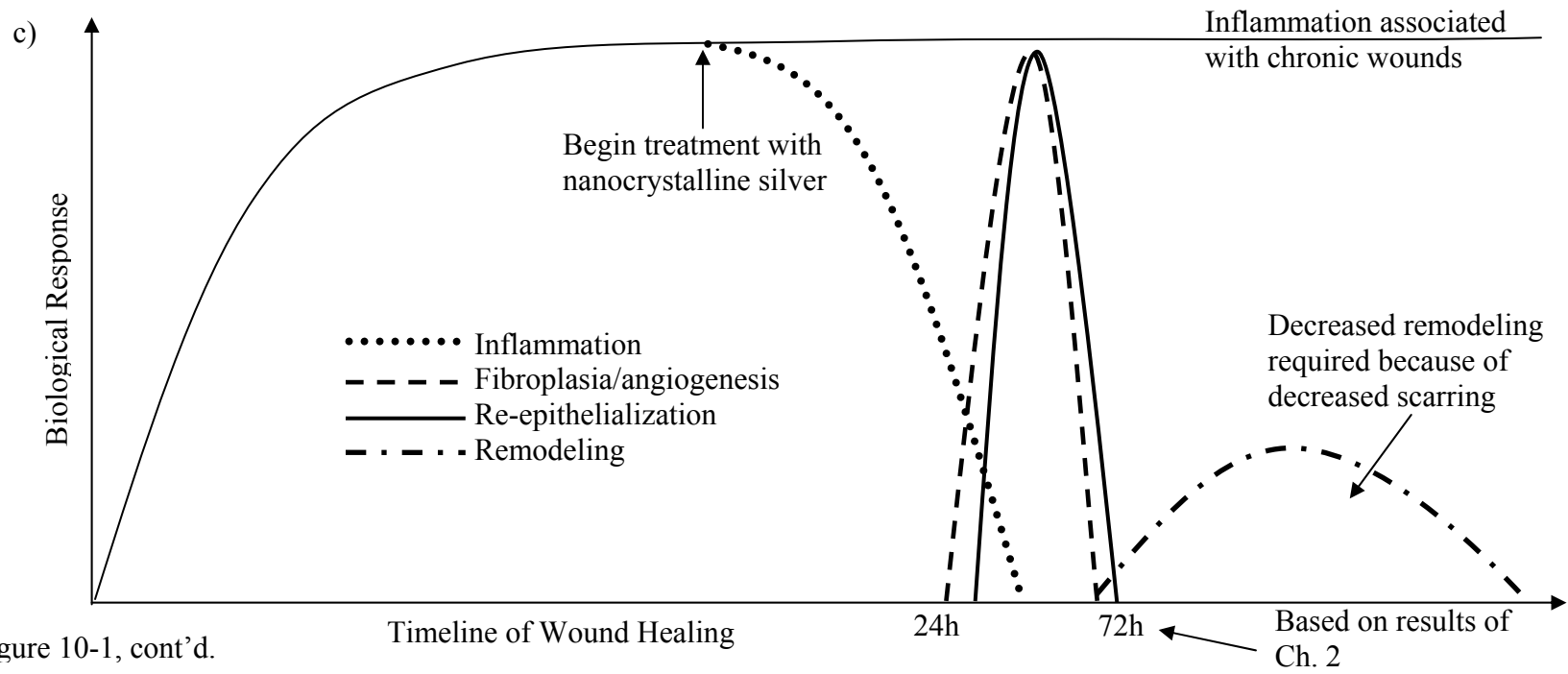
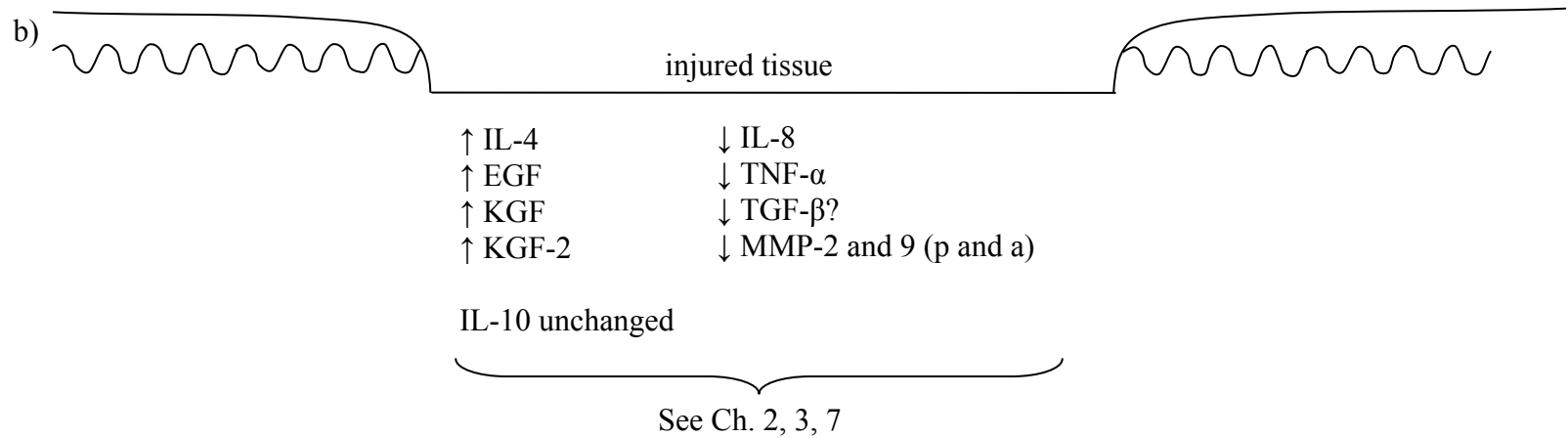


Figure 10-1, cont'd.

d)

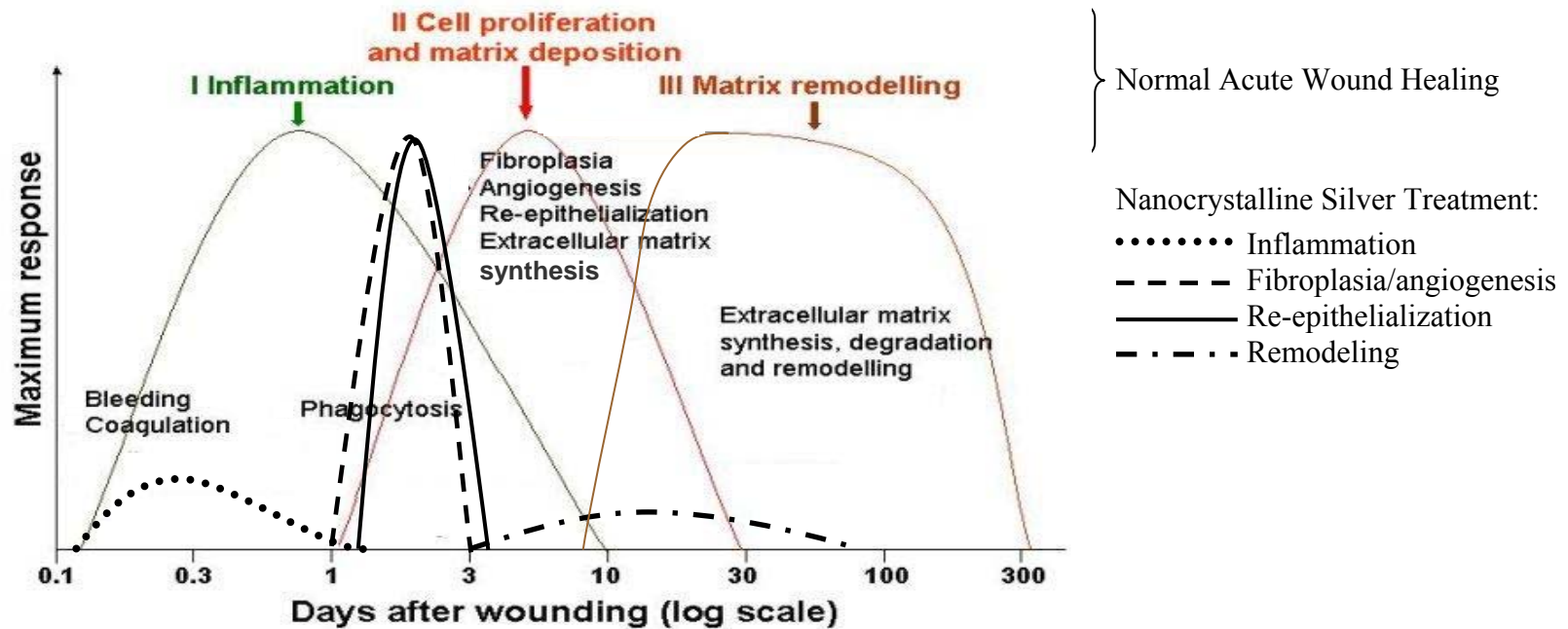


Figure 10-1, continued. Hypotheses about the mechanisms of action of nanocrystalline silver anti-inflammatory activity: Panel a) shows interactions between nanocrystalline silver and biological systems. Within the limit of detection of SIMS imaging, the nanocrystalline silver did not demonstrate further penetration of species into the tissues than silver nitrate treatments (Ag^+). The silver cluster weights showed poor penetration, even relative to such species as AgCl and AgO within the nanocrystalline silver treated animals. Based on the SIMS data, therefore, there should be less silver cluster penetration shown in this panel, but definite conclusions have not been made about this, since this conclusion is made on the basis of SIMS data alone. Therefore approximately equal amounts of all species are shown penetrating to approximately the same depth. Panel b) shows the impact on signaling molecules at sites of injury. Panel c) shows the impact of treatment with nanocrystalline silver on chronic wounds. Panel d) shows the impact of treatment of acute wounds with nanocrystalline silver (normal wound healing timescales are shown in color, modified from Ref [3], while wound healing timescales with nanocrystalline silver treatment are overlaid in black).

Future Directions

It appears that nanocrystalline silver treatment may cause an overall modulation of the inflammation process, resulting in increased rates of wound healing. However, a further understanding of what cells and signaling molecules are involved in this activity is needed. Since nanocrystalline silver appears to have very low skin penetration, it seems that the mostly likely cellular target would be keratinocytes at the wound edges, or some other cell which regularly migrates right to the surface of wounds, such as an antigen presenting cell. It would be very interesting to examine the effect of nanocrystalline silver on FGF-22, a growth factor released by keratinocytes which results in epidermal repair in an autocrine manner[4]. However, an antibody for FGF-22 was not available for immunohistochemical analyses at the time that this work was prepared.

Further study will be needed to fully understand the unusual optical properties of nanocrystalline silver-derived solutions, what these properties indicate about the species dissolved, and what the usefulness of these properties might be as methods of testing or comparing solutions generated under various conditions. Determining the identities and quantities of the various silver species dissolved in solution would be extremely valuable in the development of targeted treatments, as solutions could then be selected and tested based on the species dissolved, and the biological activities of each species could be clearly identified, and used to target specific medical conditions. Further study of the effect of dissolution of nanocrystalline silver thin films in serum would be valuable to understand the activity of nanocrystalline silver in a clinical setting.

It would also be valuable to determine whether or not placing nanocrystalline silver dressings on healthy skin could result in decreased inflammation related to joints, lungs, or other internal organs.

The effect of sputtering conditions on the anti-inflammatory activity of silver thin films should also be examined, and various conditions around those found to generate films similar to Acticoat™ could be tested to optimize antimicrobial activity or anti-inflammatory activity. It might even be possible to generate films which have high anti-inflammatory activity and low antimicrobial activity, or vice versa, which could then be used for targeted therapies. The impact of substrate on the resulting film properties should also be examined, as this would impact the ability to use the films on a variety of medical surfaces beyond HDPE mesh dressings.

It might also be valuable to determine the effect of wetting nanocrystalline silver film dressings in a basic solution prior to treating wounds, rather than using distilled water, as this might result in increased initial release of anti-inflammatory silver species into the wound.

Perhaps most importantly, nanocrystalline silver-derived solutions should be tested for their anti-inflammatory and antimicrobial effects in appropriate lung models, to examine their potential for the treatment of lung diseases such as ARDS and pneumonia. They could also be tested in an IBD model, an RA model, or any other model for which apoptosis control is important, as this appears to be a key aspect of the anti-inflammatory/pro-healing activity of nanocrystalline silver.

Bibliography

1. Demling R, Burrell RE: **The beneficial effects of nanocrystalline silver as a topical antimicrobial agent.** *Leadership Medica* 2002, **16**:10 pages.
2. Fan F, Bard AJ: **Chemical, Electrochemical, Gravimetric, and Microscopic Studies on Antimicrobial Silver Films.** *Journal of Physical Chemistry B* 2002, **106**:279-287.
3. Enoch, S, Price P. **Cellular, molecular and biochemical differences in the pathophysiology of healing between acute wounds, chronic wounds and wounds in the aged.** *World Wide Wounds* 2004. Viewed Dec. 20, 2009. <http://www.worldwidewounds.com/2004/august/Enoch/Pathophysiology-Of-Healing.html>.
4. Beyer TA, Werner S, Dickson C, Grose R: **Fibroblast growth factor 22 and its potential role during skin development and repair.** *Exp Cell Res* 2003, **287**:228-236.

HEALTH SCIENCES LABORATORY ANIMAL SERVICES
STANDARD OPERATING PROCEDURE
MEDICAL SCIENCES BUILDING NECROPSY M-B74
ABL 2/CONVENTIONAL RATS REPUTABLE SOURCE

MANAGER: Karen
TECHNICIAN: _____
INVESTIGATOR: Dr. R. Burrell

All VAF animals of known health status must be completed prior to entering this area. These animals will be infected with **PSEUDOMONAS AERUGINOSA**. This is a gram-negative aerobic rod bacterium, which is a common inhabitant of soil and water. This species is an opportunistic pathogen of humans and any persons who are immunocompromised should not be entering this area and involved with the care of these animals. This is considered a Level 2 Pathogen in the Health Canada Biosafety Guidelines. Protection is required to prevent bites, scratches, mucous membrane and/or respiratory exposure. Follow instructions within this SOP.

These rats will be housed in micro isolator caging that will be positioned near the window for observation and light source. This SOP is to be observed if it is necessary to enter for clinical health evaluation, cage change, or any other reason requiring entry while this experiment is in progress. Entry/exit to the inner necropsy can be accomplished via the cooler but must be authorized by the Clinical Pathologist.

- Street/outside lab clothing is removed in designated change rooms and facility scrubs are donned followed with a facility lab coat or back-fastening gown.
- Remove the facility lab coat or back-fastening gown at the door of the Necropsy.
- Immediately upon entering the Necropsy, don new plastic shoe covers or rubber boots.
- Wash hands with provided disinfectant kept by the sink. Prepare a 5% bleach solution (50ml bleach/1000ml water) which will be used wherever disinfection of equipment is specified in this SOP including the footbath. Contact time for this concentration is always 5 minutes.
- Don a hair bonnet (all hair tucked in), an N95 respirator (one-time use only) and protective eye goggles, clean back-fastening gown or lab coat from the bin provided and one pair of gloves, which are then secured to the cuff of the gown/lab coat with masking tape. **If rats are to be handled as required for cage changes, also don a pair of wire-mesh bite proof gloves. You may need to drape the rats also only to prevent trauma to their skin from these gloves.**
- Proceed to check the animals or change the cages. Rats are single-housed in micro-isolator cages (shoebox plus filter top). **DO NOT VENT THE CAGES.** Rats are to each have a PVC tube for enrichment and receive a piece of paper towel on top of the wire-top on each cage change.
- Complete daily room sheet and census activity (cost center is RAT/ABL/CONVENTIONAL).

- If certain that all animals are comfortable, move close to the hallway door and exit the Necropsy as follows:

REMOVE PROTECTIVE WEAR BY USING ASEPTIC TECHNIQUE: DO NOT TOUCH THE OUTSIDE OF ANY PPE BUT REMOVE BY GRASPING THE INSIDE AND TURN THE GARMENT INSIDE OUT (INCLUDES BONNET, MASK, GLOVES, GOWN/LAB COAT). Proceed as follows:

- Remove the bonnet. Remove the N95 respirator and discard (not possible to decon this without damaging integrity of the filter).
- Remove your gloves. Place in provided garbage receptacle. Remove the gown/lab coat and place in provided laundry receptacle. Remove plastic shoe covers and place in garbage. Wash your hands. Remove rubber boots as you exit the area. Dip soles of your shoes in foot bath immediately before exiting.
- Redon your initial lab coat/gown. Lock the door. Return to the change room and re-don your street/outside lab clothing.

SPECIAL PROCEDURES:

- To transfer animals to the adjoining lab M-B82, remove the water bottles. Place the cage containing the rat with filter top intact inside of a plastic autoclave bag. Twist the bag shut with a twist of masking tape and spray with 5% bleach. Cover and secure entirely with drapes. Spray again with 5% bleach. Wait 5 minutes and then transfer to the lab and immediately remove the cage from the bag inside of the BSC (always running). Repeat procedure to return rats to the animal holding room (M-B74) and remember to return the water bottles. Follow additional instructions inside the lab for cleanup of the BSC and the lab when you are done.

- Phone the Investigator/Contact regarding any morbidity and mortality. Also phone the Veterinarian-on-call and notify the manager of same.
- Carcasses are to be double-bagged (contain any leaks), secured with wrap of masking tape, identified with a completed disposal label and request for post-mortem and then placed in the Necropsy cooler for pickup by the Investigator or for a necropsy, whichever is requested. Be sure to clearly indicated "BIO HAZARD - PSEUDOMONAS AERUGINOSA" and leave a message for the Pathologist (21425) that this sample has been submitted.
- Unused water is decanted directly into the sink (place close to the drain to avoid aerosols). Follow this with a 2L flush of 5% bleach solution. No additional flush of water is required.
- Empty uneaten feed from the wire tops into the cage bottom (again avoid aerosolization of bedding, etc.). Bag all caging material securely in a plastic autoclave bag and securely close with a wrap of masking tape. Complete a disposal label and affix to the bag. Spray the bag with a 5% bleach solution. Secure all bags to transport cart under a cover that is fastened (tied/taped) to the cart and then spray again with a 5% bleach solution and after 5 minutes, transport to the MSB Bio-containment airlock for autoclaving.

- The rack holding the cages, upon the end of the experiment, is wiped down entirely with 5% bleach solution and then following a 5 minute contact time, draped and transported directly to the dirty cage wash area for cleaning.
- Upon completion of this experiment (one week duration) or once weekly if longer, following cage change all areas of wall contact are to be wiped with 5% bleach. The sink is to be disinfected the same and polished with glass cleaner along with the windows. The floor is to be mopped with 5% bleach. Following the five minute contact time, all surfaces can be rinsed with clear water and all stainless steel and glass are to be polished.

M-B82 Serology Lab Requirements of Use

- Full gown-up is expected as in the animal room.
- All bleach concentrations will be the indicated concentration and contact time within the housing area. Use the provided mouse cage, measuring cup and bleach under the cabinet to make the required solution. Use of goggles during this procedure is expected.
- The BSC must be left running at all times, however, the light may be turned off.
- All animals/caging must remain inside the cabinet after the bags are opened or during manipulation of the animals. At no time may the animals be out on the bench top open to the room air.
- The animals/caging must be prepared for transport back to the housing room or to the MSB biocontainment animal facility as indicated in the above SOP. Once the cages/animals are re-bagged the outside of the bags must be wiped down and decontaminated using the bleach solution and contact time indicated within this sop.
- All equipment brought into the BSC must be decontaminated by the same bleach solutions with the same contact time before being removed. **Do not take any equipment into the cabinet with exposure to the animals if it cannot be wiped down with the bleach solution.**
- The BSC must be decontaminated by wiping down all surfaces after removal of all animals/cages and equipment with the same bleach solutions with the same contact time.

M-B82 Serology Lab Requirements of Use Continued:

- Aseptic Technique must be followed while working within the cabinet; keeping hands within the cabinet and dipping gloves into the bleach solution (within the cabinet) before removing hands out of the cabinet.
- Do not block or cover the intake grills of the BSC at any time. Ensure the sash is down and in place before opening the bags containing the animals.
- All needles and sharps must be disposed in the sharps container provided within the BSC. Ensure that a new Sharps container is replaced after each animal event that uses the BSC.
- After each event that has animals within the BSC, the Sharps container must be bagged in an autoclave bag by the PI staff and sealed with tape(as in the above sop) and following decontamination procedures with bleach solution, remove it from the BSC. The sharps container can then be sent to MSB biocontainment for autoclaving prior to disposal.

- Concluding use of the room; all counter tops and the floor must be wiped with the indicated bleach solutions and then rinsed with fresh water as indicated within the main sop.
- Return the cleaning supplies to the storage area under the sink.

Clinical Pathologist Manager	Investigator Signature	Manager of Operations, HMRC/MSB Complex	Investigator	Services
---------------------------------	------------------------	---	--------------	----------

CC Dr. Dan Dragon

I:\home\donna\word\2007 MSB Bio SOP\pseudomonas aeruginosa

Appendix 2 - Lipopolysaccharide Isolation

Lipopolysaccharide isolation was attempted following methods in the literature[1-3], in hopes of using it for the inflammatory lung studies in Chapter 6.

Collection of Biomass and Lyophilization

3 colonies of *Pseudomonas aeruginosa* were transferred from an MHA plate into 100 mL of TSB. This was incubated overnight at 37°C in a shaker incubator. Simultaneously, a fermentor was sterilized and loaded with 30 L TSB. 6 flasks of 100 mL TSB were inoculated with 1 mL each of the inoculum grown overnight. The newly inoculated flasks were incubated in the shaker incubator at 37°C for 4 hours. This inoculum was added to the fermentor, which was run at a flow rate of 18 L/min and a temperature of 37°C overnight. Data from the run is shown in Figure A2-1. The resulting bacterial growth was poured into 20 centrifuge buckets and centrifuged for 20 minutes at 1700 rpm. The supernatant was poured off, and the pellets were resuspended and combined. Approximately 20 mL was used per pellet, with a little extra for rinsing each bucket, for a total of about 700 mL. The resulting suspension was centrifuged again, and this procedure was repeated twice for a total of three washes of the collected bacteria. Based on the optical density of the original material, a total wet weight of 1.78 kg was estimated. However, when the pellets were weighed, the wet weight was estimated to be 500-600 g. The pellets were frozen at -20°C. Four days later they were allowed to thaw at 4°C. Approximately 200 mL of PBS was added to each bottle containing pelleted material, and then this suspension was divided into round bottomed flasks (approximately 80 mL per flask). The flasks were placed

in dry ice/methanol bathes and spun until the bacteria-containing suspension froze in a thin layer on the sides of the flasks. The flasks were attached to a Freezeomatic freeze dryer, and exposed to the vacuum. The samples were allowed to freeze dry overnight. At the completion of the freeze drying, the samples were no longer cold, flaked easily, and had shrunk away from the sides of the flasks. The lyophilized material was recovered from the flasks, at which point the dry weight was 91.0g, and powdered in a fumehood using a mortar and pestle, after which the dry weight was 90.3g, indicating some loss of powder during the powdering process. If the dry weight is 20% of the wet weight (personal communication, Nick Allan, October 23, 2007), this suggests the original wet weight was 455 g.

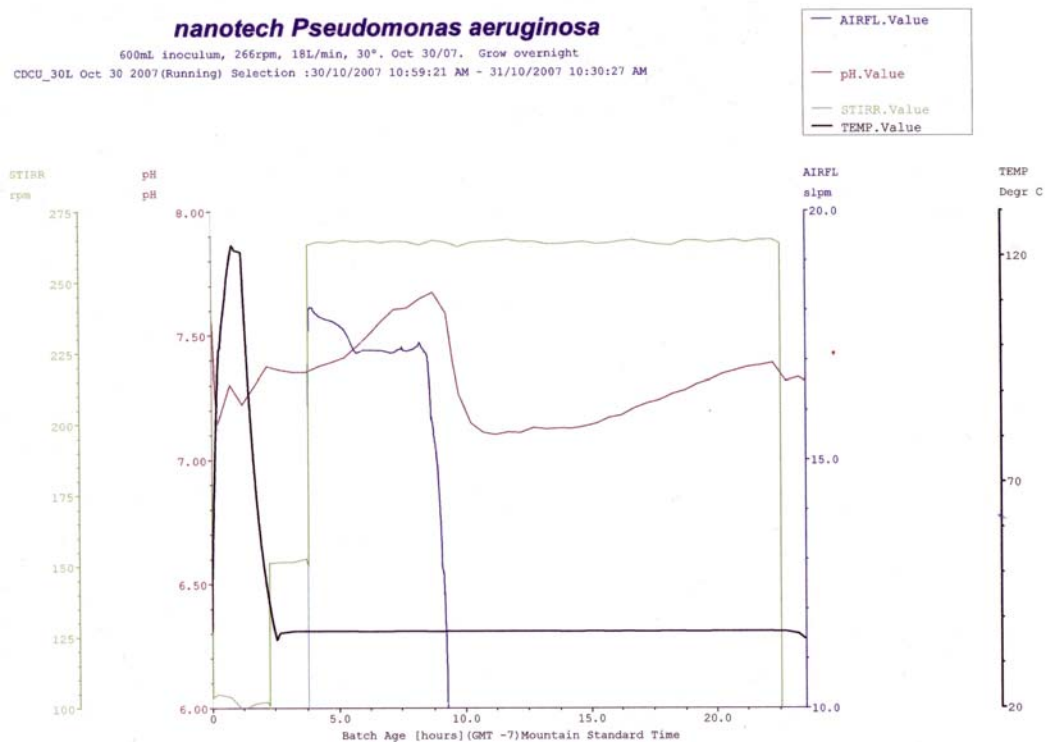


Figure A2-1. pH, temperature, airflow, and stirring data over time for *Pseudomonas aeruginosa* growth in a fermentor.

LPS Extraction with Hot Phenol

Powdered *Pseudomonas aeruginosa* was gradually added to Millipore water at 70°C, until 30 g had been mixed with 300 mL of water. The temperature was maintained close to 70°C while the *Pseudomonas aeruginosa* was resuspended in the water using a heated stir-plate. 350 mL of phenol was heated to 70°C in a water bath, and was then slowly added to the bacterial suspension with vigorous stirring, while maintaining the temperature of the emulsion as close to 70°C as possible. Stirring at 70°C was continued for 3 hours.

At the end of the extraction period, the mixture was removed from heat, and allowed to cool to room temperature for 4 hours. Then it was packed on ice overnight to begin phase separation.

The suspension was centrifuged (8300 rpm, 20 min, 4°C) to promote good phase separation. As the layers did not separate well, the suspension was centrifuged a second time (8281 g, 4°C, 20 min). An upper aqueous layer and a lower phenol layer resulted, with cell debris at the bottom. The cell debris was discarded. Approximately 300 mL of the aqueous layer was recovered.

Removal of Phenol from the LPS-Rich Aqueous Layer by Dialysis

60 cm of dialysis tubing (3500 MWCO) was soaked in distilled water for 20 minutes. It was then rinsed three times with distilled water. The bottom of the tube was clamped and the aqueous layer was loaded into the tubing. The tube was clamped at the top, and placed in a container of cold slow flowing tap water in a fumehood, to remove the phenol from the aqueous phase. The following day, the tubing was quite full, despite 10% initial allowance. A second piece of tubing

was prepared as described above, and approximately half of the liquid was transferred from the first tube to the second one. After seven days, any lumps in the material in the tubing were broken up to enhance phenol removal, and the material was transferred to two fresh dialysis tubes prepared as described above. It took 12 days for no more phenol to be detected (by smell) and the sample was dialysed for a further two days to ensure that no phenol was left.

Concentration of the LPS-Rich Aqueous Layer Via Centrifugation

When the dialysis was complete, the sample was frozen at -80°C and then lyophilized.

Reduction of Contaminants via Enzymatic Digestion

At this point, the next step would have been to resuspend the sample for enzymatic degradation, however the procedure was shut down due to safety concerns related to the use of the ultracentrifuges in subsequent steps (see below). The intention was to resuspend the lyophilised material in nanopure water at a concentration of 1-10 mg/mL, and then perform enzymatic digestions. The first digestion would have been done using bovine pancreatic deoxyribonuclease I (DNase I, Sigma) and RNase A Type I-A (Sigma), both at concentrations of 10 $\mu\text{g/mL}$, in the presence of 10 mM MgCl_2 , for one hour at 37°C . The second digestion would have been done with proteinase K (10 $\mu\text{g/mL}$), at 56°C for two hours.

Final Centrifugation for Purification and Isolation of LPS

After digestion, the material would have been allowed to cool, and then would have been centrifuged. The centrifugation would have removed unwanted

material and concentrated the LPS. Low speed spins of about 12 000 g for about 20 min at 4°C would have been used to remove cell debris such as murein. The supernatant (LPS-rich) layer would have been retained via collection with a pipette, and this would have been repeated five times. This would have been followed by high speed spins at 100 000 g for up to 18 hours at 4°C to pellet out the LPS and leave the digested DNA, RNA, and protein in the supernatant. If the LPS pellet was not transparent at this point, the low speed spins, and then the high speed spins, would have been repeated. The pellet would then have been re-suspended in a small volume of water, lyophilised, and stored at 2-8°C.

Assessment of LPS Purity

To assess the purified LPS, a concentration of 1 mg/mL of the final LPS product, supplemented with SDS at a final concentration of 0.1% (w/v), would have been analyzed using a BCA assay, similar to that described in Chapter 2.

Bibliography

1. Westphal O, Jann K: **Bacterial lipopolysaccharides.** *Methods Carb Chem* 1965, **5**:83-91.
2. Heckels JE, Virji M: **Separation and purification of cell surface components.** In: *Bacterial Cell Surface Techniques* Edited by Hancock I, Poxton I. Chichester, UK: John Wiley and Sons; 1988: 91-95.
3. Sprott DG, Koval SF, Schnaitman CA. In: *Methods for General and Molecular Bacteriology* Edited by Gerhardt P, Murray RGE, Wood WA, Krieg NR. Washington, D.C., USA: ASM Press; 1994: 88-93.